NASA Contractor Report 3097

Rotary Balance Data for a Typical Single-Engine General Aviation Design for an Angle-of-Attack Range of 8° to 90°

I - High-Wing Model B

William Bihrle, Jr., and Randy S. Hultberg

CONTRACT NAS1-14849
SEPTEMBER 1979

NASA

NASA Contractor Report 3097

Rotary Balance Data for a Typical Single-Engine General Aviation Design for an Angle-of-Attack Range of 8° to 90°

I - High-Wing Model B

William Bihrle, Jr., and Randy S. Hultberg
Bihrle Applied Research, Inc.
Jericho, New York

Prepared for
Langley Research Center
under Contract NAS1-14849

NASA
National Aeronautics
and Space Administration

Scientific and Technical
Information Branch

1979

SUMMARY

Aerodynamic characteristics obtained in a rotational flow environment utilizing a rotary balance located in the Langley spin tunnel are presented in plotted form for a 1/6.5-scale, single-engine, high-wing, general aviation airplane model. The configurations tested included the basic airplane, various wing leading-edge devices, tail designs, and rudder control settings as well as airplane components. Data are presented without analysis for an angle-of-attack range of 8^{o} to 90^{o} and clockwise and counter-clockwise rotations covering an $\frac{\Omega b}{2V}$ range from 0 to 0.85.

INTRODUCTION

The NASA Langley Research Center has initiated a broad general aviation stall/spin research program which includes spin-tunnel and free-flight radio control model tests, as well as full-scale flight tests for a number of configurations typical of light, general aviation airplanes. To support this effort, rotary balance wind tunnel force tests covering these same configurations will be conducted to establish a data base for analysis of model and full-scale flight results, and to develop design charts for desirable stall/spin characteristics.

A 1/6.5-scale, single-engine, general aviation airplane model, referred to as model B, having a high-wing location was tested in a rotational flow environment utilizing a rotary balance located in the Langley spin tunnel. This report presents the data obtained for the basic configuration, various wing leading-edge devices, tail designs and rudder control settings as well as airplane components. Data for model B having a low-wing location are presented in reference 1.

SYMBOLS

The units for physical quantities used herein are presented in the International System of Units (SI) and U.S. Customary Units. The measurements were made in the U.S. Customary Units; equivalent dimensions were determined by using the conversion factors given in reference 2.

b wing span, m (ft)

$\bar{c}$ mean aerodynamic chord, cm (in.)

C_L lift-force coefficient, $\frac{\text{Lift force}}{qS}$

C_N normal-force coefficient, $\frac{\text{Normal force}}{qS}$

C_A axial-force coefficient, $\frac{\text{Axial force}}{qS}$

C_Y side-force coefficient, $\frac{\text{Side force}}{qS}$

C_ℓ rolling moment coefficient, $\frac{\text{Rolling moment}}{qSb}$

C_m pitching-moment coefficient, $\frac{\text{Pitching moment}}{qS\bar{c}}$

C_n yawing-moment coefficient, $\frac{\text{Yawing moment}}{qSb}$

q free-stream dynamic pressure, N/m^2 (lb/ft^2)

S wing area, m^2 (ft^2)

V free-stream velocity, m/sec (ft/sec)

α angle of attack, deg

β angle of sideslip, deg

Ω angular velocity about spin axis, rad/sec

$\frac{\Omega b}{2V}$ spin coefficient, positive for clockwise spin

δ_a aileron deflection, positive when right aileron is down

$(\delta_{a_{right}} - \delta_{a_{left}})/2$, deg

δ_e elevator deflection, positive when trailing edge is down, deg

δ_r rudder deflection, positive when trailing edge is to left, deg

Abbreviations:

cg center of gravity

LE leading edge

SR spin radius

TE trailing edge

TEST EQUIPMENT

A rotary balance measures the forces and moments acting on an airplane while subjected to rotational flow conditions; the background for this apparatus is discussed in reference 3. A photograph and sketch of the rotary balance apparatus installed in the Langley spin tunnel are shown in figures 1 and 2, respectively. The rotating portion of the balance system, mounted on a horizontal supporting boom which is hinged at the wall, is moved from the wall to the center of the tunnel by cables. The rotary arm of the balance system, which rotates about a vertical axis, is attached to the outer end of the horizontal supporting boom and is driven by a drive shaft through couplings and gears.

A test model is mounted on a strain gauge balance which is affixed to the bottom of the rotary balance apparatus. Controls located outside the tunnel are used to activate motors on the rig which position the model to the desired attitude. The angle-of-attack range of the rig is 8 to 90 degrees and the sideslip angle range is ± 15 degrees. The spin radius and the lateral displacement motors allow the operator to position the moment center of

the balance on the spin axis or at a specific distance from the spin axis. This is done for each combination of angle of attack and sideslip angle. The general practice is to mount the moment center of the balance at the cg location about which the aerodynamic moments are desired. Electrical current from the balance, and to the motors on the rig, is conducted through slip-rings located at the rig head. Examples of how the rig is positioned for different angle of attack and sideslip angles are shown in figures 2a and 2b, respectively.

The model can be rotated up to 90 rpm in either direction. By using different rotational speeds and a specific airflow in the tunnel, the motions of a steady spinning airplane can be simulated. The aerodynamic forces and moments can then be measured for values of $\frac{\Omega b}{2V}$, including the case of $\frac{\Omega b}{2V} = 0$, where static aerodynamic forces and moments can be obtained.

A NASA six-component strain gauge balance is mounted inside the model and measures the normal, lateral and longitudinal forces and the yawing, rolling and pitching moments acting about the mode body axis. The interactions that exist between the six components are available from balance calibration tests and are accounted for after the balance voltages are converted to forces and moments.

The data acquisition, reduction and presentation system for the rotary balance set-up is composed of a 12-channel scanner/voltmeter, a mini-computer and a plotter. With this equipment,

on-line digital print-out and/or graphical plots of data are possible.

TEST PROCEDURES

Rotary aerodynamic data are obtained in two steps. The first step is to record the inertial forces and moments (tares) acting on the model at different attitudes and rotational speeds. To accomplish this, a covered bird-cage like structure is mounted to the upper rig which encloses the model without touching it. In this manner, the air immediately surrounding the model is rotated with it. As the rig is rotated at the desired attitude and rate, the inertial forces and moments generated by the model are measured and stored on magnetic tape for later use.

The second step in the data-gathering process is to measure aerodynamic and inertial forces at different attitudes and rotational speeds for a selected tunnel velocity with, of course, the cage structure removed. The tares are subtracted from these values, and the remaining aerodynamic forces and moments are then converted to coefficient form and stored on magnetic tape.

MODEL

A 1/6.5-scale fiberglass/aluminum model of a configuration considered to be a typical high-wing, single-engine, light general aviation airplane was tested in the present study. A three-view drawing of this model is shown in figure 3, dimensional characteristics of the model are presented in Table I, and a photograph of the model installed on the rotary balance located in the Langley spin tunnel is presented in figure 1.

The model was fabricated such that various airplane components were removable for component build-up tests and for testing alternate wing leading edges and tail configurations. In addition, allowance was made for attaching various fuselage modifications.

The four tail configurations tested involved different locations of the horizontal tail as shown in figure 4. The fuselage shape and wing leading-edge modifications tested are shown in figures 5 and 6, respectively.

The model control surfaces could be set at any position prior to the test. The maximum deflections for the control surfaces were:

Elevator, deg	28 up, 23 down
Rudder, deg	25 right, 25 left
Aileron, deg	20 up, 15 down

TEST CONDITIONS

The tests were conducted in the spin tunnel at a tunnel velocity of 7.62 m/sec (25 ft/sec) which corresponds to a Reynolds number of 119,378 based on the model mean aerodynamic chord. Unless noted otherwise in Table II, all the configurations were tested through an angle-of-attack range of 8 to 90° at a zero sideslip angle with the spin axis passing through the full-scale airplane cg location of .25$\bar{c}$ for angles of attack above 30°. For angles of attack below 35°, the spin axis was set 99 cm (39 in.) forward of the cg. Consequently, data was obtained for both a 0 and 99 cm (39 in.) spin radius at angles of attack of 30 and 35°. At each spin attitude, measurements

were obtained for nominal $\frac{\Omega b}{2V}$ values of .1, .2, .3, .4, .45, .55, .65, .75 and .85 in both clockwise and counter-clockwise directions, as well as for $\frac{\Omega b}{2V}$ =0 (static value).

DATA PRESENTATION

Table II identifies the configurations tested and the corresponding appendix figure numbers which present the aerodynamic data. The aerodynamic coefficients vs. $\frac{\Omega b}{2V}$ are presented for each configuration in six sequentially numbered figures in the following order: C_n, C_ℓ, C_m, C_N, C_Y and C_A. Each figure, in turn, consists of four pages which present the subject aerodynamic coefficient vs. $\frac{\Omega b}{2V}$ for the following angles of attack and spin radii, unless noted otherwise in Table II.

a) α= 8, 10, 12, 14, 16 deg SR= 99 cm (39 in.)

b) α= 18, 20, 25, 30, 35 deg SR= 99 cm (39 in.)

c) α= 30, 35, 40, 45, 50 deg SR= 0

d) α= 55, 60, 70, 80, 90 deg SR= 0

All the moment data are presented for a cg position of 0.25$\bar{c}$.

Lift coefficient as a function of angle of attack for zero rotation rate is presented at the end of the Appendix for several configurations cited in Table II.

REFERENCES

1. Bihrle, William, Jr.; Hultberg, Randy S.: Rotary Balance Data for a Typical Single-Engine General Aviation Design for an Angle-of-Attack Range of 8° to 90°. II- Low-Wing Model B. NASA CR 3098, 1979.

2. Mechtly, E.A.: The International System of Units - Physical Constants and Conversion Factors. NASA SP-7012, 1973.

3. Bihrle, William, Jr.; Hultberg, Randy S.; and Mulcay, William: Rotary Balance Data for a Typical Single-Engine Low-Wing General Aviation Design for an Angle-of-Attack Range of 30° to 90°. NASA CR 2972, 1978.

TABLE I.- DIMENSIONAL CHARACTERISTICS OF THE BASIC MODEL

Overall length, m (ft)	1.24 (4.05)
Wing:	
Span, m (ft)	1.68 (5.51)
Area, m^2 (ft^2)	.38 (4.12)
Root chord, cm (in.)	25.02 (9.85)
Tip chord, cm (in.)	17.39 (6.85)
Mean aerodynamic chord, cm (in.)	22.81 (8.98)
Leading edge of $\bar{c}$, distance rearward of leading edge of root chord, cm (in.)	.53 (.21)
Aspect ratio	7.37
Dihedral at 0.25 $\bar{c}$ along top surface, deg	1.7
Incidence:	
Root, deg	1.5
Tip, deg	-1.5
Airfoil section	NACA 2412
Horizontal tail:	
Span, m (ft)	0.53 (1.74)
Incidence, deg	-3.5
Airfoil section:	
Root	NACA 0009
Tip	NACA 0006
Vertical tail:	
Airfoil section:	
Root	NACA 0009
Tip	NACA 0006

TABLE II.- CONFIGURATIONS TESTED AND FIGURE INDEX

(Unless noted otherwise, all configurations tested through α= 8 to 90° at β= 0°.)

FIGURE NO.	CONFIGURATION	δ_e deg	δ_a deg	δ_r deg	REMARKS
[a]A1-A6	Basic	0	0	0	
A7-A12	↓	↓	↓	↓	β= 10°
A13-A18	↓	↓	↓	-25	
A19-A24	↓	23	↓	↓	
A25-A30	#1 Horizontal tail	0	↓	0	
A31-A36	↓	↓	↓	-25	
A37-A42	#2 Horizontal tail	↓	↓	0	
A43-A48	↓	↓	↓	-25	
A49-A54	T tail	↓	↓	0	
A55-A60	↓	↓	↓	-25	
A61-A66	Horizontal tail off	↓	↓	0	
A67-A72	Vertical tail off	↓	↓	↓	
A73-A78	#2 Horizontal tail with vertical tail off	↓	↓	↓	
A79-A84	Sharp-edged fuselage bottom aft of wing TE	↓	↓	↓	
A85-A90	Sharp-edged fuselage bottom aft of engine cowling	↓	↓	↓	
[a]A91-A96	Full-span LE wing droop having moderate nose radius	↓	↓	↓	
[a]A97-A102	Segmented LE wing droop	↓	↓	↓	
[b]A103-A108	Outboard LE wing droop extended inboard 33.8cm (13.3in)	↓	↓	↓	
[a]A109-A114	Outboard wing Kruger flap	↓	↓	↓	α=8-35° only
[b]A115-A120	Outboard LE wing droop extended inboard 42.7cm (16.8in)	↓	↓	↓	α=8-35° only
[b]A121-A126	45.2cm (17.8in)	↓	↓	↓	α=16-30° only
[b]A127-A132	47.8cm (18.8in)	↓	↓	↓	α=16-30° only
[b]A133-A138	42.7cm (16.8in) and having moderate nose radius	↓	↓	↓	α=16-30° only

[a] C_L vs. α presented in figure A139.

[b] C_L vs. α presented in figure A140.

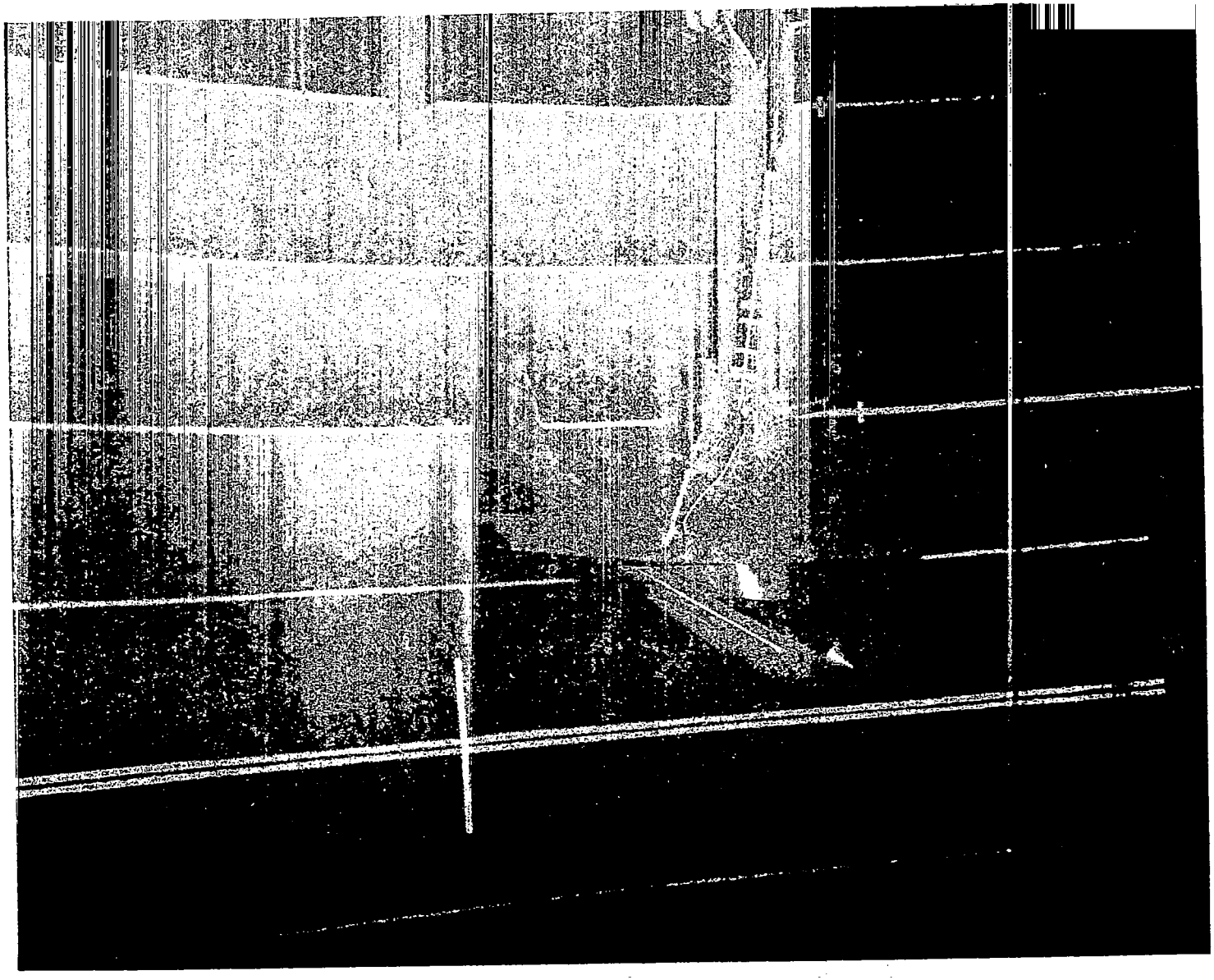

Figure 1.- Photograph of 1/6.5-scale model installed on rotary balance apparatus.

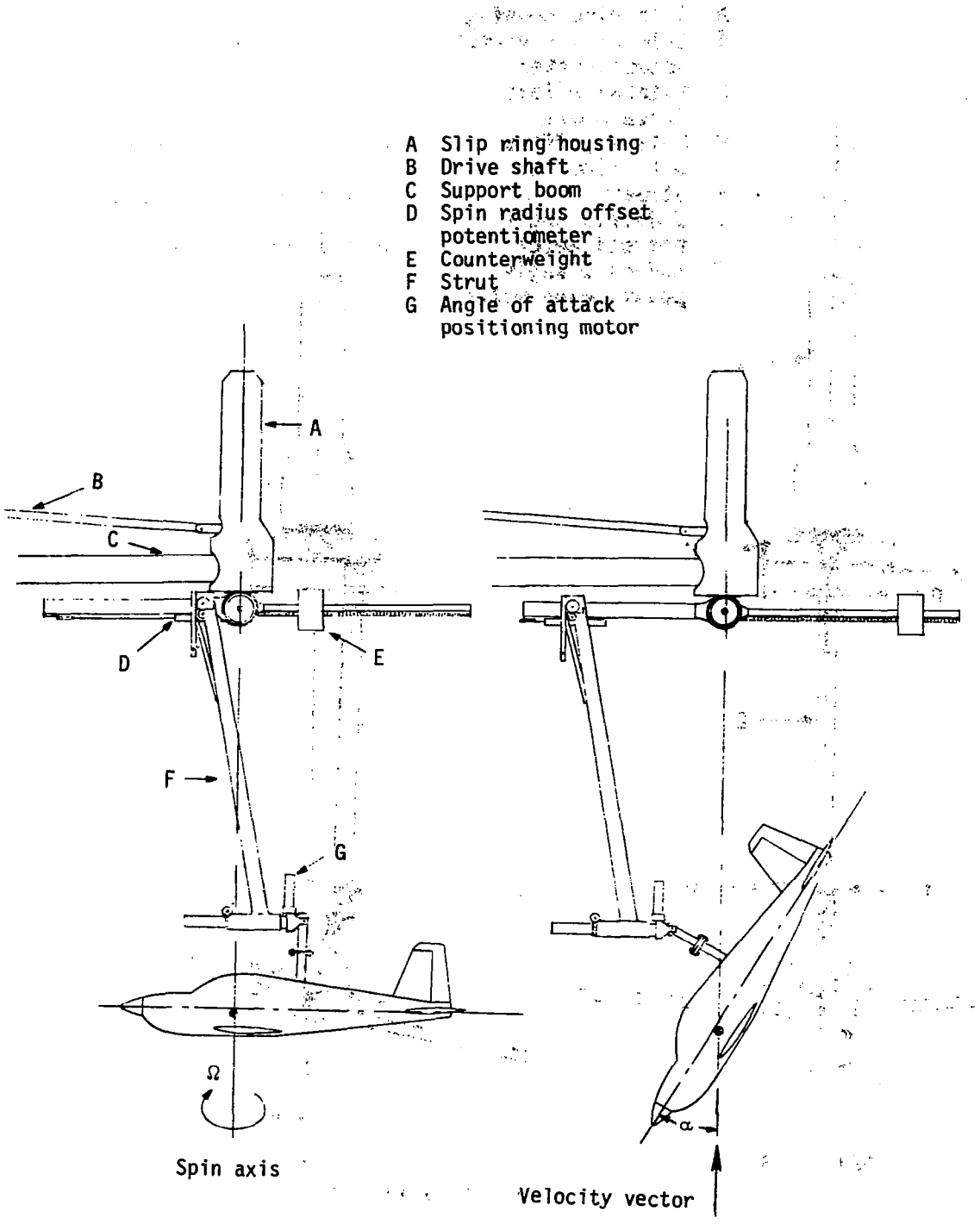

(a) Side view of model.

Figure 2.- Sketch of rotary balance apparatus.

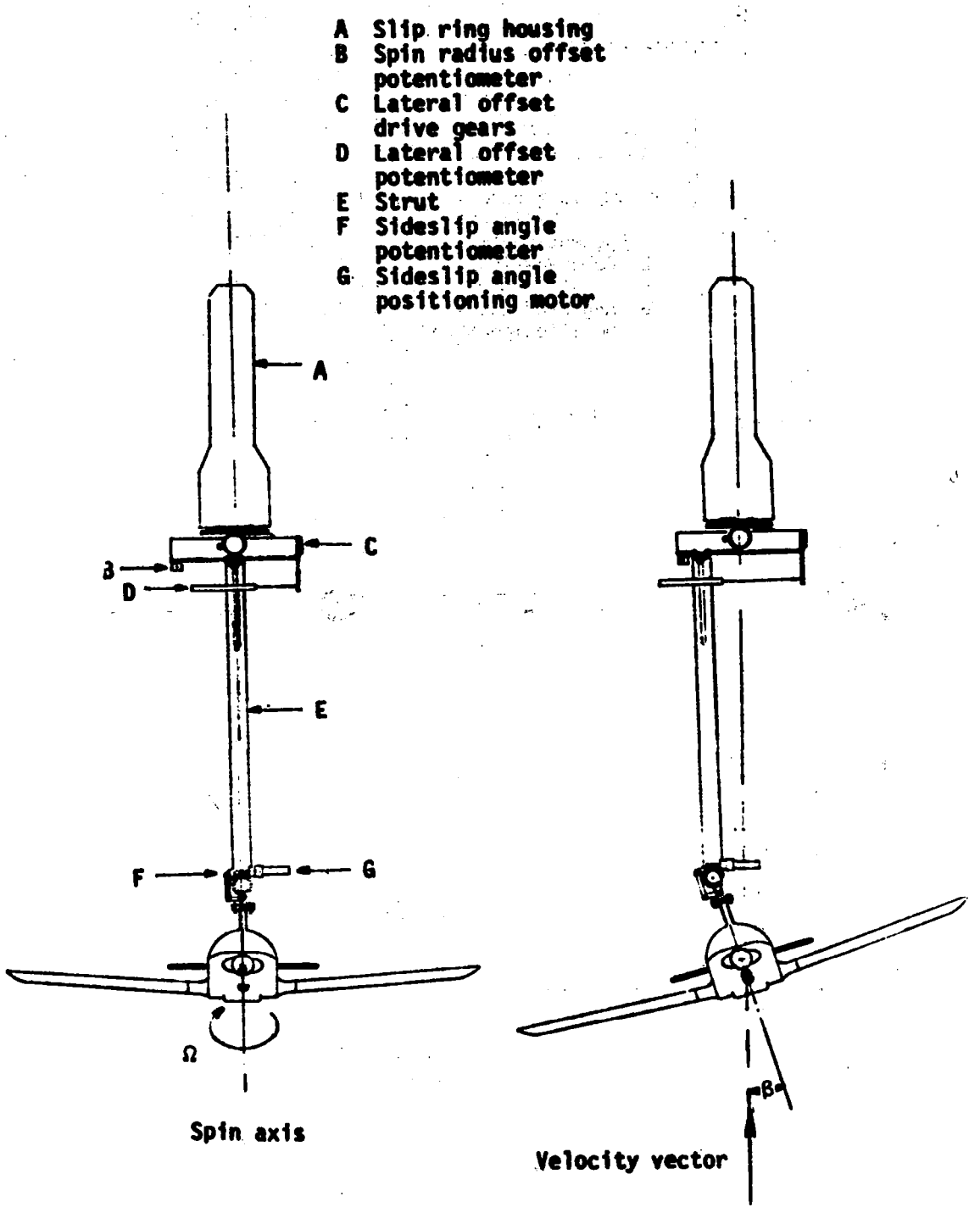

(b) Front view of model.

Figure 2.- Concluded.

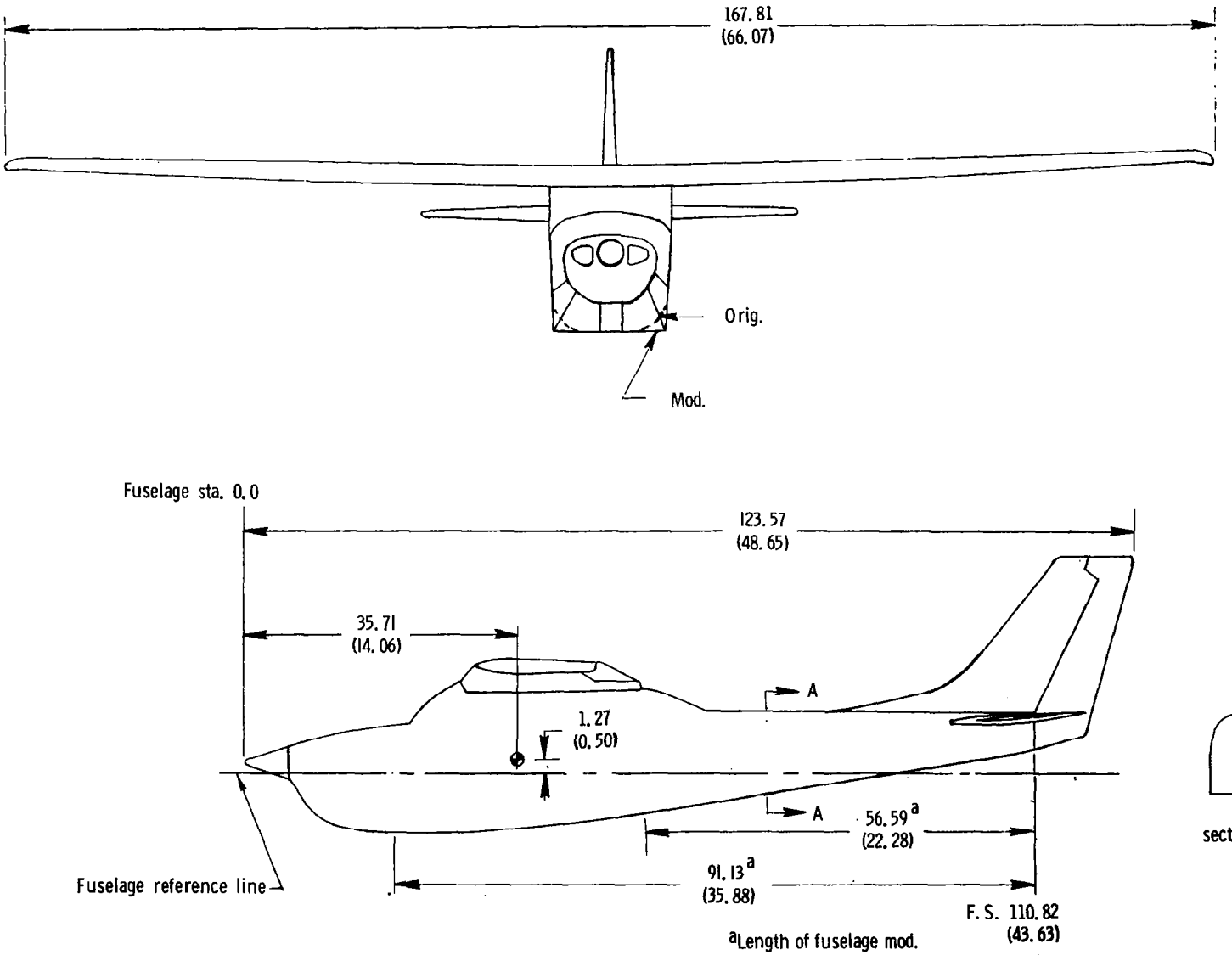

Figure 5. - Fuselage shape modifications tested on model. Dimensions are given in centimeters (inches), model scale.

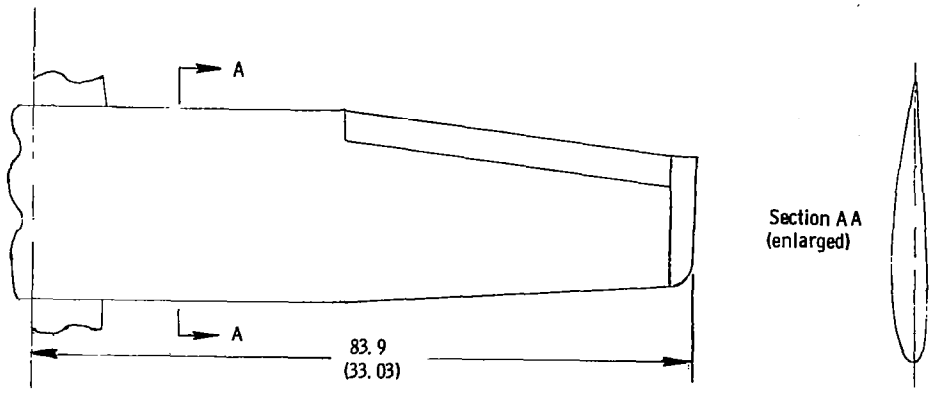

(a) Basic wing

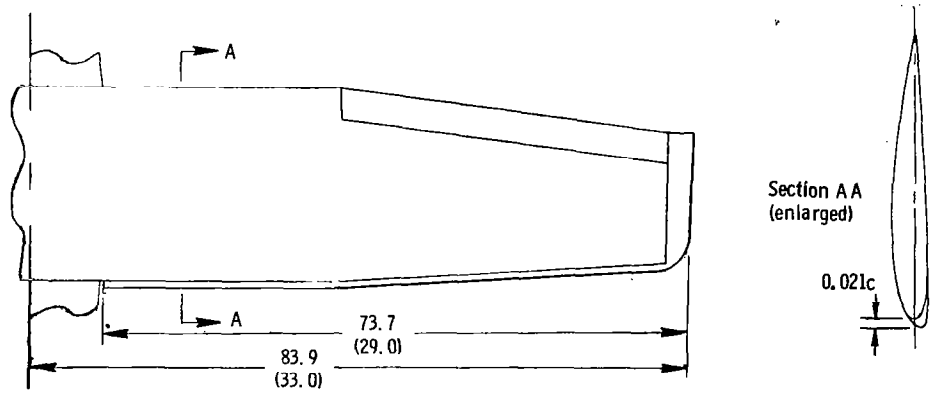

(b) Full-span LE wing droop having moderate nose radius.

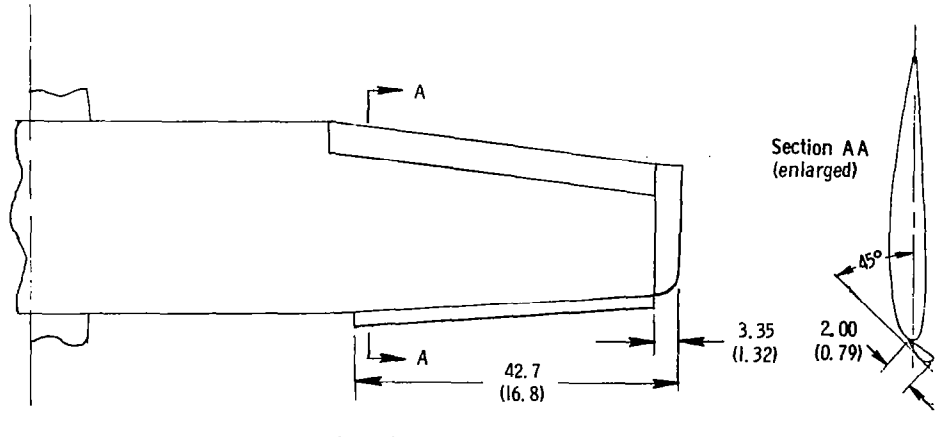

(c) Outboard LE wing Kruger flap.

Figure 6. - Wing leading-edge modifications tested on model. Dimensions are given in centimeters (inches), model scale.

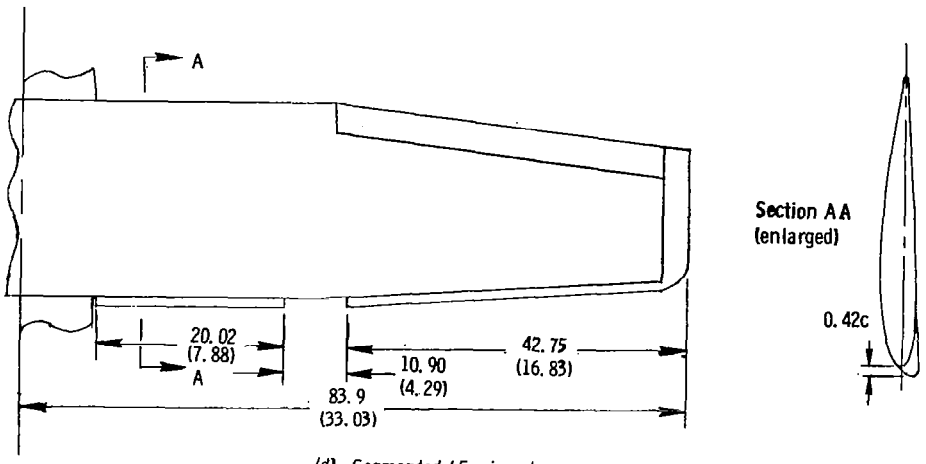

(d) Segmented LE wing droop.

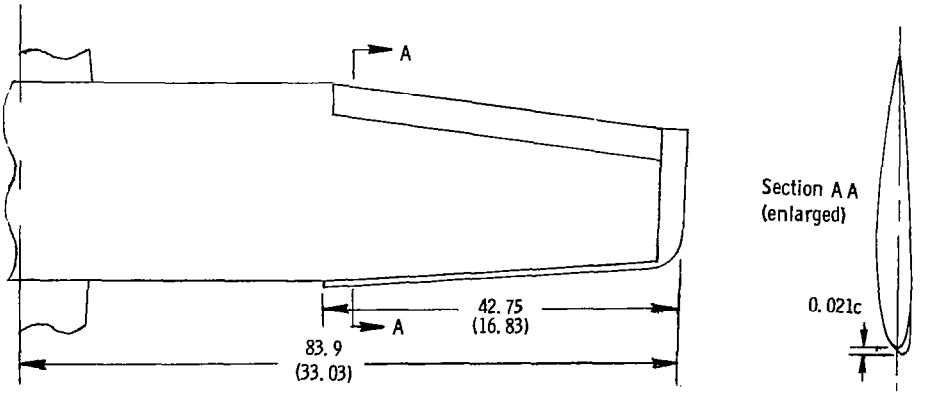

(e) Outboard LE wing droop having moderate nose radius.

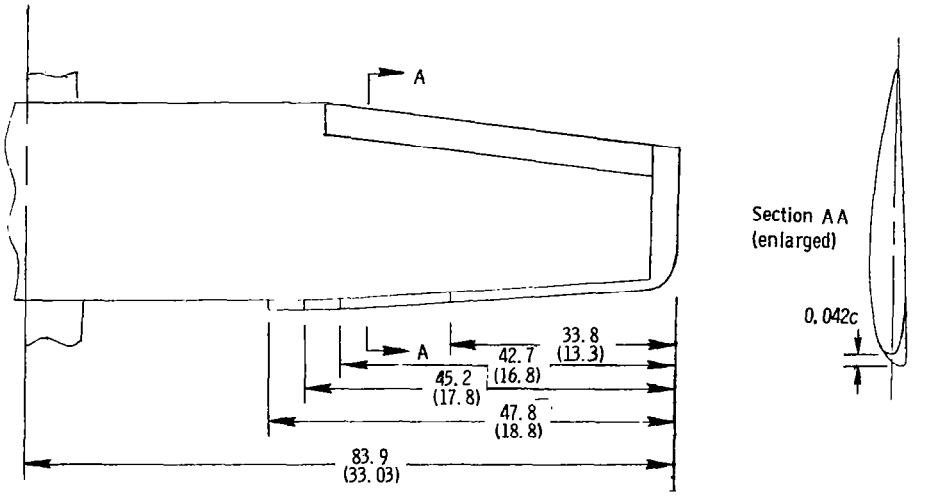

(f) Outboard LE wing droop.

Figure 6. -Concluded.

APPENDIX

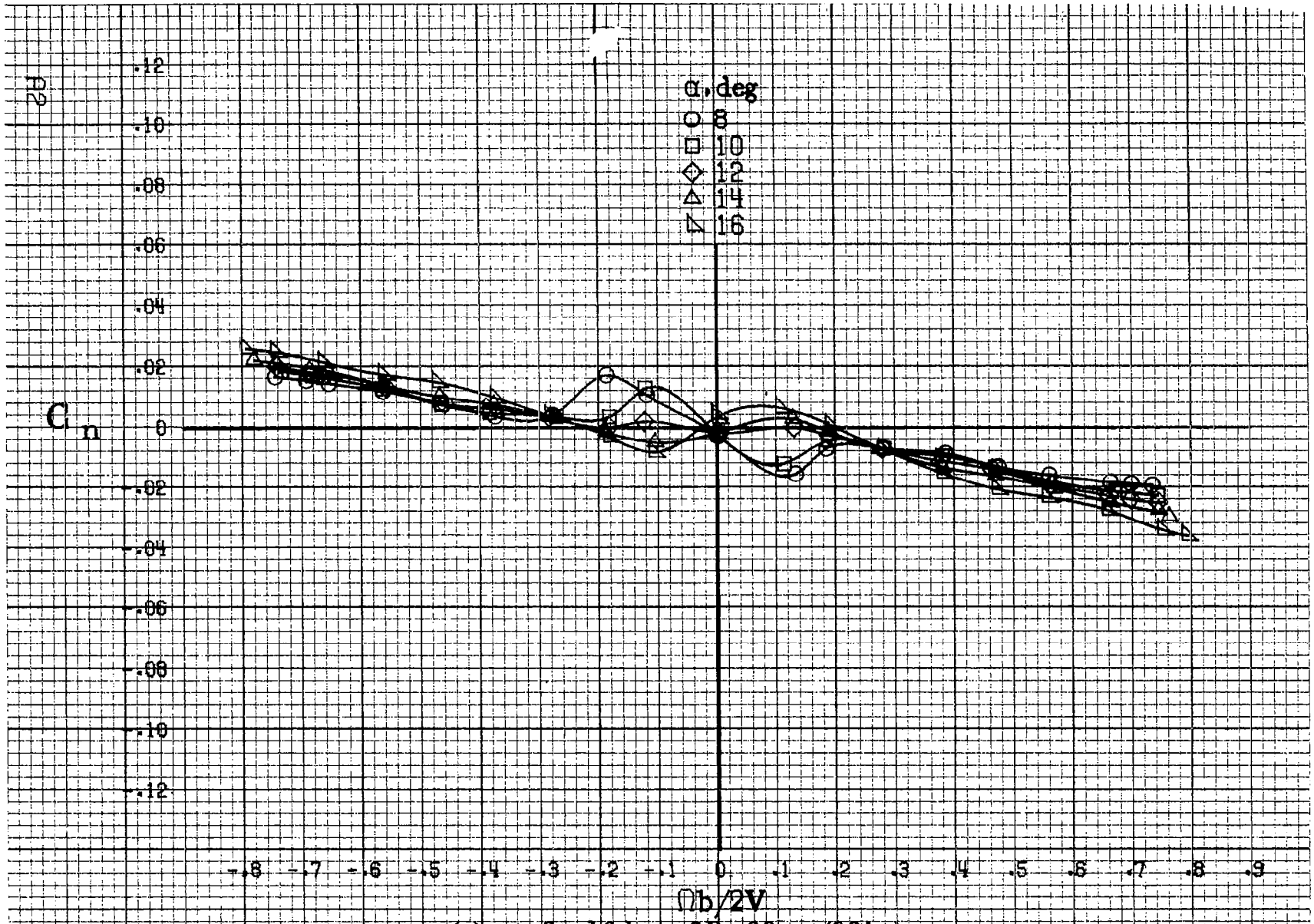

(a) α=8to16deg, SR=99cm(39in).

Figure A1.-Effect of rotation rate and angle of attack on yawing-moment coefficient for basic configuration. $\phi_e = 0°$, $\delta_a = 0°$, $\delta_r = 0°$, $\beta = 0°$.

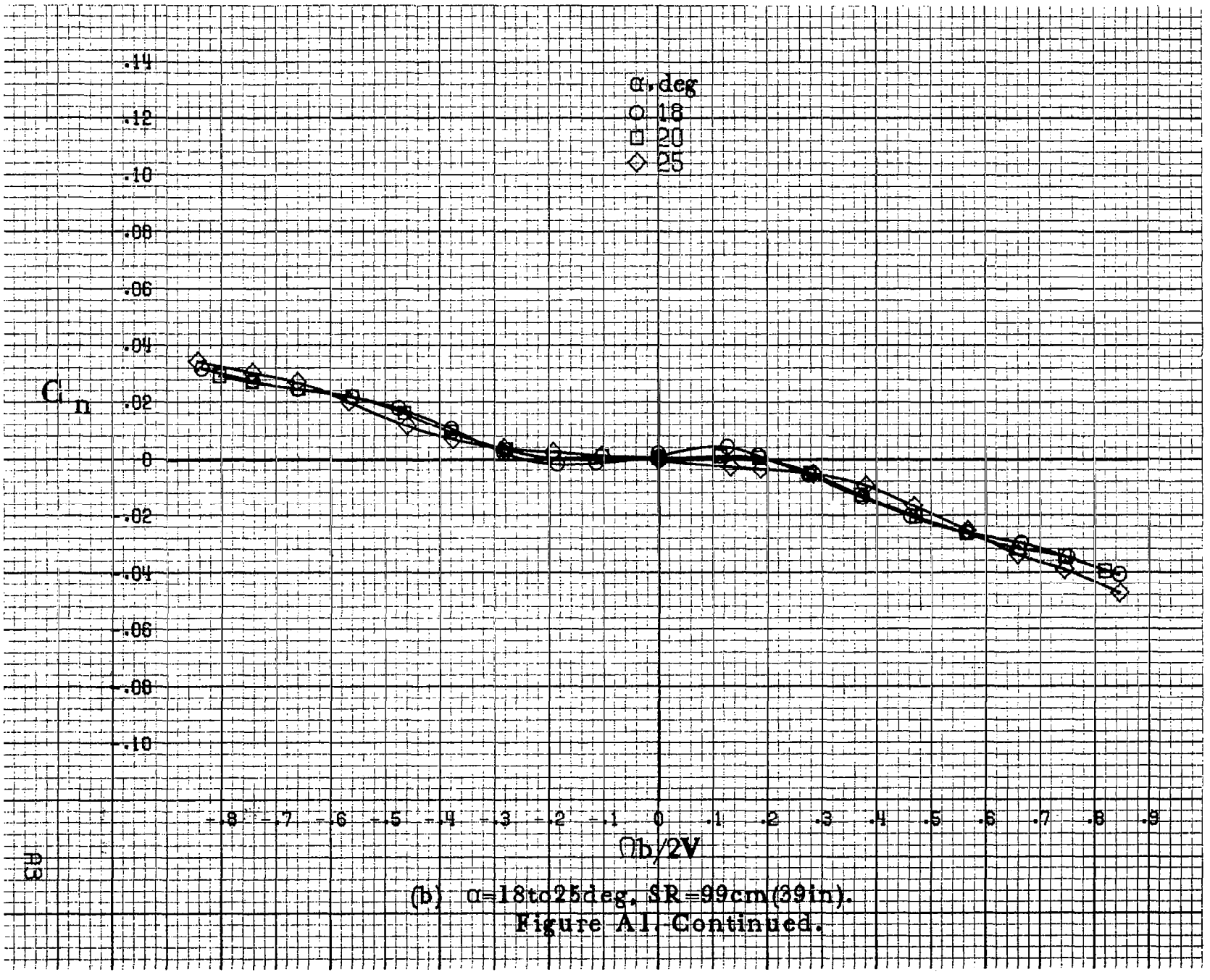

(b) α=18to25deg, SR=99cm(39in).

Figure A1. Continued.

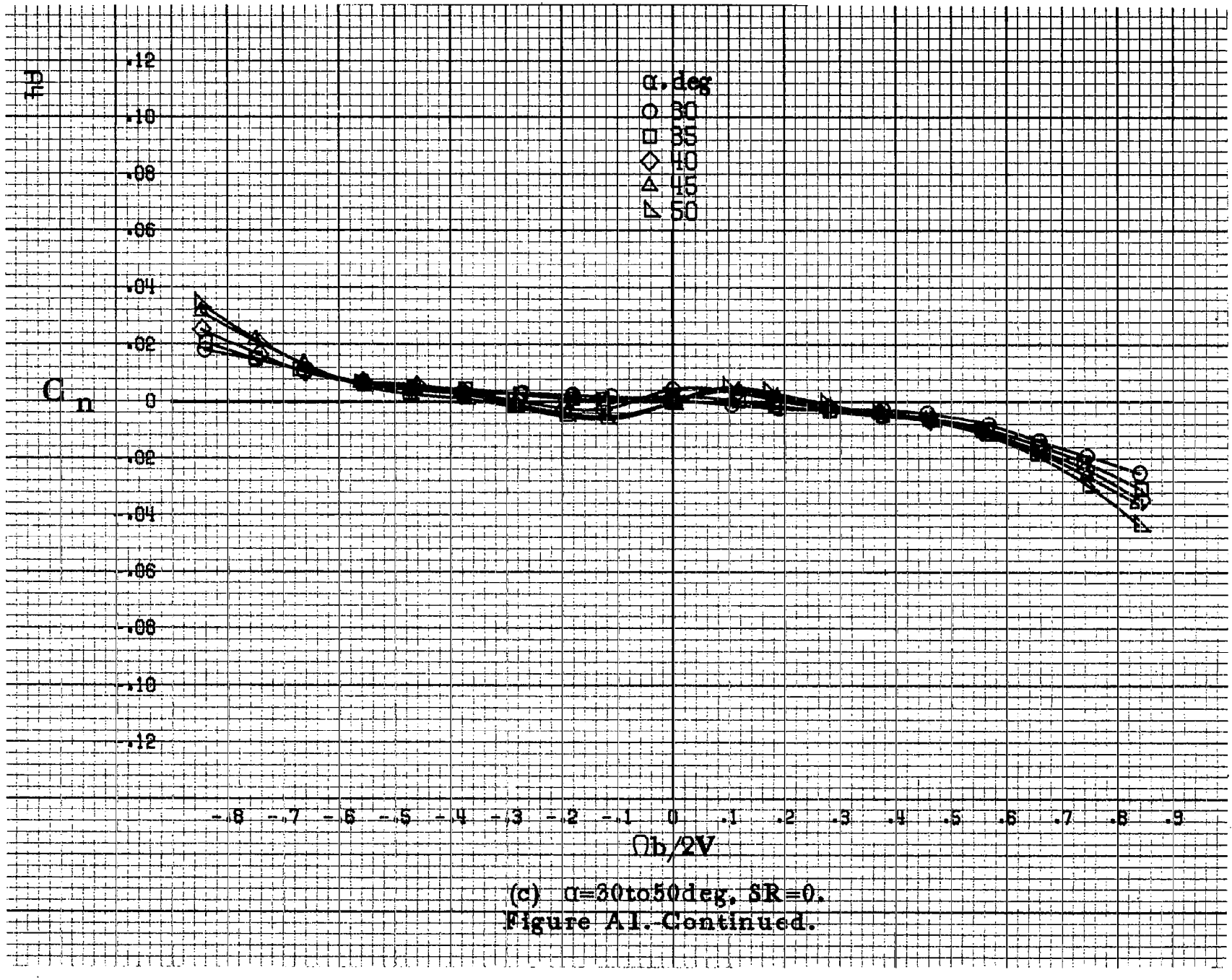

(c) α=30to50deg, SR=0.

Figure A1.-Continued.

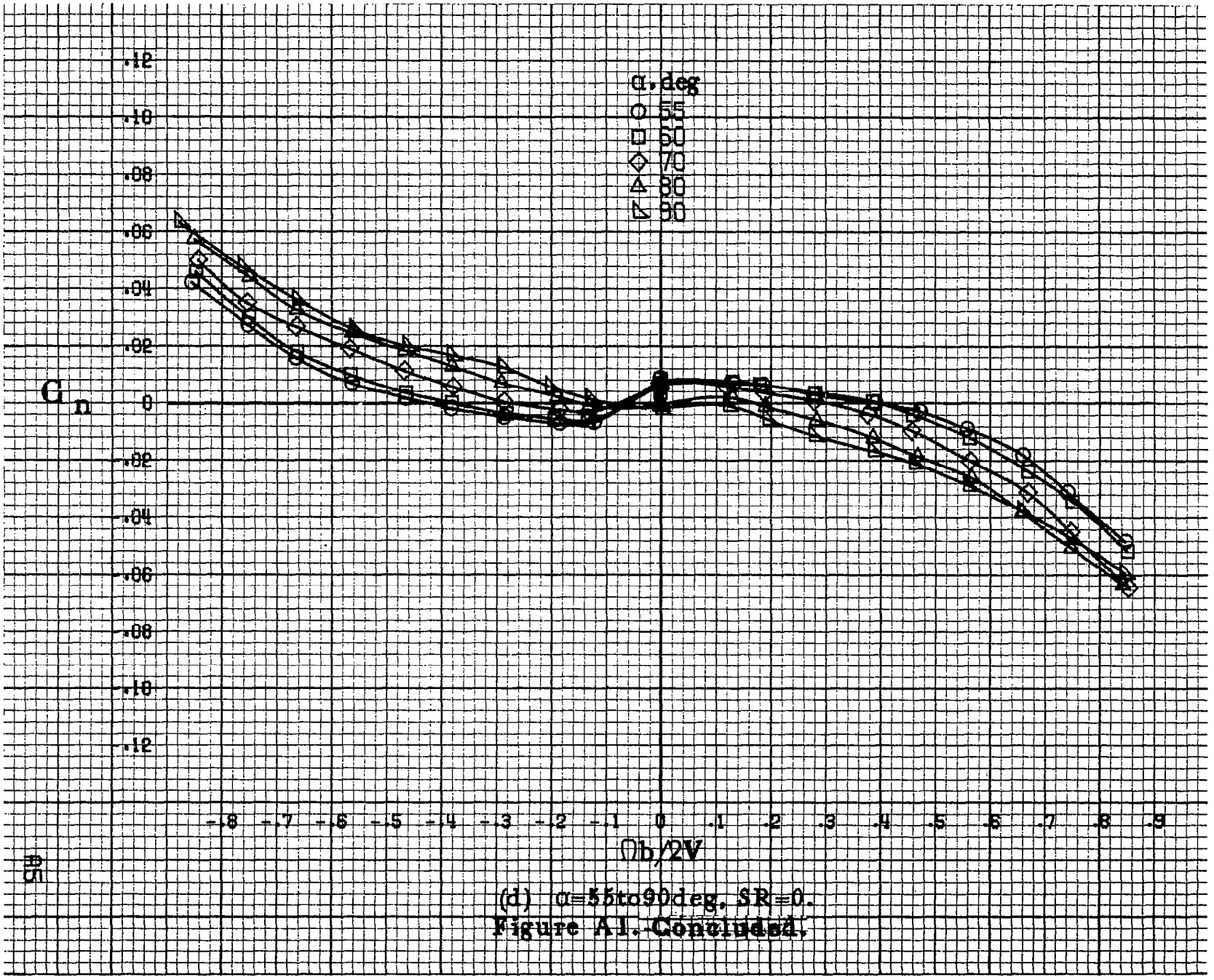

(d) α=55to90deg, SR=0.

Figure A1.-Concluded.

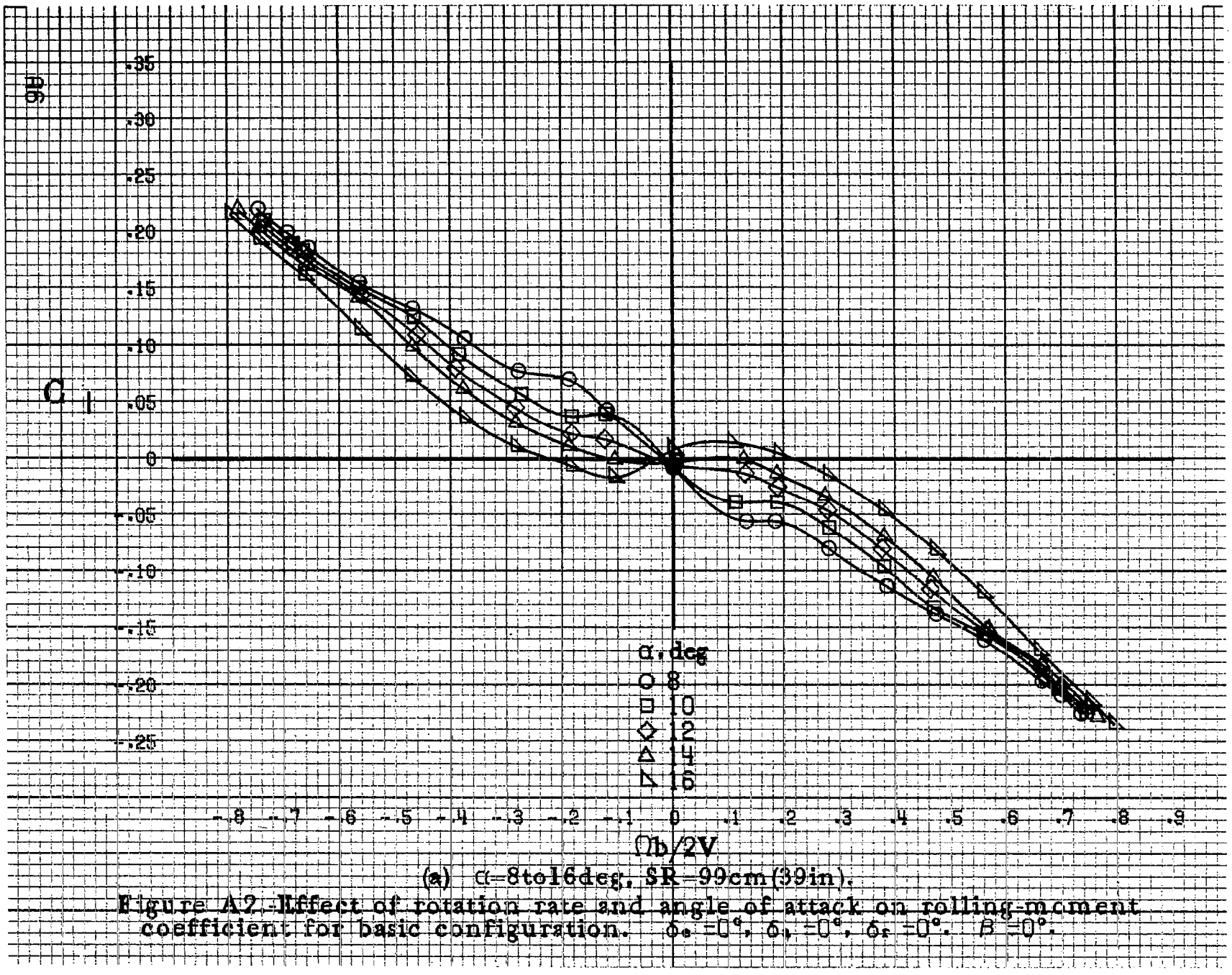

(a) α=8to16deg, $R=99cm(39in).

Figure A2.-Effect of rotation rate and angle of attack on rolling-moment coefficient for basic configuration. $\delta_a = 0°$, $\delta_e = 0°$, $\delta_r = 0°$. $\beta = 0°$.

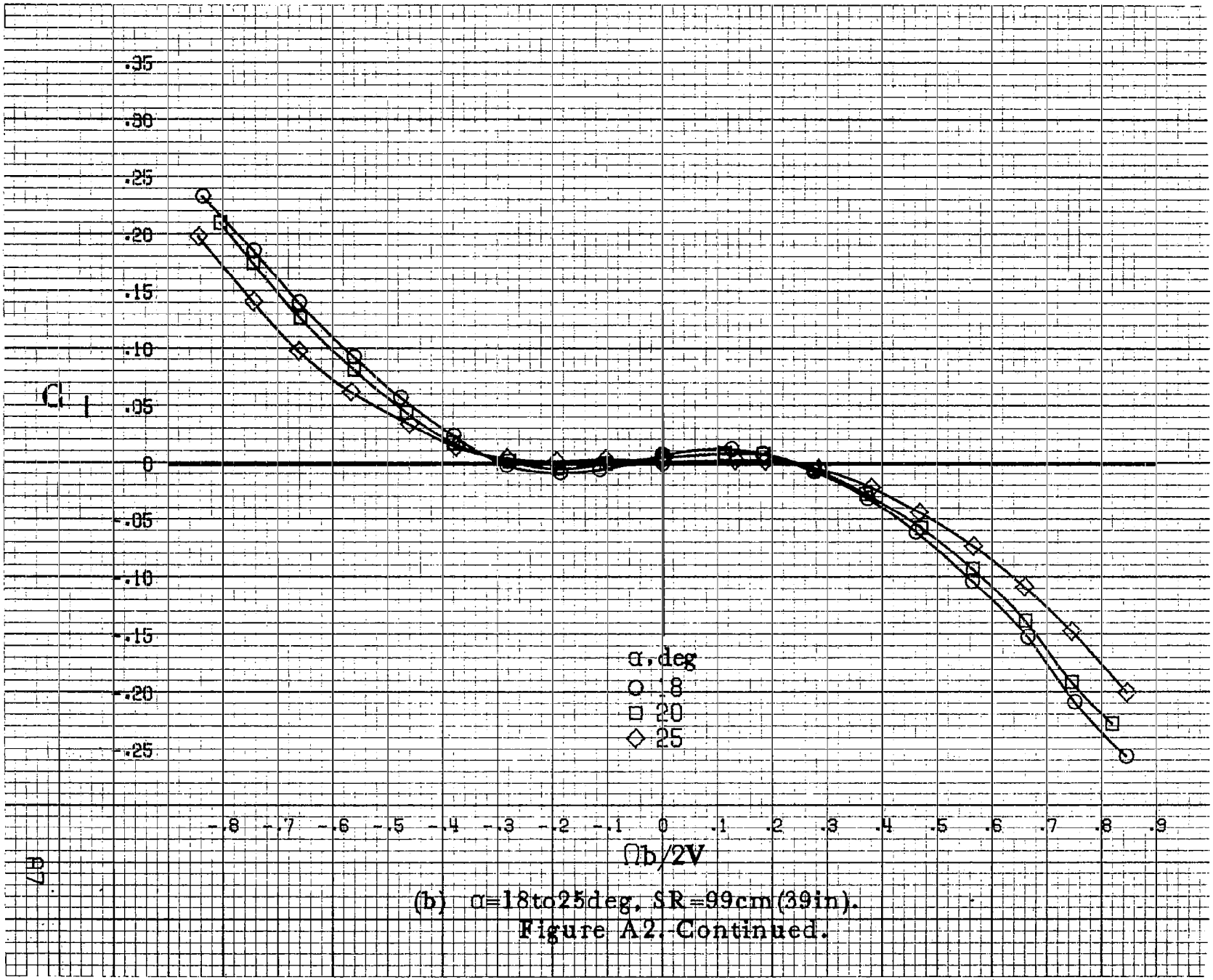

(b) α=18to25deg, SR=99cm(39in).

Figure A2.-Continued.

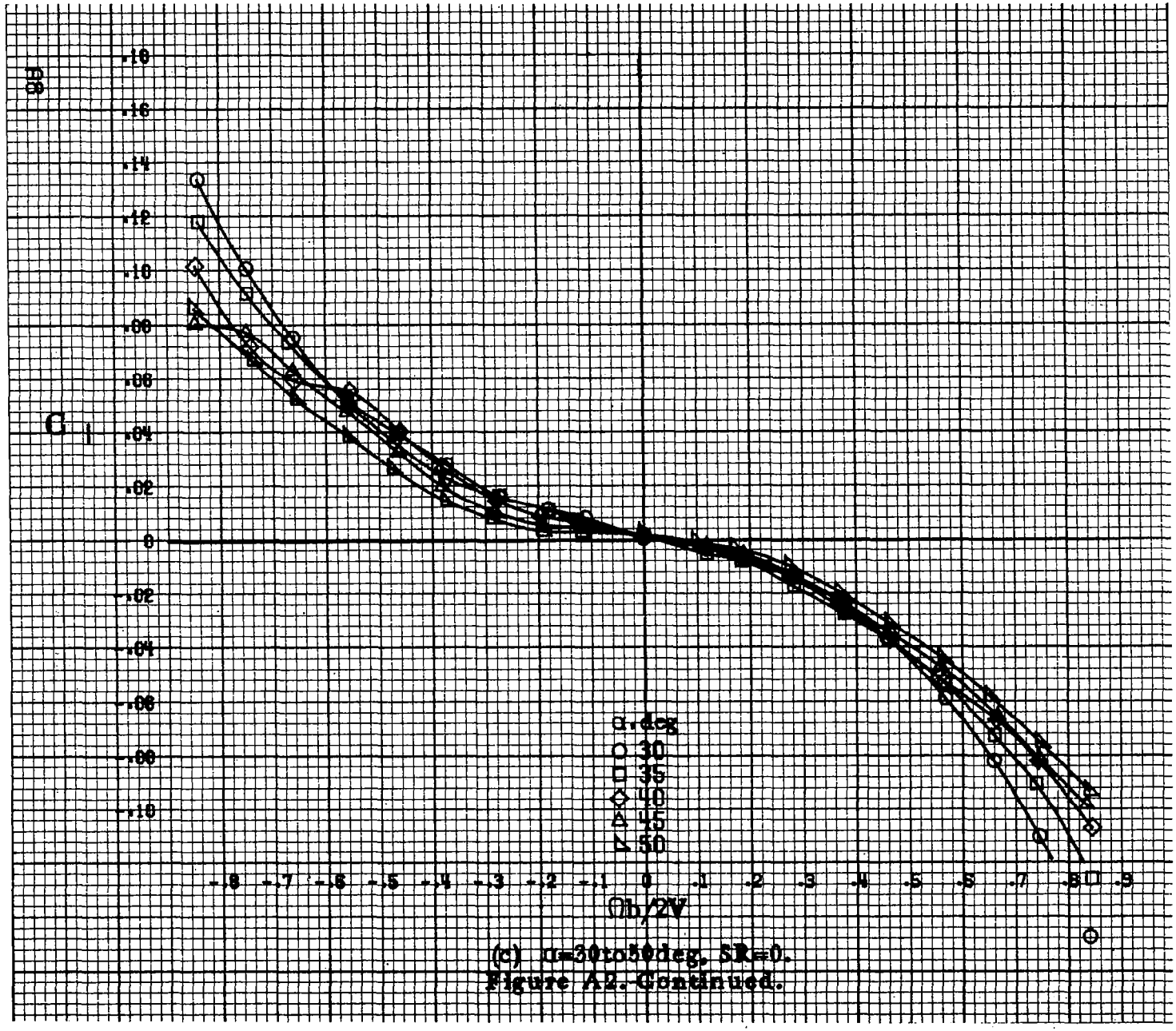

(c) α=30to50deg, SR=0.

Figure A2. Continued.

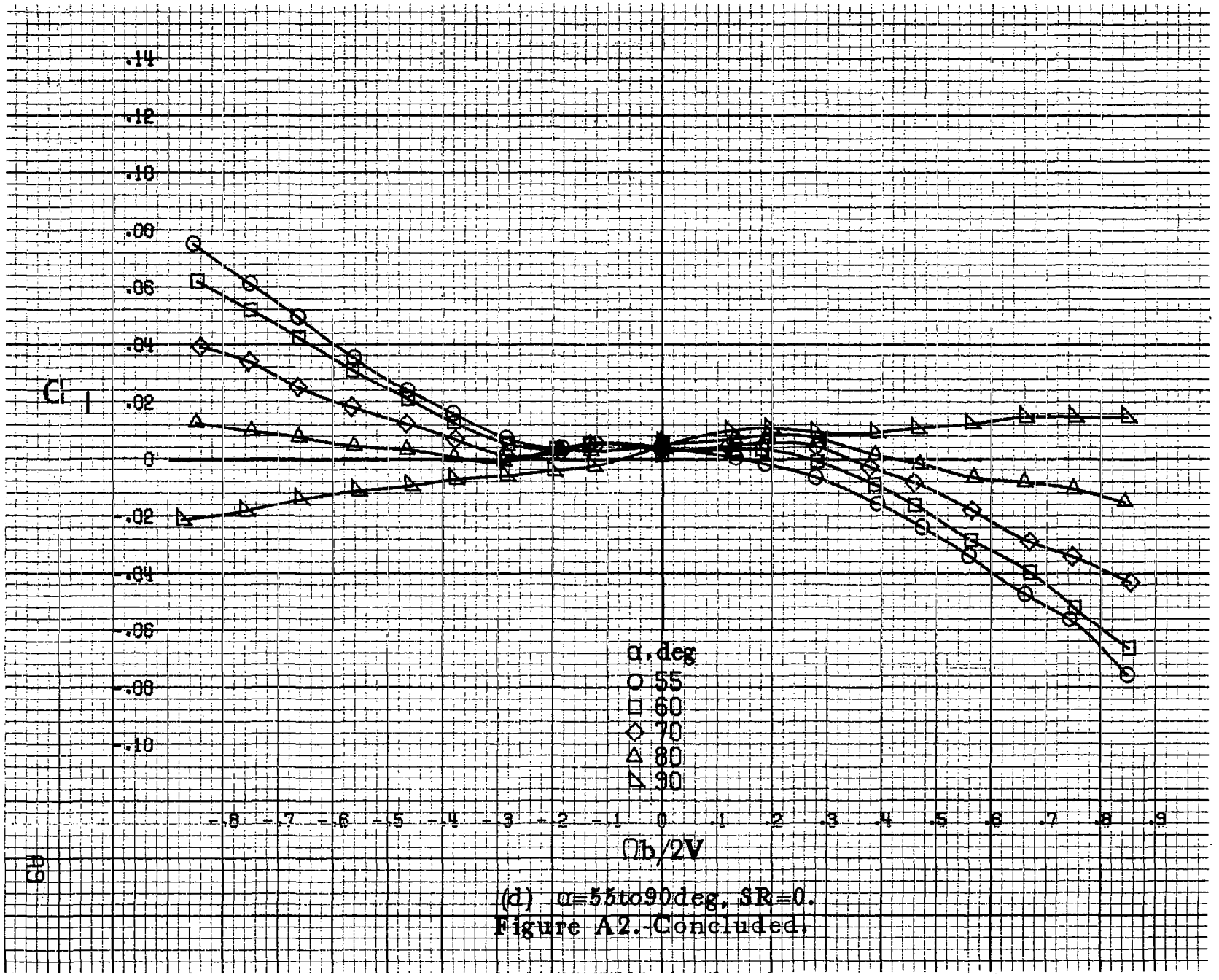

(d) $\alpha = 55$ to 90 deg, SR = 0.

Figure A2. Concluded.

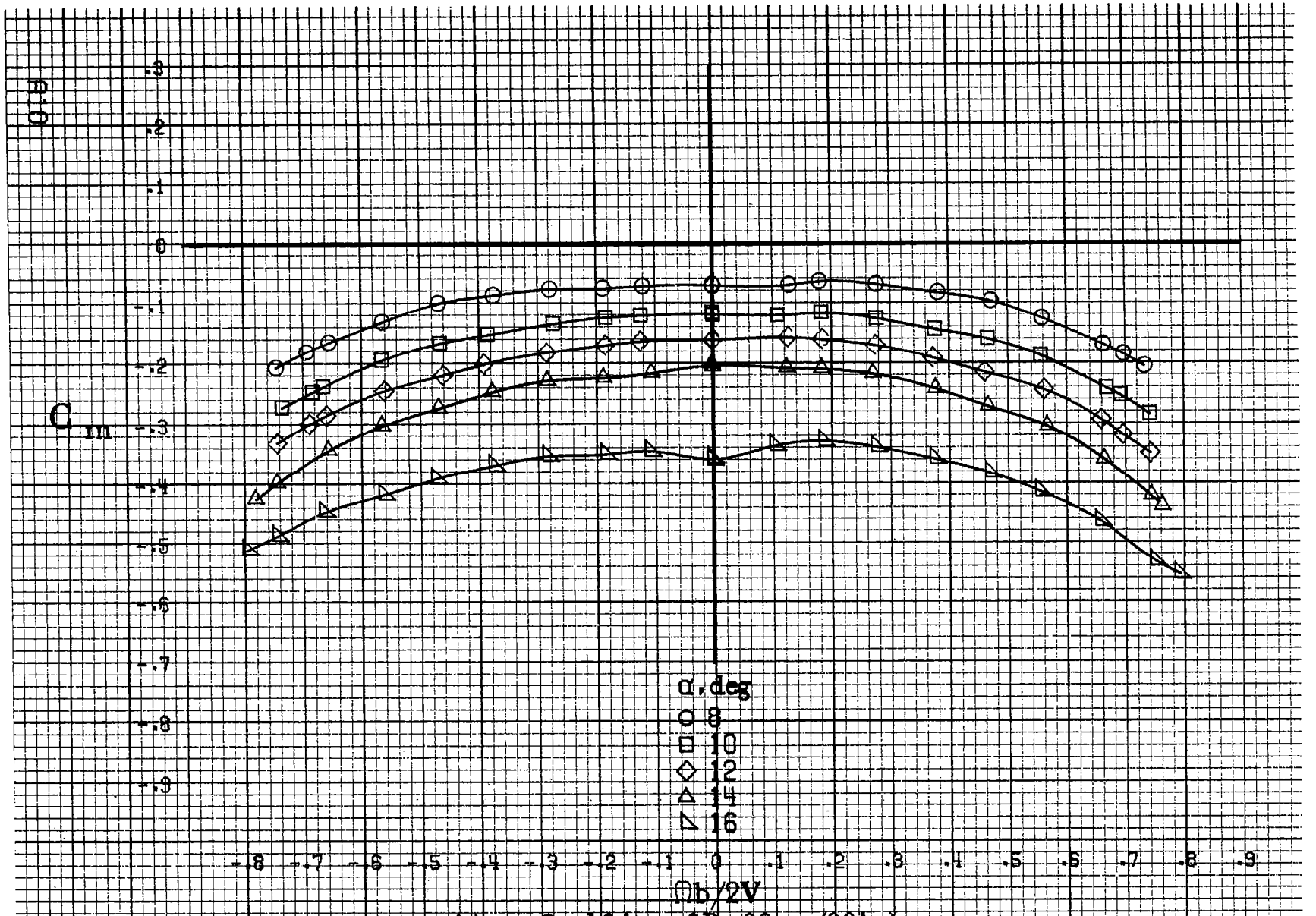

(a) α=8to16deg, SR=99cm(39in).

Figure A3.-Effect of rotation rate and angle of attack on pitching-moment coefficient for basic configuration. δ_e =0°, δ_a =0°, δ_r =0°, β =0°.

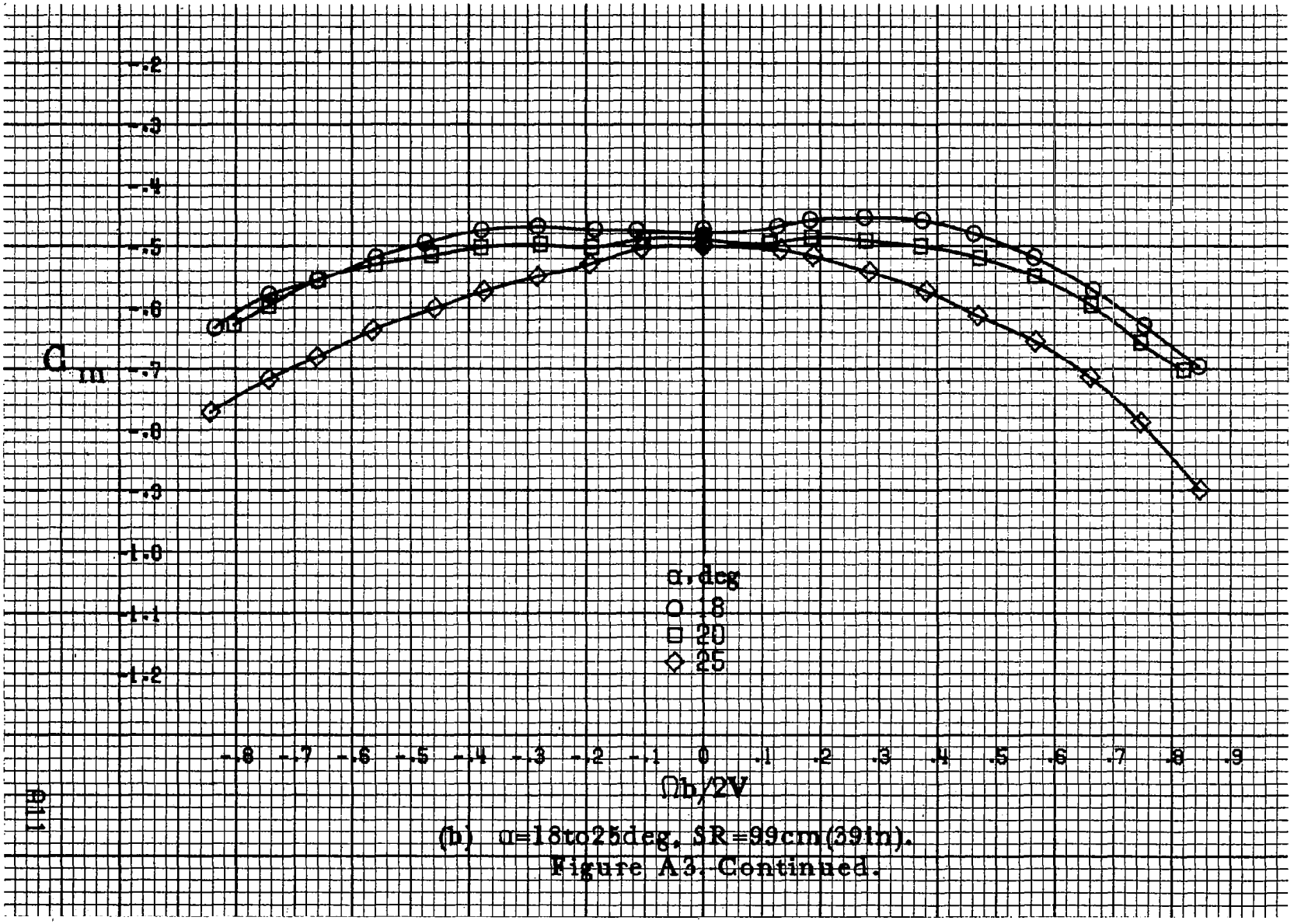

(b) α=18to25deg, SR=99cm(39in).

Figure A3. Continued.

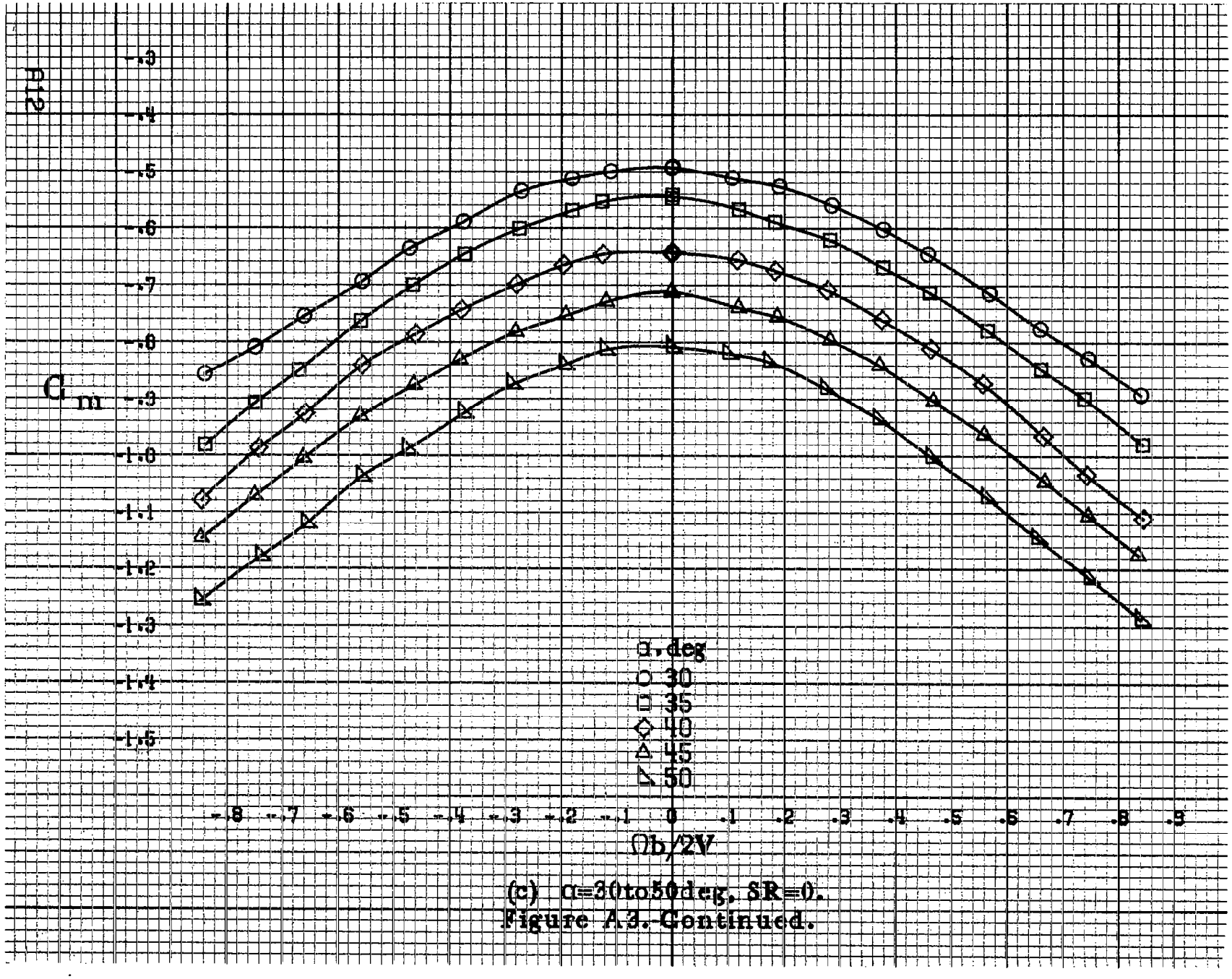

(c) α=30to50deg, δR=0.

Figure A.3.-Continued.

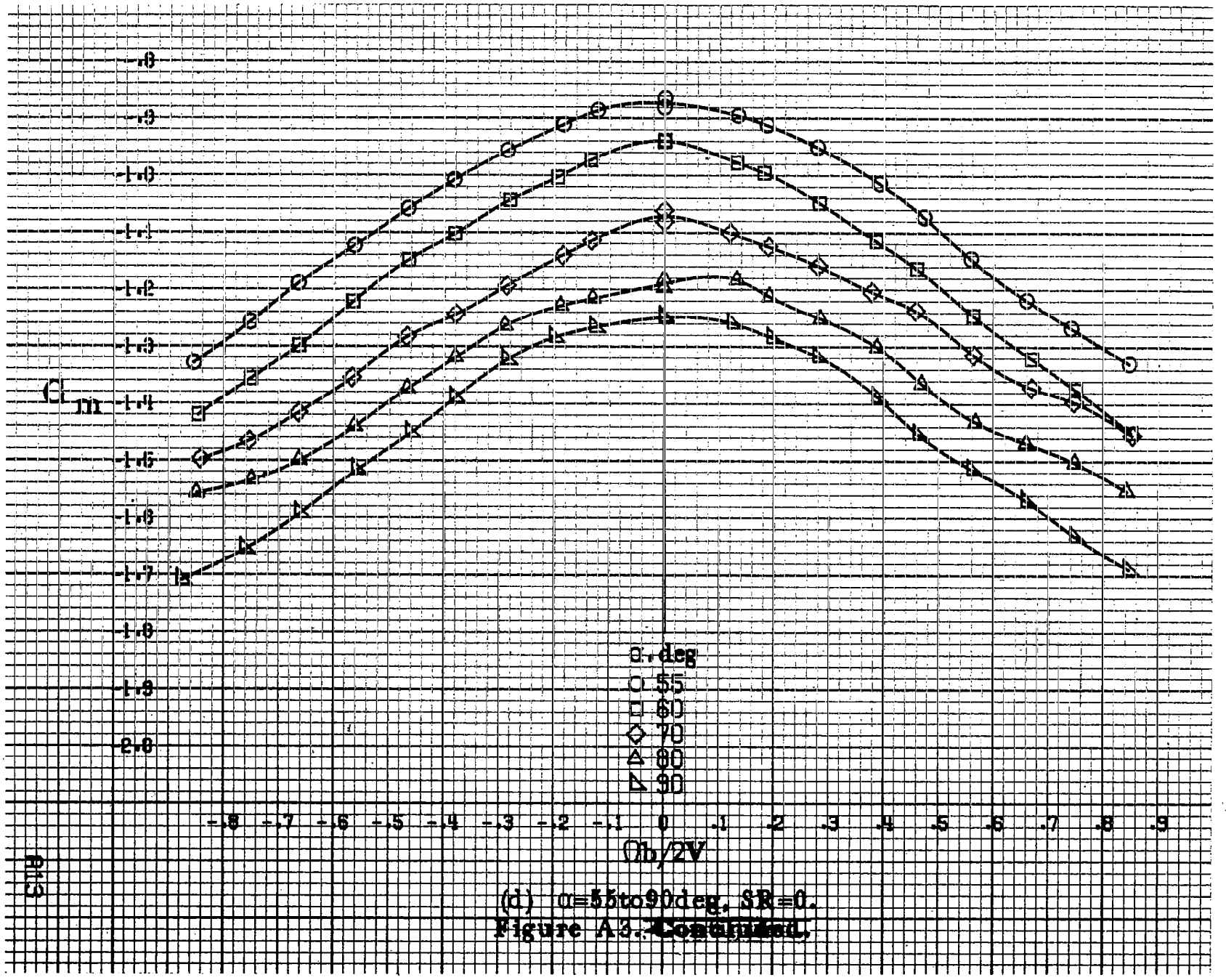

(d) α=55to90deg, SR=0.

Figure A3. Concluded.

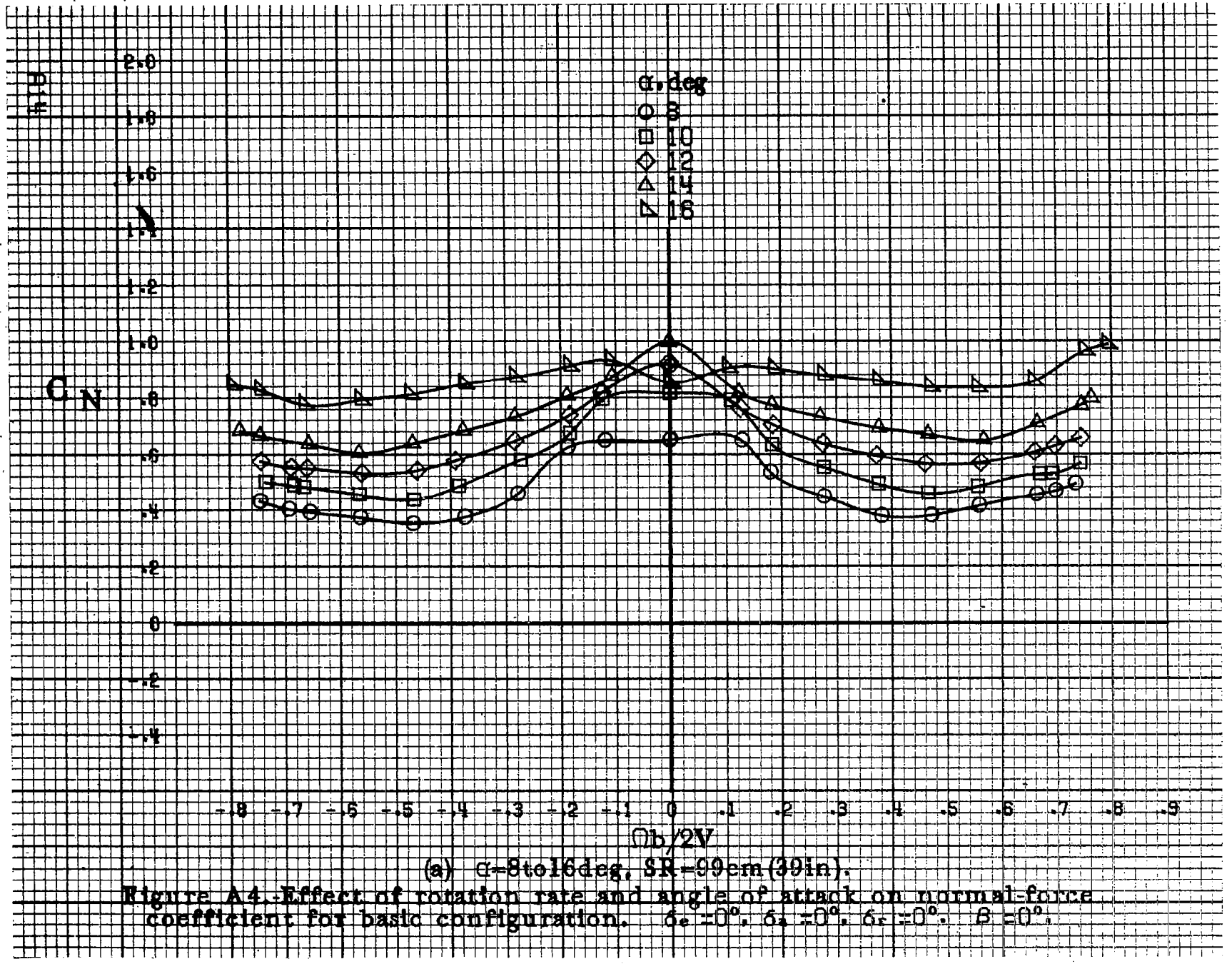

(a) α=8to16deg, SR=99cm(39in).

Figure A4.-Effect of rotation rate and angle of attack on normal-force coefficient for basic configuration. $\delta_e = 0°$, $\delta_a = 0°$, $\delta_r = 0°$, $\beta = 0°$.

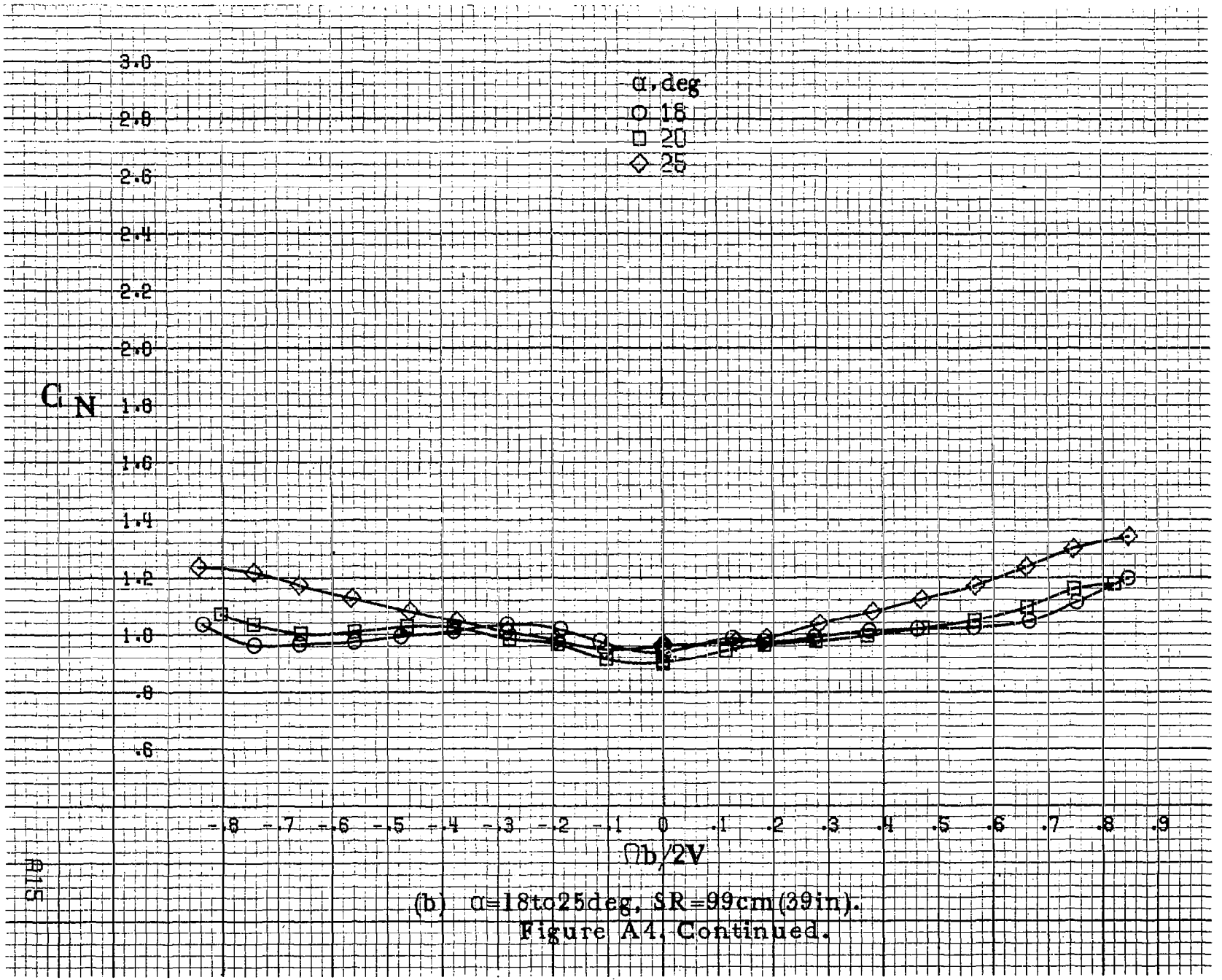

(b) α=18to25deg, SR=99cm(39in).

Figure A4. Continued.

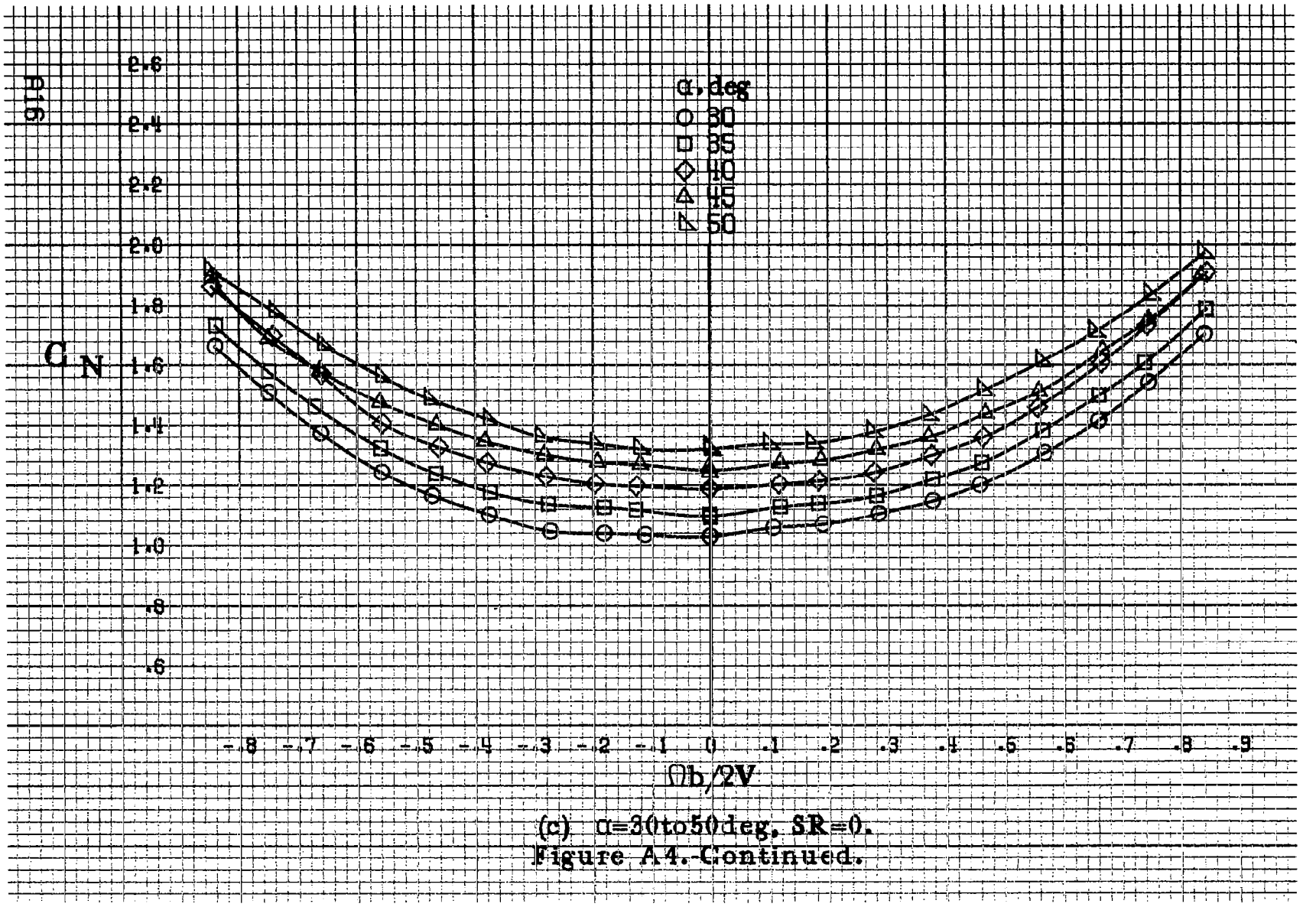

(c) α=30to50deg, SR=0.

Figure A4.-Continued.

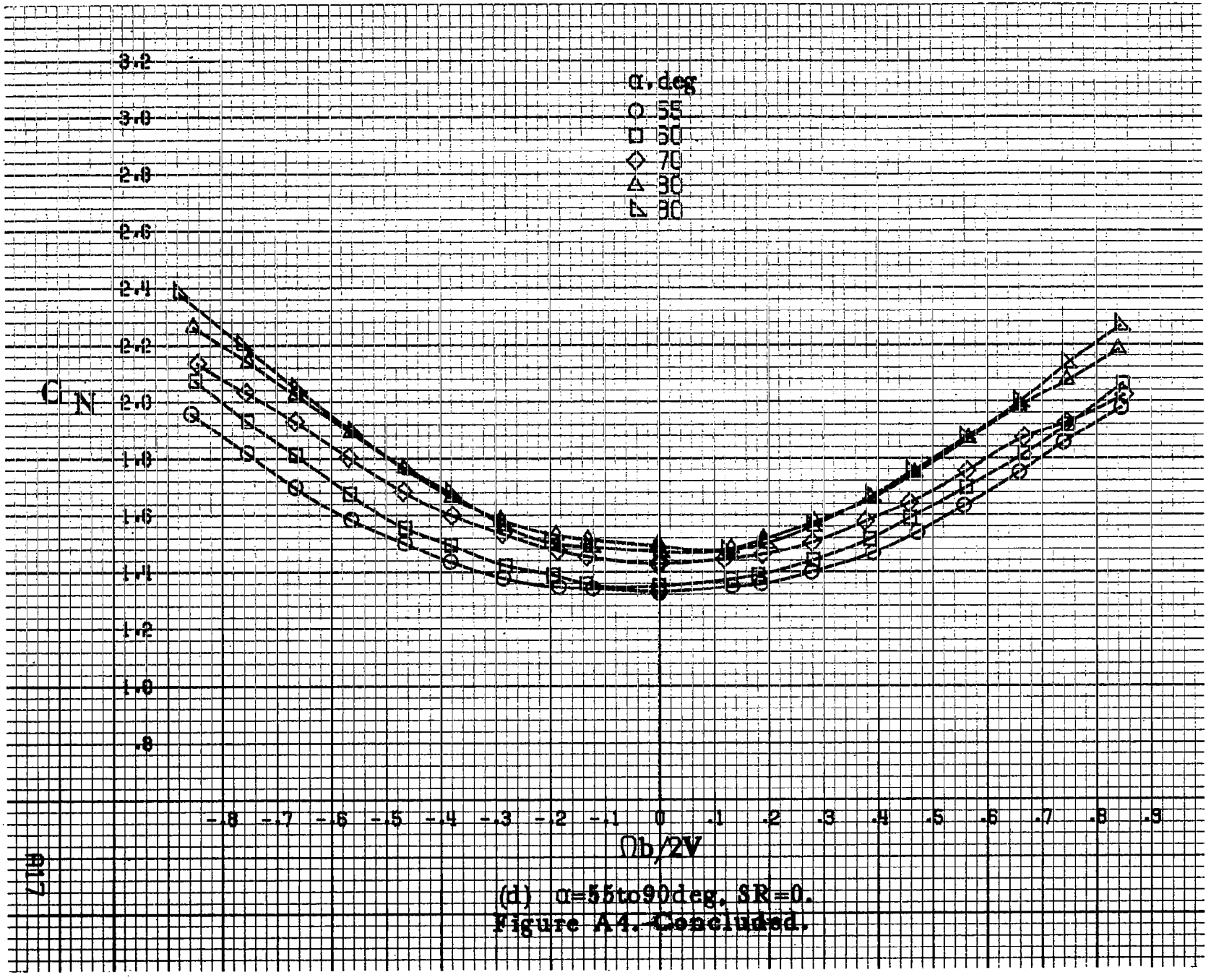

(d) α=55to90deg, SR=0.

Figure A4.-Concluded.

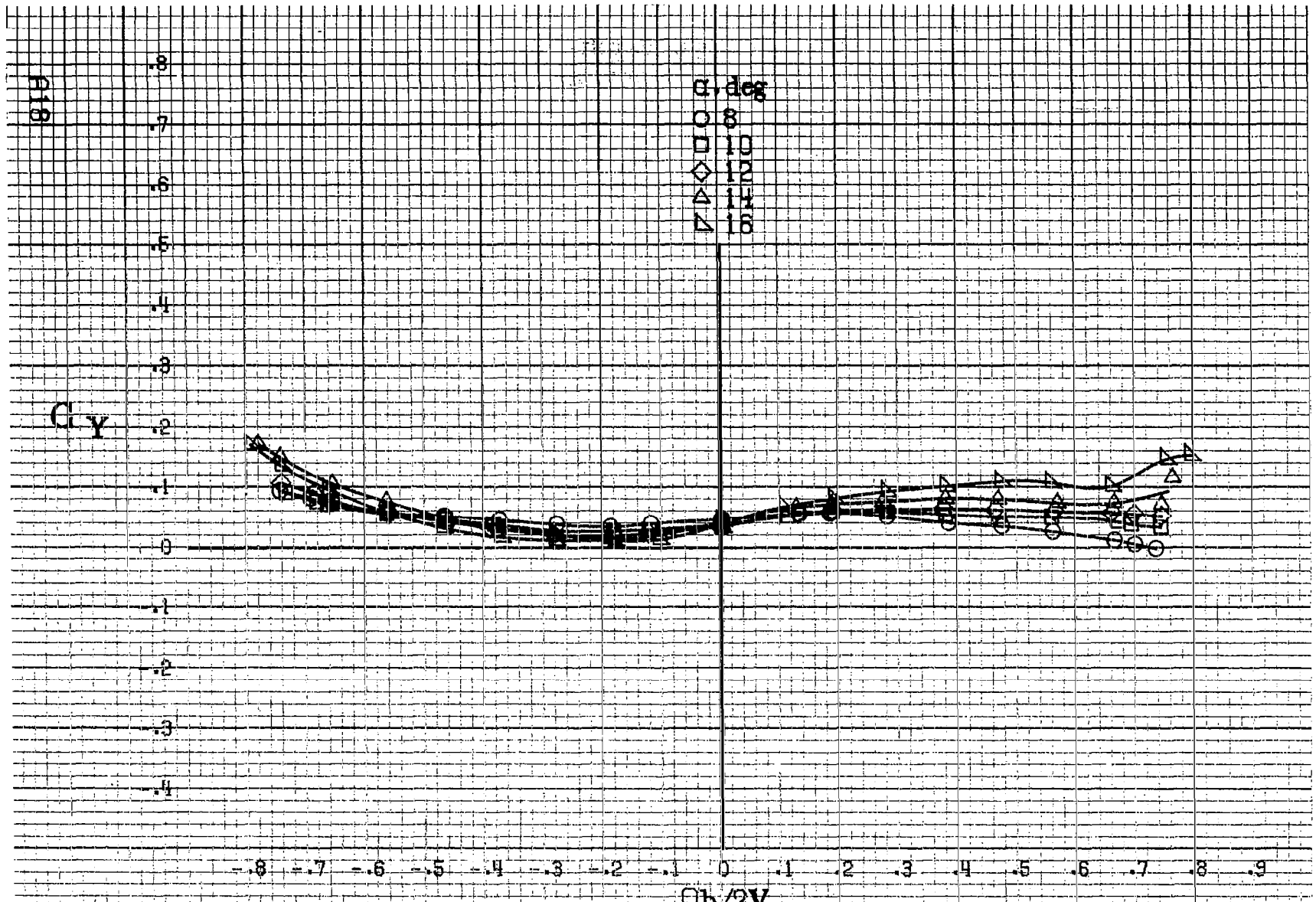

(a) α=8to16deg, SR=99cm(39in).

Figure A5.-Effect of rotation rate and angle of attack on side-force coefficient for basic configuration. $\delta_e = 0°$, $\delta_a = 0°$, $\delta_r = 0°$, $\beta = 0°$.

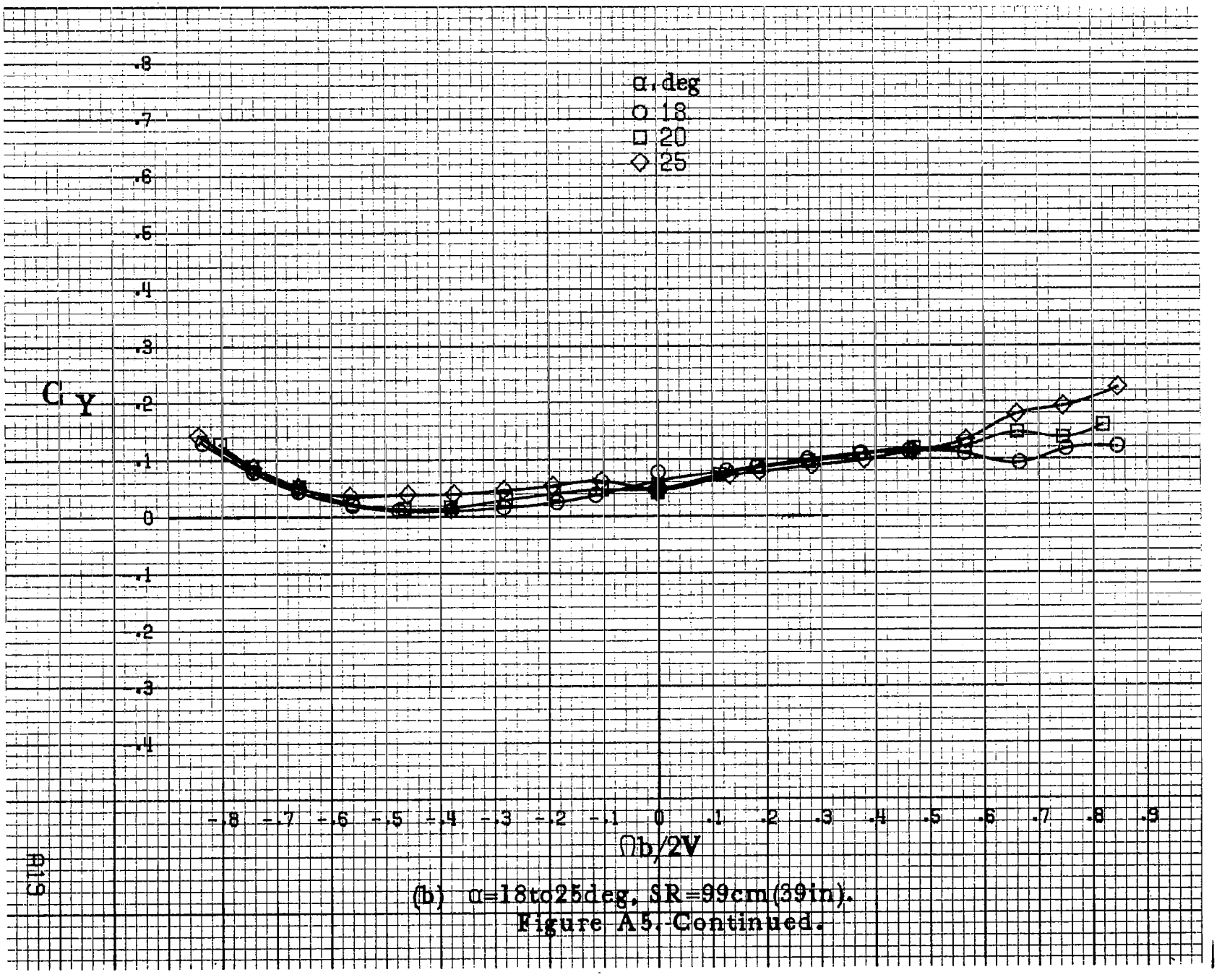

(b) α=18to25deg, SR=99cm(39in).

Figure A5.-Continued.

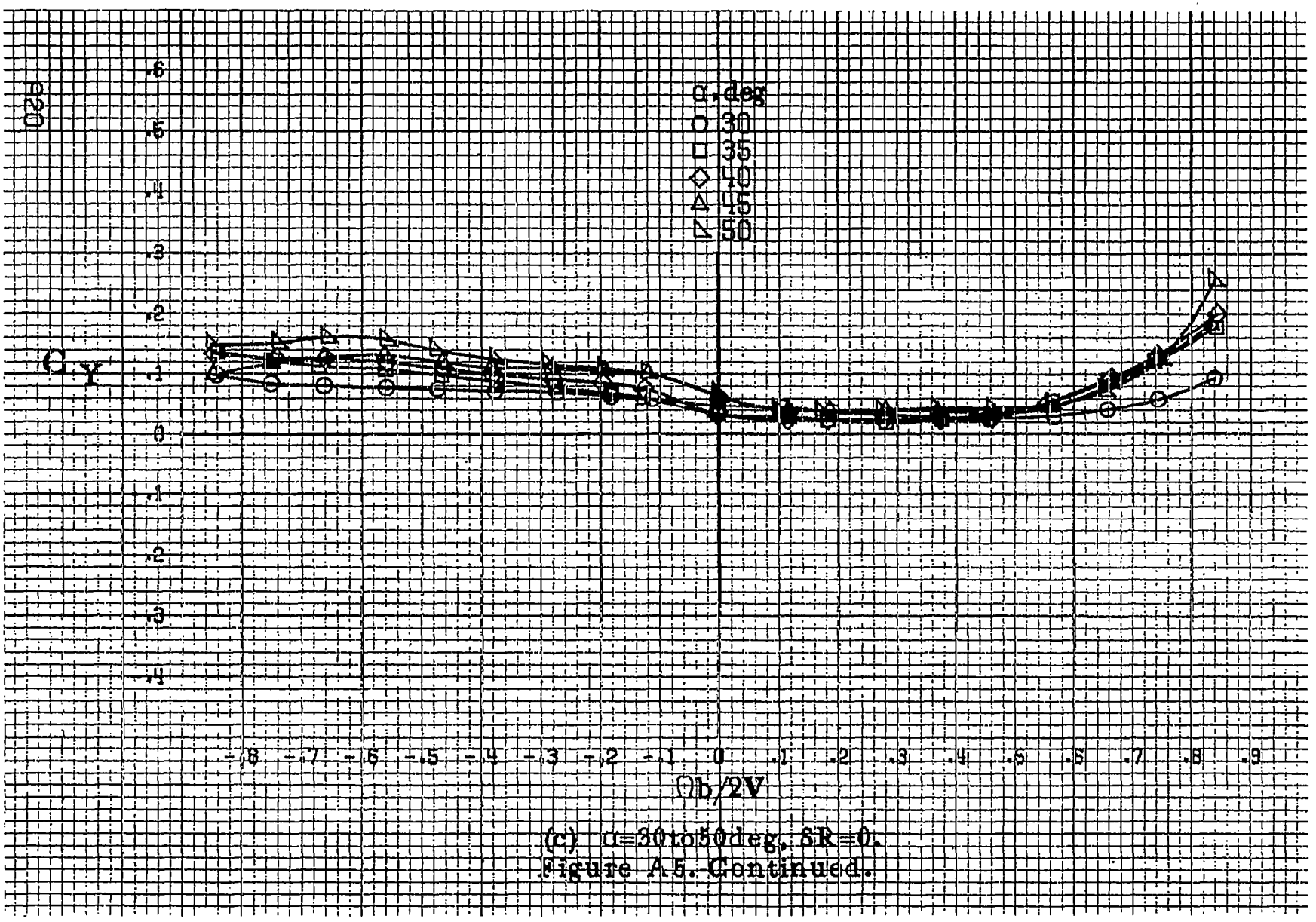

(c) α=30to50deg, δR=0.

Figure A.5. Continued.

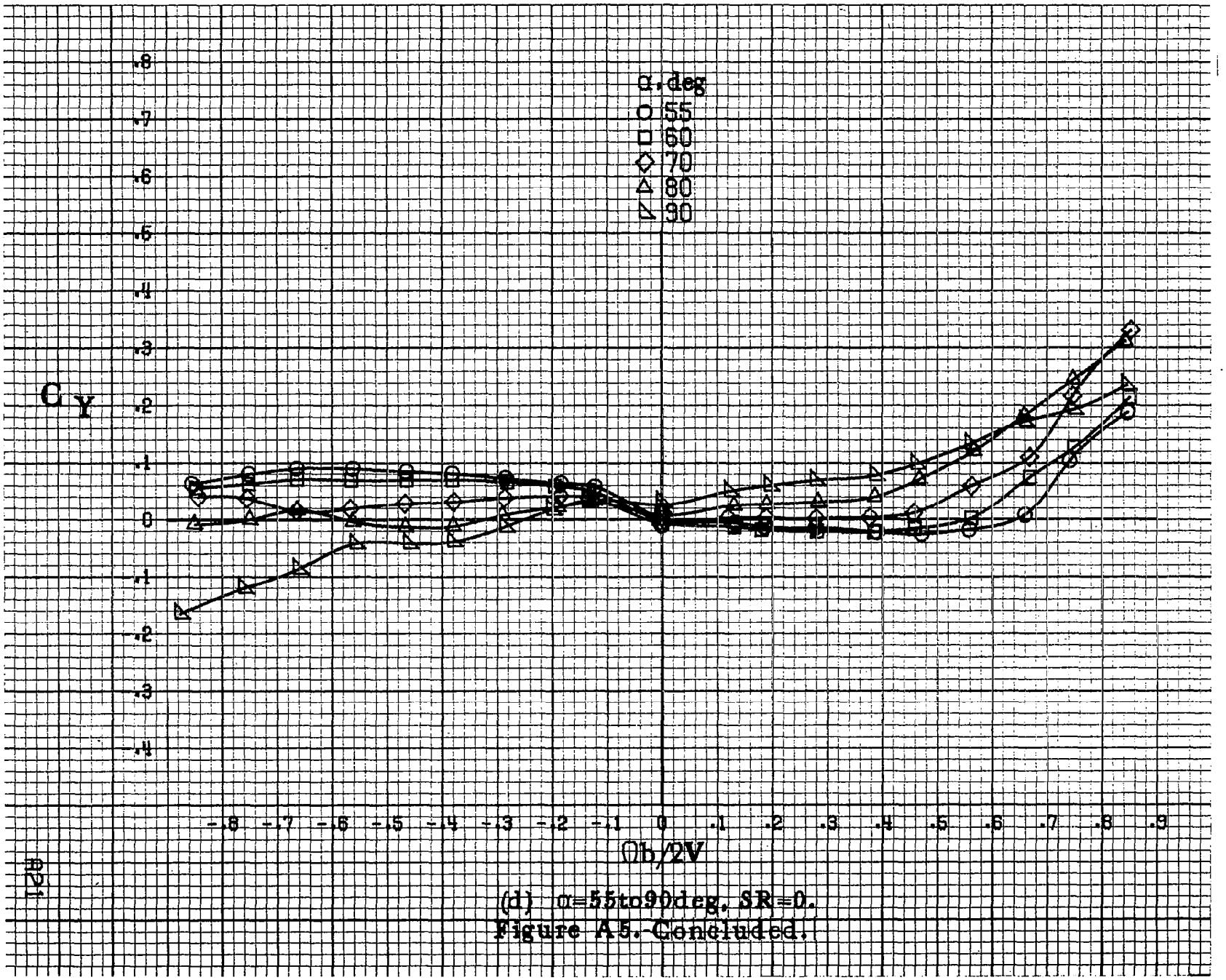

(d) α=55to90deg, SR=0.

Figure A5.-Concluded.

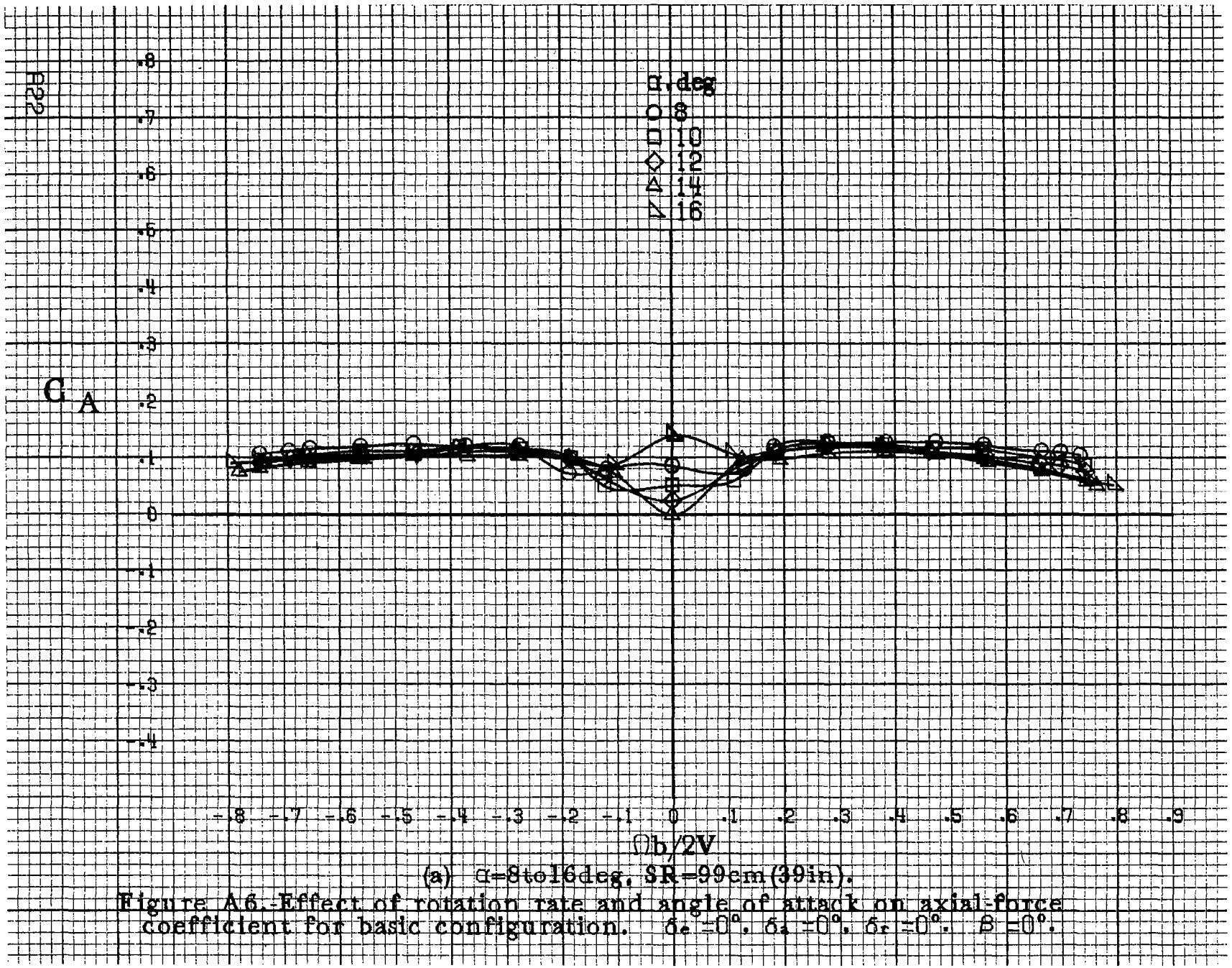

(a) α=8to16deg, SR=99cm(39in).

Figure A6.-Effect of rotation rate and angle of attack on axial-force coefficient for basic configuration. $\delta_e = 0°$, $\delta_a = 0°$, $\delta_r = 0°$, $\beta = 0°$.

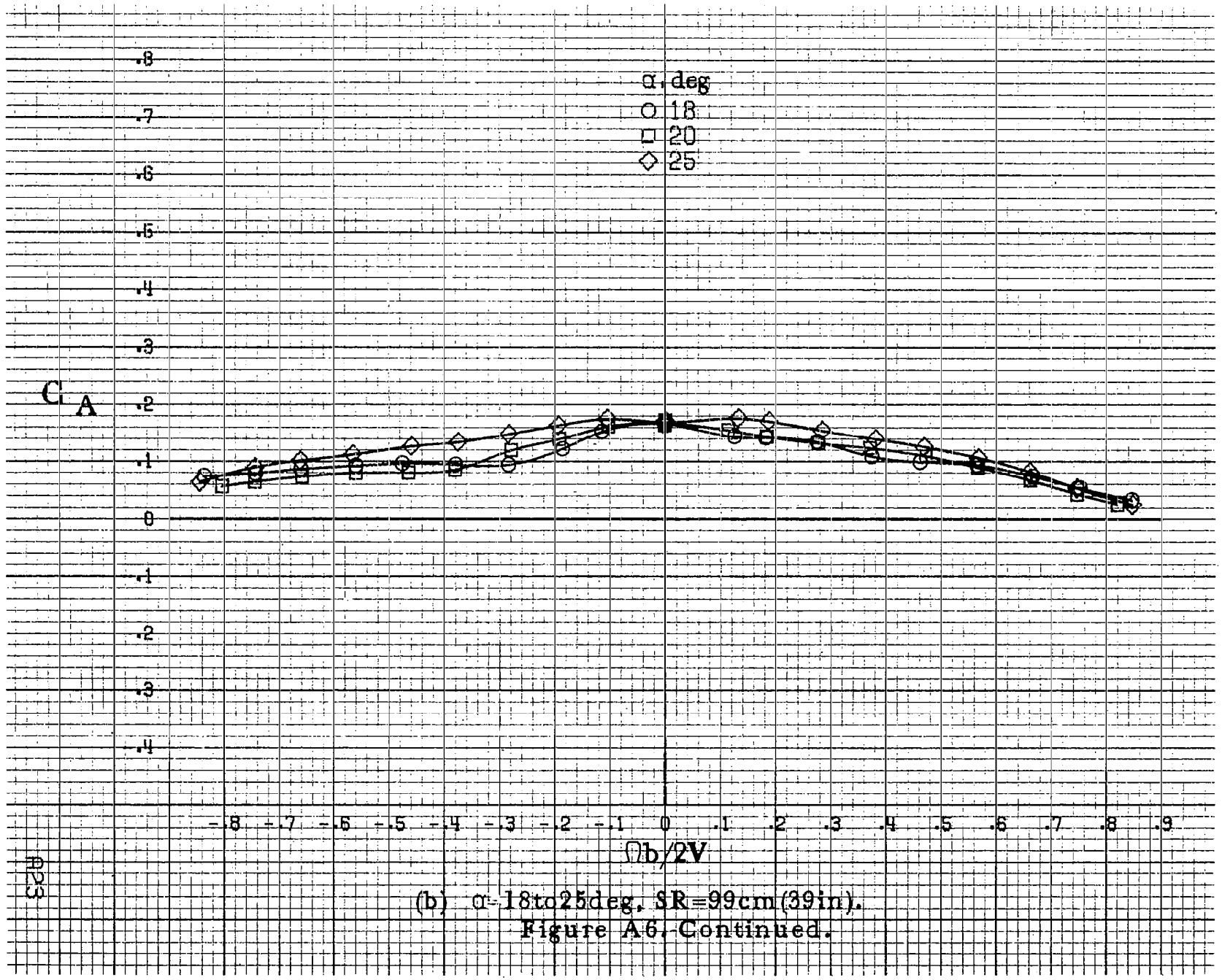

(b) α=18to25deg, SR=99cm(39in).

Figure A6. Continued.

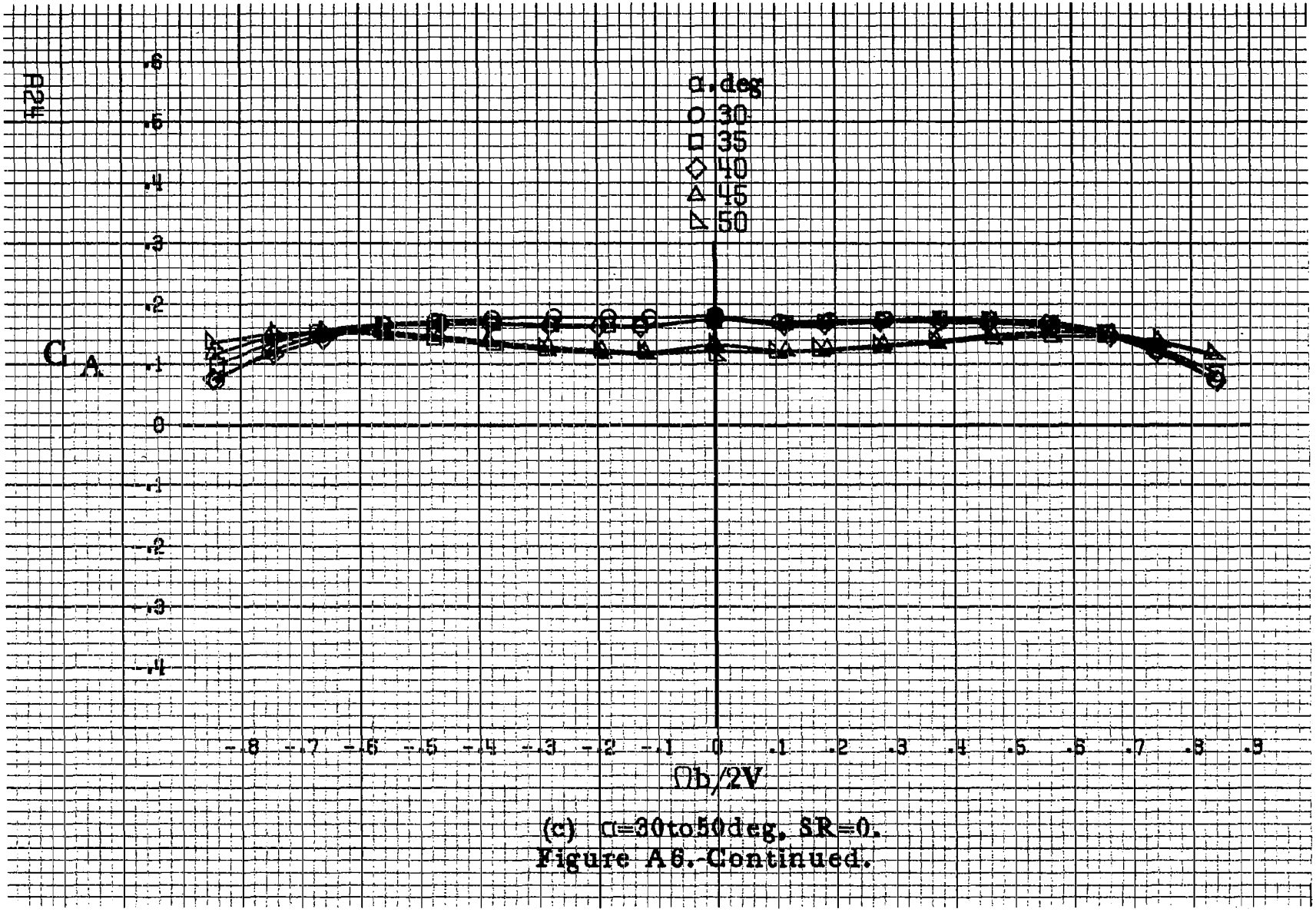

(c) α=30to50deg, SR=0.

Figure A6.-Continued.

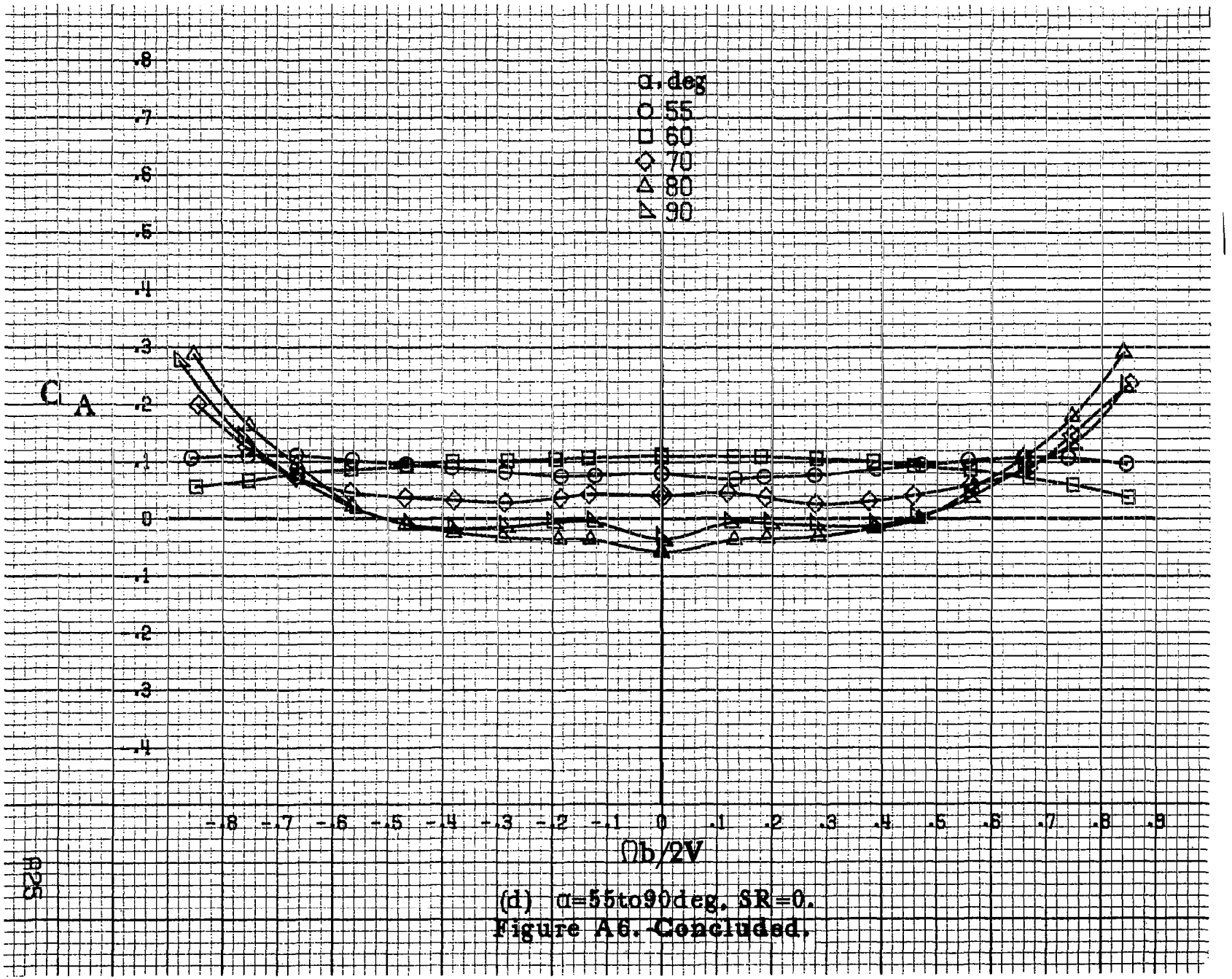

(d) α=55to90deg, SR=0.

Figure A6. Concluded.

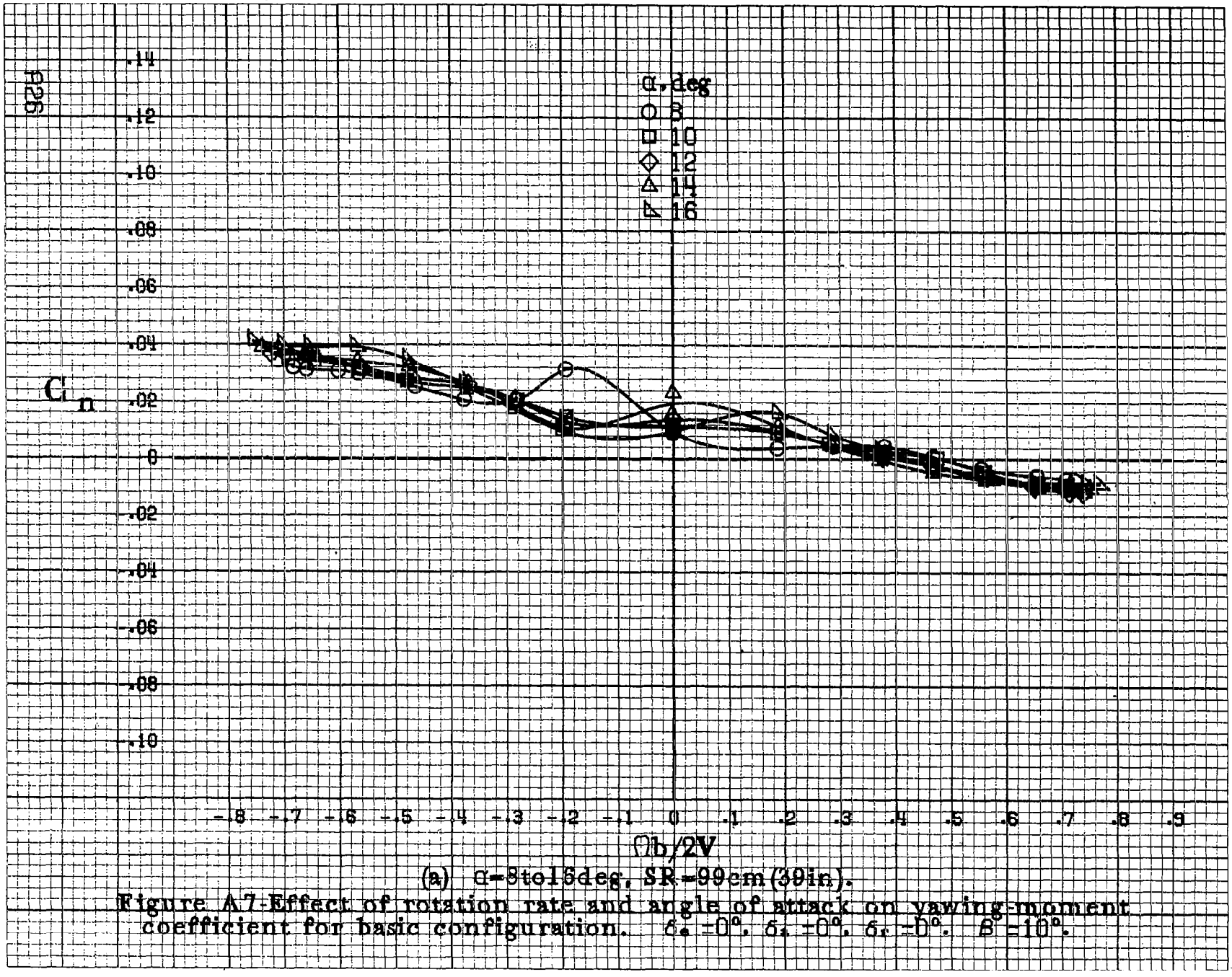

(a) α=8to16deg, SR=99cm(39in).

Figure A7-Effect of rotation rate and angle of attack on yawing-moment coefficient for basic configuration. $\delta_e = 0°$, $\delta_a = 0°$, $\delta_r = 0°$, $\beta = 10°$.

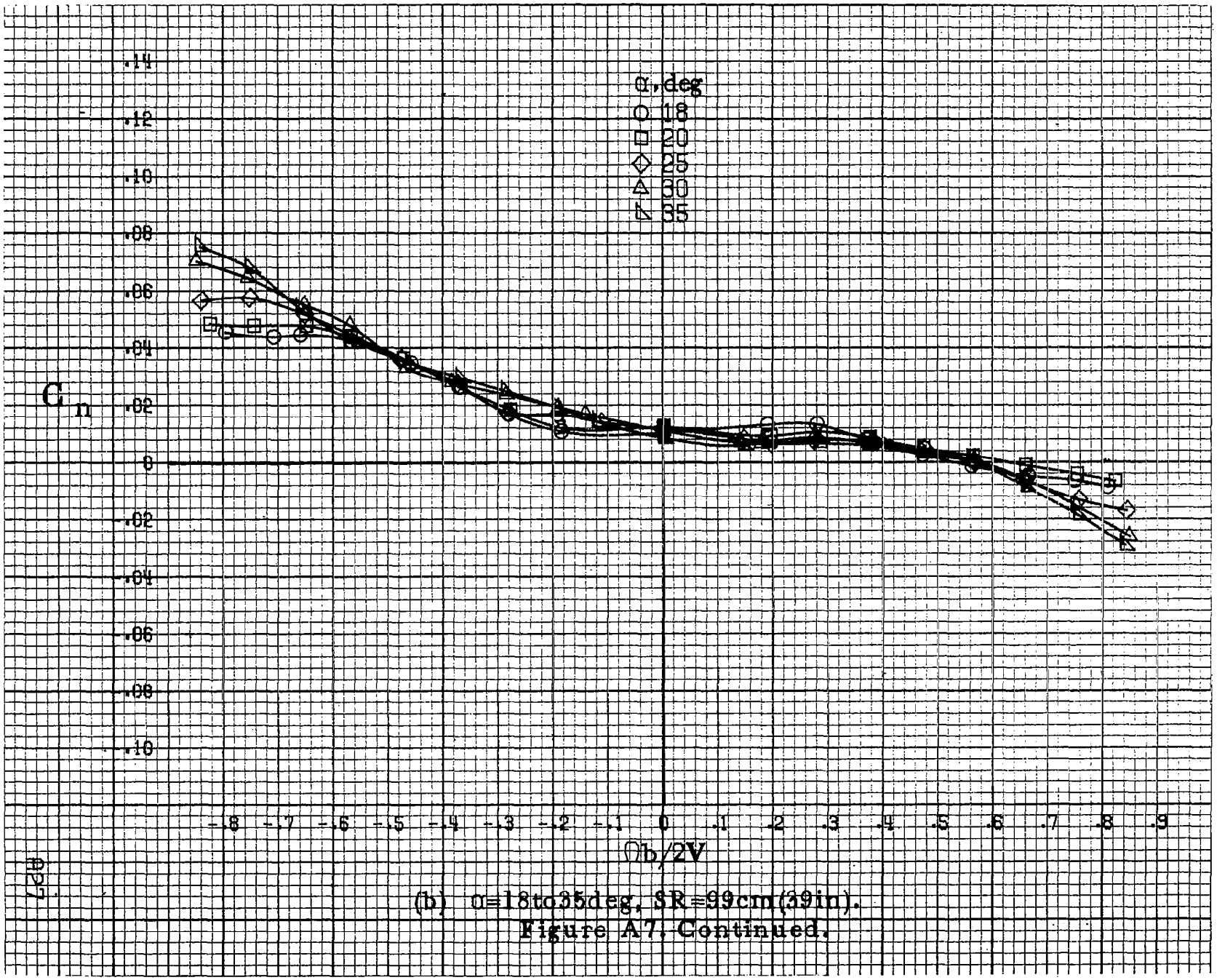

(b) α=18to35deg, SR=99cm(39in).

Figure A7. Continued.

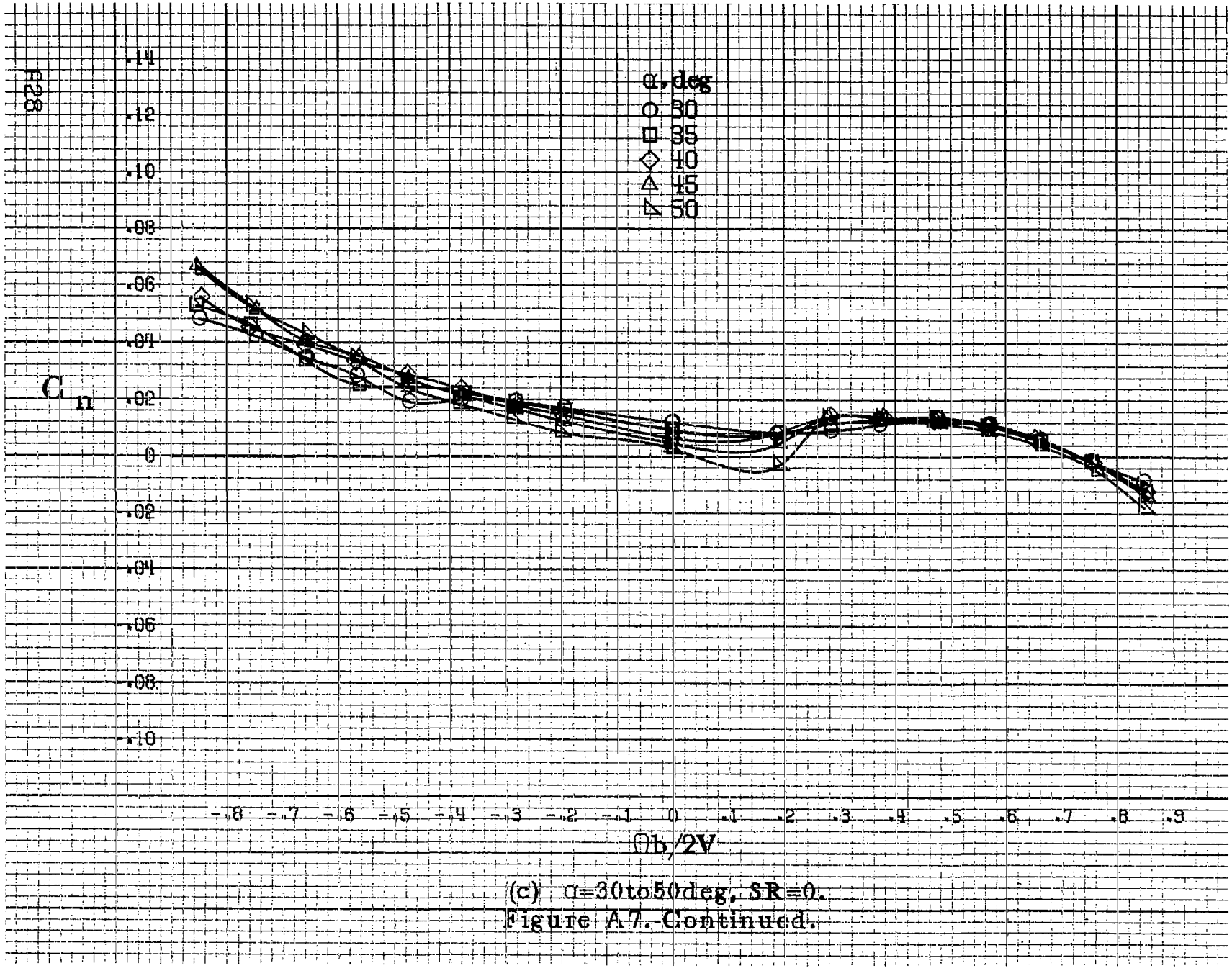

(c) α=30to50deg, SR=0.

Figure A7.-Continued.

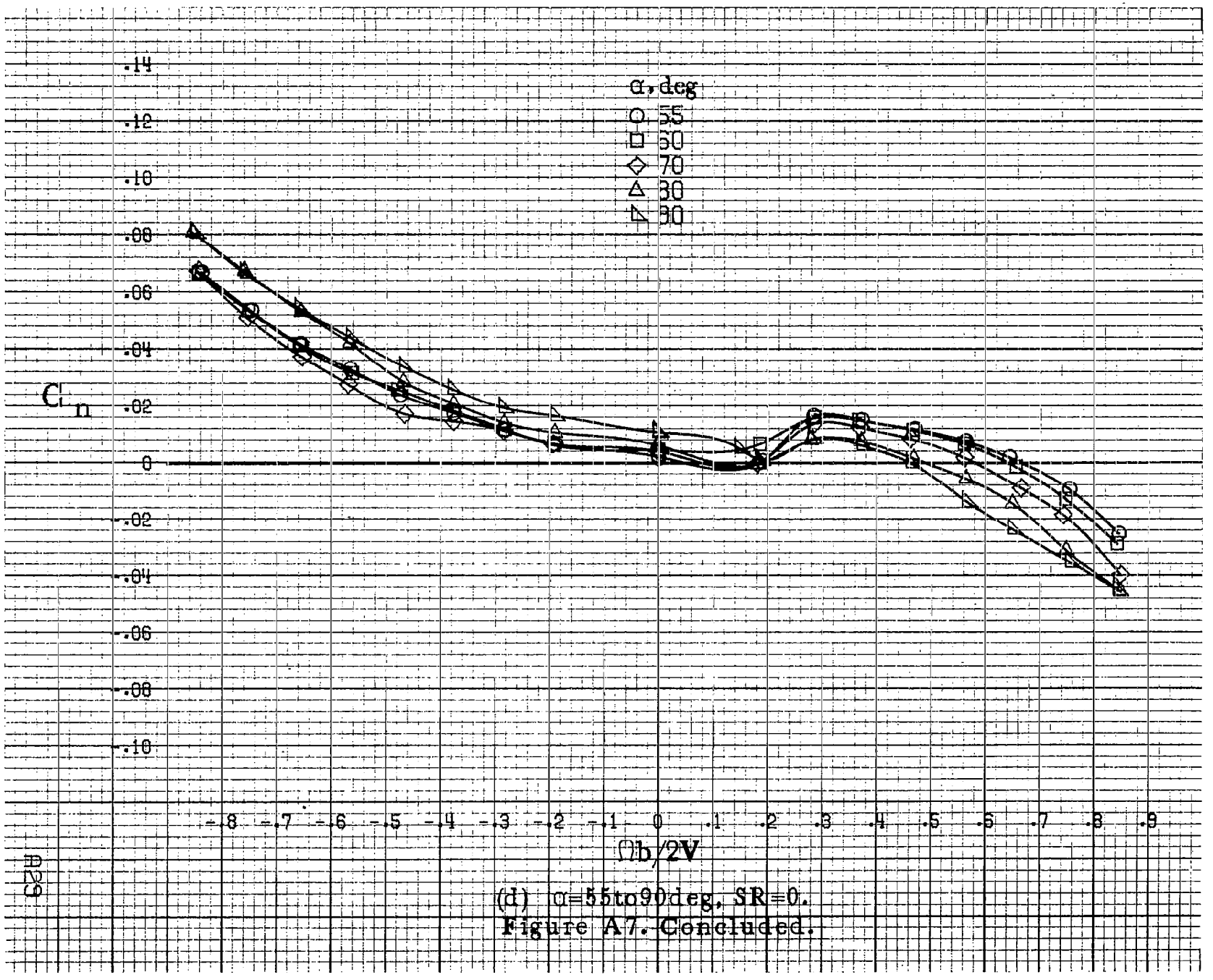

(d) α=55to90deg, SR=0.

Figure A7. Concluded.

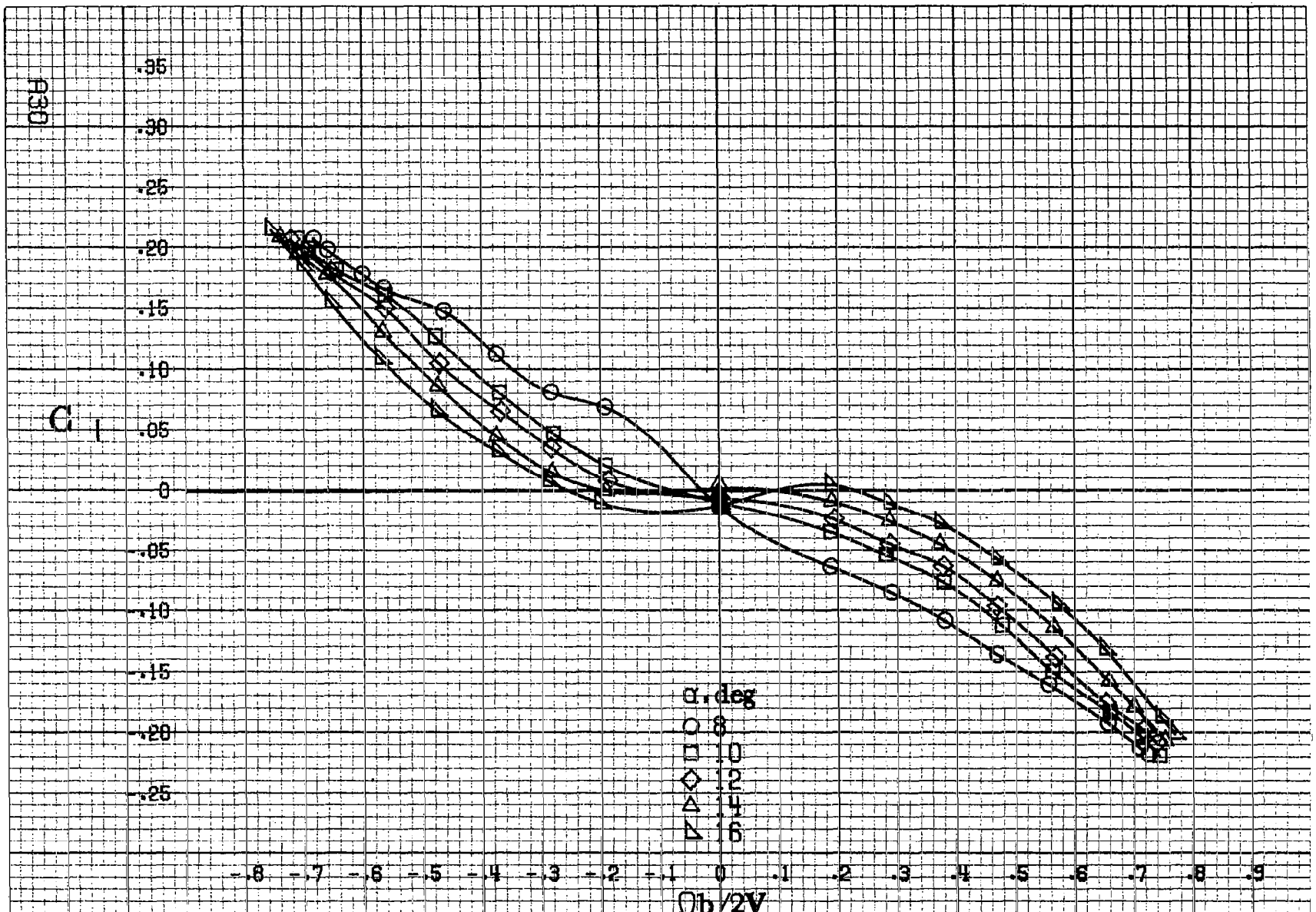

(a) α=8to16deg, SR=99cm(39in).

Figure A8.-Effect of rotation rate and angle of attack on rolling-moment coefficient for basic configuration. $\delta_e = 0°$, $\delta_a = 0°$, $\delta_r = 0°$, $\beta = 10°$.

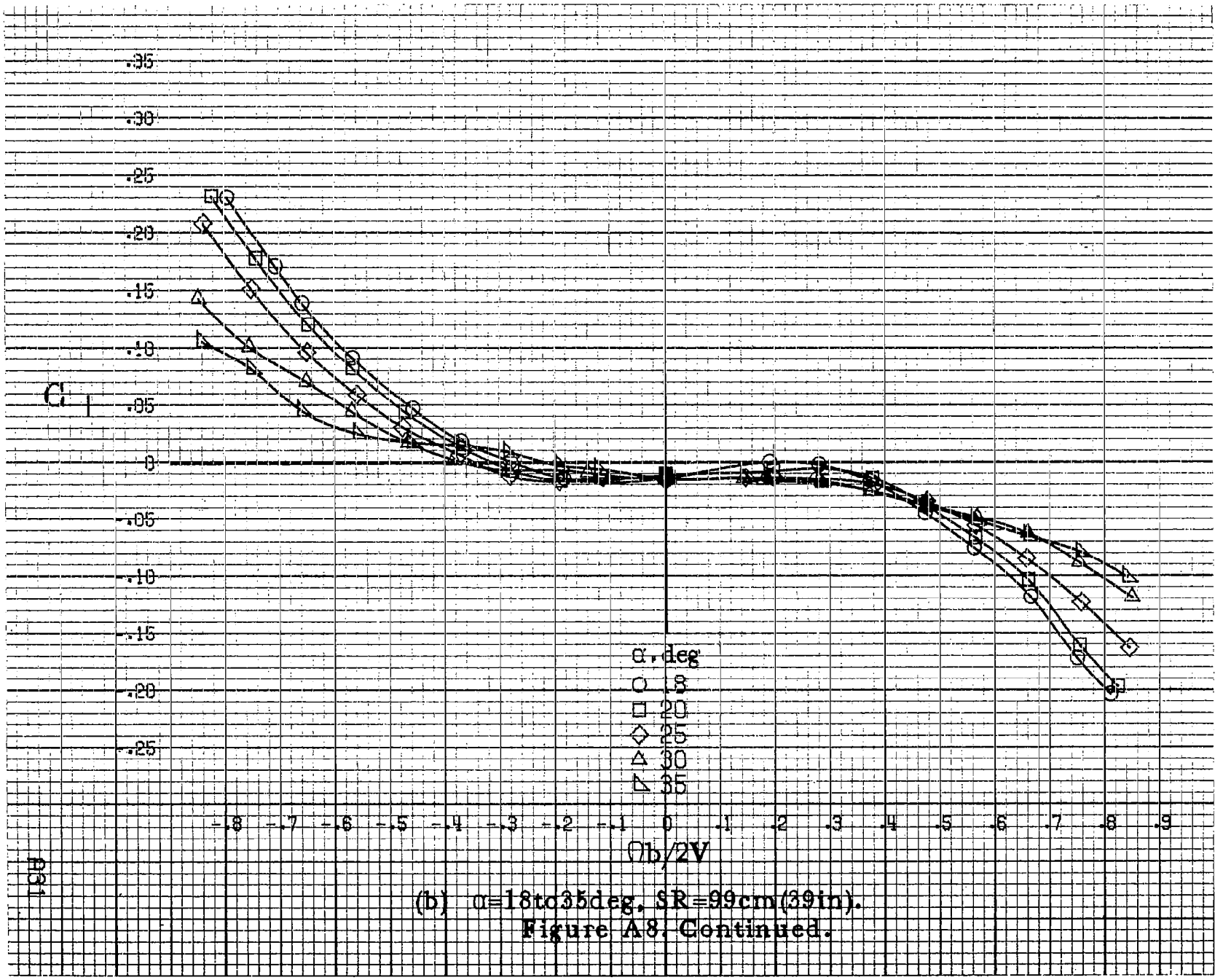

(b) α=18to35deg, SR=99cm(39in).

Figure A8. Continued.

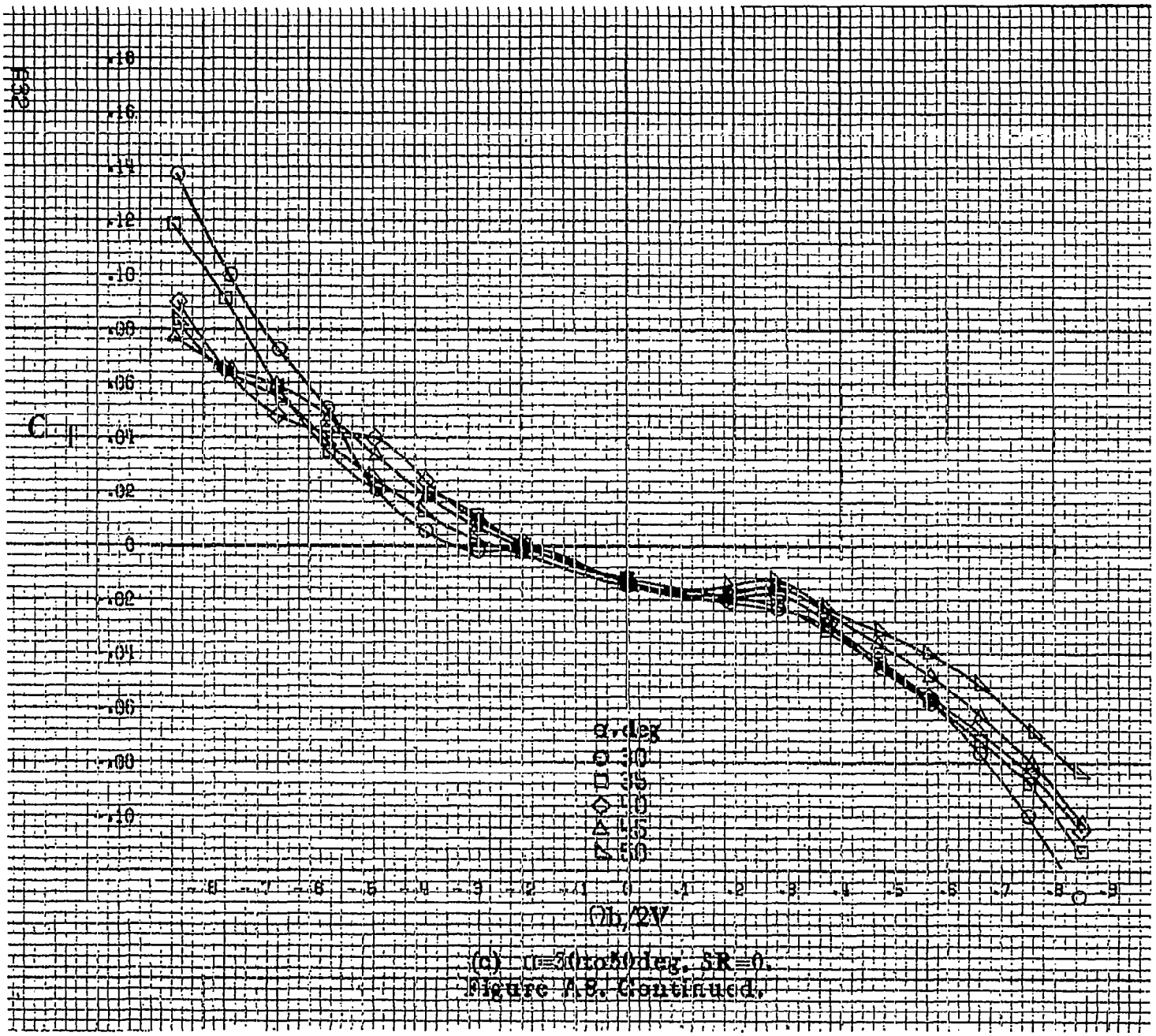

(a) $\Gamma = 3(\cos^2)$deg, SR = 0.

Figure A.8. Continued.

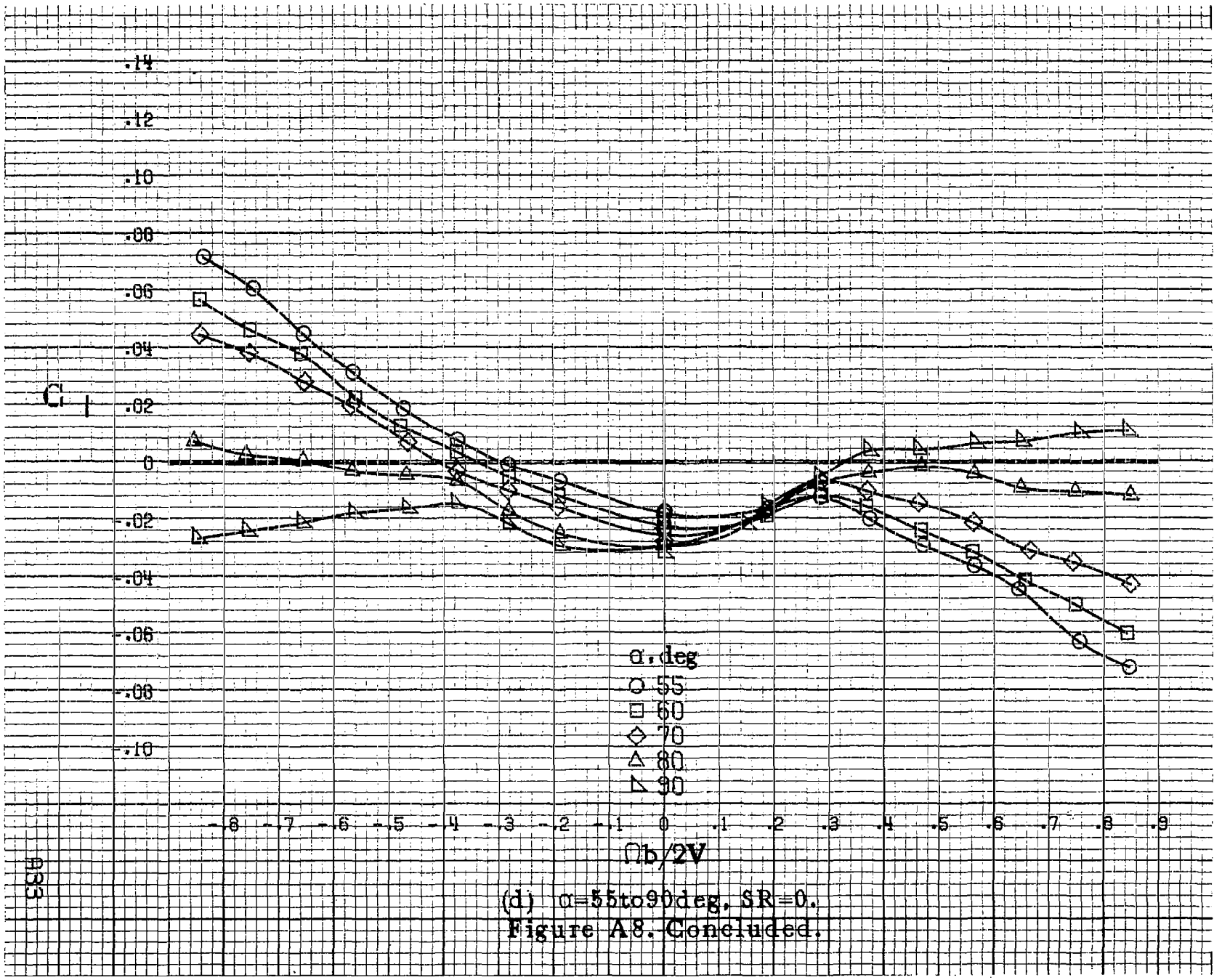

(d) α=55to90deg, SR=0.

Figure A8. Concluded.

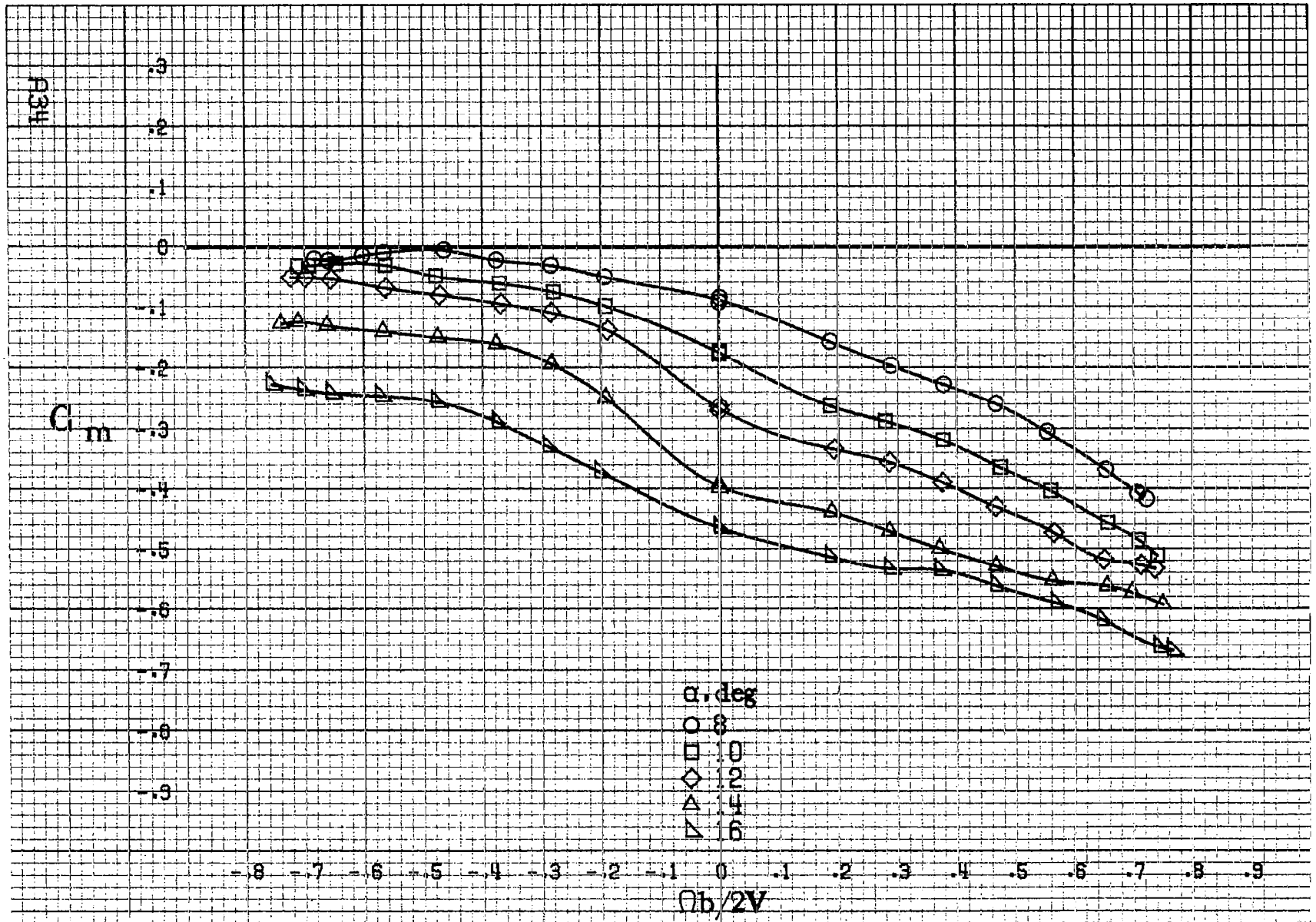

(a) α=8to16deg, SR=99cm(39in).

Figure A9.-Effect of rotation rate and angle of attack on pitching-moment coefficient for basic configuration. $\delta_e = 0°$, $\delta_a = 0°$, $\delta_r = 0°$, $\beta = 0°$.

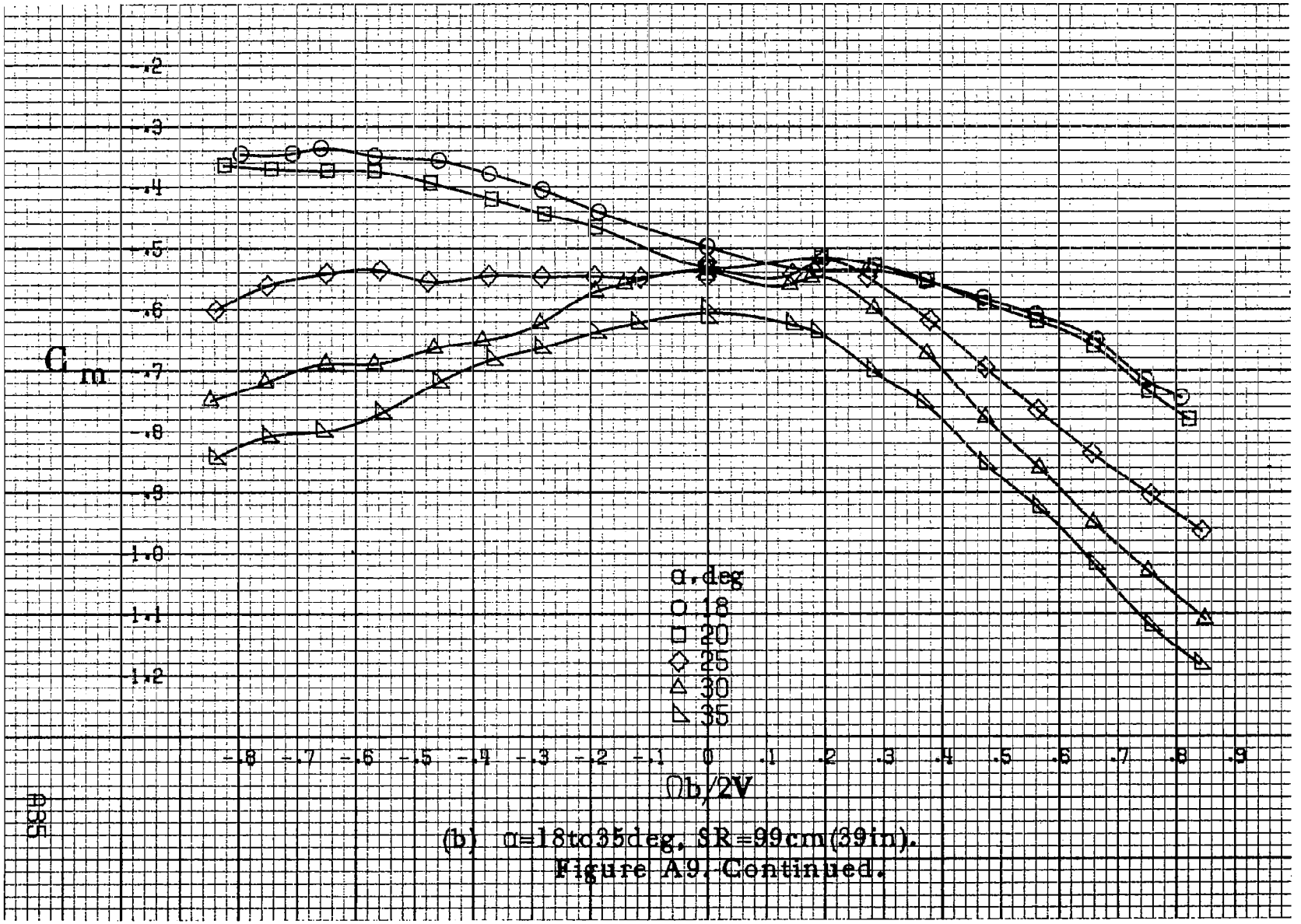

(b) α=18to35deg, SR=99cm(39in).

Figure A9. Continued.

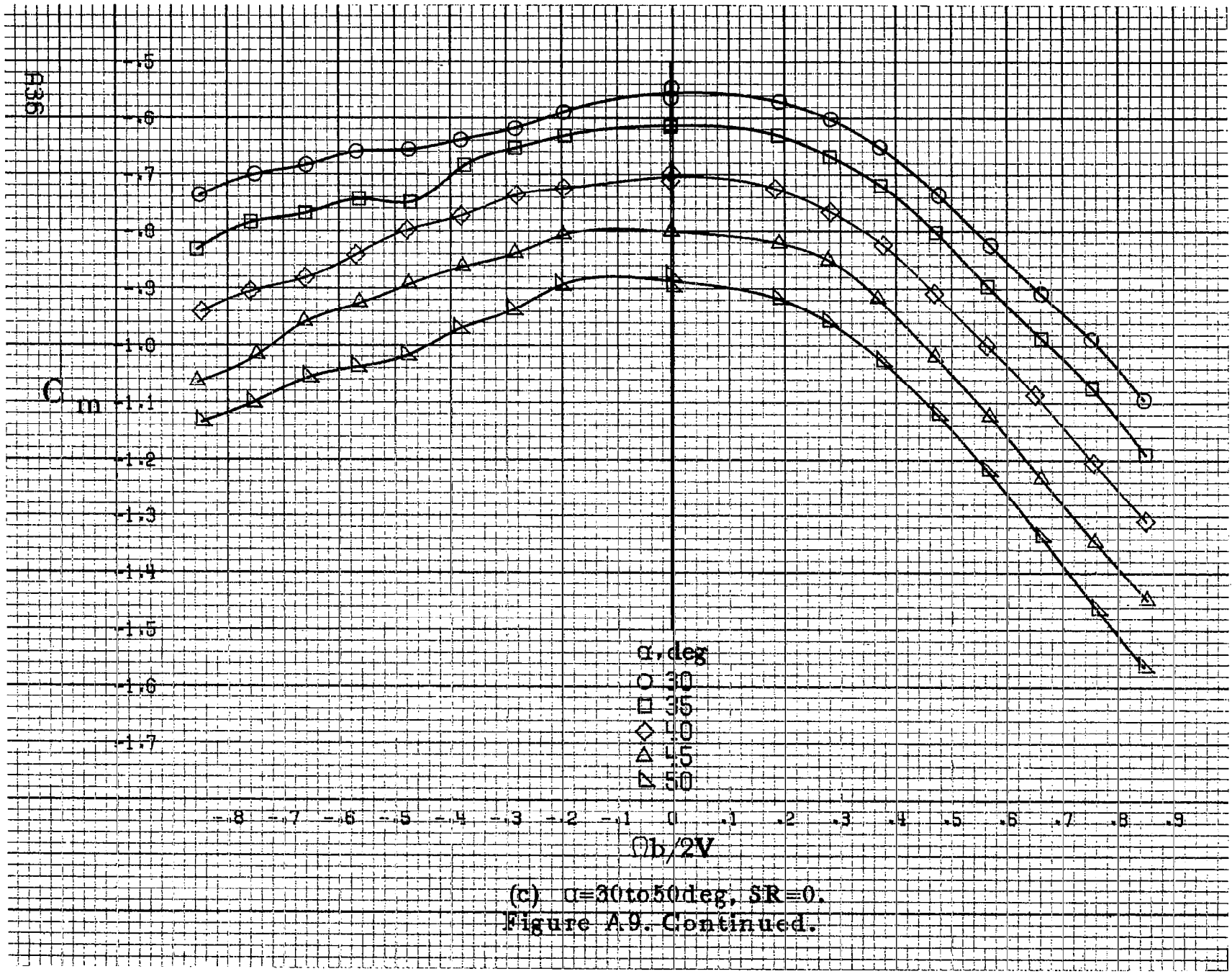

(c) α=30to50deg, SR≡0.

Figure A.9. Continued.

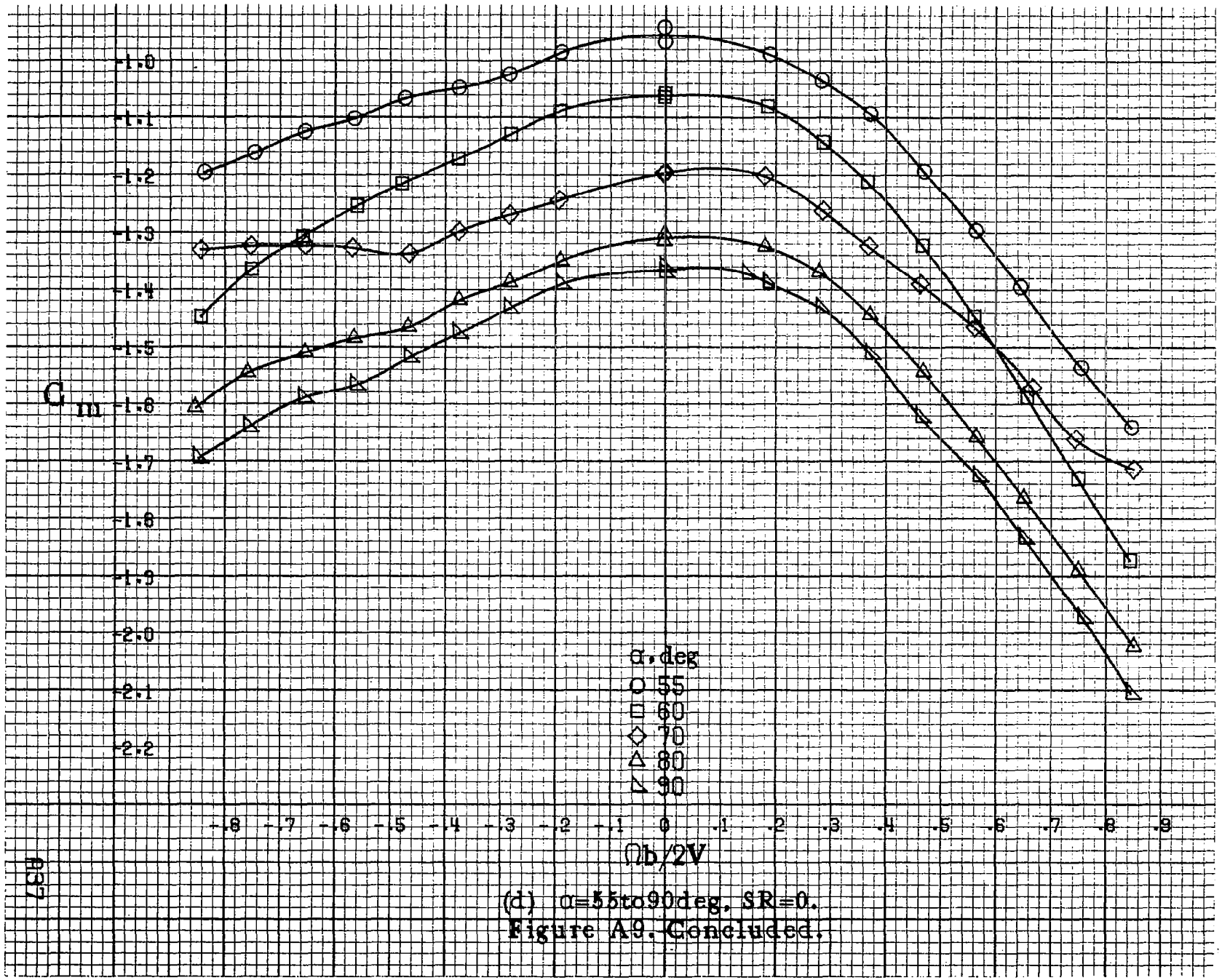

(d) α=55to90deg, SR=0.

Figure A9. Concluded.

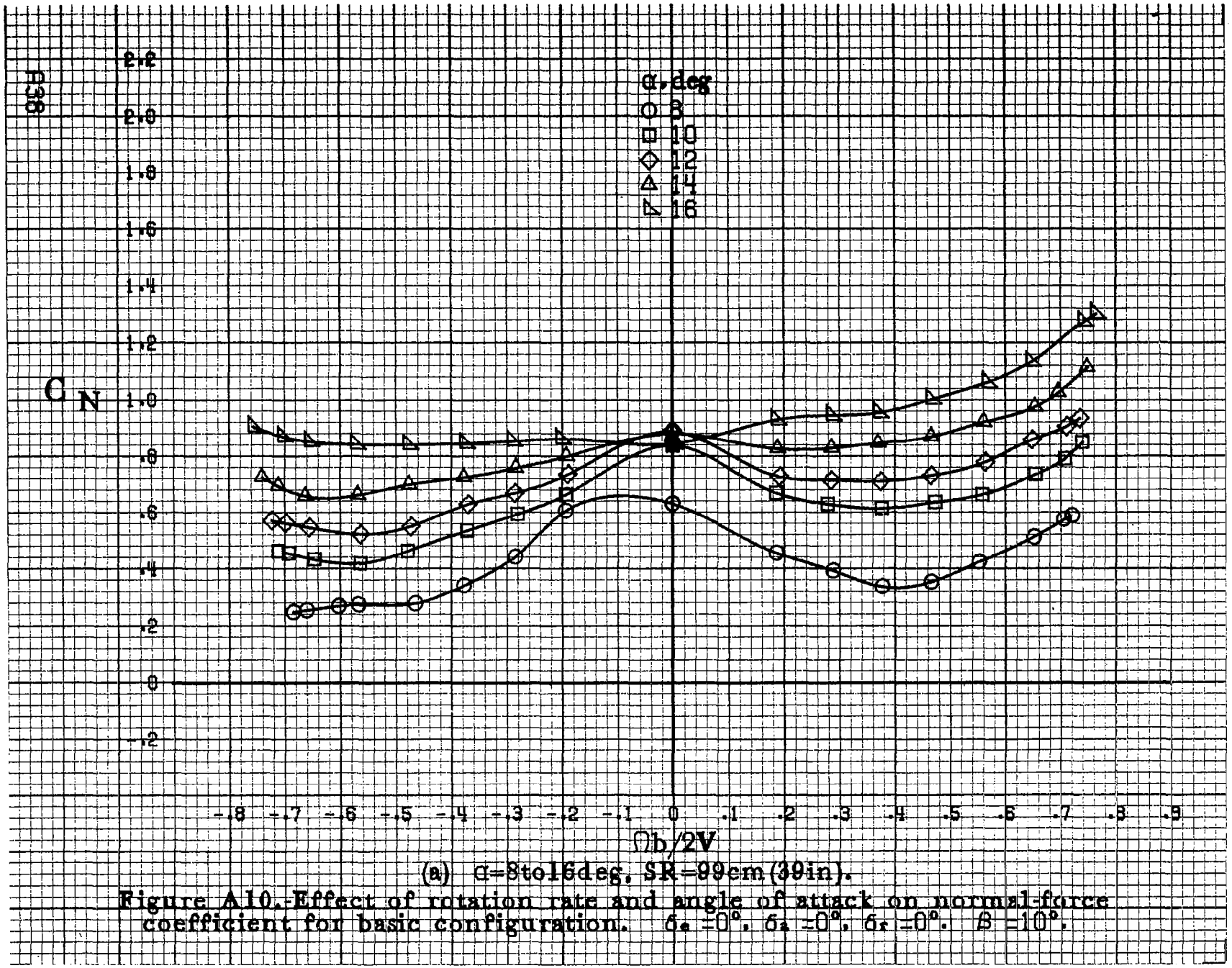

(a) α=8to16deg, SR=99cm(39in).

Figure A10.-Effect of rotation rate and angle of attack on normal-force coefficient for basic configuration. δ_e =0°, δ_a =0°, δ_r =0°. β =10°.

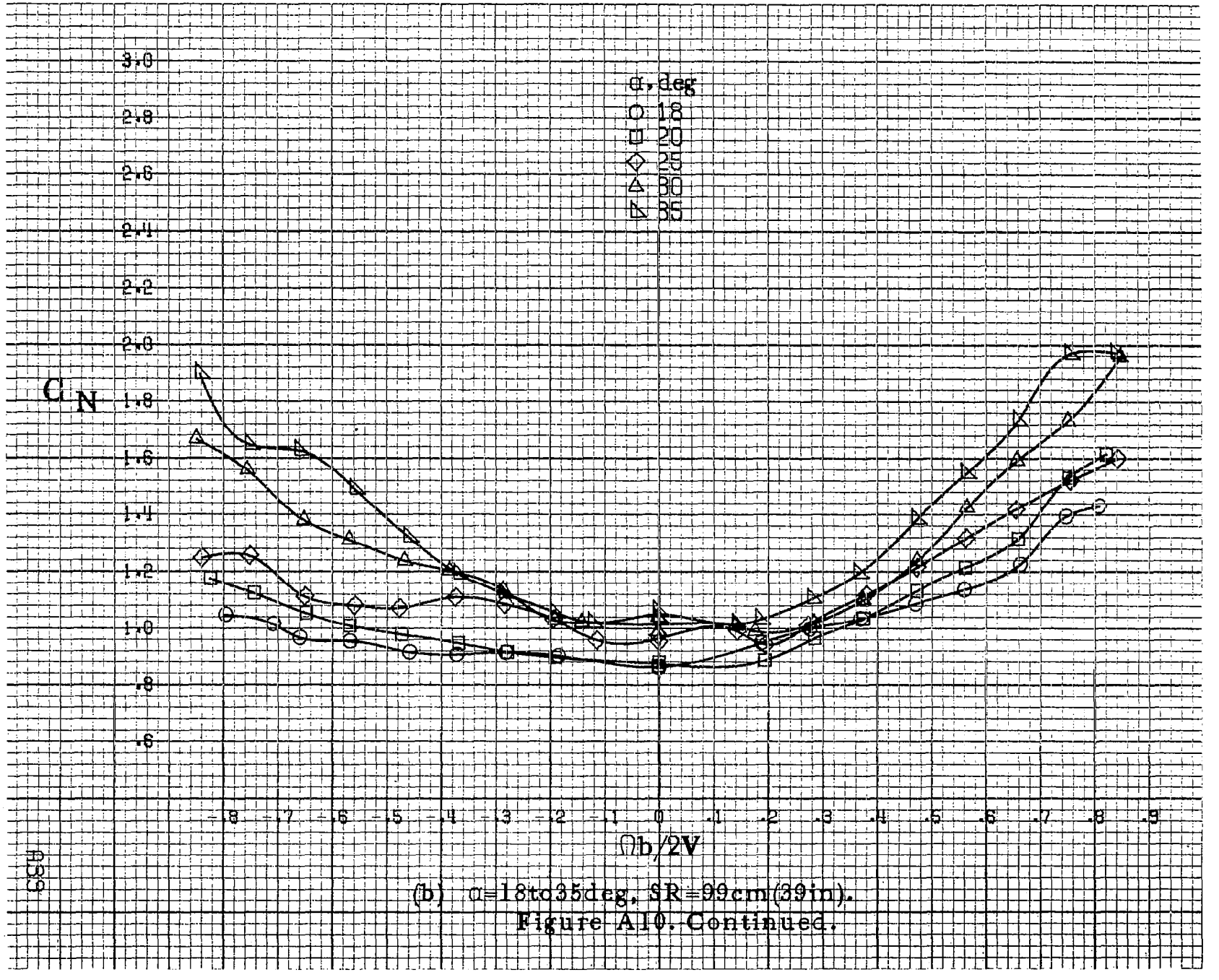

(b) α=18to35deg, SR=99cm(39in).

Figure A10. Continued.

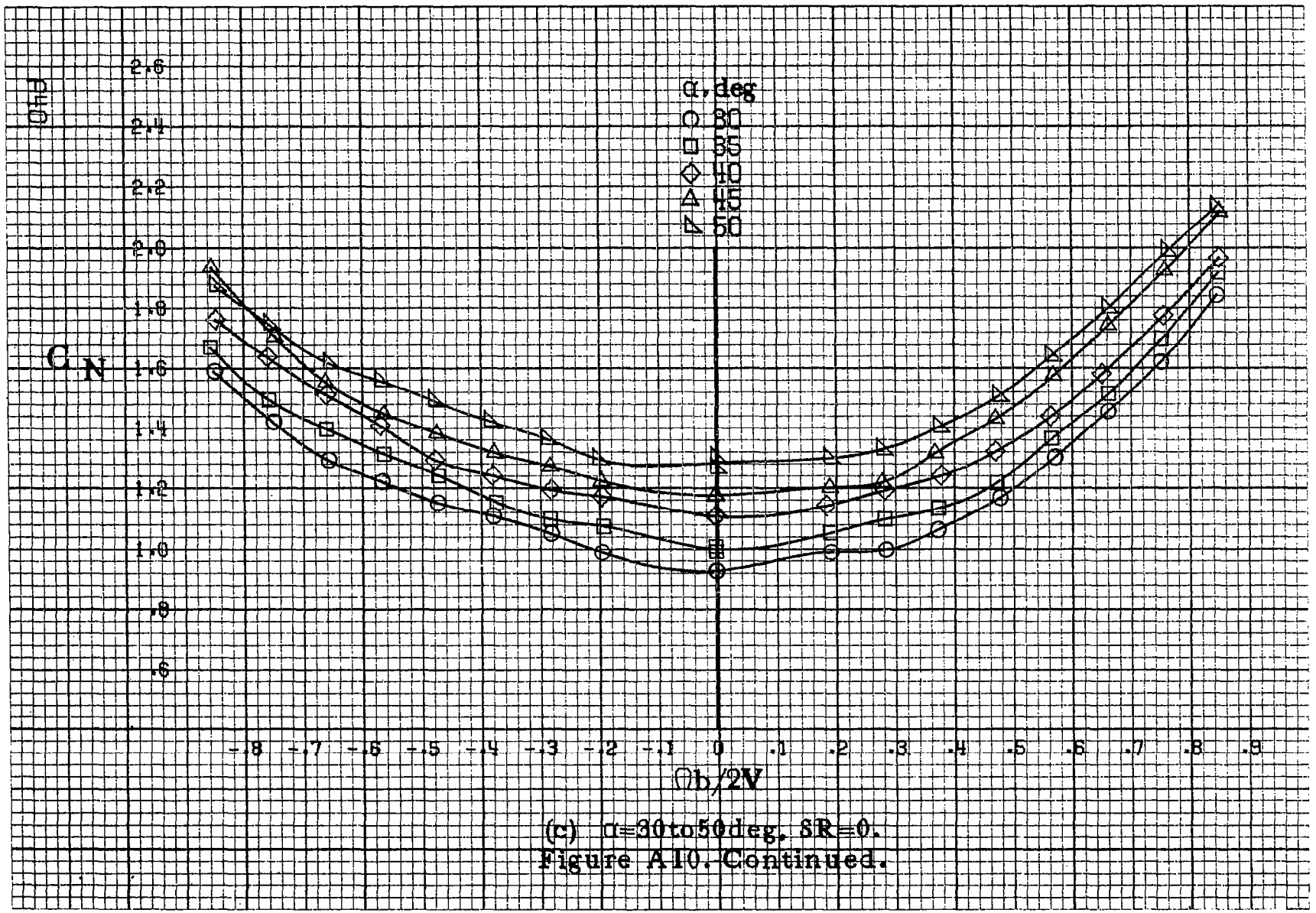

(c) α=30to50deg, δR=0.

Figure A10. Continued.

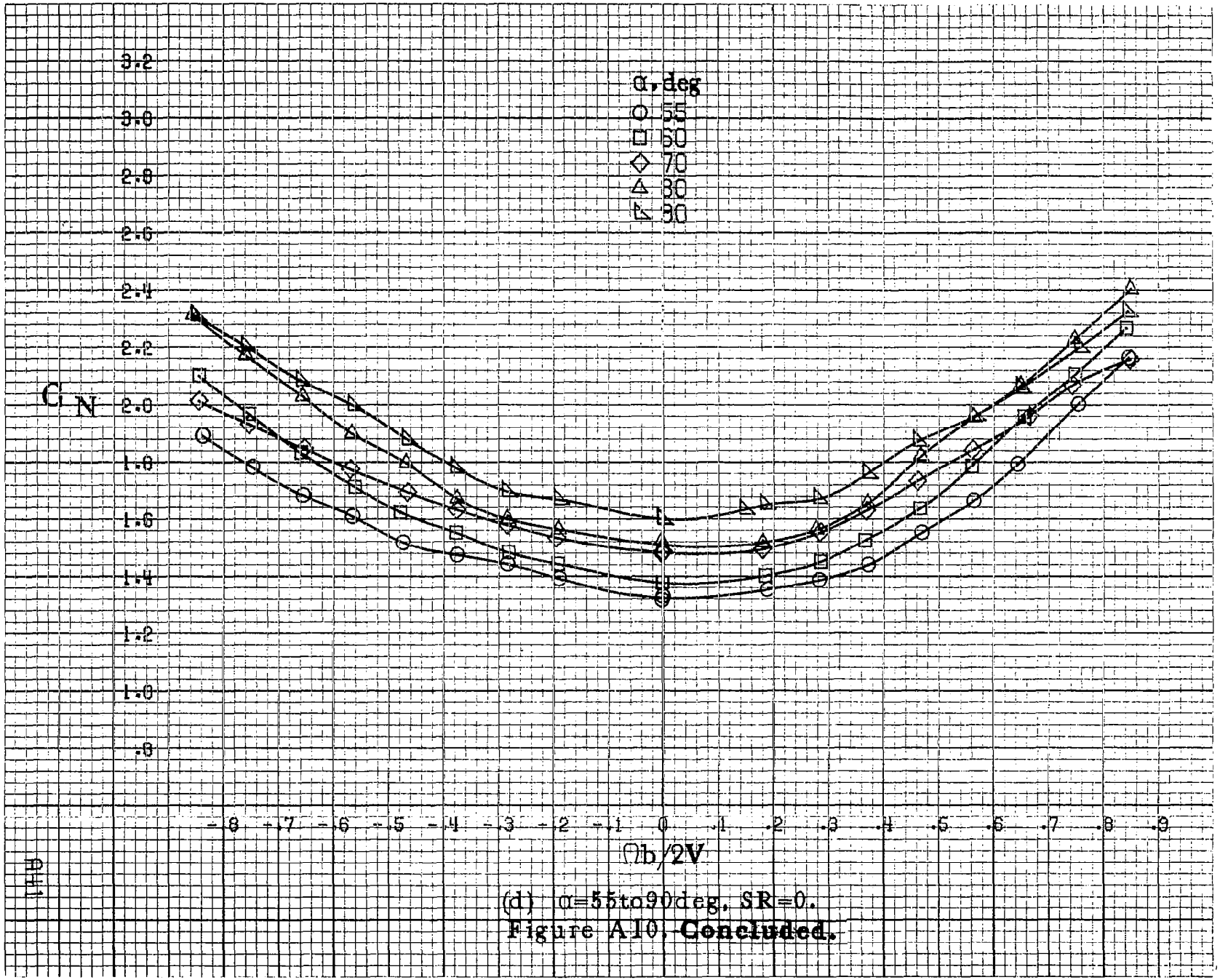

(d) α=55 to 90 deg, SR=0.

Figure A10. Concluded.

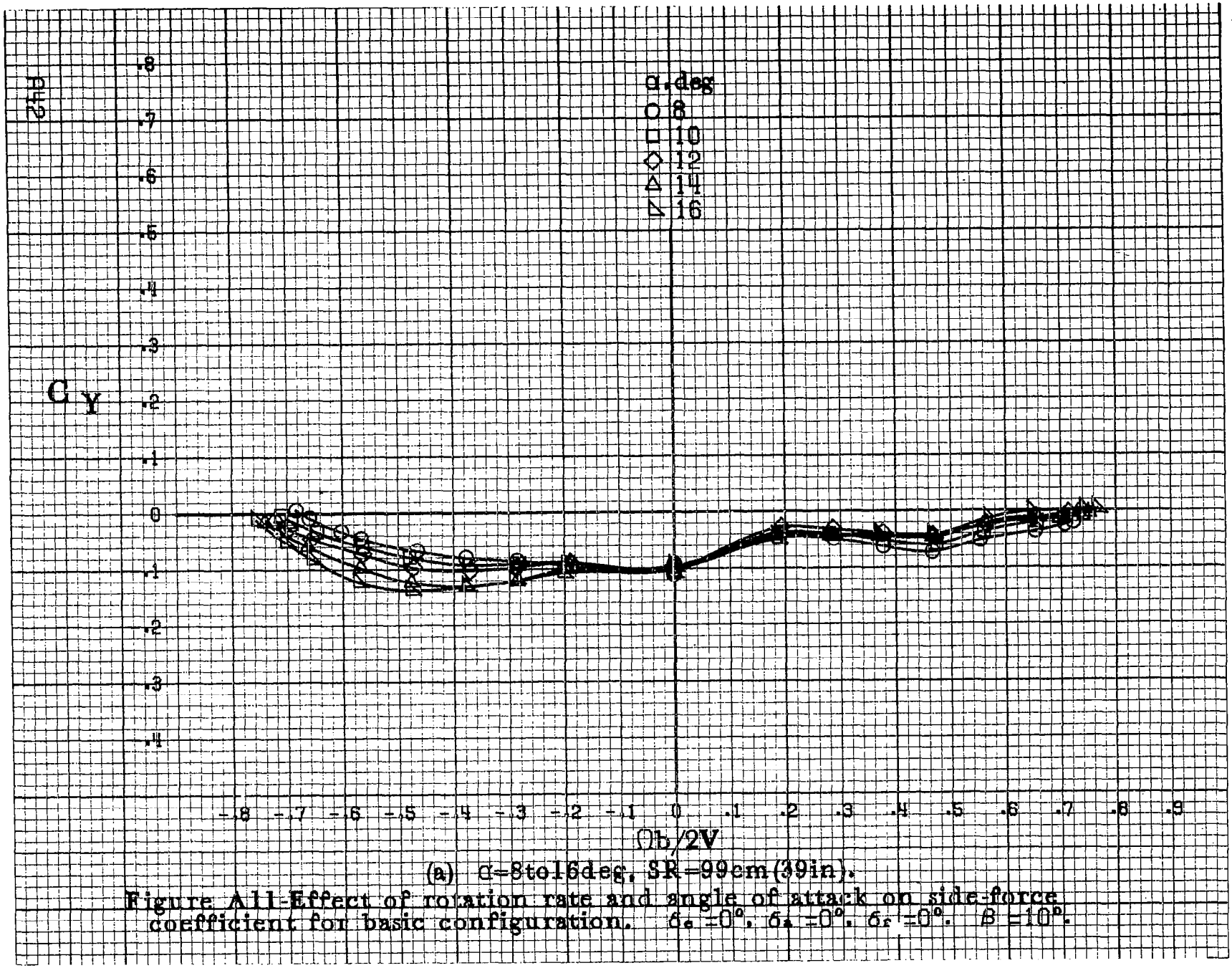

(a) α=8to16deg, SR=99cm(39in).

Figure All-Effect of rotation rate and angle of attack on side-force coefficient for basic configuration. $\delta_e = 0°$, $\delta_a = 0°$, $\delta_r = 0°$. $\beta = 10°$.

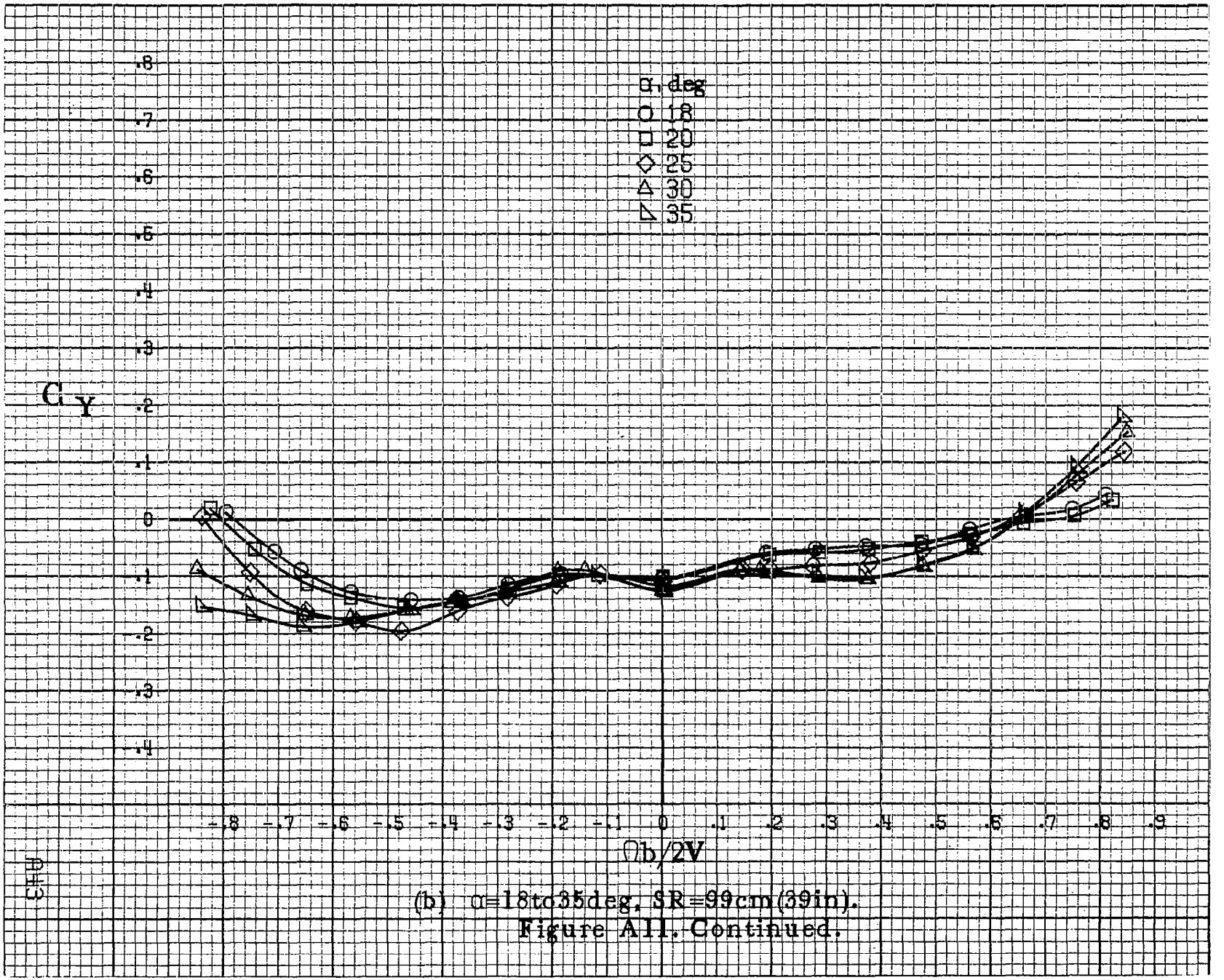

(b) α=18to35deg, SR=99cm(39in).

Figure A11. Continued.

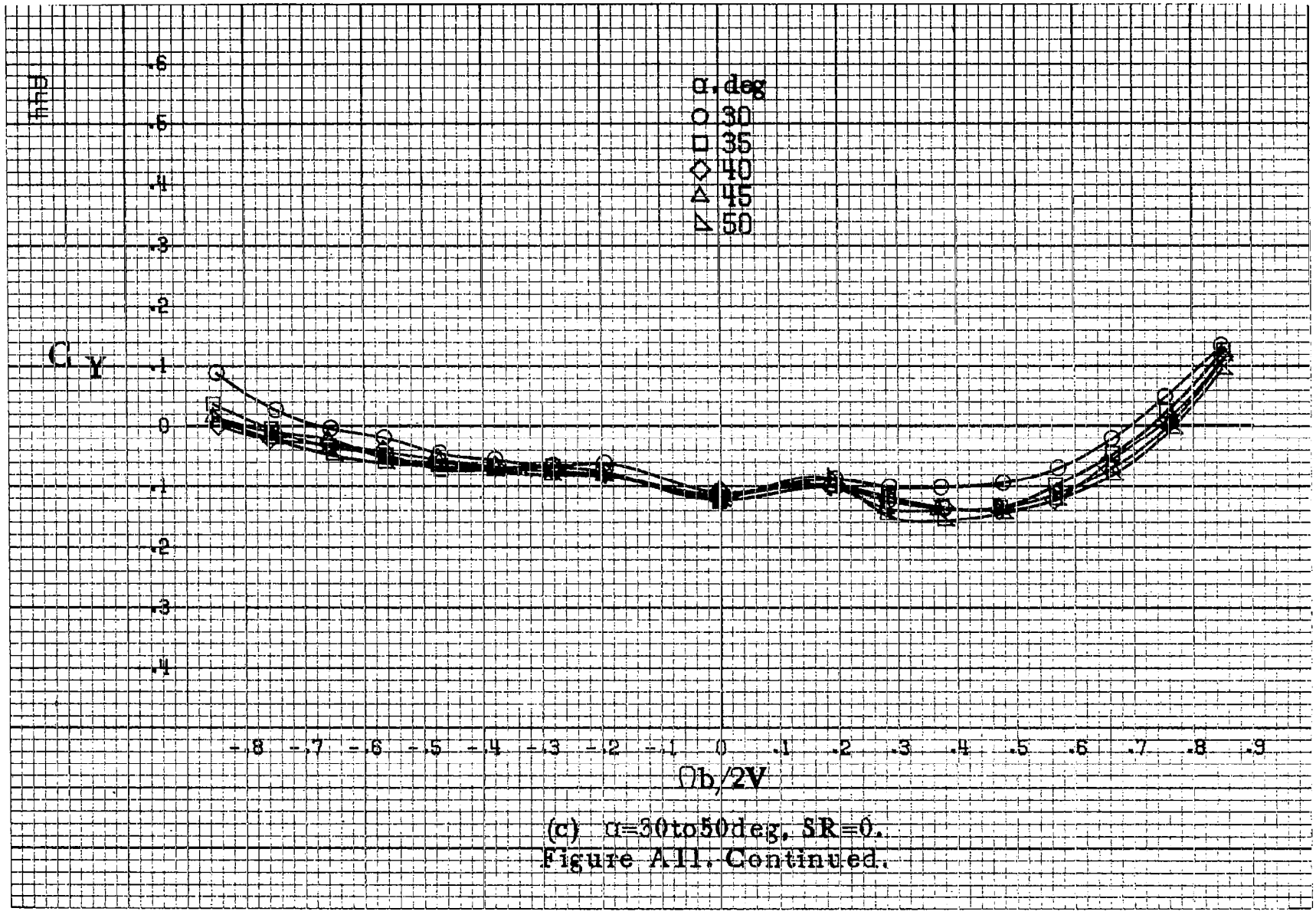

(c) α=30to50deg, SR=0.

Figure A11. Continued.

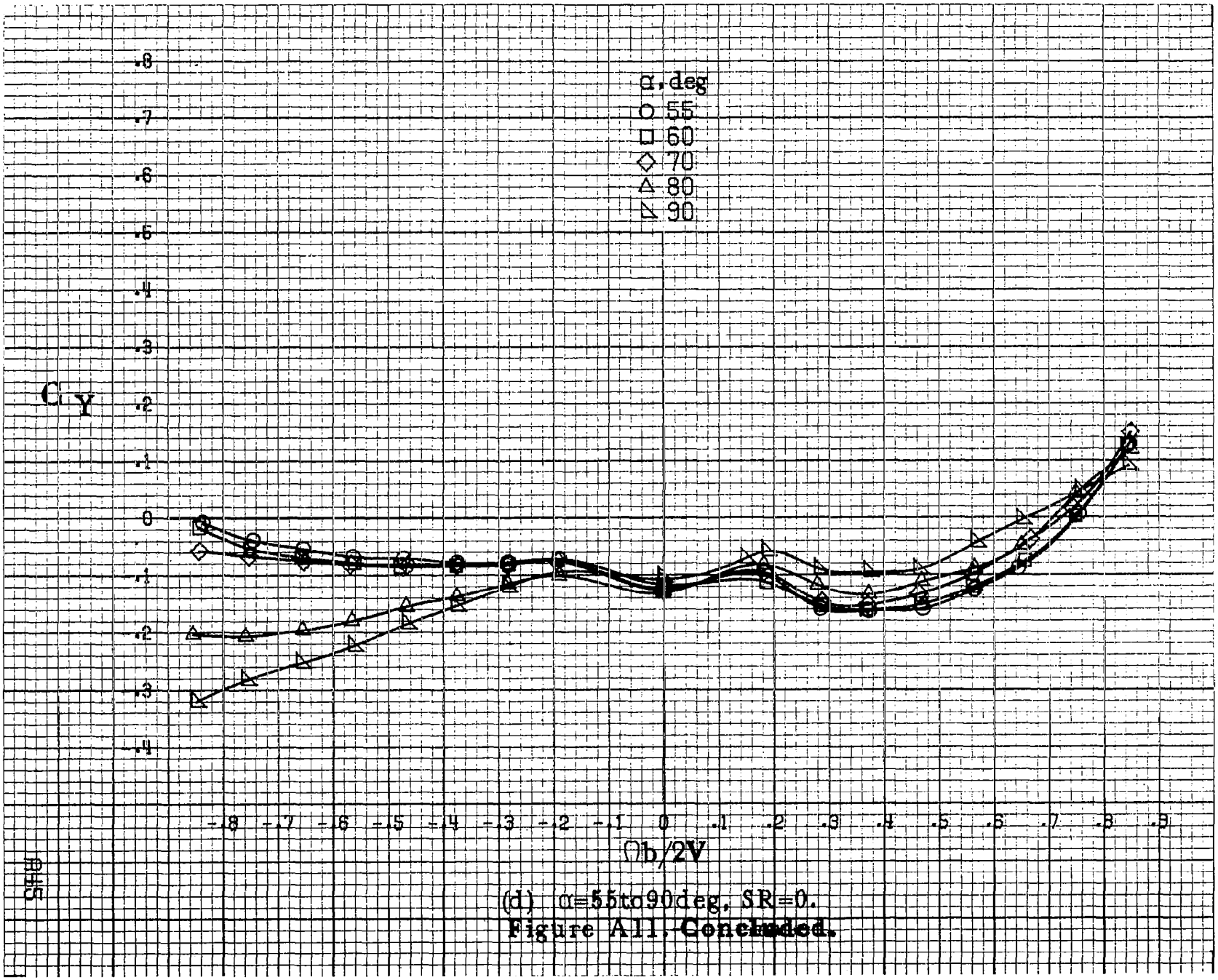

(d) α=55 to 90 deg, SR=0.

Figure A11. Concluded.

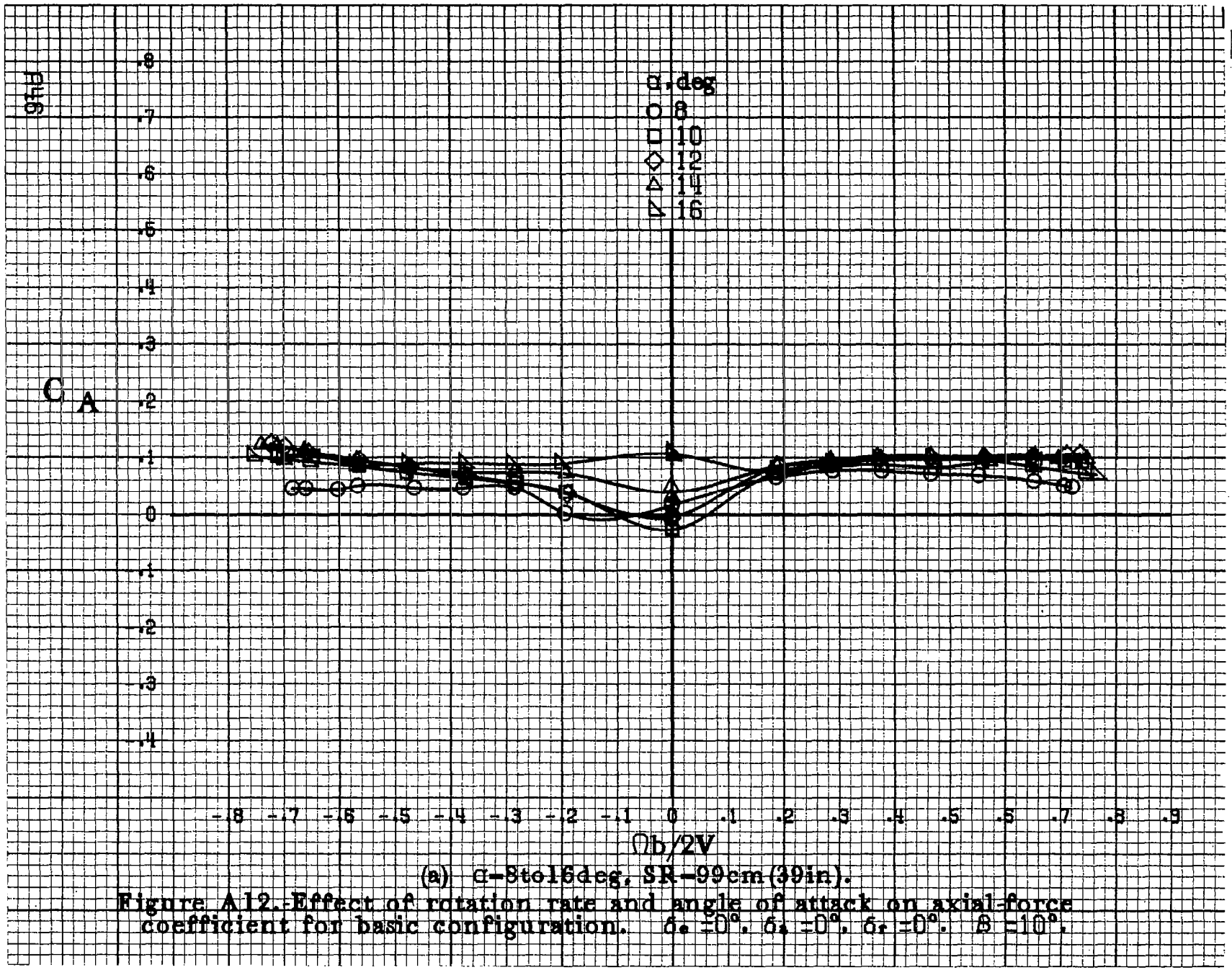

(a) α=8to16deg, SR=99cm(39in).

Figure A12.-Effect of rotation rate and angle of attack on axial-force coefficient for basic configuration. $\delta_e = 0°$, $\delta_a = 0°$, $\delta_r = 0°$, $\beta = 10°$.

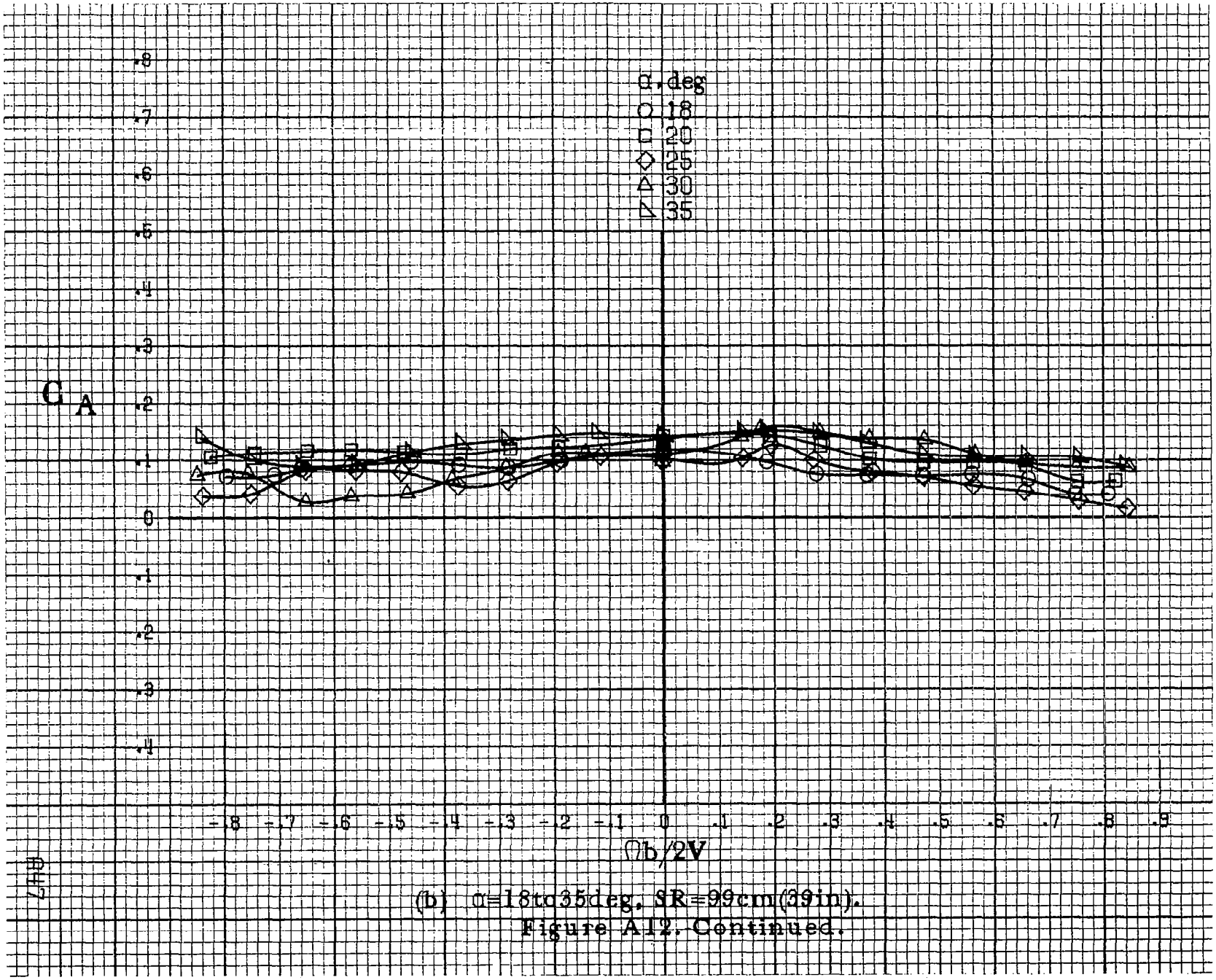

(b) α=18 to 35 deg, SR=99 cm (39 in).

Figure A12. Continued.

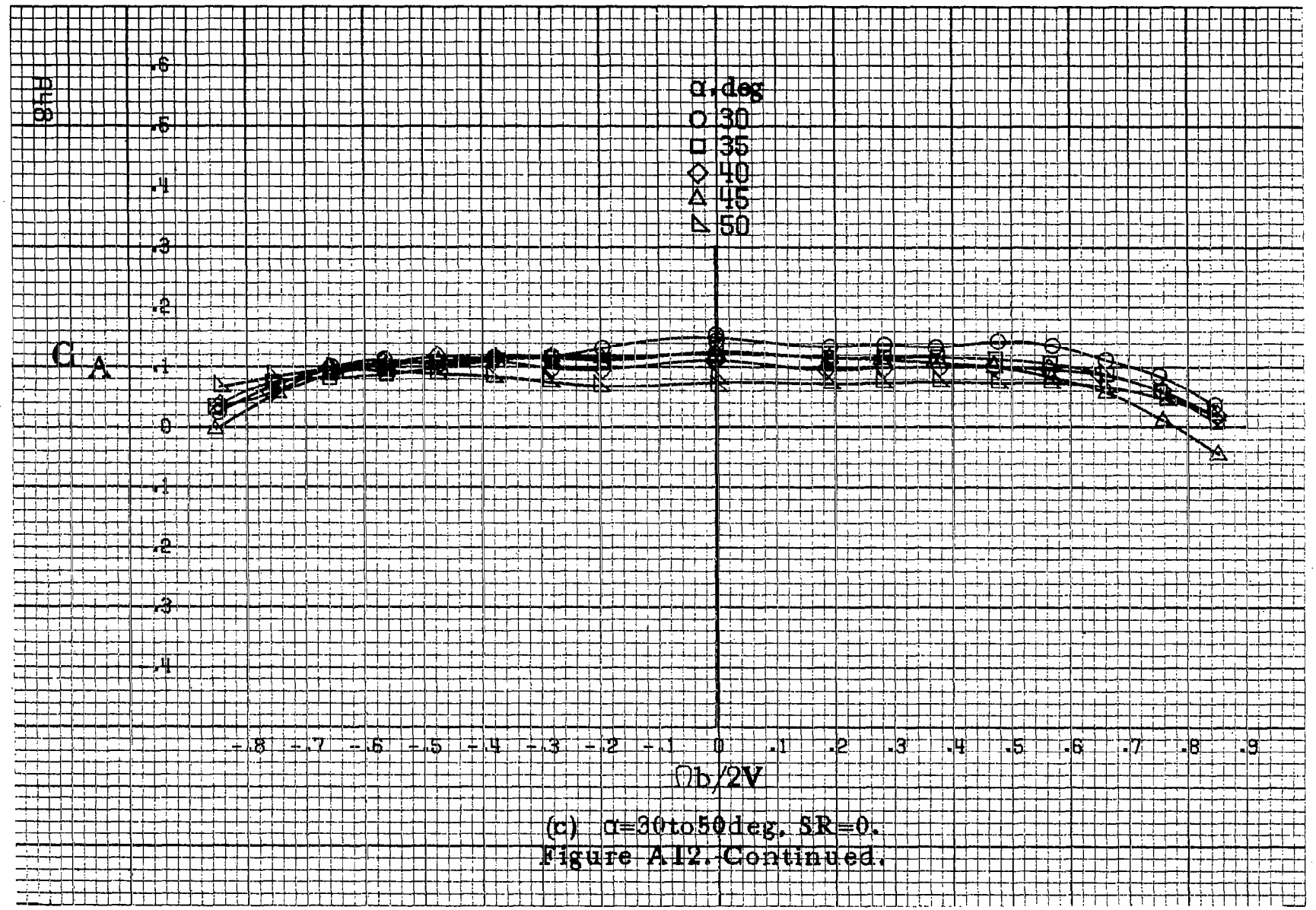

(c) α=30to50deg, SR=0.

Figure A12. Continued.

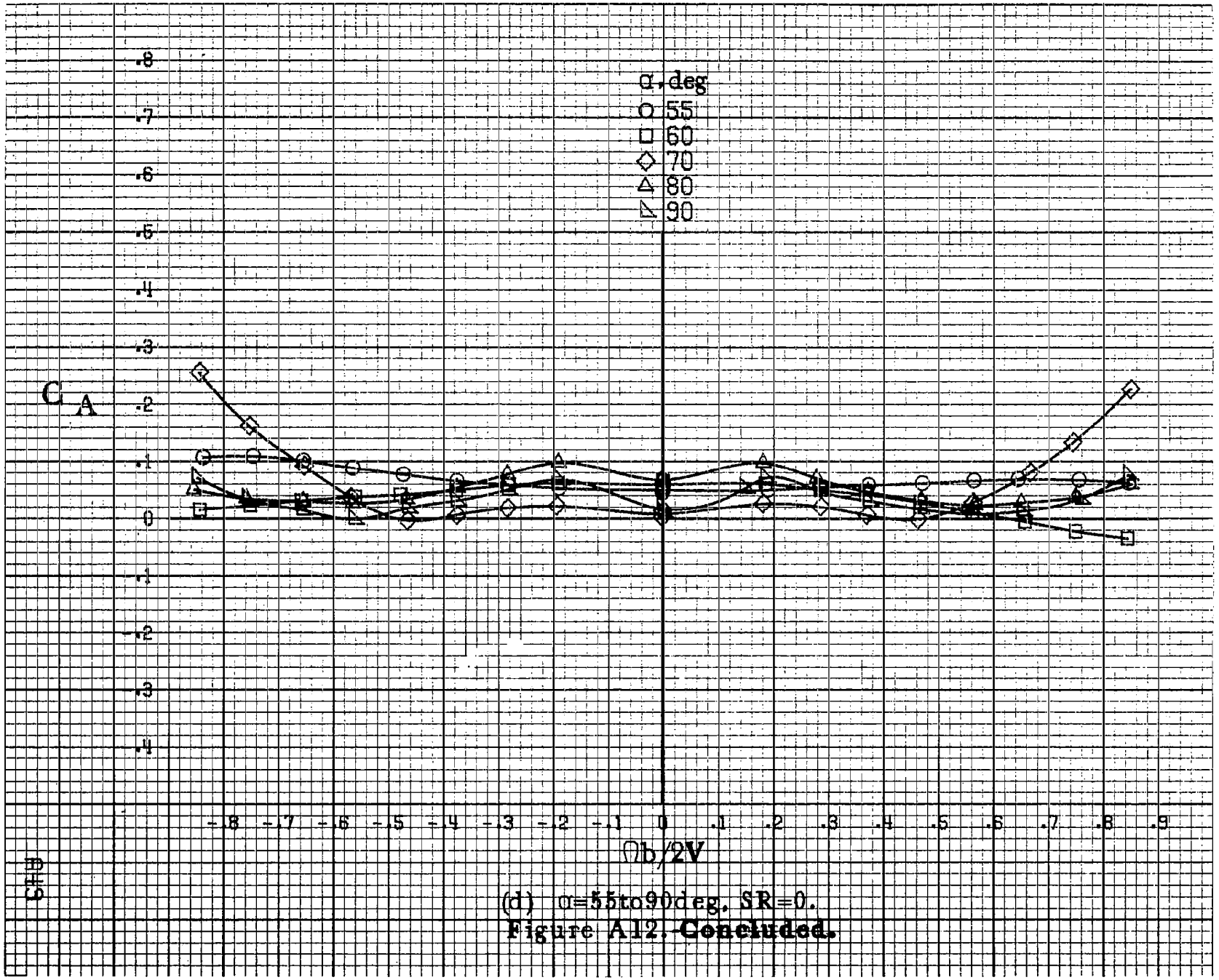

(d) α=55 to 90 deg, SR=0.

Figure A12.-Concluded.

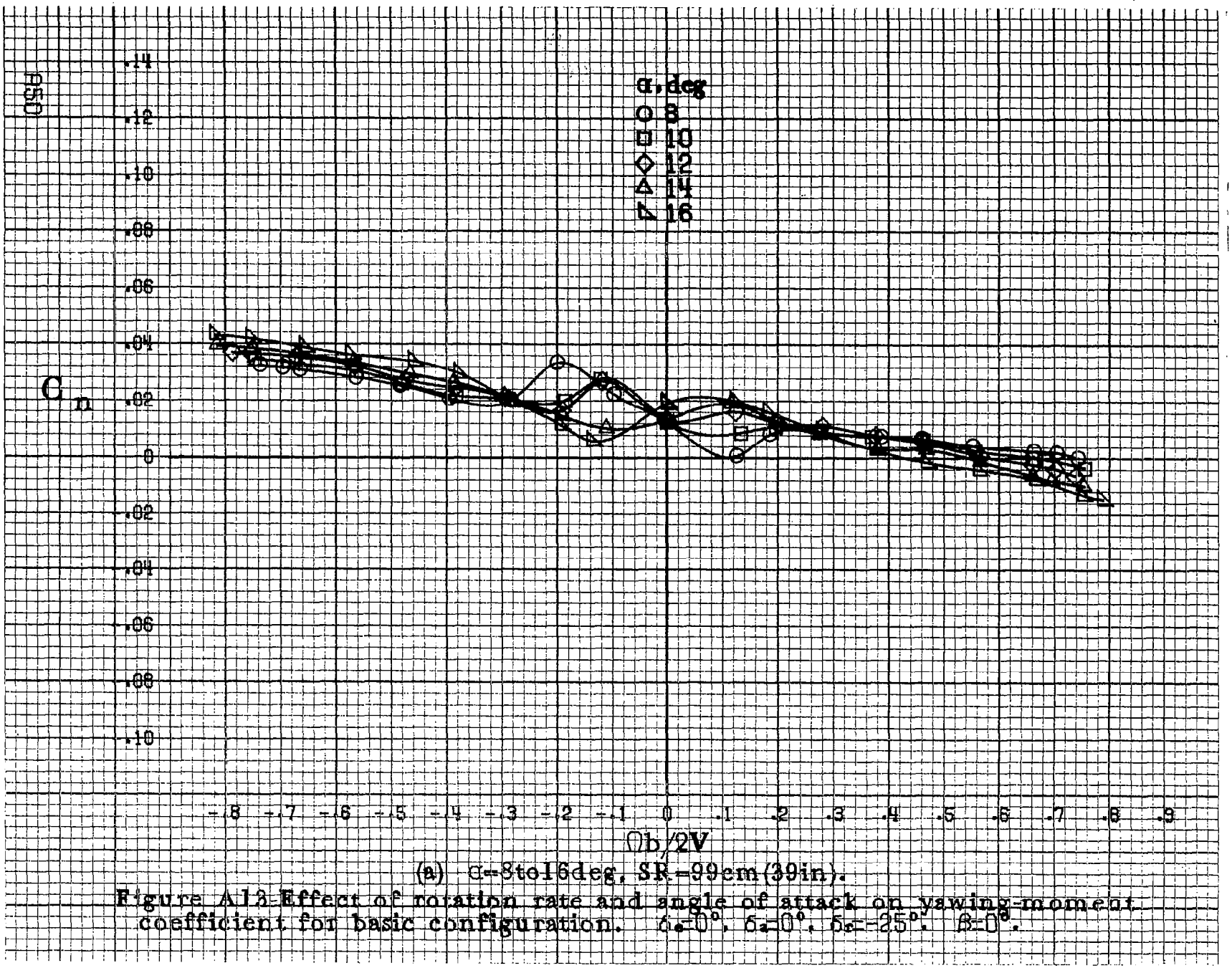

(a) α=-8to16deg, SR=99cm(39in).

Figure A13 Effect of rotation rate and angle of attack on yawing-moment coefficient for basic configuration. δ_e=0°, δ_a=0°, δ_r=-25°, β=0°.

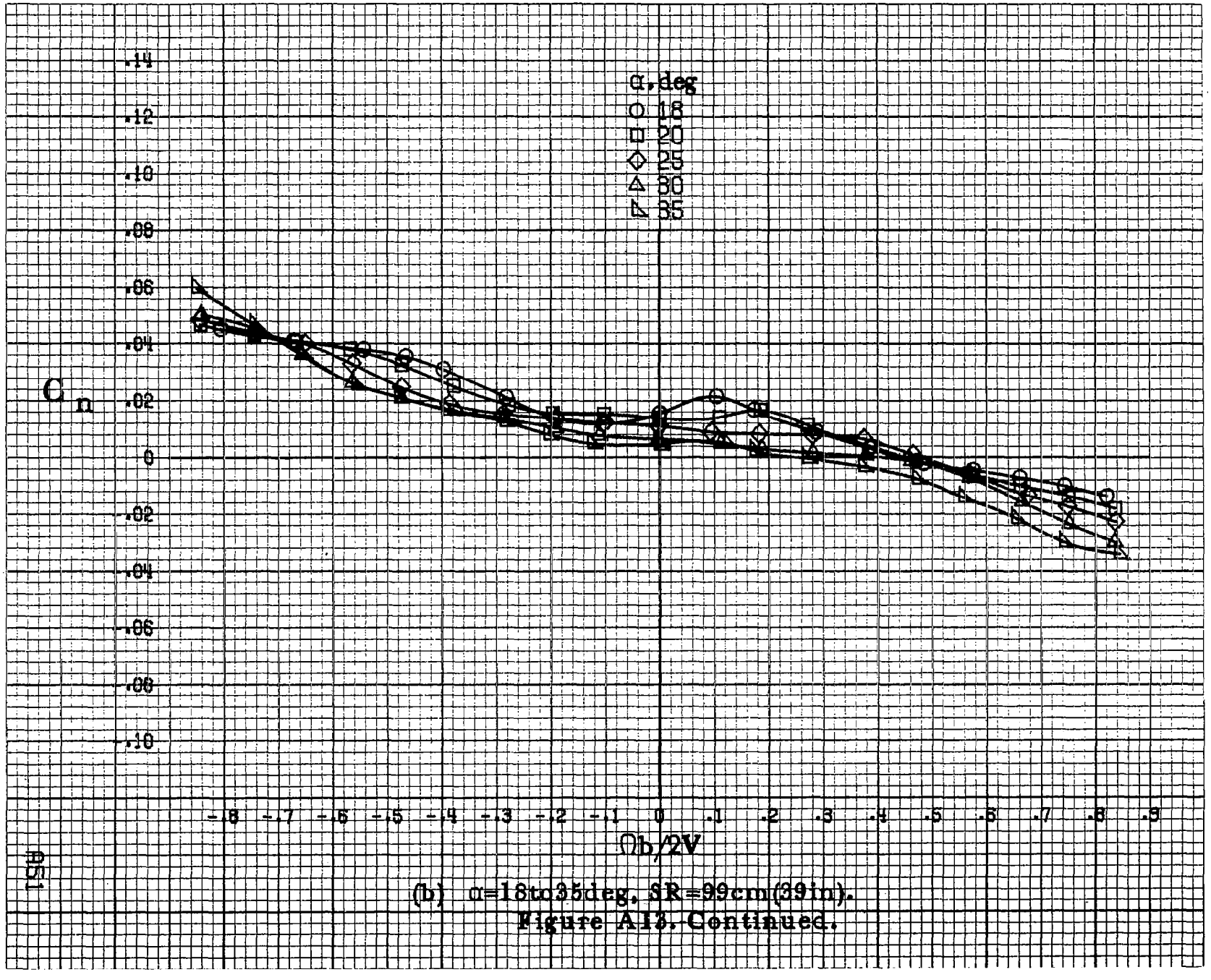

(b) α=18to35deg, SR=99cm(39in).

Figure A13.-Continued.

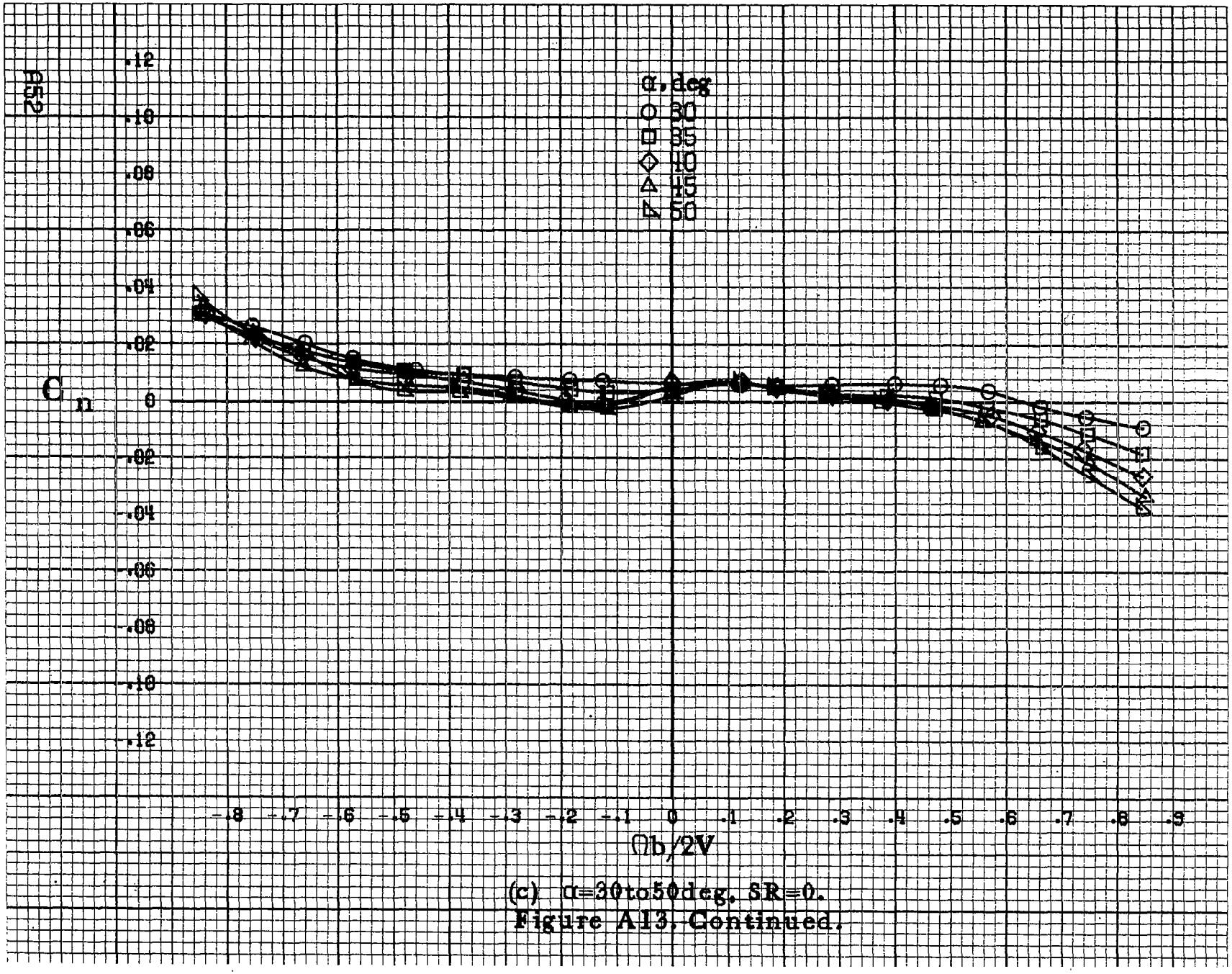

(c) α=30to50deg, δR=0.

Figure A13.-Continued.

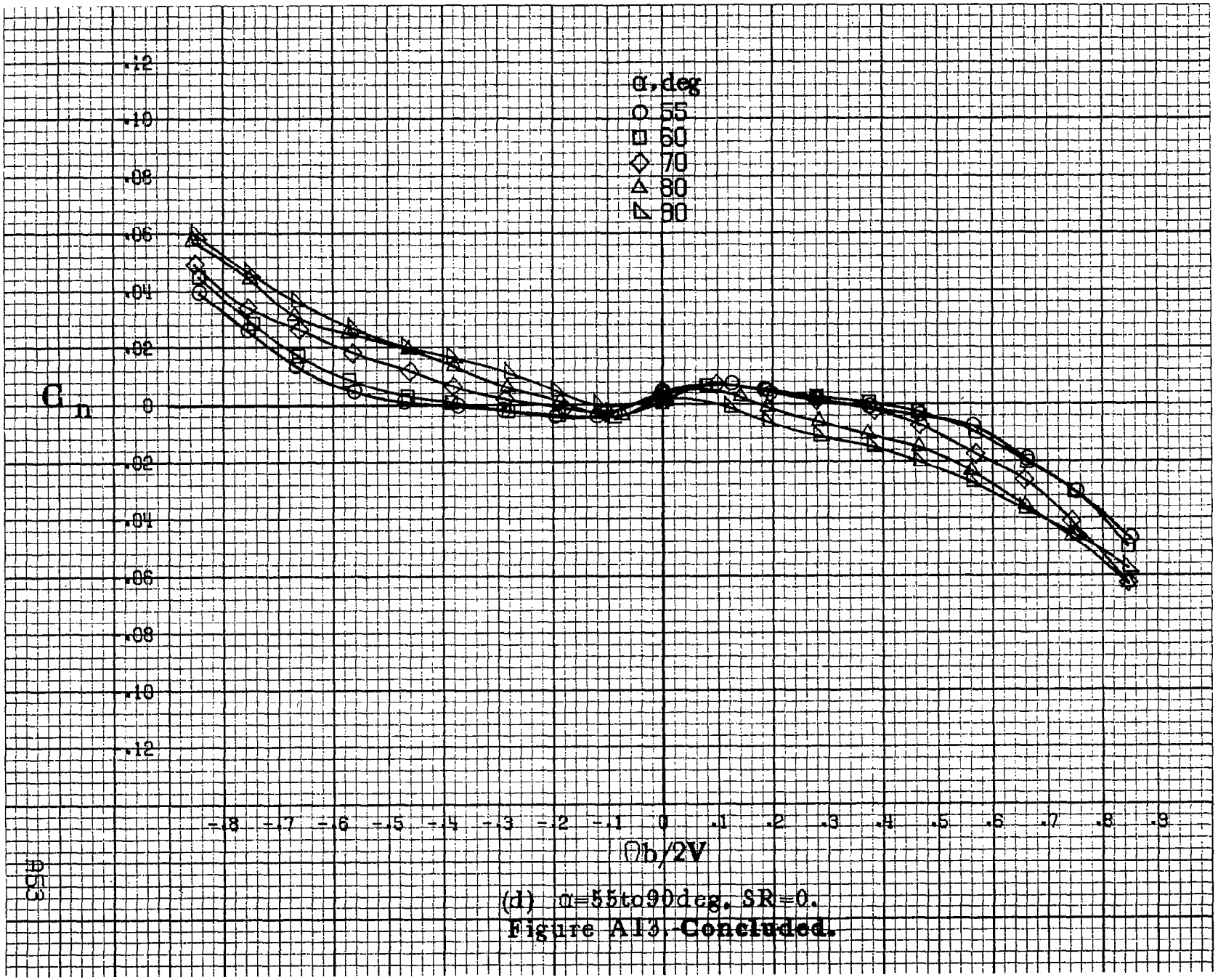

(d) α=55to90deg, SR=0.

Figure A13.-Concluded.

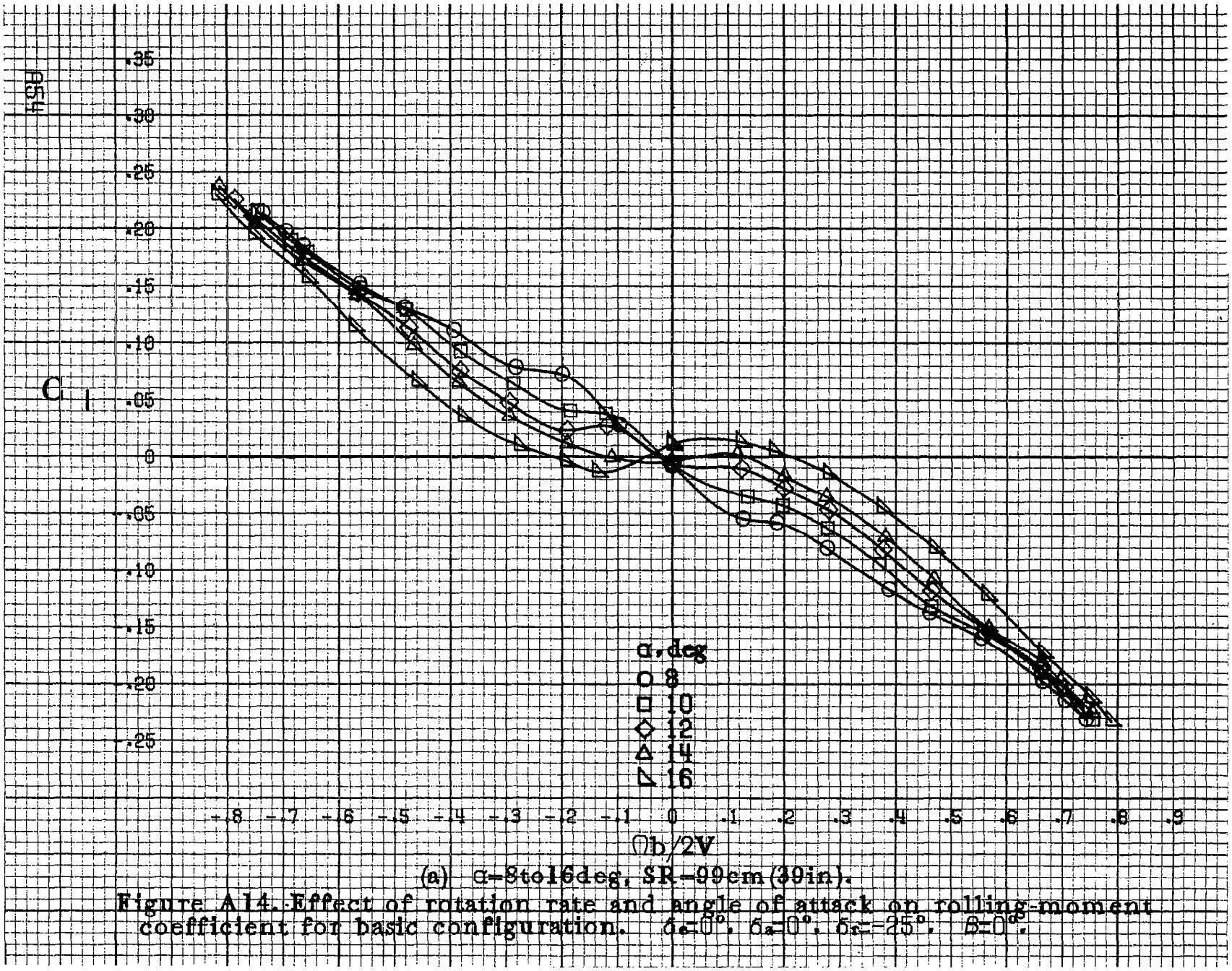

(a) α=8to16deg, SR=99cm(39in).

Figure A14. Effect of rotation rate and angle of attack on rolling-moment coefficient for basic configuration. δ_e=0°, δ_a=0°, δ_r=25°, β=0°.

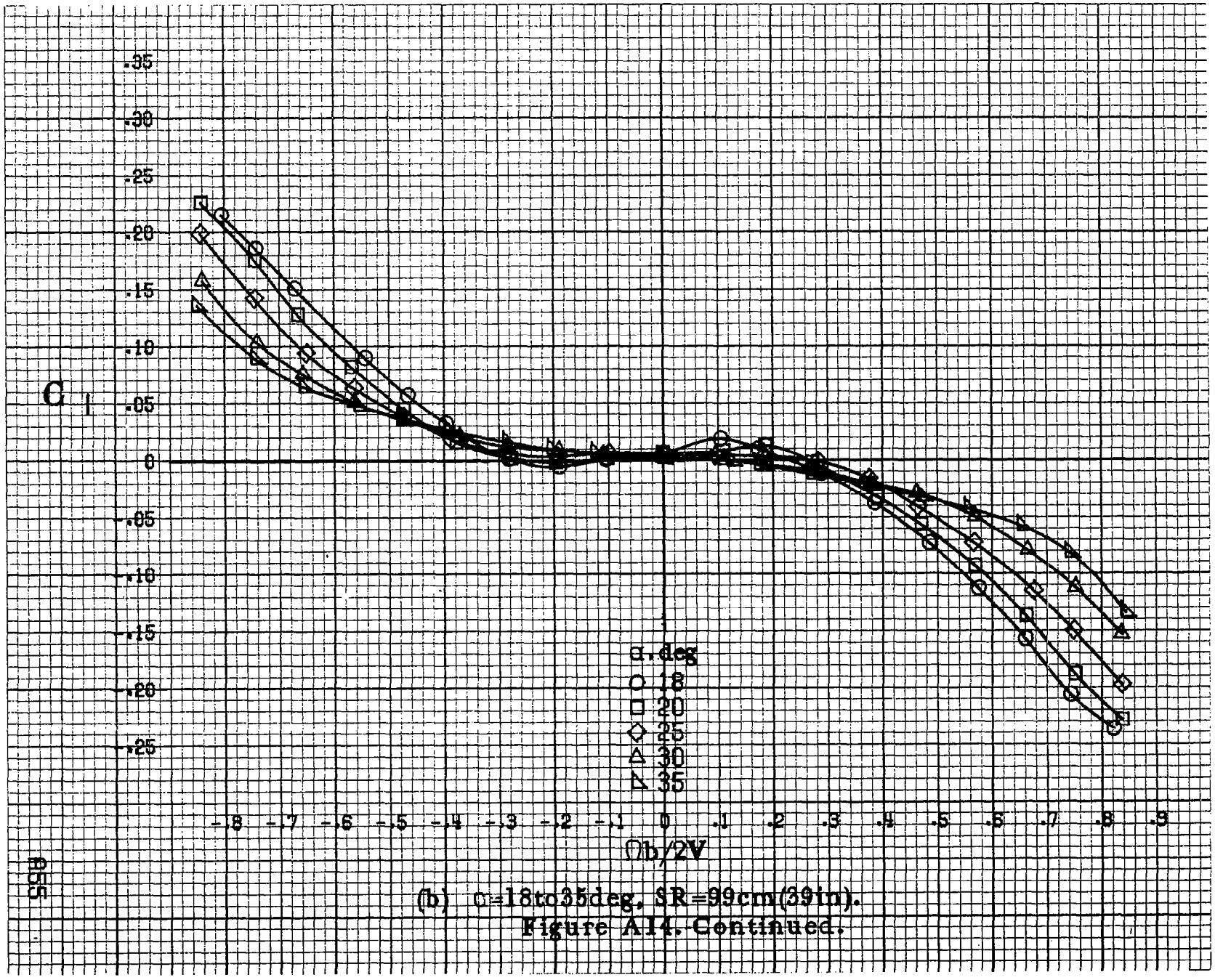

(b) α=18to35deg. SR=99cm(39in).

Figure A14. Continued.

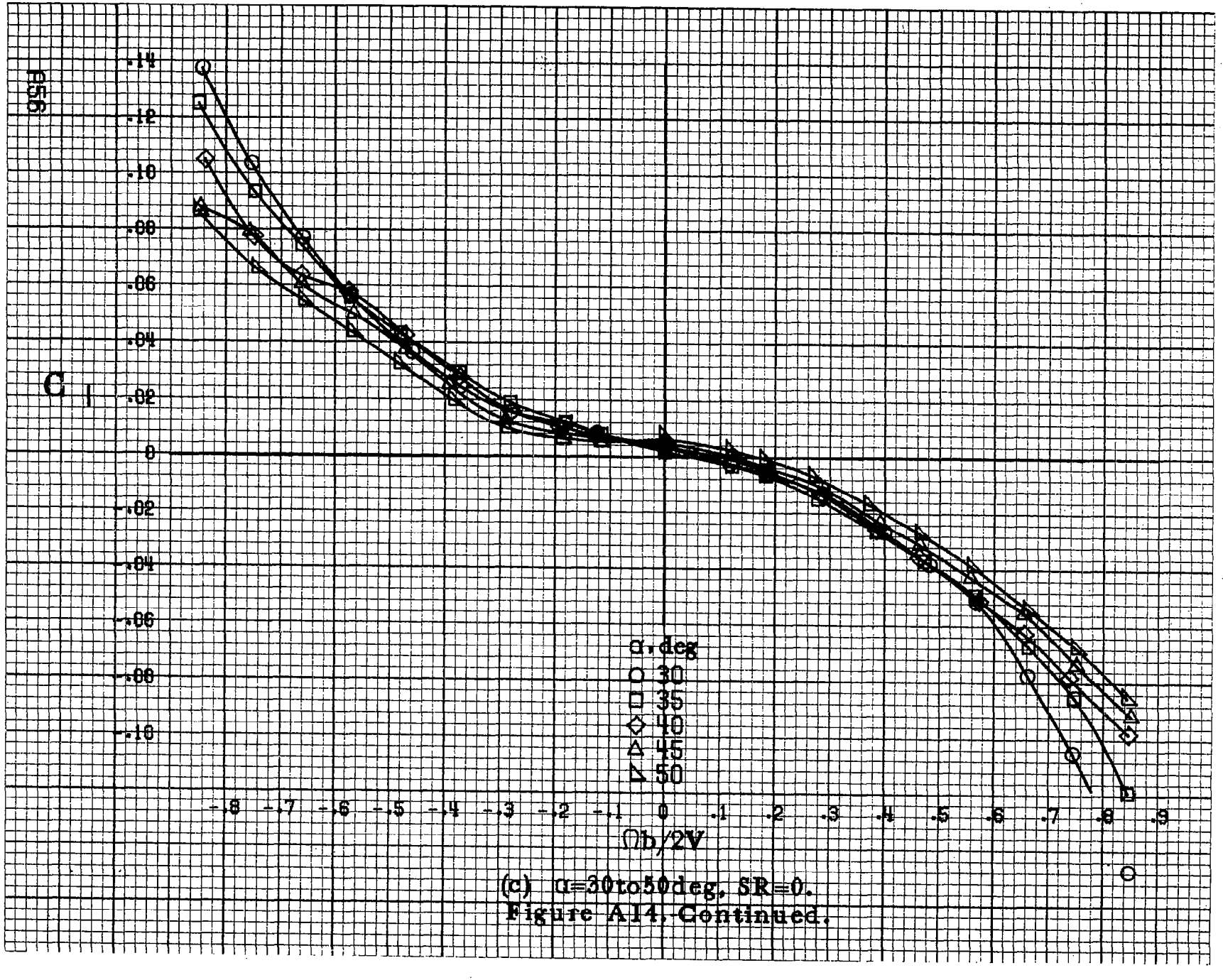

(c) α=30to50deg, SR=0.

Figure A14.-Continued.

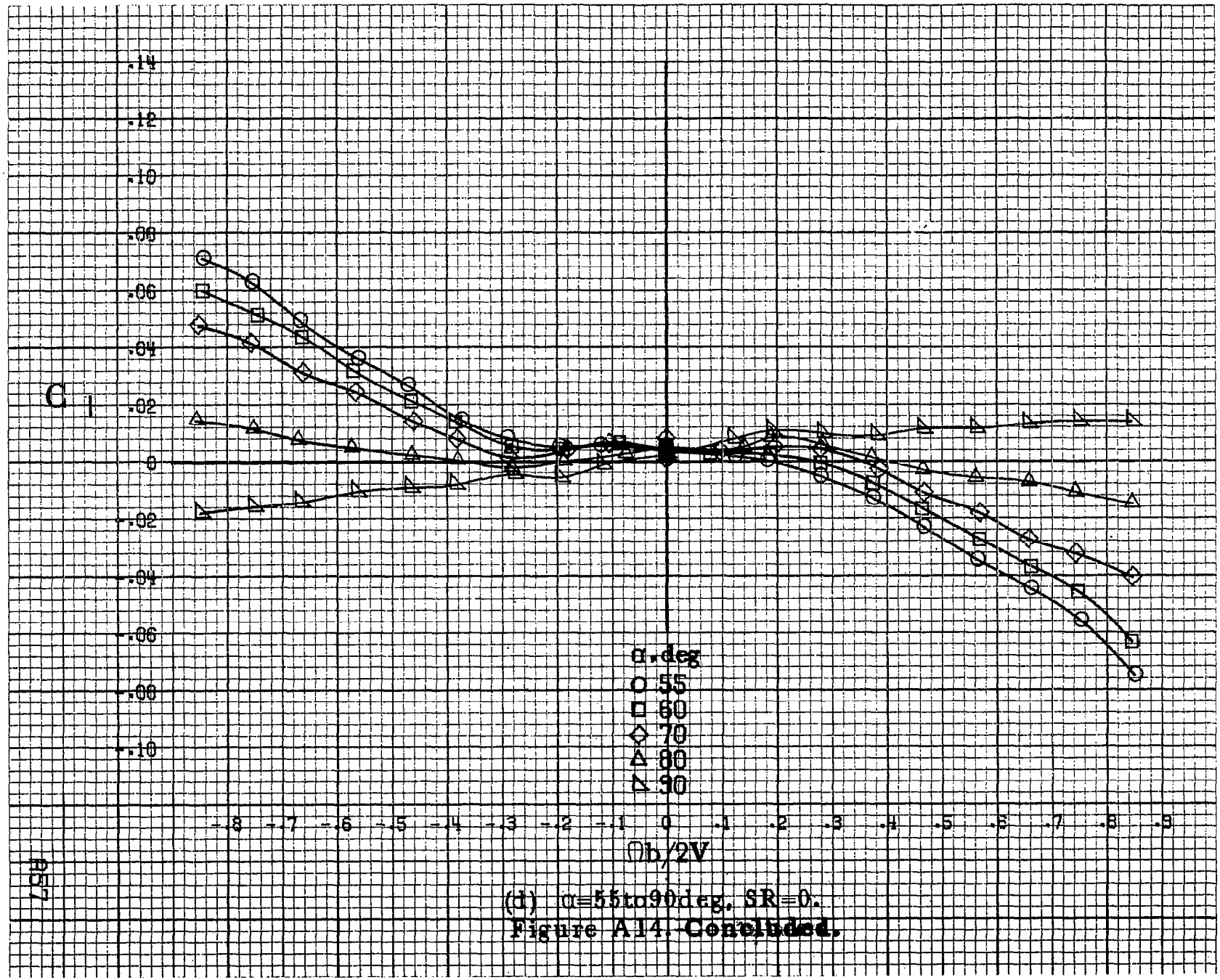

(d) α=55 to 90 deg, SR=0.

Figure A14.- Concluded.

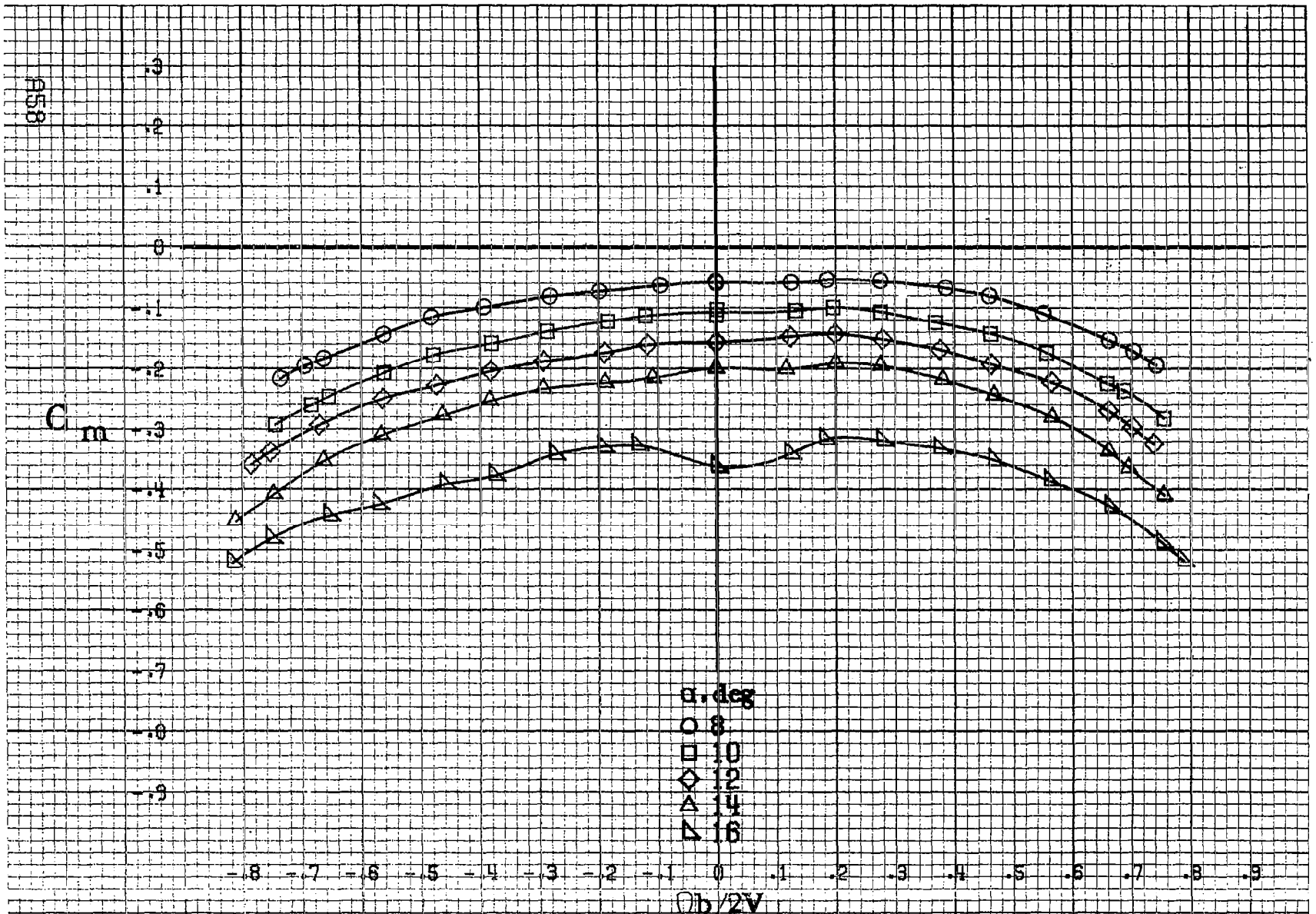

(a) α=8to16deg, SR=99cm(39in).

Figure A15. Effect of rotation rate and angle of attack on pitching-moment coefficient for basic configuration. δ_e=0°, δ_a=0°, δ_r=-25°, β=0°.

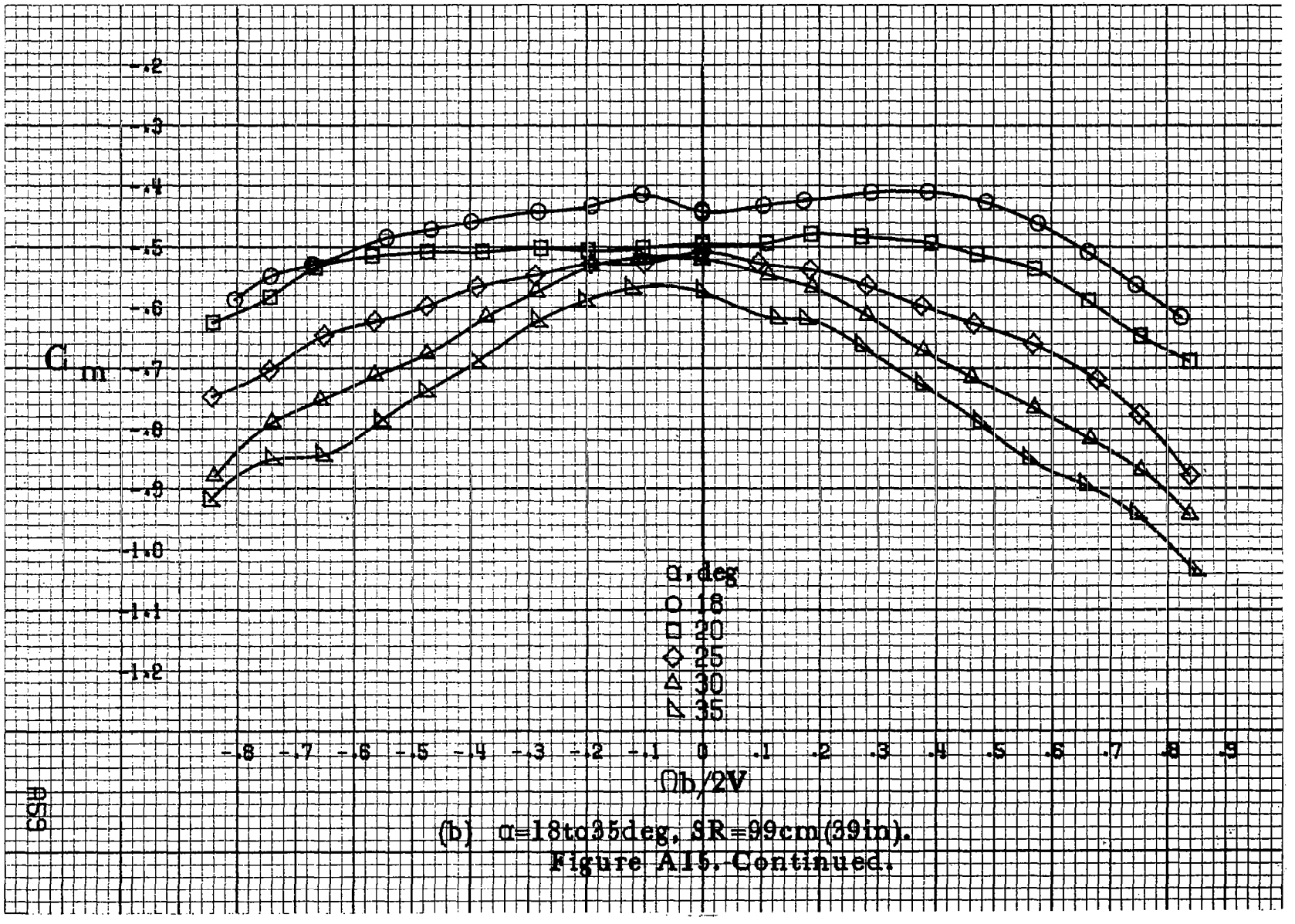

(b) α=18to35deg, SR=99cm(39in).

Figure A15. Continued.

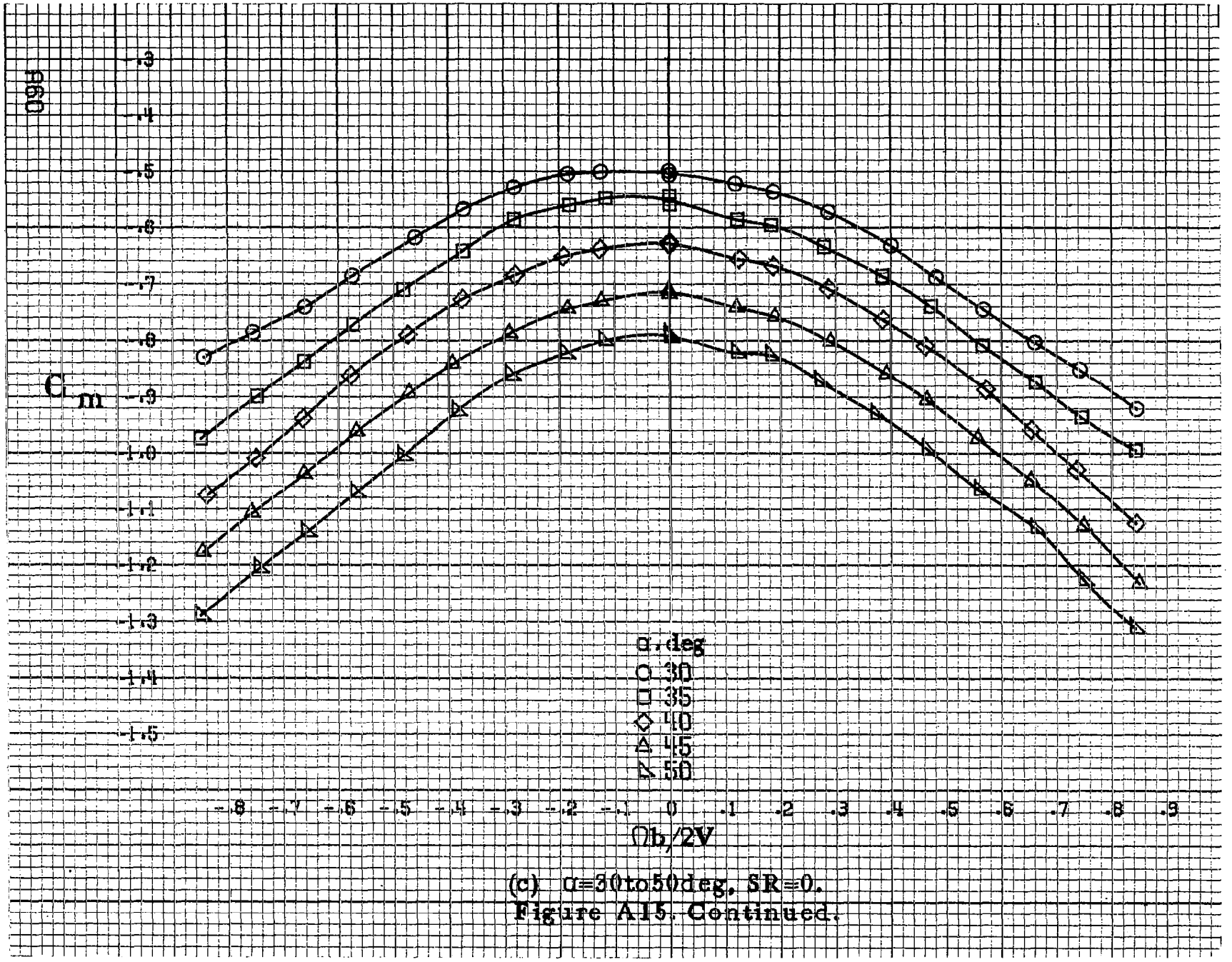

(c) α=30to50deg, SR=0.

Figure A15. Continued.

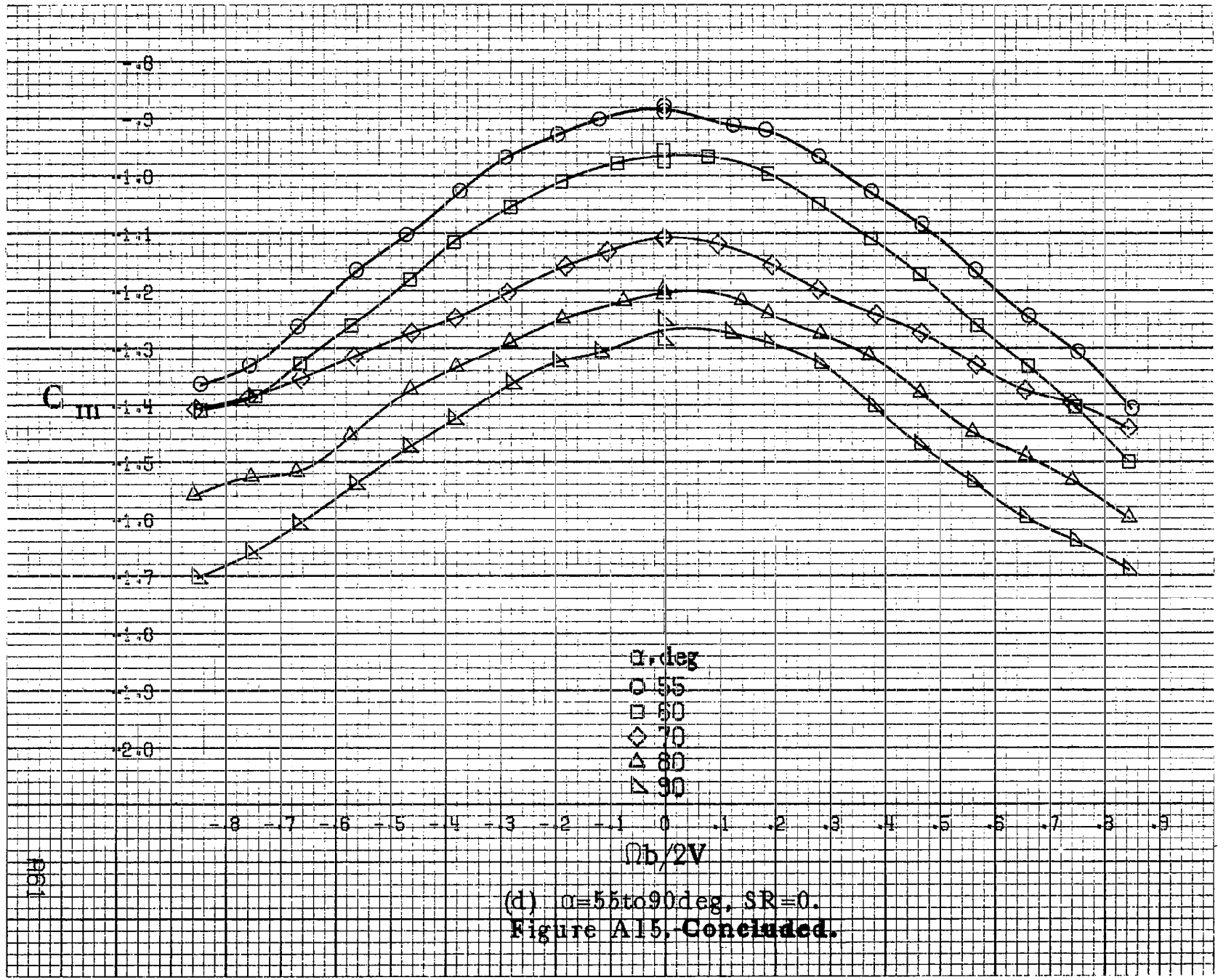

(d) α=55to90deg, SR=0.

Figure A15.-Concluded.

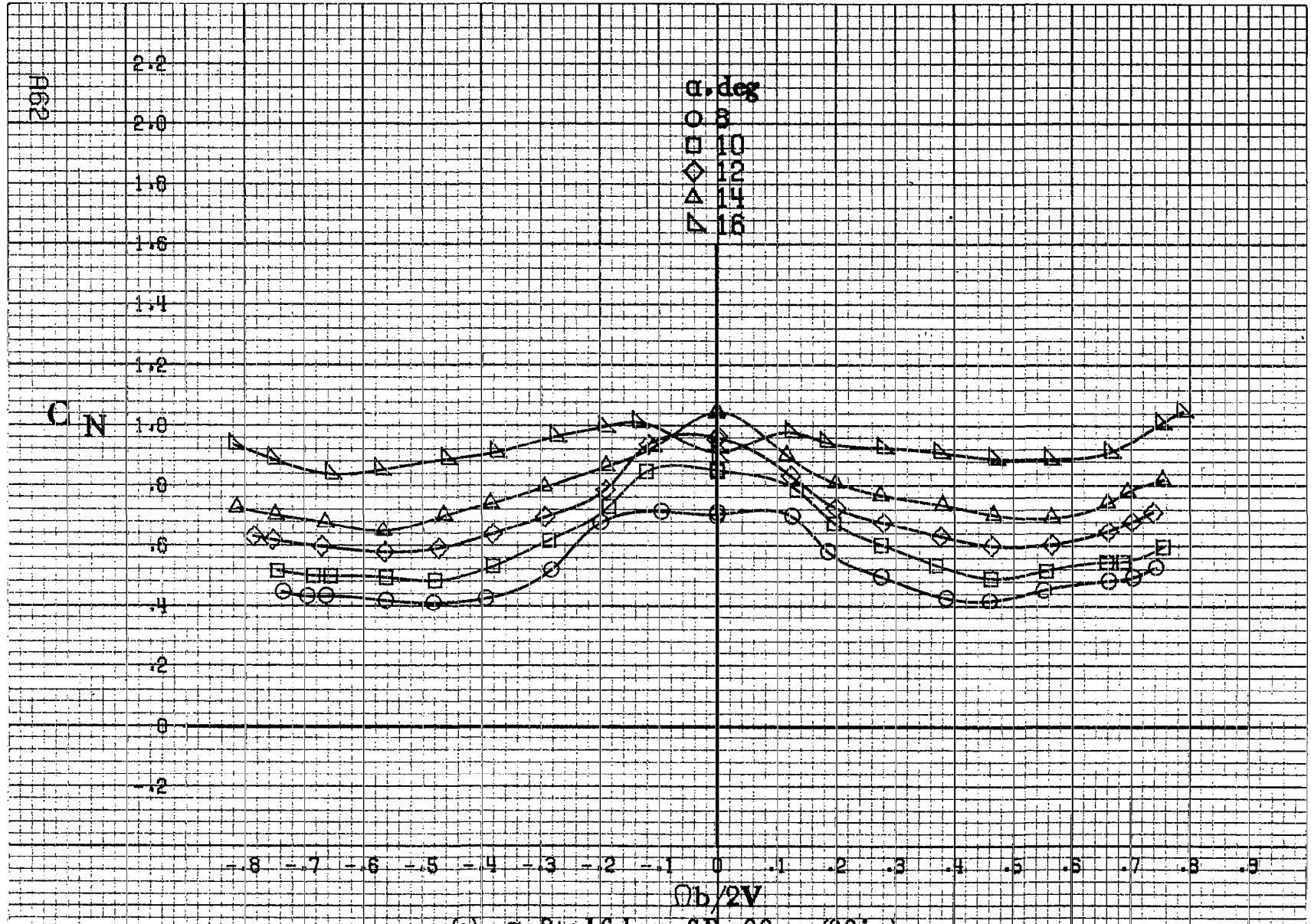

(a) α=8to16deg, SR=99cm(39in).

Figure A16.-Effect of rotation rate and angle of attack on normal-force coefficient for basic configuration. δ_e=0°, δ_a=0°, δ_r=-25°. β=0°.

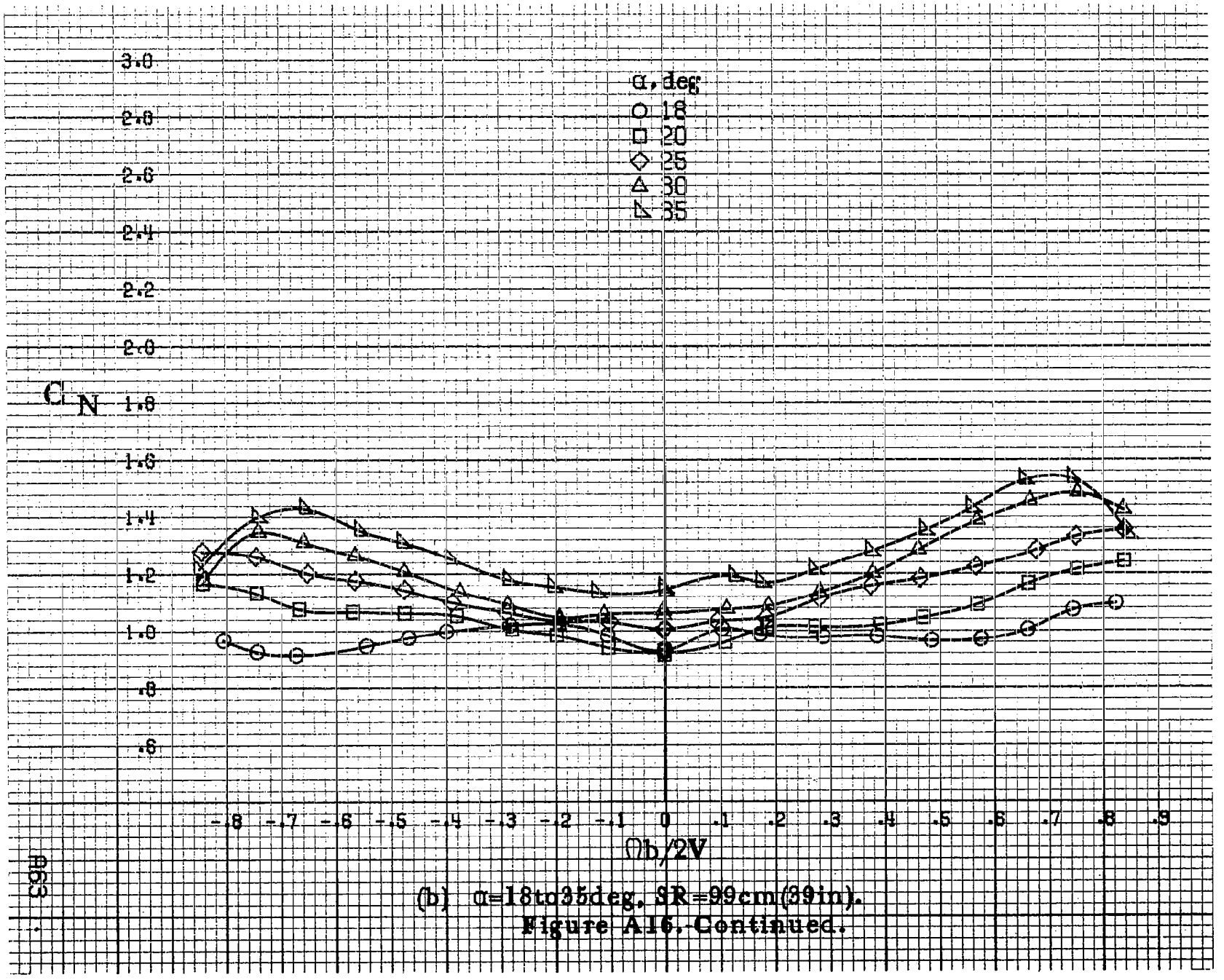

(b) α=18to35deg, SR=99cm(39in).

Figure A16. Continued.

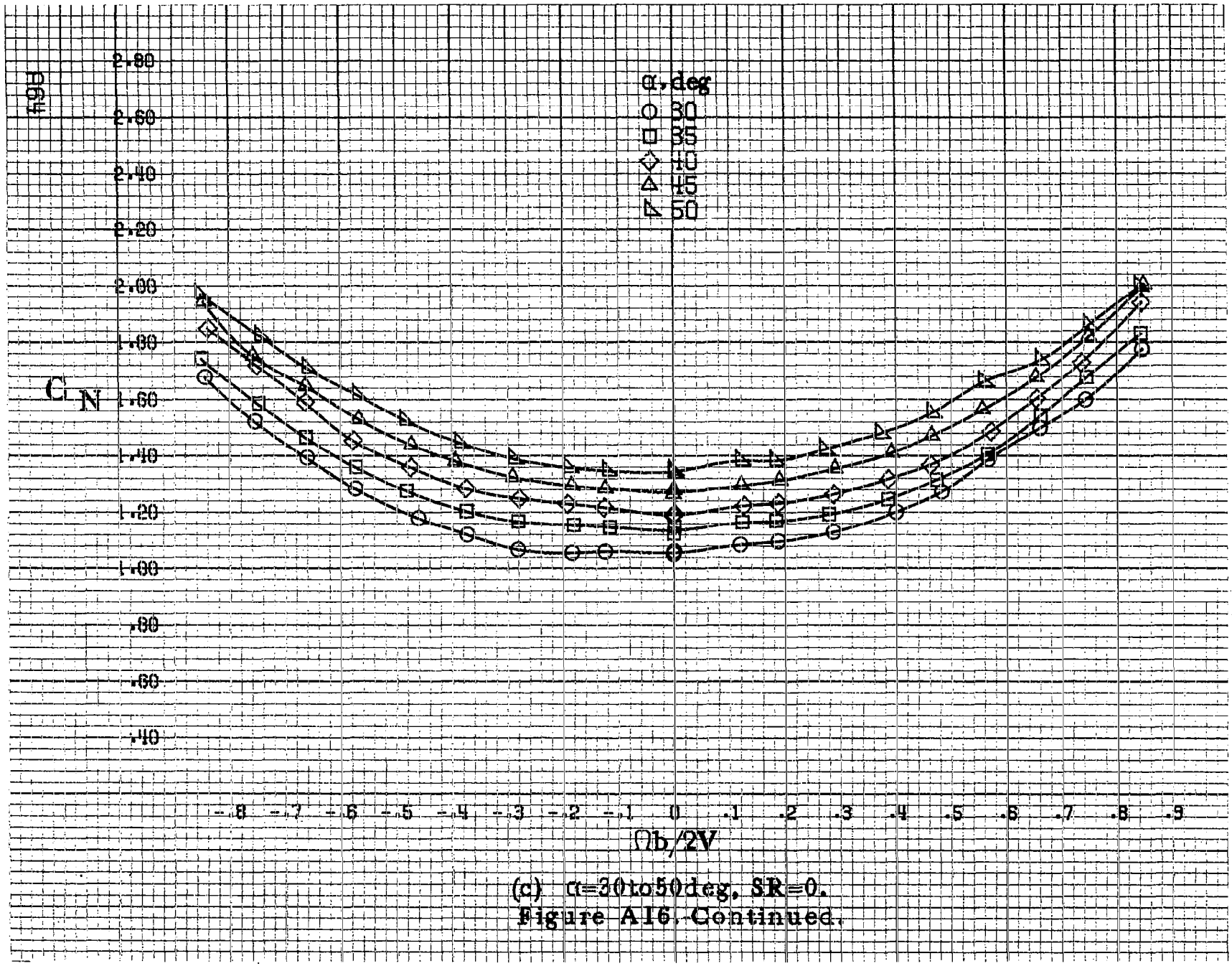

(c) α=30to50deg, SR=0.

Figure A16. Continued.

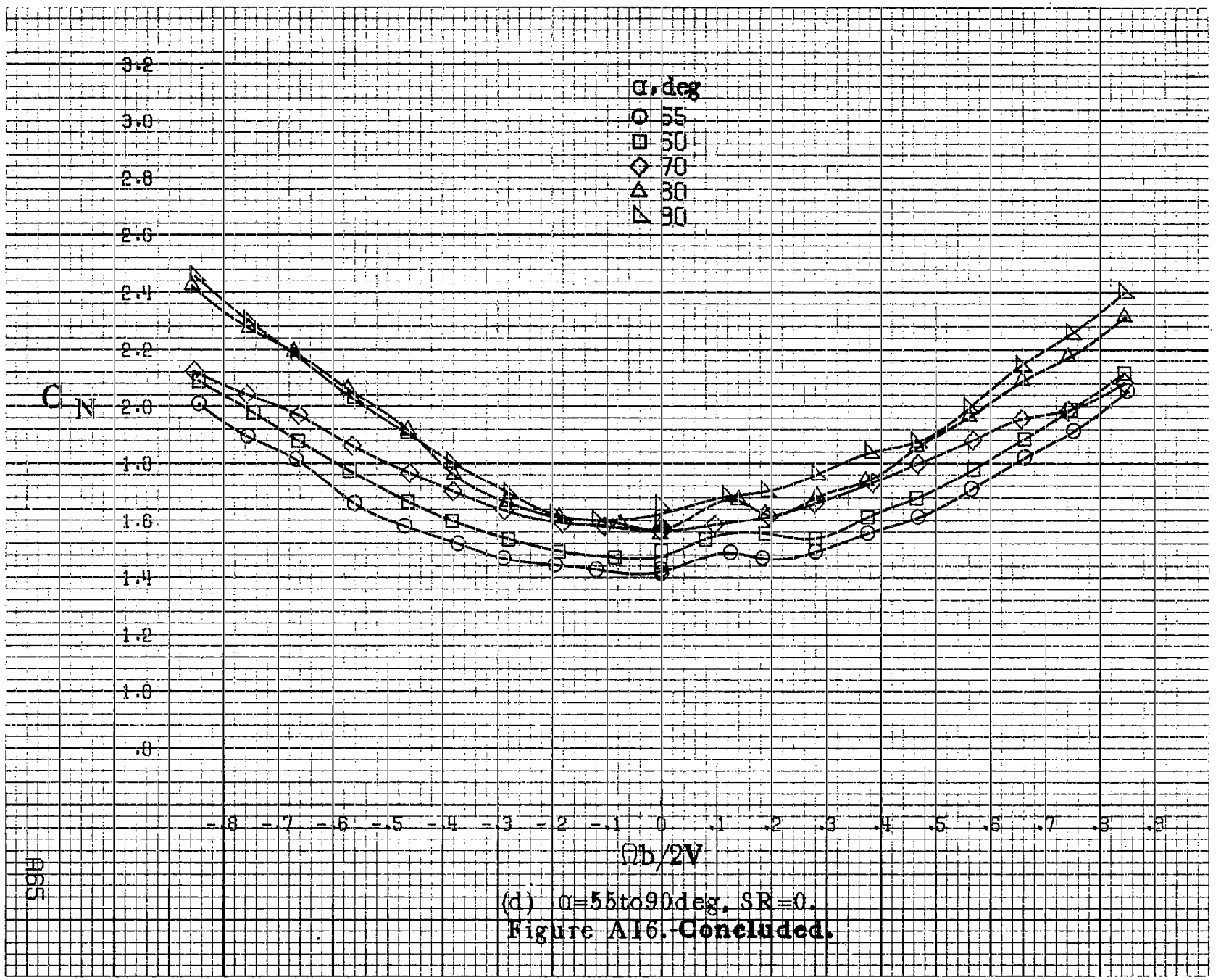

(d) α=55to90deg, SR=0.

Figure A16.-Concluded.

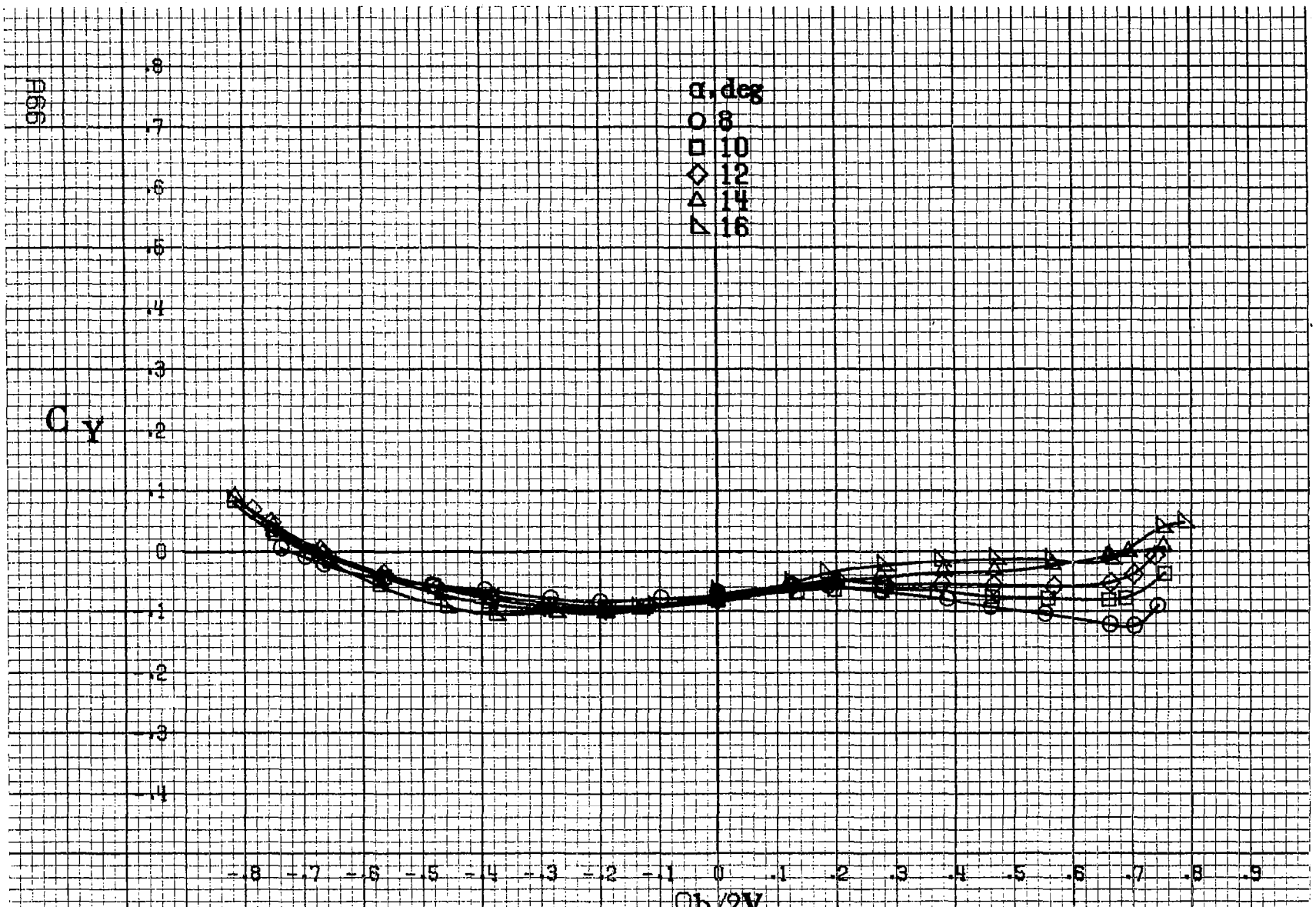

(a) α=8to16deg, SR=99cm(39in).

Figure A17-Effect of rotation rate and angle of attack on side-force coefficient for basic configuration. δ_e=0°, δ_a=0°, δ_r=-25°, β=0°.

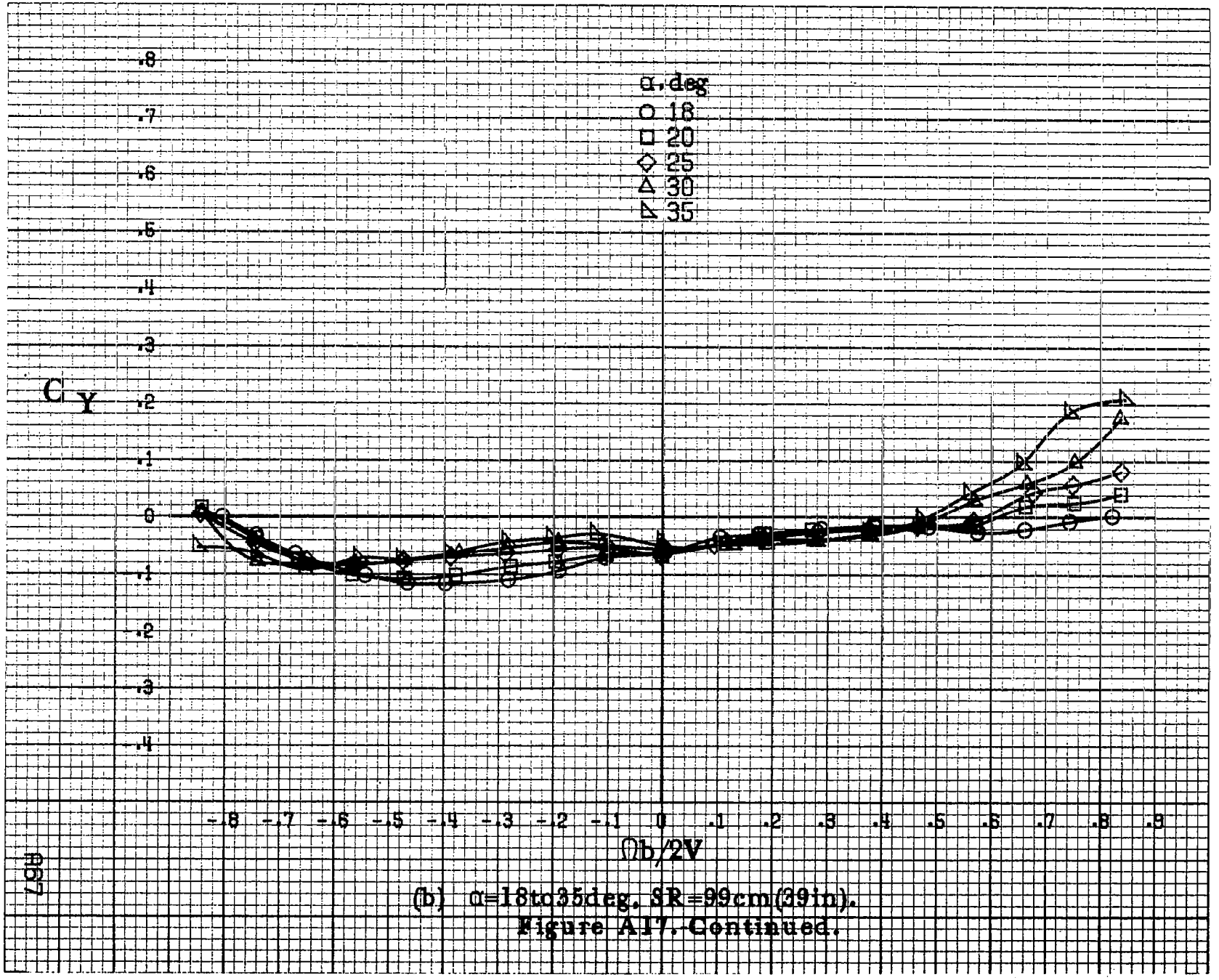

(b) α=18to35deg, SR=99cm(39in).

Figure A17.-Continued.

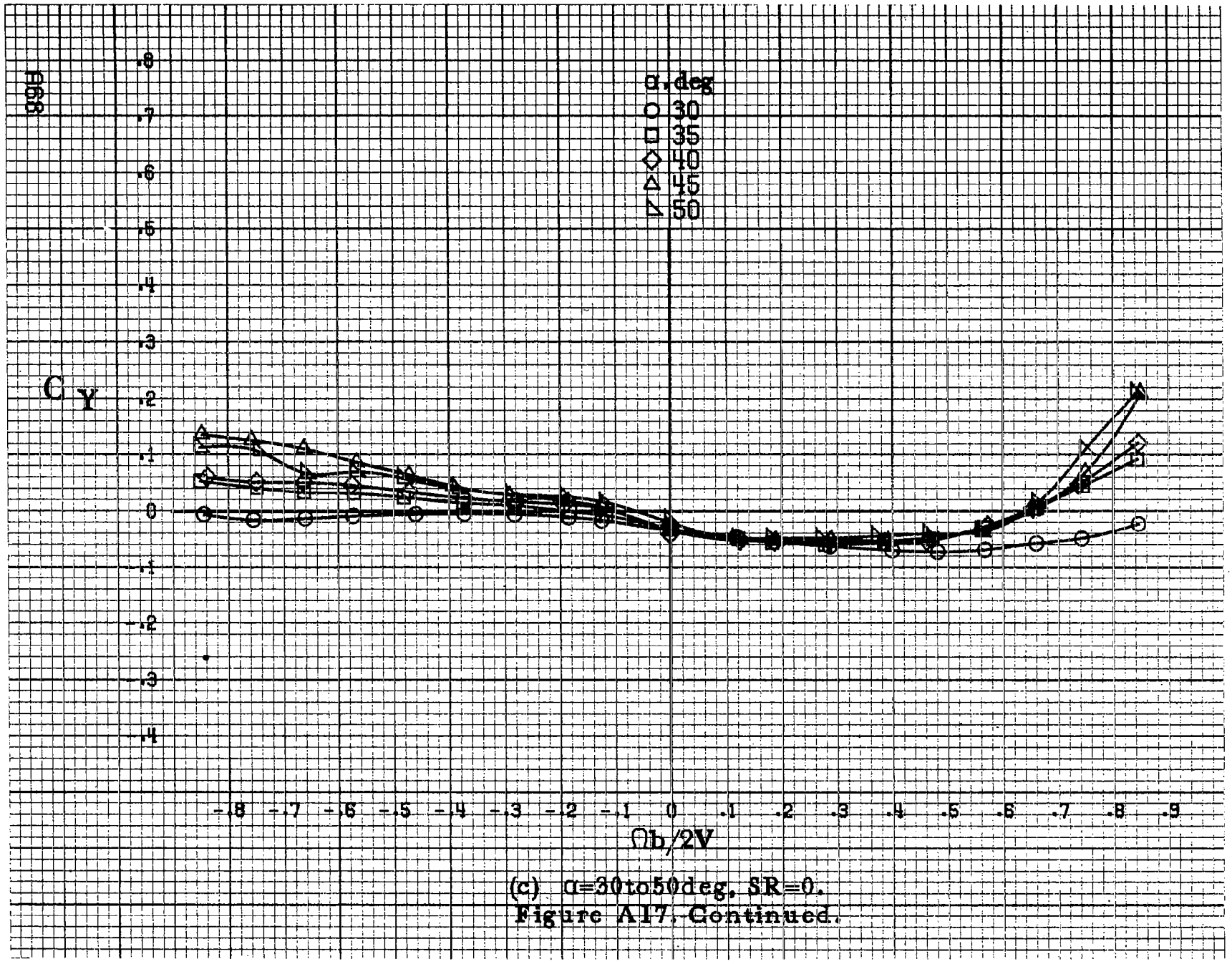

(c) α=30to50deg, SR=0.

Figure A17. Continued.

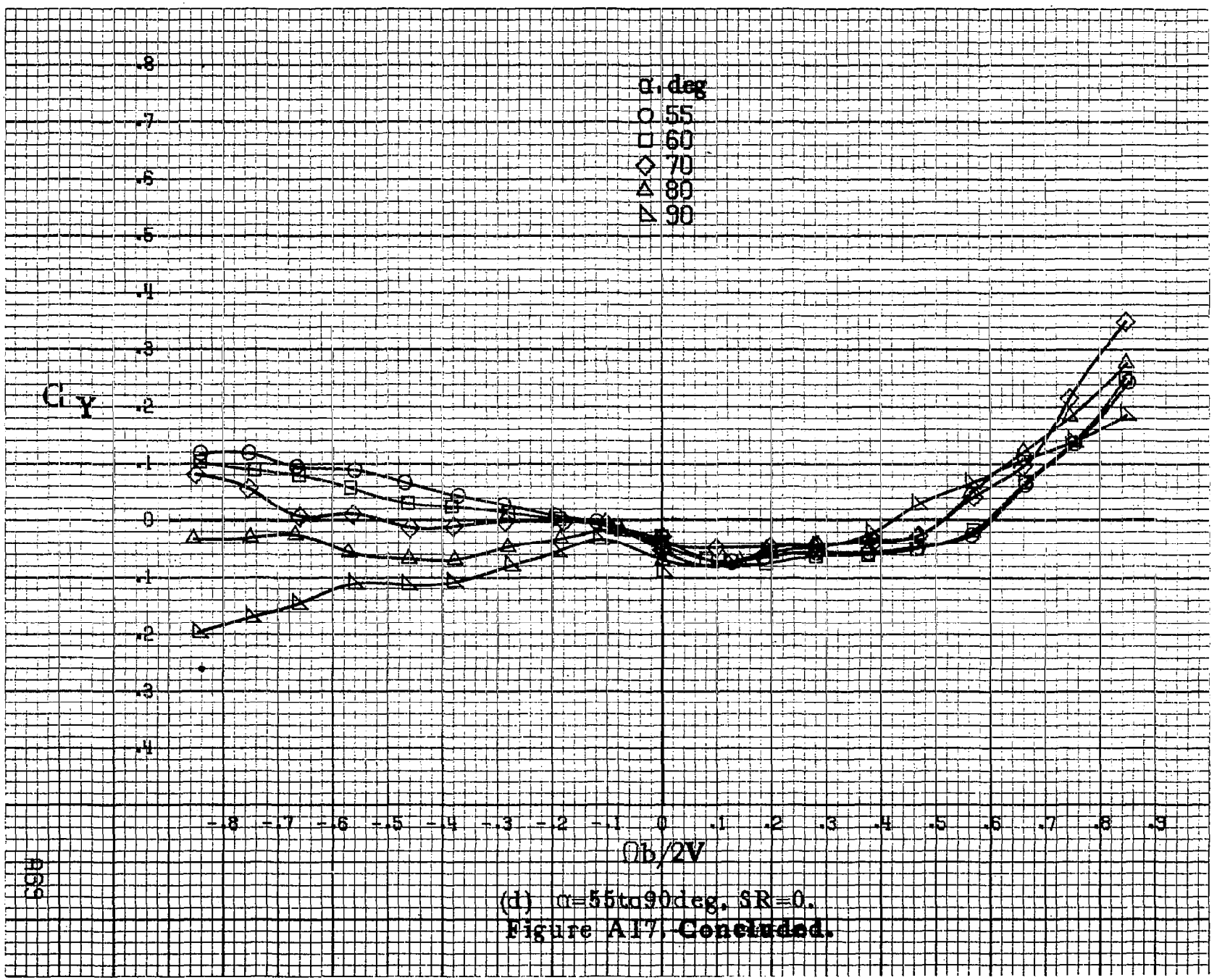

(d) α=55to90deg, SR=0.

Figure A17. Concluded.

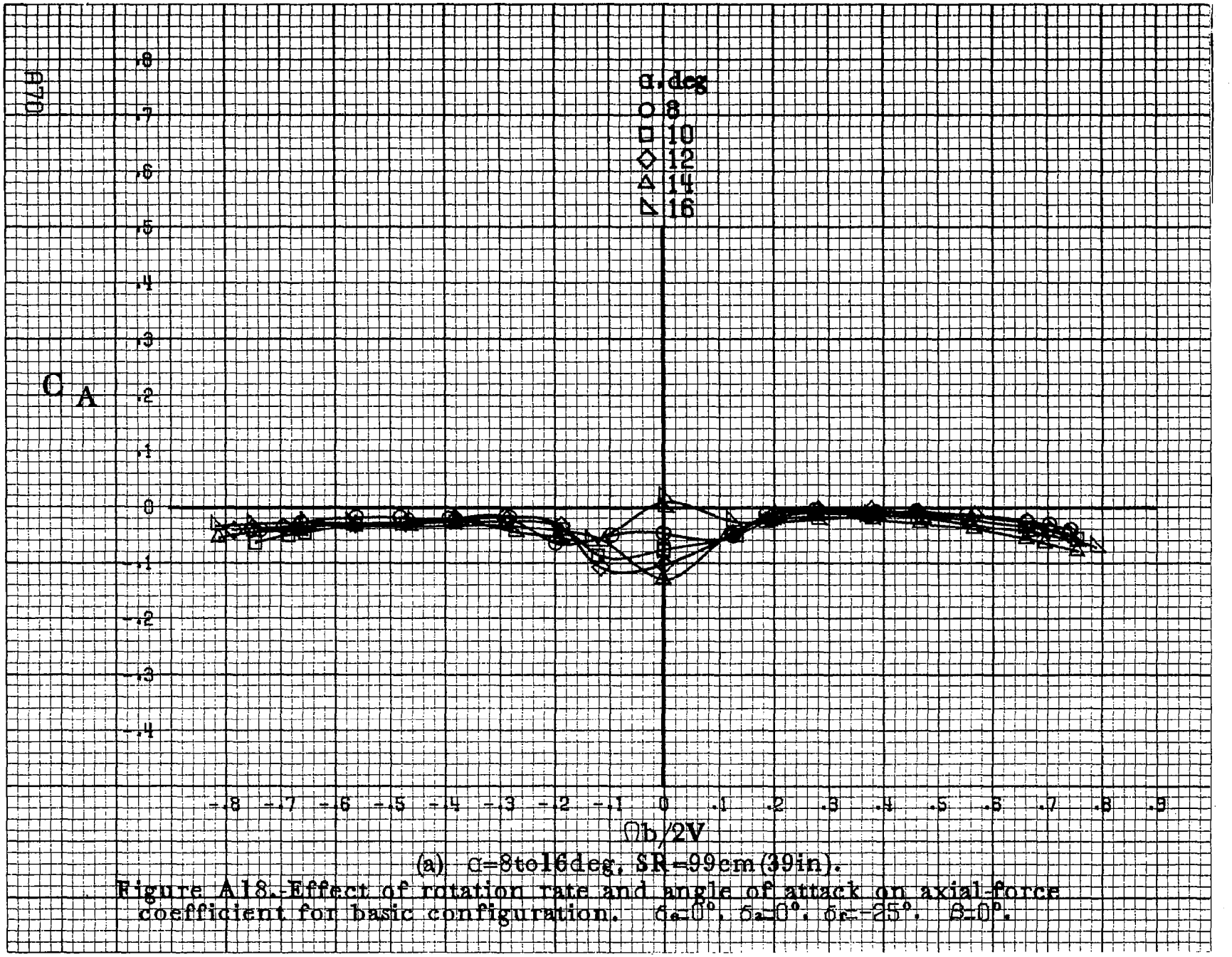

(a) α=8to16deg, SR=99cm(39in).

Figure A18.-Effect of rotation rate and angle of attack on axial-force coefficient for basic configuration. $\delta_e=0°$, $\delta_a=0°$, $\delta_r=-25°$, $\beta=0°$.

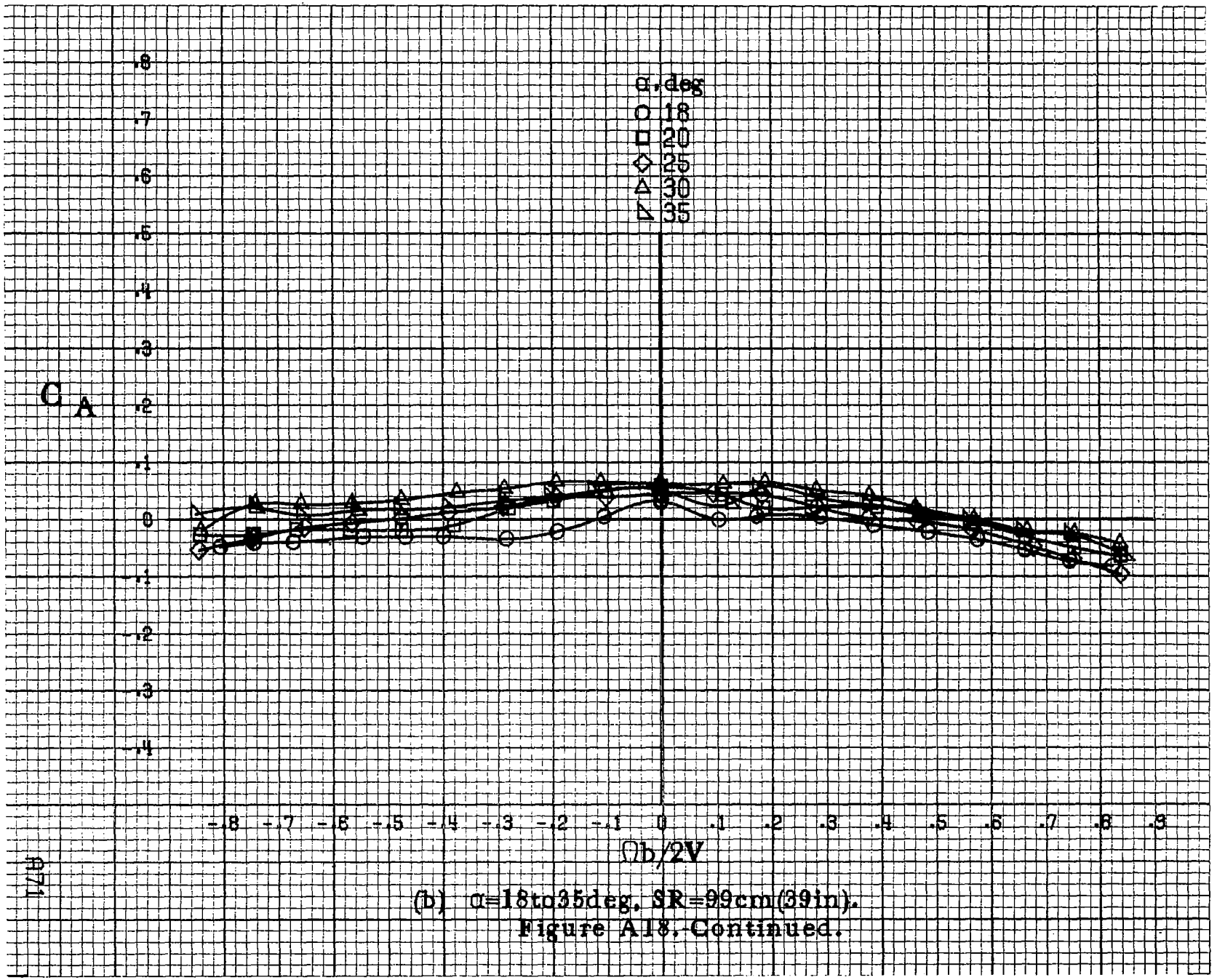

(b) α=18to35deg, SR=99cm(39in).

Figure A18. Continued.

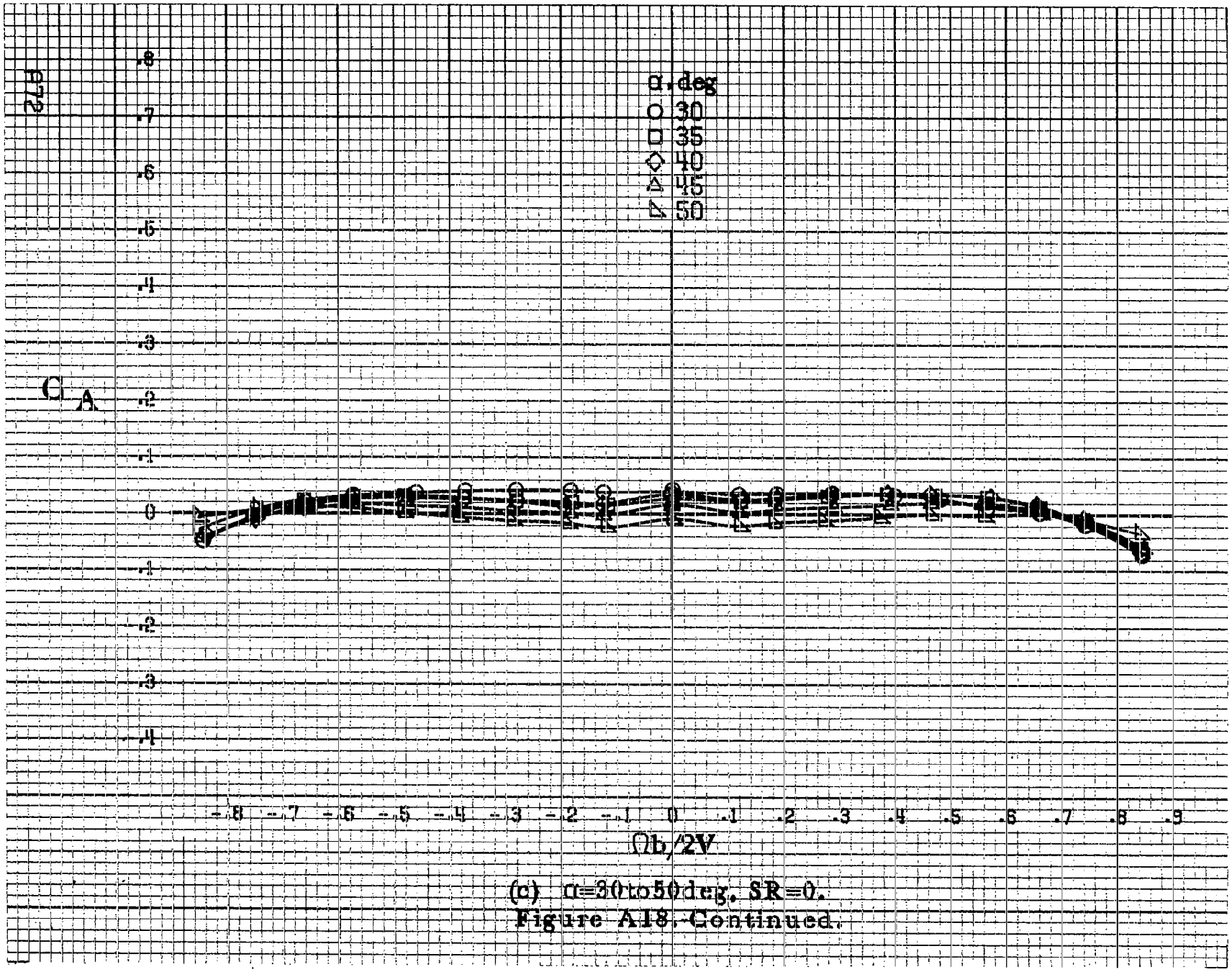

(c) α=30 to 50 deg, SR=0.

Figure A18.-Continued.

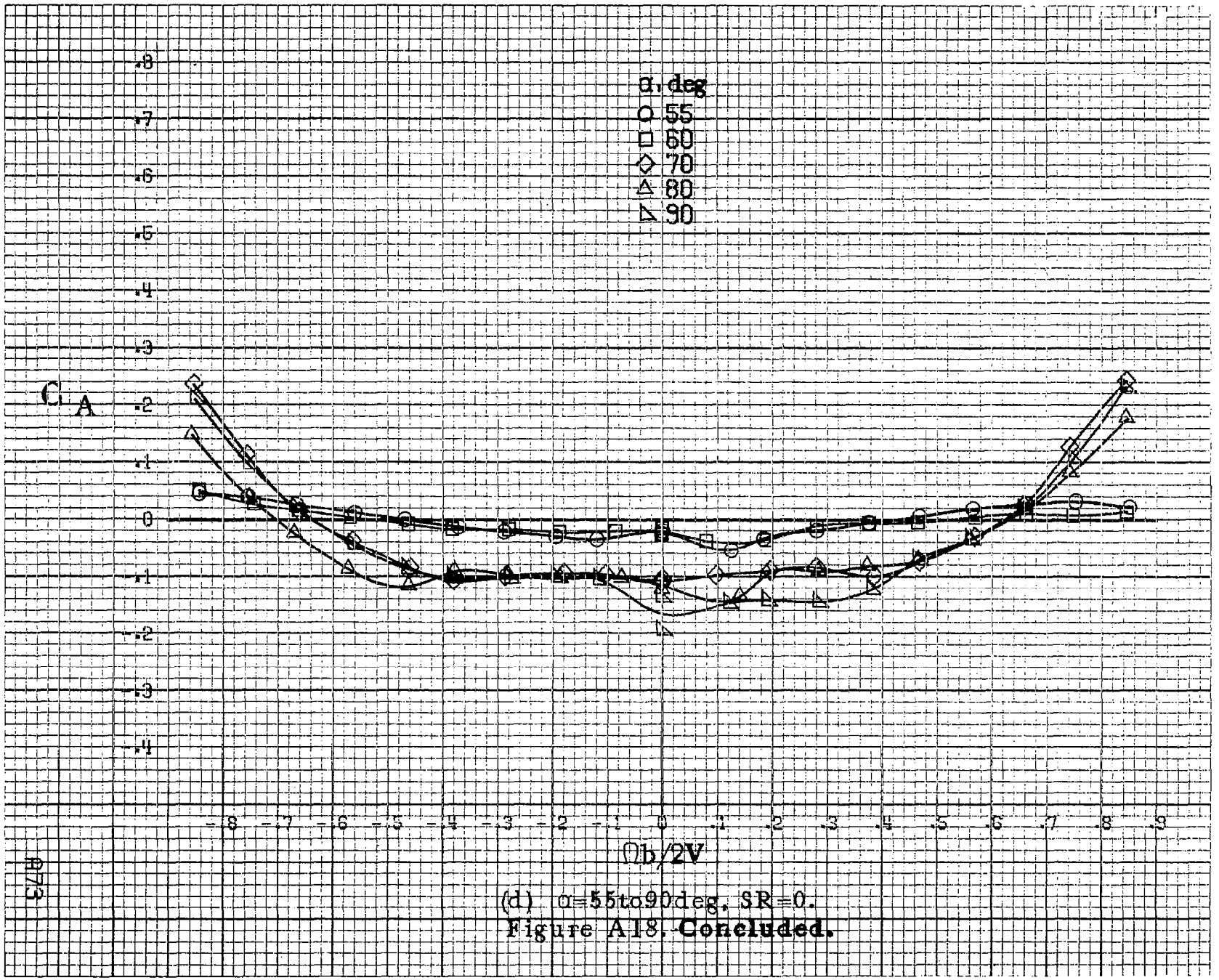

(d) α=55to90deg, SR=0.

Figure A18. Concluded.

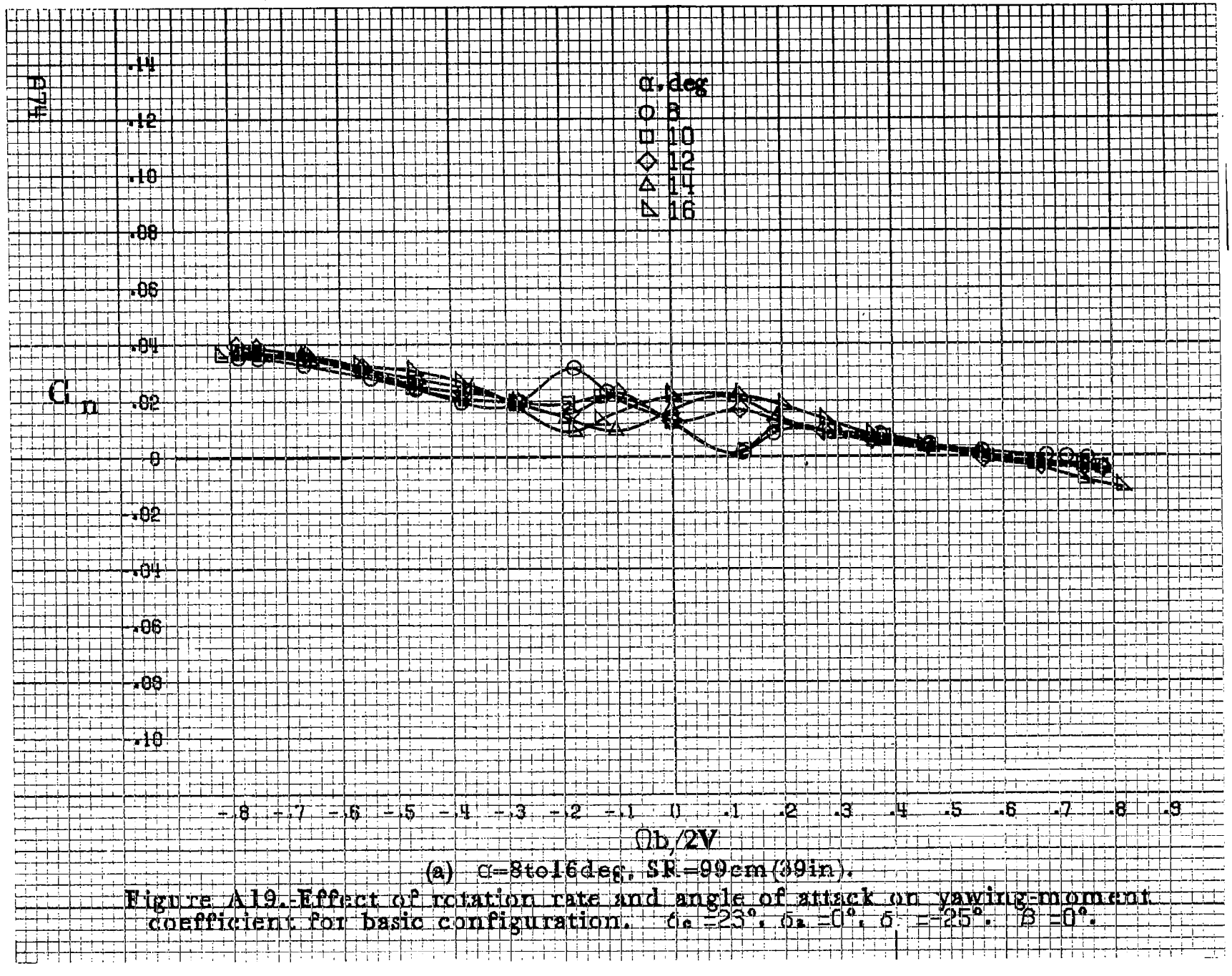

(a) α=8to16deg, SR=99cm(39in).

Figure A19.-Effect of rotation rate and angle of attack on yawing-moment coefficient for basic configuration. δ_e=23°, δ_a=0°, δ_r=-25°, β=0°.

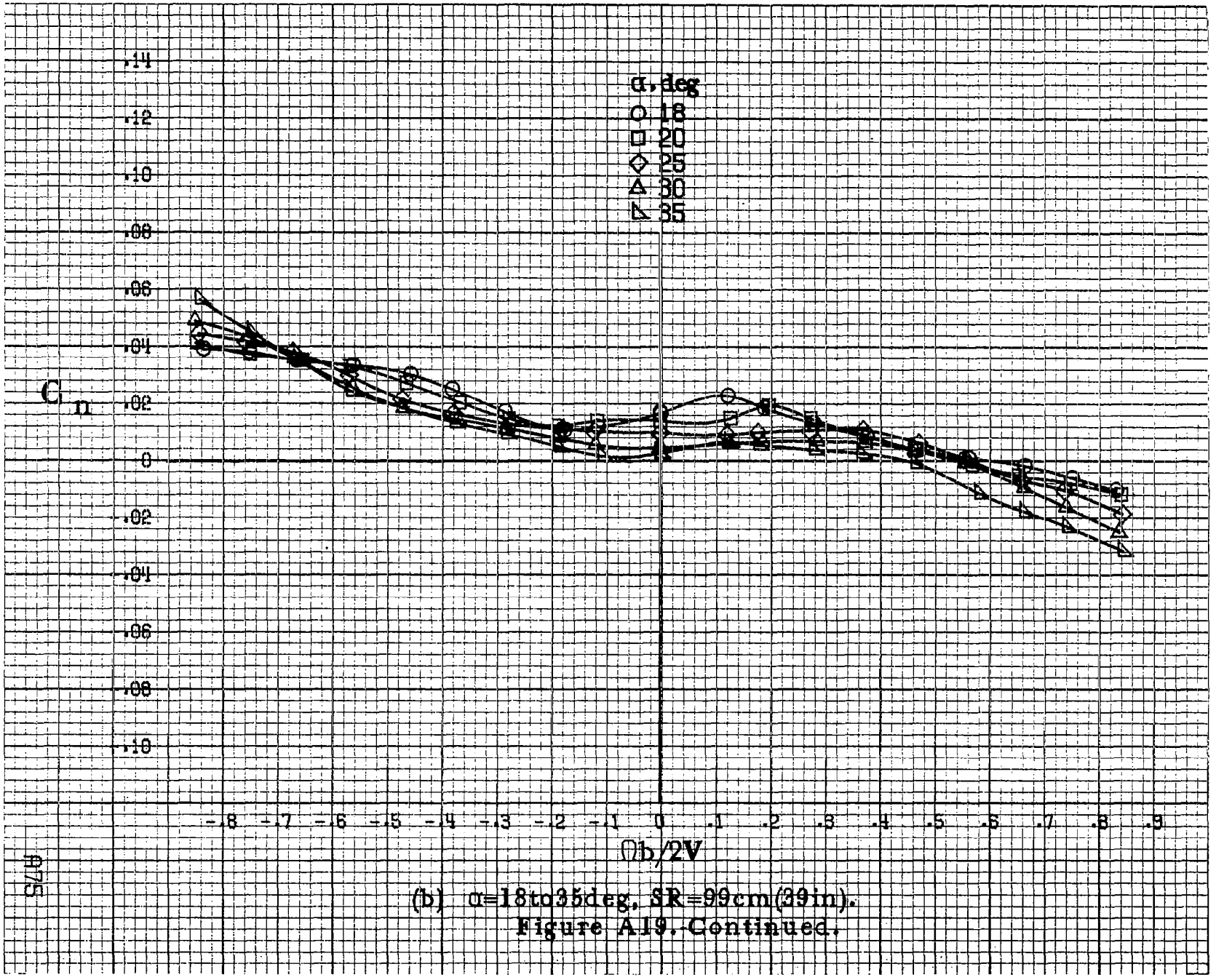

(b) α=18to35deg, SR=99cm(39in).

Figure A19.-Continued.

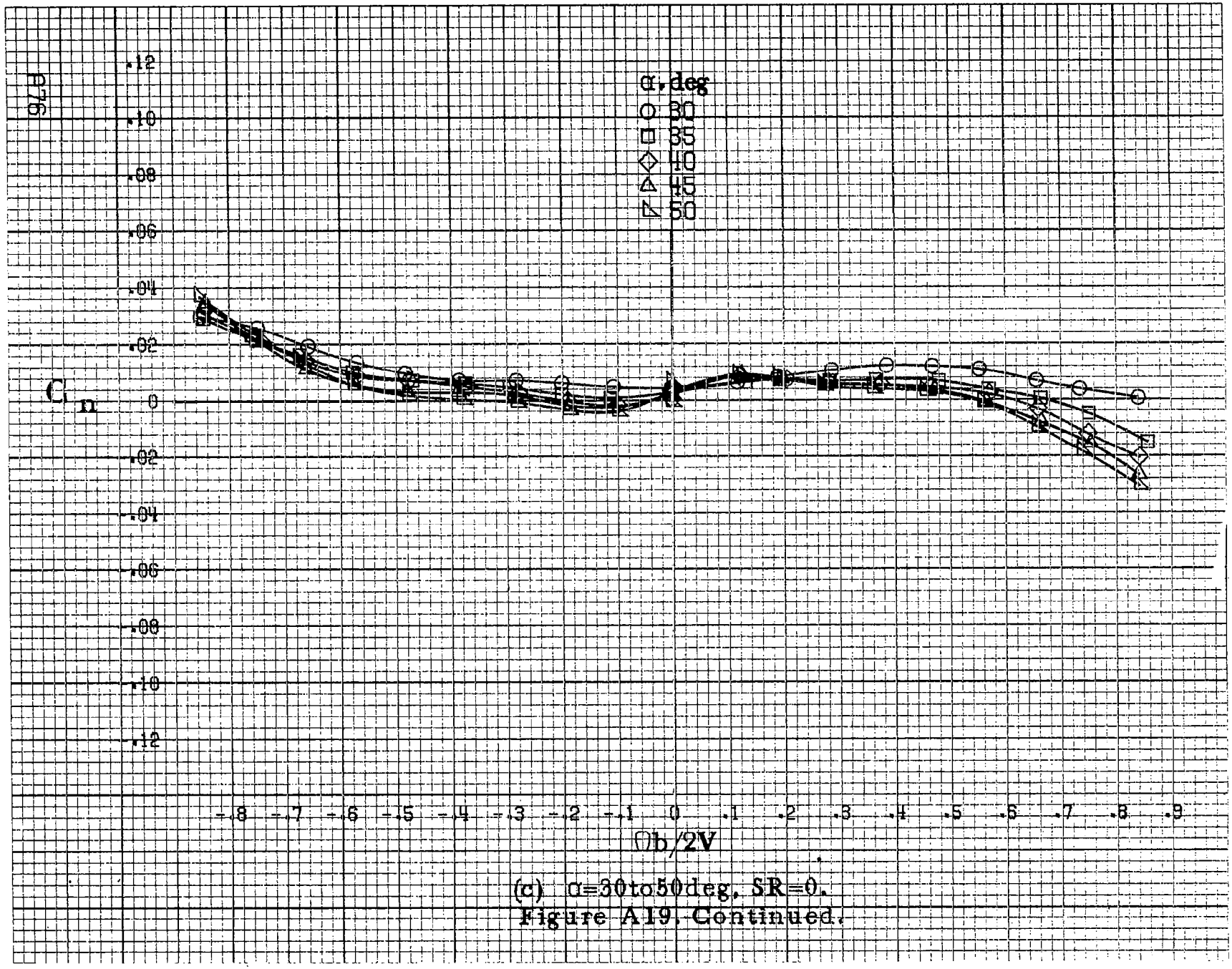

(c) α=30to50deg, SR=0.

Figure A19. Continued.

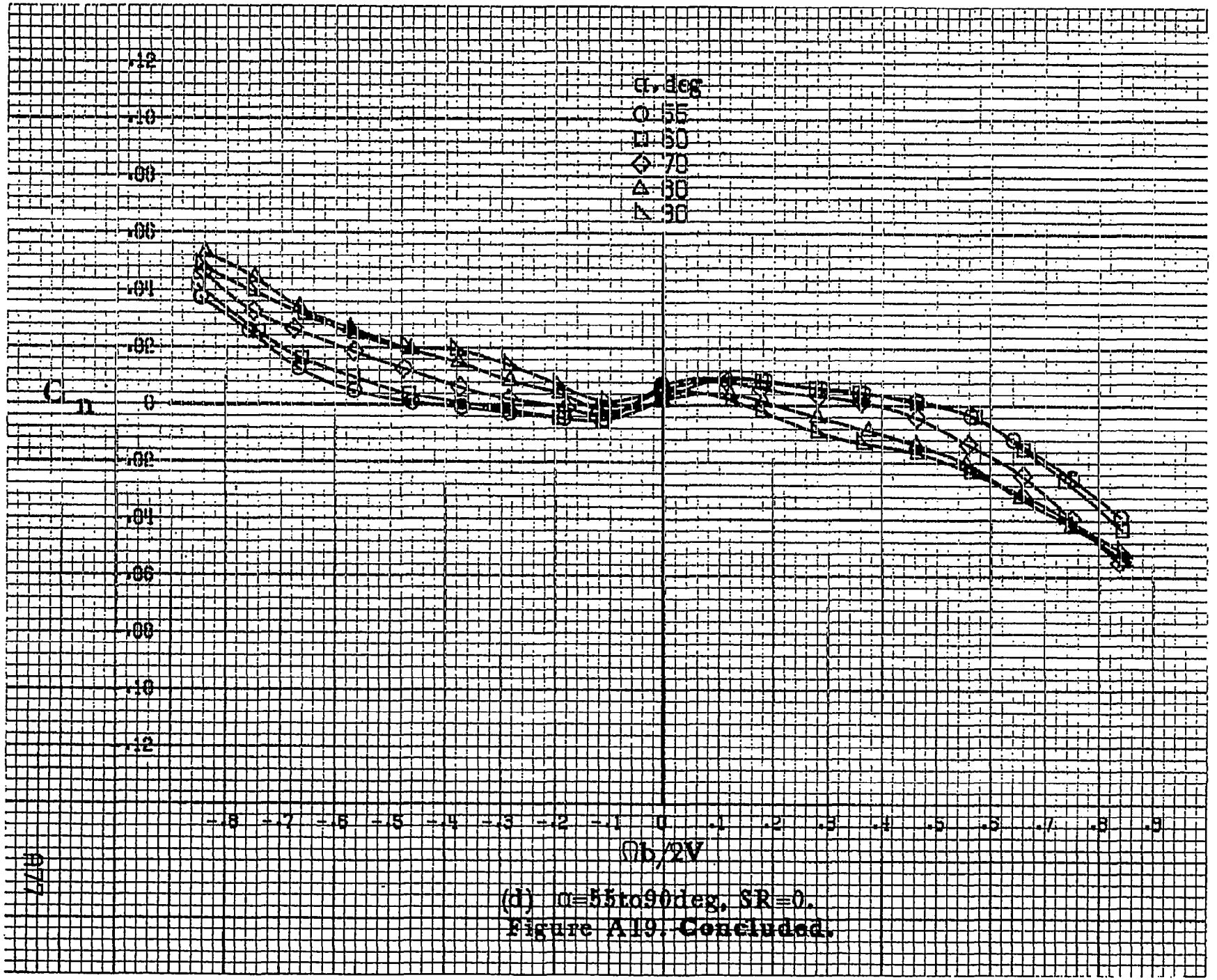

(d) α=55to90deg, SR=0.

Figure A19. Concluded.

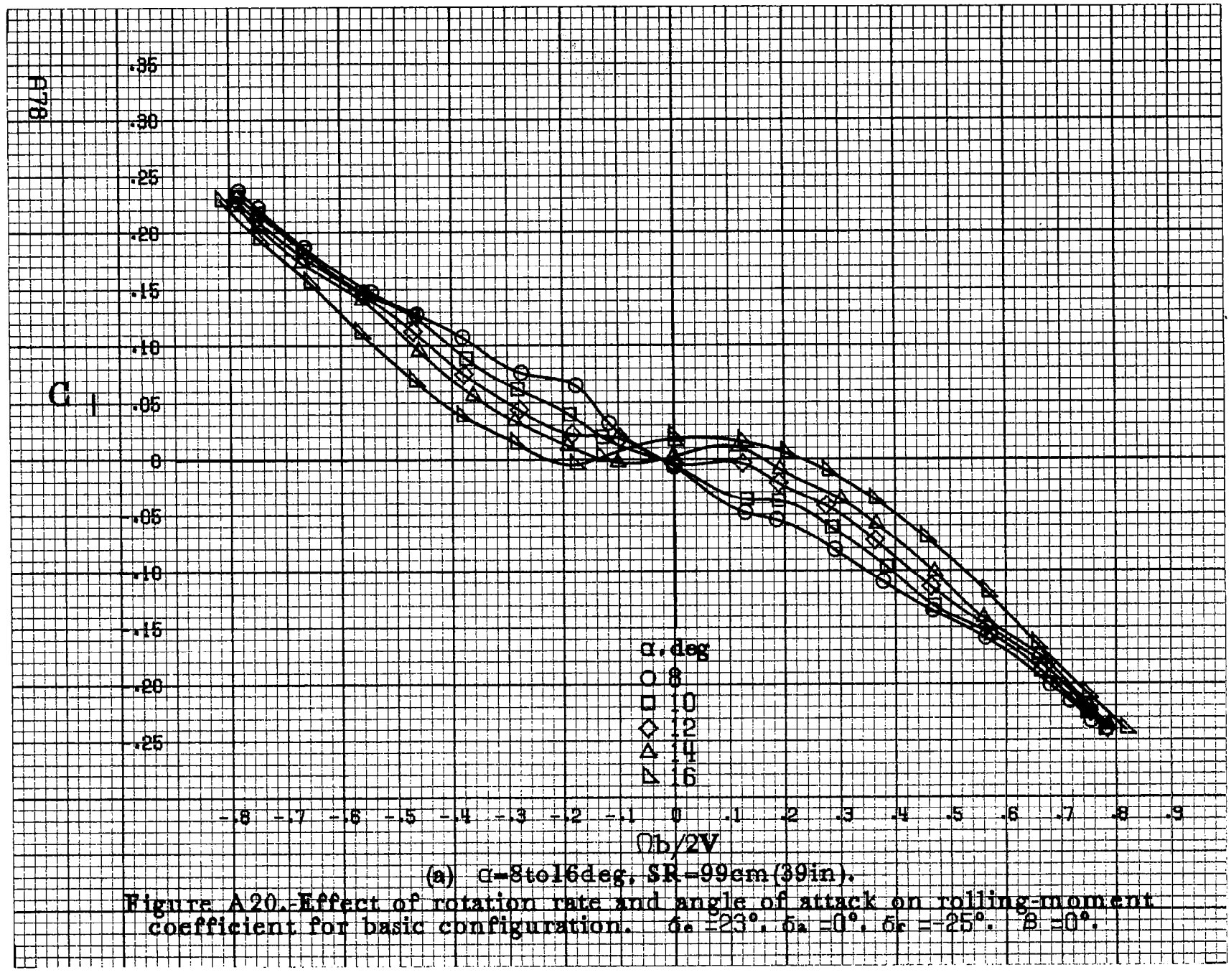

(a) α=8to16deg, SR=99cm(39in).

Figure A20. Effect of rotation rate and angle of attack on rolling-moment coefficient for basic configuration. δ_e =23°, δ_a =0°, δ_r =-25°. β =0°.

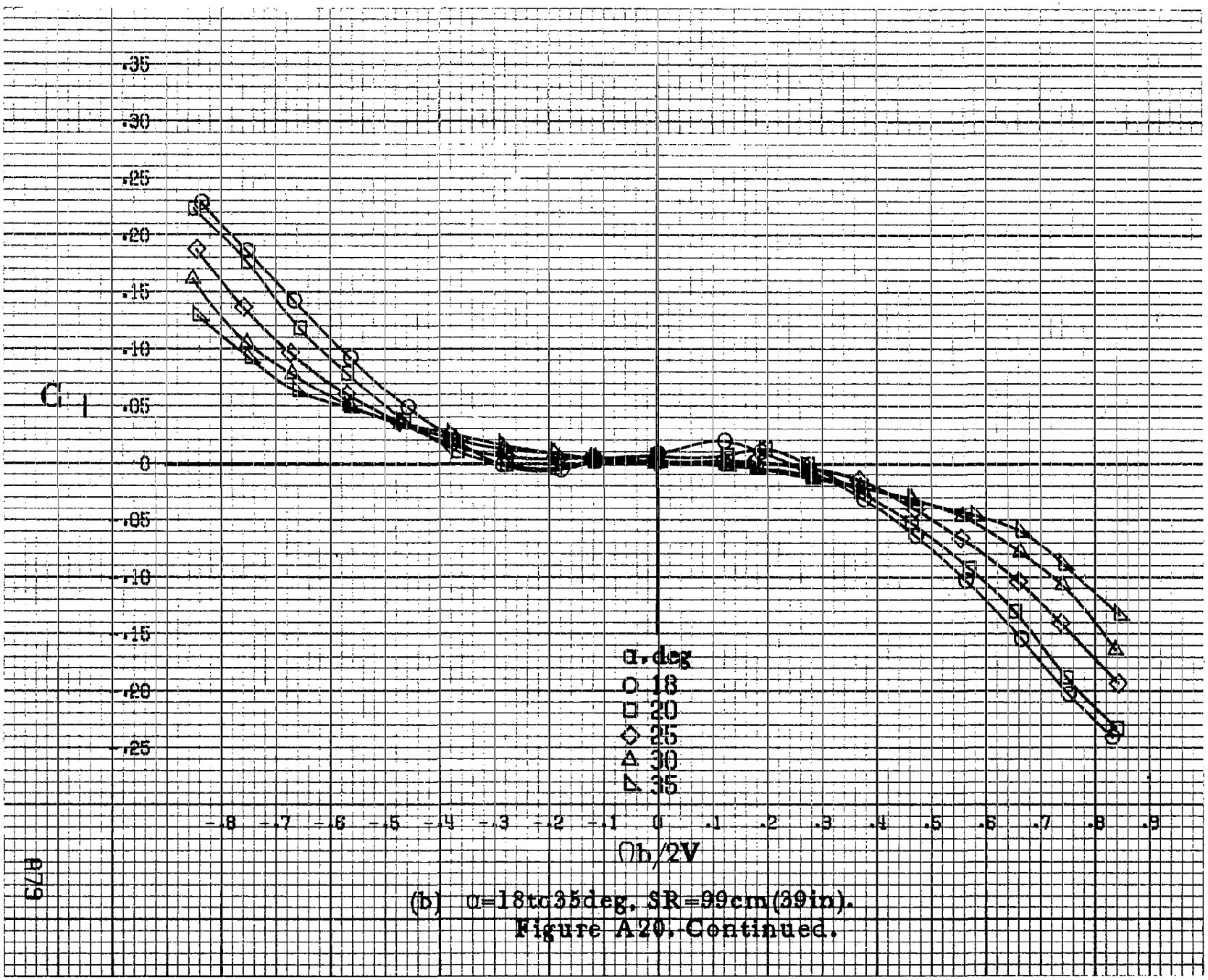

(b) α=18tc35deg. SR=99cm(39in).

Figure A20.-Continued.

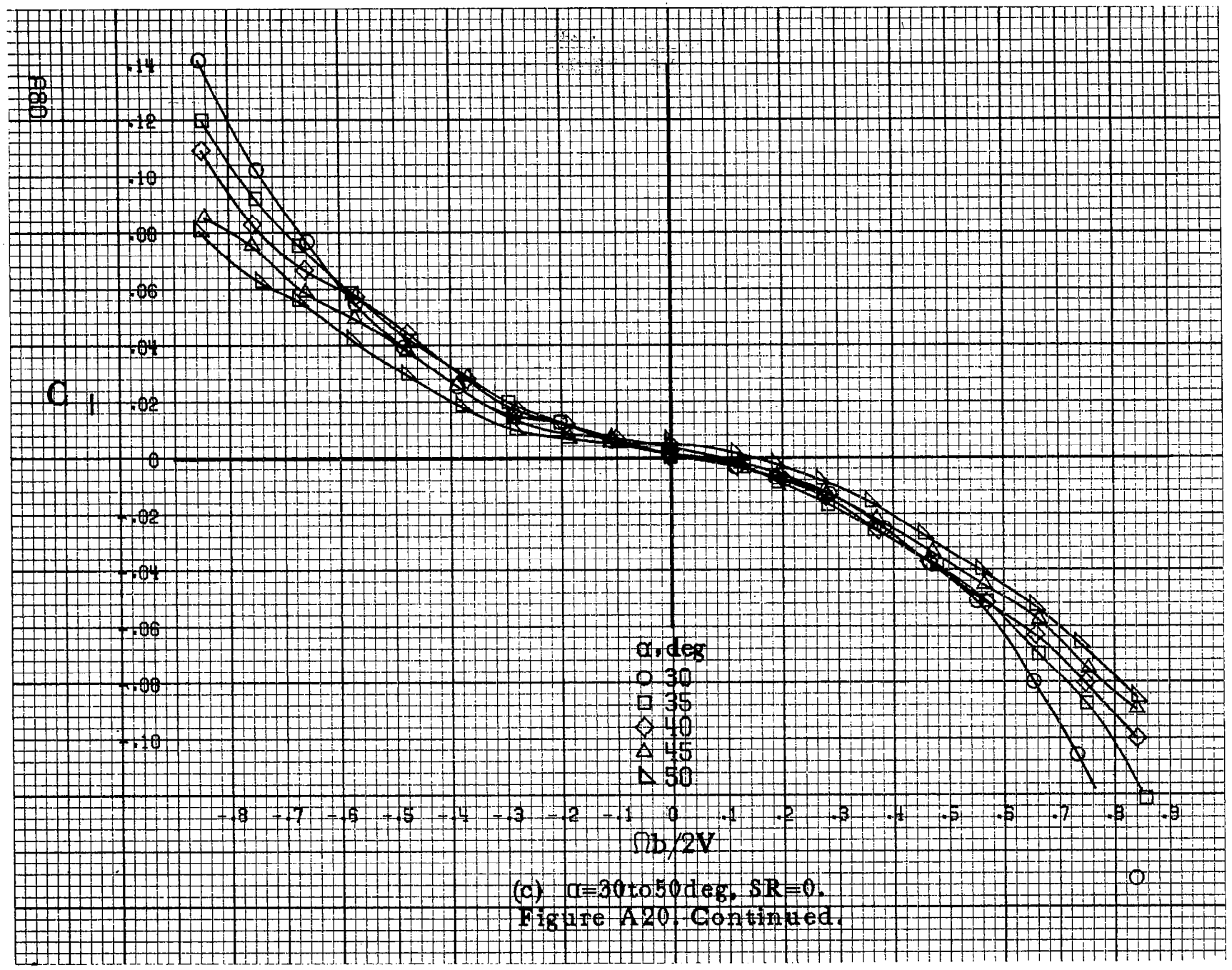

(c) α=30to50deg, SR=0.

Figure A20. Continued.

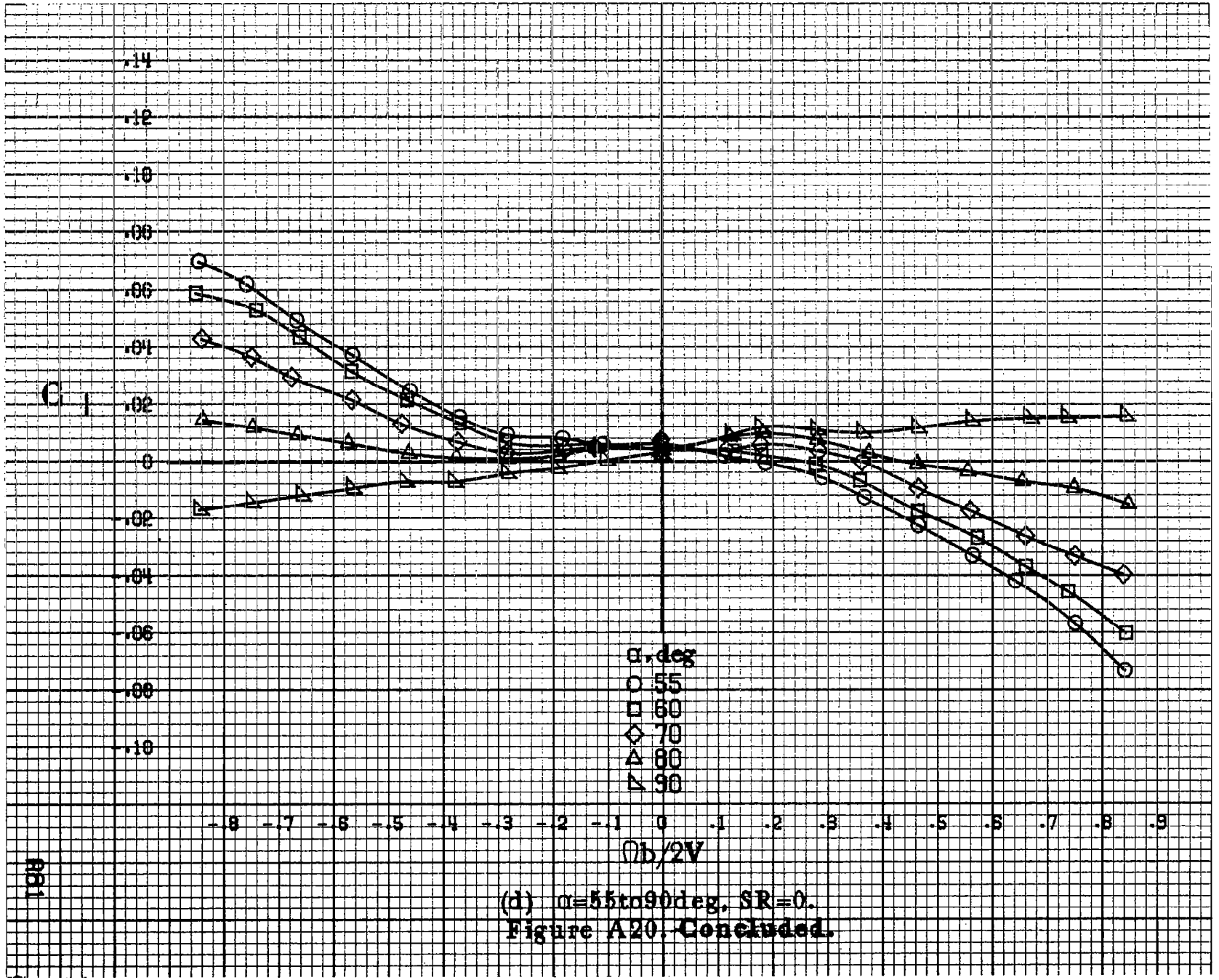

(d) α=55to90deg, SR=0.

Figure A20.-Concluded.

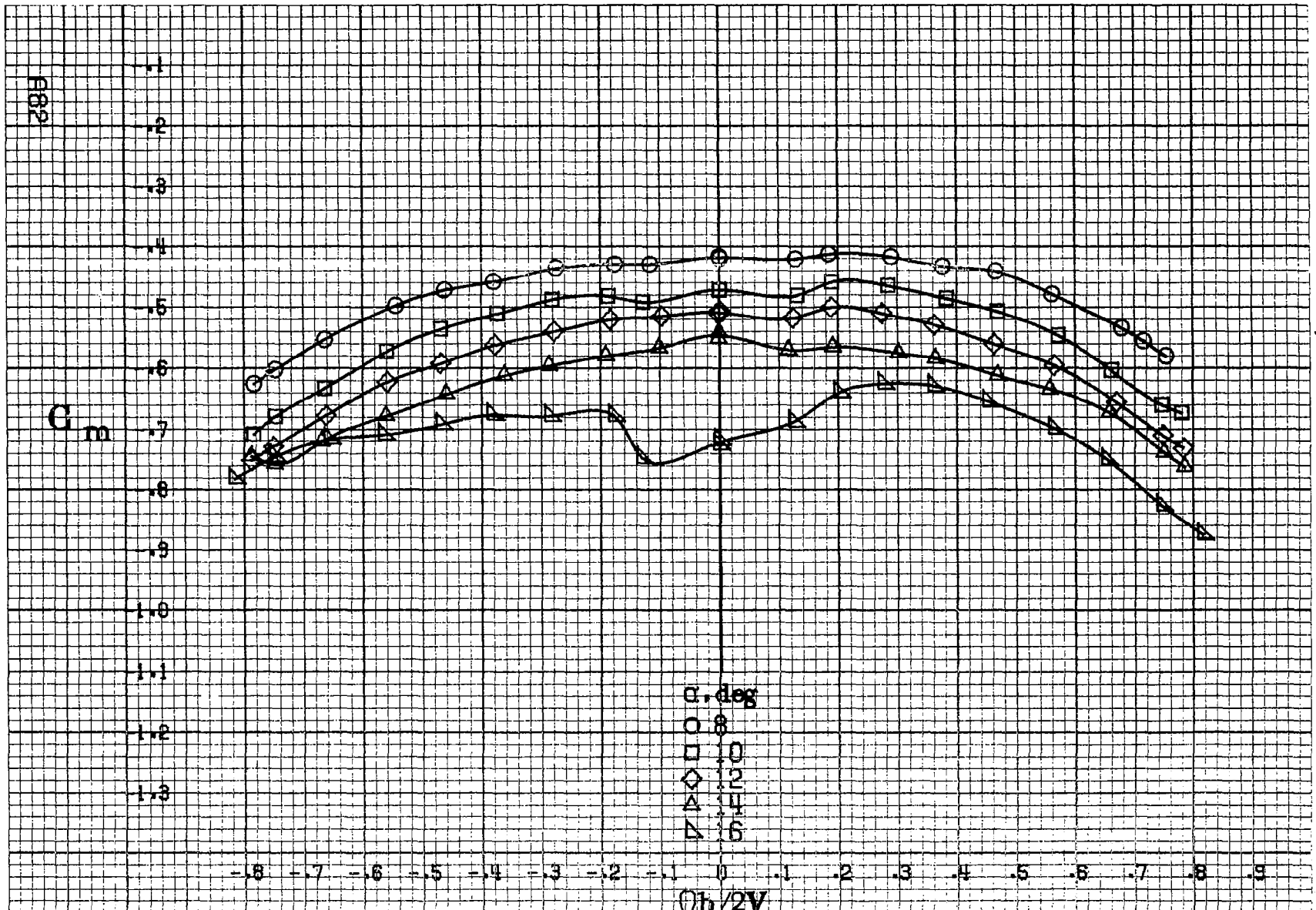

(a) α=8to16deg, SR=99cm(39in).

Figure A21.-Effect of rotation rate and angle of attack on pitching-moment coefficient for basic configuration. $\delta_e = 23°$, $\delta_a = 0°$, $\delta_r = -25°$, $\beta = 0°$.

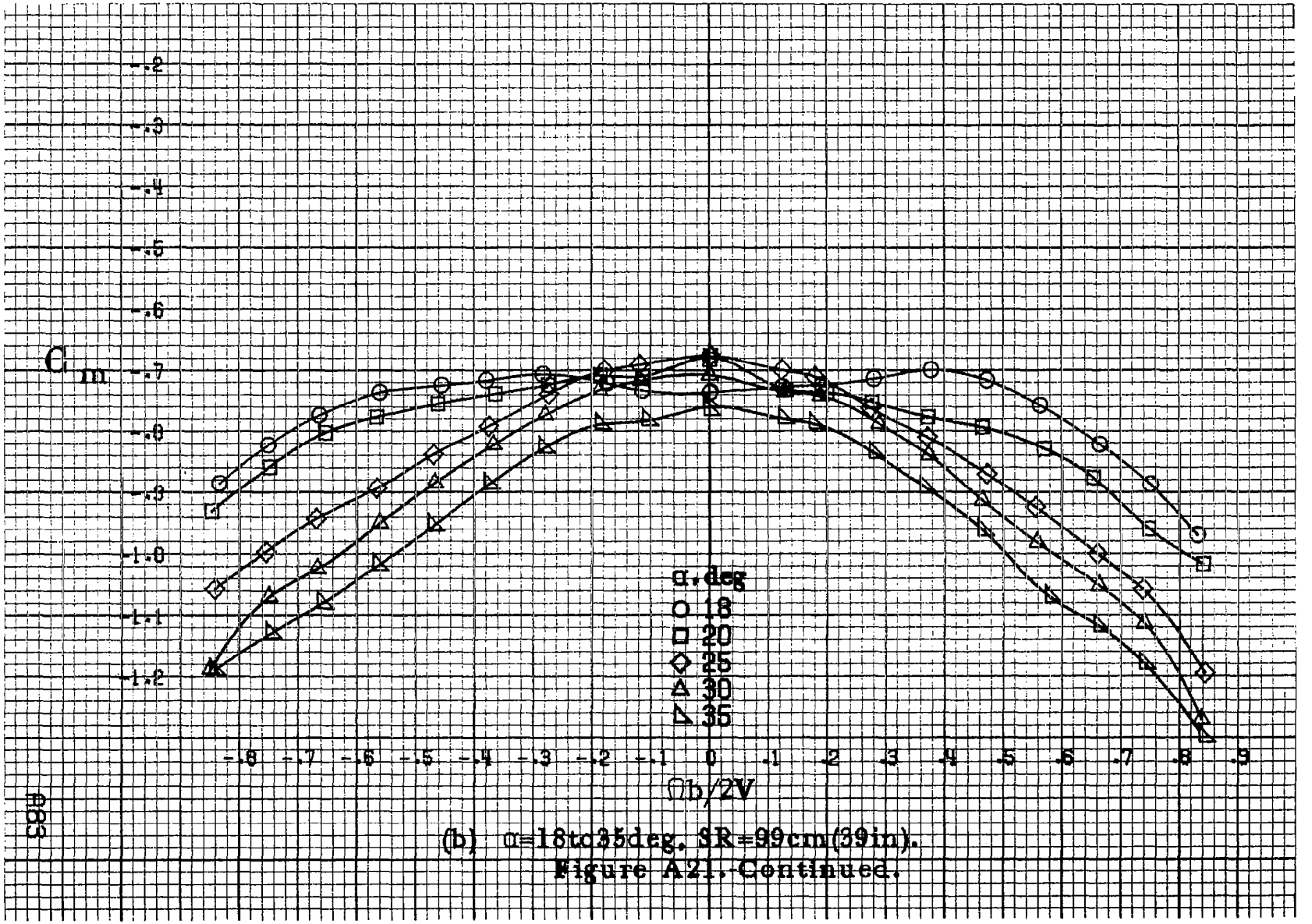

(b) α=18to35deg. SR=99cm(39in).

Figure A21.-Continued.

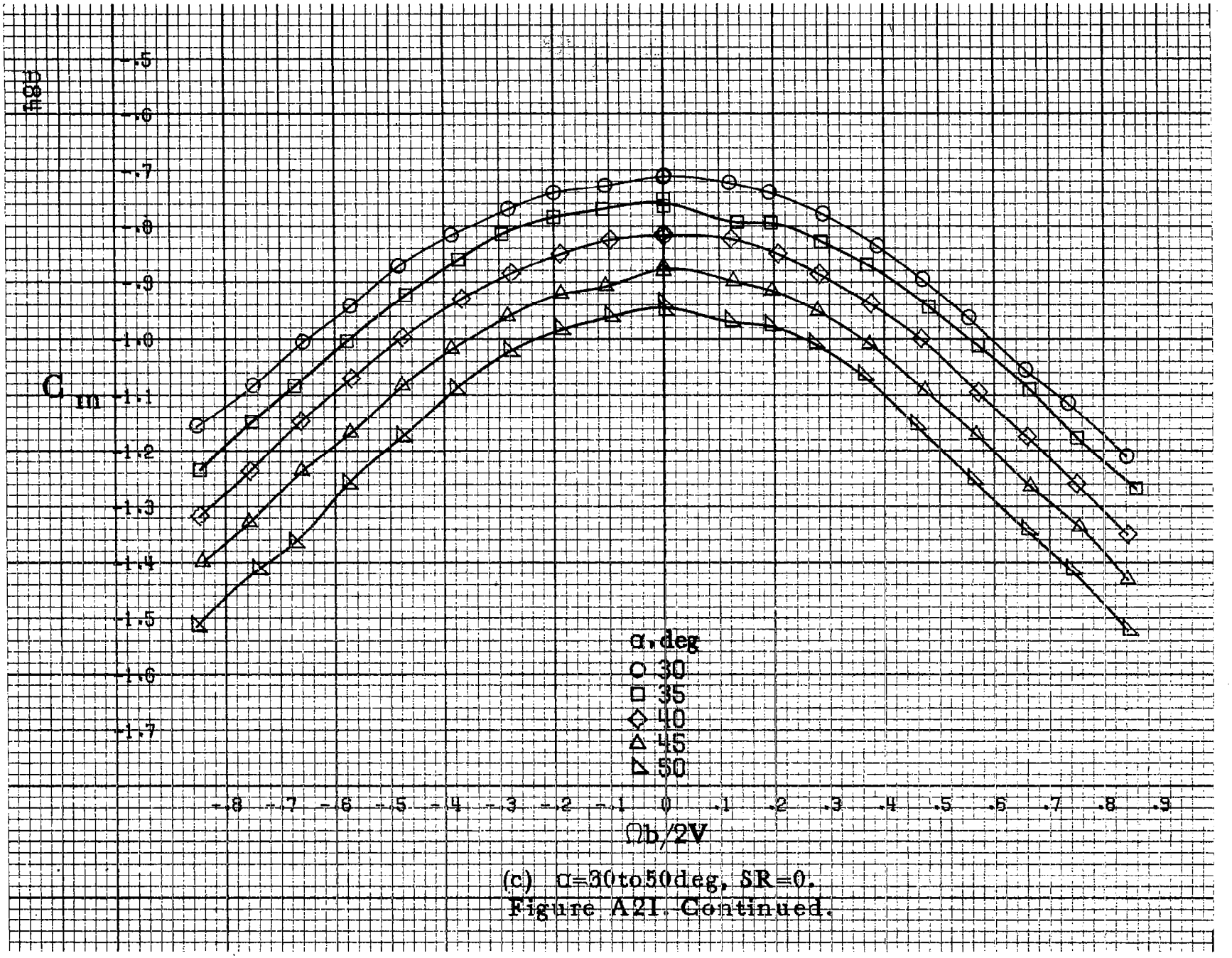

(c) α=30to50deg, SR=0.

Figure A21. Continued.

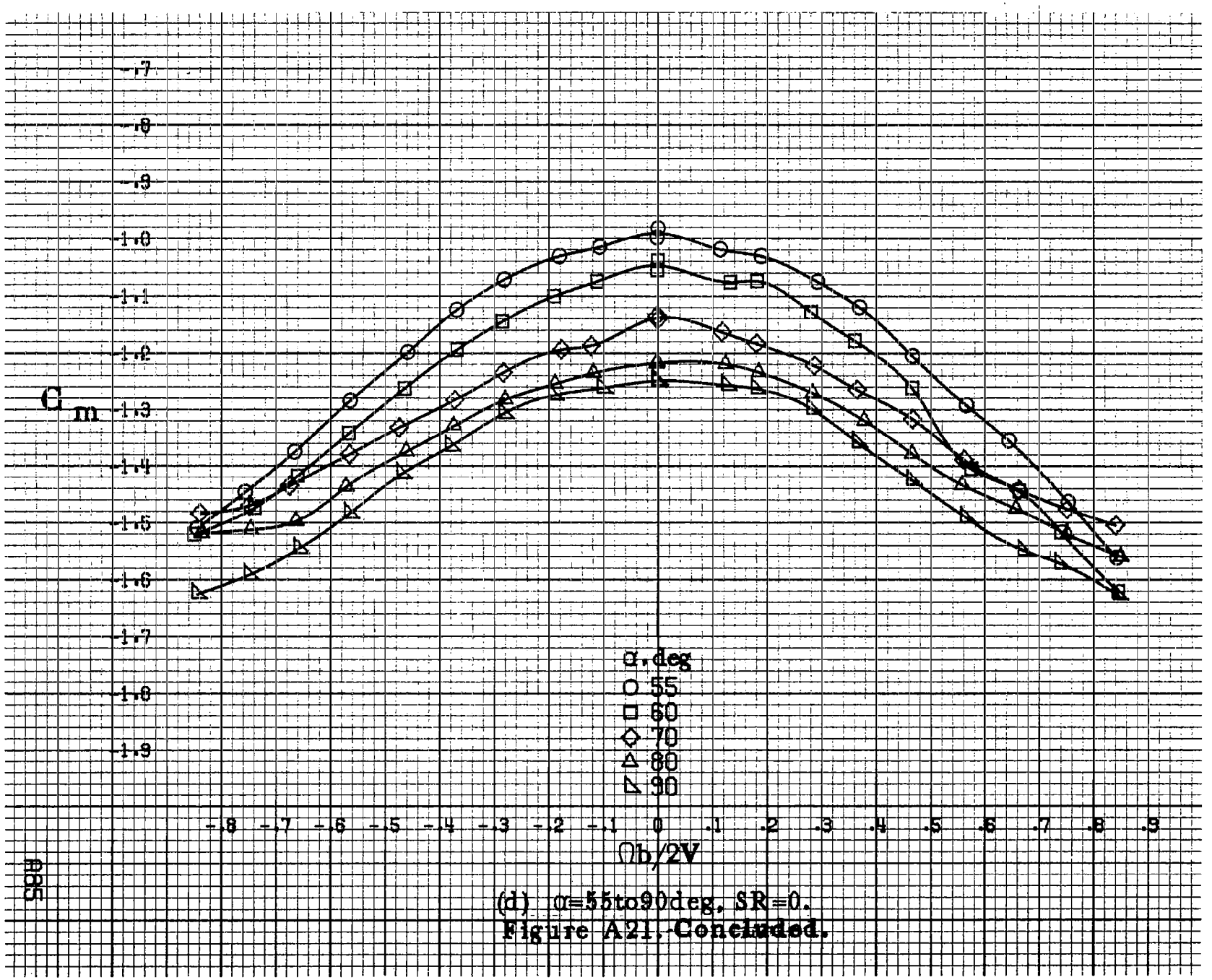

(d) α=55to90deg, SR=0.

Figure A21. Concluded.

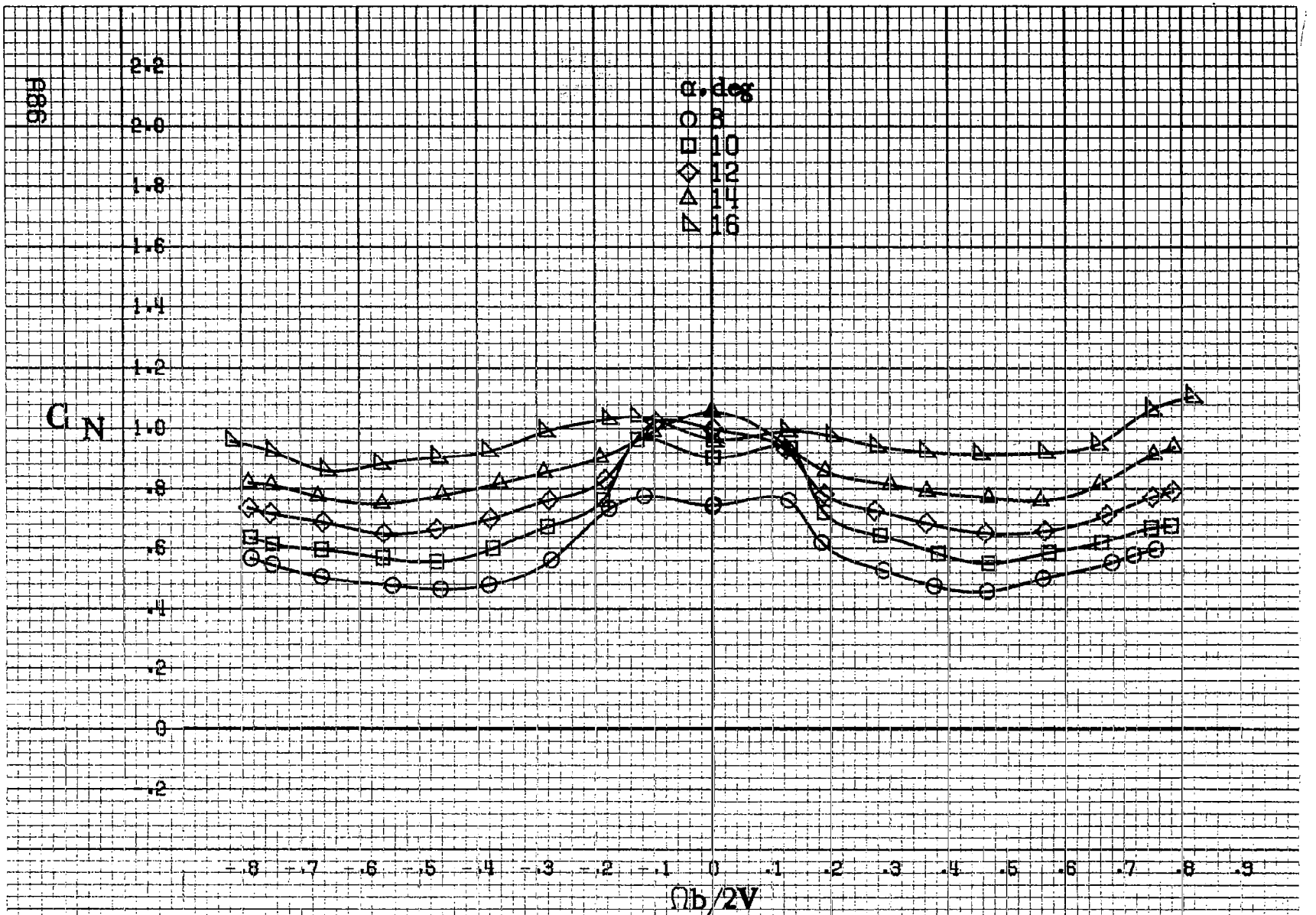

(a) α=8to16deg, SR=99cm(39in).

Figure A22.-Effect of rotation rate and angle of attack on normal-force coefficient for basic configuration. $\delta_e = 23°$, $\delta_a = 0°$, $\delta_r = -25°$, $\beta = 0°$.

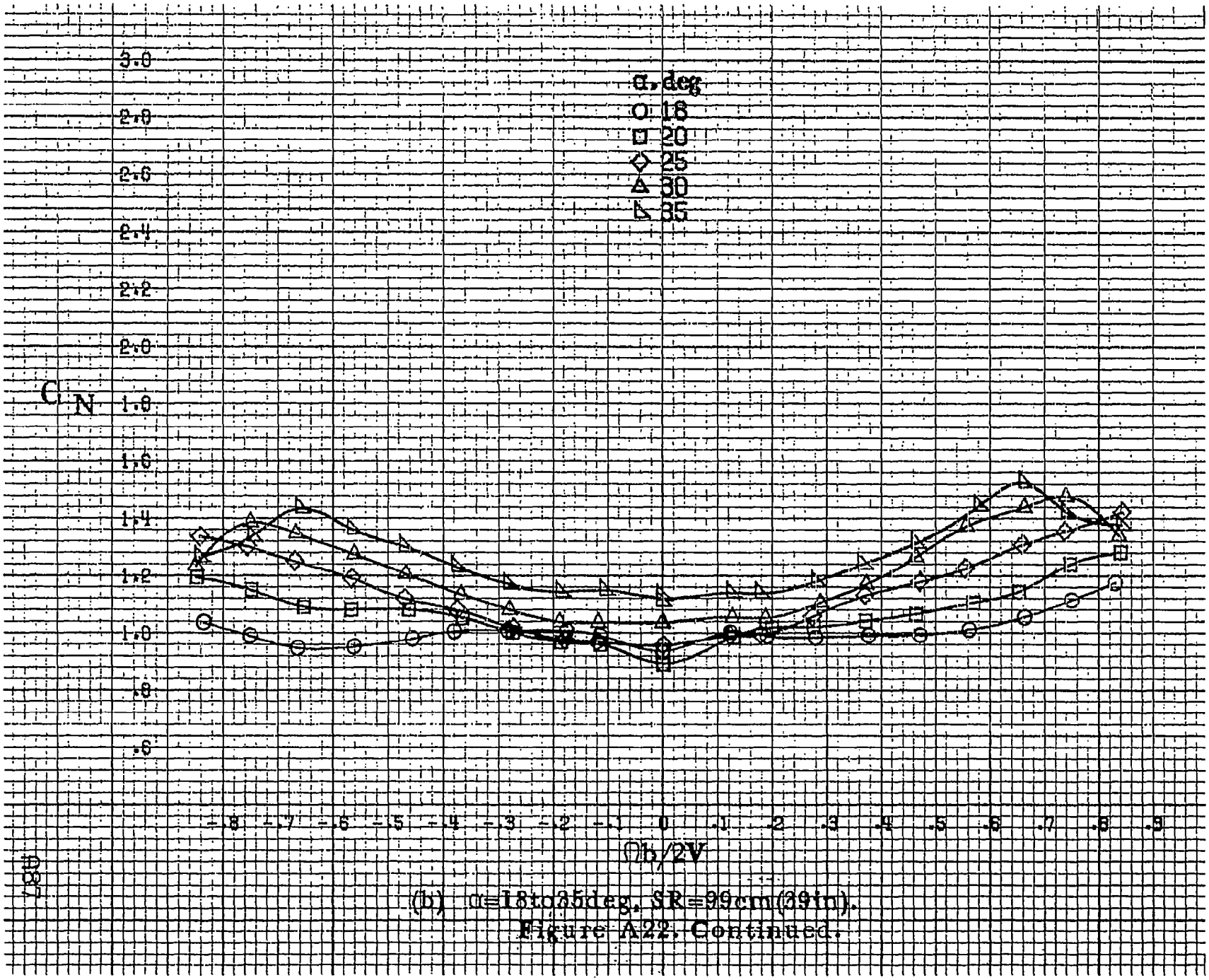

(b) α=18to35deg, SR=99cm(39in).

Figure A22. Continued.

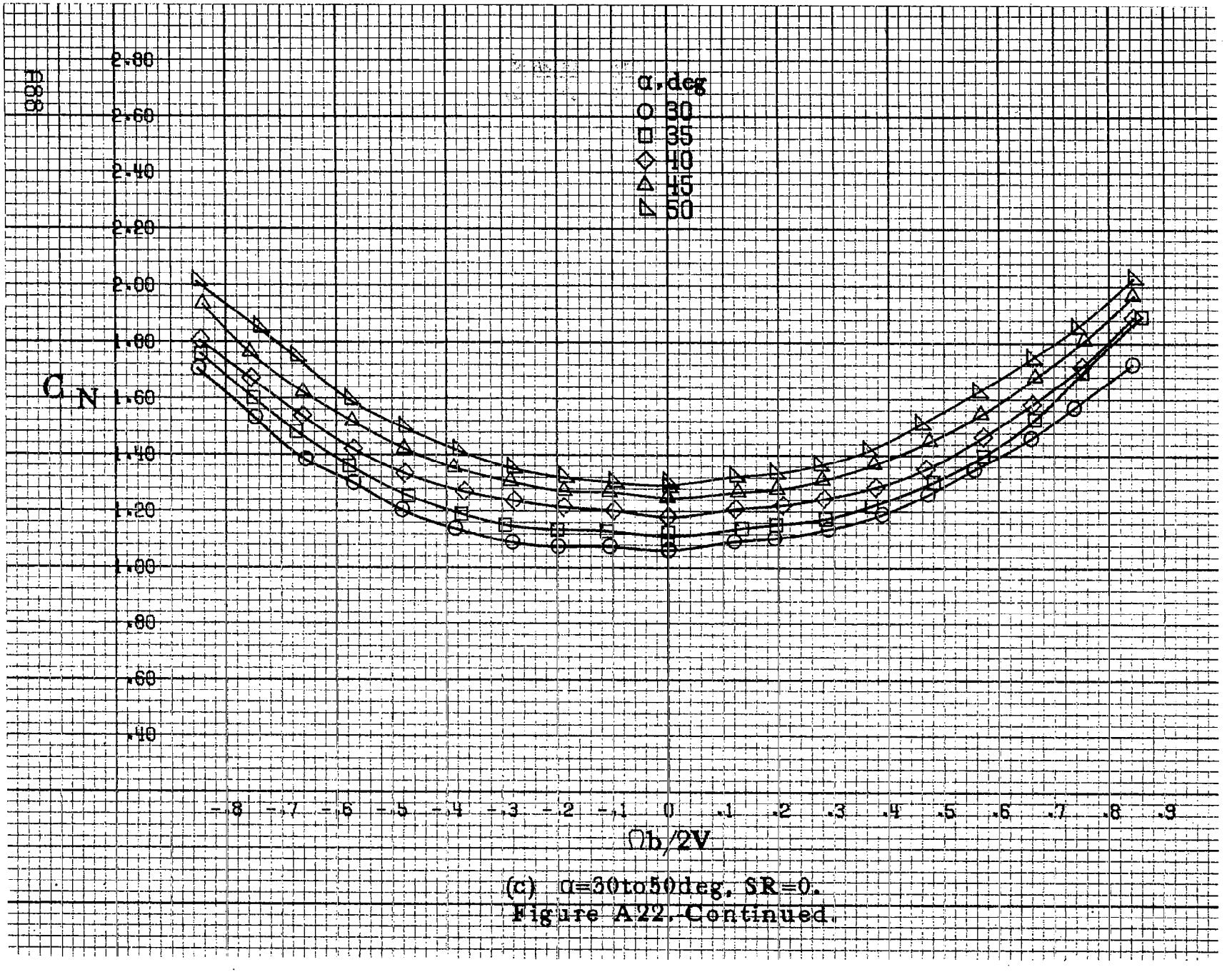

(c) α=30to50deg, SR=0.

Figure A22.-Continued.

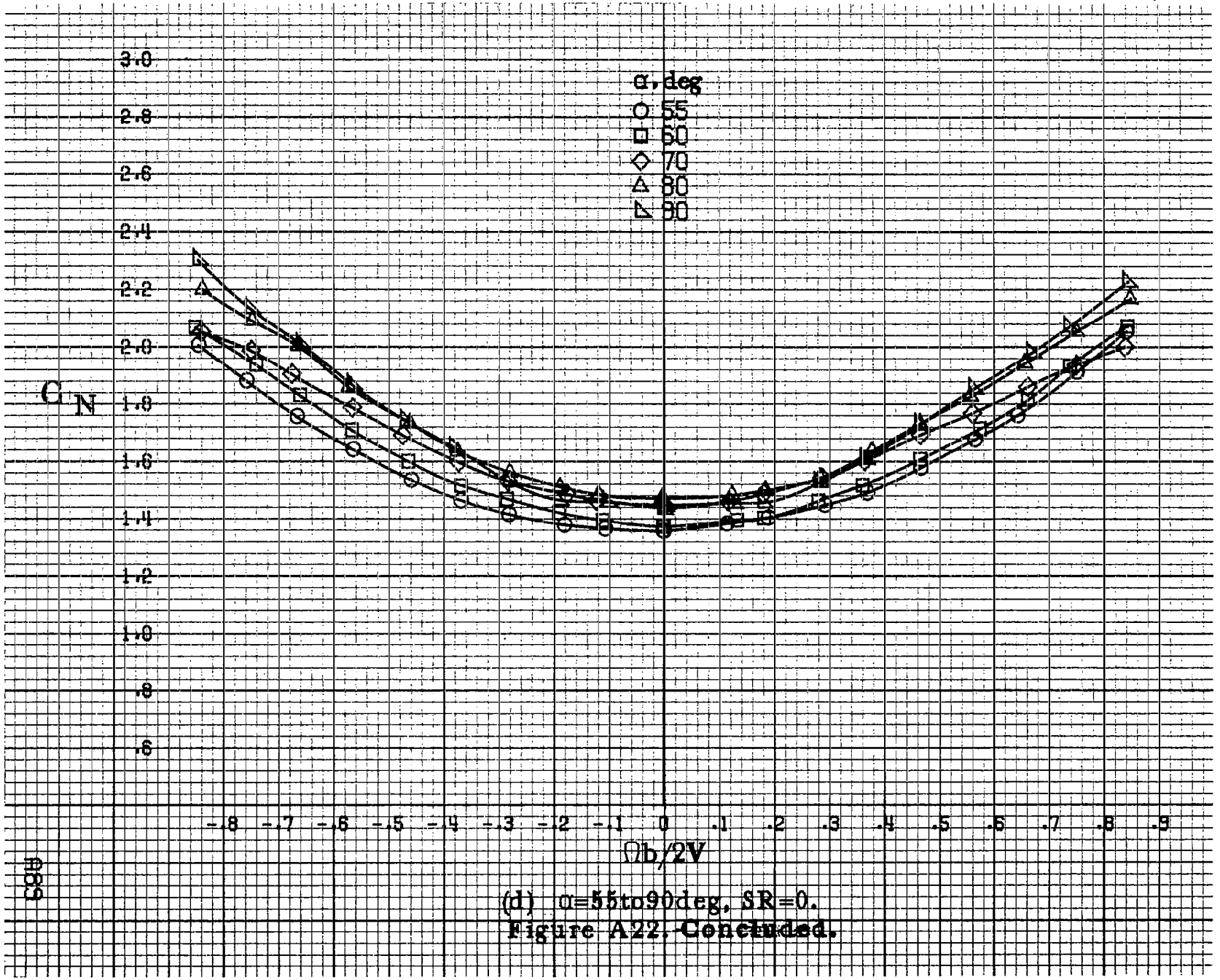

(d) α=55to90deg, SR=0.

Figure A22.-Concluded.

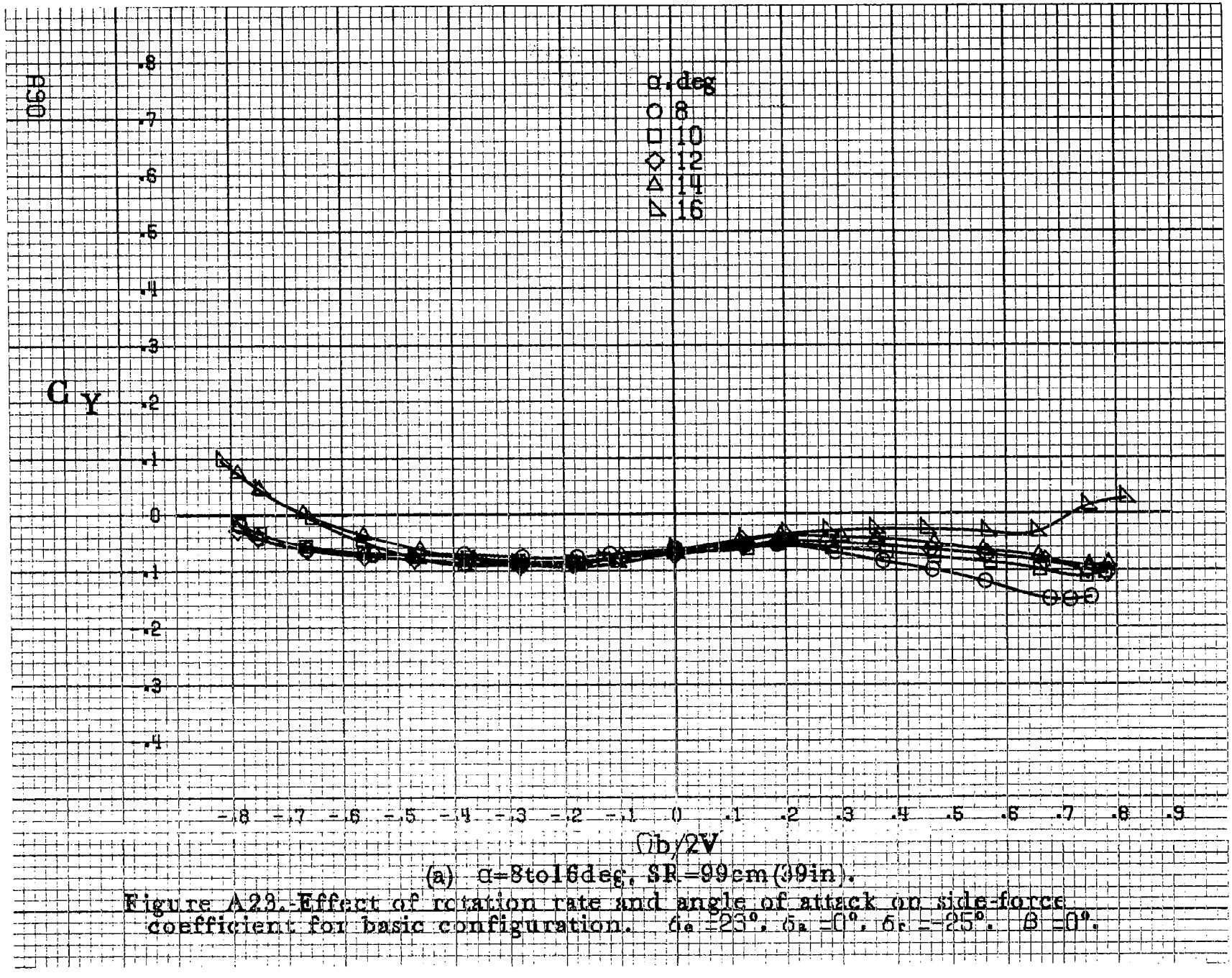

(a) α=8to16deg, SR=99cm(39in).

Figure A23.-Effect of rotation rate and angle of attack on side-force coefficient for basic configuration. δ_e=23°, δ_a=0°, δ_r=-25°, β=0°.

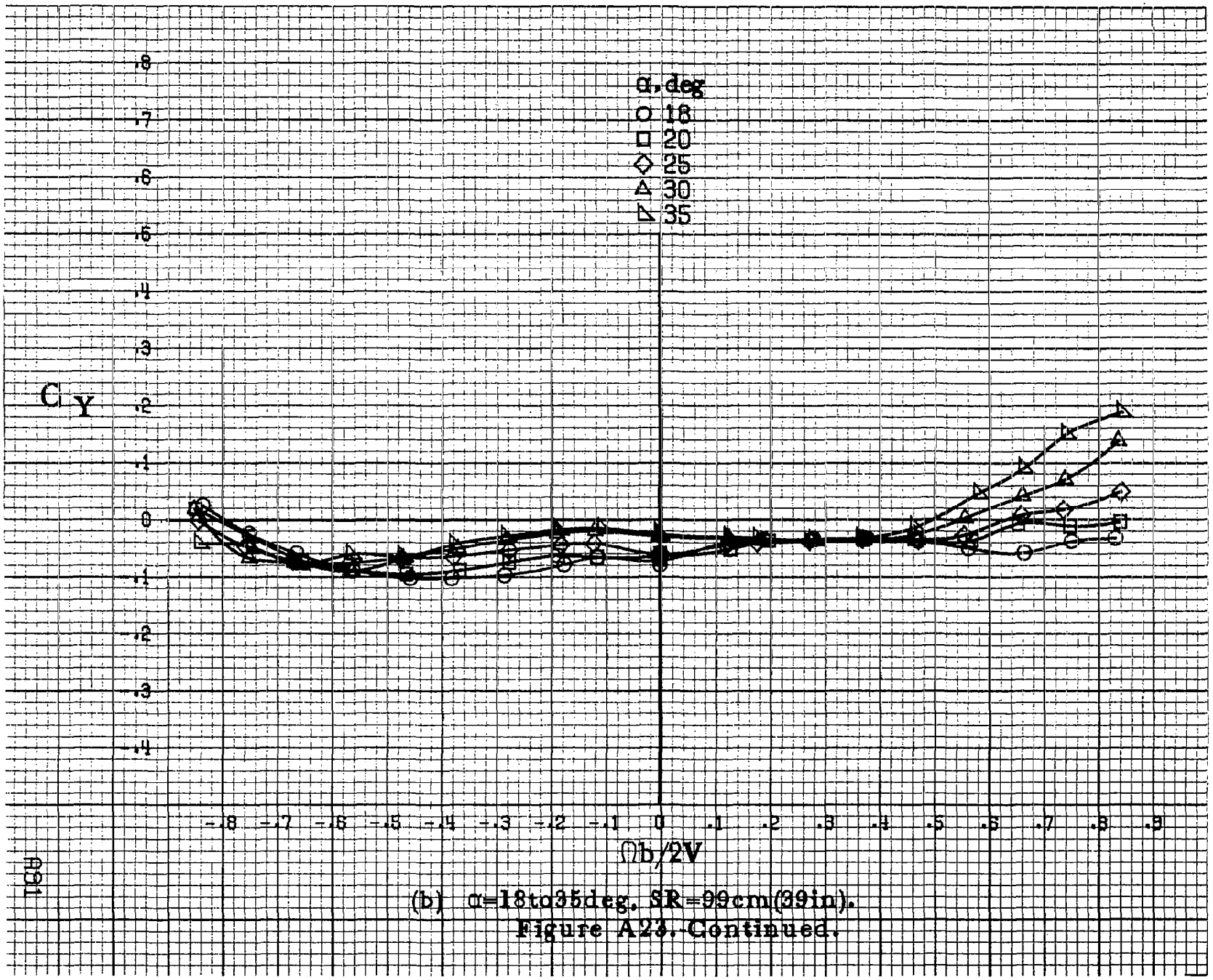

(b) α=18to35deg. SR=99cm(39in).

Figure A23.-Continued.

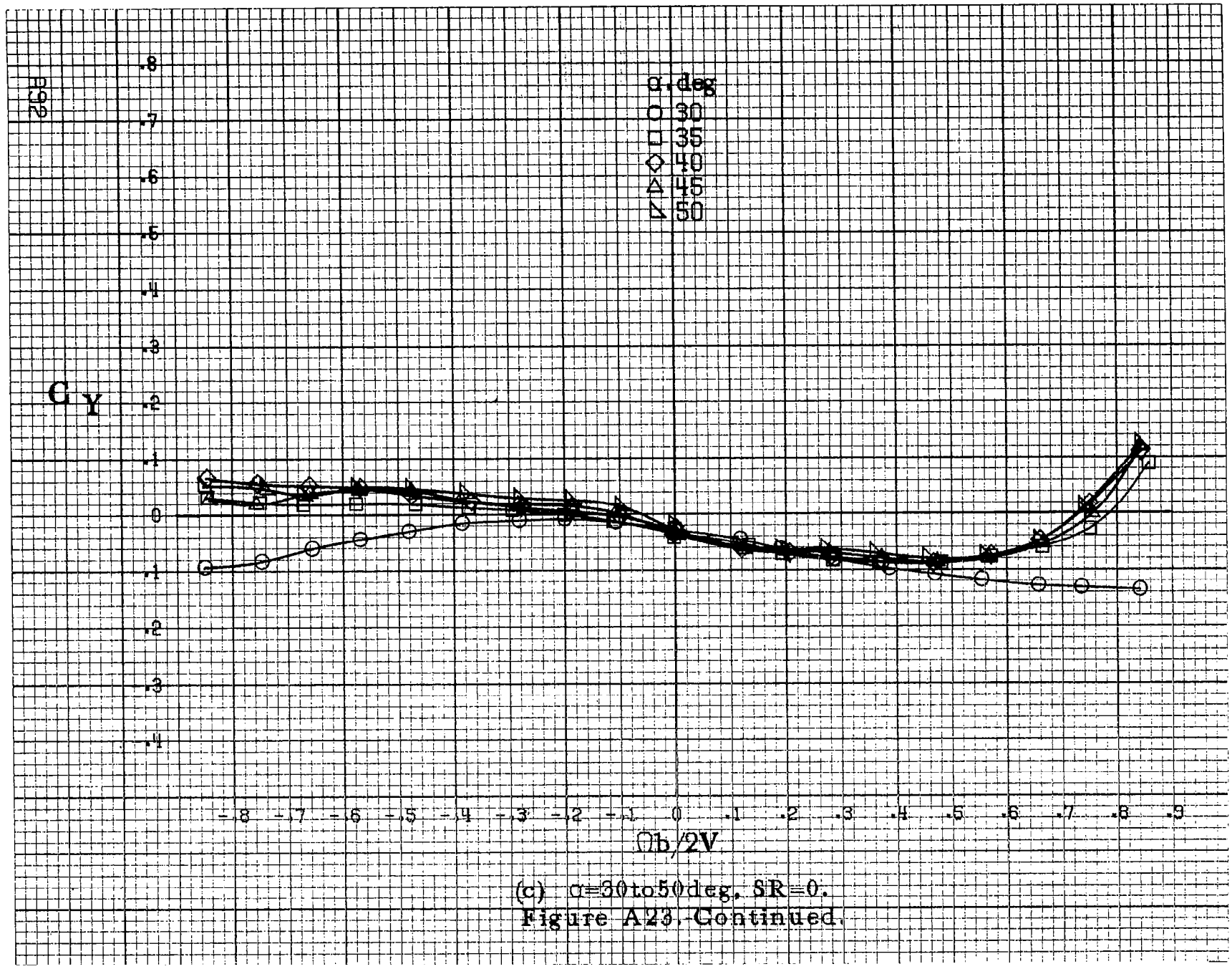

(c) α=30to50deg, SR=0.

Figure A23.-Continued.

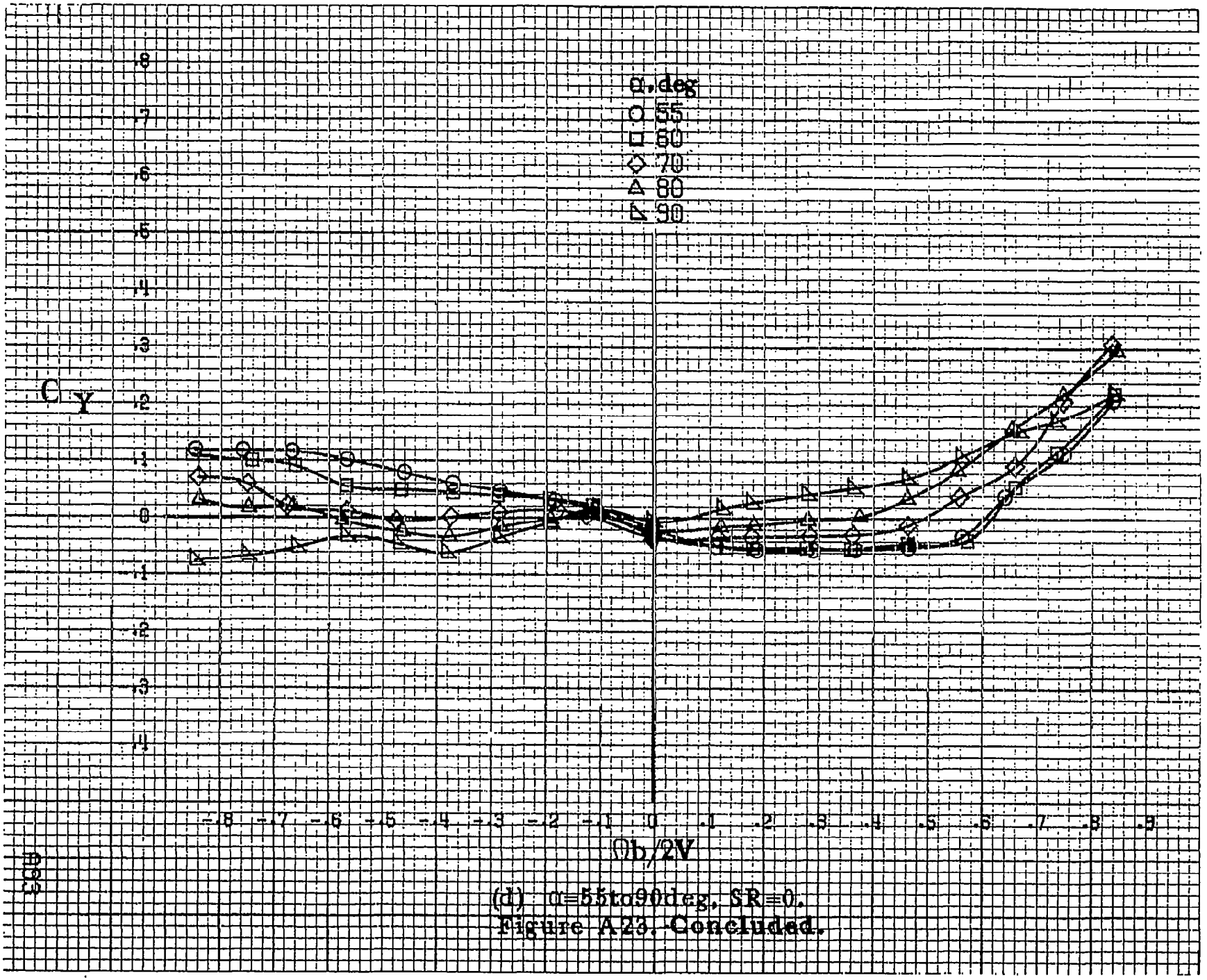

(d) $\alpha = 55$ to 90 deg, $SR = 0$.

Figure A23.-Concluded.

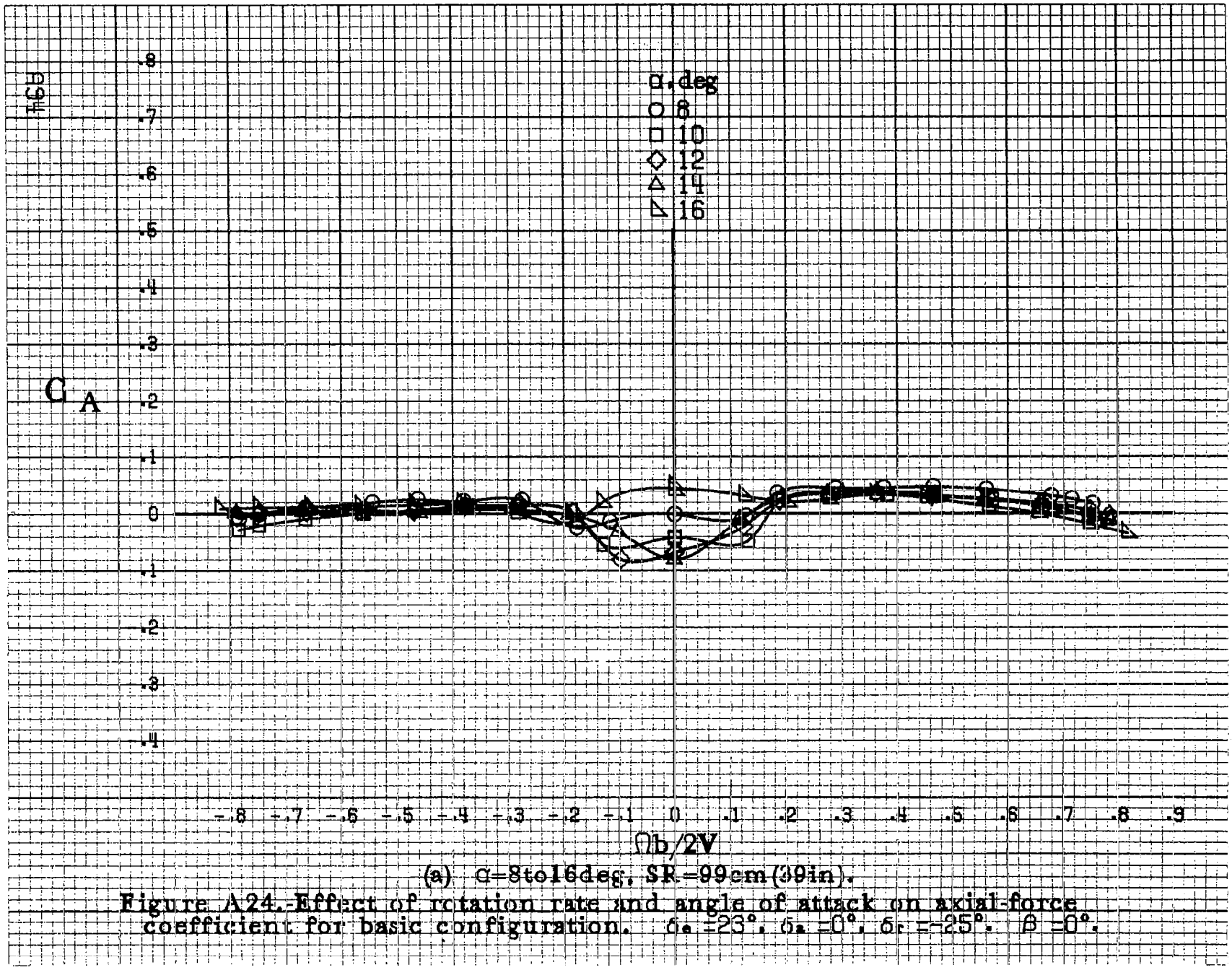

(a) α=8to16deg, SR=99cm(39in).

Figure A24.-Effect of rotation rate and angle of attack on axial-force coefficient for basic configuration. $\delta_e = 23°$, $\delta_a = 0°$, $\delta_r = -25°$, $\beta = 0°$.

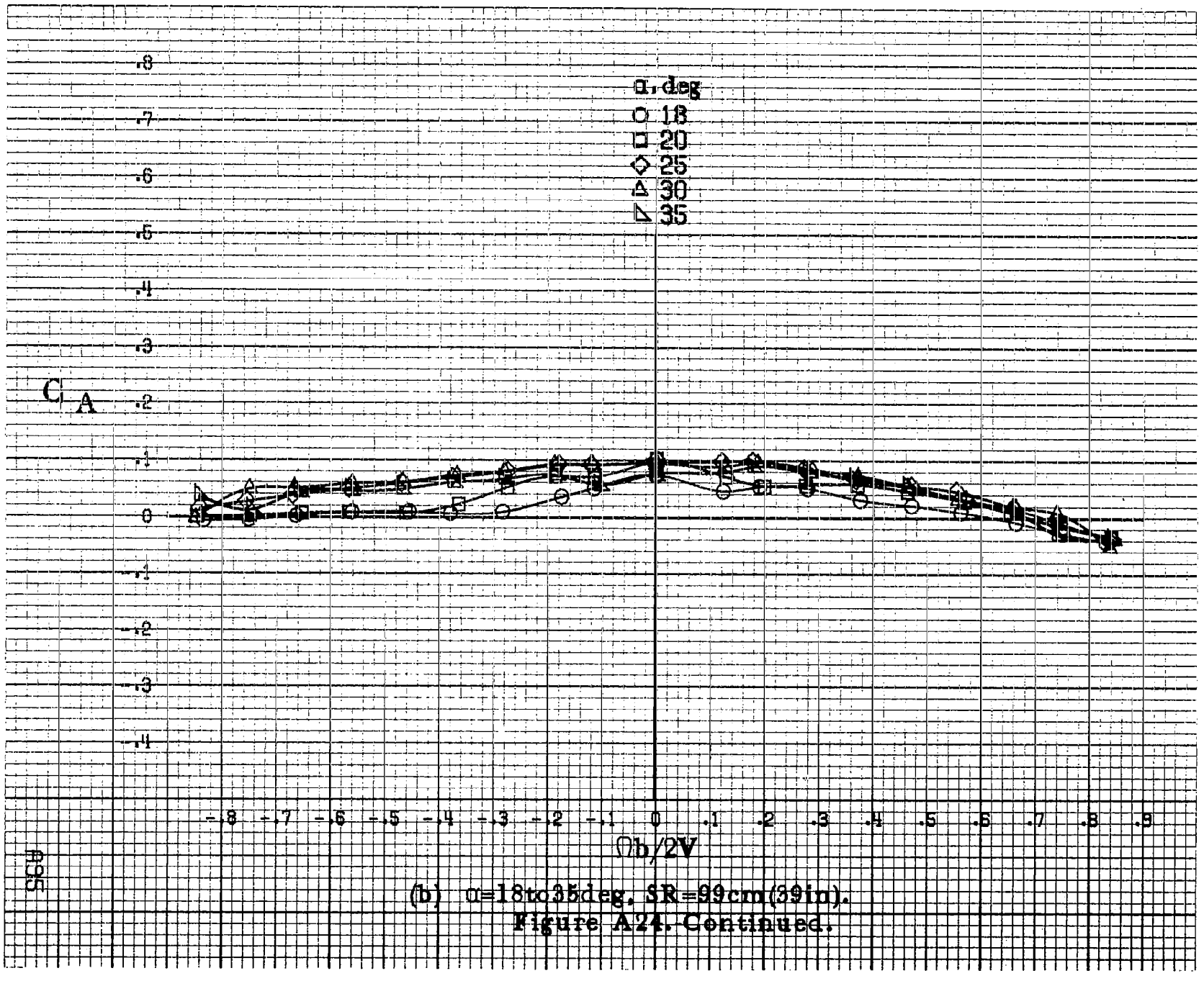

(b) α=18to35deg, SR=99cm(39in).

Figure A24.-Continued.

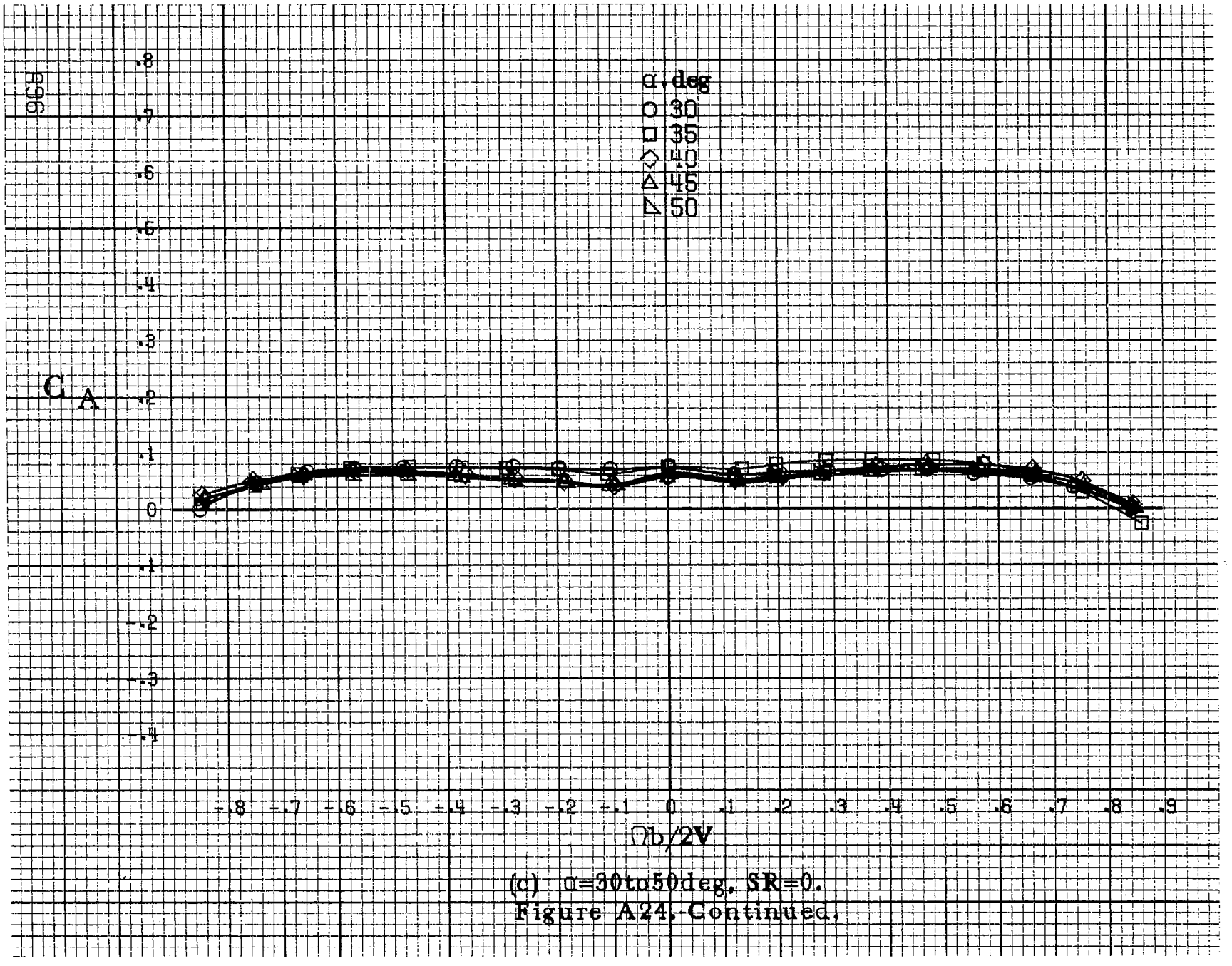

(c) α=30to50deg, SR=0.

Figure A24.-Continued.

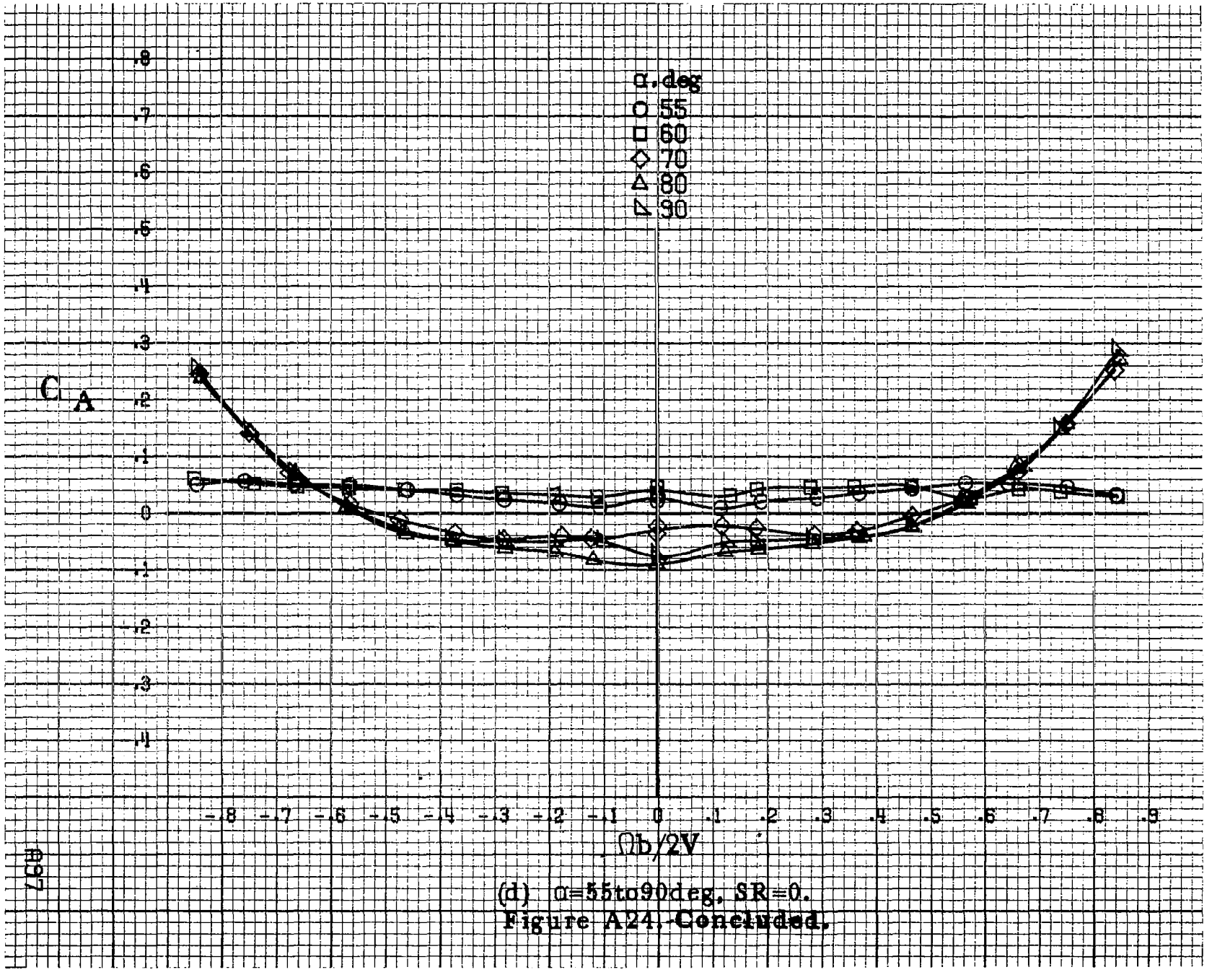

(d) α=55to90deg, SR=0.

Figure A24.-Concluded.

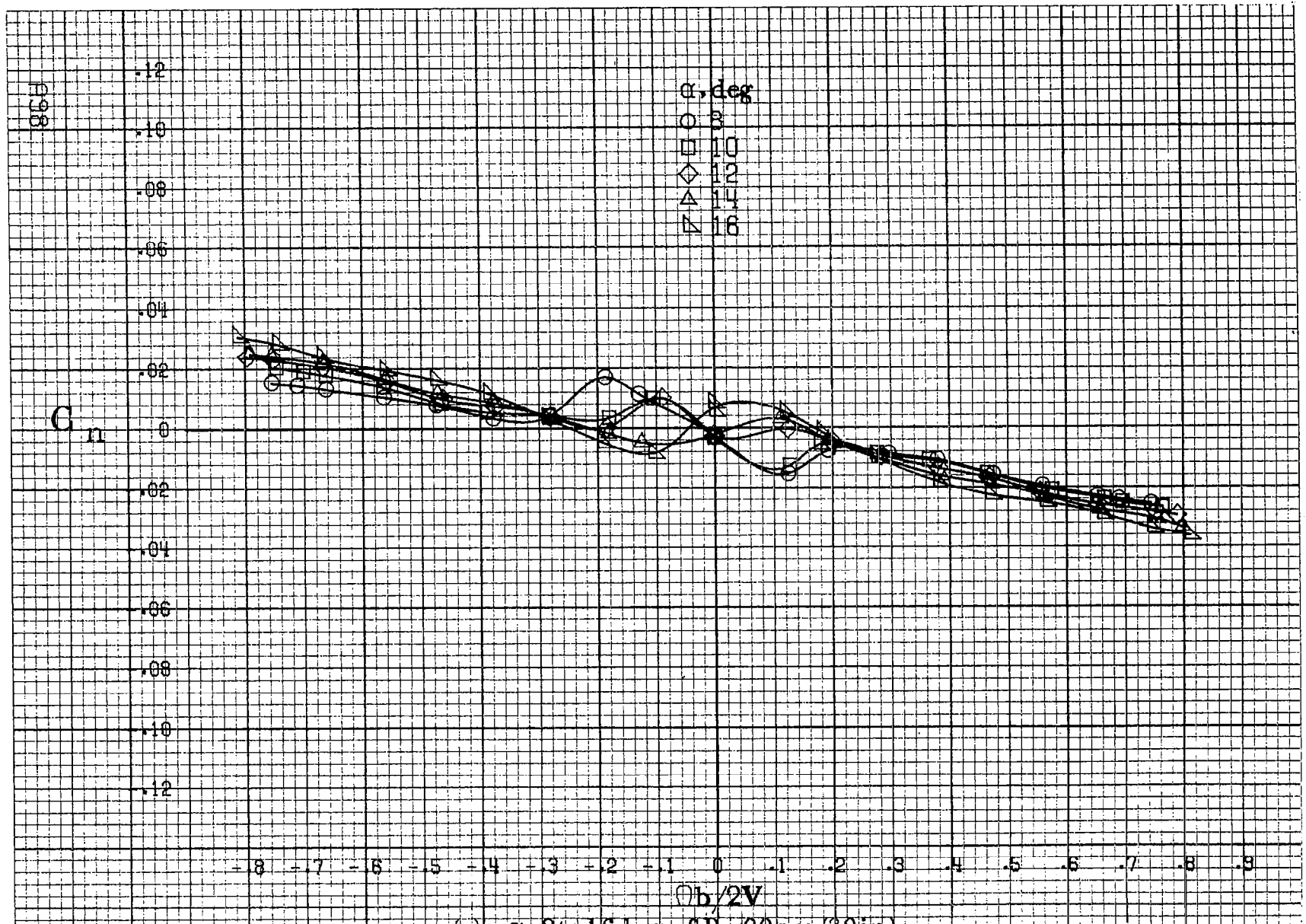

(a) α=8to16deg, SR=99cm(39in).

Figure A25. Effect of rotation rate and angle of attack on yawing-moment coefficient for no. 1 horizontal tail configuration. δ_e ±0°, δ_a ±0°, δ_r ±0°, β ±0°.

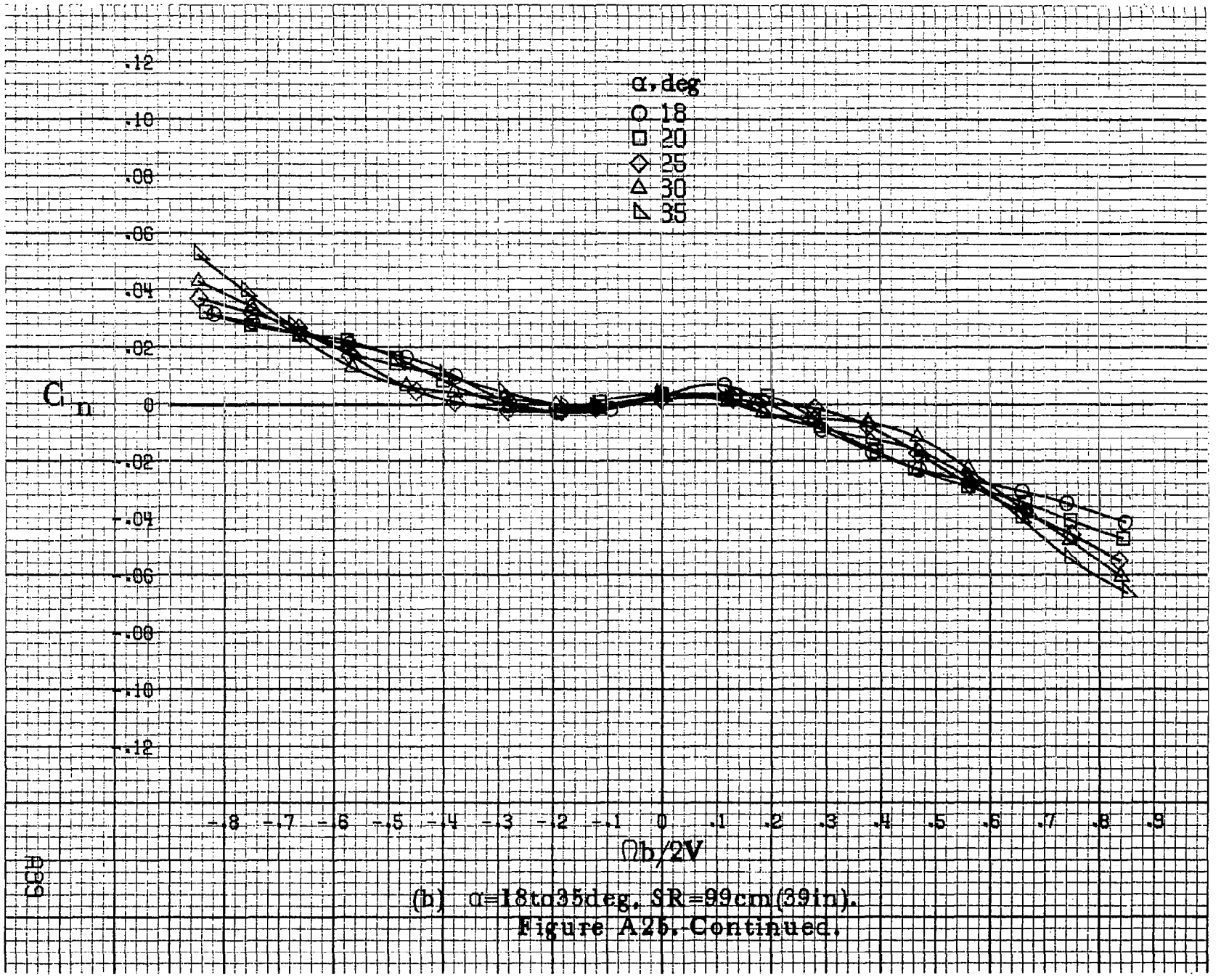

(b) α=18to35deg, SR=99cm(39in).

Figure A26.-Continued.

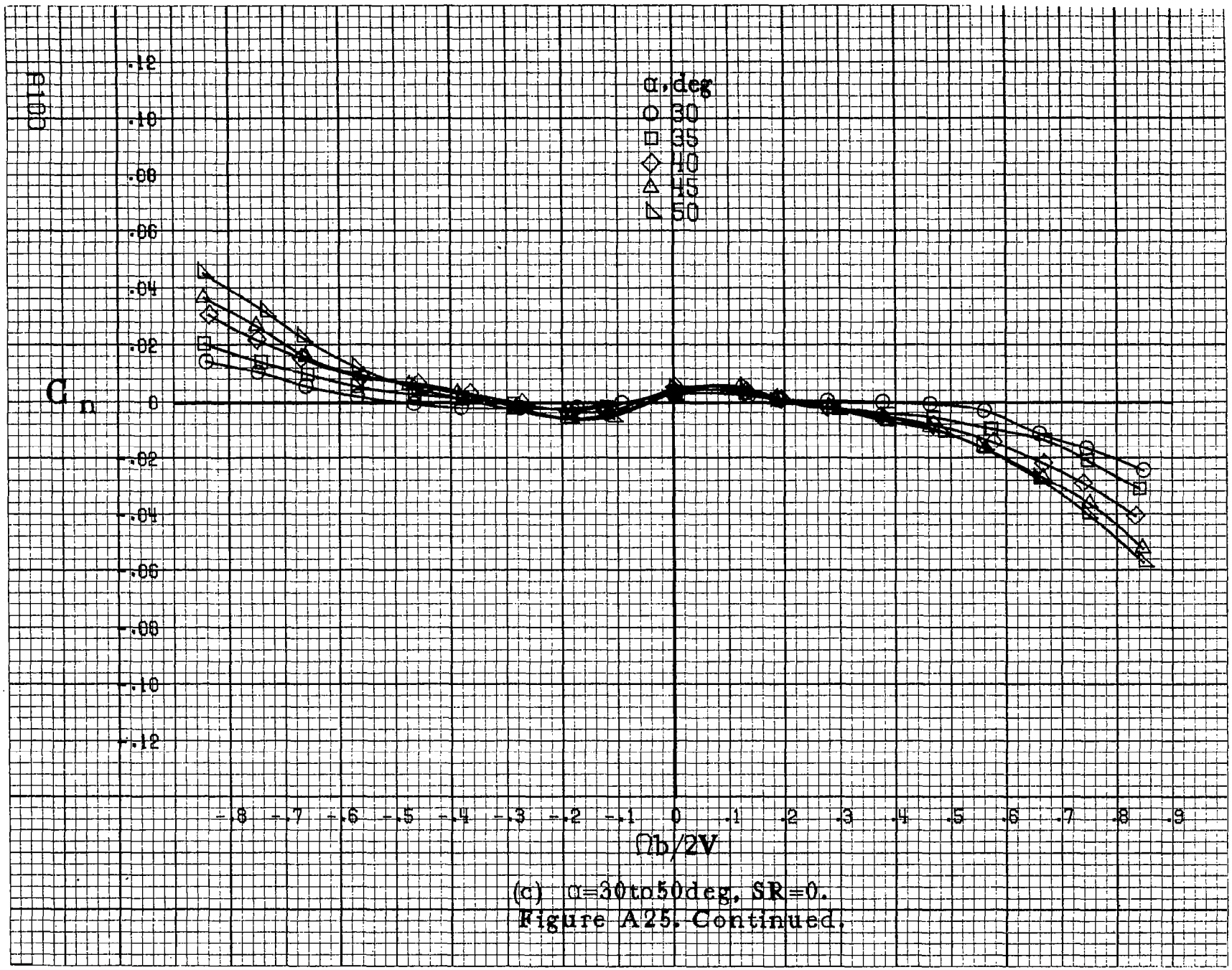

(c) α=30to50deg, SR=0.

Figure A25. Continued.

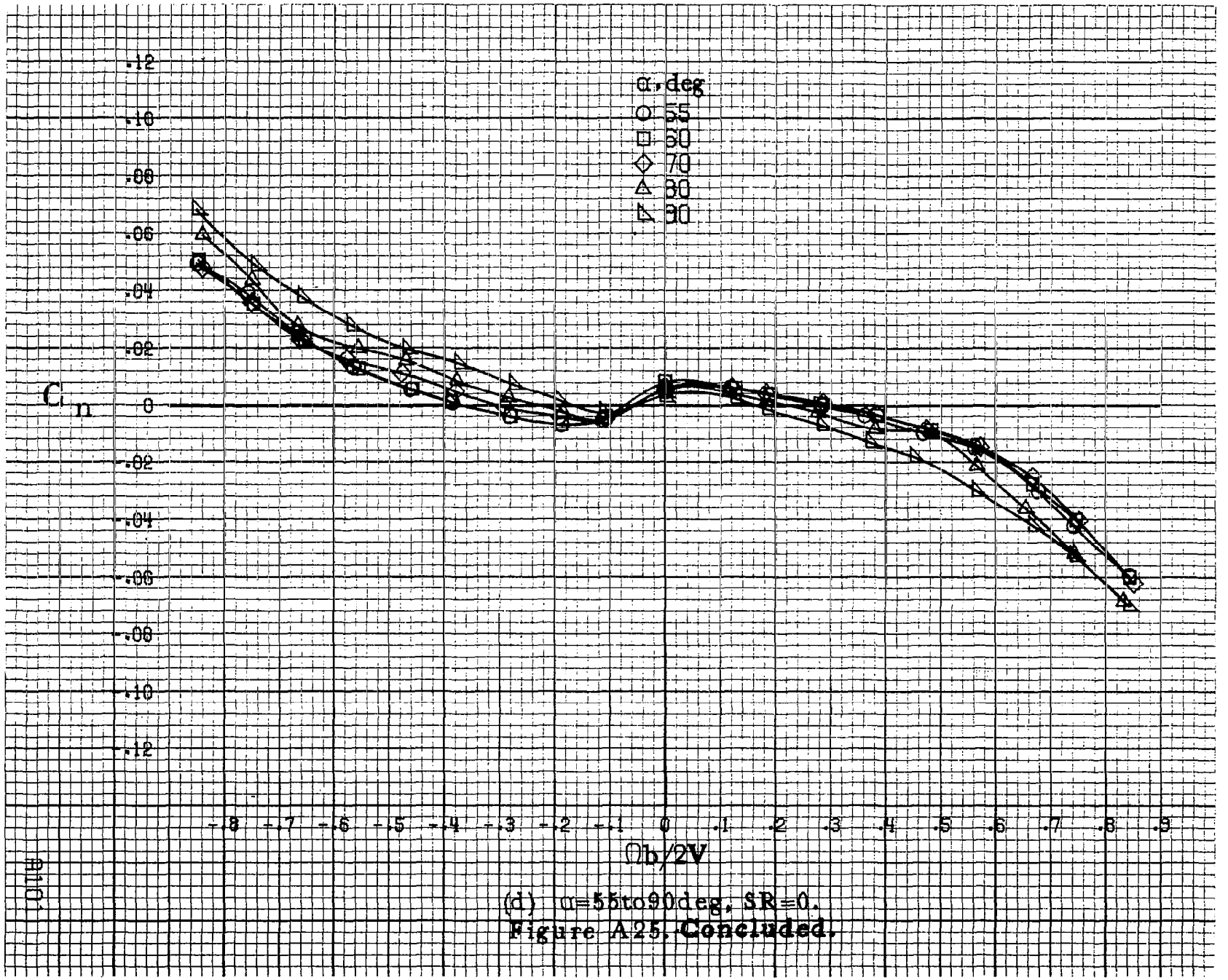

(d) α=55to90deg, SR=0.

Figure A25. Concluded.

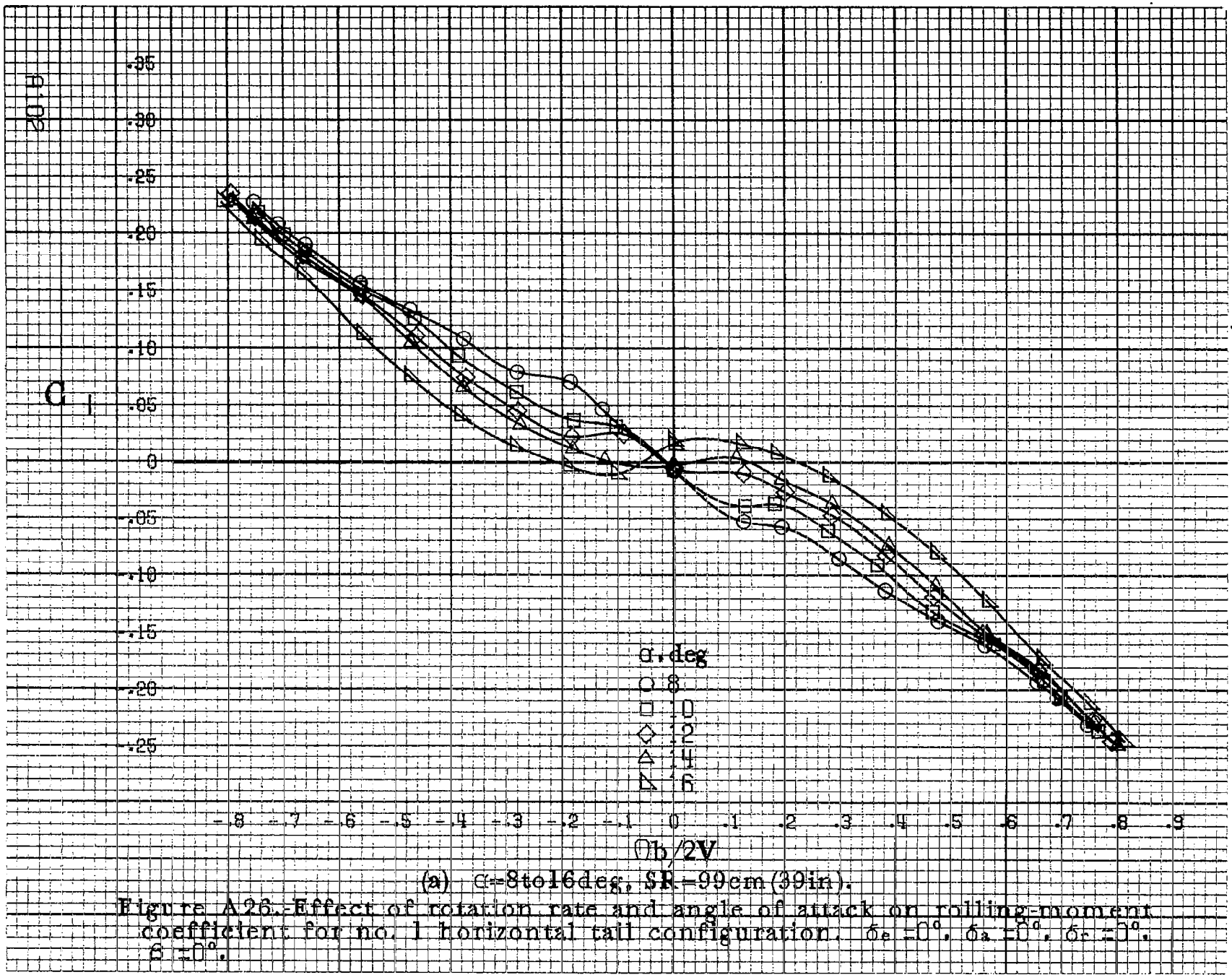

(a) $\alpha = 8$ to 16 deg; SR = 99 cm (39 in).

Figure A26.- Effect of rotation rate and angle of attack on rolling-moment coefficient for no. 1 horizontal tail configuration. $\delta_e = 0°$, $\delta_a = 0°$, $\delta_r = 0°$, $\beta = 0°$.

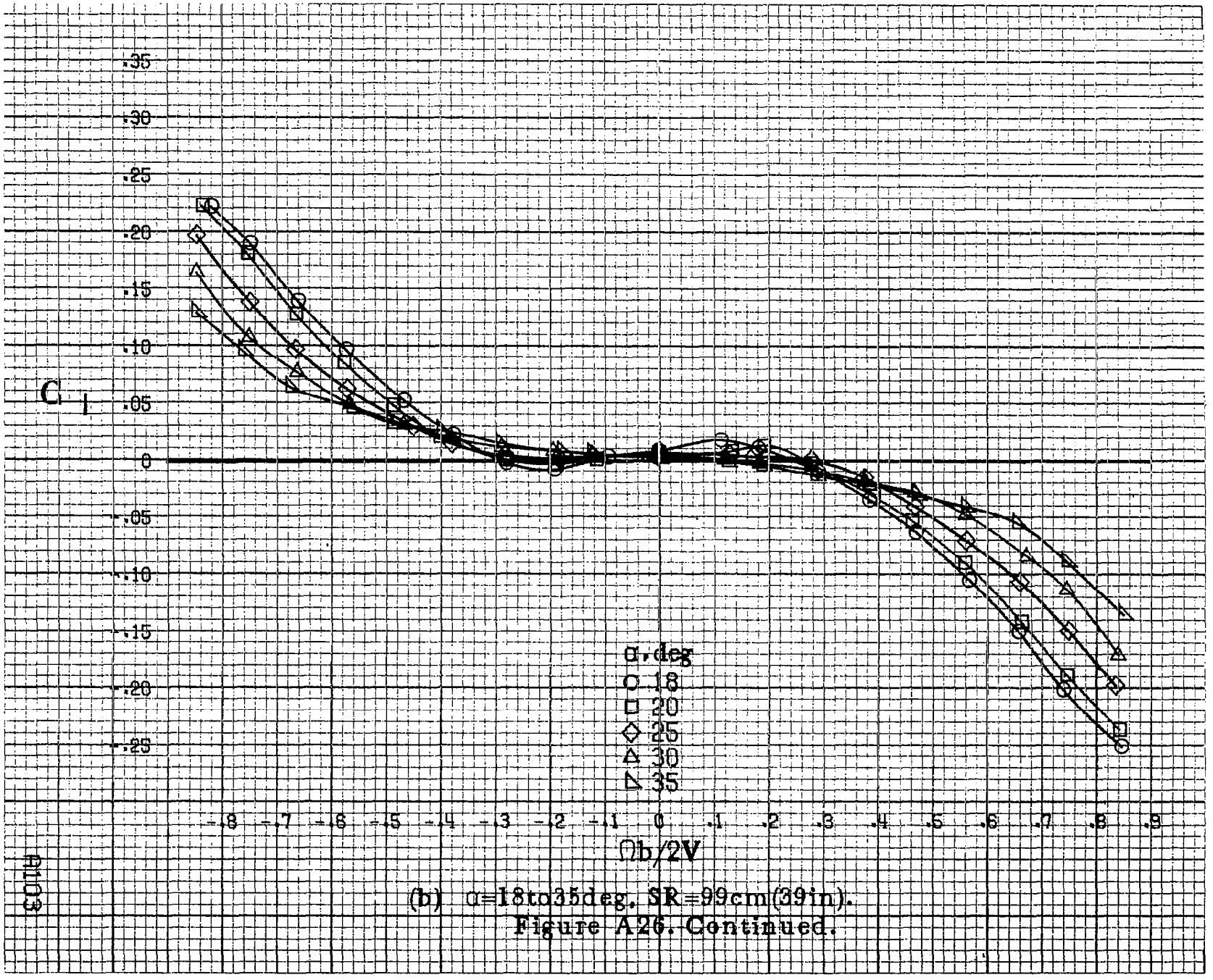

(b) α=18to35deg, SR=99cm(39in).

Figure A26. Continued.

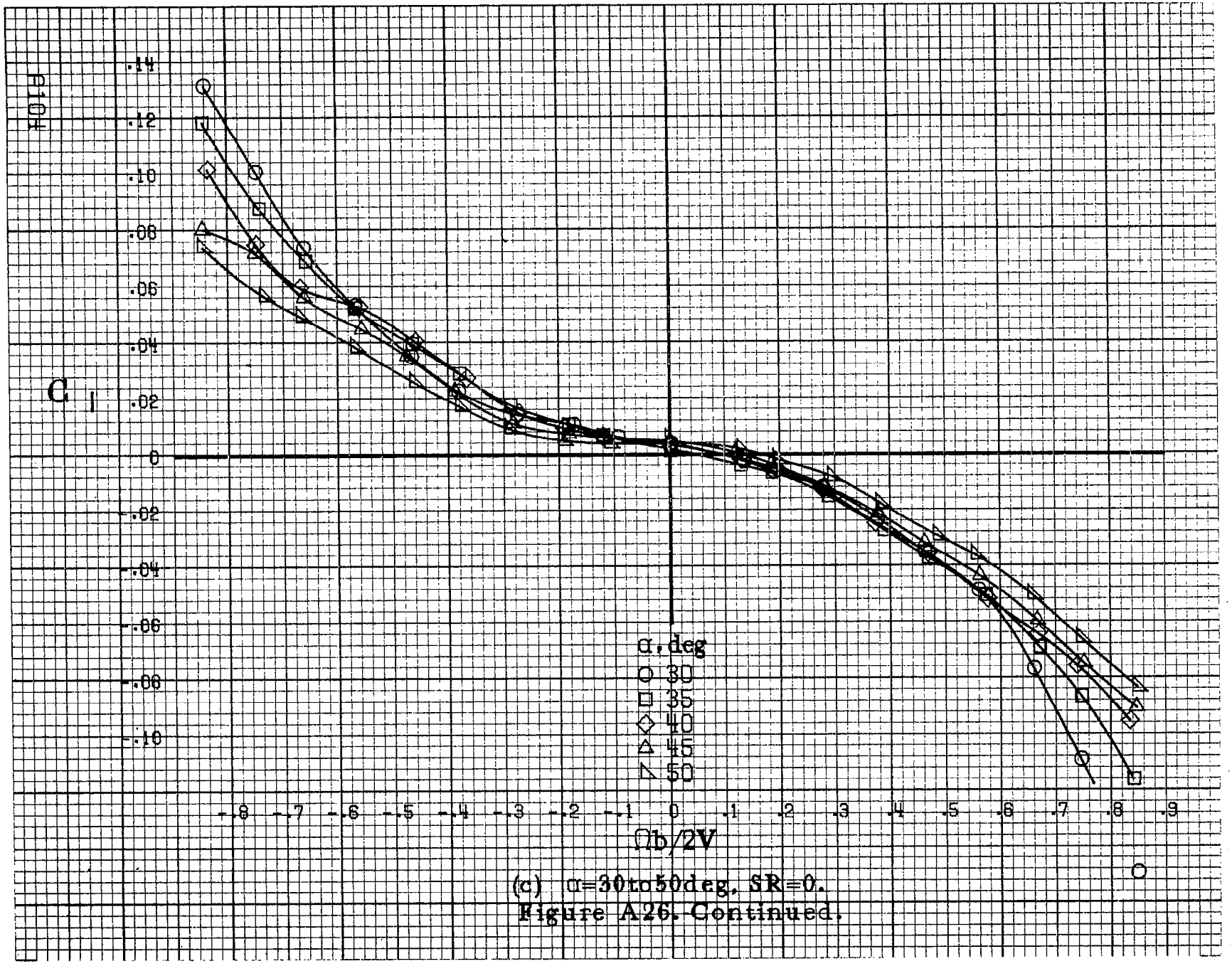

(c) α=30 to 50 deg, SR=0.

Figure A26. Continued.

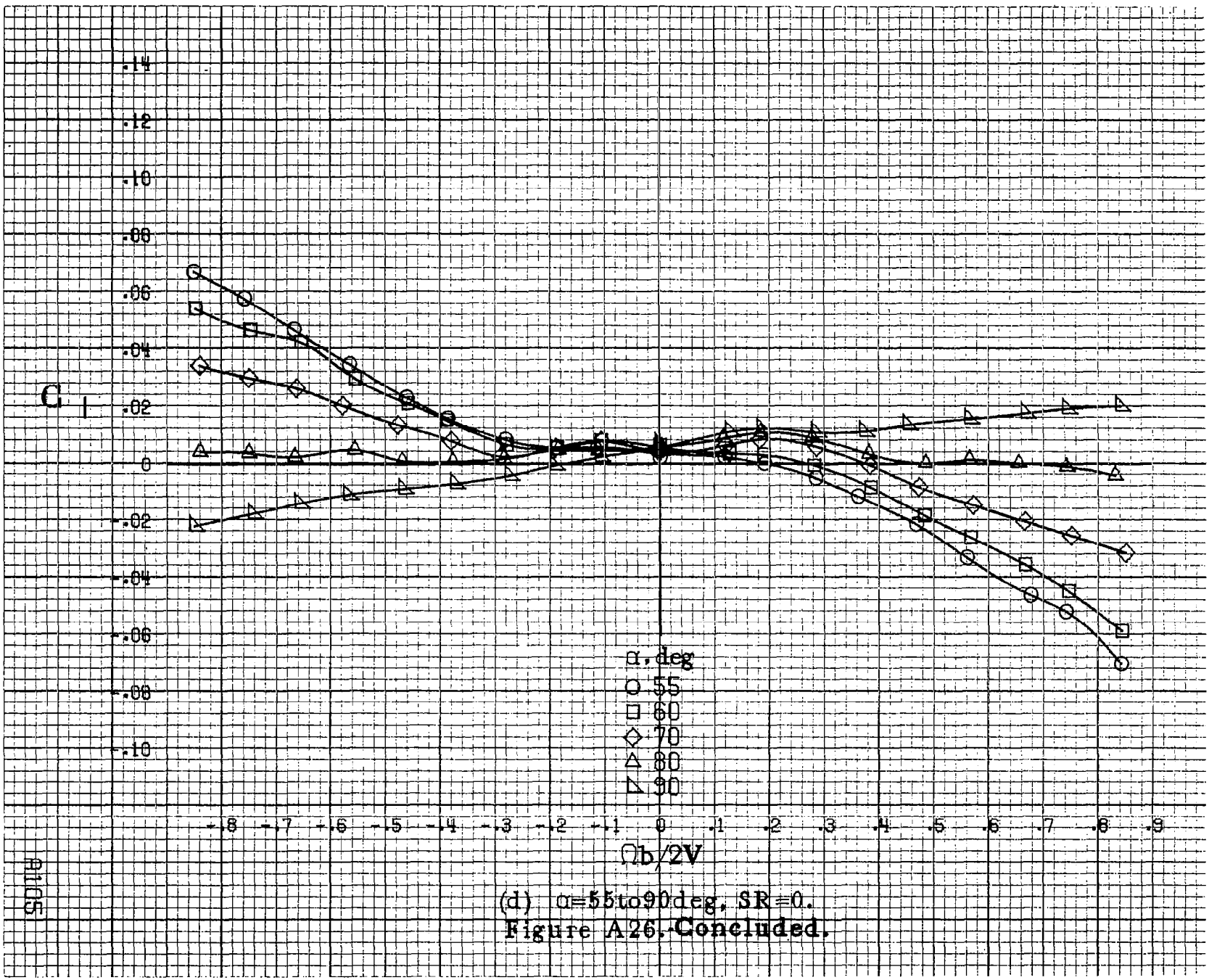

(d) α=55to90deg, SR=0.

Figure A26.-Concluded.

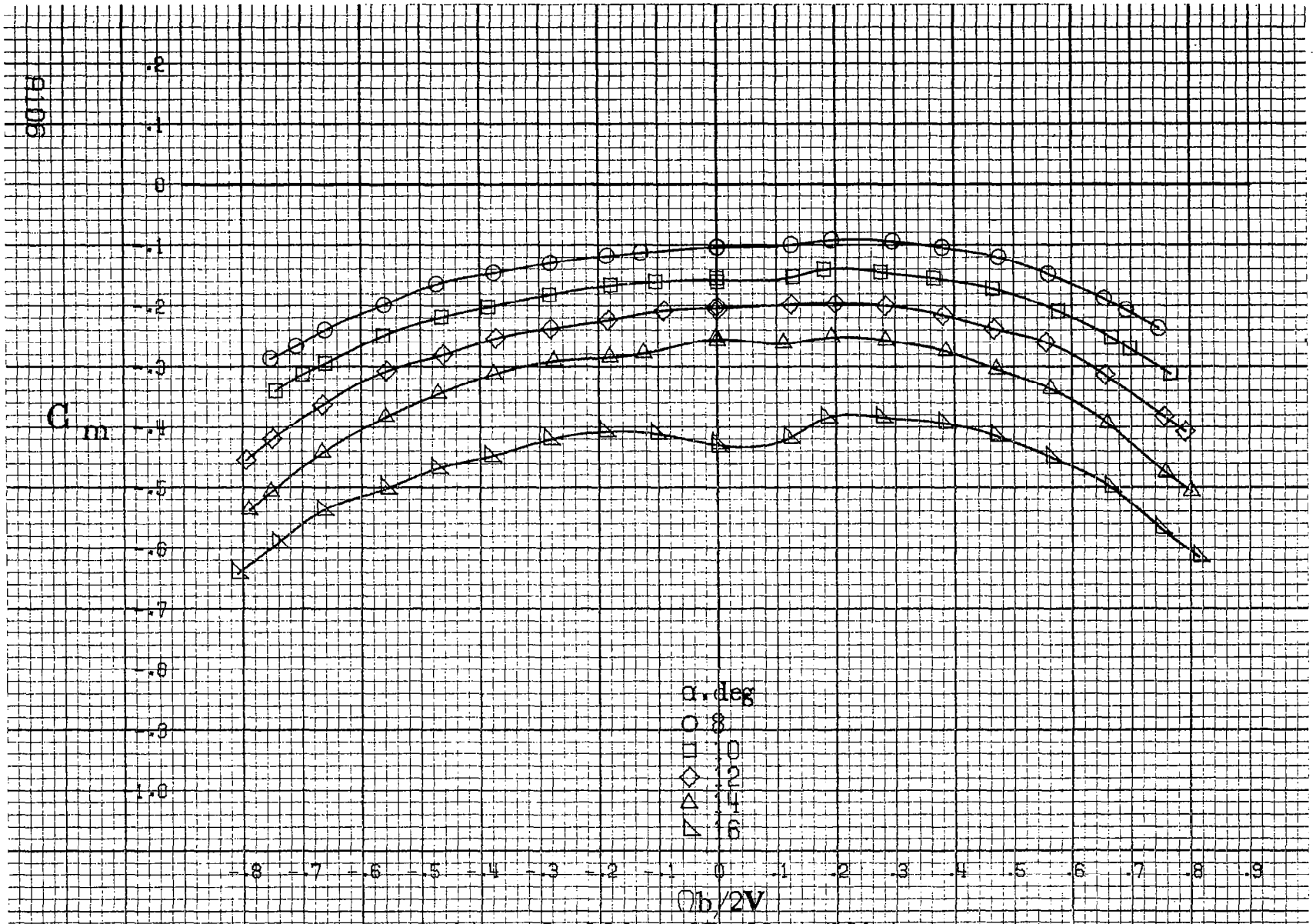

(a) α=8to16deg, SR=99cm(39in).

Figure A27. Effect of rotation rate and angle of attack on pitching-moment coefficient for no. 1 horizontal tail configuration. $\delta_e = 0°$, $\delta_a = 0°$, $\delta_r = 0°$, $\beta = 0°$.

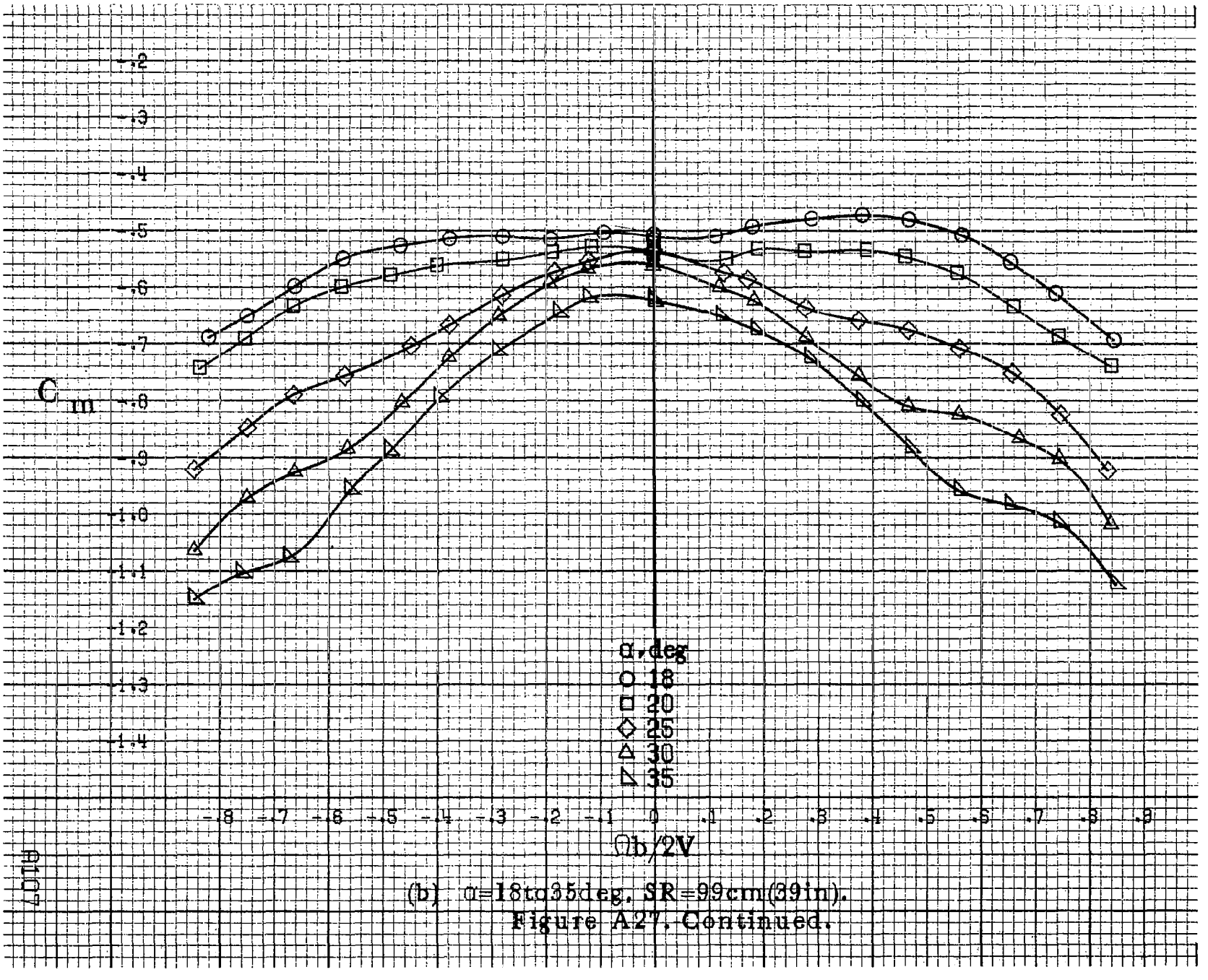

(b) α=18to35deg, SR=99cm(39in).

Figure A27. Continued.

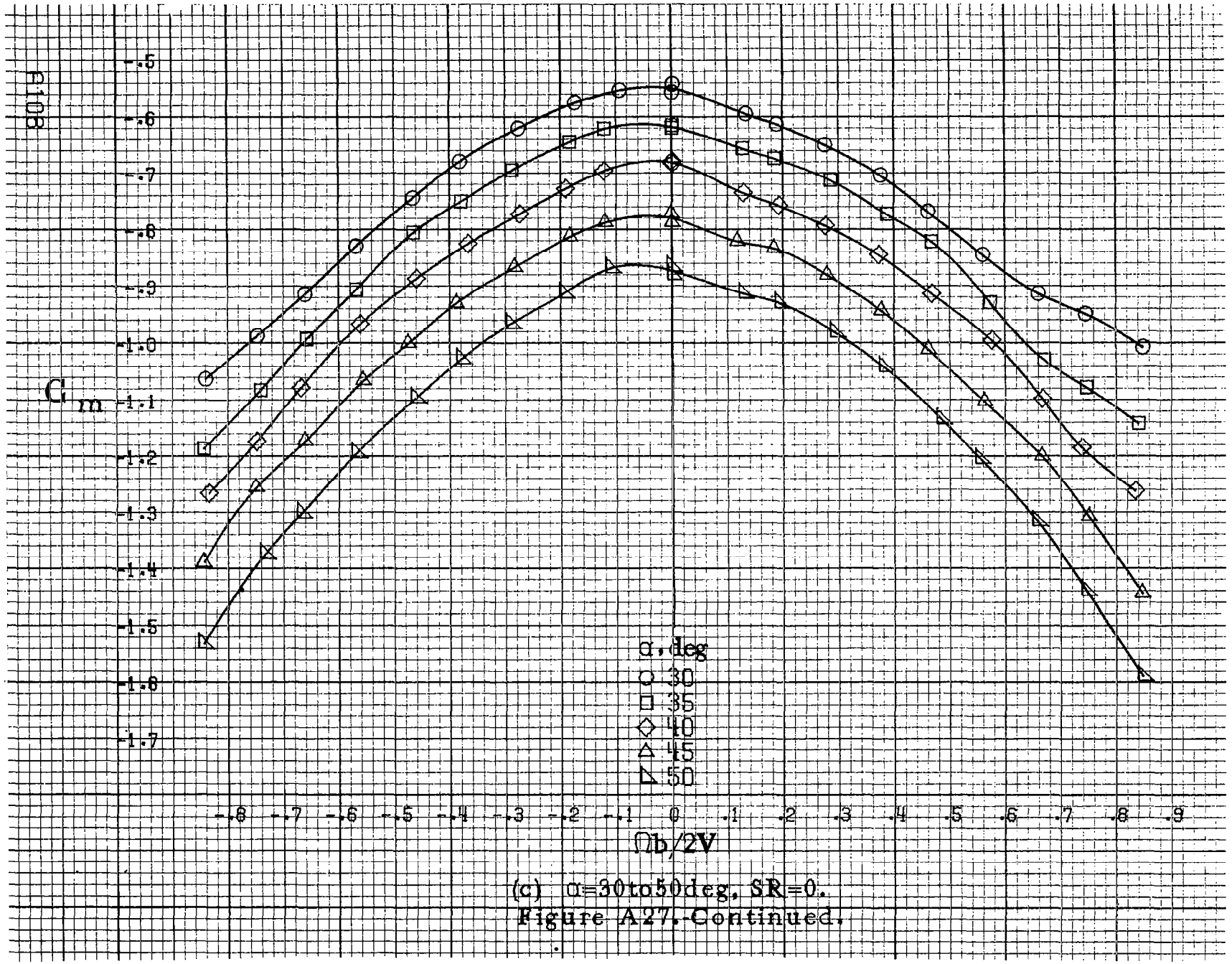

(c) α=30to50deg, SR=0.

Figure A27.-Continued.

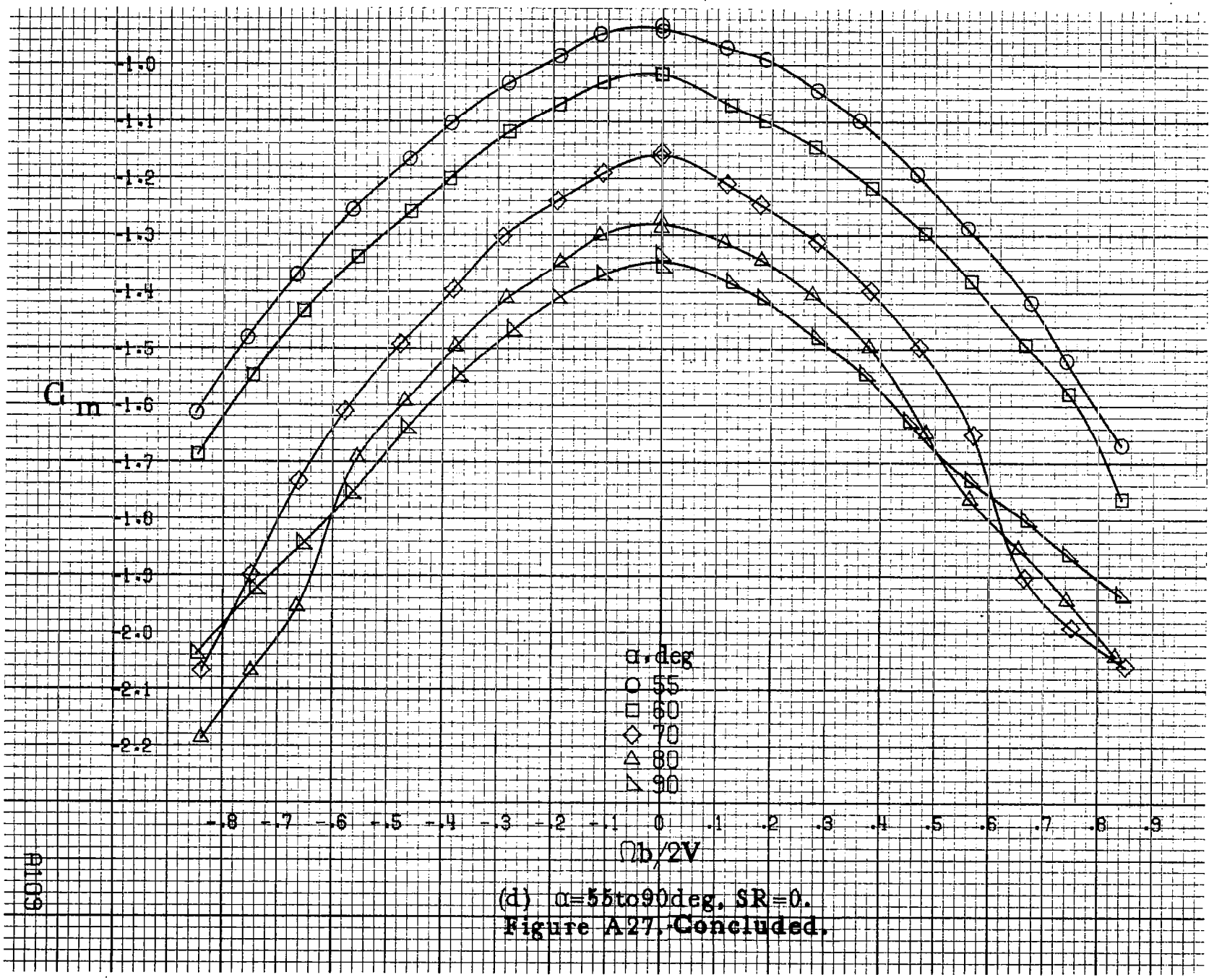

(d) α=55to90deg, SR=0.

Figure A27.-Concluded.

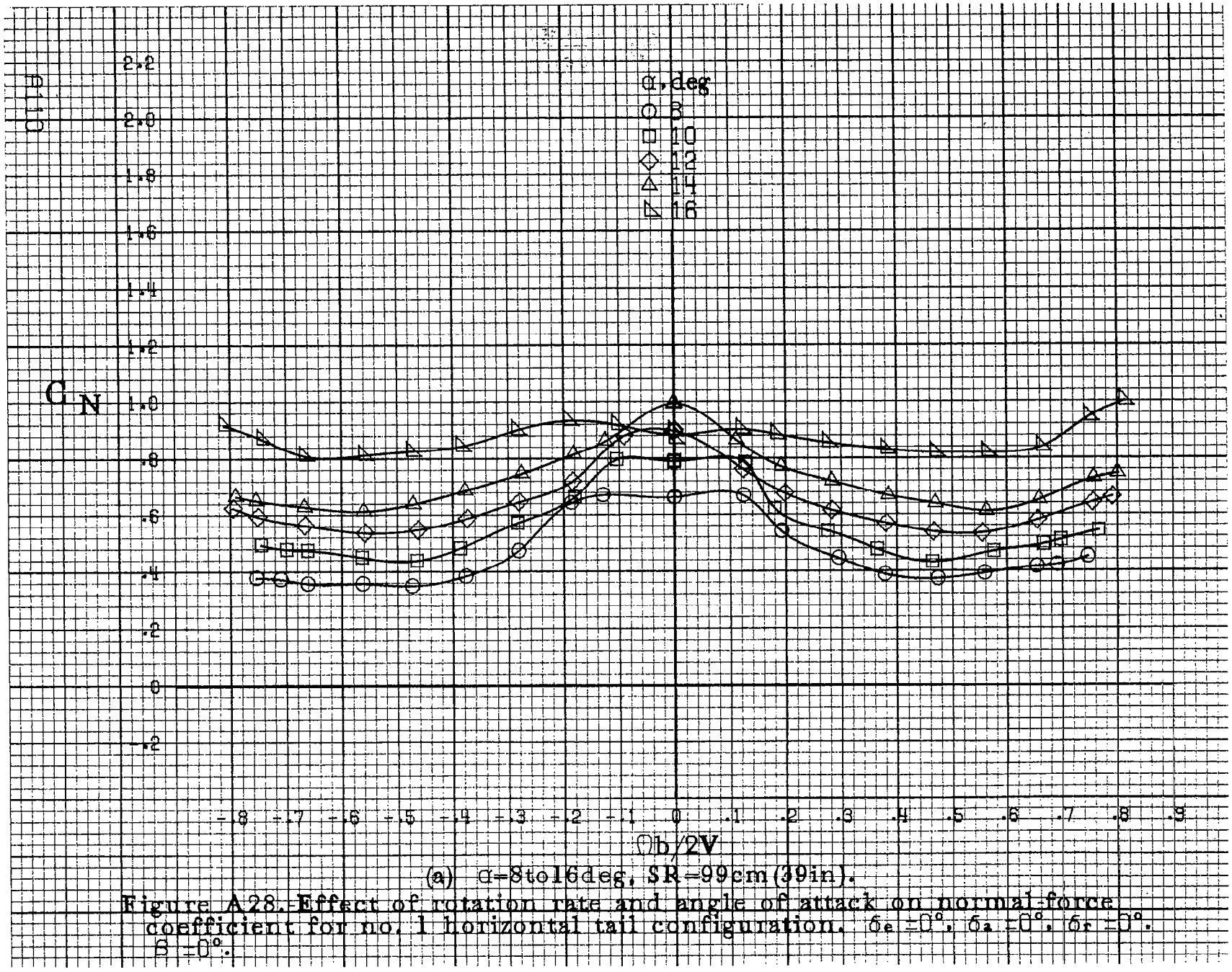

(a) α=8to16deg, SR=99cm(39in).

Figure A28.- Effect of rotation rate and angle of attack on normal-force coefficient for no. 1 horizontal tail configuration. $\delta_e = 0°$, $\delta_a = 0°$, $\delta_r = 0°$, $\beta = 0°$.

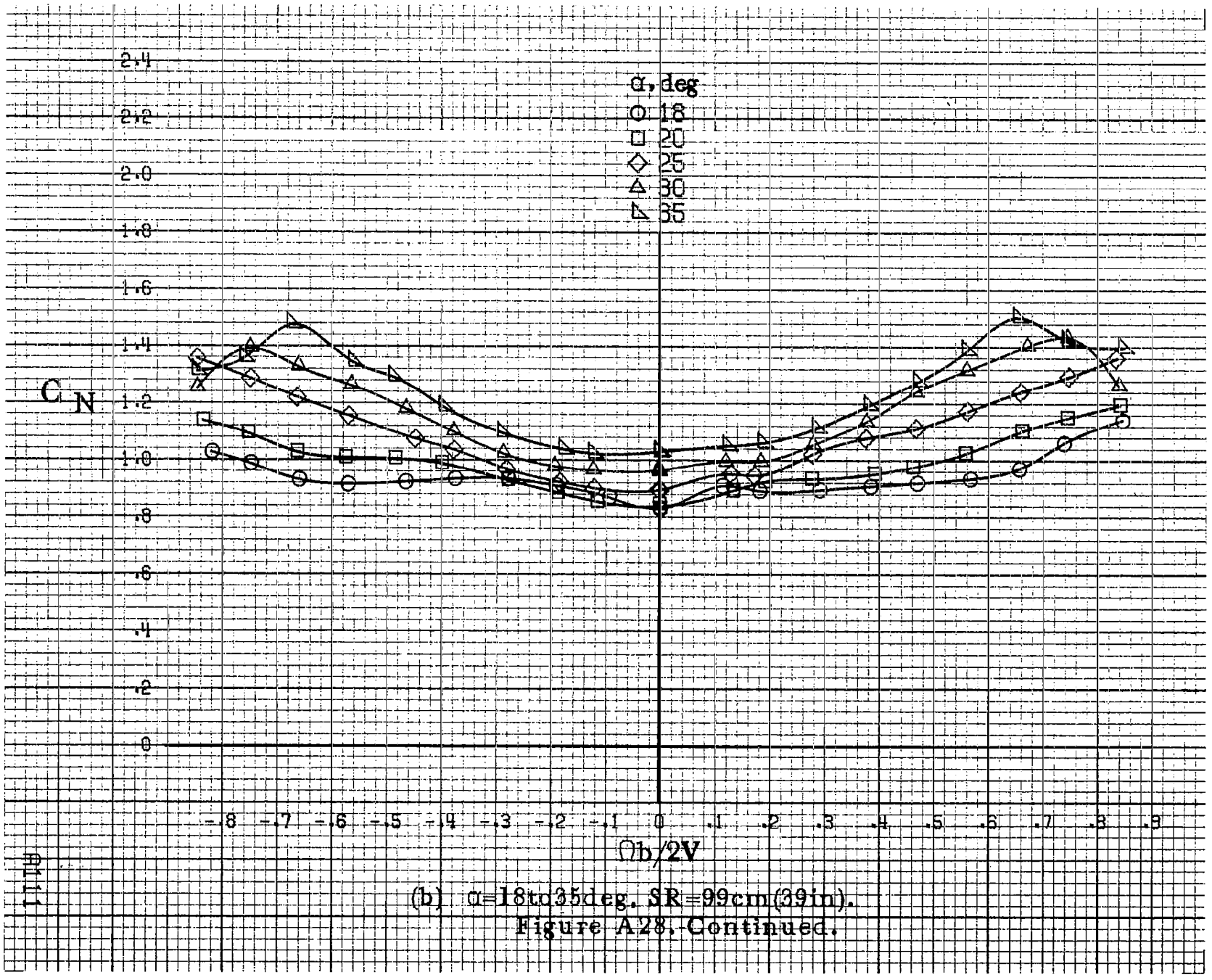

(b) α=18to35deg, SR=99cm(39in).

Figure A28. Continued.

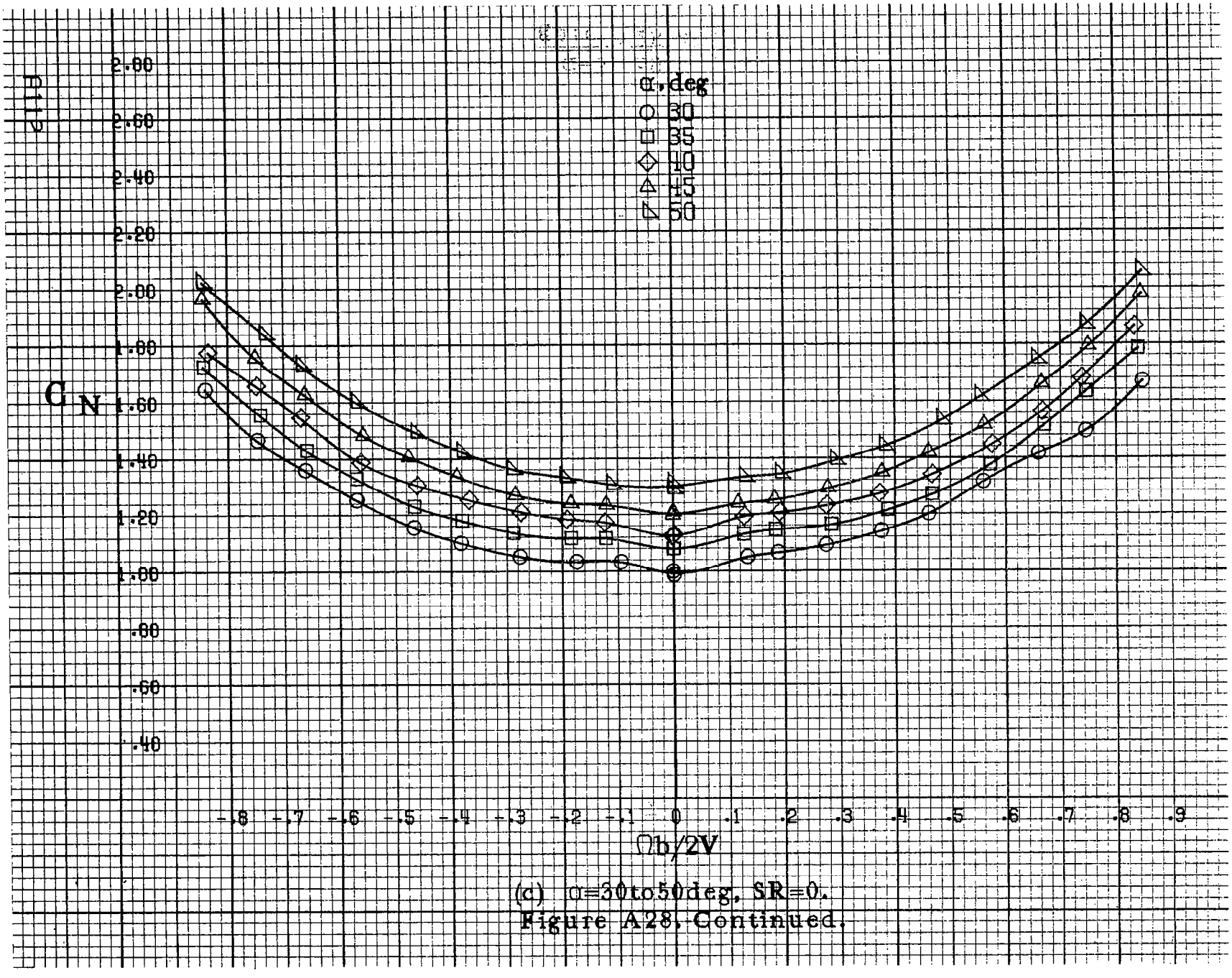

(c) α=30to50deg, SR=0.

Figure A28. Continued.

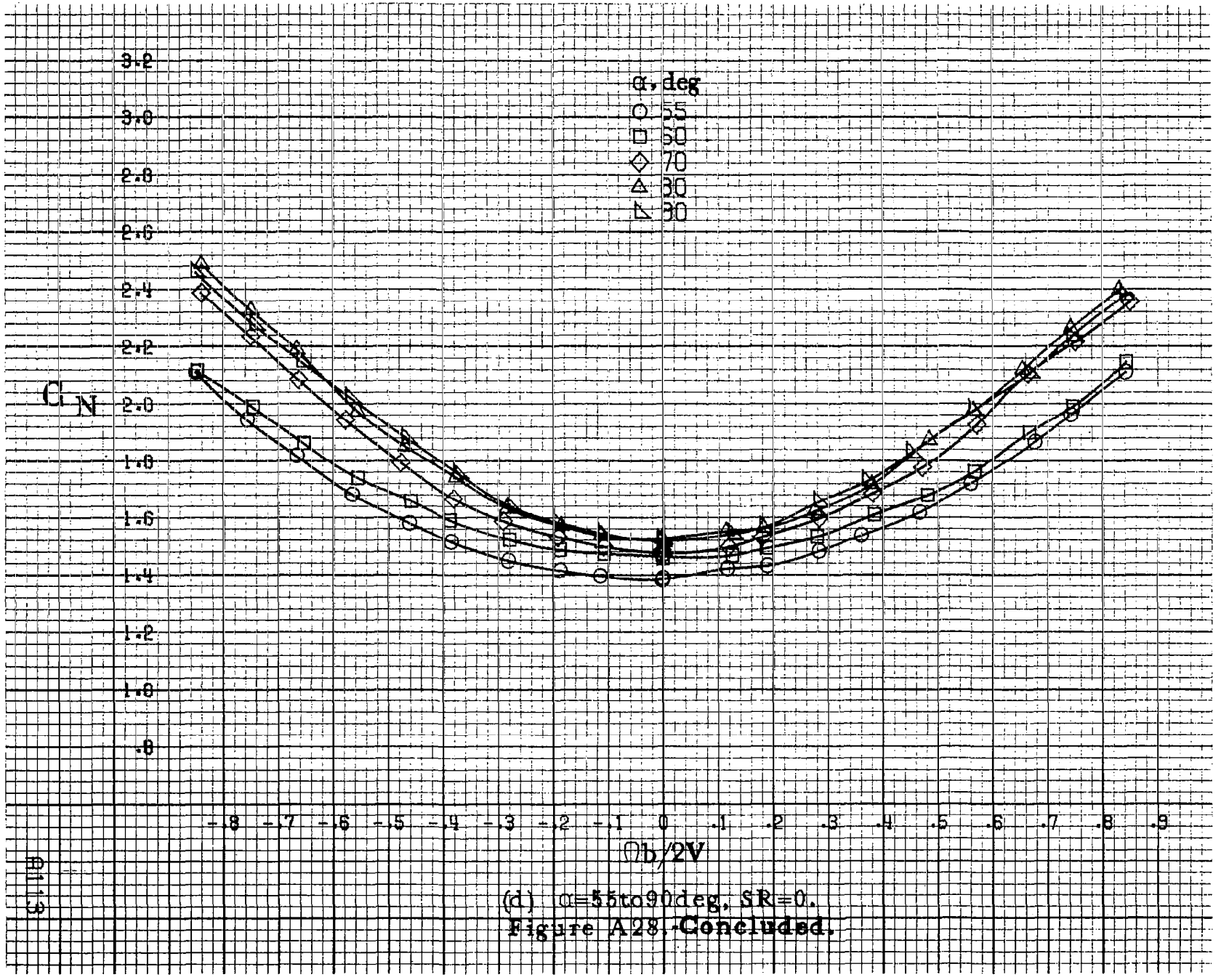

(d) α=55 to 90 deg, SR=0.

Figure A28.-Concluded.

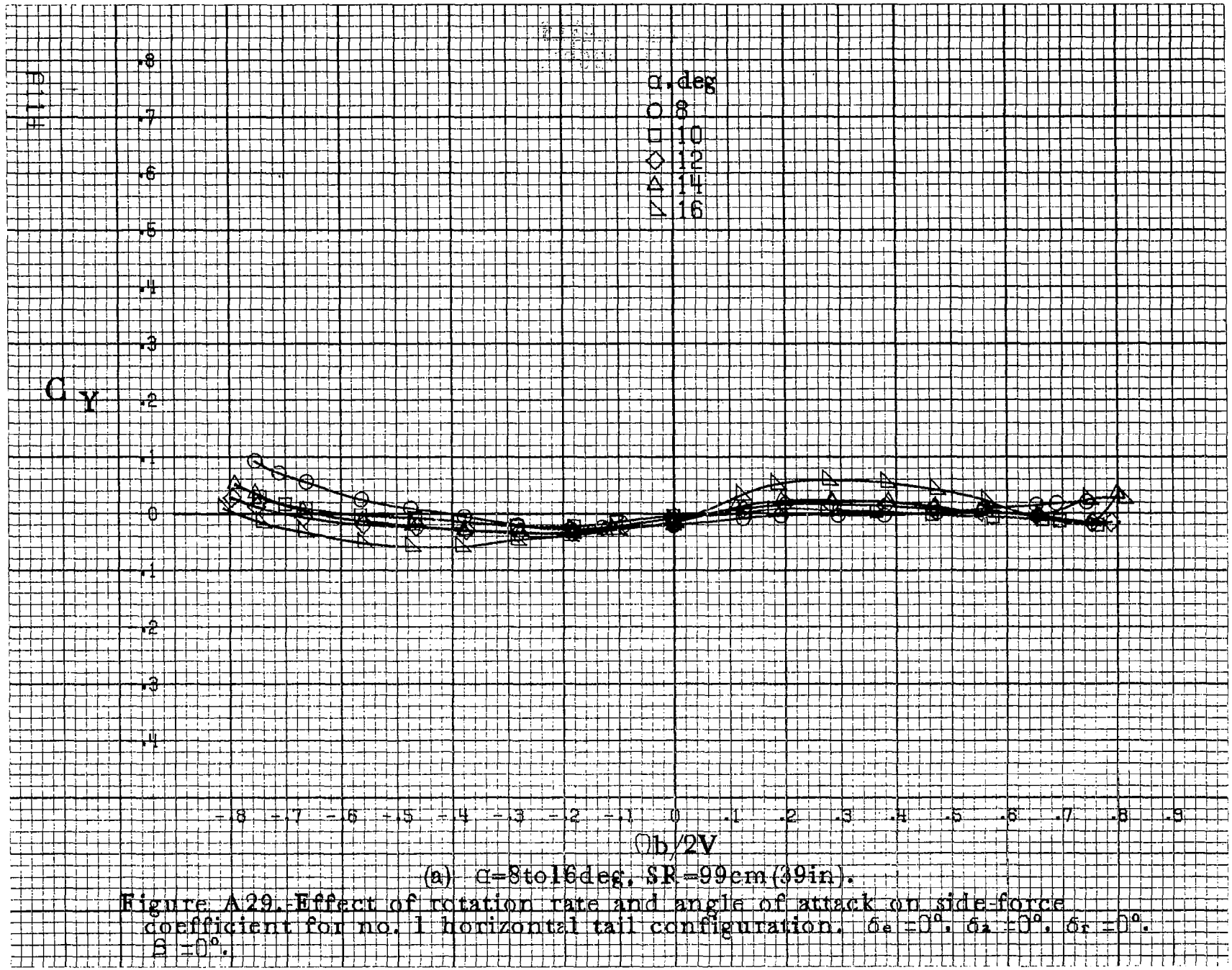

(a) α=8to16deg, SR=99cm(39in).

Figure A29.-Effect of rotation rate and angle of attack on side-force coefficient for no. 1 horizontal tail configuration. $\delta_e = 0°$, $\delta_a = 0°$, $\delta_r = 0°$, $\beta = 0°$.

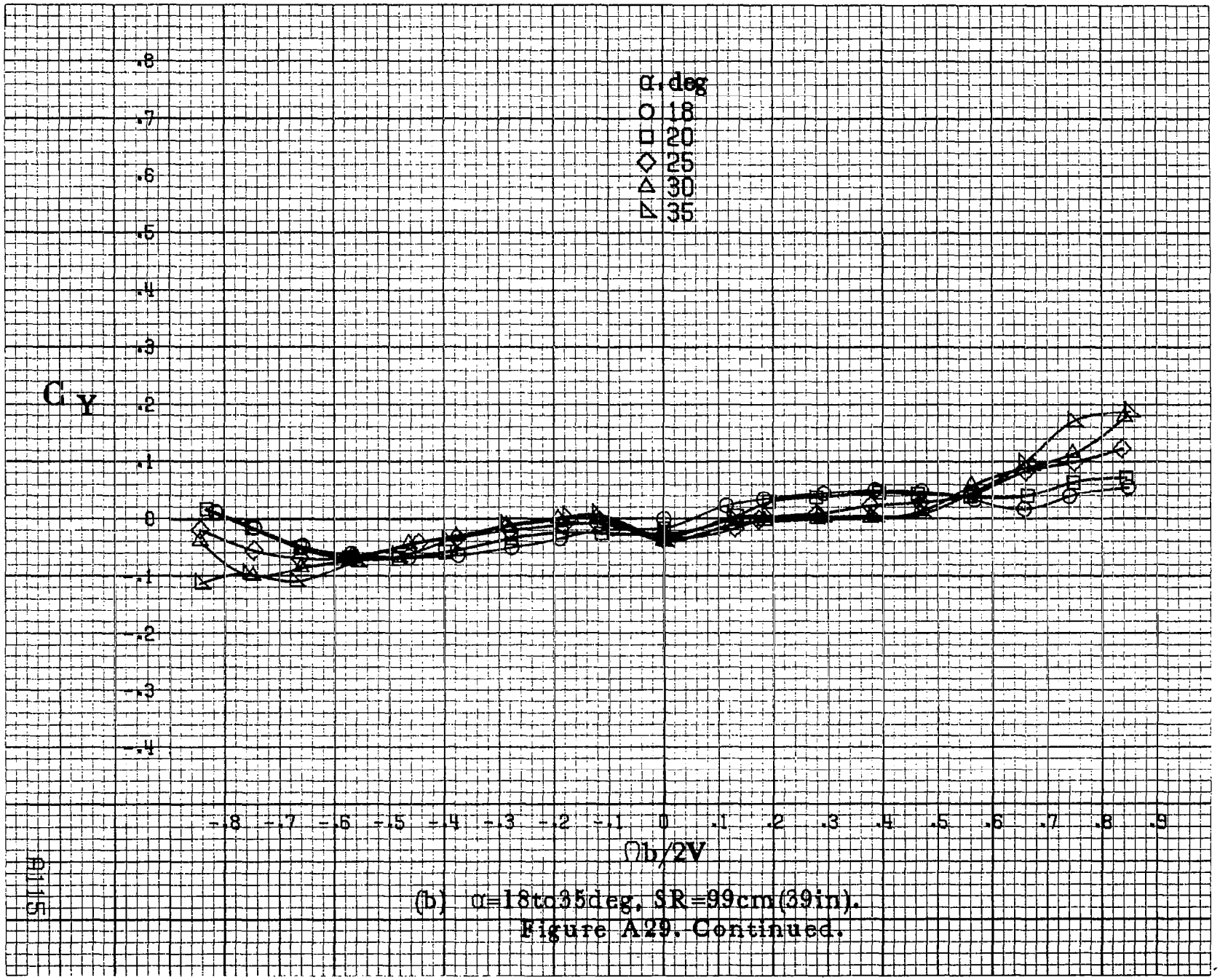

(b) α=18to35deg, SR=99cm(39in).

Figure A29. Continued.

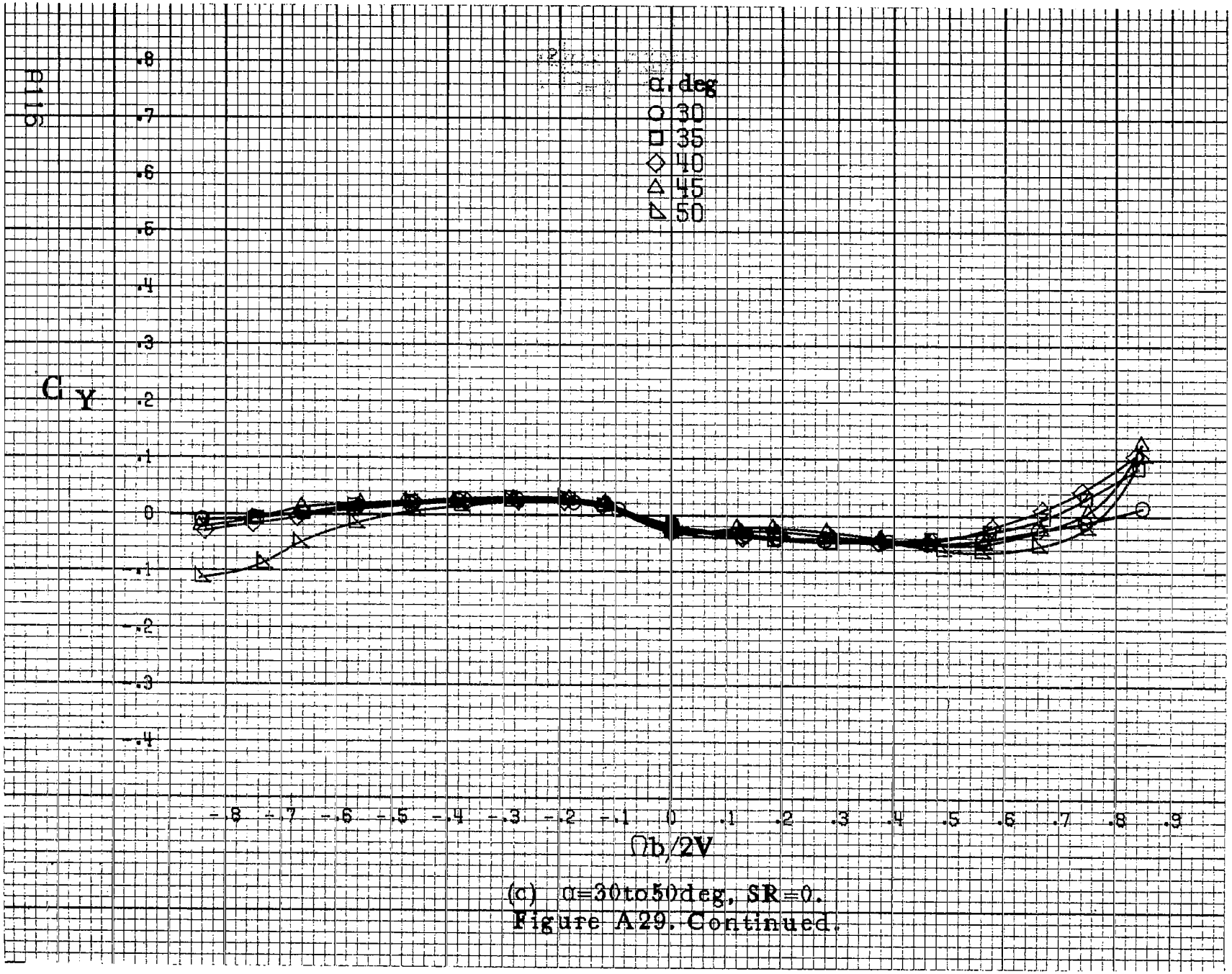

(c) α=30 to 50 deg, SR=0.

Figure A29. Continued.

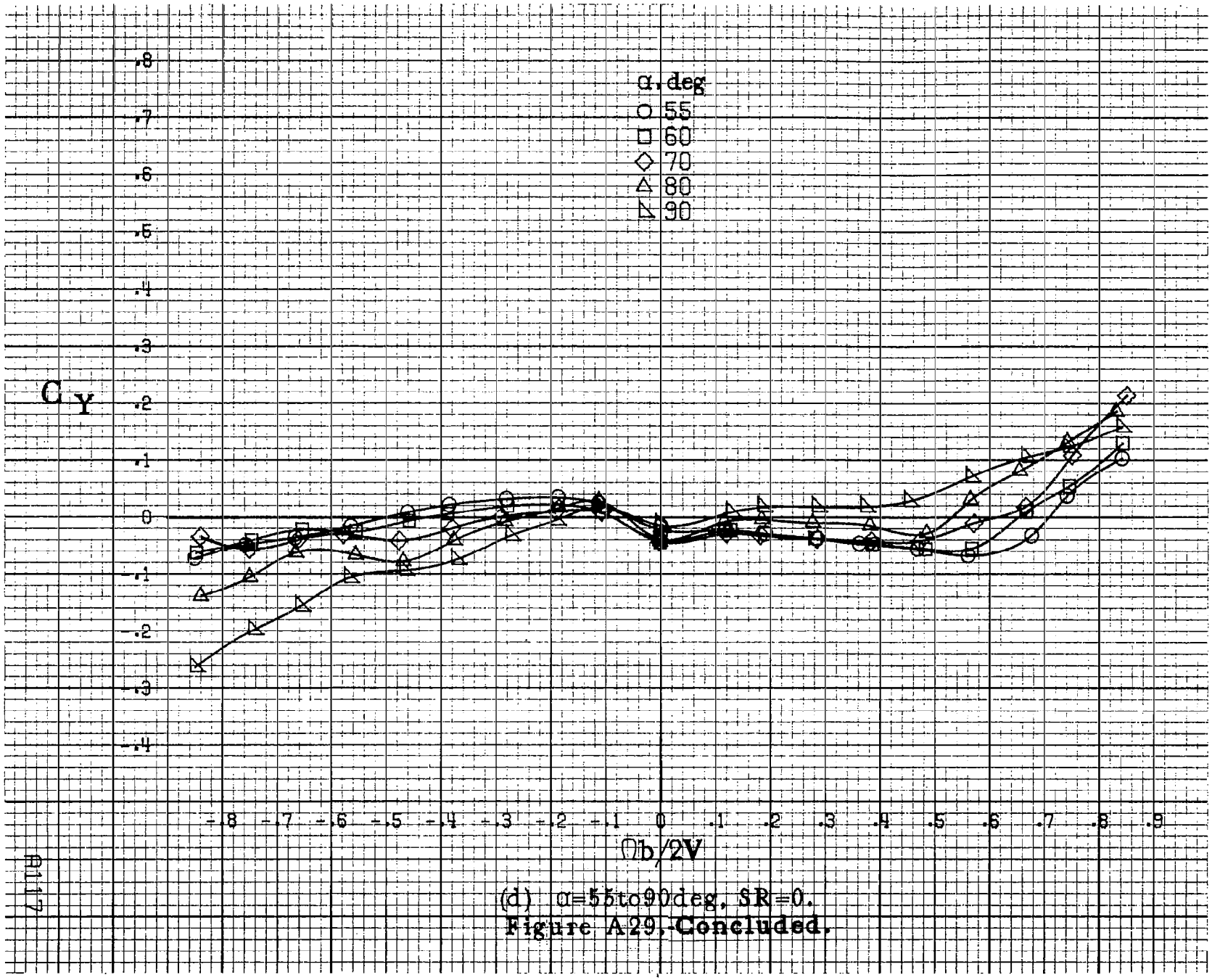

(d) α=55to90deg, SR=0.

Figure A29. Concluded.

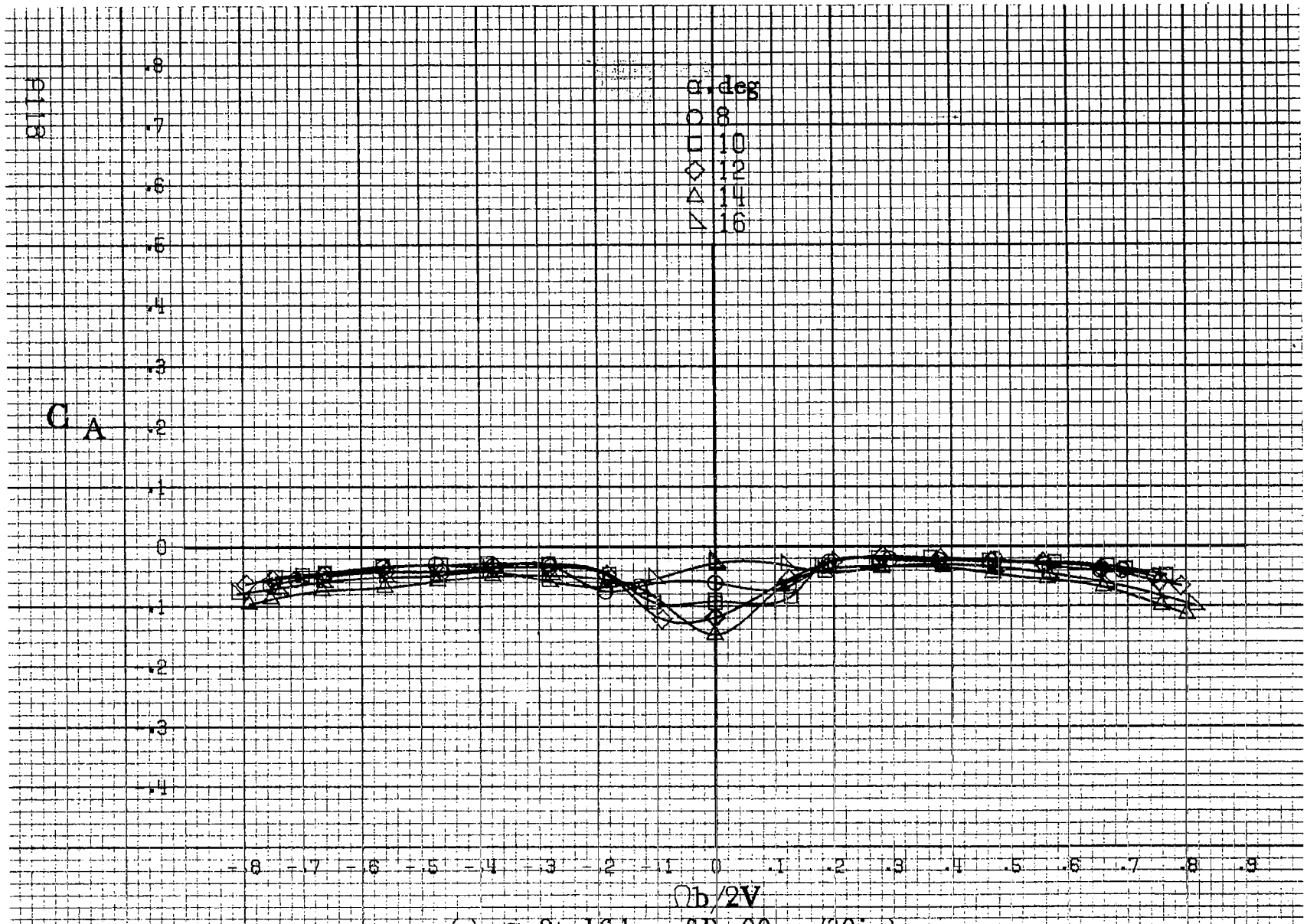

(a) α=8to16deg, SR=99cm(39in).

Figure A30.- Effect of rotation rate and angle of attack on axial-force coefficient for no. 1 horizontal tail configuration. $\delta_e = 0°$, $\delta_a = 0°$, $\delta_r = 0°$, $\beta = 0°$.

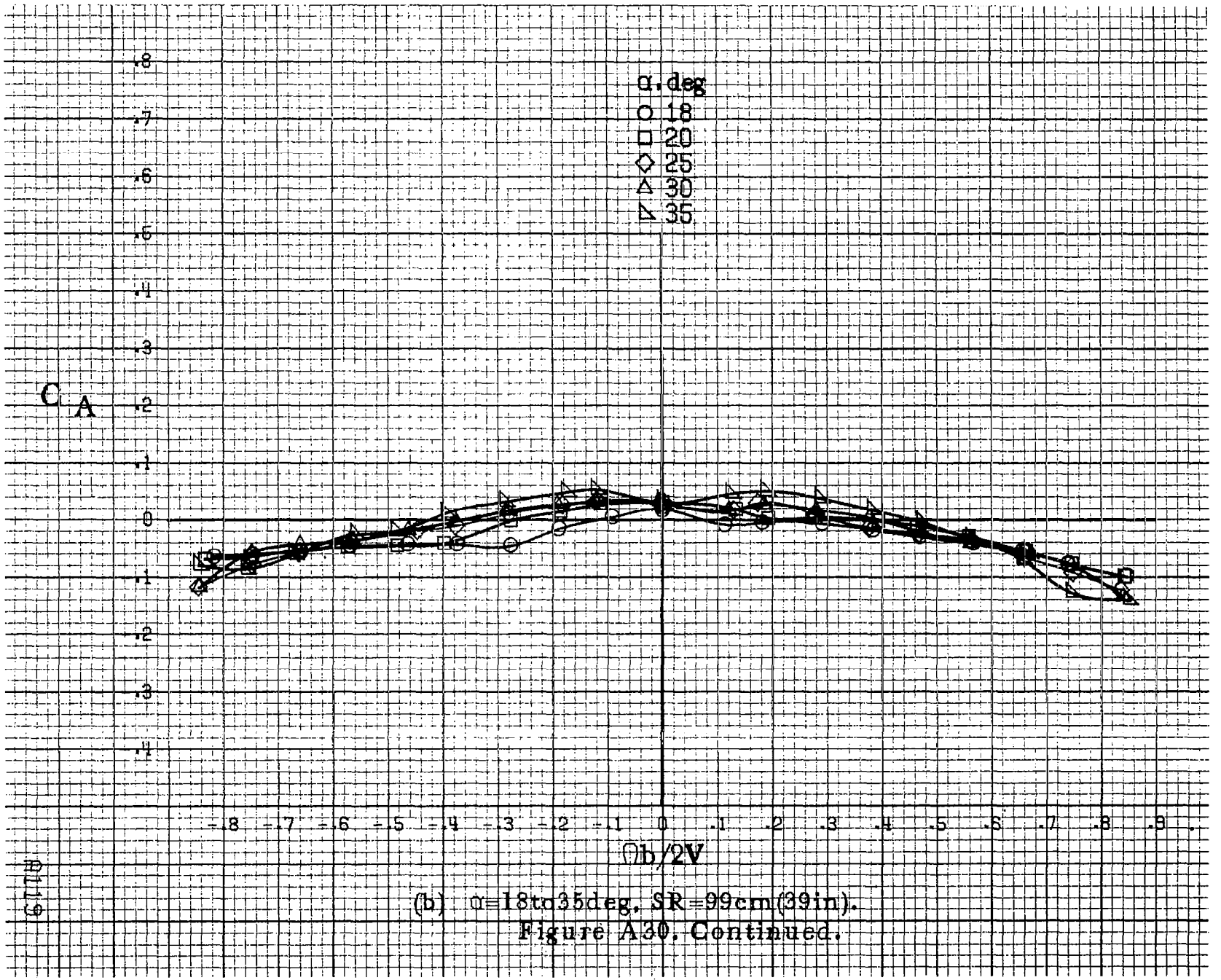

(b) α=18to35deg, SR=99cm(39in).

Figure A30. Continued.

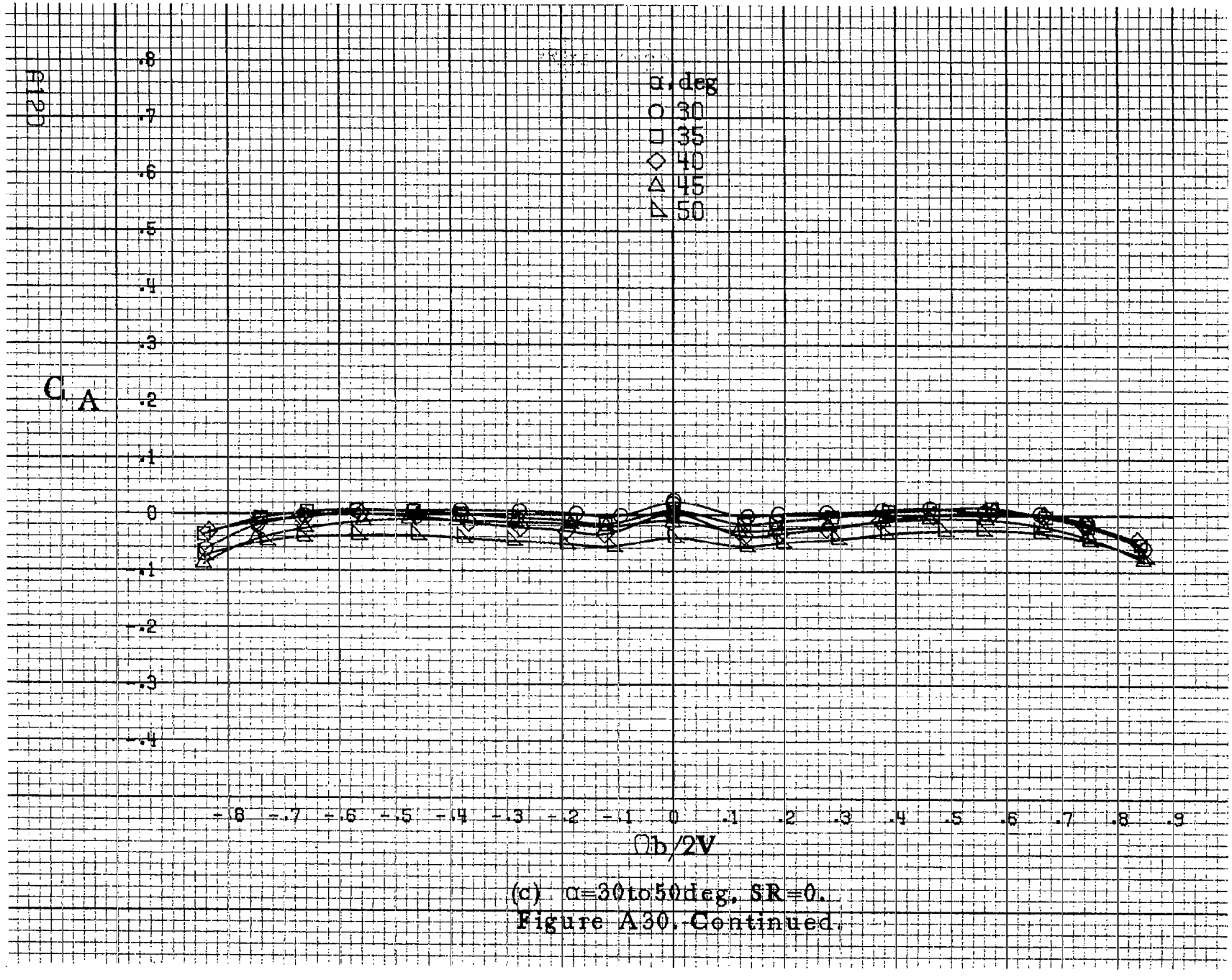

(c) α=30 to 50 deg, SR=0.

Figure A30. Continued.

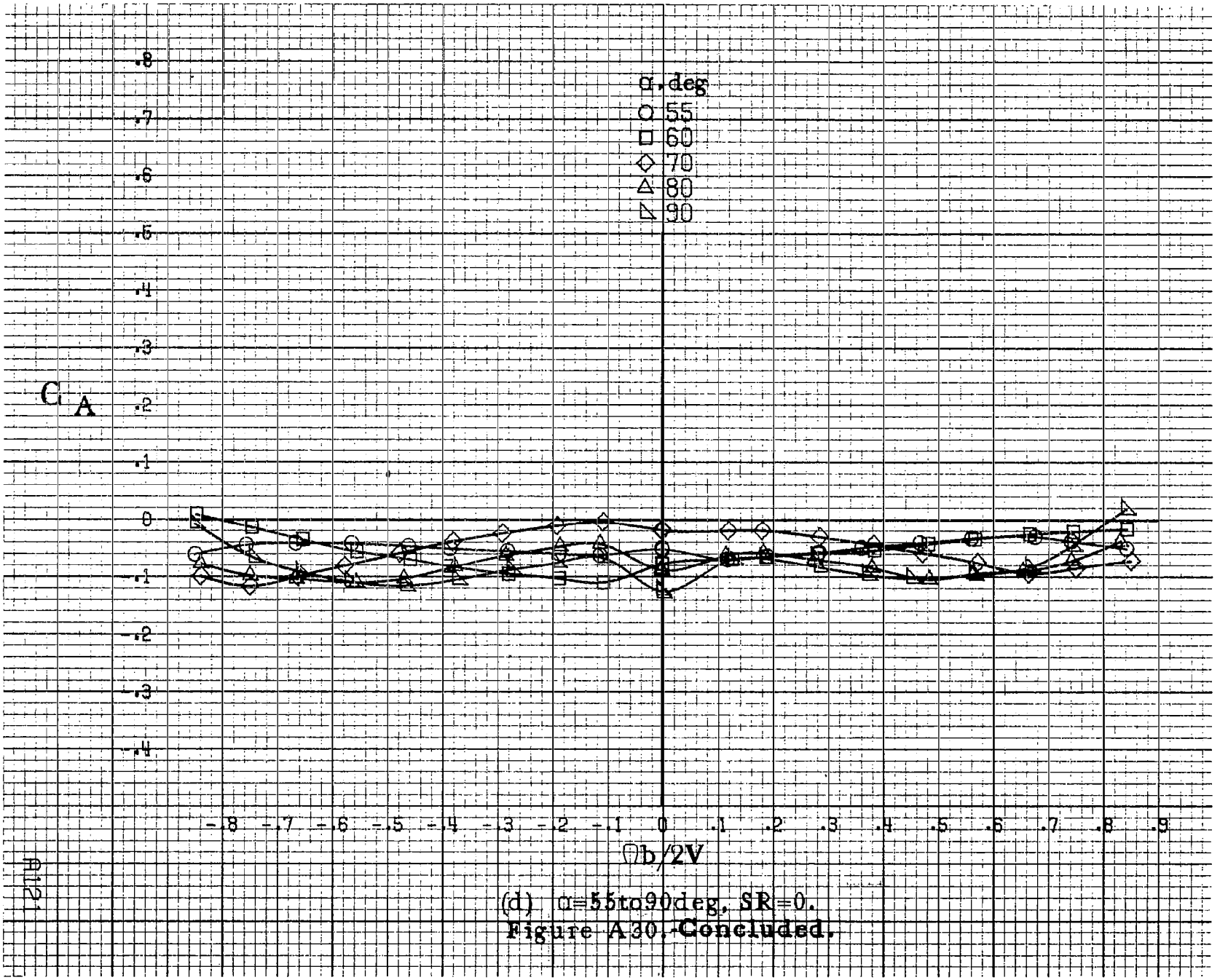

(d) α=55to90deg, SR=0.

Figure A30.-Concluded.

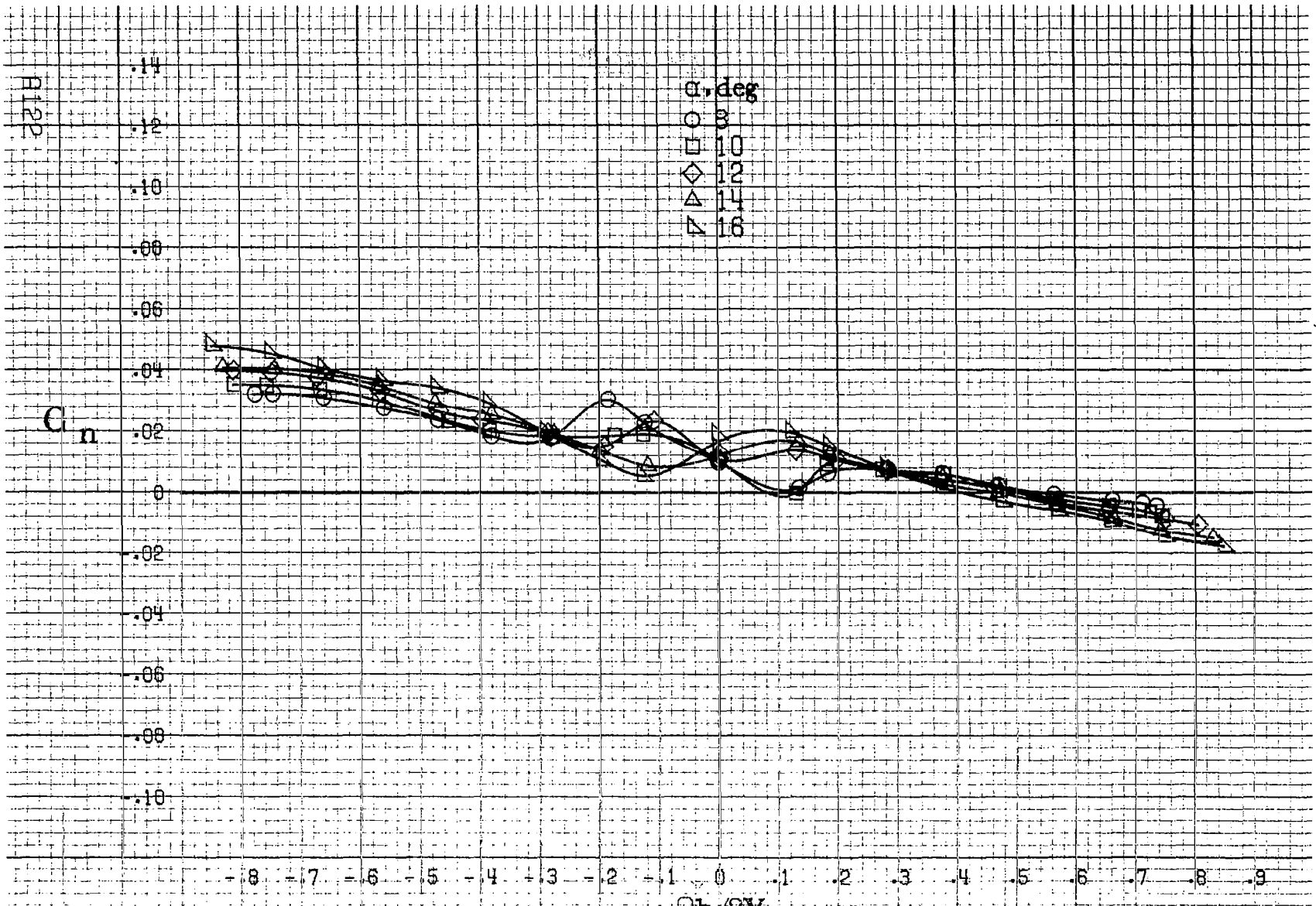

(a) α=8to16deg, S_R=99cm(39in).

Figure A31.- Effect of rotation rate and angle of attack on yawing-moment coefficient for no. 1 horizontal tail configuration. $\delta_e = 0°$, $\delta_a = 0°$, $\delta_r = -25°$, $\beta = 0°$.

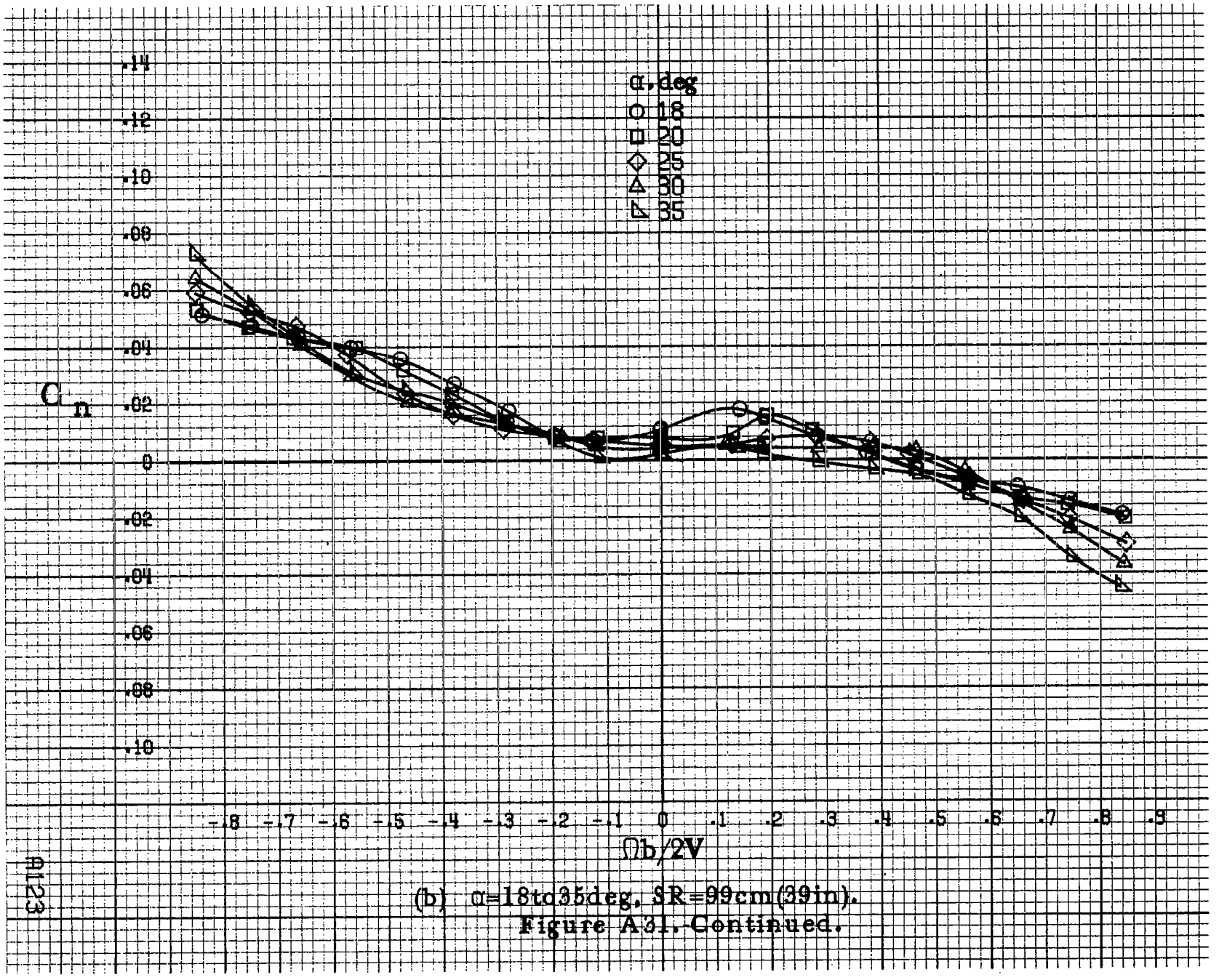

(b) α=18to35deg, SR=99cm(39in).

Figure A31.-Continued.

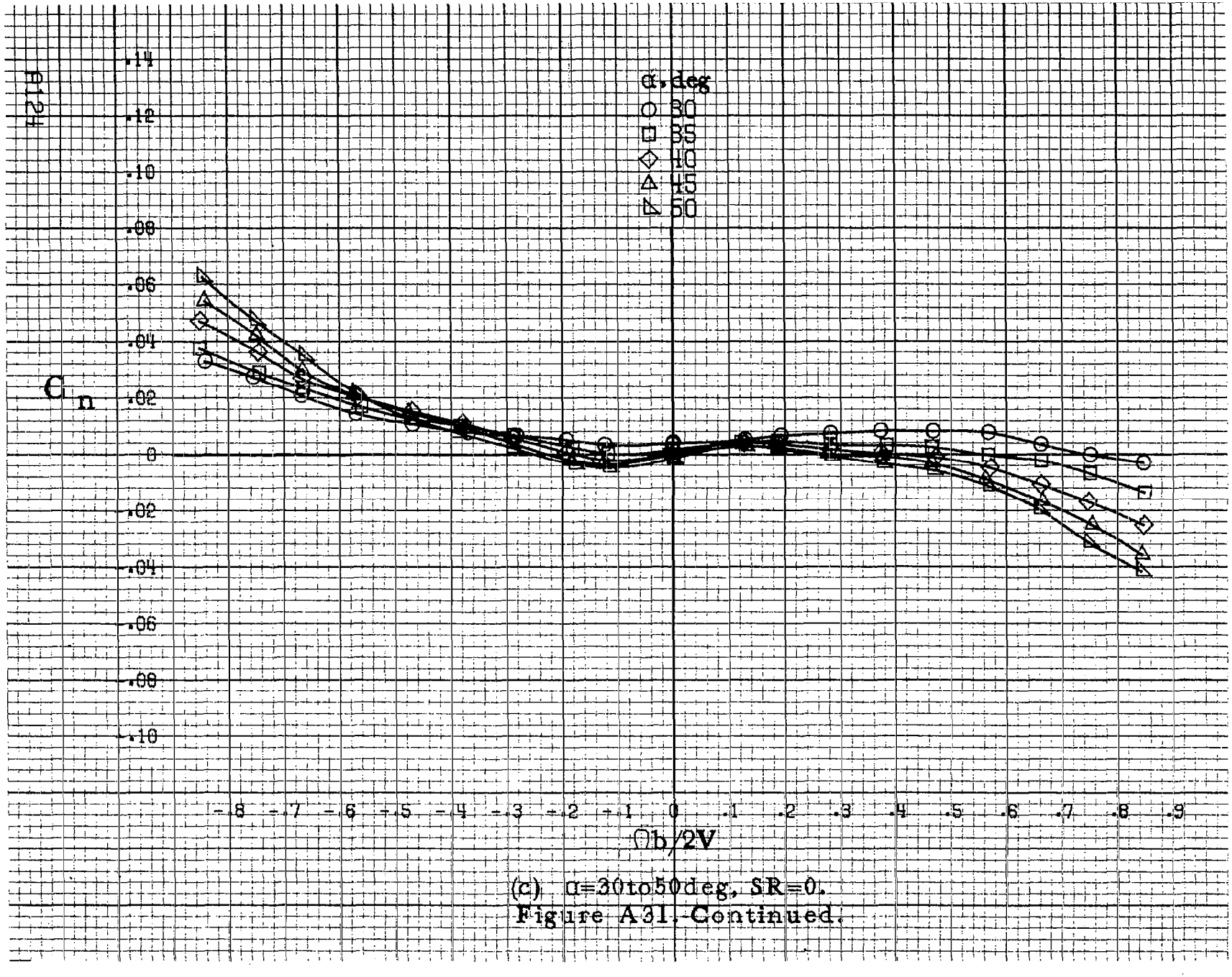

(c) α=30to50deg, SR=0.

Figure A31. Continued.

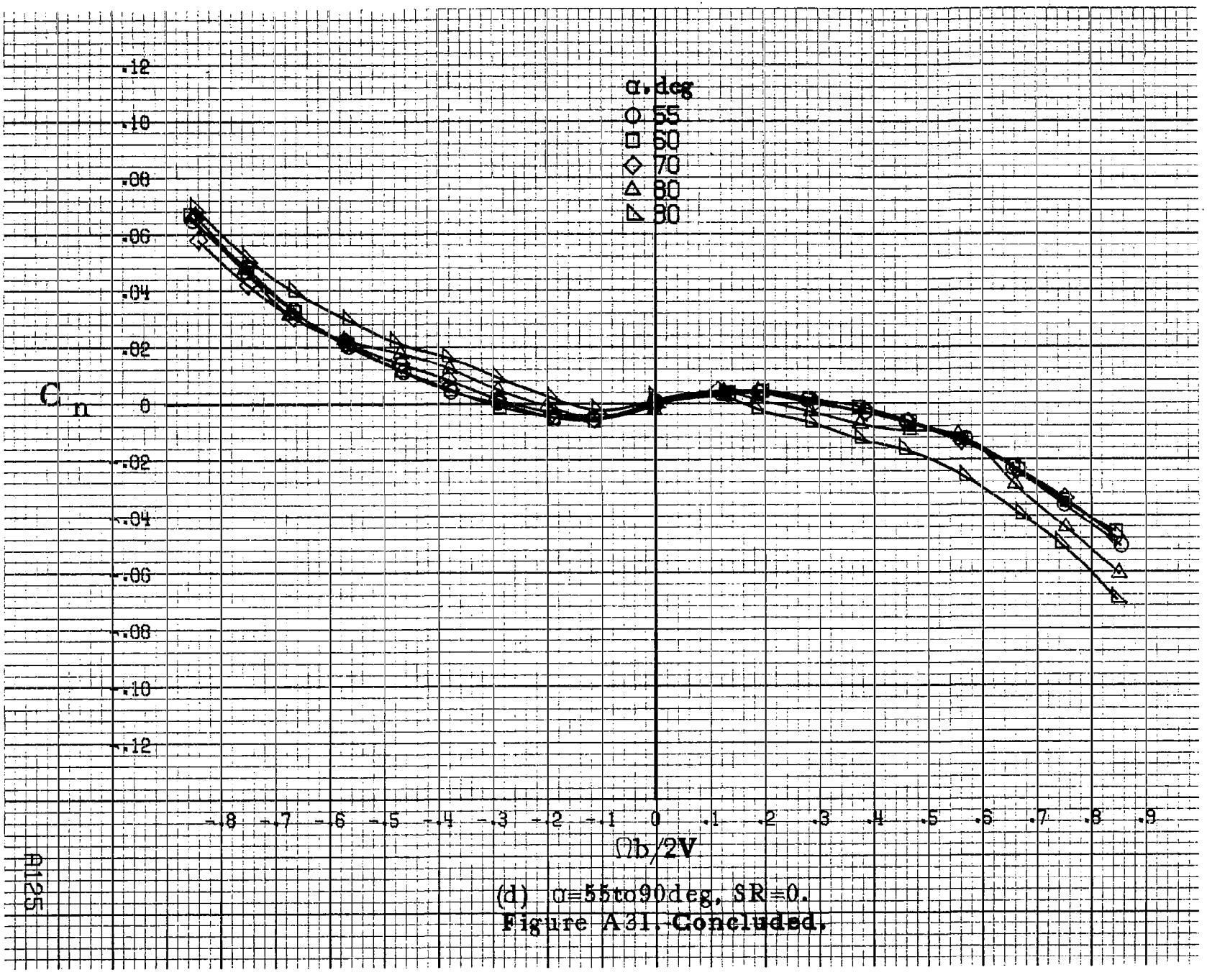

(d) $\alpha = 55$ to 90 deg, SR = 0.

Figure A31. Concluded.

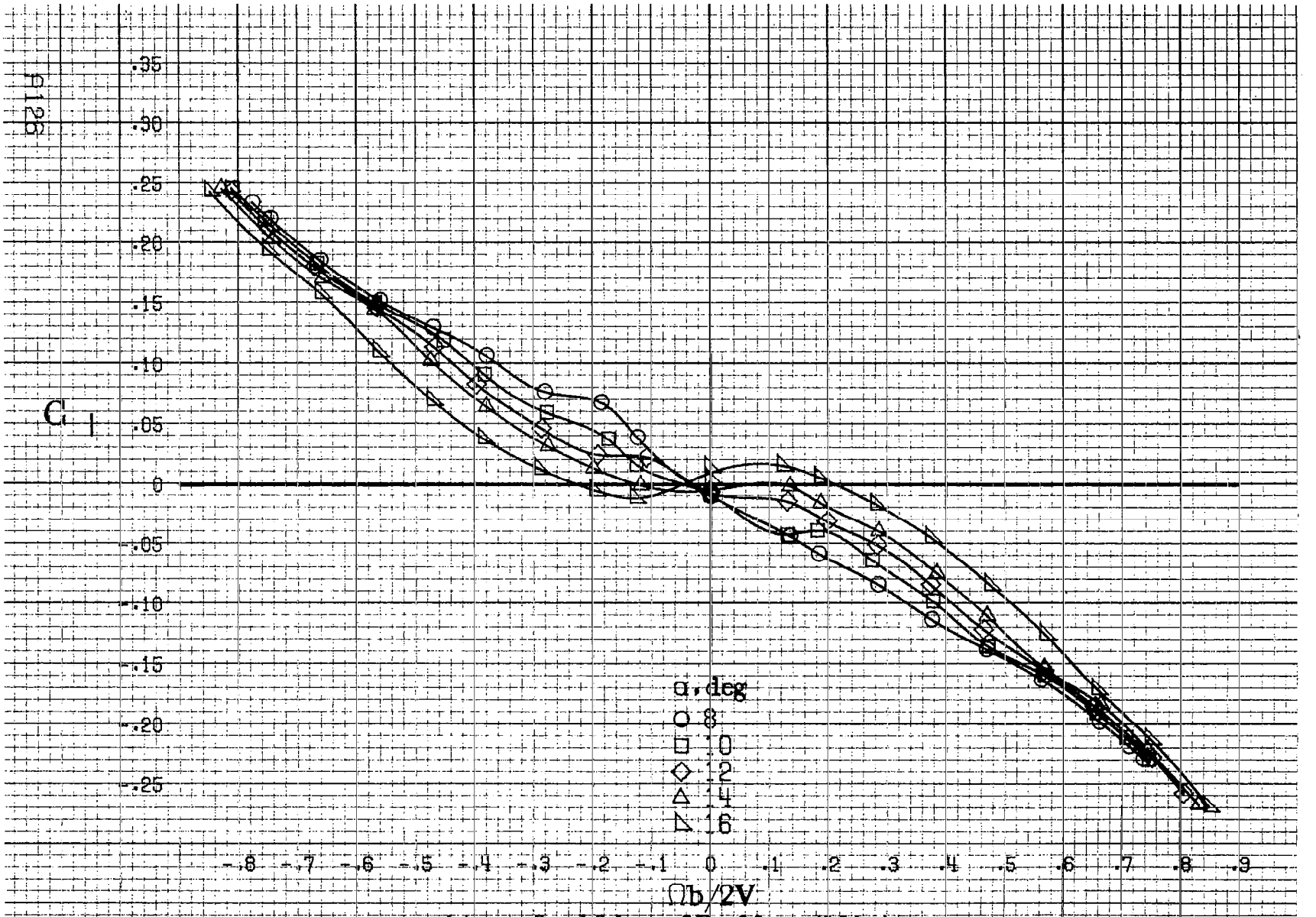

(a) α=8to16deg, SR=99cm(39in).

Figure A32.-Effect of rotation rate and angle of attack on rolling-moment coefficient for no. 1 horizontal tail configuration. $\delta_e = 0°$, $\delta_a = 0°$, $\delta_r = -25°$, $\beta = 0°$.

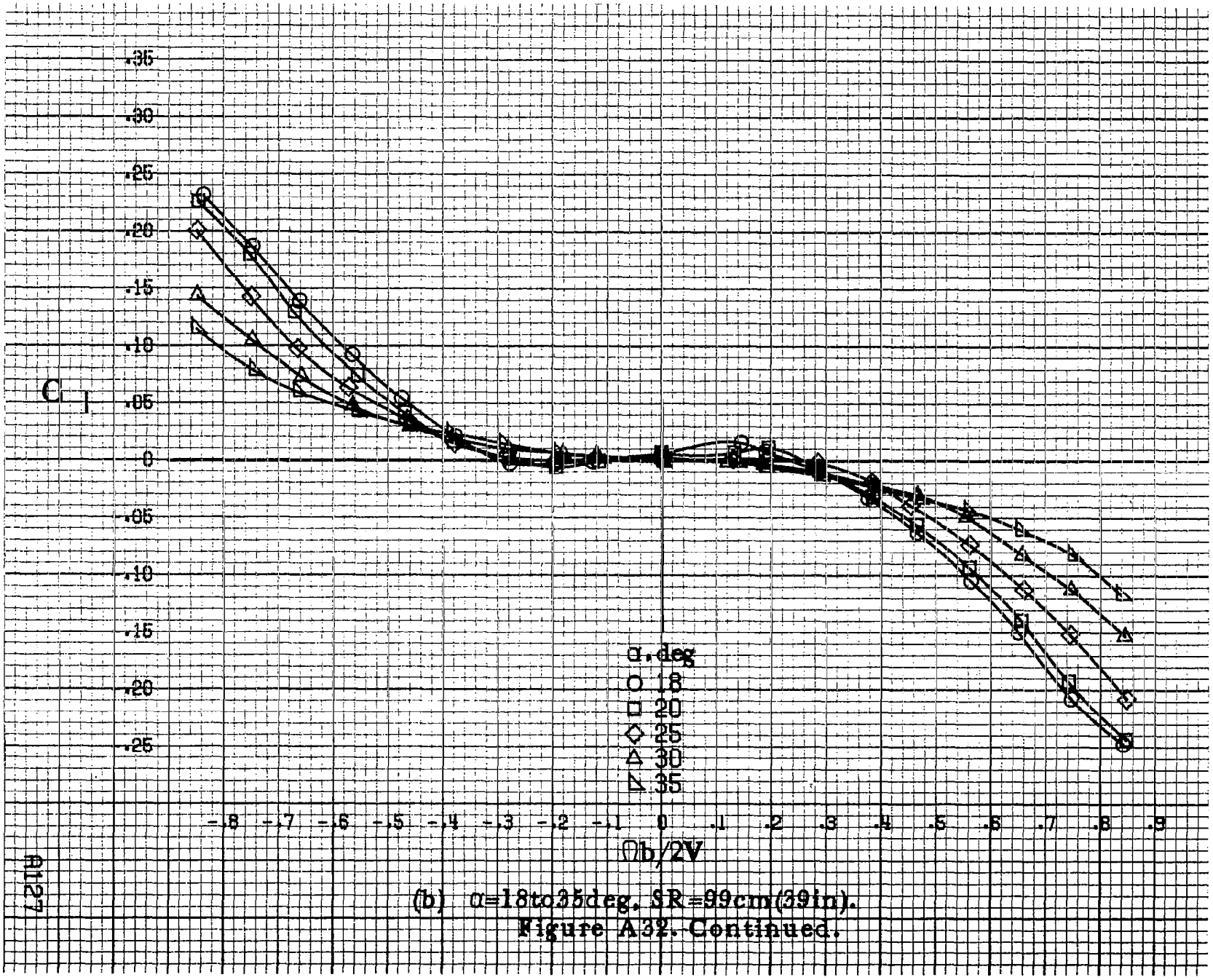

(b) α=18to35deg, SR=99cm(39in).

Figure A32. Continued.

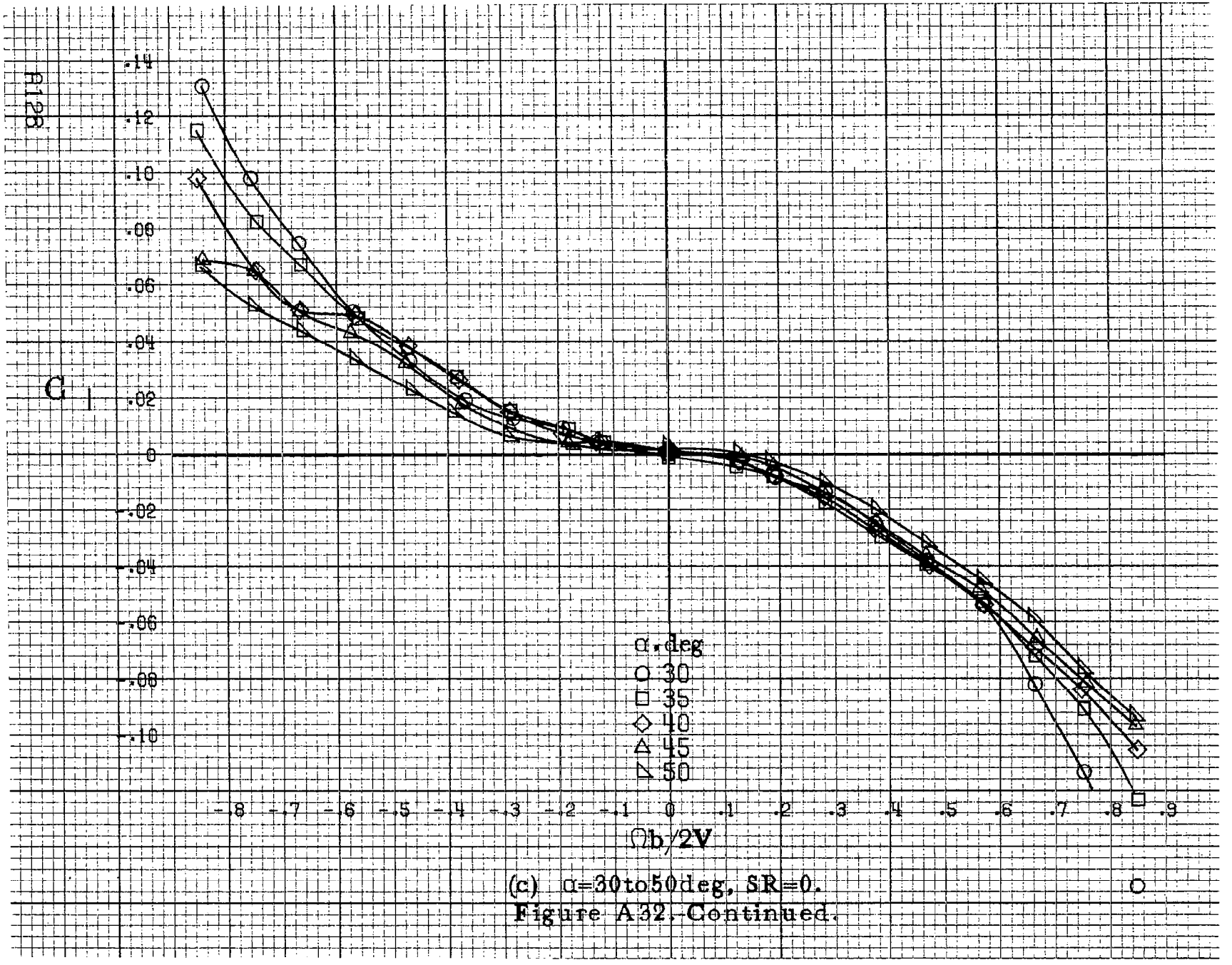

(c) α=30 to 50 deg, SR=0.

Figure A32.-Continued.

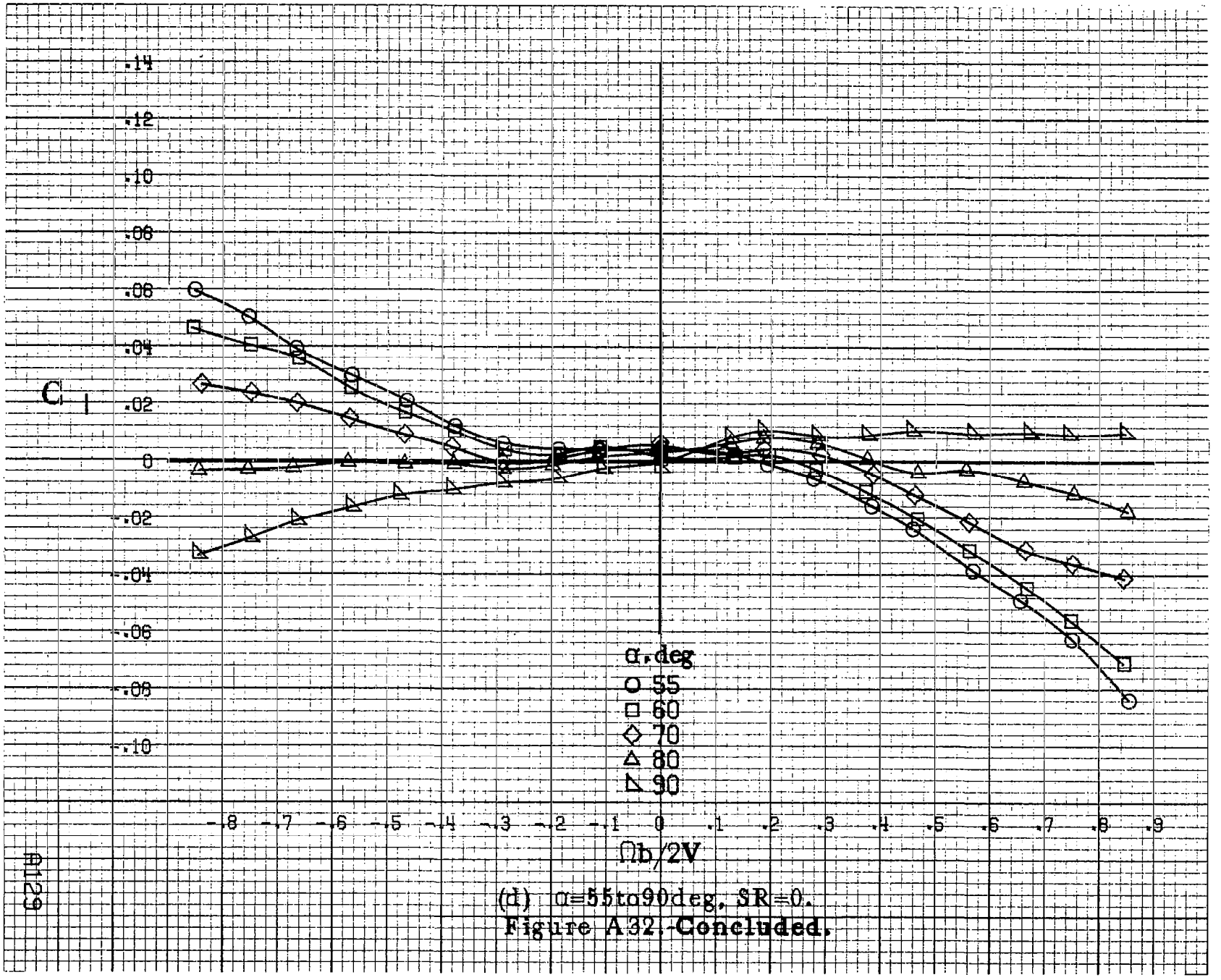

(d) α=55 to 90 deg, SR=0.

Figure A32.-Concluded.

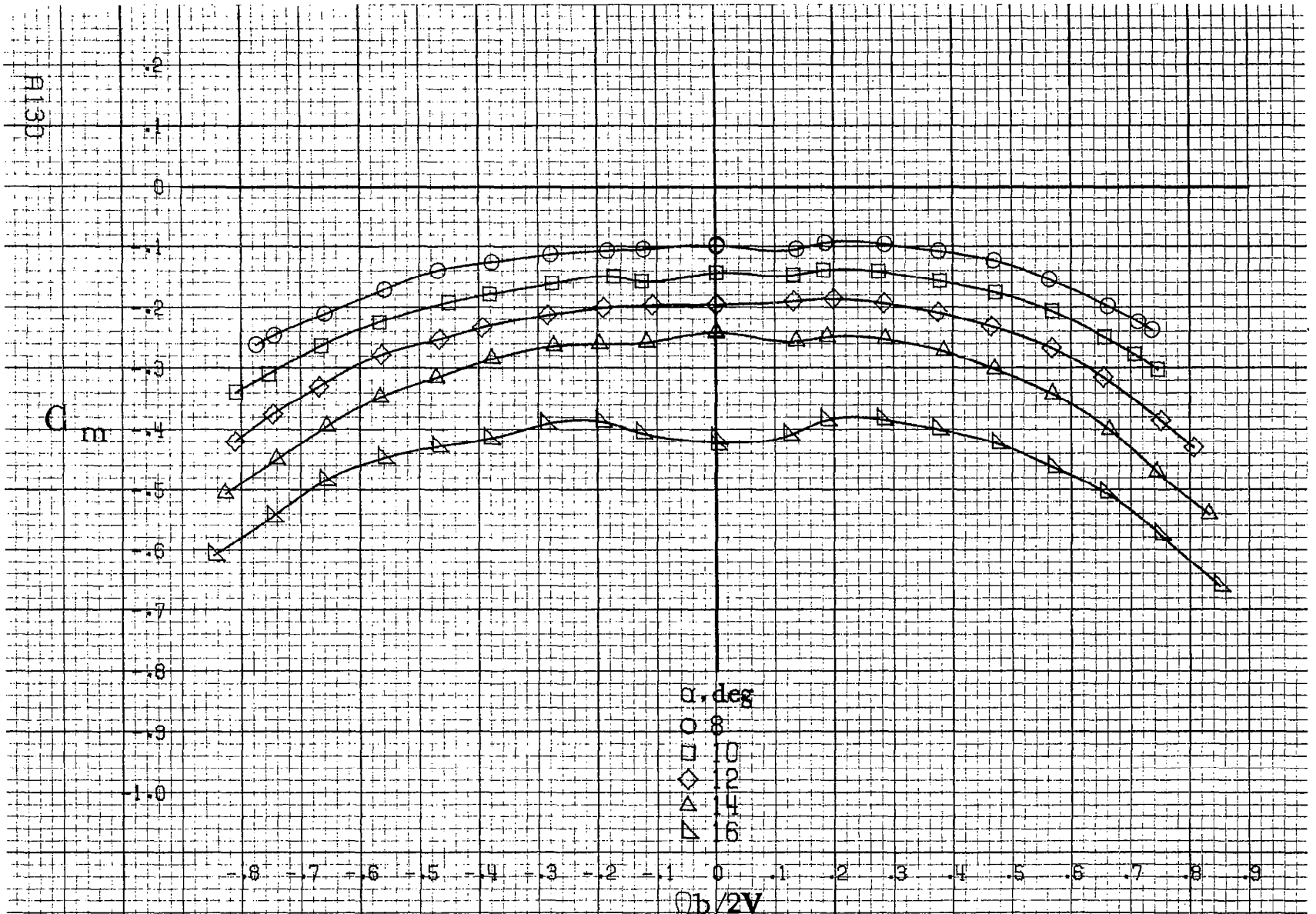

(a) α=8to16deg, SR=99cm(39in).

Figure A33.-Effect of rotation rate and angle of attack on pitching-moment coefficient for no. 1 horizontal tail configuration. $\delta_e = 0°$, $\delta_a = 0°$, $\delta_r = -25°$, $\beta = 0°$.

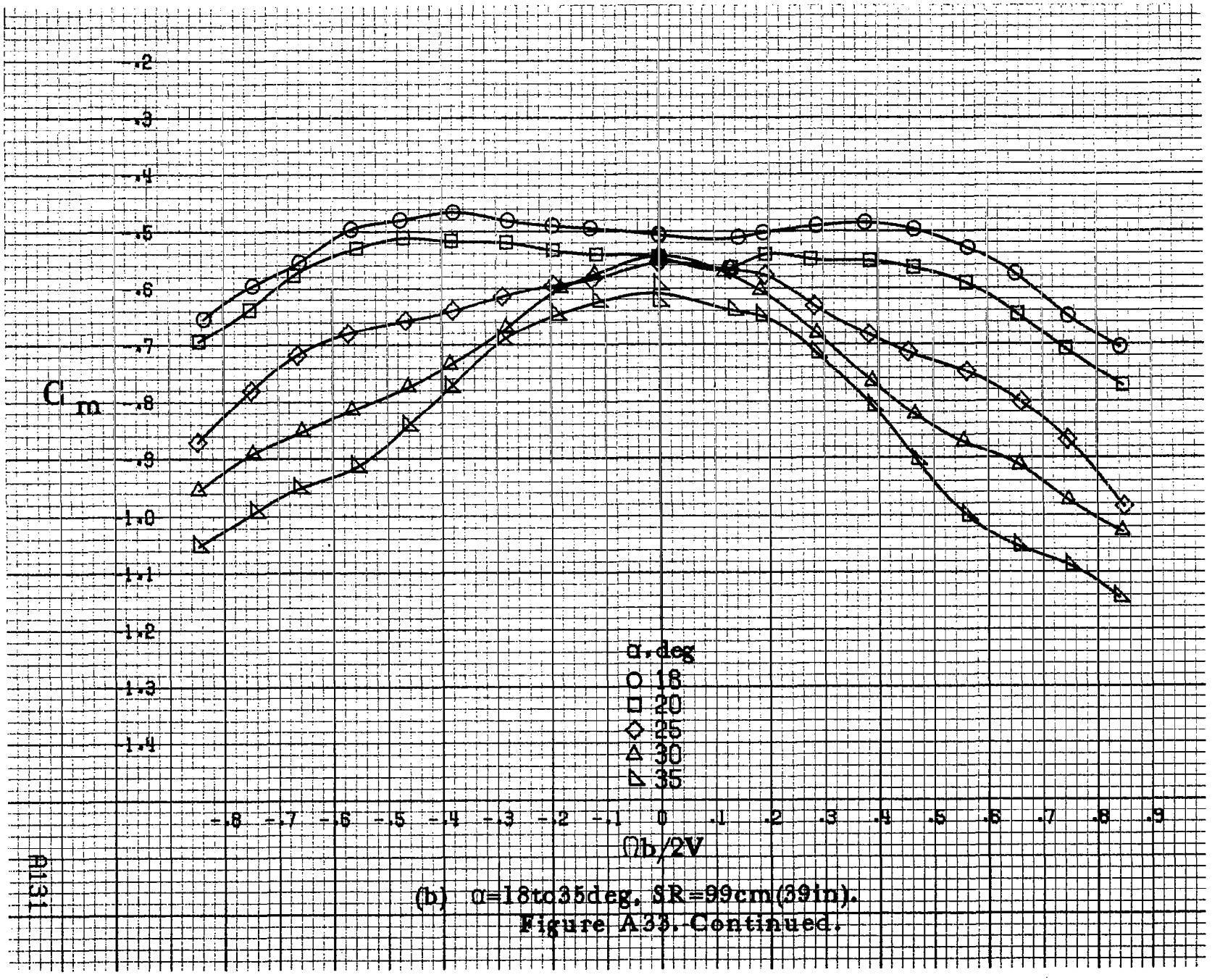

(b) α=18 to 35 deg, SR=99 cm (39 in).

Figure A33. Continued.

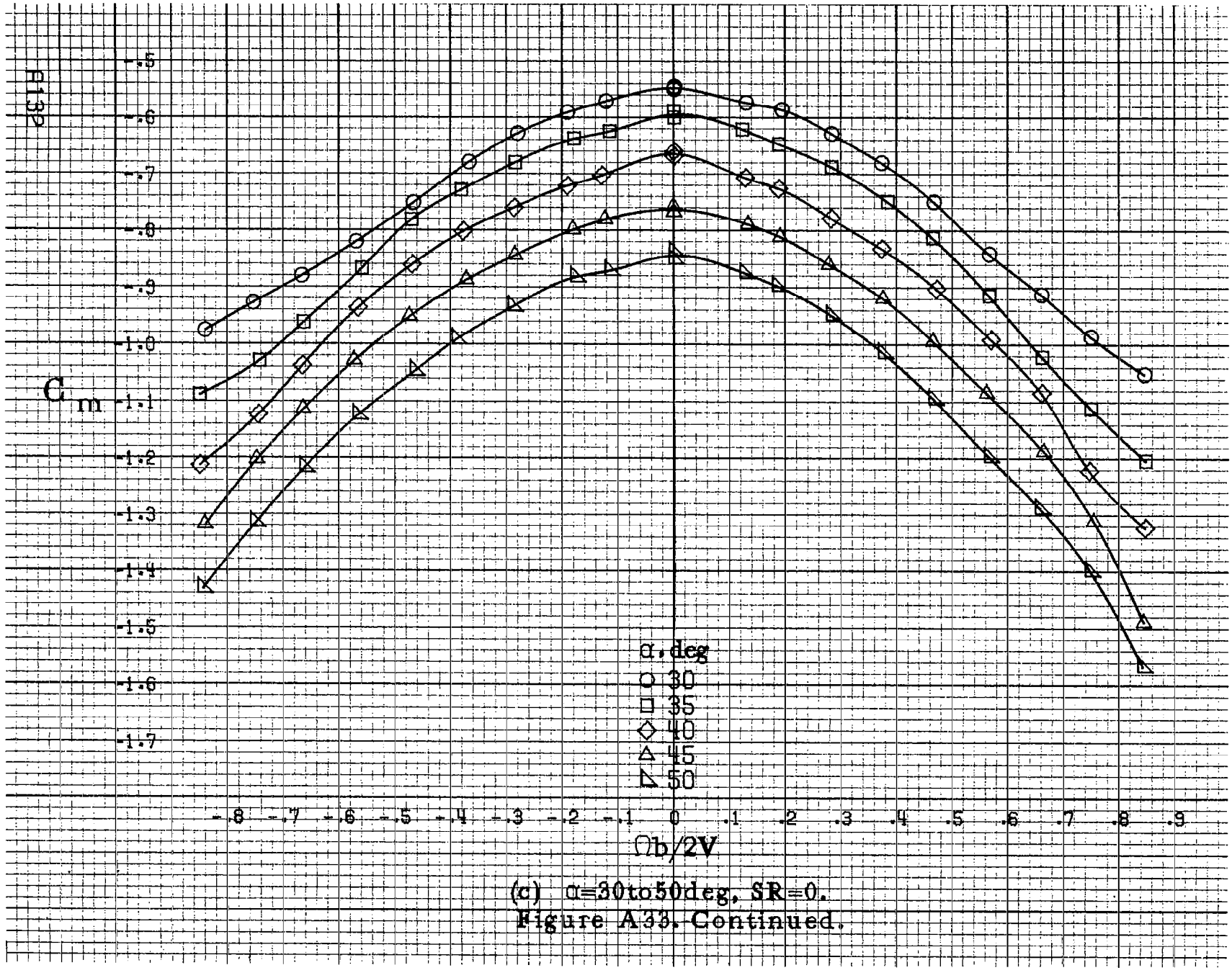

(c) α=30to50deg, SR=0.

Figure A33. Continued.

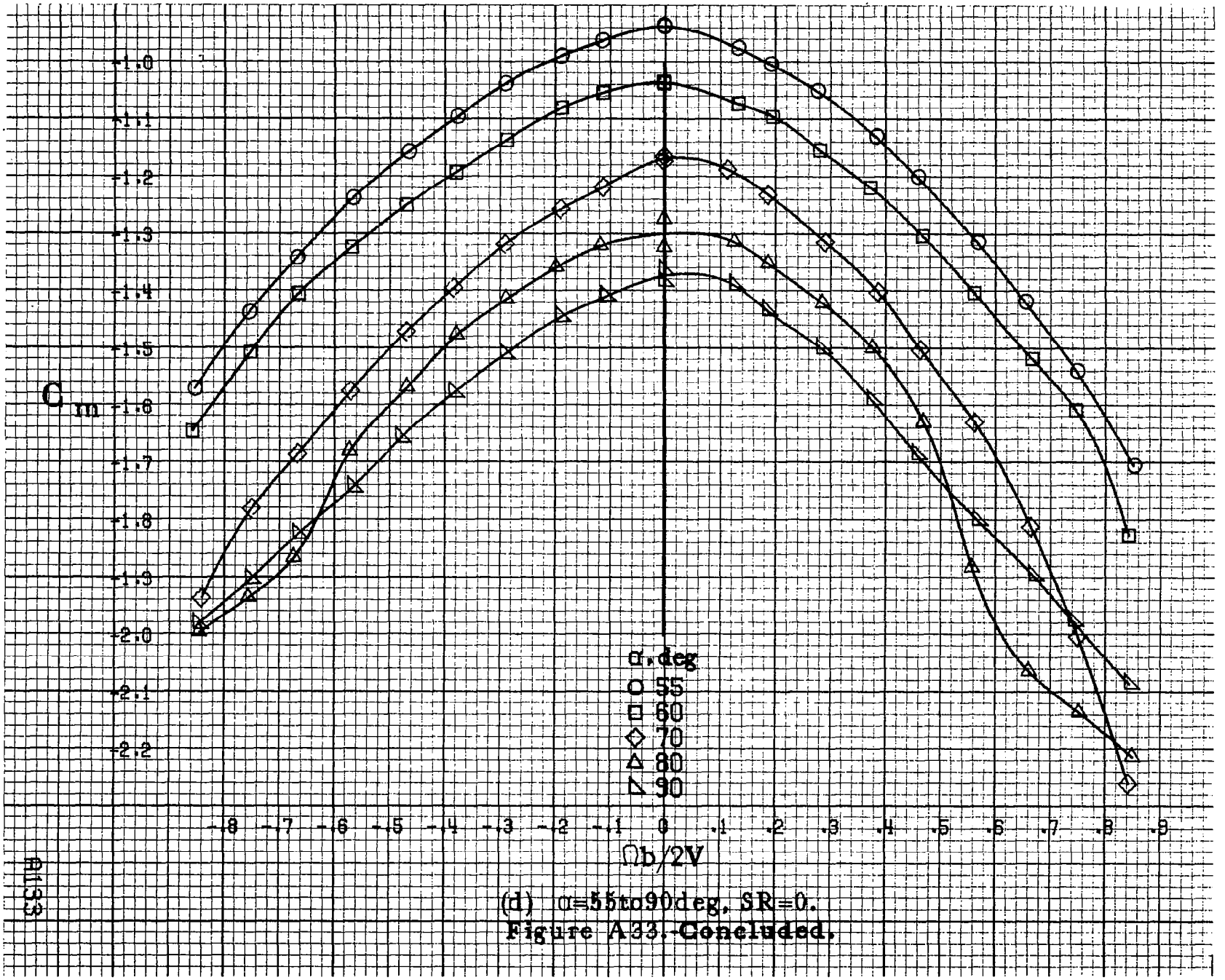

(d) α=55to90deg, SR=0.

Figure A33.-Concluded.

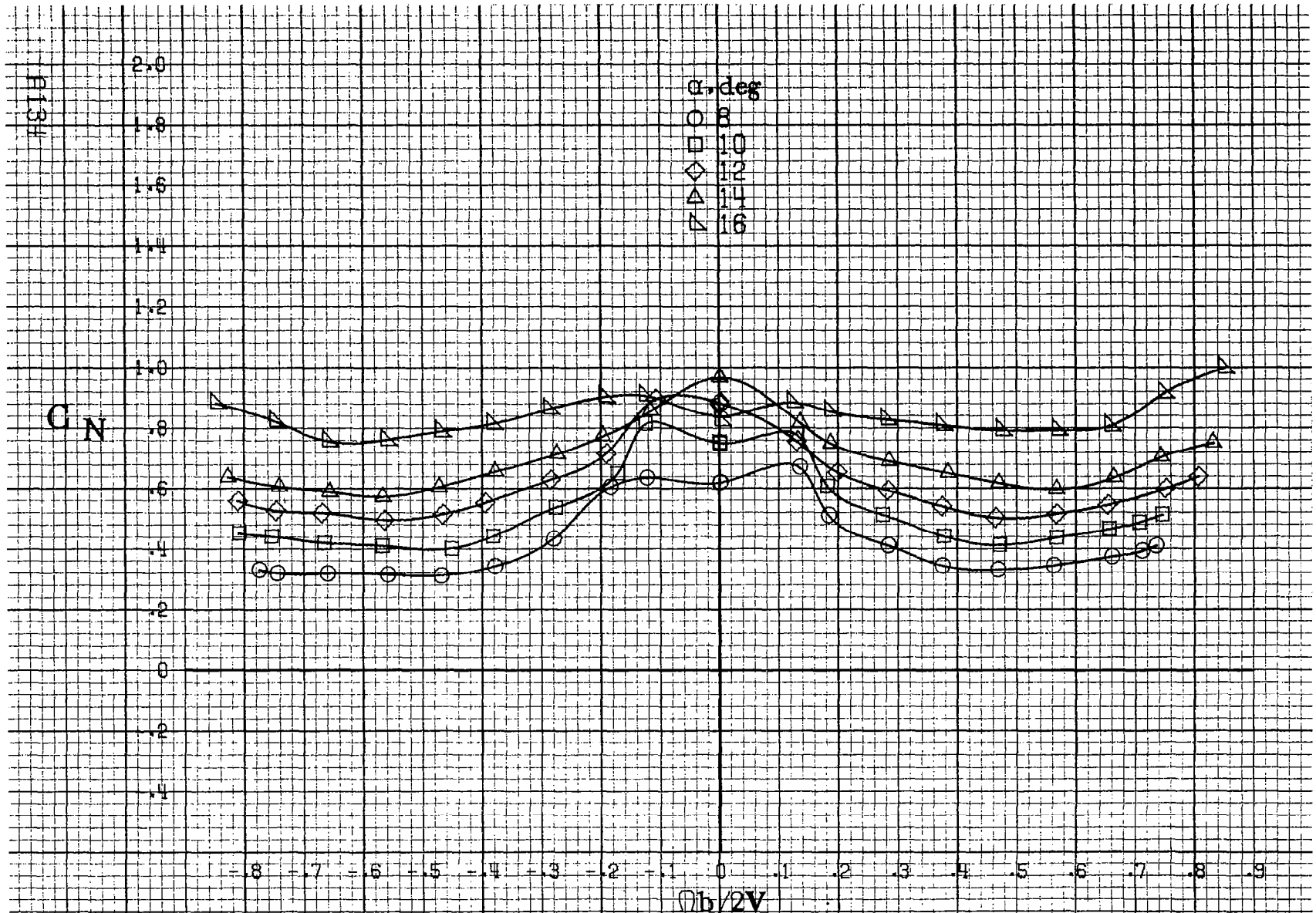

(a) α=8to16deg, SR=99cm(39in).

Figure A.34.-Effect of rotation rate and angle of attack on normal-force coefficient for no. 1 horizontal tail configuration. δ_e =0°, δ_a =0°, δ_r =-25°, β =0°.

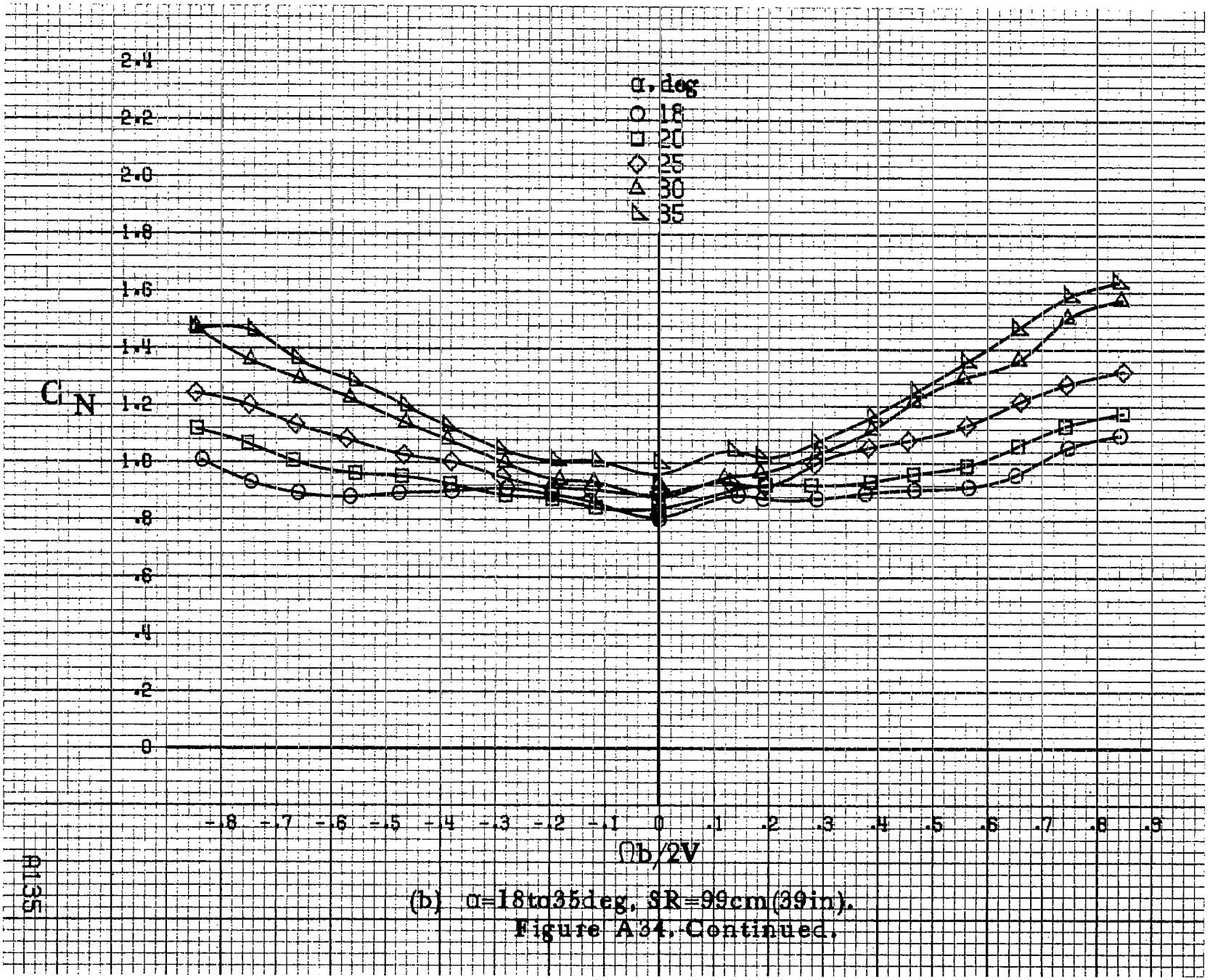

(b) α=18to35deg, SR=99cm(39in).

Figure A34. Continued.

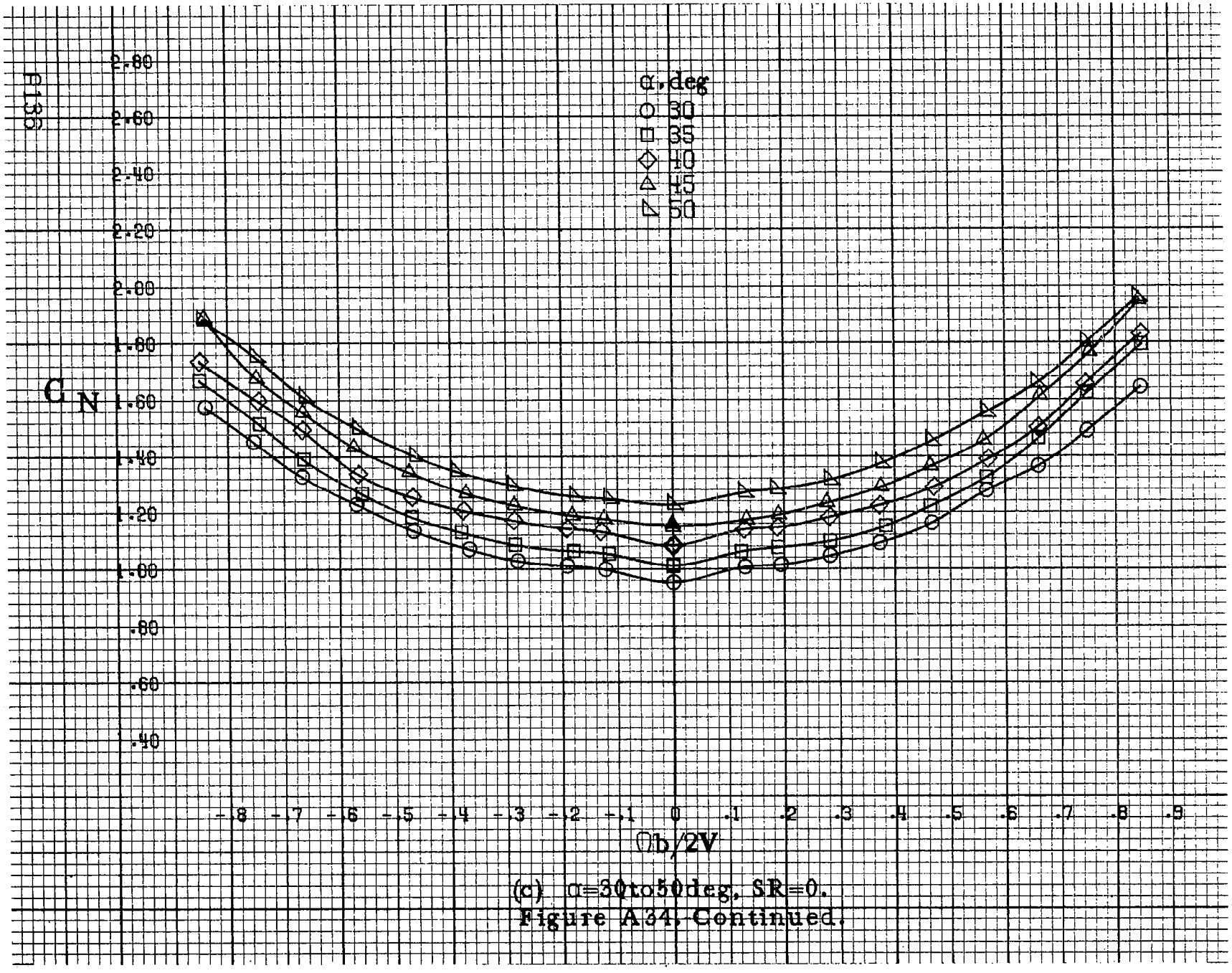

(c) α=30to50deg, SR=0.

Figure A34. Continued.

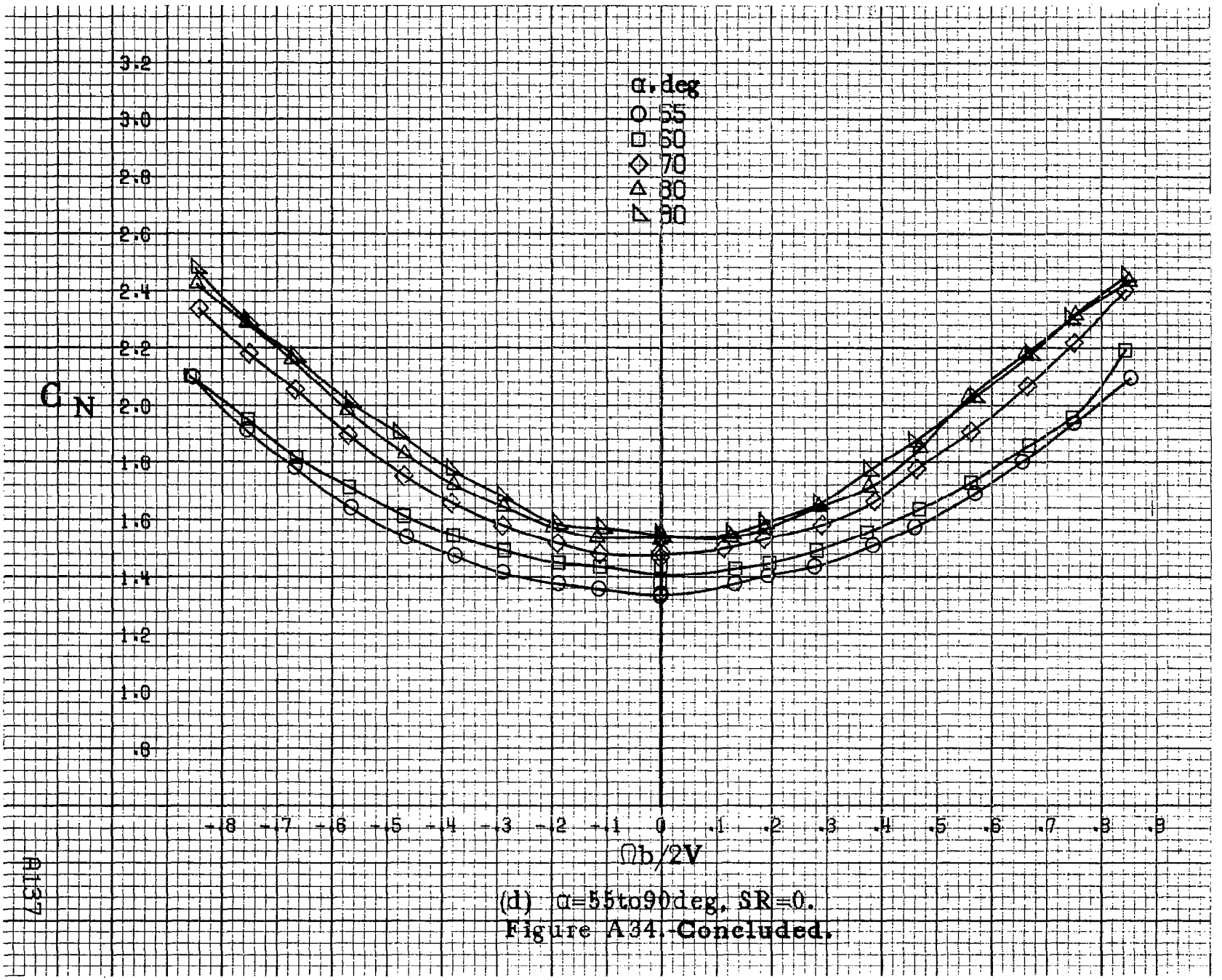

(d) α=55to90deg, SR=0.

Figure A34.-Concluded.

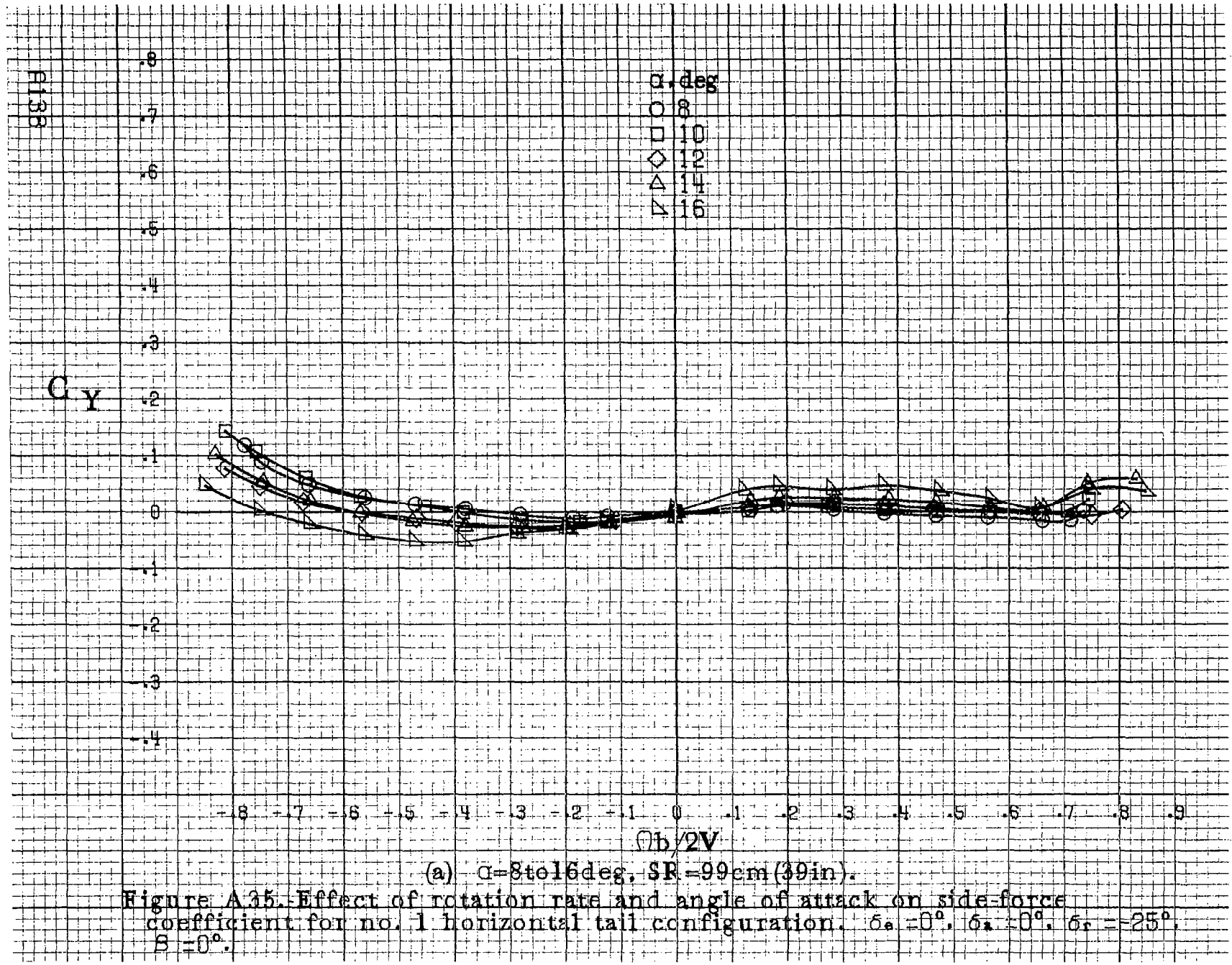

(a) α=8to16deg, $R=99cm(39in).

Figure A.35.-Effect of rotation rate and angle of attack on side-force coefficient for no. 1 horizontal tail configuration. $\delta_e = 0°$, $\delta_a = 0°$, $\delta_r = -25°$, $\beta = 0°$.

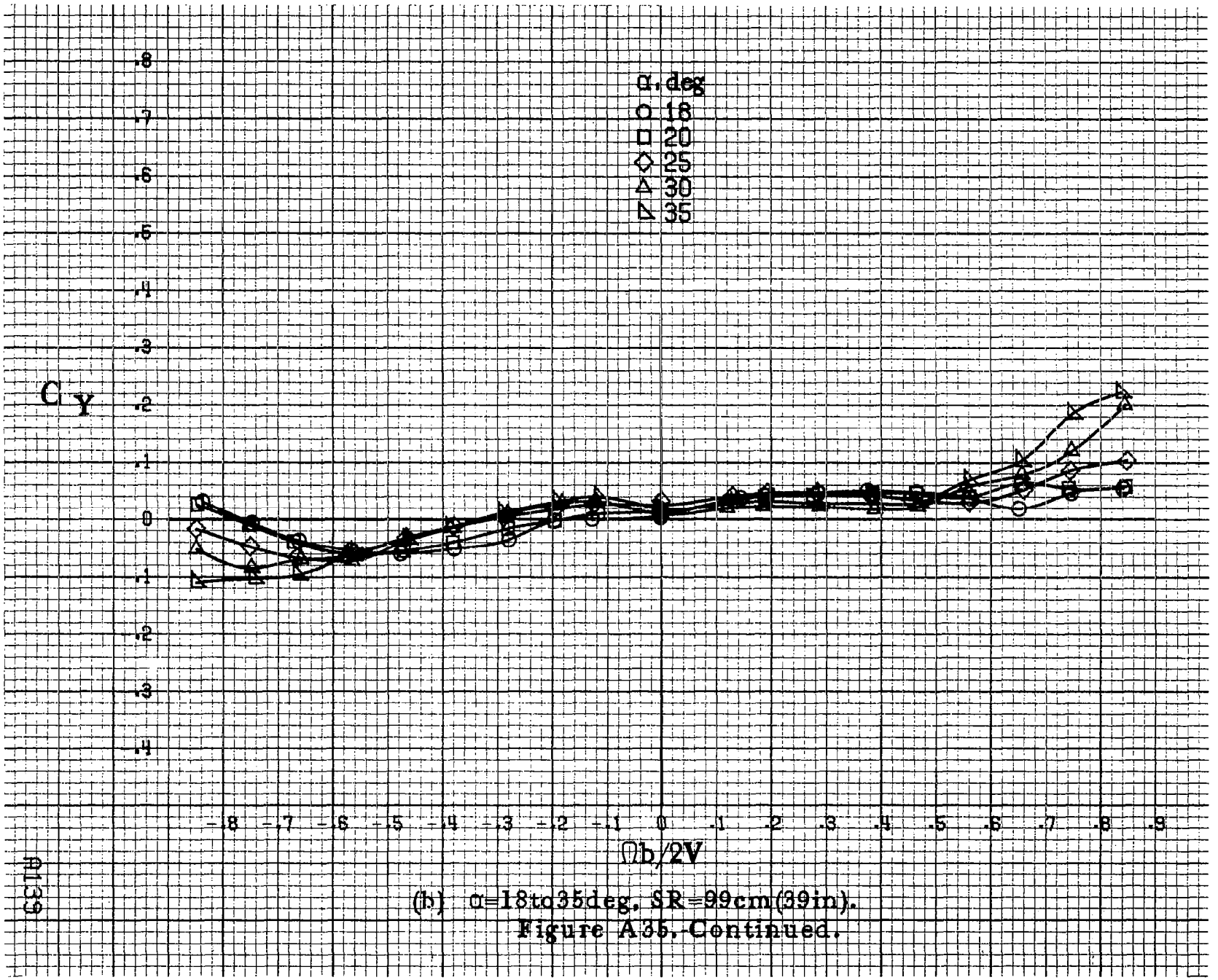

(b) α=18 to 35 deg, SR=99 cm (39 in).

Figure A35.-Continued.

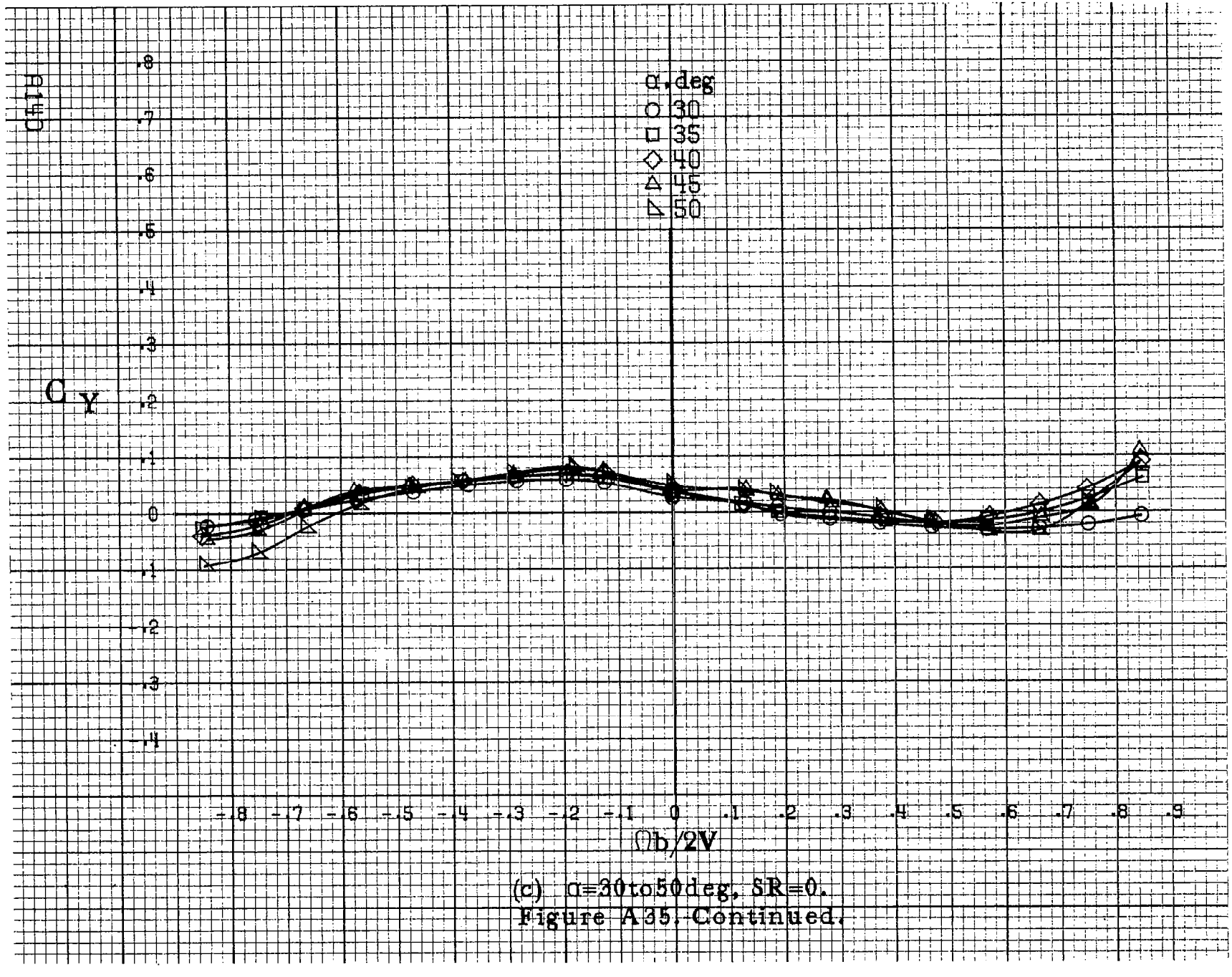

(c) α=30 to 50 deg, SR=0.

Figure A35. Continued.

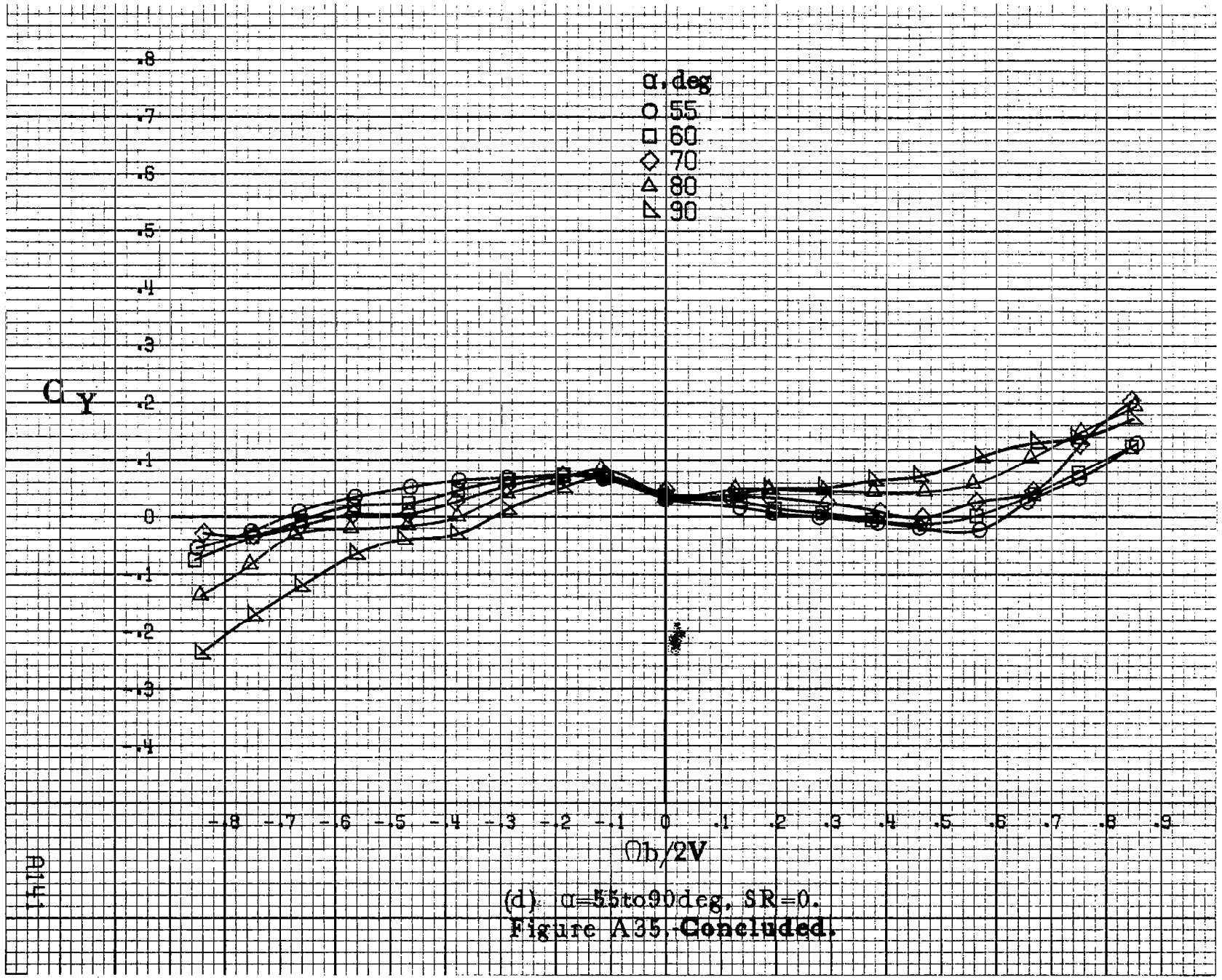

(d) α=55 to 90 deg, SR=0.

Figure A35. Concluded.

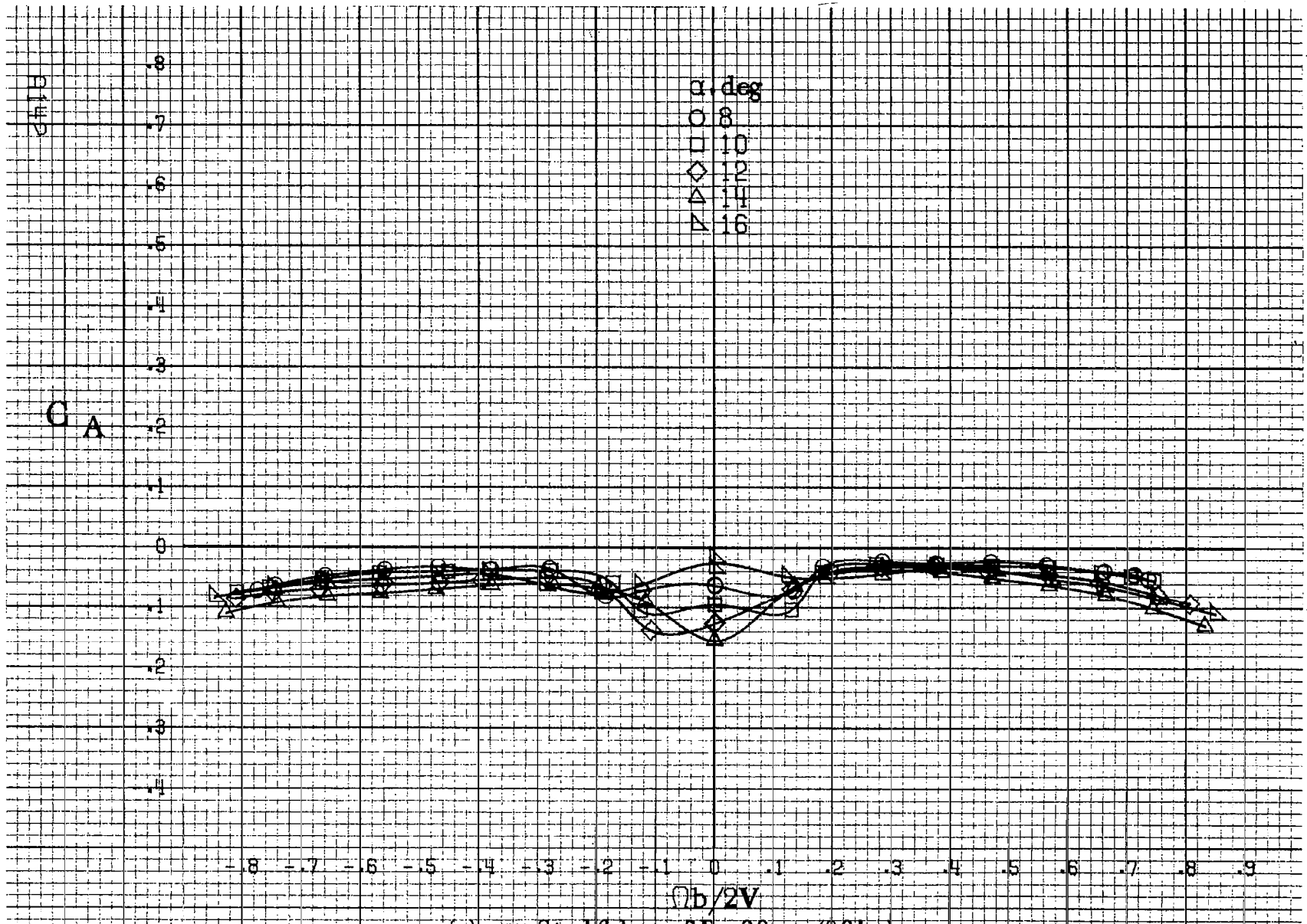

(a) α=8to16deg, SR=99cm(39in).

Figure A36.-Effect of rotation rate and angle of attack on axial-force coefficient for no. 1 horizontal tail configuration. $\delta_e = 0°$, $\delta_a = 0°$, $\delta_r = -25°$, $\beta = 0°$.

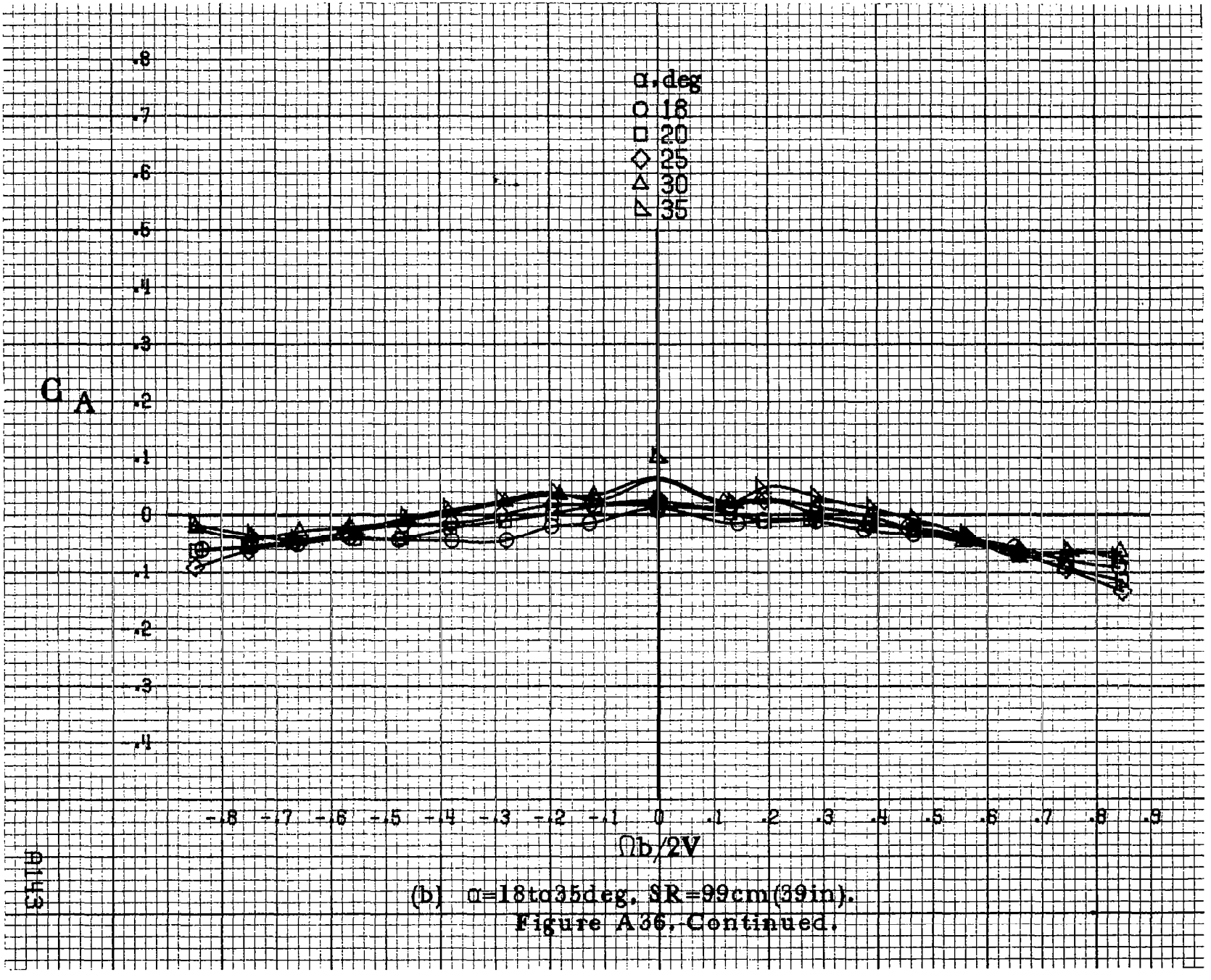

(b) α=18to35deg, SR=99cm(39in).

Figure A36. Continued.

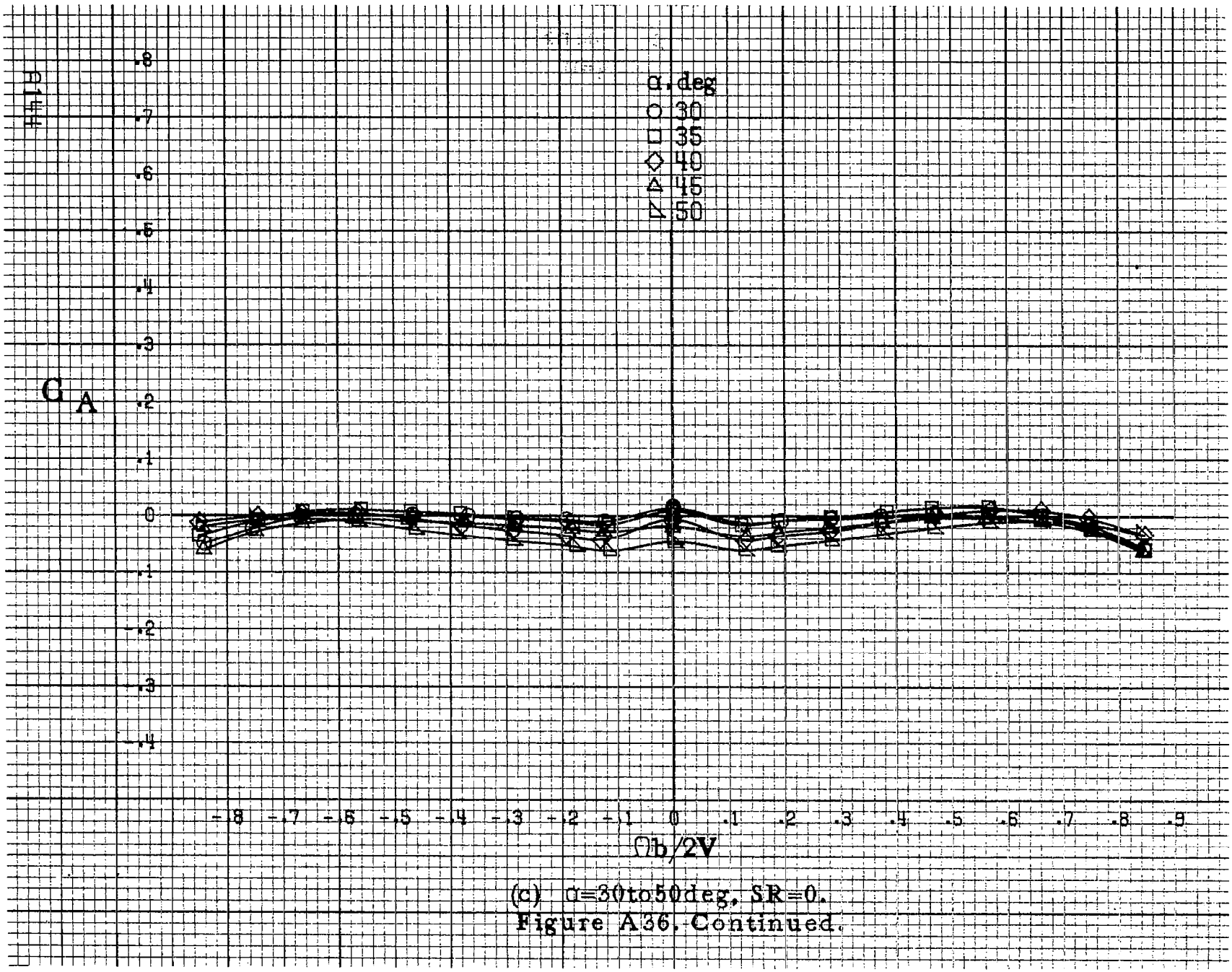

(c) α=30to50deg, SR=0.

Figure A36. Continued.

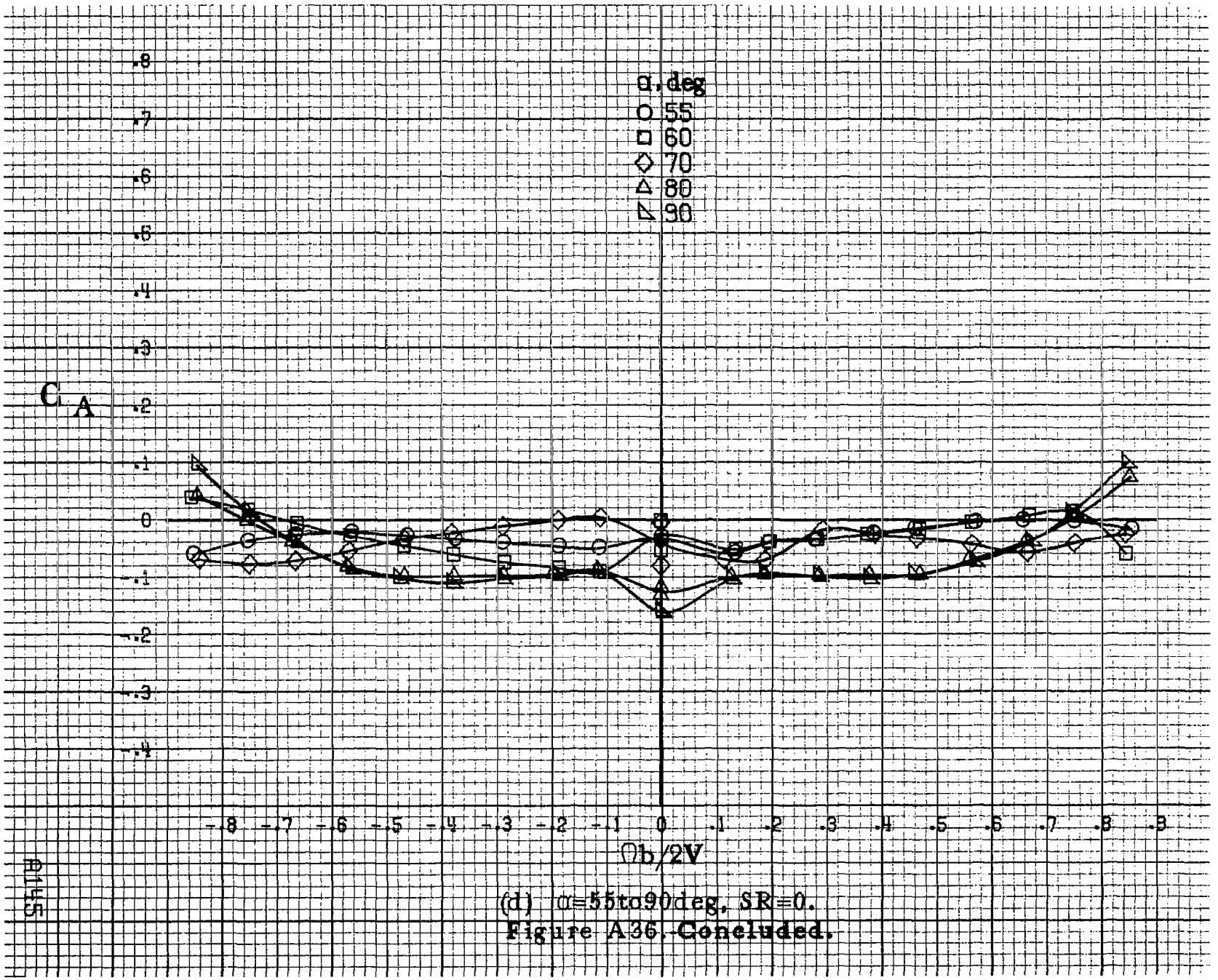

(d) $\alpha = 55$ to 90 deg, SR = 0.

Figure A36.- Concluded.

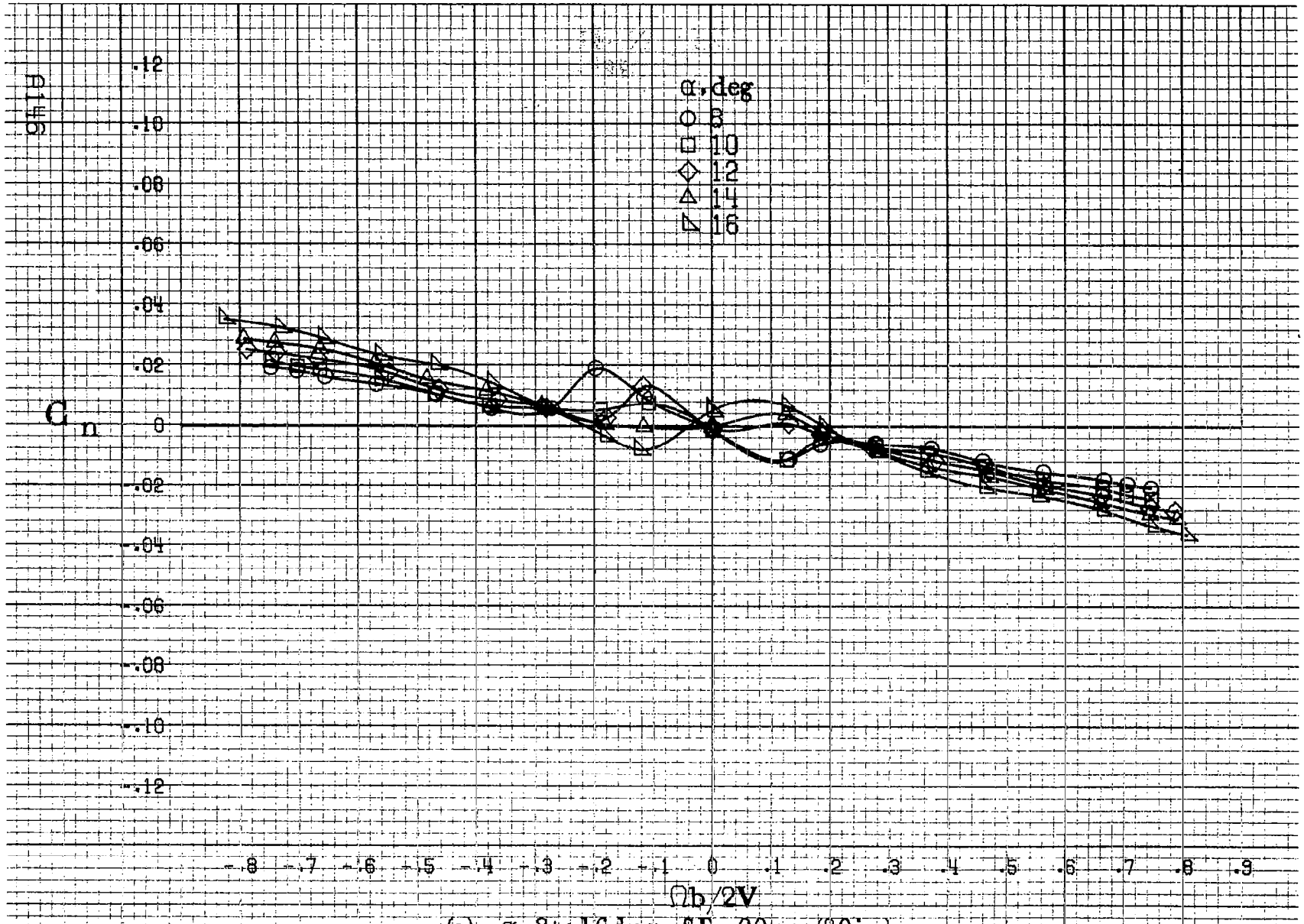

(a) α=8to16deg, SR=99cm(39in).

Figure A37. Effect of rotation rate and angle of attack on yawing-moment coefficient for no. 2 horizontal tail configuration. $\delta_e = 0°$, $\delta_a = 0°$, $\delta_r = 0°$, $\beta = 0°$.

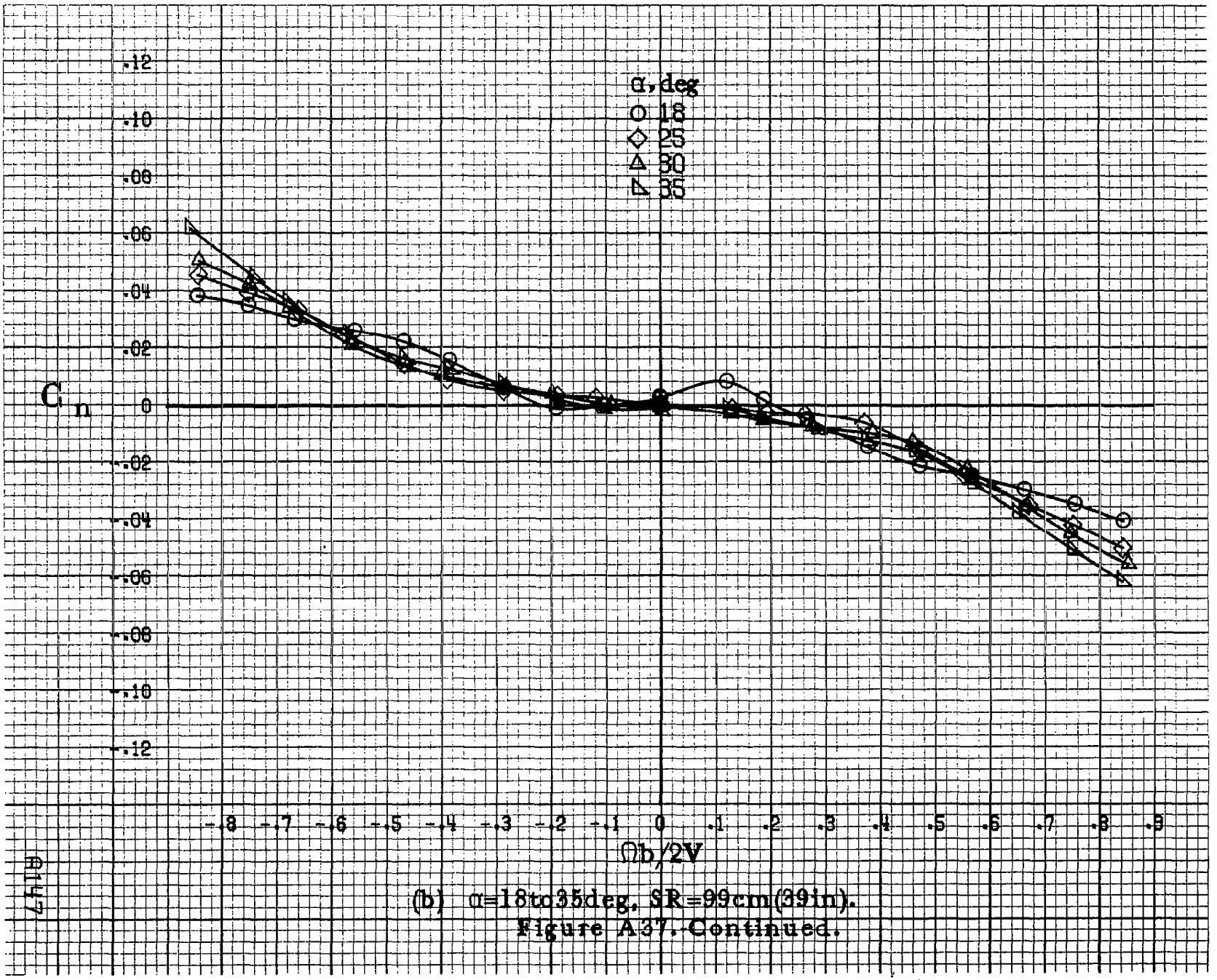

(b) α=18to35deg, SR=99cm(39in).

Figure A37.-Continued.

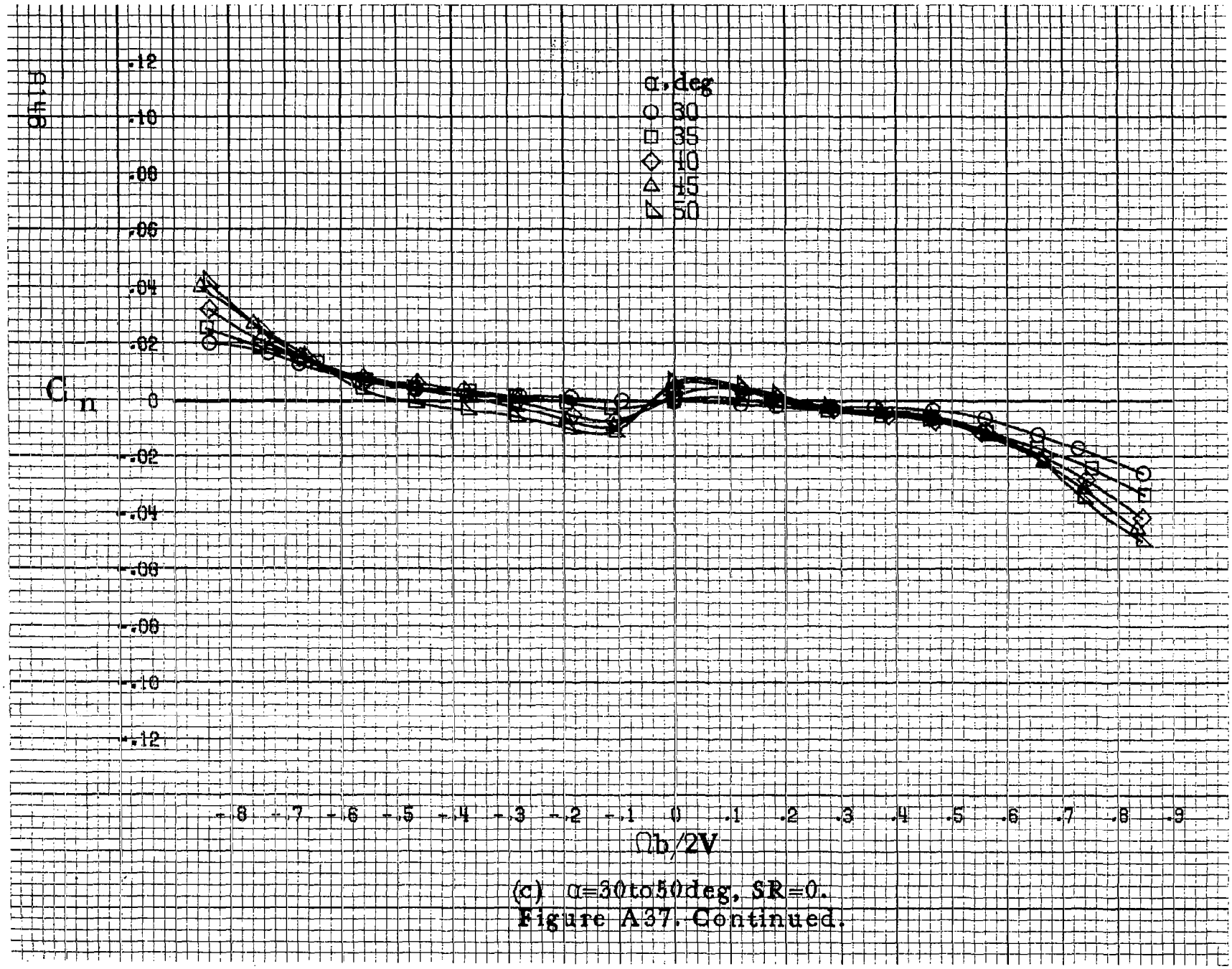

(c) α=30to50deg, SR=0.

Figure A37. Continued.

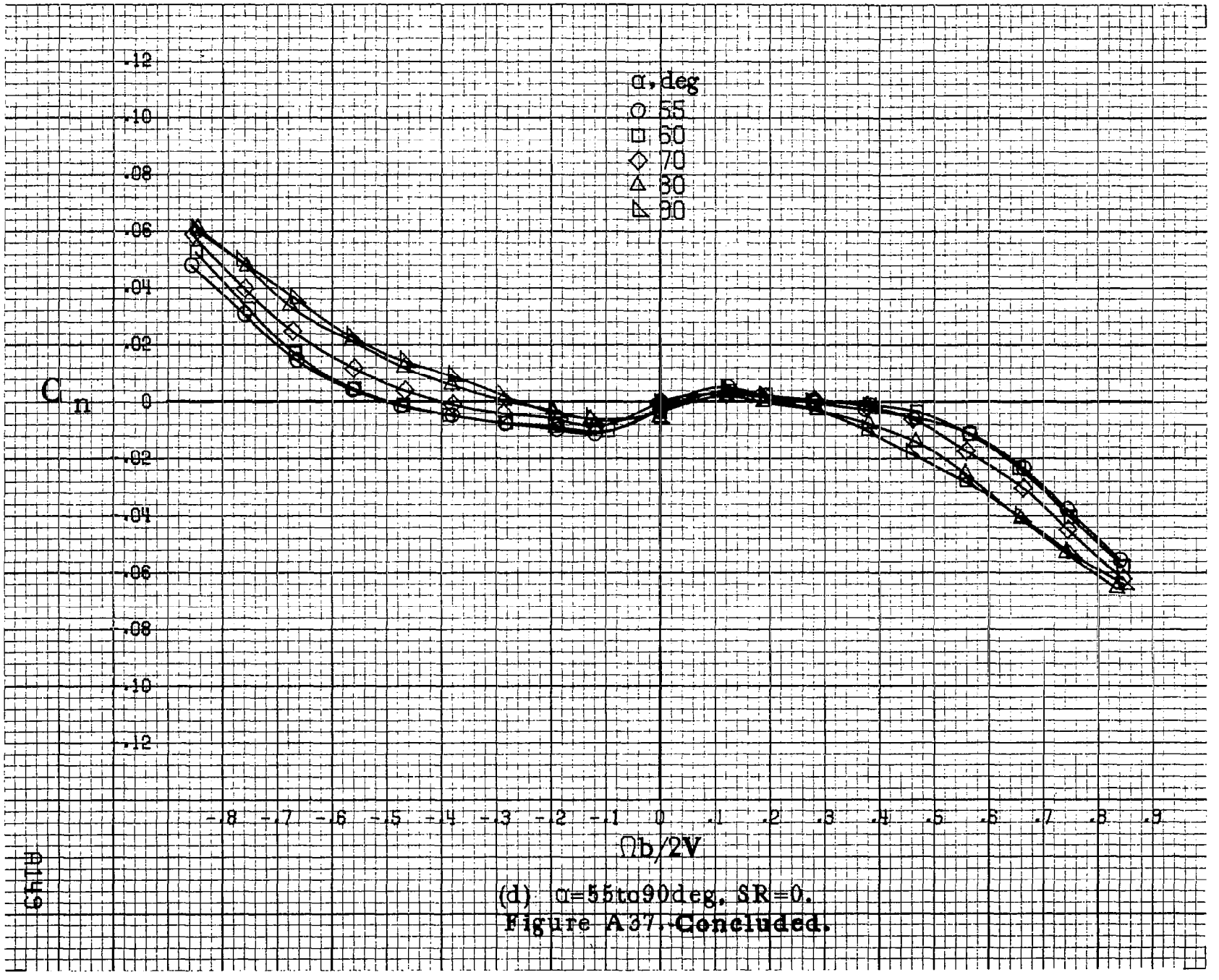

(d) α=55to90deg, SR=0.

Figure A37.-Concluded.

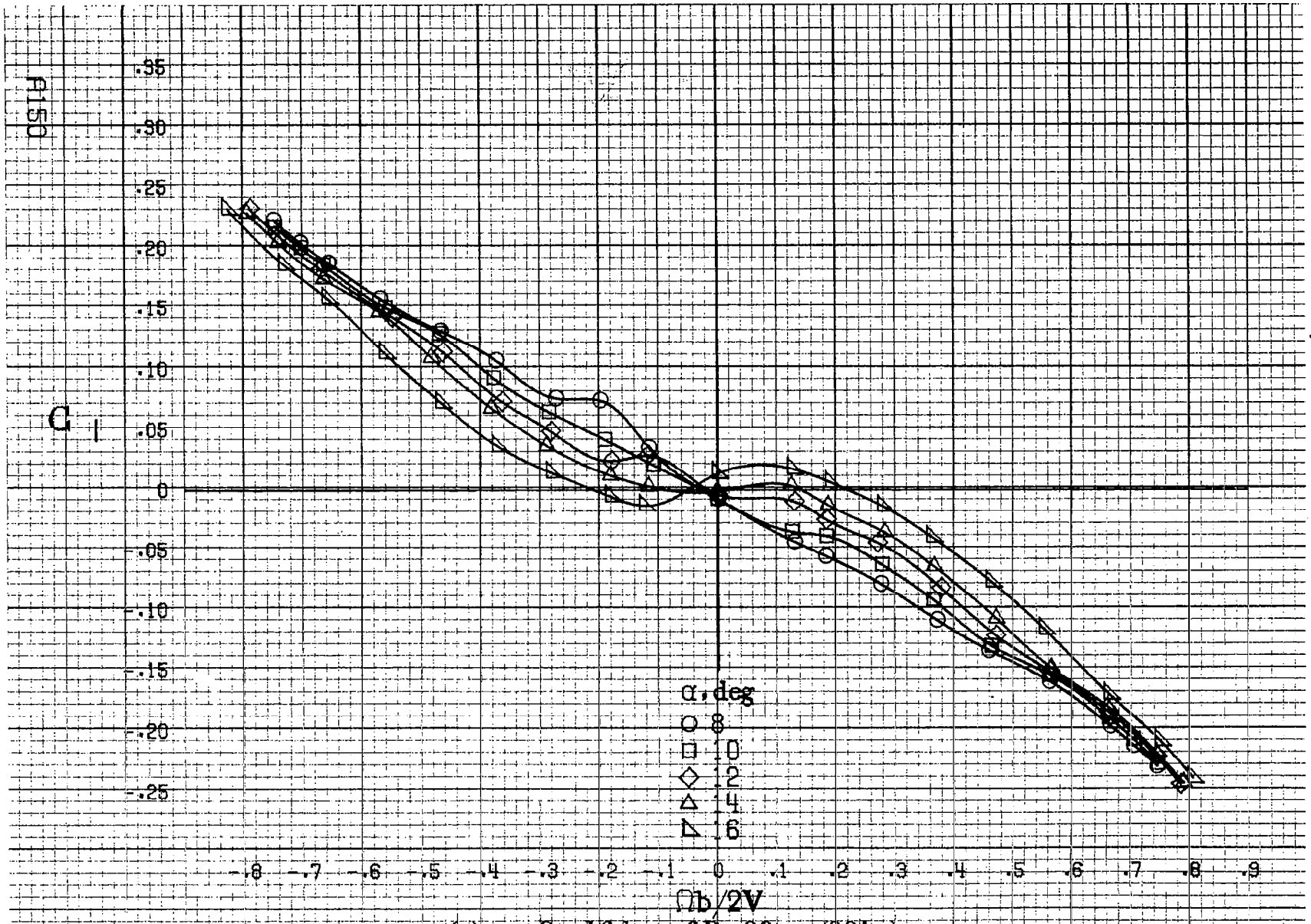

(a) α=8to16deg, SR=99cm(39in).

Figure A38. Effect of rotation rate and angle of attack on rolling-moment coefficient for no. 2 horizontal tail configuration. $\delta_e = 0°$, $\delta_a = 0°$, $\delta_r = 0°$, $\beta = 0°$.

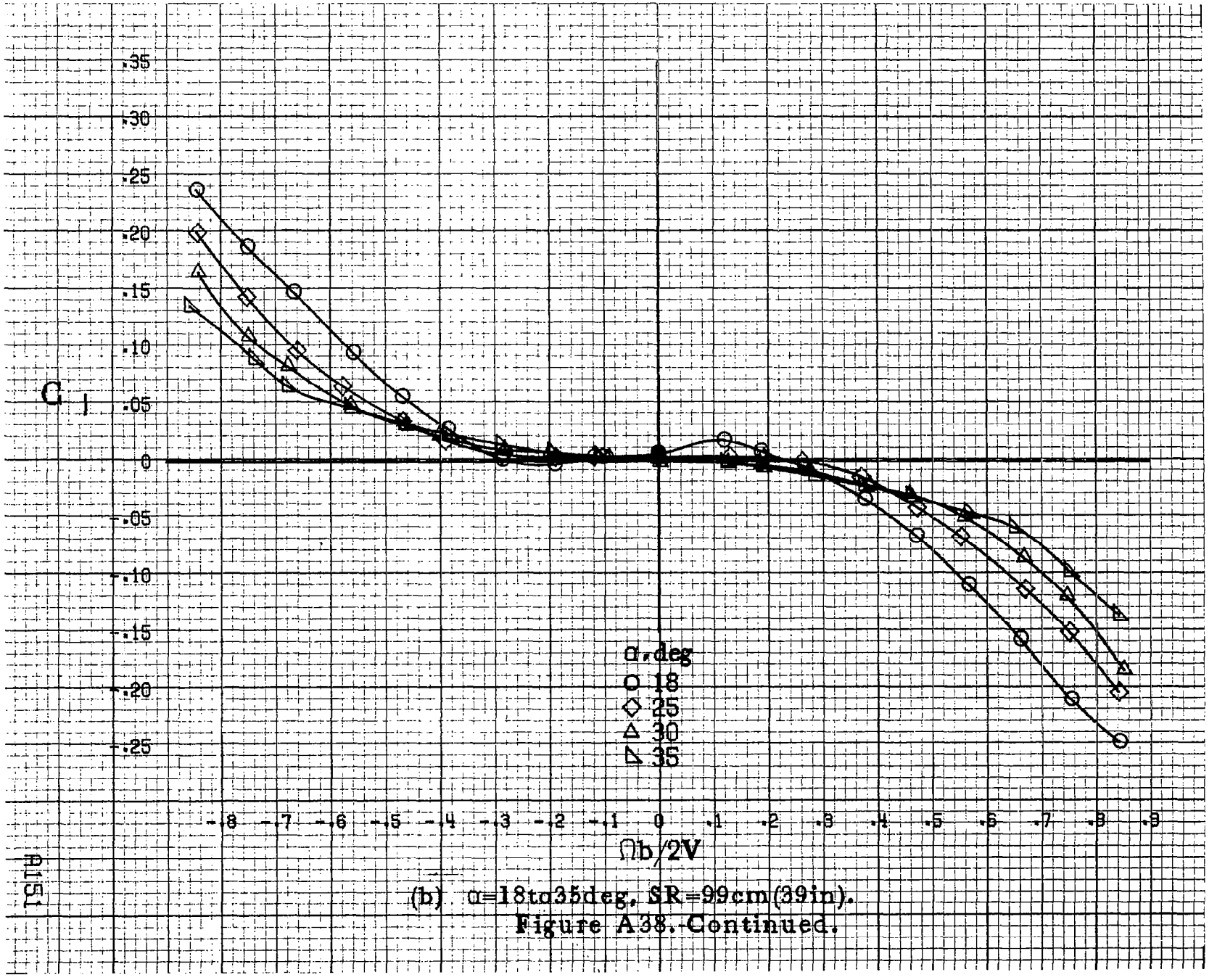

(b) α=18 to 35 deg, SR=99 cm (39 in).

Figure A38.-Continued.

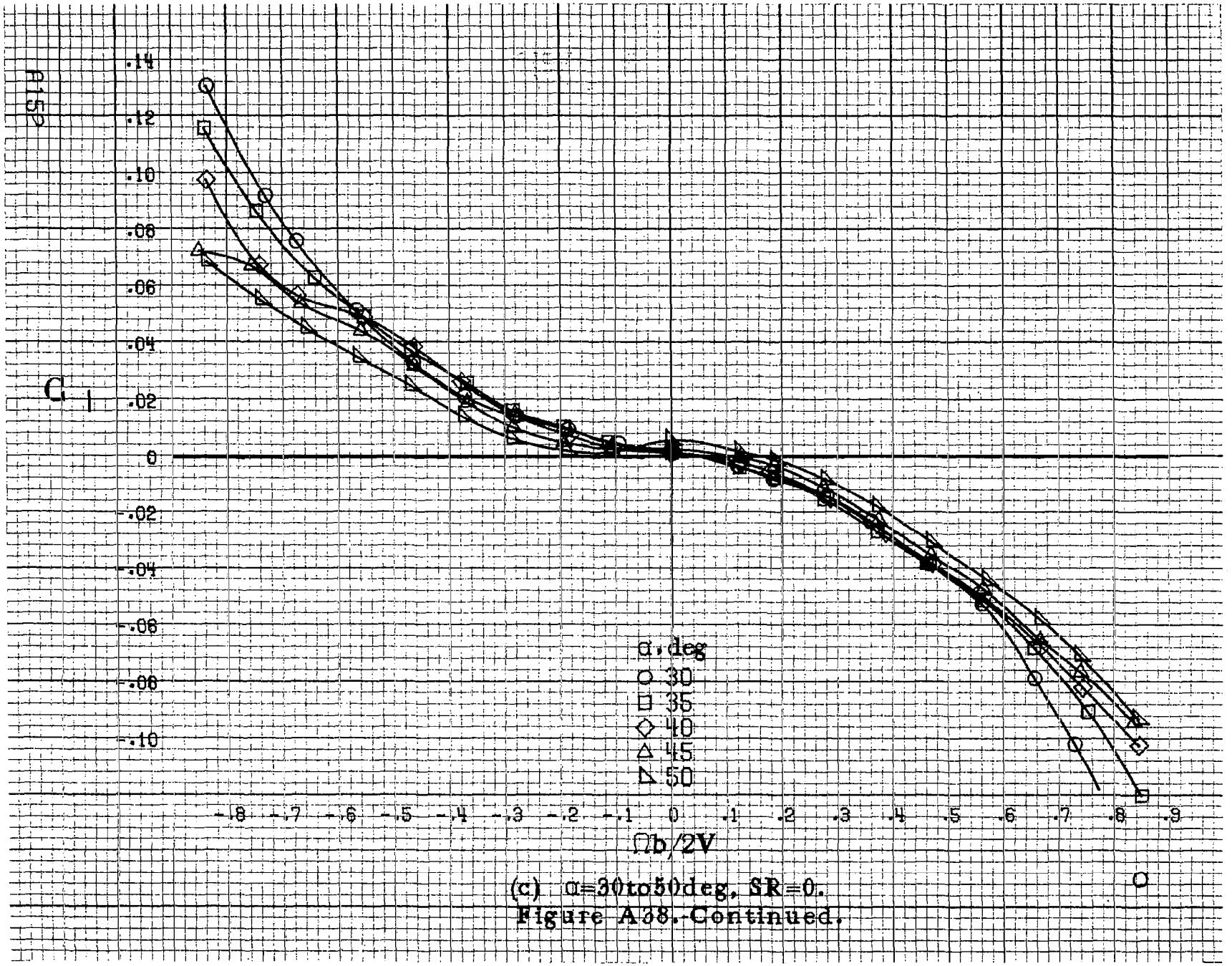

(c) α=30to50deg, SR=0.

Figure A38.-Continued.

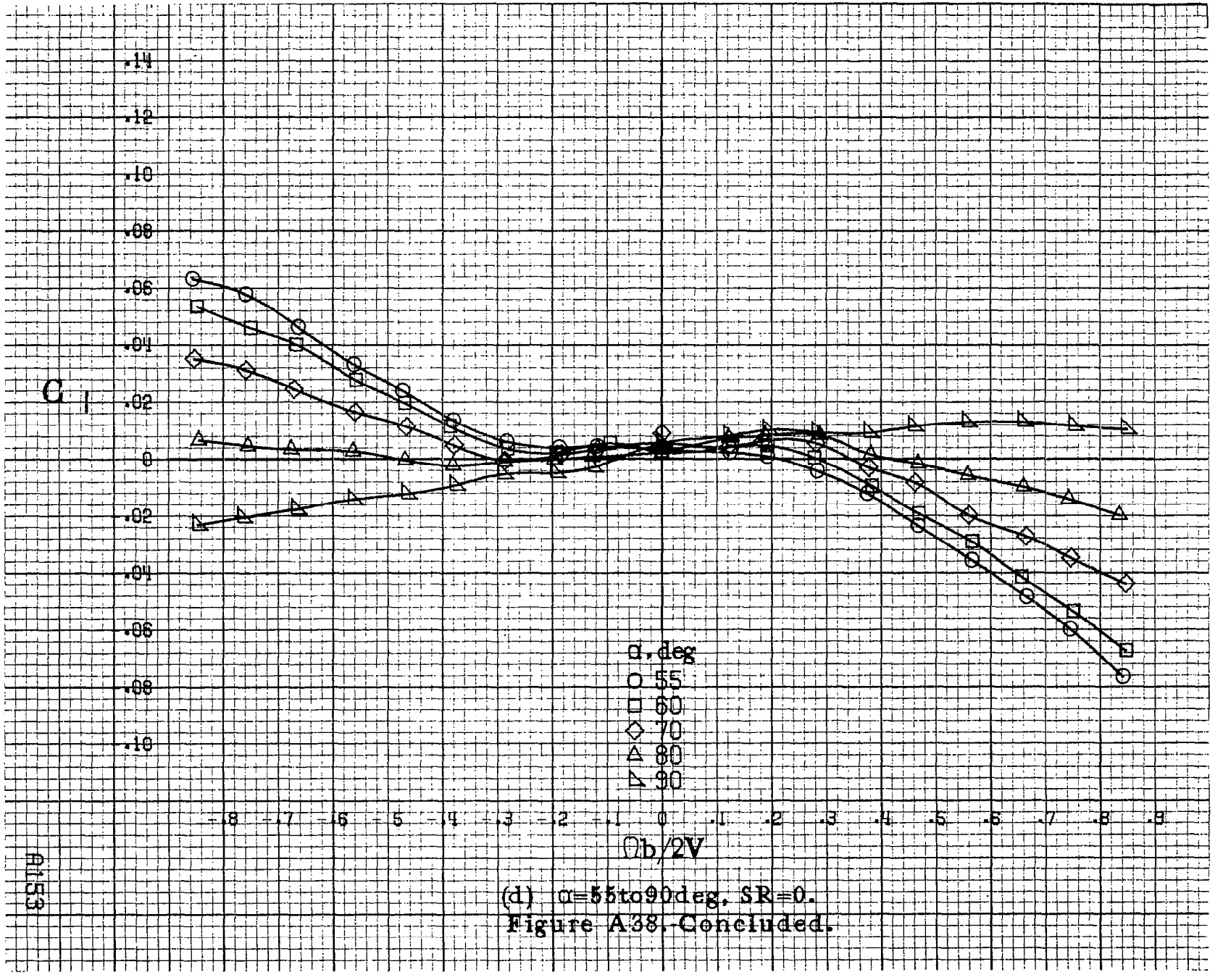

(d) α=55to90deg, SR=0.

Figure A38. Concluded.

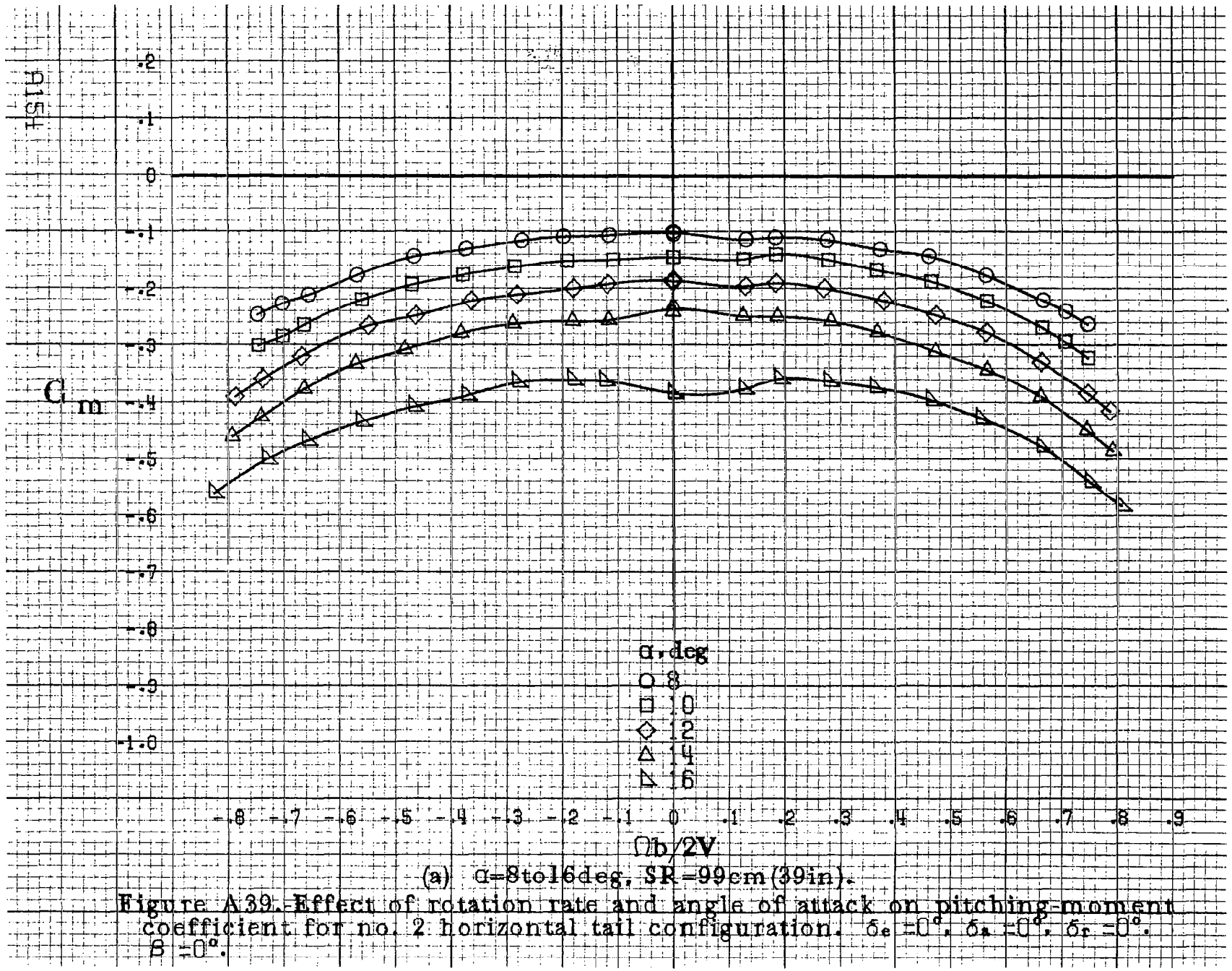

(a) α=8to16deg, SR=99cm(39in).

Figure A39.-Effect of rotation rate and angle of attack on pitching-moment coefficient for no. 2 horizontal tail configuration. $\delta_e = 0°$, $\delta_a = 0°$, $\delta_r = 0°$, $\beta = 0°$.

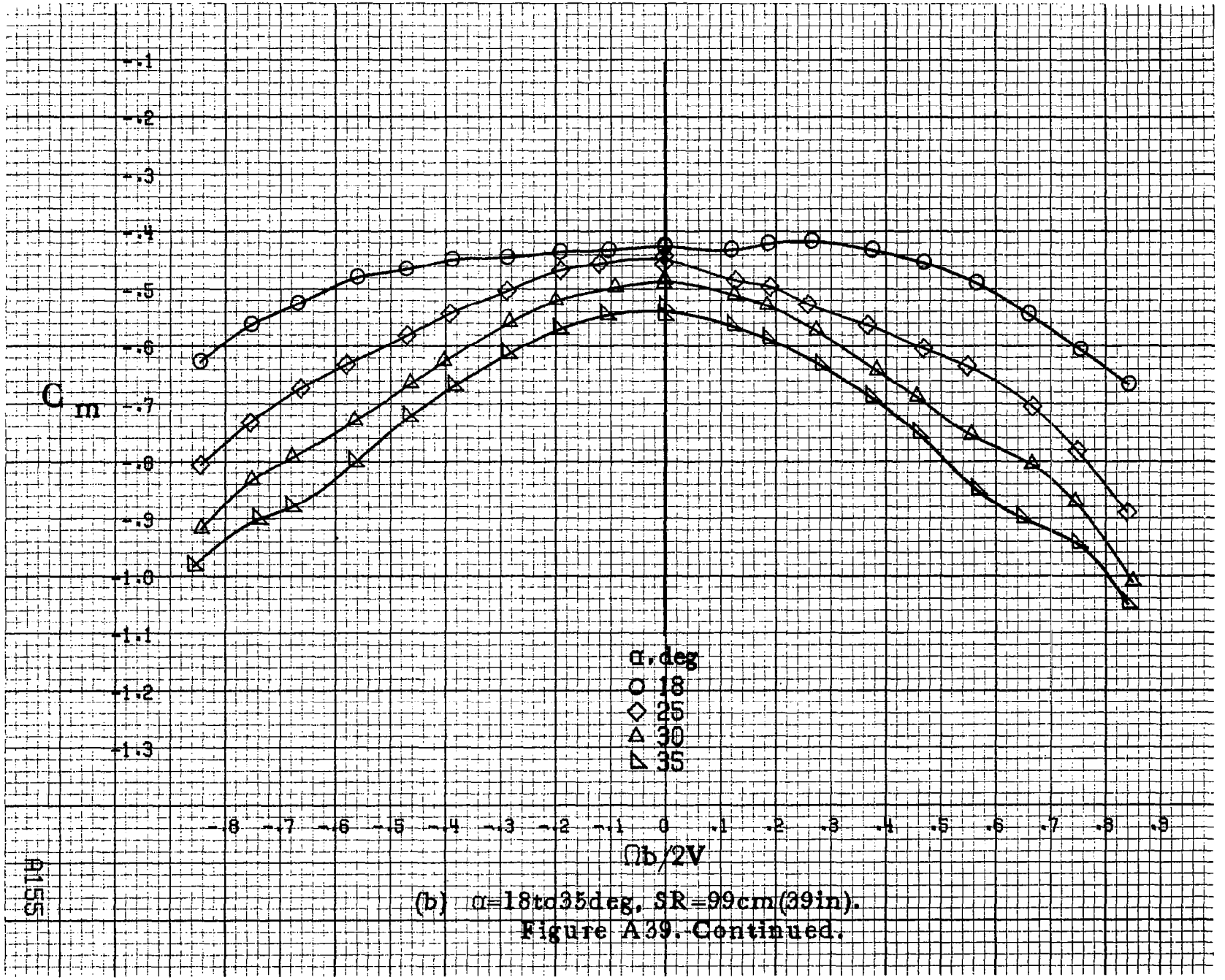

D155

(b) α=18to35deg, SR=99cm(39in).

Figure A39. Continued.

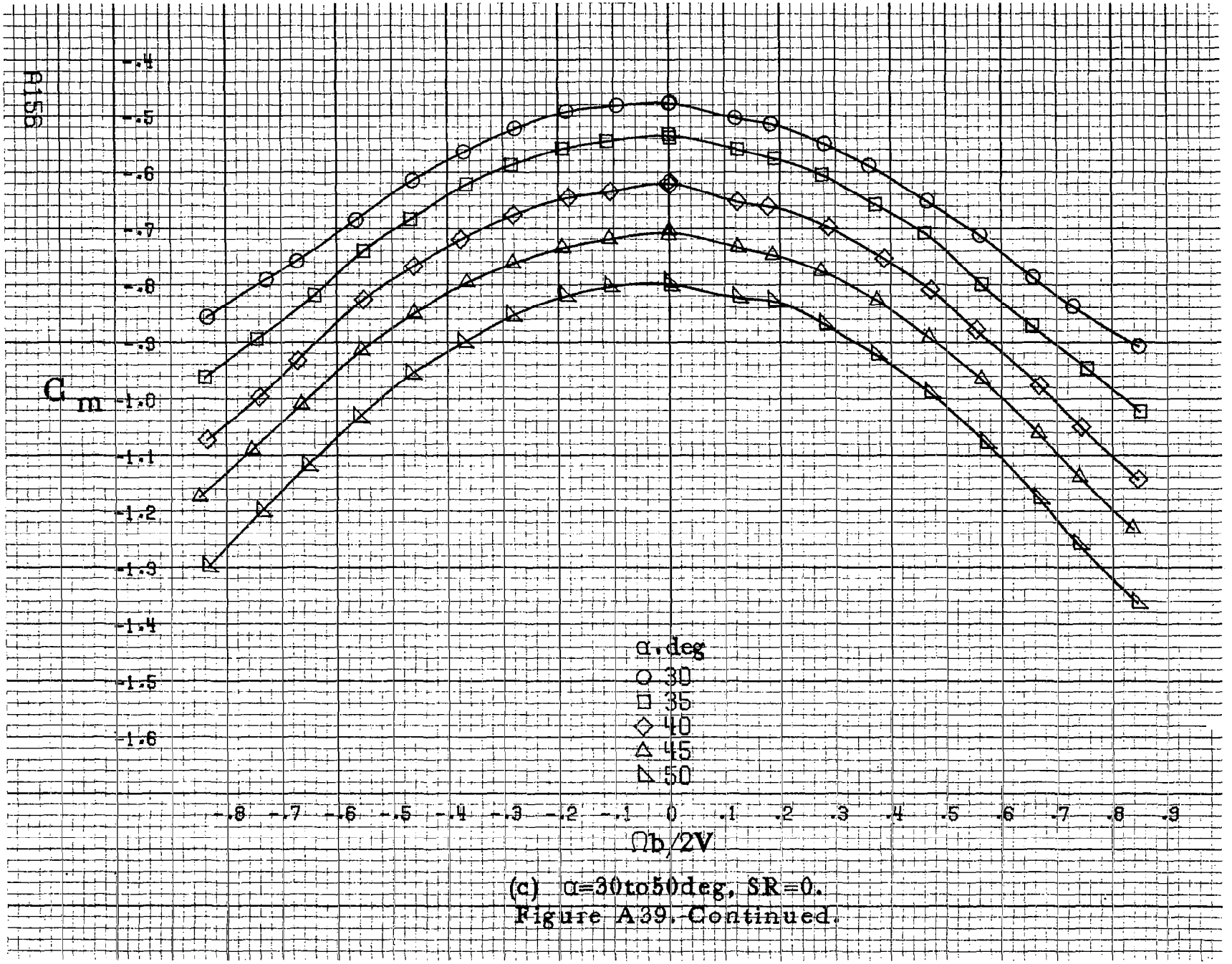

(c) α=30to50deg, SR=0.

Figure A39.-Continued.

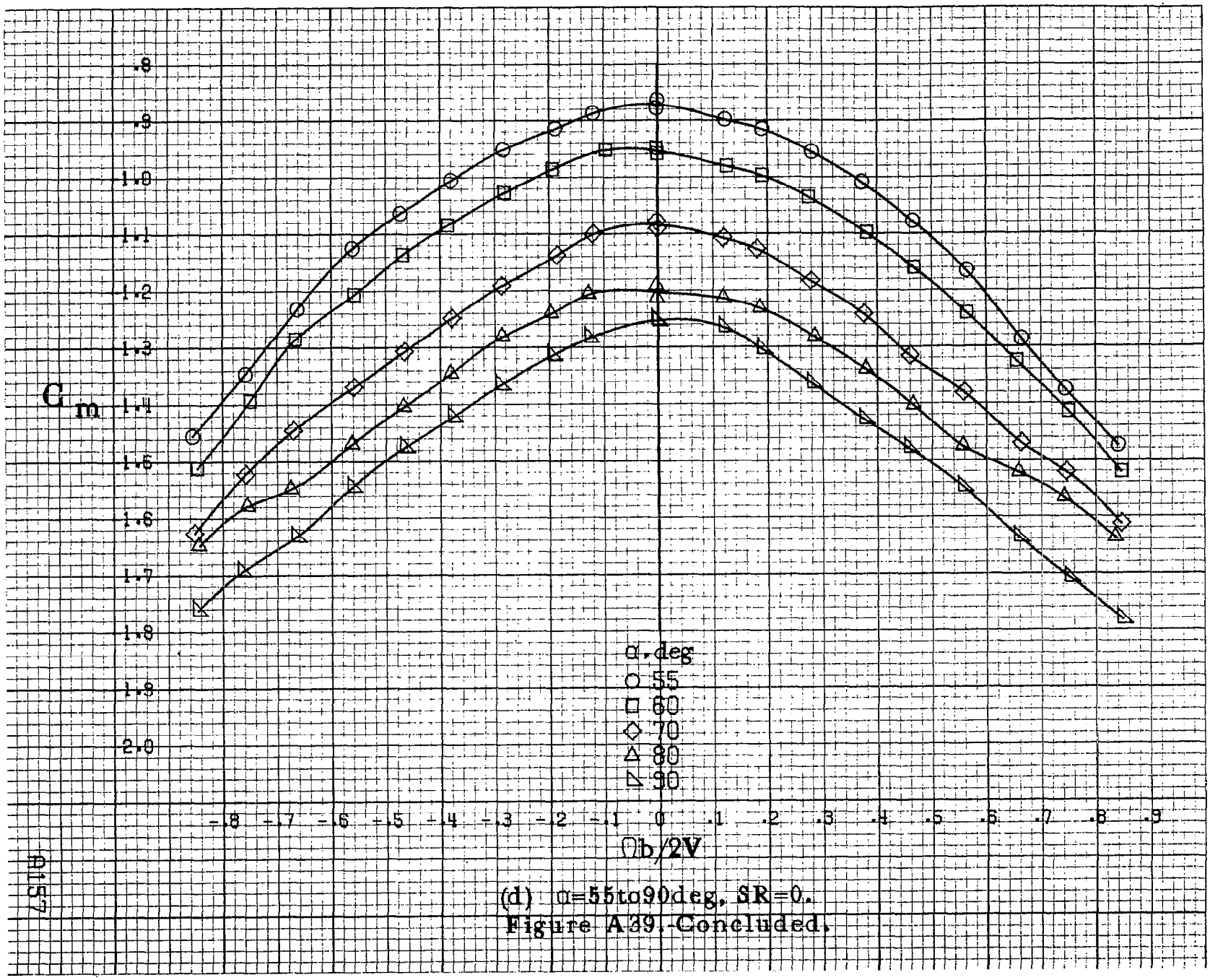

(d) α=55to90deg, SR=0.

Figure A39.-Concluded.

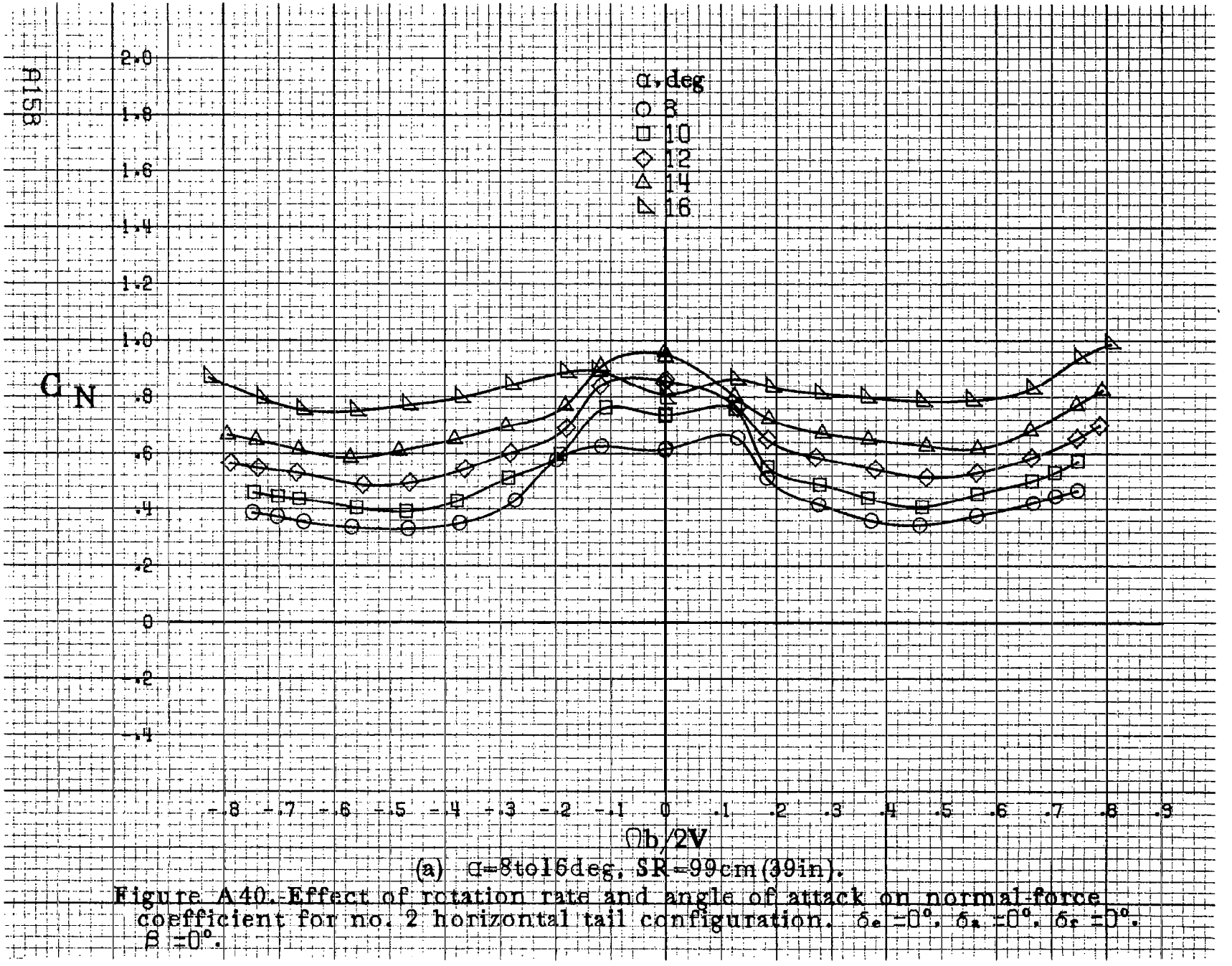

(a) α=8to16deg, SR=99cm(39in).

Figure A40. Effect of rotation rate and angle of attack on normal-force coefficient for no. 2 horizontal tail configuration. $\delta_e = 0°$, $\delta_a = 0°$, $\delta_r = 0°$, $\beta = 0°$.

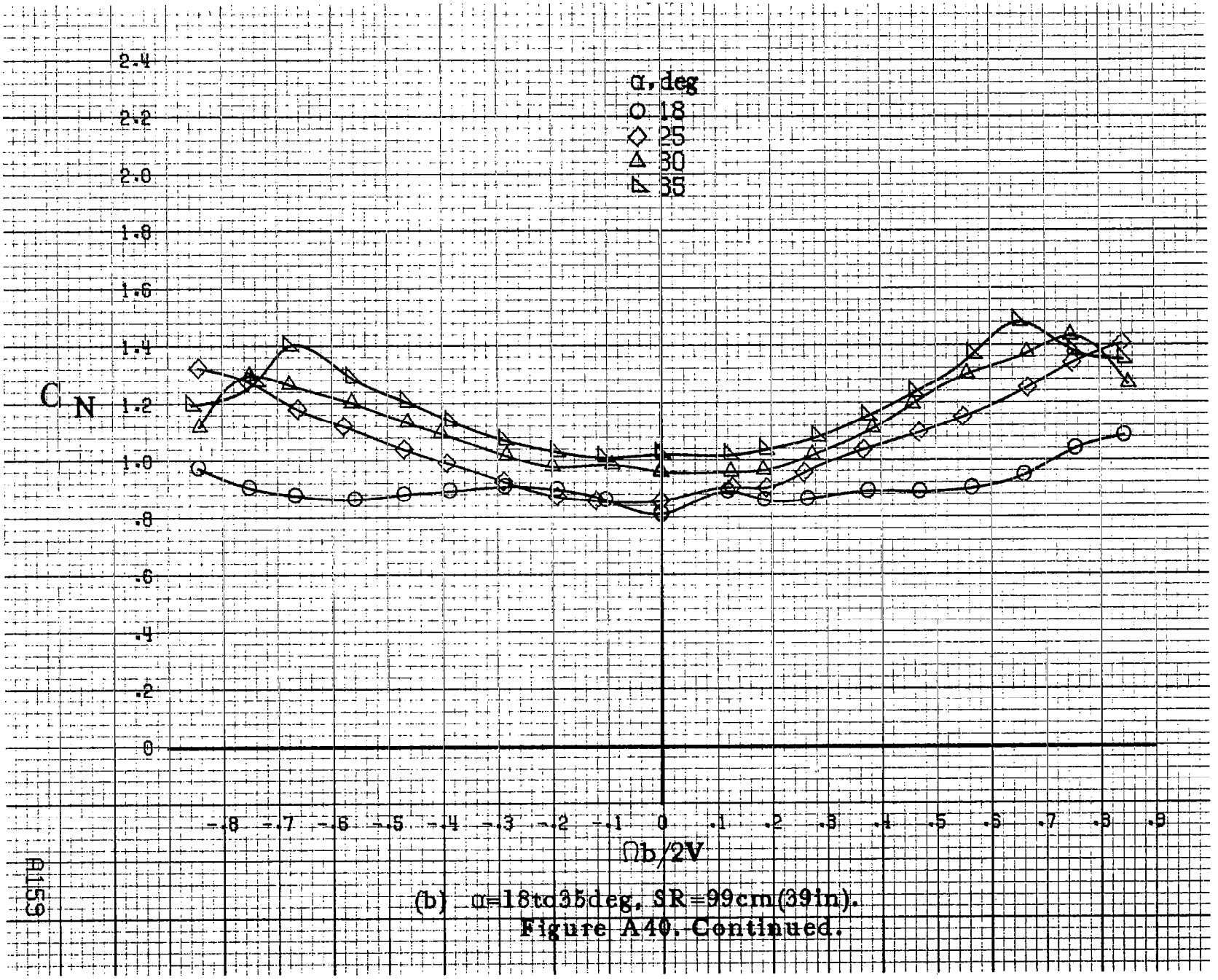

B156

(b) α=18to35deg, SR=99cm(39in).

Figure A40. Continued.

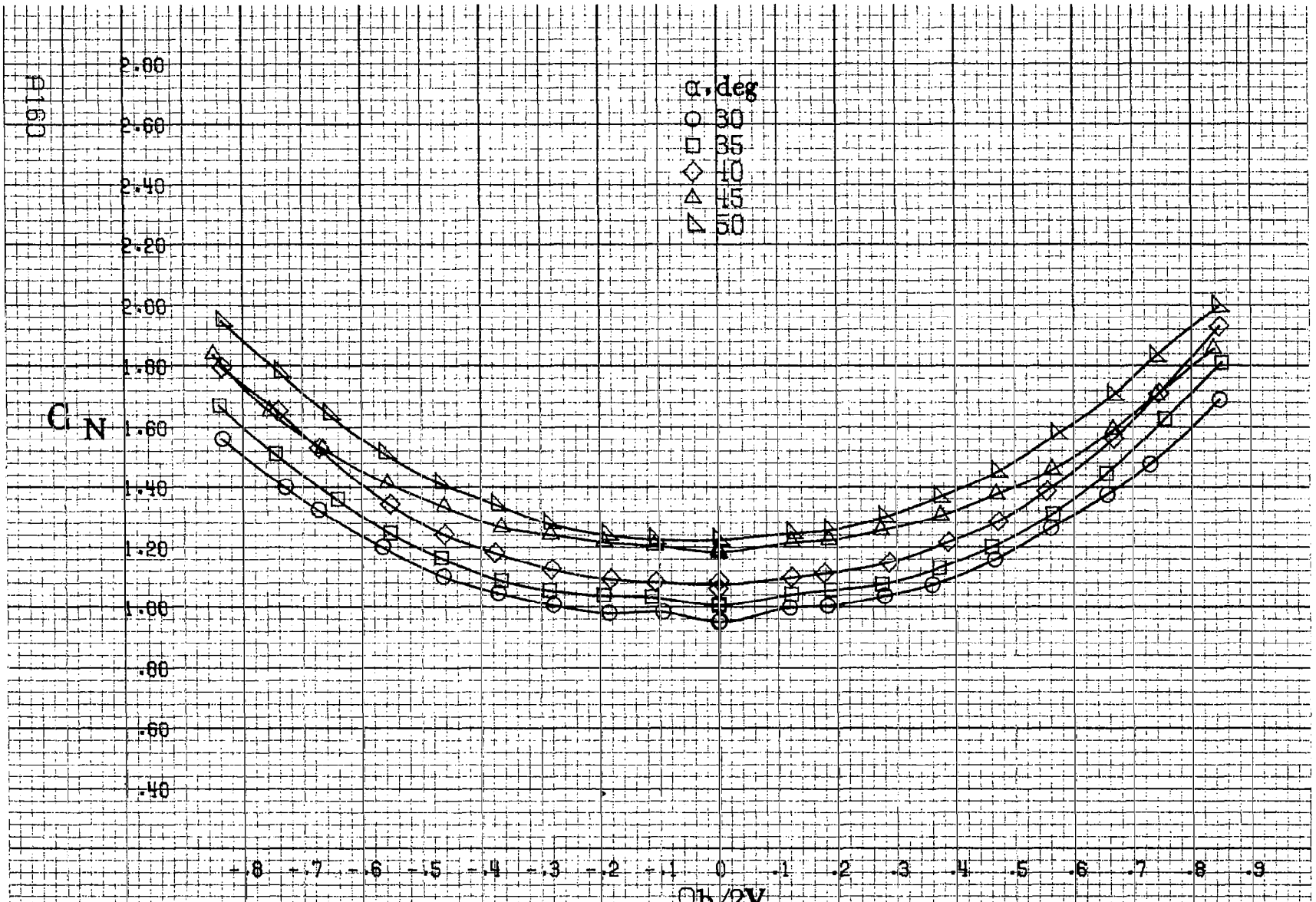

(c) α=30 to 50 deg, SR=0.

Figure A40.-Continued.

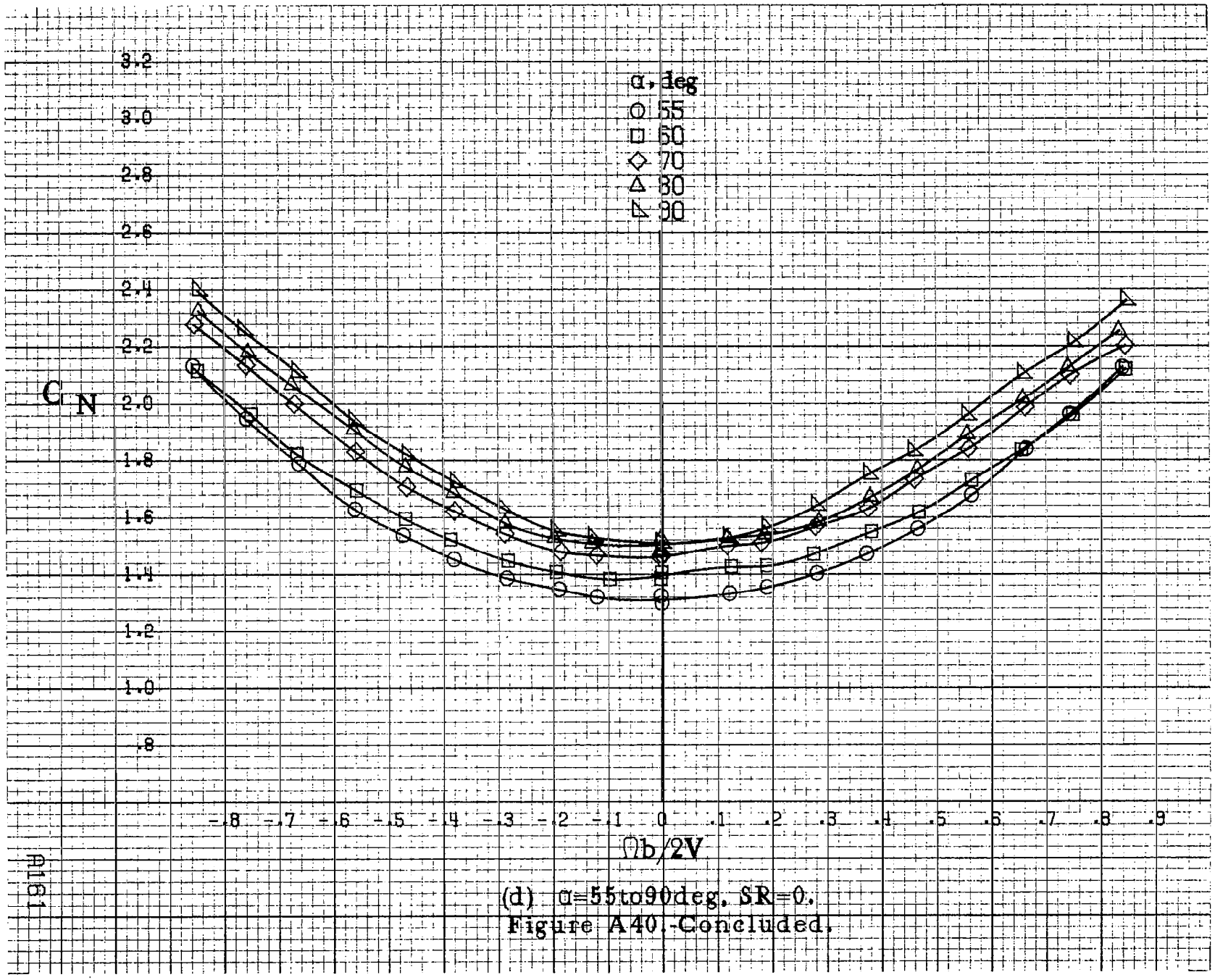

(d) α=55to90deg, SR=0.

Figure A40.-Concluded.

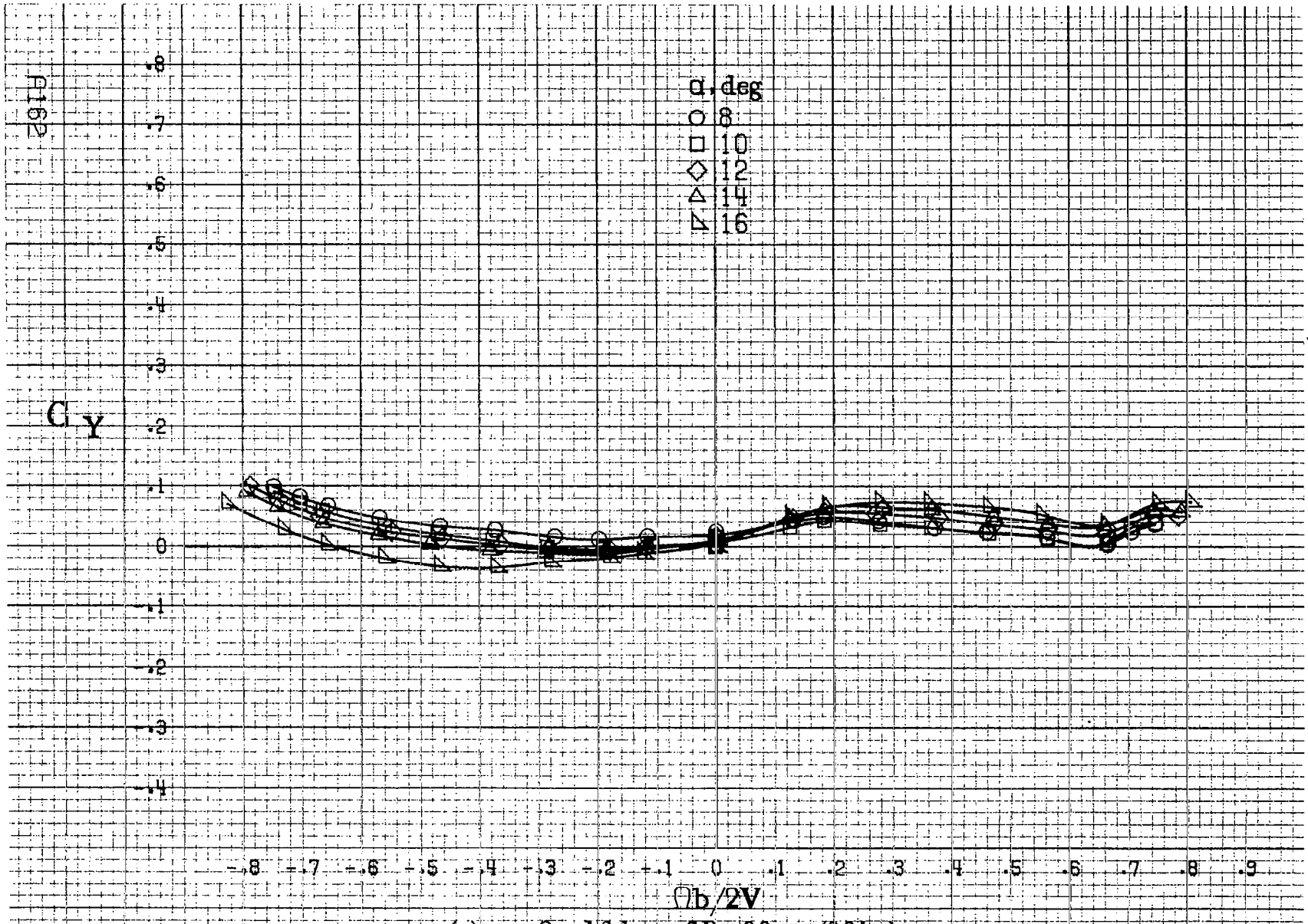

(a) α=8to16deg, SR=99cm(39in).

Figure A41. Effect of rotation rate and angle of attack on side-force coefficient for no. 2 horizontal tail configuration. $\delta_e = 0°$, $\delta_a = 0°$, $\delta_r = 0°$, $\beta = 0°$.

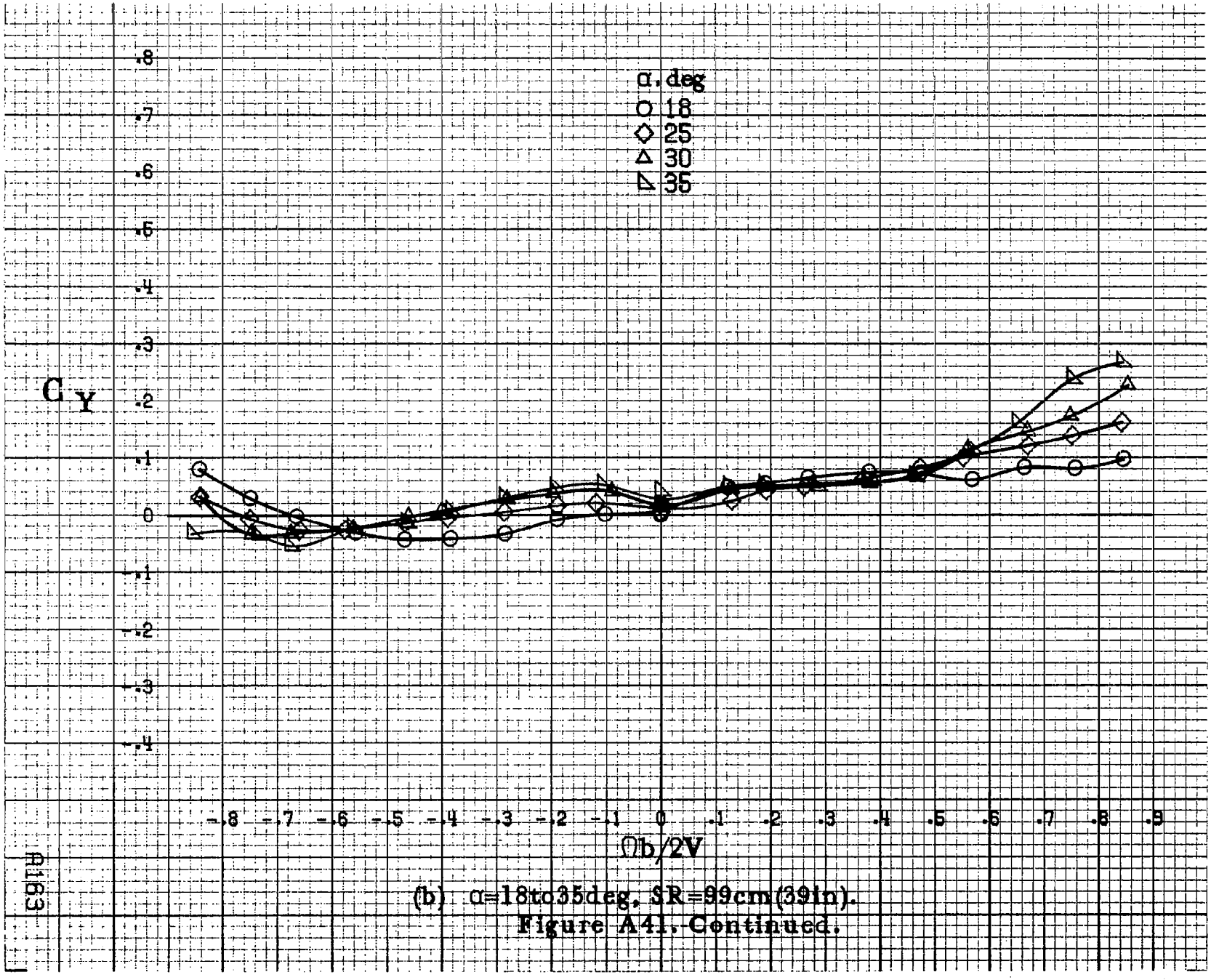

R1163

(b) α=18to35deg, SR=99cm(39in).

Figure A41.-Continued.

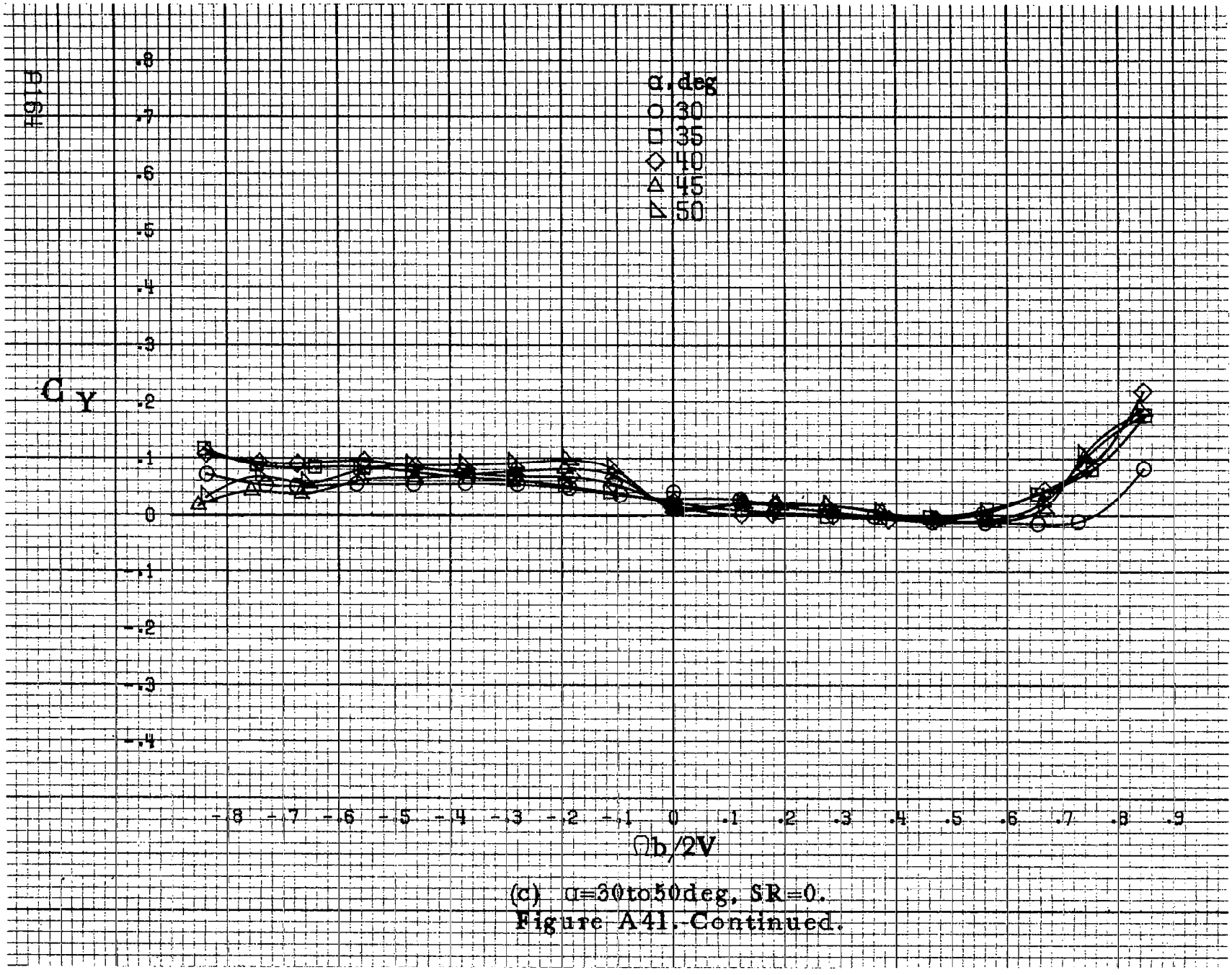

(c) α=30to50deg, SR=0.

Figure A41.-Continued.

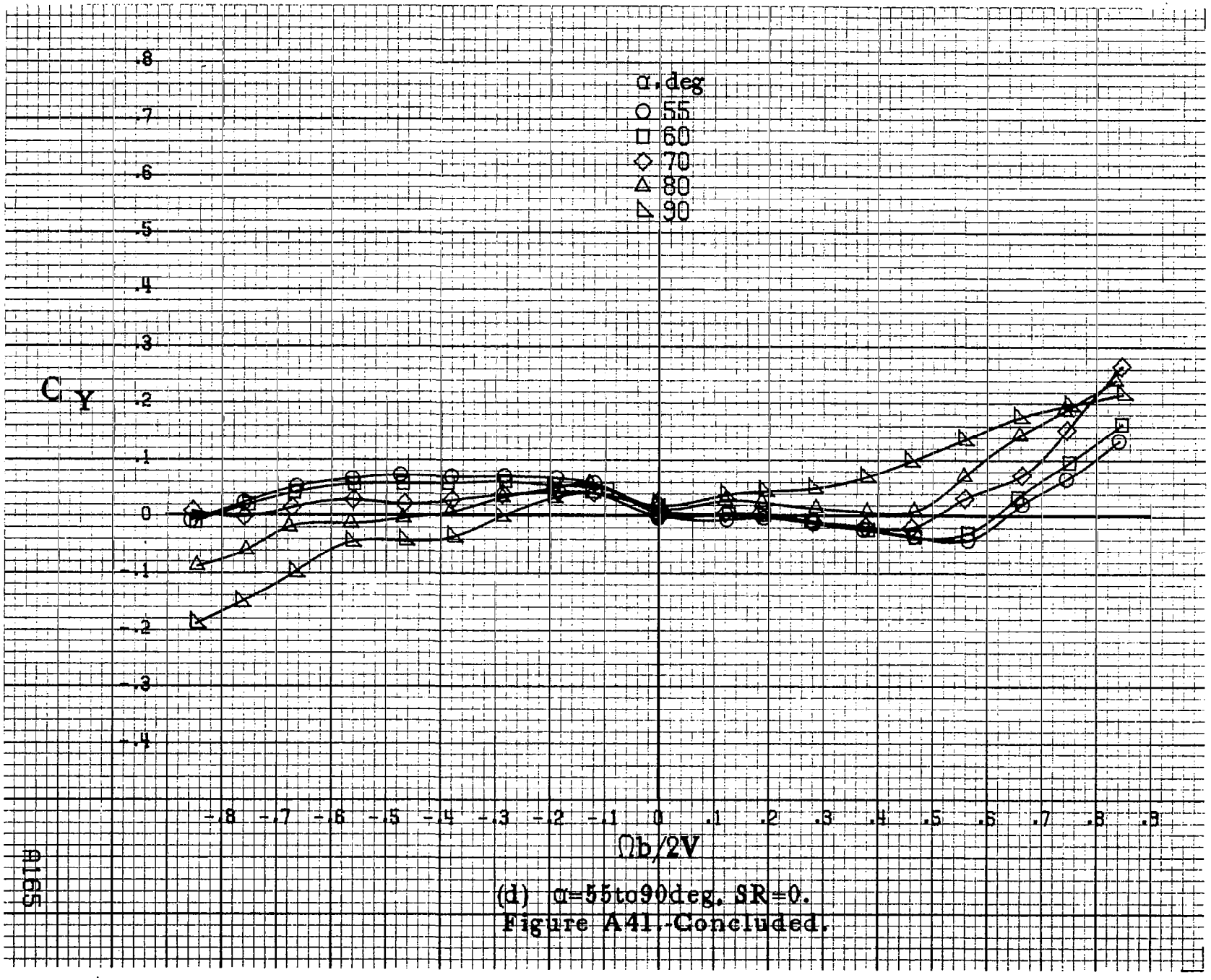

(d) α=55to90deg. SR=0.

Figure A41.-Concluded.

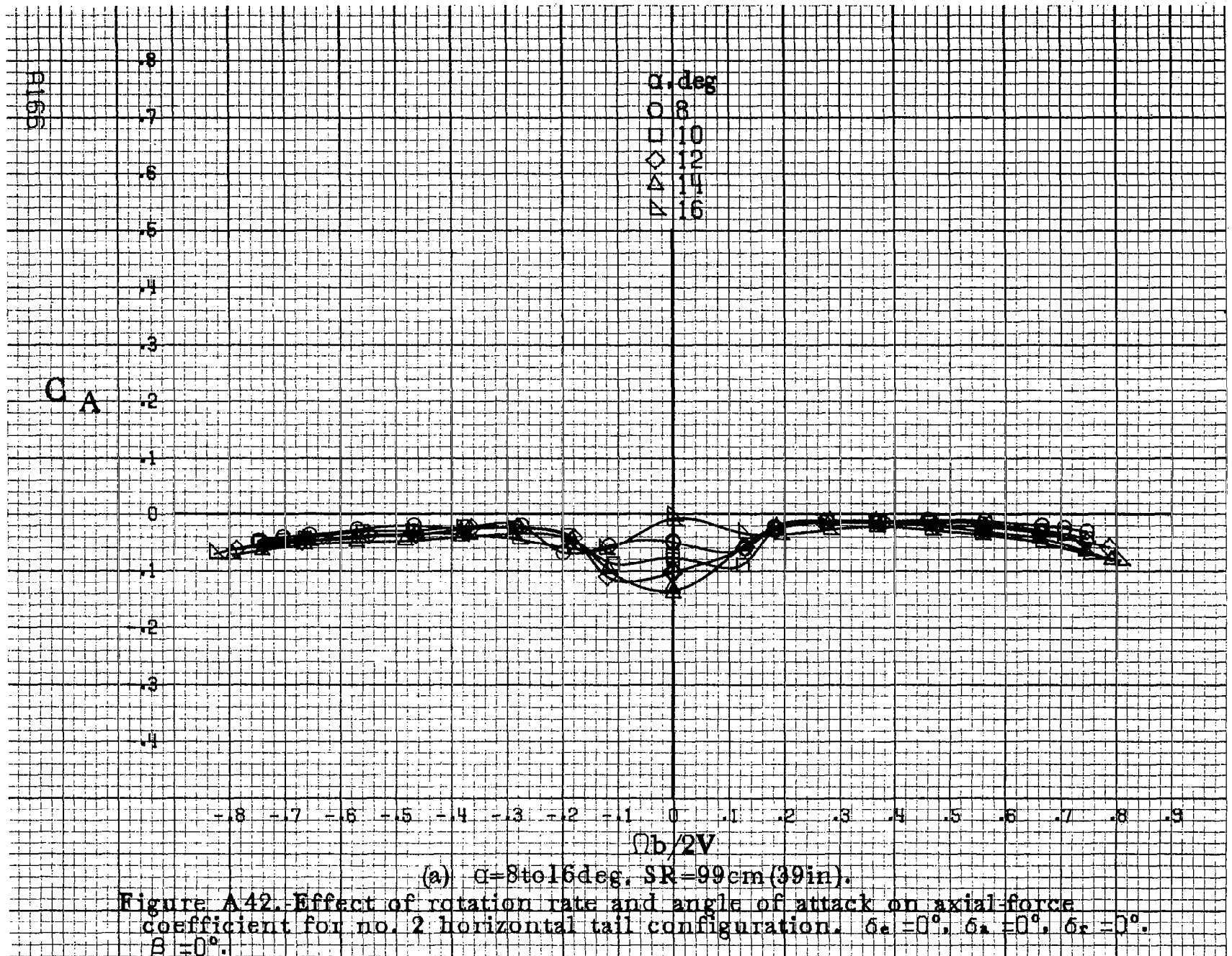

(a) α=8to16deg, SR=99cm(39in).

Figure A42.-Effect of rotation rate and angle of attack on axial-force coefficient for no. 2 horizontal tail configuration. $\delta_e = 0°$, $\delta_a = 0°$, $\delta_r = 0°$, $\beta = 0°$.

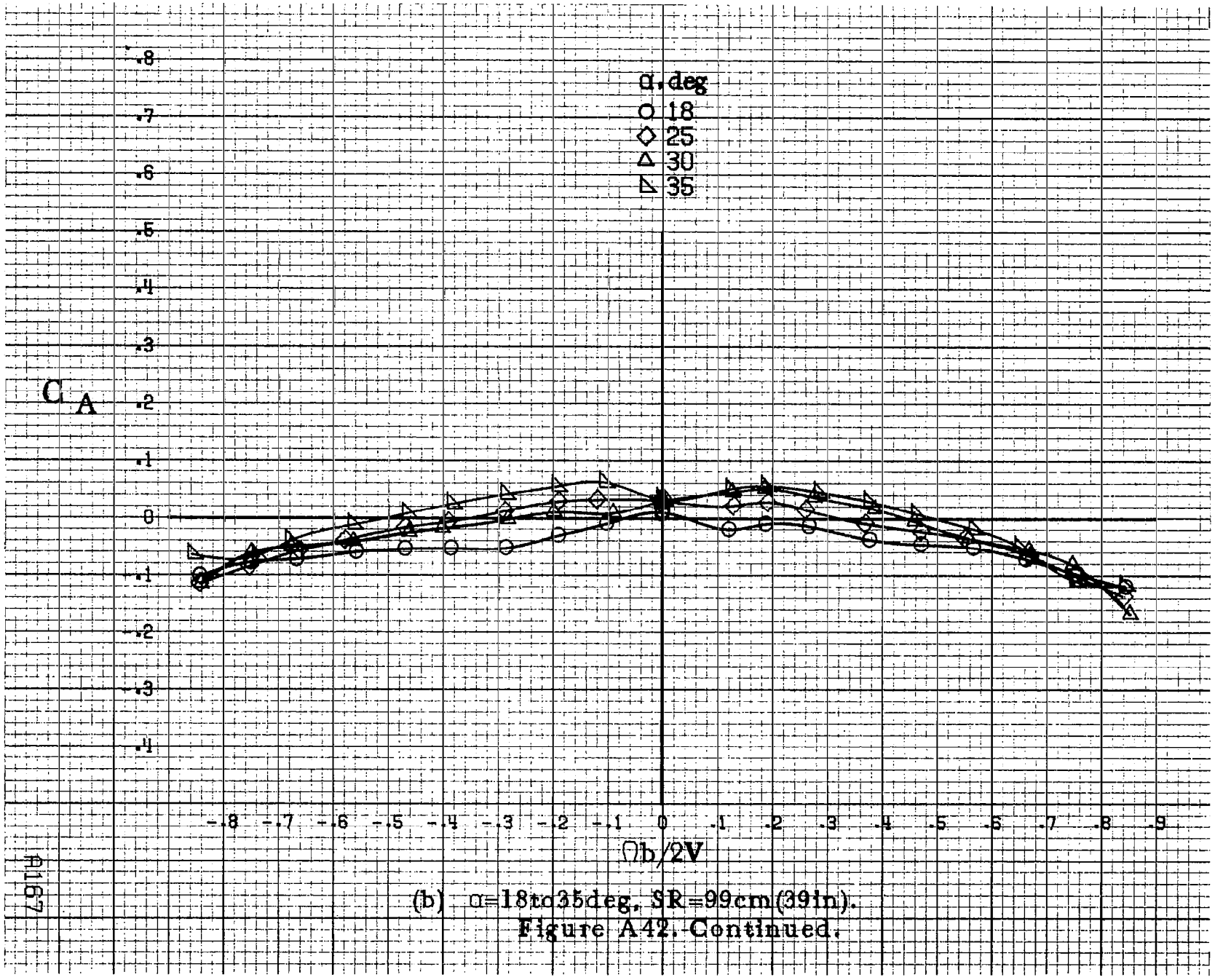

(b) α=18to35deg, SR=99cm(39in).

Figure A42. Continued.

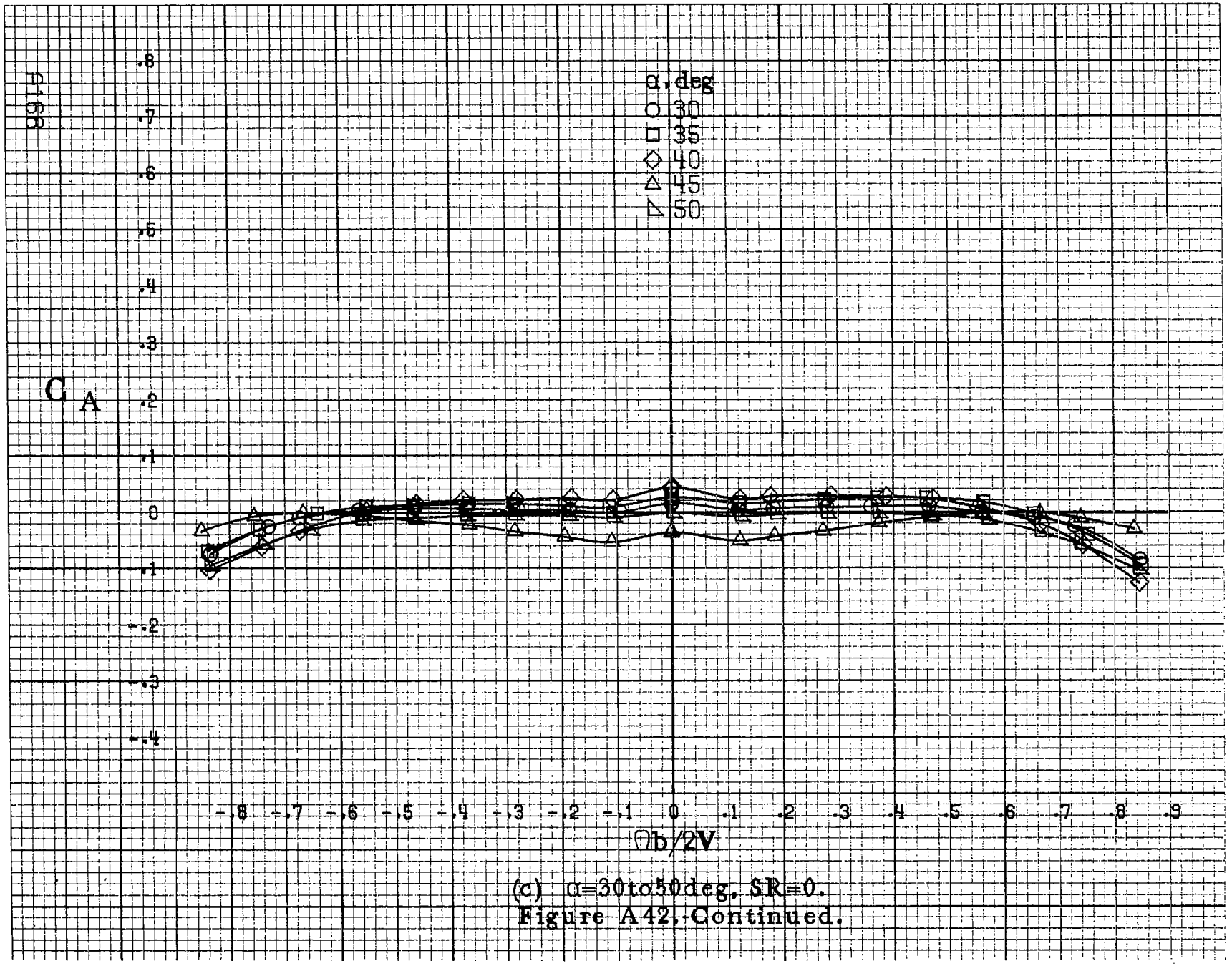

(c) α=30 to 50 deg, SR=0.

Figure A42.-Continued.

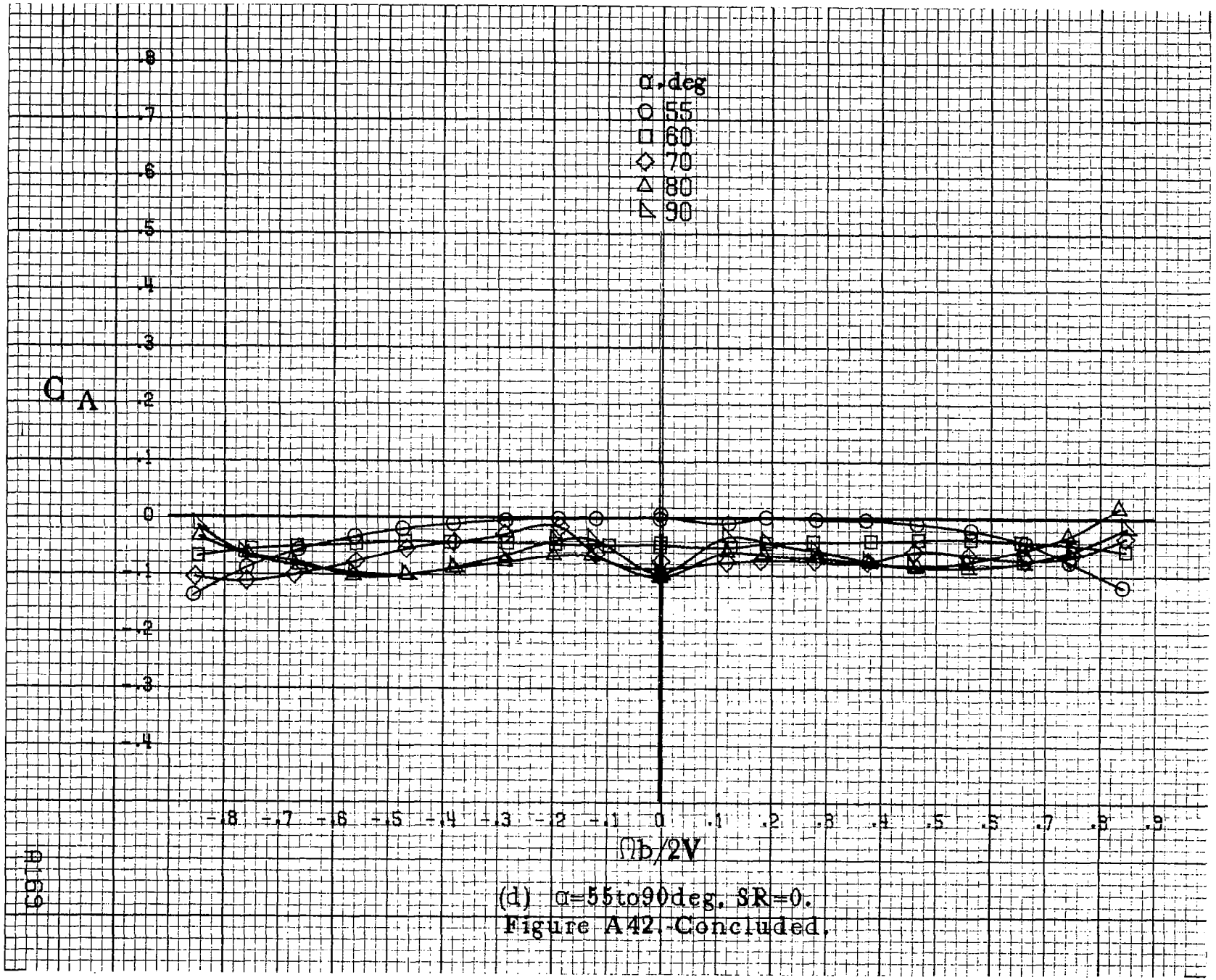

(d) α=55to90deg. SR=0.

Figure A42. Concluded.

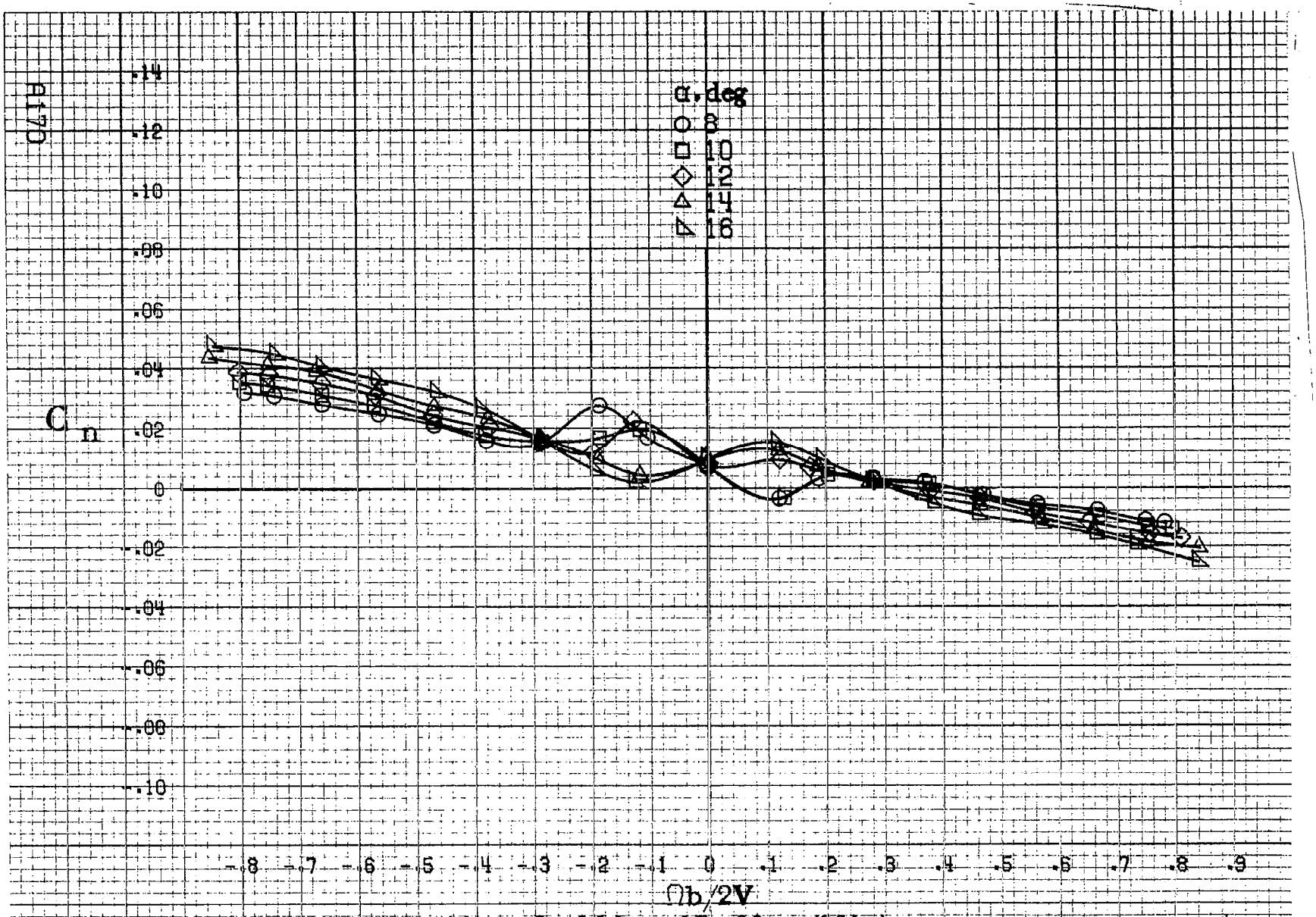

(a) α=8to16deg, SR=99cm(39in).

Figure A43. Effect of rotation rate and angle of attack on yawing-moment coefficient for no. 2 horizontal tail configuration. $\delta_e = 0°$, $\delta_a = 0°$, $\delta_r = -25°$, $\beta = 0°$.

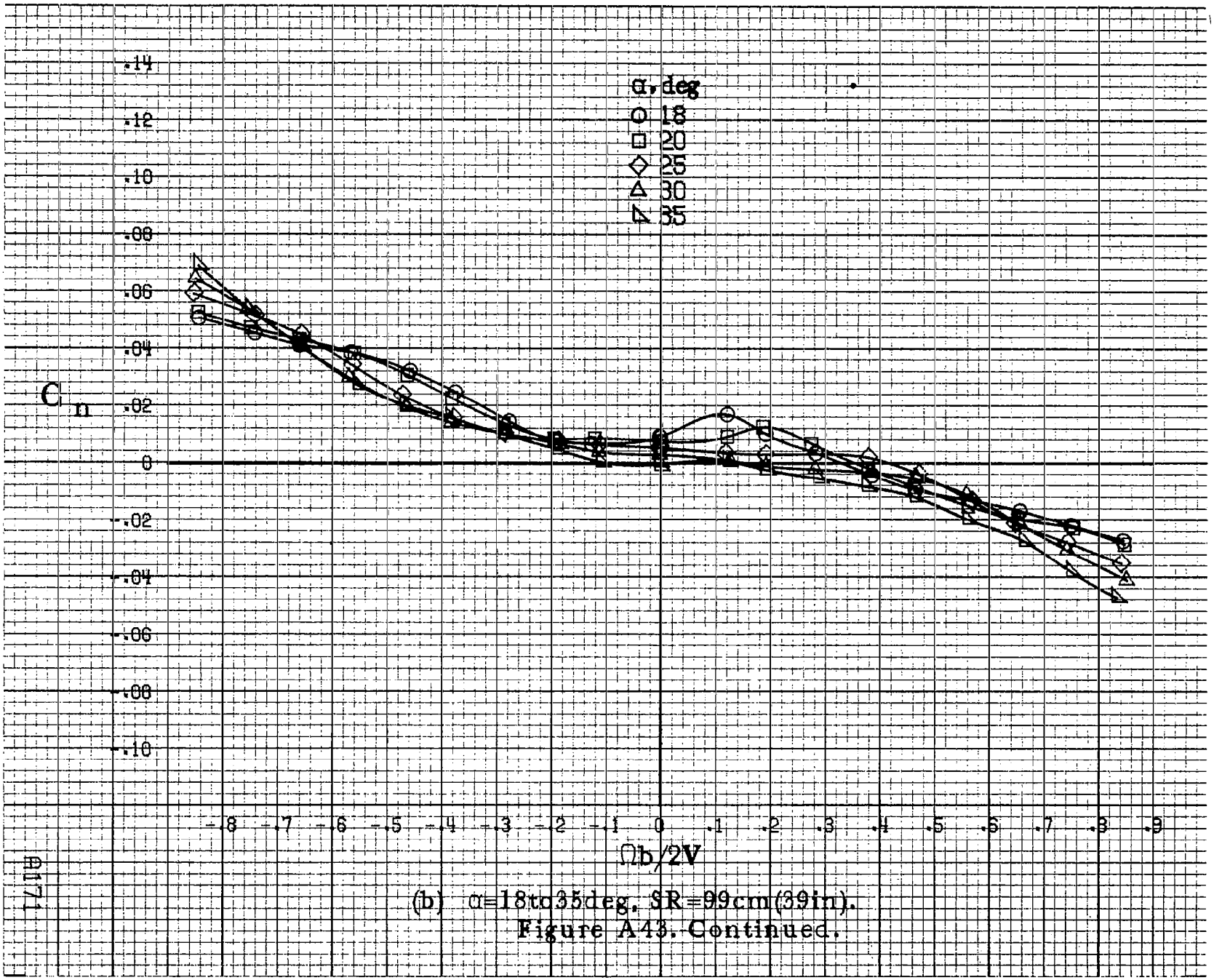

(b) α=18to35deg. SR=99cm(39in).

Figure A43. Continued.

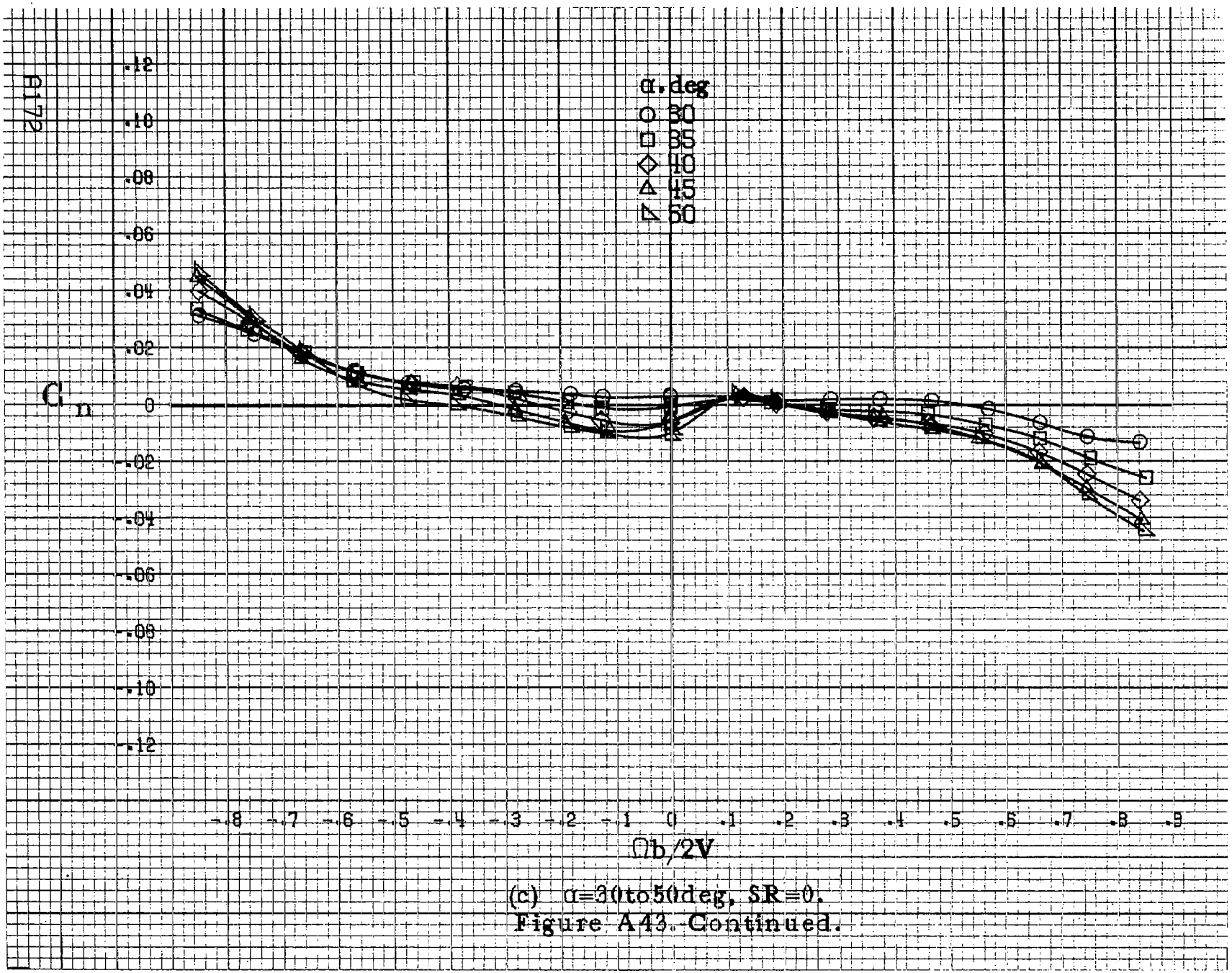

(c) α=30to50deg, SR=0.

Figure A43. Continued.

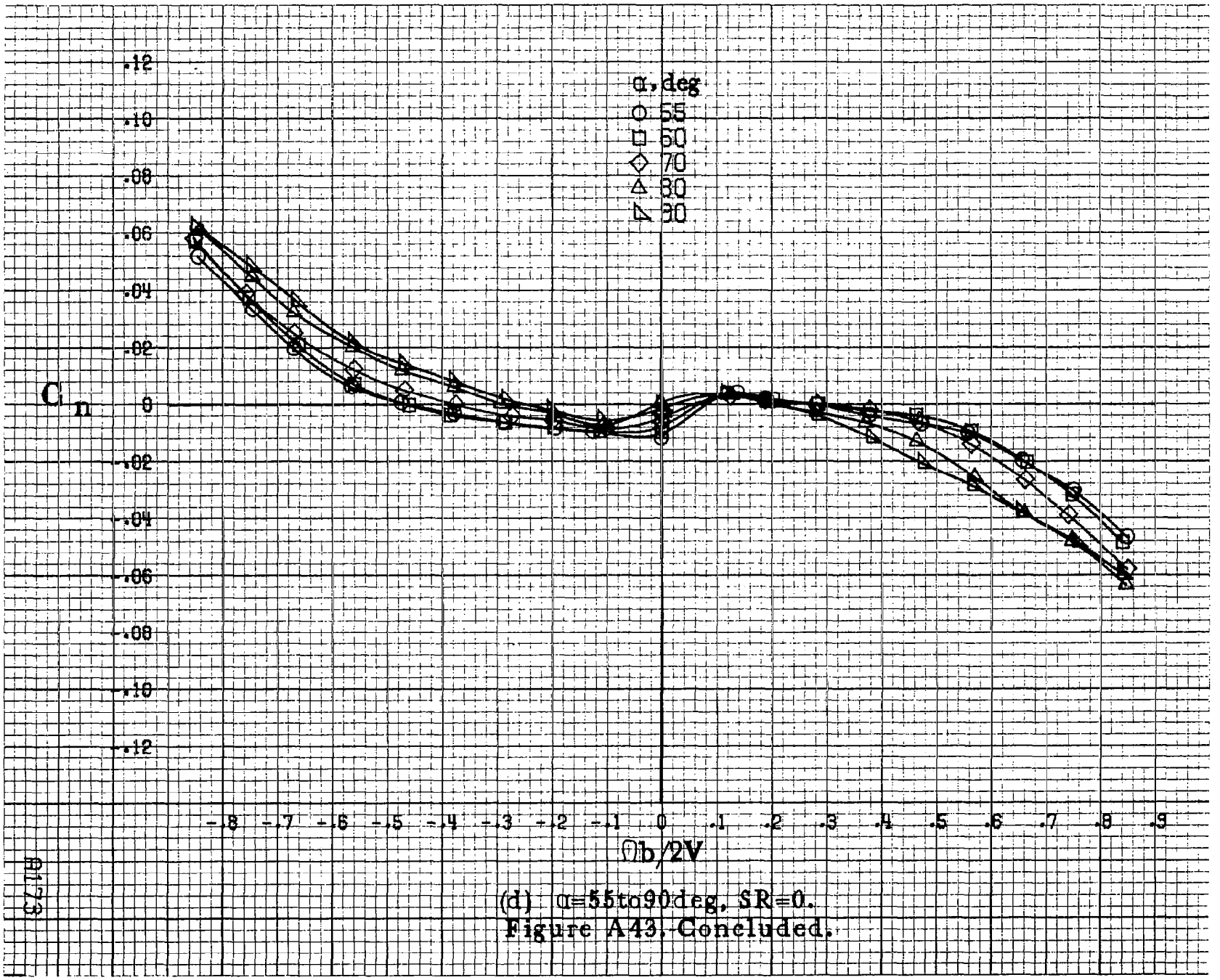

(d) α=55 to 90 deg, SR=0.

Figure A43. Concluded.

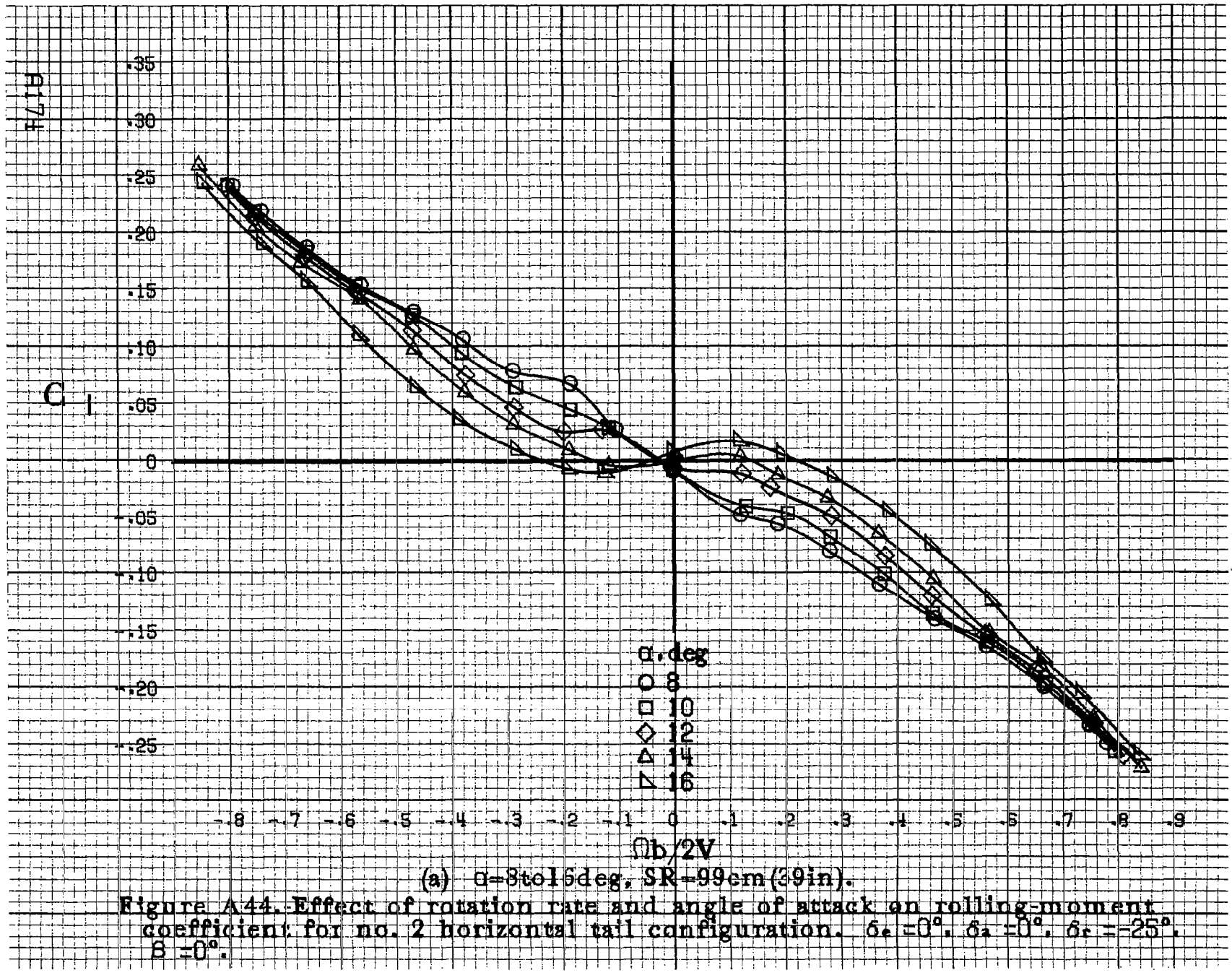

(a) α=8to16deg, SR=99cm(39in).

Figure A44.-Effect of rotation rate and angle of attack on rolling-moment coefficient for no. 2 horizontal tail configuration. $\delta_e = 0°$, $\delta_a = 0°$, $\delta_r = -25°$, $\beta = 0°$.

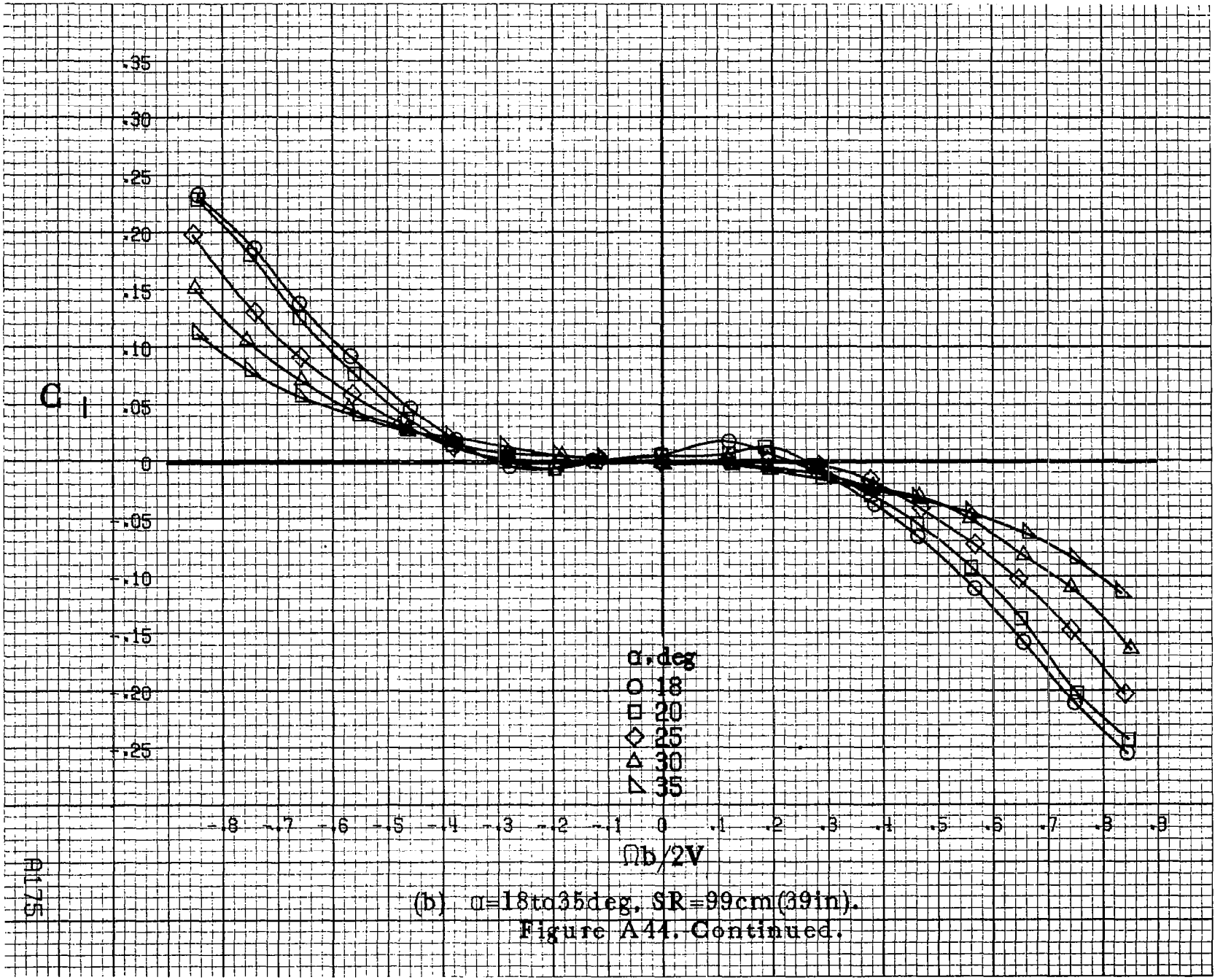

(b) α=18to35deg, SR=99cm(39in).

Figure A44. Continued.

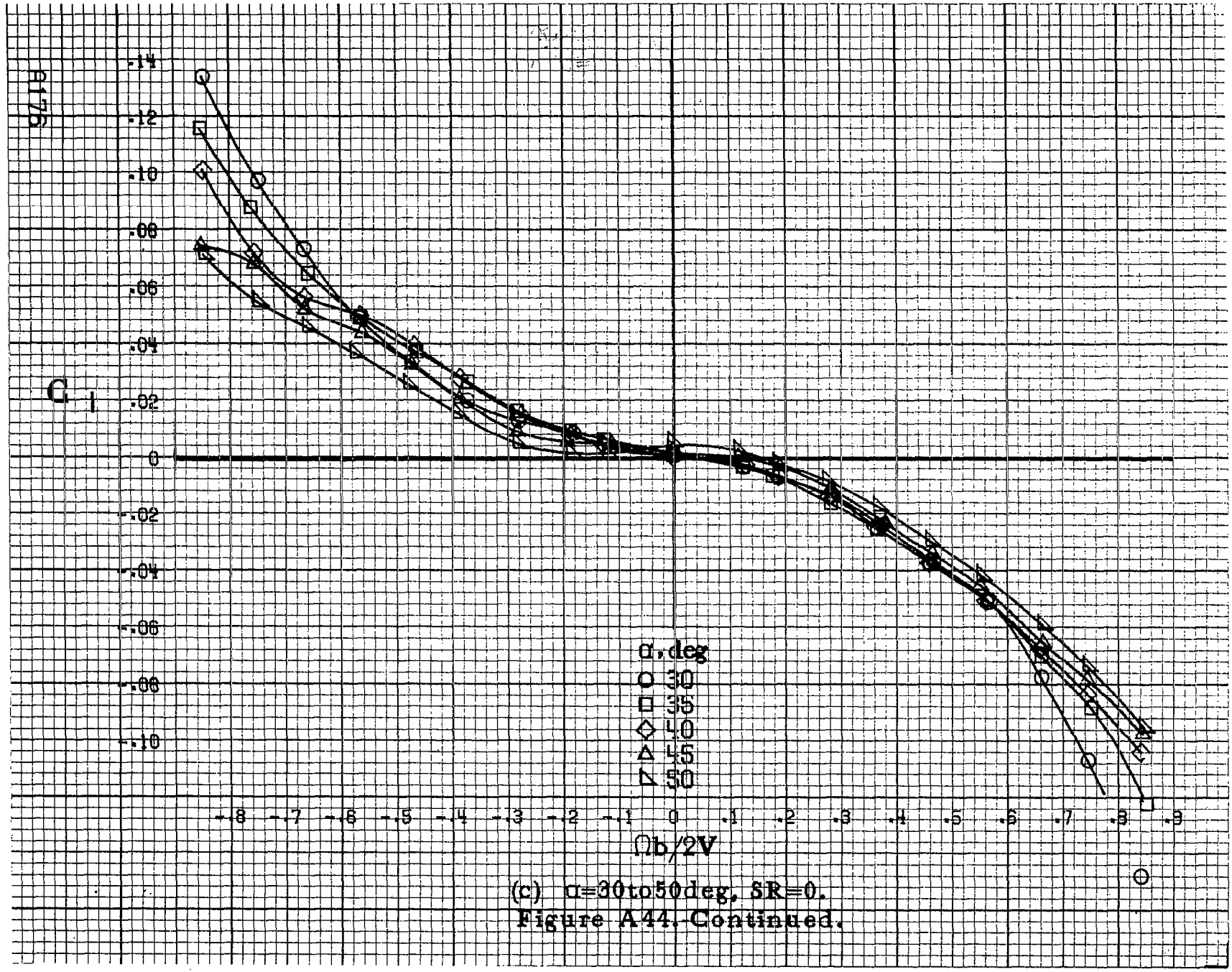

(c) α=30to50deg, SR=0.

Figure A44.-Continued.

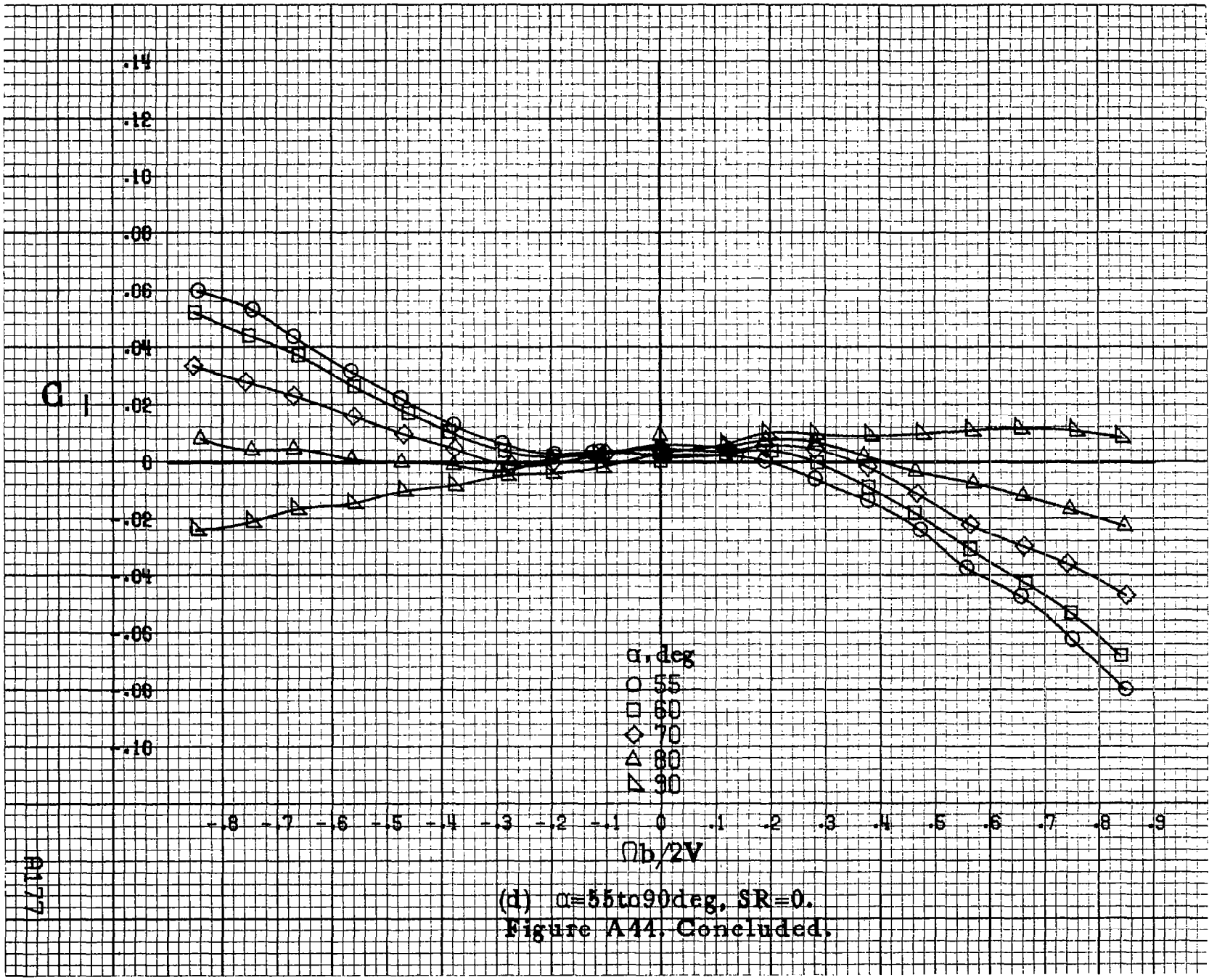

(d) α=55to90deg, SR=0.

Figure A44. Concluded.

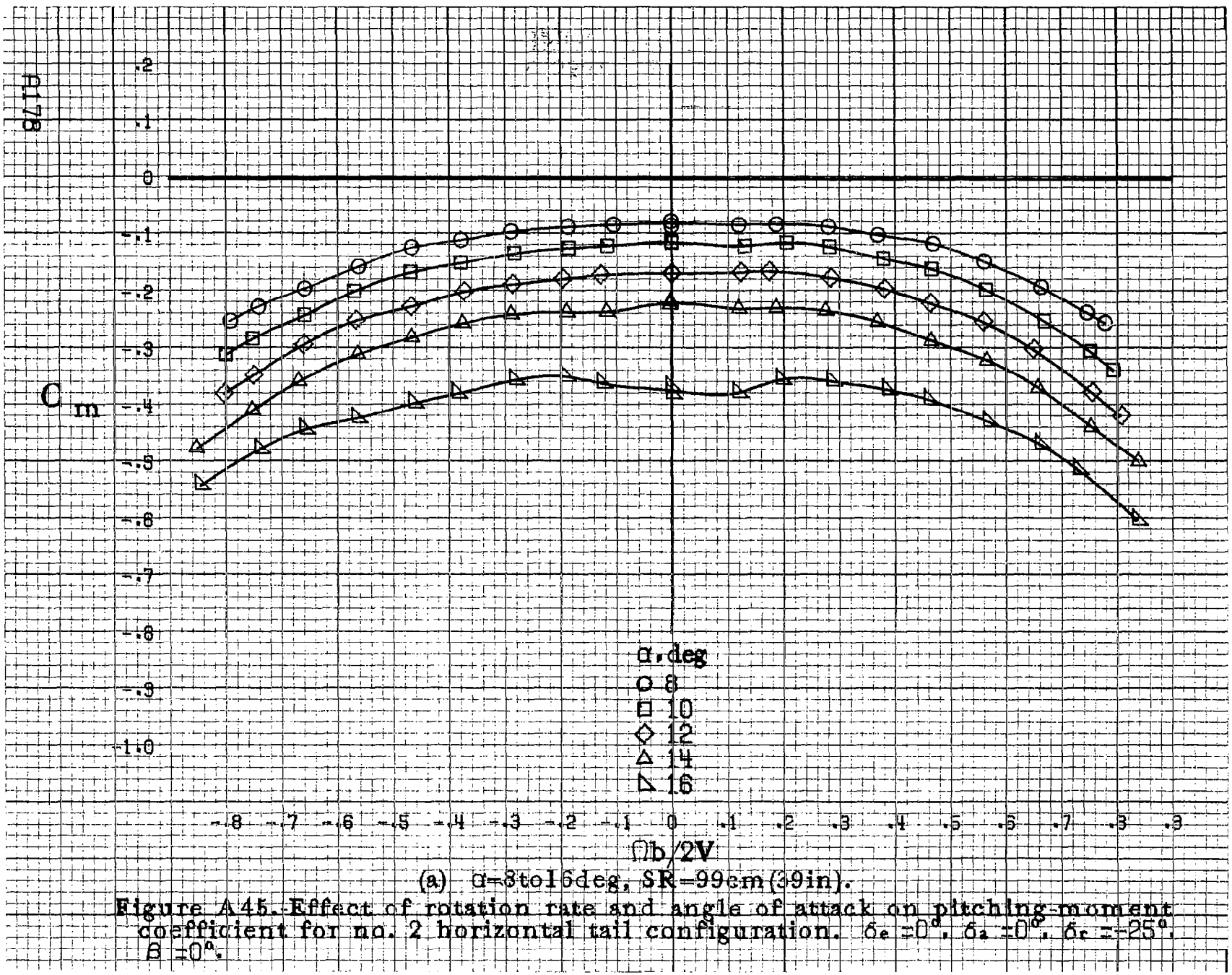

(a) α=8to16deg, SR=99cm(39in).

Figure A45.-Effect of rotation rate and angle of attack on pitching-moment coefficient for no. 2 horizontal tail configuration. $\delta_e = 0^\circ$, $\delta_a = 0^\circ$, $\delta_r = -25^\circ$, $\beta = 0^\circ$.

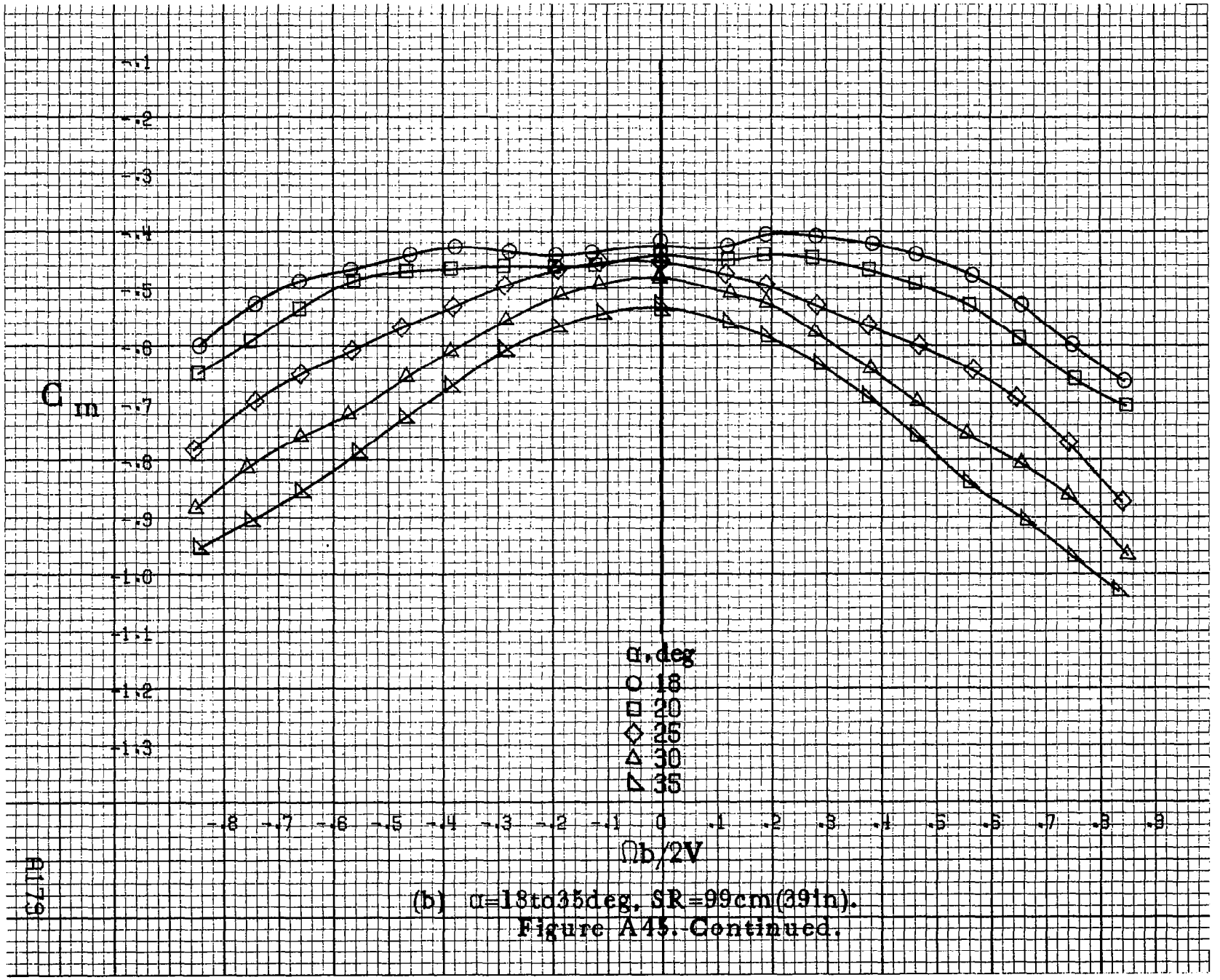

(b) α=18to35deg, SR=99cm(39in).

Figure A45.-Continued.

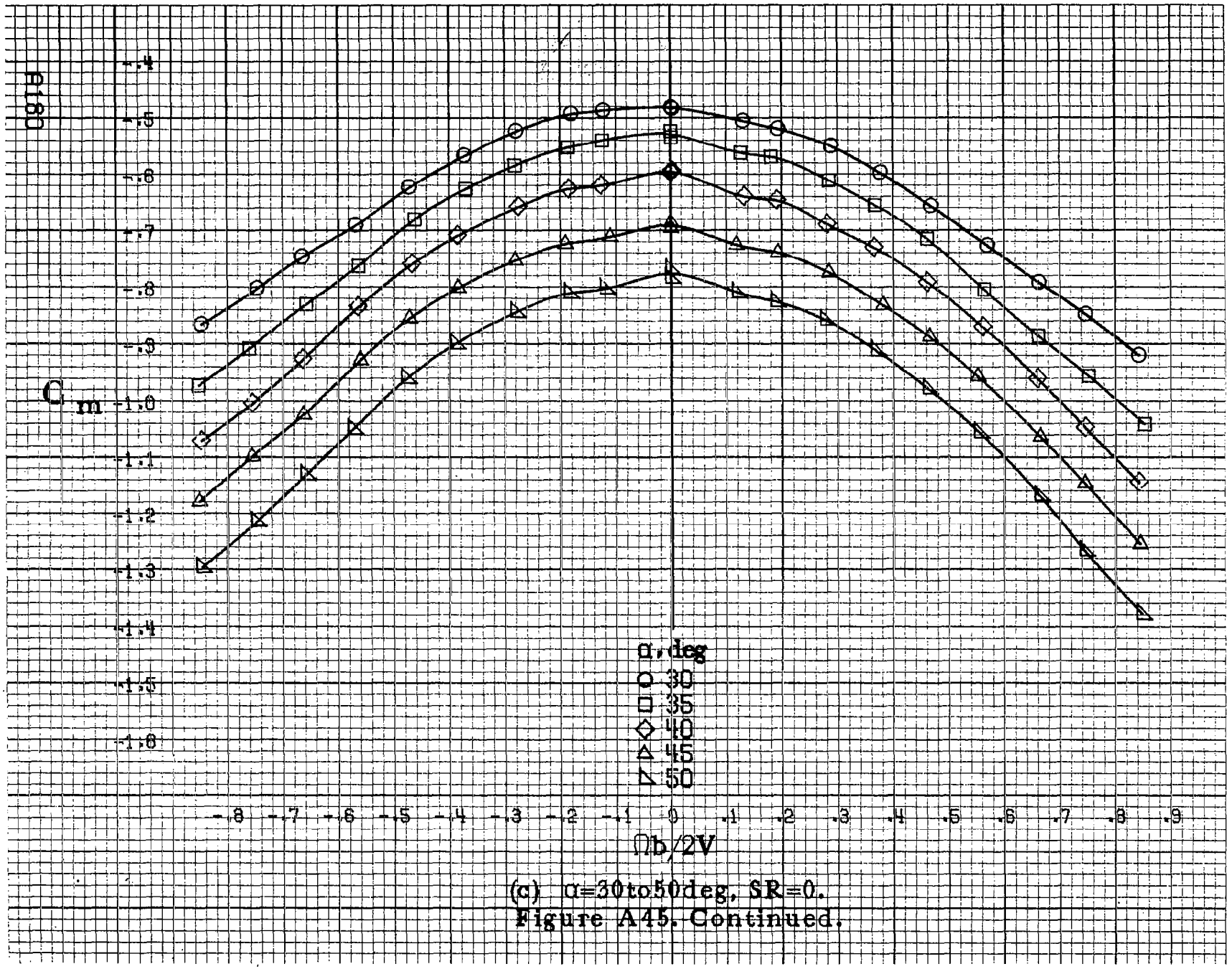

(c) α=30to50deg, SR=0.

Figure A45. Continued.

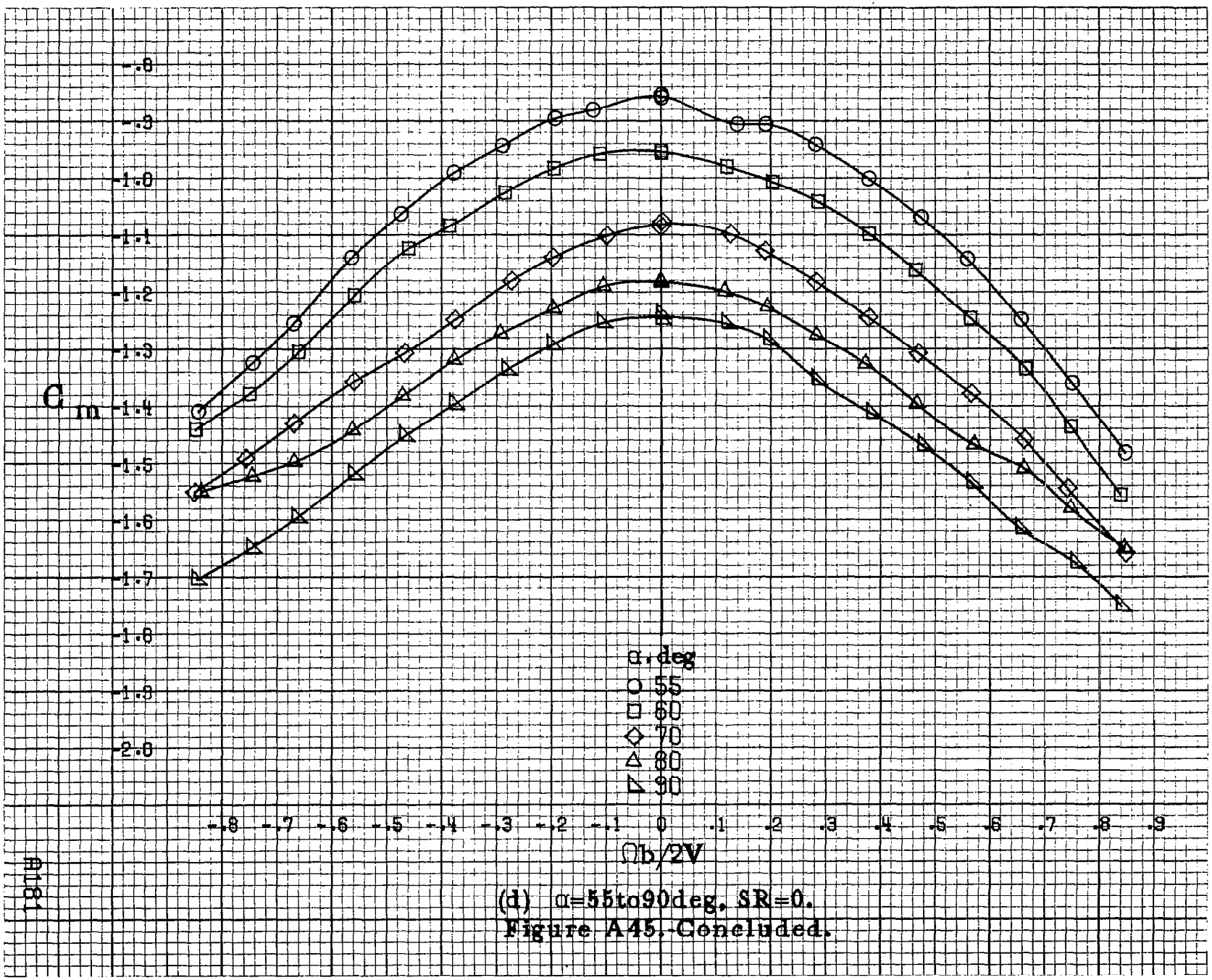

(d) α=55to90deg, SR=0.

Figure A45.-Concluded.

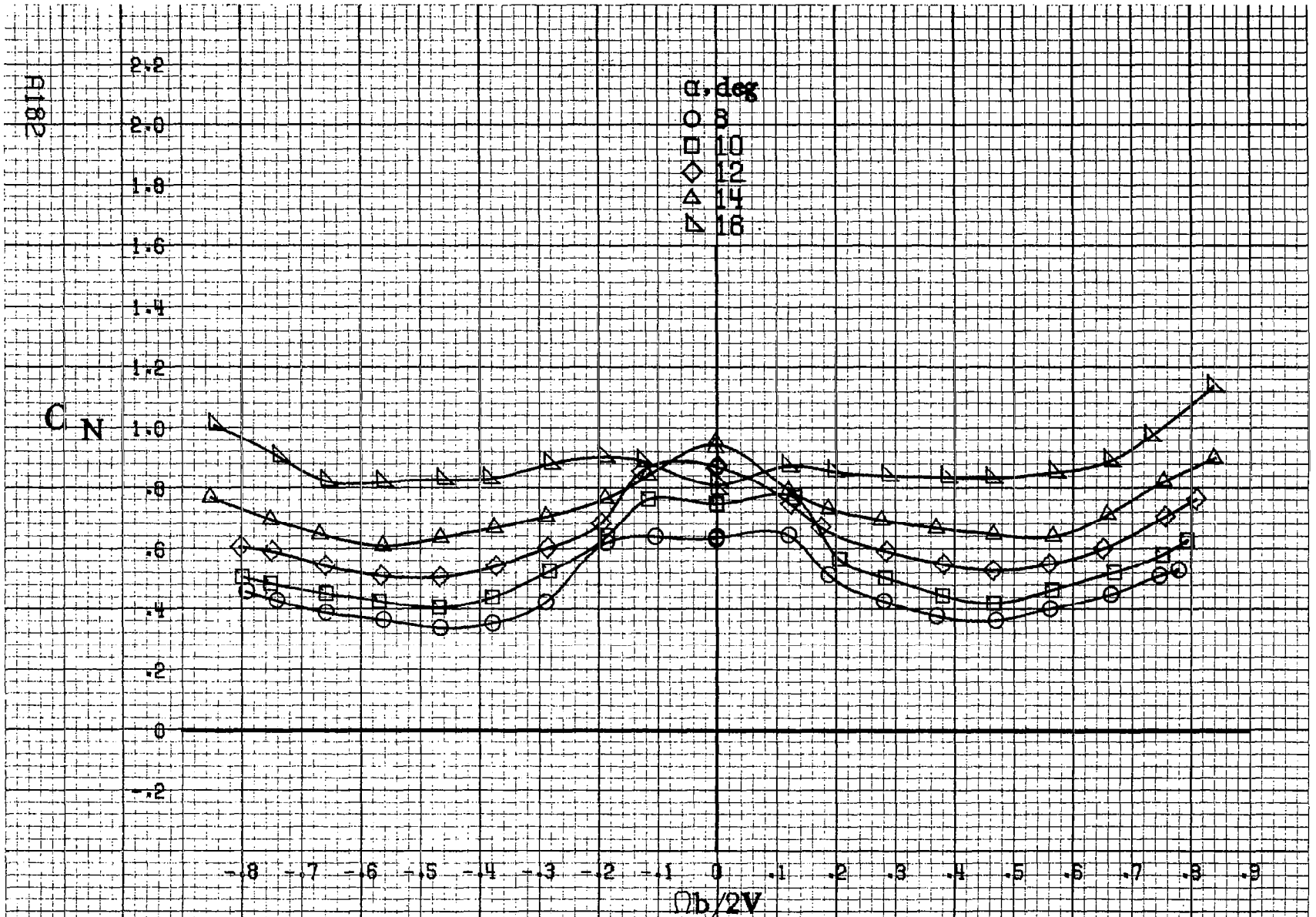

(a) α=8to16deg, SR=99cm(39in).

Figure A46.-Effect of rotation rate and angle of attack on normal-force coefficient for no. 2 horizontal tail configuration. δ_e =0°, δ_a =0°, δ_r =-25°, β =0°.

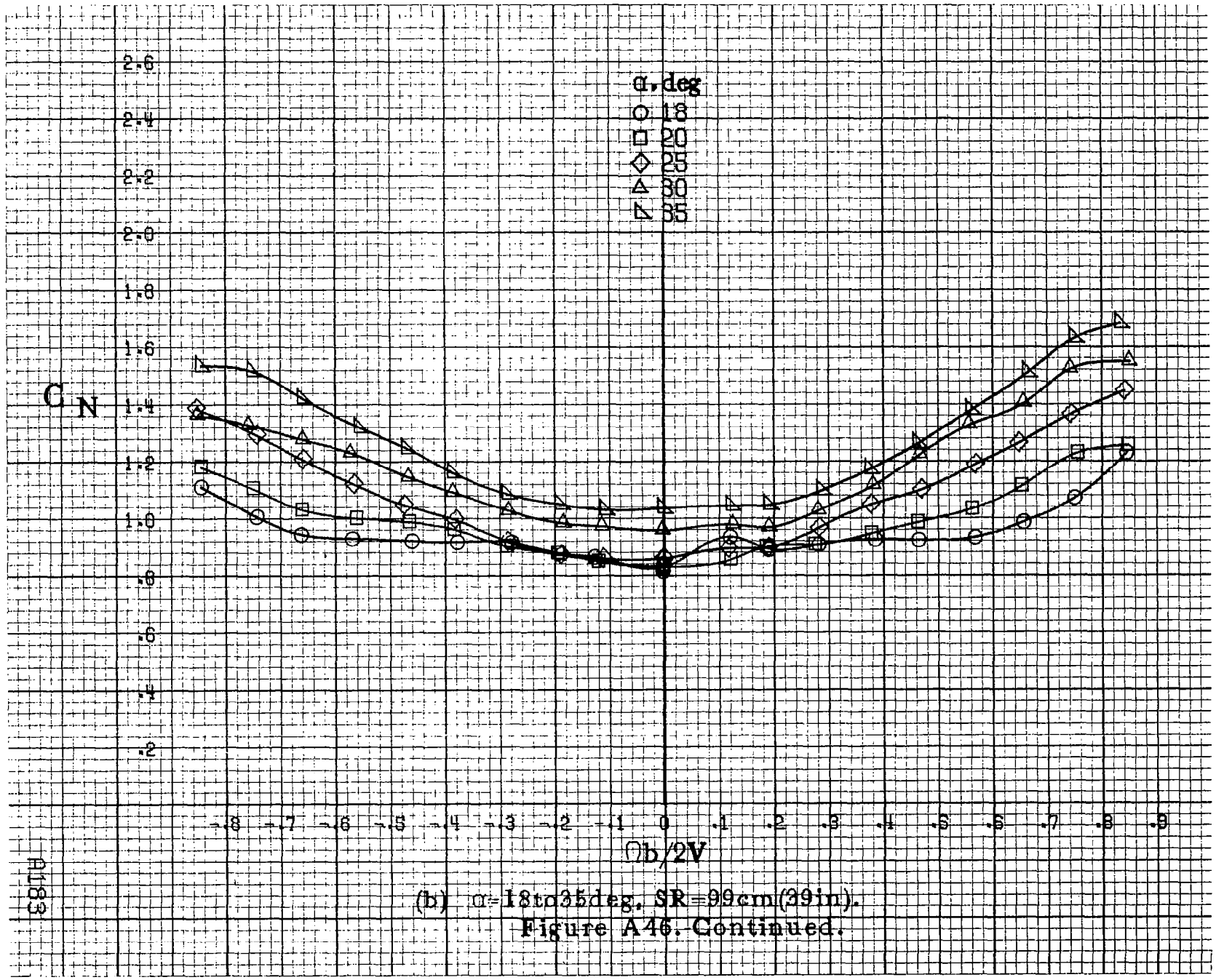

(b) α=18to35deg. SR=99cm(39in).

Figure A46. Continued.

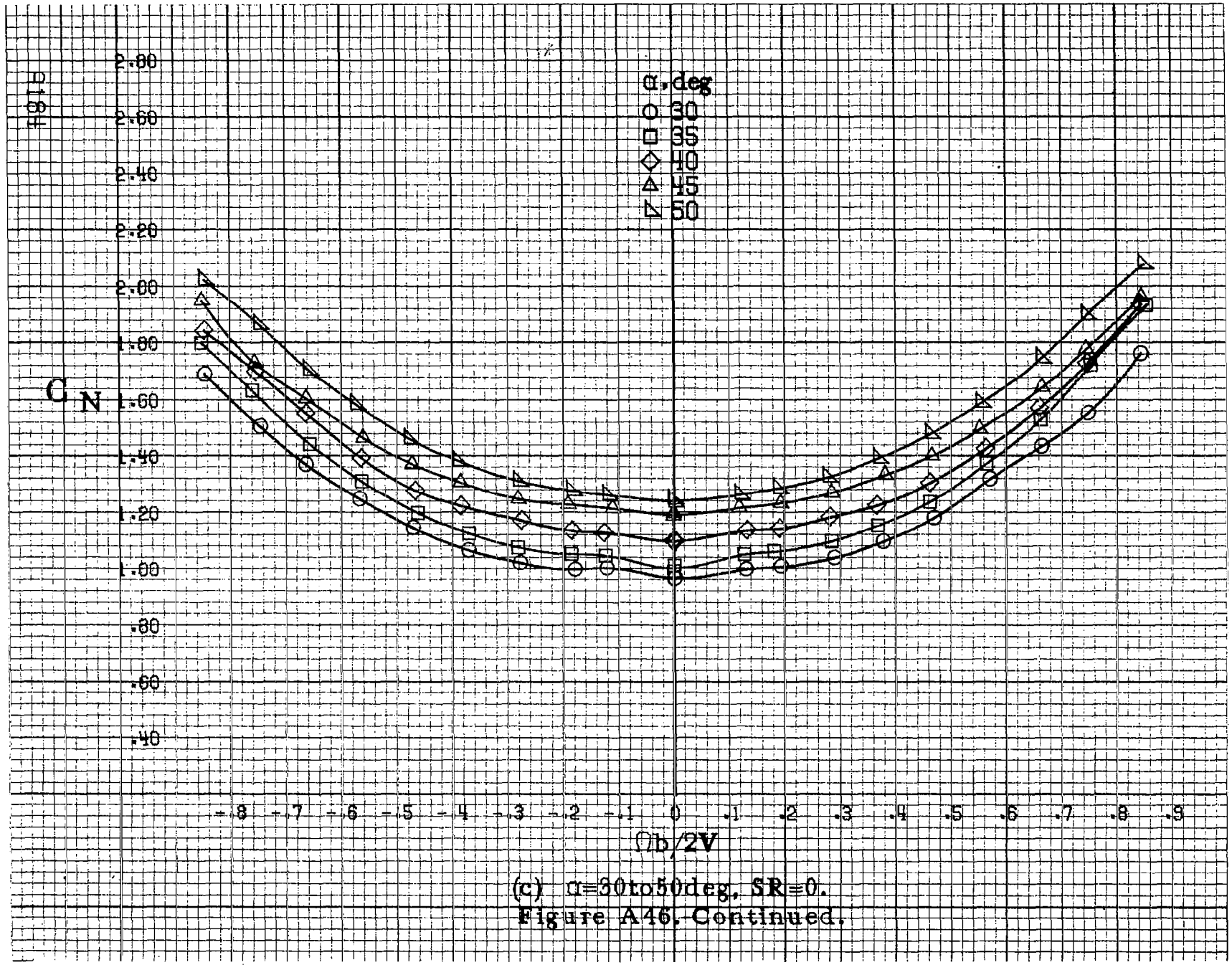

(c) α=30to50deg, SR=0.

Figure A46. Continued.

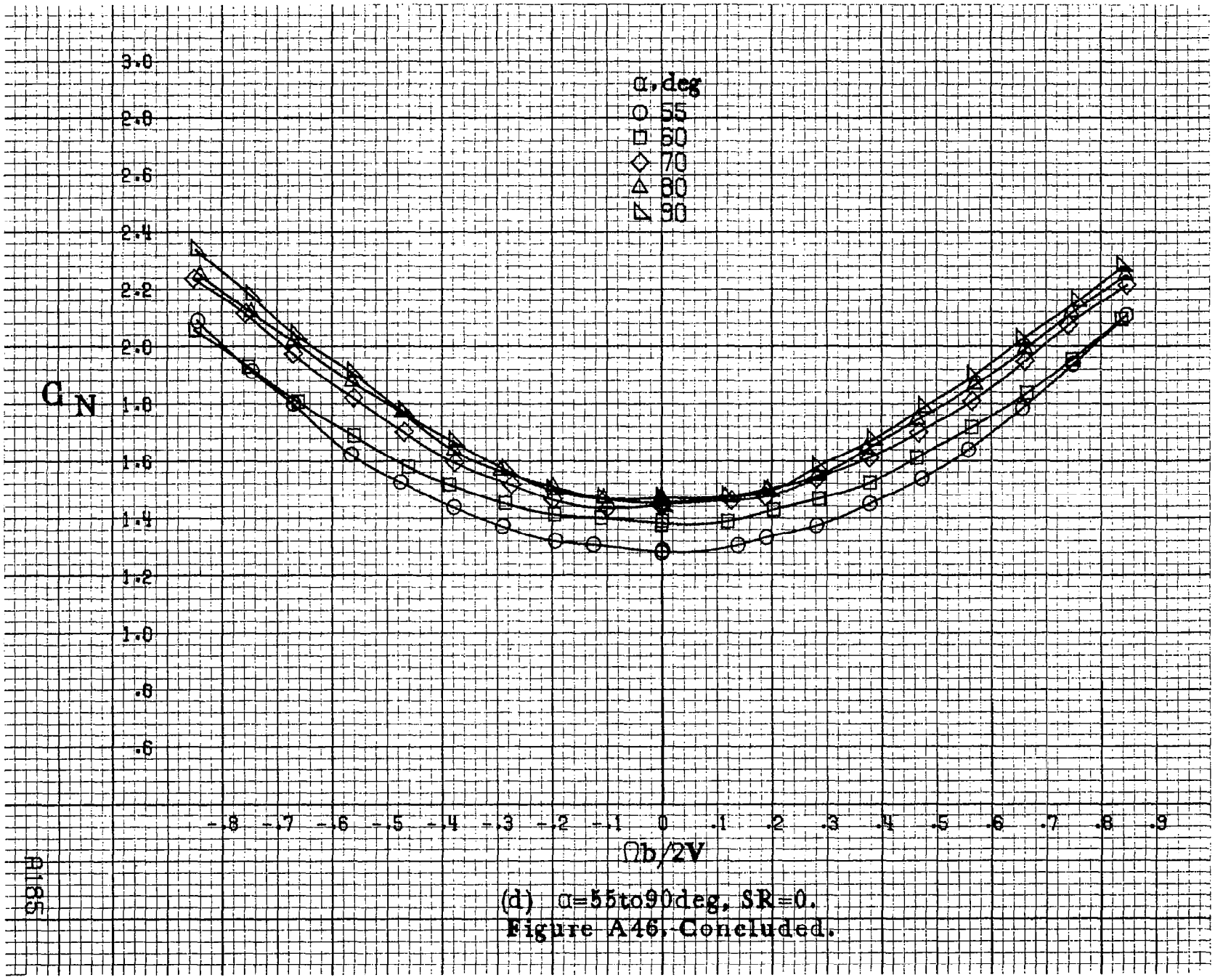

(d) α=55to90deg, SR=0.

Figure A46. Concluded.

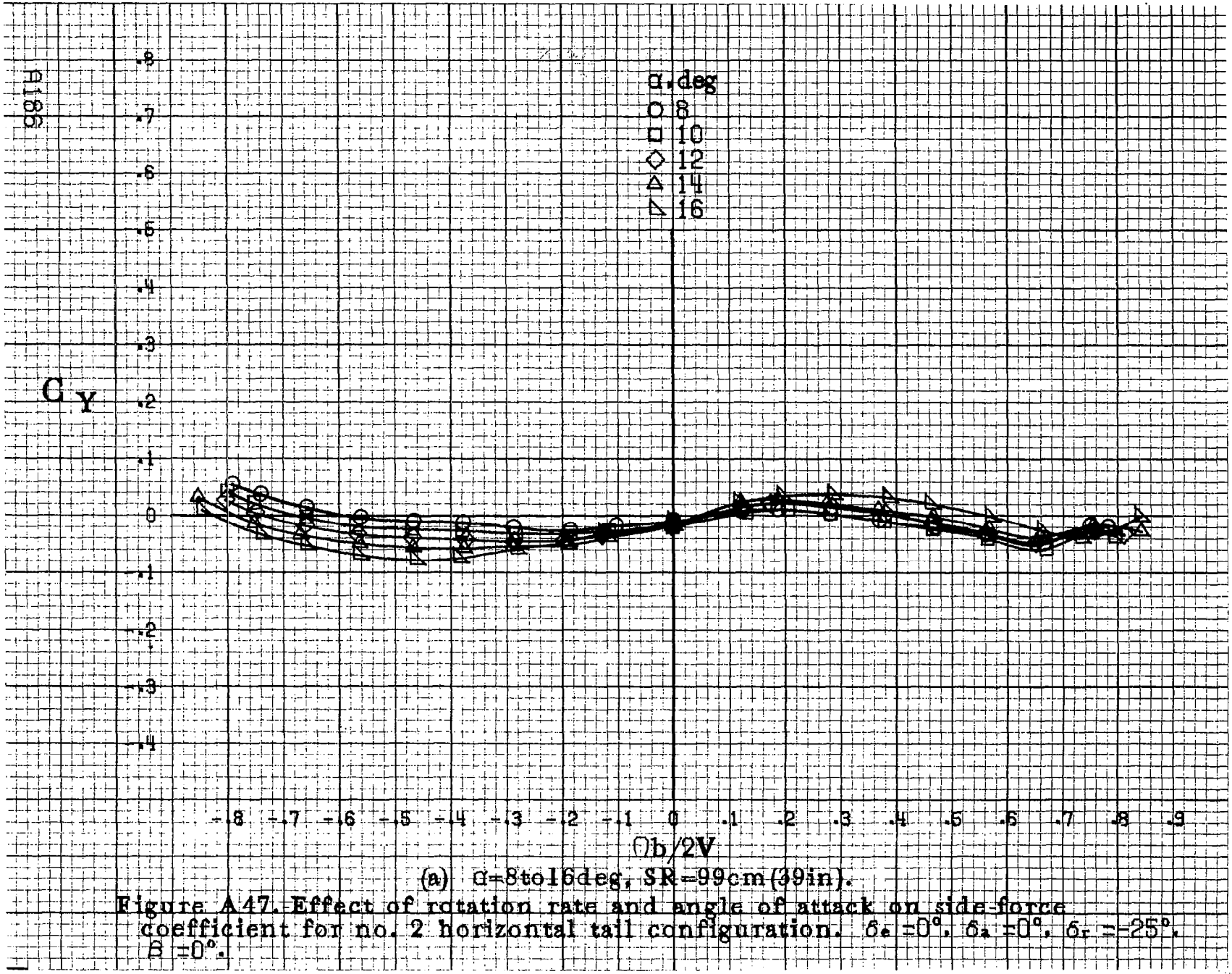

(a) α=8to16deg, SR=99cm(39in).

Figure A47. Effect of rotation rate and angle of attack on side-force coefficient for no. 2 horizontal tail configuration. $\delta_e = 0°$, $\delta_a = 0°$, $\delta_r = -25°$, $\beta = 0°$.

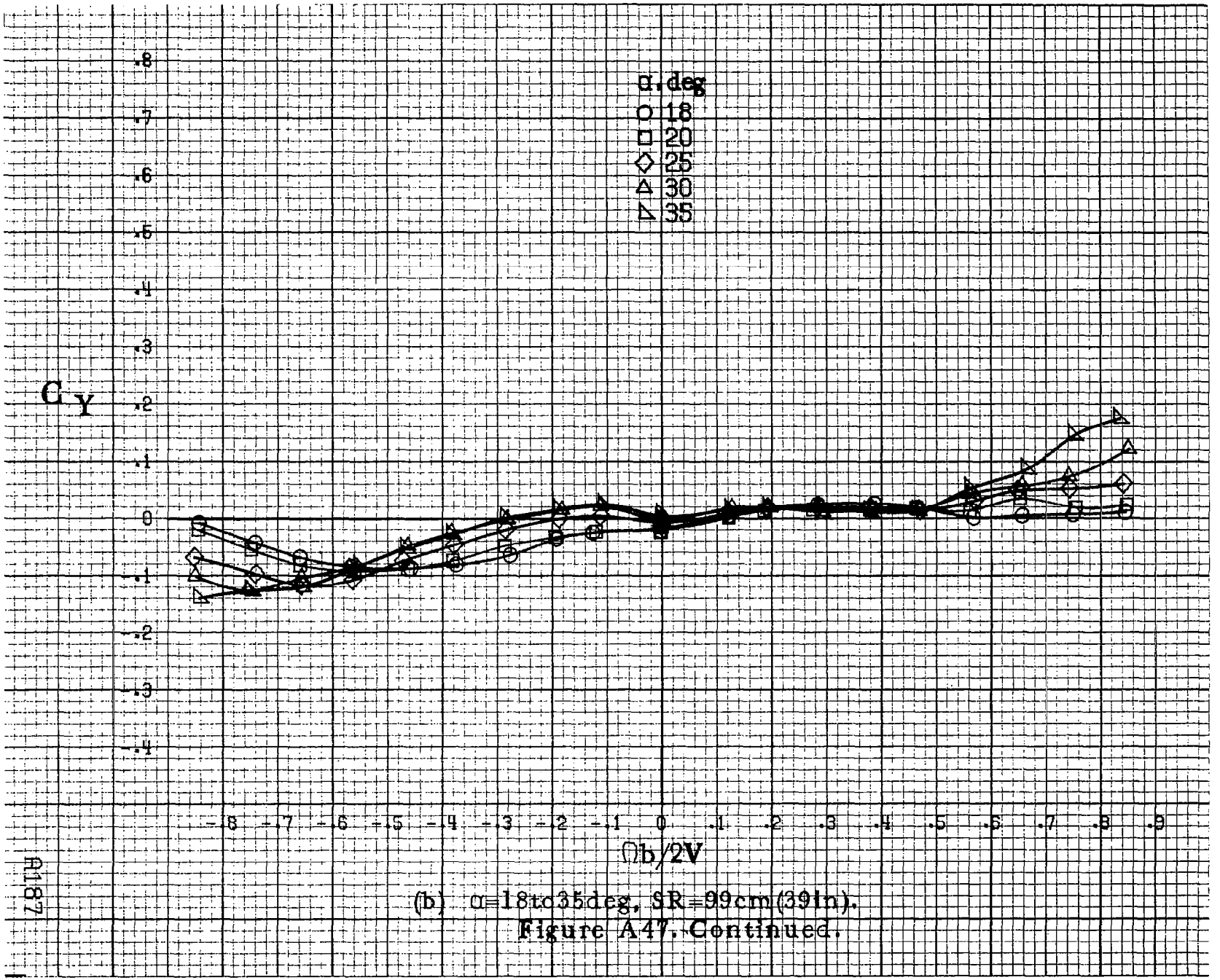

(b) α=18to35deg, SR=99cm(39in).

Figure A47. Continued.

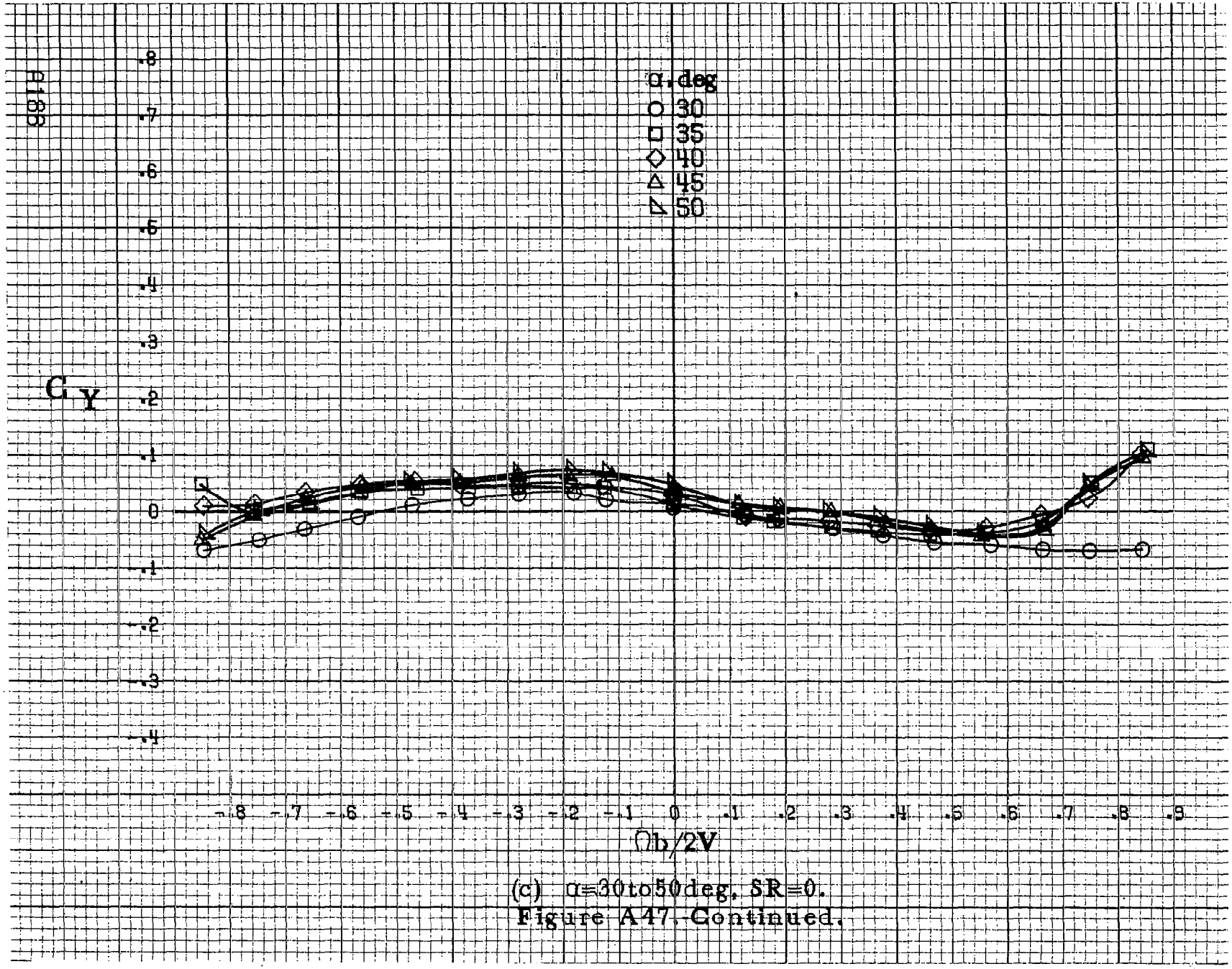

(c) α=30 to 50 deg, SR=0.

Figure A47.-Continued.

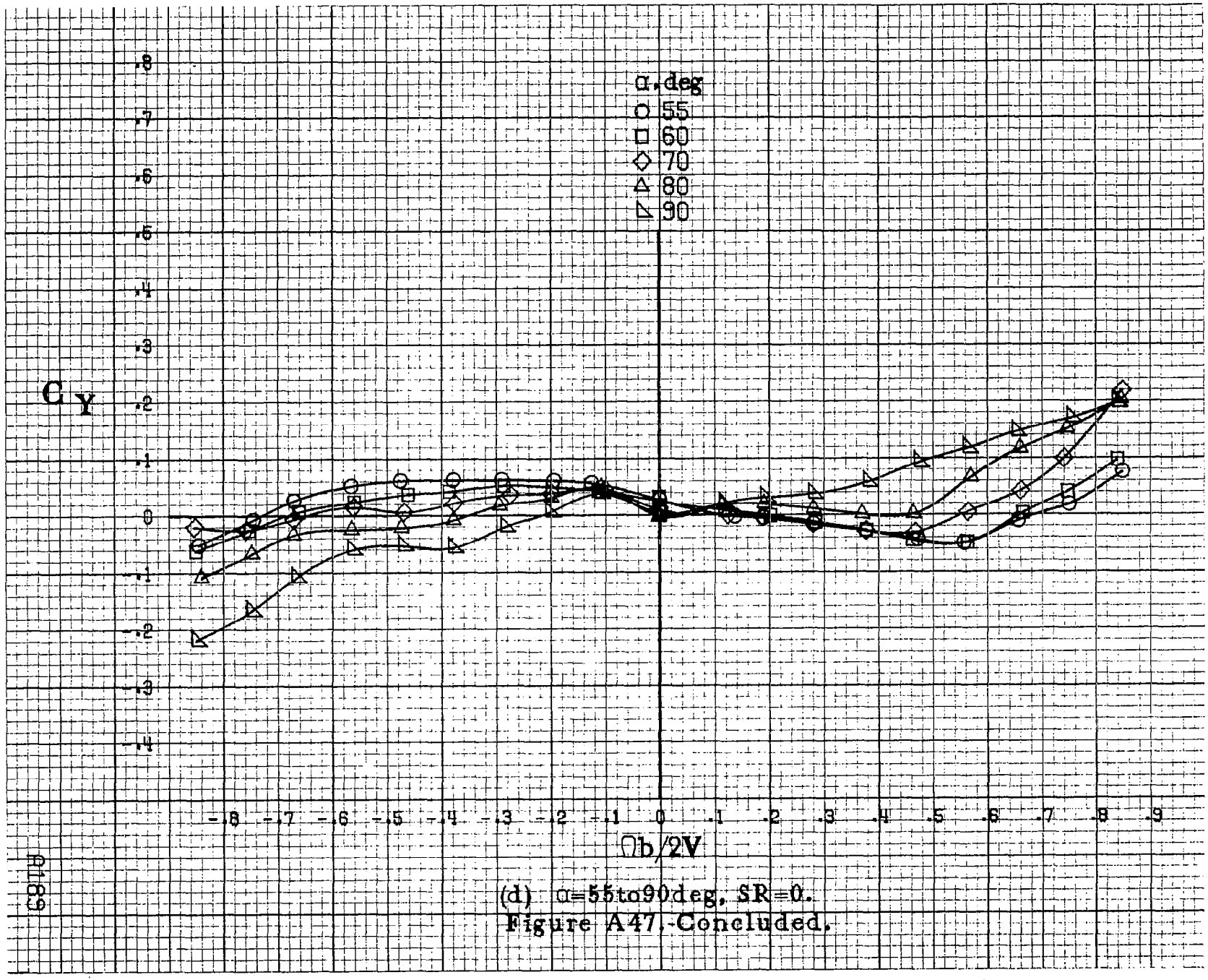

(d) α=55to90deg, SR=0.

Figure A47.-Concluded.

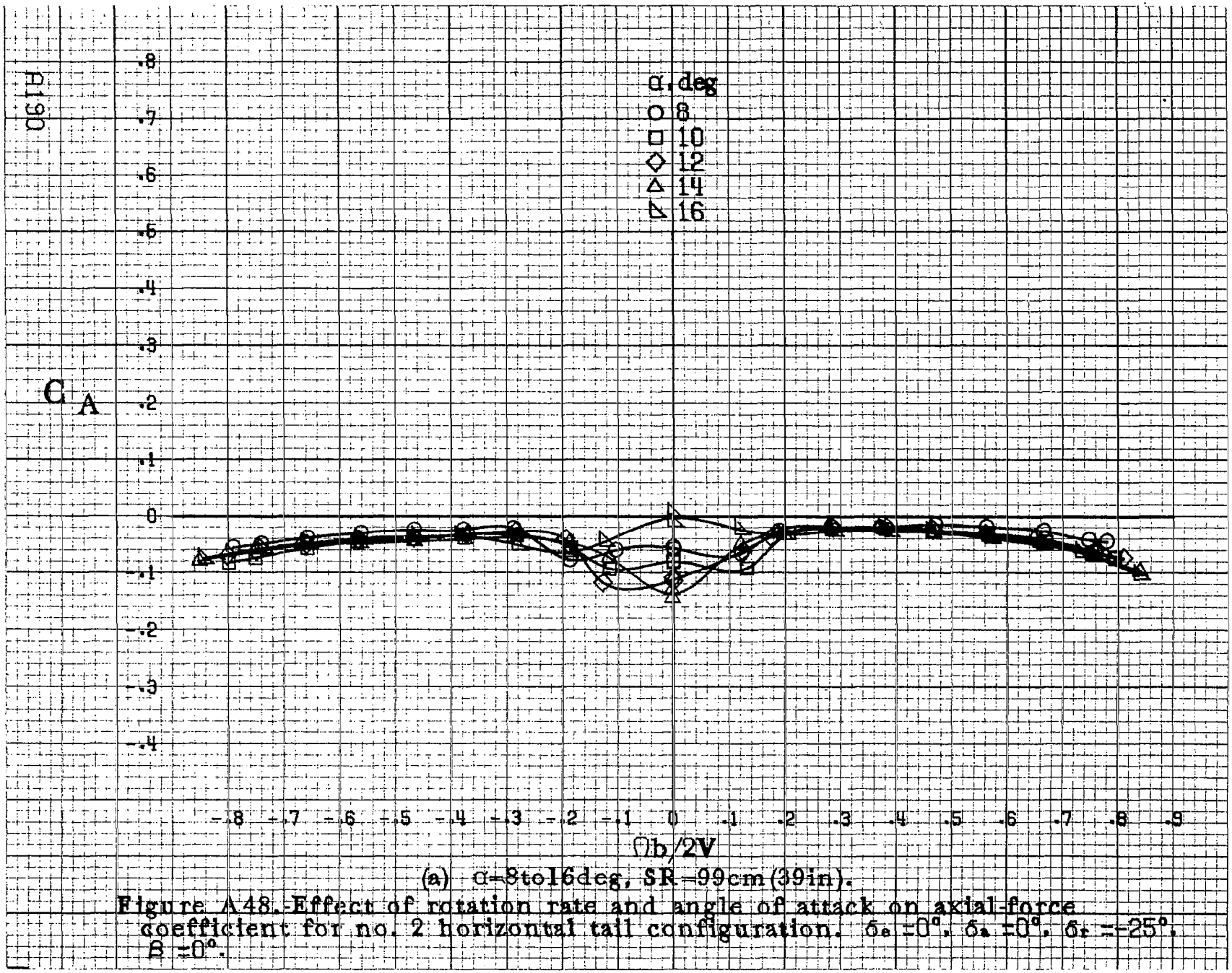

(a) α=8to16deg, SR=99cm(39in).

Figure A48.-Effect of rotation rate and angle of attack on axial-force coefficient for no. 2 horizontal tail configuration. $\delta_e = 0°$, $\delta_a = 0°$, $\delta_r = -25°$, $\beta = 0°$.

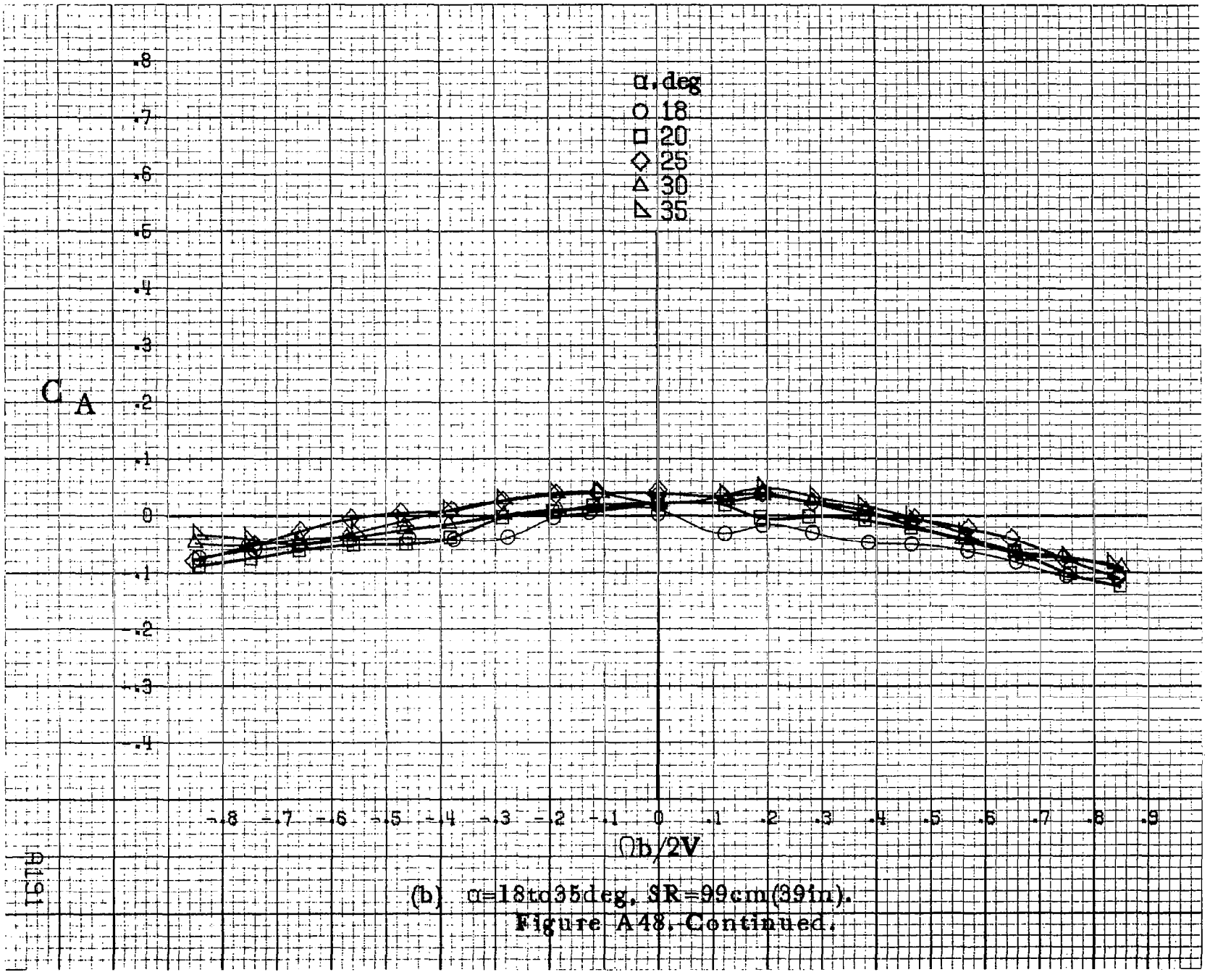

(b) α=18 to 35 deg, SR=99 cm (39 in).

Figure A48. Continued.

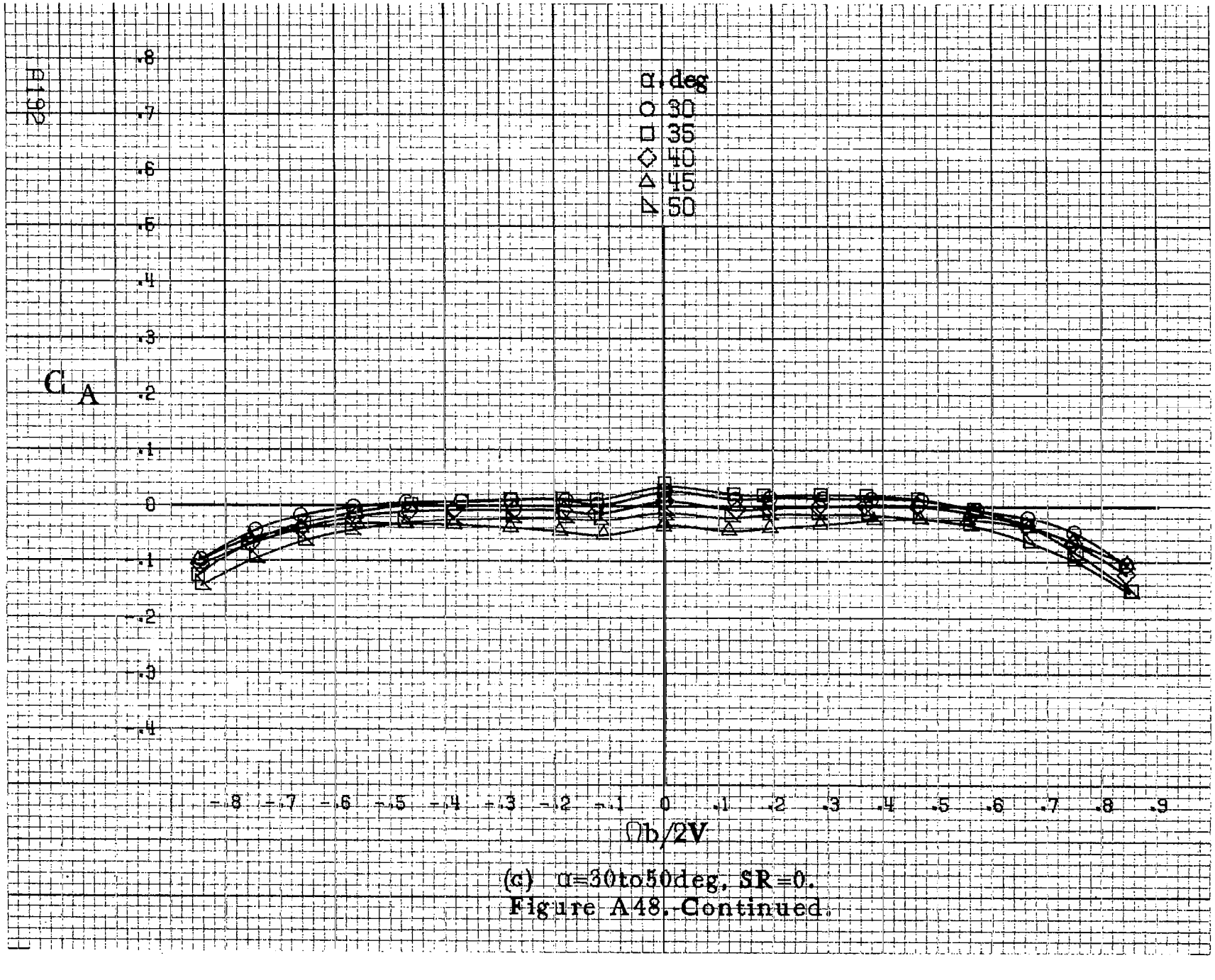

(c) α=30to50deg, SR=0.

Figure A48.-Continued.

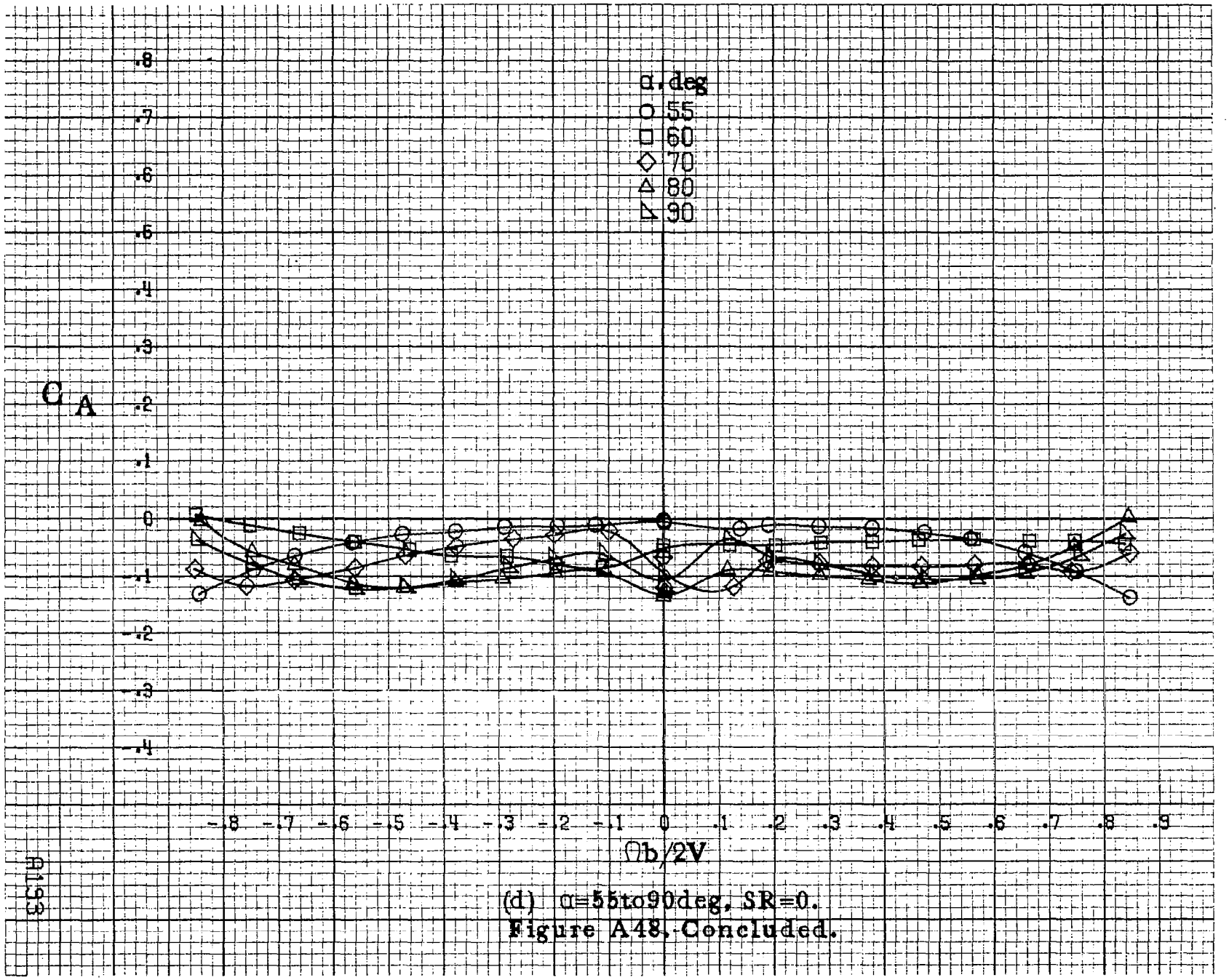

(d) α=55to90deg, SR=0.

Figure A48.-Concluded.

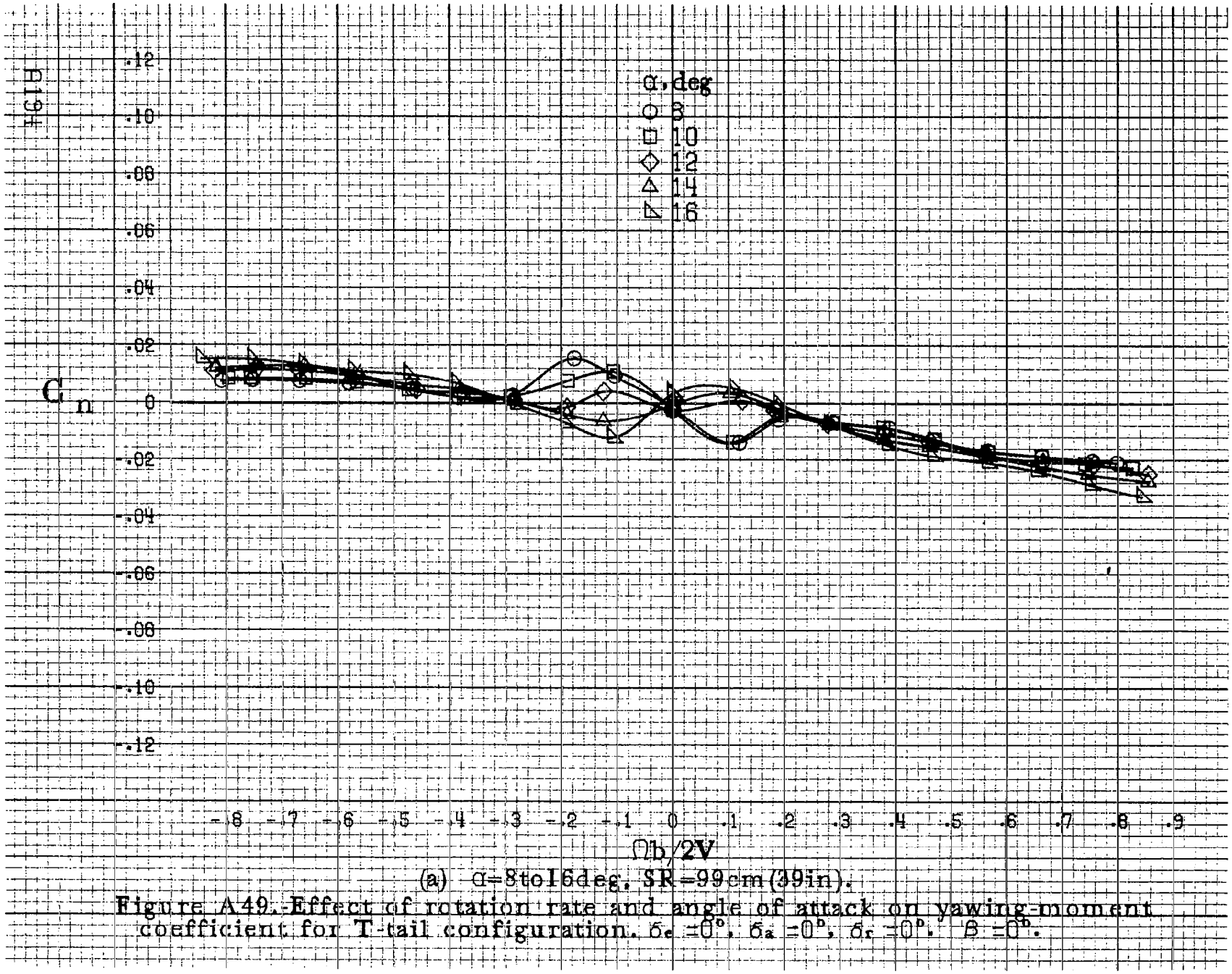

(a) α=8to16deg, SR=99cm(39in).

Figure A49.-Effect of rotation rate and angle of attack on yawing-moment coefficient for T-tail configuration. $\delta_e = 0°$, $\delta_a = 0°$, $\delta_r = 0°$, $\beta = 0°$.

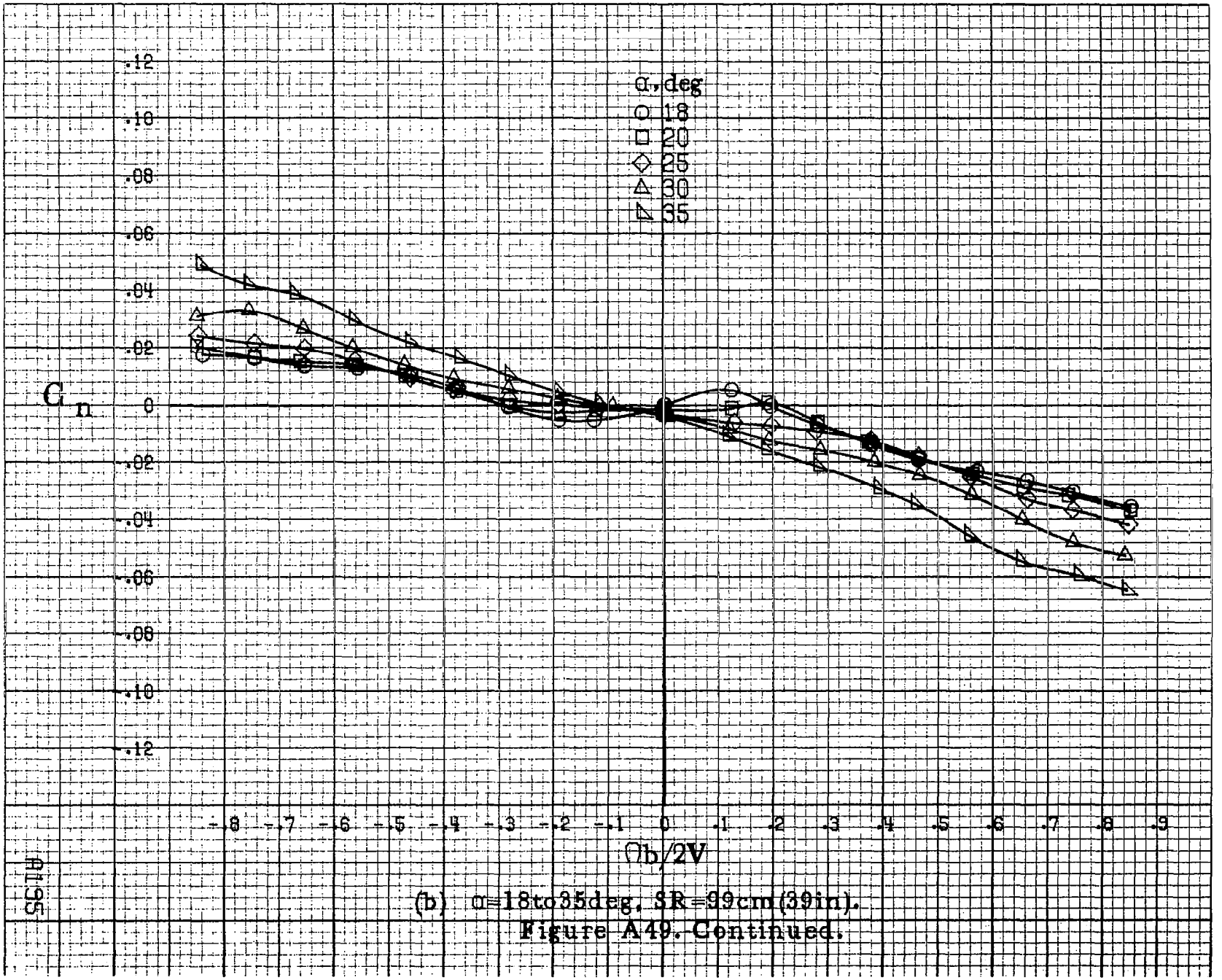

(b) α=18to35deg, SR=99cm(39in).

Figure A49.-Continued.

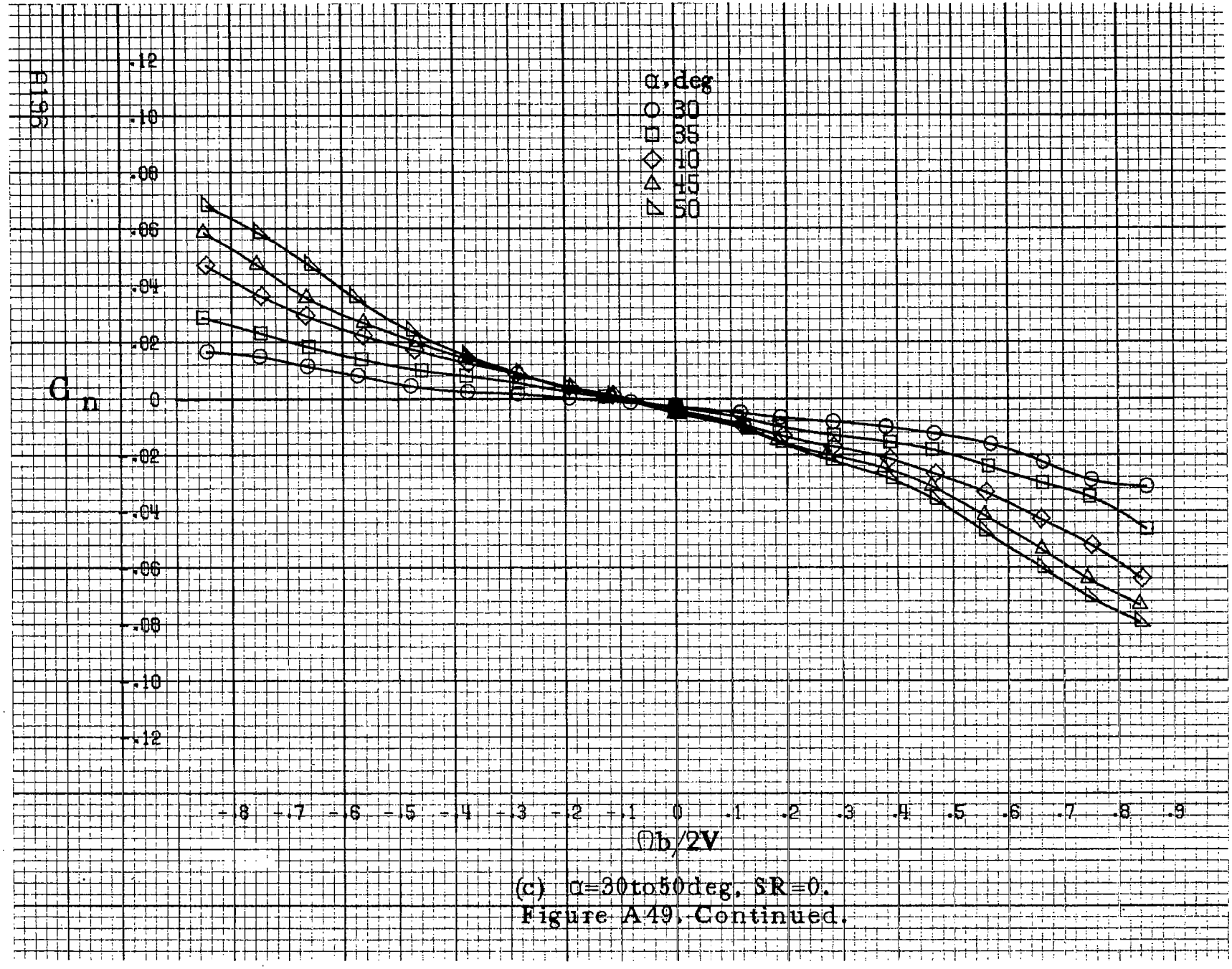

(c) α=30to50deg, SR=0.

Figure A49. Continued.

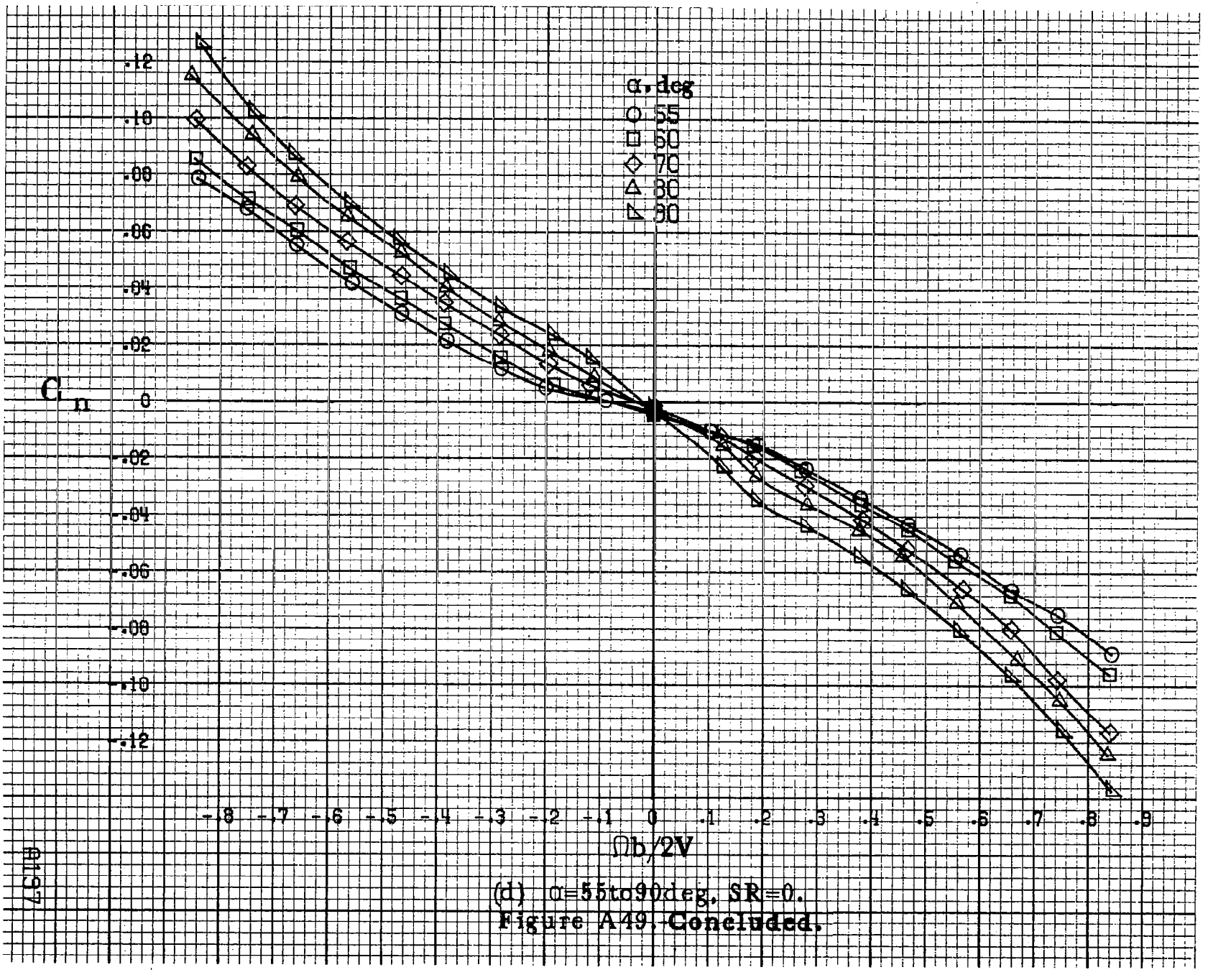

(d) α=55to90deg, SR=0.

Figure A49.-Concluded.

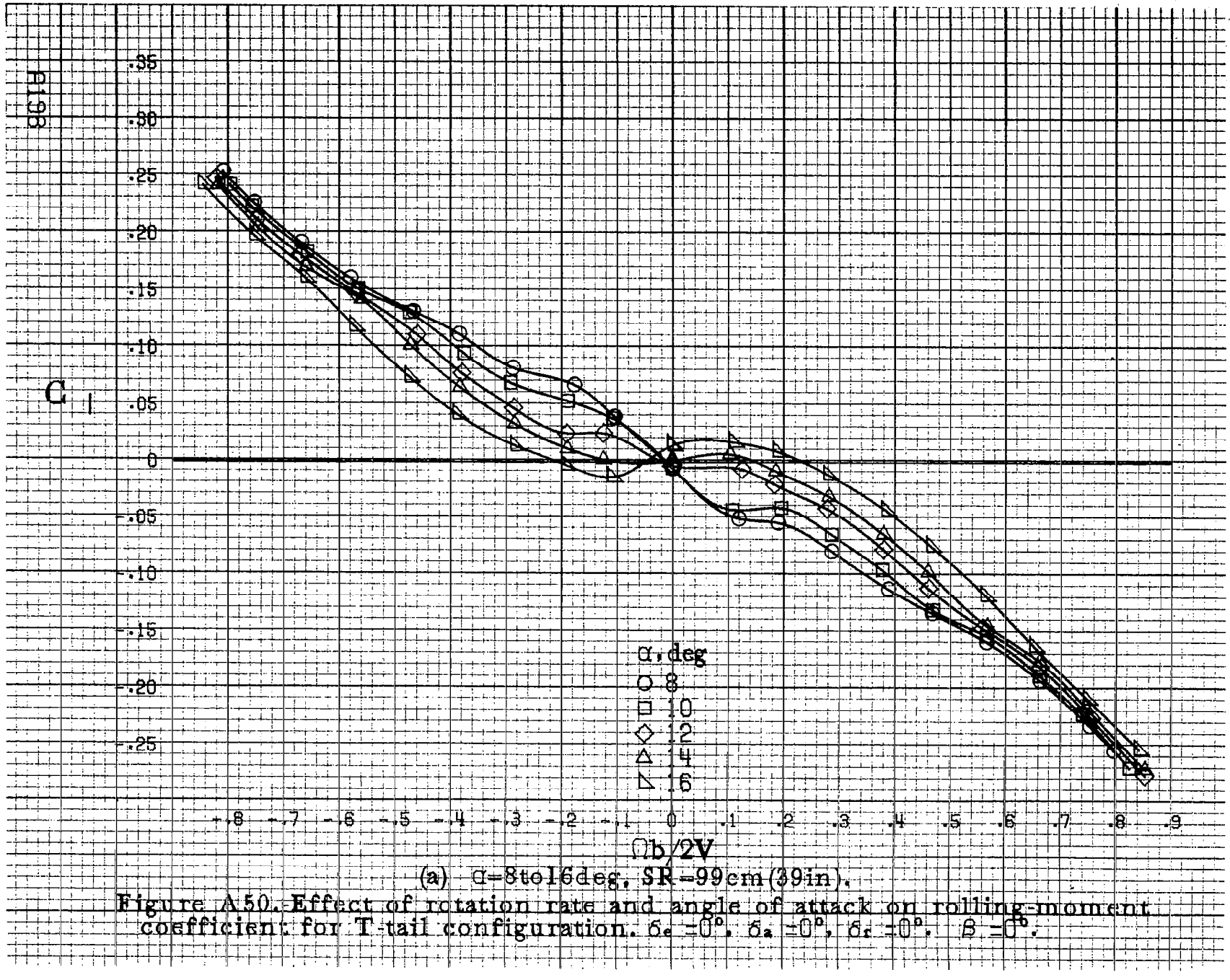

(a) α=8to16deg, SR=99cm(39in).

Figure A50.-Effect of rotation rate and angle of attack on rolling-moment coefficient for T-tail configuration. $\delta_e = 0^\circ$, $\delta_a = 0^\circ$, $\delta_r = 0^\circ$, $\beta = 0^\circ$.

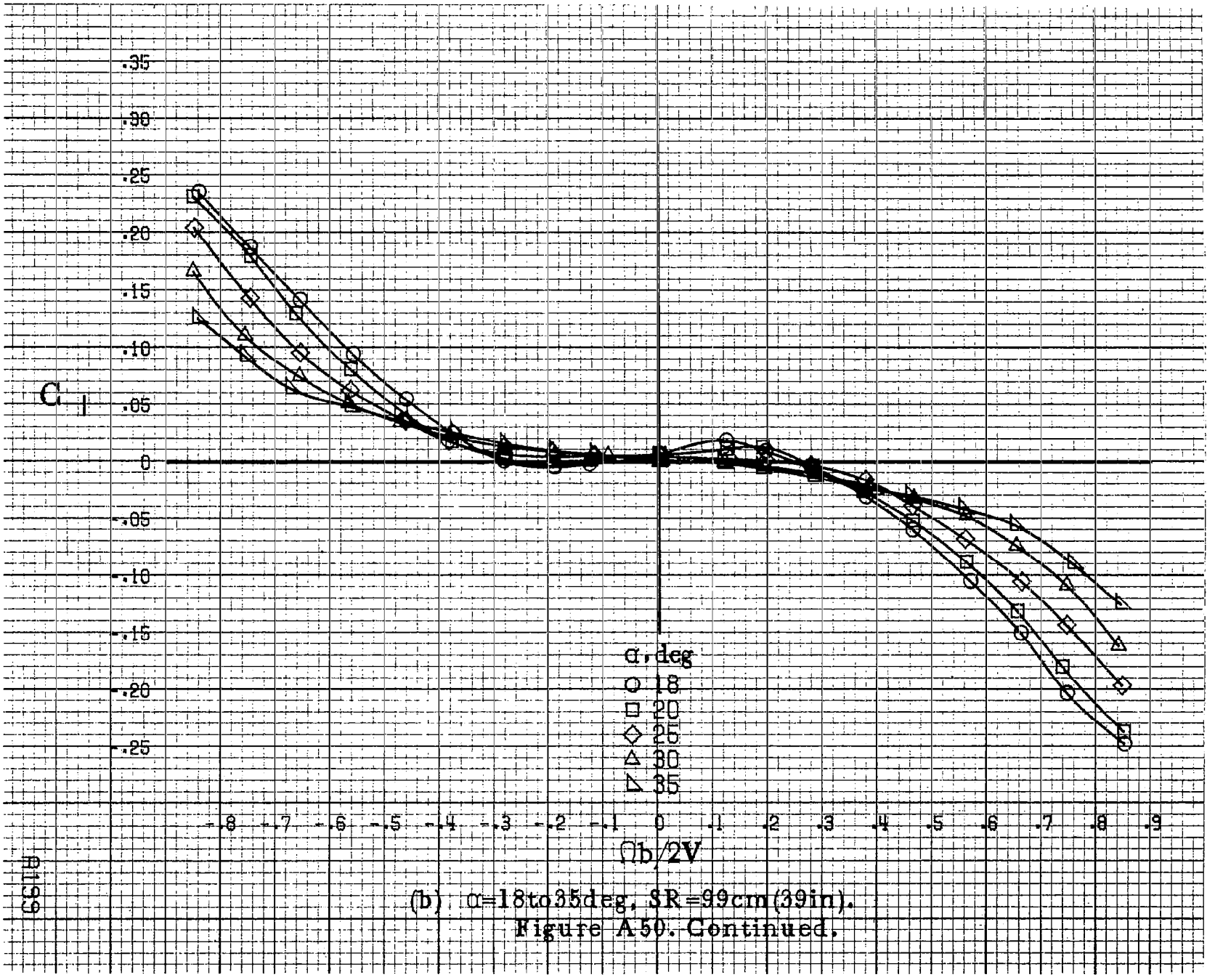

(b) α=18to35deg, SR=99cm(39in).

Figure A50. Continued.

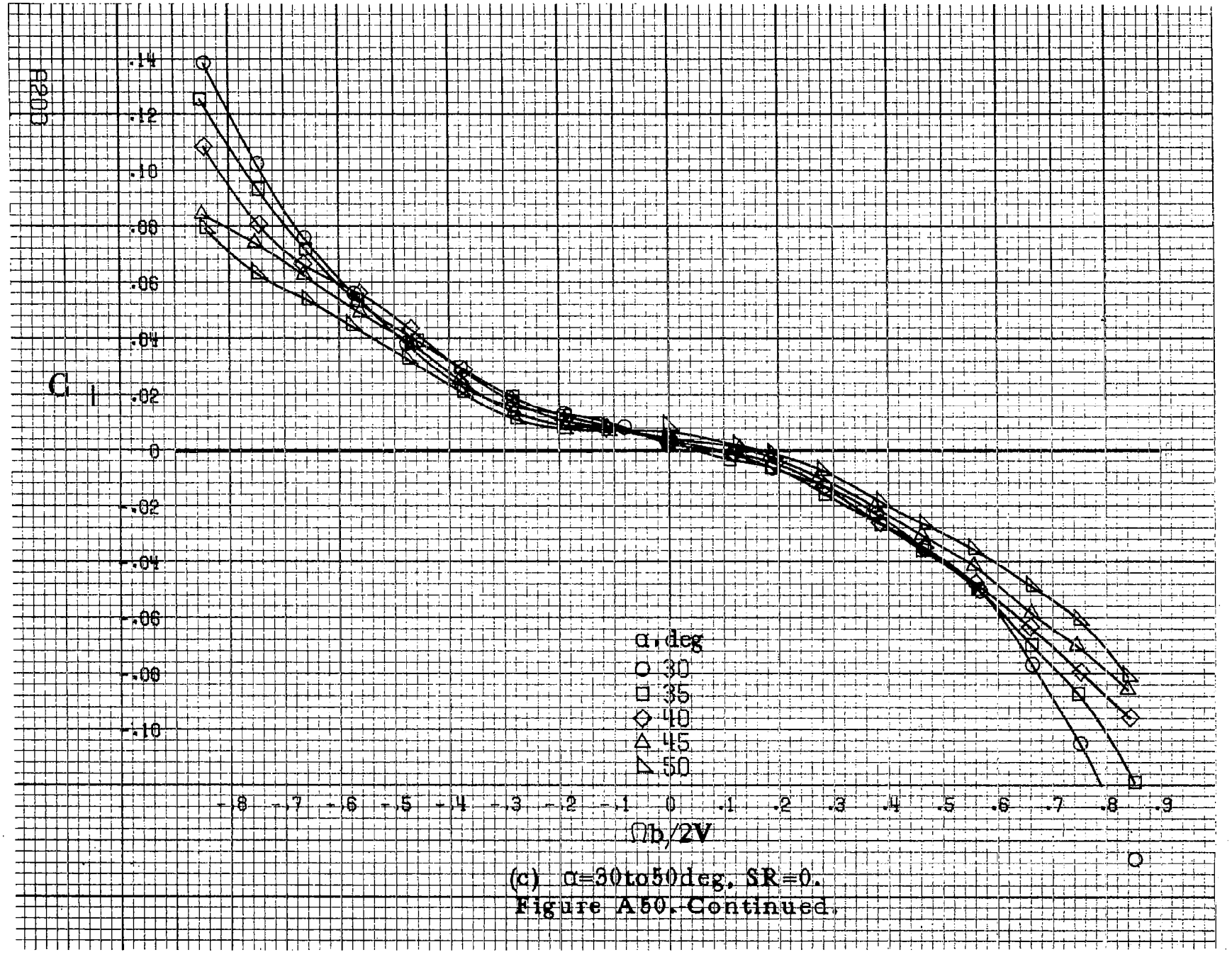

(c) α=30to50deg. SR=0.

Figure A50. Continued.

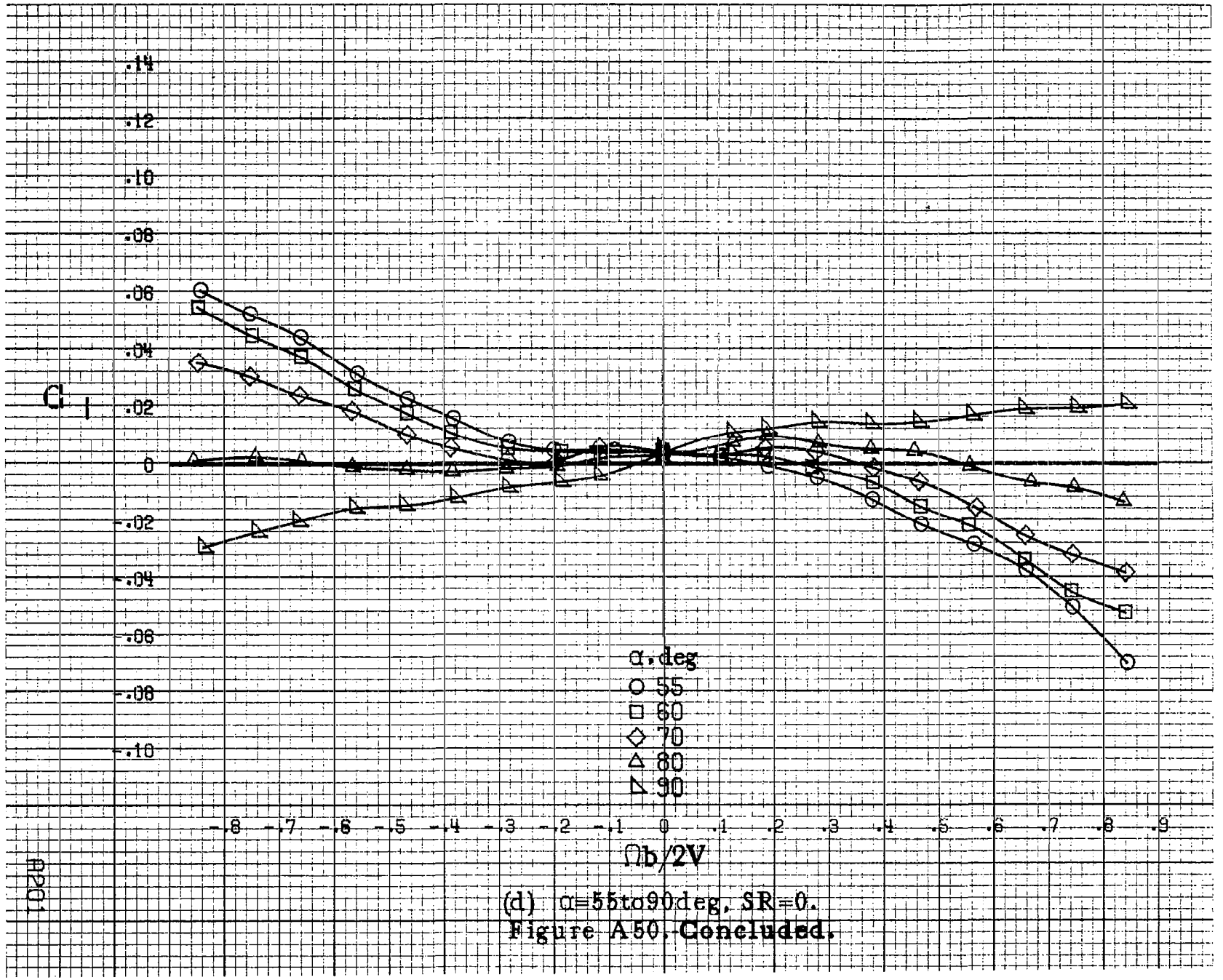

(d) α=55 to 90 deg, SR=0.

Figure A50. Concluded.

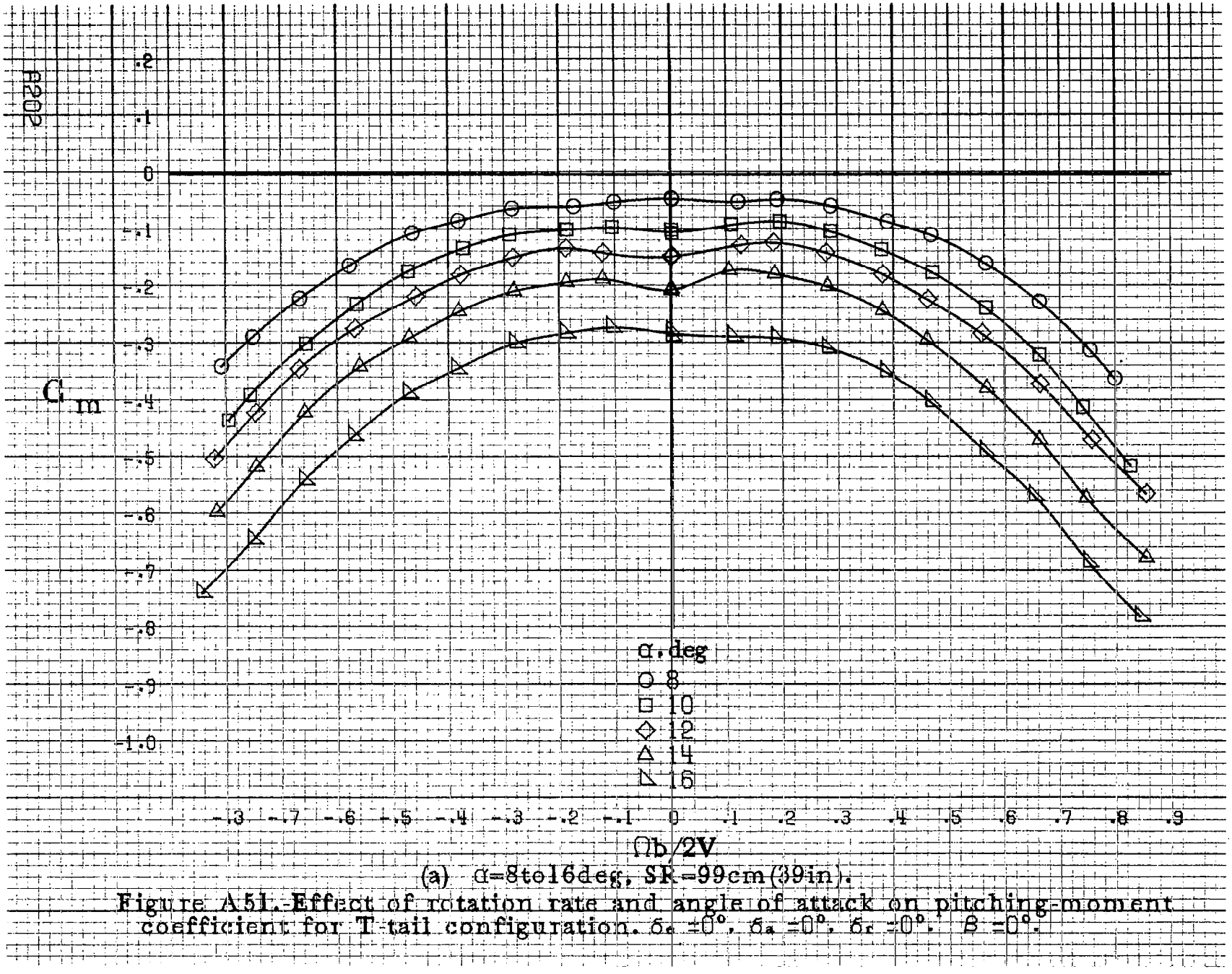

(a) α=8to16deg, SR=99cm(39in).

Figure A51.-Effect of rotation rate and angle of attack on pitching-moment coefficient for T-tail configuration. δ_e =0°, δ_a =0°, δ_r =0°, β =0°.

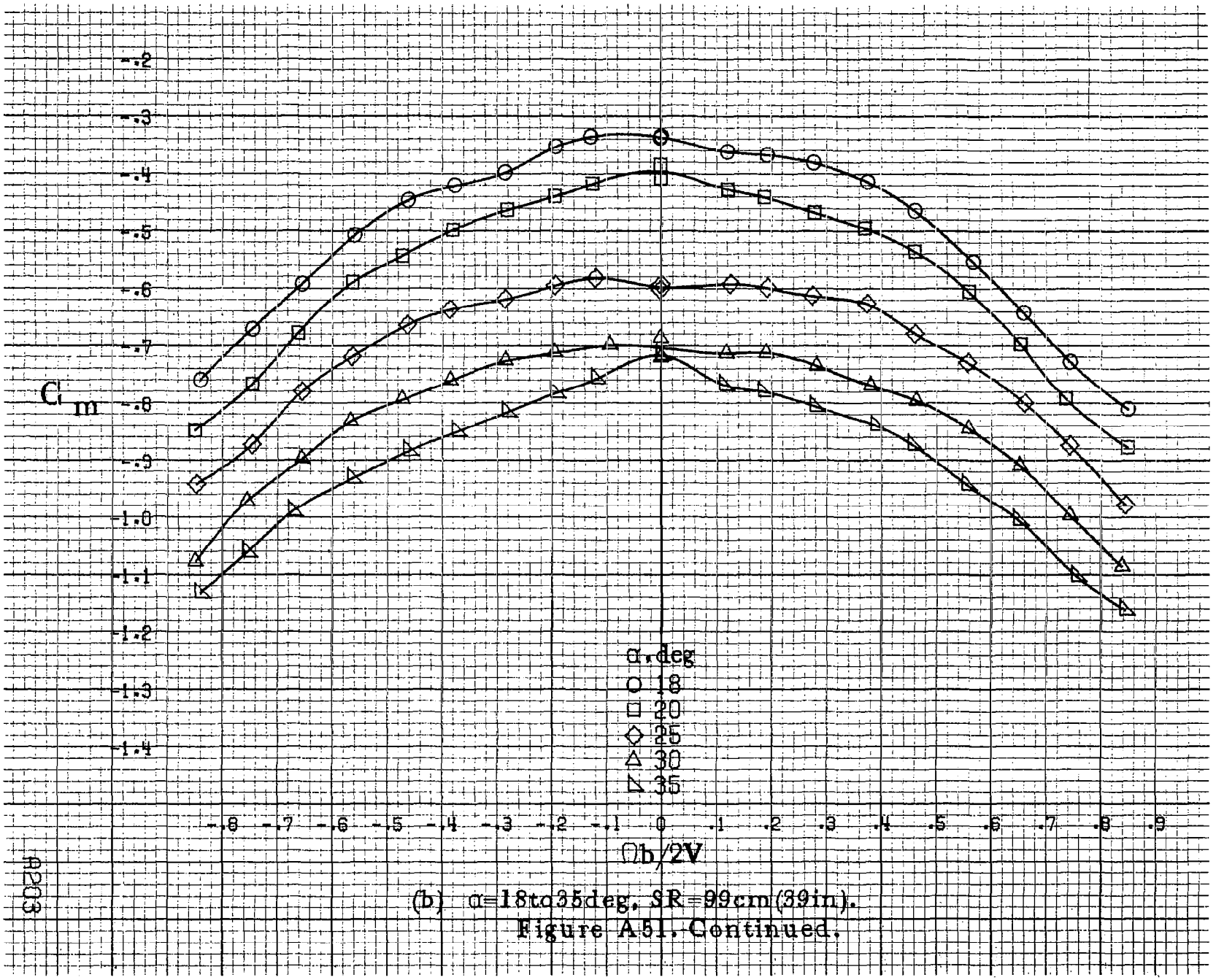

(b) α=18to35deg, SR=99cm(39in).

Figure A51. Continued.

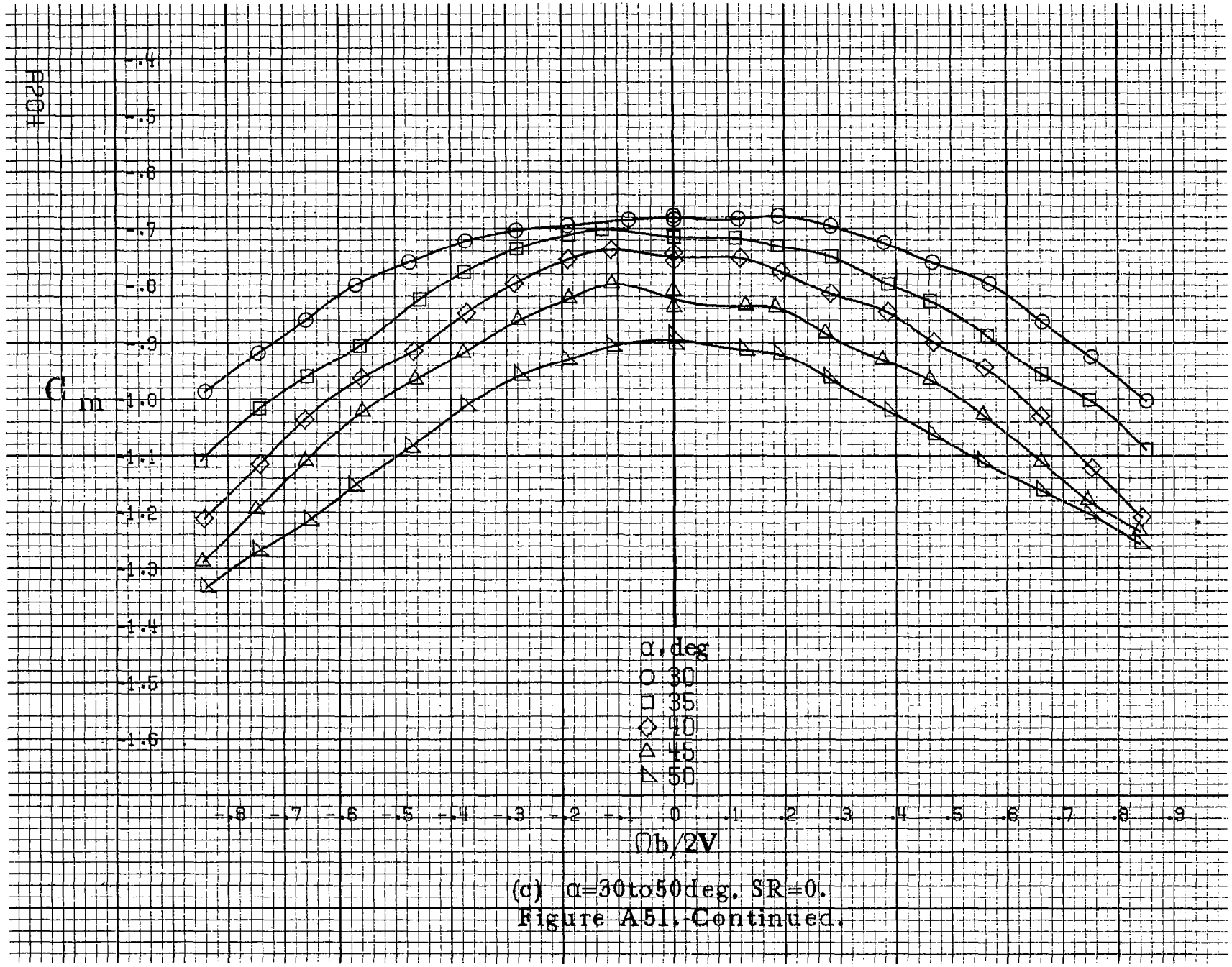

(c) α=30 to 50 deg, SR=0.

Figure A51.-Continued.

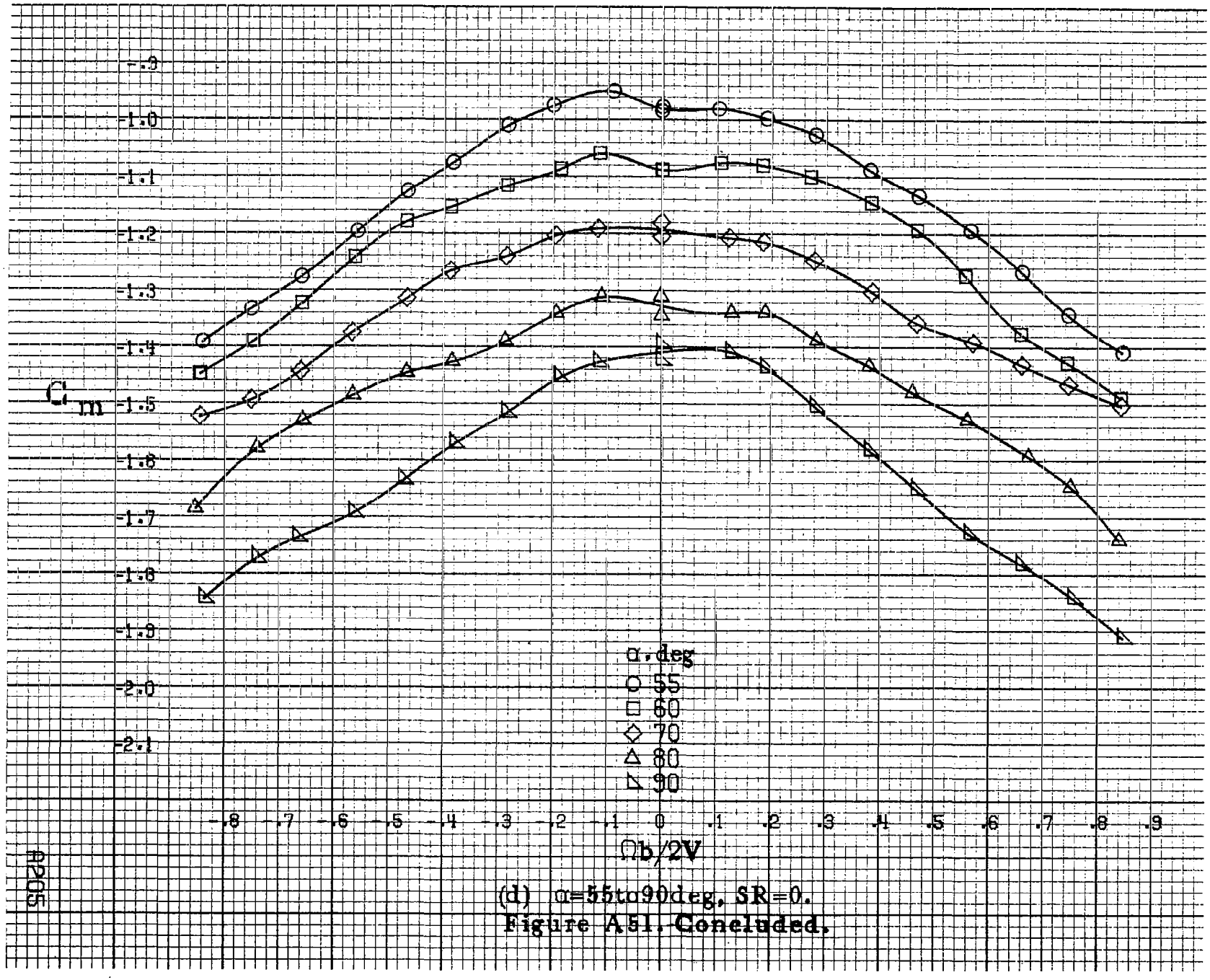

(d) α=55 to 90 deg, SR=0.

Figure A51. Concluded.

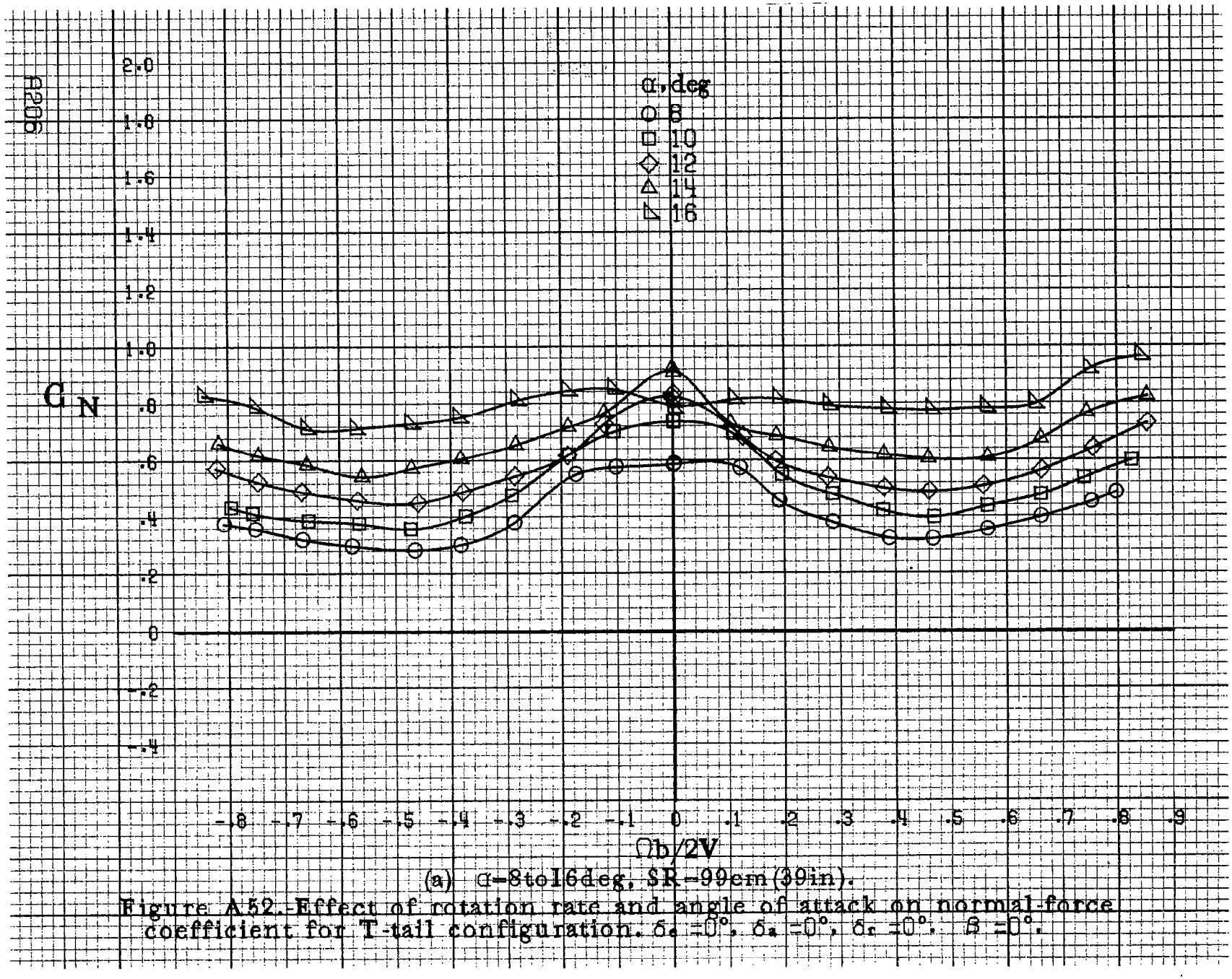

(a) α=8to16deg, $R=99cm(39in).

Figure A52.-Effect of rotation rate and angle of attack on normal-force coefficient for T-tail configuration. δ_e =0°, δ_a =0°, δ_r =0°, β =0°.

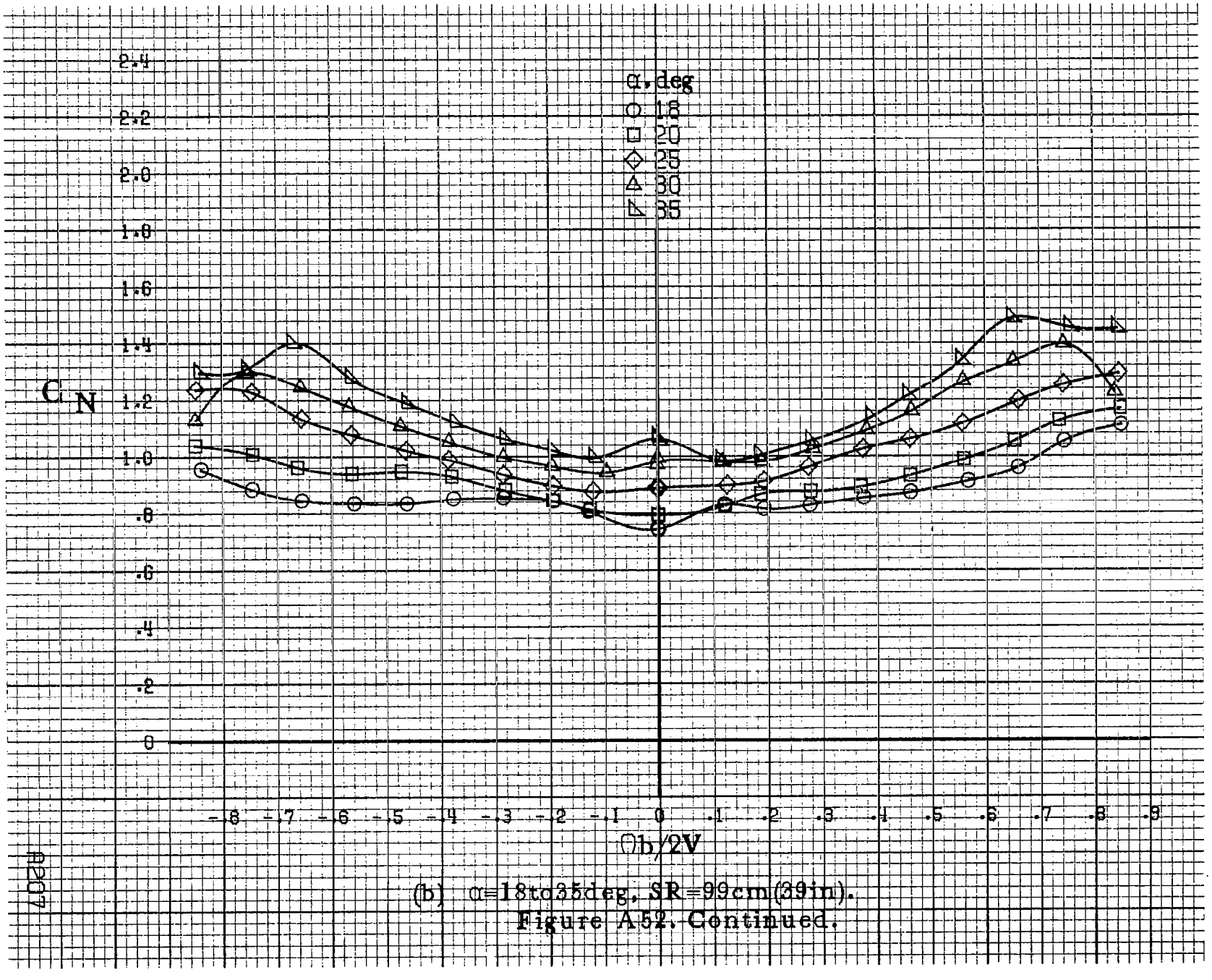

(b) α=18to35deg, SR=99cm(39in).

Figure A52. Continued.

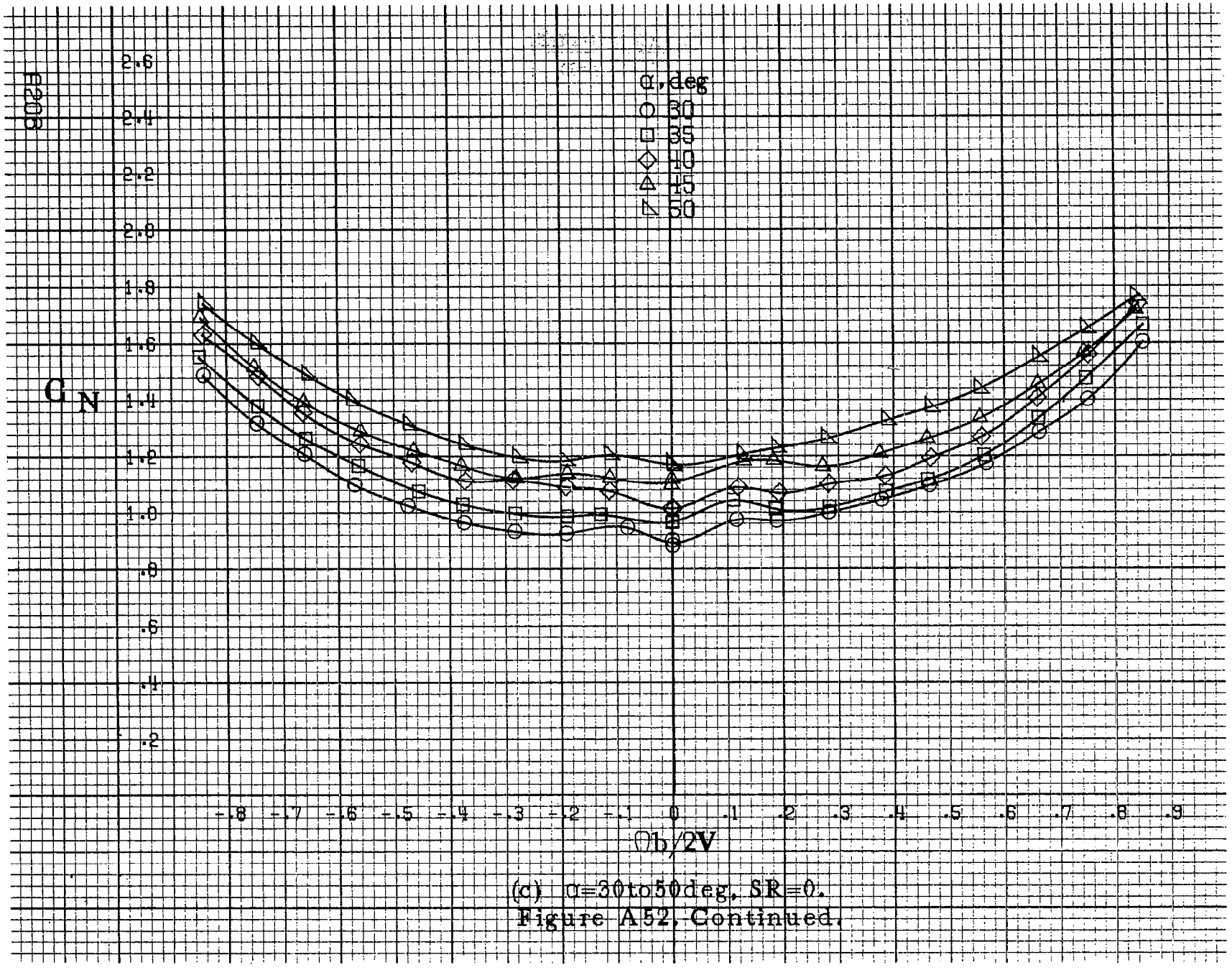

(c) α=30to50deg, SR=0.

Figure A52. Continued.

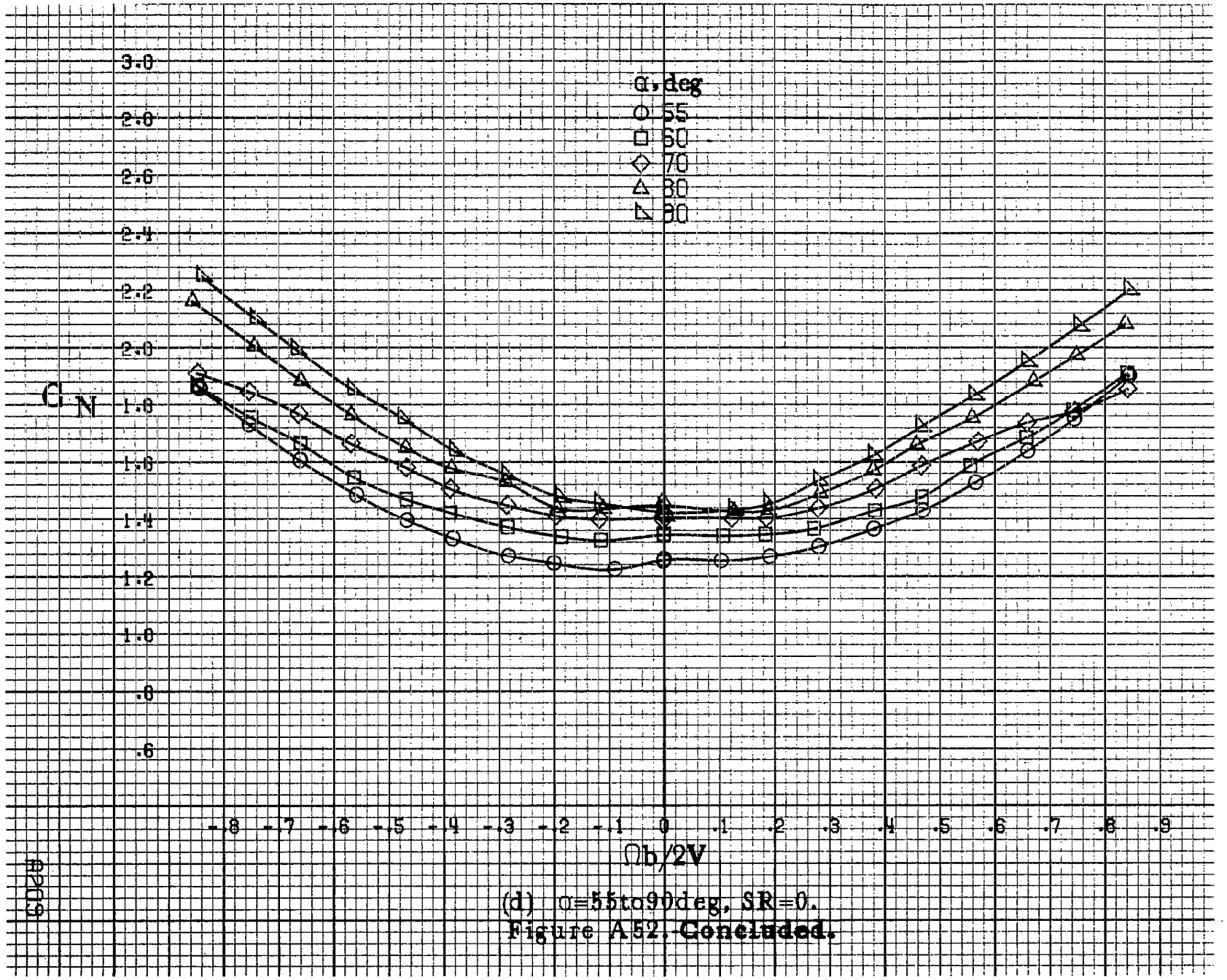

(d) α=55 to 90 deg, SR=0.

Figure A52. Concluded.

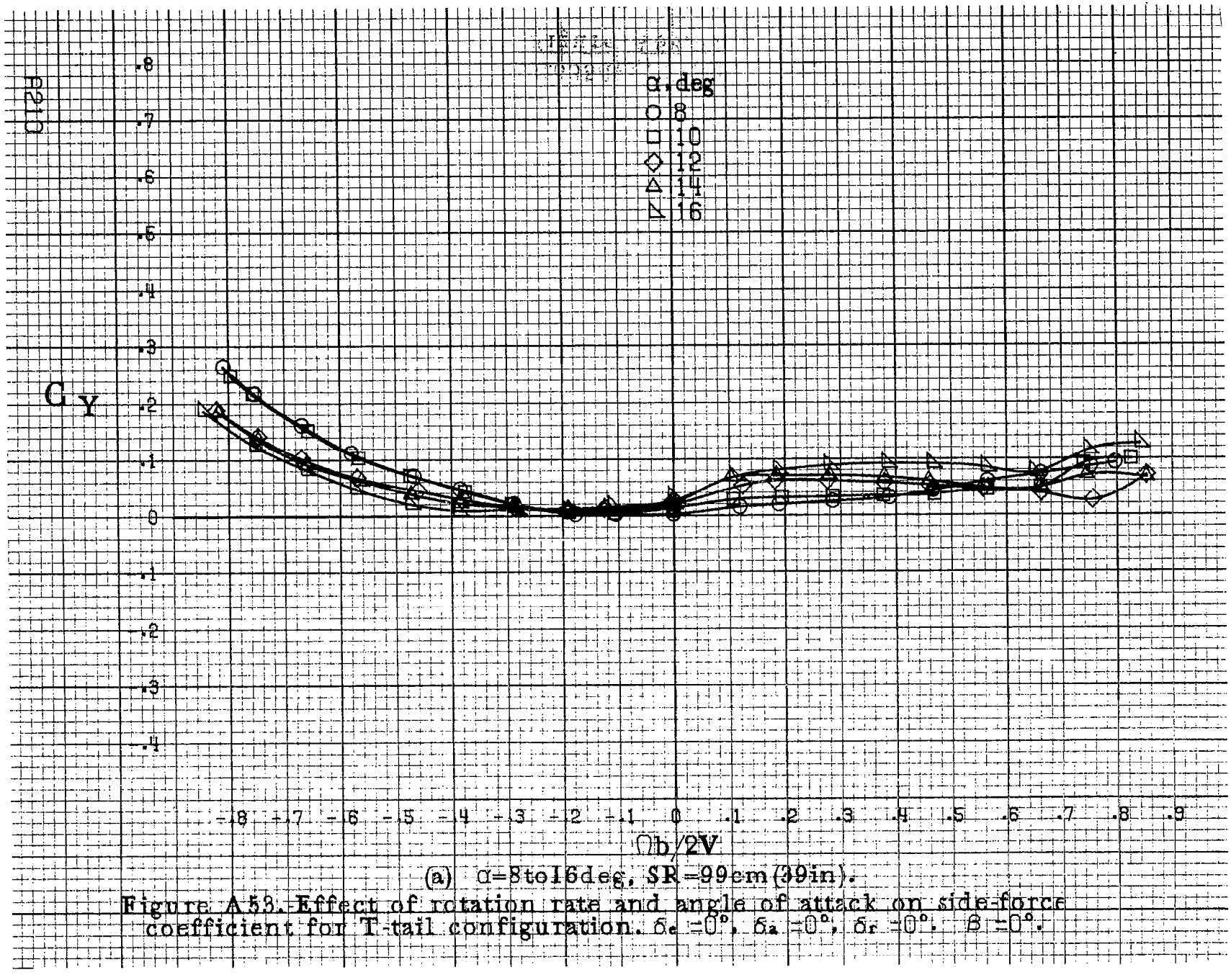

(a) α=8to16deg, SR=99cm(39in).

Figure A.53. Effect of rotation rate and angle of attack on side-force coefficient for T-tail configuration. $\delta_e = 0°$, $\delta_a = 0°$, $\delta_r = 0°$, $\beta = 0°$.

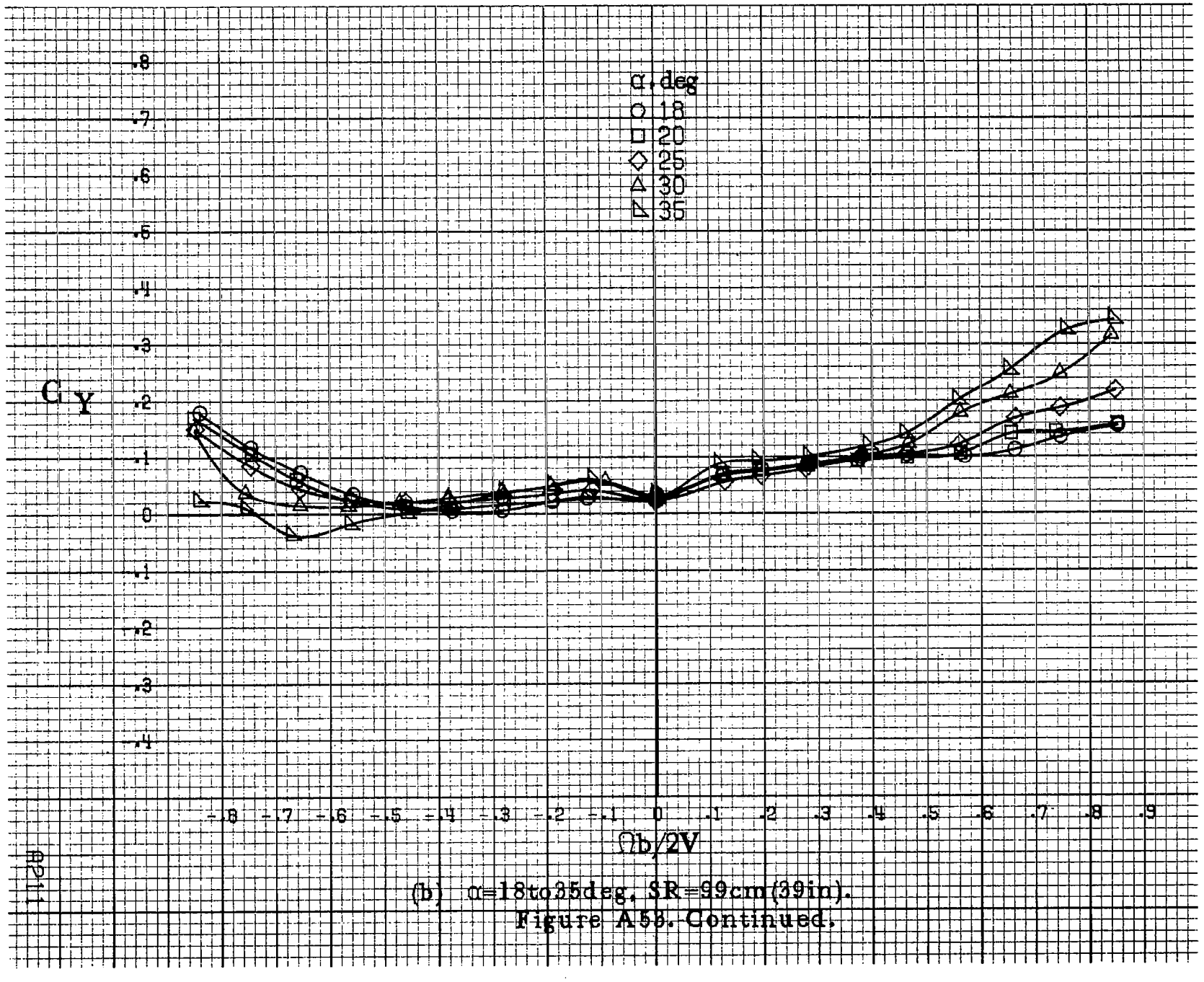

(b) α=18to35deg, SR=99cm(39in).

Figure A56. Continued.

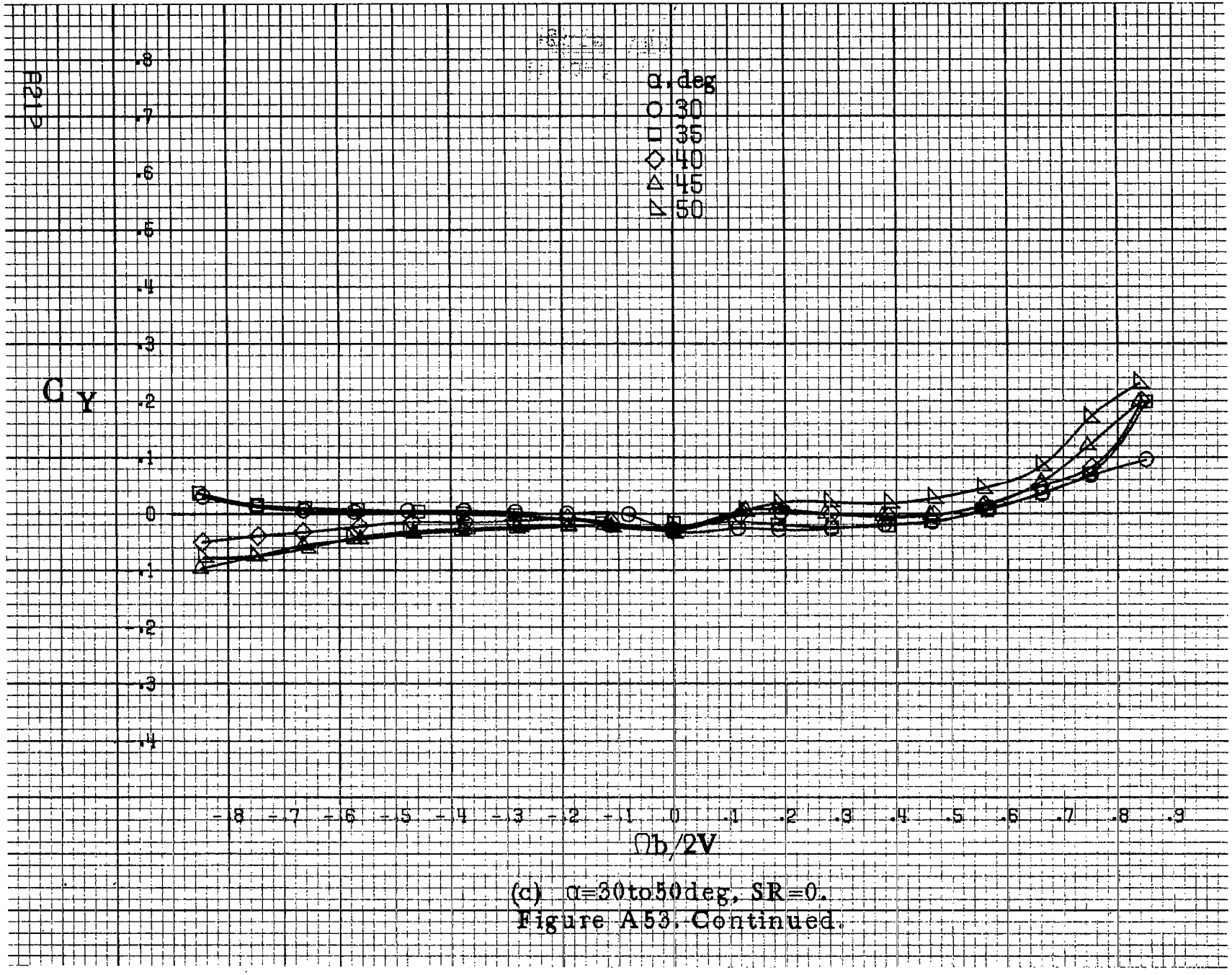

(c) α=30to50deg, SR=0.

Figure A53. Continued.

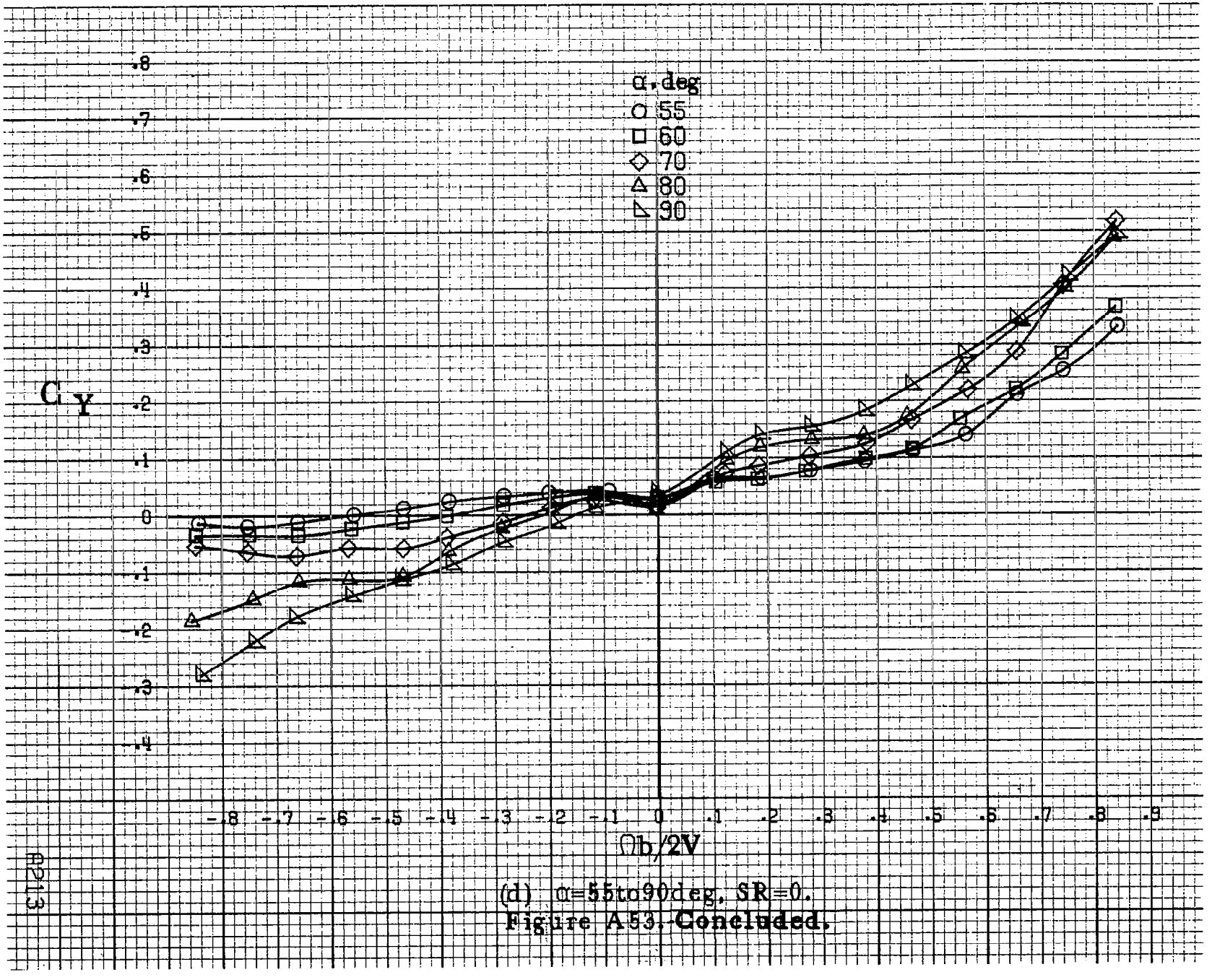

(d) α=55to90deg, SR=0.

Figure A53.-Concluded.

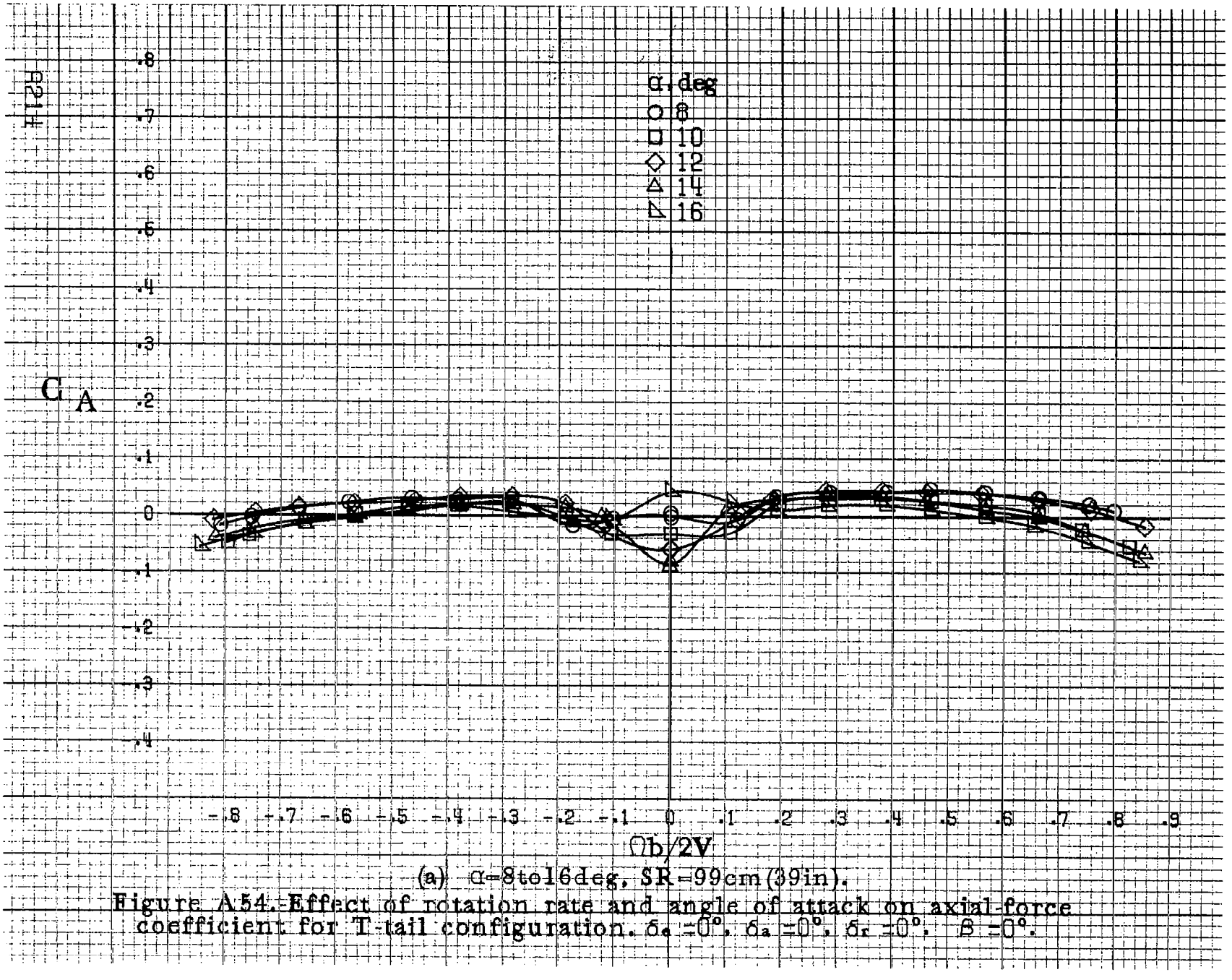

(a) α=8to16deg, SR=99cm(39in).

Figure A54. Effect of rotation rate and angle of attack on axial-force coefficient for T-tail configuration. $\delta_e = 0°$, $\delta_a = 0°$, $\delta_r = 0°$, $\beta = 0°$.

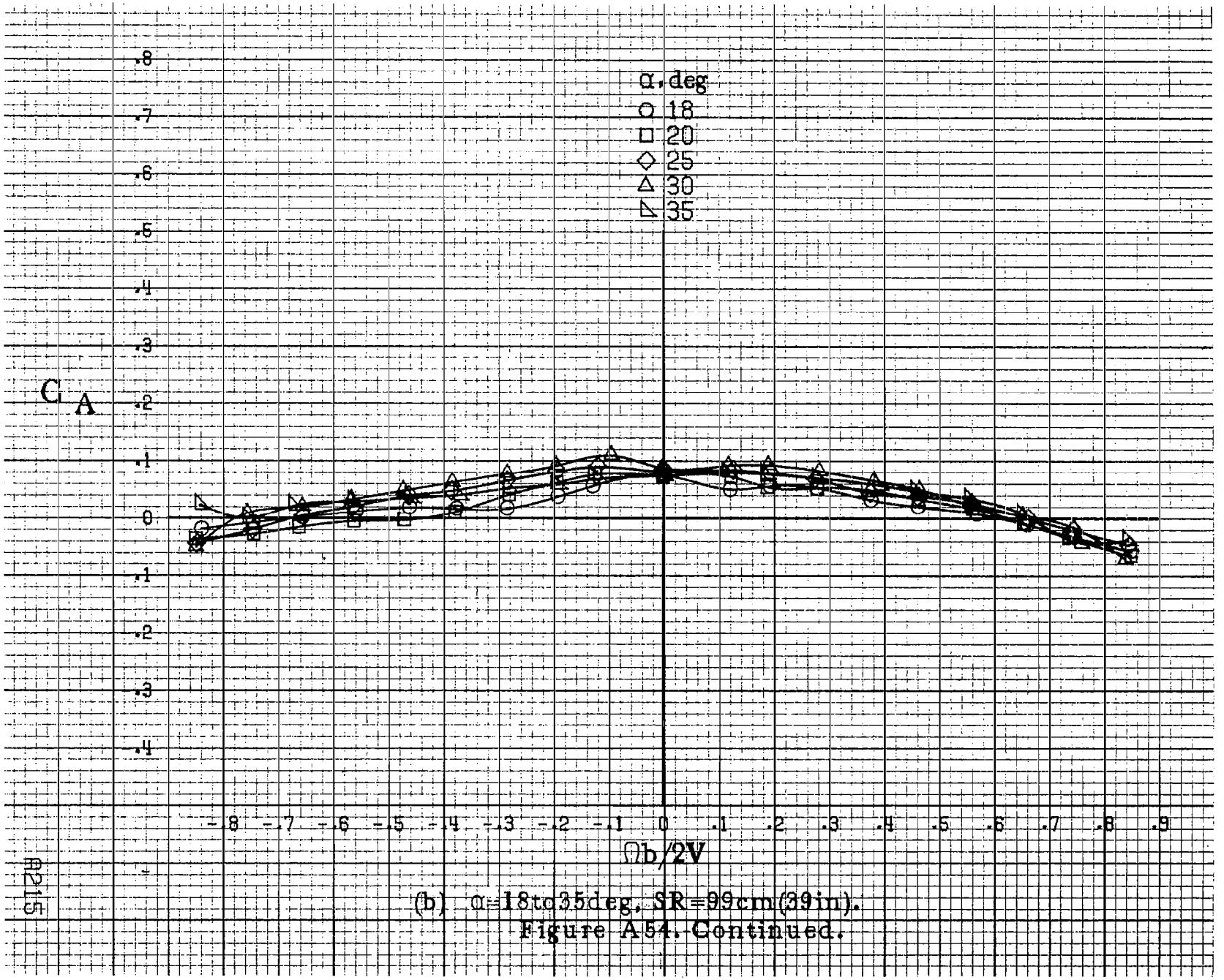

(b) α=18to35deg, SR=99cm(39in).

Figure A54.-Continued.

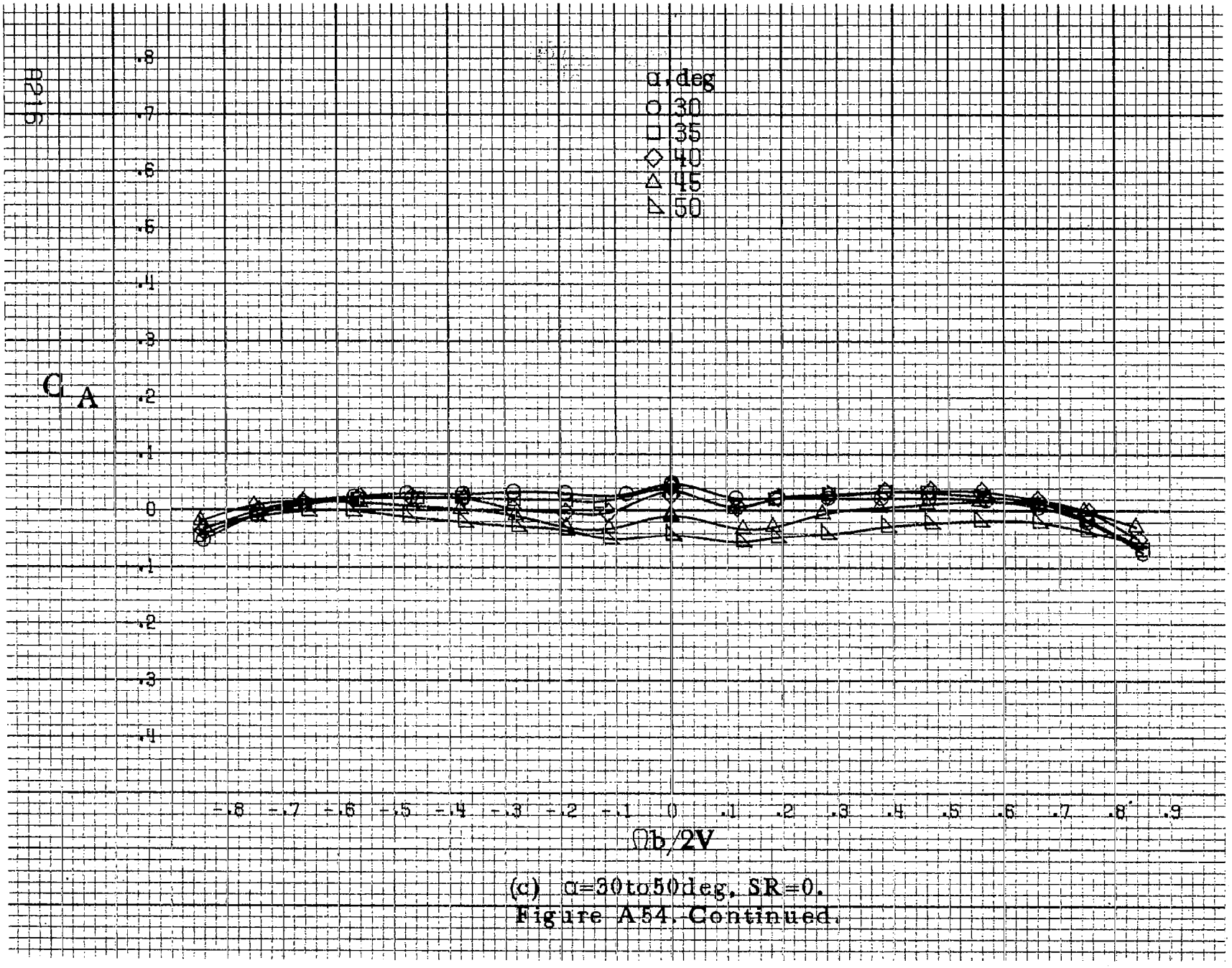

(c) α=30 to 50 deg, SR=0.

Figure A54. Continued.

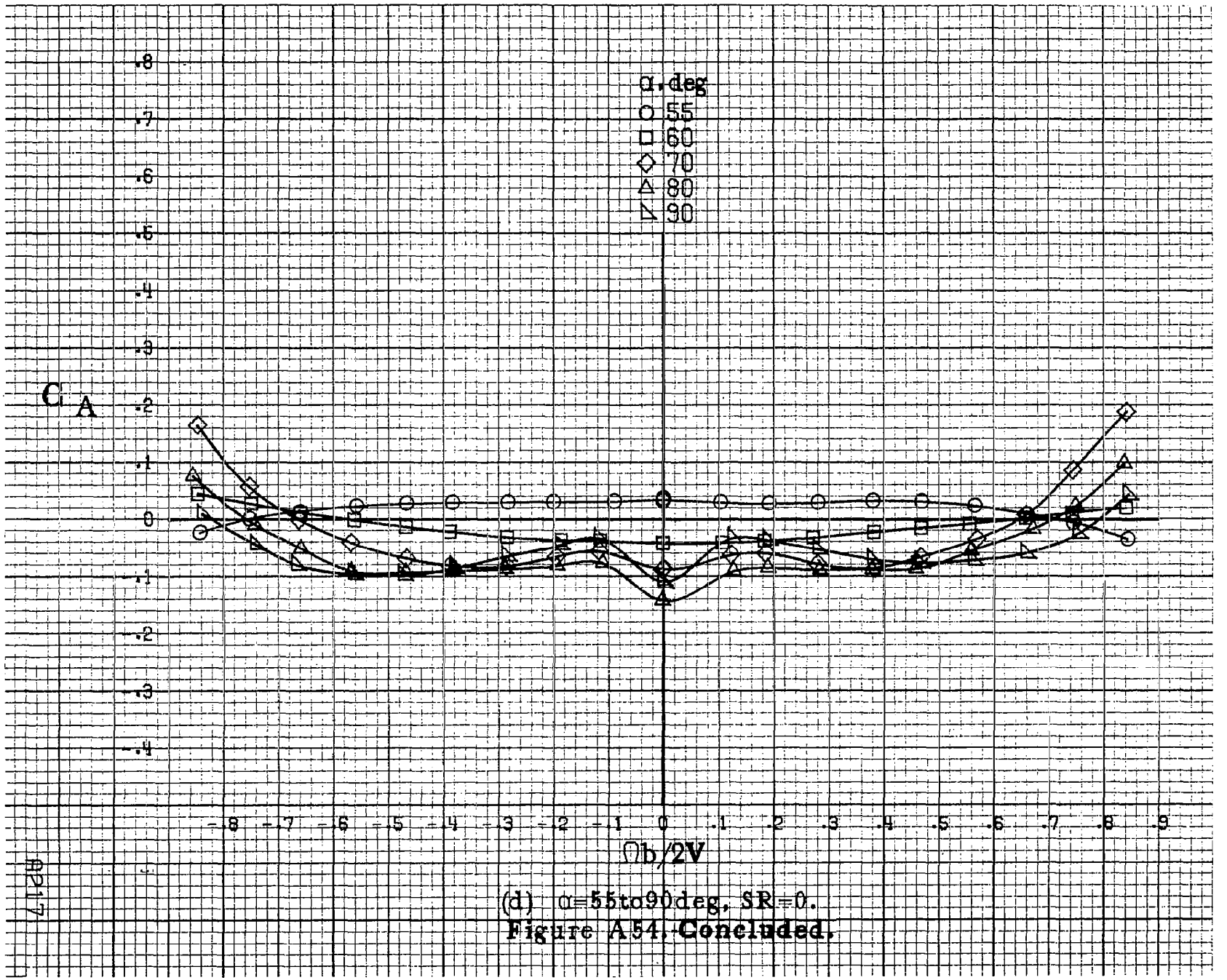

(d) α=55 to 90 deg, SR=0.

Figure A54. Concluded.

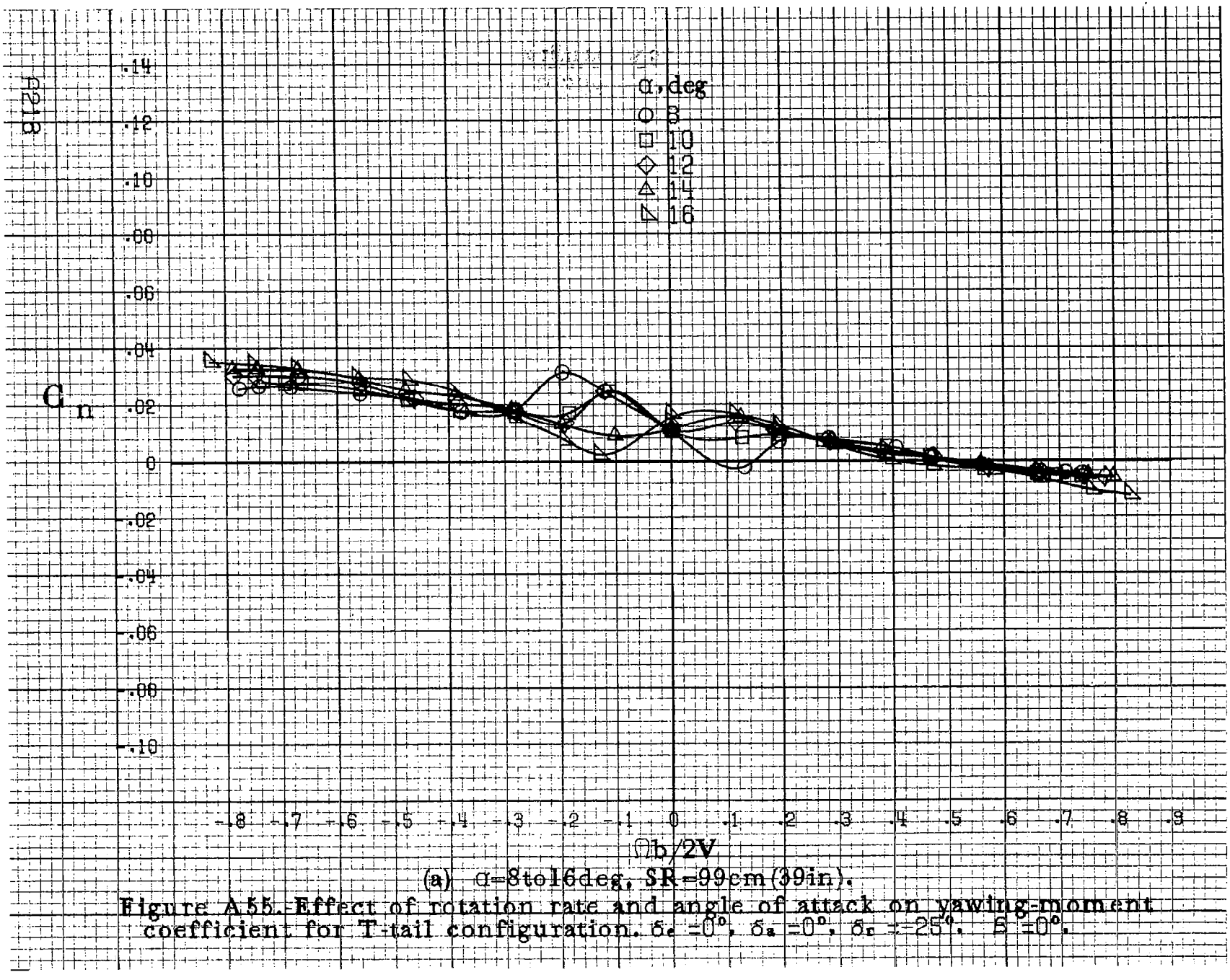

(a) α=8to16deg, SR=99cm(39in).

Figure A55.-Effect of rotation rate and angle of attack on yawing-moment coefficient for T-tail configuration. $\delta_e = 0°$, $\delta_a = 0°$, $\delta_r = -25°$, $\beta = 0°$.

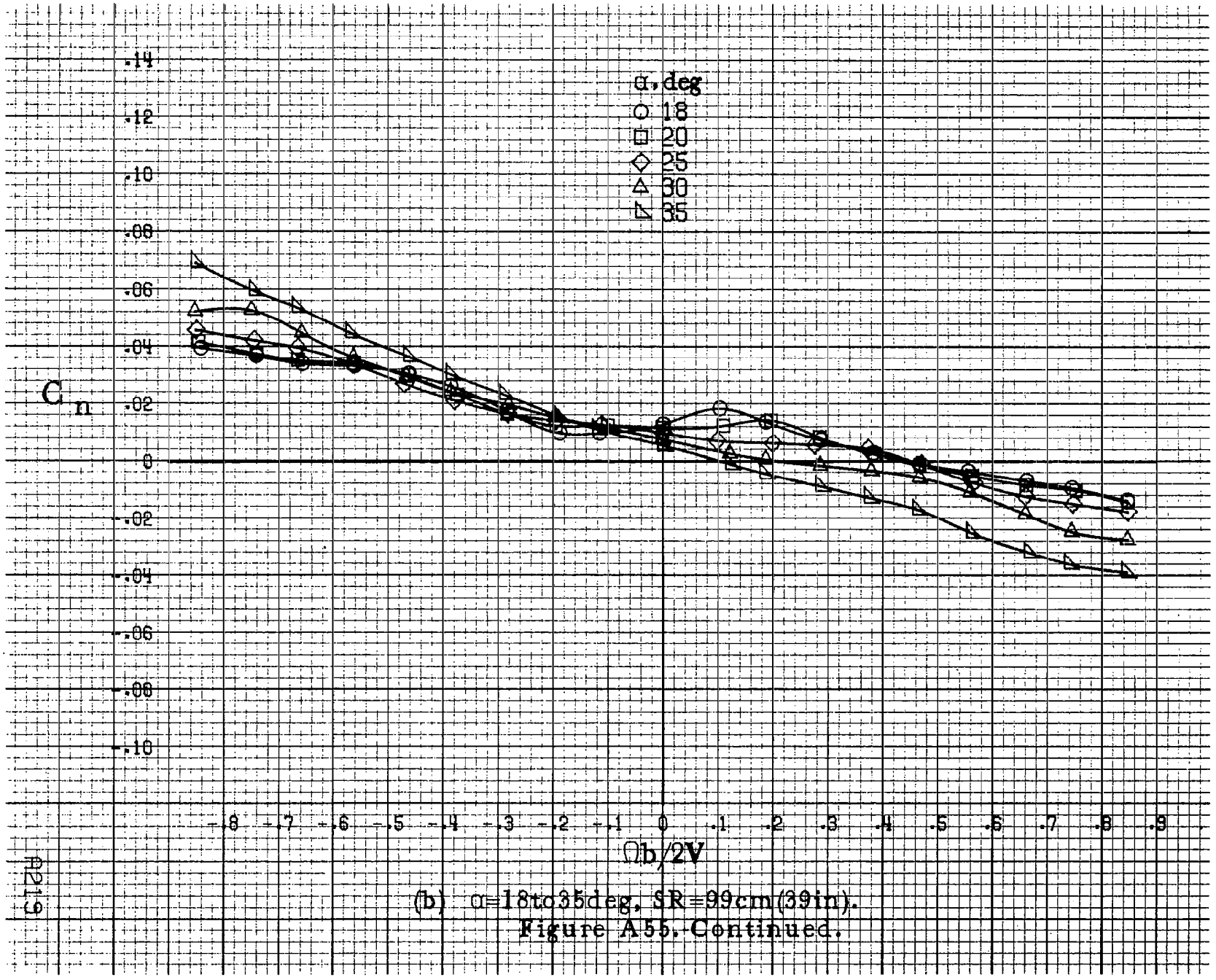

(b) α=18to35deg, SR=99cm(39in).

Figure A55.-Continued.

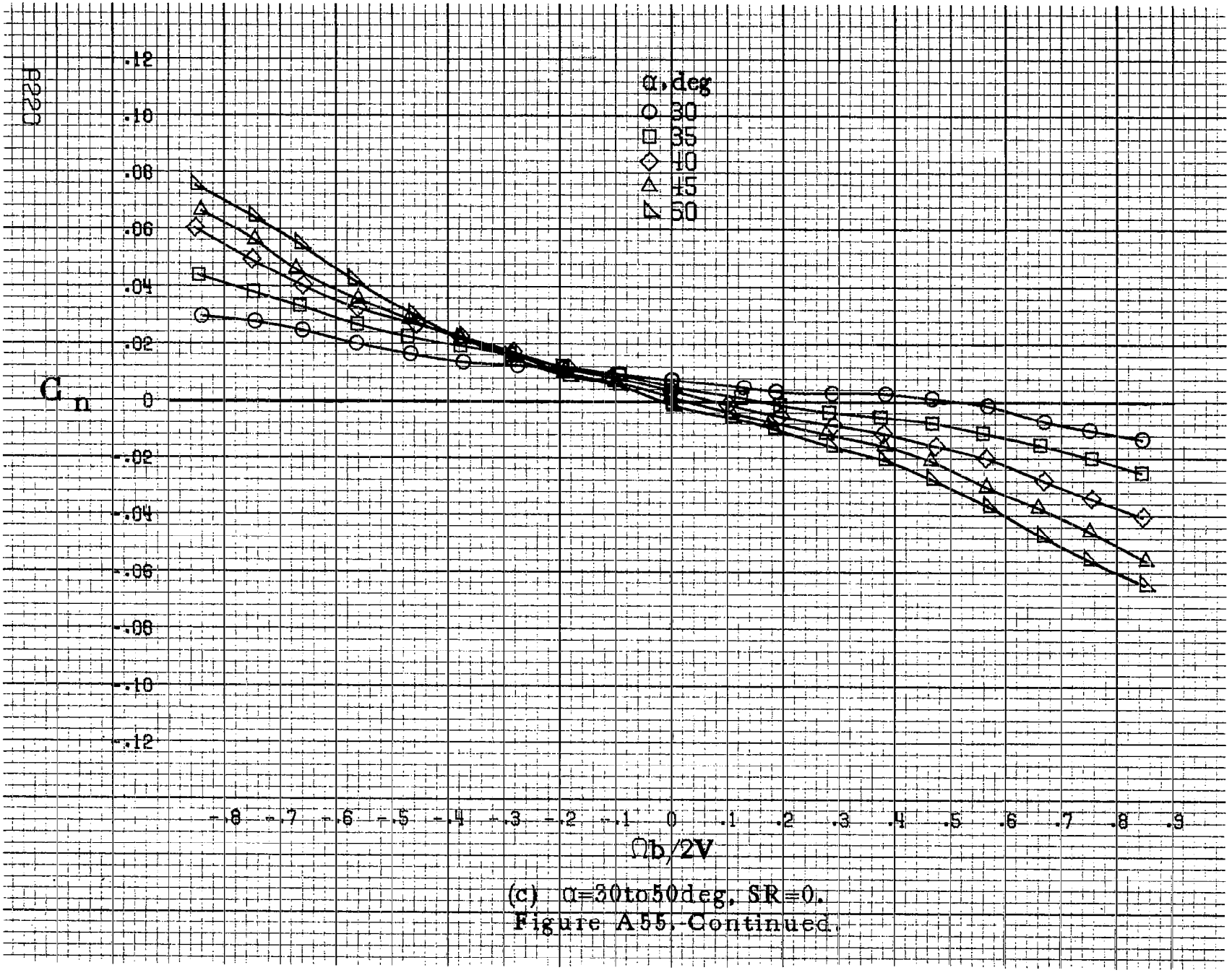

(c) α=30to50deg, SR=0.

Figure A55.-Continued.

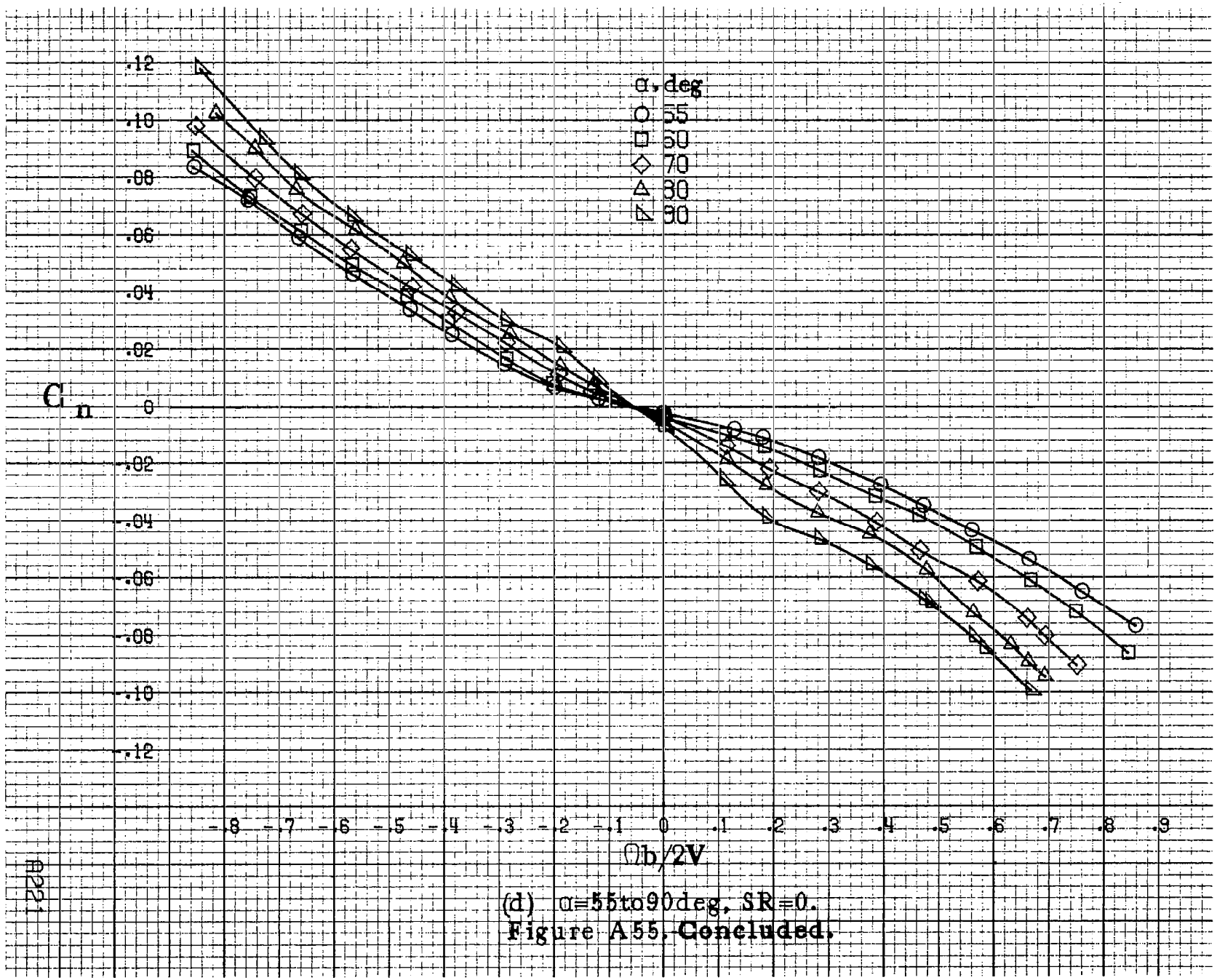

(d) α=55to90deg, SR=0.

Figure A55. Concluded.

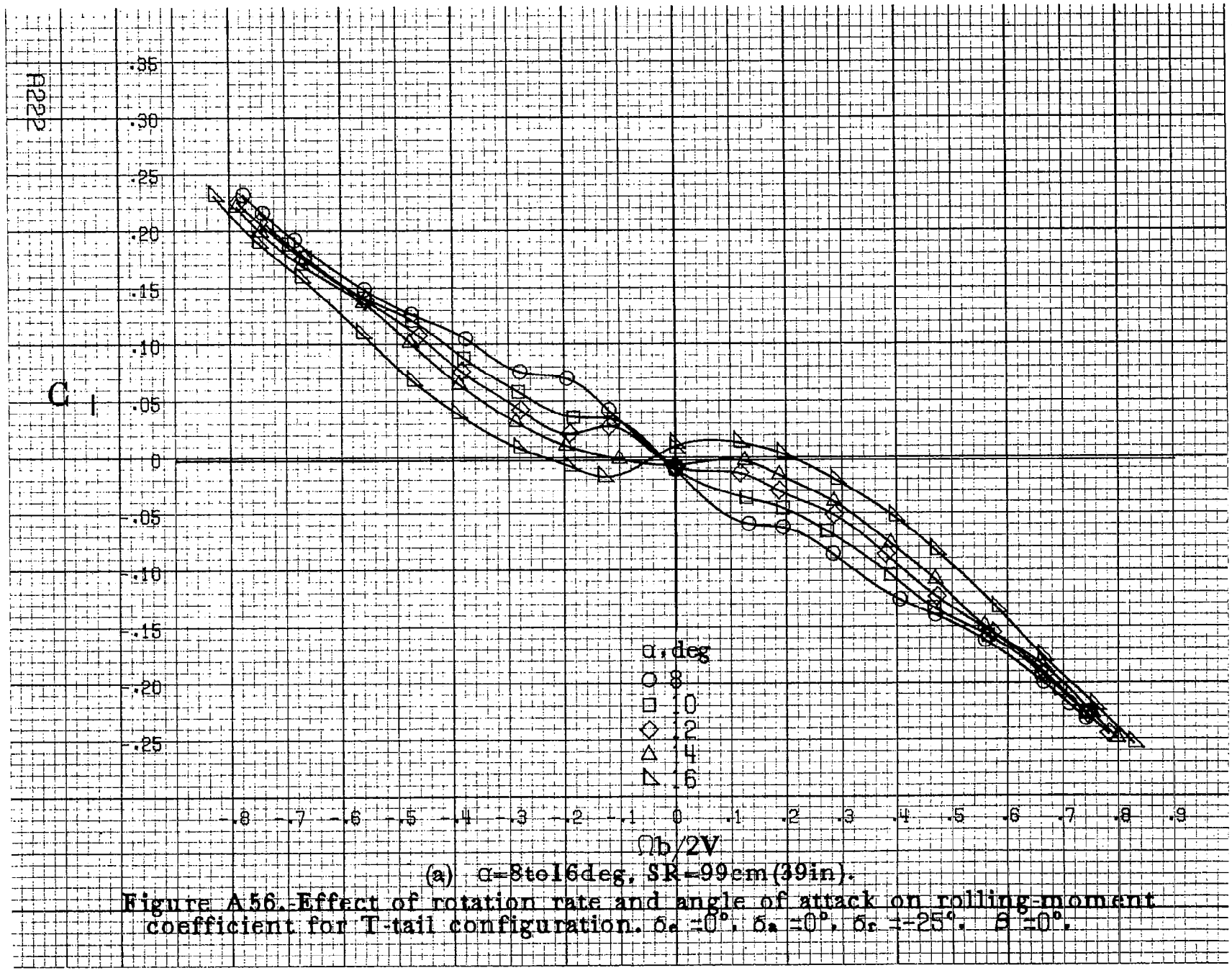

(a) α=8to16deg, SR=99cm(39in).

Figure A56.-Effect of rotation rate and angle of attack on rolling-moment coefficient for T-tail configuration. δ_e =0°, δ_a =0°, δ_r =-25°, β =0°.

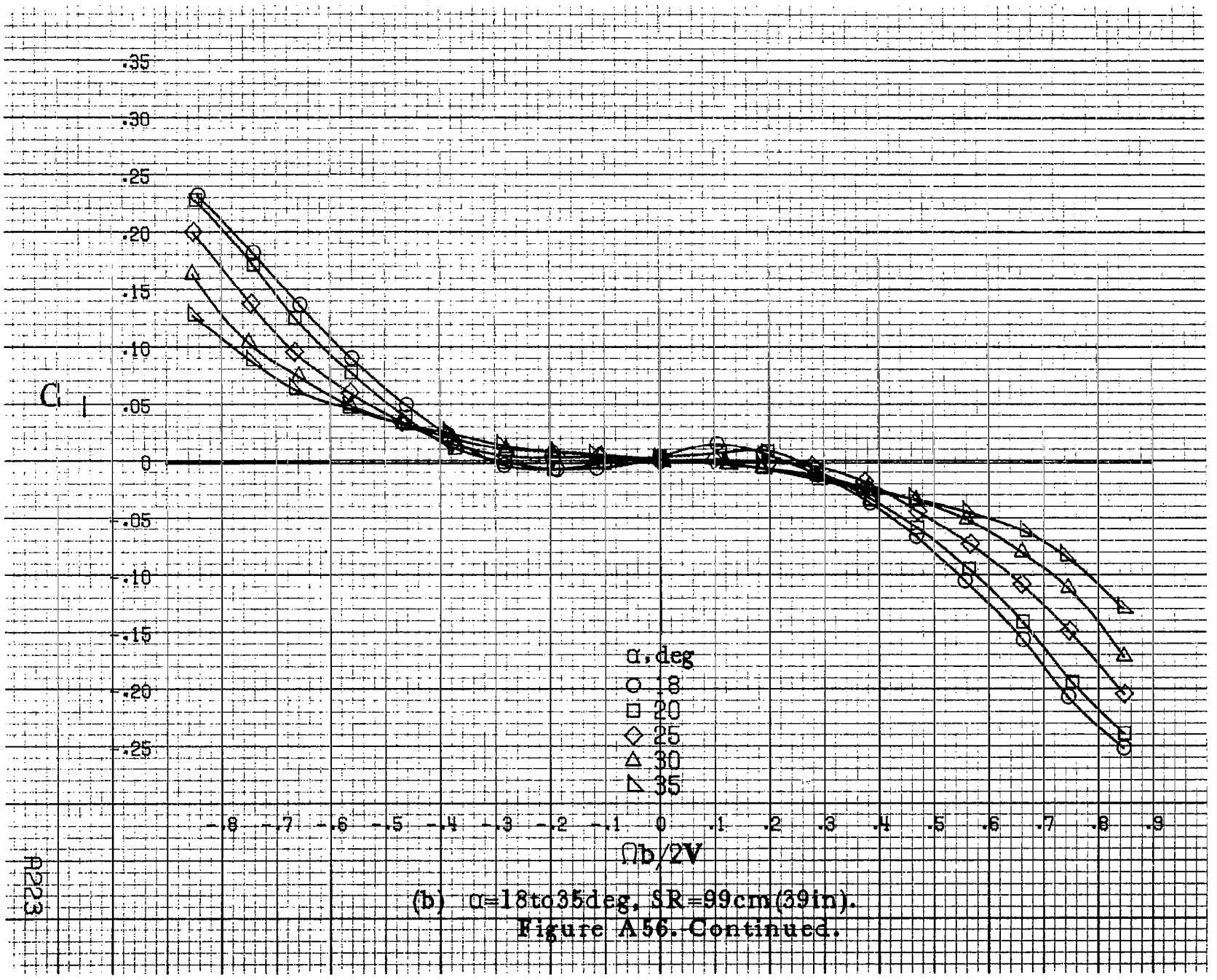

(b) α=18to35deg, SR=99cm(39in).

Figure A56. Continued.

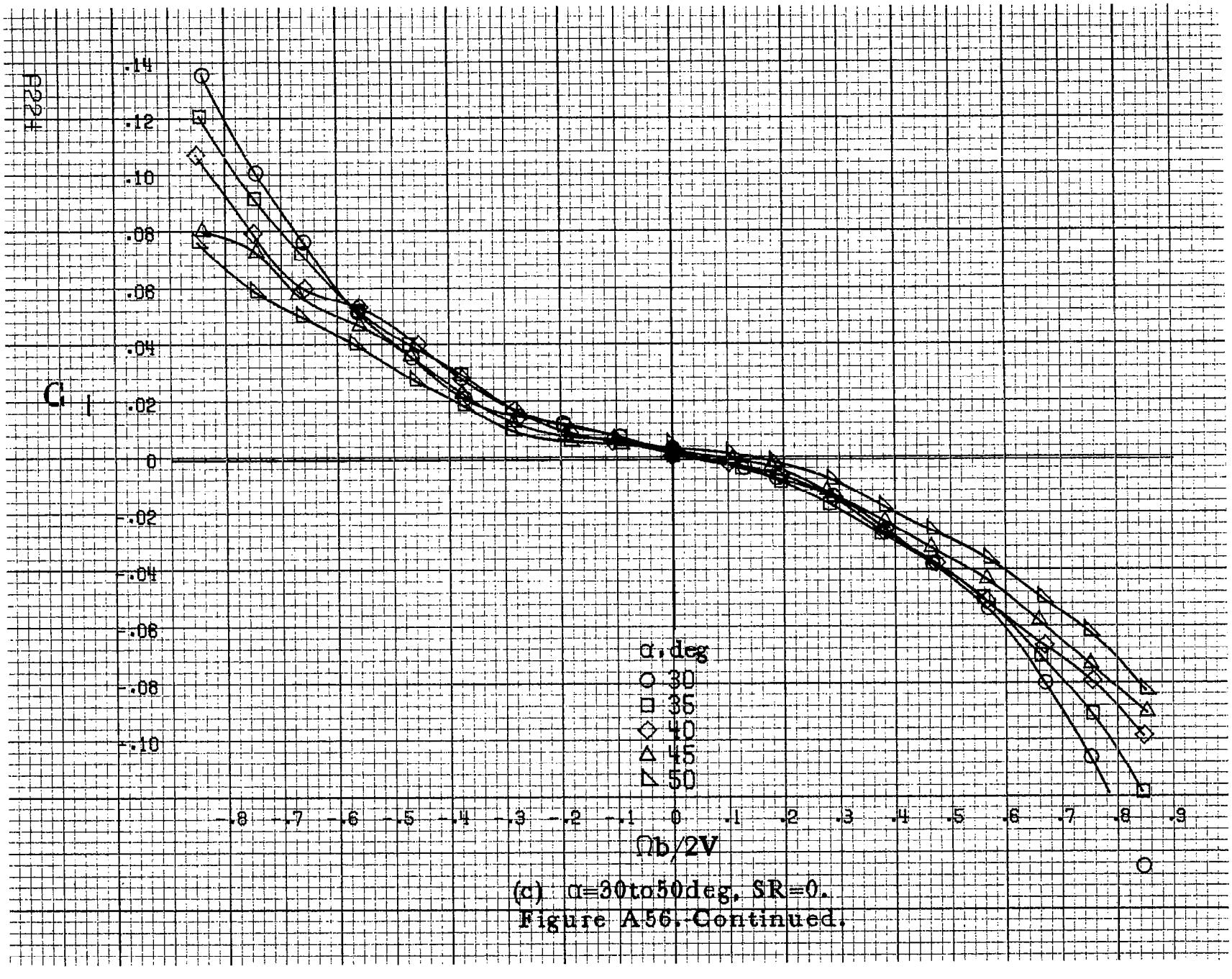

(d) α=30to50deg, SR=0.

Figure A56.-Continued.

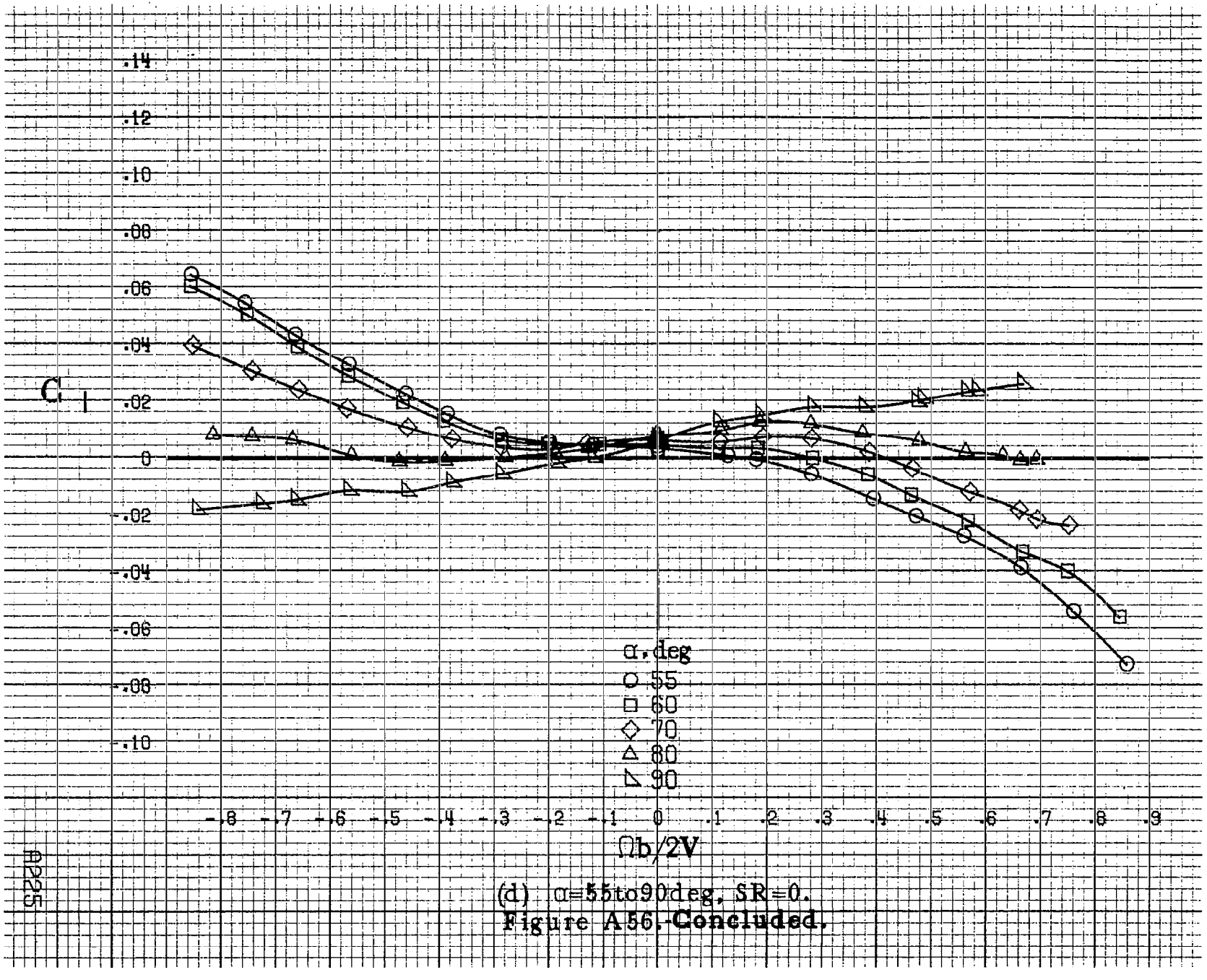

(d) α=55to90deg, SR=0.

Figure A56. Concluded.

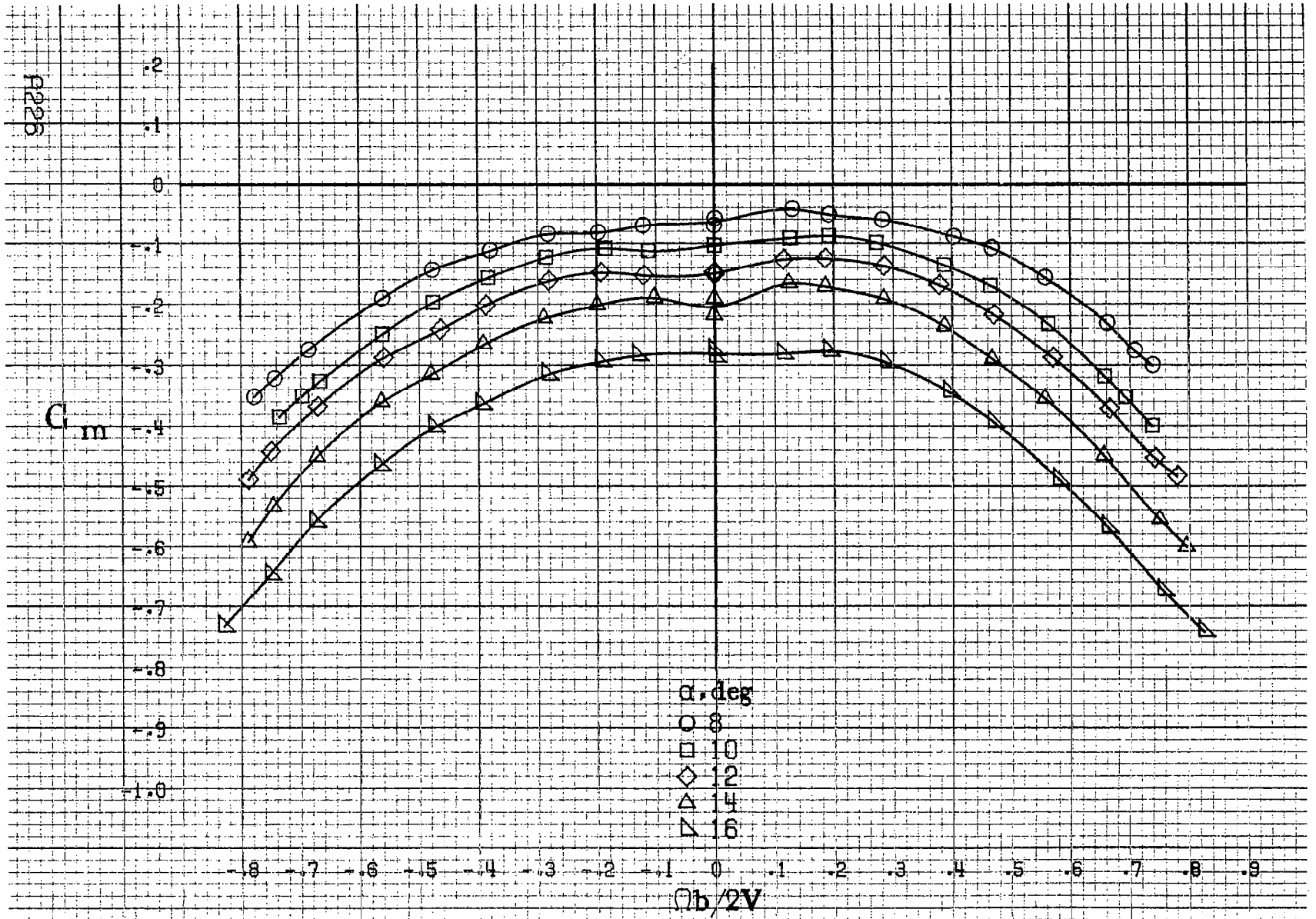

(a) α=8to16deg, SR=99cm(39in).

Figure A57.-Effect of rotation rate and angle of attack on pitching-moment coefficient for T-tail configuration. $\delta_e = 0°$, $\delta_a = 0°$, $\delta_r = -25°$, $\beta = 0°$.

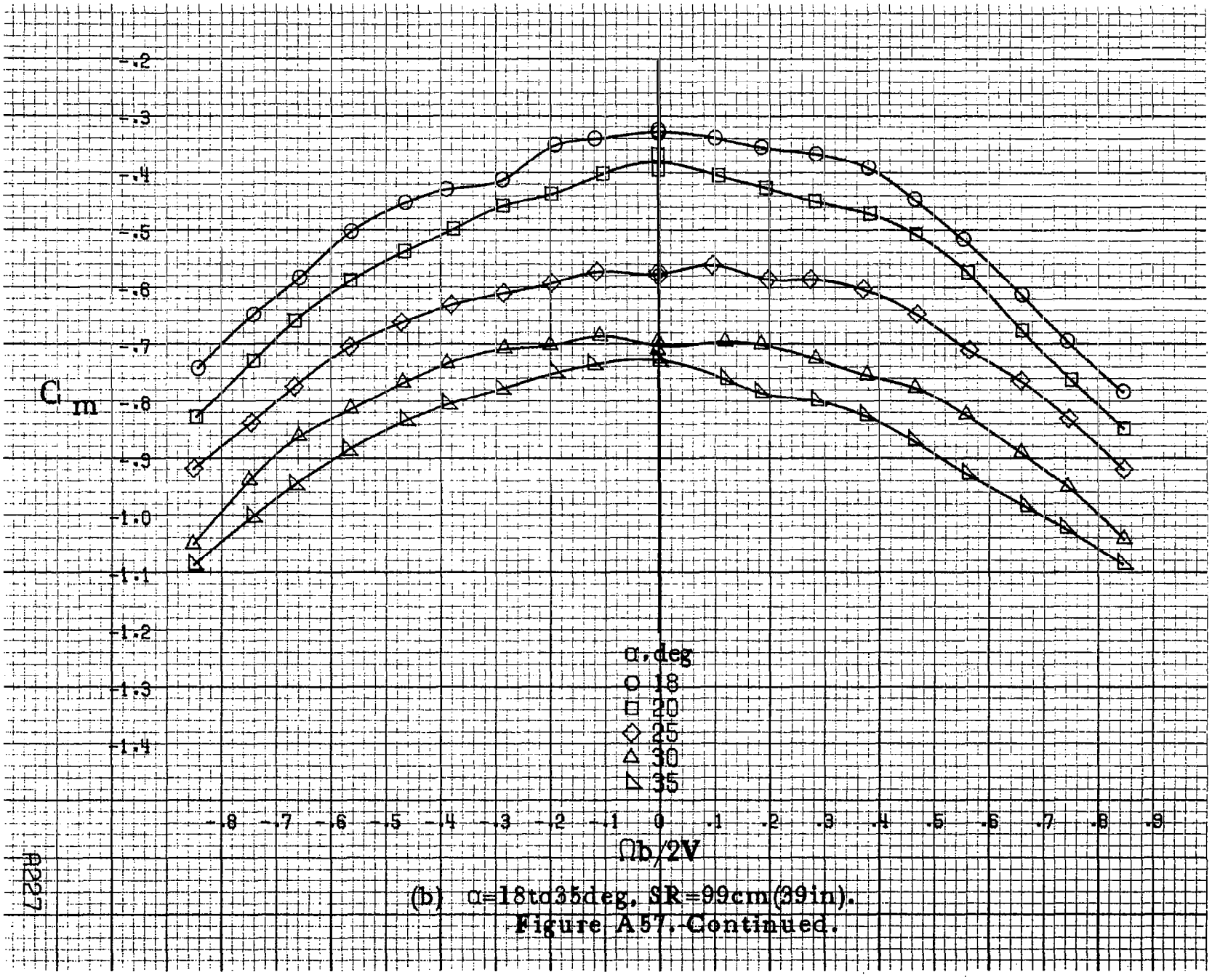

(b) α=18to35deg, SR=99cm(39in).

Figure A57.-Continued.

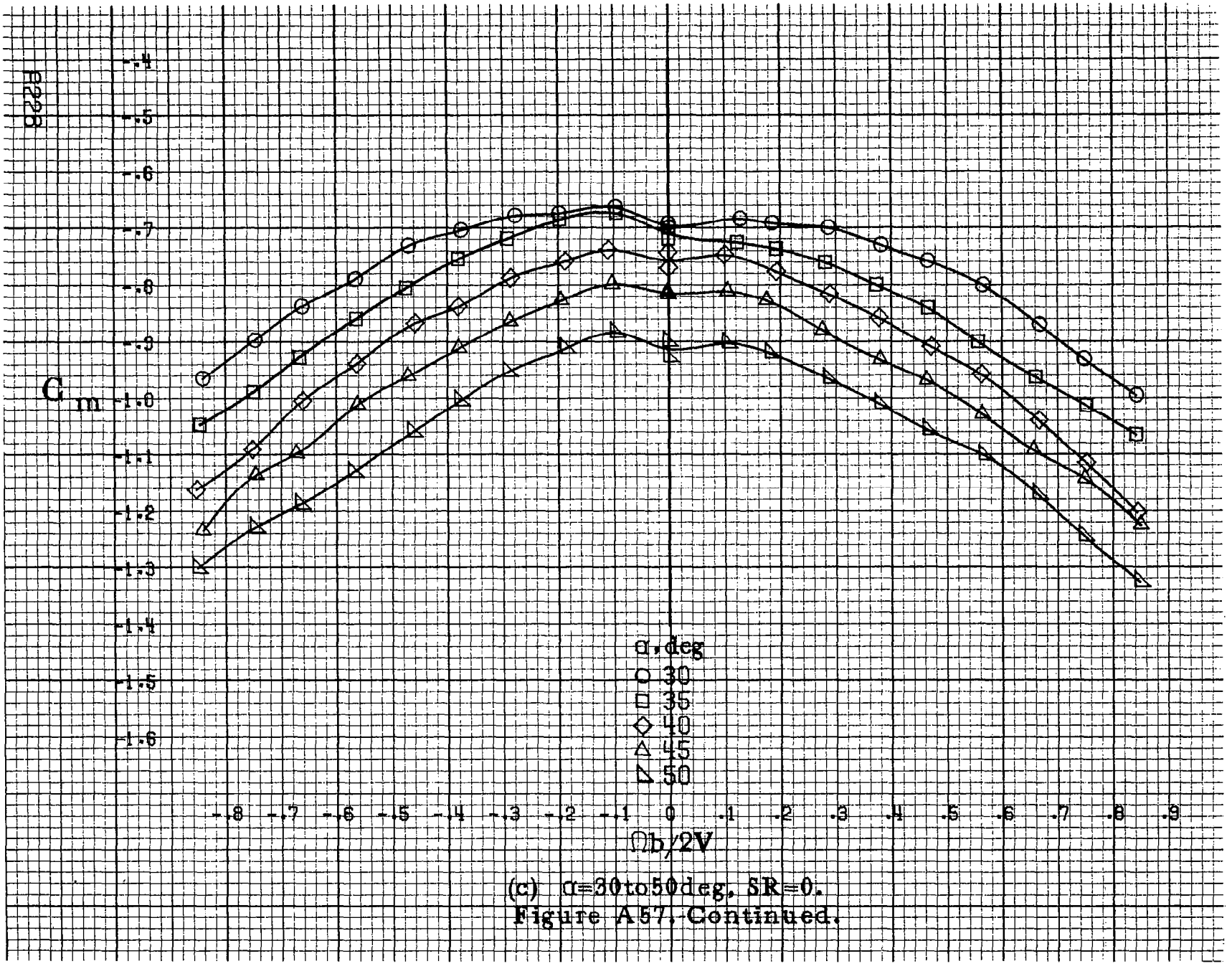

(c) α=30to50deg, δR=0.

Figure A57. Continued.

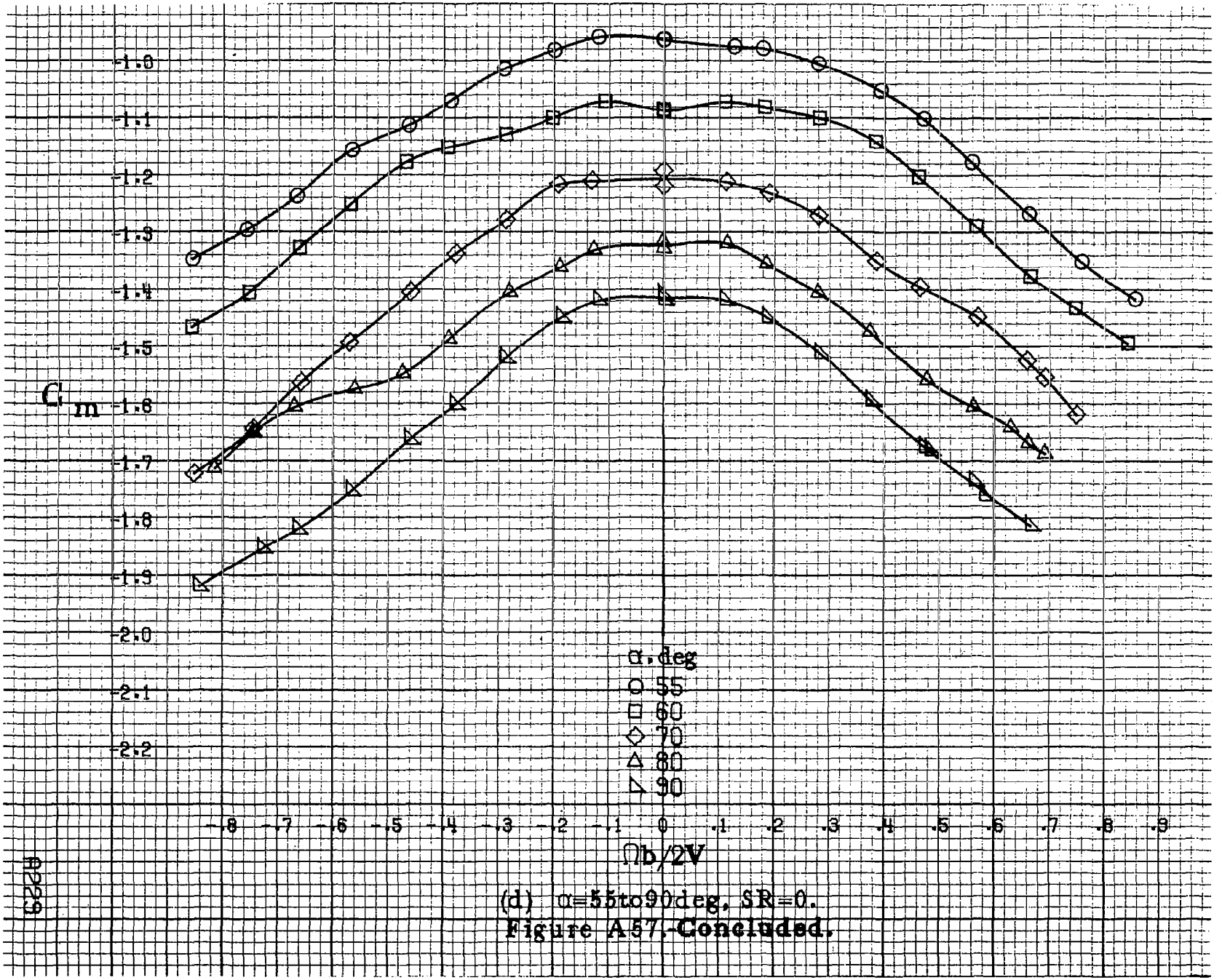

(d) α=55to90deg, SR=0.

Figure A57.-Concluded.

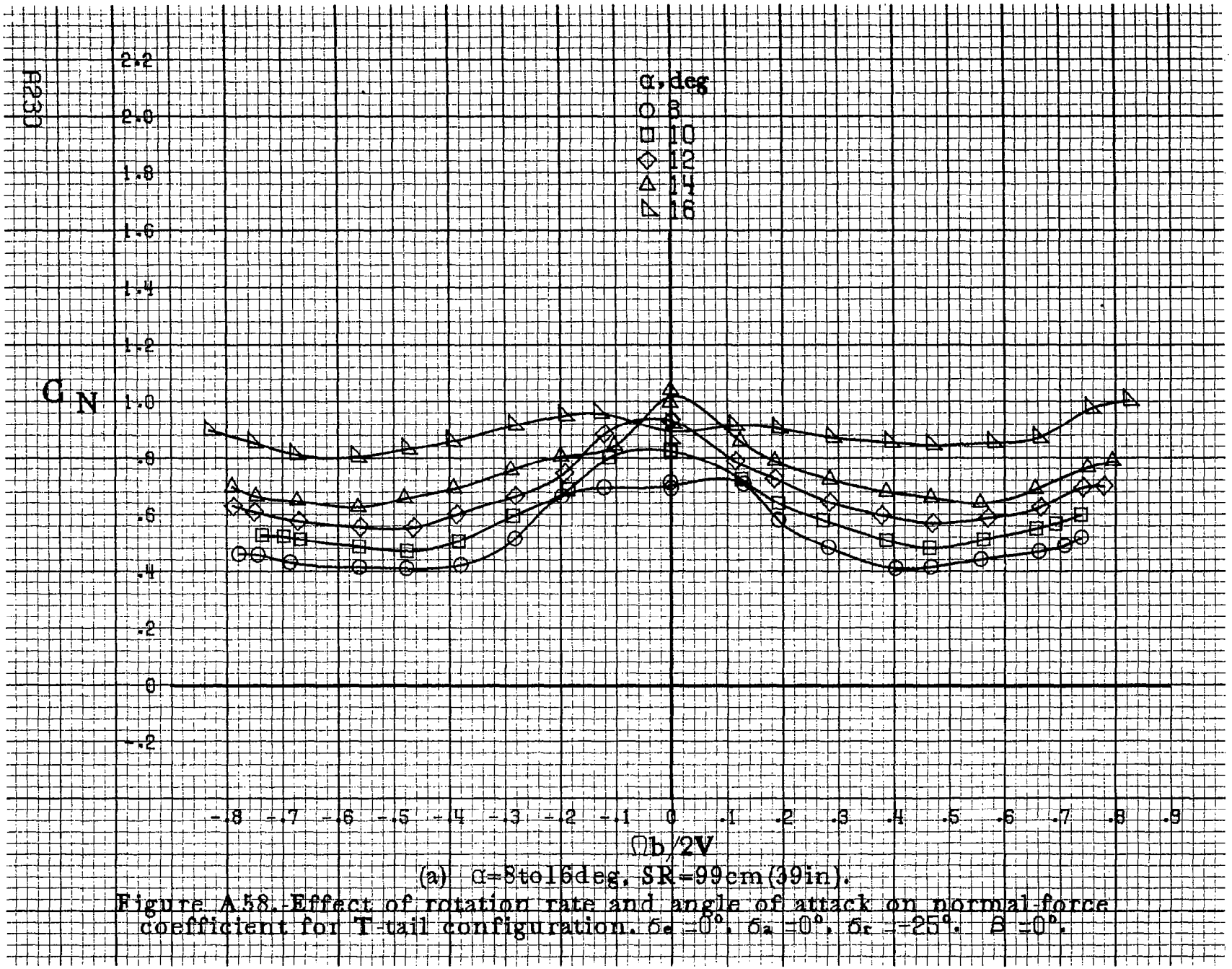

(a) α=8to16deg, SR=99cm(39in).

Figure A.58.-Effect of rotation rate and angle of attack on normal-force coefficient for T-tail configuration. $\delta_e = 0°$, $\delta_a = 0°$, $\delta_r = -25°$, $\beta = 0°$.

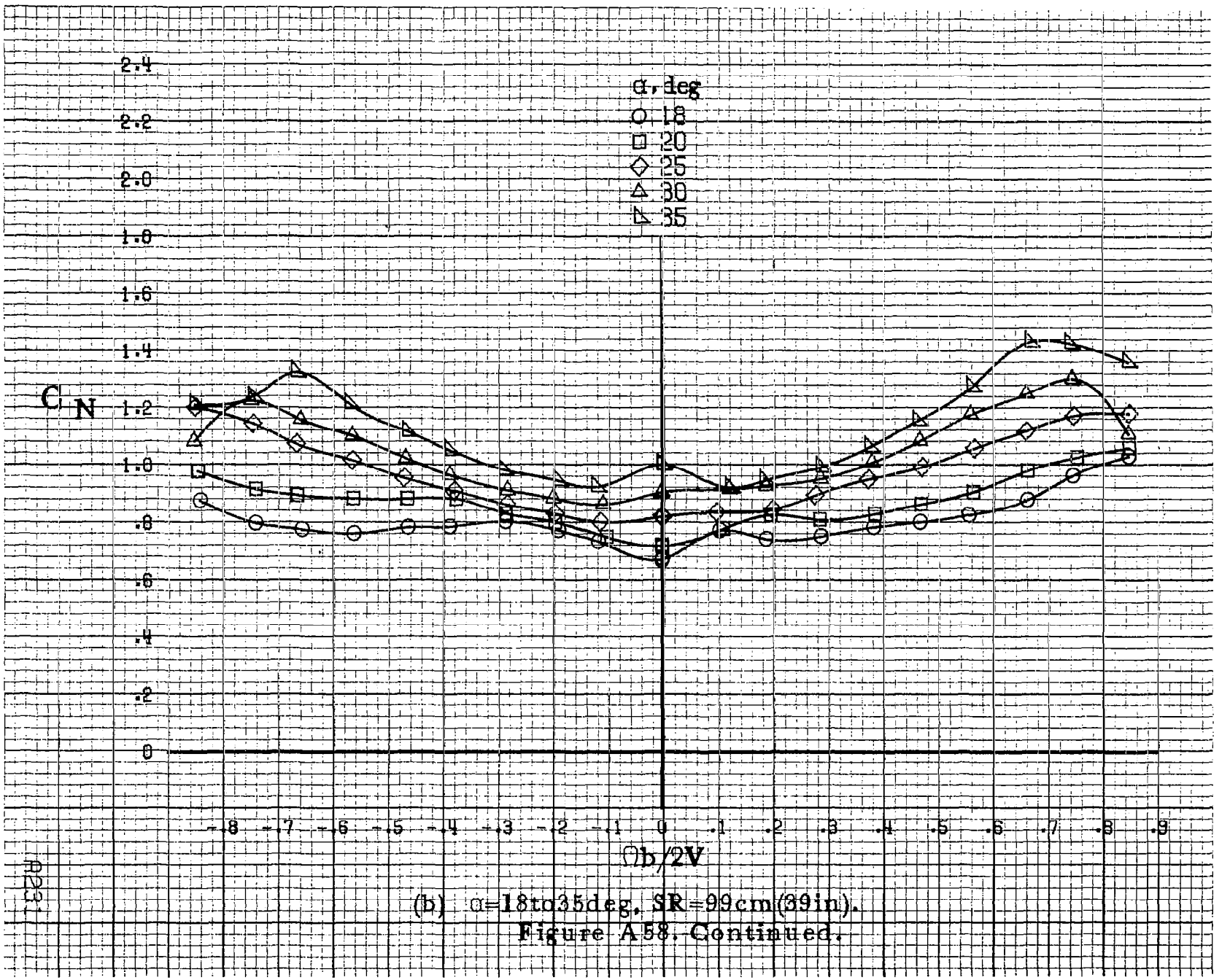

(b) α=18to35deg, SR=99cm(39in).

Figure A58. Continued.

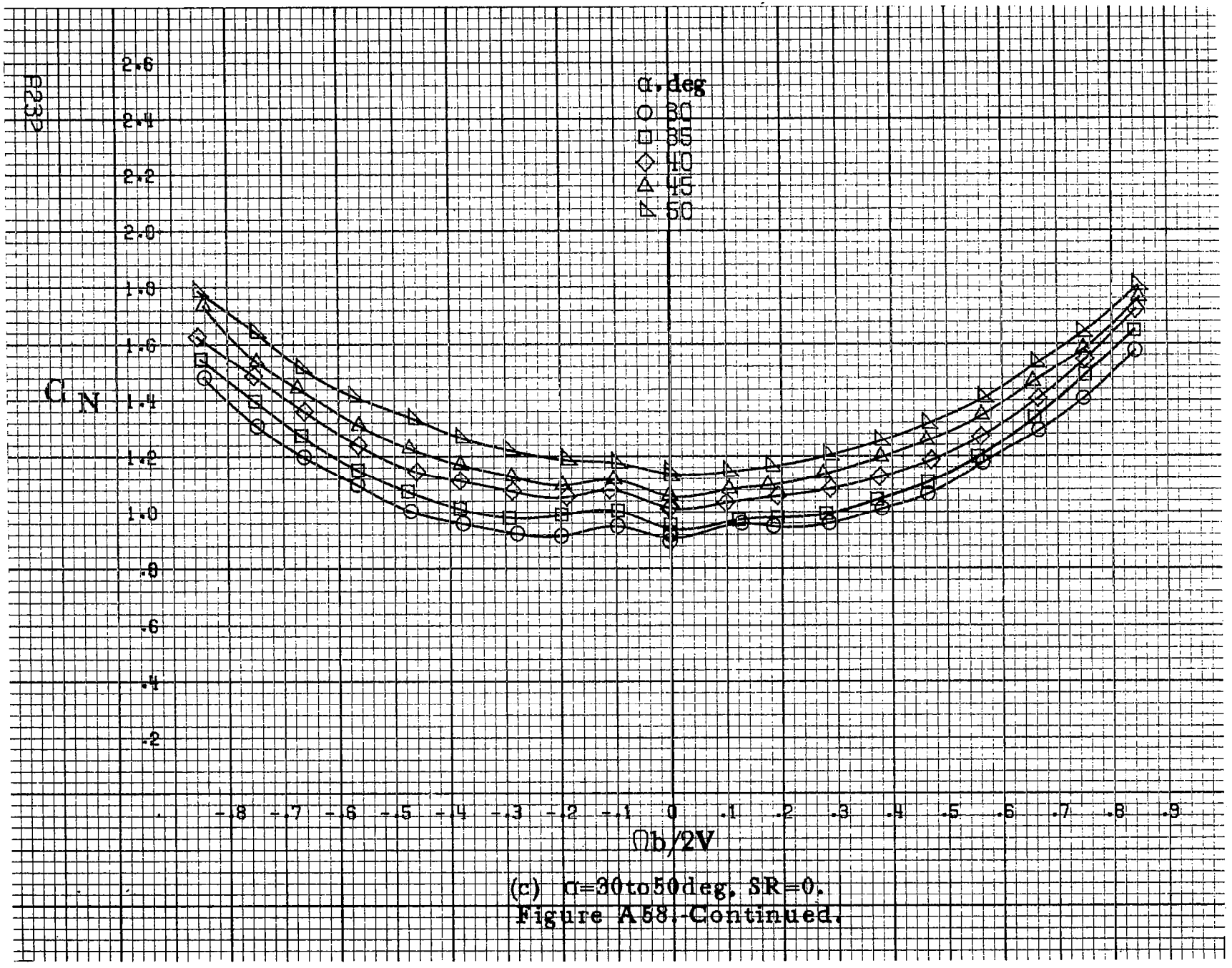

(c) α=30 to 50 deg, SR=0.

Figure A58.-Continued.

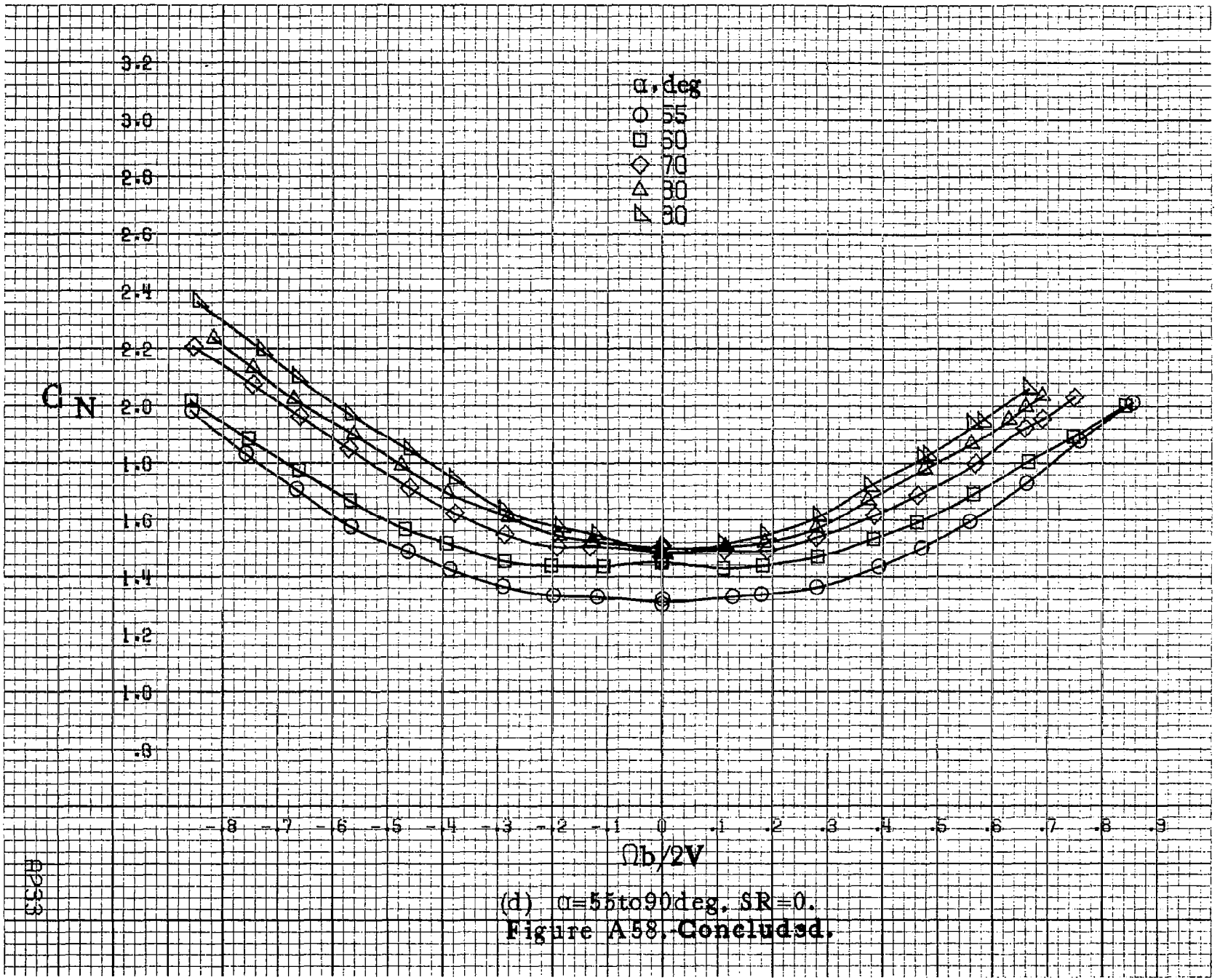

(d) α=55to90deg, SR=0.

Figure A58.-Concluded.

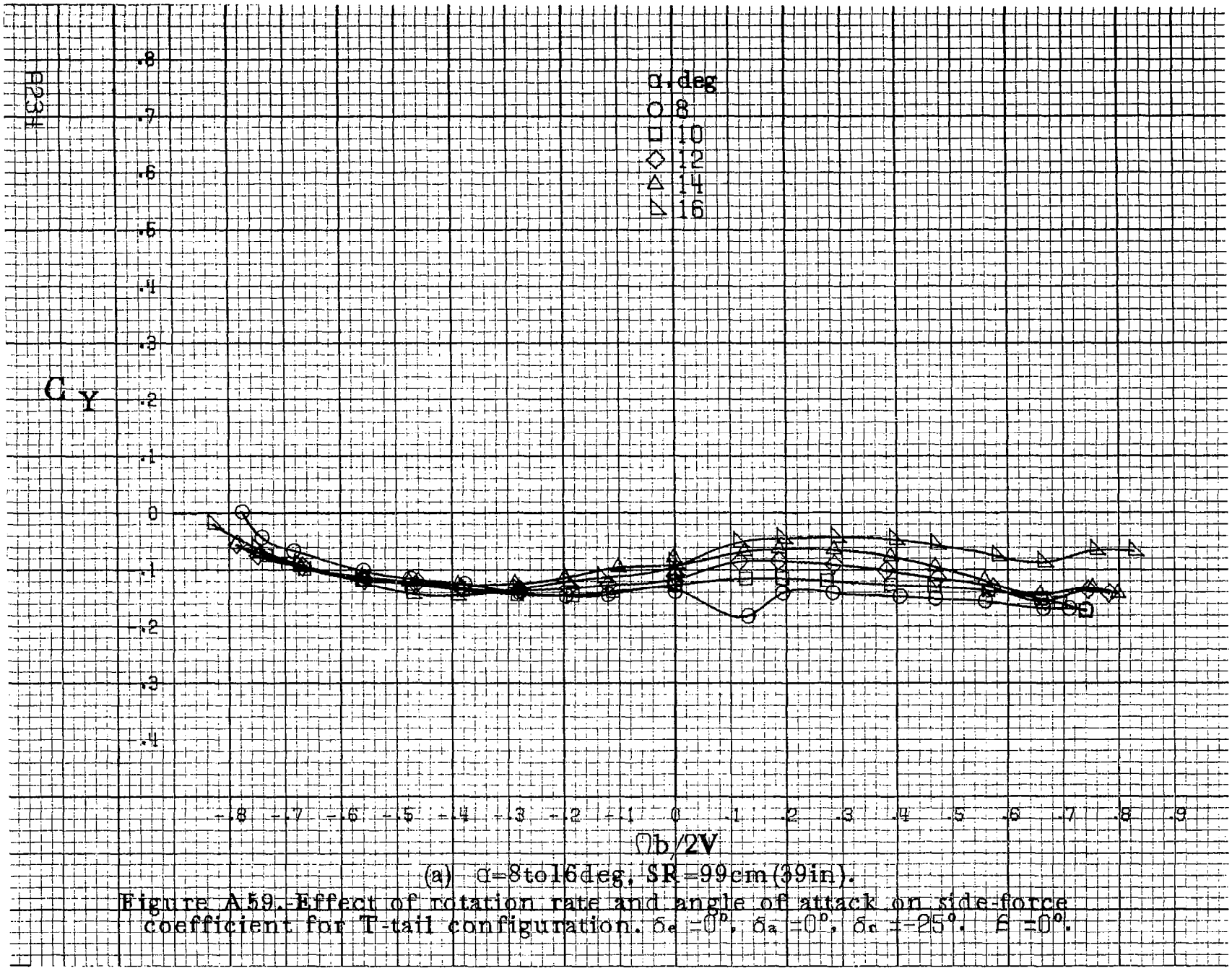

(a) α=8to16deg, $R=99cm(39in).

Figure A59.-Effect of rotation rate and angle of attack on side-force coefficient for T-tail configuration. $\delta_e = 0^\circ$, $\delta_a = 0^\circ$, $\delta_r = -25^\circ$. $\beta = 0^\circ$.

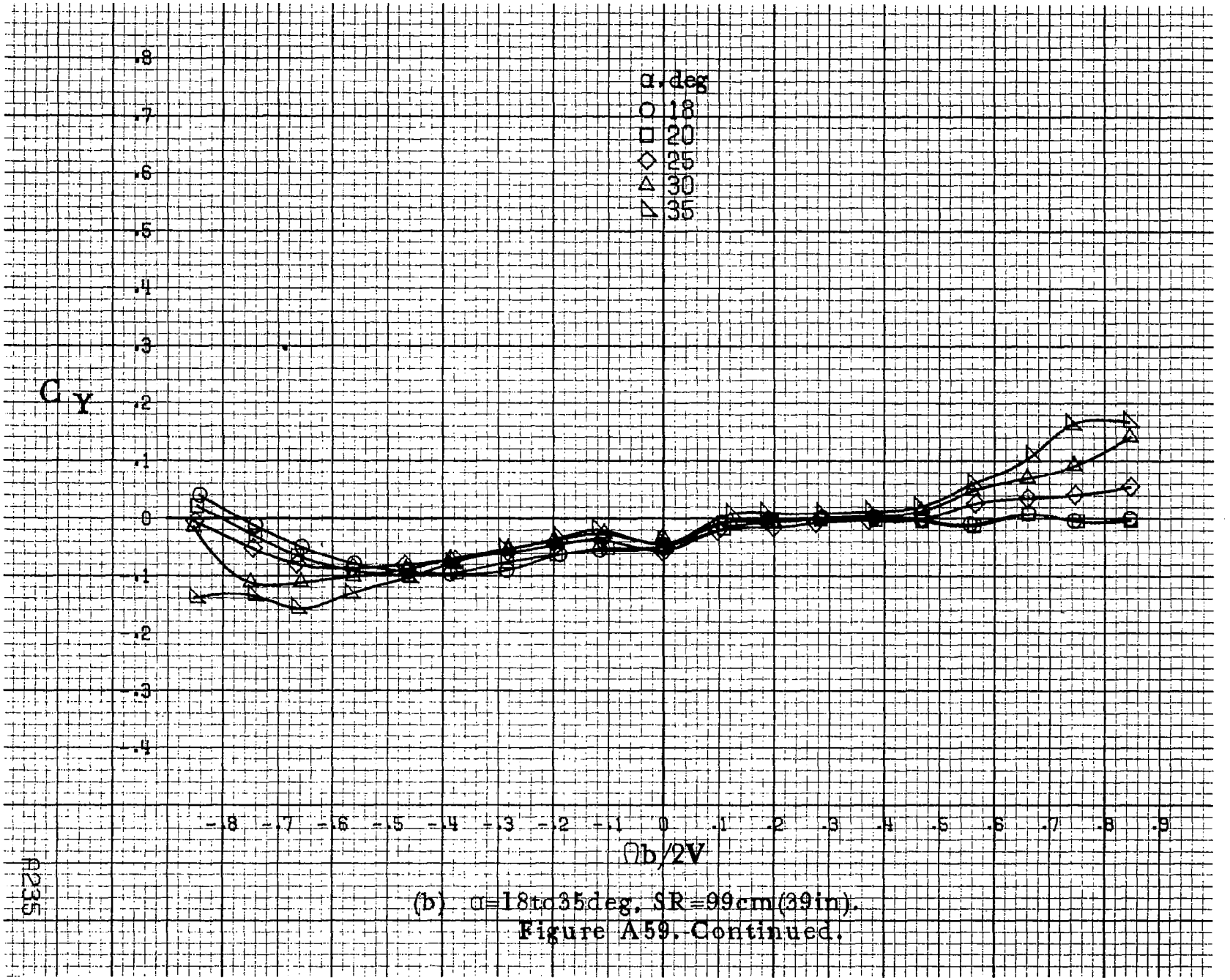

(b) α=18to35deg, SR=99cm(39in).

Figure A59.-Continued.

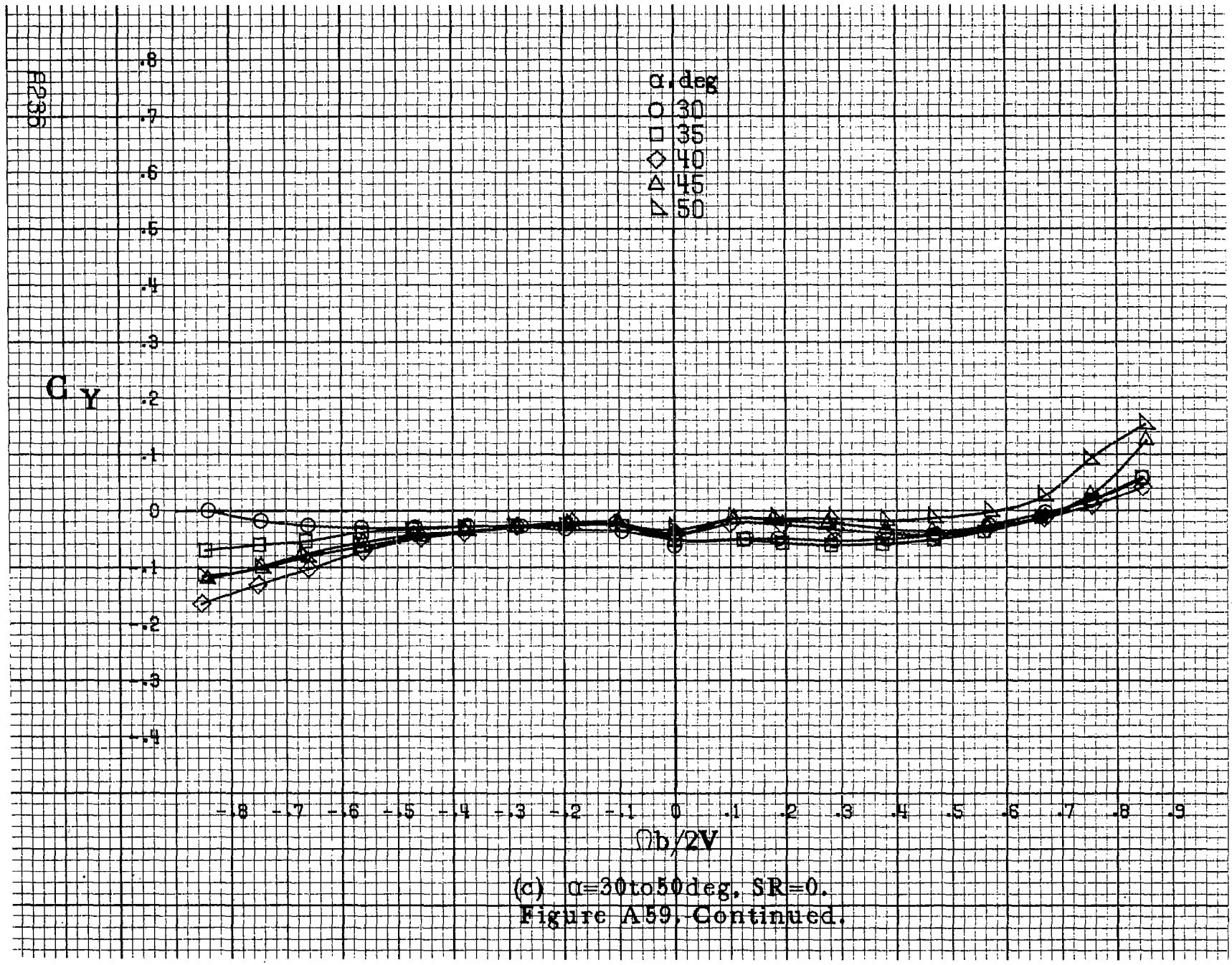

(c) α=30to50deg, SR=0.

Figure A59. Continued.

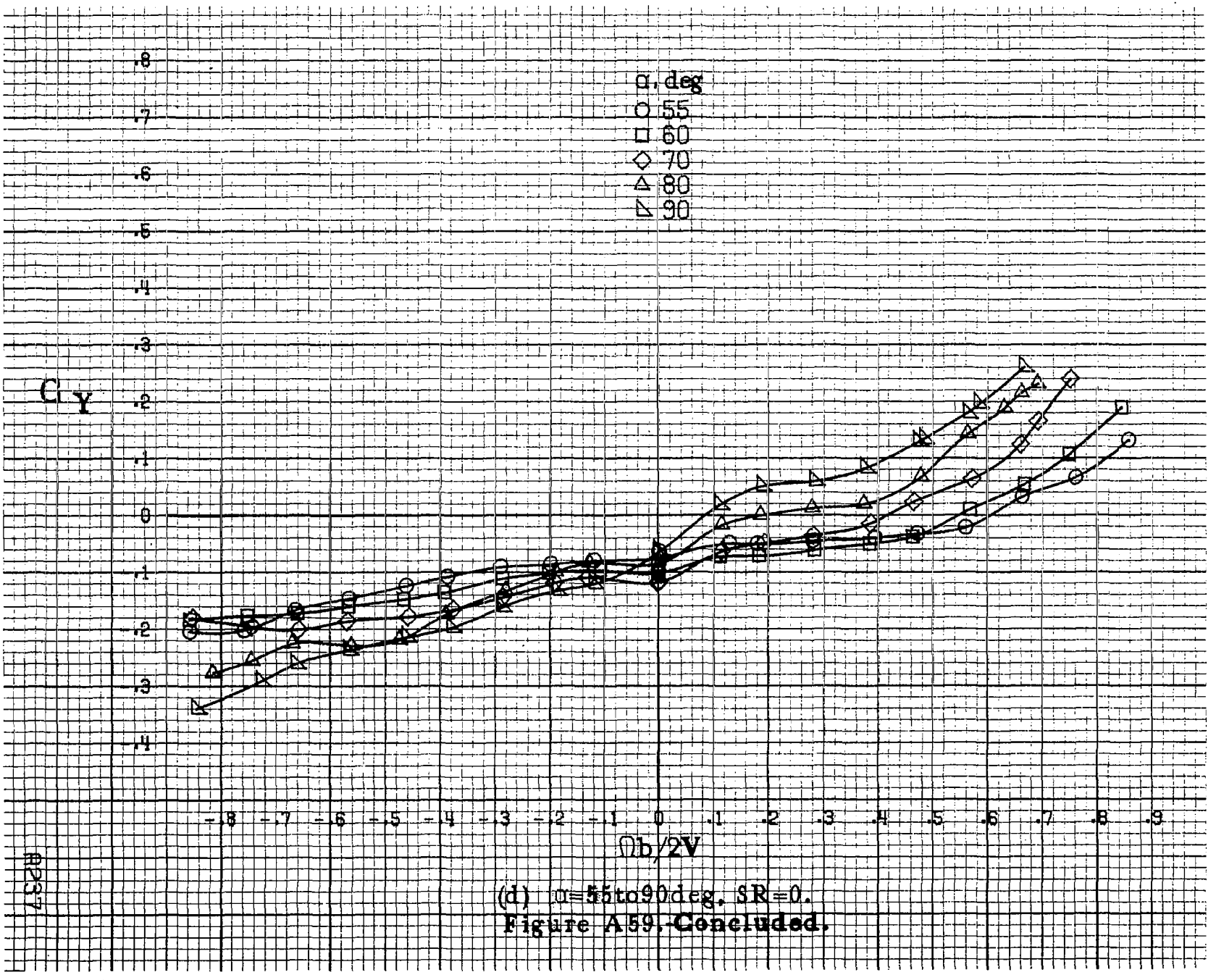

(d) α=55to90deg, SR=0.

Figure A59. Concluded.

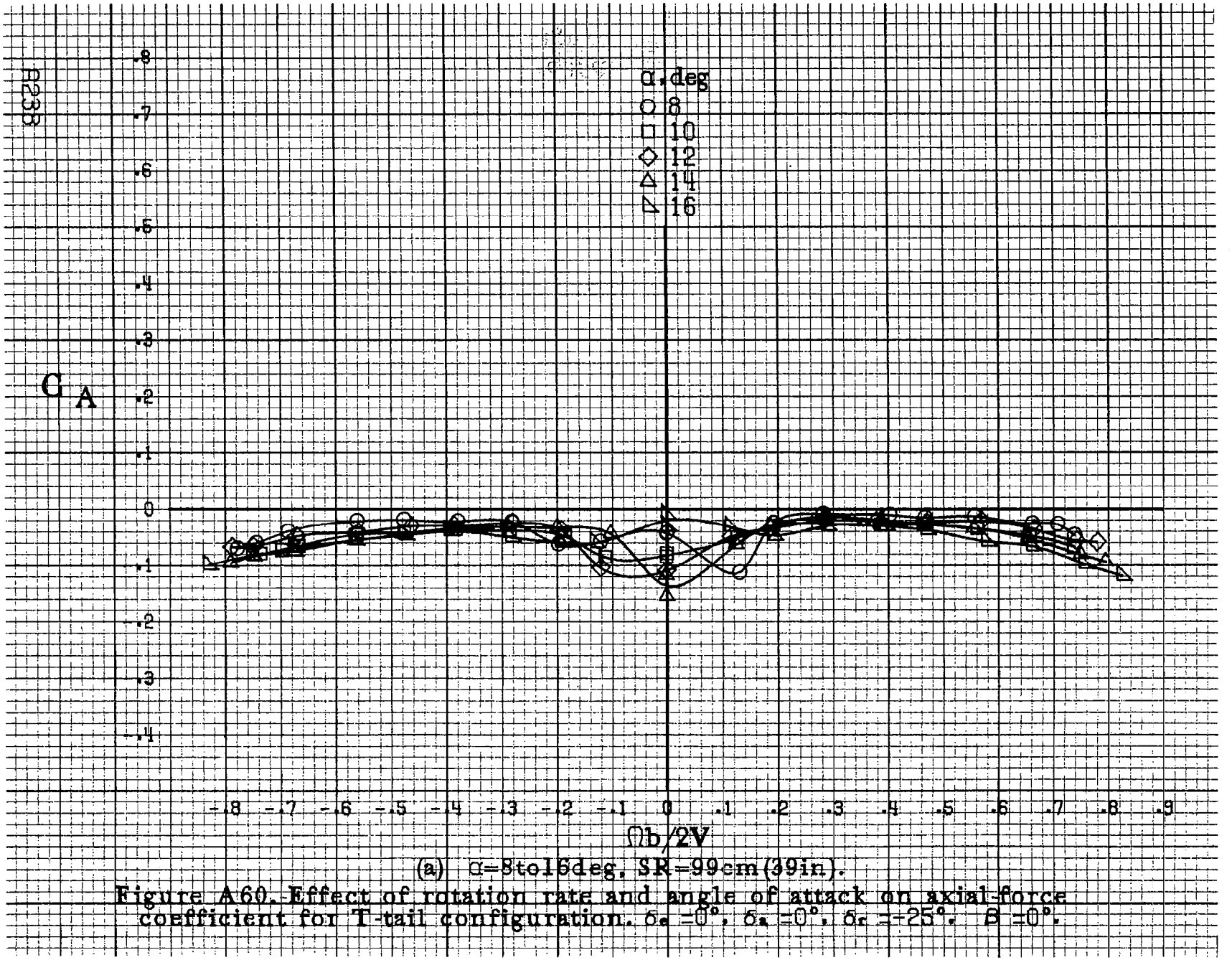

(a) α=8to16deg, SR=99cm(39in).

Figure A60. Effect of rotation rate and angle of attack on axial-force coefficient for T-tail configuration. $\delta_e = 0°$, $\delta_a = 0°$, $\delta_r = -25°$. $\beta = 0°$.

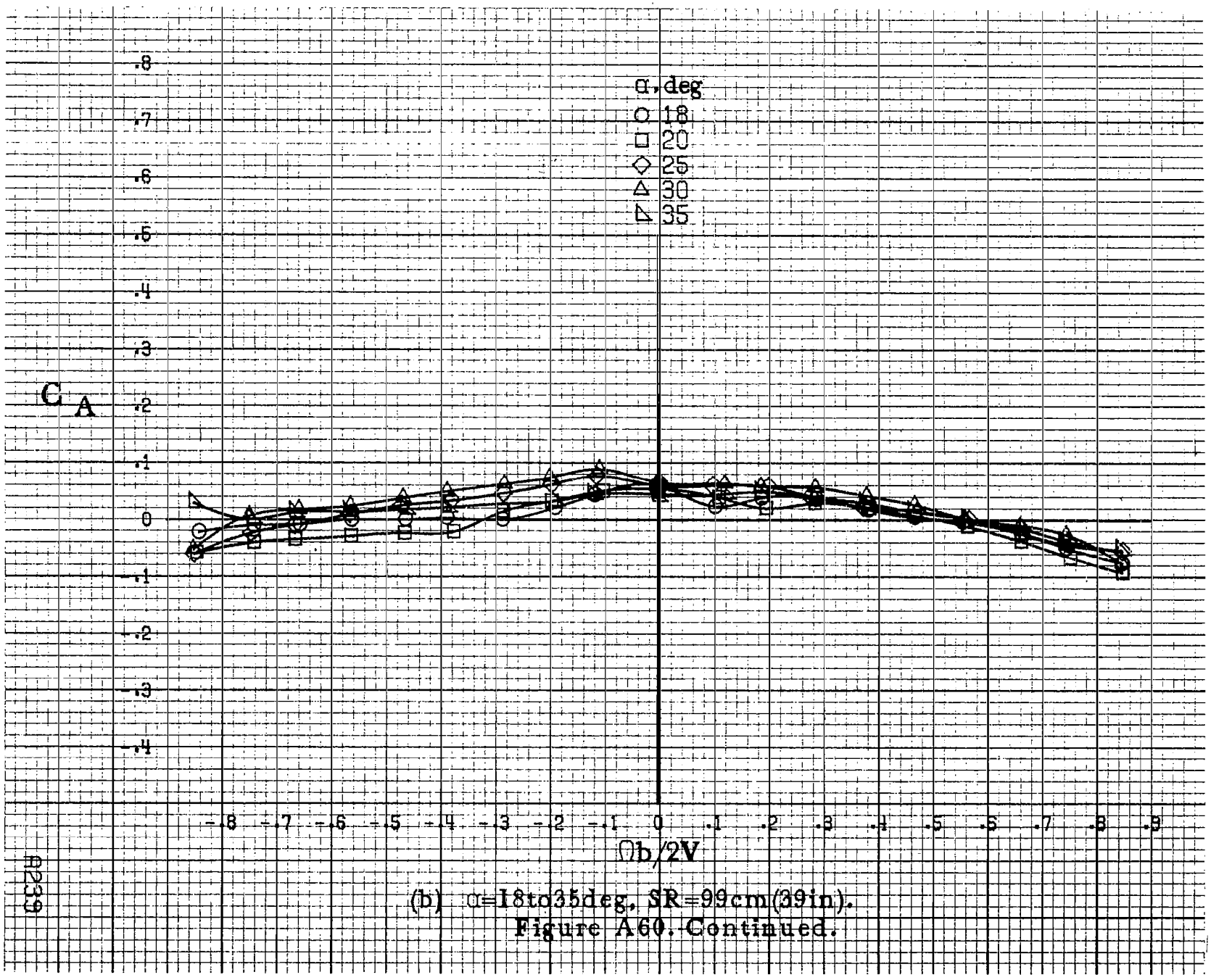

(b) α=18to35deg, SR=99cm(39in).

Figure A60. Continued.

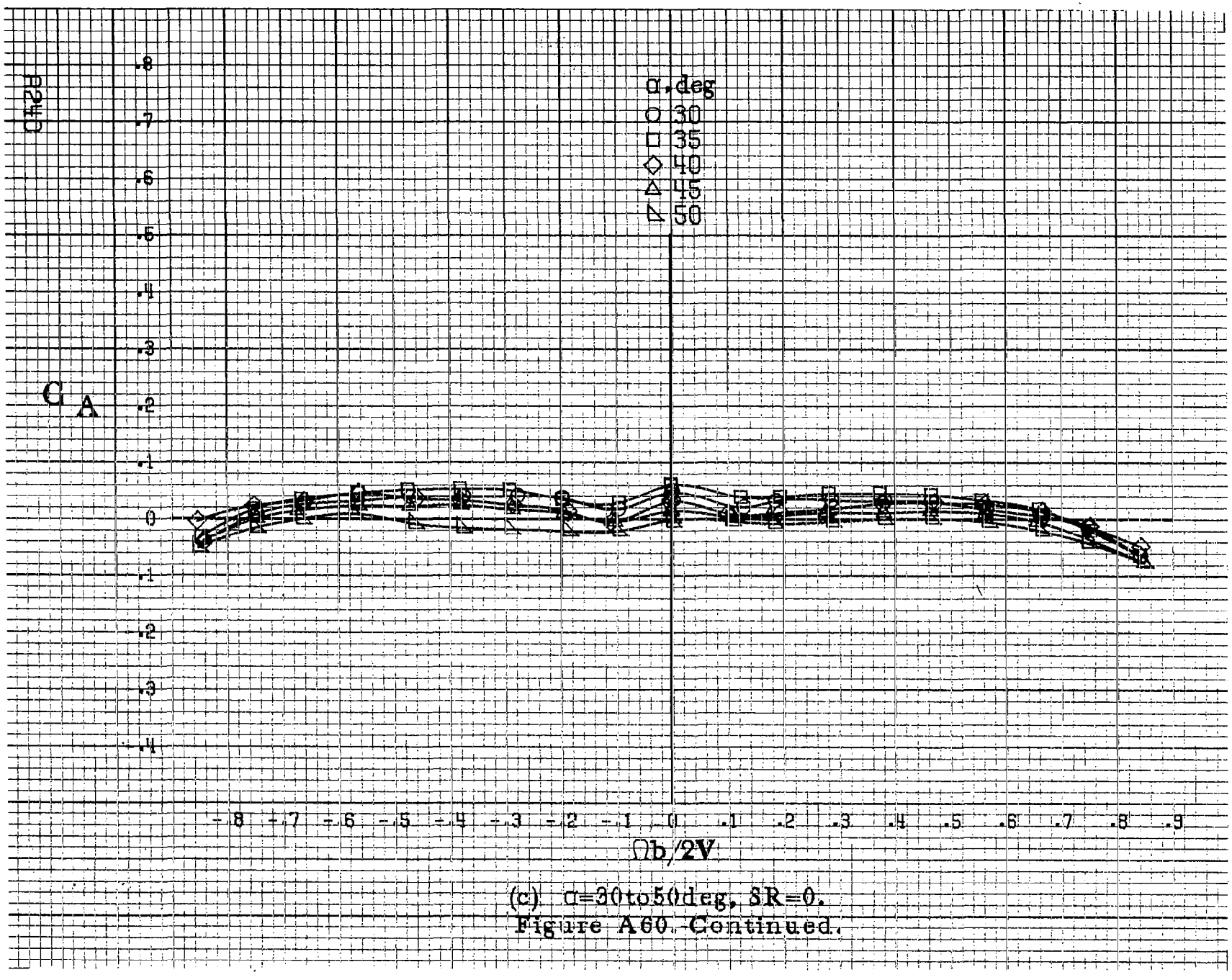

(c) α=30to50deg, δR=0.

Figure A60.-Continued.

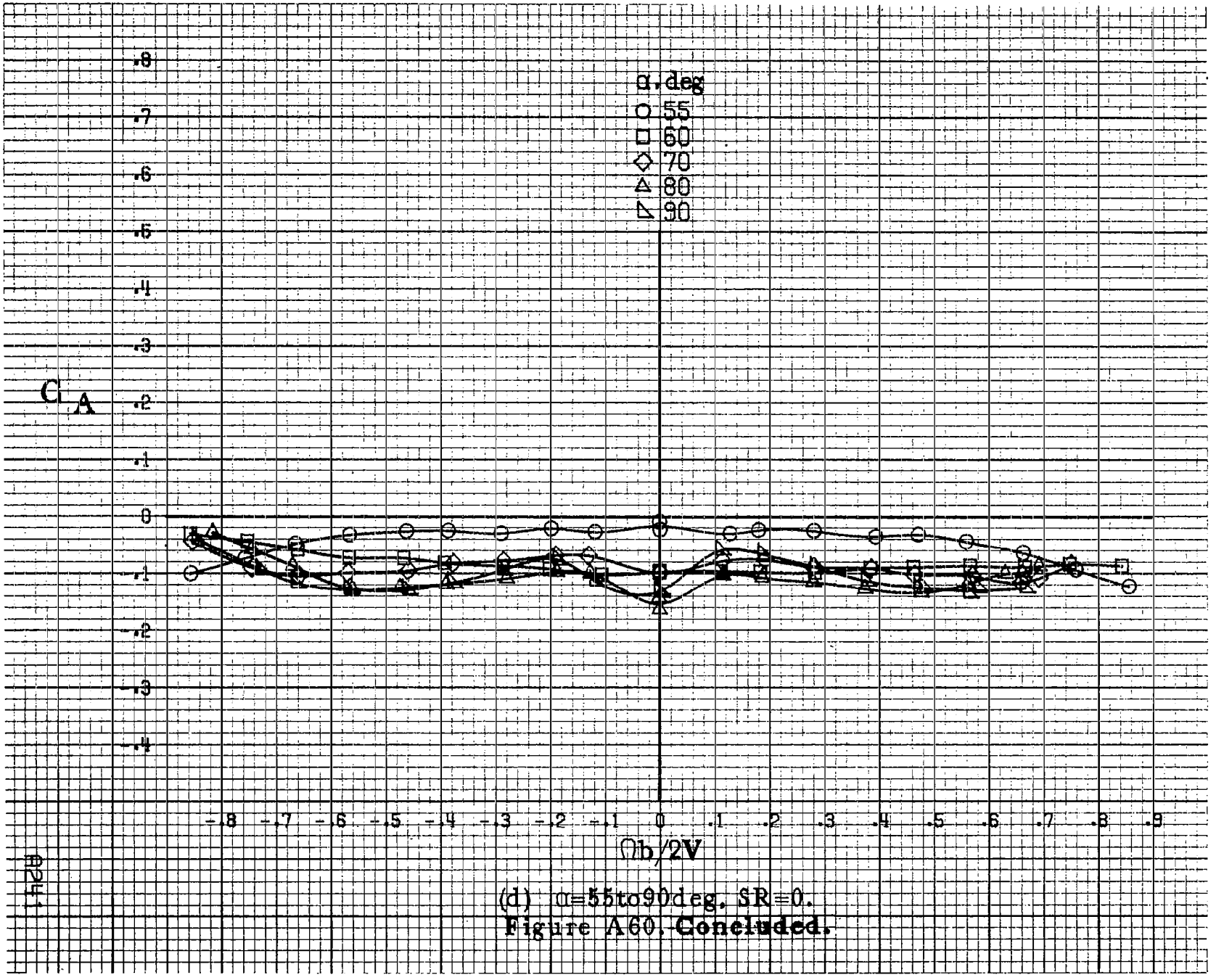

(d) α=55to90deg, SR=0.

Figure A60. Concluded.

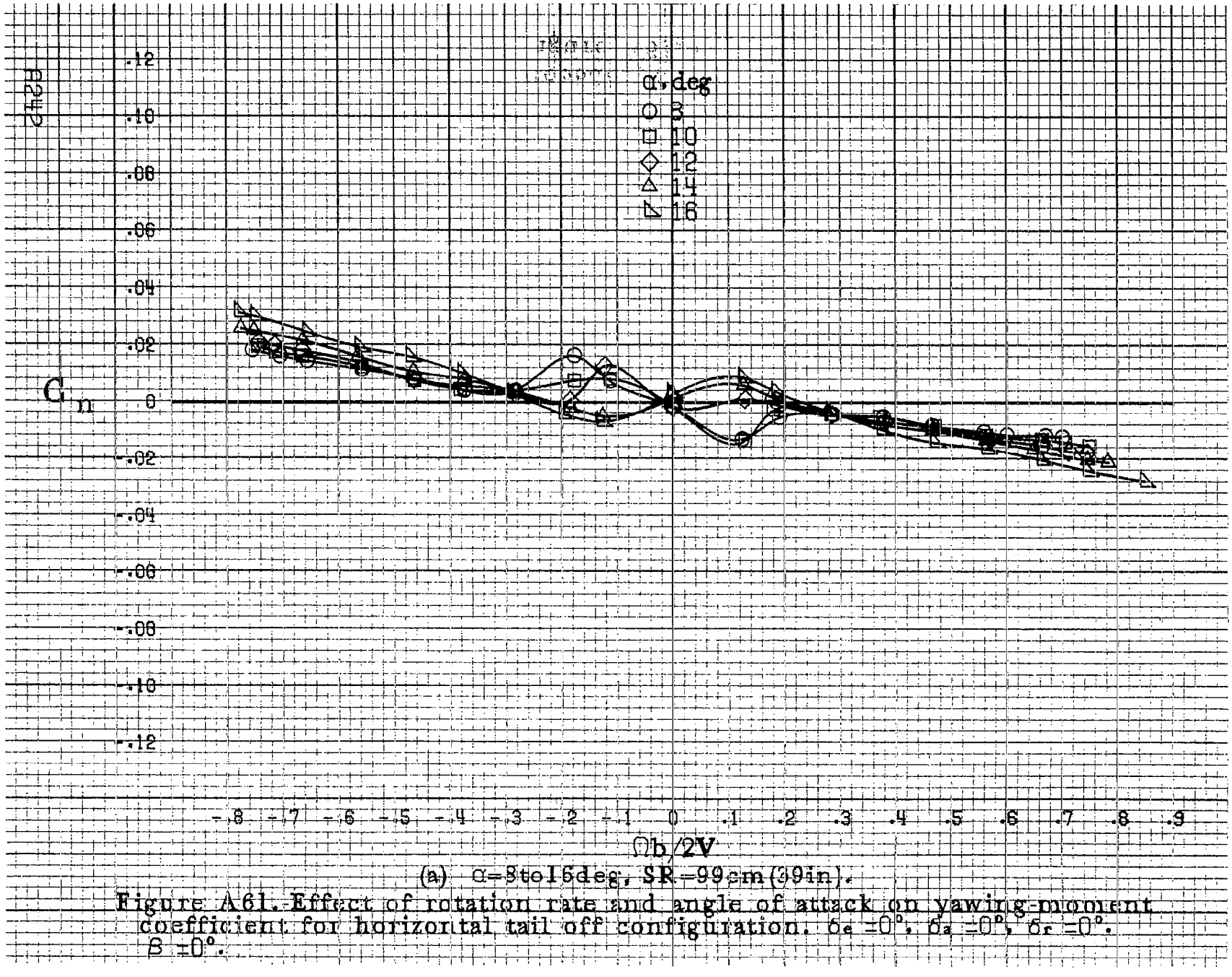

(a) α=8to16deg, SR=99cm(39in).

Figure A61. Effect of rotation rate and angle of attack on yawing-moment coefficient for horizontal tail off configuration. $\delta_e = 0°$, $\delta_a = 0°$, $\delta_r = 0°$. $\beta = 0°$.

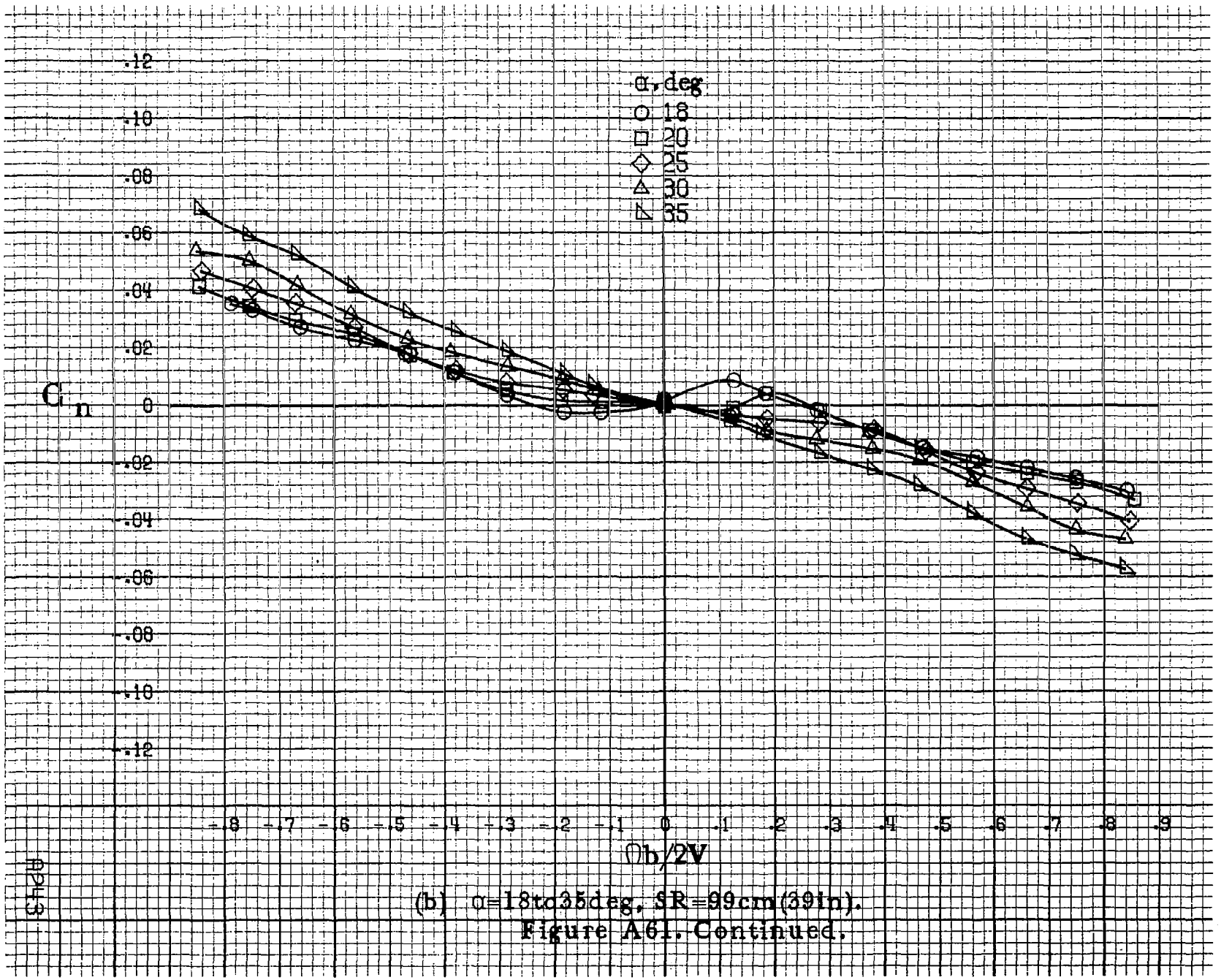

(b) α=18 to 35 deg, SR=99 cm (39 in).

Figure A61. Continued.

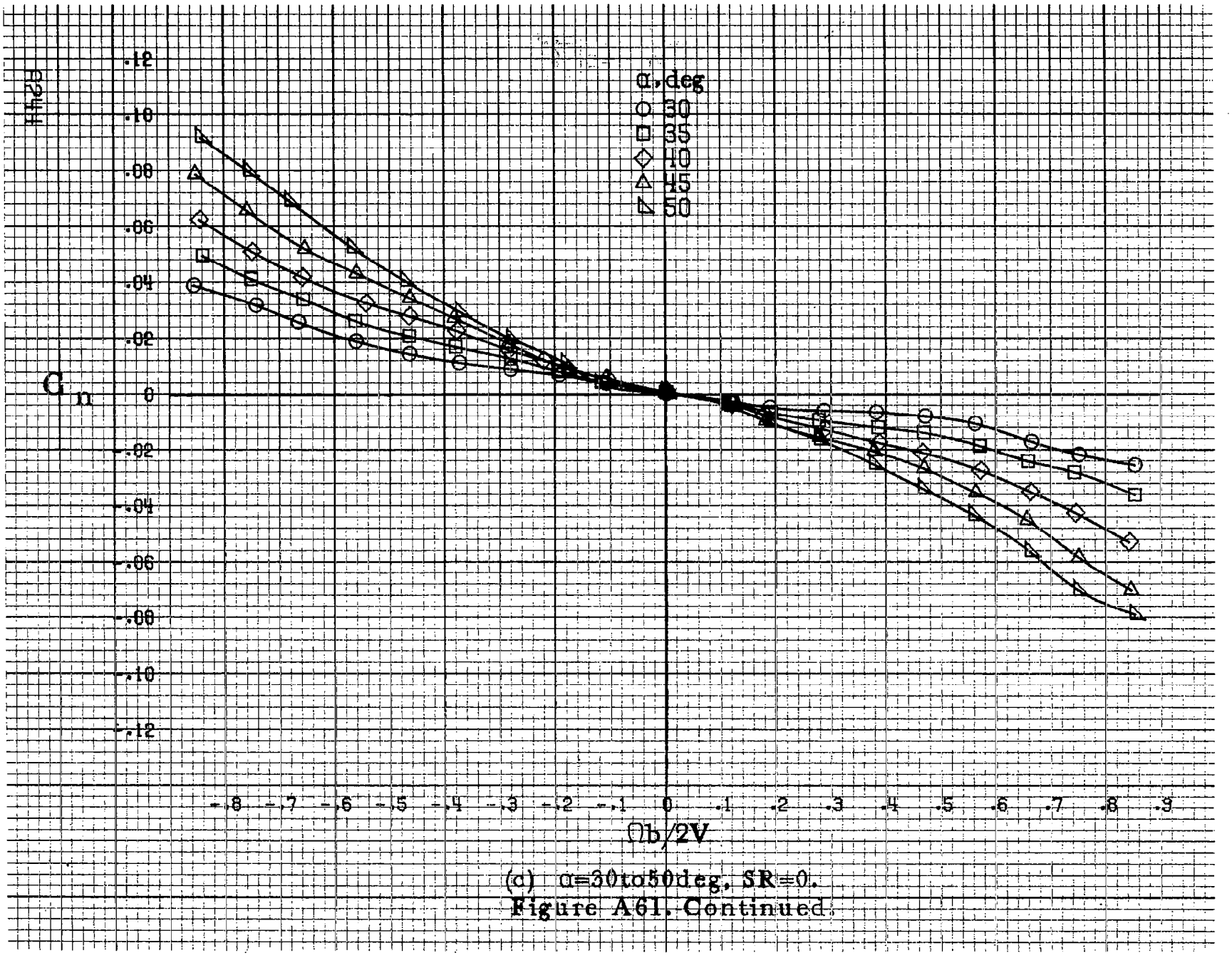

(c) α=30to50deg, SR=0.

Figure A61. Continued.

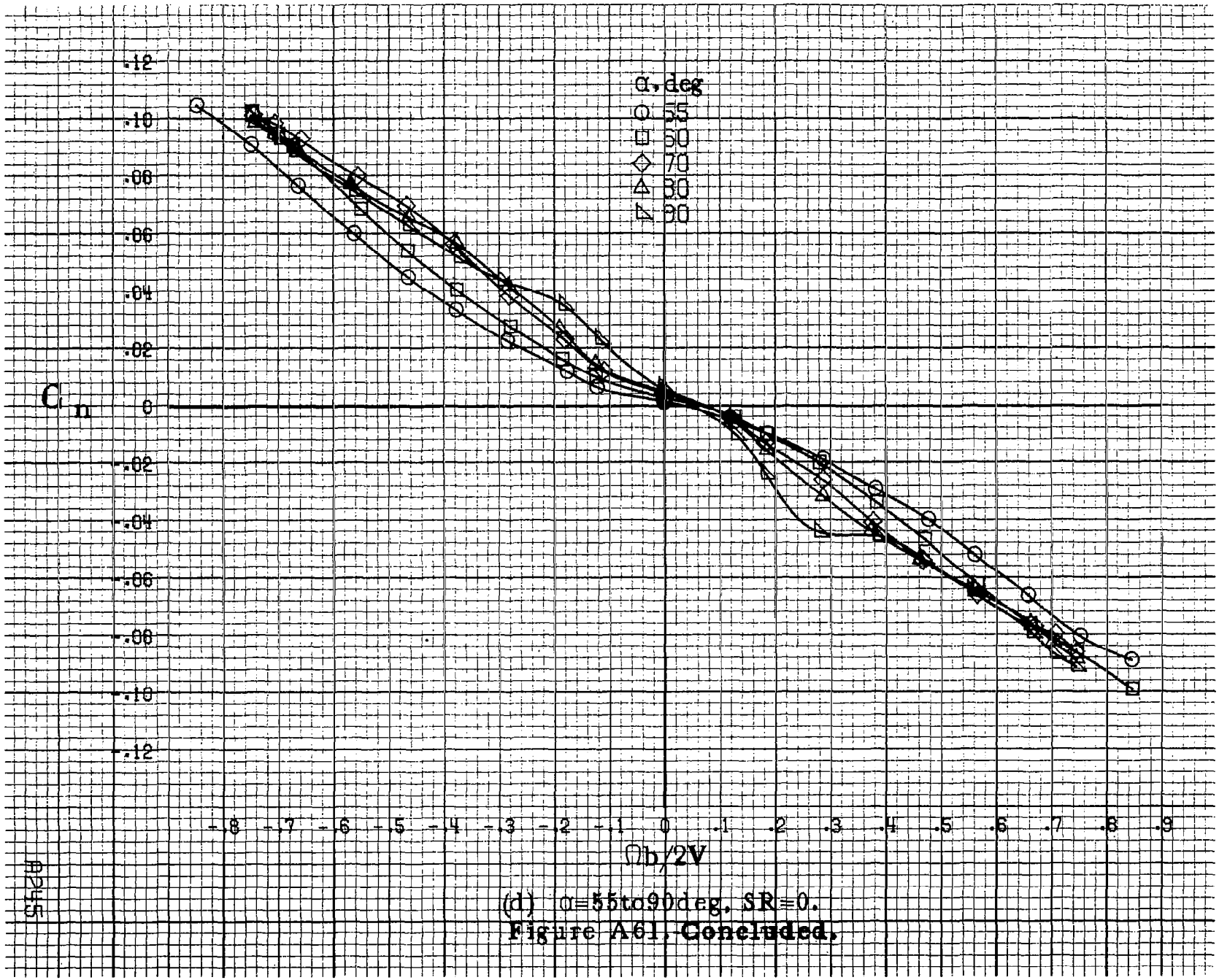

(d) α=55to90deg, SR=0.

Figure A61. Concluded.

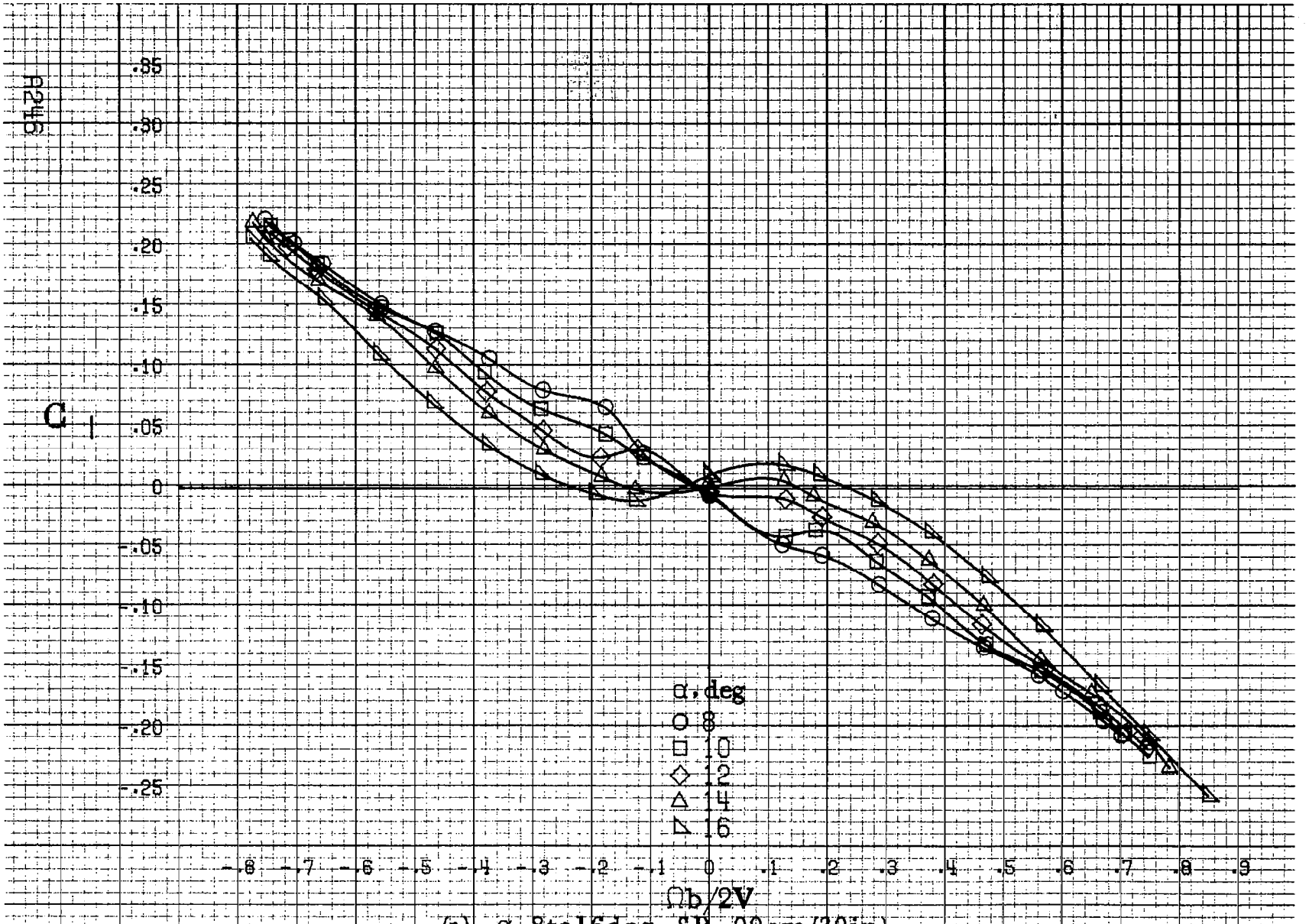

(a) α=8to16deg, SR=99cm(39in).

Figure A62.-Effect of rotation rate and angle of attack on rolling-moment coefficient for horizontal tail off configuration. $\delta_e = 0°$, $\delta_a = 0°$, $\delta_r = 0°$, $\beta = 0°$.

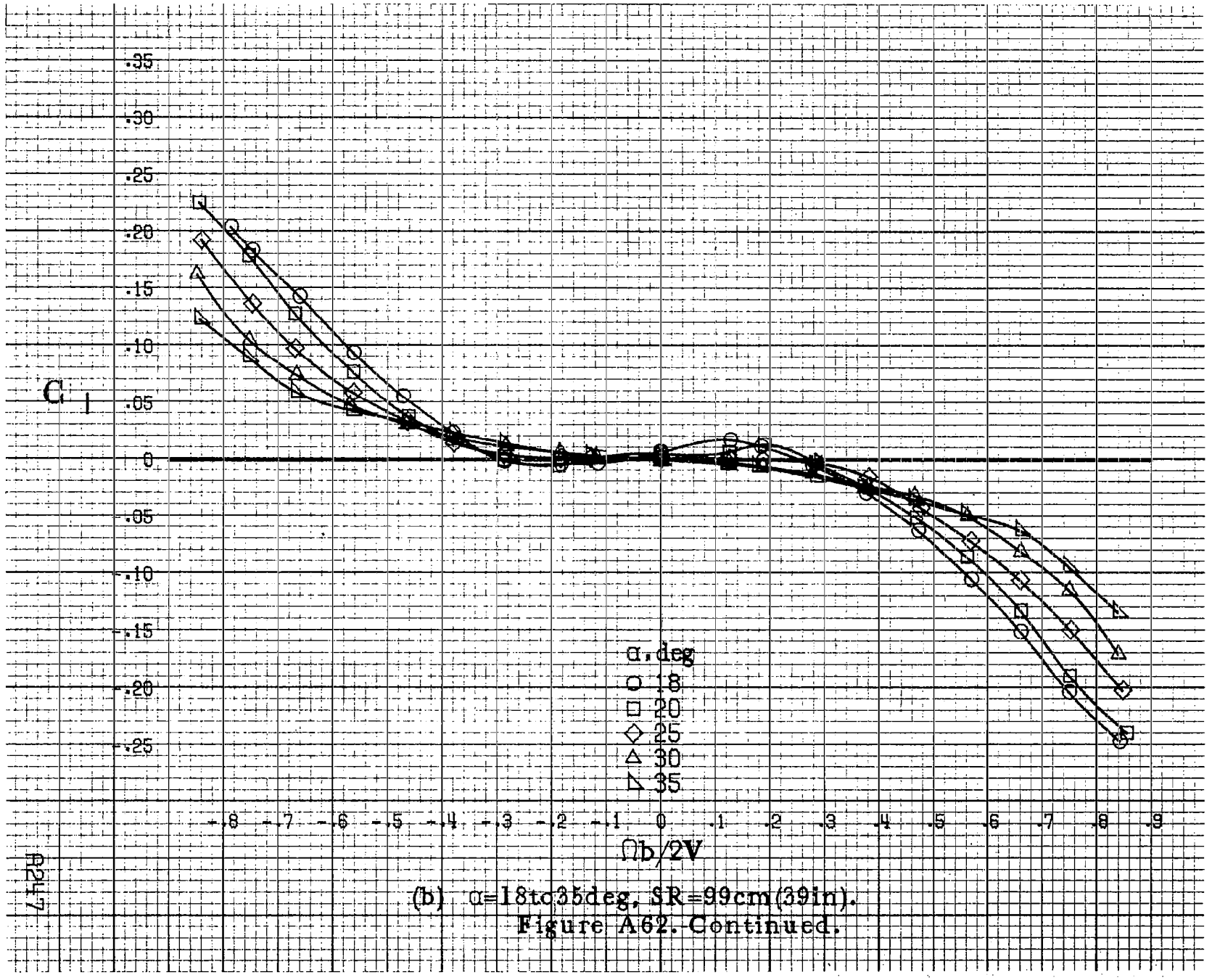

(b) α=18to35deg, SR=99cm(39in).

Figure A62.-Continued.

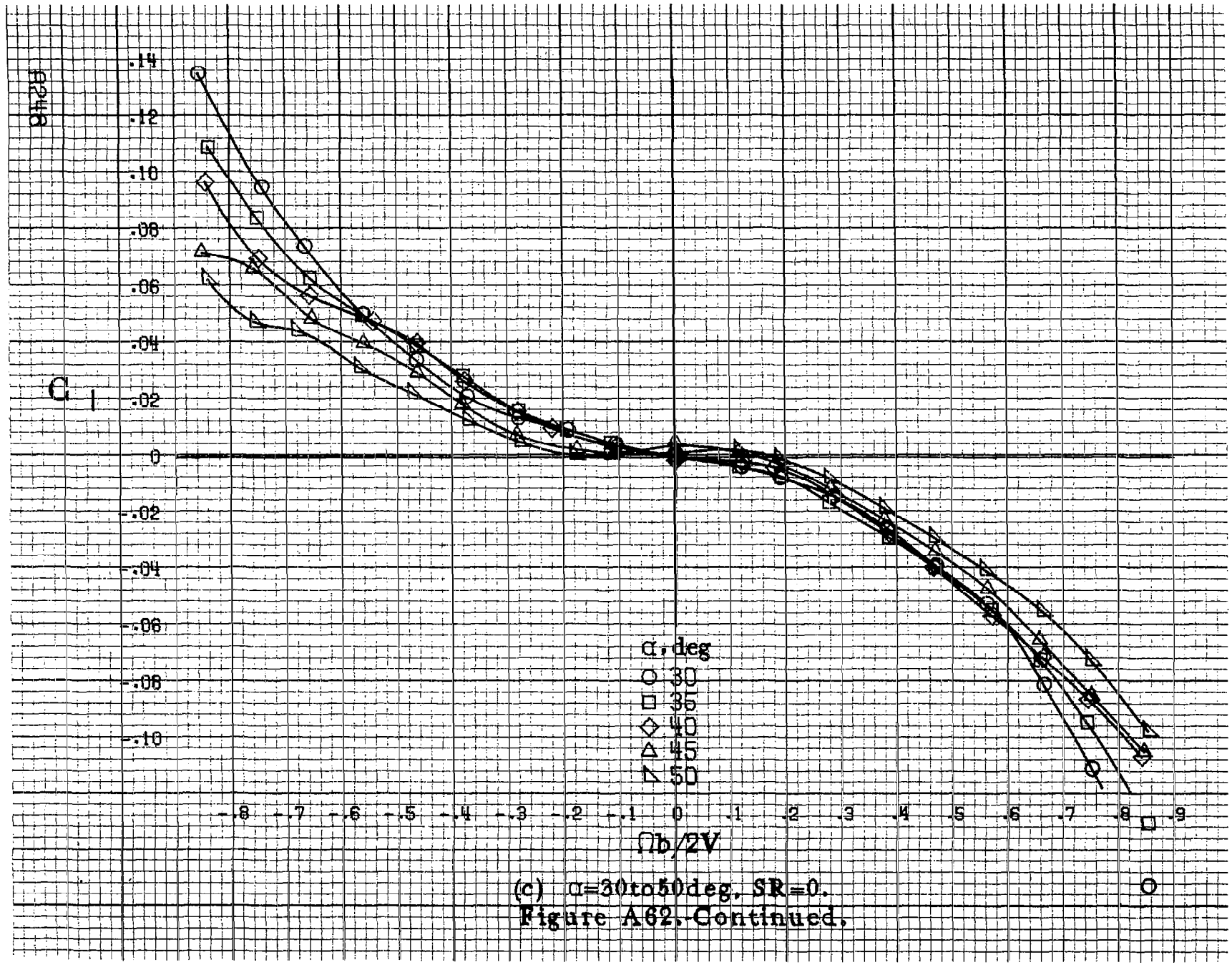

(c) α=30to50deg, SR=0.

Figure A62.-Continued.

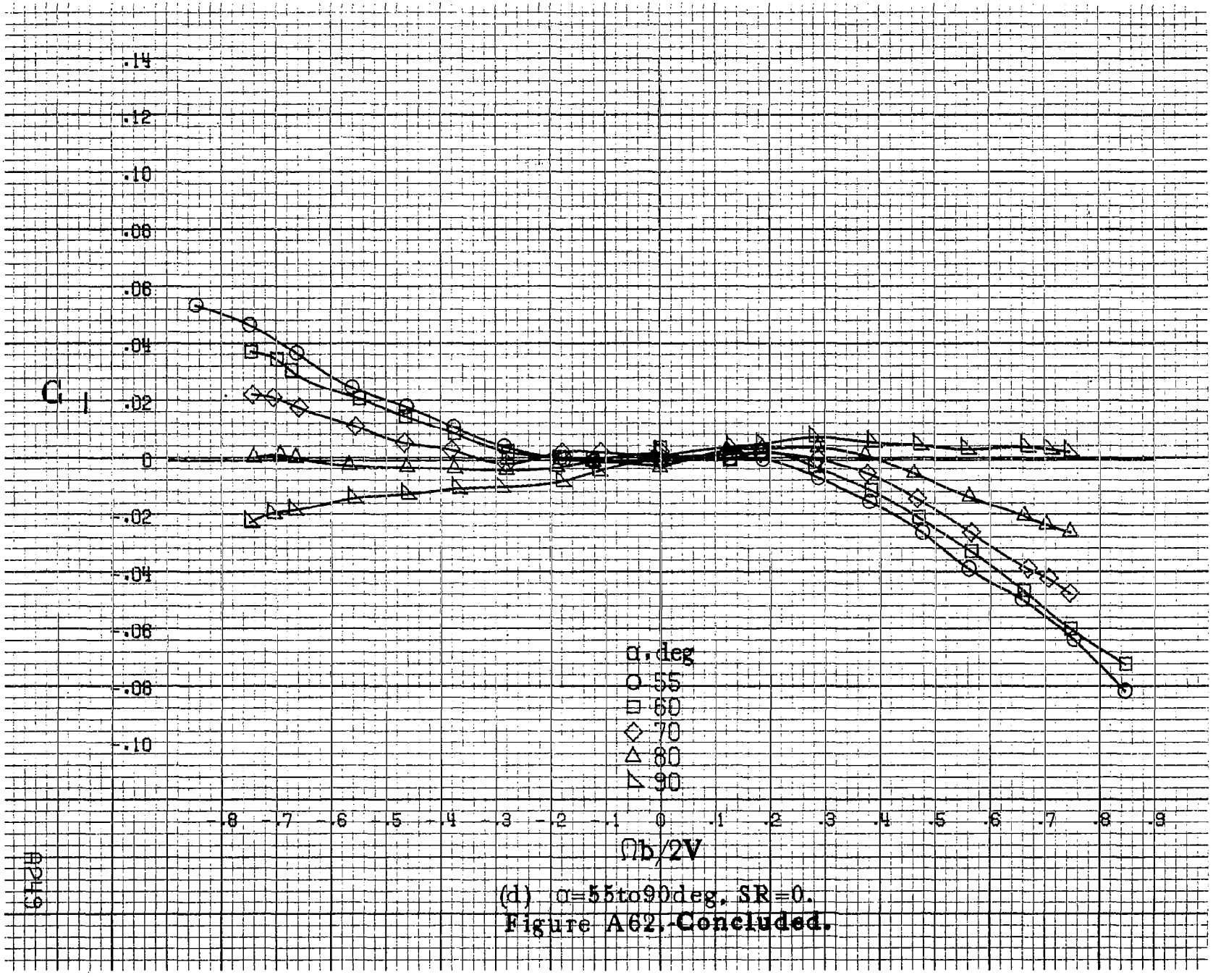

Figure A62.-Concluded.

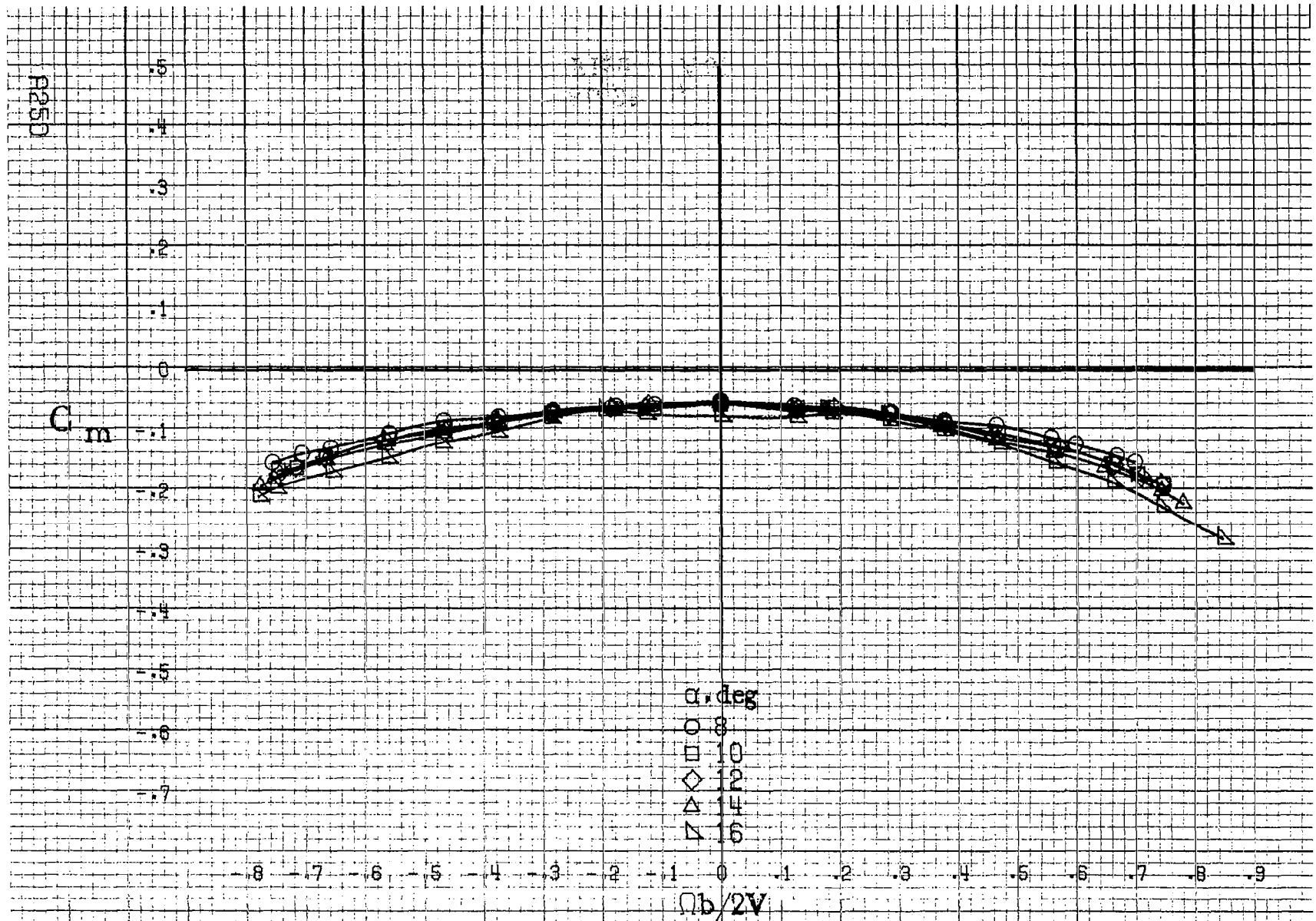

(a) α=8to16deg, SR=99cm(39in).

Figure A63. Effect of rotation rate and angle of attack on pitching-moment coefficient for horizontal tail off configuration. $\delta_e = 0°$, $\delta_a = 0°$, $\delta_r = 0°$, $\beta = 0°$.

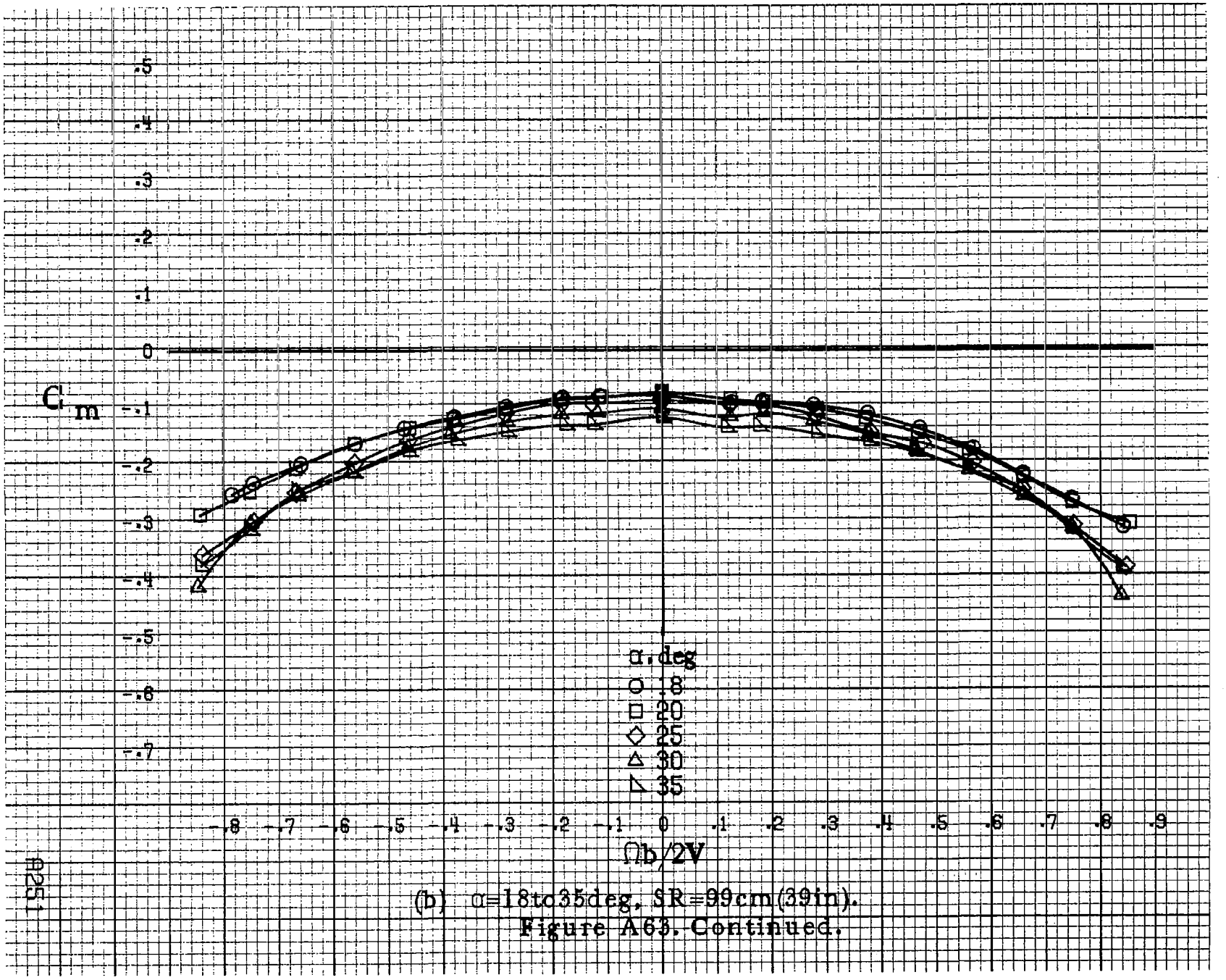

(b) α=18to35deg, SR=99cm(39in).

Figure A63. Continued.

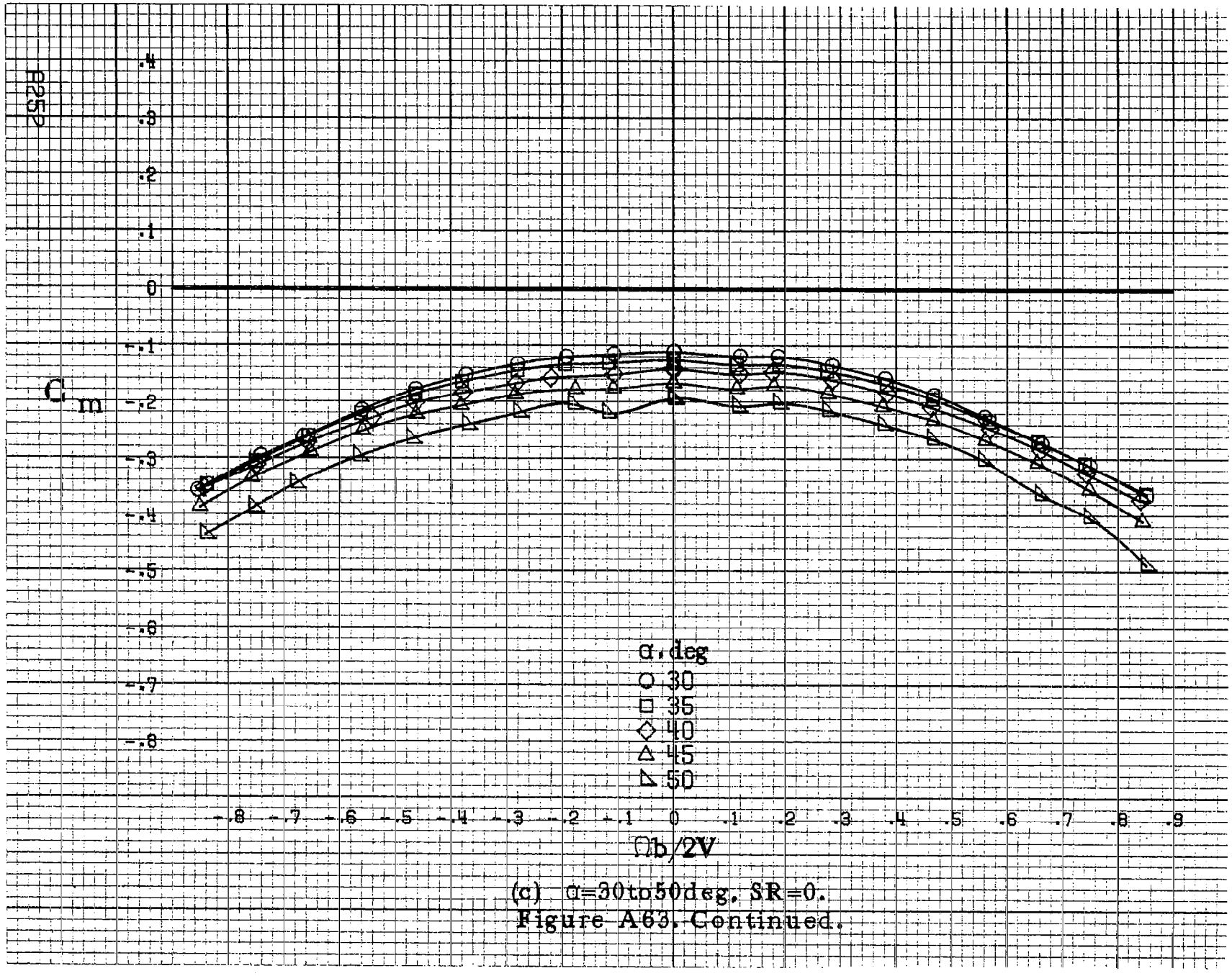

(c) α=30to50deg, SR=0.

Figure A63. Continued.

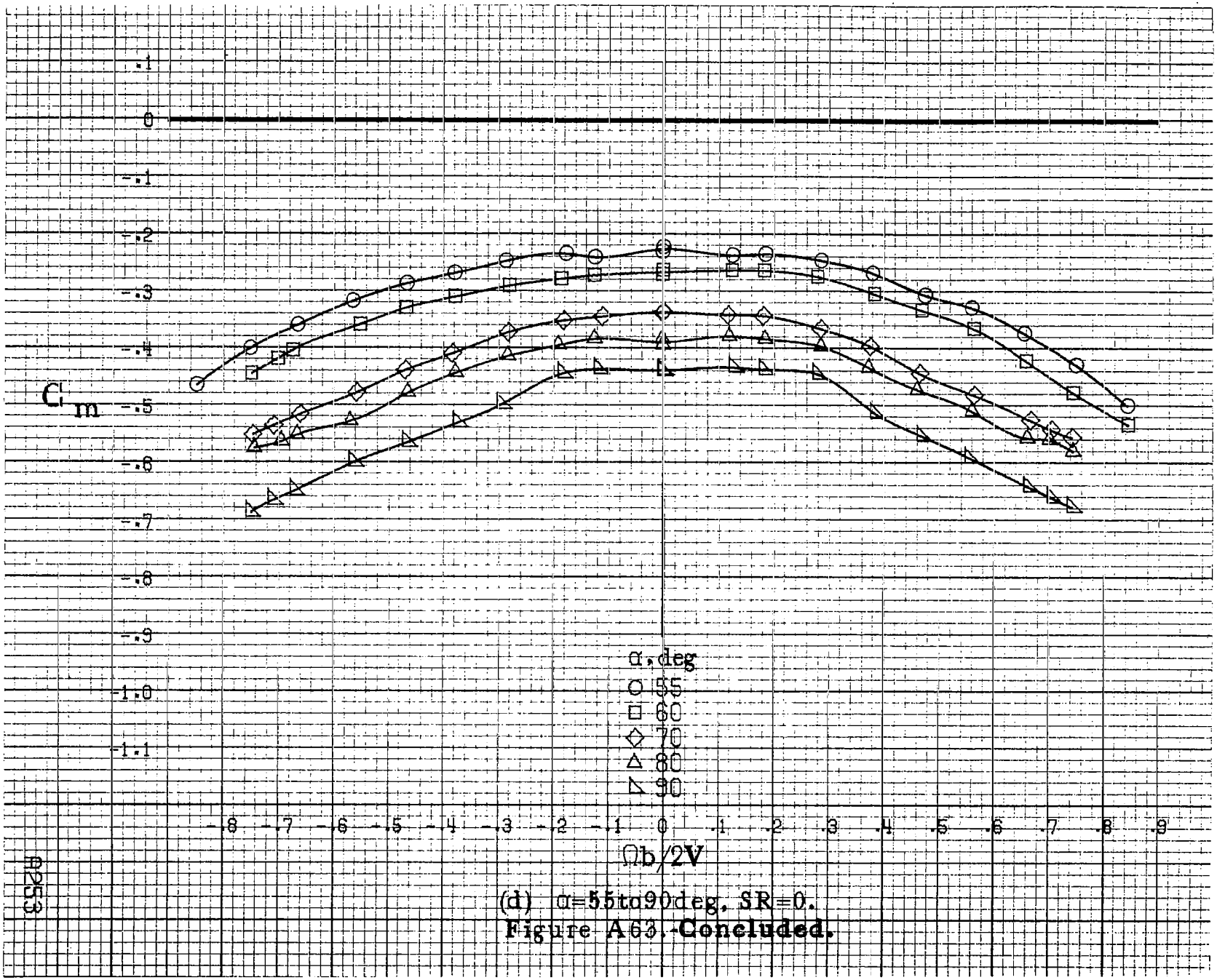

(d) α=55to90deg, SR=0.

Figure A63.-Concluded.

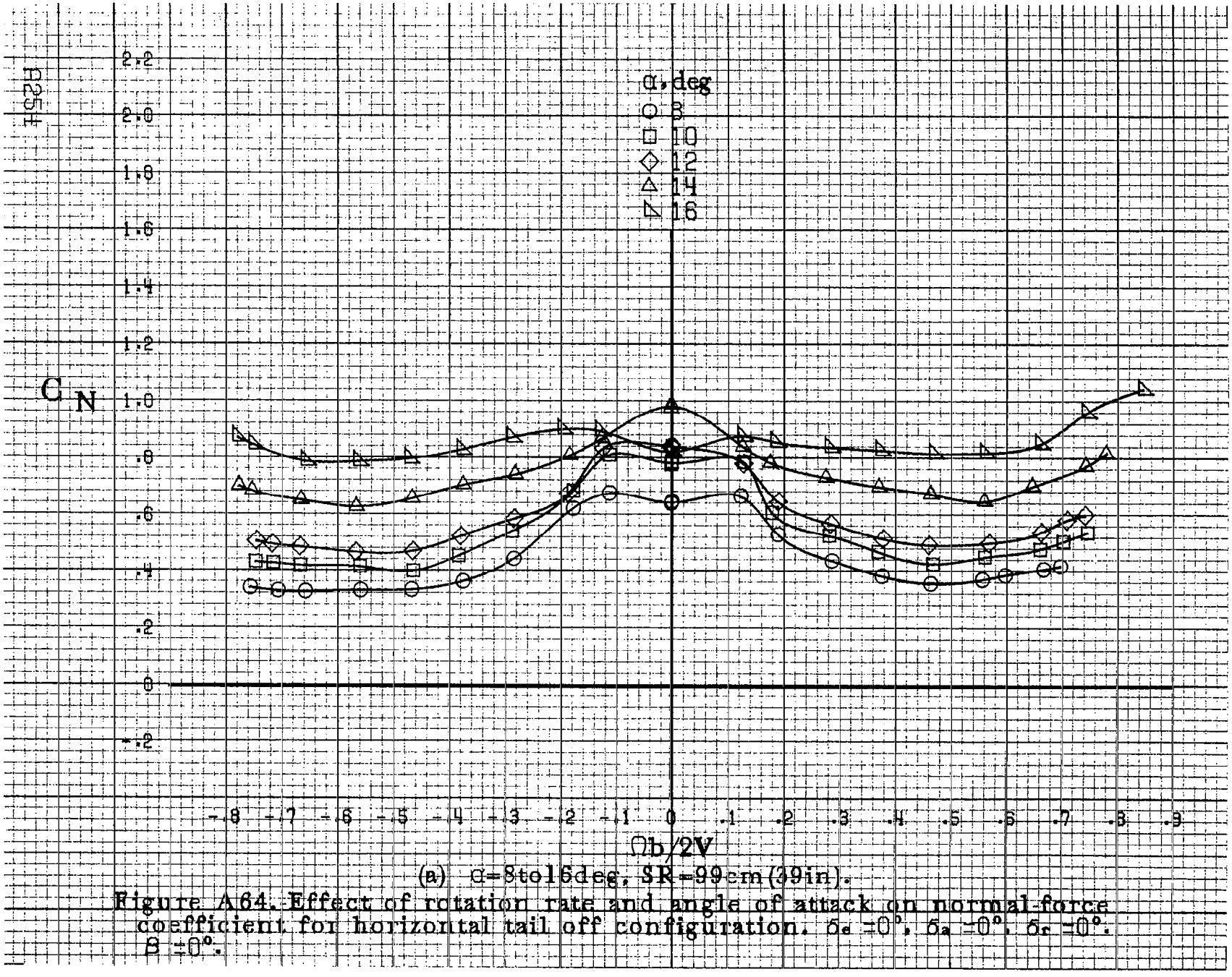

(a) α=8to16deg, SR=99cm(39in).

Figure A64. Effect of rotation rate and angle of attack on normal-force coefficient for horizontal tail off configuration. $\delta_e = 0°$, $\delta_a = 0°$, $\delta_r = 0°$. $\beta = 0°$.

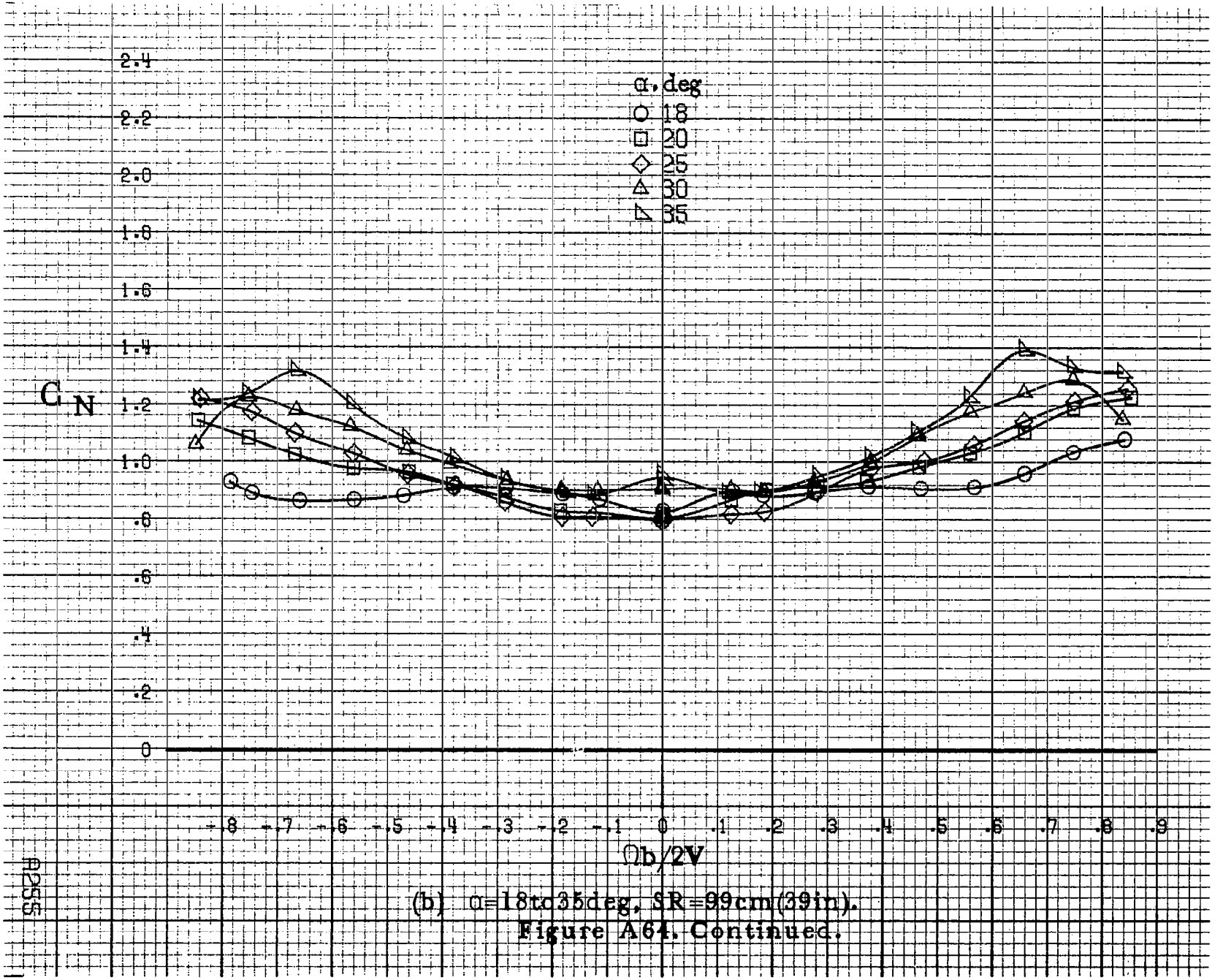

(b) α=18to35deg, SR=99cm(39in).

Figure A64. Continued.

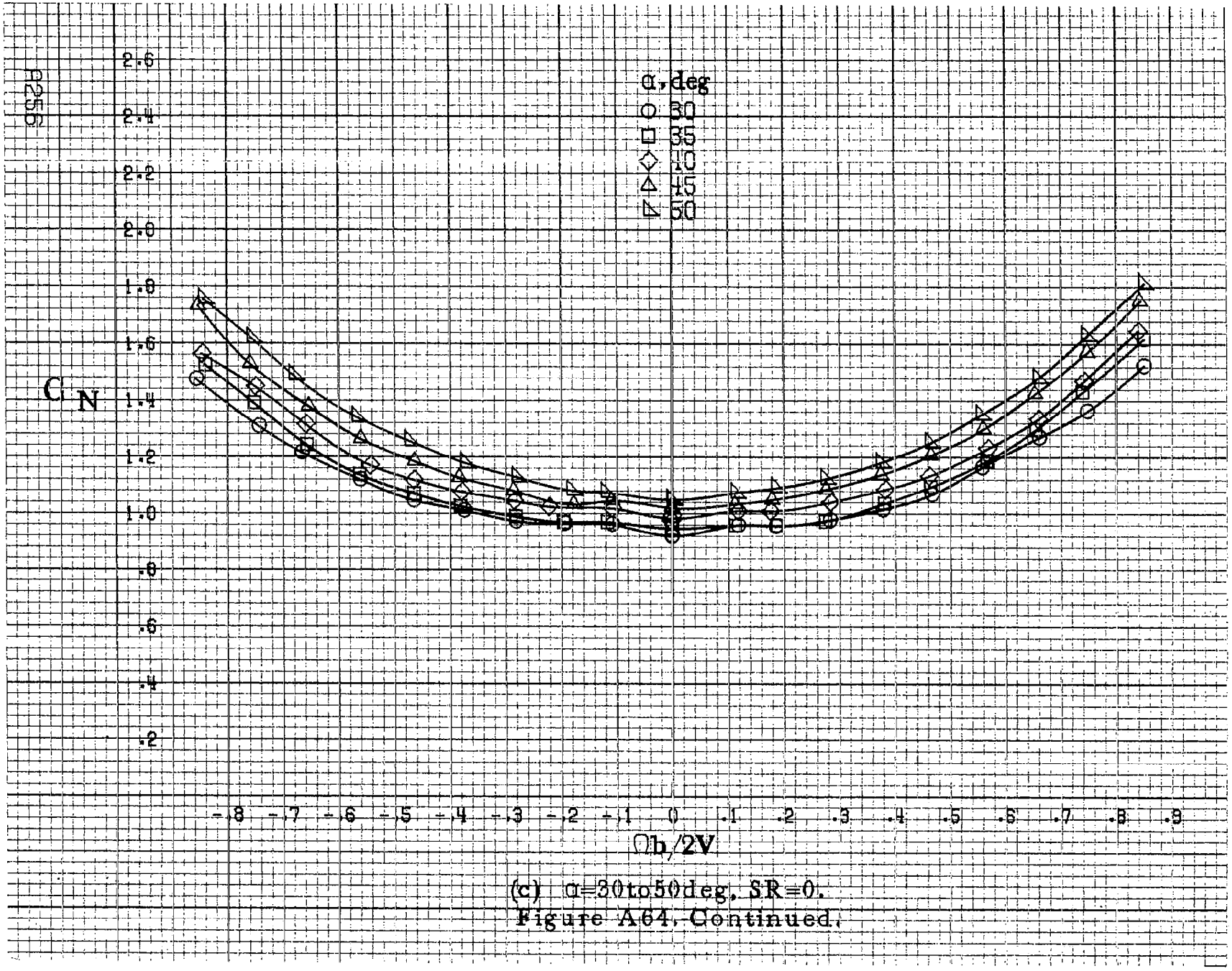

(c) α=30to50deg, SR=0.

Figure A64. Continued.

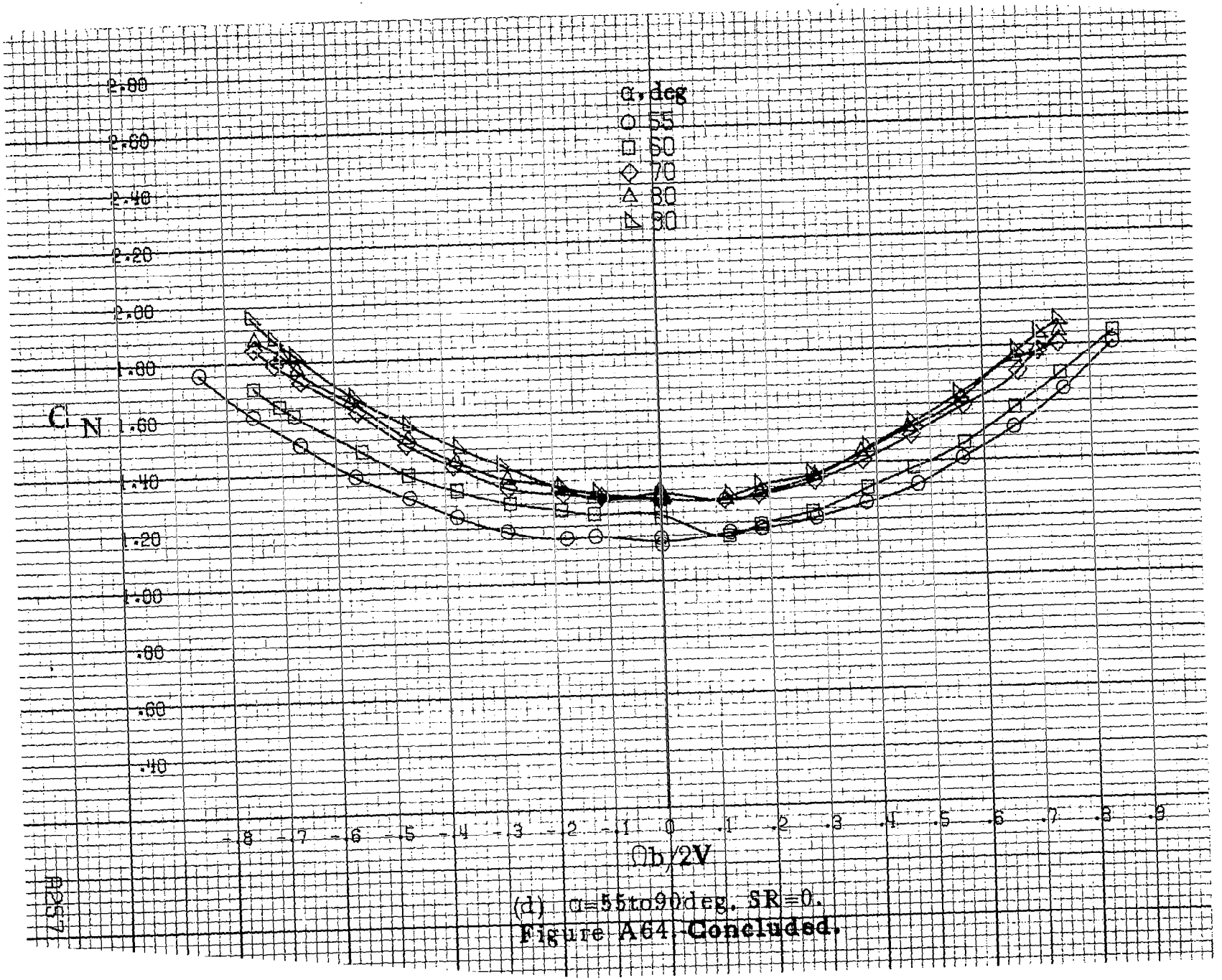

(d) α=55to90deg. SR=0.

Figure A64. Concluded.

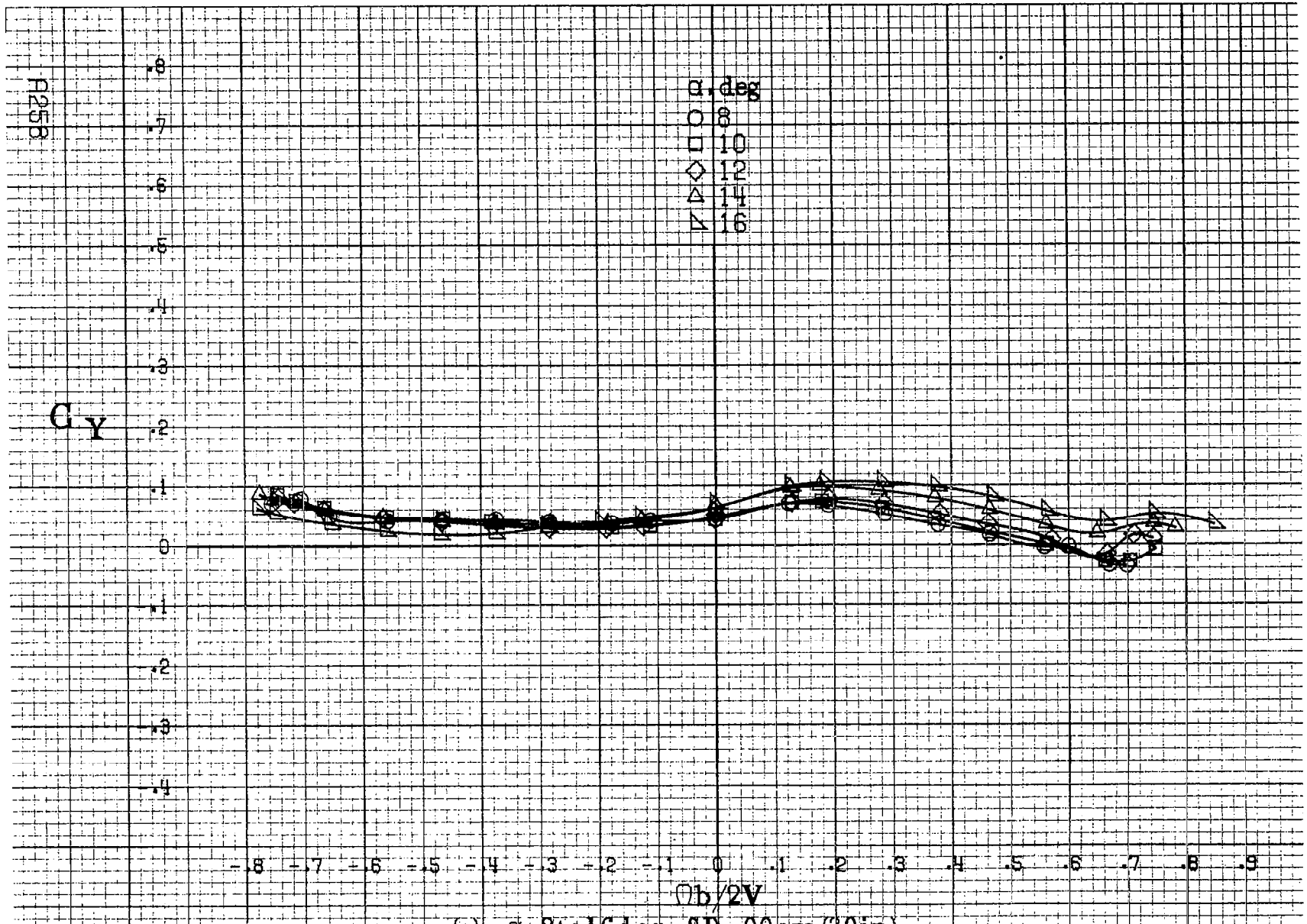

(a) α=8to16deg, SR=99cm(39in).

Figure A65.-Effect of rotation rate and angle of attack on side-force coefficient for horizontal tail off configuration. $\delta_e = 0°$, $\delta_a = 0°$, $\delta_r = 0°$, $\beta = 0°$.

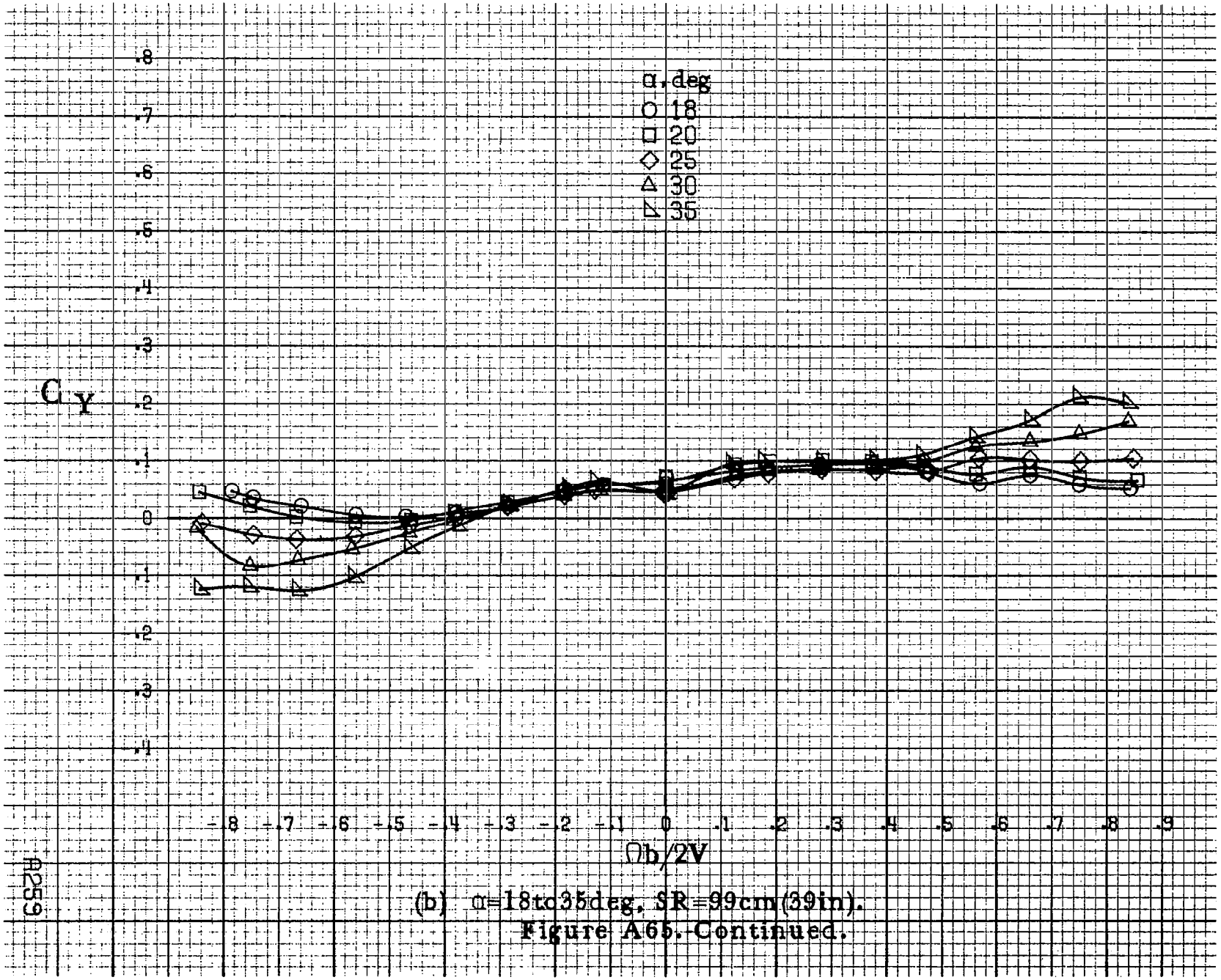

(b) α=18to35deg, SR=99cm(39in).

Figure A65.-Continued.

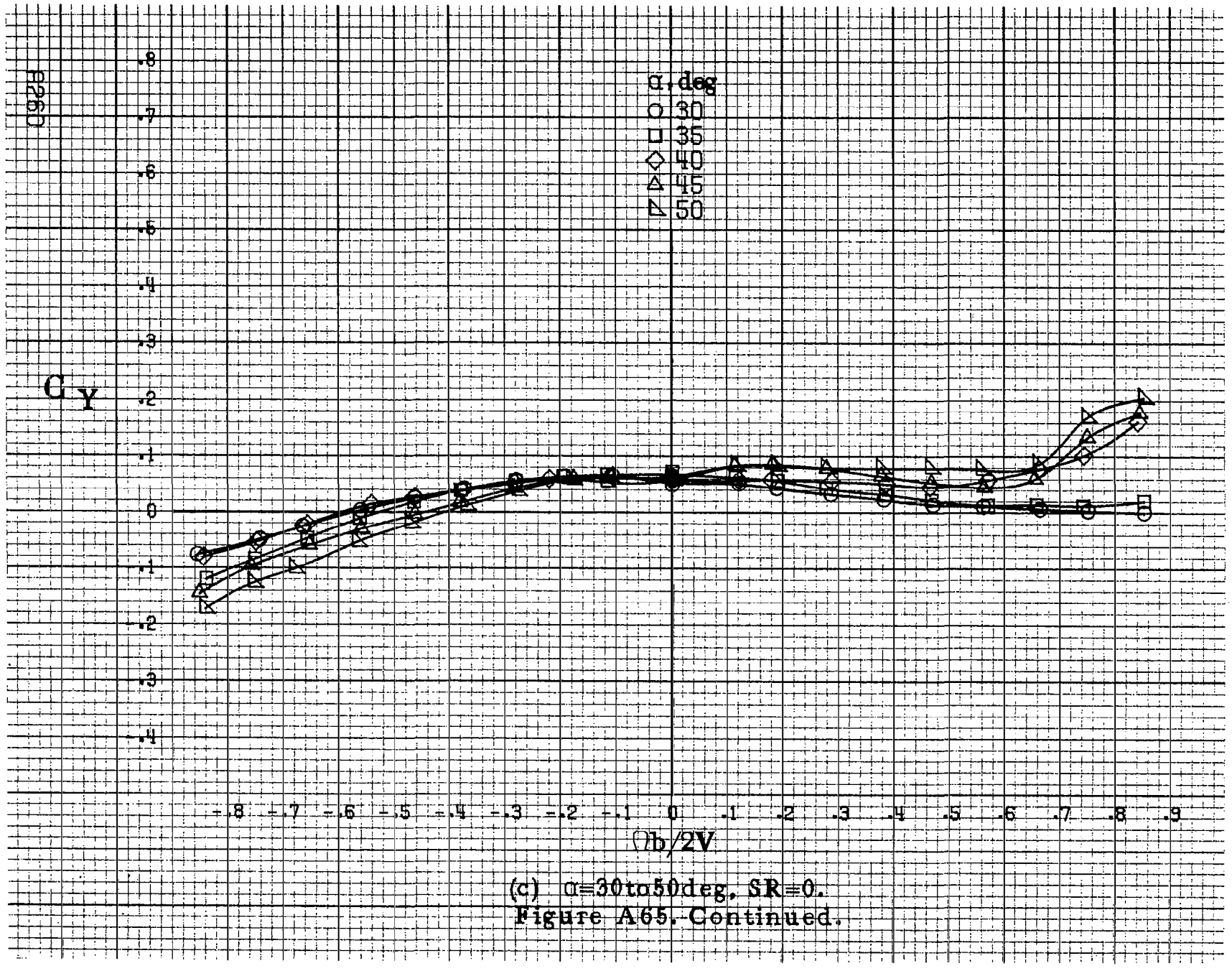

(c) α=30to50deg, SR=0.

Figure A65. Continued.

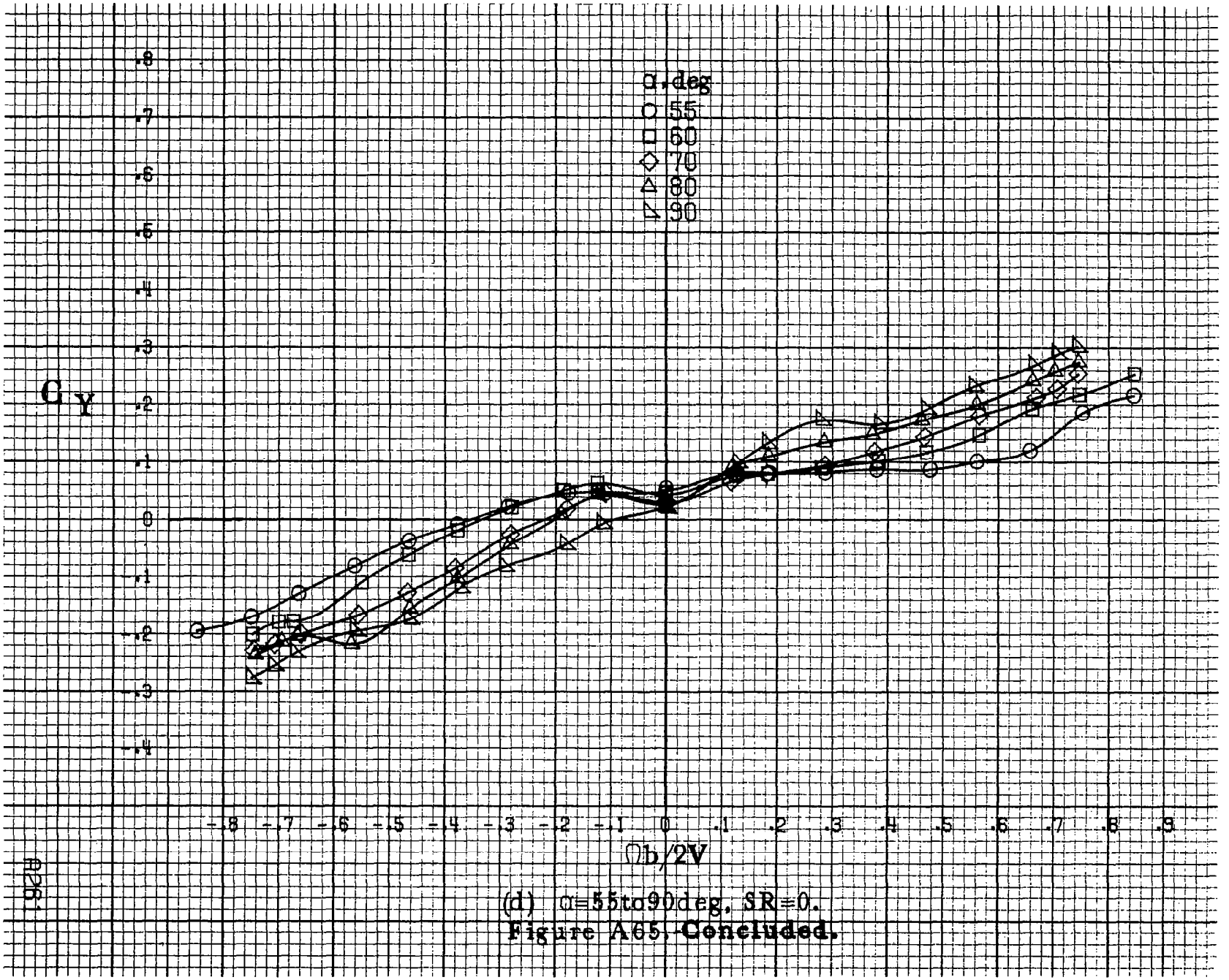

(d) $\alpha = 55$ to 90 deg, SR = 0.

Figure A65.- Concluded.

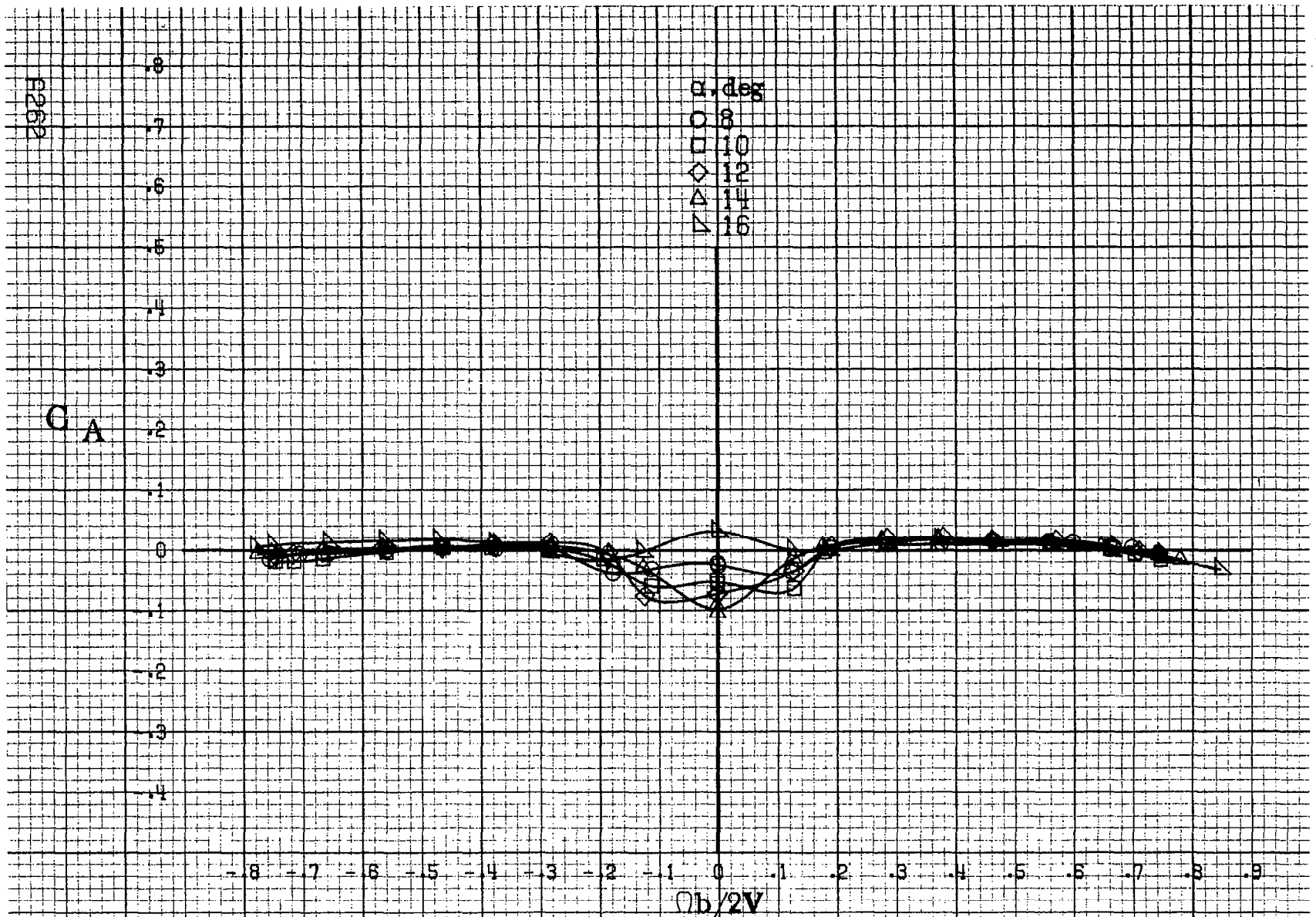

(a) α=8to16deg, SR=99cm(39in).

Figure A66.-Effect of rotation rate and angle of attack on axial-force coefficient for horizontal tail off configuration. $\delta_e = 0°$, $\delta_a = 0°$, $\delta_r = 0°$, $\beta = 0°$.

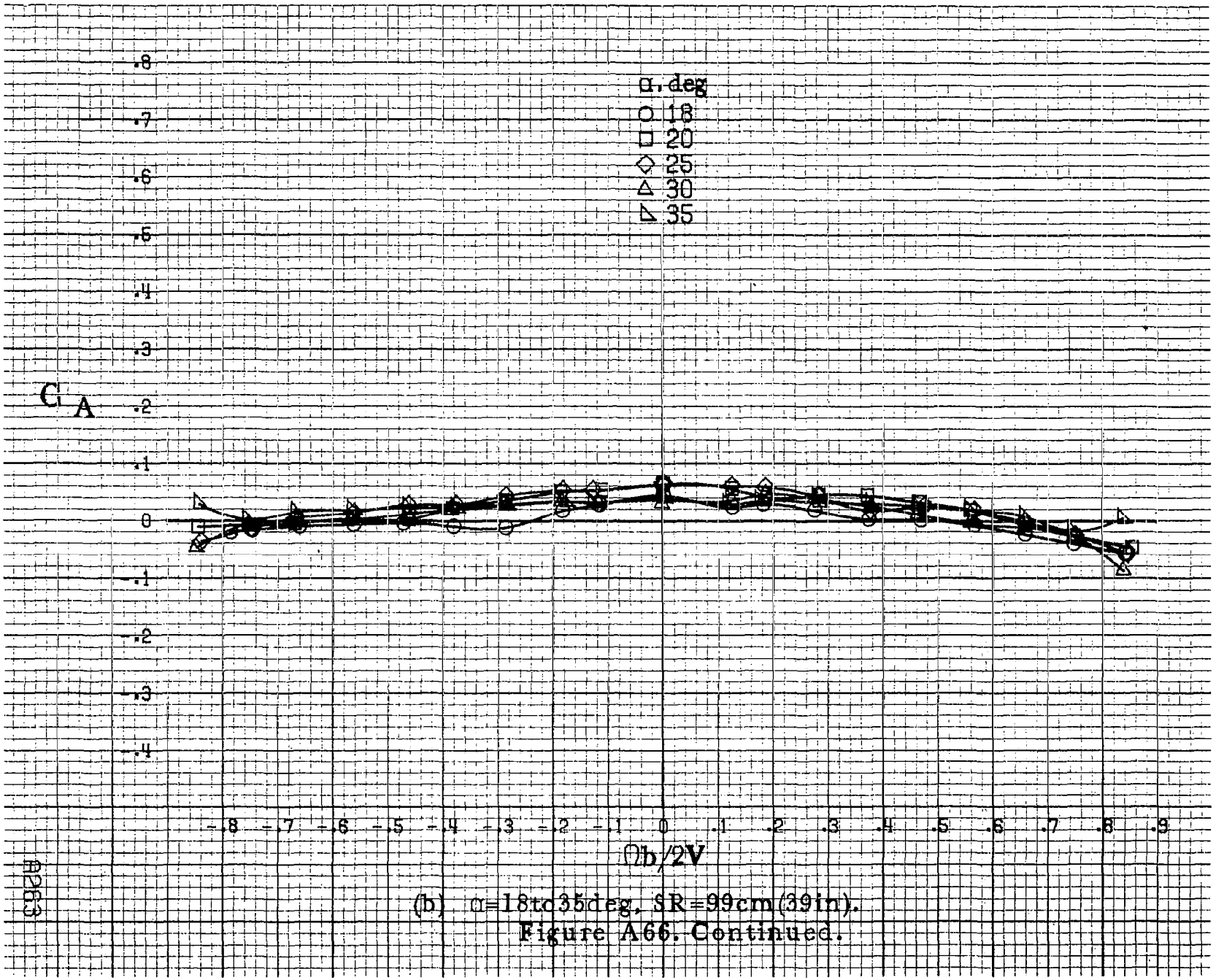

B263

(b) α=18to35deg, SR=99cm(39in).

Figure A66. Continued.

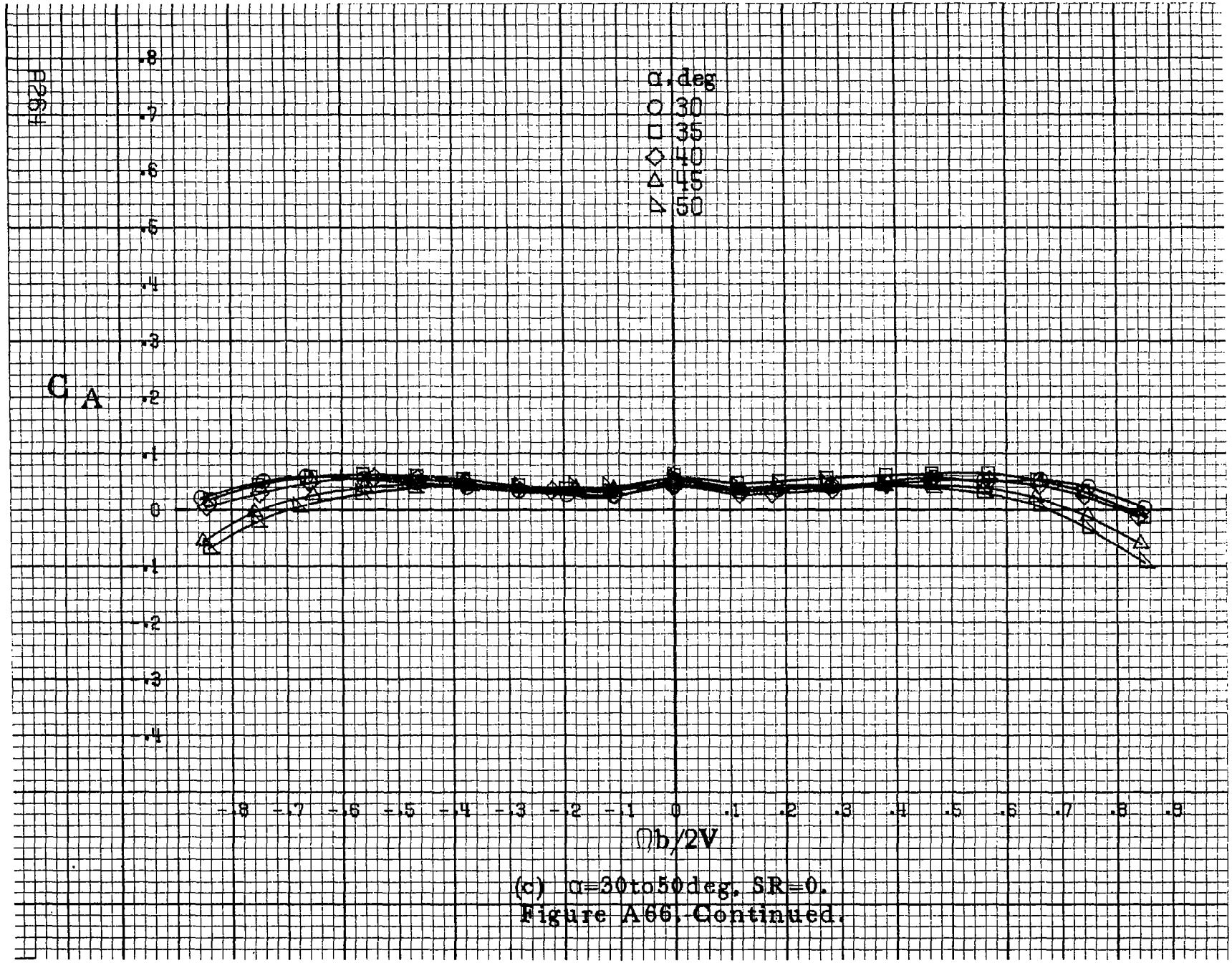

(c) α=30to50deg, SR=0.

Figure A66. Continued.

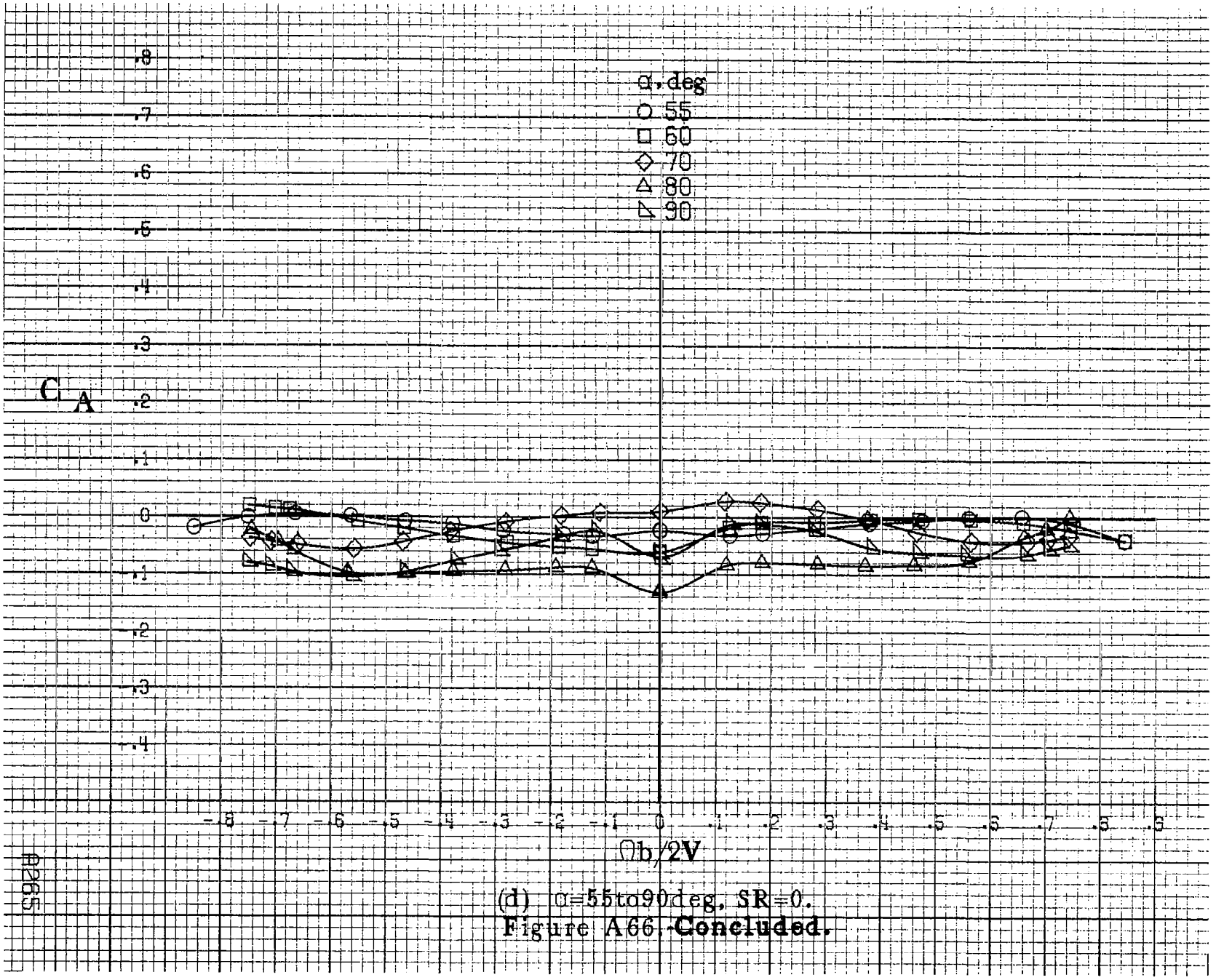

(d) α=55to90deg, SR=0.

Figure A66. Concluded.

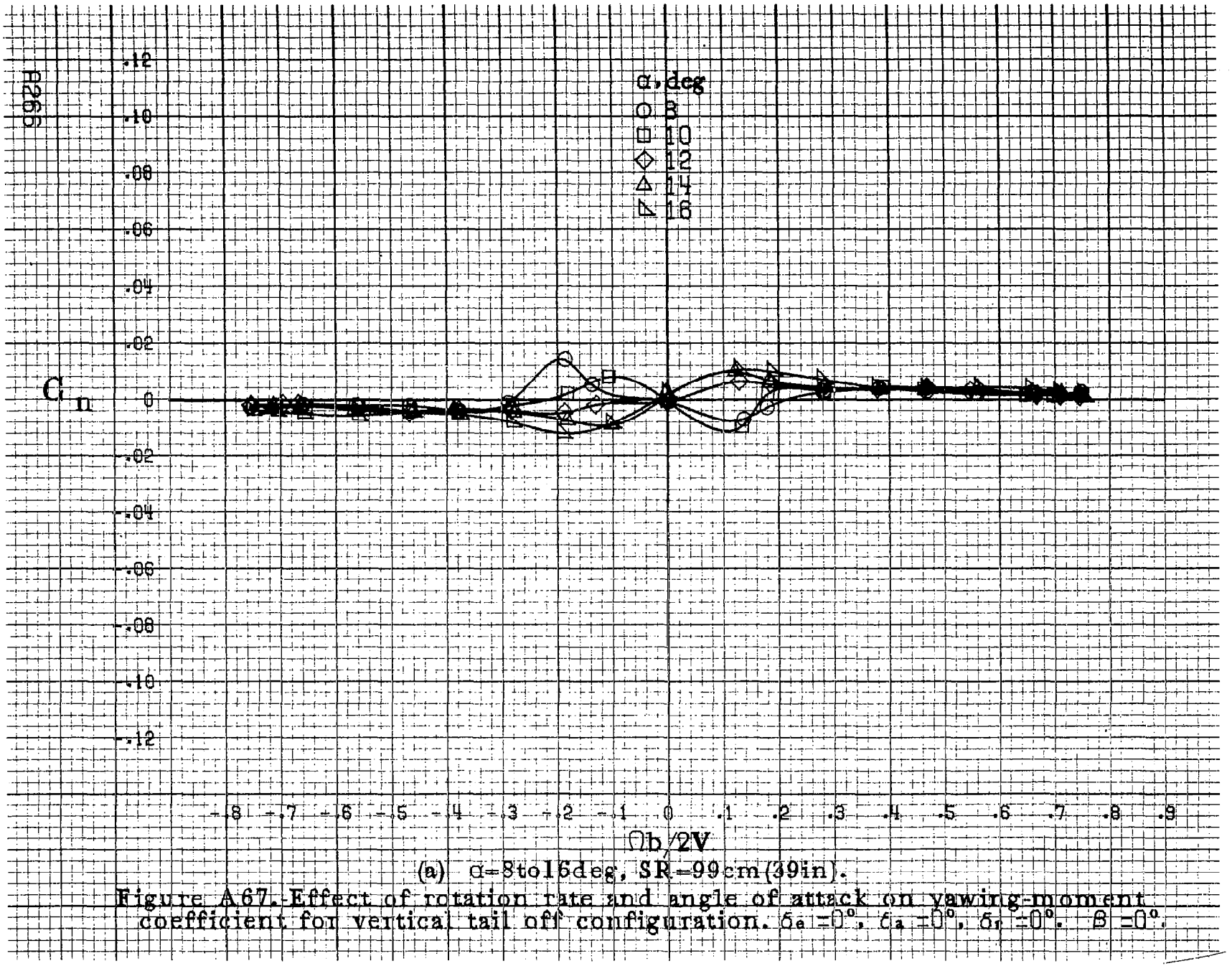

(a) α=8to16deg, SR=99cm(39in).

Figure A67.-Effect of rotation rate and angle of attack on yawing-moment coefficient for vertical tail off configuration. $\delta_{a_l}=0°$, $\delta_{a_r}=0°$, $\delta_r=0°$, $\beta=0°$.

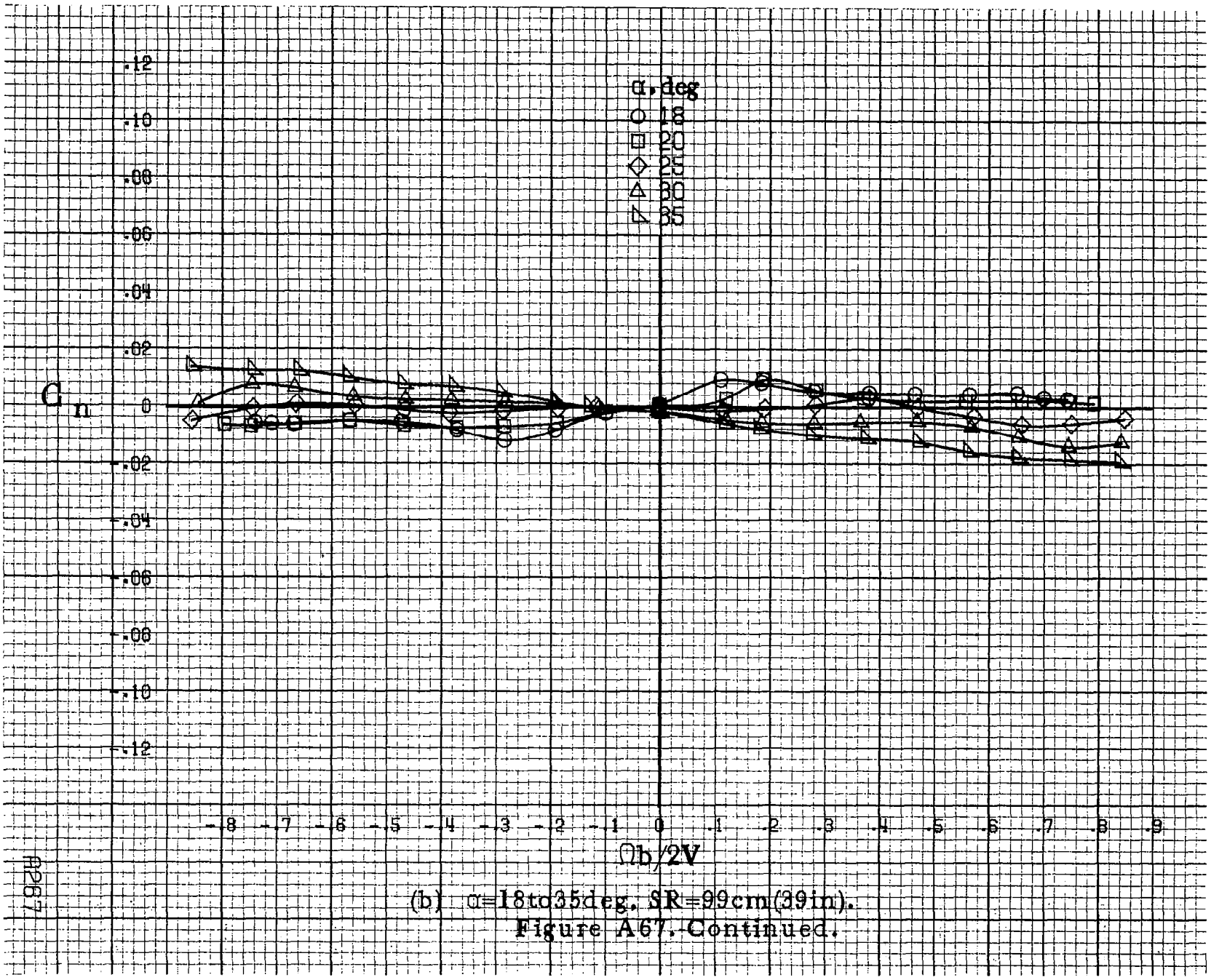

(b) α=18to35deg, SR=99cm(39in).

Figure A67.-Continued.

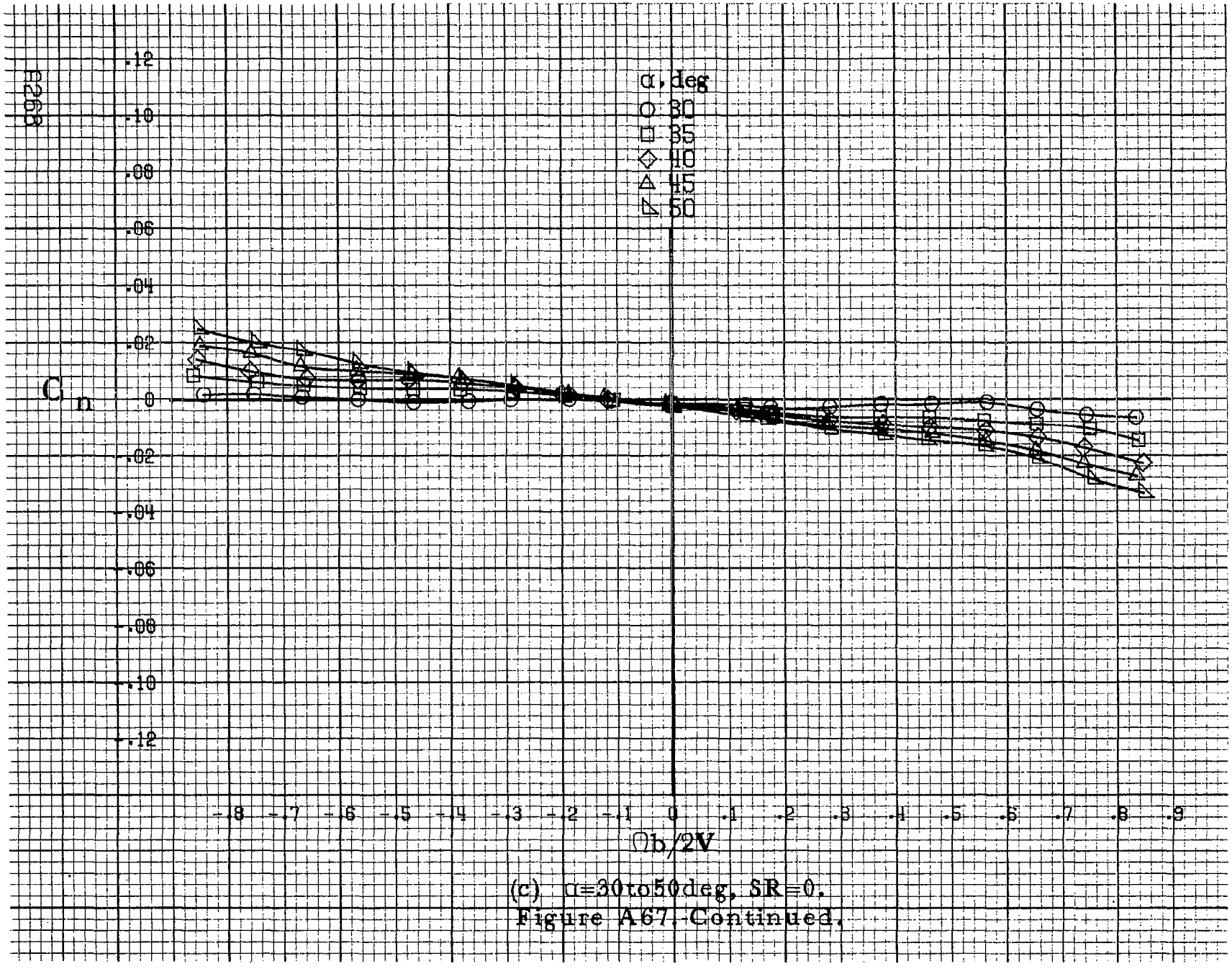

(c) α=30to50deg, SR=0.

Figure A67.-Continued.

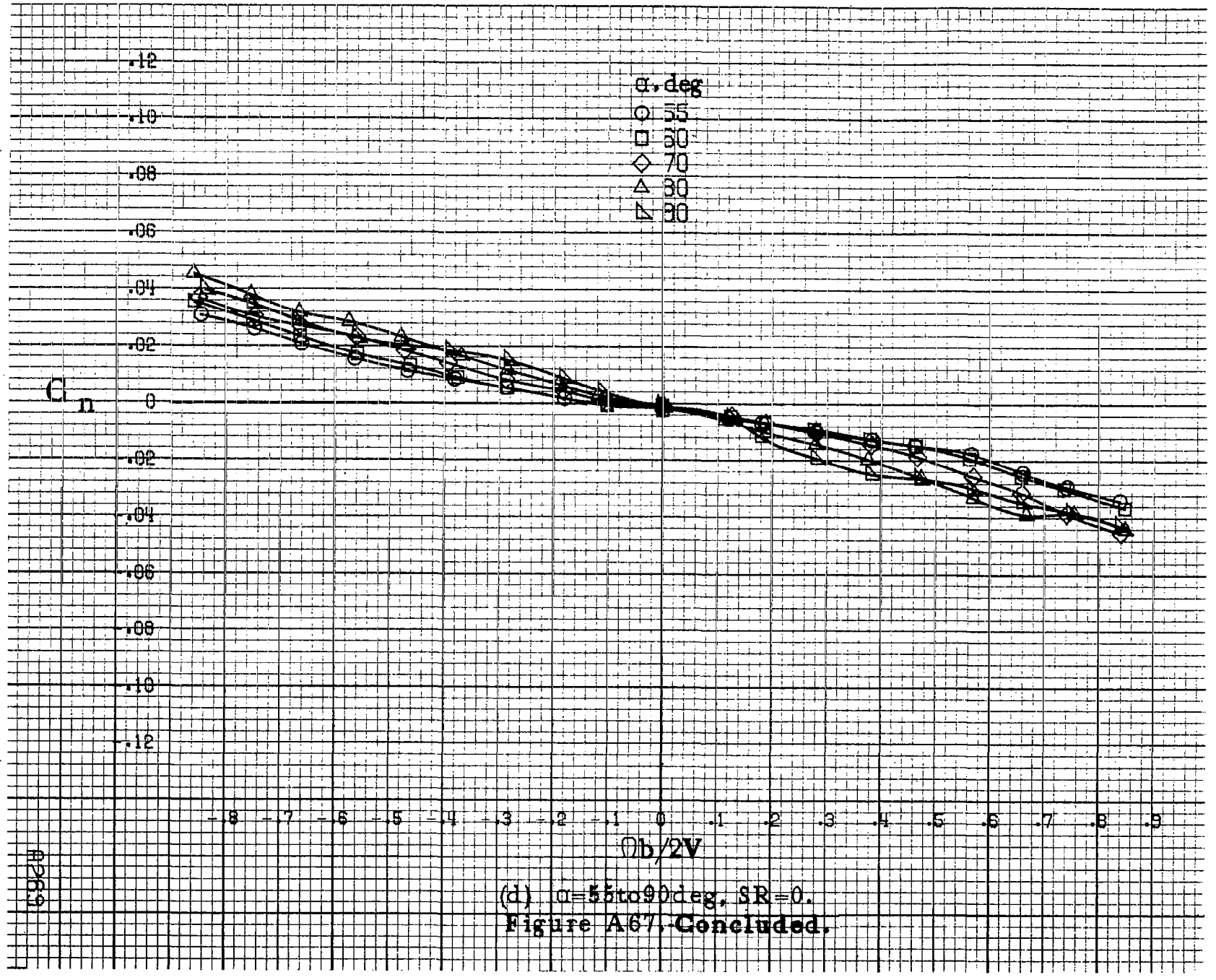

(d) α=55to90deg, SR=0.

Figure A67.-Concluded.

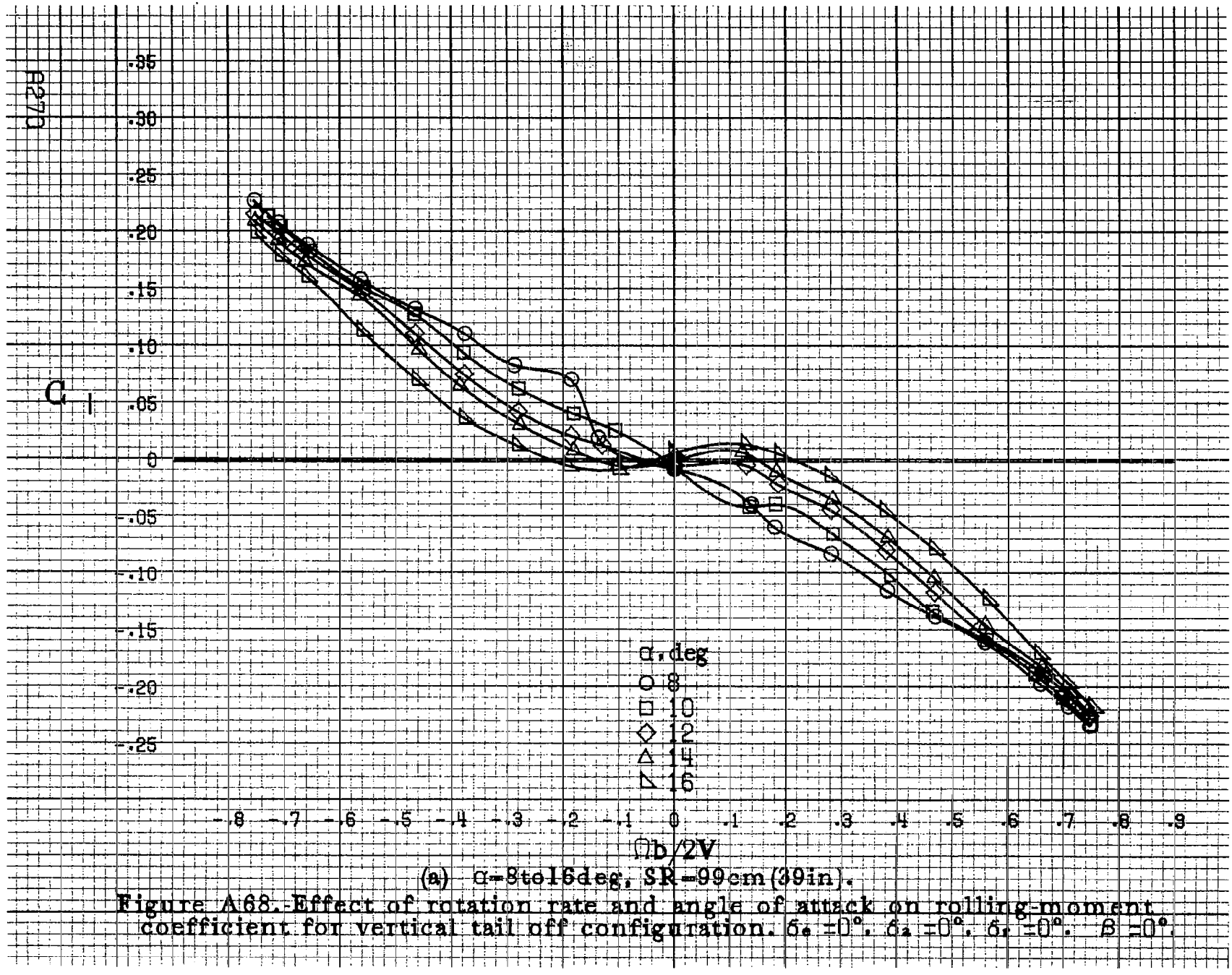

(a) α=8to16deg, SR=99cm(39in).

Figure A68.-Effect of rotation rate and angle of attack on rolling-moment coefficient for vertical tail off configuration. δ_e =0°, δ_a =0°, δ_r =0°. β =0°.

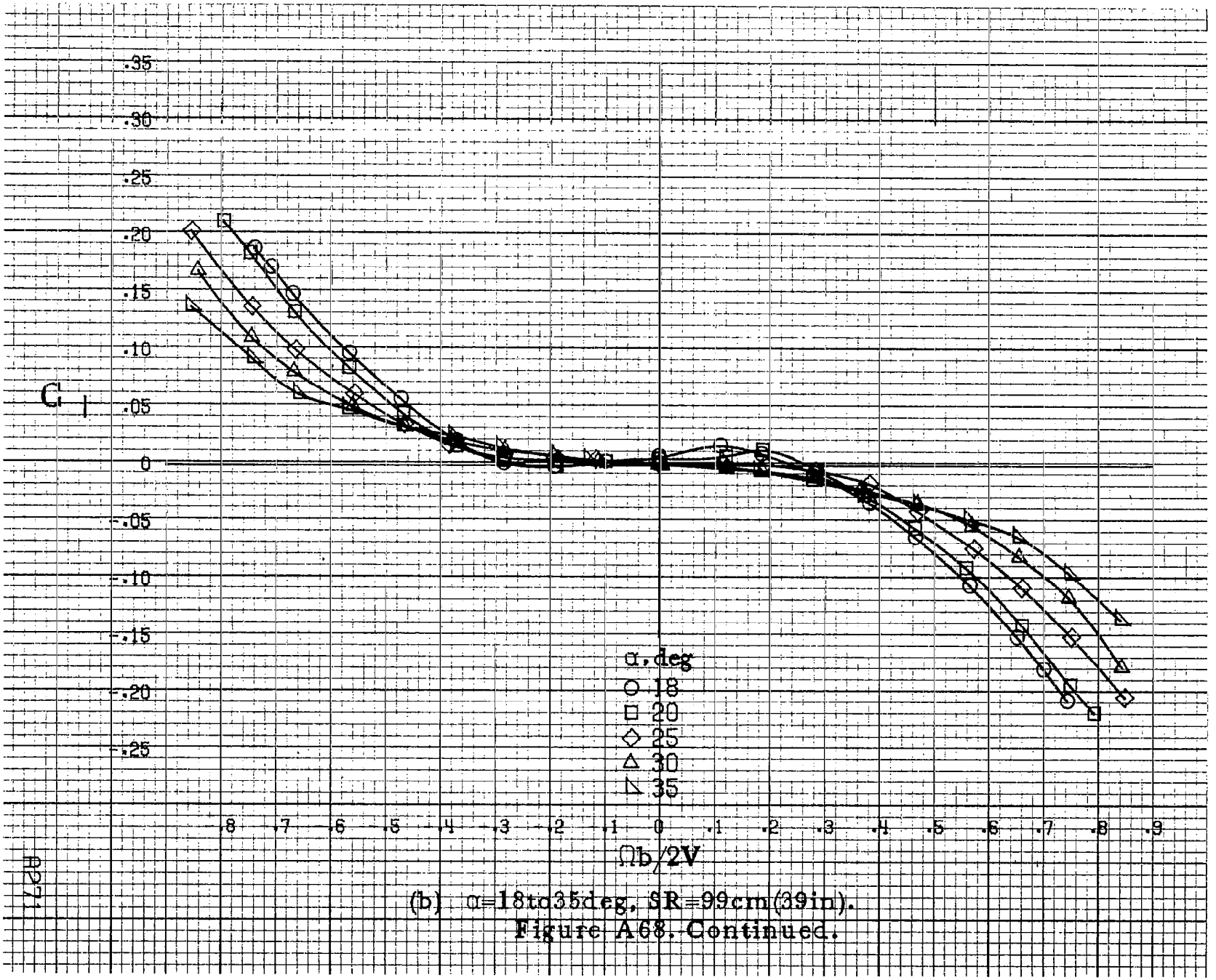

(b) α=18to35deg, SR=99cm(39in).

Figure A68. Continued.

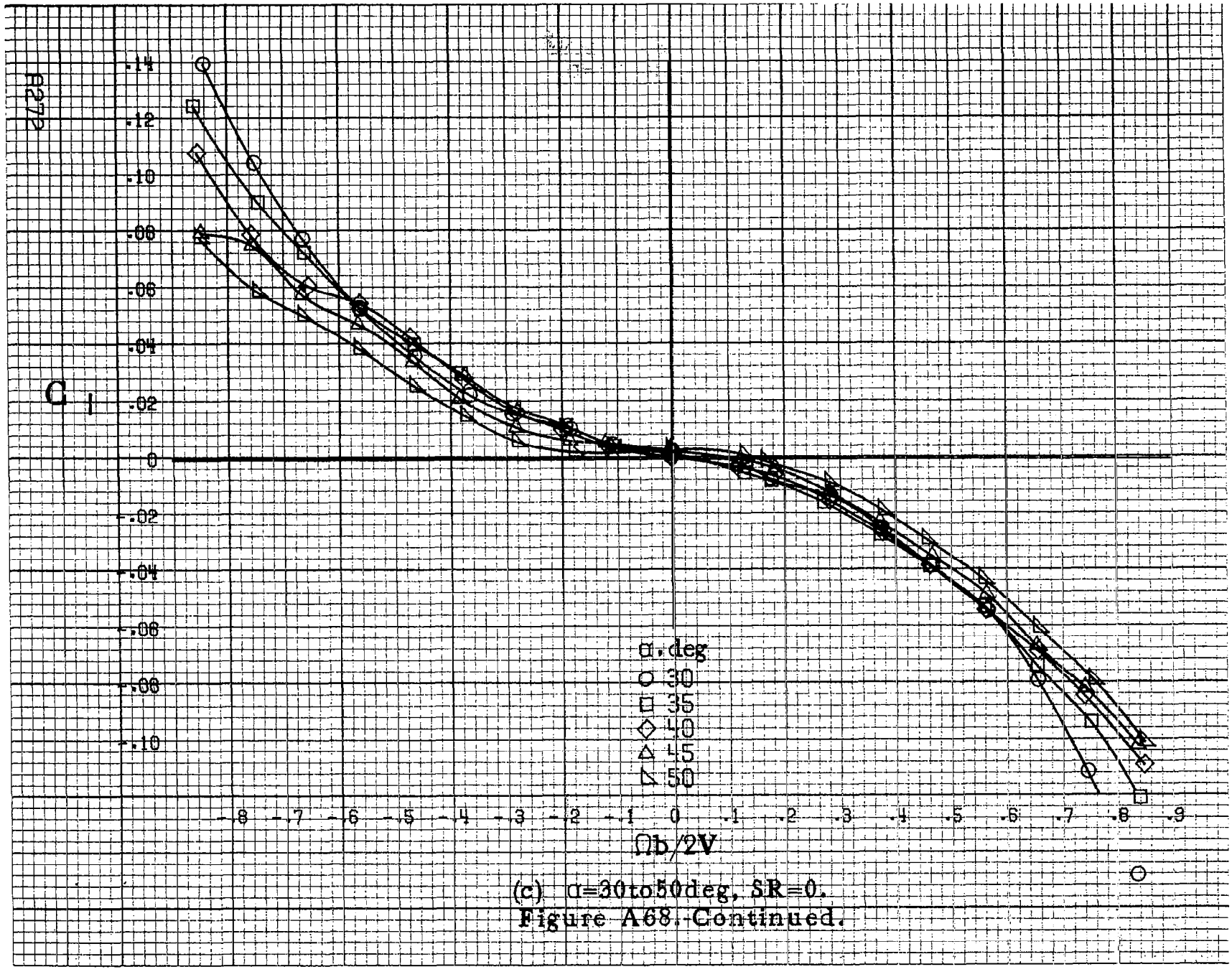

(c) α=30to50deg, SR=0.

Figure A68.-Continued.

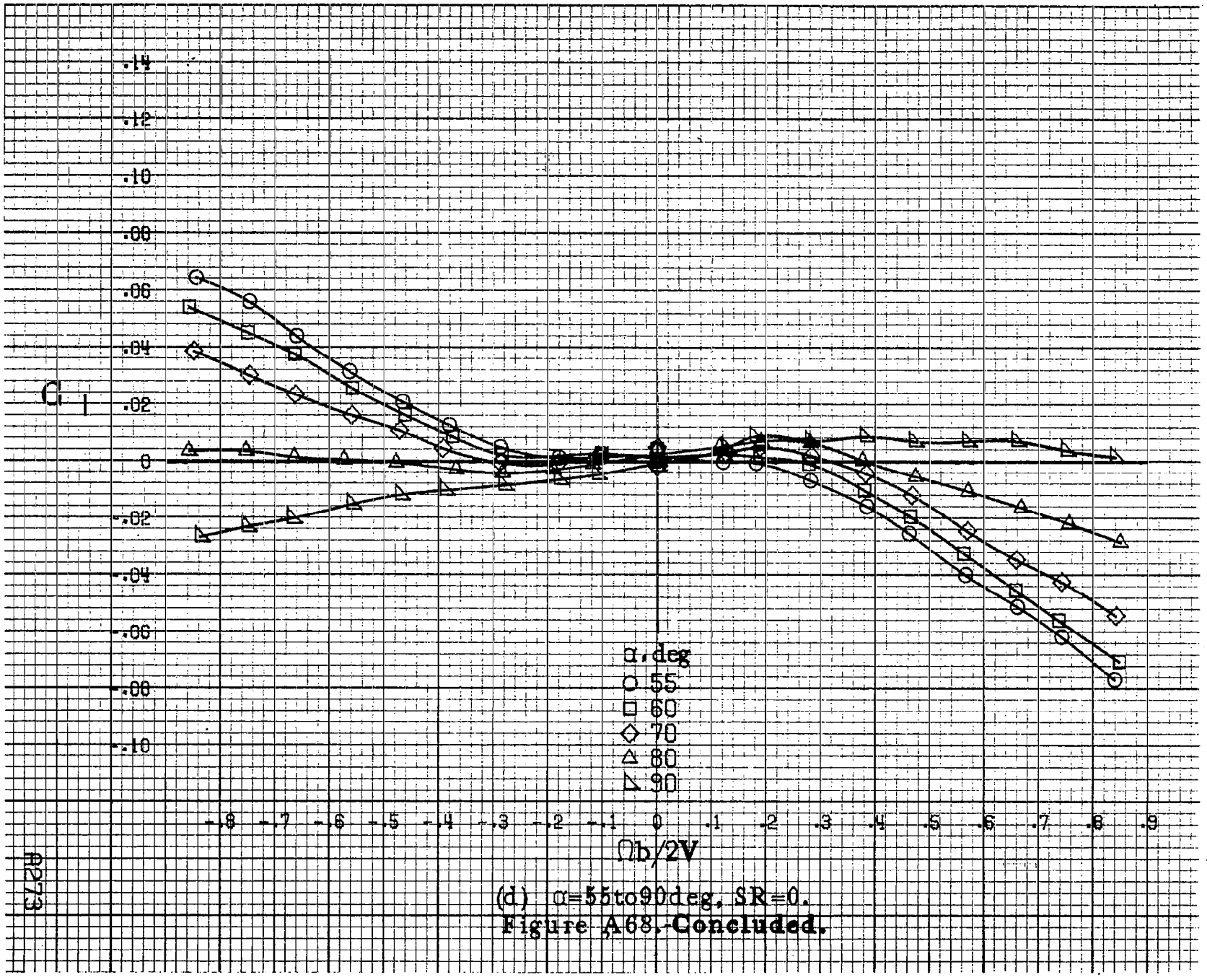

(d) α=55to90deg, SR=0.

Figure A68.-Concluded.

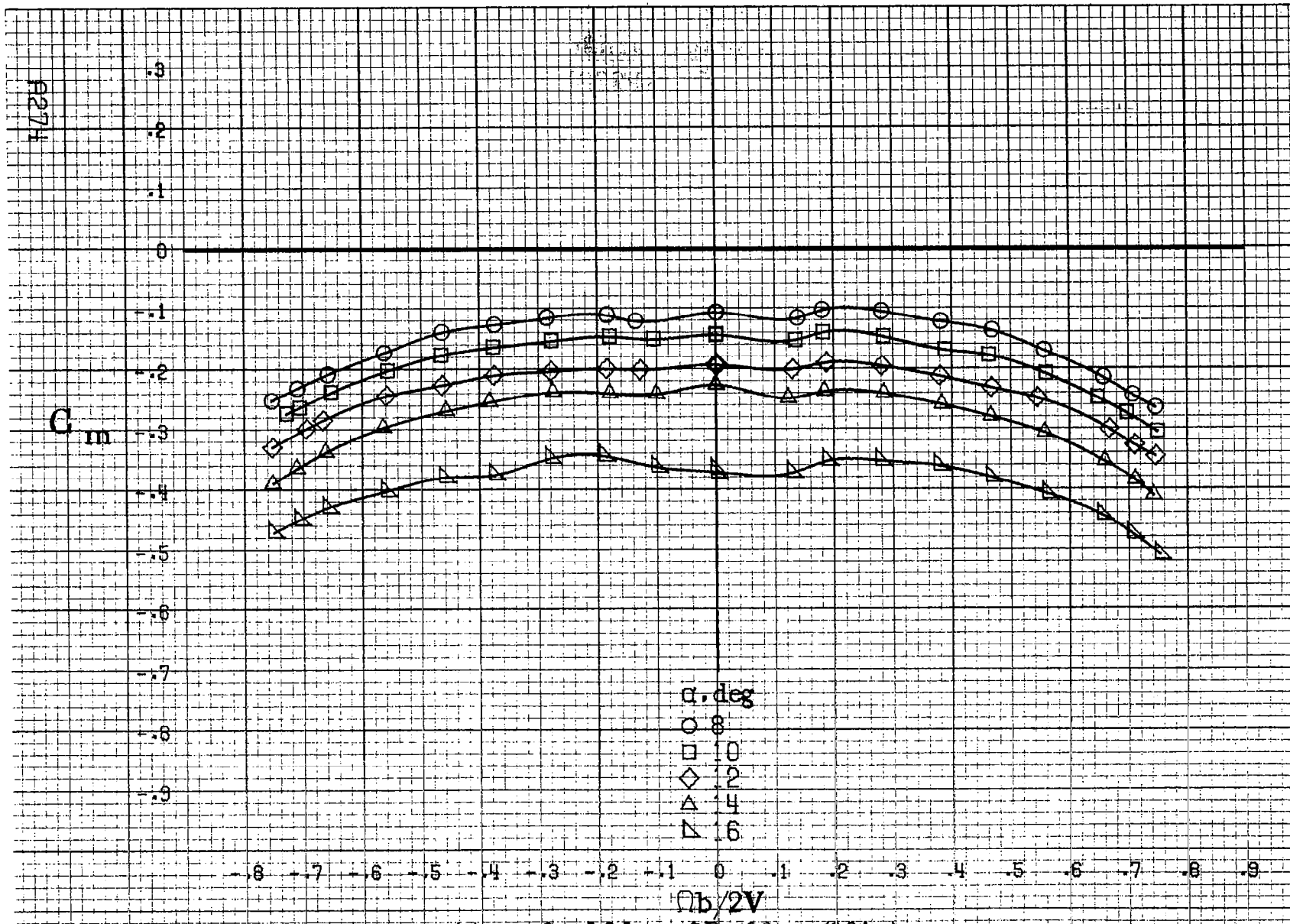

(a) α=8to16deg, SR=99cm(39in).

Figure A69.-Effect of rotation rate and angle of attack on pitching-moment coefficient for vertical tail off configuration. δ_e =0°, δ_a =0°, δ_r =0°, β =0°.

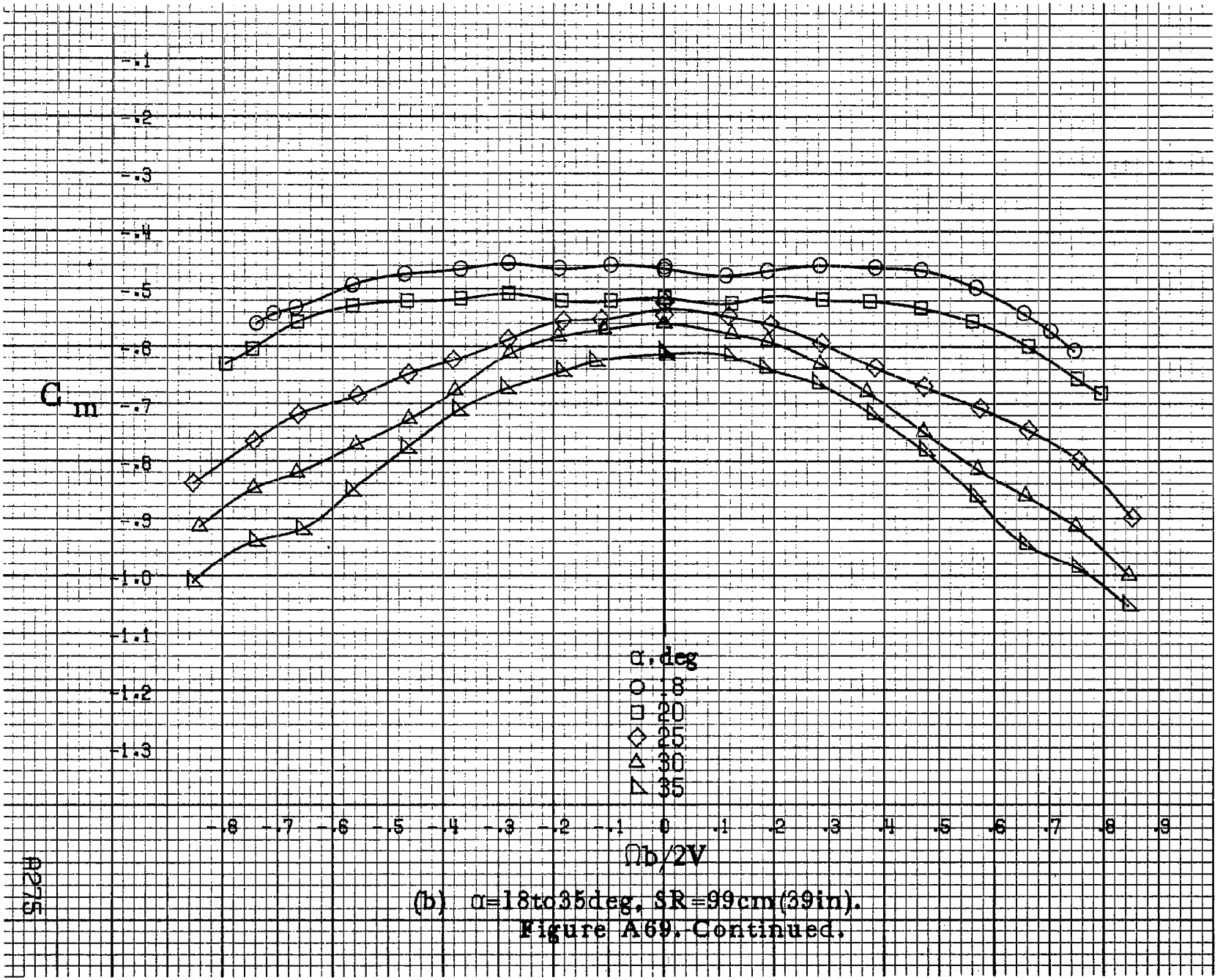

(b) α=18to35deg, SR=99cm(39in).

Figure A69. Continued.

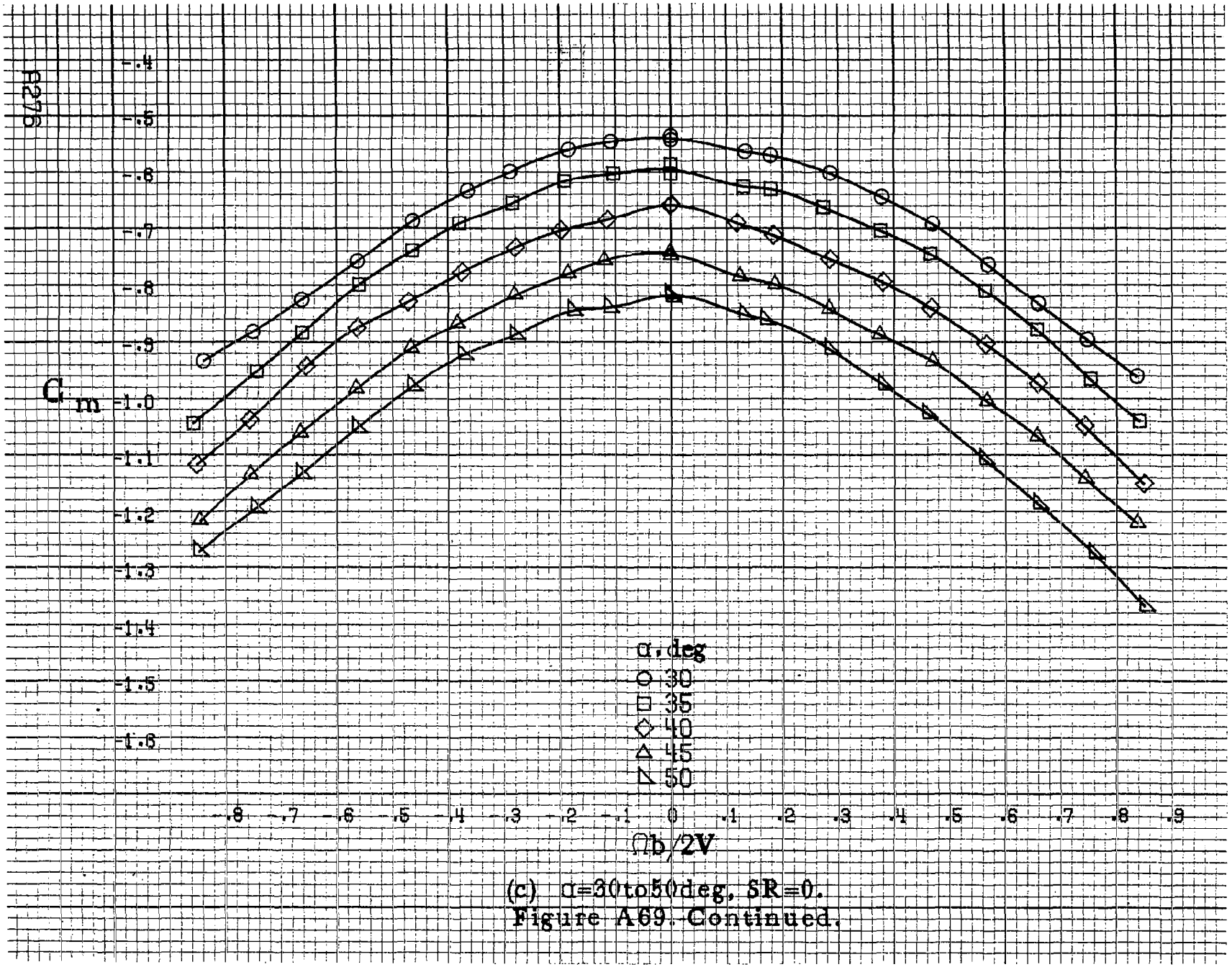

(c) α=30to50deg, δR=0.

Figure A69.-Continued.

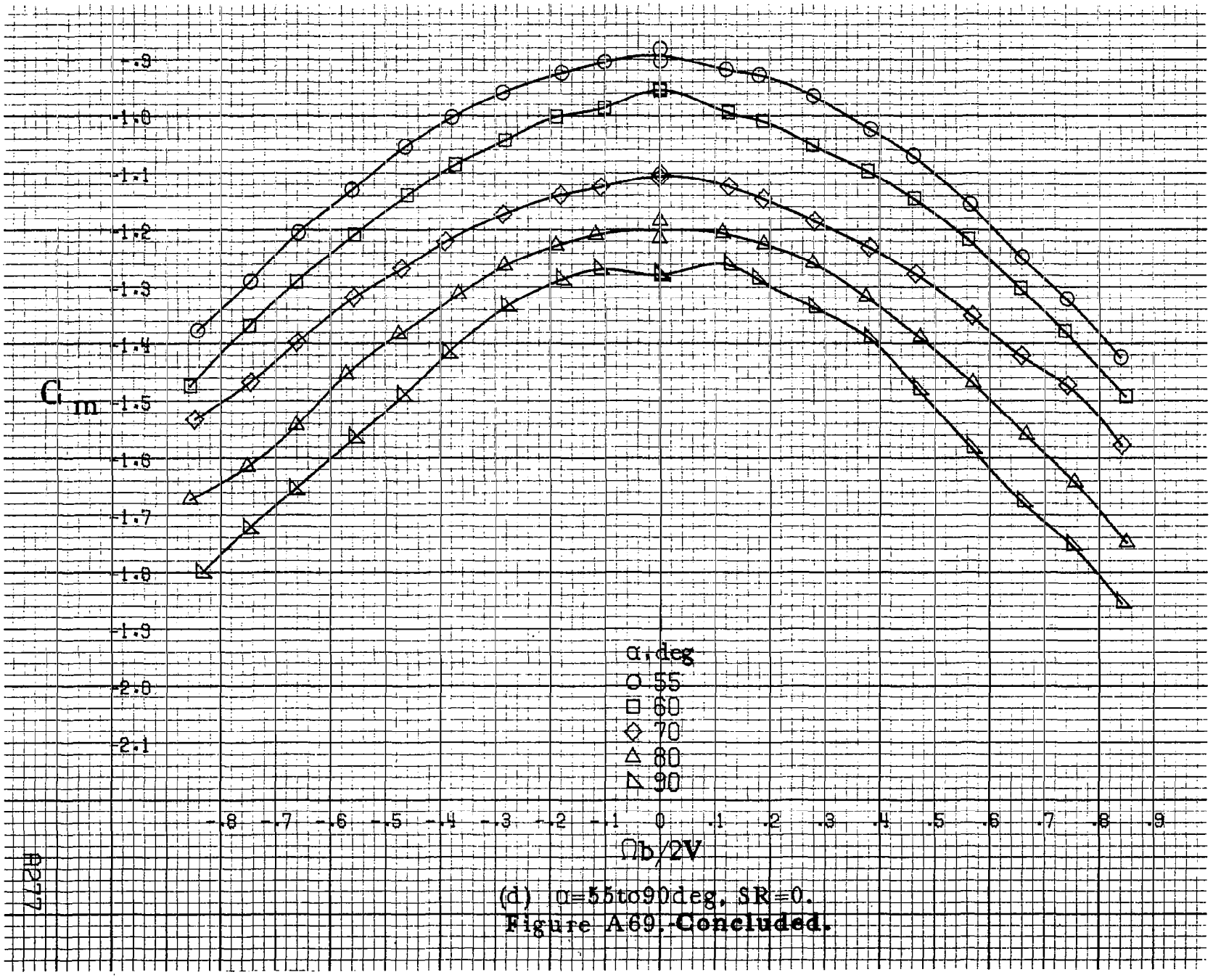

(d) α≡55to90deg, SR≡0.

Figure A69. Concluded.

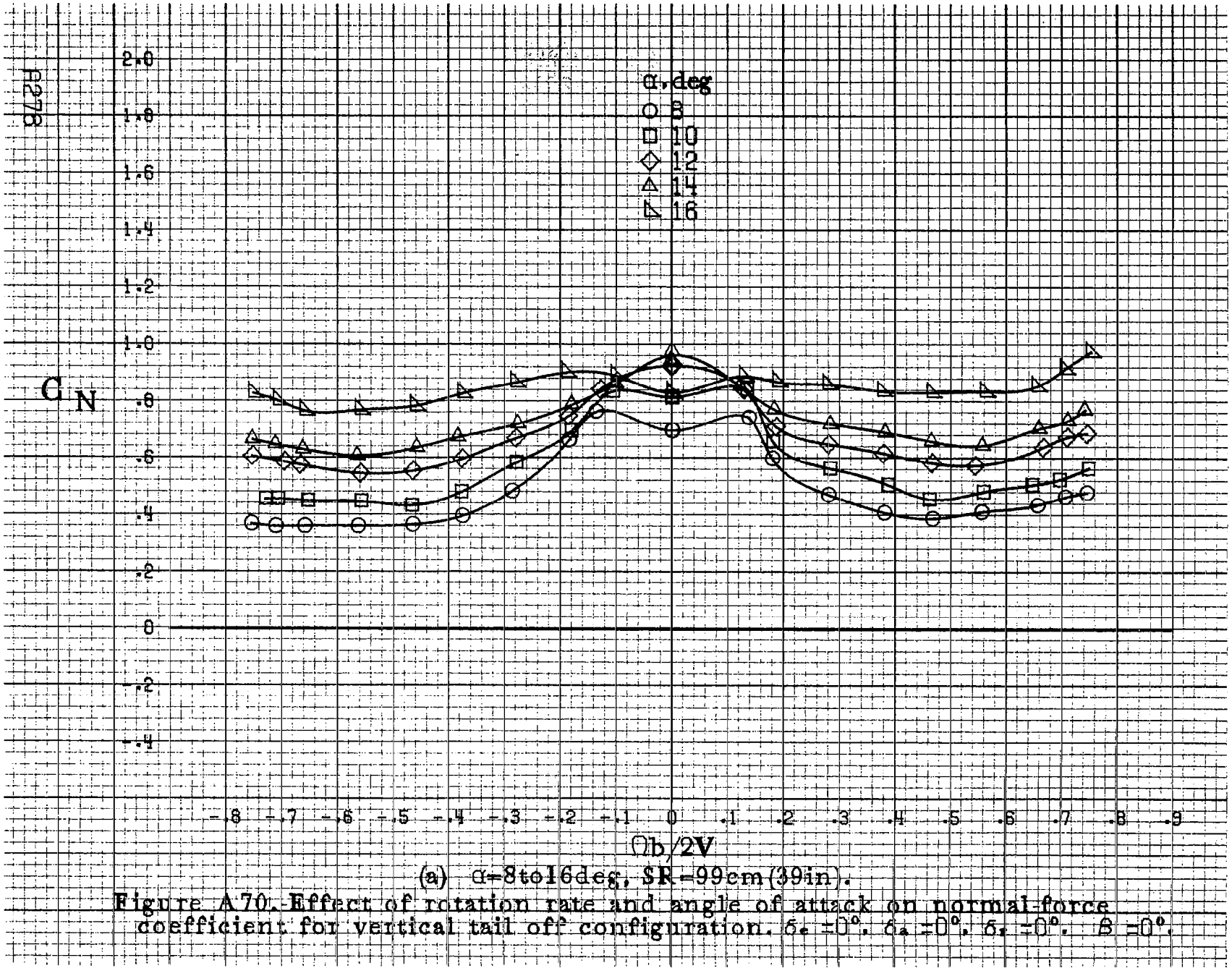

(a) α=8to16deg, $R=99cm(39in).

Figure A70. Effect of rotation rate and angle of attack on normal-force coefficient for vertical tail off configuration. $\delta_e = 0°$, $\delta_a = 0°$, $\delta_r = 0°$, $\beta = 0°$.

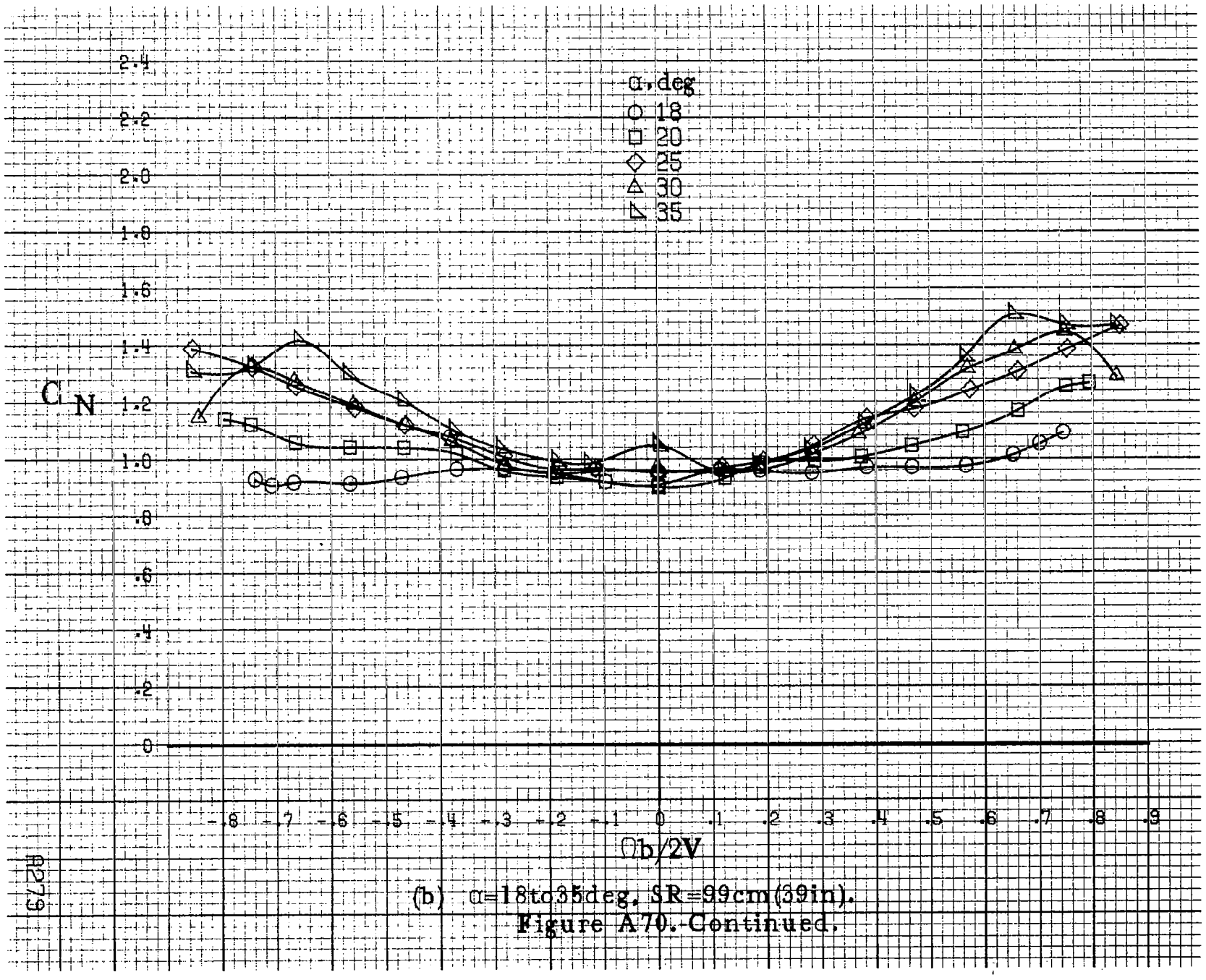

B27-69

(b) α=18to35deg, SR=99cm(39in).

Figure A70.-Continued.

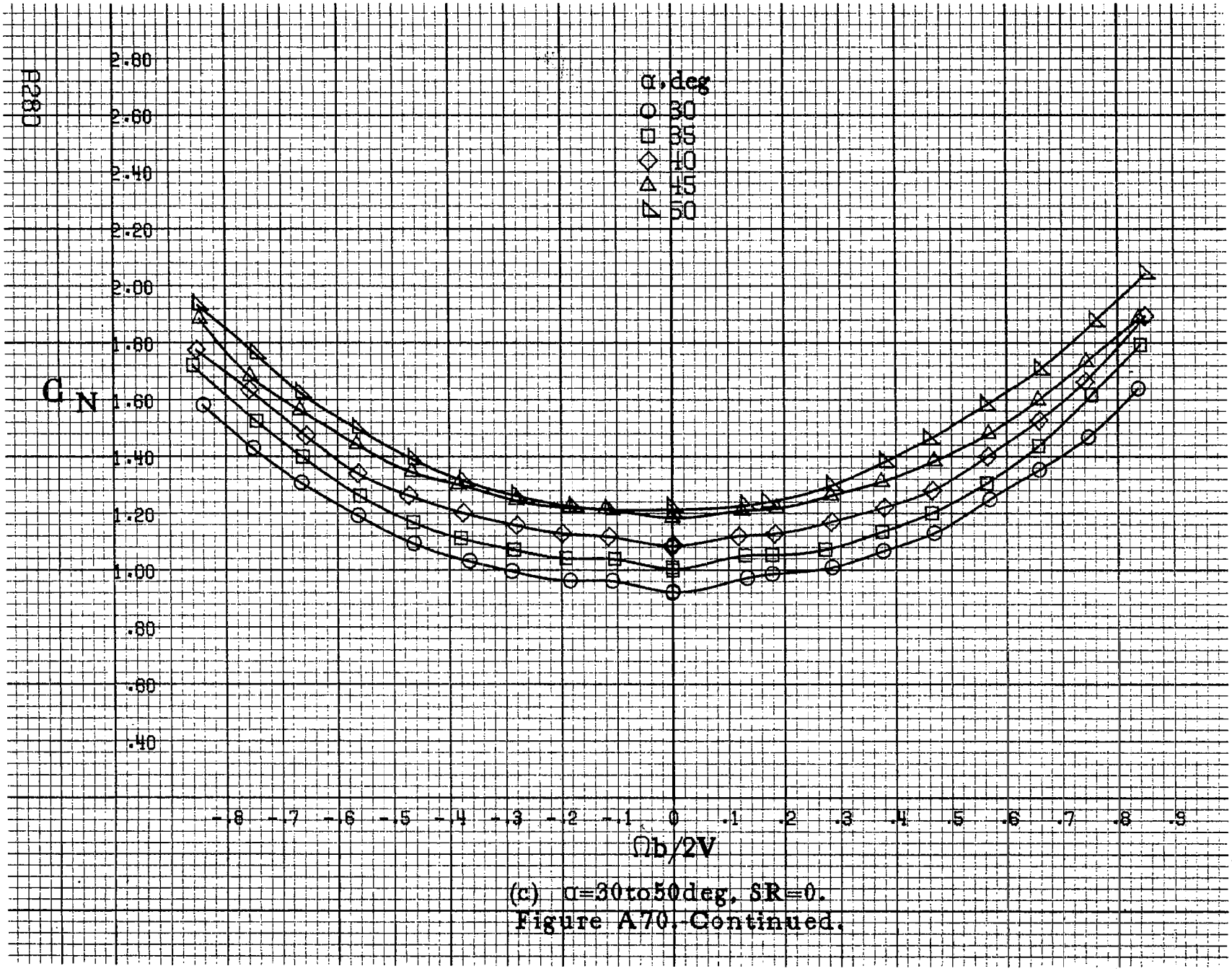

(c) α=30to50deg, δR=0.

Figure A70.-Continued.

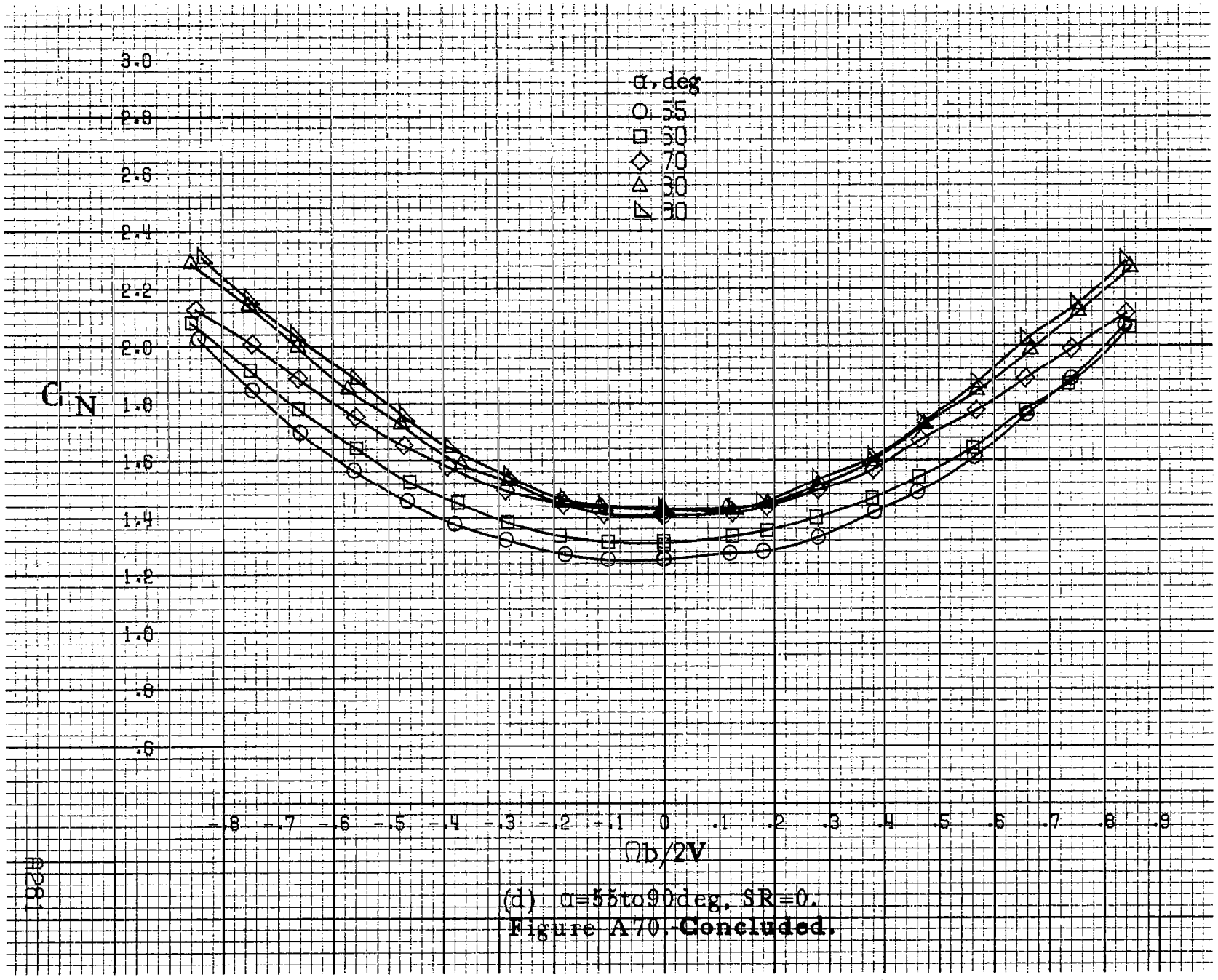

(d) α=55 to 90 deg, SR=0.

Figure A70.-Concluded.

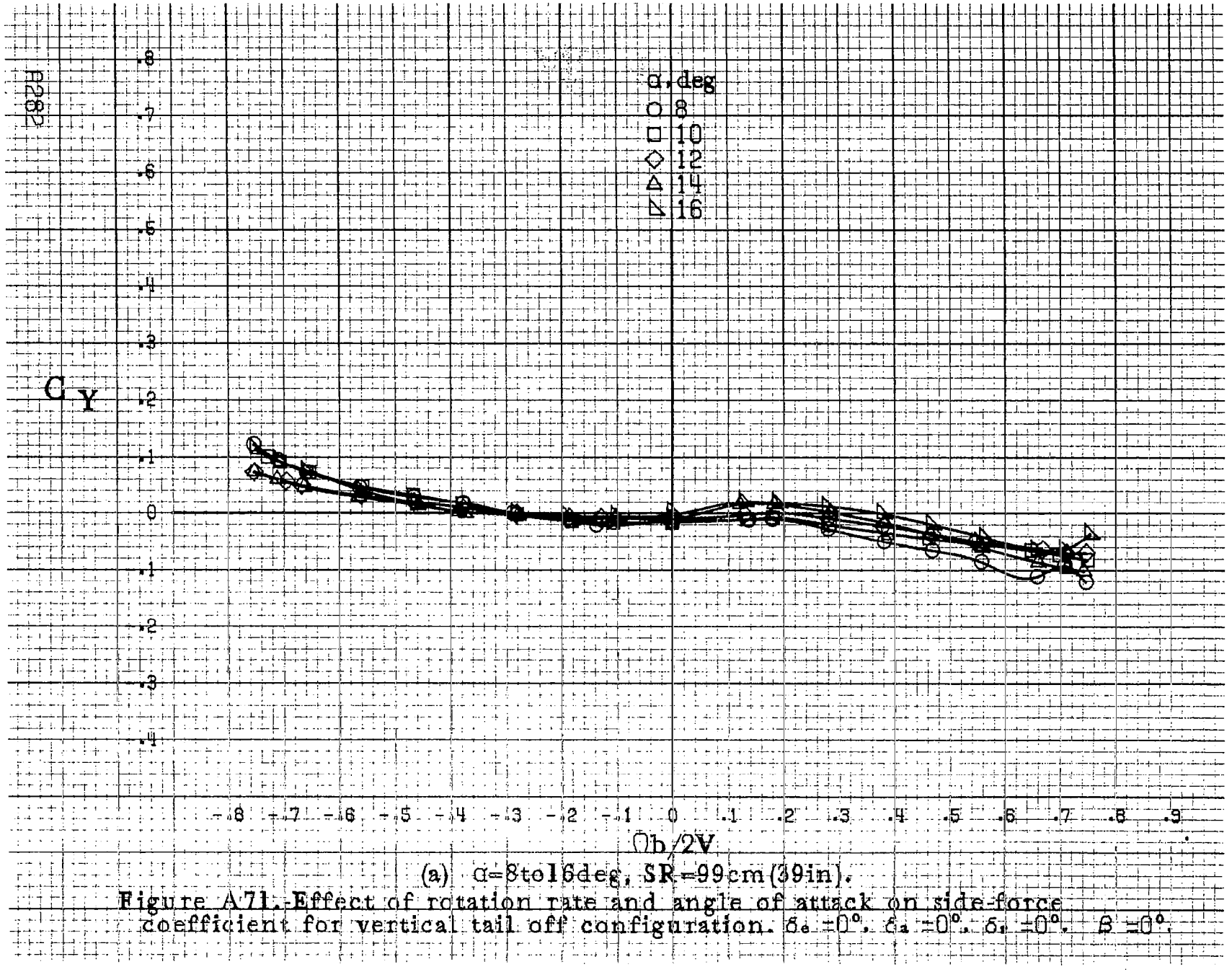

(a) α=8to16deg, SR=99cm(39in).

Figure A71.-Effect of rotation rate and angle of attack on side-force coefficient for vertical tail off configuration. $\delta_e = 0°$, $\delta_a = 0°$, $\delta_r = 0°$, $\beta = 0°$.

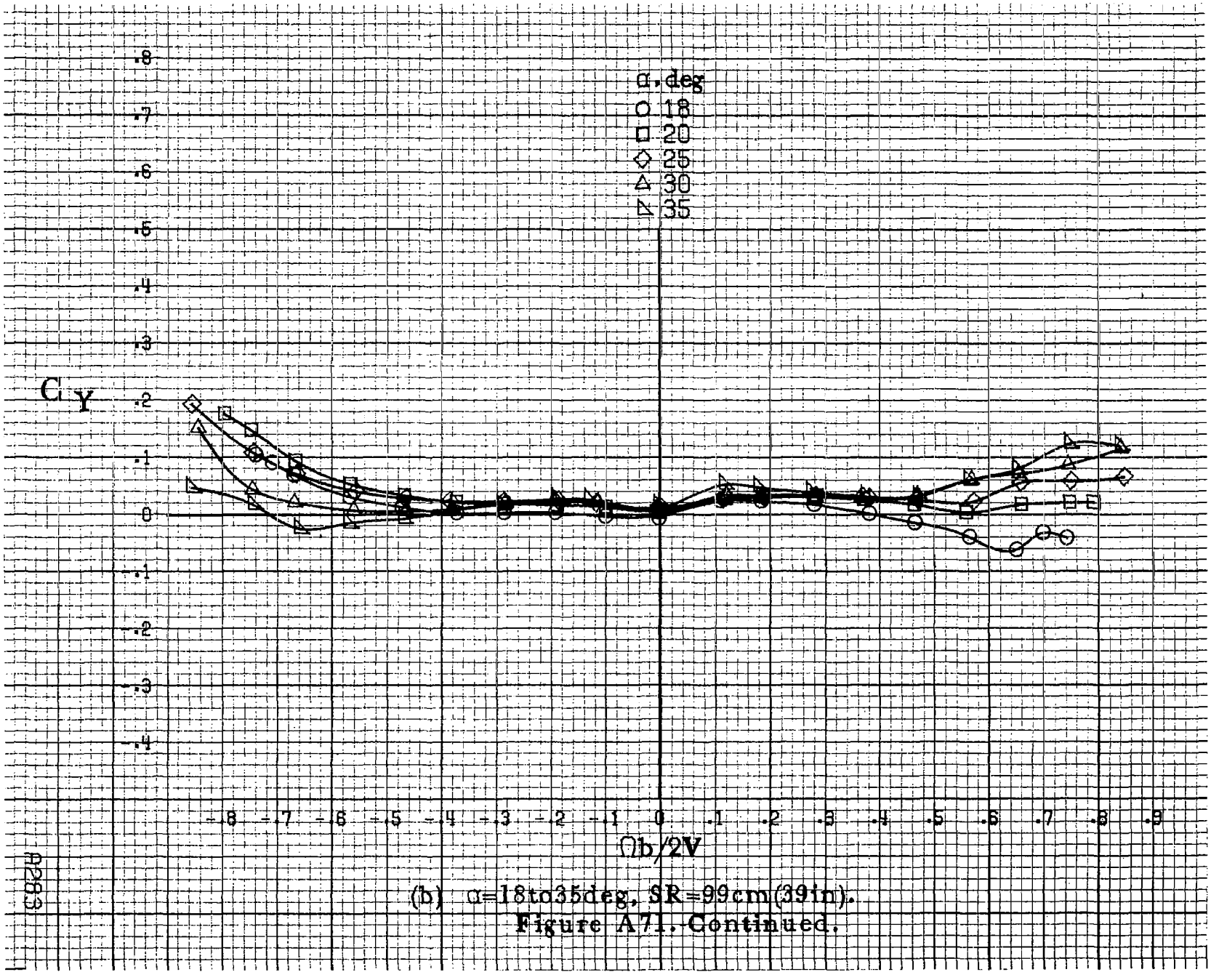

(b) α=18to35deg, SR=99cm(39in).

Figure A71.-Continued.

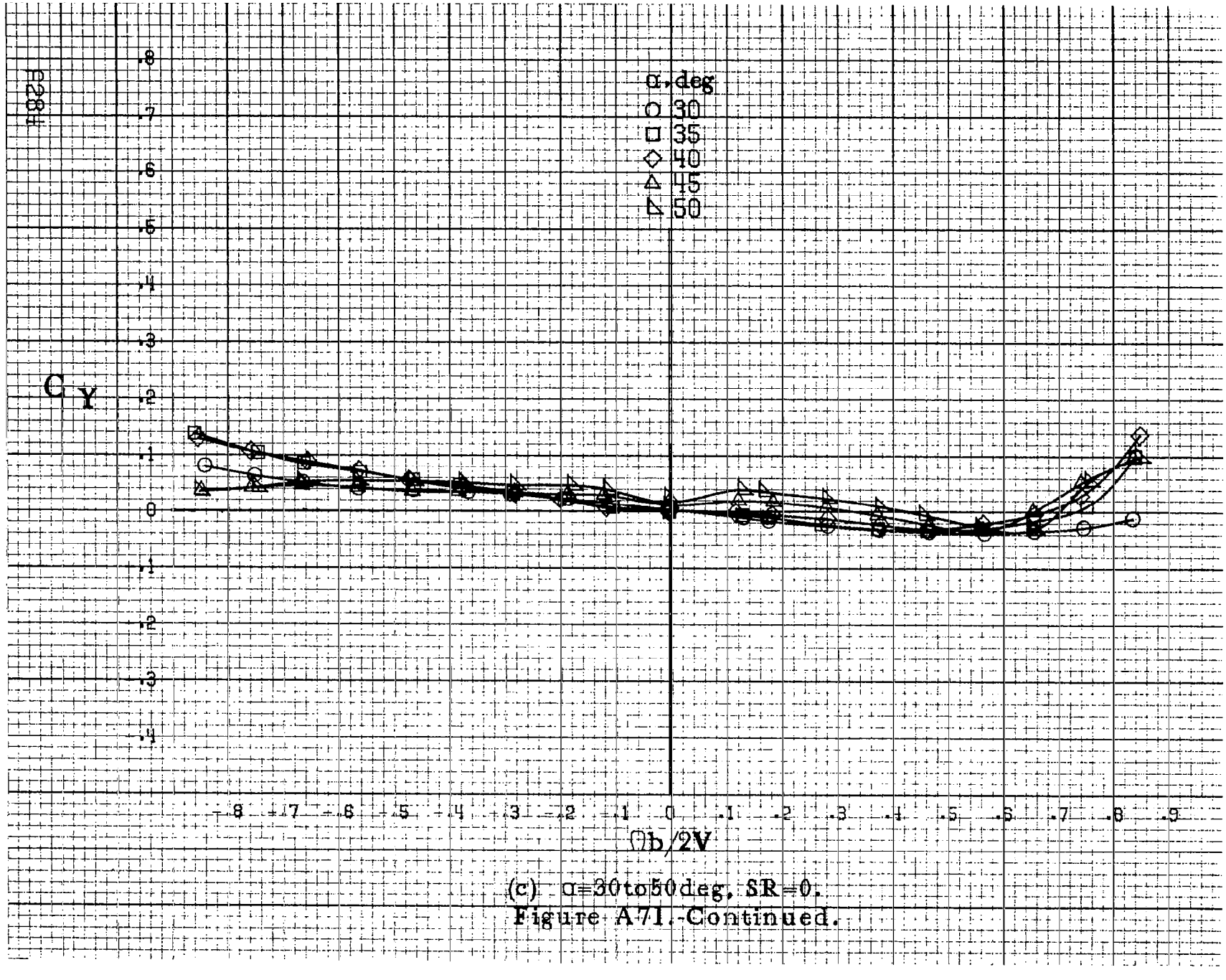

(c) α=30 to 50 deg, SR=0.

Figure A71.-Continued.

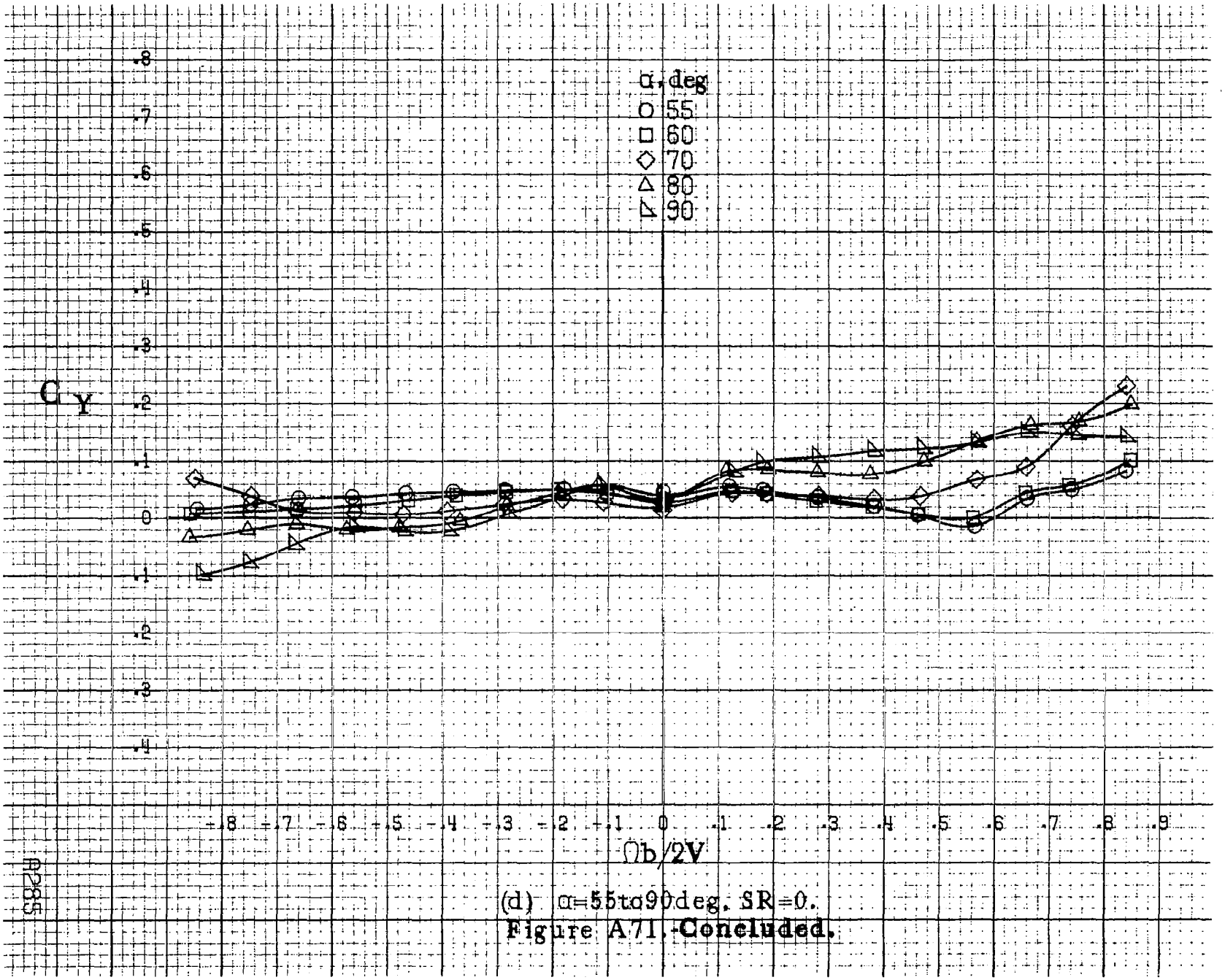

(d) α=55to90deg. SR=0.

Figure A71.-Concluded.

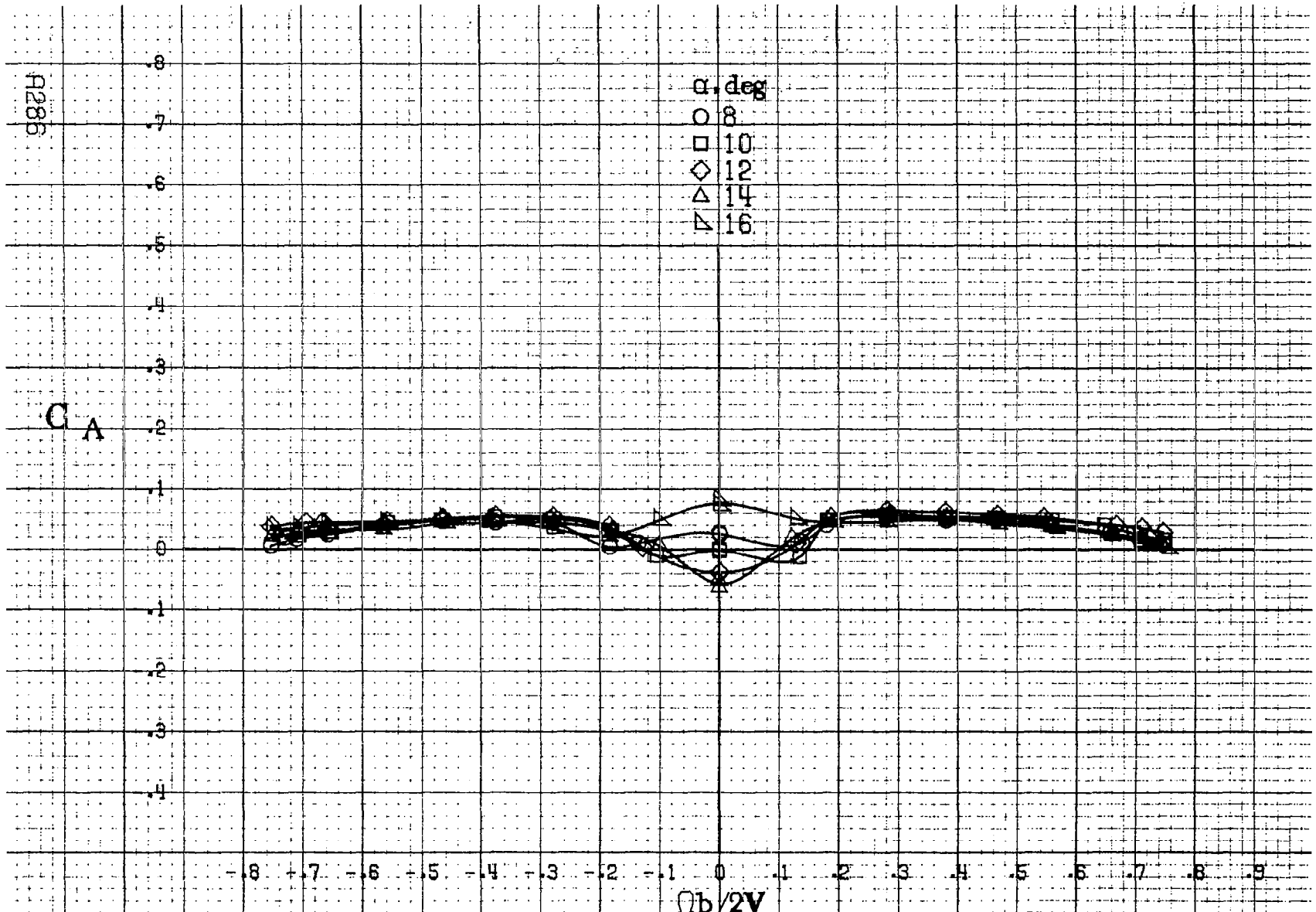

(a) α=8to16deg, SR=99cm(39in).

Figure A72.-Effect of rotation rate and angle of attack on axial force coefficient for vertical tail off configuration. $\delta_e = 0°$, $\delta_a = 0°$, $\delta_r = 0°$, $\beta = 0°$.

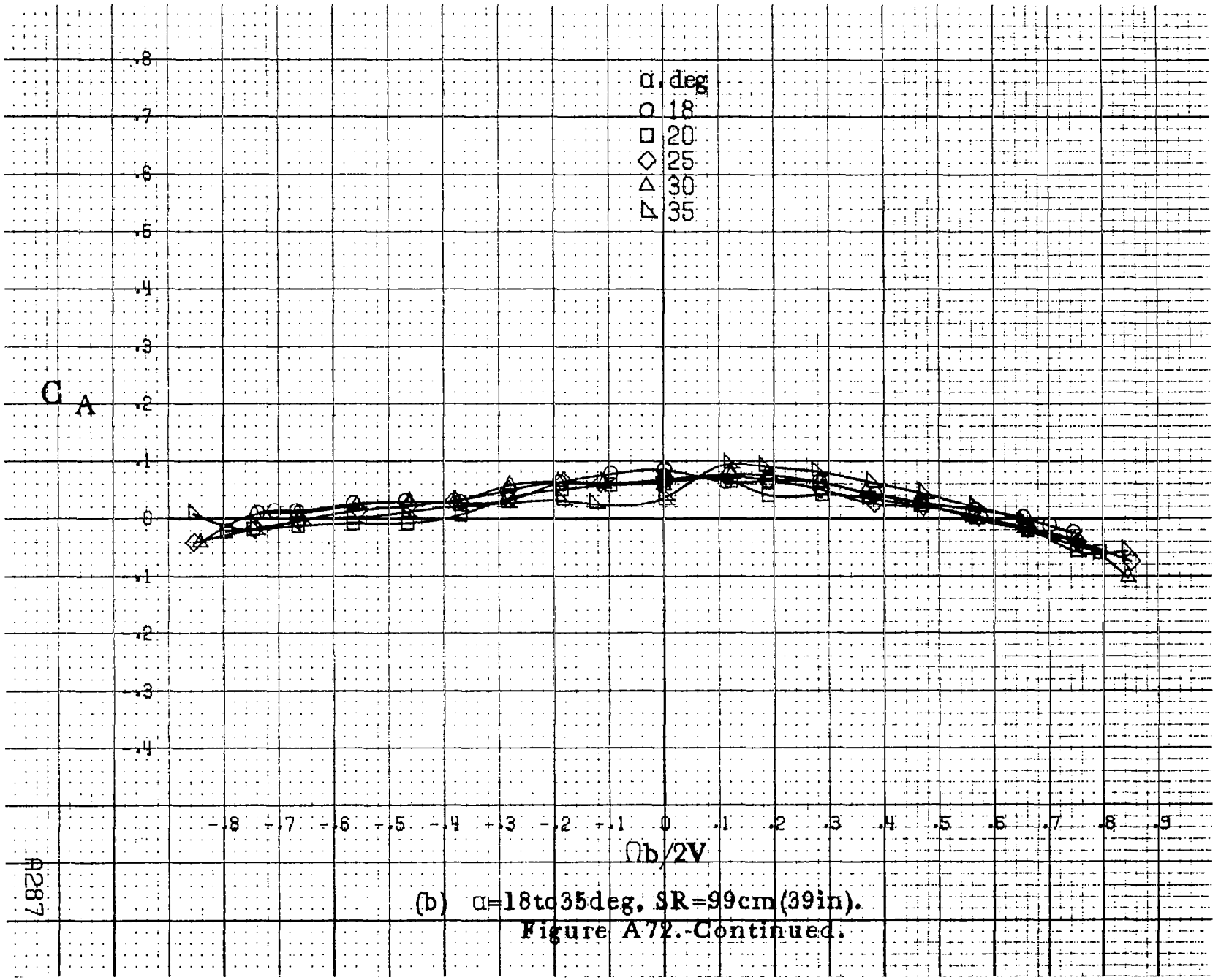

A287

(b) α=18to35deg, SR=99cm(39in).

Figure A72.-Continued.

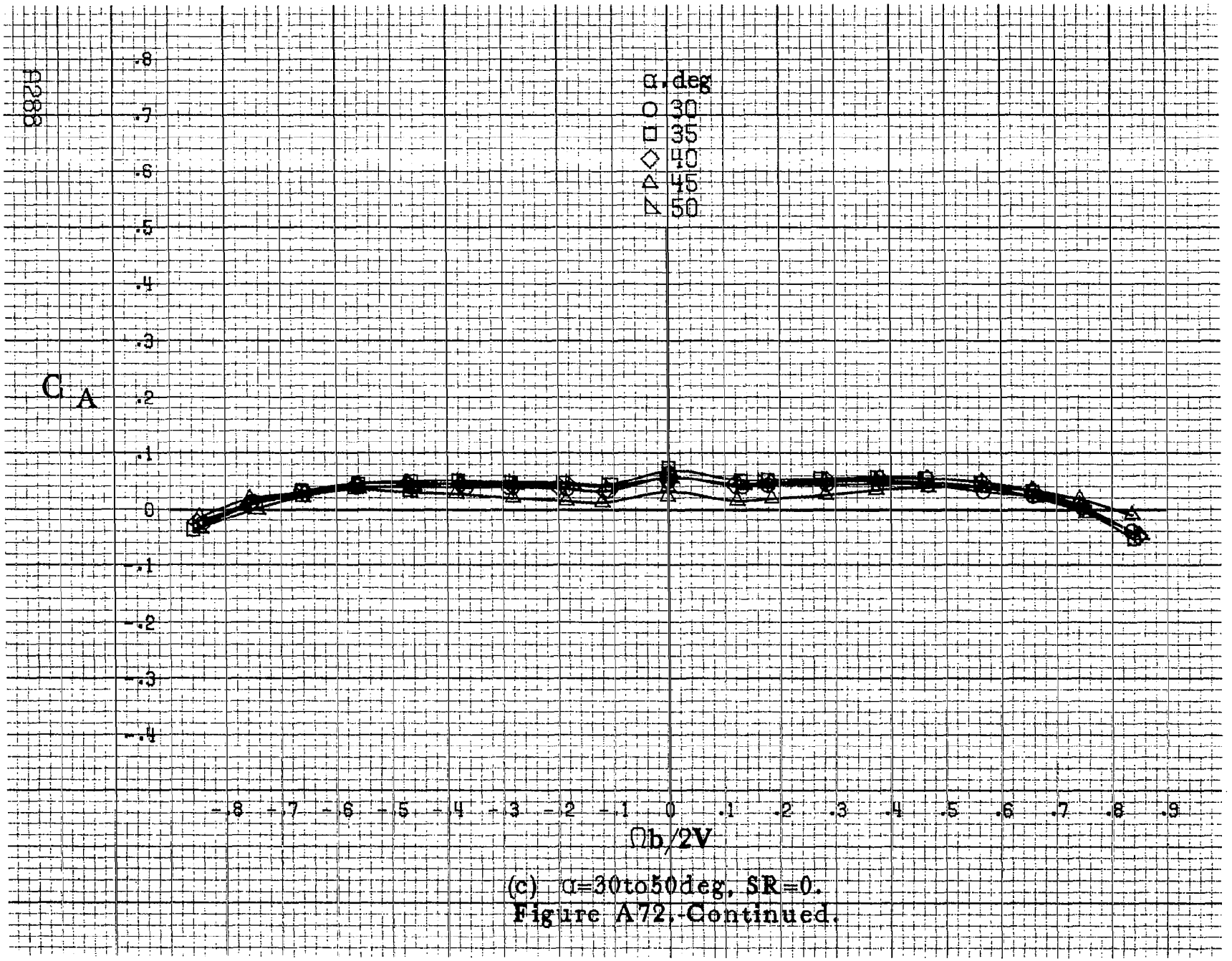

(c) α=30to50deg, SR=0.

Figure A72.-Continued.

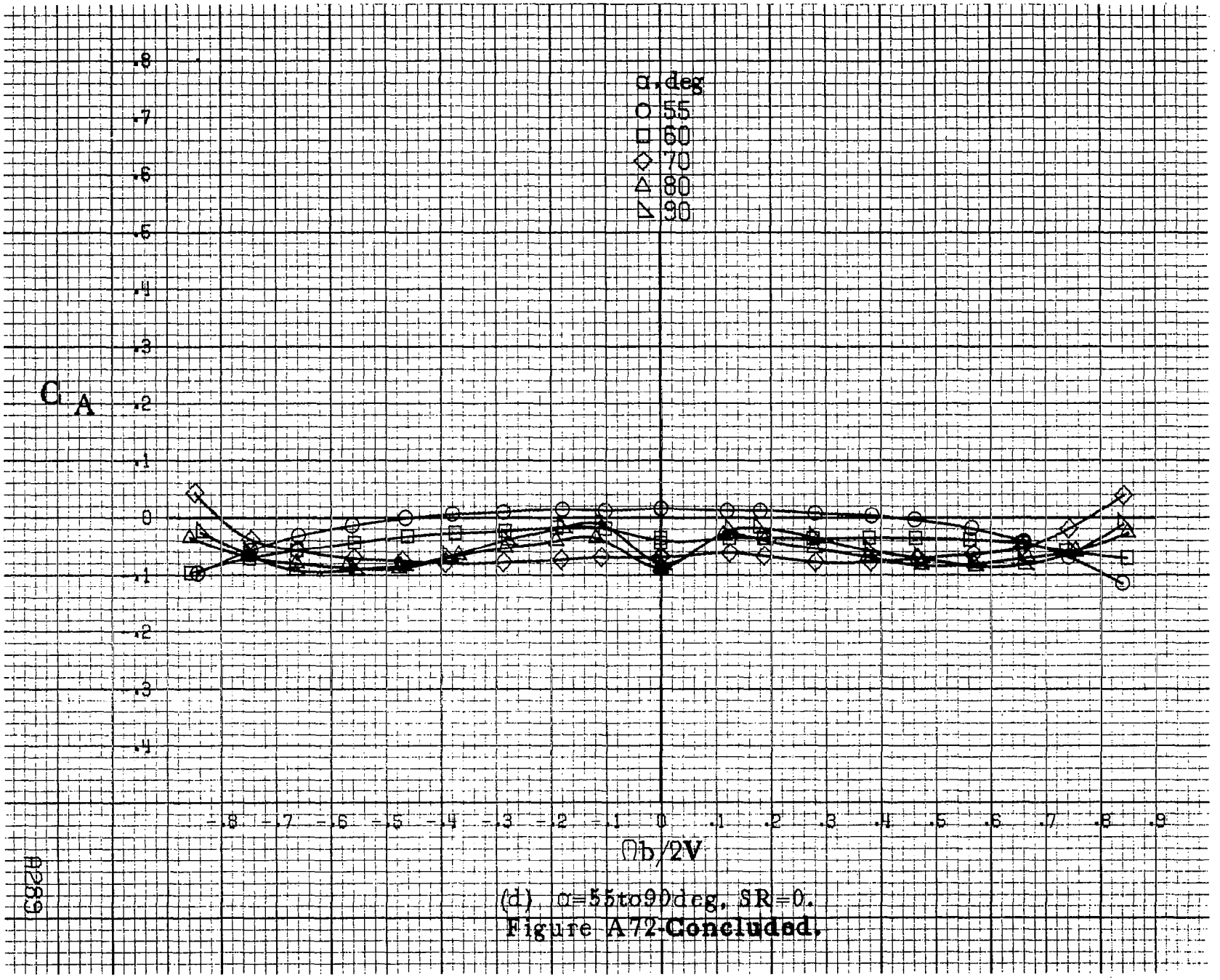

(d) α=55 to 90 deg, SR=0.

Figure A72-Concluded.

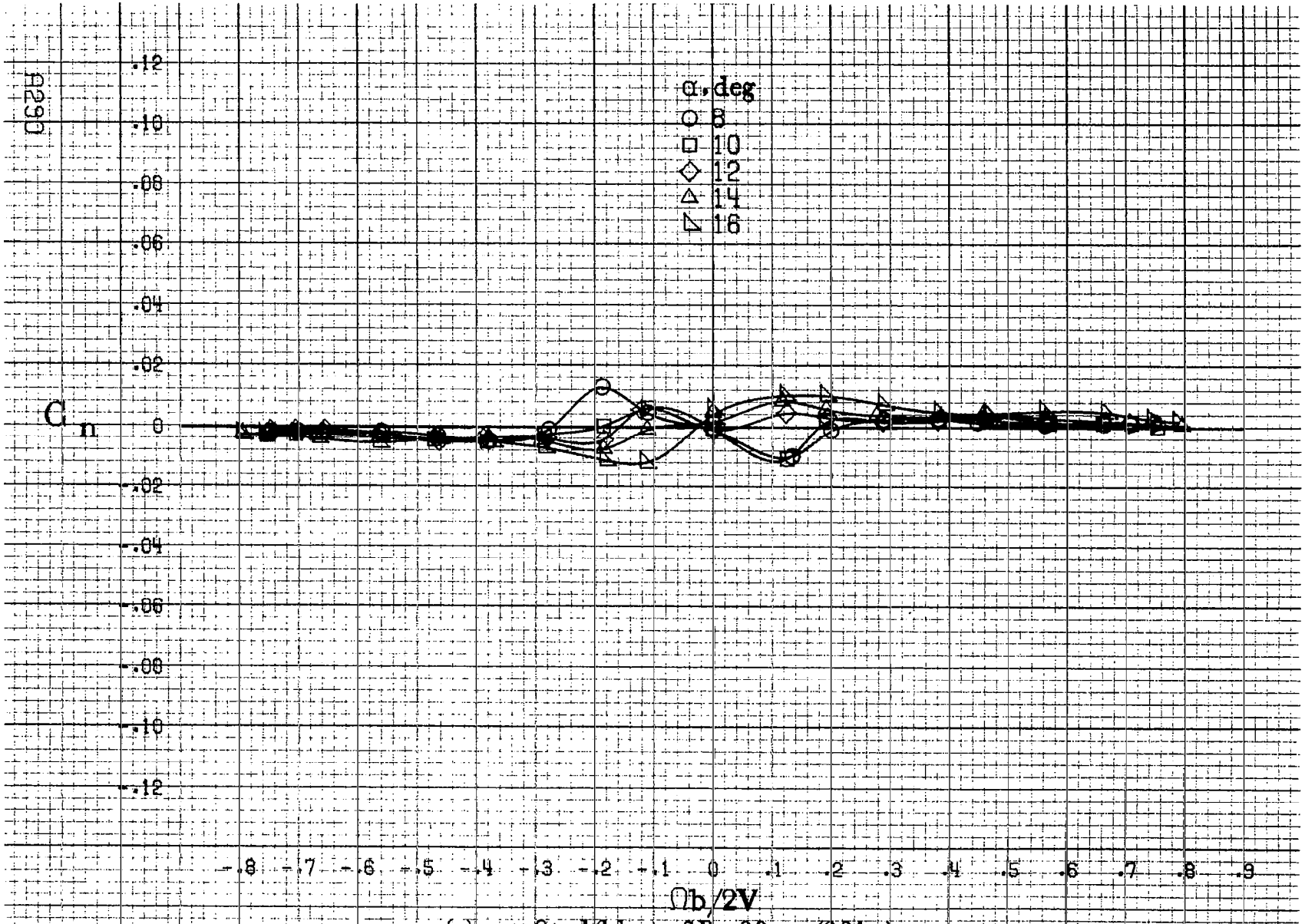

(a) α=8to16deg, SR=99cm(39in).

Figure A73. Effect of rotation rate and angle of attack on yawing-moment coefficient for no. 2 horizontal tail configuration with vertical tail off. $\delta_e = 0°$, $\delta_a = 0°$, $\delta_r = 0°$, $\beta = 0°$.

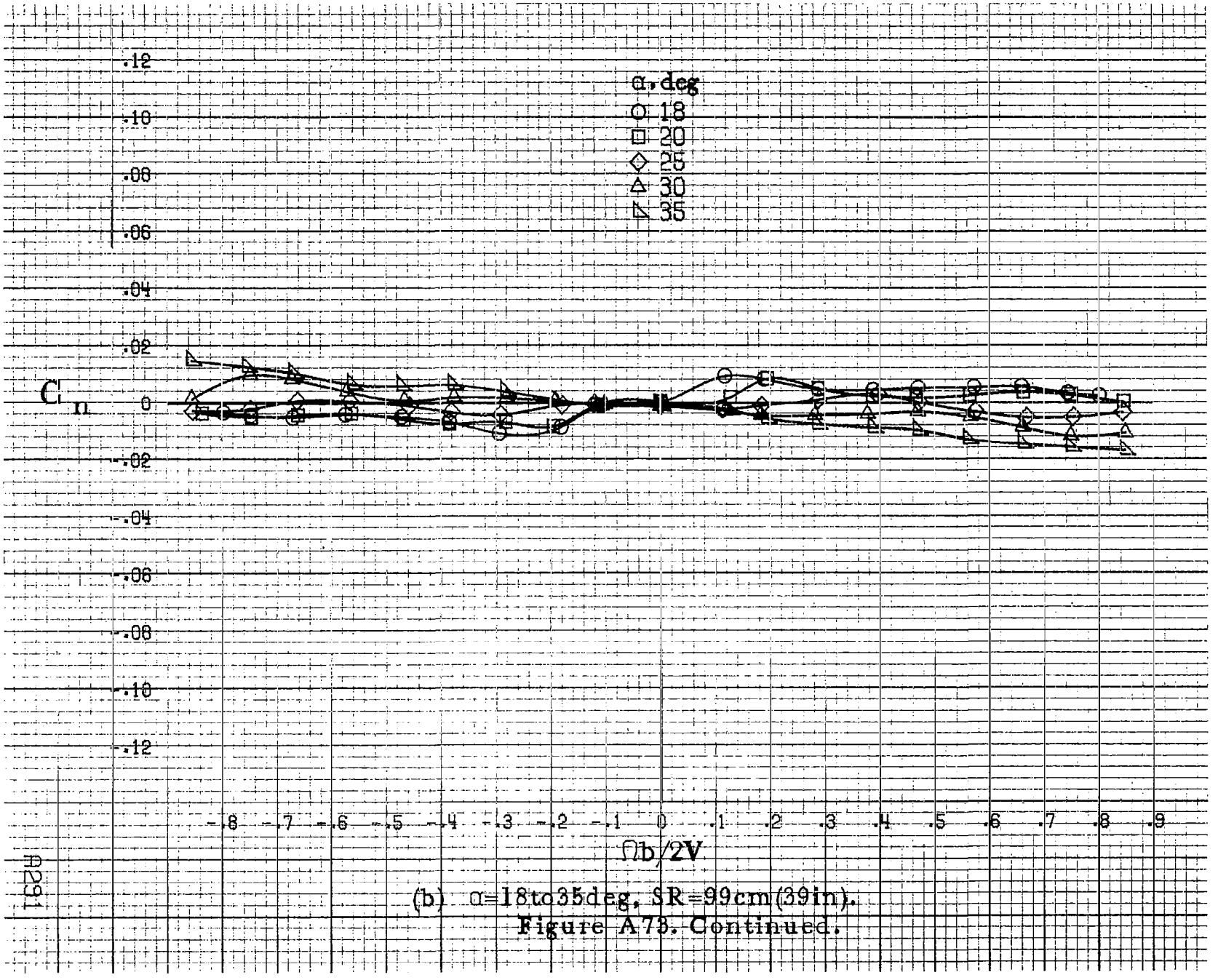

(b) α=18to35deg, SR=99cm(39in).

Figure A73. Continued.

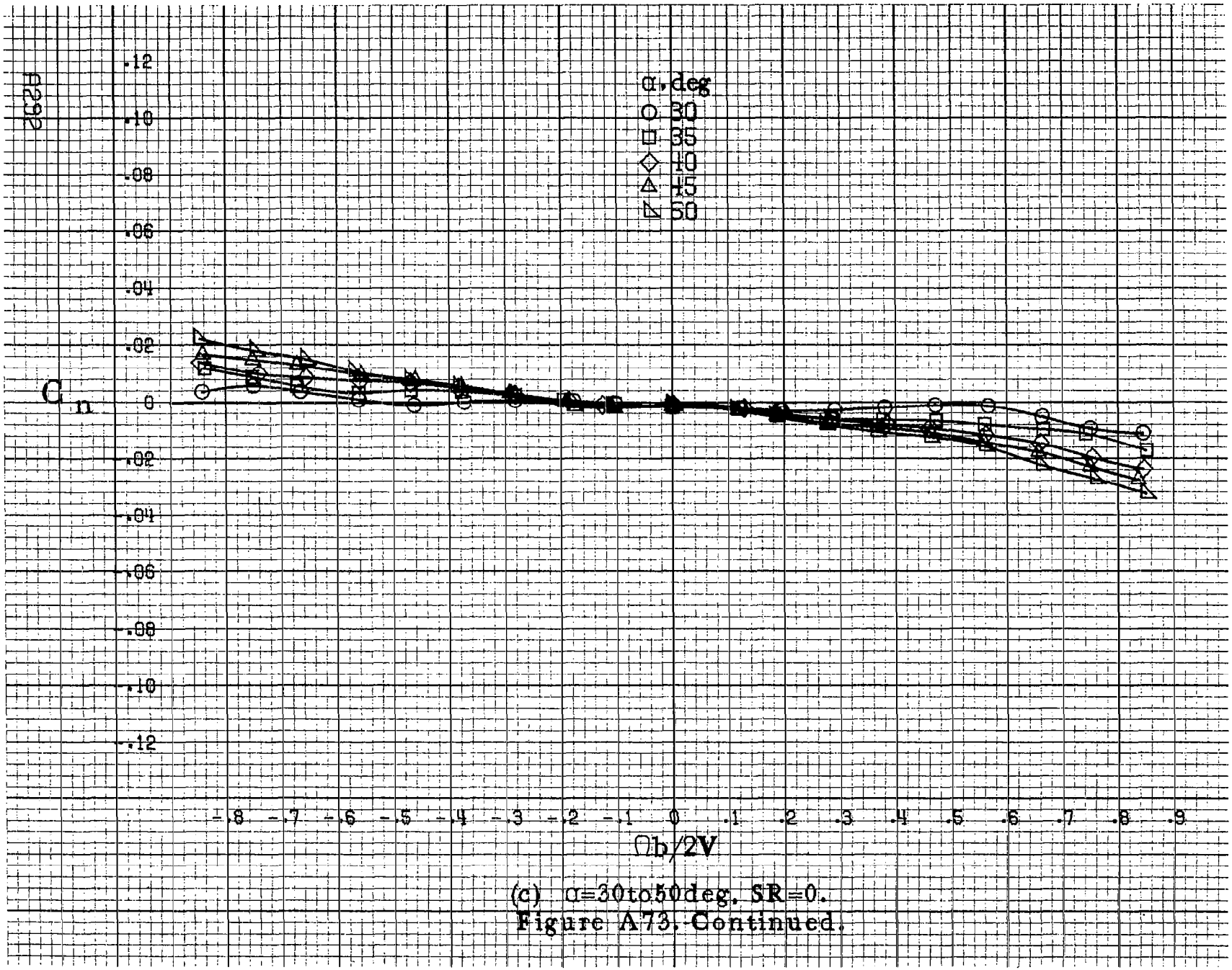

(c) α=30to50deg, SR=0.

Figure A73. Continued.

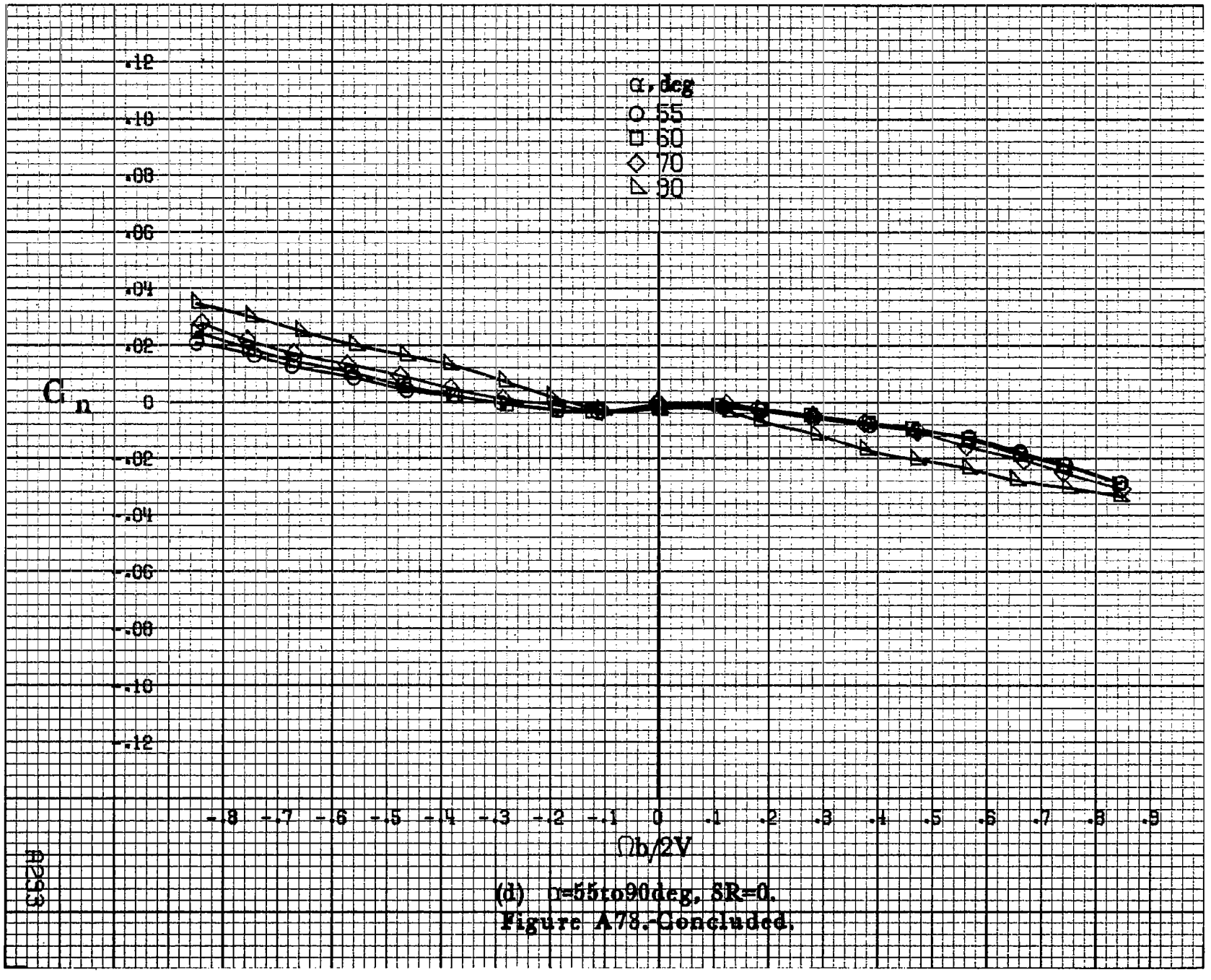

(d) α=55to90deg, δR=0.

Figure A78.-Concluded.

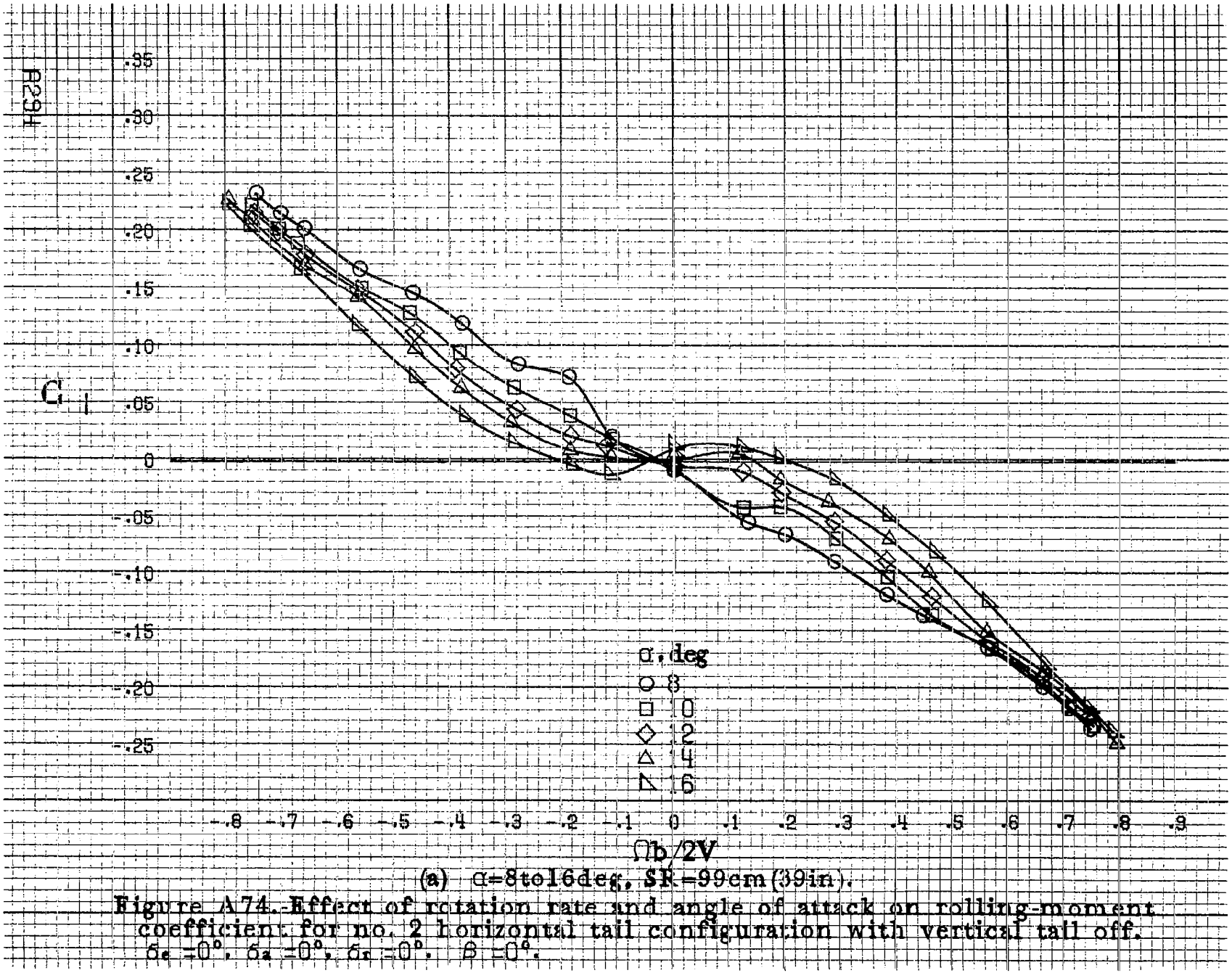

(a) α=8to16deg, SR=99cm(39in).

Figure A74.-Effect of rotation rate and angle of attack on rolling-moment coefficient for no. 2 horizontal tail configuration with vertical tail off. $\delta_e = 0°$, $\delta_a = 0°$, $\delta_r = 0°$, $\beta = 0°$.

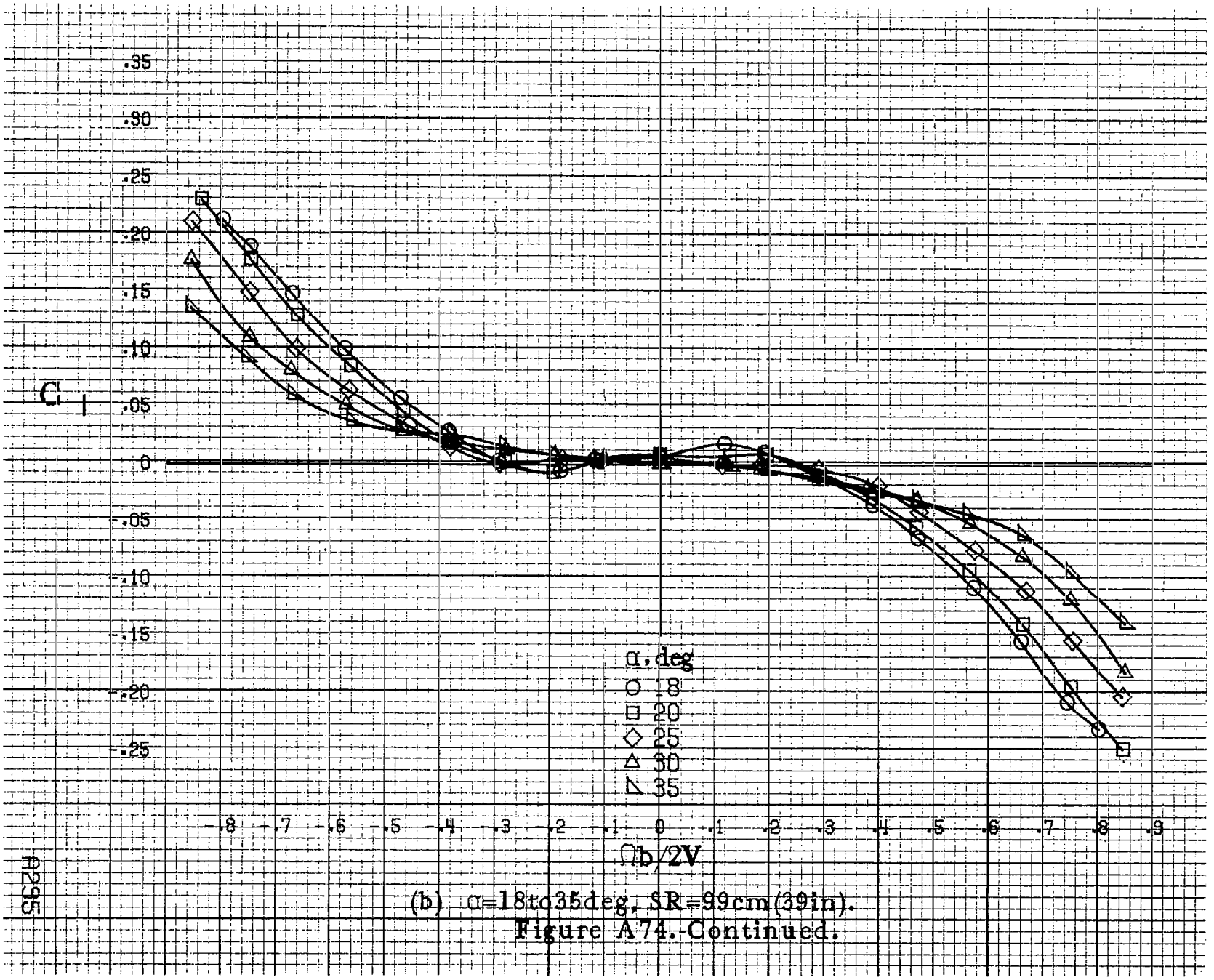

(b) α=18to35deg, SR=99cm(39in).

Figure A74.-Continued.

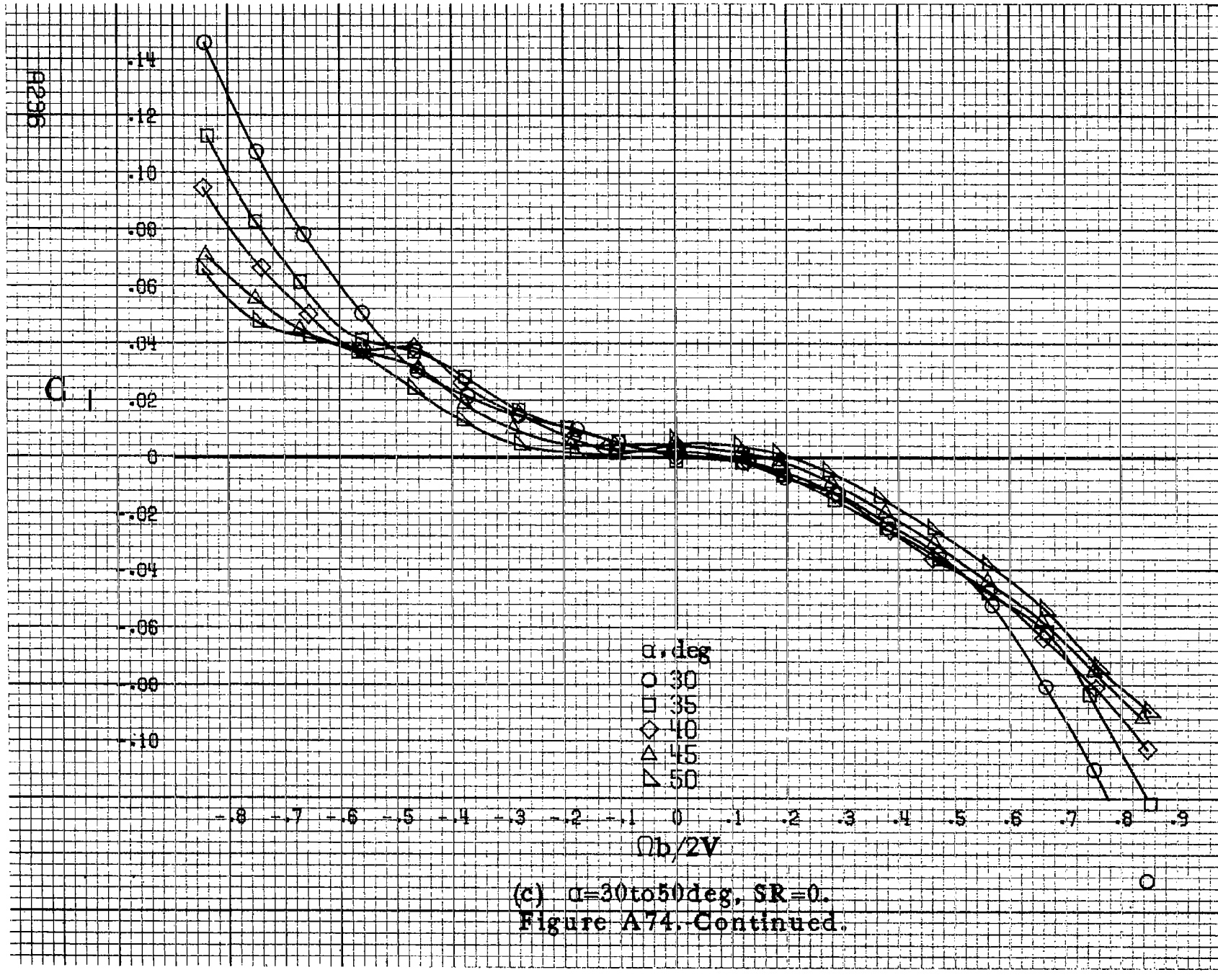

(c) α=30to50deg, SR=0.

Figure A74.-Continued.

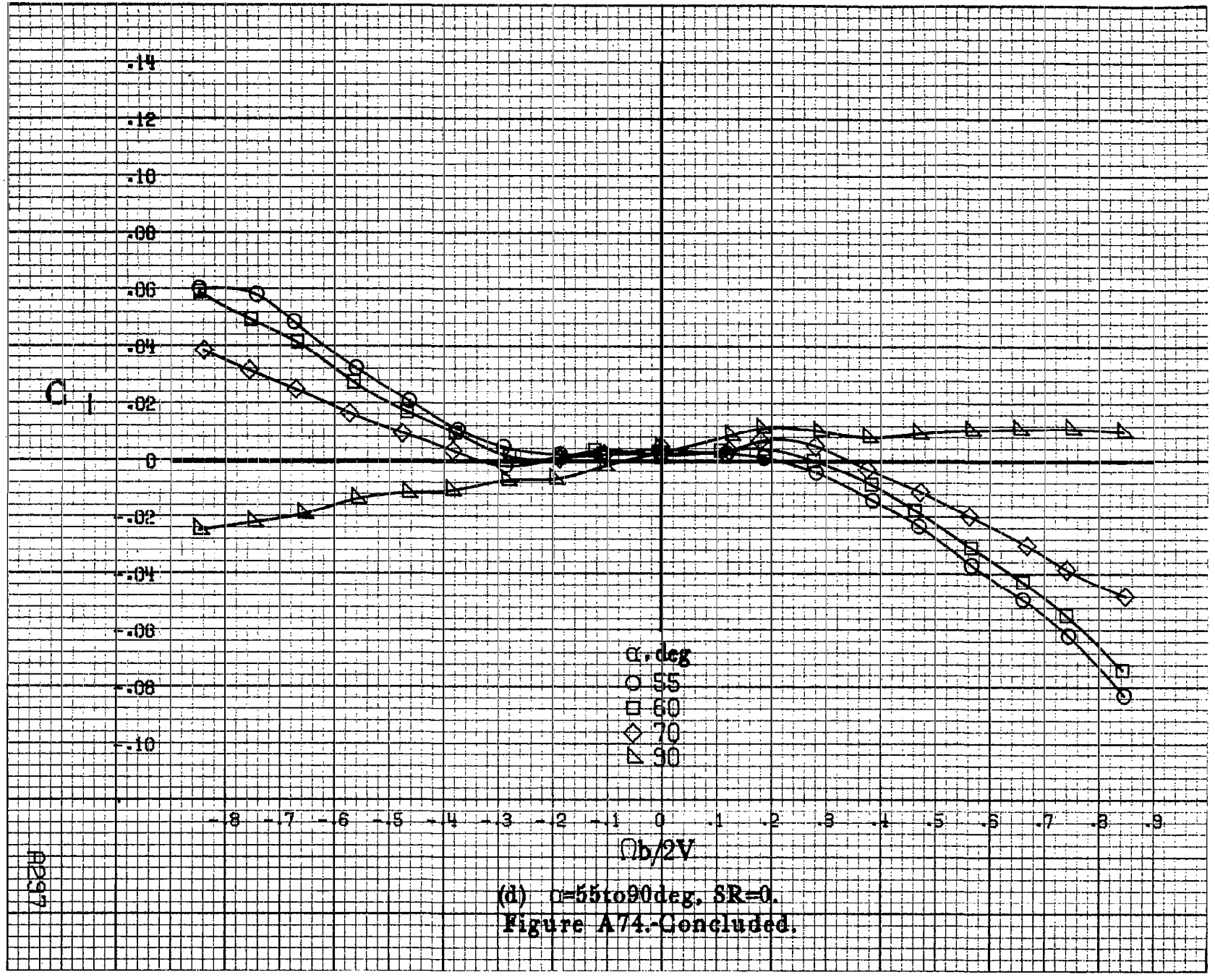

(d) α=55to90deg, SR=0.

Figure A74.-Concluded.

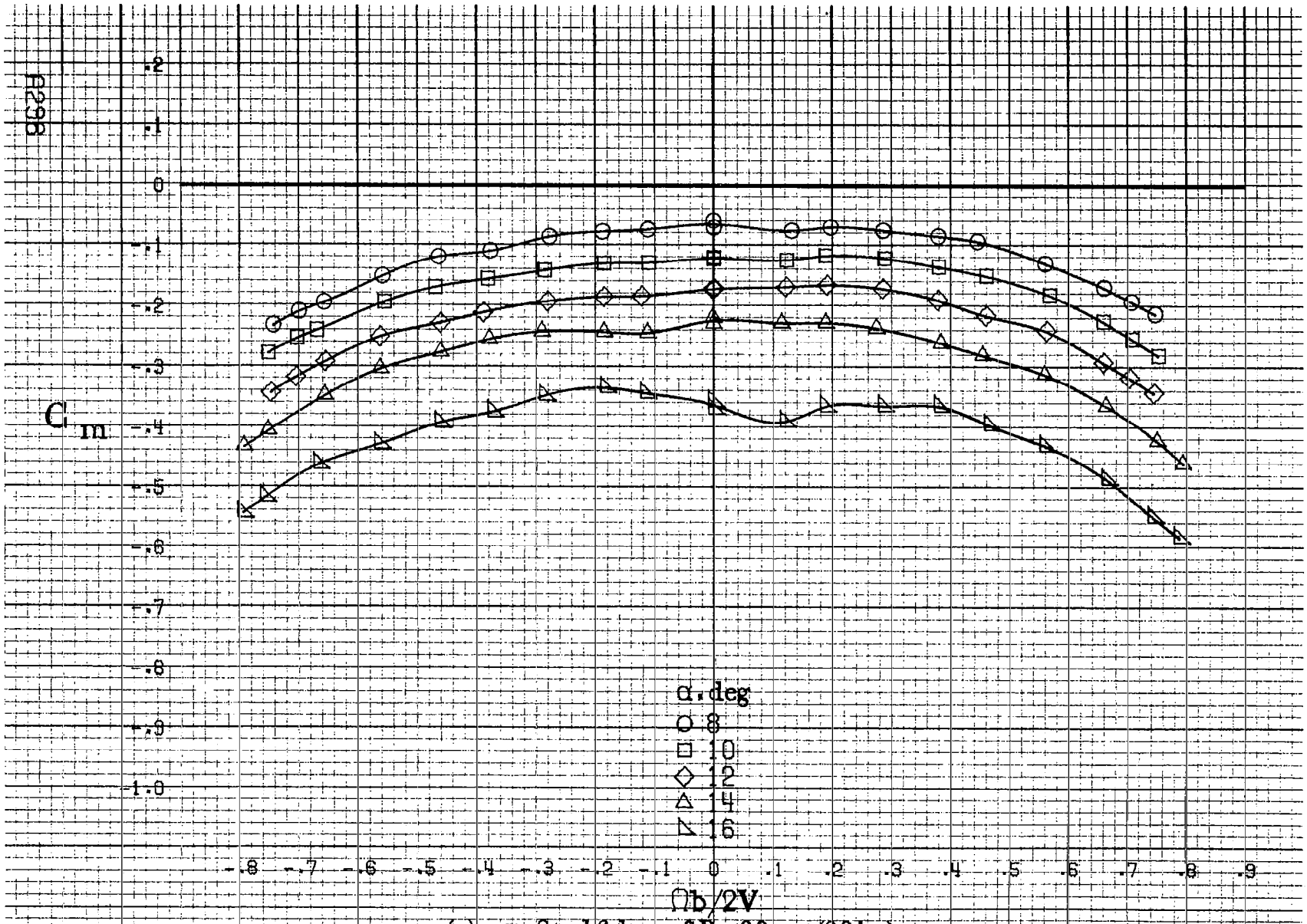

(a) α=8to16deg, $R=99cm(39in).

Figure A75.-Effect of rotation rate and angle of attack on pitching-moment coefficient for no. 2 horizontal tail configuration with vertical tail off. $\delta_e = 0°$, $\delta_a = 0°$, $\delta_r = 0°$, $\beta = 0°$.

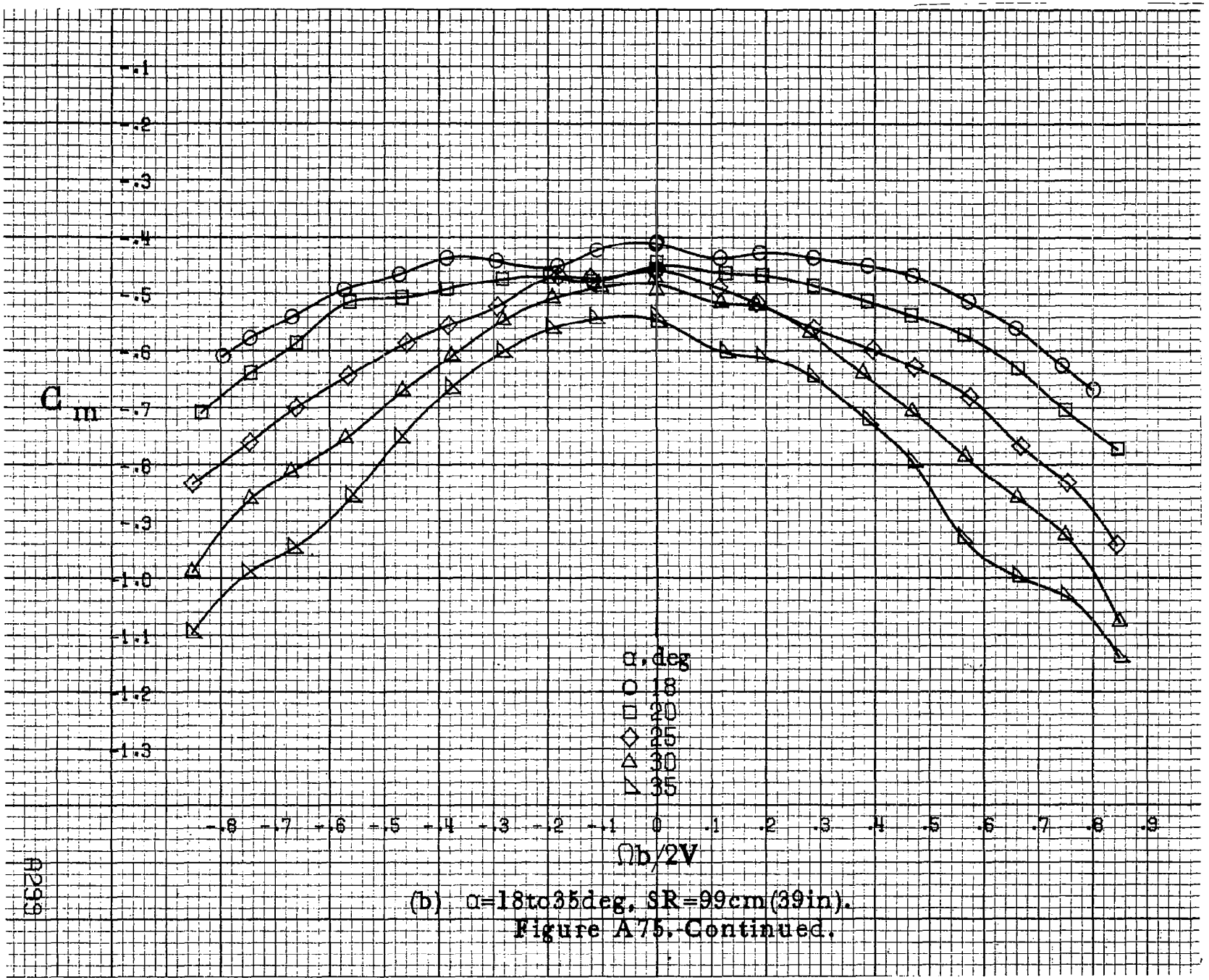

(b) α=18to35deg, SR=99cm(39in).

Figure A75.-Continued.

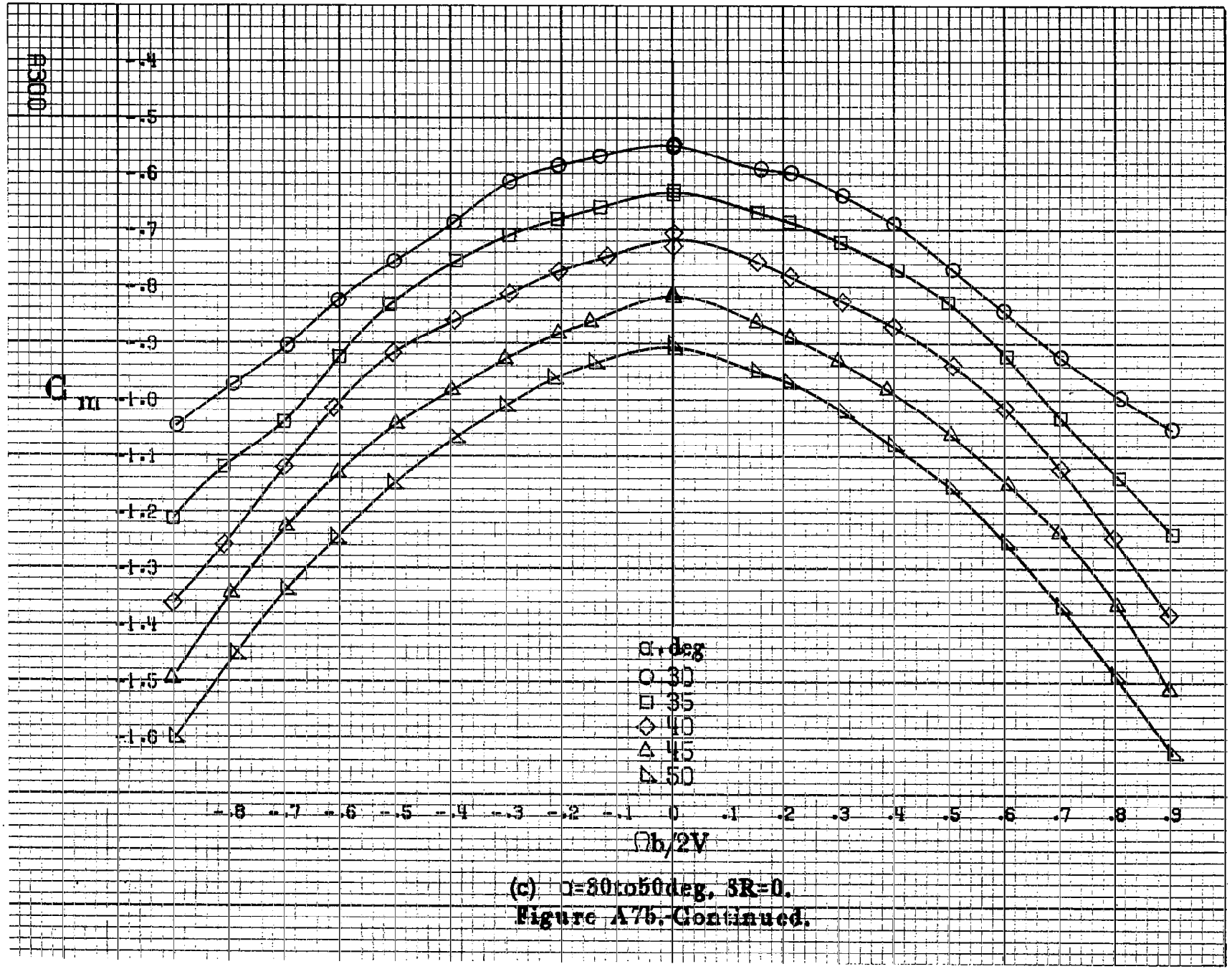

(c) Λ=30 to 50 deg, δR=0.

Figure A75.-Continued.

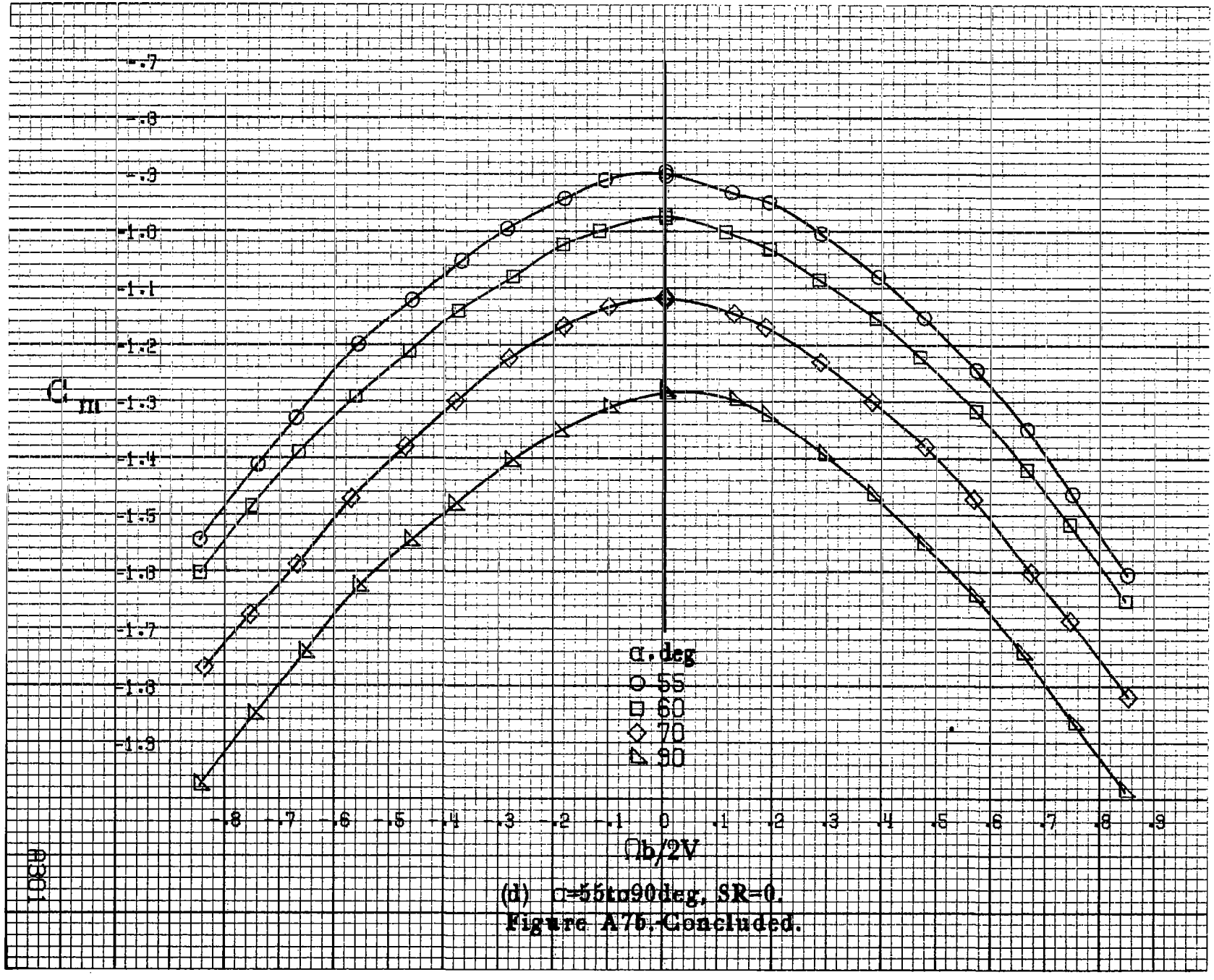

(d) α=55to90deg, SR=0.

Figure A76.-Concluded.

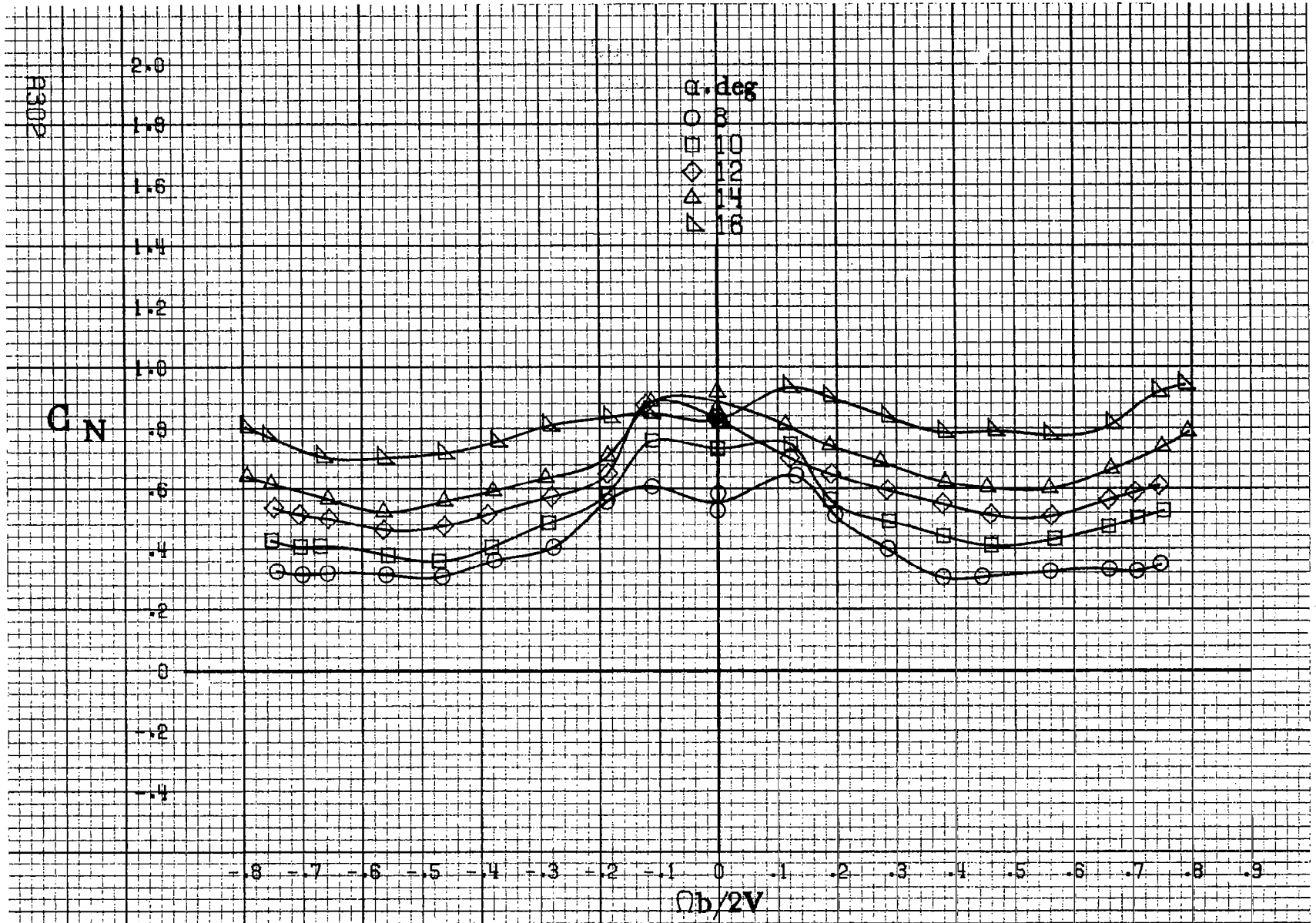

(a) α=8to16deg, SR=99cm(39in).

Figure A76.-Effect of rotation rate and angle of attack on normal-force coefficient for no. 2 horizontal tail configuration with vertical tail off. $\delta_e = 0°$, $\delta_a = 0°$, $\delta_r = 0°$, $\beta = 0°$.

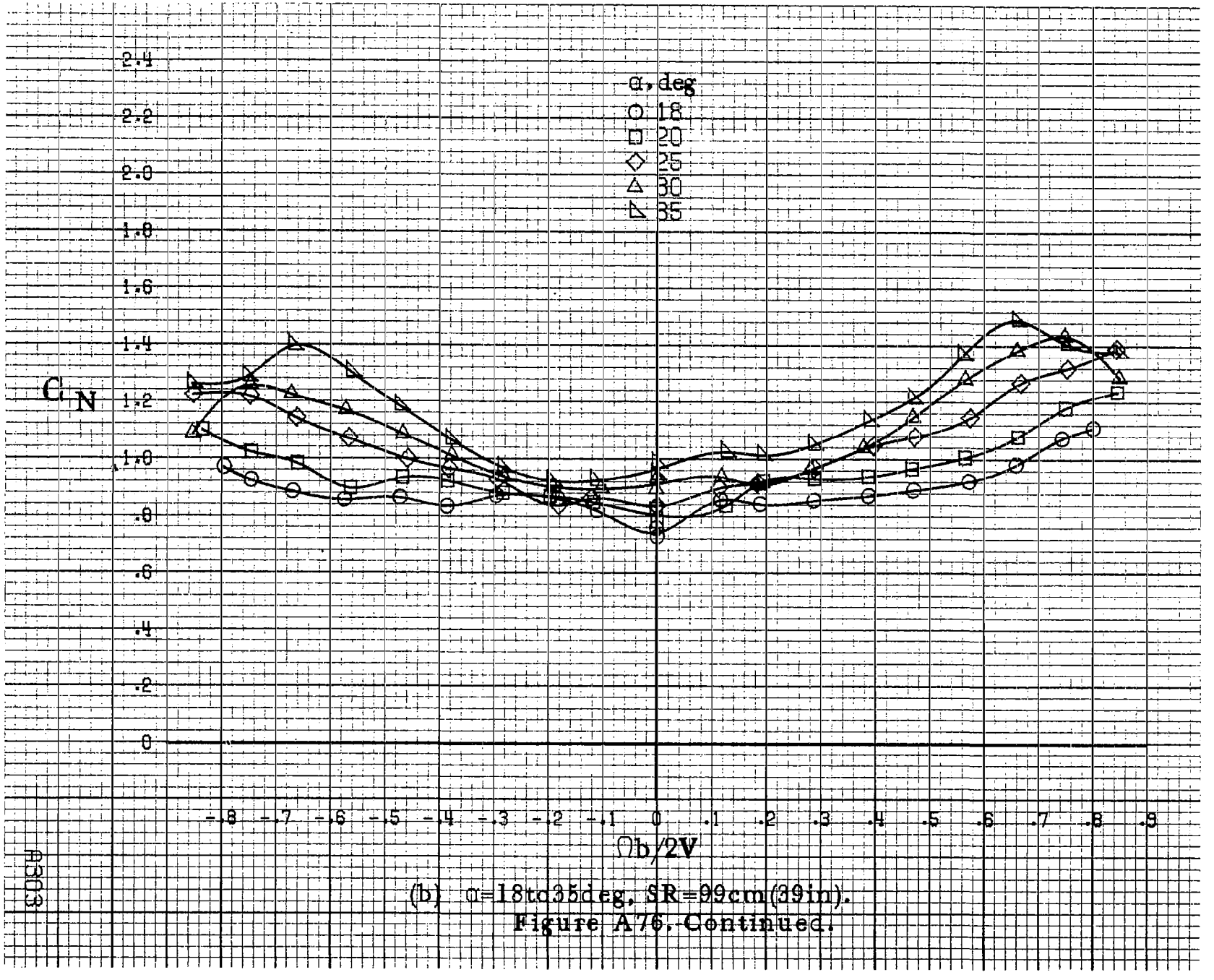

(b) α=18 to 35 deg, SR=99cm(39in).

Figure A76. Continued.

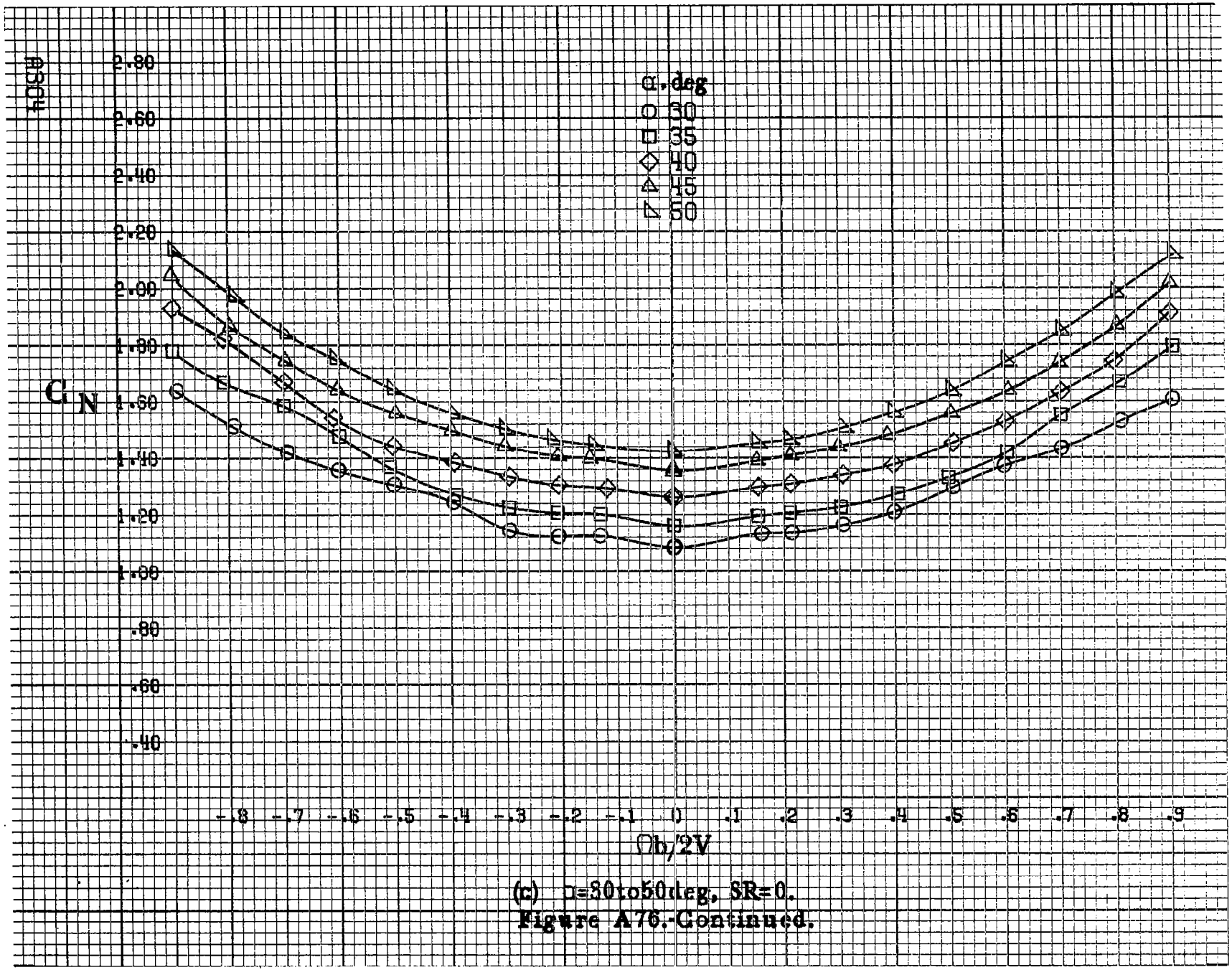

(c) α=30to50deg, SR=0.

Figure A76.-Continued.

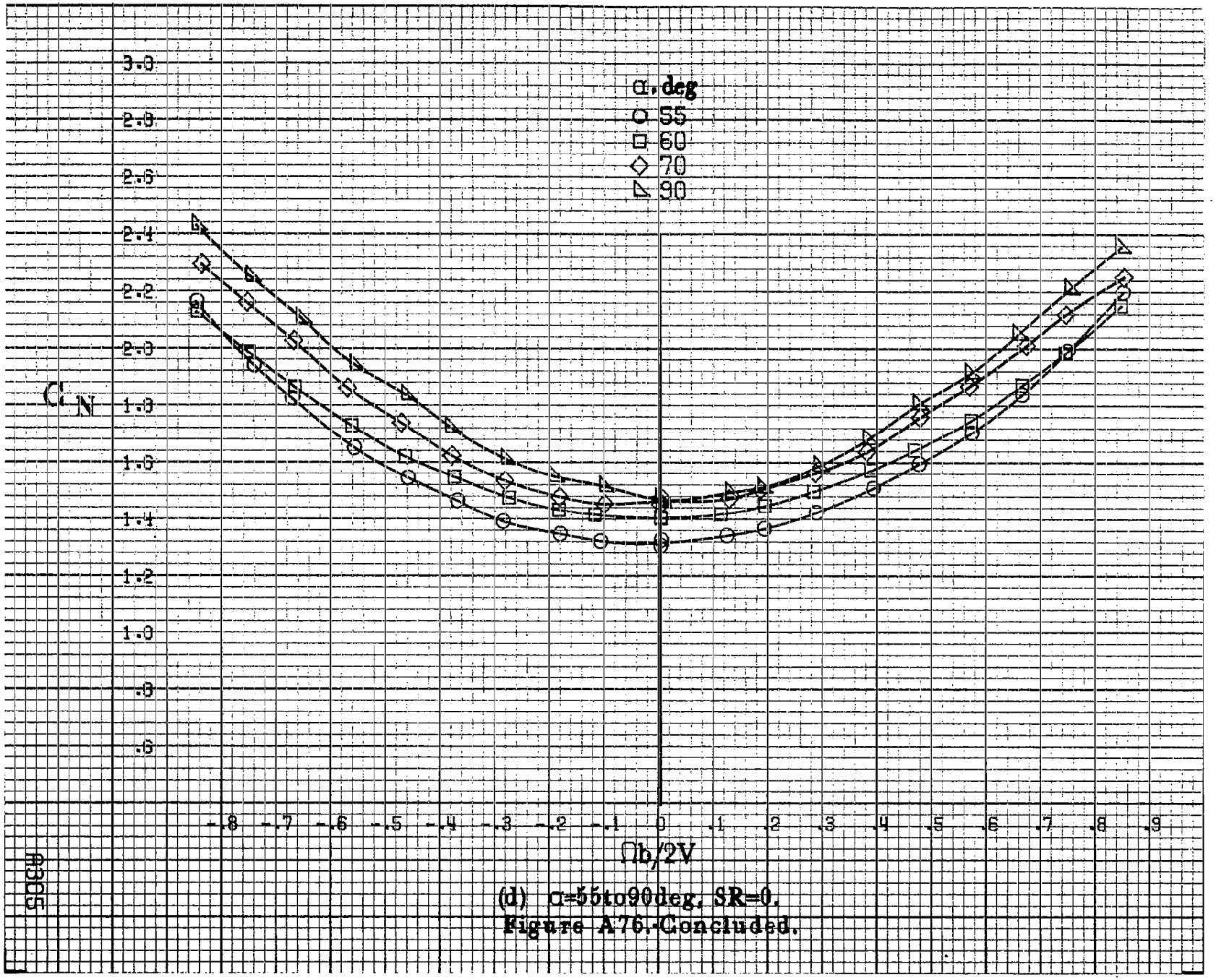

(d) α=55to90deg, SR=0.

Figure A76.-Concluded.

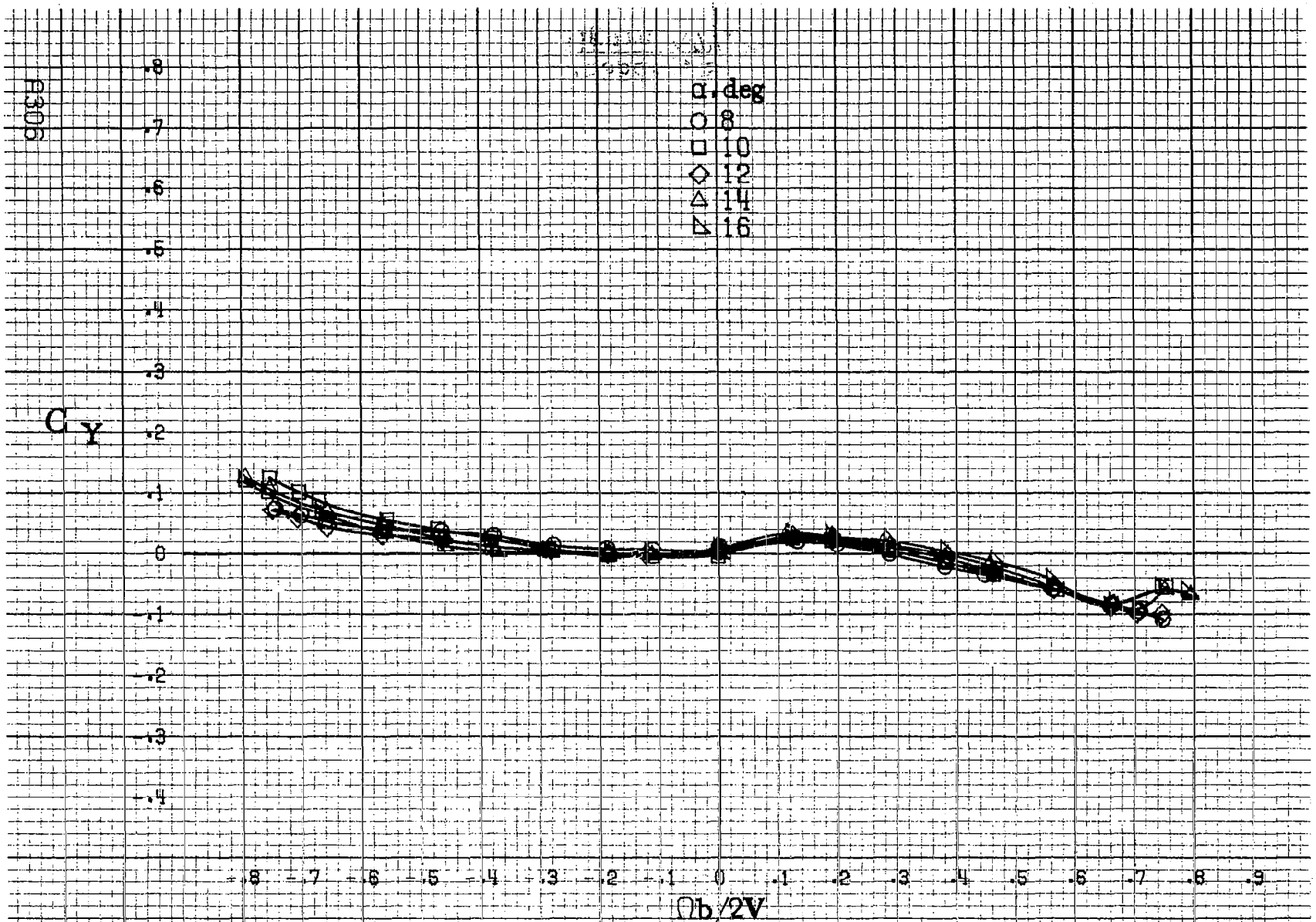

(a) α=8to16deg, SR=99cm(39in).

Figure A77.-Effect of rotation rate and angle of attack on side-force coefficient for no. 2 horizontal tail configuration with vertical tail off. $\delta_e = 0°$, $\delta_a = 0°$, $\delta_r = 0°$, $\beta = 0°$.

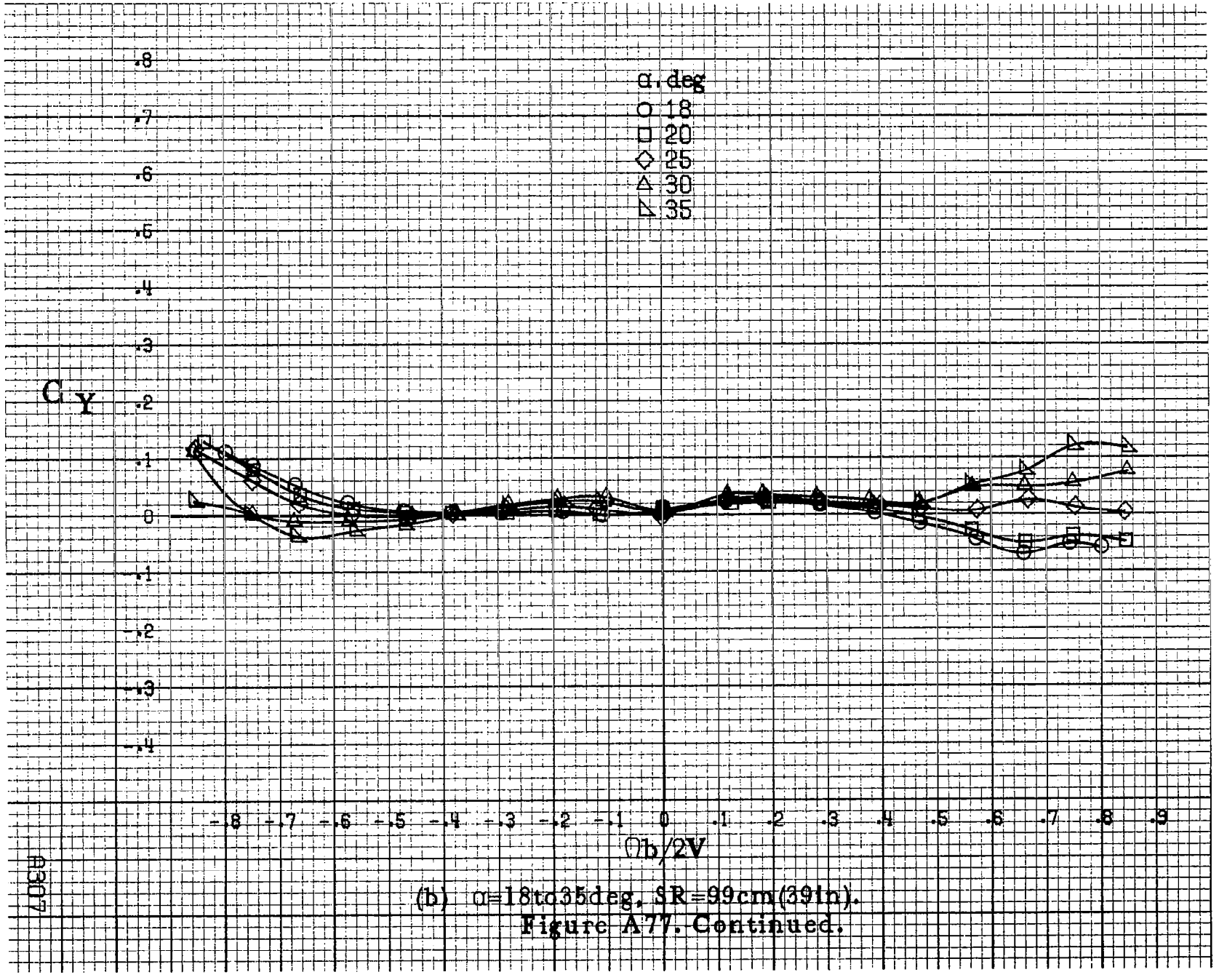

(b) α=18to35deg, SR=99cm(39in).

Figure A77. Continued.

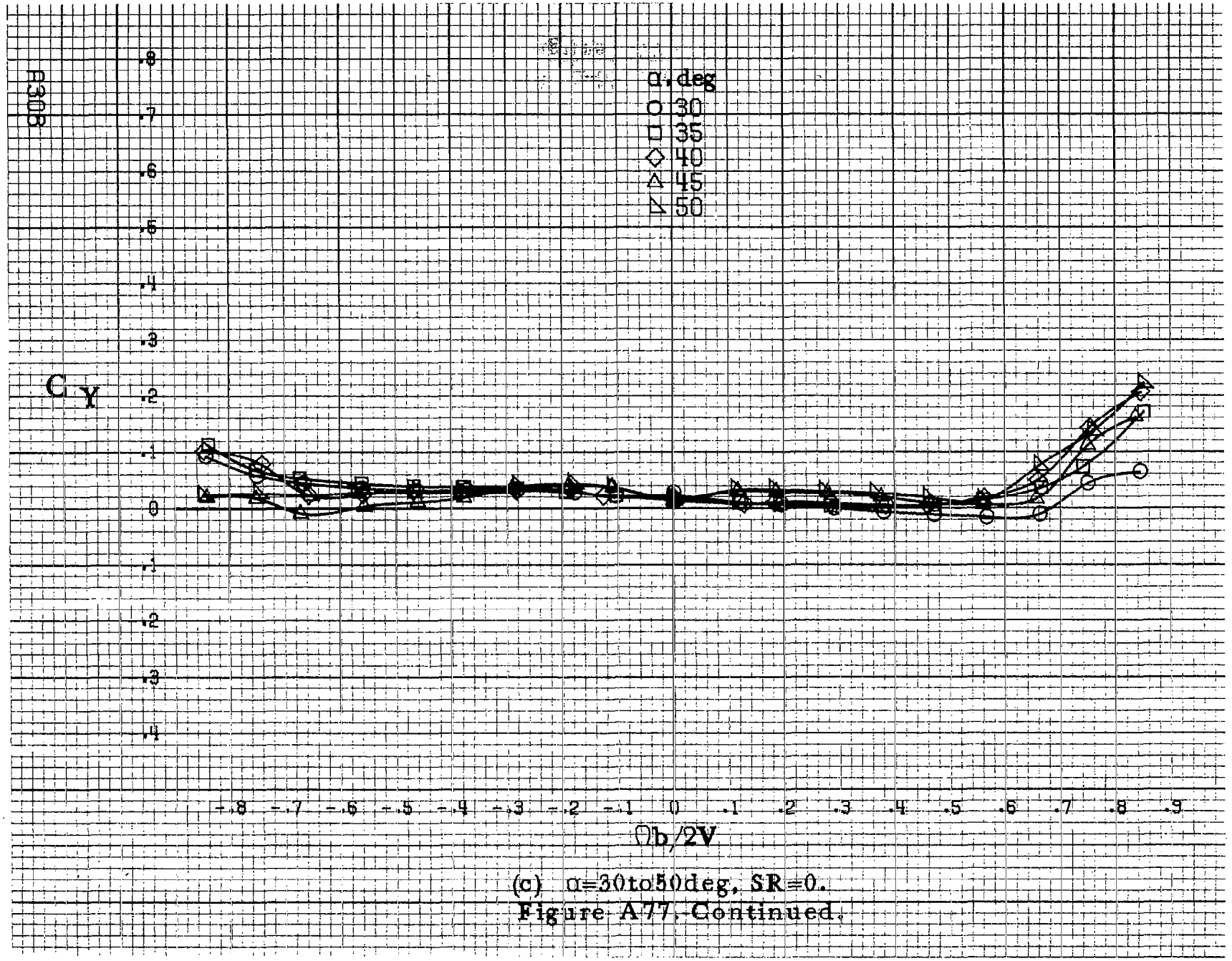

(c) α=30to50deg, SR=0.

Figure A77.-Continued.

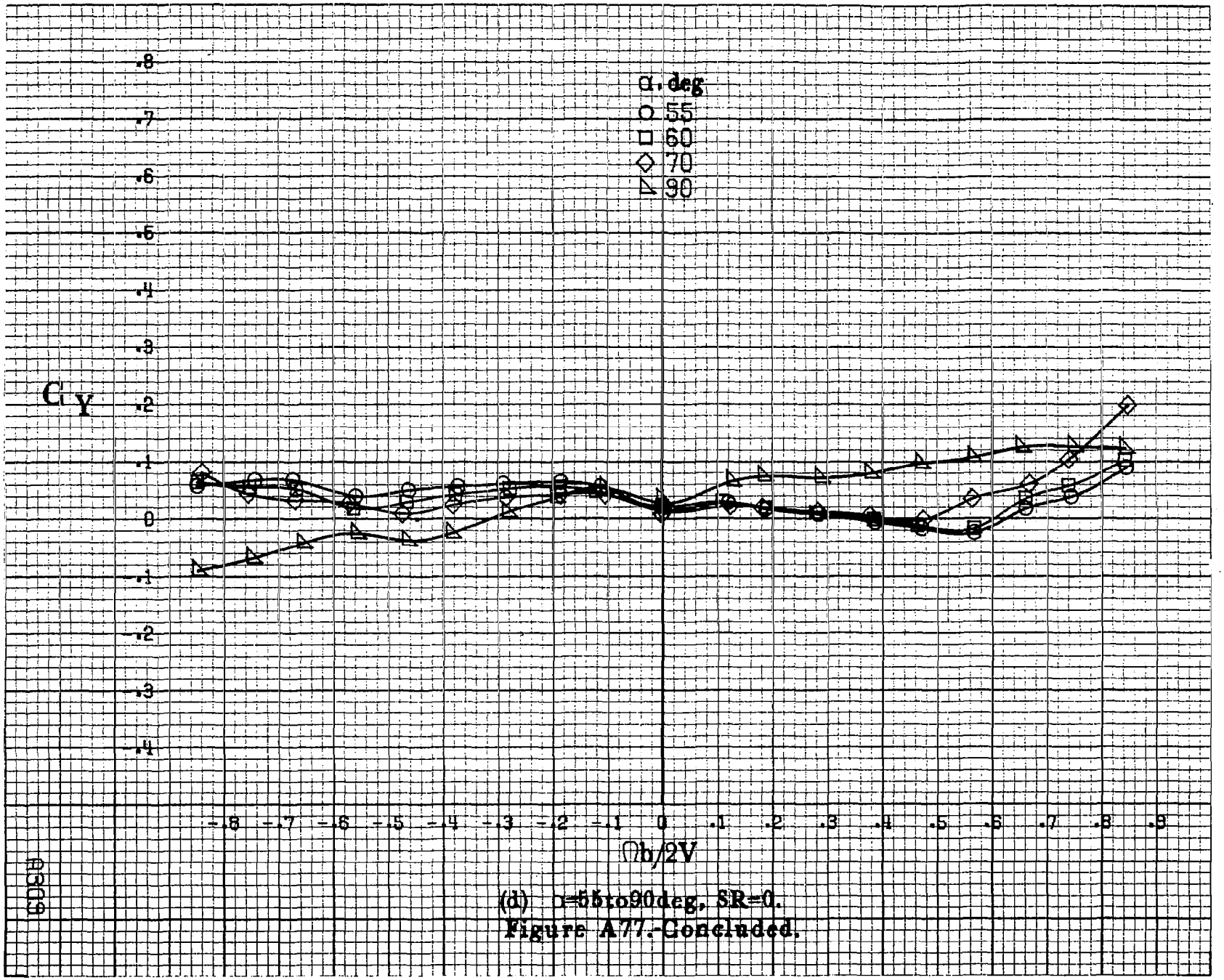

(d) α=55to90deg, SR=0.

Figure A77.-Concluded.

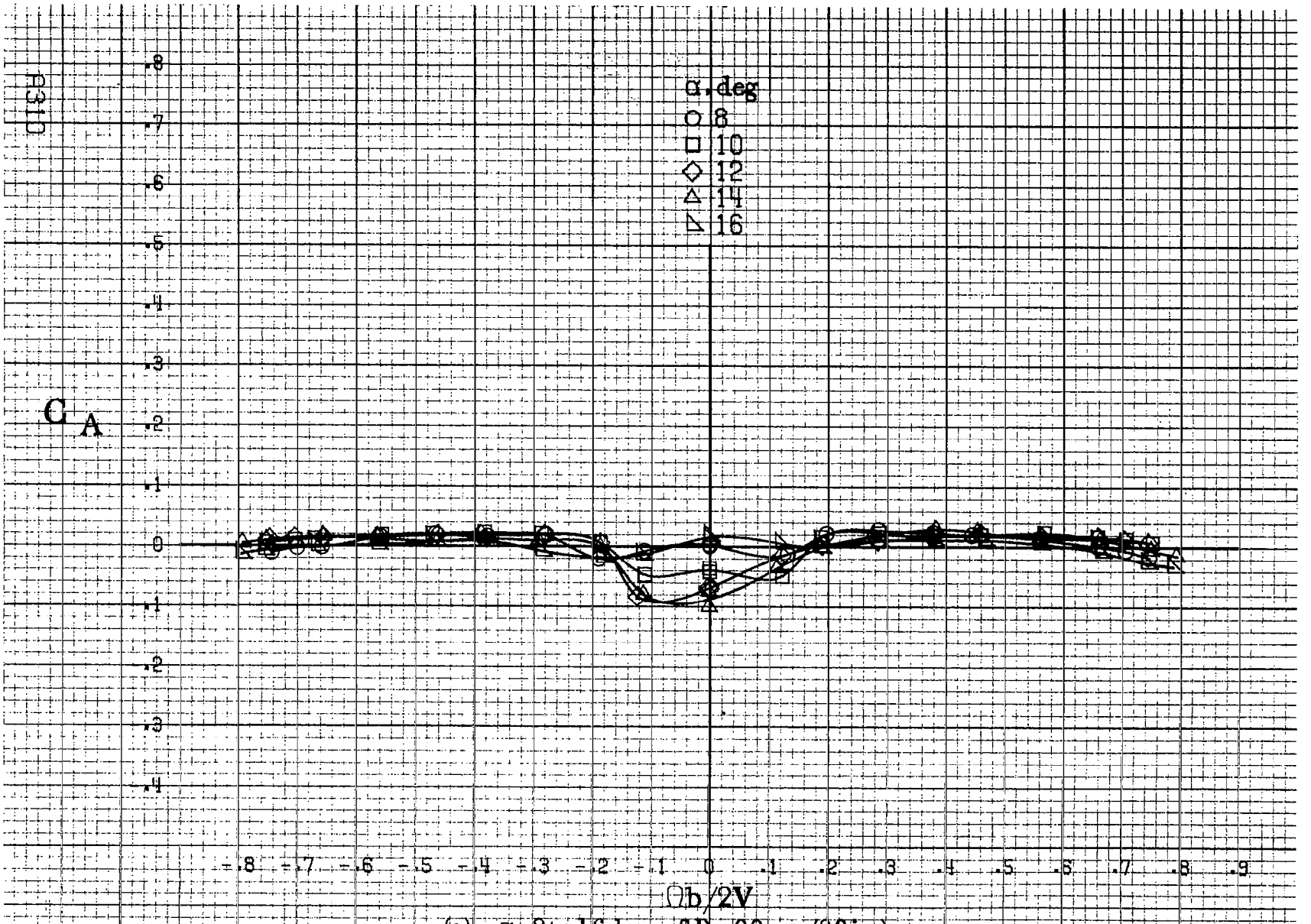

(a) α=8to16deg, SR=99cm(39in).

Figure A78.-Effect of rotation rate and angle of attack on axial-force coefficient for no. 2 horizontal tail configuration with vertical tail off. $\delta_e = 0°$, $\delta_a = 0°$, $\delta_r = 0°$, $\beta = 0°$.

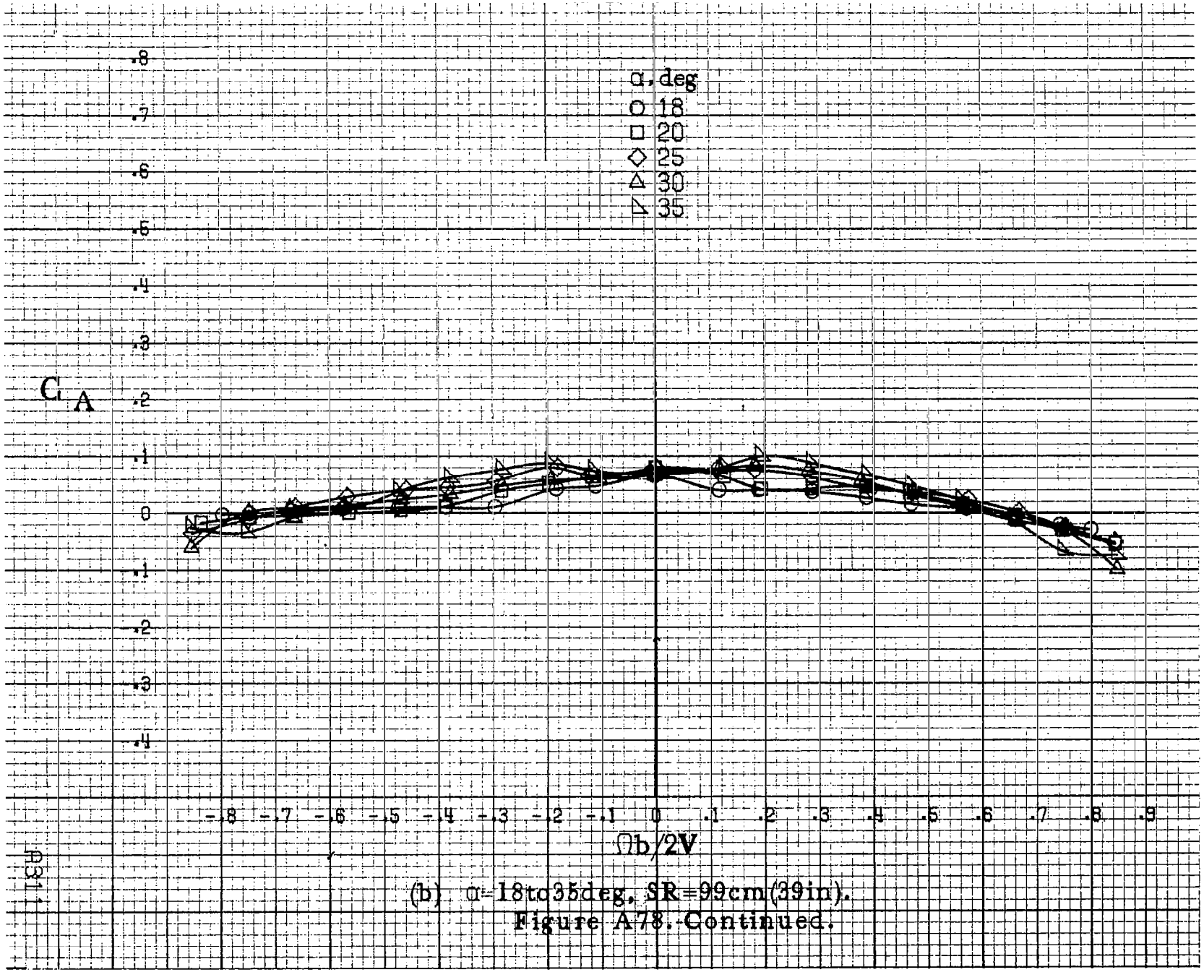

(b) α=18to35deg, SR=99cm(39in).

Figure A78.-Continued.

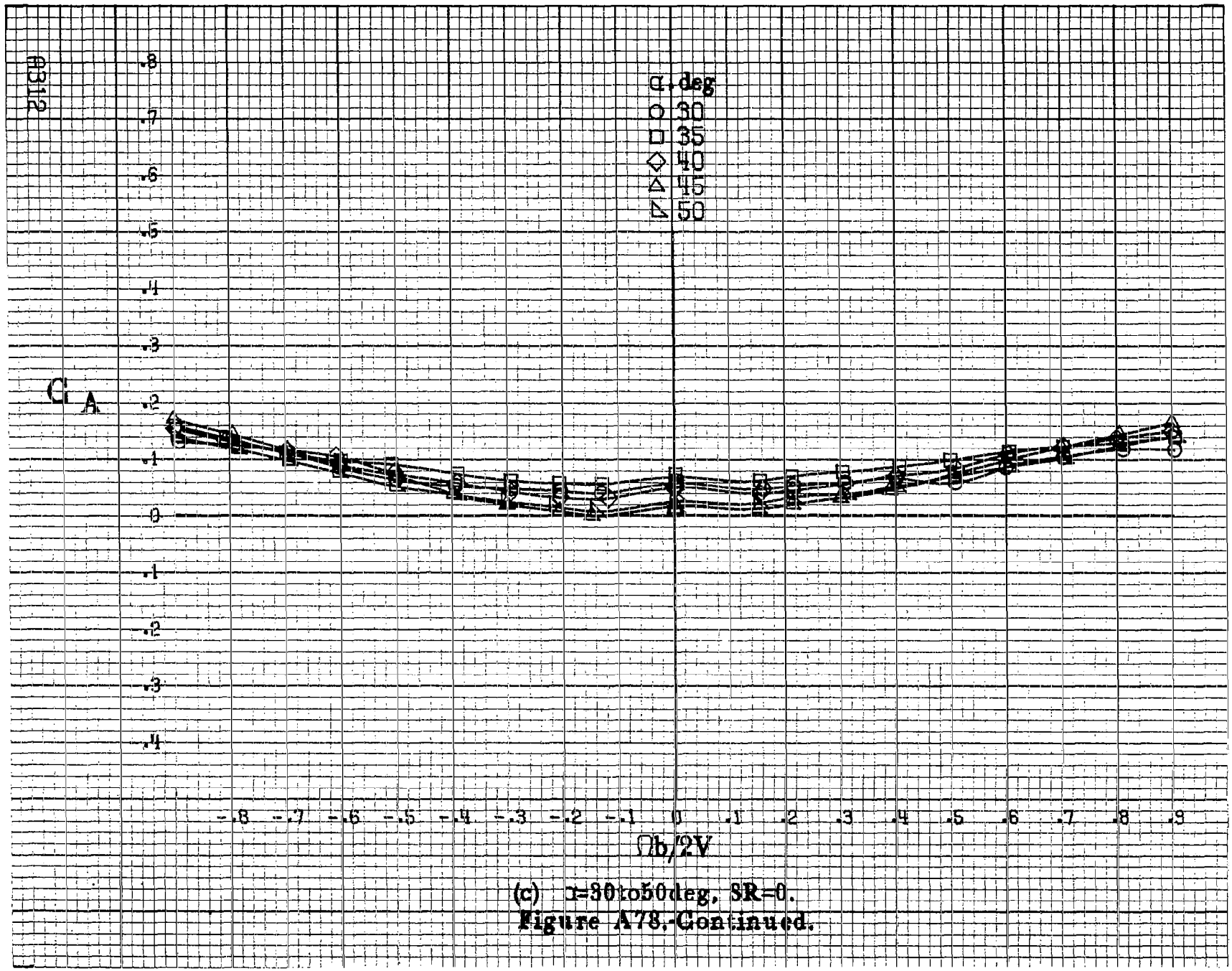

(c) α=30 to 50 deg, SR=0.

Figure A78.-Continued.

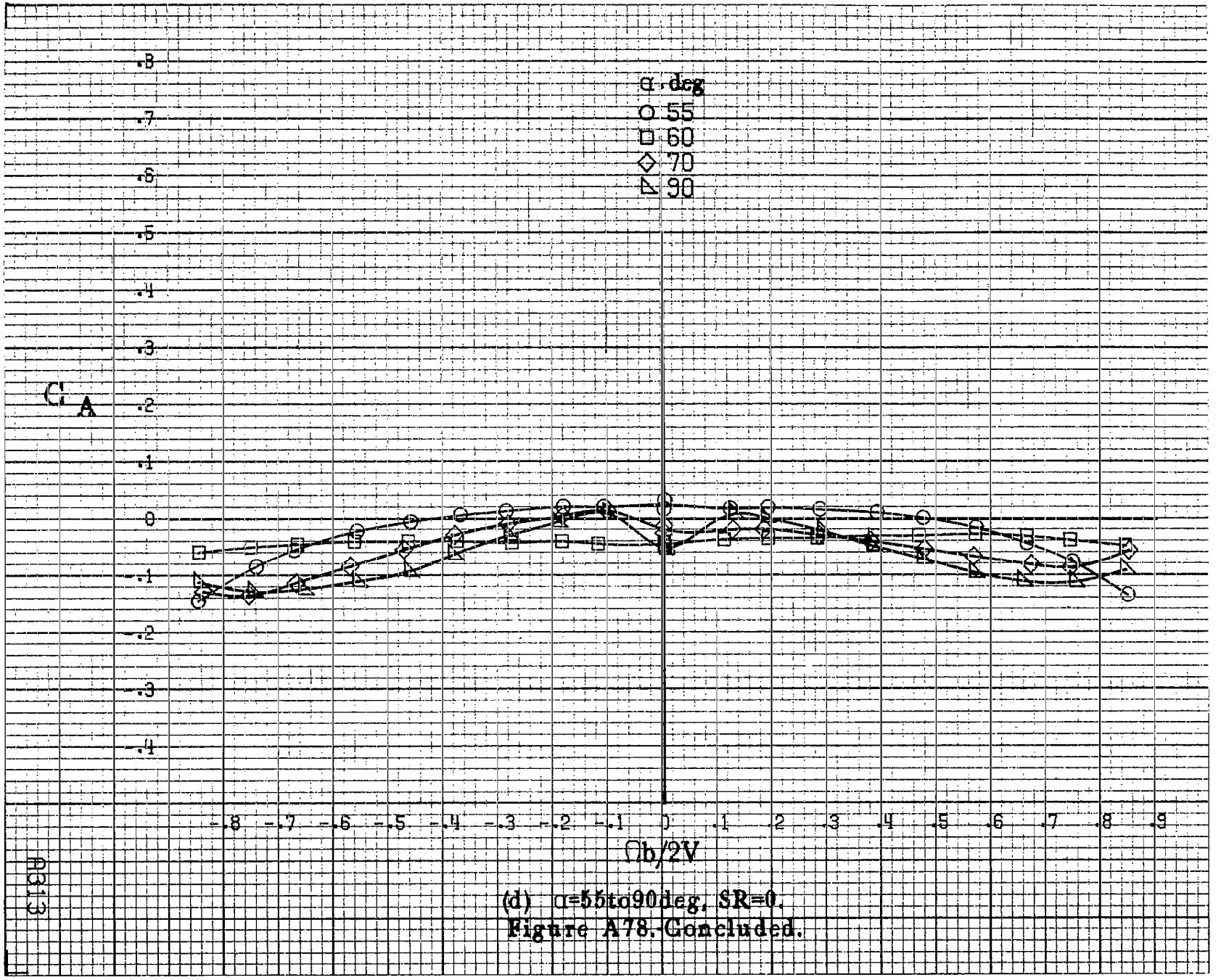

(d) α=55to90deg, SR=0.

Figure A78. Concluded.

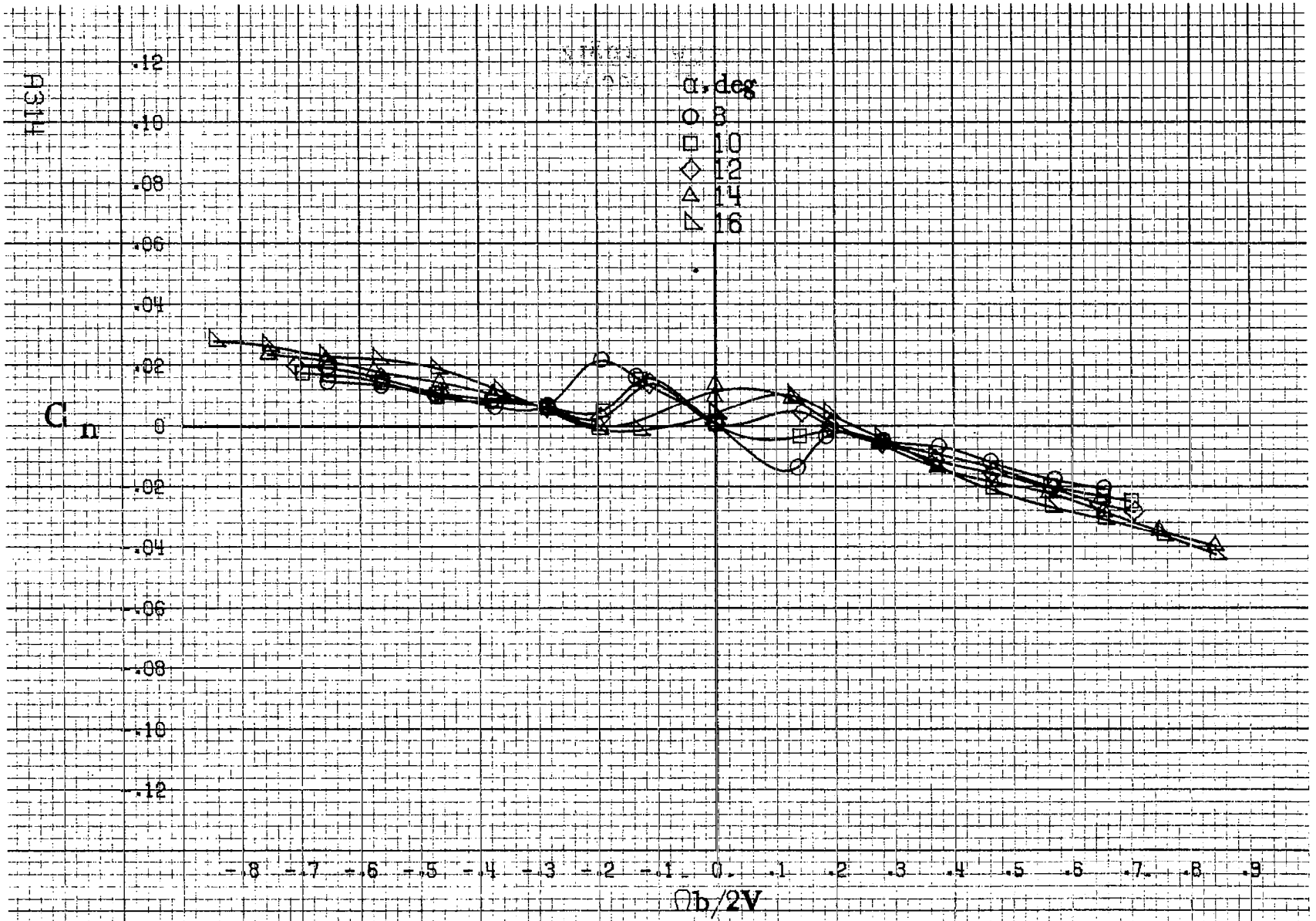

(a) α=8to16deg, SR=99cm(39in).

Figure A79.-Effect of rotation rate and angle of attack on yawing-moment coefficient for configuration having sharp-edged fuselage bottom aft of wing TE. $\delta_e = 0^\circ$, $\delta_a = 0^\circ$, $\delta_r = 0^\circ$, $\beta = 0^\circ$.

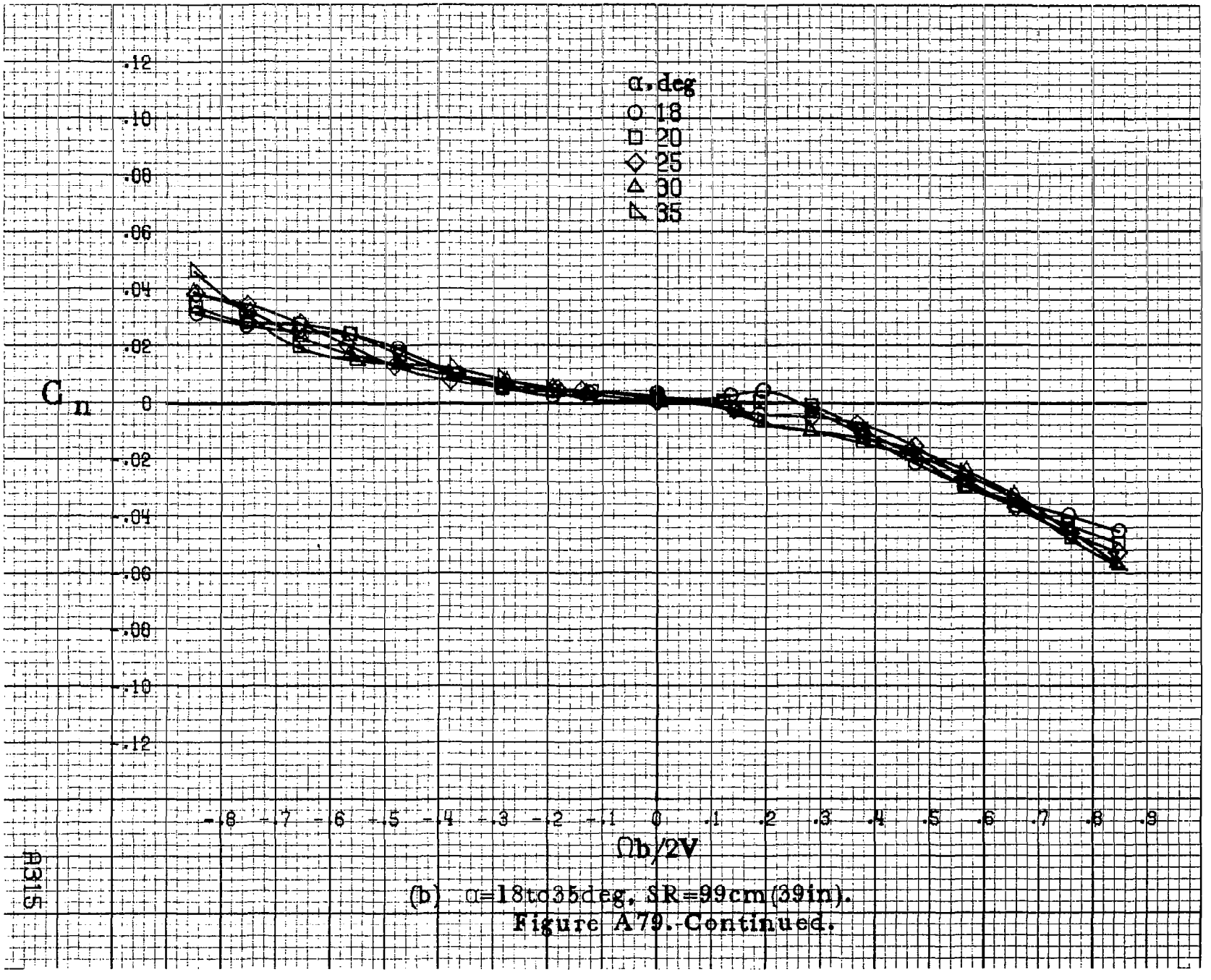

(b) α=18to35deg, SR=99cm(39in).

Figure A79. Continued.

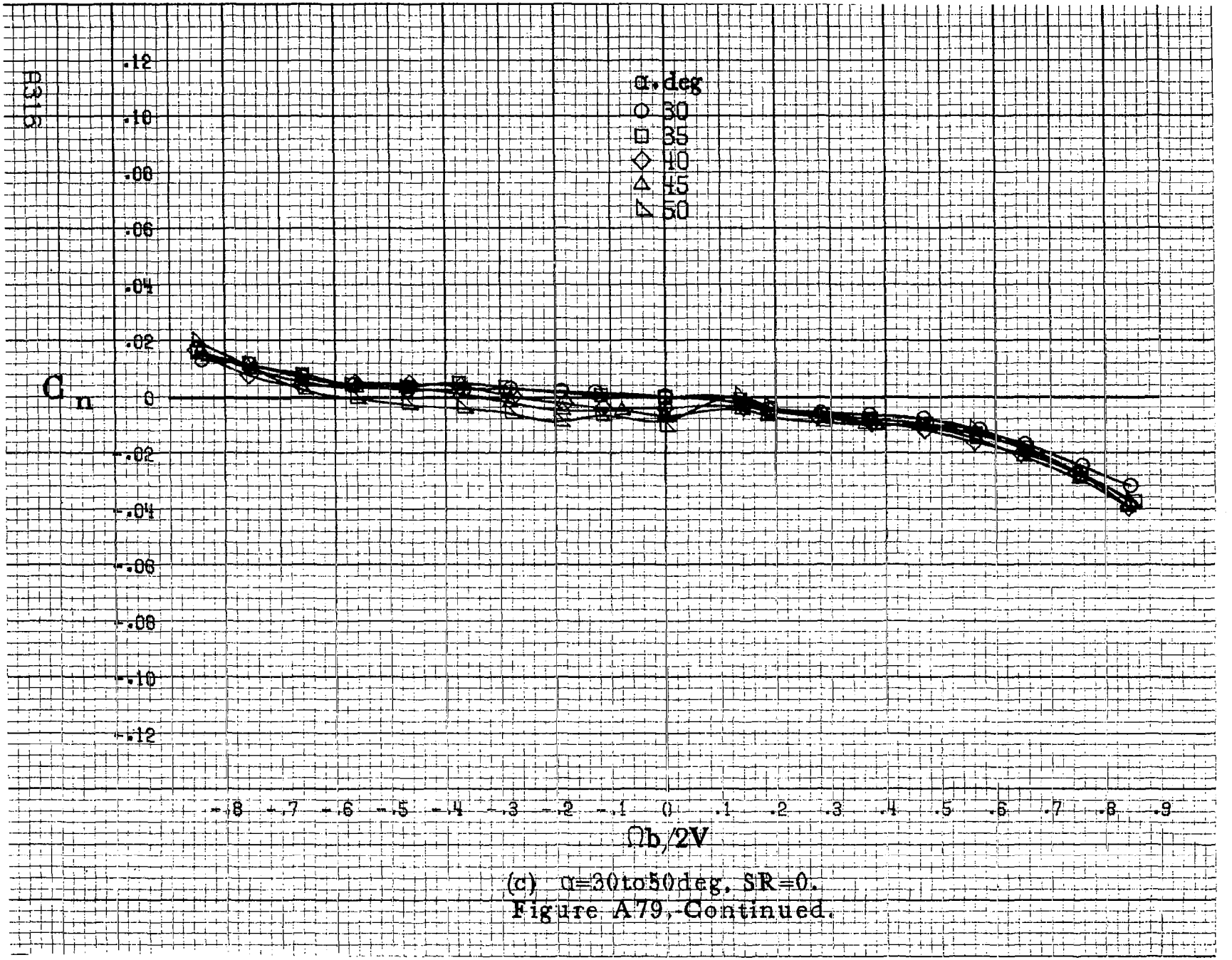

(c) α=30to50deg, SR=0.

Figure A79.-Continued.

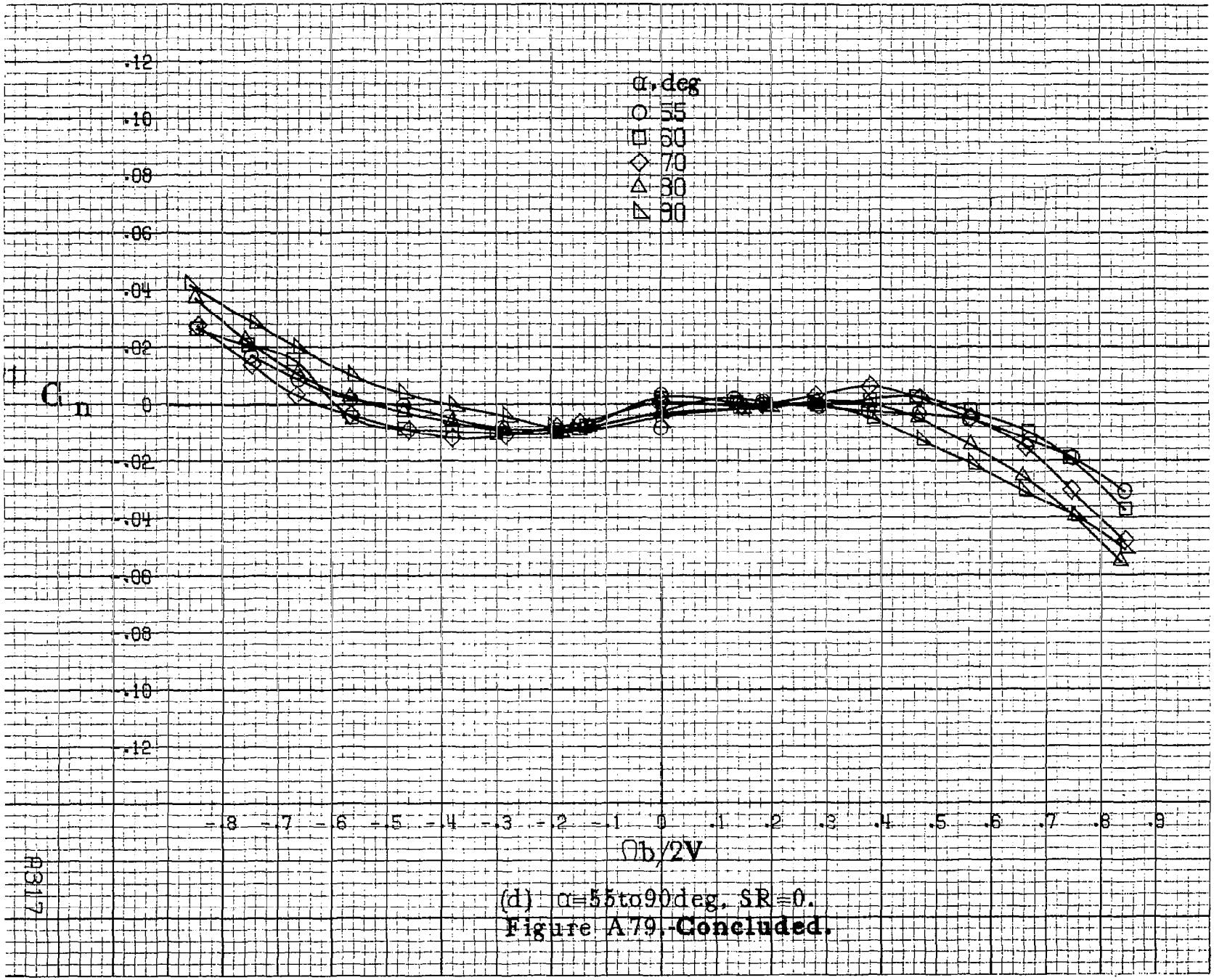

(d) α=55to90deg. SR=0.

Figure A79.-Concluded.

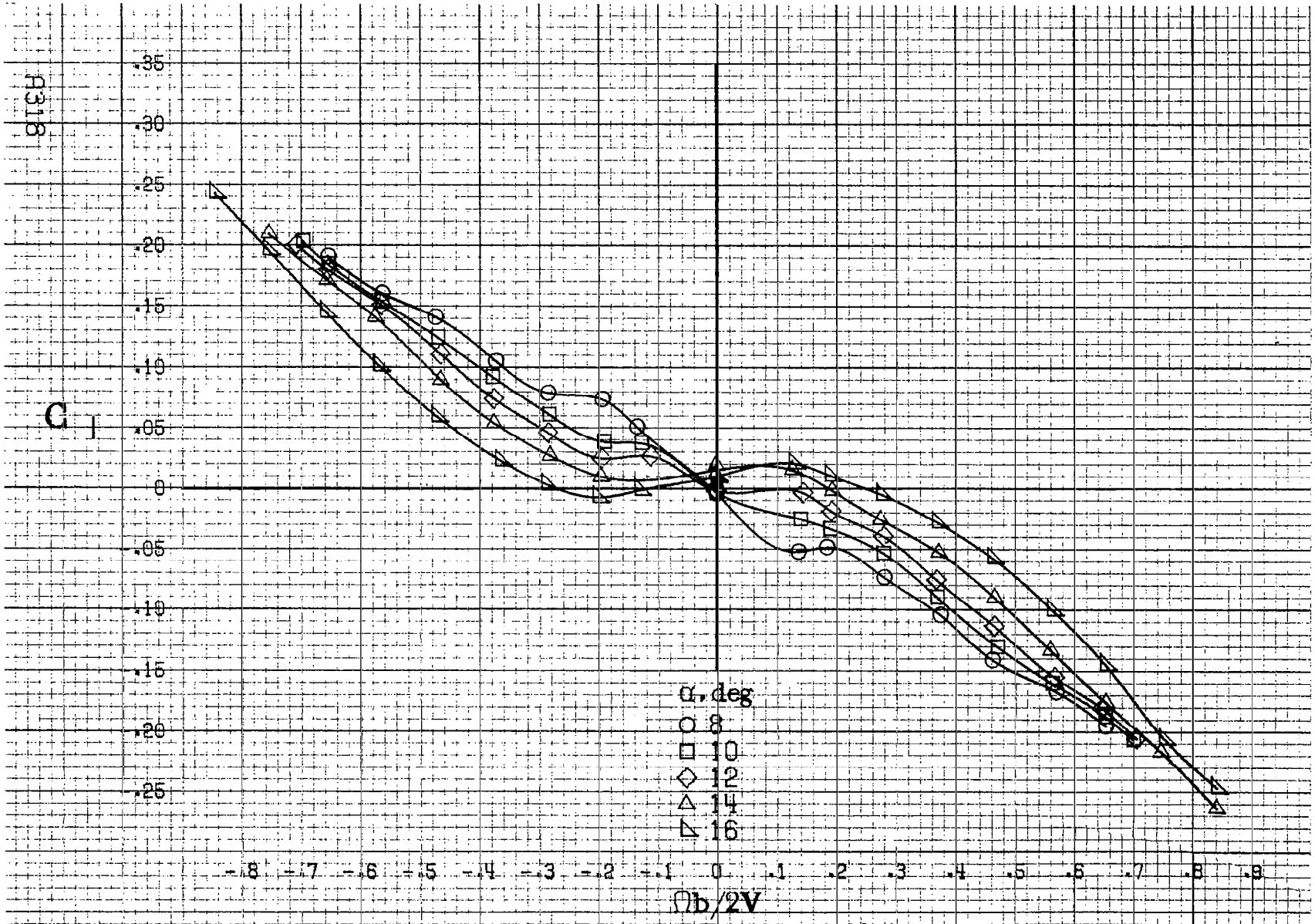

(a) α=8to16deg, SR=99cm(39in).

Figure A80.-Effect of rotation rate and angle of attack on rolling-moment coefficient for configuration having sharp-edged fuselage bottom aft of wing TE. $\delta_e = 0°$, $\delta_a = 0°$, $\delta_r = 0°$, $\beta = 0°$.

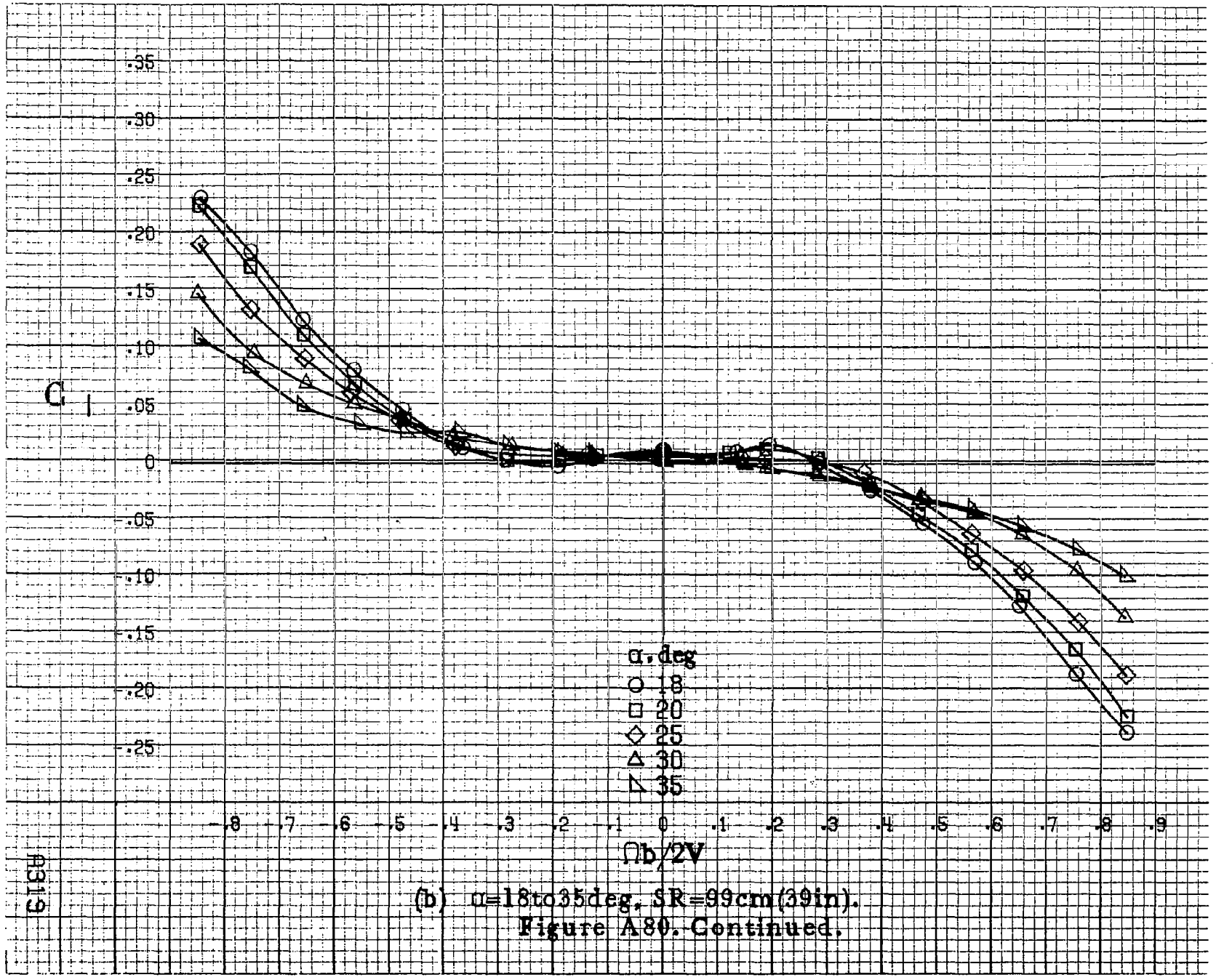

(b) α=18to35deg, SR=99cm(39in).

Figure A80.-Continued.

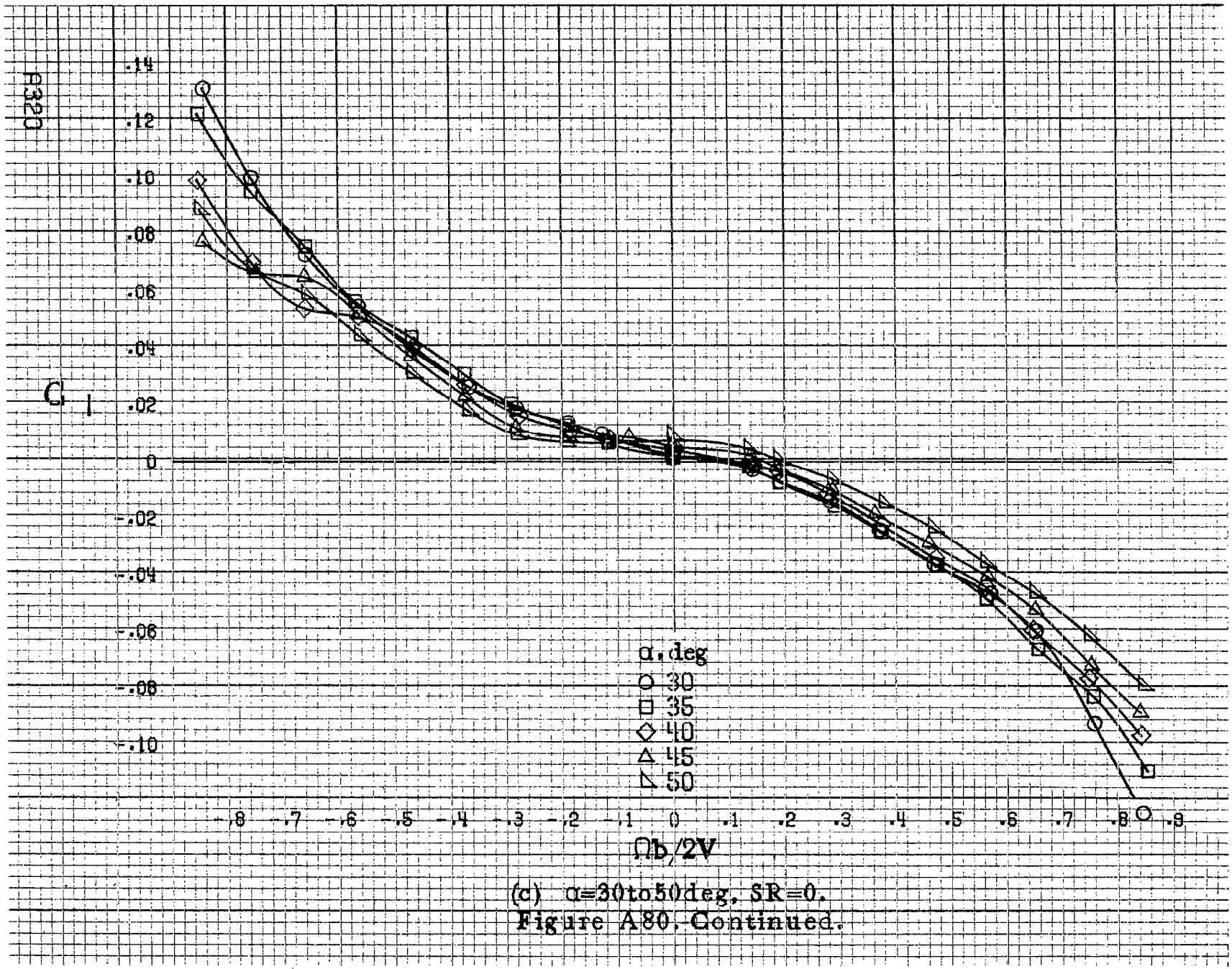

(c) α=30to50deg, SR=0.

Figure A80.-Continued.

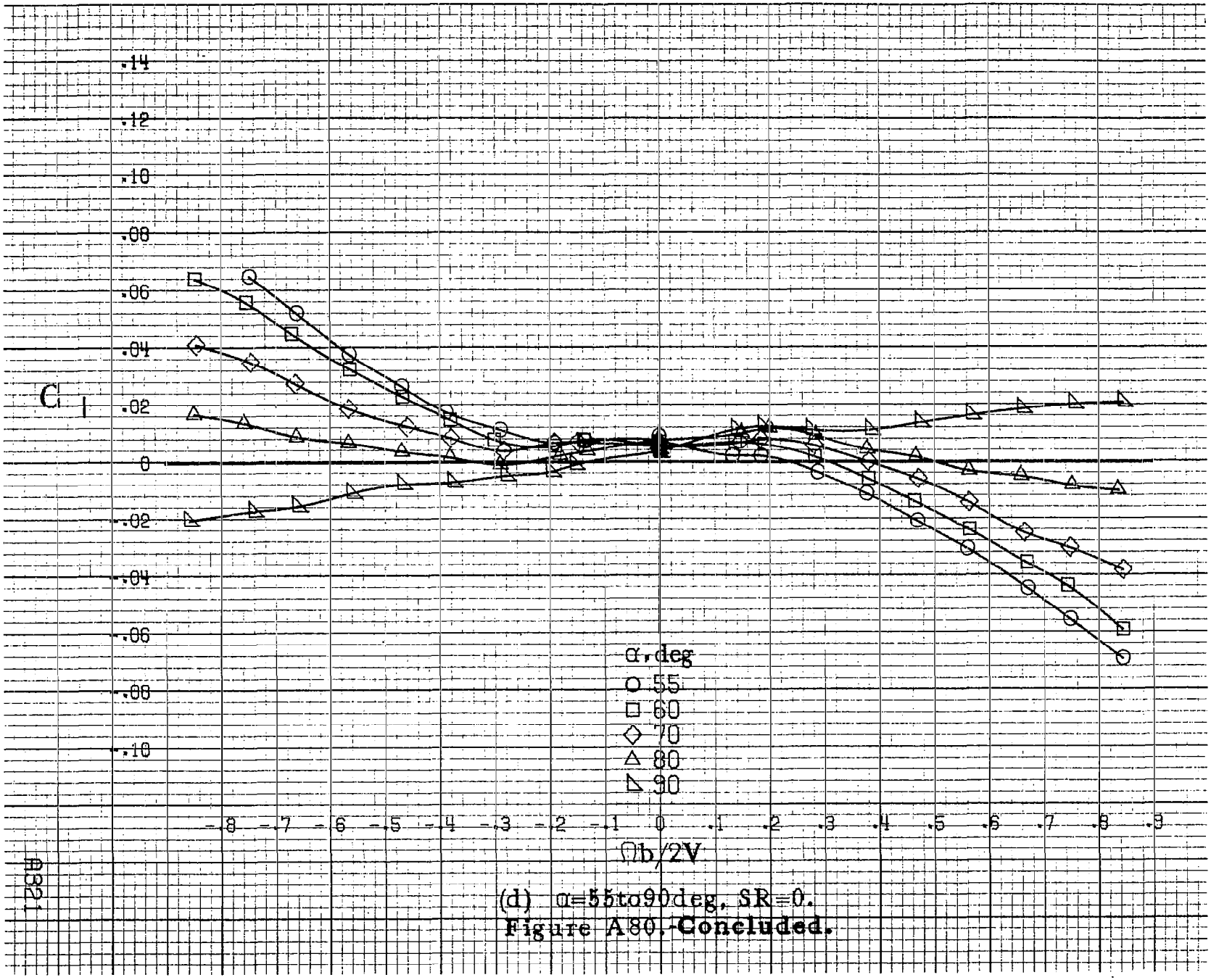

(d) α=55 to 90 deg, SR=0.

Figure A80. Concluded.

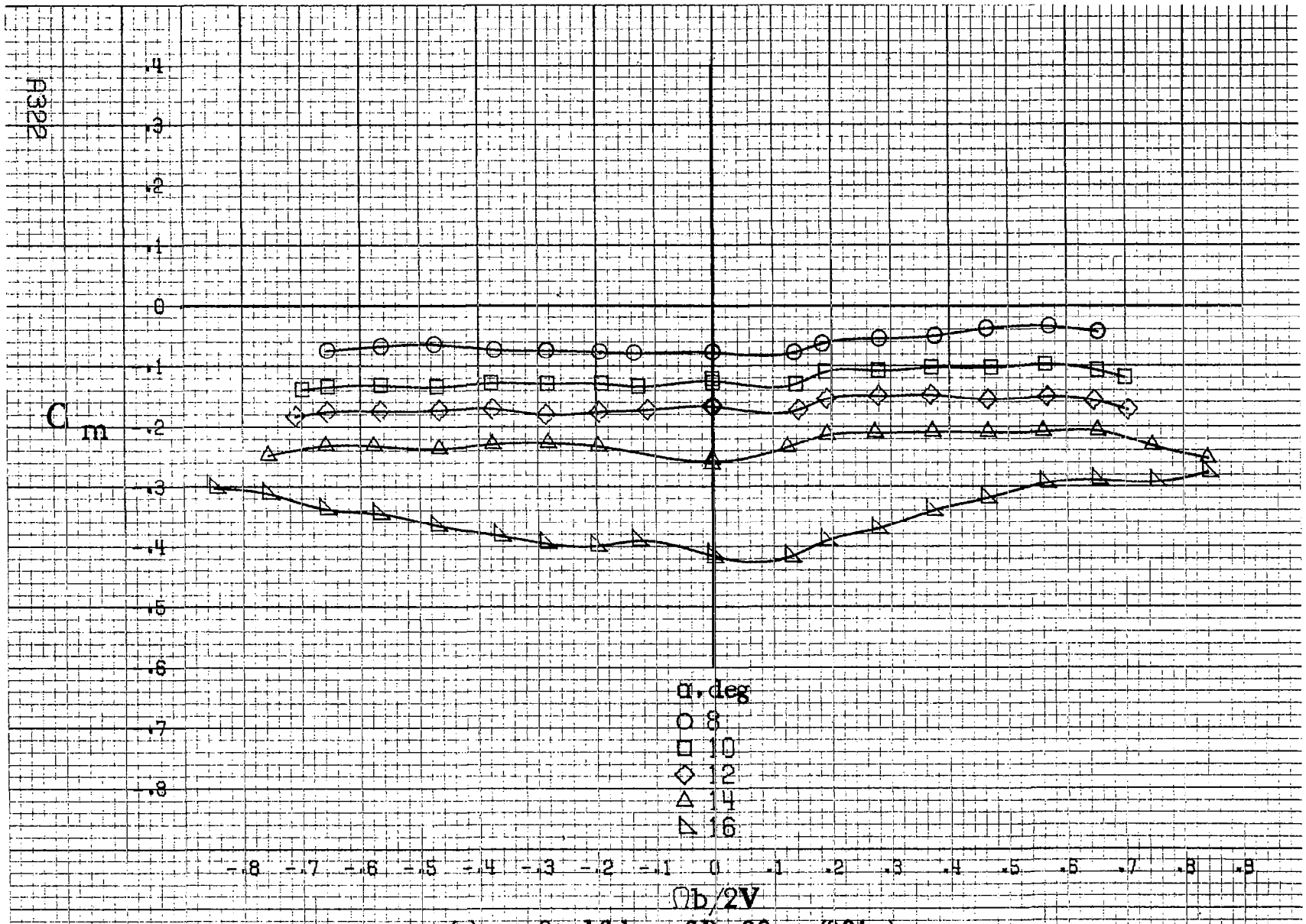

(a) α=8to16deg, SR=99cm(39in).

Figure A81.-Effect of rotation rate and angle of attack on pitching-moment coefficient for configuration having sharp-edged fuselage bottom aft of wing TE. $\delta_e = 0°$, $\delta_a = 0°$, $\delta_r = 0°$, $\beta = 0°$.

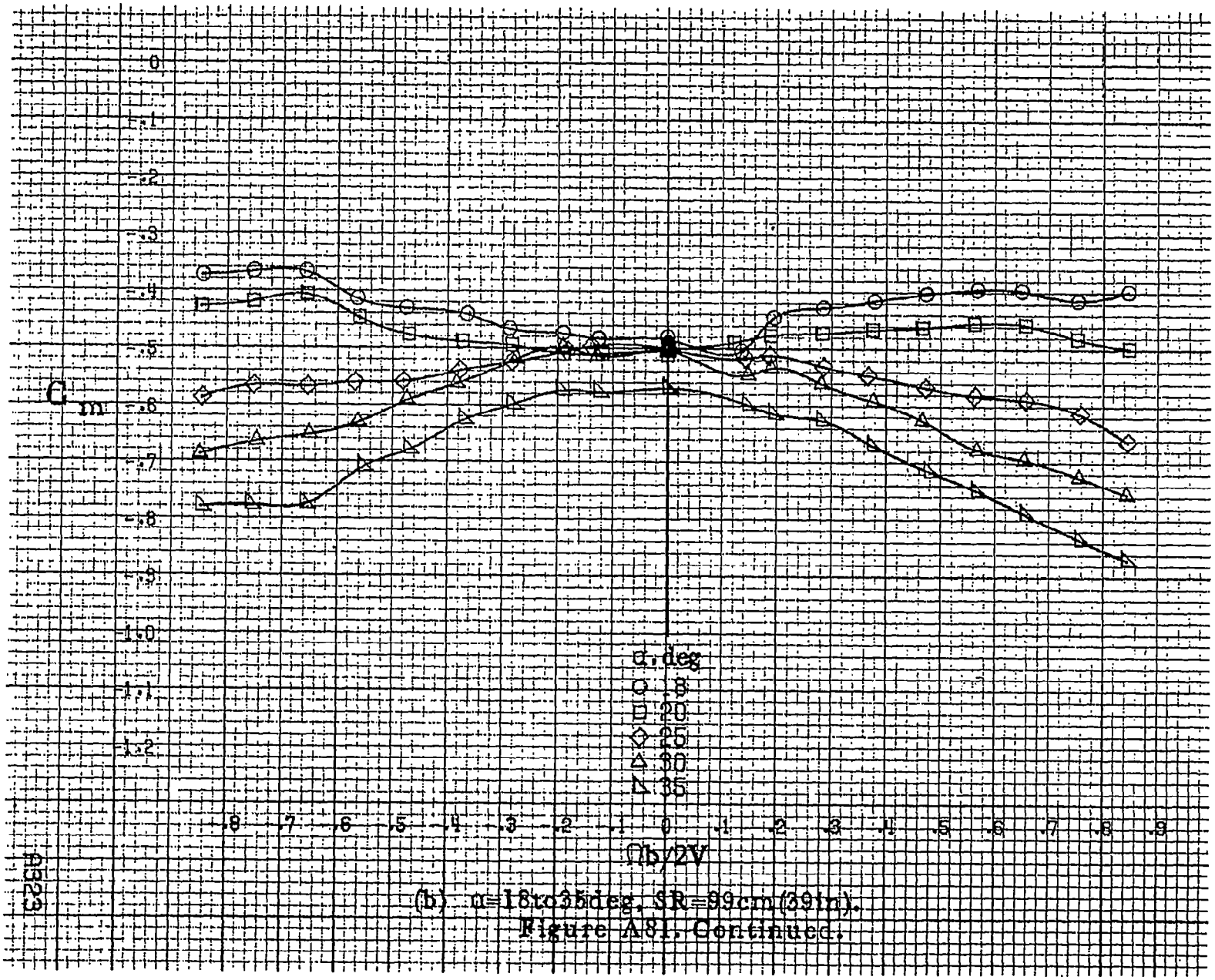

(b) α=18to35deg, SR=99cm(39in).

Figure A81. Continued.

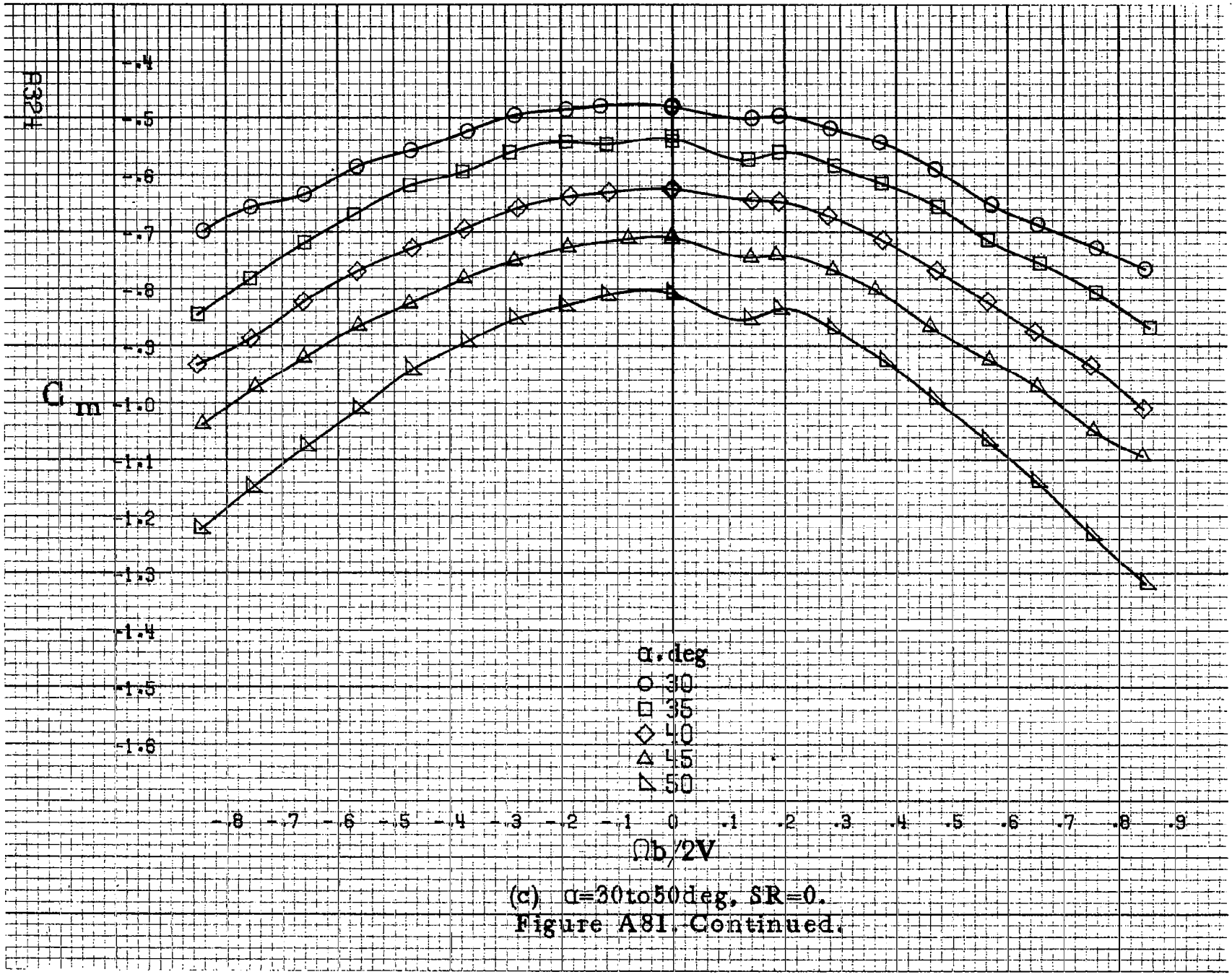

(c) α=30to50deg, SR=0.

Figure A81. Continued.

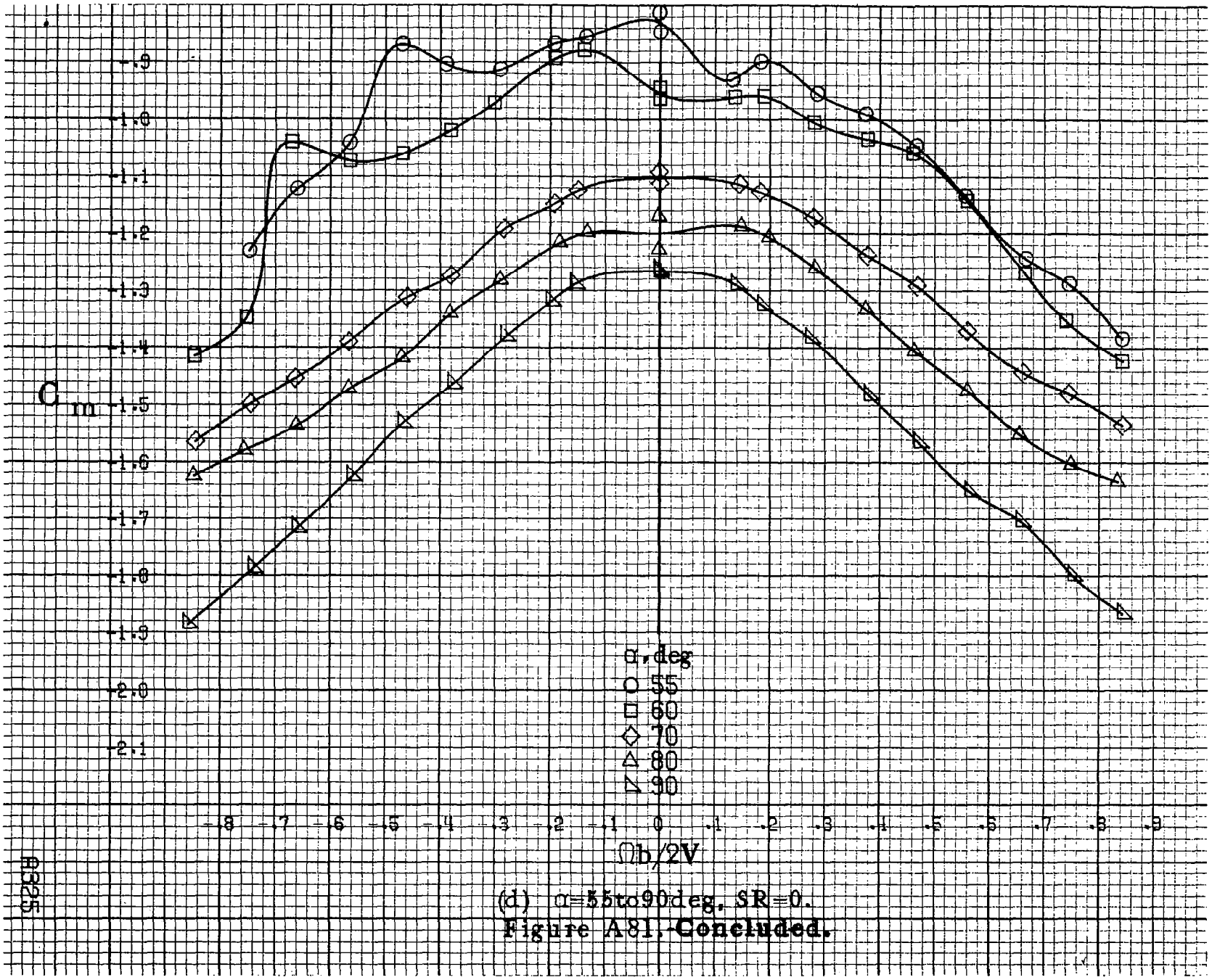

(d) α=55to90deg, SR=0.

Figure A81.-Concluded.

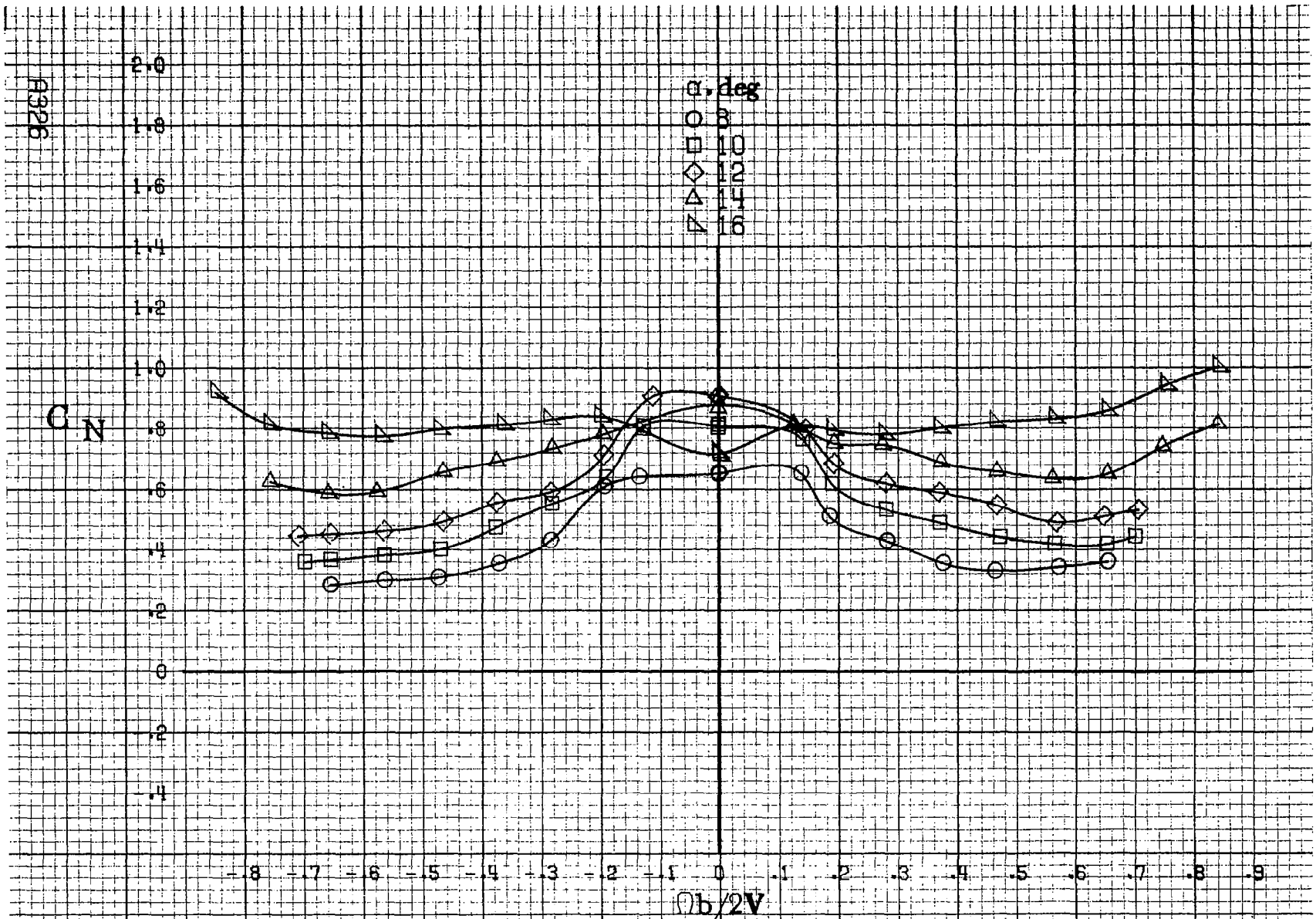

(a) α=8to16deg, SR=99cm(39in).

Figure A82.-Effect of rotation rate and angle of attack on normal-force coefficient for configuration having sharp-edged fuselage bottom aft of wing TE. $\delta_e = 0°$, $\delta_a = 0°$, $\delta_r = 0°$, $\beta = 0°$.

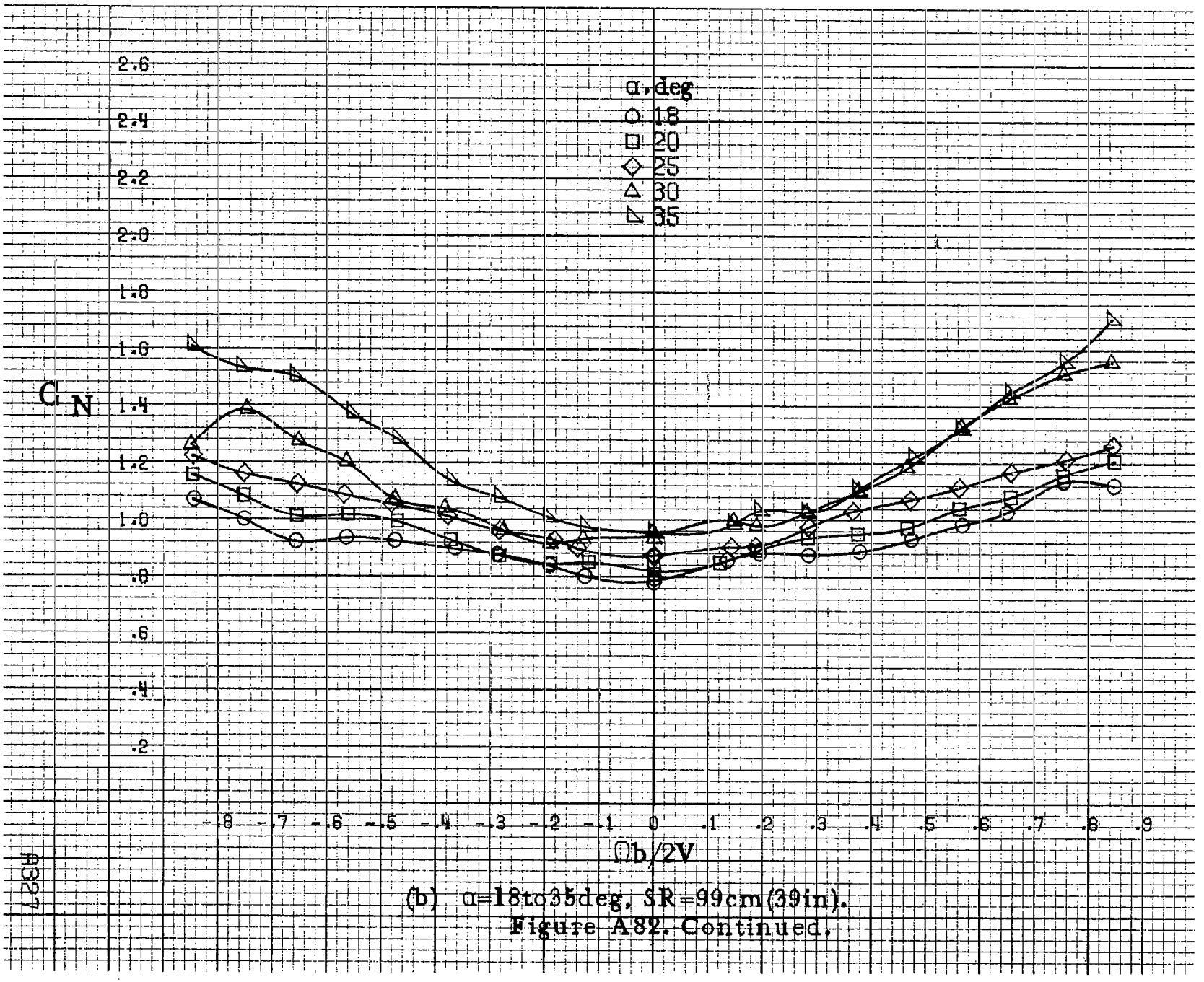

(b) α=18to35deg, SR=99cm(39in).

Figure A82. Continued.

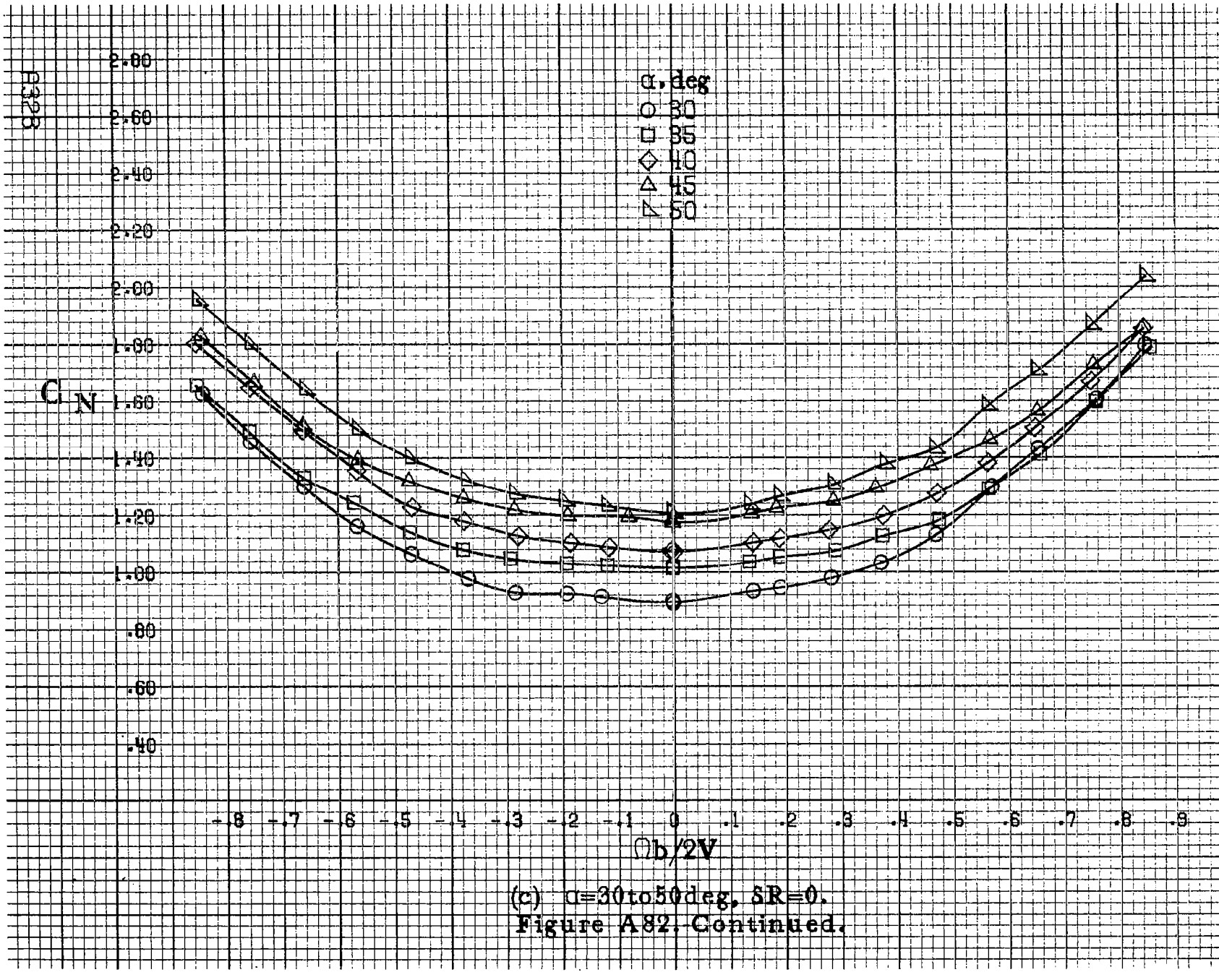

(c) α=30to50deg, δR=0.

Figure A82. Continued.

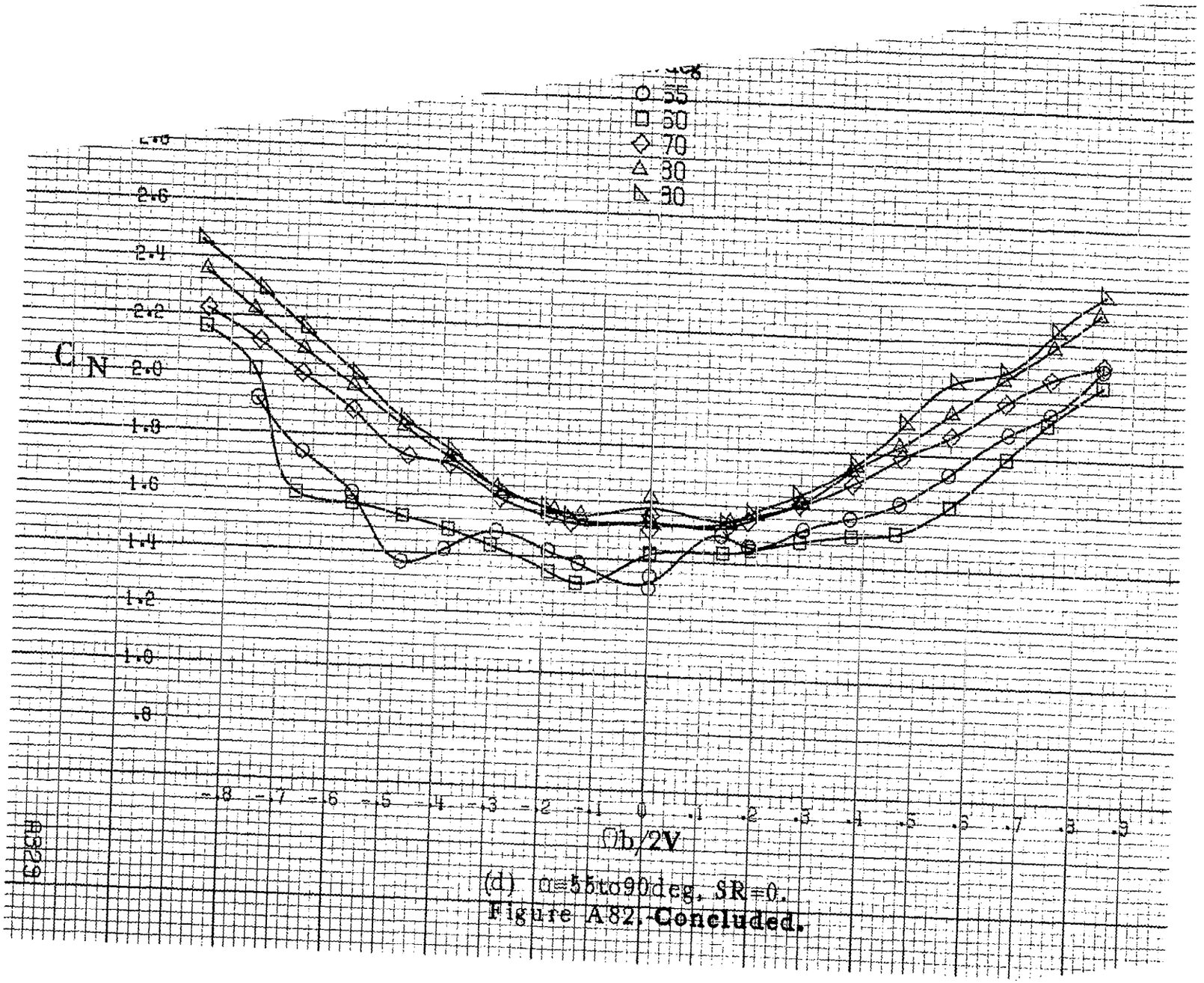

(d) $\alpha = 55$ to 90 deg, SR = 0.

Figure A82. Concluded.

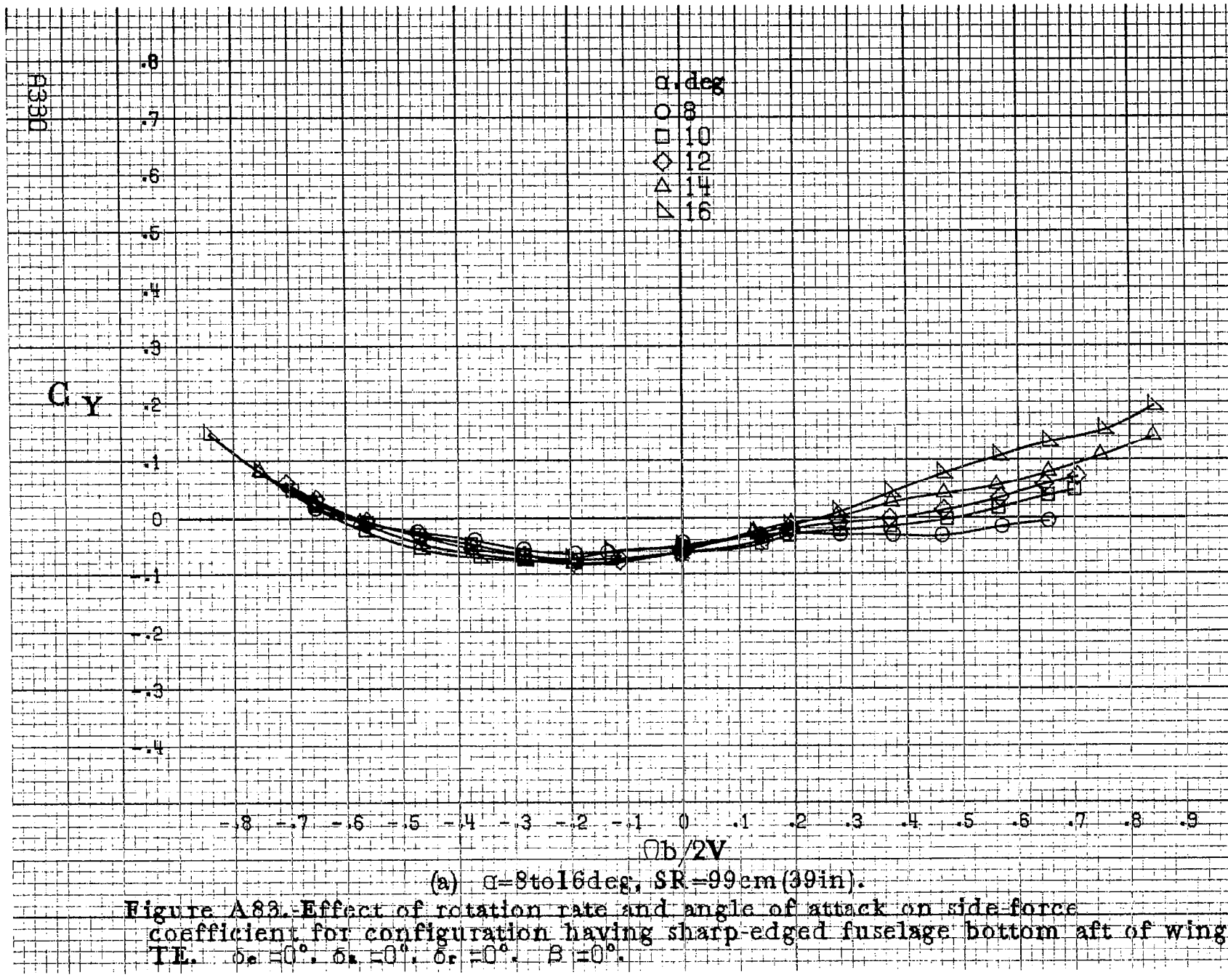

(a) α=8to16deg, SR=99cm(39in).

Figure A83.-Effect of rotation rate and angle of attack on side-force coefficient for configuration having sharp-edged fuselage bottom aft of wing TE. $\delta_e = 0°$, $\delta_a = 0°$, $\delta_r = 0°$, $\beta = 0°$.

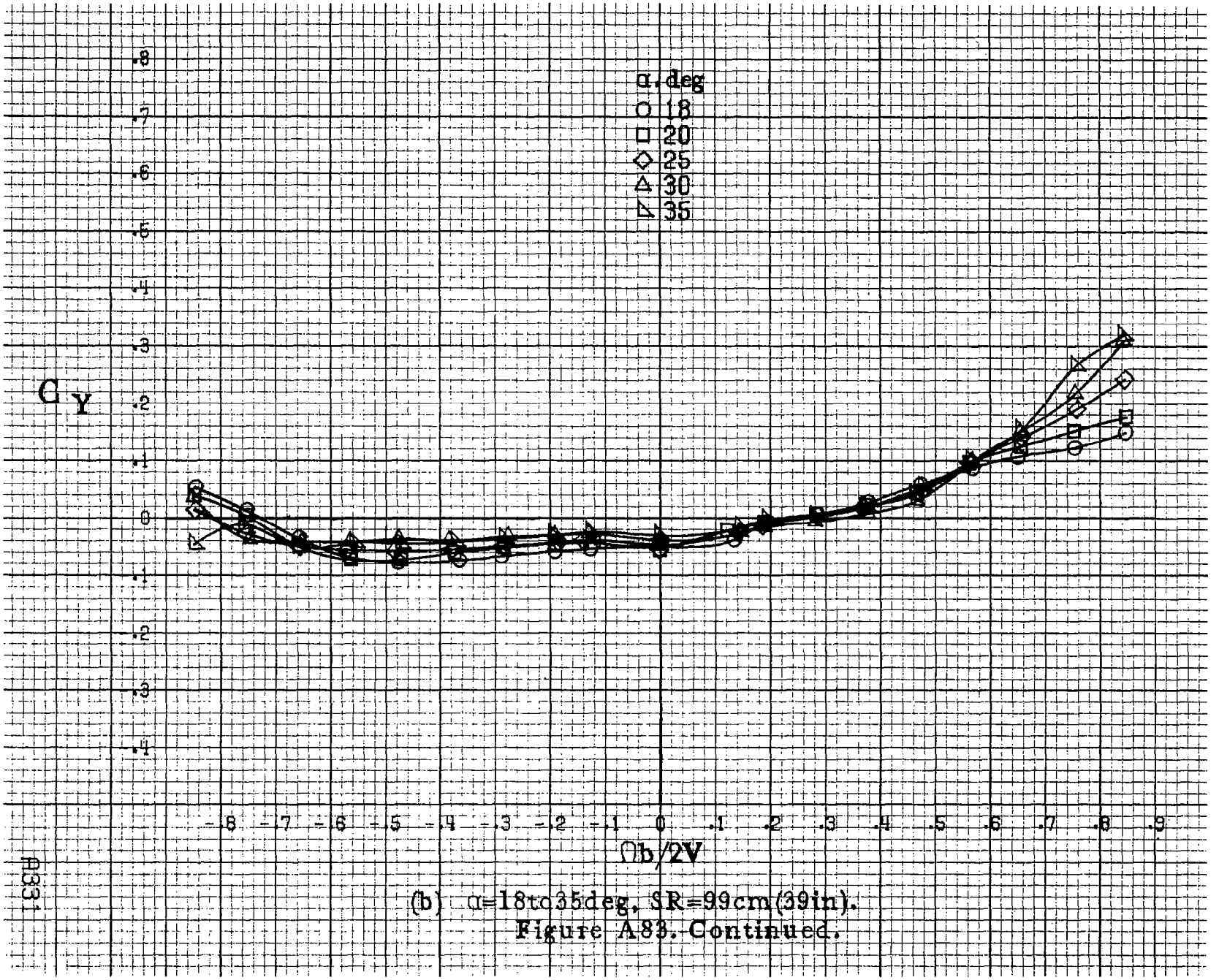

(b) α=18to35deg, SR=99cm(39in).

Figure A83.-Continued.

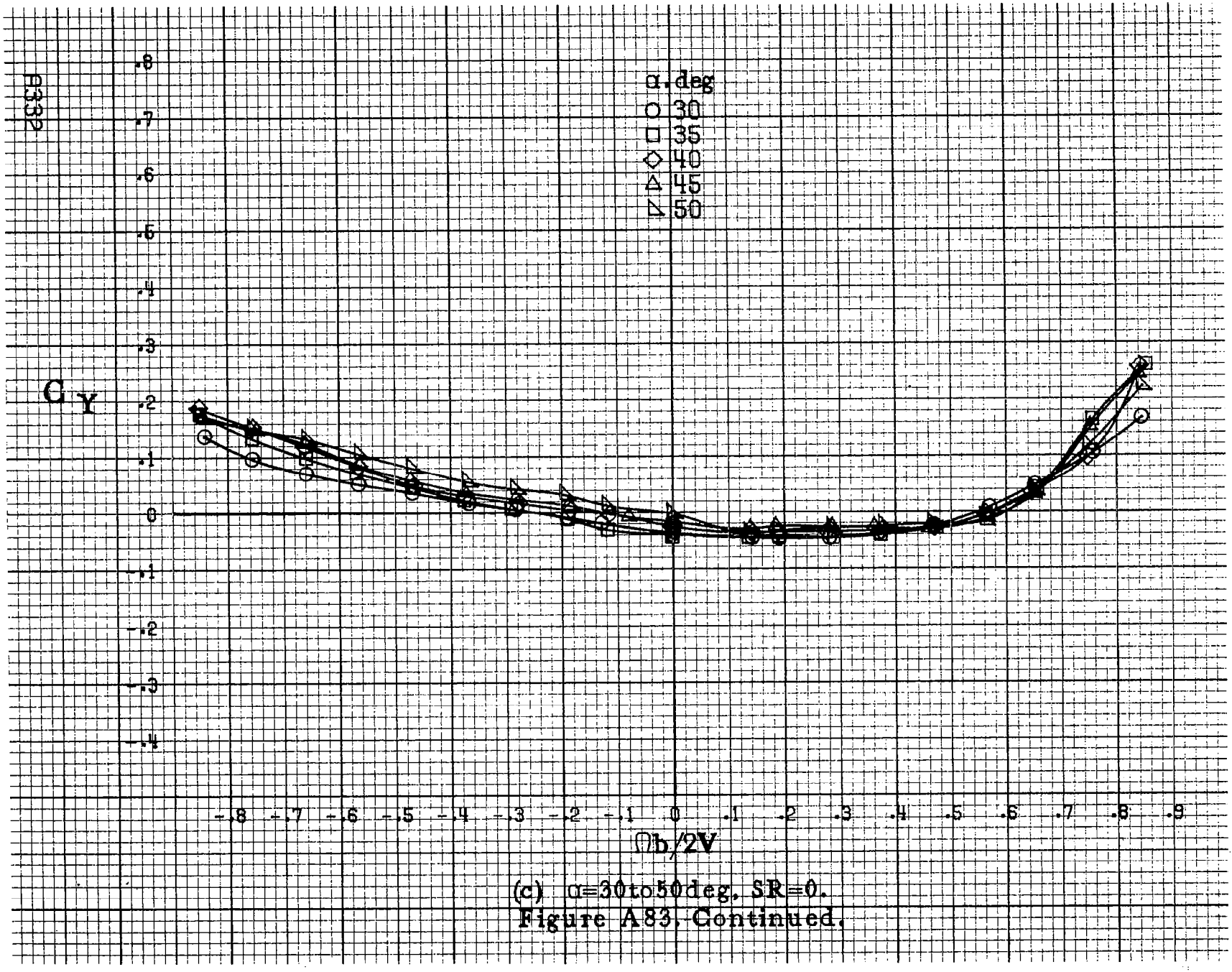

(c) α=30to50deg, SR=0.

Figure A83. Continued.

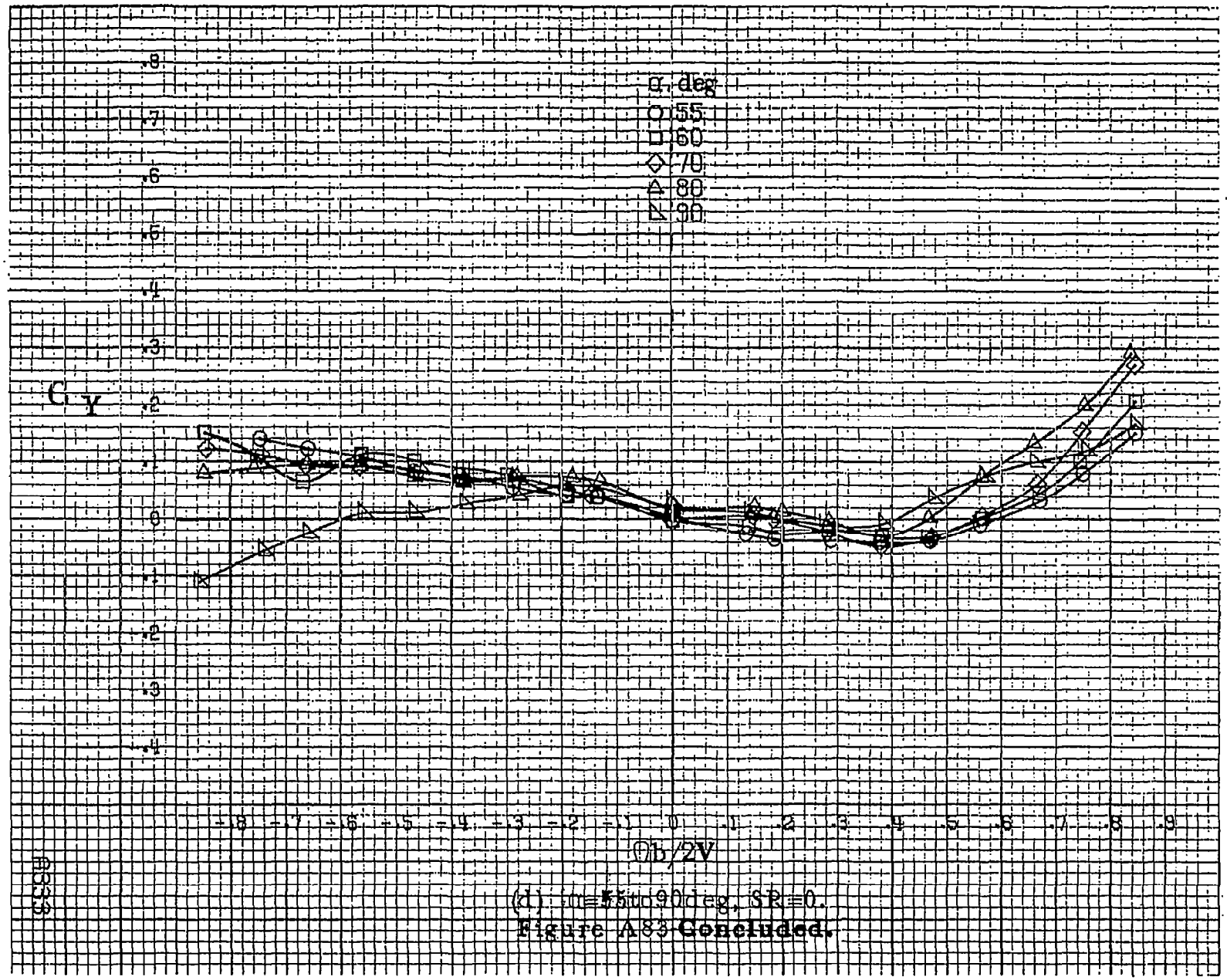

(d) $\alpha = 55$ to 90 deg, $SR = 0$.

Figure A83. Concluded.

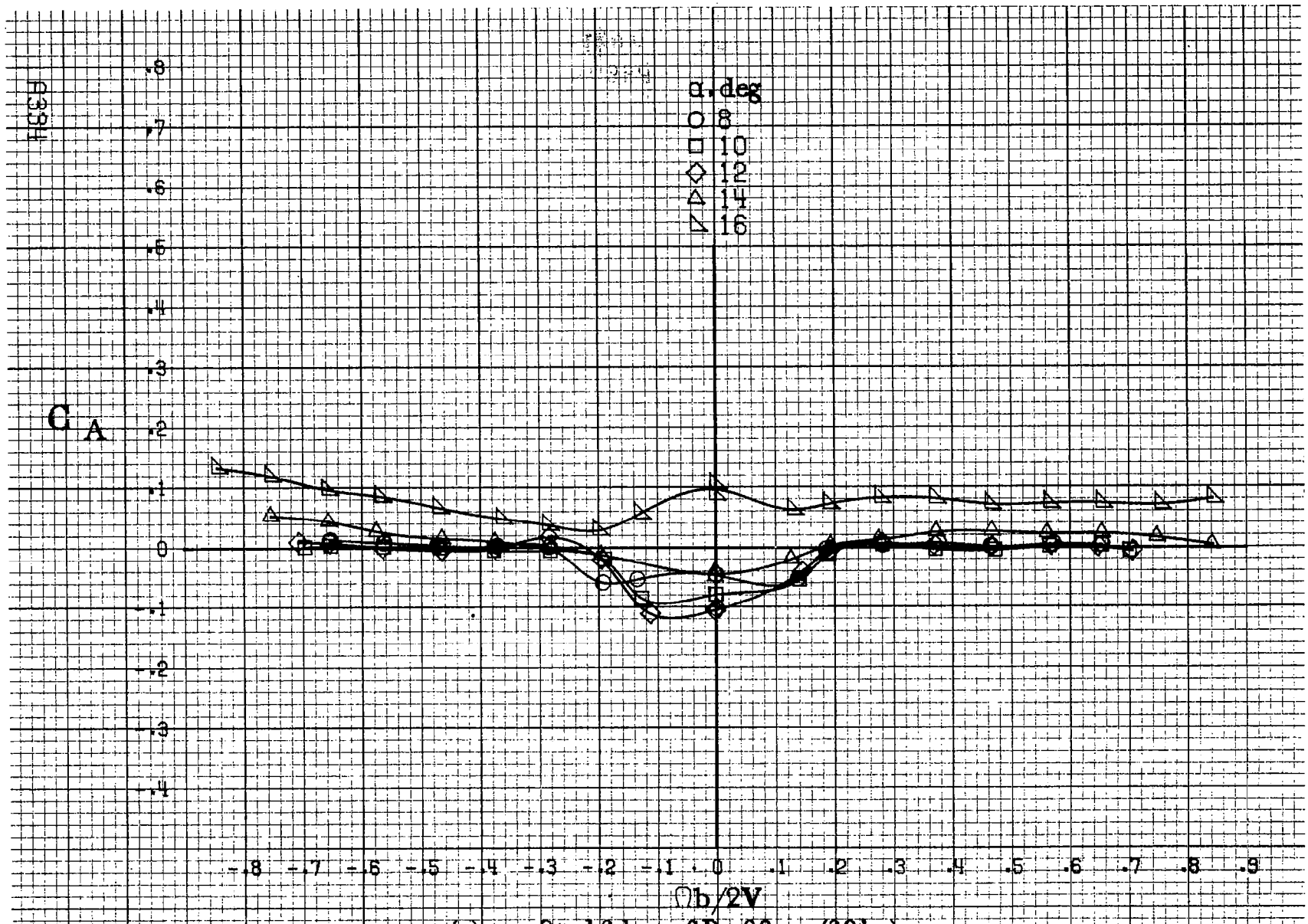

(a) α=8to16deg, SR=99cm(39in).

Figure A84. Effect of rotation rate and angle of attack on axial-force coefficient for configuration having sharp-edged fuselage bottom aft of wing TE. $\delta_a = 0°$, $\delta_s = 0°$, $\delta_r = 0°$, $\beta = 0°$.

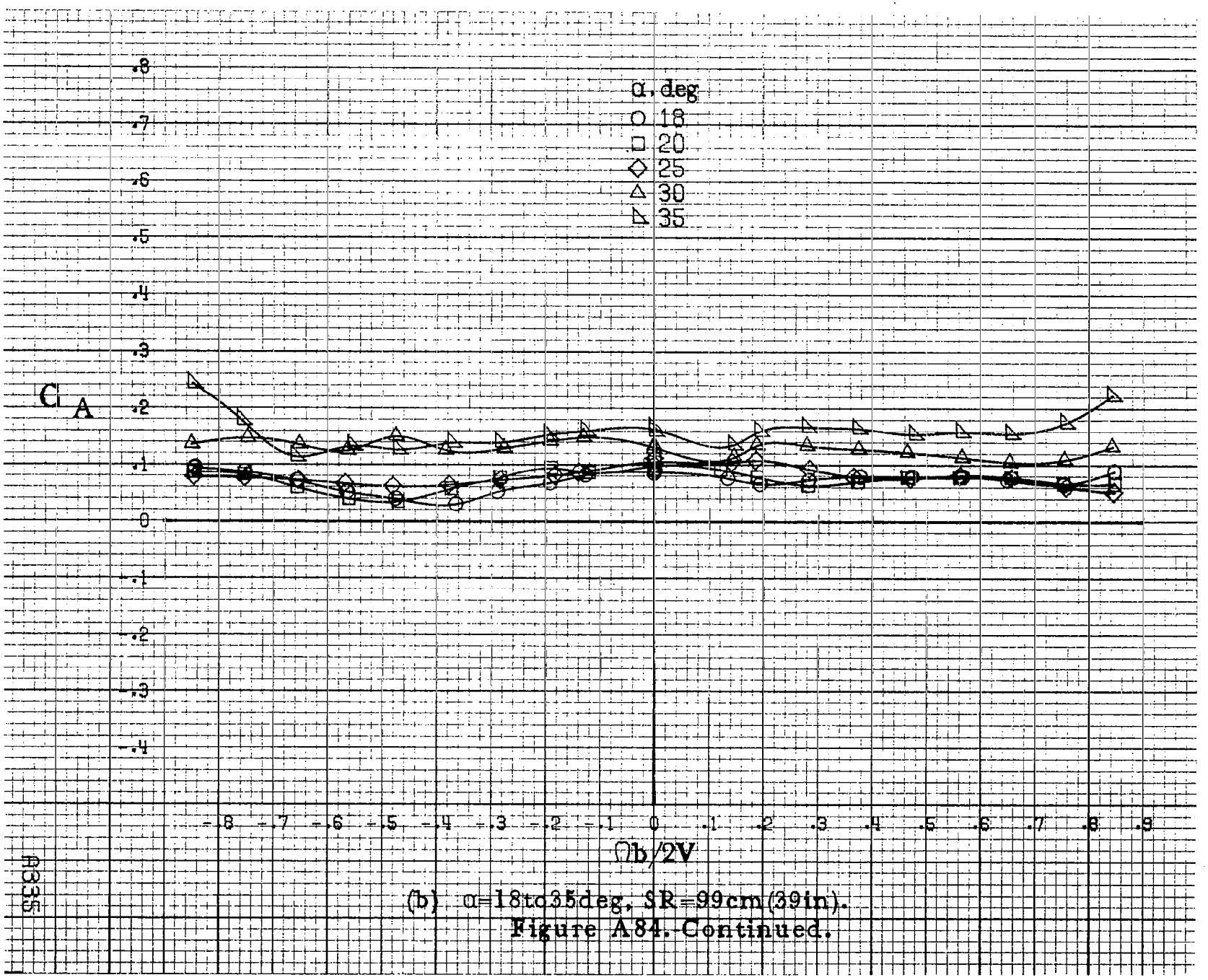

R335

(b) α=18to35deg, SR=99cm(39in).

Figure A84.-Continued.

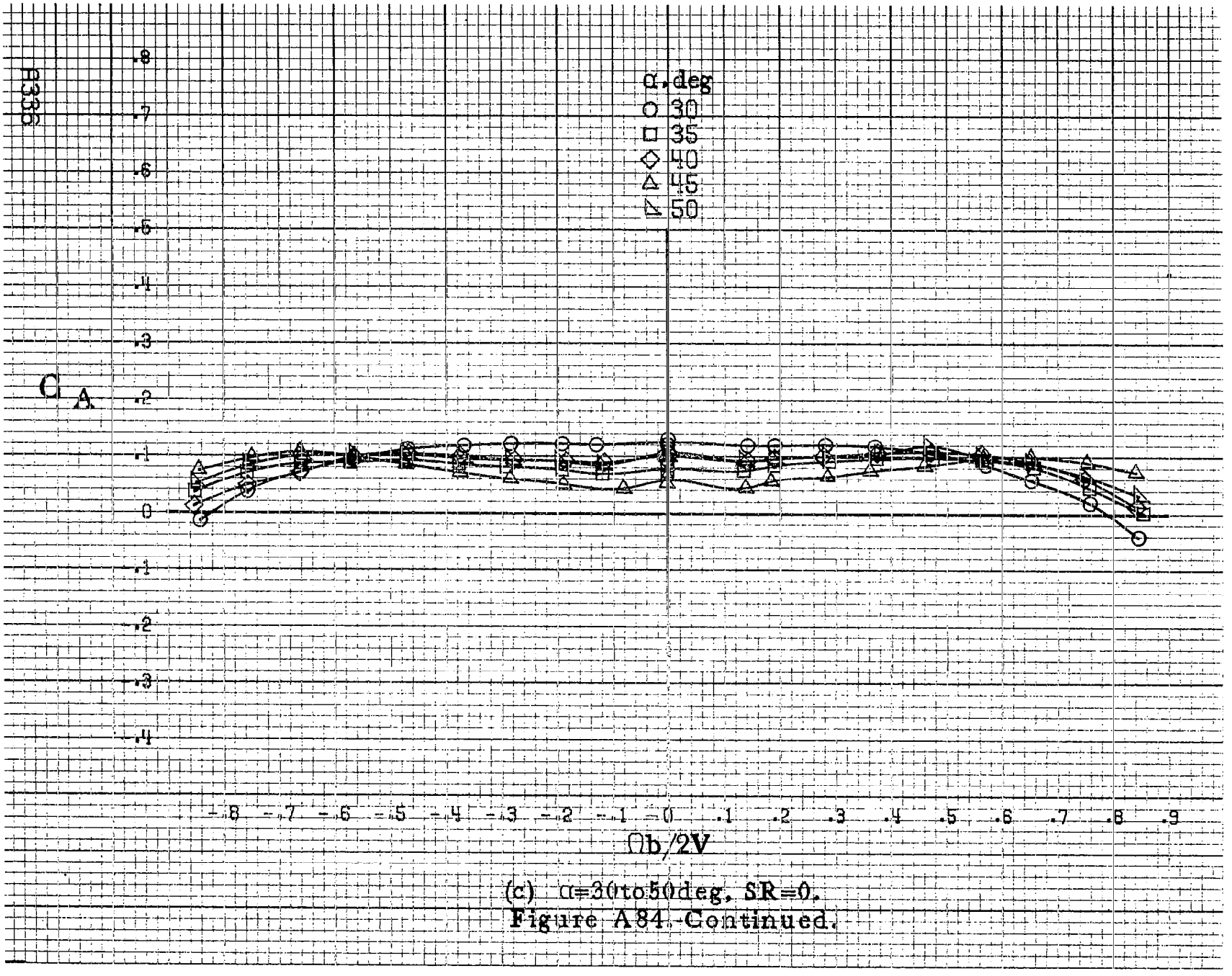

(c) α=30to50deg, SR=0.

Figure A84. Continued.

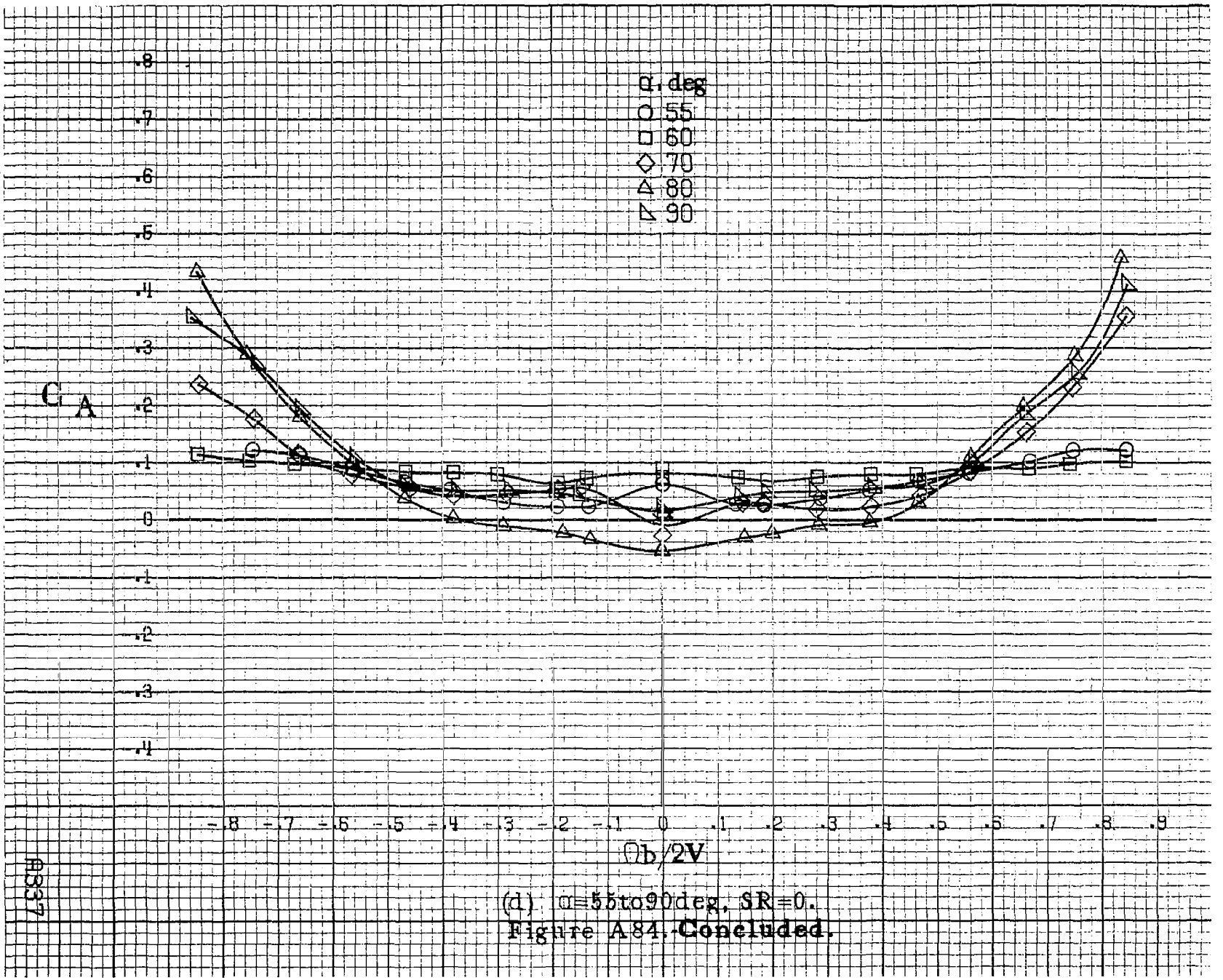

(d) α=55to90deg, SR=0.

Figure A84. **Concluded.**

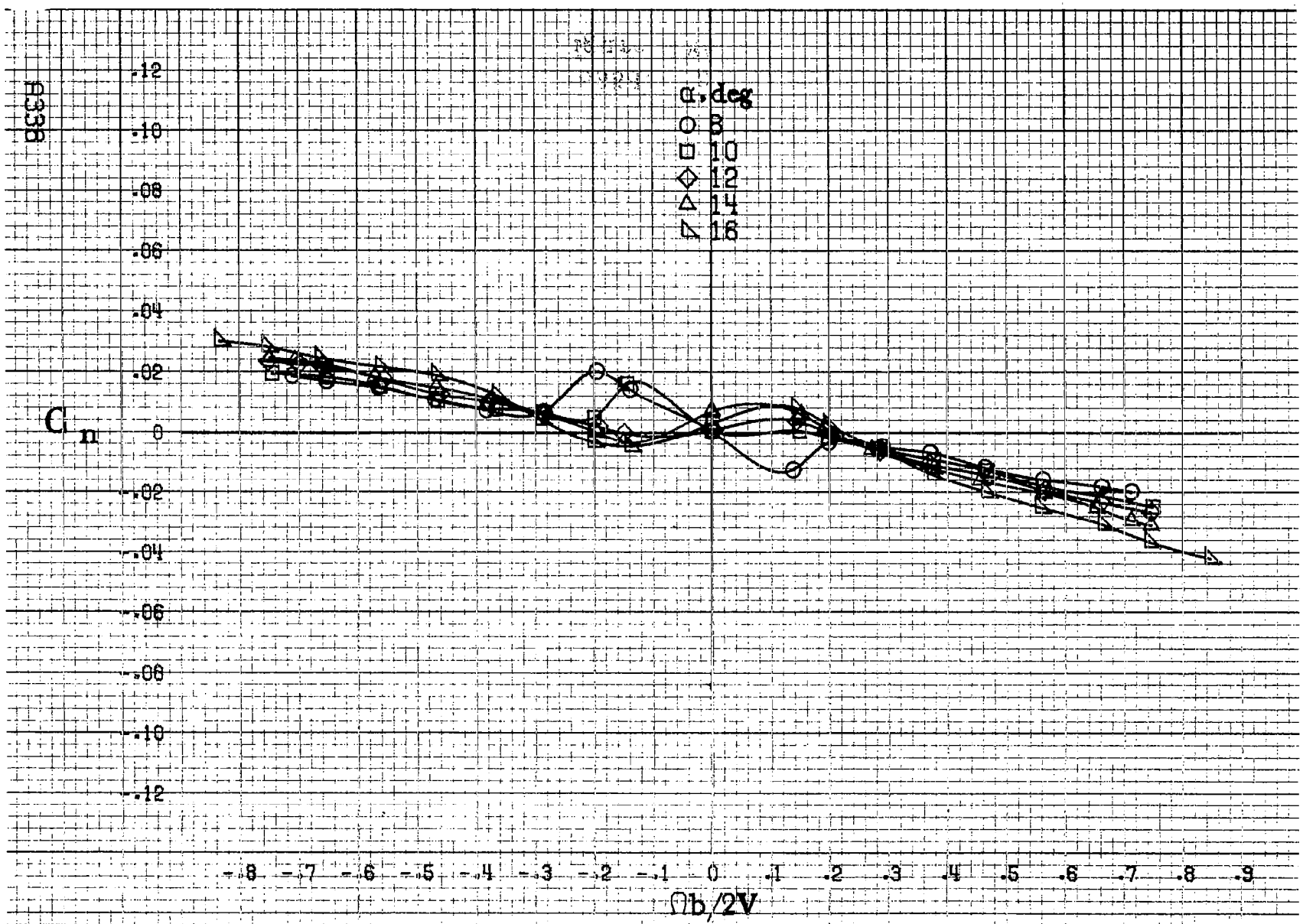

(a) α=8to16deg, SR=99cm(39in).

Figure A85. Effect of rotation rate and angle of attack on yawing-moment coefficient for configuration having sharp-edged fuselage bottom aft of engine cowling. $\delta_e = 0°$, $\delta_a = 0°$, $\delta_r = 0°$, $\beta = 0°$.

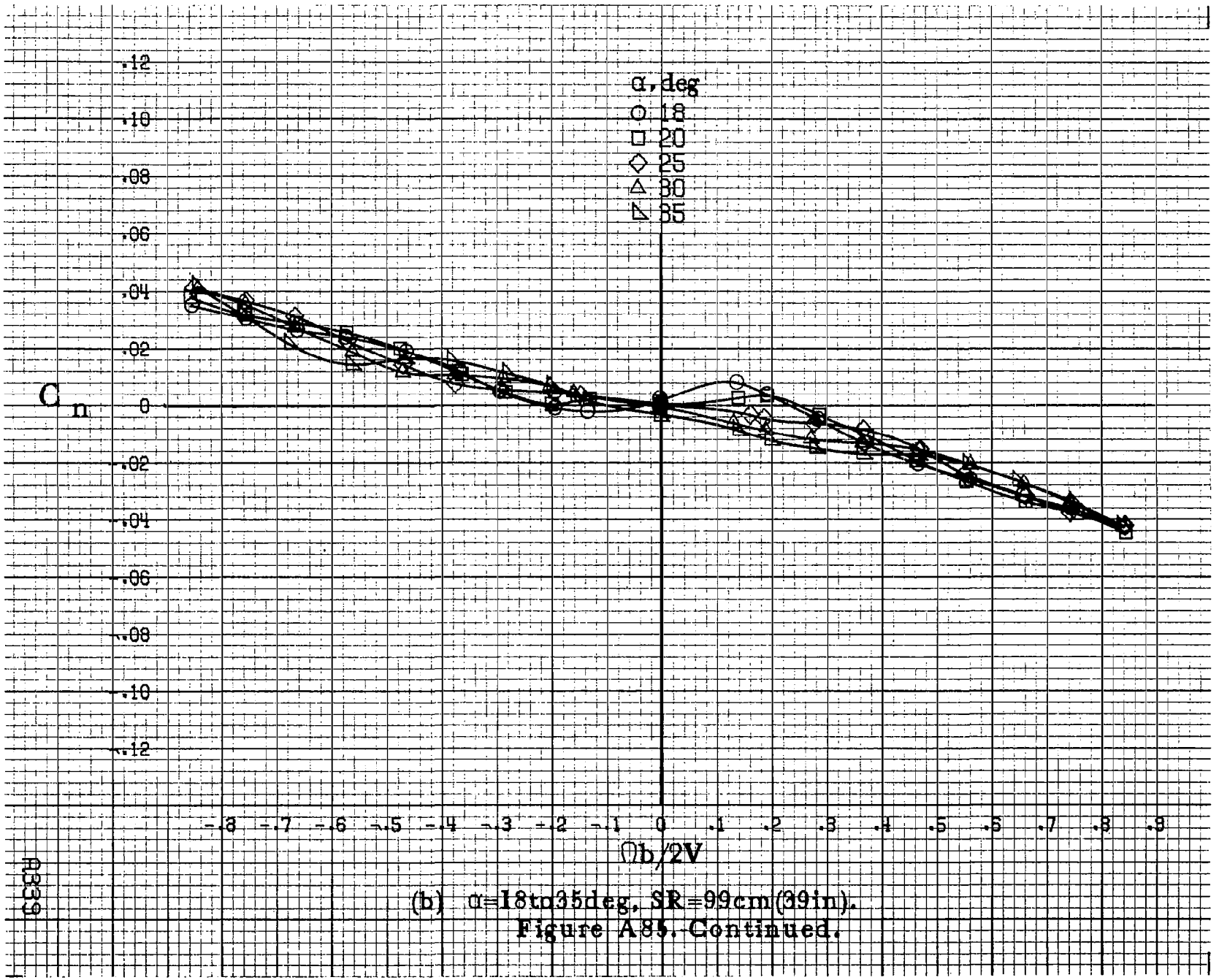

(b) α=18to35deg, SR=99cm(39in).

Figure A85. Continued.

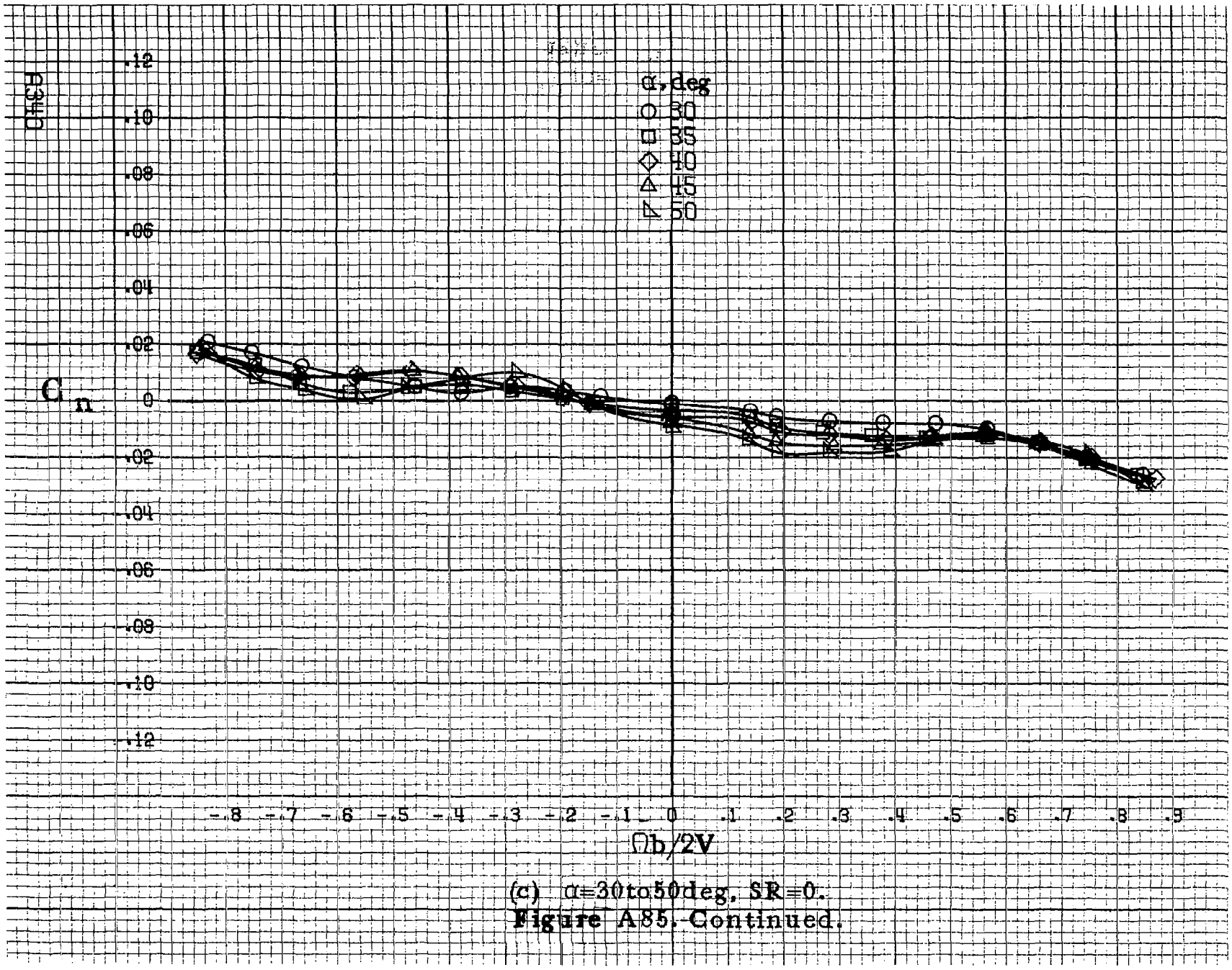

(c) α=30to50deg, SR=0.

Figure A85.-Continued.

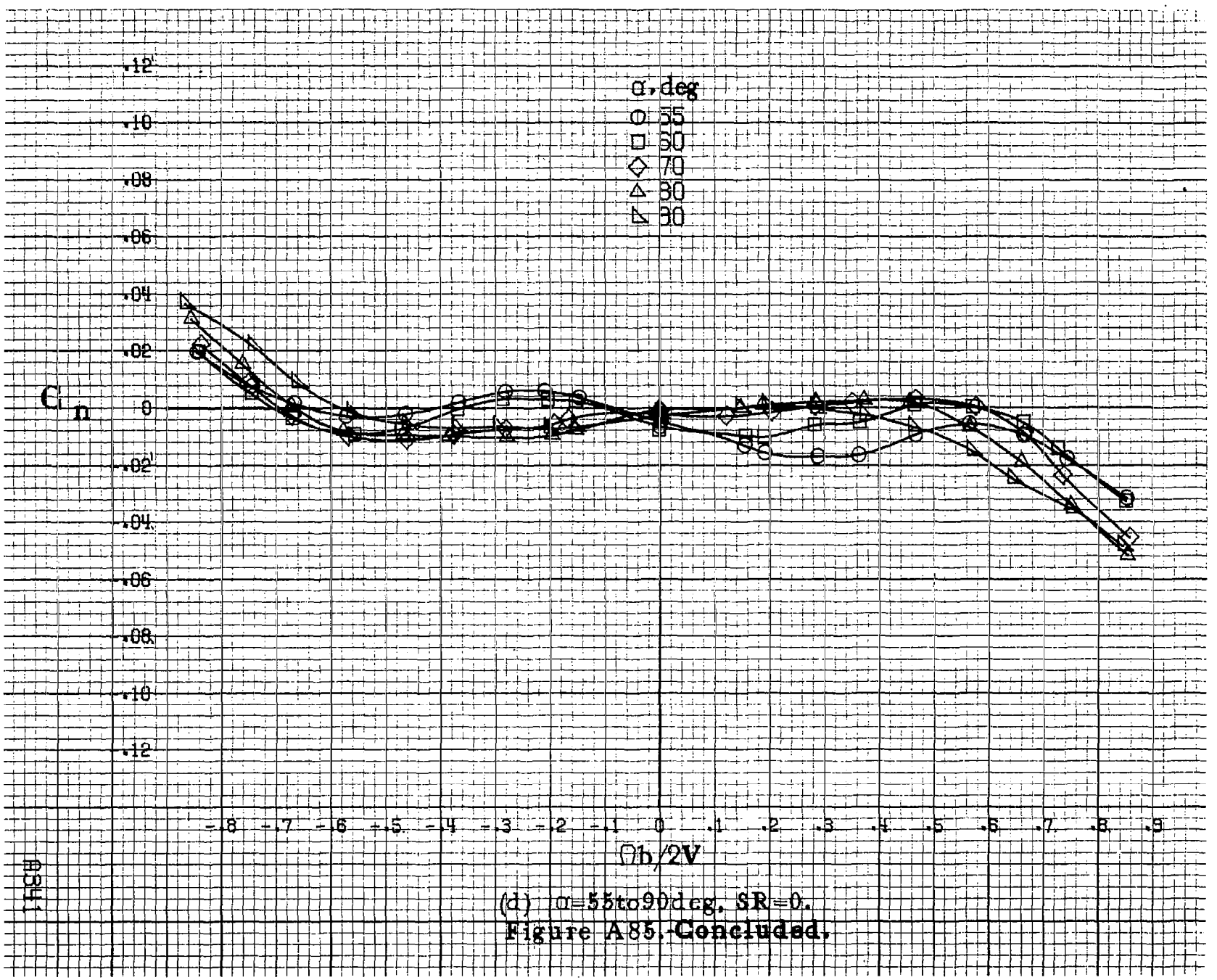

(d) $\alpha = 55$ to 90 deg, SR = 0.

Figure A85.-Concluded.

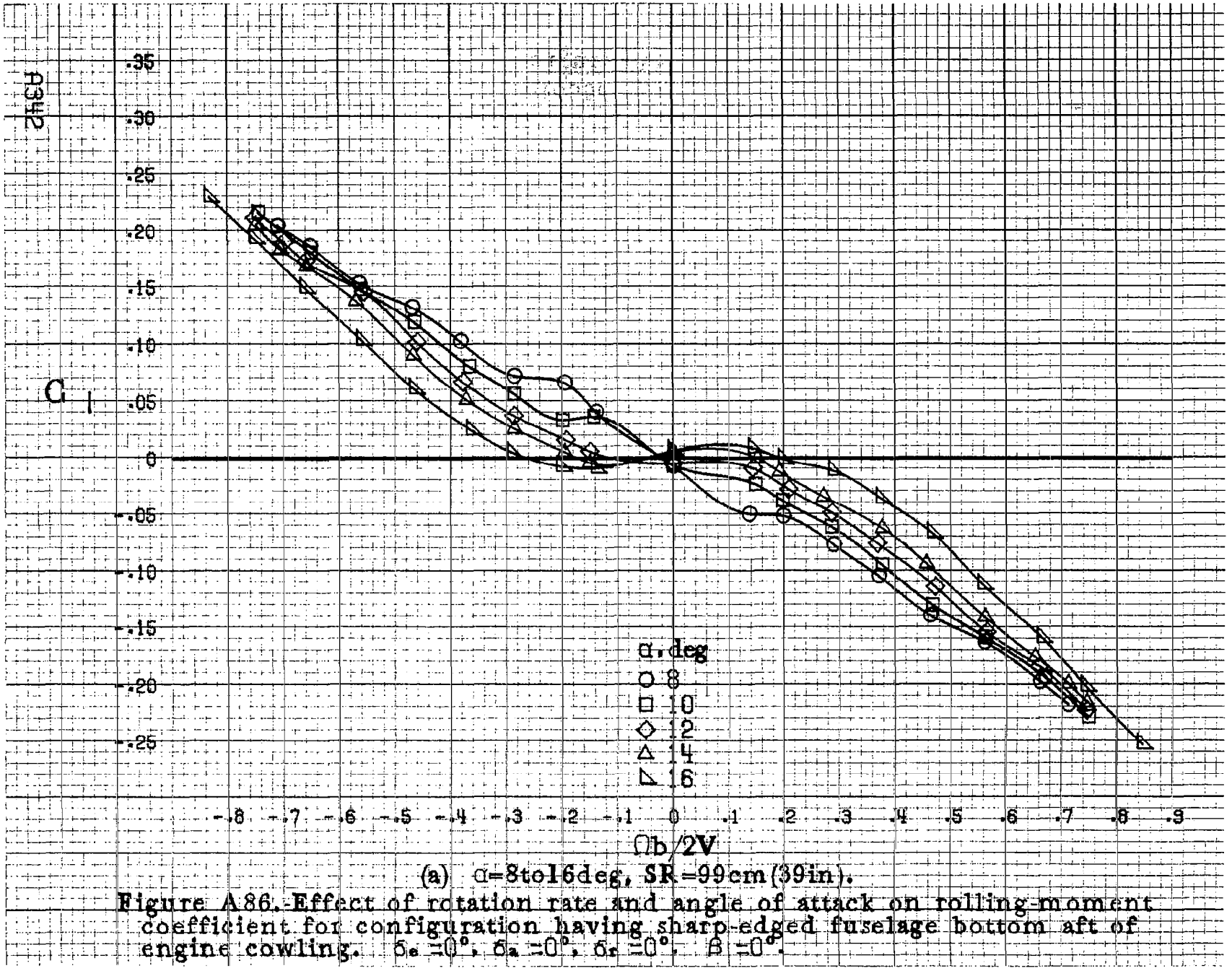

(a) α=8to16deg, SR=99cm(39in).

Figure A86.-Effect of rotation rate and angle of attack on rolling-moment coefficient for configuration having sharp-edged fuselage bottom aft of engine cowling. $\delta_e = 0°$, $\delta_a = 0°$, $\delta_r = 0°$, $\beta = 0°$.

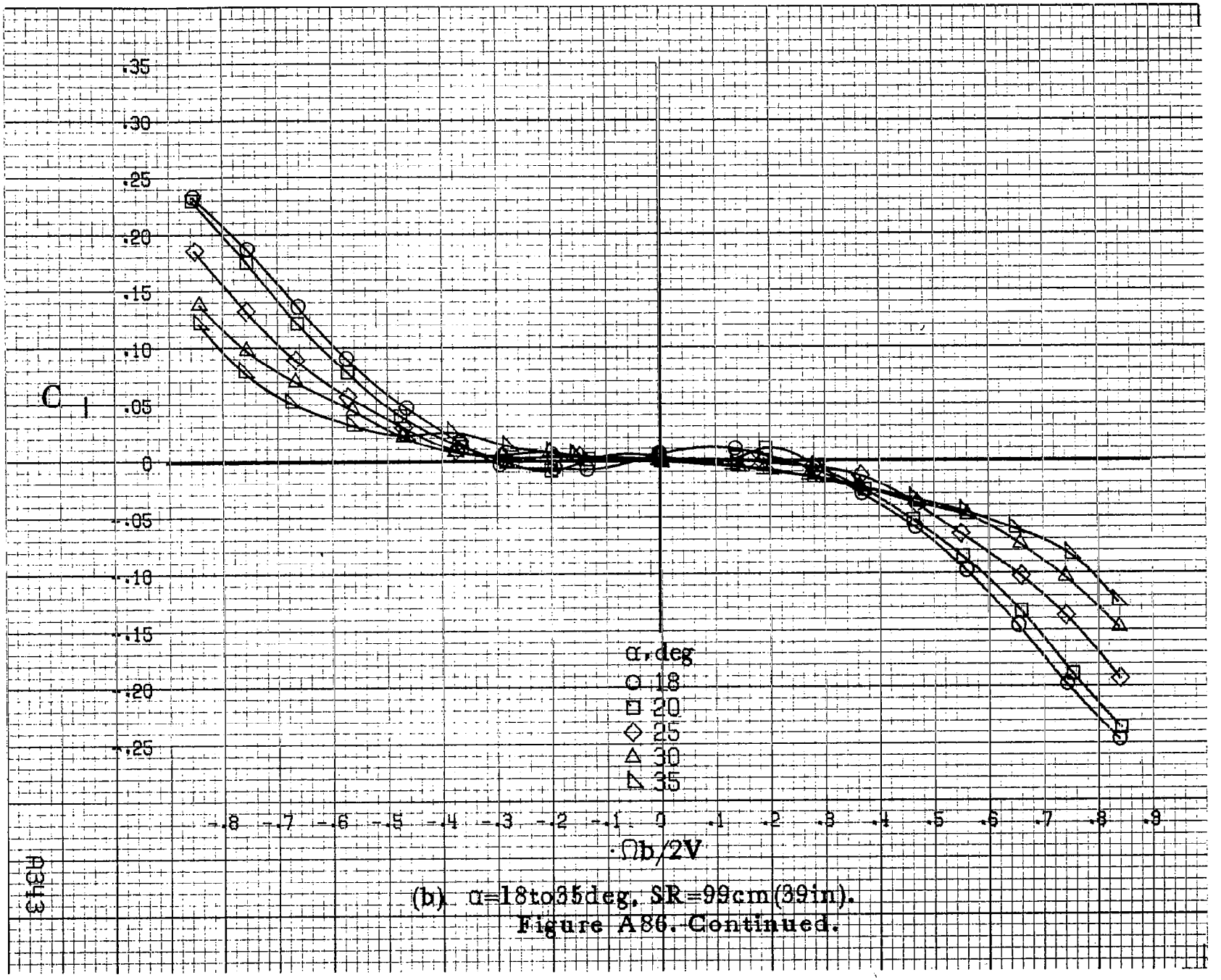

(b) α=18to35deg, SR=99cm(39in).

Figure A86. Continued.

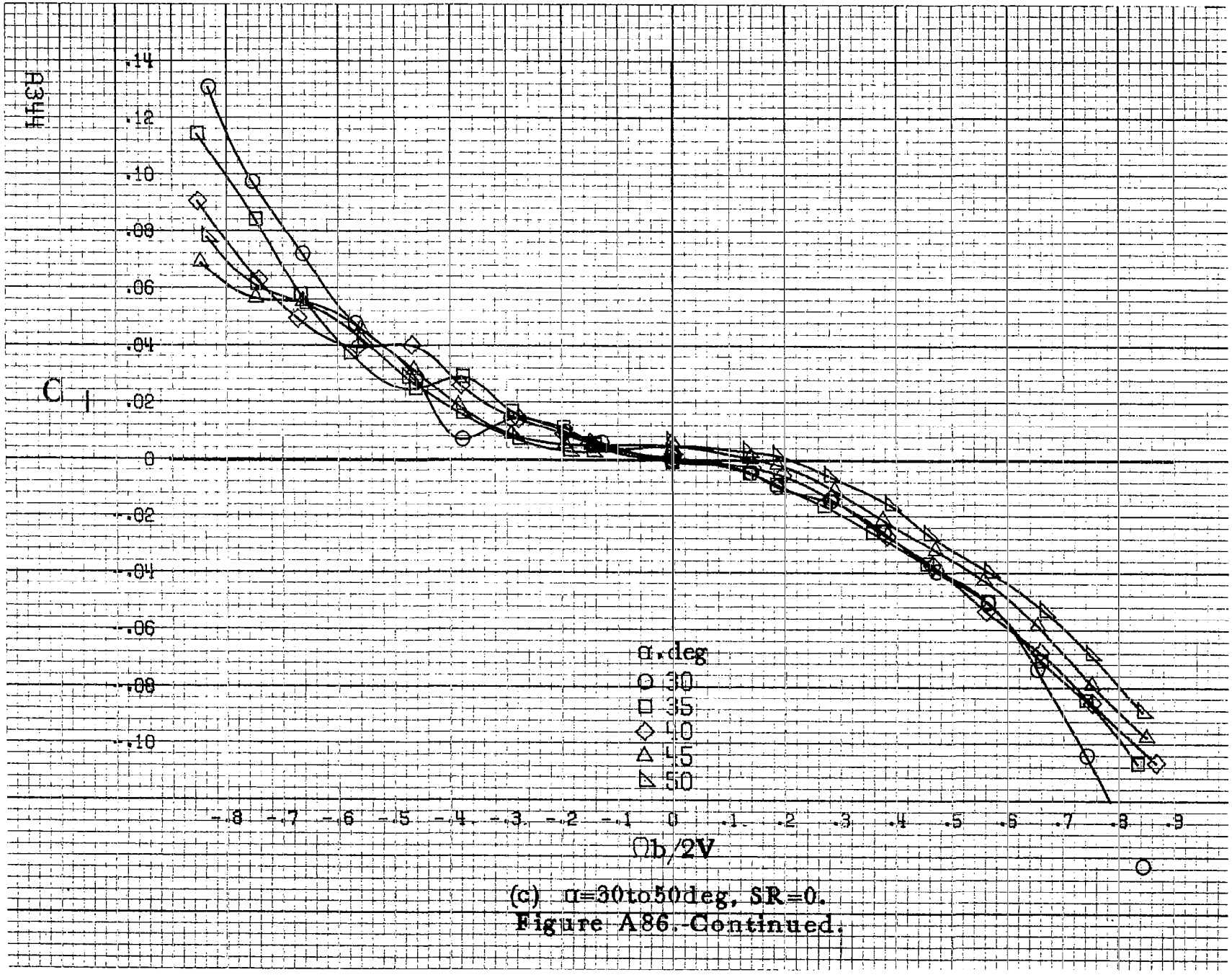

(c) α=30to50deg, SR=0.

Figure A86.-Continued.

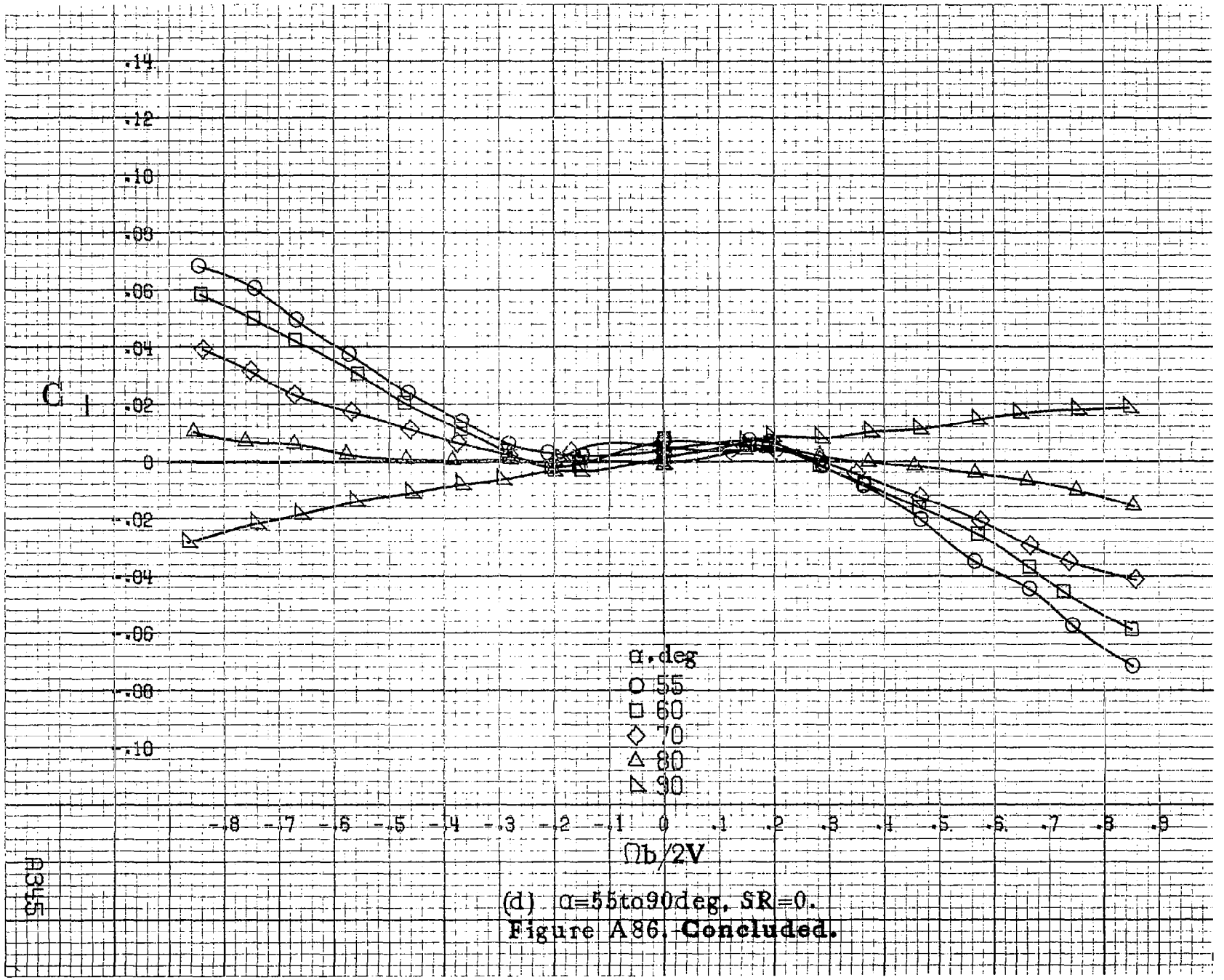

(d) α=55to90deg, SR=0.

Figure A86. Concluded.

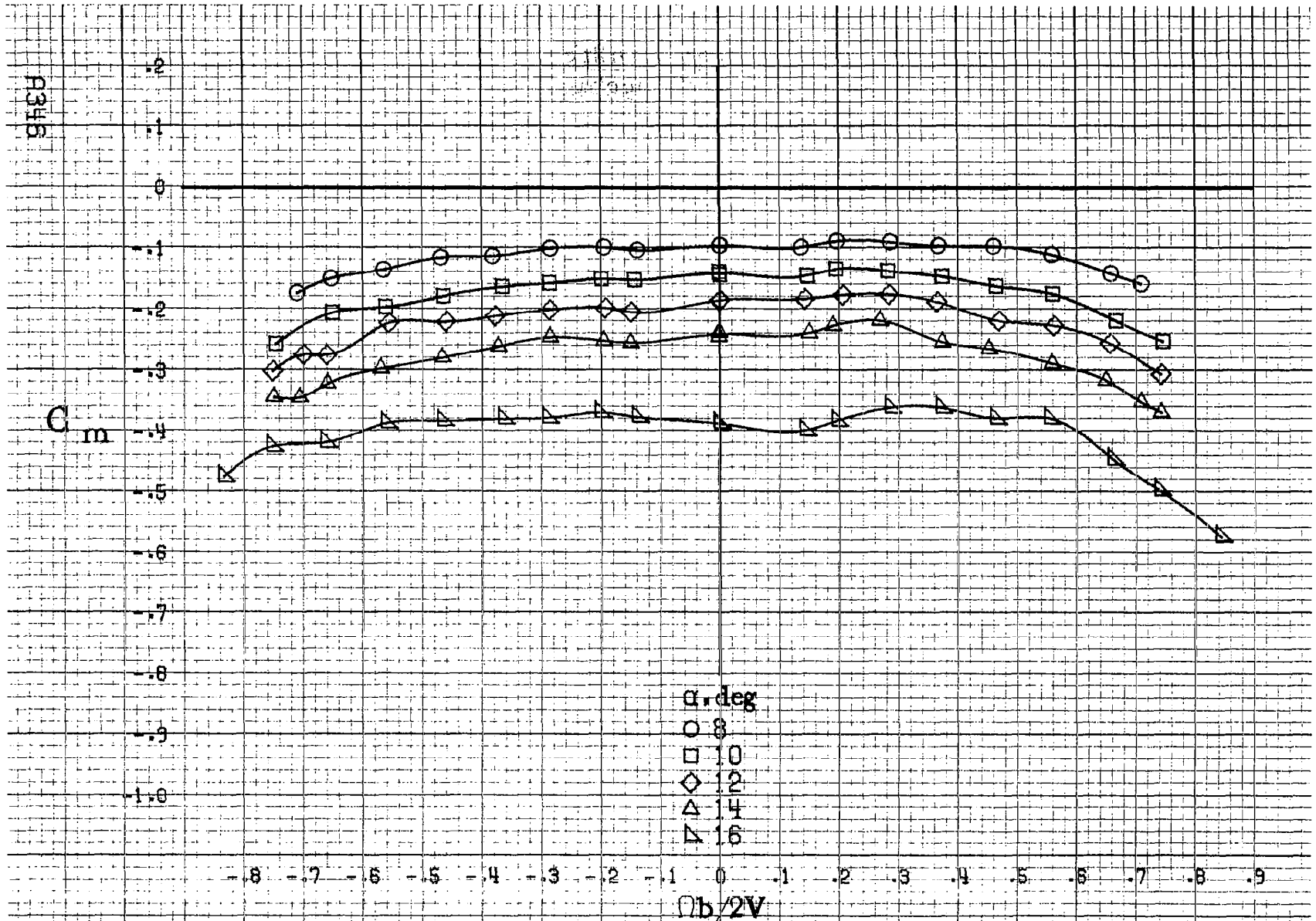

(a) α=8to16deg, SR=99cm(39in).

Figure A87.-Effect of rotation rate and angle of attack on pitching-moment coefficient for configuration having sharp-edged fuselage bottom aft of engine cowling. $\delta_e = 0°$, $\delta_a = 0°$, $\delta_r = 0°$, $\beta = 0°$.

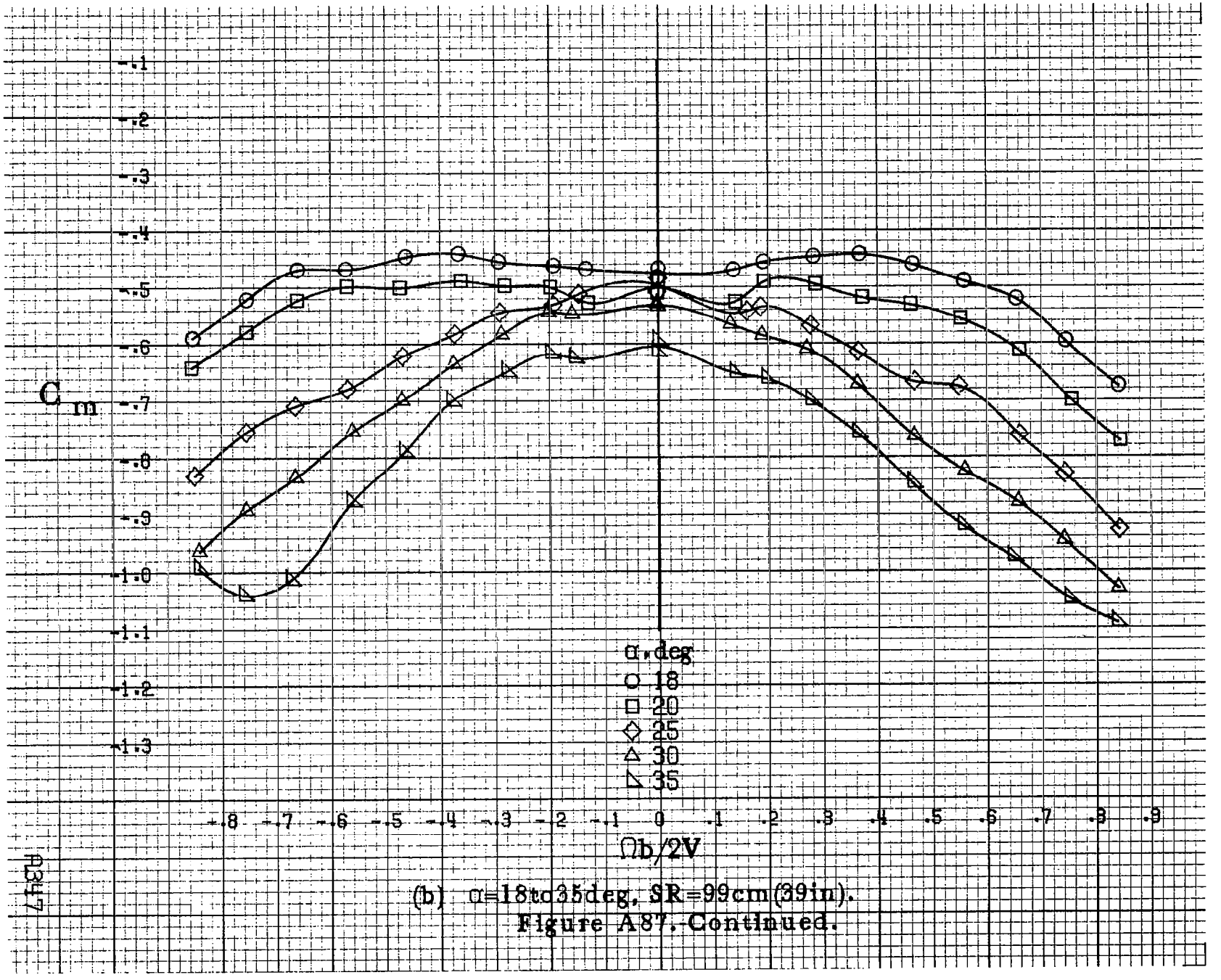

(b) α=18to35deg, SR=99cm(39in).

Figure A87.-Continued.

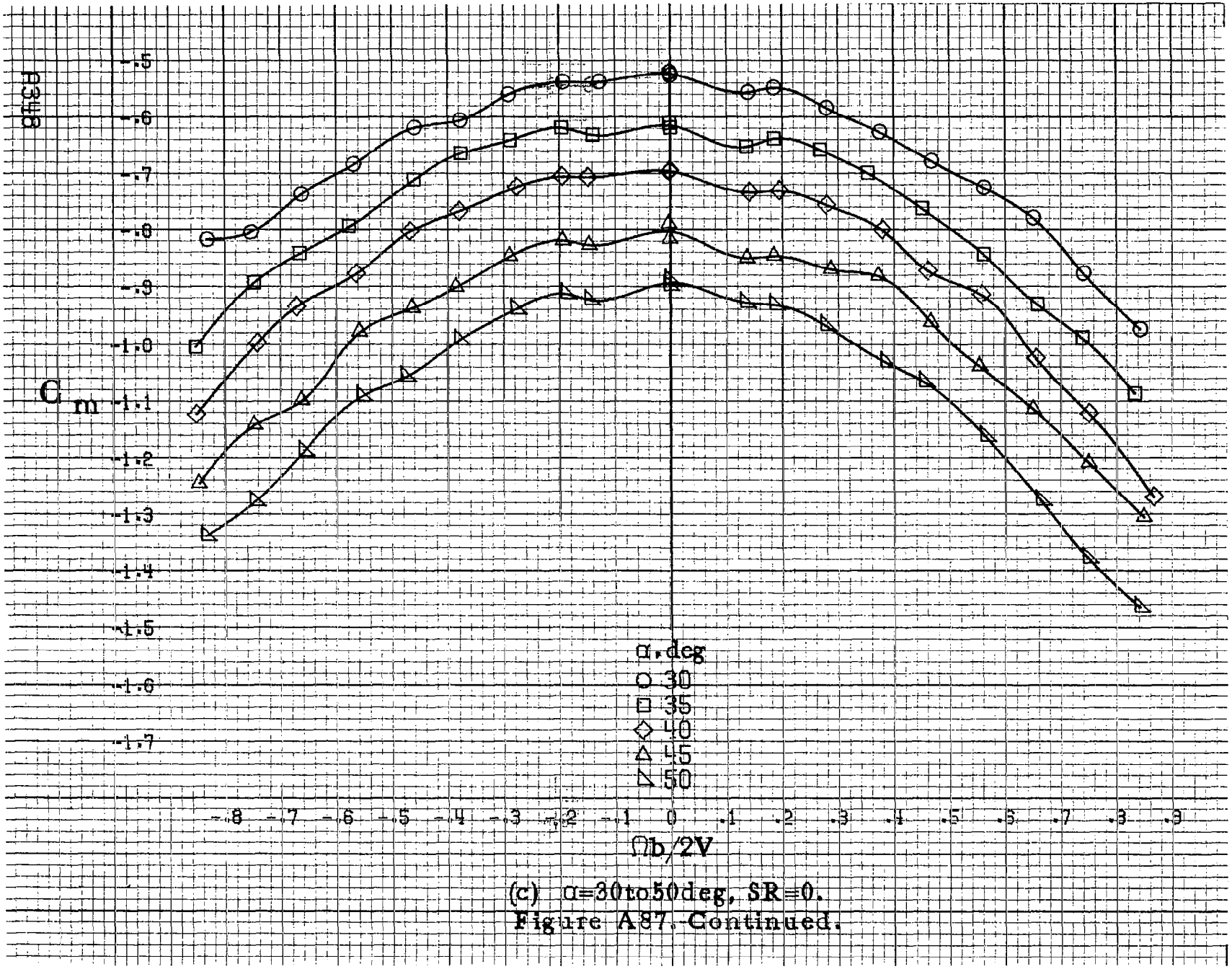

(c) α=30to50deg, SR=0.

Figure A87.-Continued.

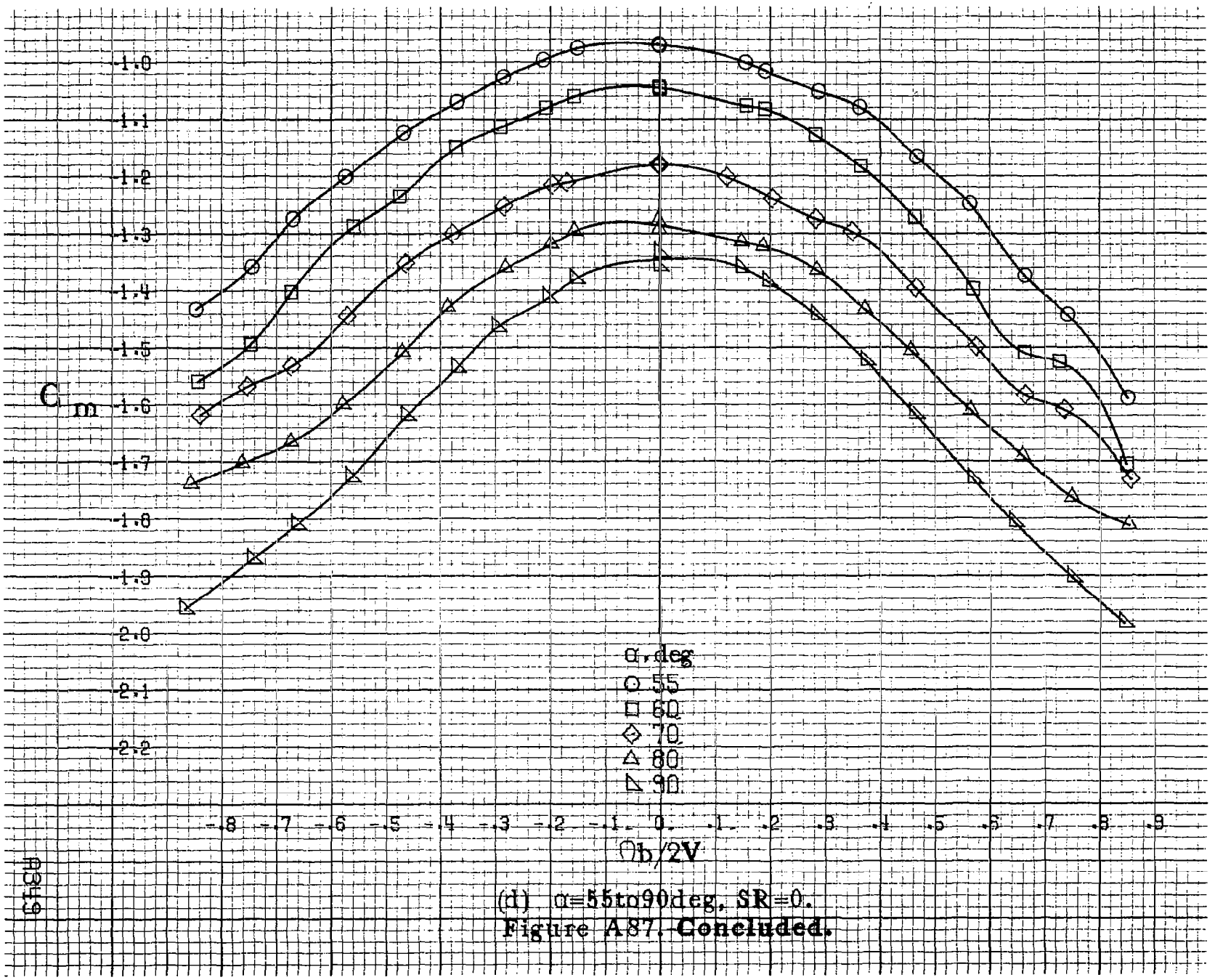

Figure A87. Concluded.

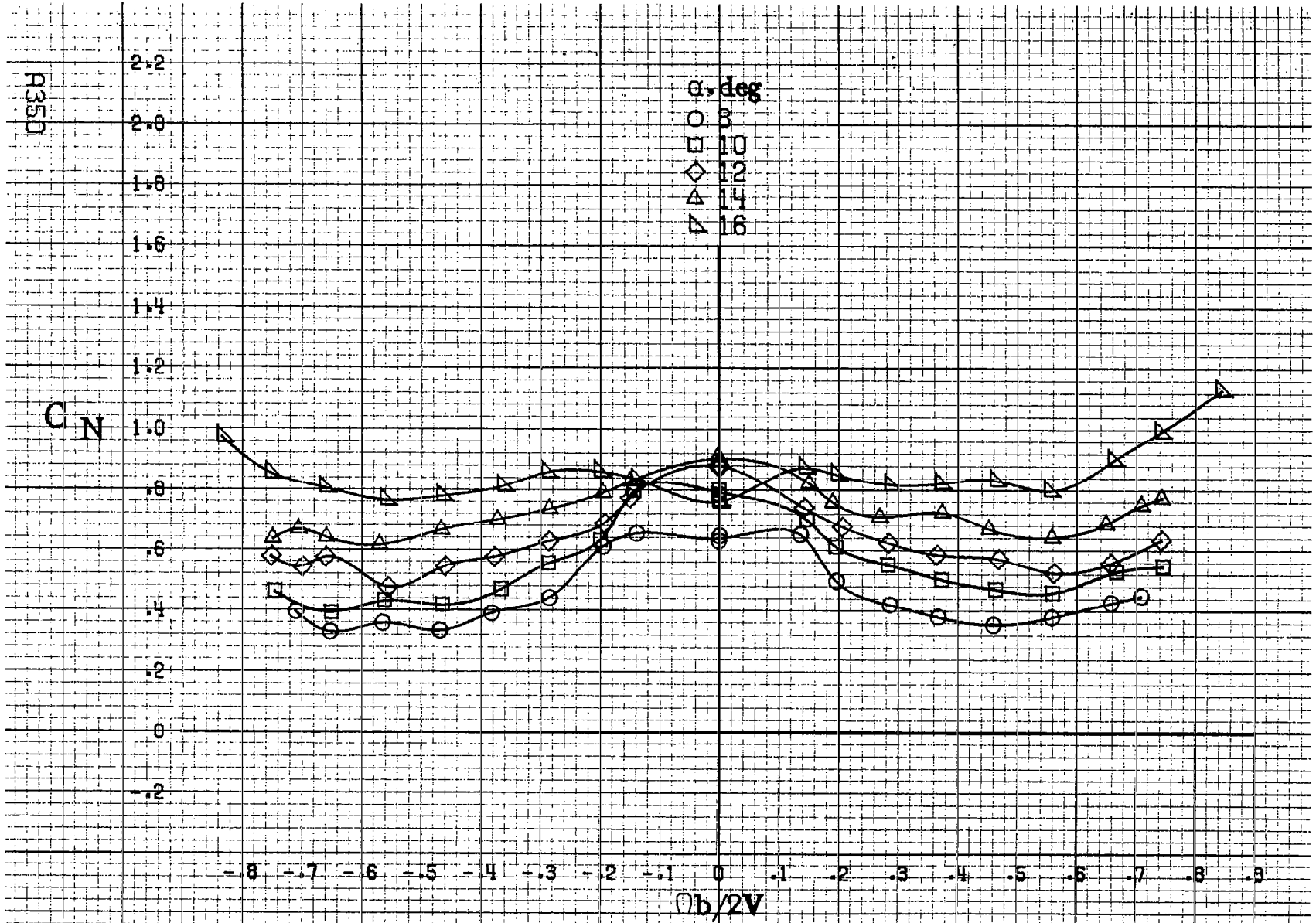

(a) α=8to16deg, SR=99cm(39in).

Figure A88.-Effect of rotation rate and angle of attack on normal-force coefficient for configuration having sharp-edged fuselage bottom aft of engine cowling. $\delta_a = 0°$, $\delta_a = 0°$, $\delta_r = 0°$, $\beta = 0°$.

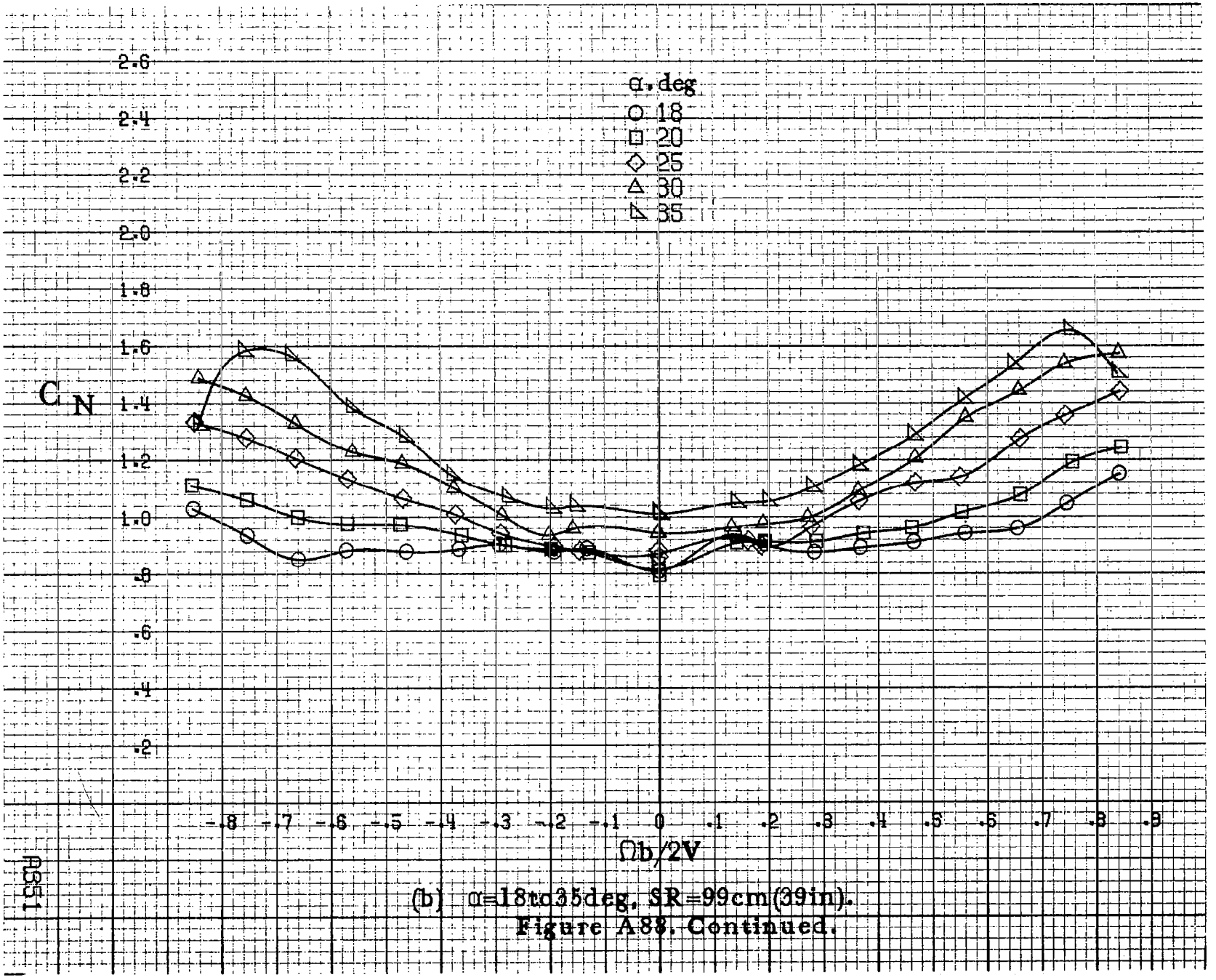

(b) α=18to35deg, SR=99cm(39in).

Figure A88. Continued.

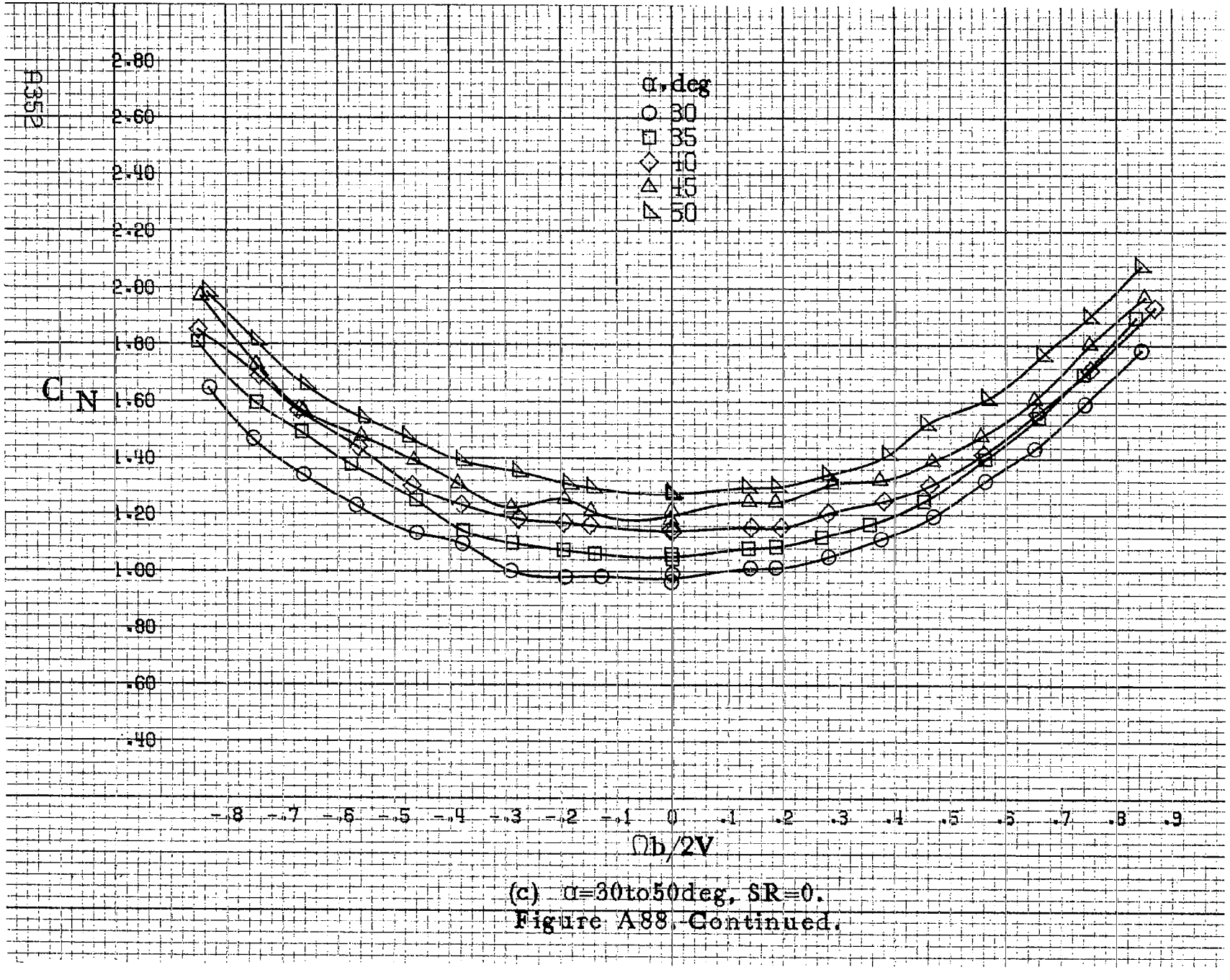

(c) α=30to50deg, SR=0.

Figure A88.-Continued.

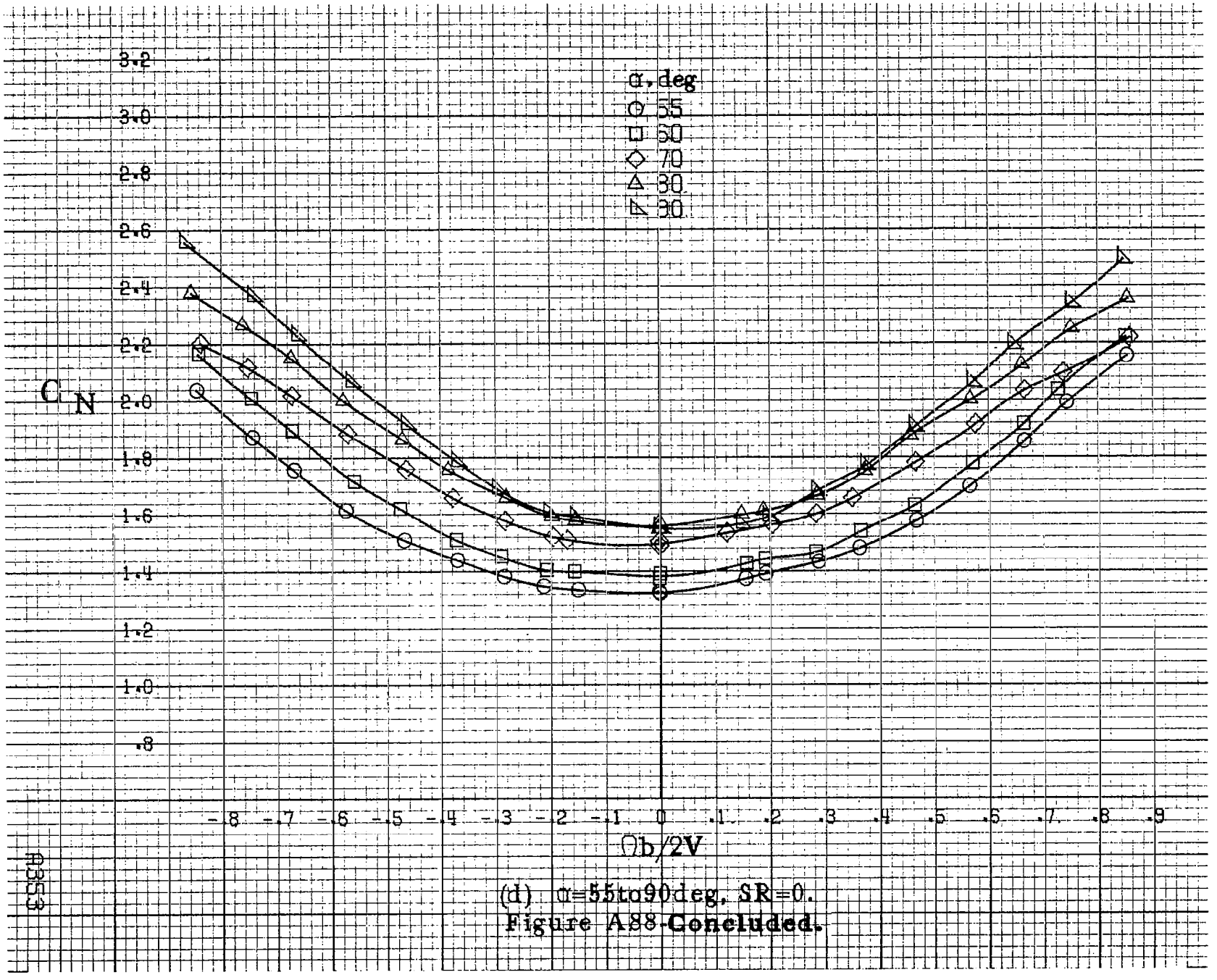

(d) α=55to90deg, SR=0.

Figure A88-Concluded.

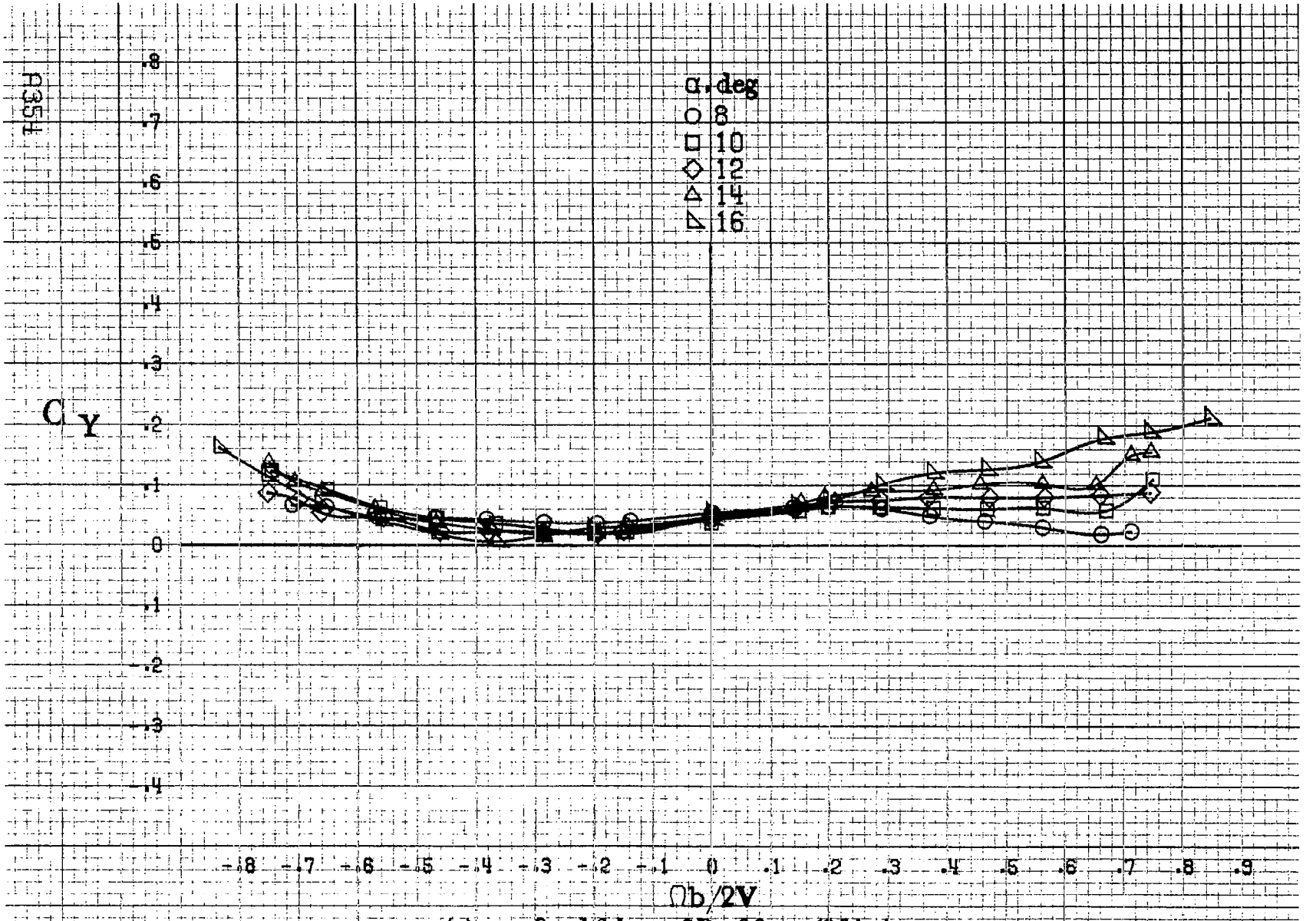

(a) α=8to16deg, SR=99cm(39in).

Figure A89.-Effect of rotation rate and angle of attack on side-force coefficient for configuration having sharp-edged fuselage bottom aft of engine cowling. $\delta_a = 0°$, $\delta_a = 0°$, $\delta_r = 0°$, $\beta = 0°$.

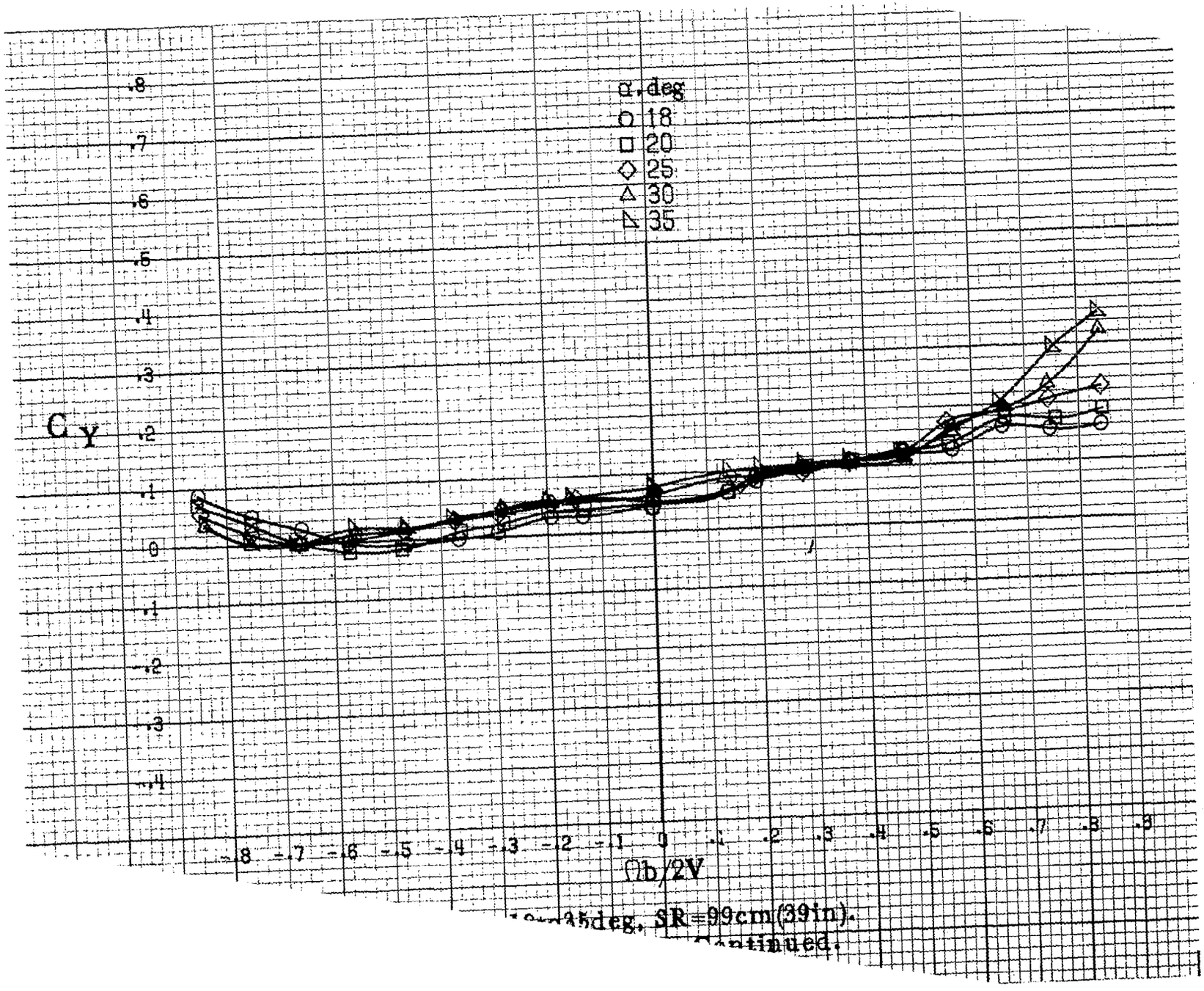

deg, SR=99cm(39in).

Continued.

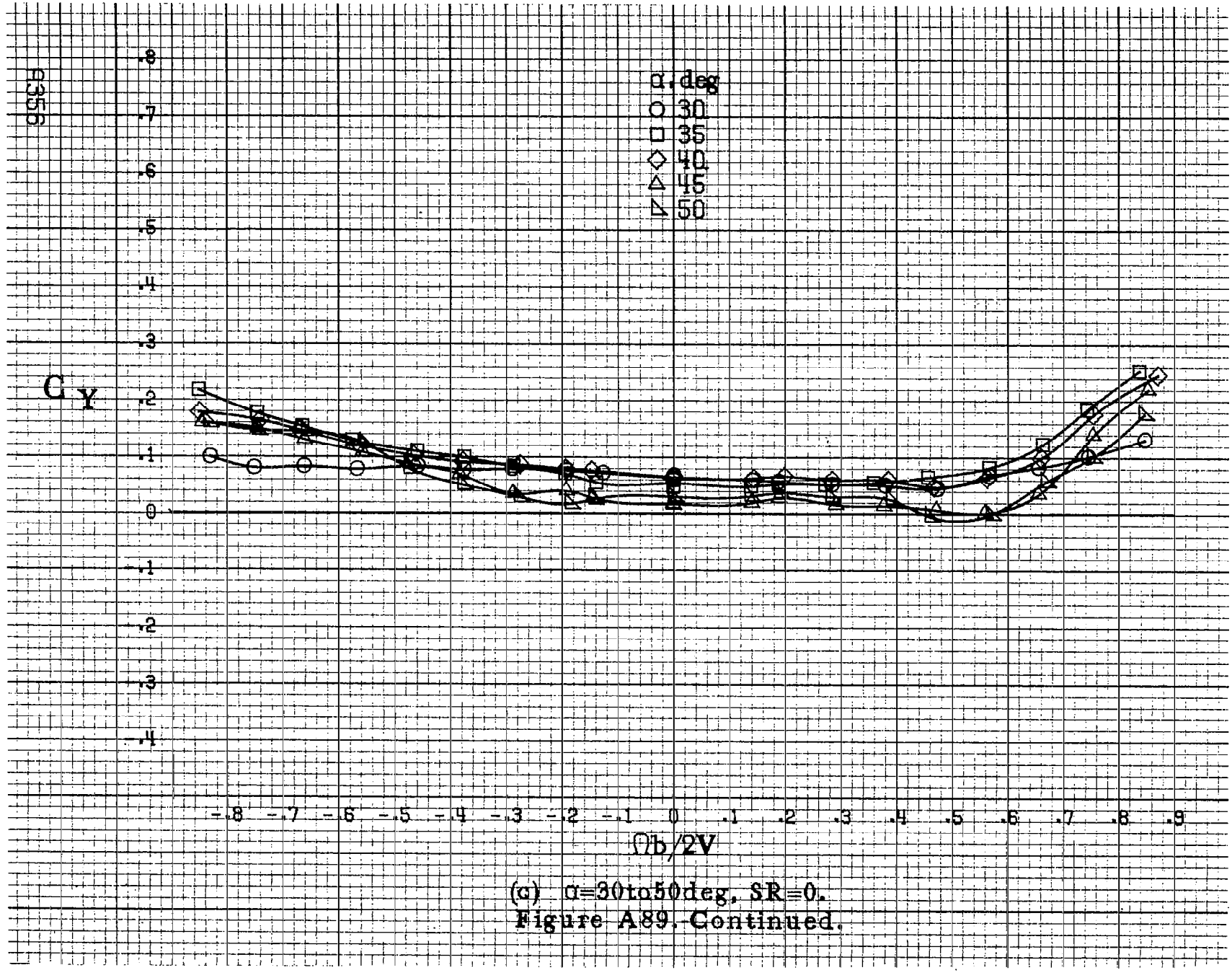

(c) α=30to50deg, SR=0.

Figure A89. Continued.

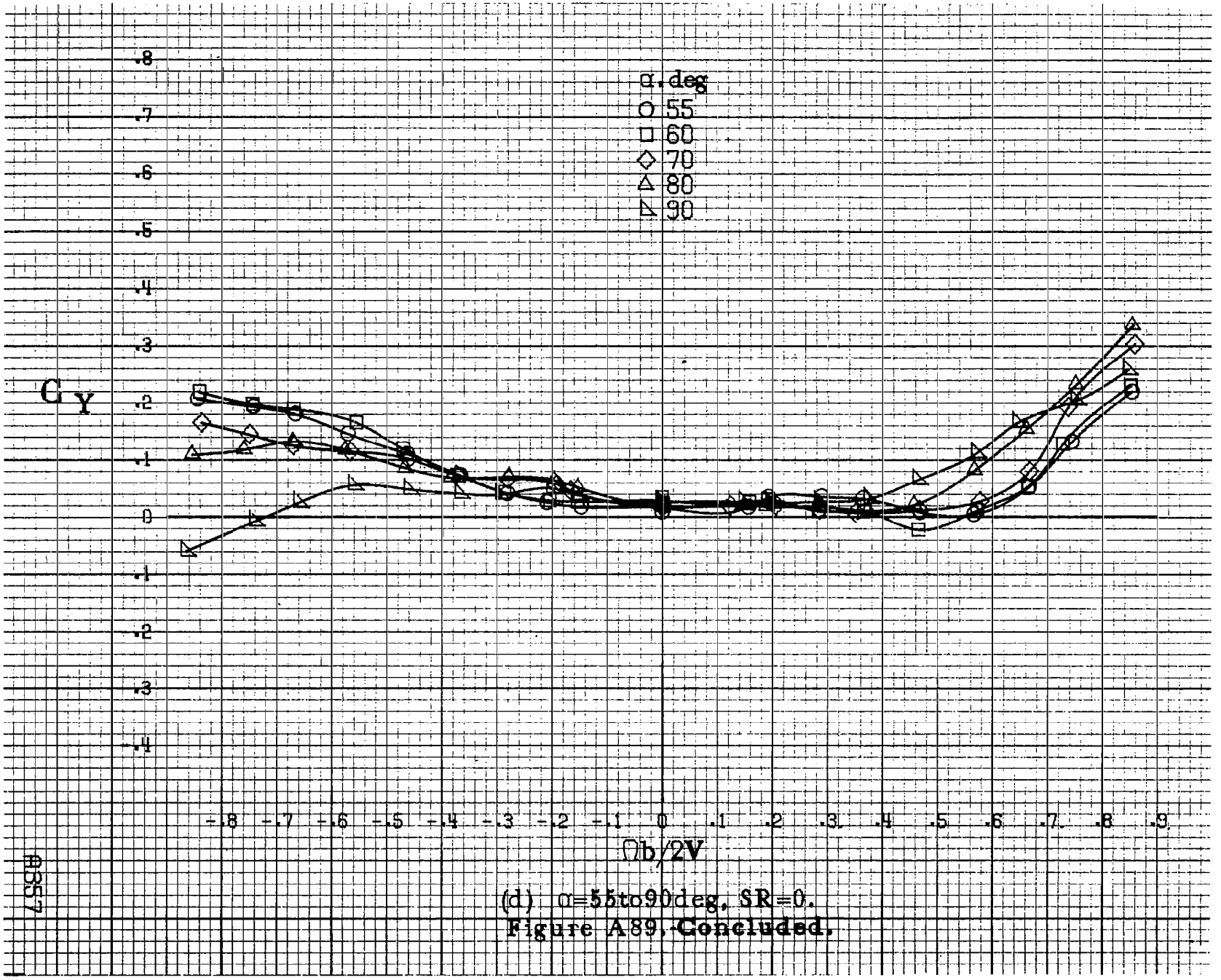

B957

(d) α=55to90deg, SR=0.

Figure A89.-Concluded.

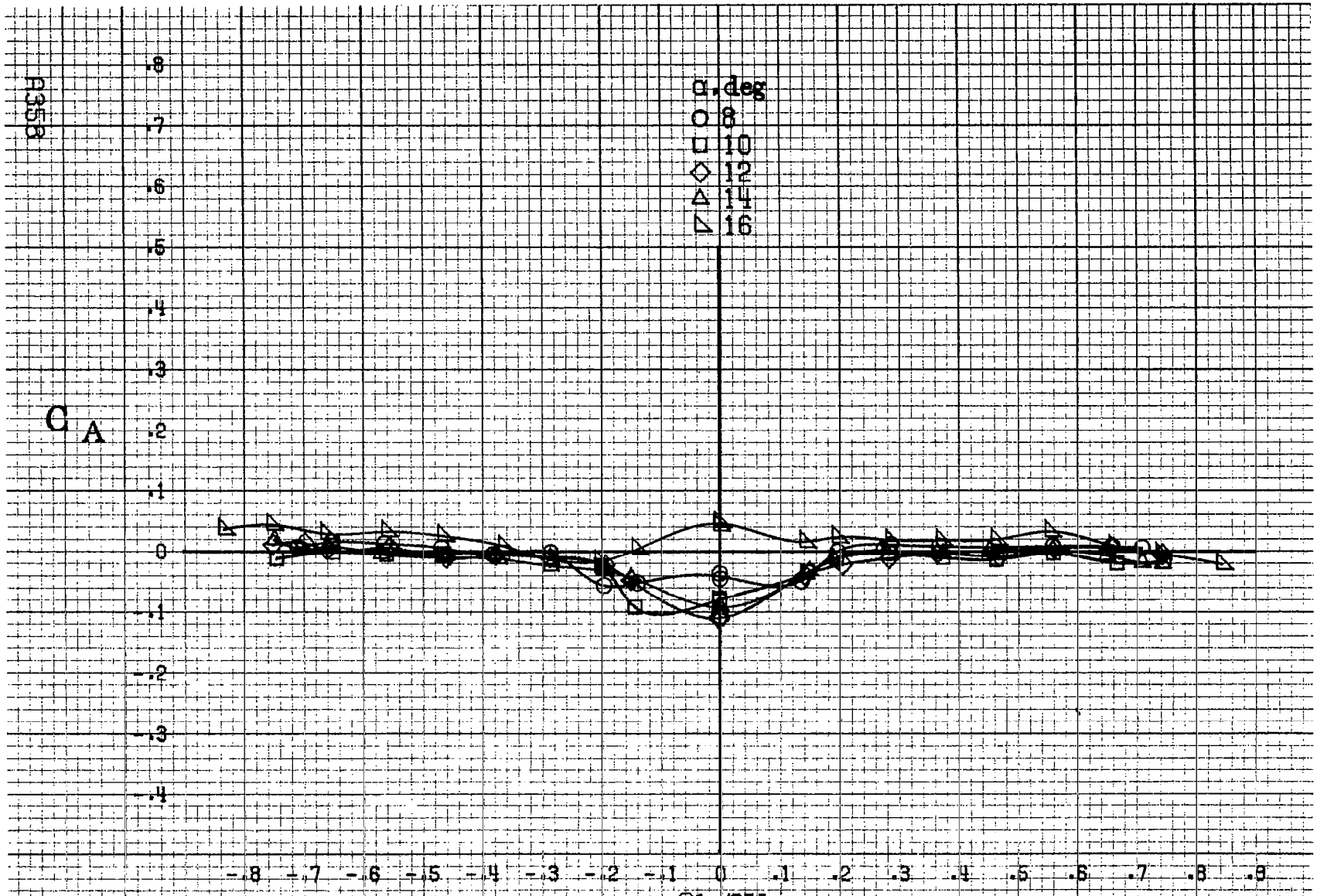

(a) α=8to16deg, SR=99cm(39in).

Figure A90. Effect of rotation rate and angle of attack on axial-force coefficient for configuration having sharp-edged fuselage bottom aft of engine cowling. $\delta_e = 0°$, $\delta_a = 0°$, $\delta_r = 0°$, $\beta = 0°$.

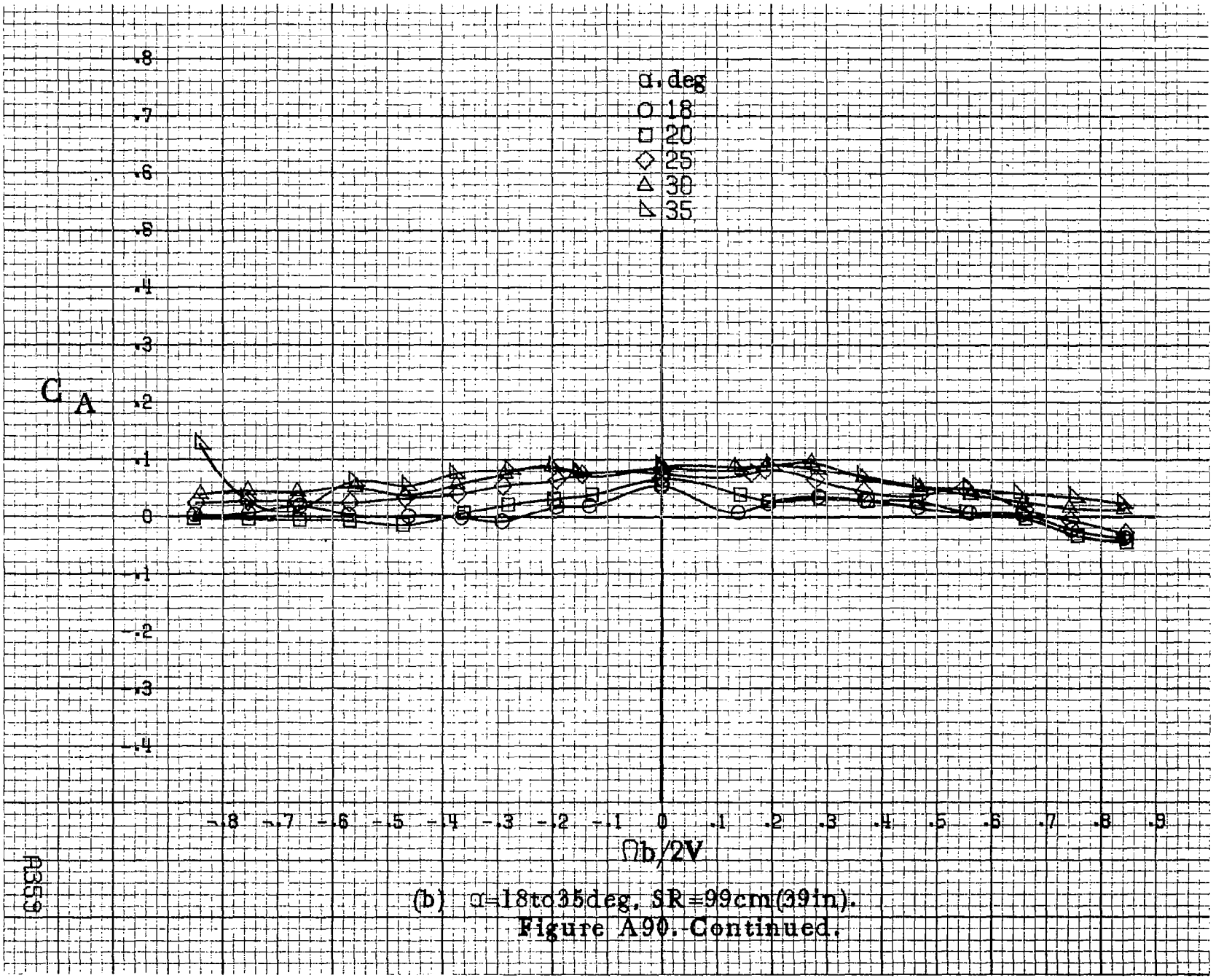

(b) α=18to35deg, SR=99cm(39in).

Figure A90.-Continued.

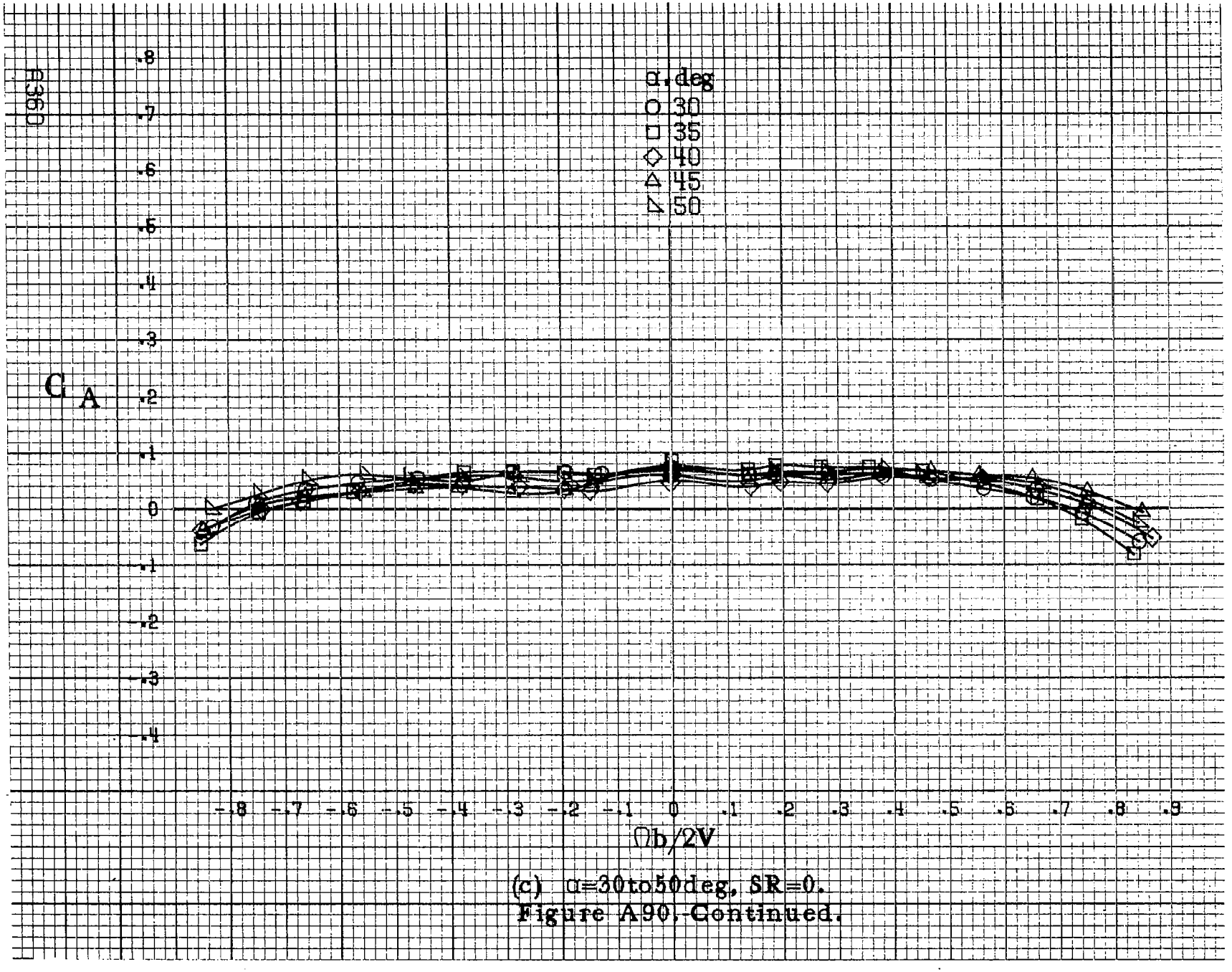

(c) α=30to50deg, SR=0.

Figure A90.-Continued.

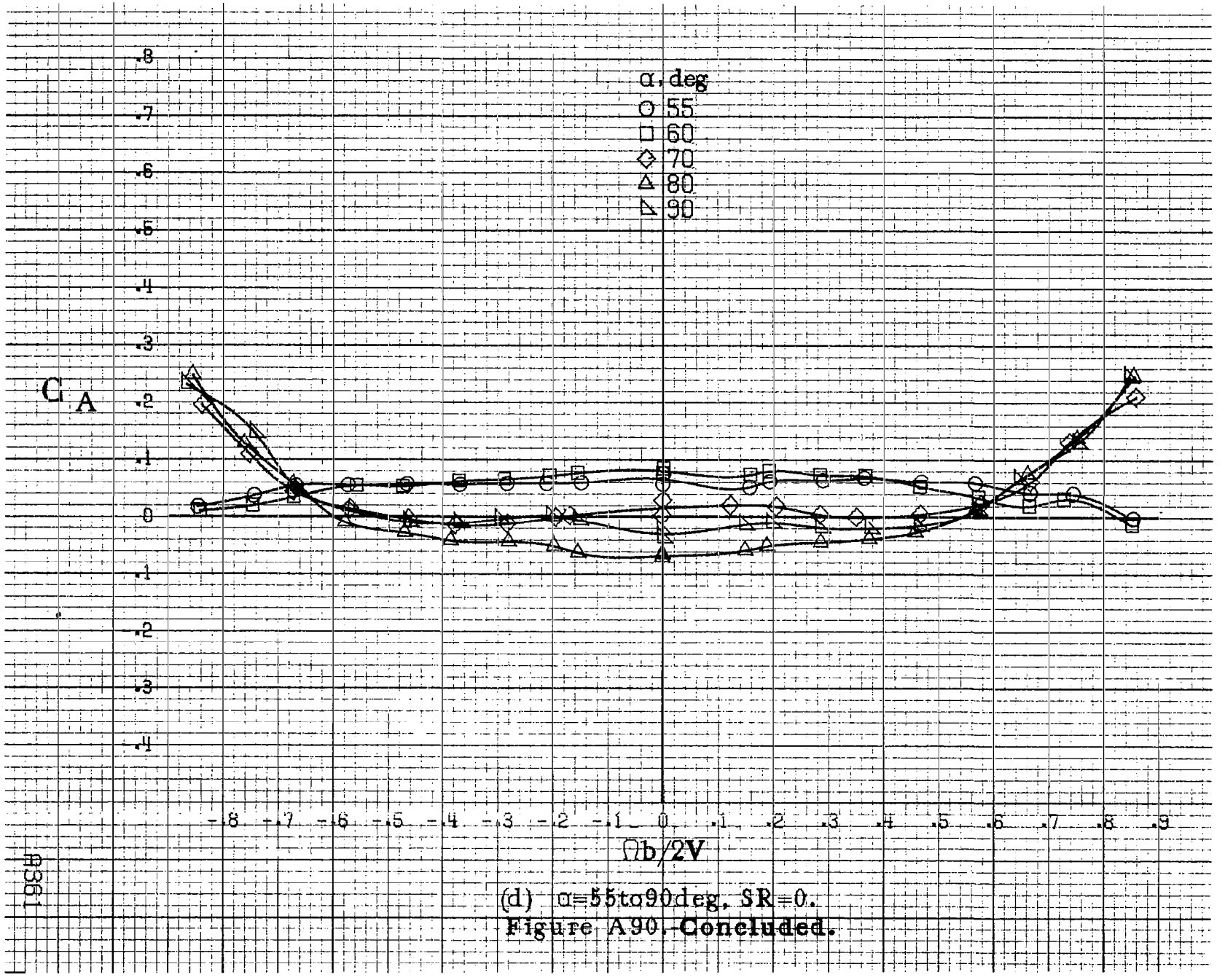

(d) α=55 to 90 deg, SR=0.

Figure A90. Concluded.

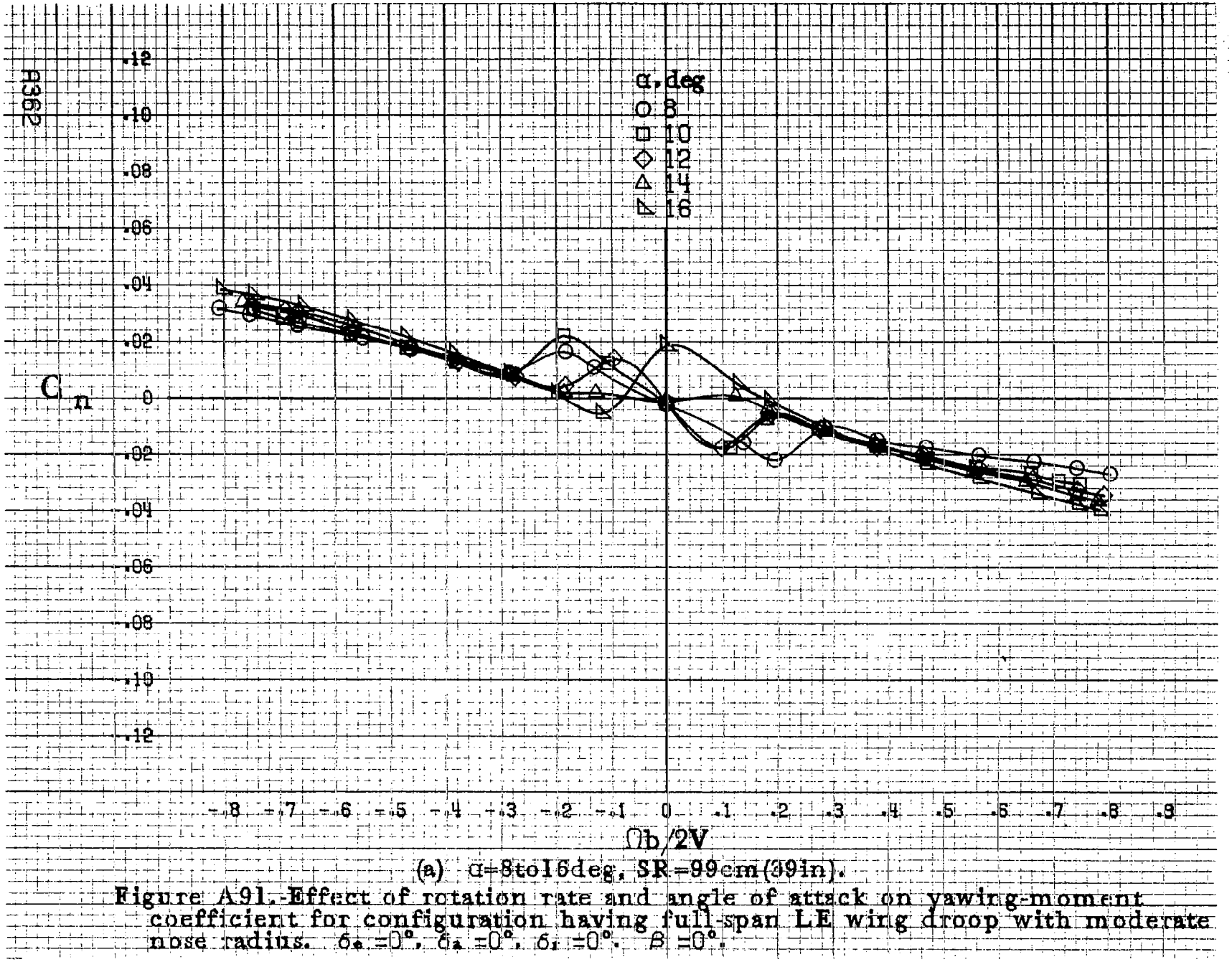

(a) α=8to16deg, SR=99cm(39in).

Figure A91.-Effect of rotation rate and angle of attack on yawing-moment coefficient for configuration having full-span LE wing droop with moderate nose radius. $\delta_e = 0°$, $\delta_a = 0°$, $\delta_r = 0°$, $\beta = 0°$.

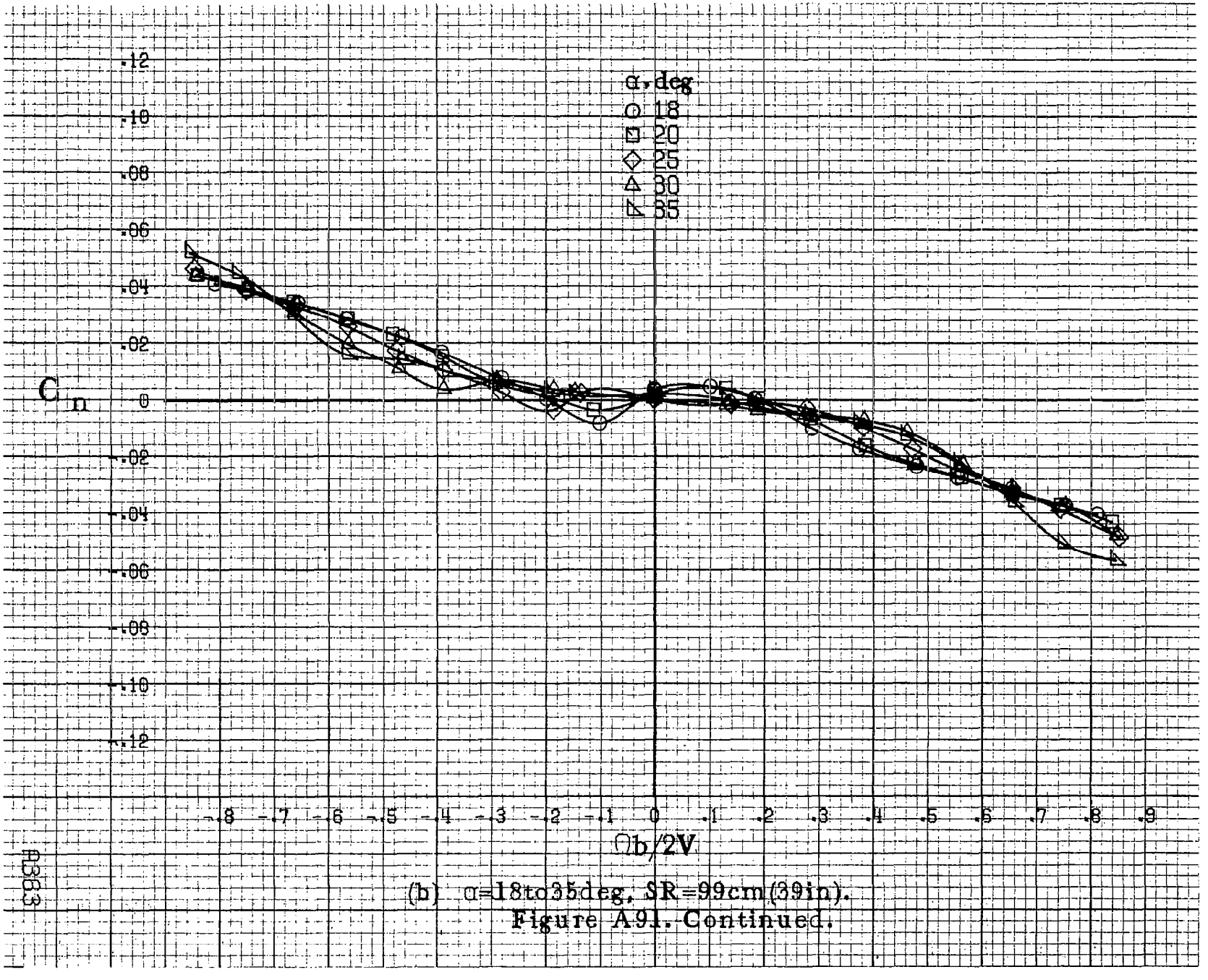

(b) α=18to35deg, SR=99cm(39in).

Figure A91. Continued.

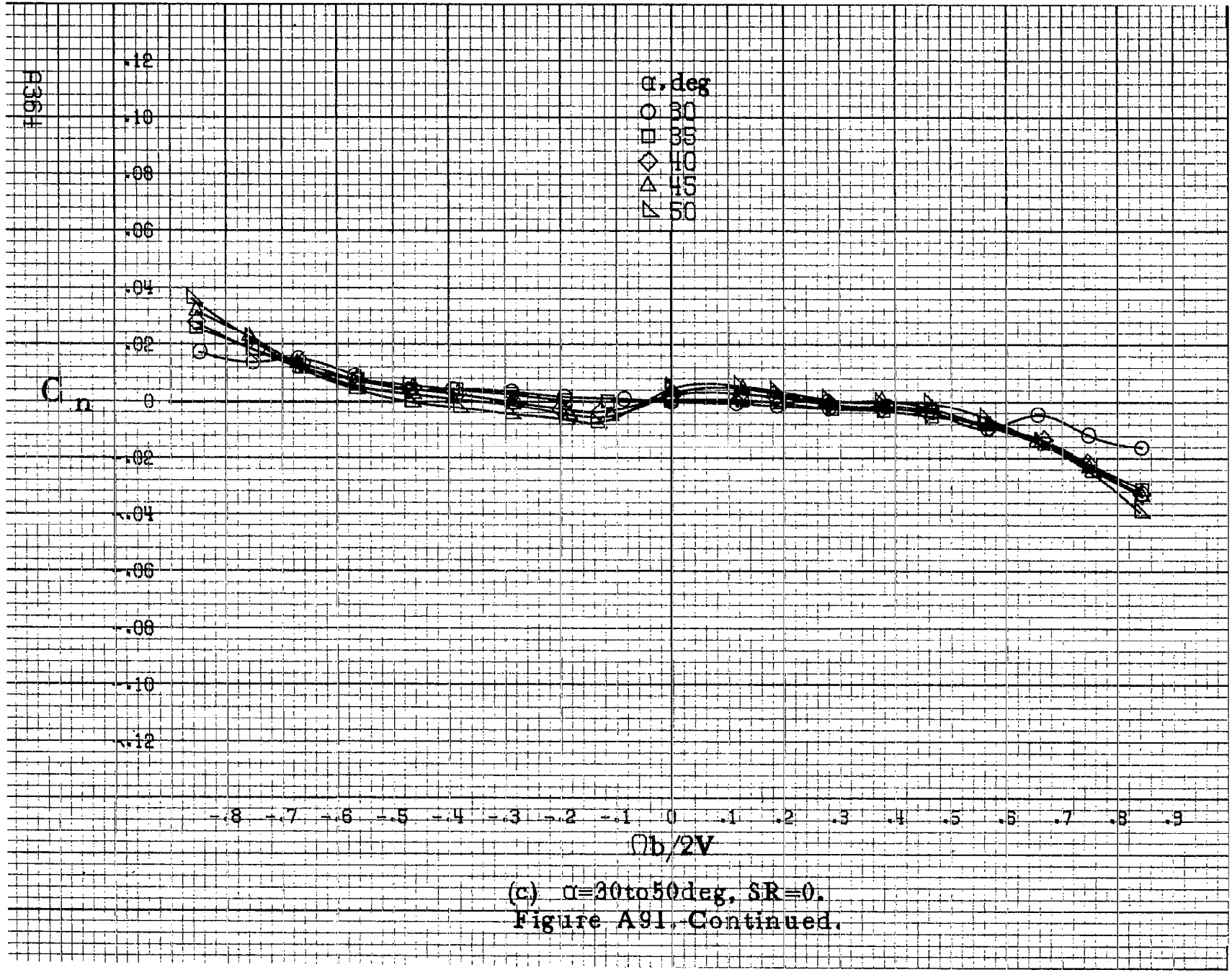

(c) α=30to50deg, SR=0.

Figure A91. Continued.

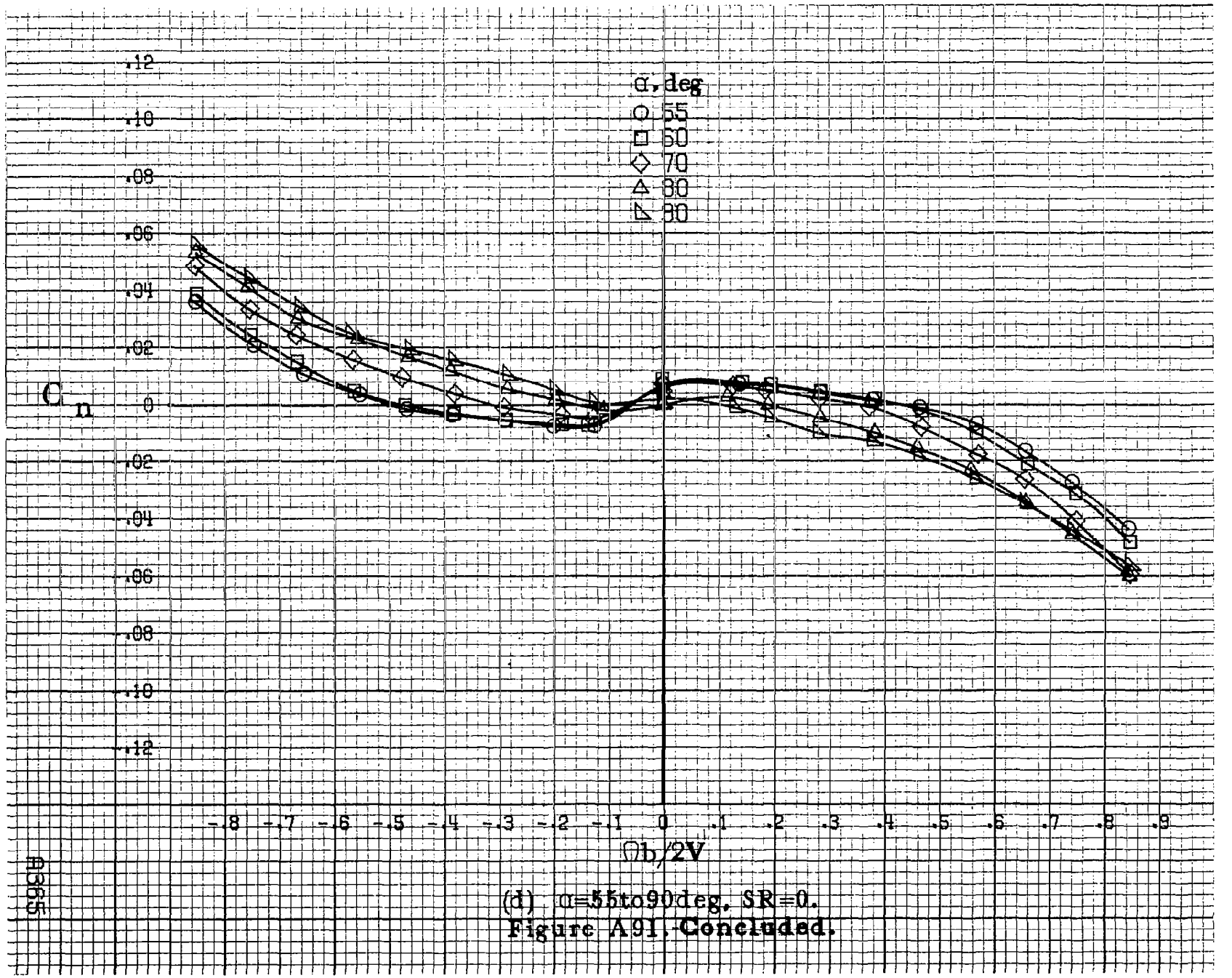

(d) α=55to90deg, SR=0.

Figure A91.-Concluded.

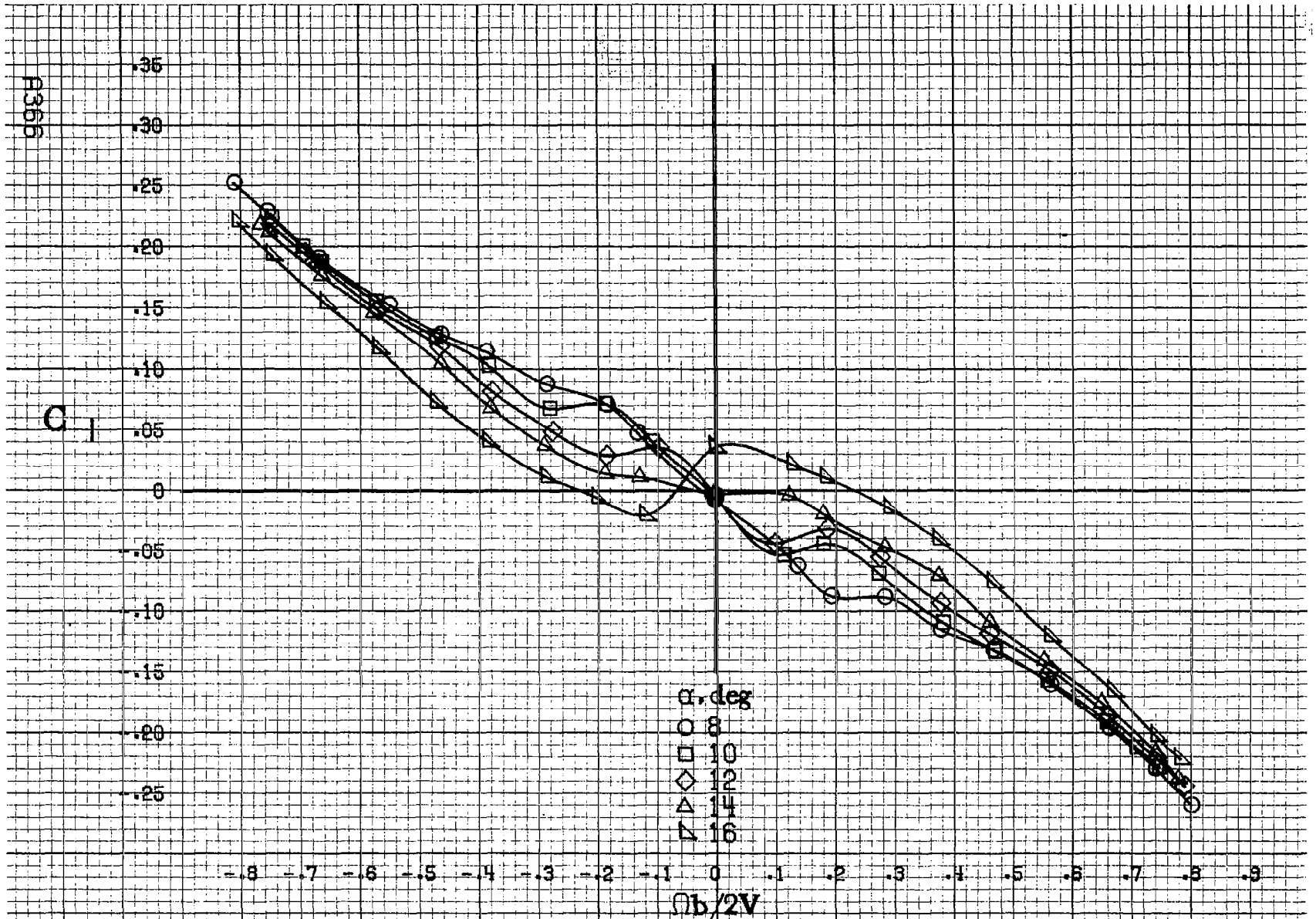

(a) α=8to16deg, SR=99cm(39in).

Figure A92.-Effect of rotation rate and angle of attack on rolling-moment coefficient for configuration having full-span LE wing droop with moderate nose radius. $\delta_e = 0°$, $\delta_a = 0°$, $\delta_r = 0°$, $\beta = 0°$.

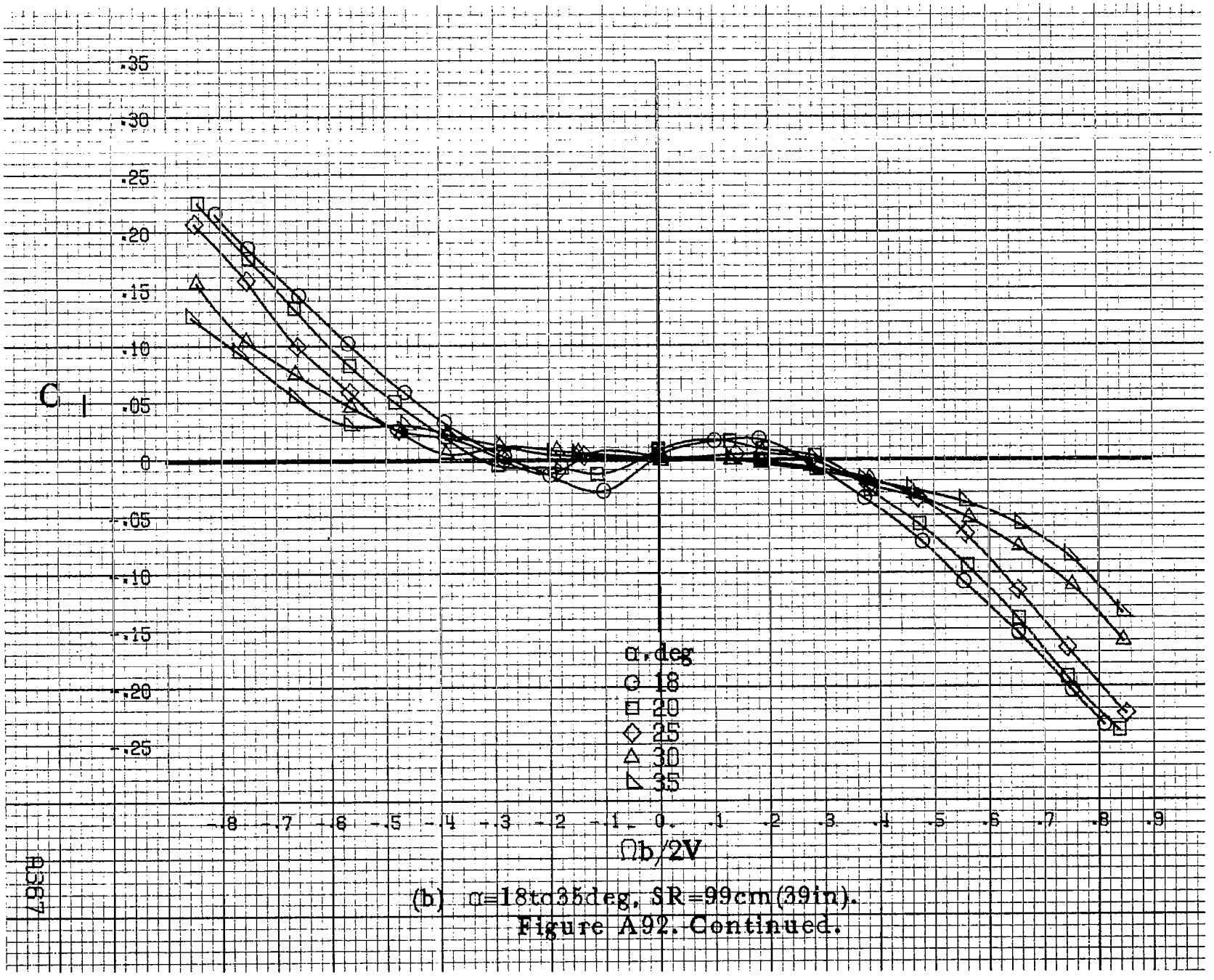

(b) α=18to35deg, SR=99cm(39in).

Figure A92. Continued.

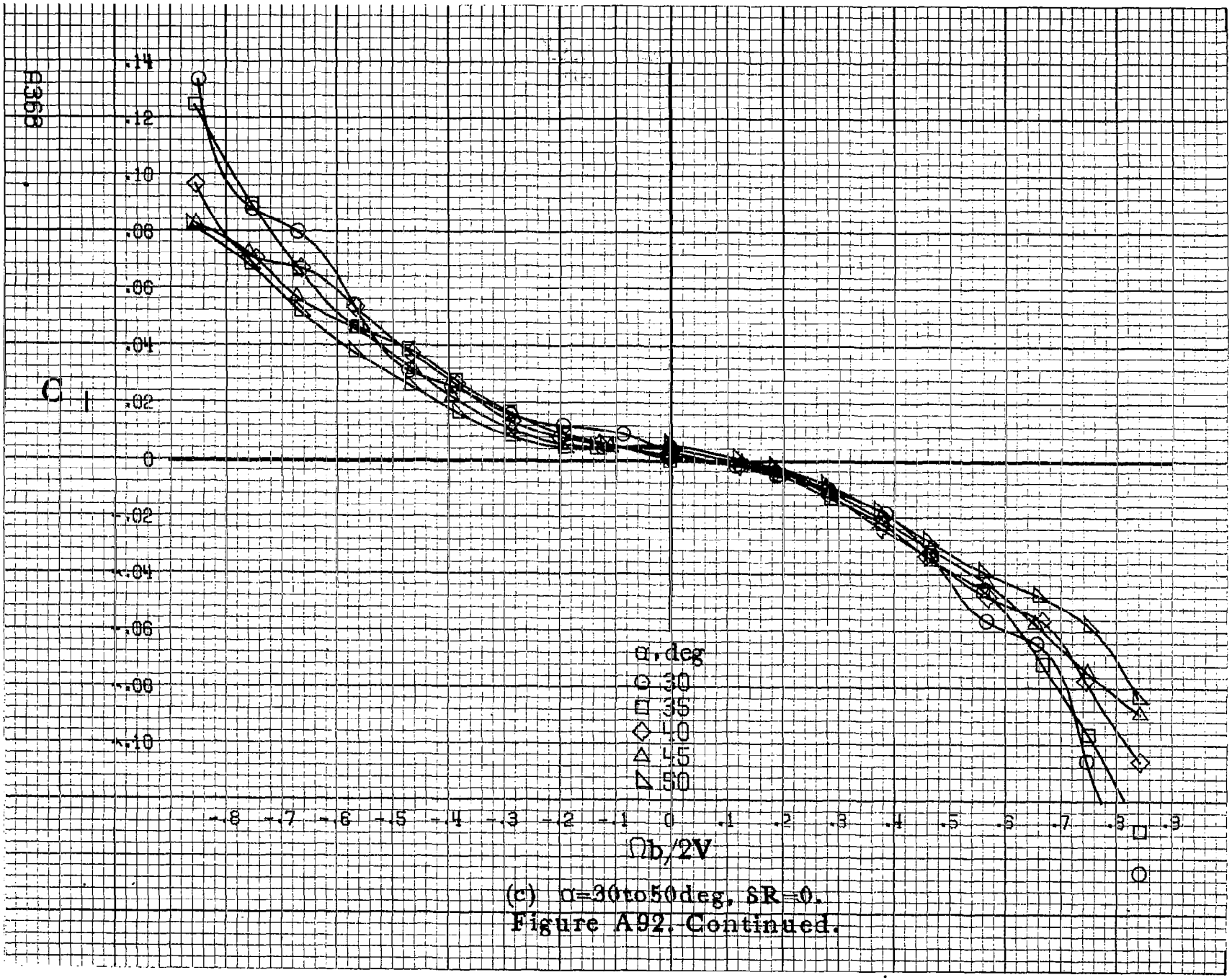

(c) α=30 to 50 deg, δR=0.

Figure A92. Continued.

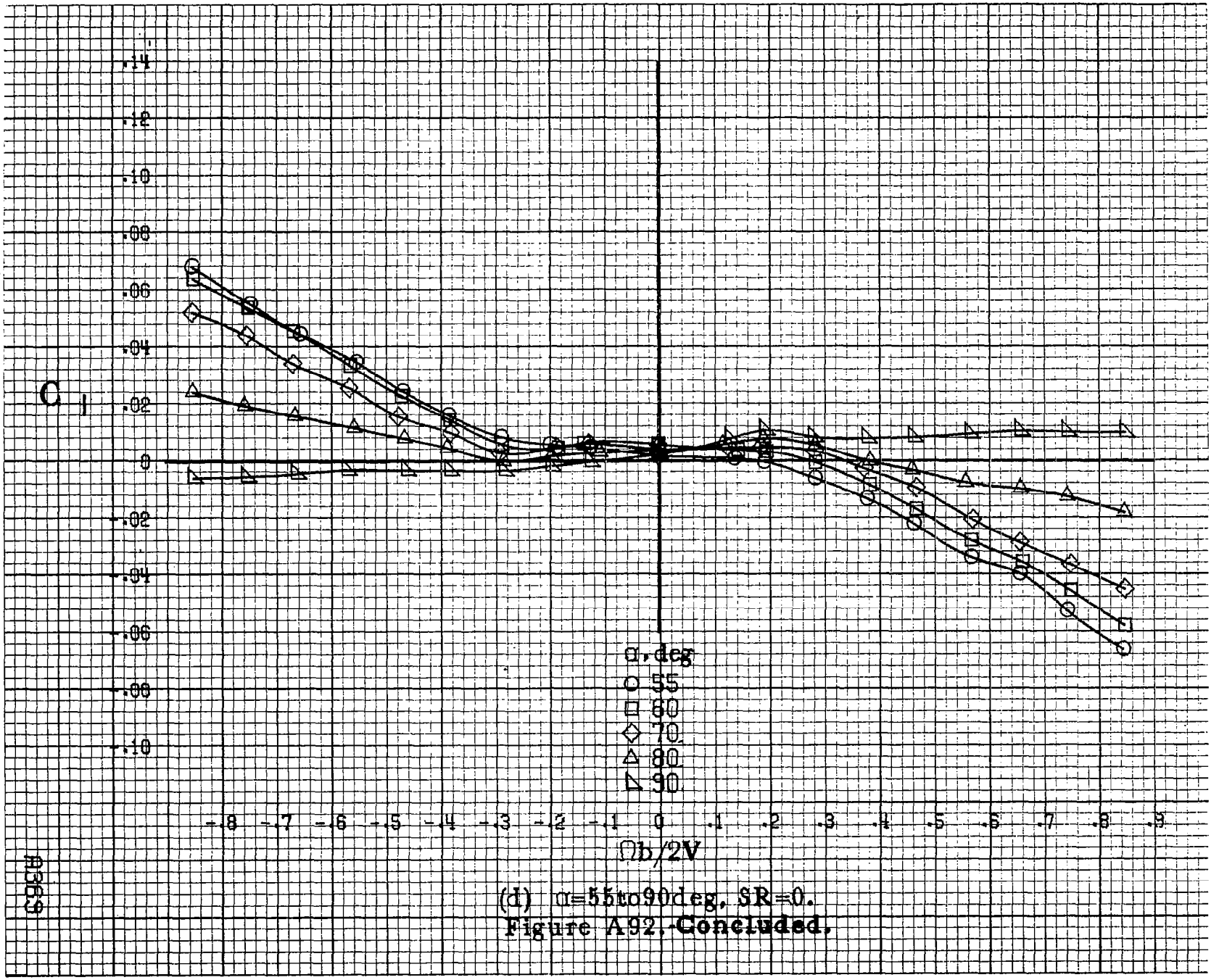

(d) α=55to90deg, SR=0.

Figure A92.-Concluded.

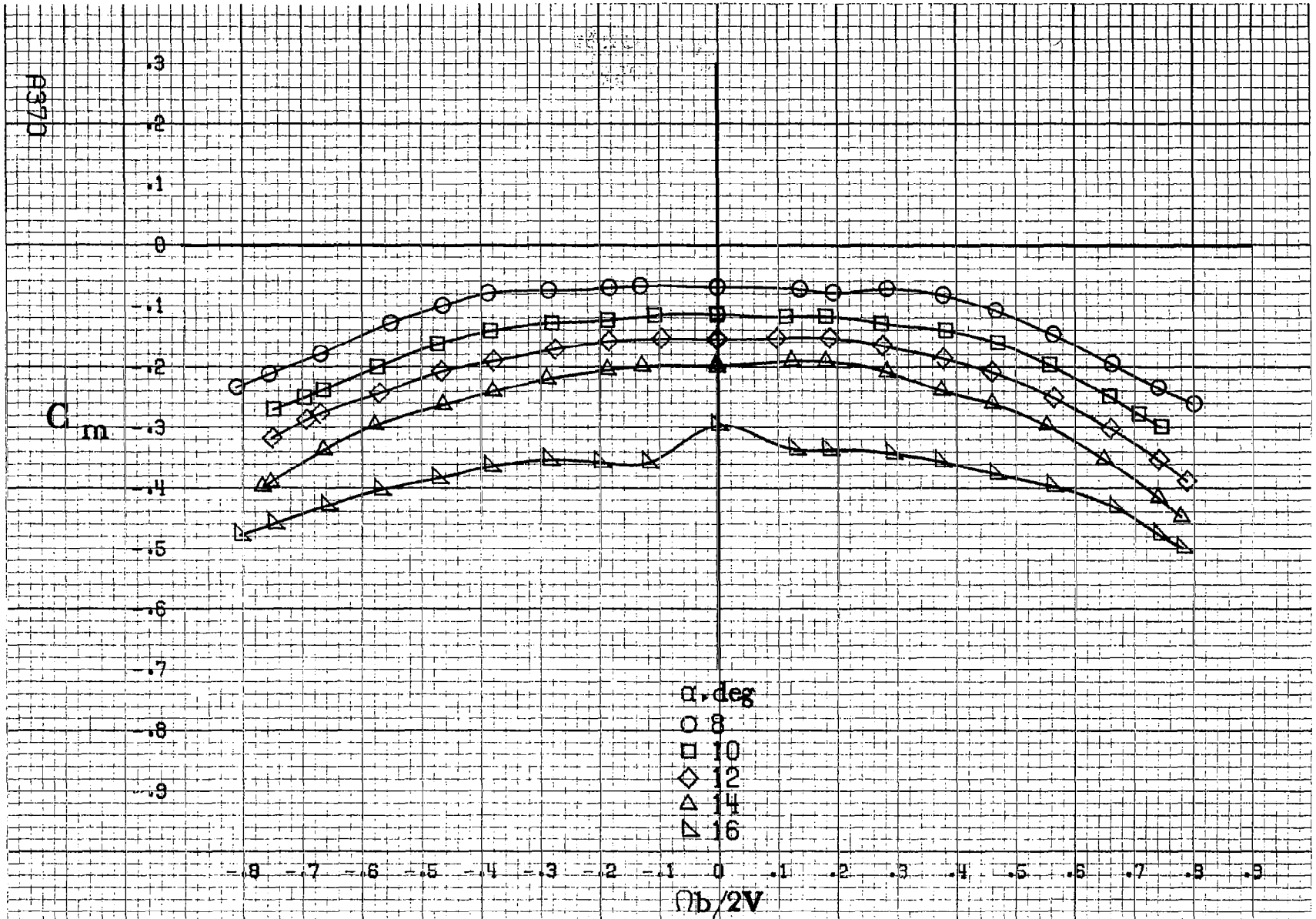

(a) α=8to16deg, SR=99cm(39in).

Figure A93. Effect of rotation rate and angle of attack on pitching-moment coefficient for configuration having full-span LE wing droop with moderate nose radius. $\delta_e = 0°$, $\delta_a = 0°$, $\delta_r = 0°$, $\beta = 0°$.

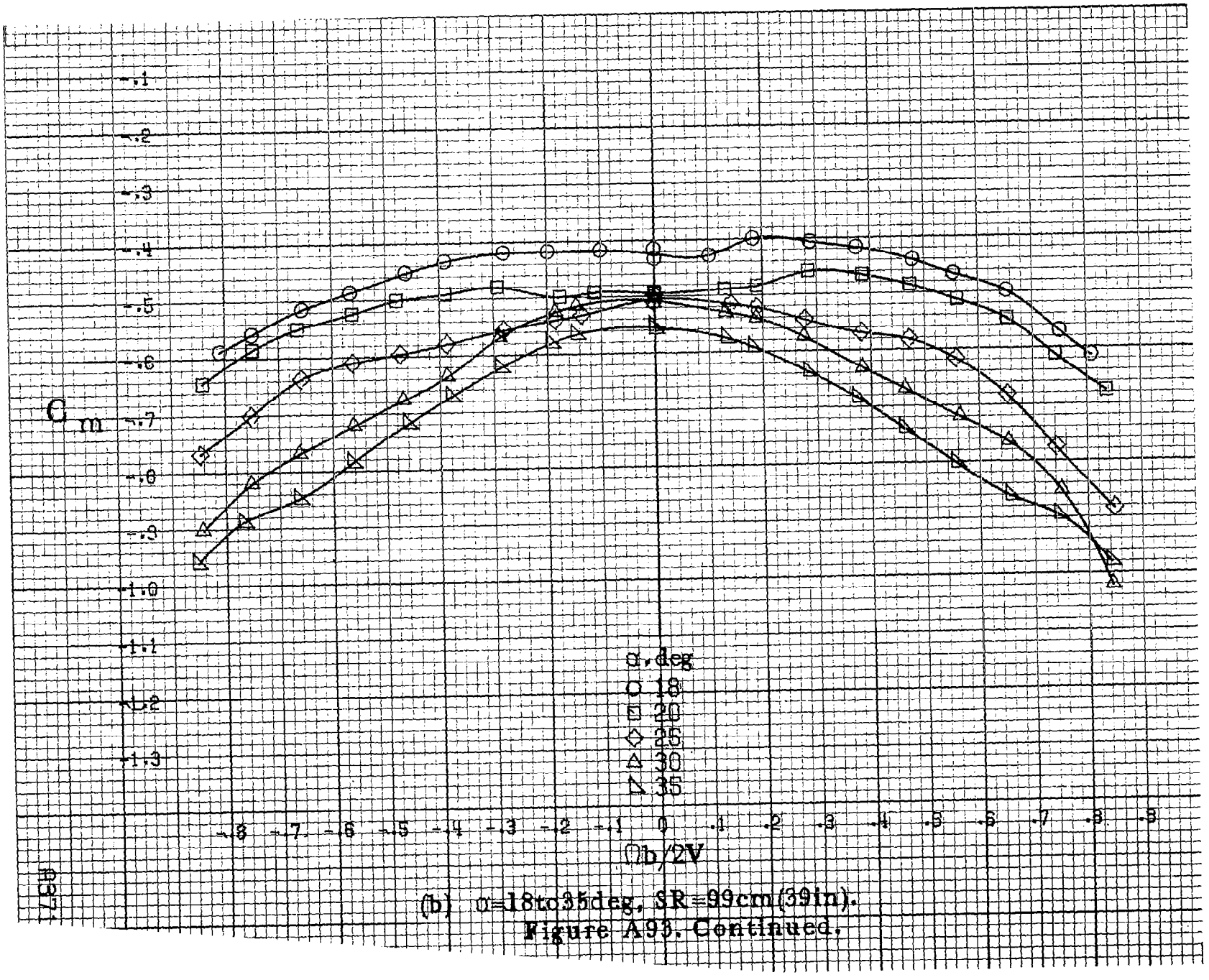

(b) α=18to35deg, SR=99cm(39in).

Figure A93. Continued.

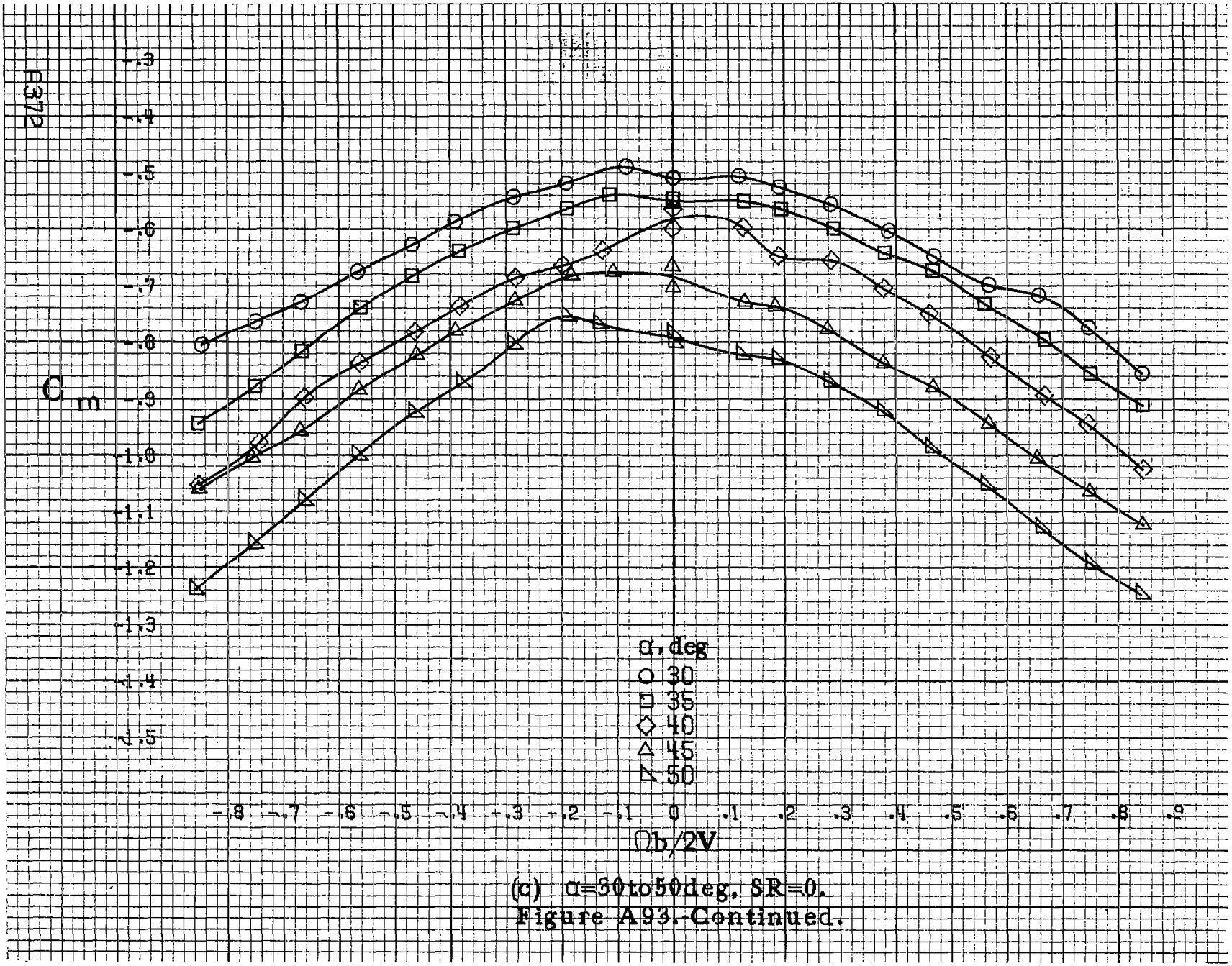

(c) α=30to50deg, SR=0.

Figure A93.-Continued.

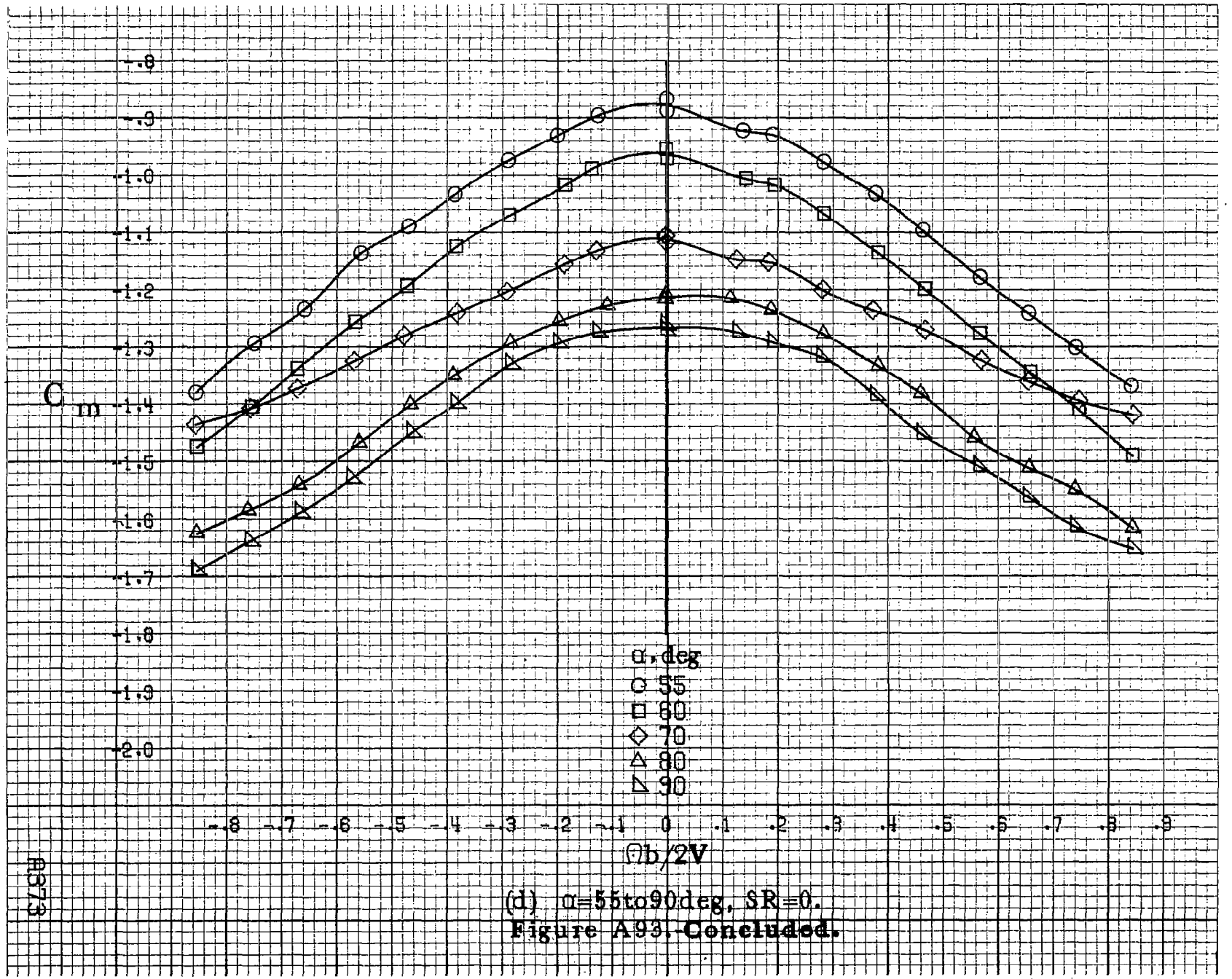

(d) α=55 to 90 deg, SR=0.

Figure A93.-Concluded.

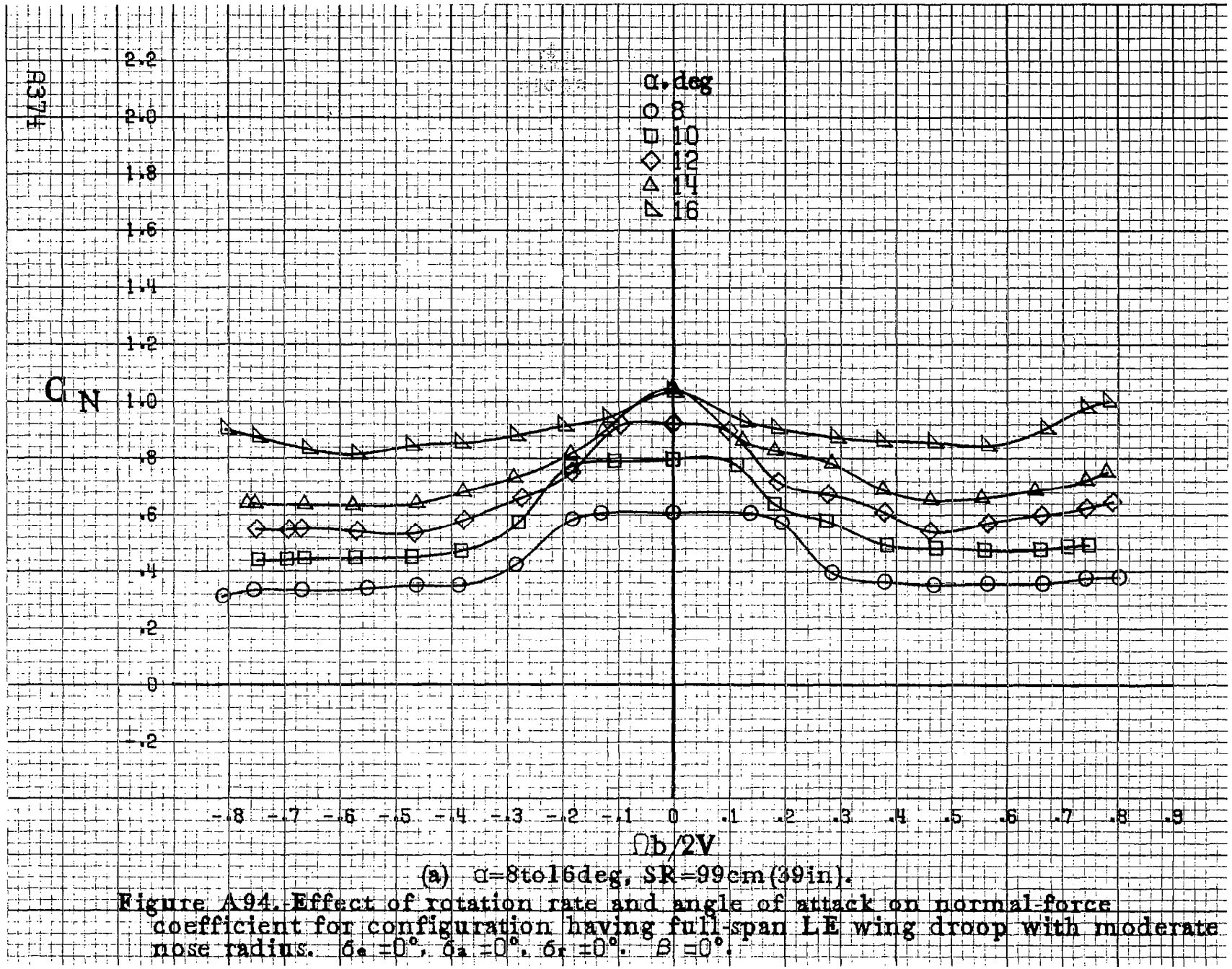

(a) α=8to16deg, SR=99cm(39in).

Figure A94. Effect of rotation rate and angle of attack on normal-force coefficient for configuration having full-span LE wing droop with moderate nose radius. $\delta_e = 0°$, $\delta_a = 0°$, $\delta_r = 0°$, $\beta = 0°$.

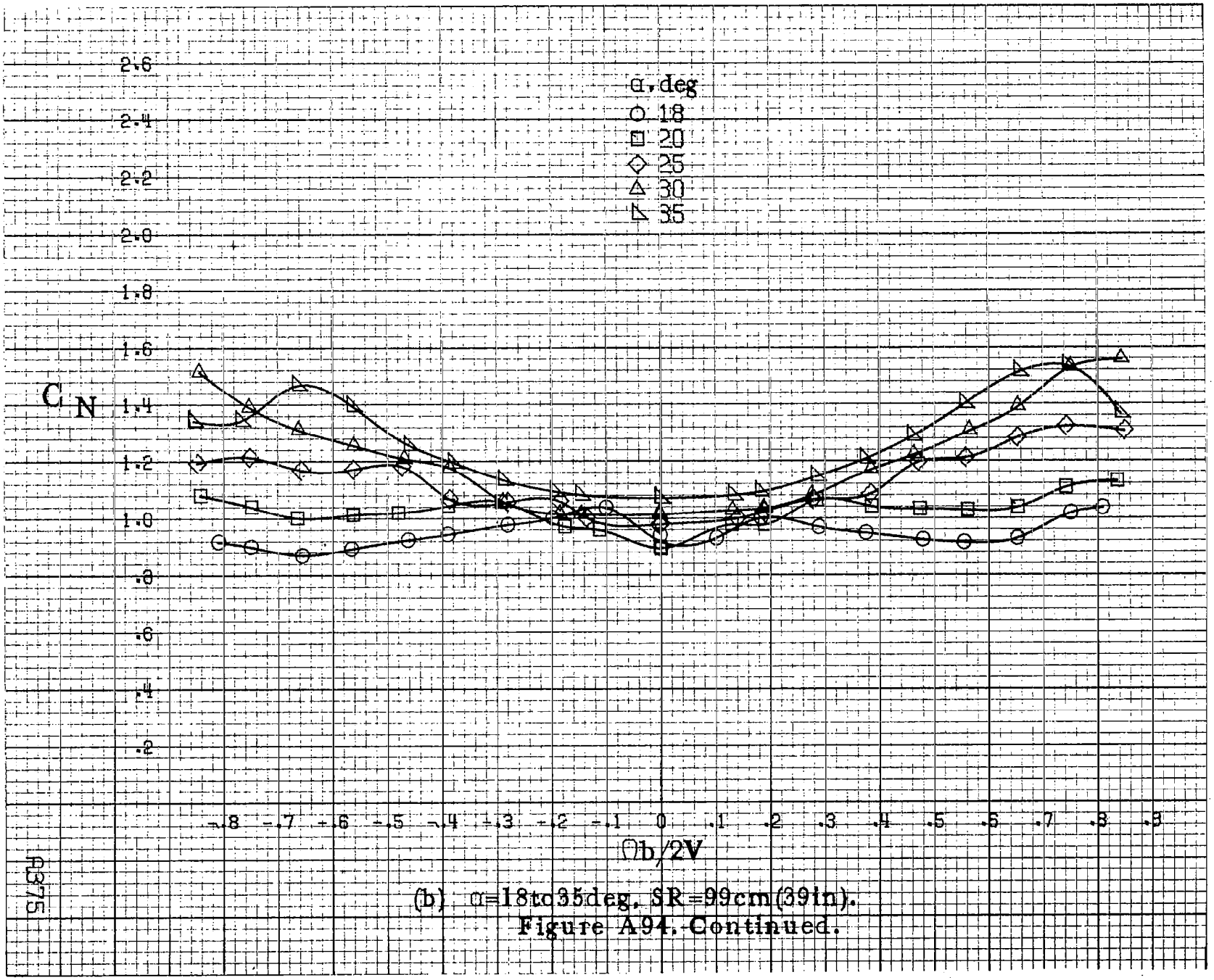

(b) α=18to35deg, SR=99cm(39in).

Figure A94. Continued.

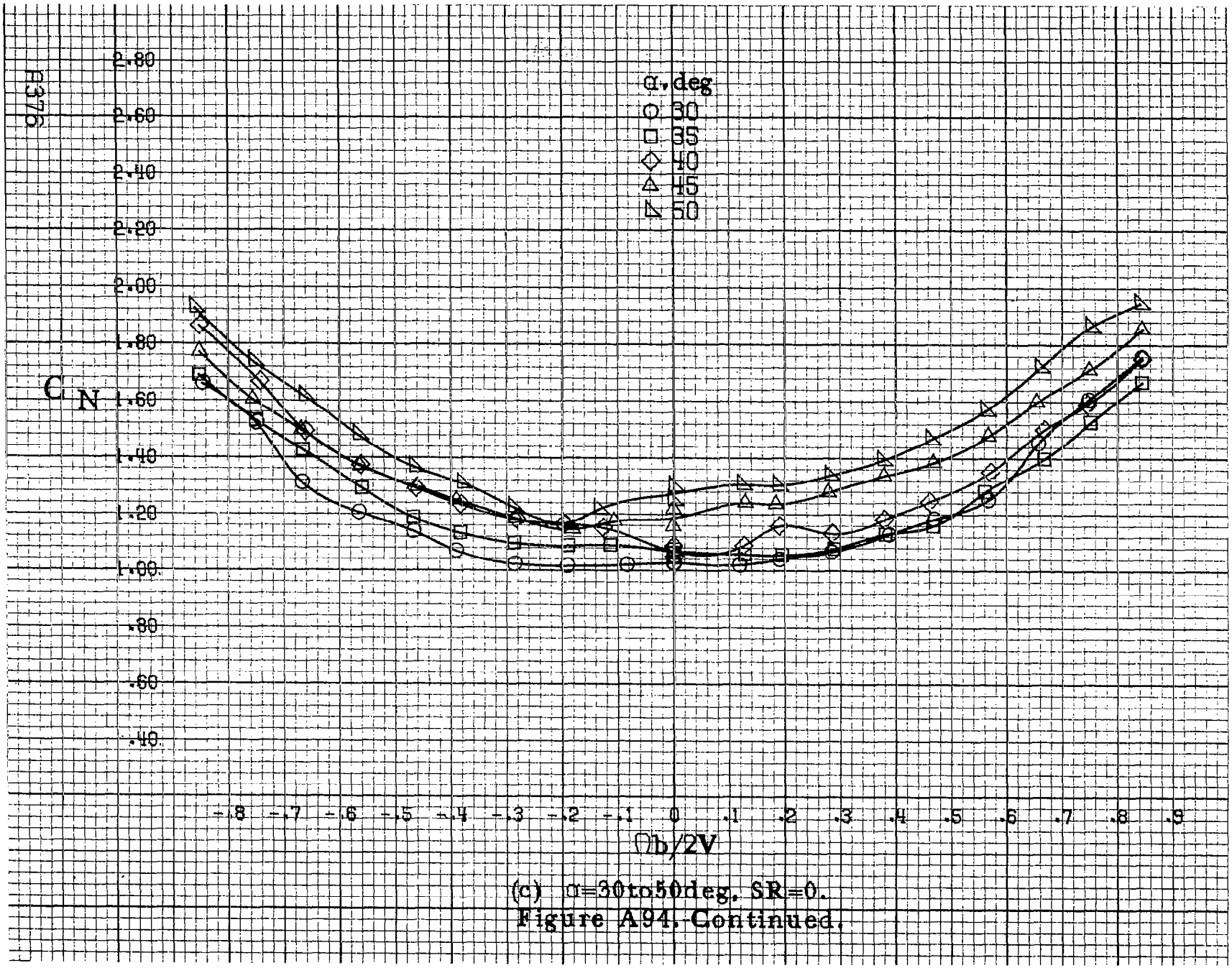

(c) α=30to50deg, SR=0.

Figure A94. Continued.

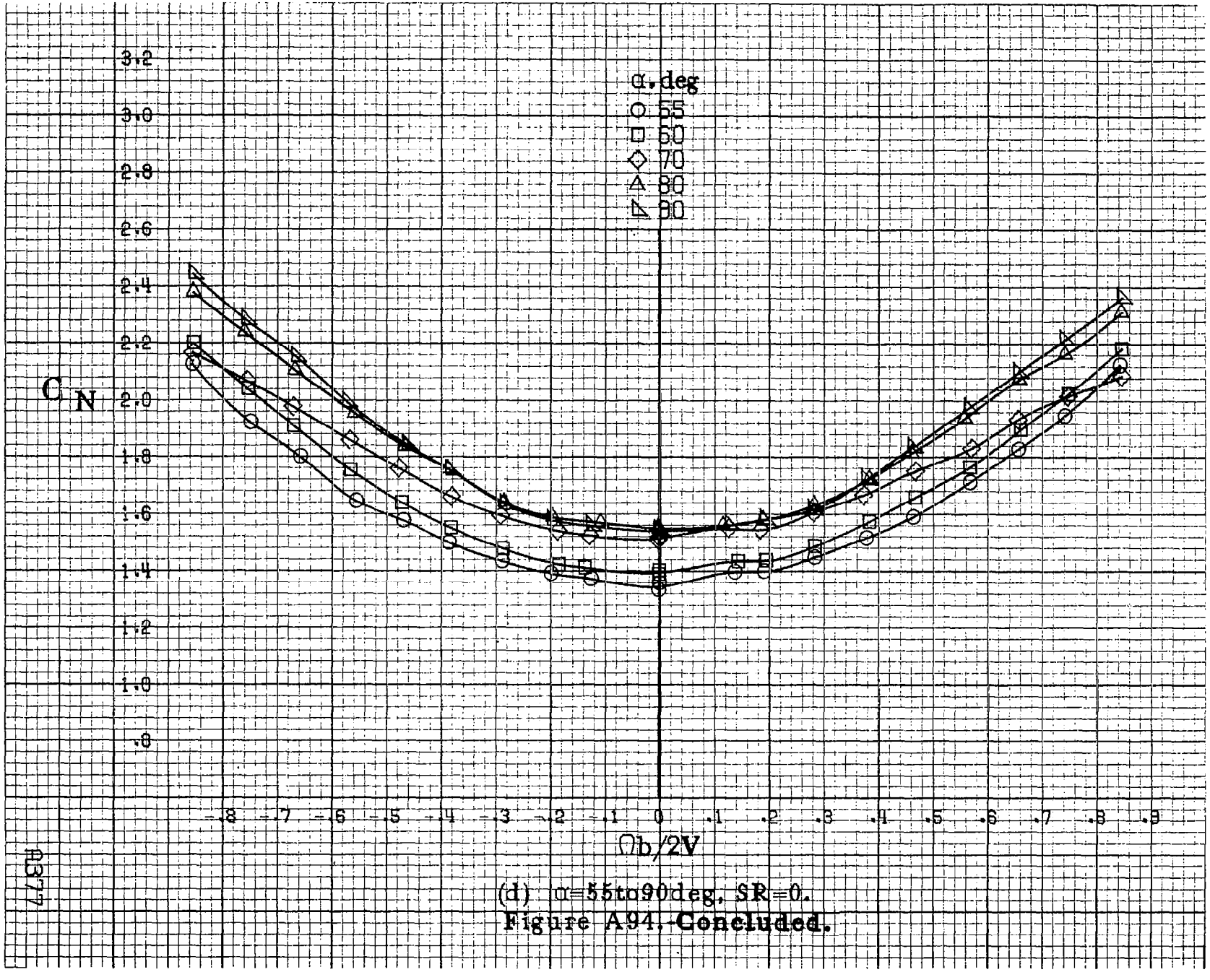

(d) α=55to90deg, SR=0.

Figure A94.-Concluded.

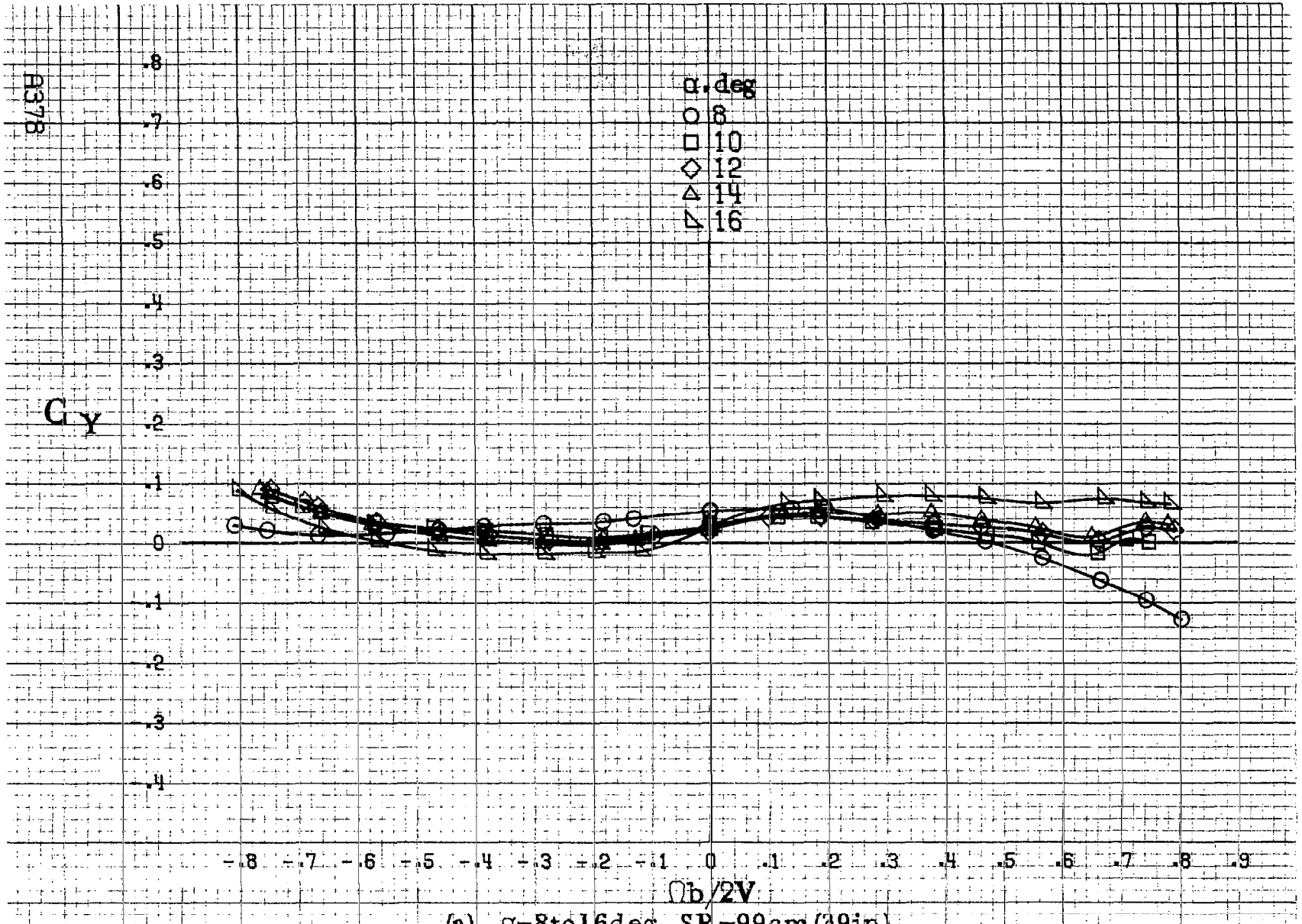

(a) α=8to16deg, SR=99cm(39in).

Figure A95. Effect of rotation rate and angle of attack on side-force coefficient for configuration having full-span LE wing droop with moderate nose radius. $\delta_e = 0°$, $\delta_a = 0°$, $\delta_r = 0°$, $\beta = 0°$.

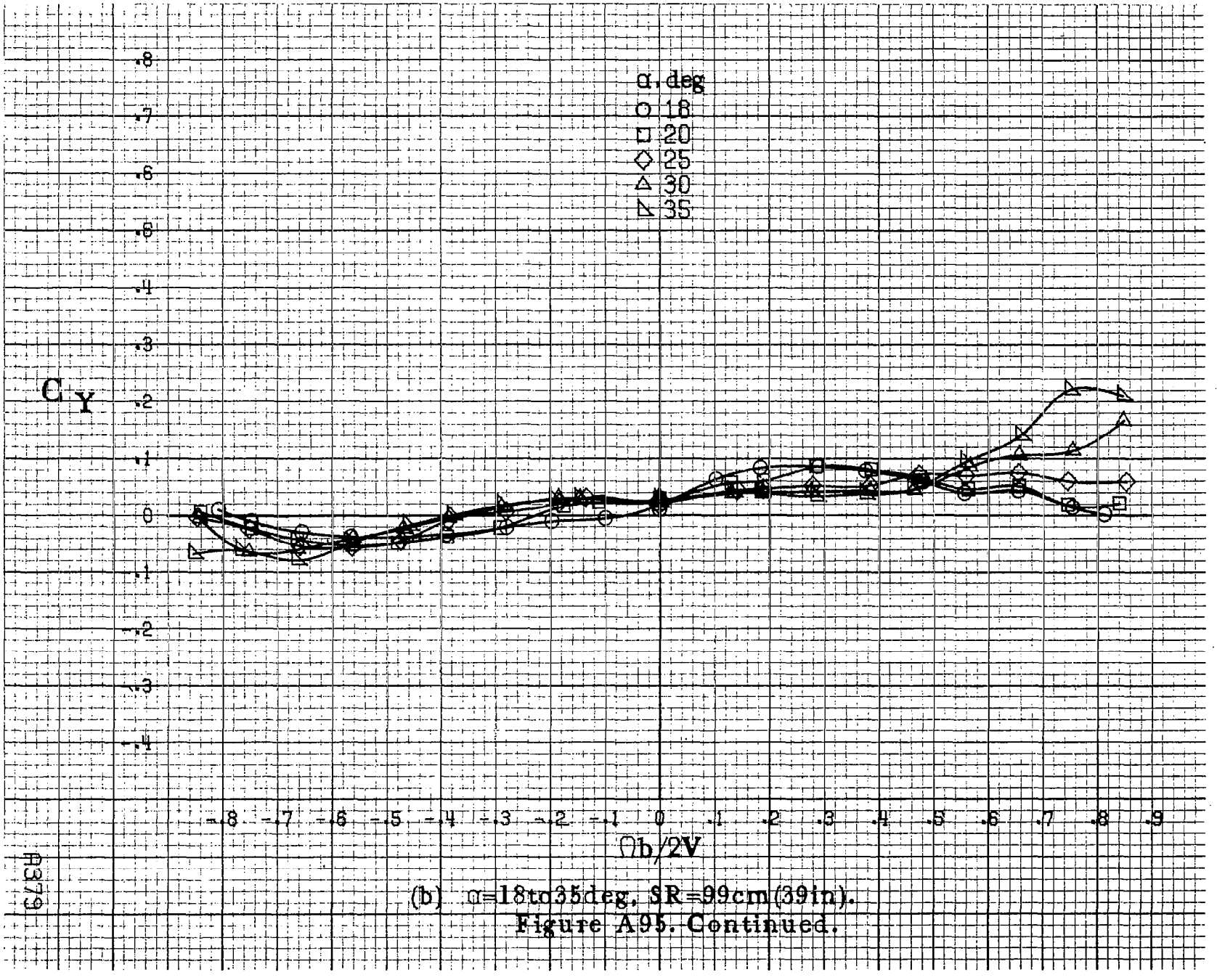

R376

(b) α=18to35deg, SR=99cm(39in).

Figure A95. Continued.

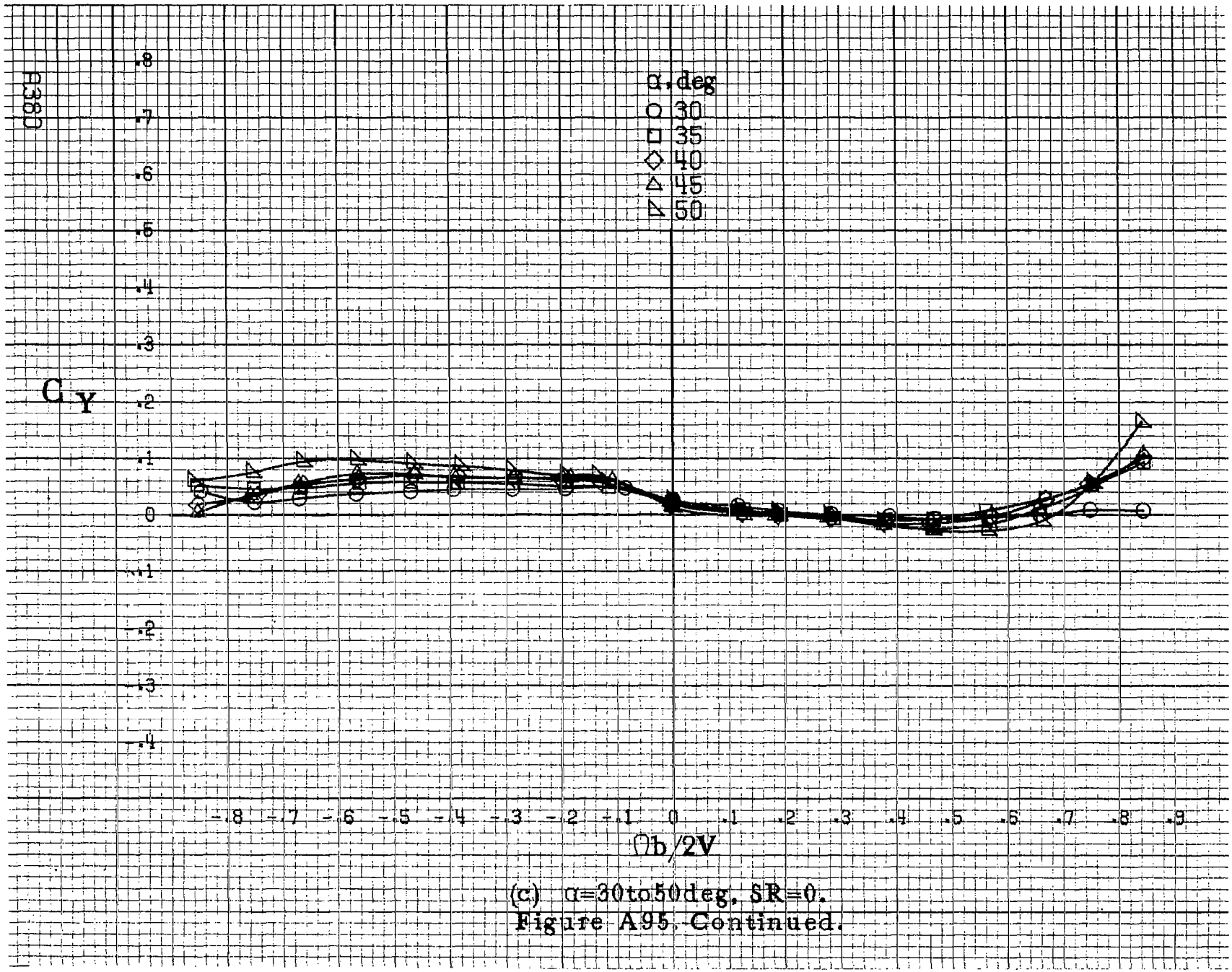

(c) α=30to50deg, δR=0.

Figure A95 Continued.

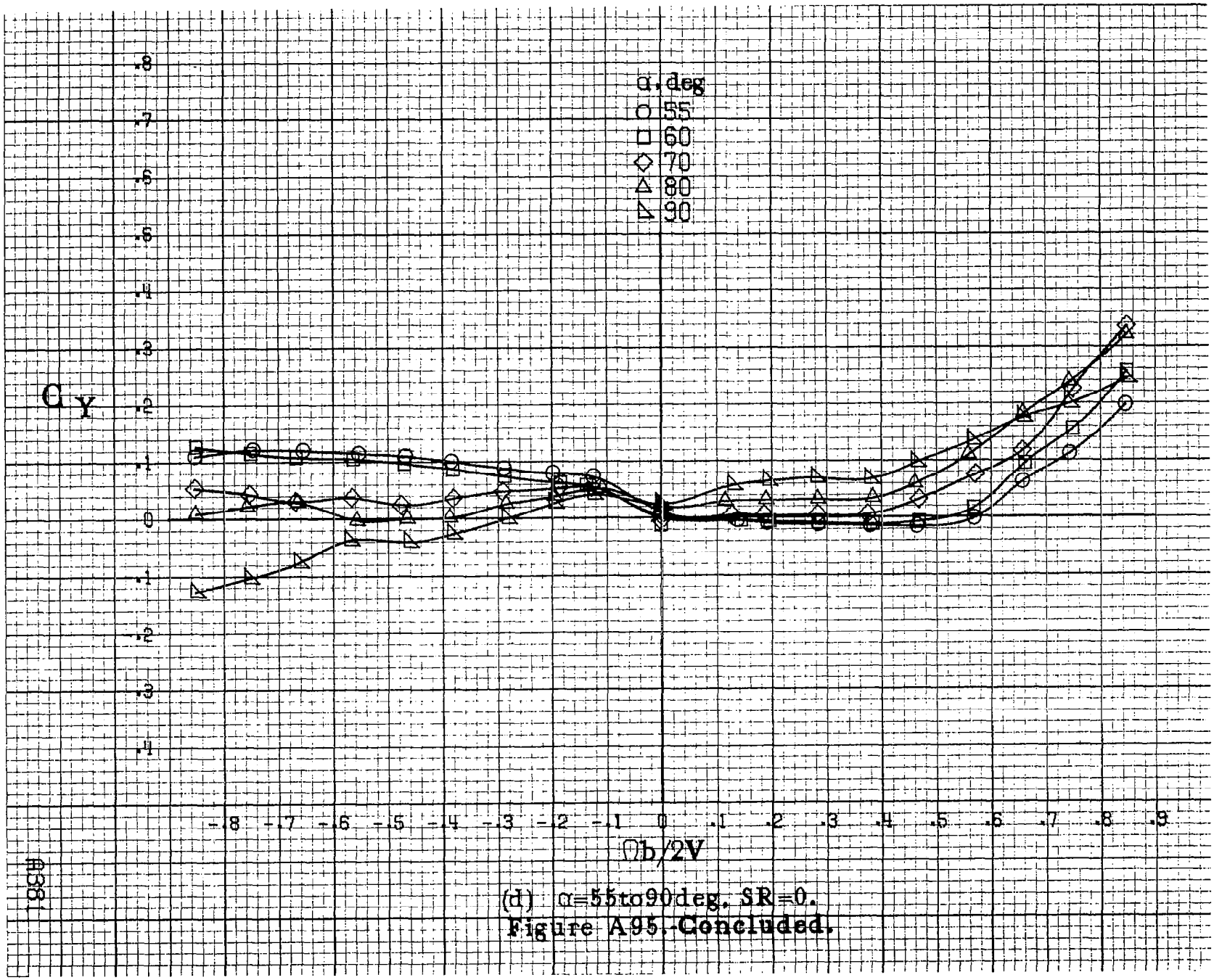

(d) α=55 to 90 deg, SR=0.

Figure A95.-Concluded.

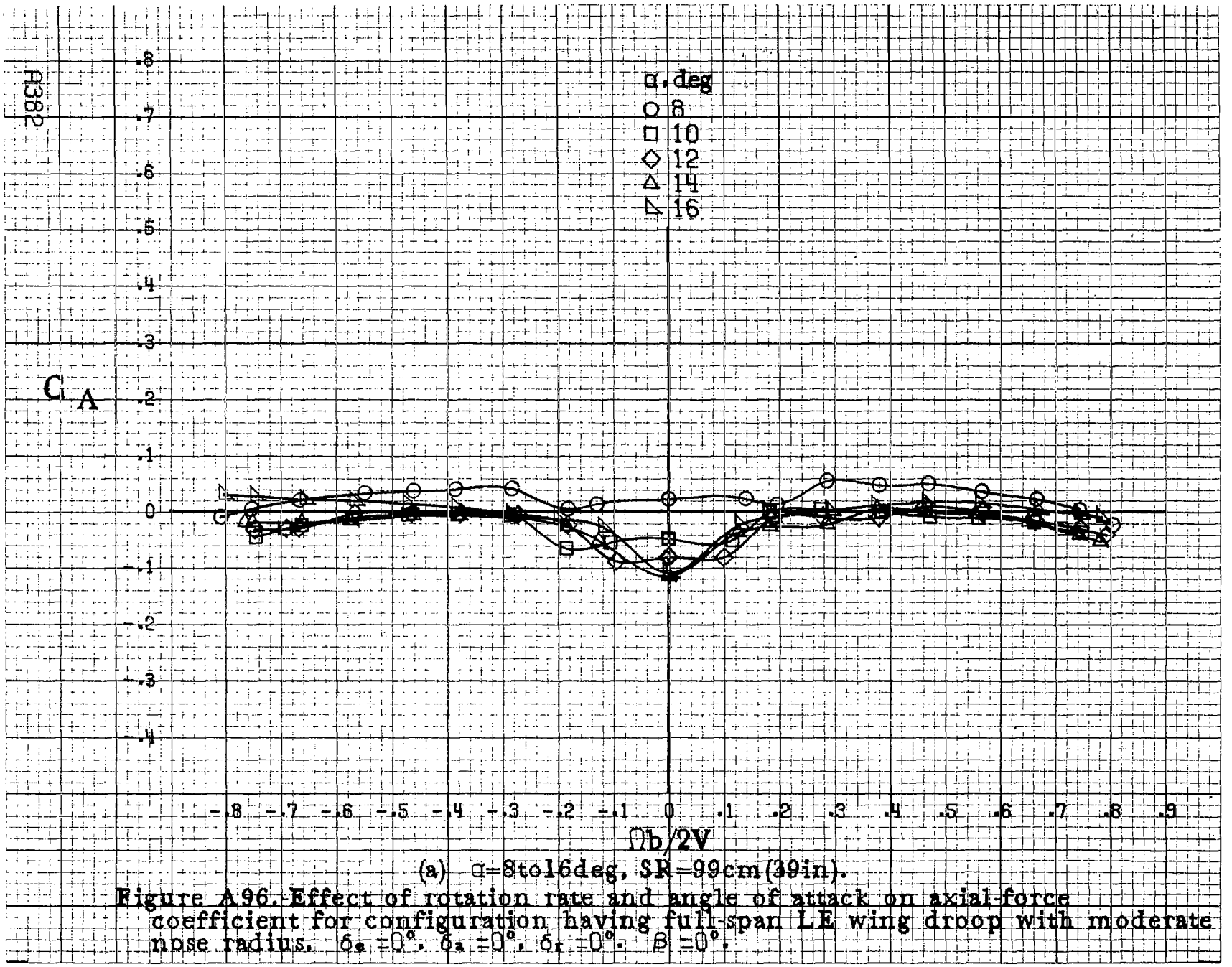

(a) α=8to16deg, SR=99cm(39in).

Figure A96.-Effect of rotation rate and angle of attack on axial-force coefficient for configuration having full-span LE wing droop with moderate nose radius. $\delta_e = 0°$, $\delta_a = 0°$, $\delta_r = 0°$, $\beta = 0°$.

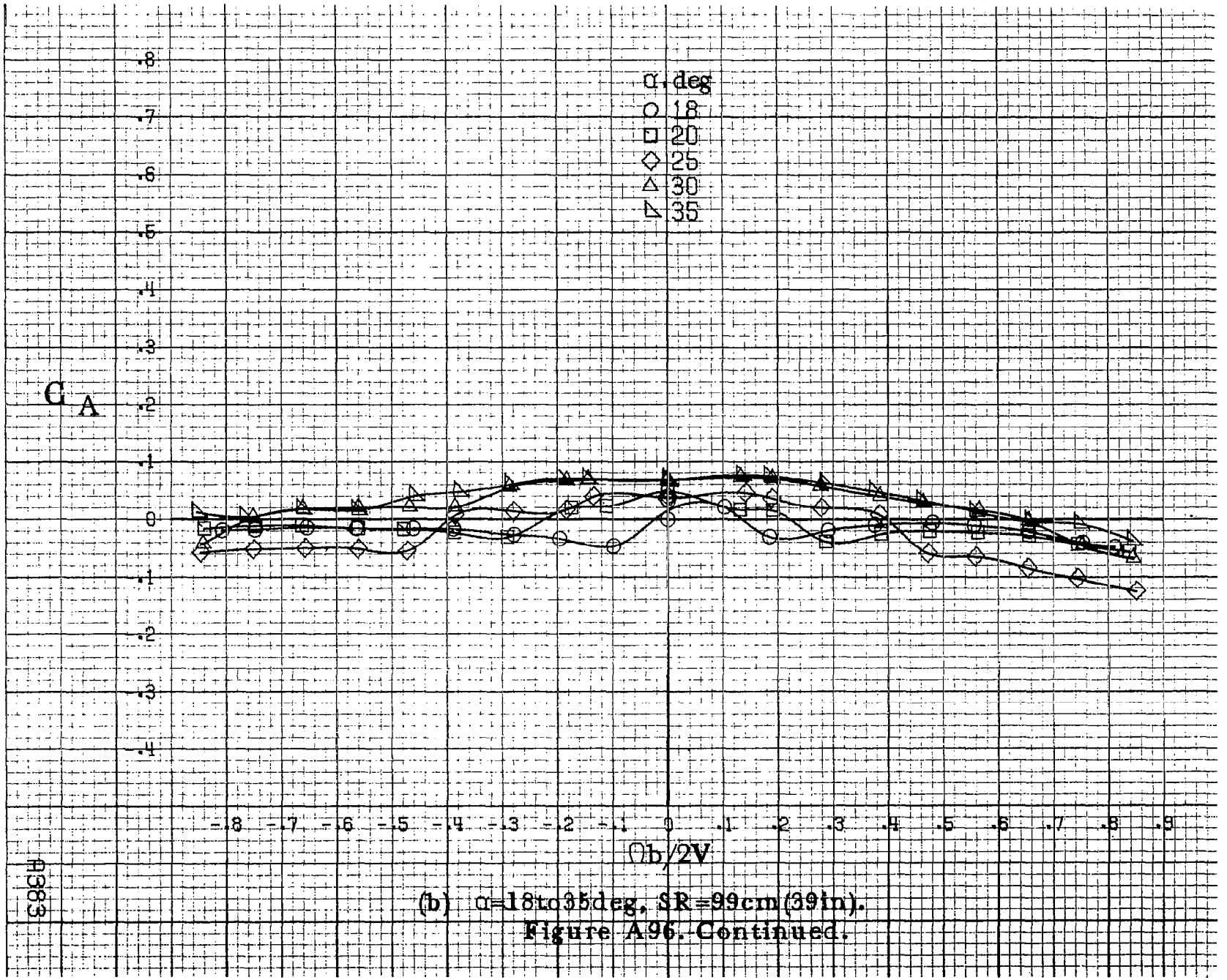

(b) α=18to35deg, SR=99cm(39in).

Figure A96.-Continued.

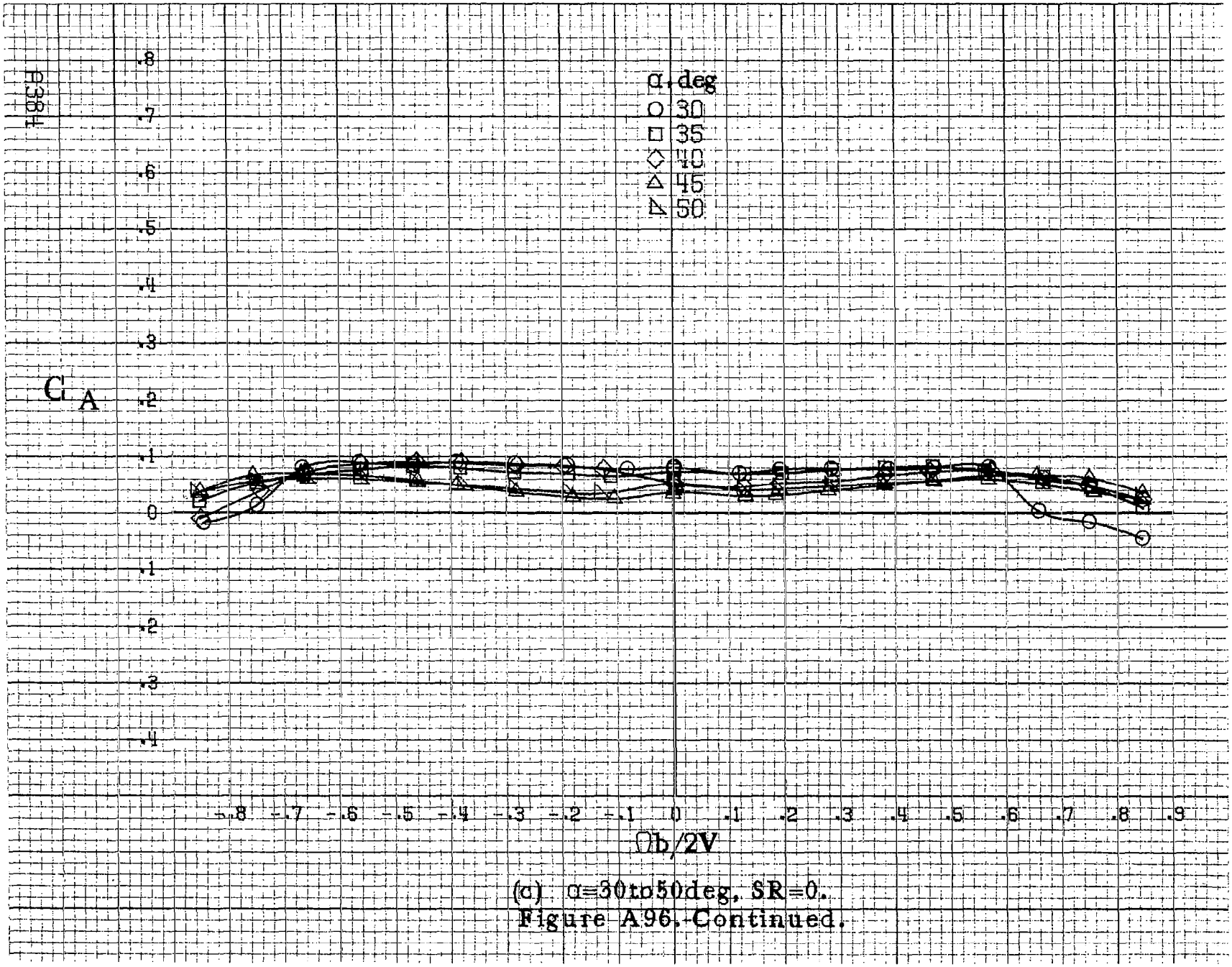

(c) α=30to50deg, SR=0.

Figure A96.-Continued.

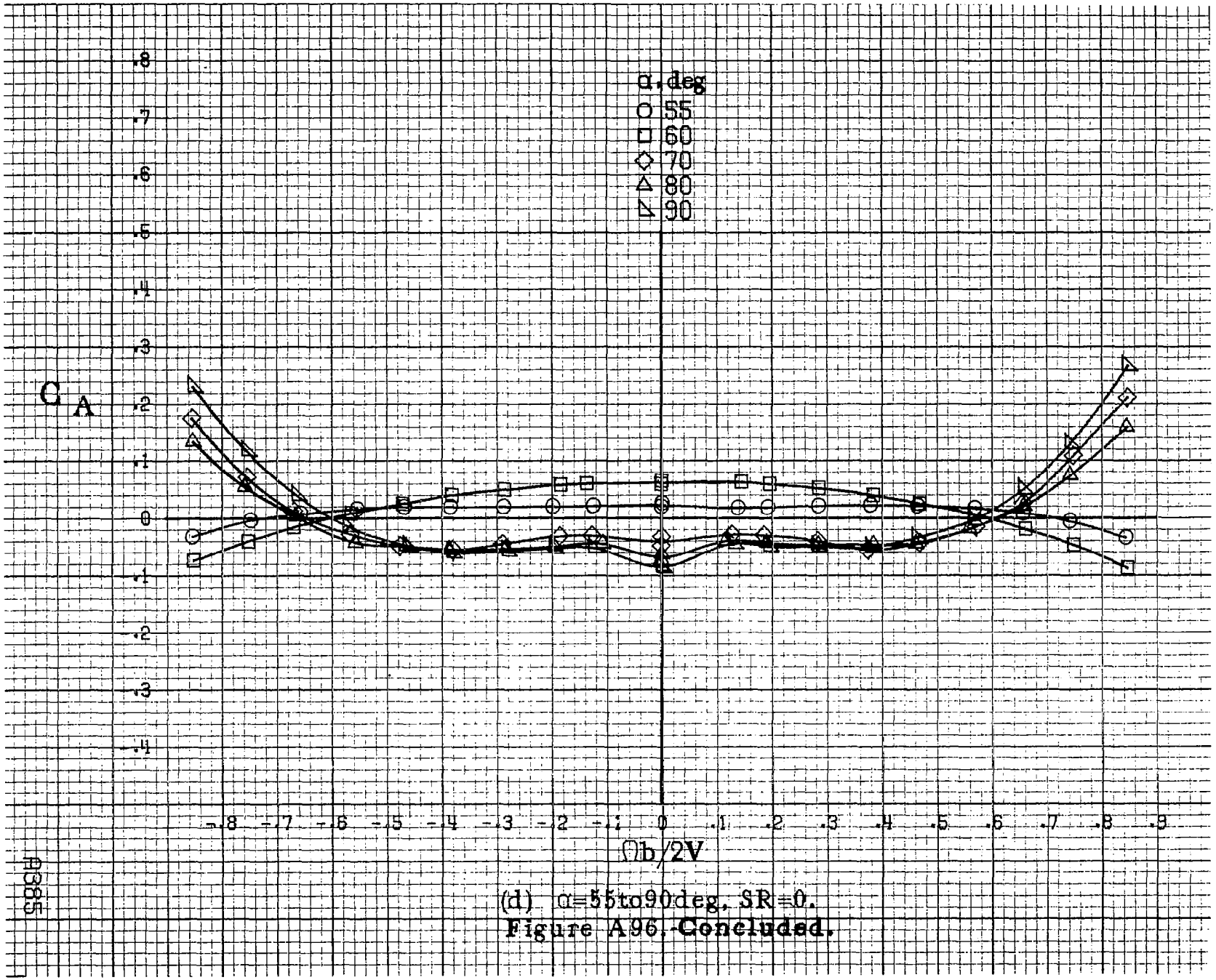

(d) α=55to90deg, SR=0.

Figure A96.-Concluded.

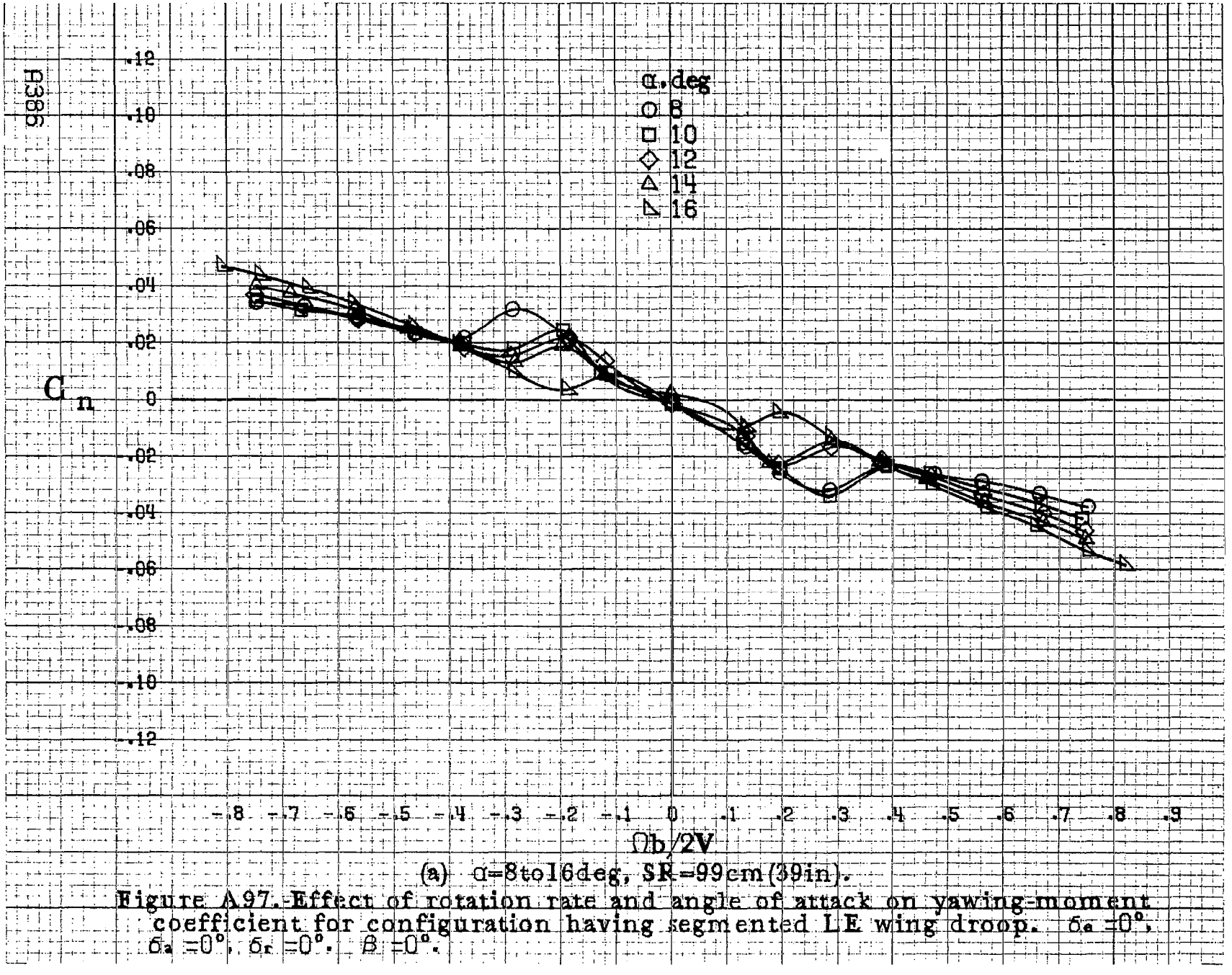

(a) α=8to16deg, SR=99cm(39in).

Figure A97.-Effect of rotation rate and angle of attack on yawing-moment coefficient for configuration having segmented LE wing droop. $\delta_e = 0°$, $\delta_a = 0°$, $\delta_r = 0°$, $\beta = 0°$.

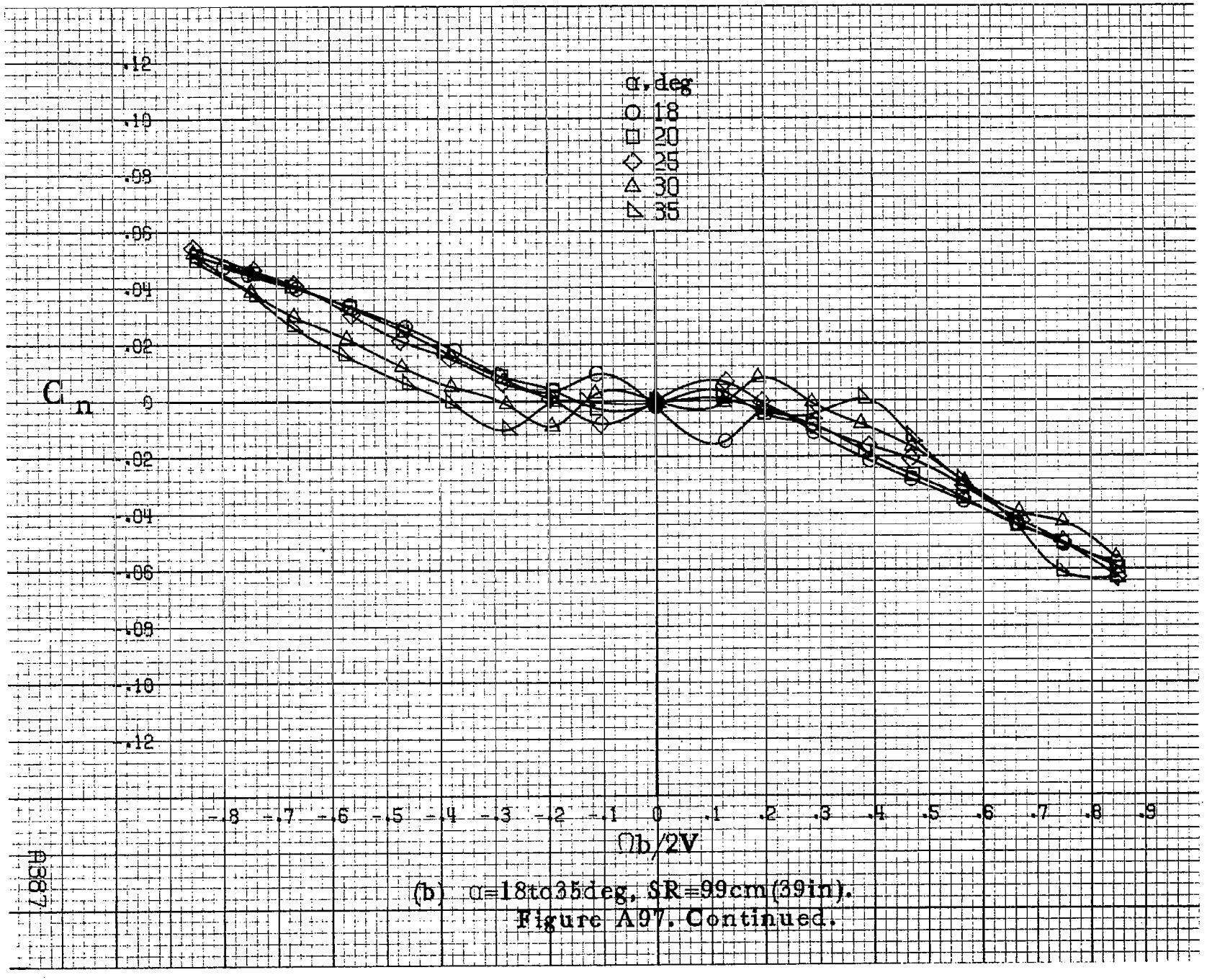

(b) α=18to35deg, SR=99cm(39in).

Figure A97. Continued.

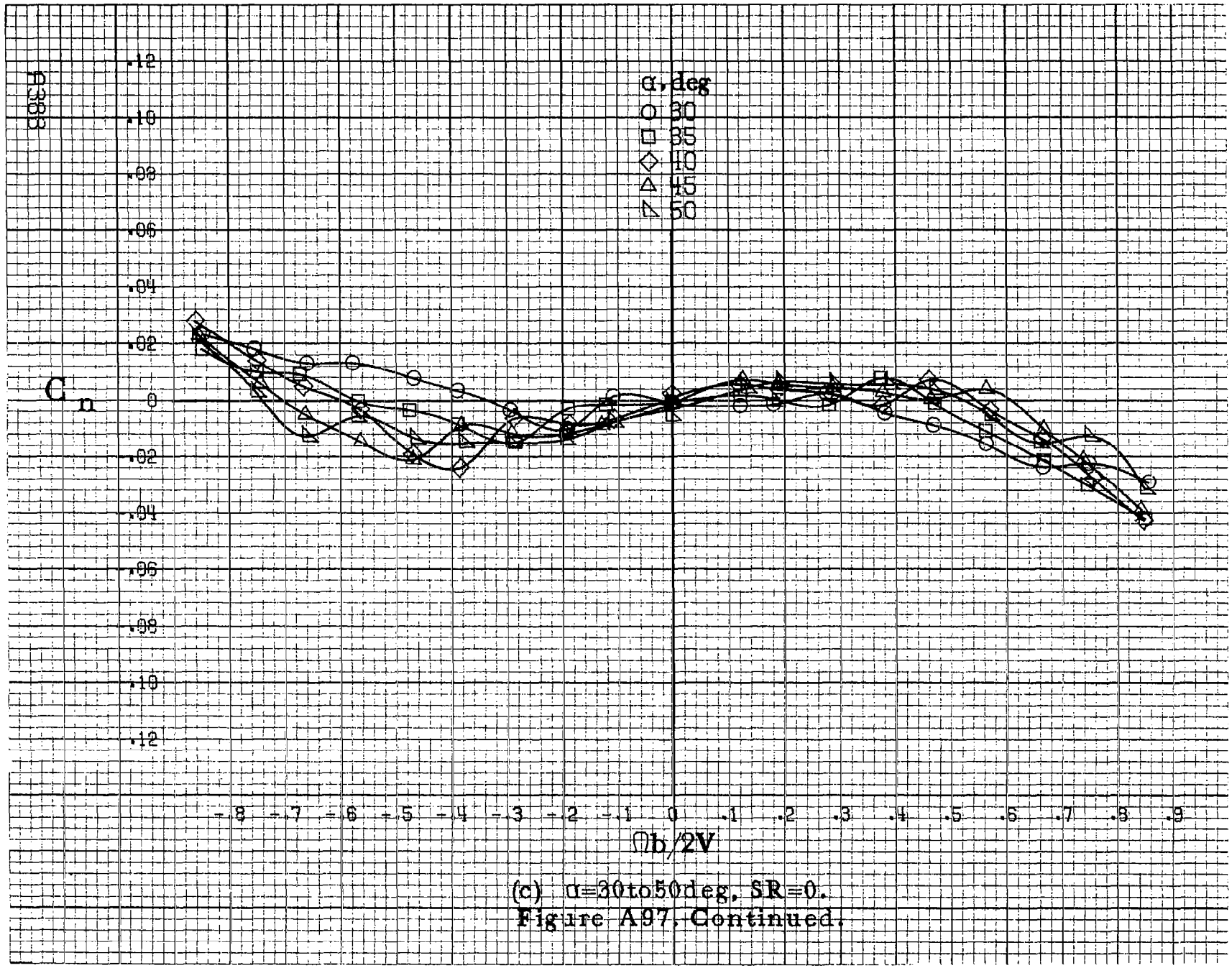

(c) α=30to50deg, SR=0.

Figure A97. Continued.

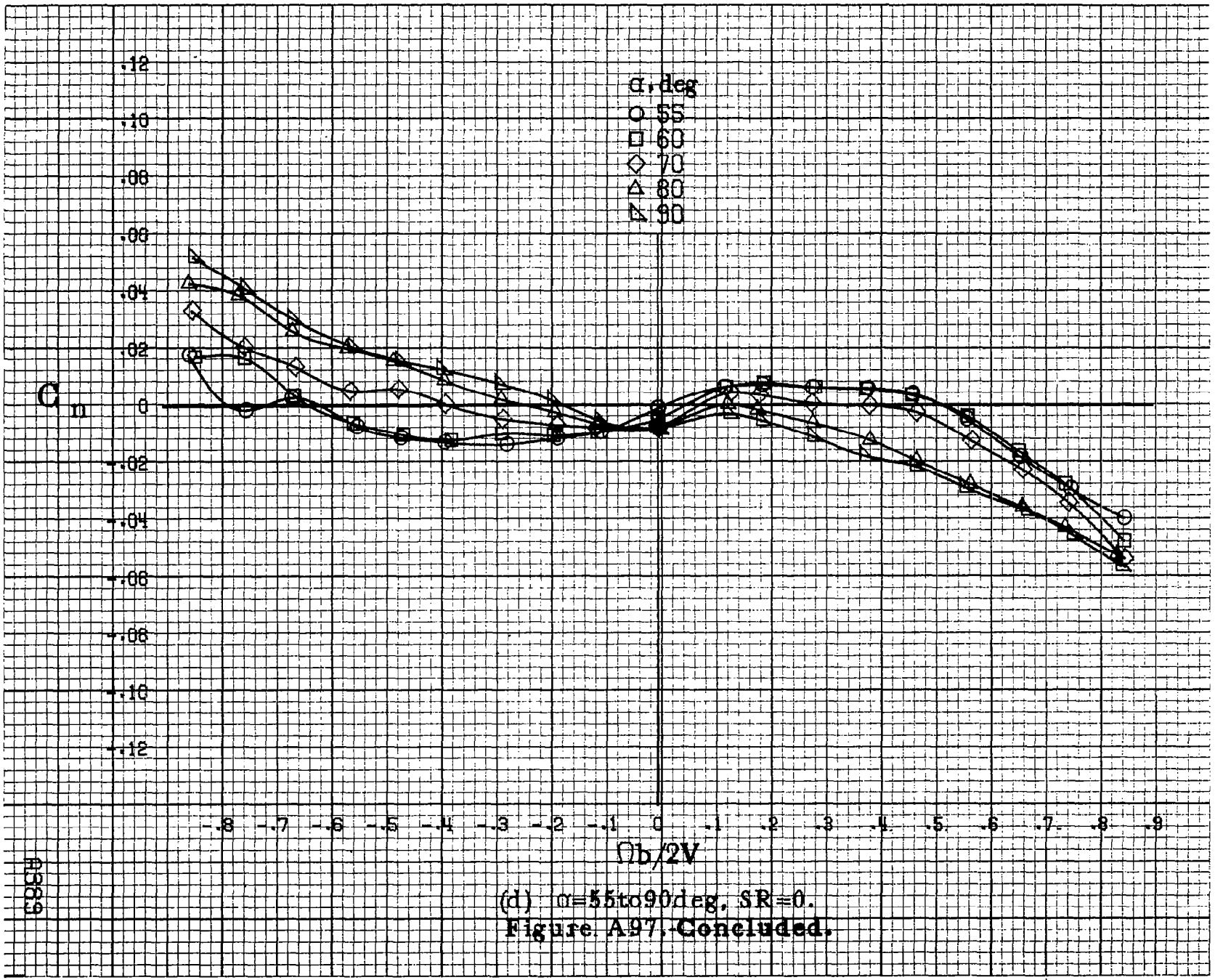

(d) α=55to90deg, SR=0.

Figure A97.-Concluded.

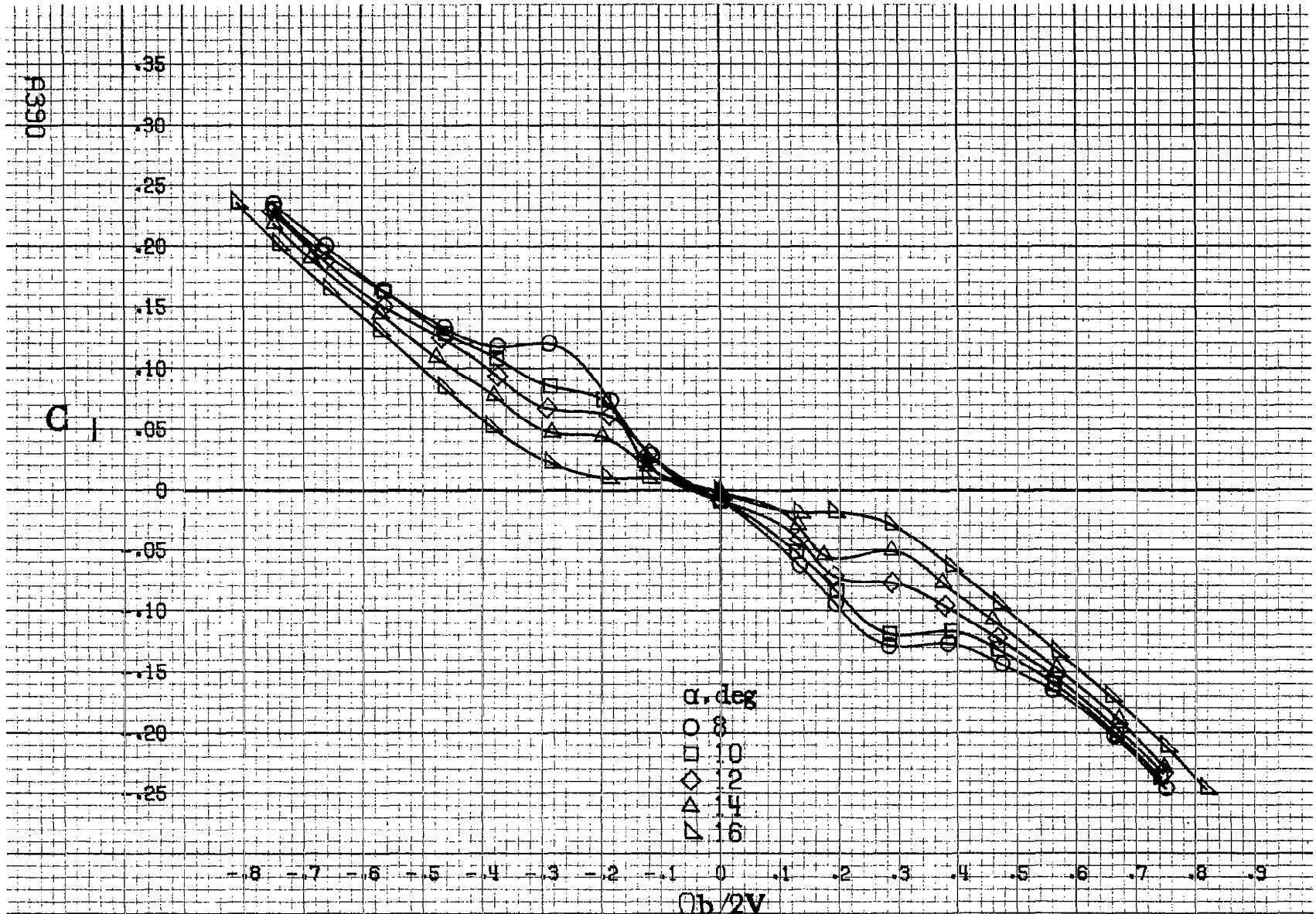

(a) α=8to16deg, SR=99cm(39in).

Figure A98.-Effect of rotation rate and angle of attack on rolling-moment coefficient for configuration having segmented LE wing droop. $\delta_e = 0°$, $\delta_a = 0°$, $\delta_r = 0°$, $\beta = 0°$.

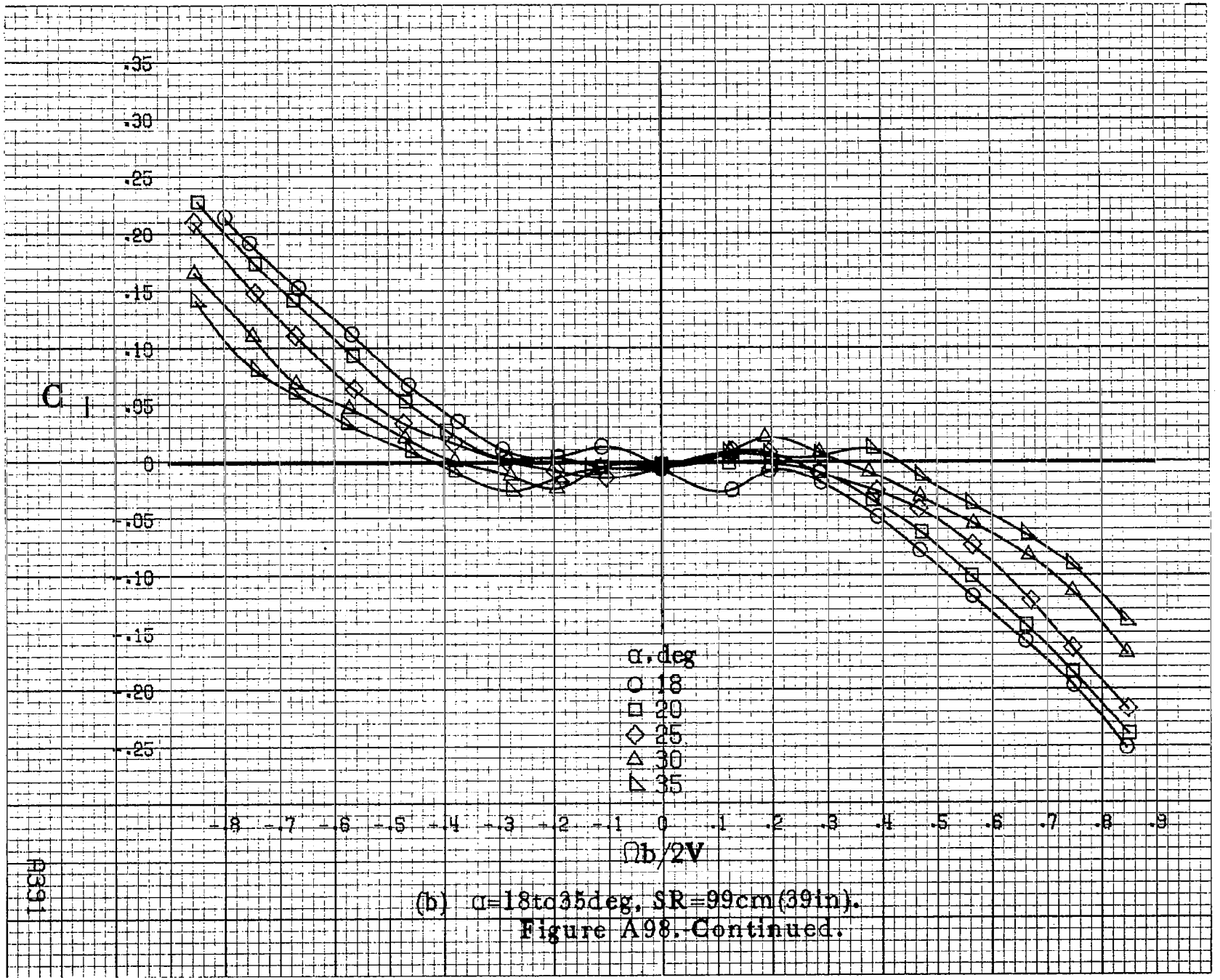

(b) α=18to35deg, SR=99cm(39in).

Figure A98.-Continued.

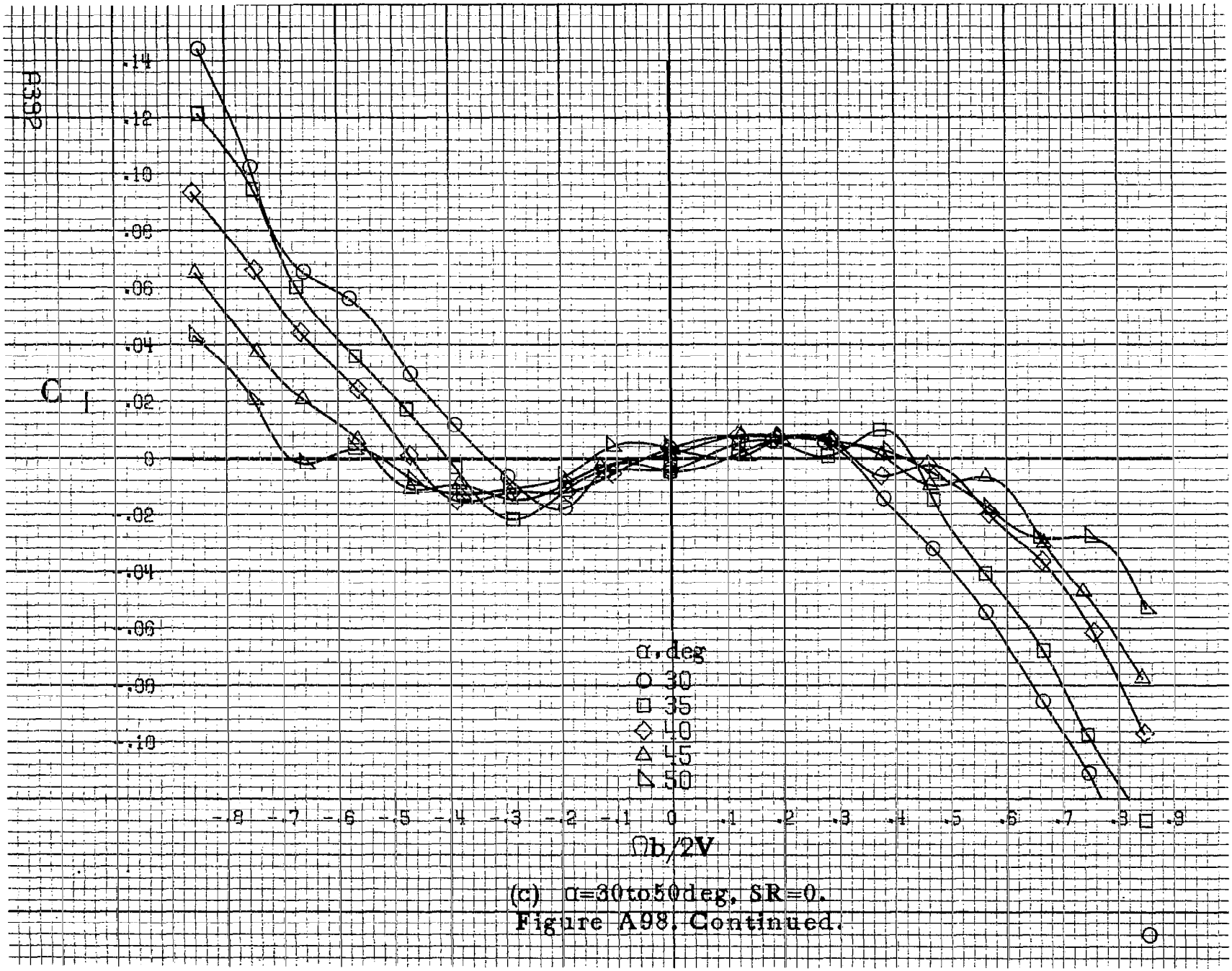

(c) α=30to50deg, δR=0.

Figure A98. Continued.

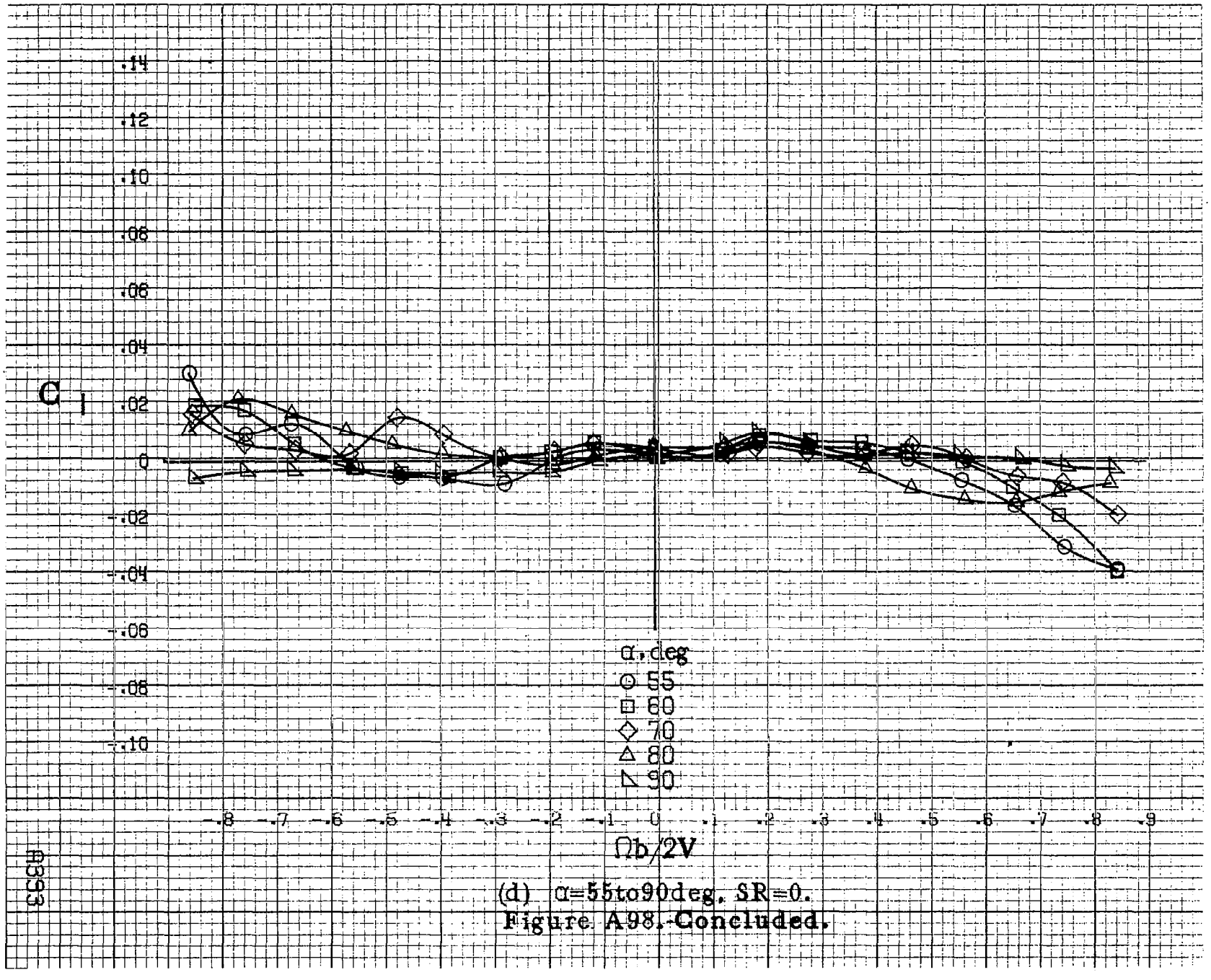

(d) α=55to90deg. SR=0.

Figure A98.-Concluded.

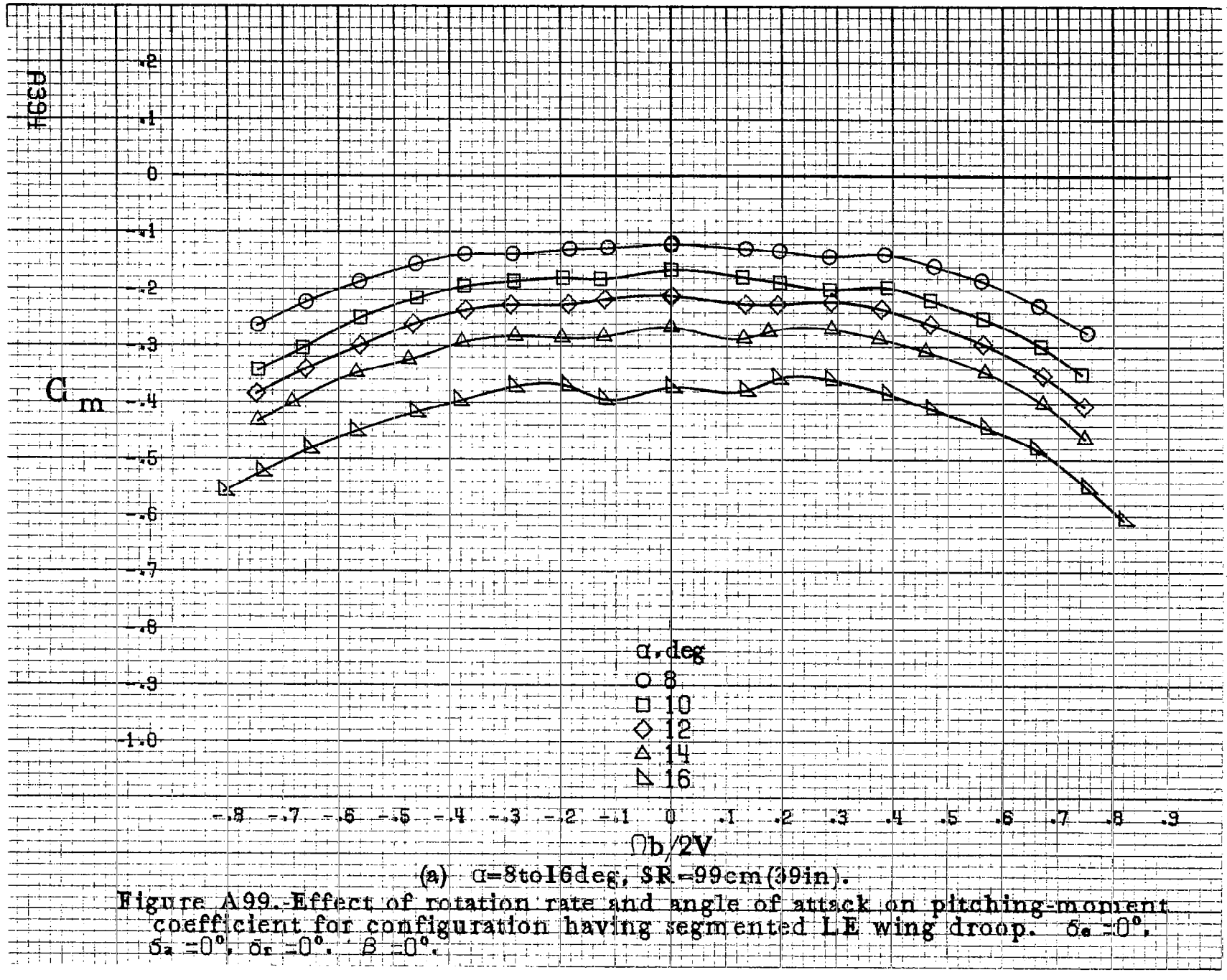

(a) α=8to16deg, SR=99cm(39in).

Figure A99.-Effect of rotation rate and angle of attack on pitching-moment coefficient for configuration having segmented LE wing droop. $\delta_e = 0°$, $\delta_a = 0°$, $\delta_r = 0°$, $\beta = 0°$.

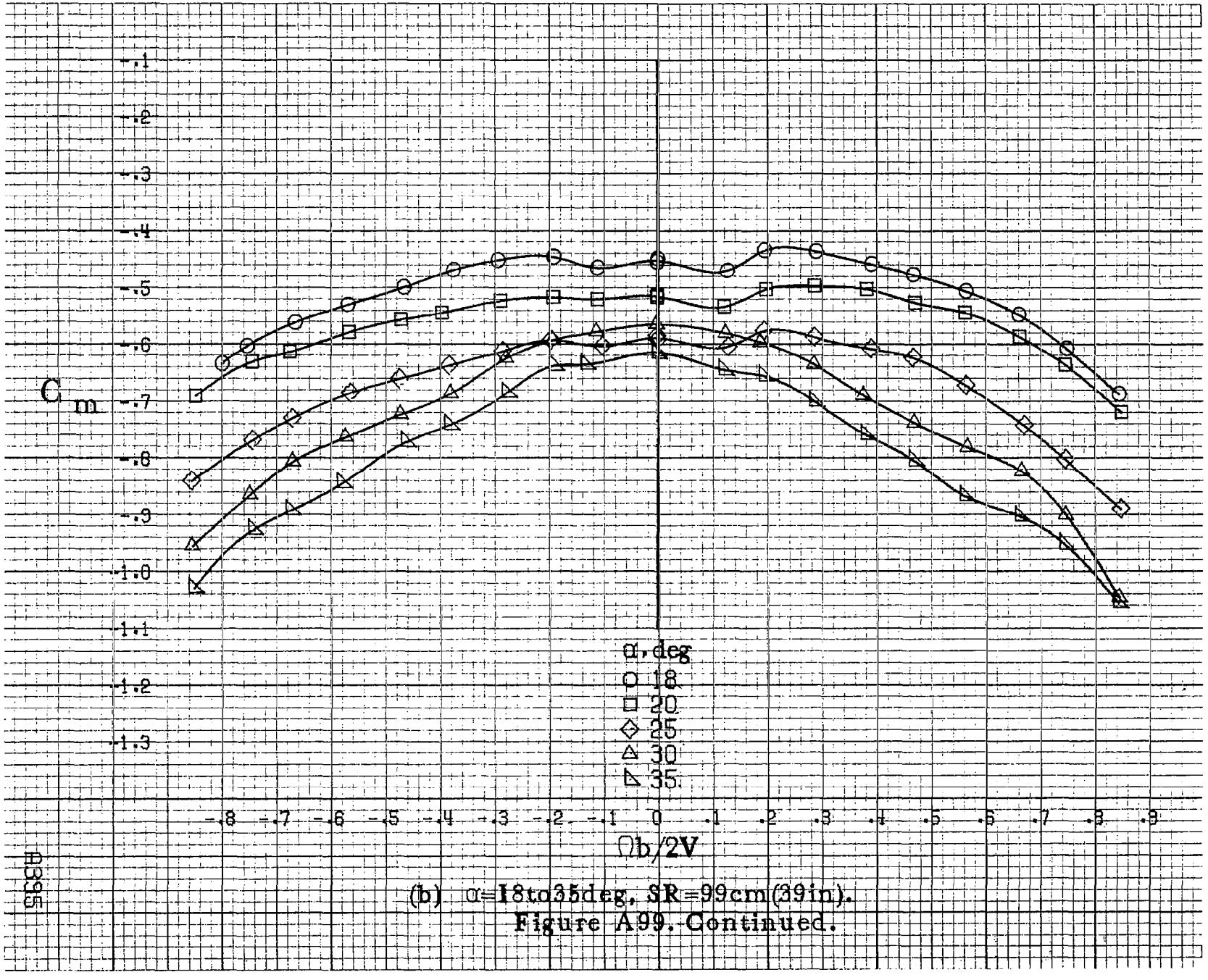

(b) α=18to35deg, SR=99cm(39in).

Figure A99.-Continued.

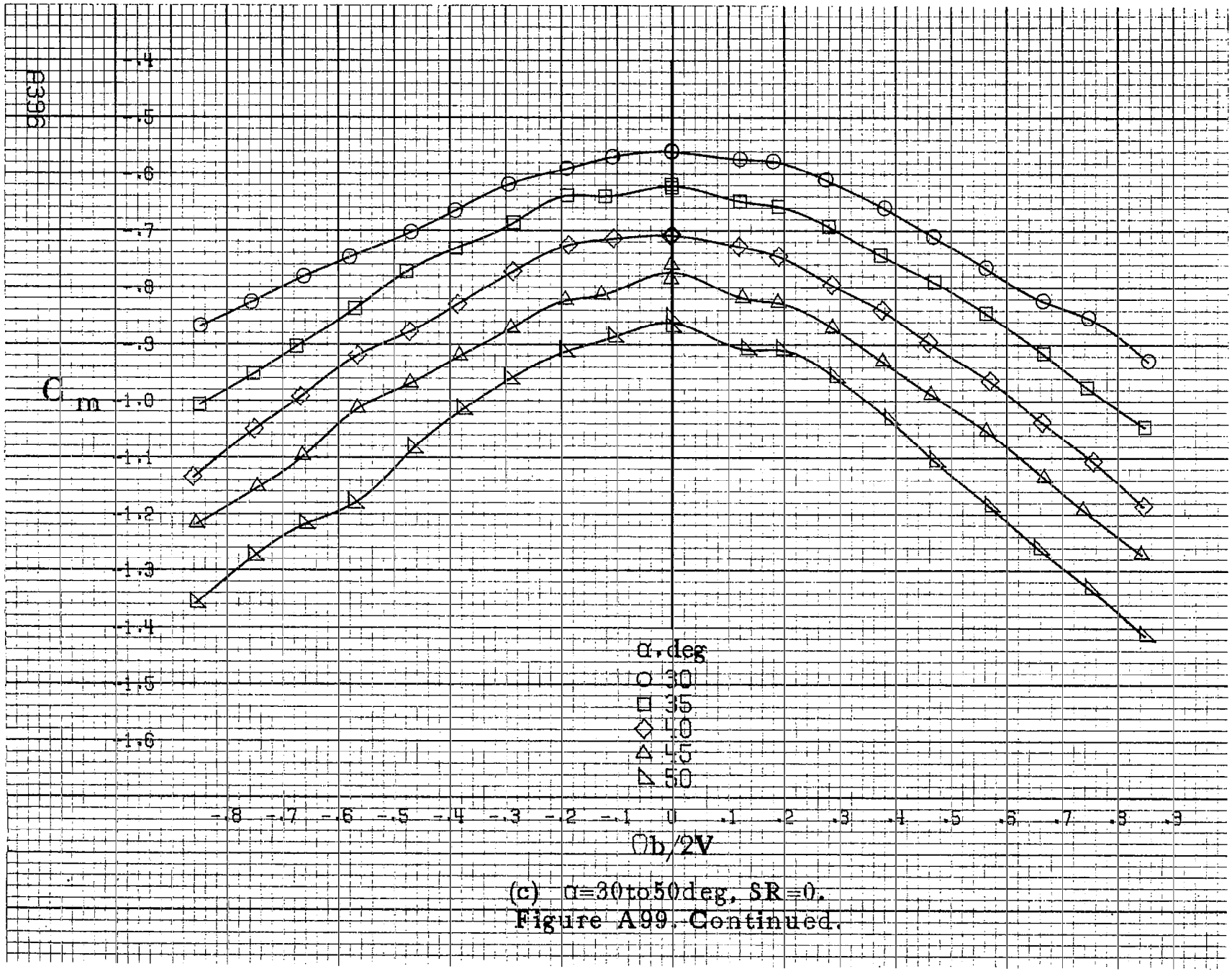

(c) α=30to50deg, SR=0.

Figure A99. Continued.

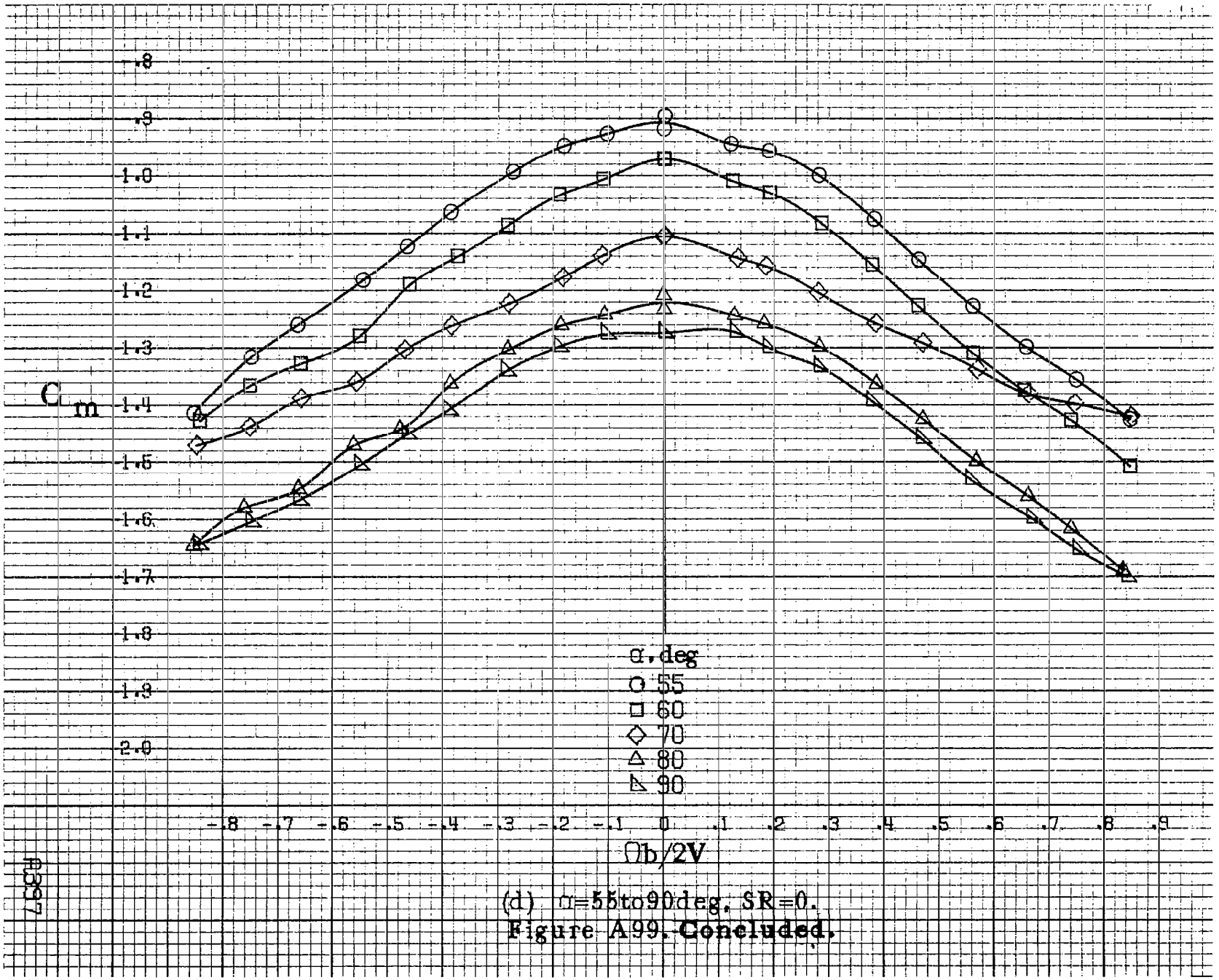

(d) α=55to90deg, SR=0.

Figure A99.-Concluded.

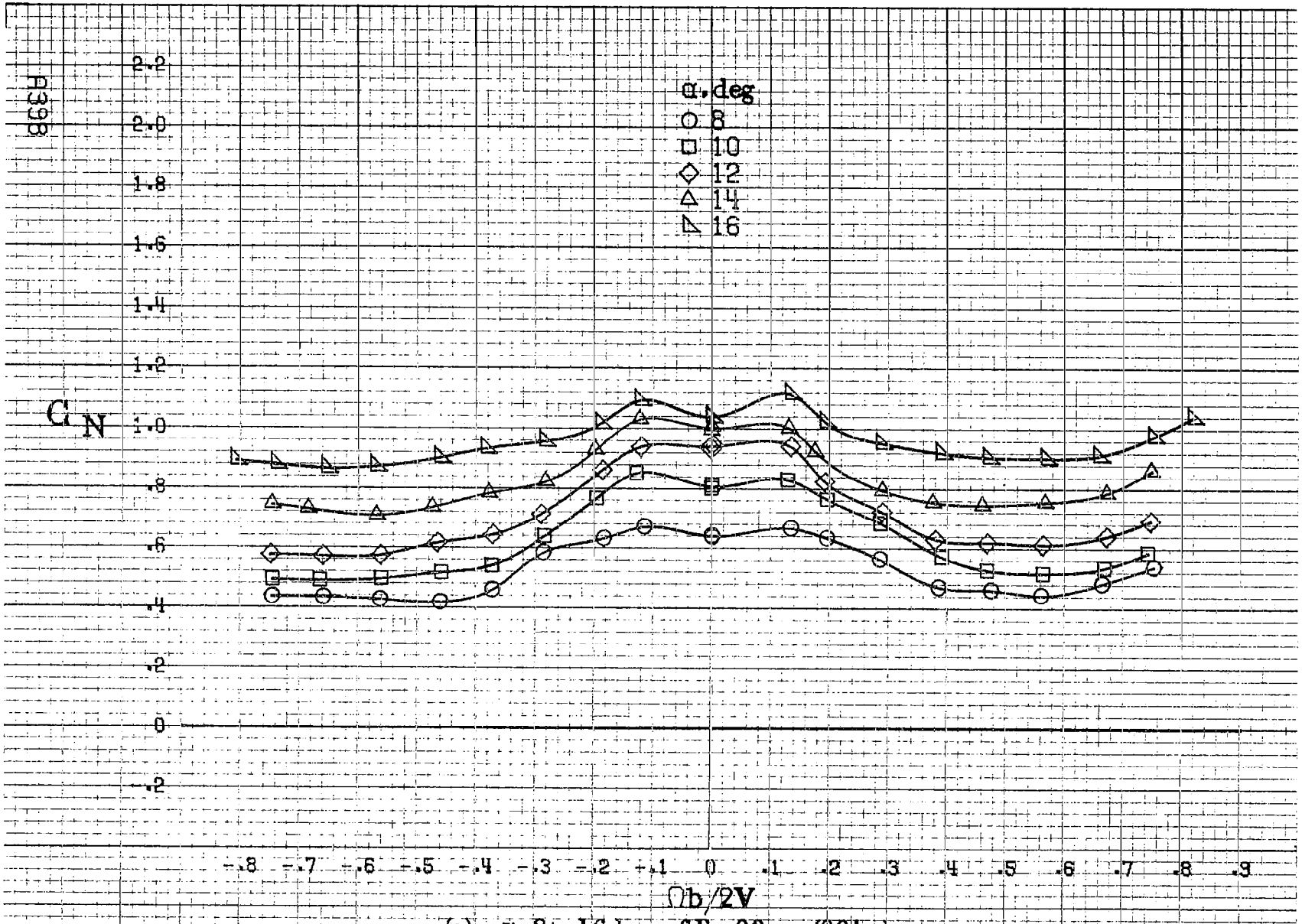

(a) α=8to16deg, SR=99cm(39in).

Figure A100.-Effect of rotation rate and angle of attack on normal-force coefficient for configuration having segmented LE wing droop. δ_e =0°, δ_a =0°, δ_r =0°, β =0°.

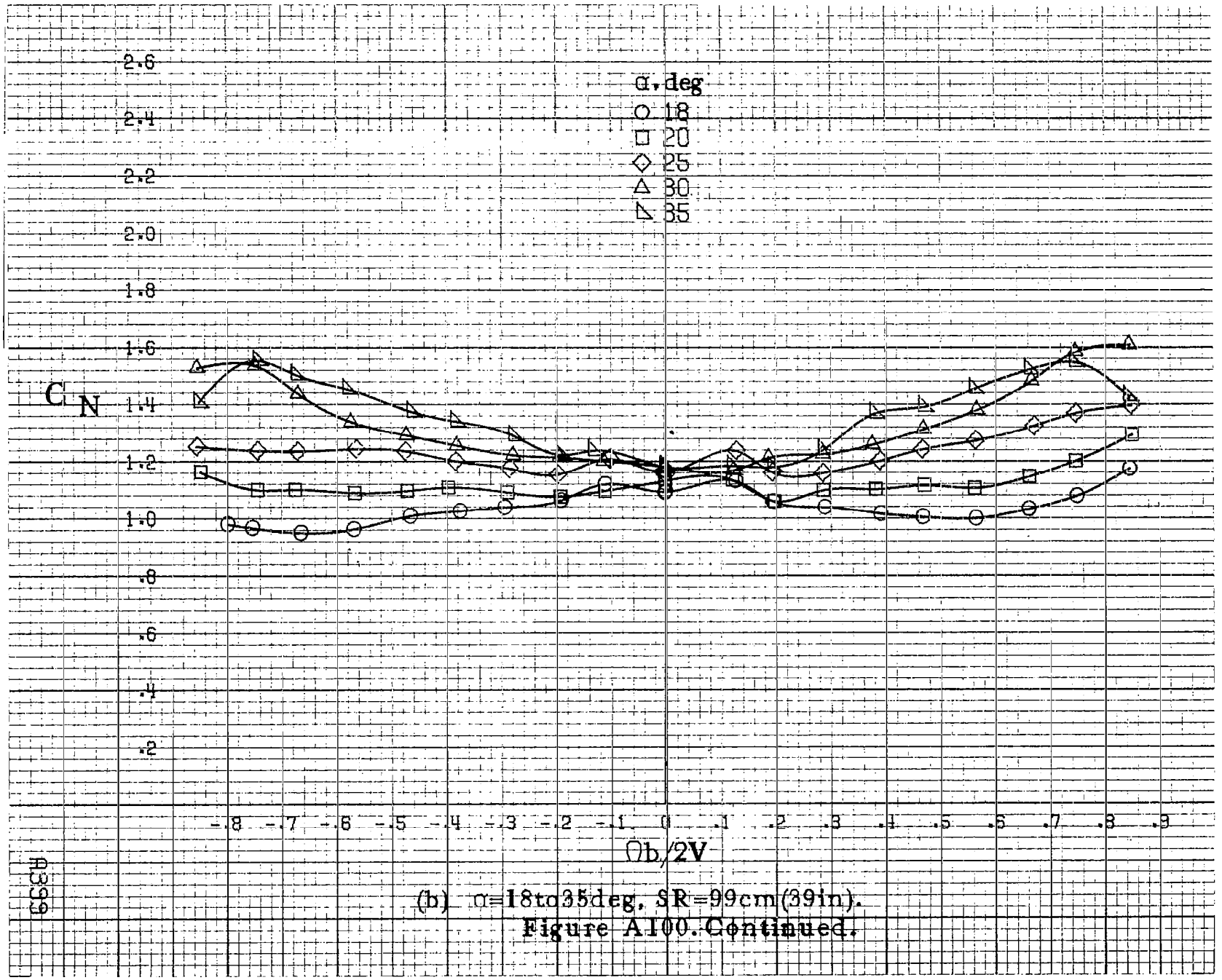

(b) α=18to35deg, SR=99cm(39in).

Figure A100. Continued.

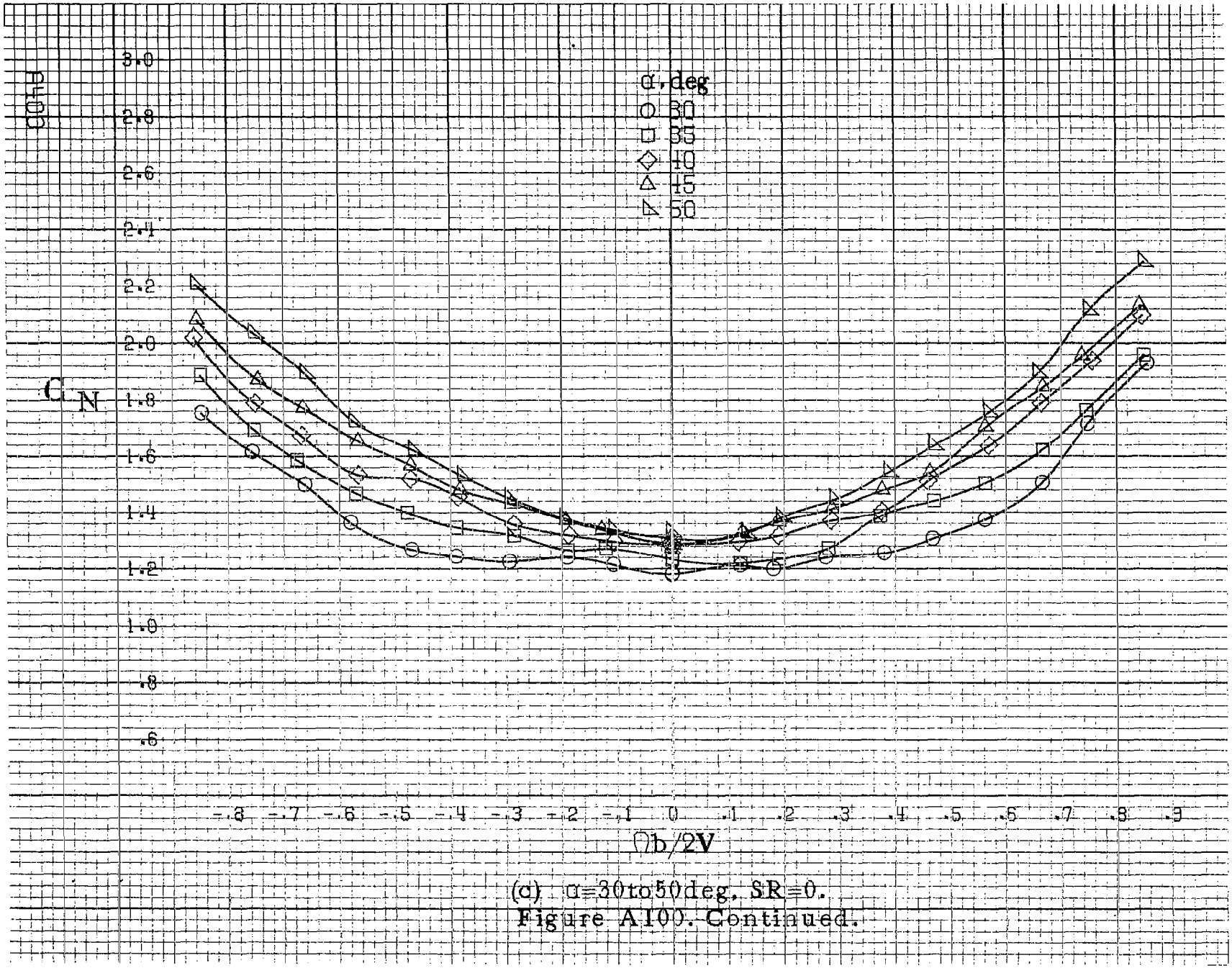

(d) α=30to50deg, SR=0.

Figure A100. Continued.

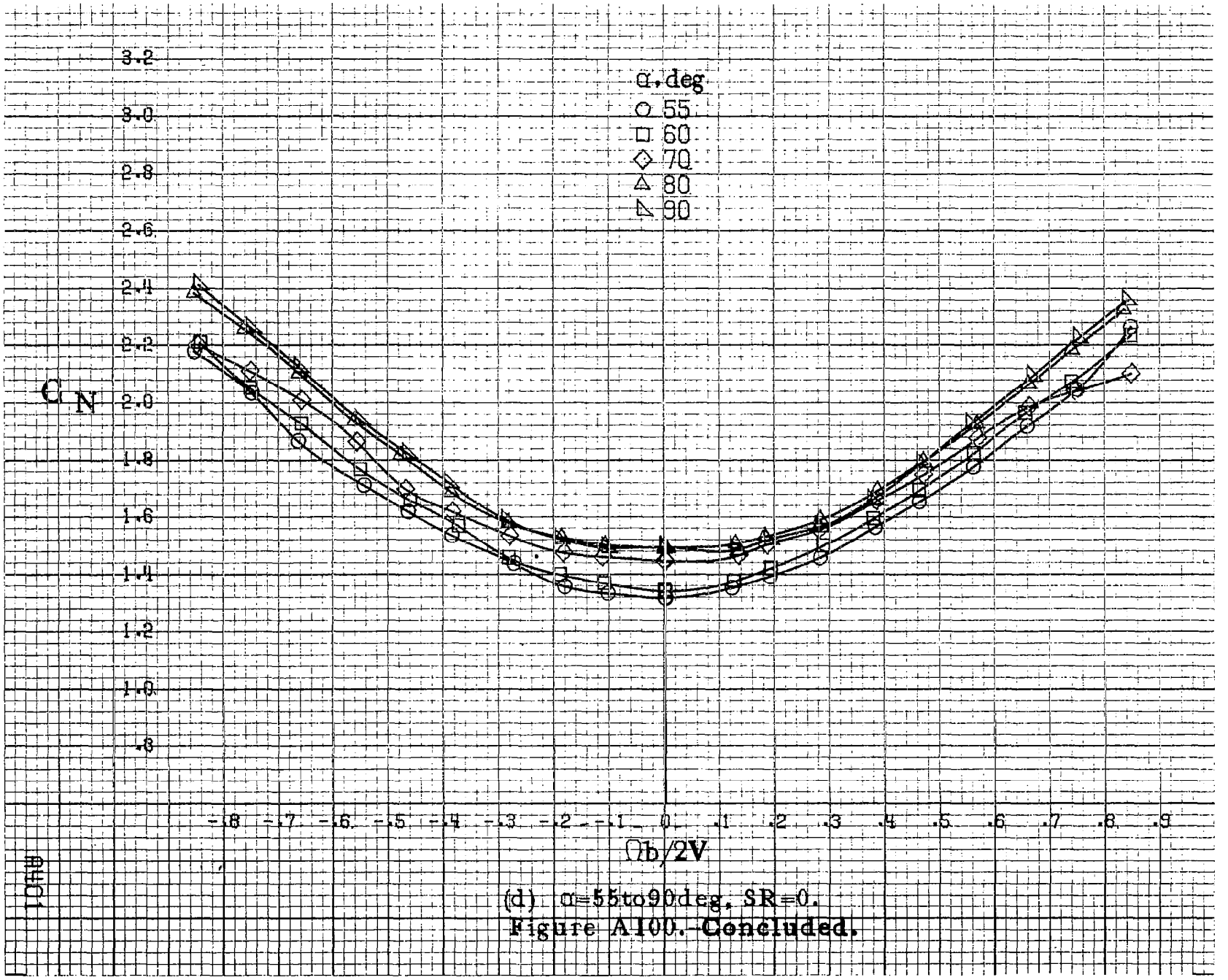

(d) α=55to90deg, SR=0.

Figure A100.-Concluded.

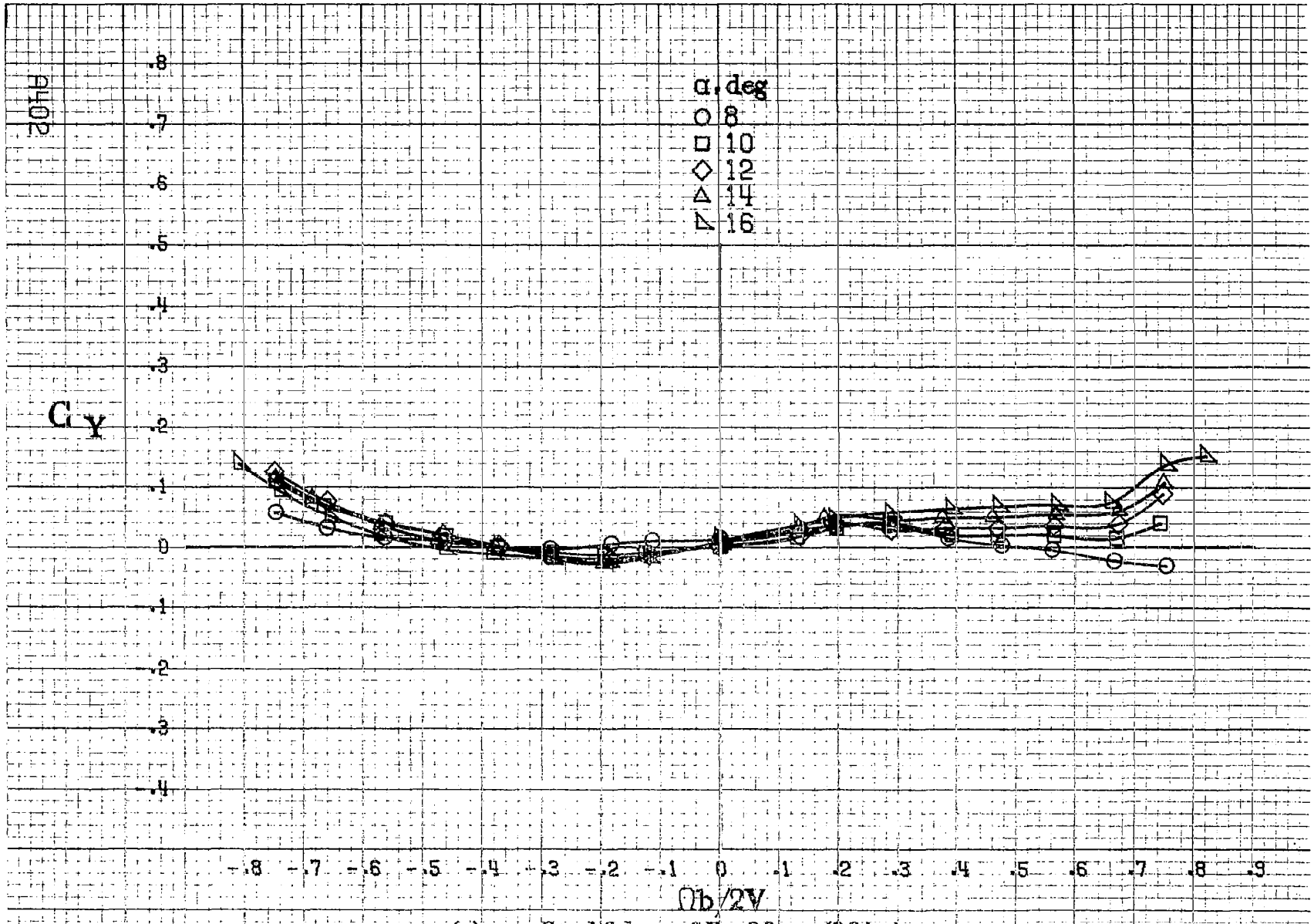

(a) α=8to16deg, SR=99cm(39in).

Figure A101. Effect of rotation rate and angle of attack on side-force coefficient for configuration having segmented LE wing droop. $\delta_e = 0°$, $\delta_a = 0°$, $\delta_r = 0°$, $\beta = 0°$.

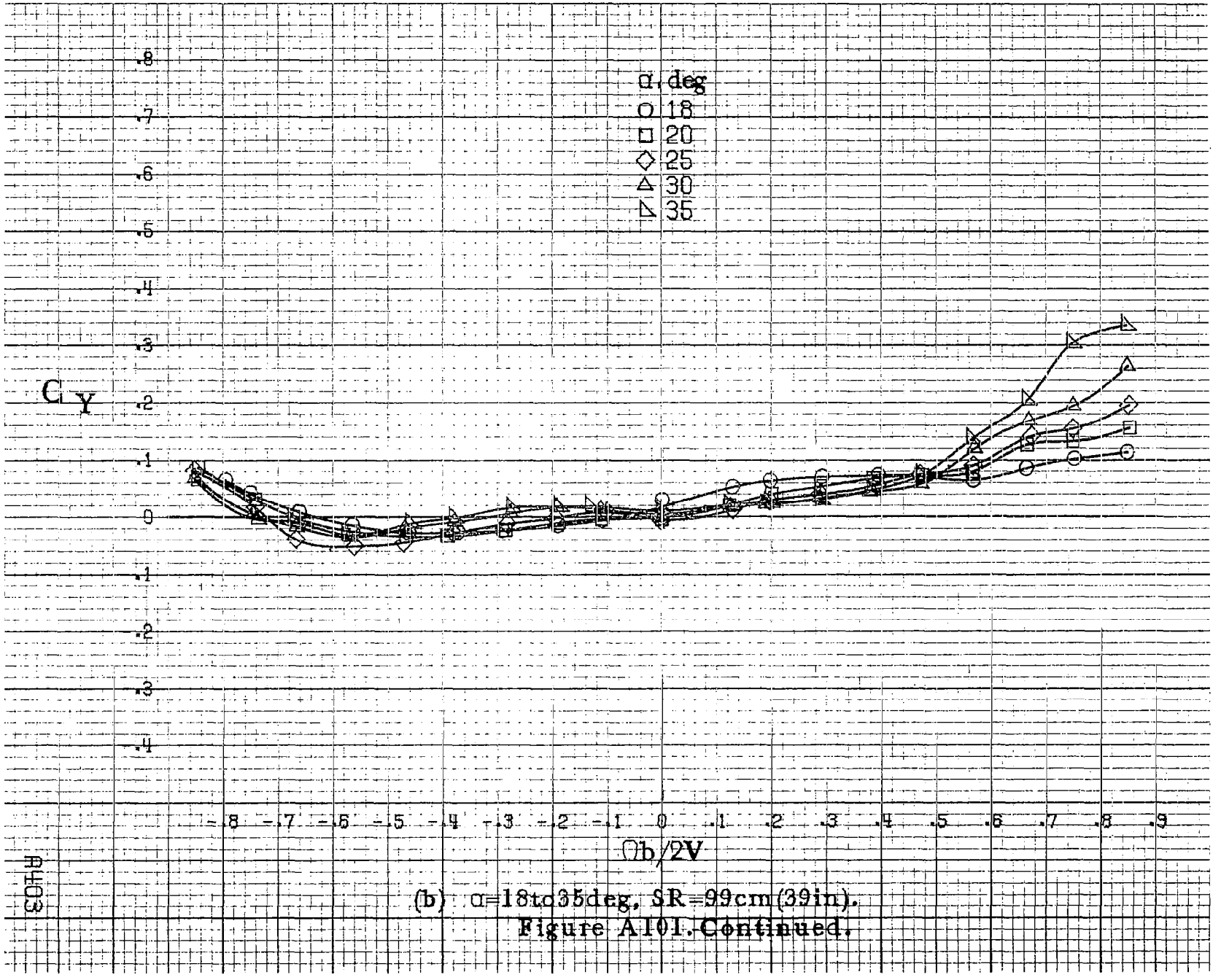

(b) α=18to35deg, SR=99cm(39in).

Figure A101.Continued.

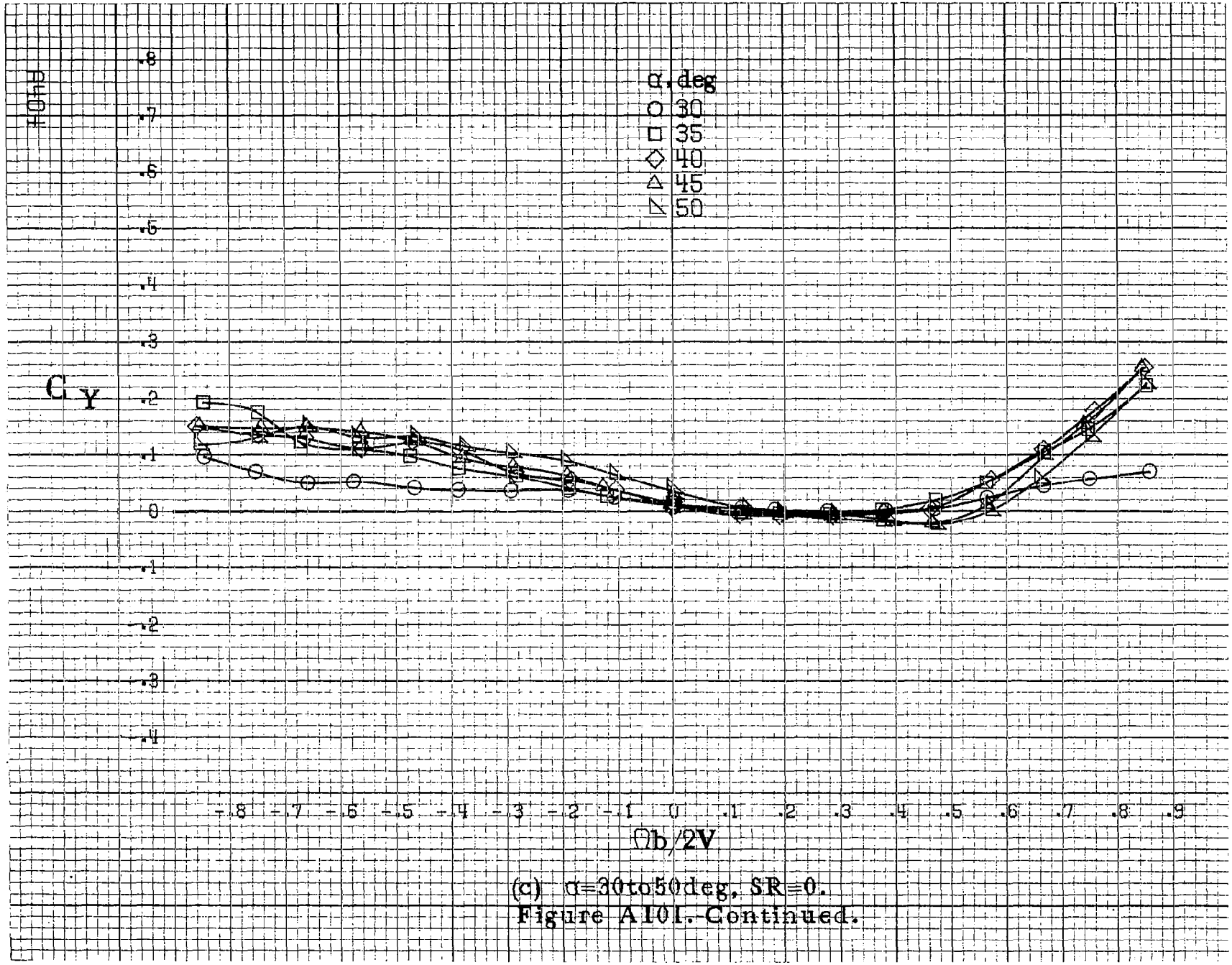

(c) α=30to50deg, SR=0.

Figure A101.-Continued.

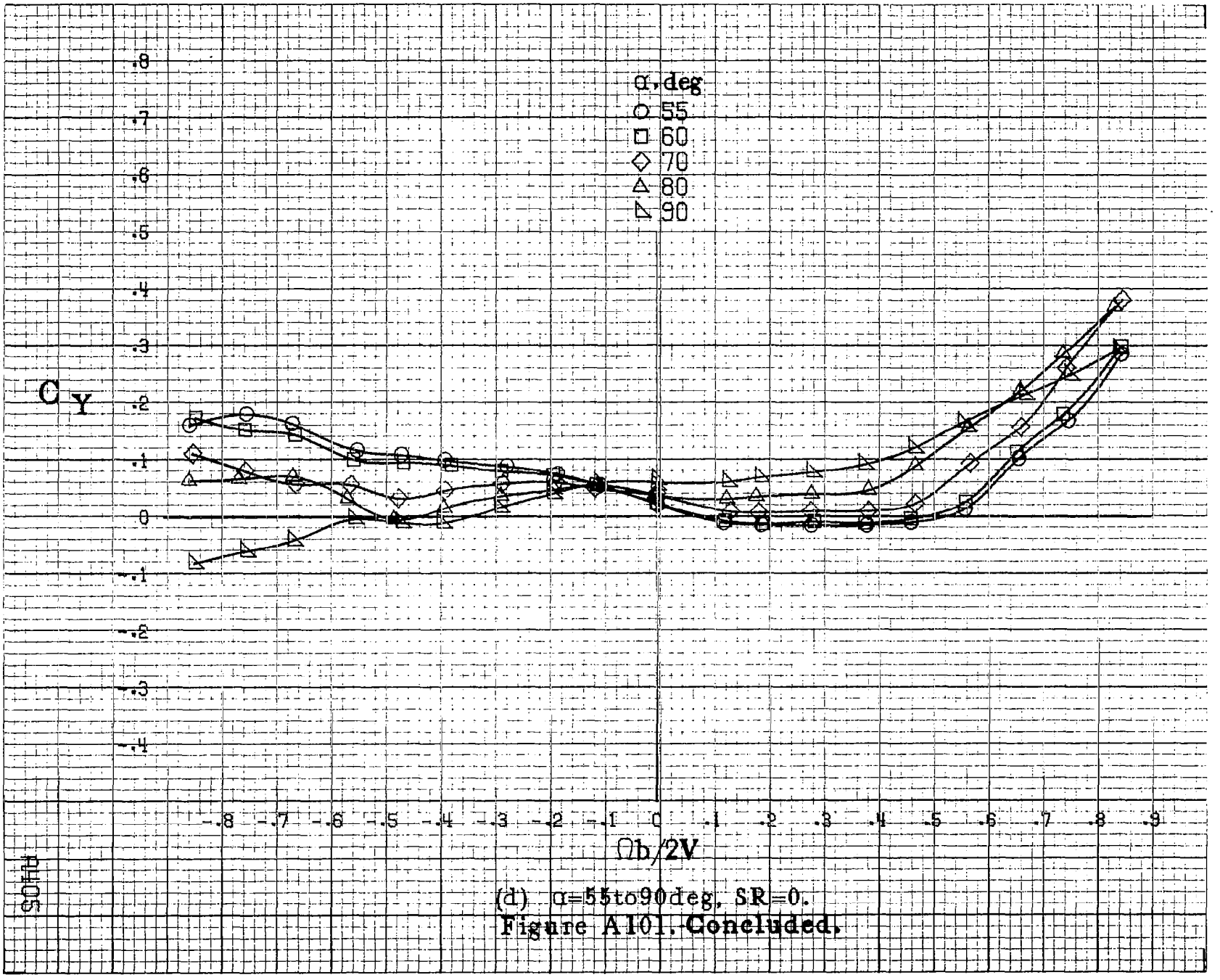

(d) α=55 to 90 deg, SR=0.

Figure A101. Concluded.

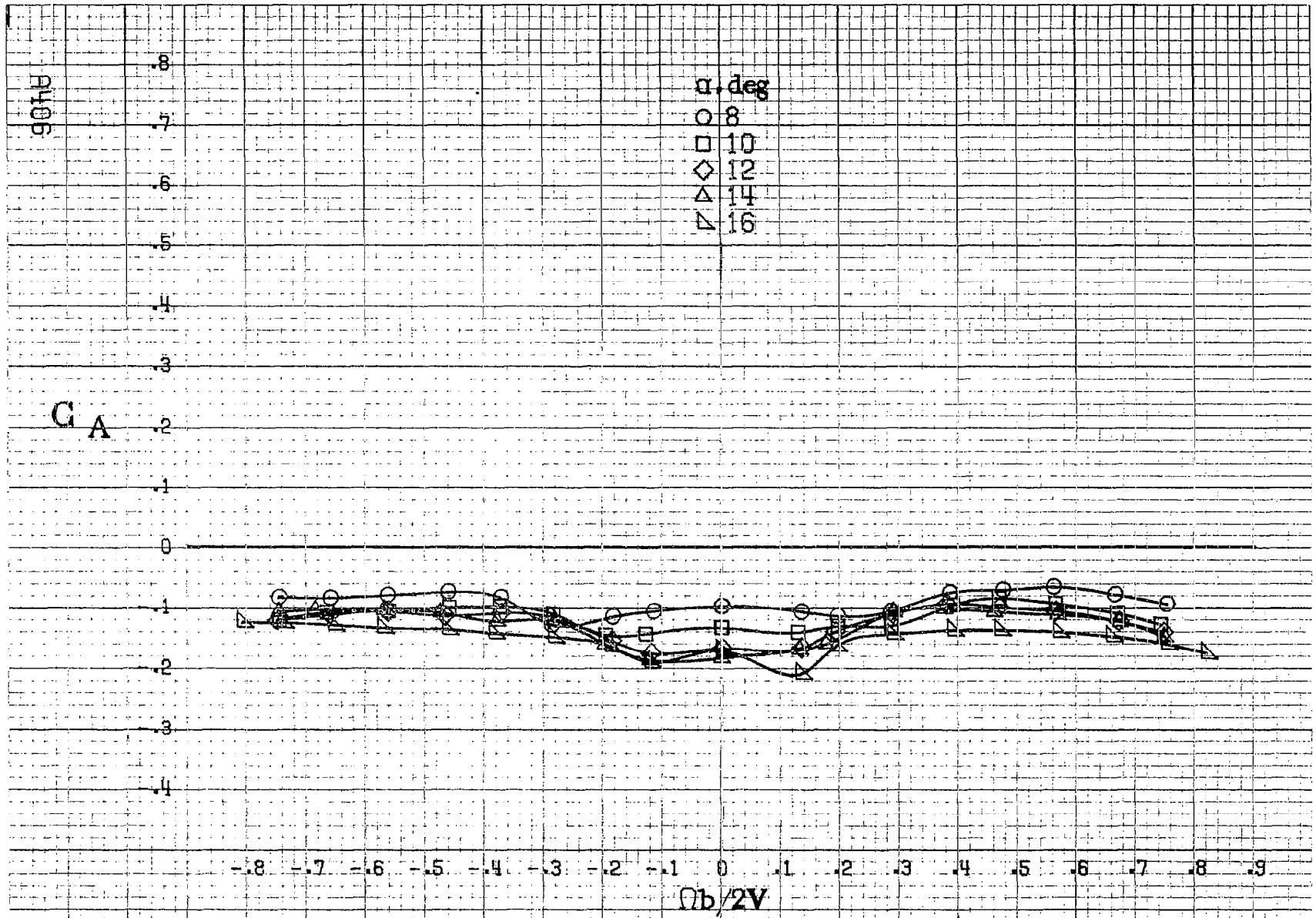

(a) α=8to16deg, SR=99cm(39in).

Figure A102.-Effect of rotation rate and angle of attack on axial-force coefficient for configuration having segmented LE wing droop. $\delta_a = 0°$, $\delta_s = 0°$, $\delta_r = 0°$, $\beta = 0°$.

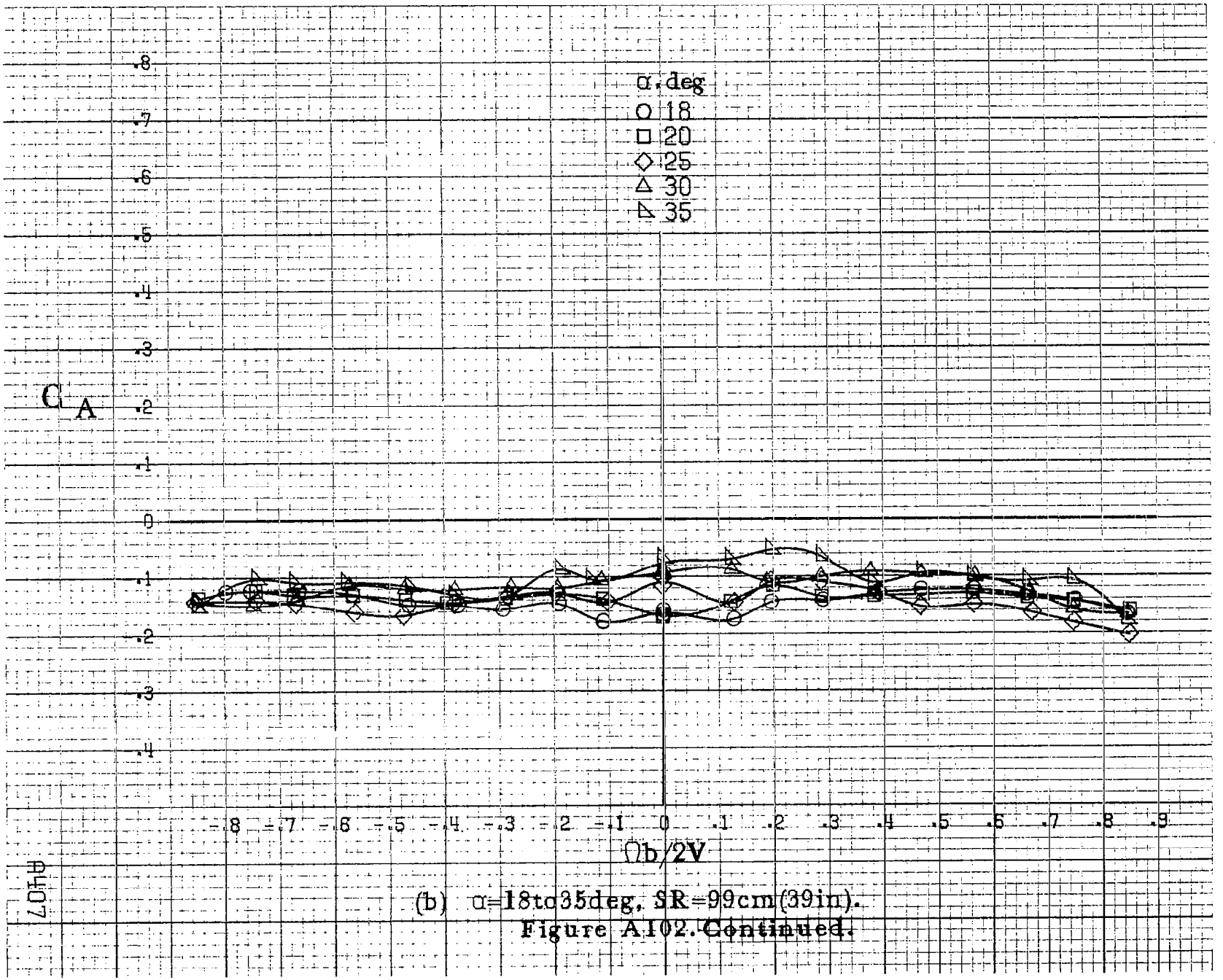

(b) α=18to35deg, SR=99cm(39in).

Figure A102. Continued.

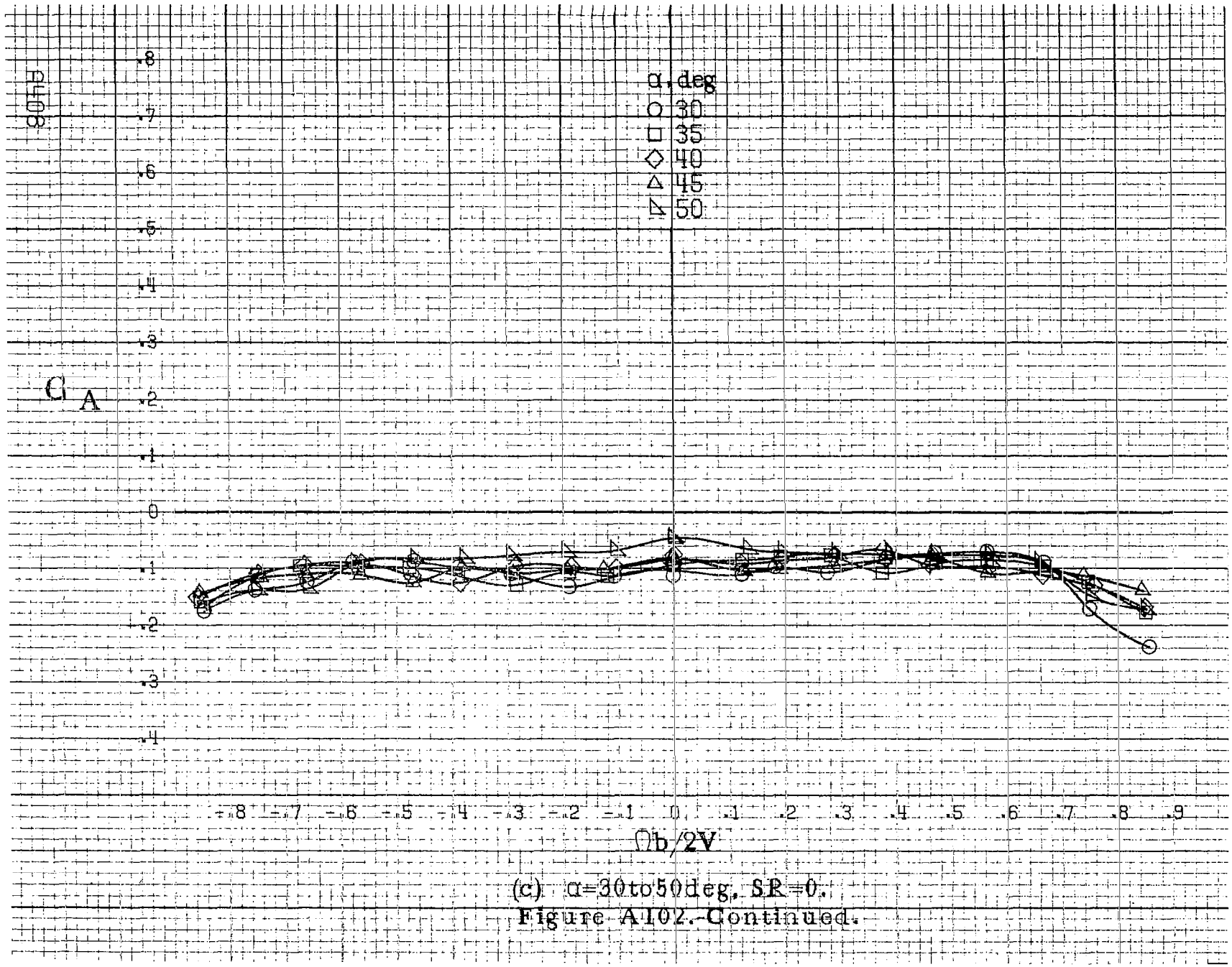

(c) α=30to50deg, SR=0.

Figure A102.-Continued.

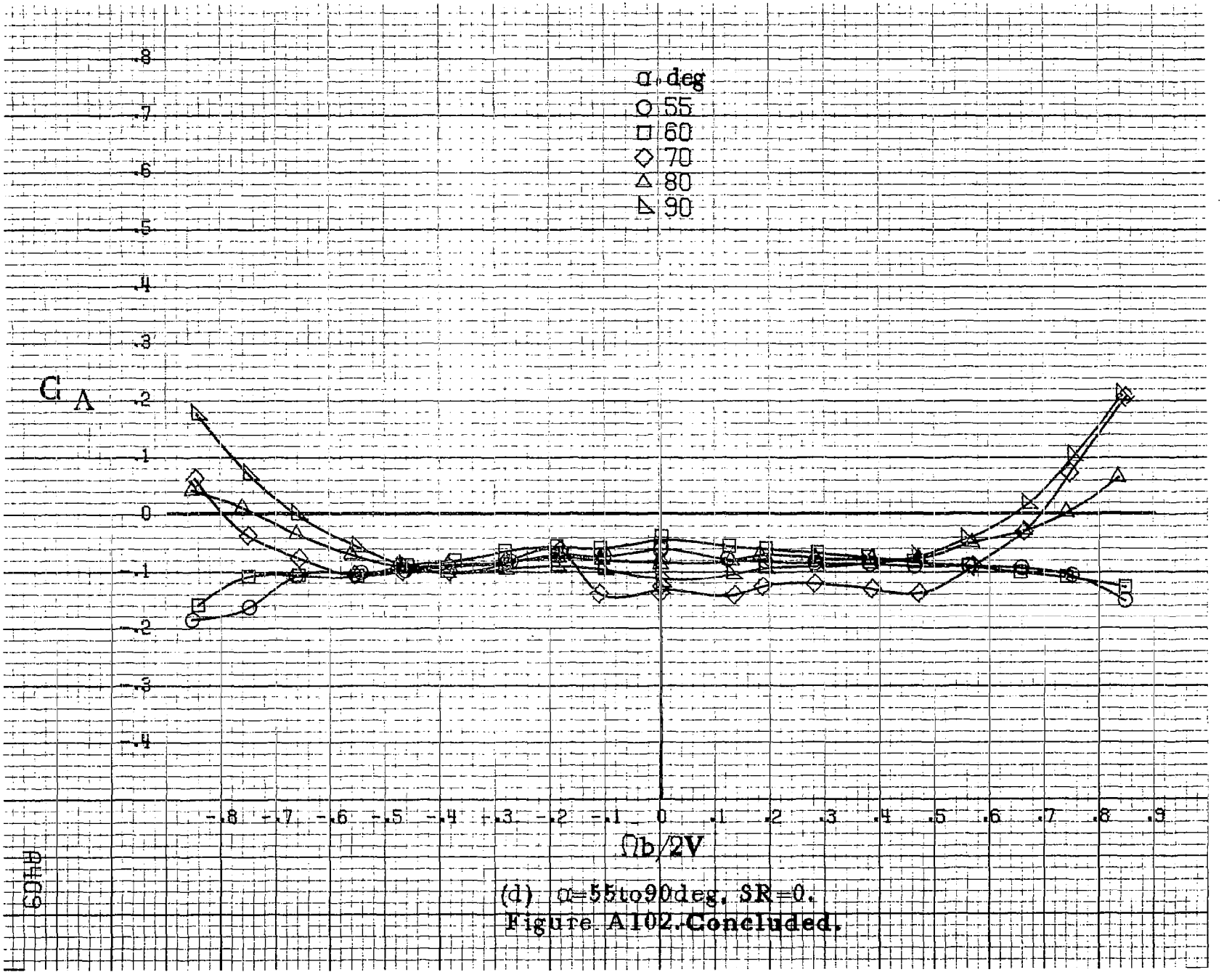

(d) α=55to90deg, SR=0.

Figure A102.Concluded.

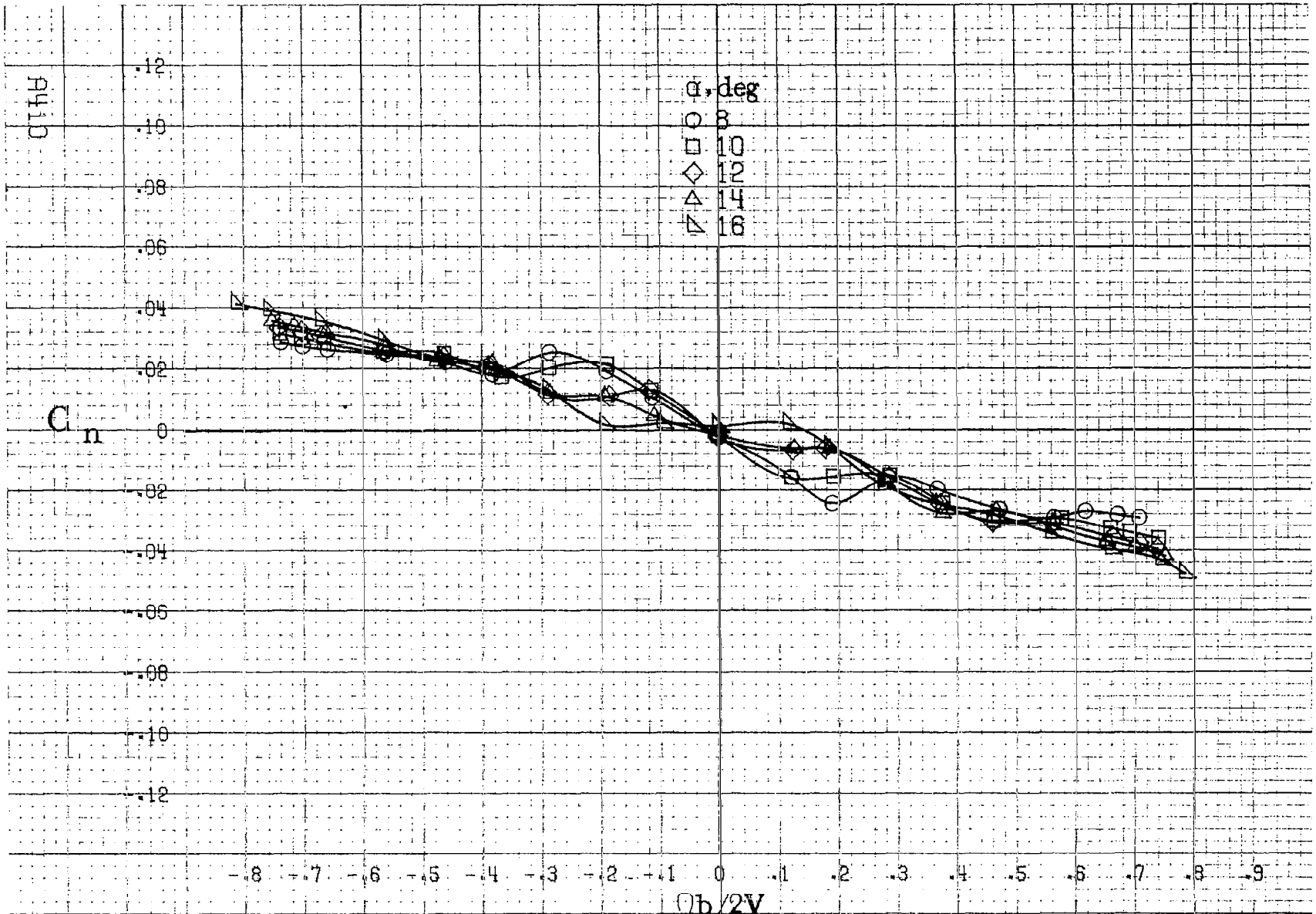

(a) α=8to16deg, SR=99cm(39in).

Figure A103.-Effect of rotation rate and angle of attack on yawing-moment coefficient for configuration having outboard LE wing droop extended inboard 33.8cm(13.3in). δ_e =0°, δ_a =0°, δ_r =0°. β =0°.

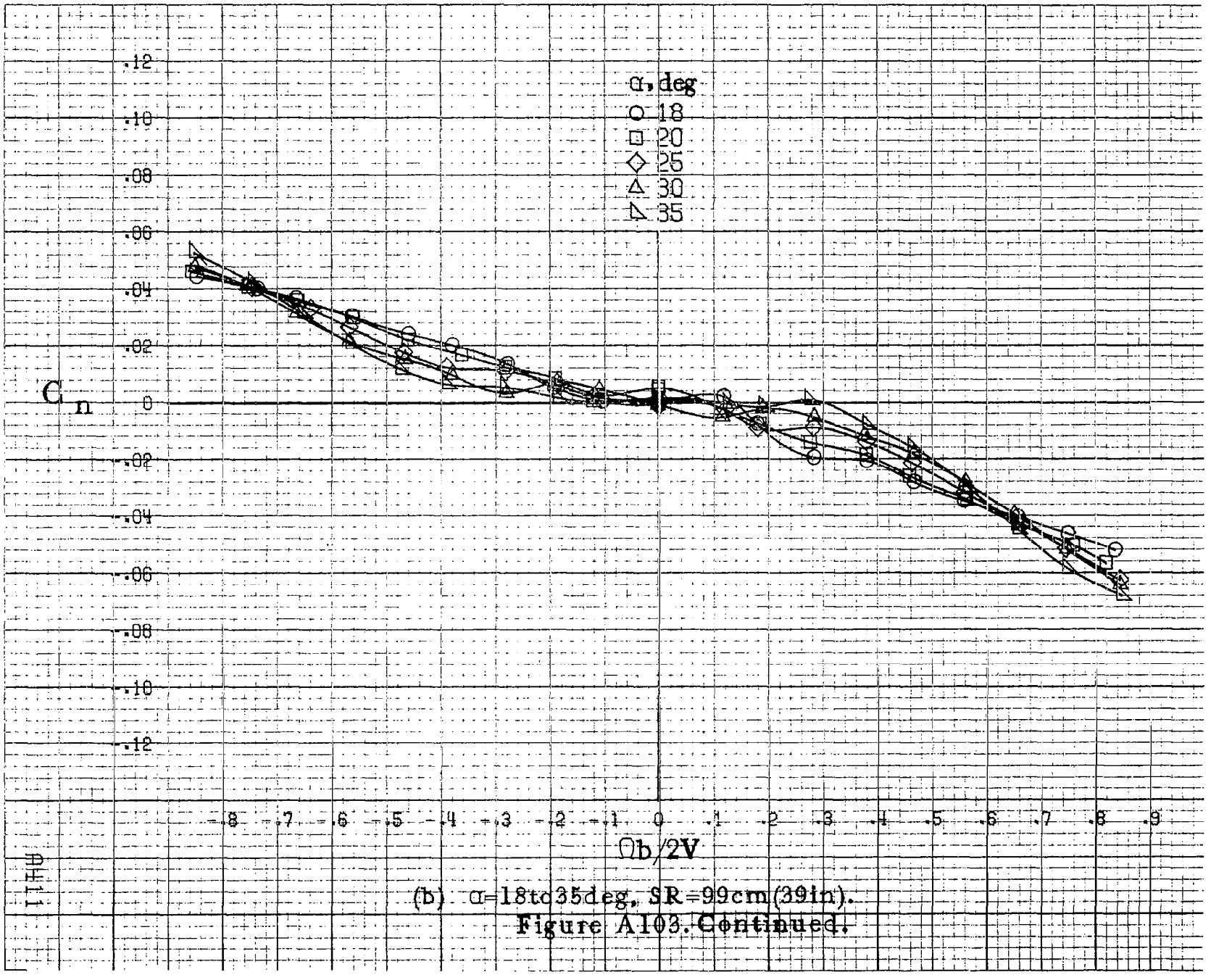

(b) α=18to35deg, SR=99cm(39in).

Figure A103.Continued.

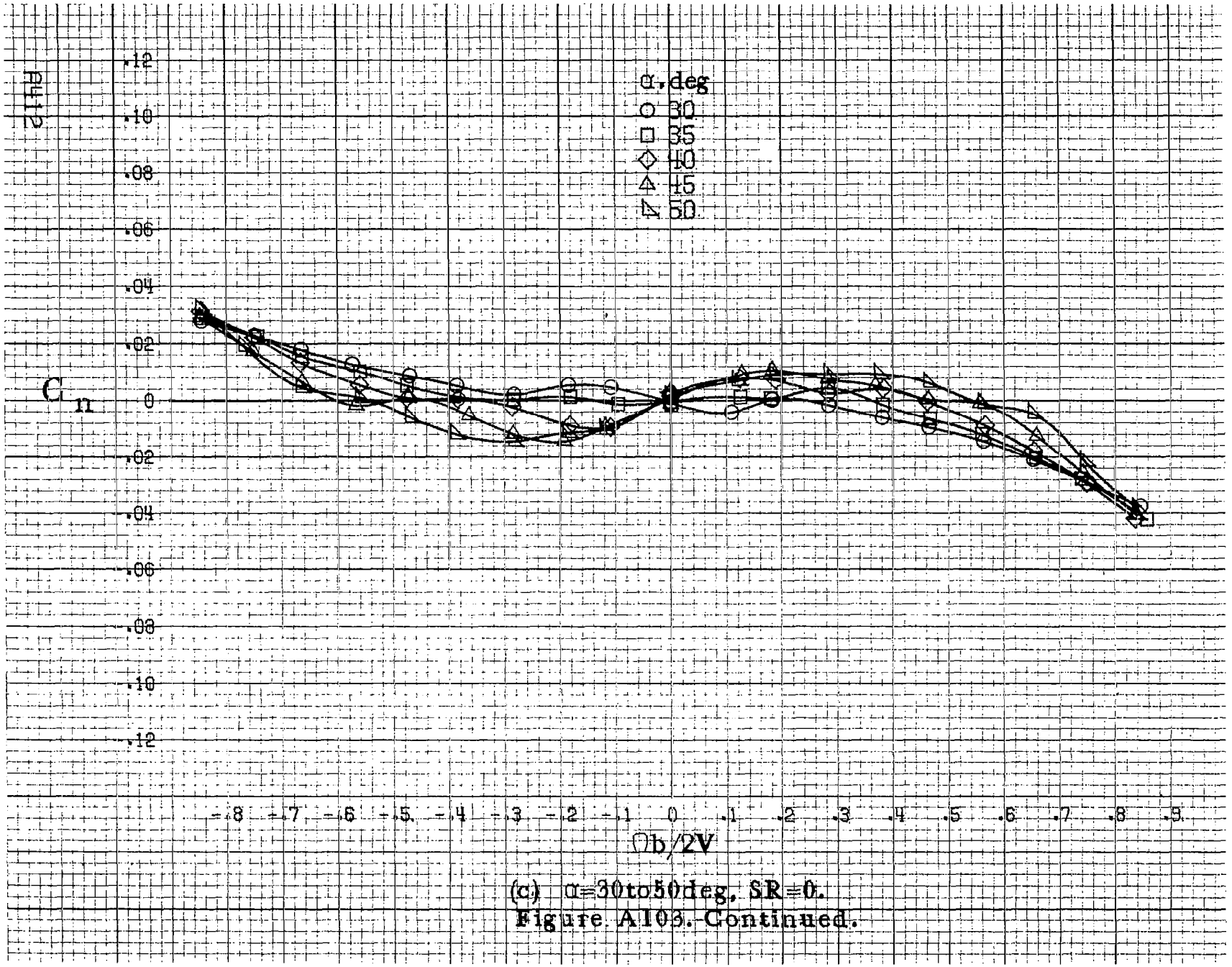

(c) α=30to50deg, SR=0.

Figure A103.-Continued.

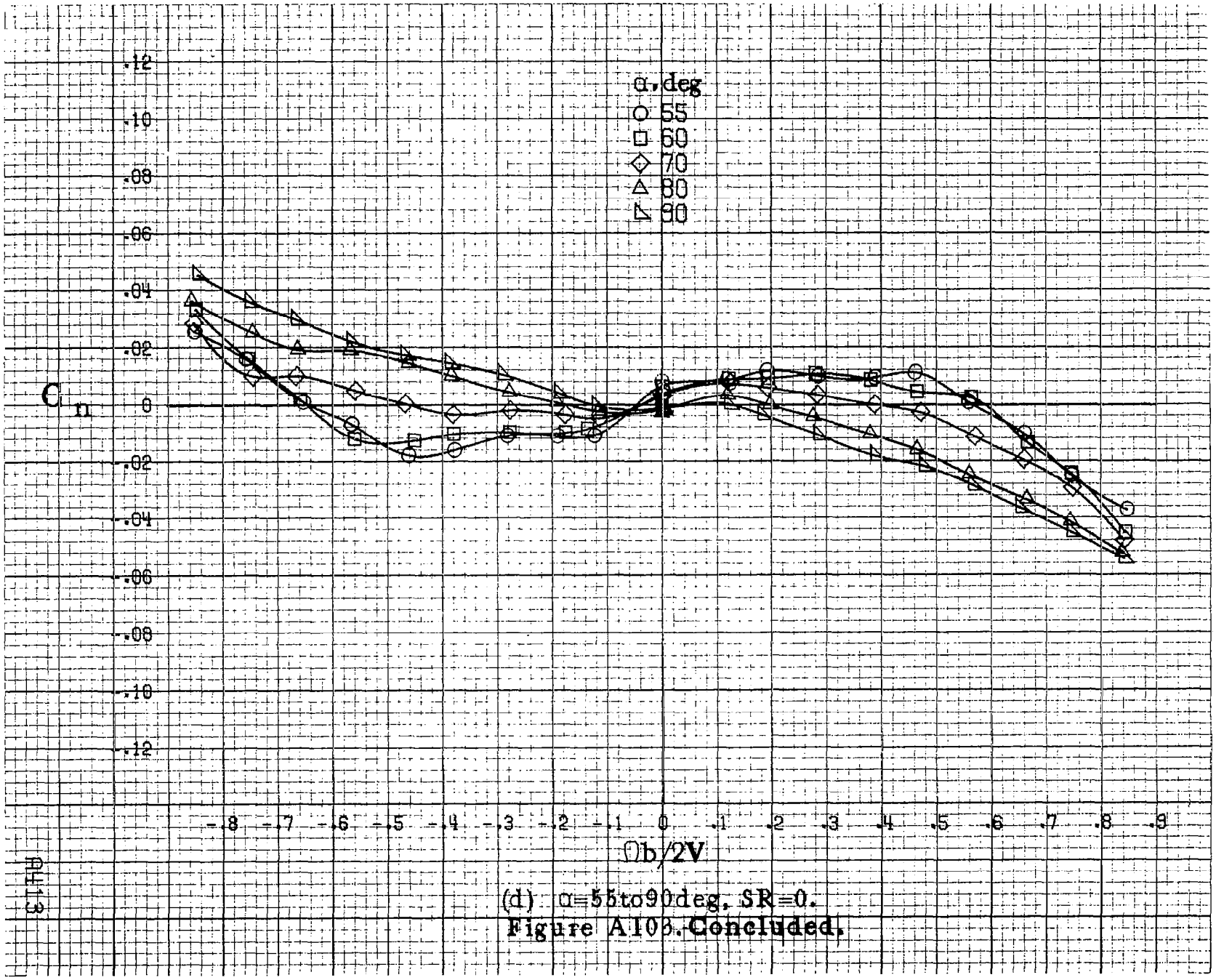

(d) α=55to90deg, SR=0.

Figure A103.Concluded.

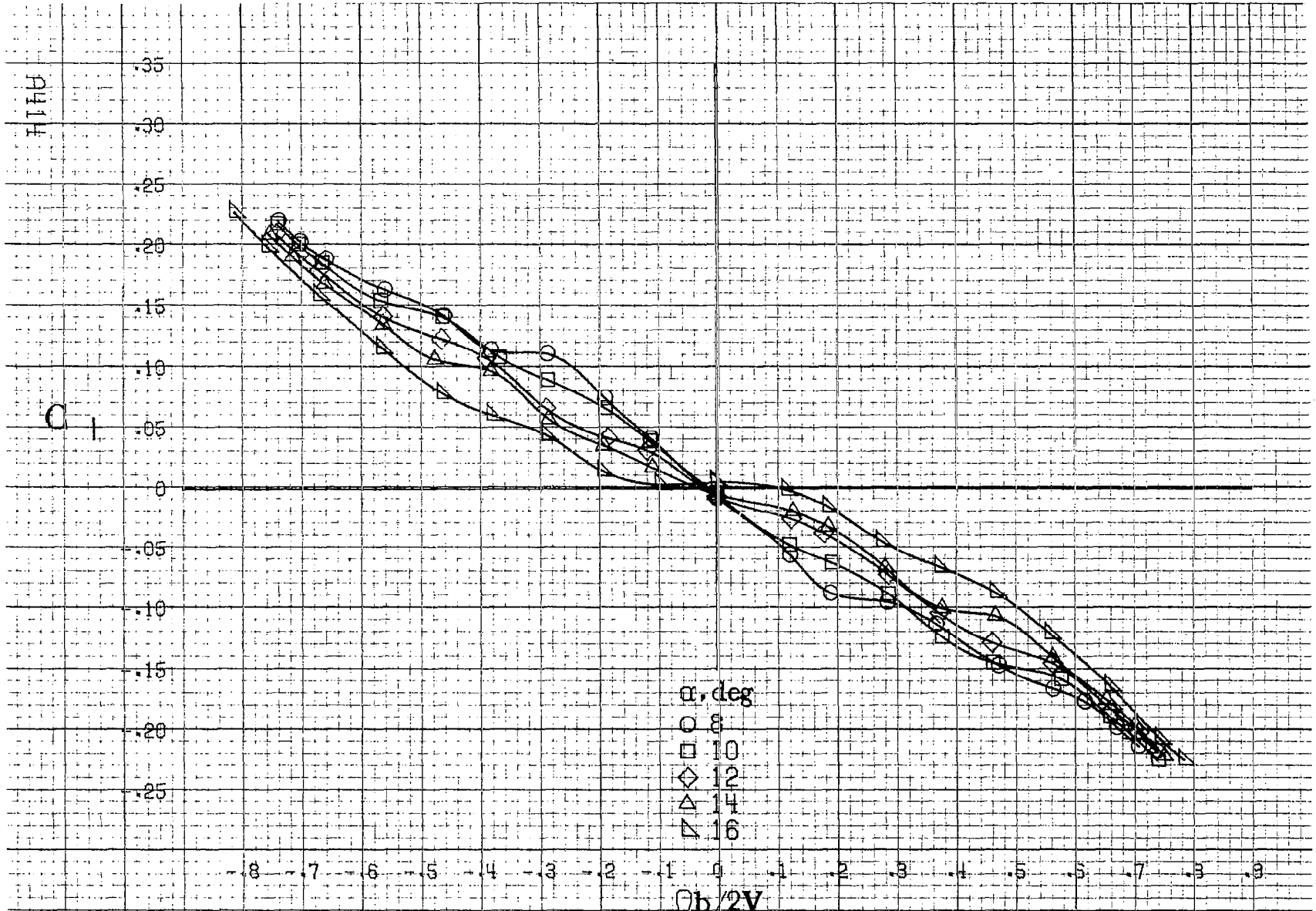

(a) α=8to16deg, SR=99cm(39in).

Figure A104.-Effect of rotation rate and angle of attack on rolling-moment coefficient for configuration having outboard LE wing droop extended inboard 33.8cm(13.3in). δ_e=0°, δ_a=0°, δ_r=0°, β=0°.

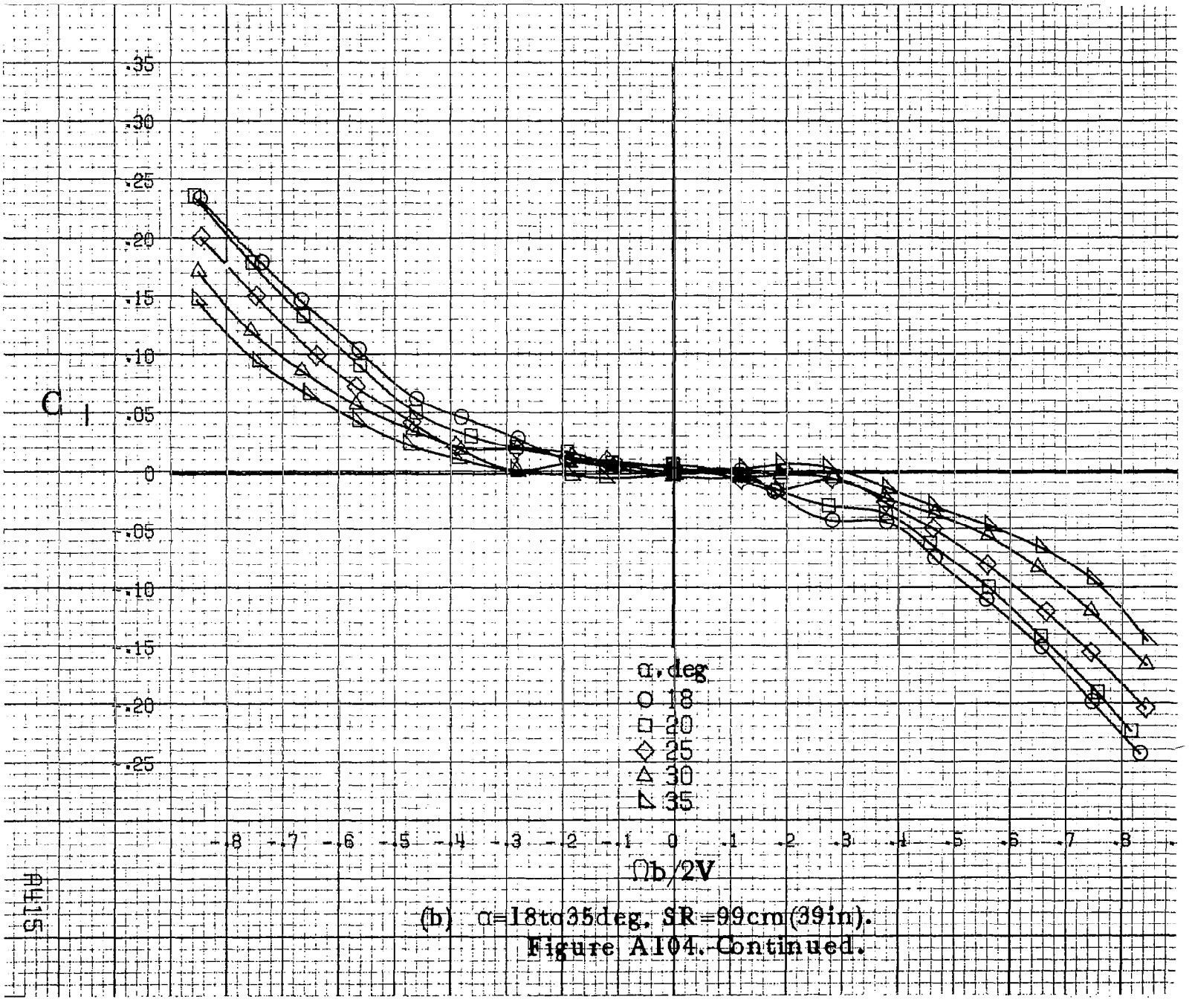

(b) α=18toα35deg. SR=99cm(39in).

Figure A104.-Continued.

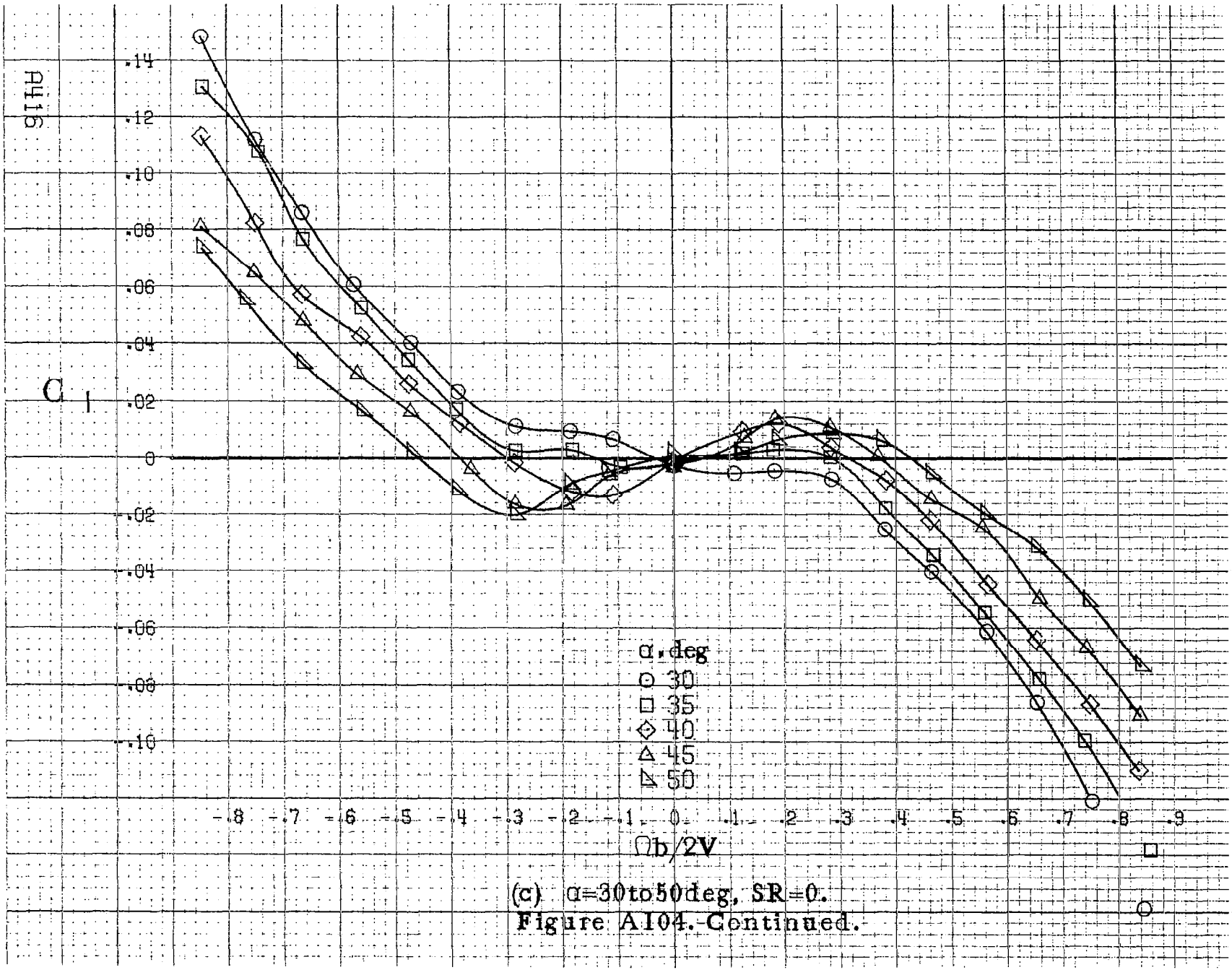

(c) α=30to50deg, SR=0.

Figure A104.-Continued.

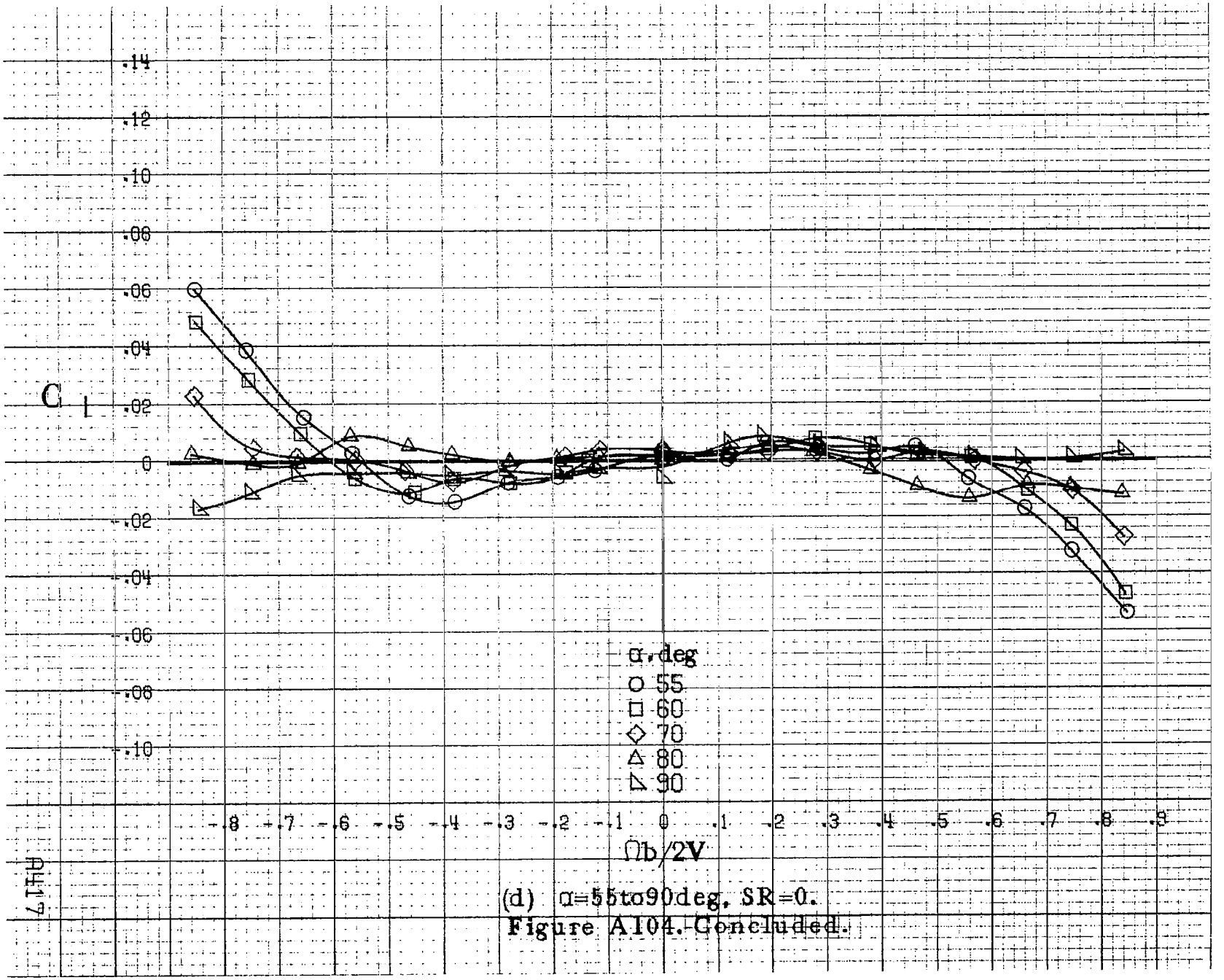

(d) α=55to90deg, SR=0.

Figure A104.-Concluded.

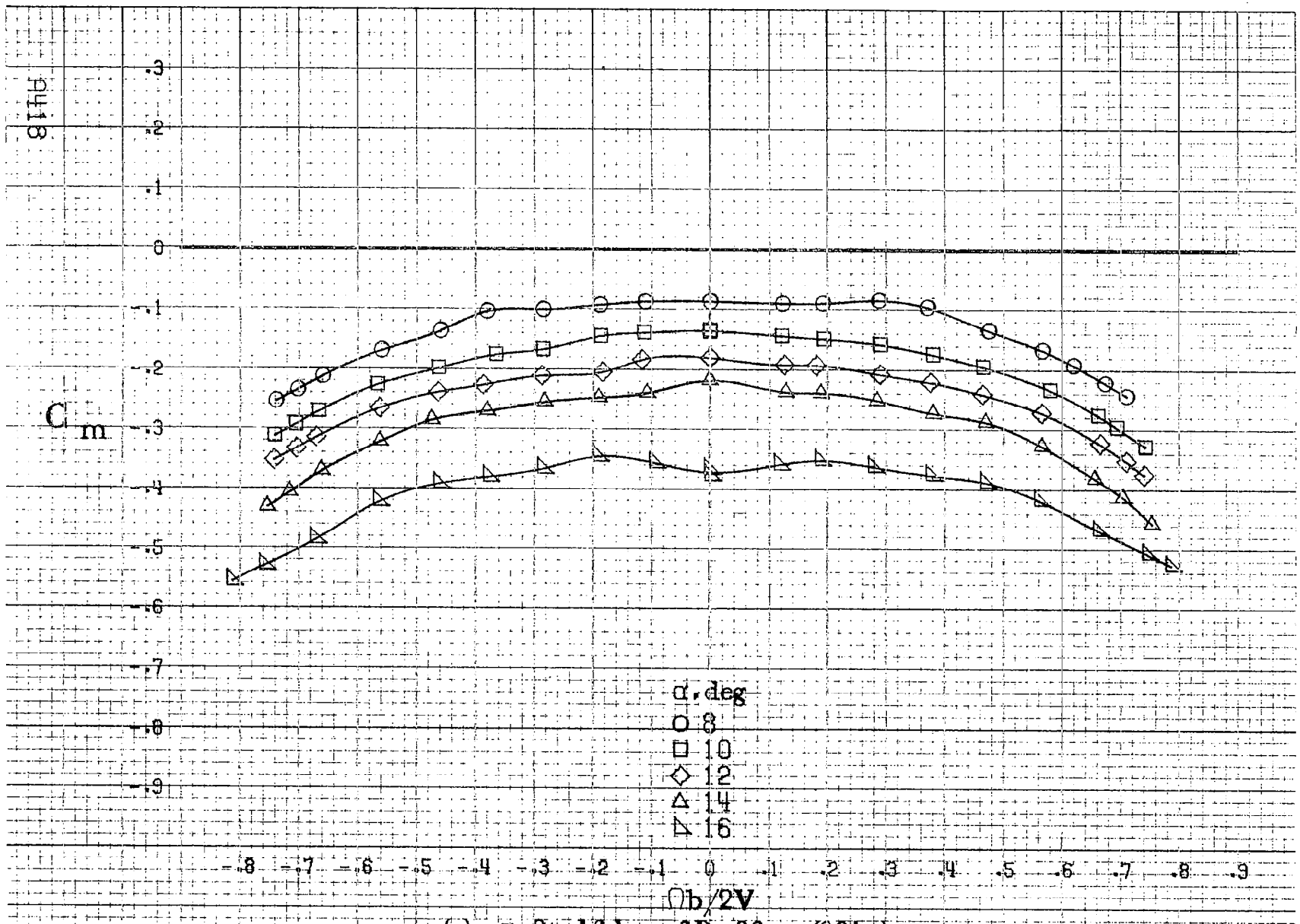

(a) α=8to16deg, SR=99cm(39in).

Figure A105. Effect of rotation rate and angle of attack on pitching-moment coefficient for configuration having outboard LE wing droop extended inboard 33.8cm(13.3in). δ_e =0°, δ_a =0°, δ_r =0°, β =0°.

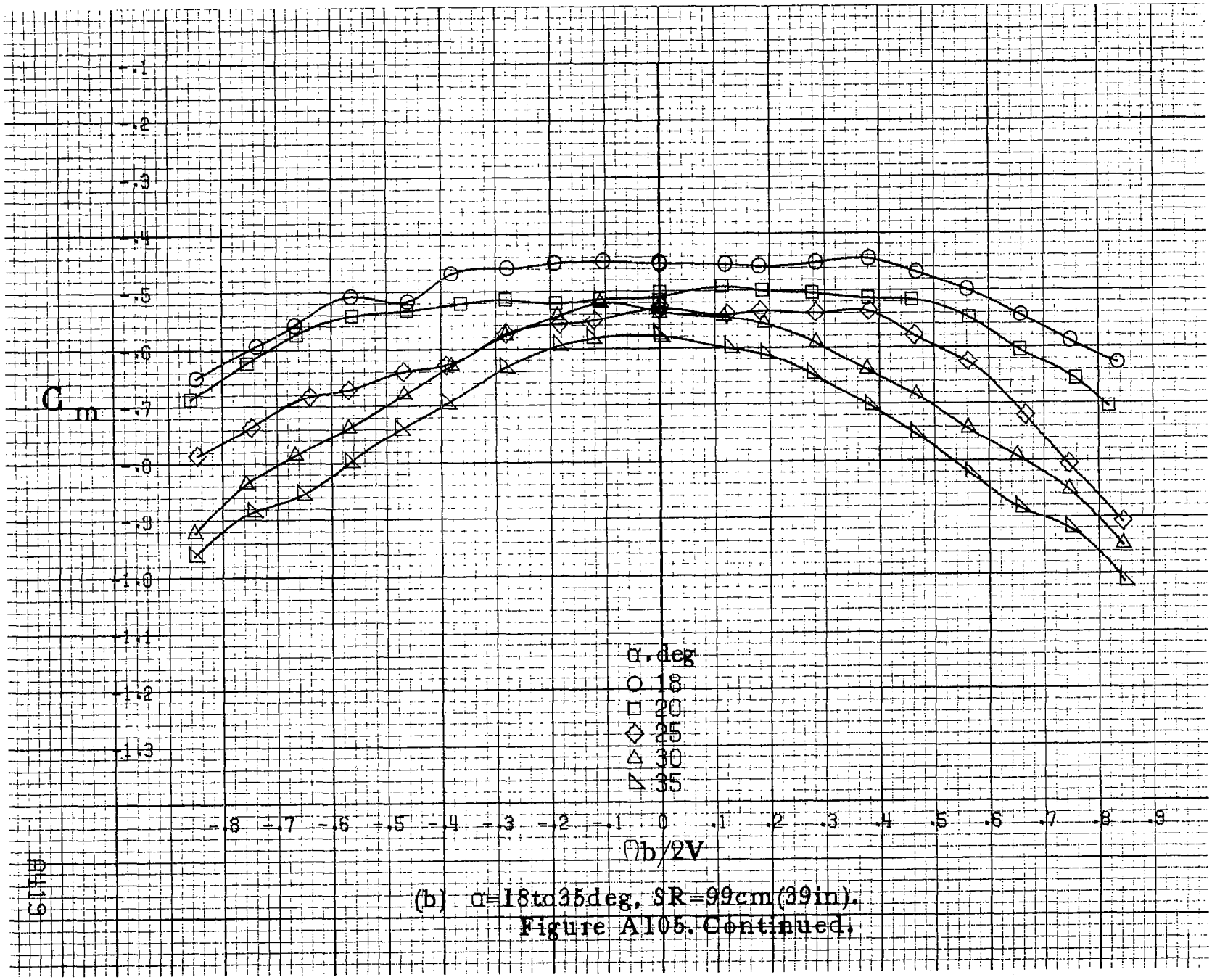

(b) α=18to35deg, SR=99cm(39in).

Figure A105. Continued.

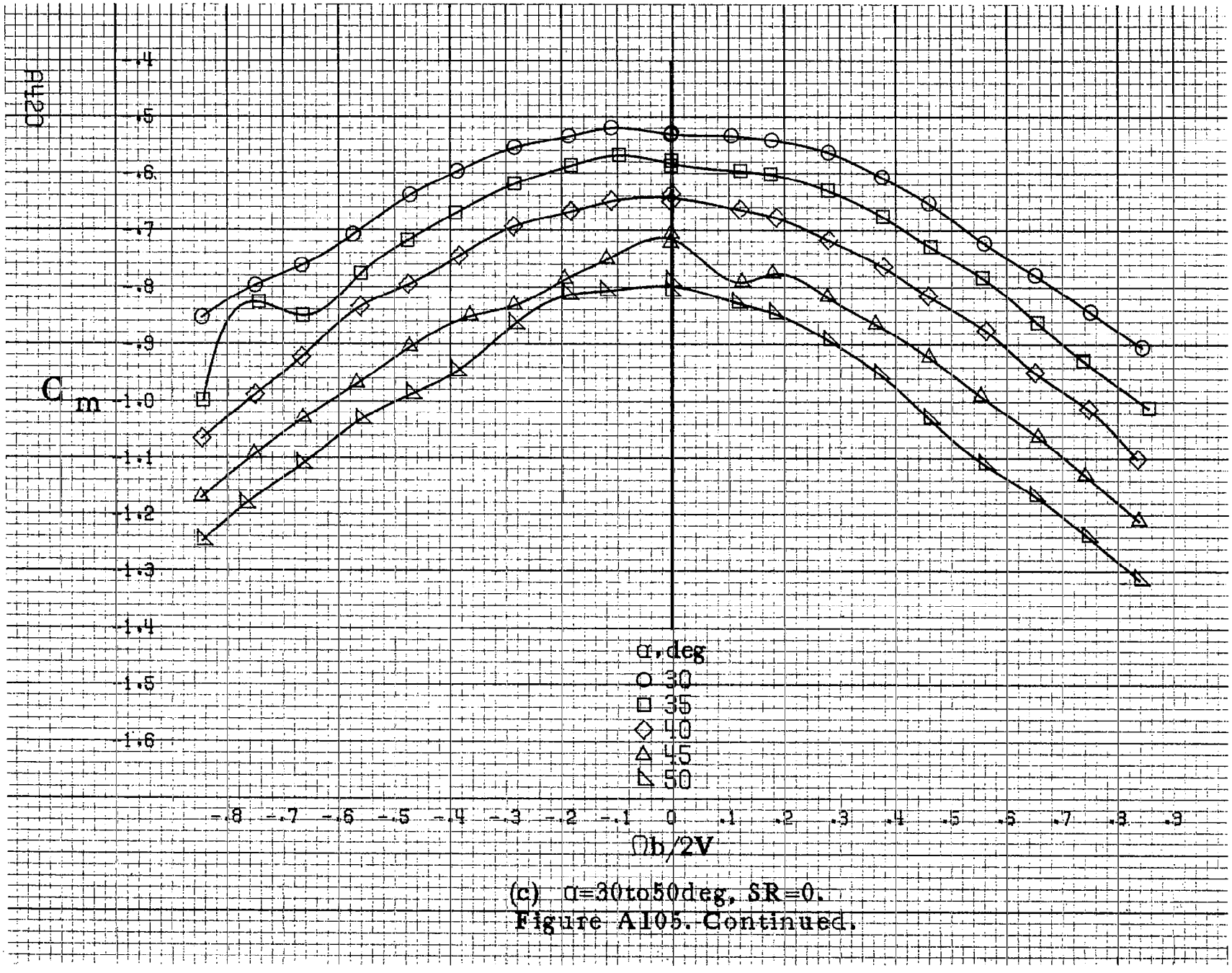

(c) α=30to50deg, SR=0.

Figure A105. Continued.

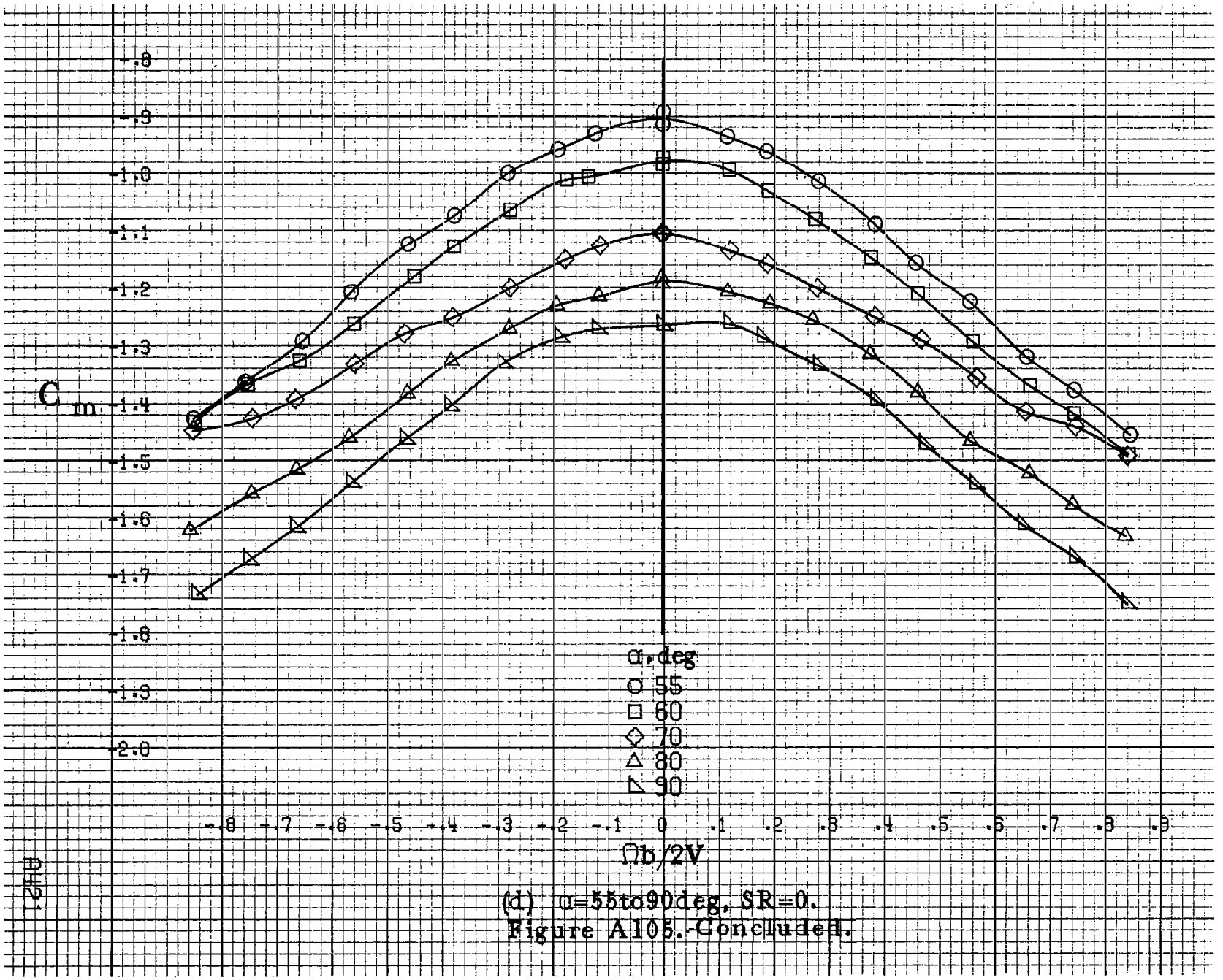

(d) α=55to90deg, SR=0.

Figure A105.-Concluded.

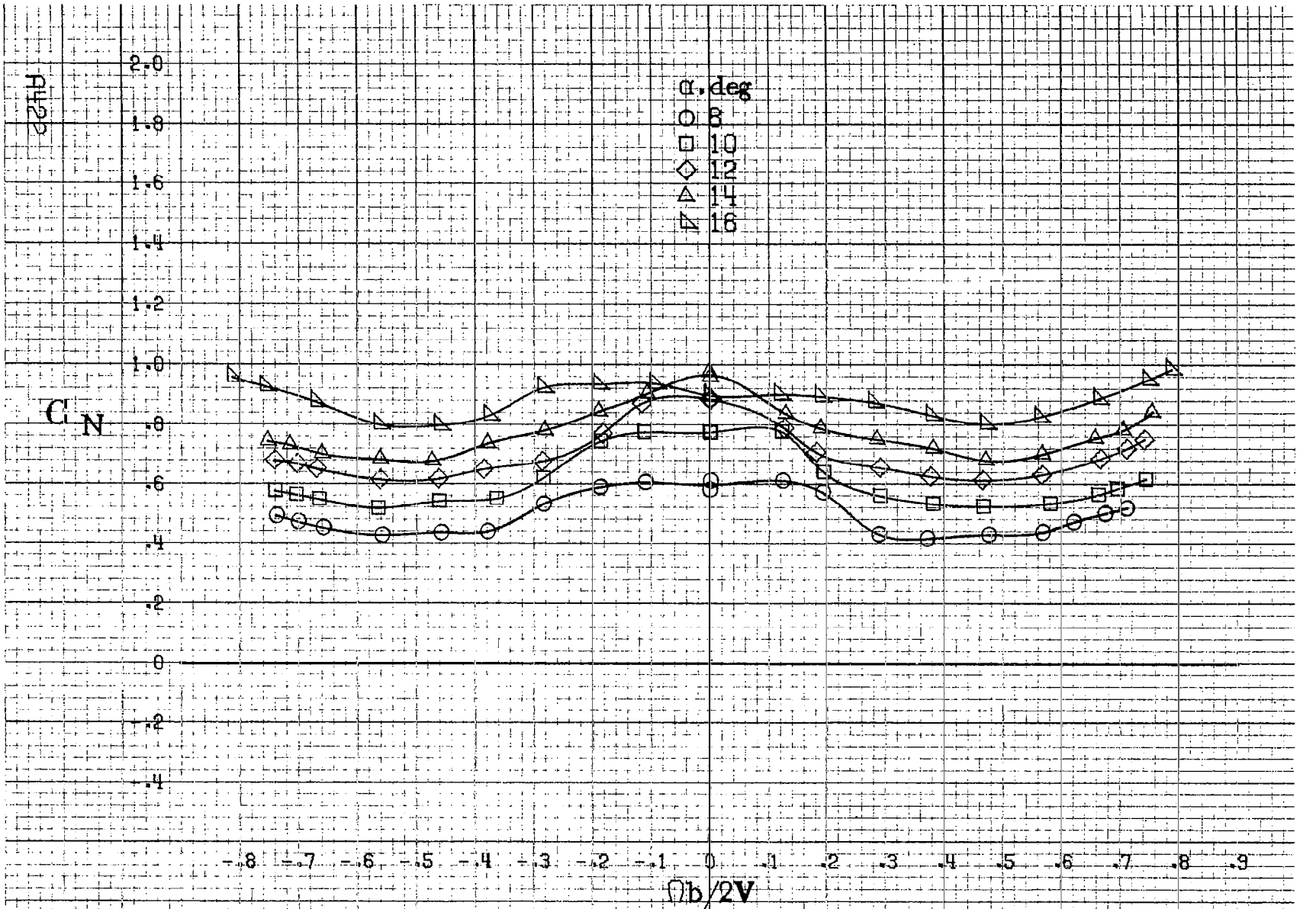

(a) α=8to16deg, $R=99cm(39in).

Figure A106. Effect of rotation rate and angle of attack on normal-force coefficient for configuration having outboard LE wing droop extended inboard 33.8cm(13.3in). $\delta_e = 0°$, $\delta_a = 0°$, $\delta_r = 0°$. $\beta = 0°$.

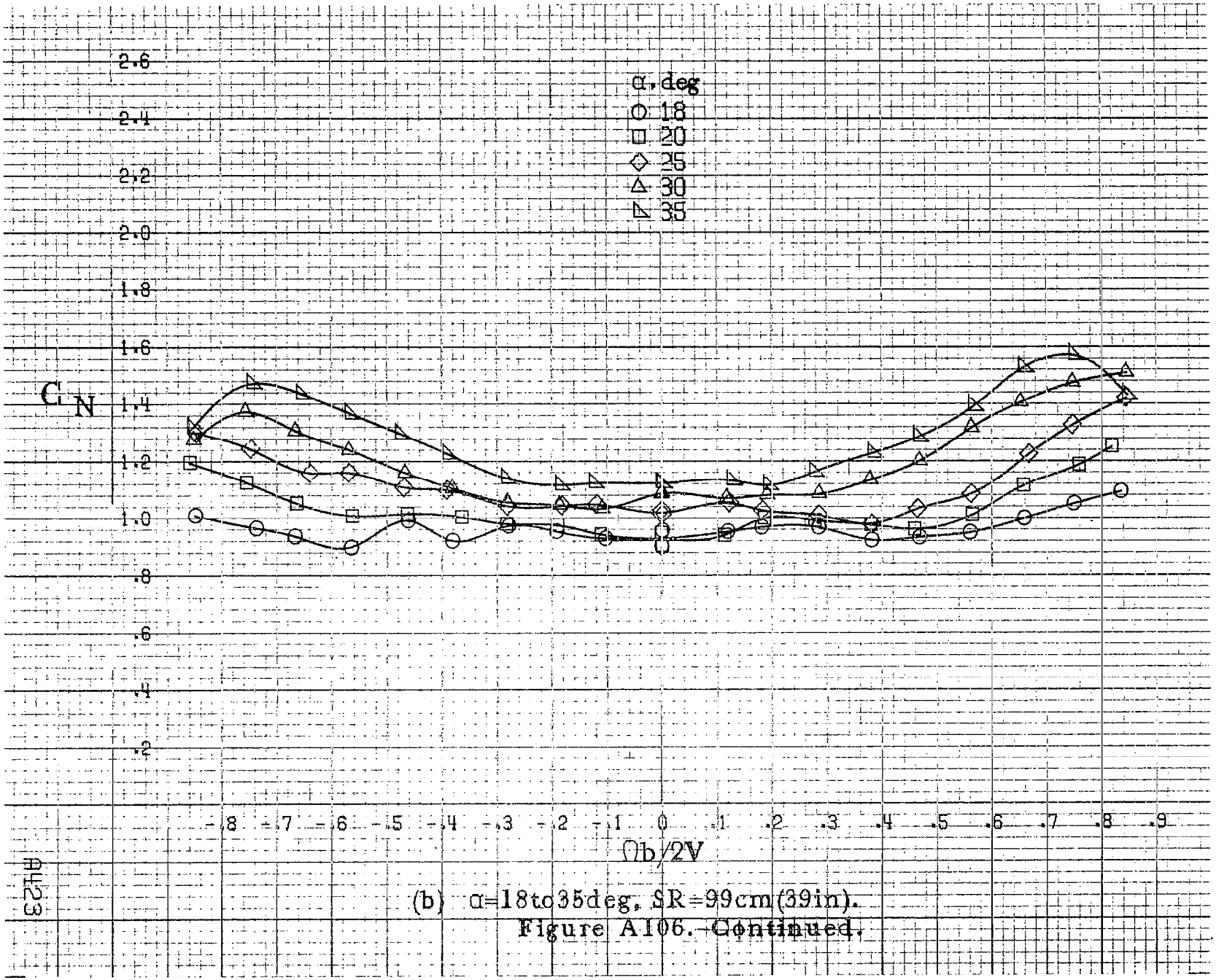

(b) α=18to35deg. SR=99cm(39in).

Figure A106.-Continued.

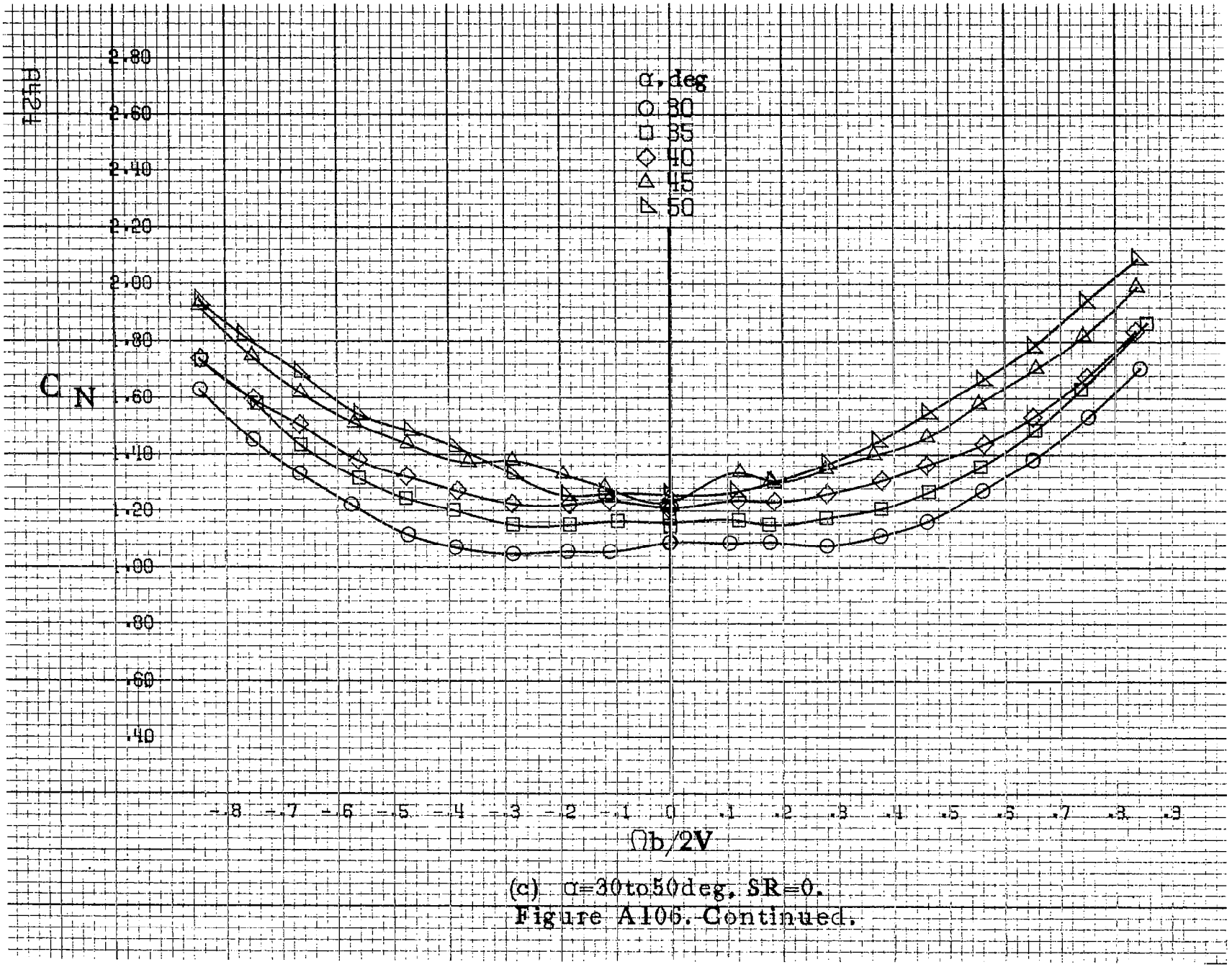

(c) $\alpha = 30$ to 50 deg, SR = 0.

Figure A106. Continued.

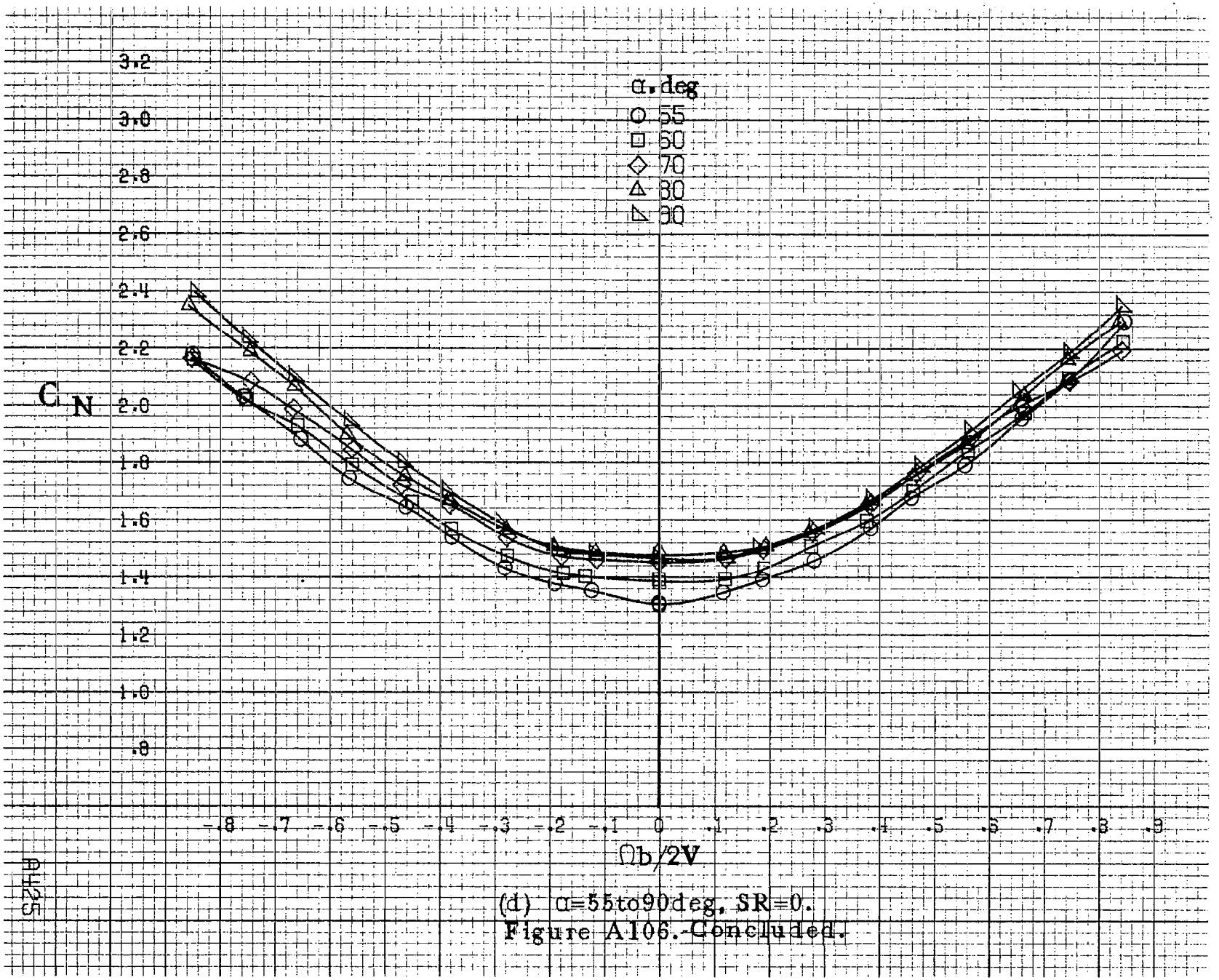

(d) α=55to90deg, SR=0.

Figure A106.-Concluded.

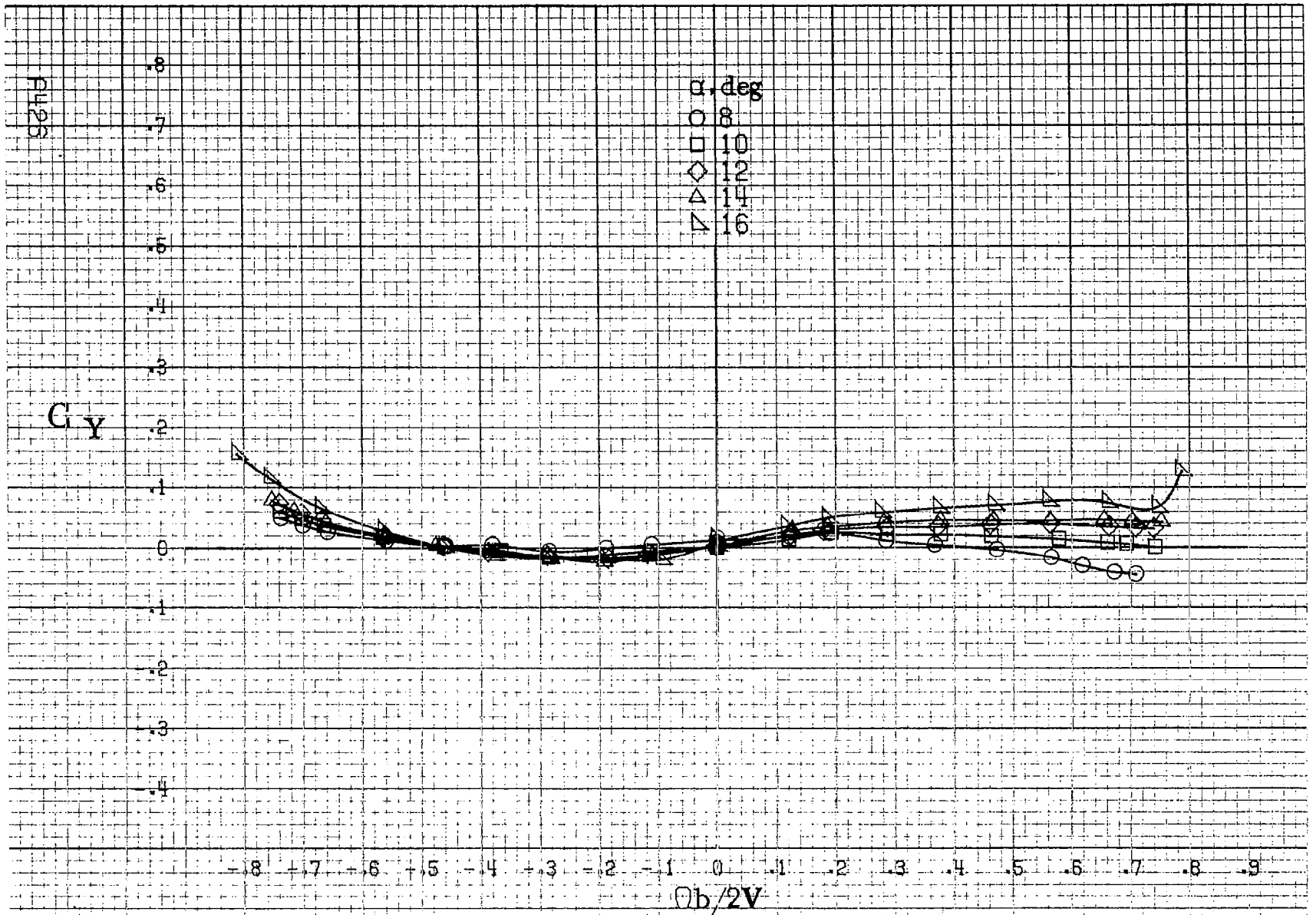

(a) α=8to16deg, SR=99cm(39in).

Figure A107.-Effect of rotation rate and angle of attack on side-force coefficient for configuration having outboard LE wing droop extended inboard 33.8cm(13.3in). $\delta_e = 0°$, $\delta_a = 0°$, $\delta_r = 0°$, $\beta = 0°$.

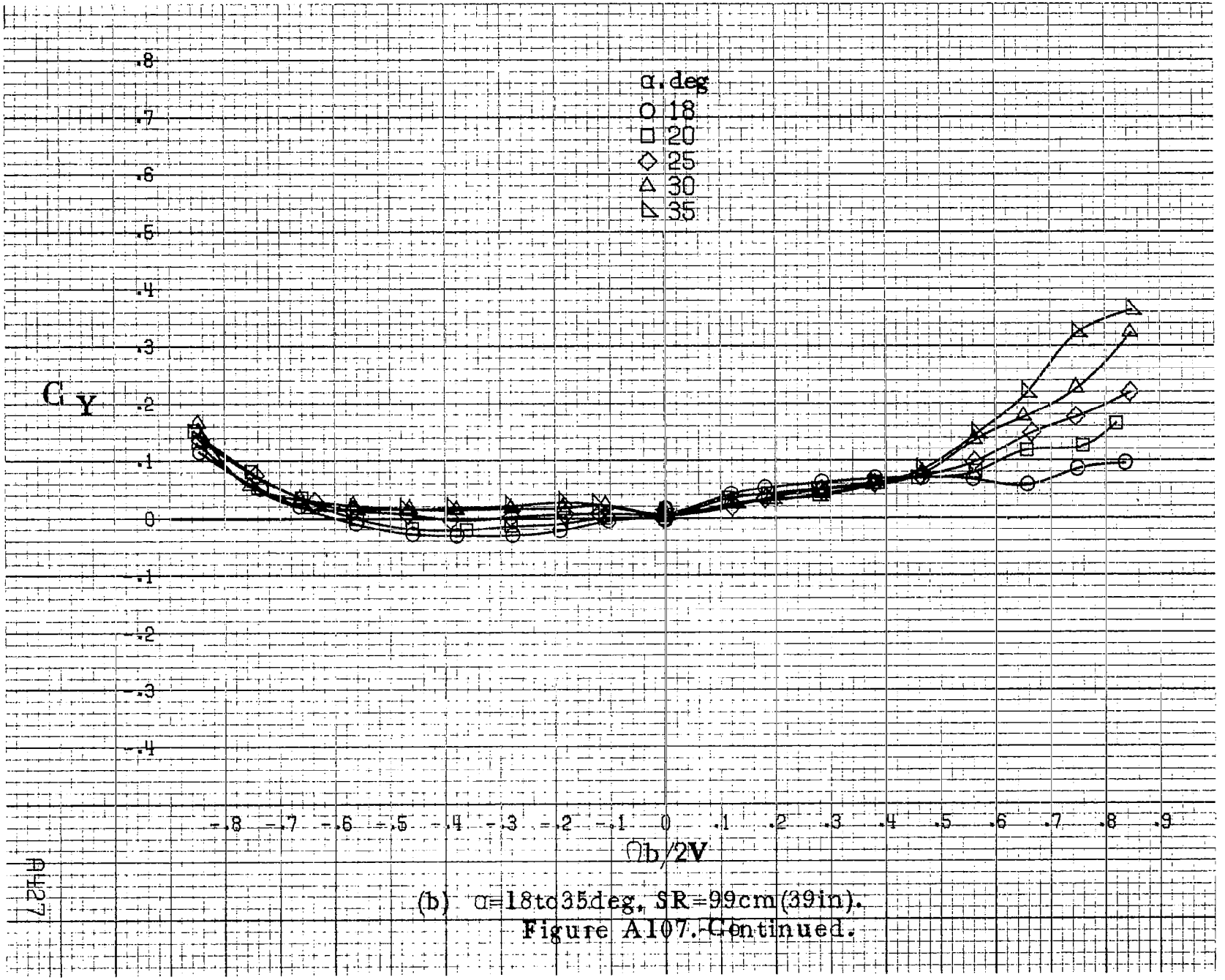

AH27

(b) α=18to35deg, SR=99cm(39in).

Figure A107. Continued.

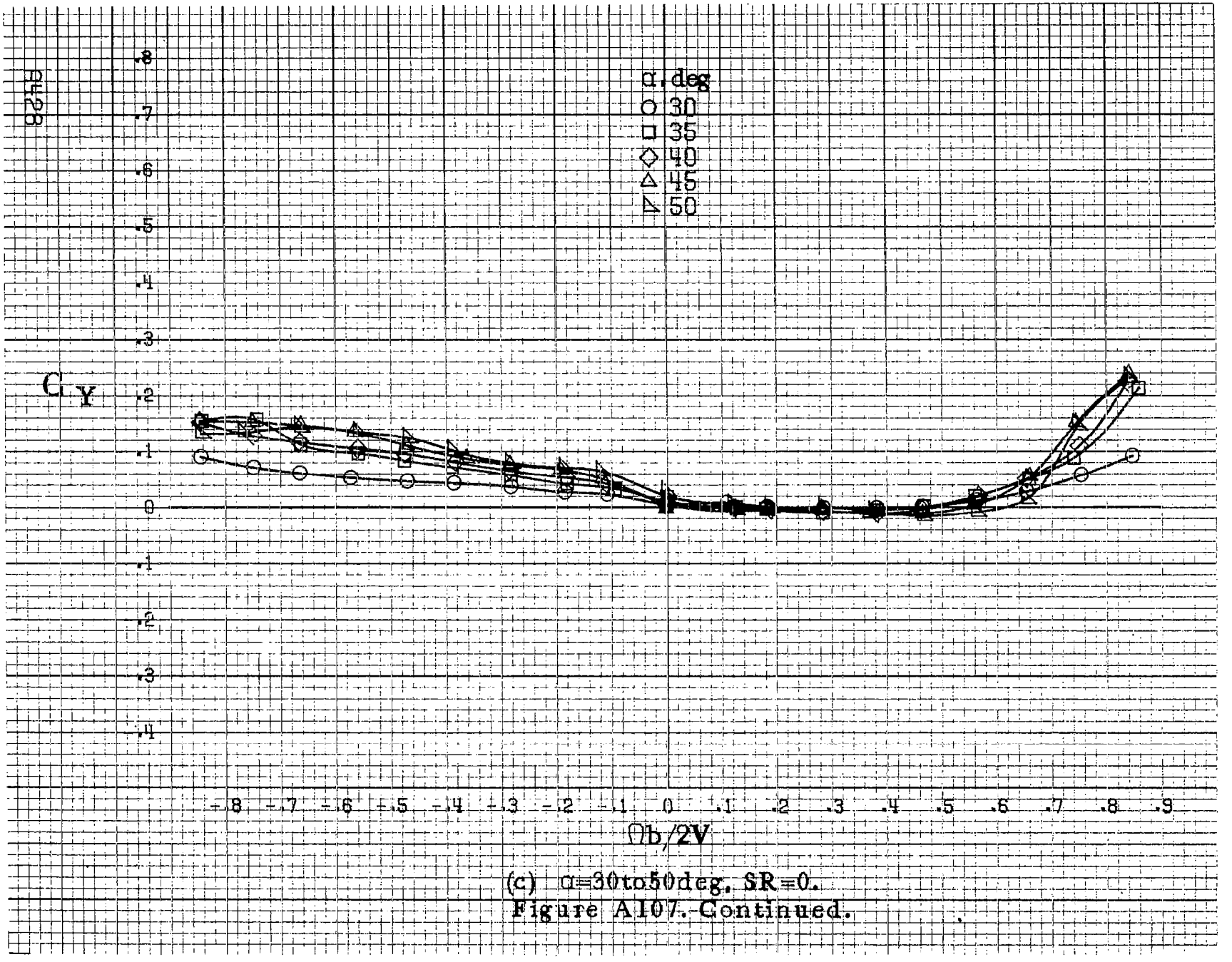

(c) α=30to50deg. SR=0.

Figure A107.-Continued.

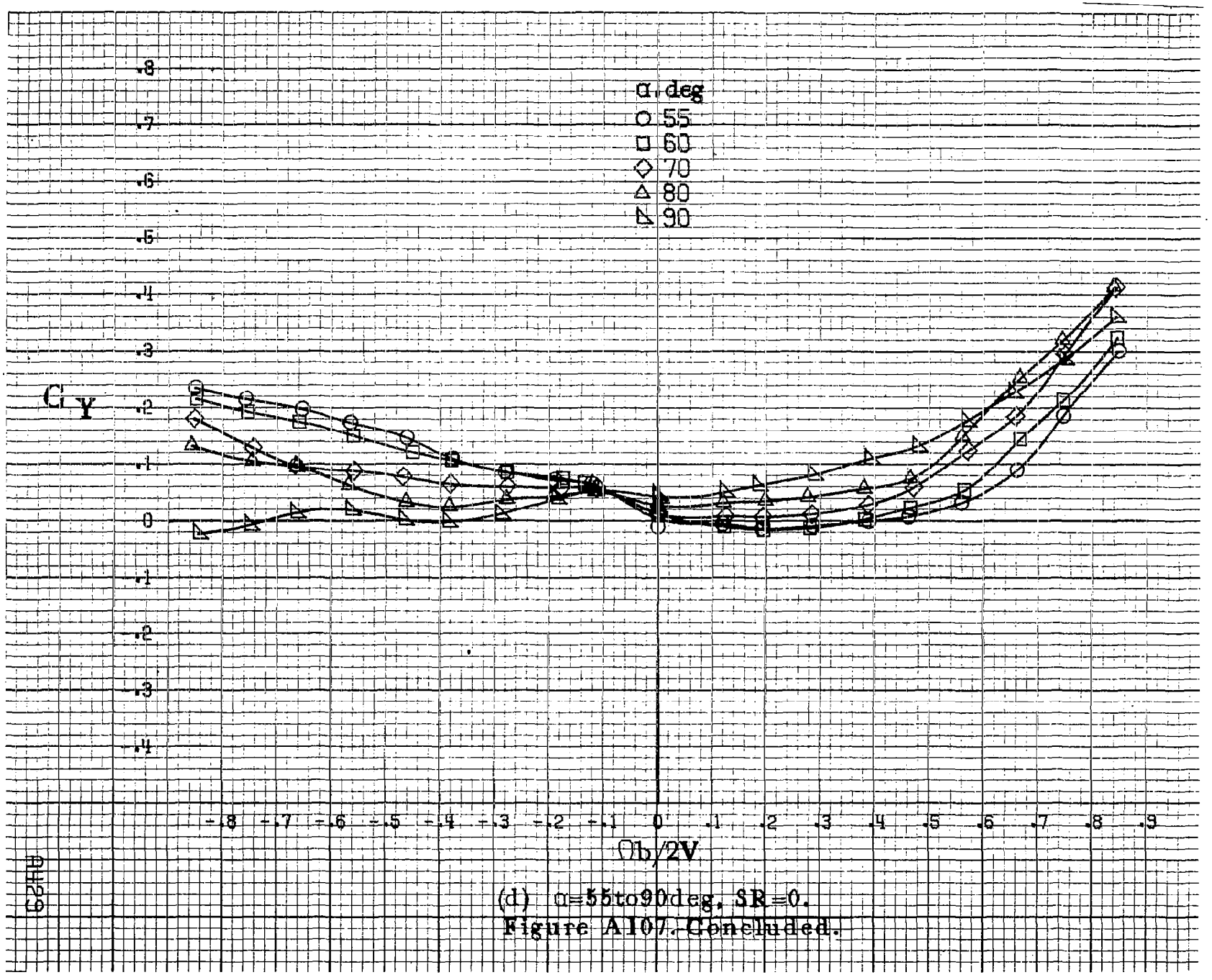

(d) α=55to90deg, SR=0.

Figure A107. Concluded.

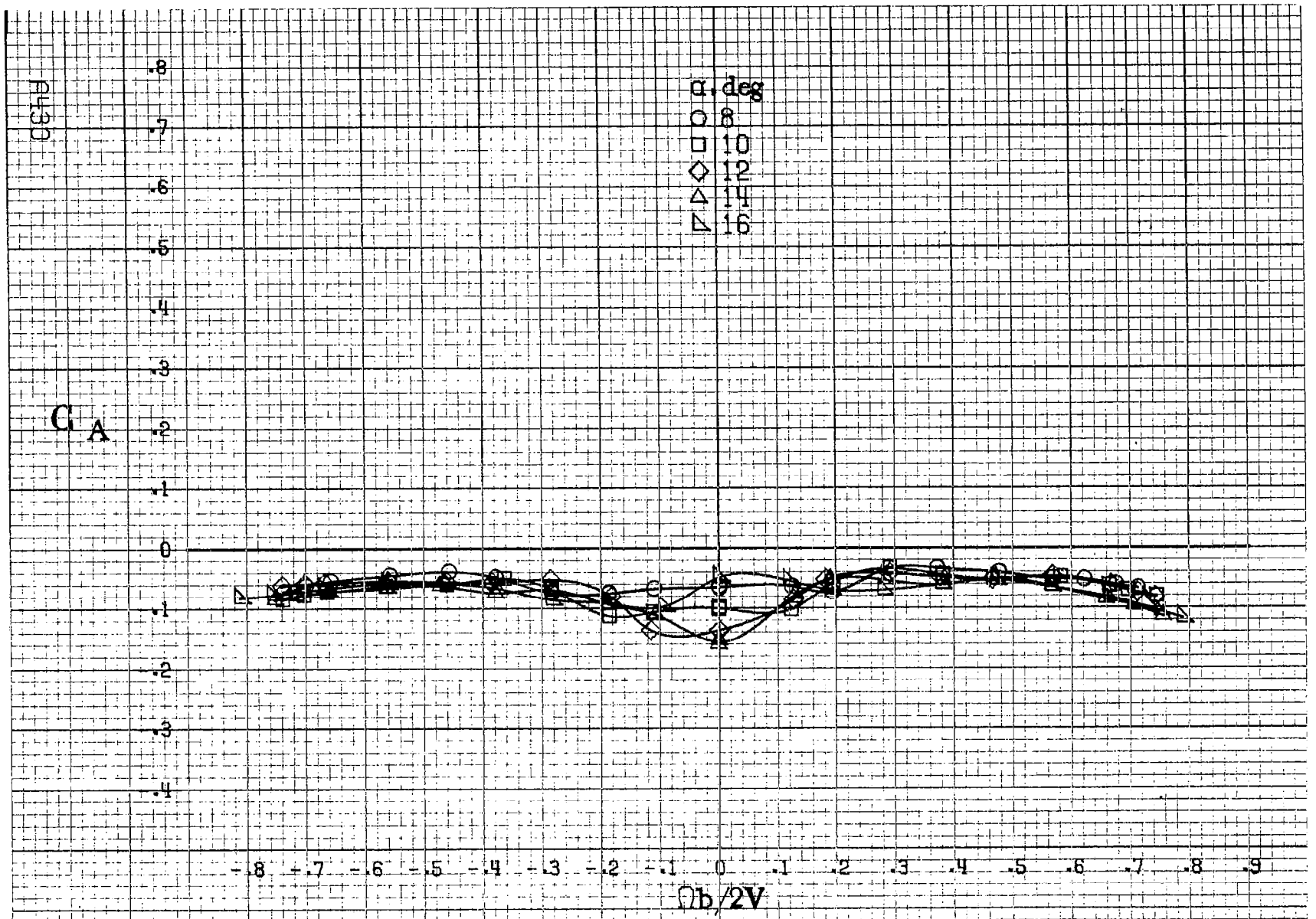

(a) α=8to16deg, $R=99cm(39in).

Figure A108. Effect of rotation rate and angle of attack on axial-force coefficient for configuration having outboard LE wing droop extended inboard 33.8cm(13.3in). δ_e=0°, δ_a=0°, δ_r=0°. β=0°.

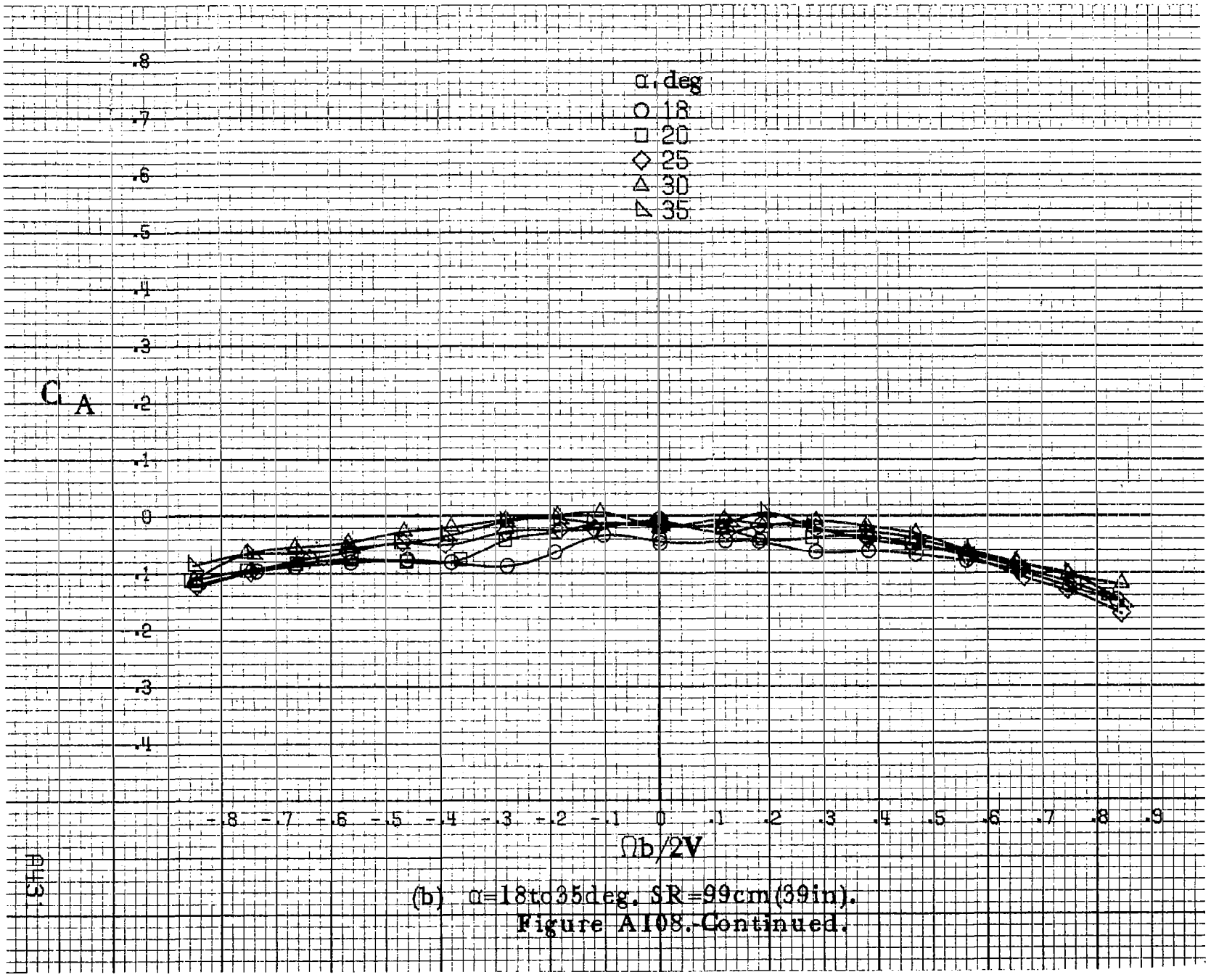

(b) α=18to35deg, SR=99cm(39in).

Figure A108.-Continued.

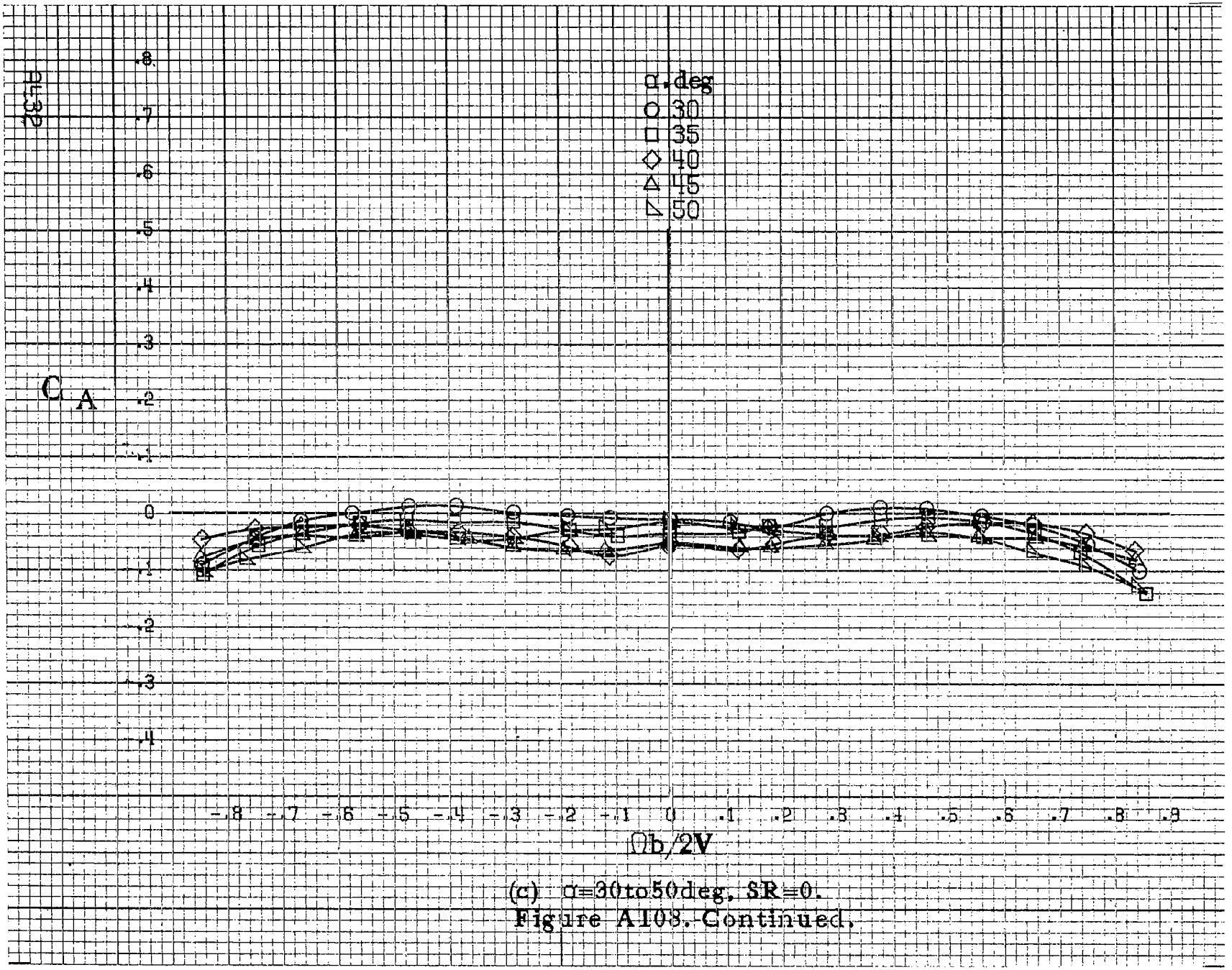

(c) α=30to50deg, SR=0.

Figure A108. Continued.

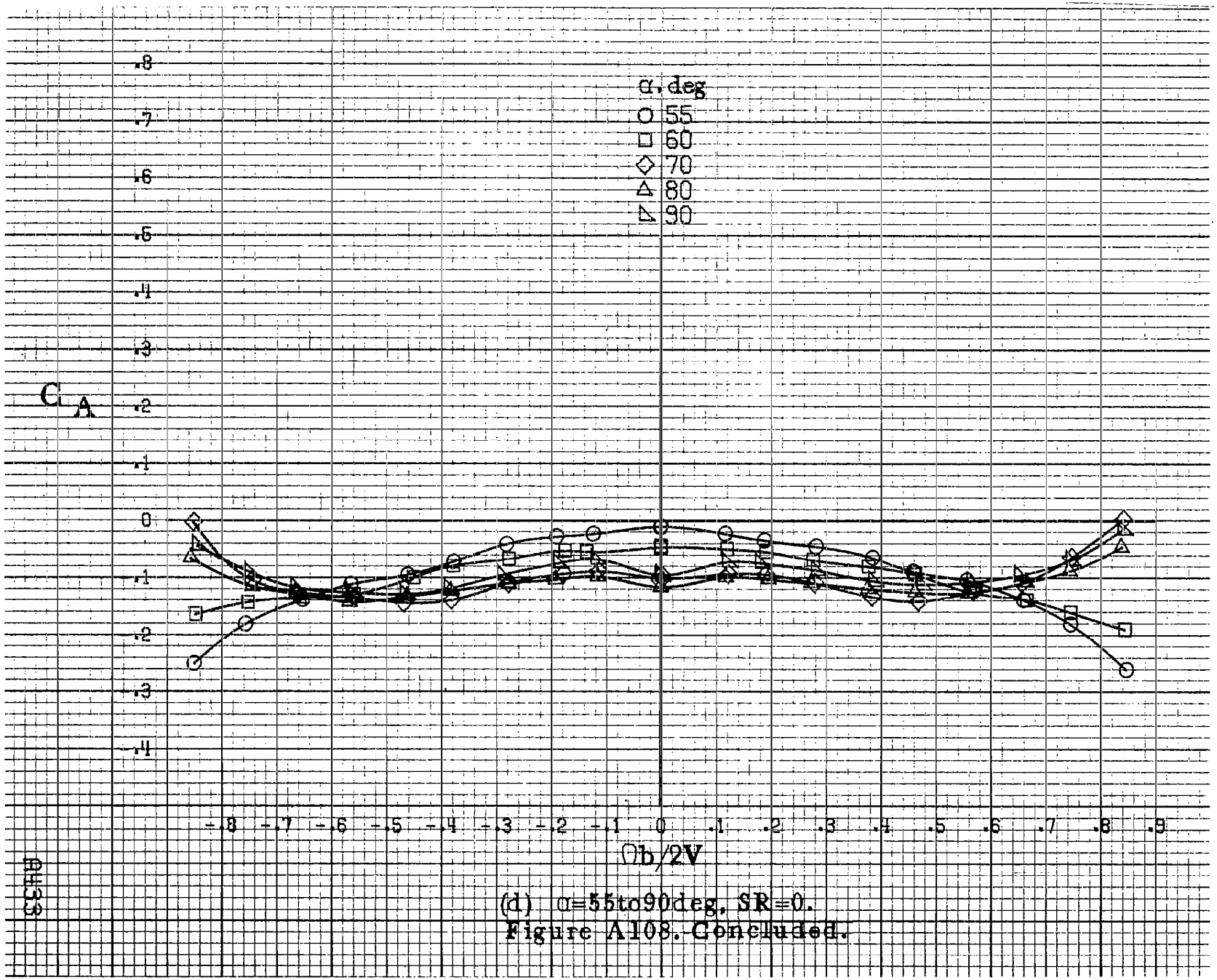

(d) α=55to90deg, SR=0.

Figure A108. Concluded.

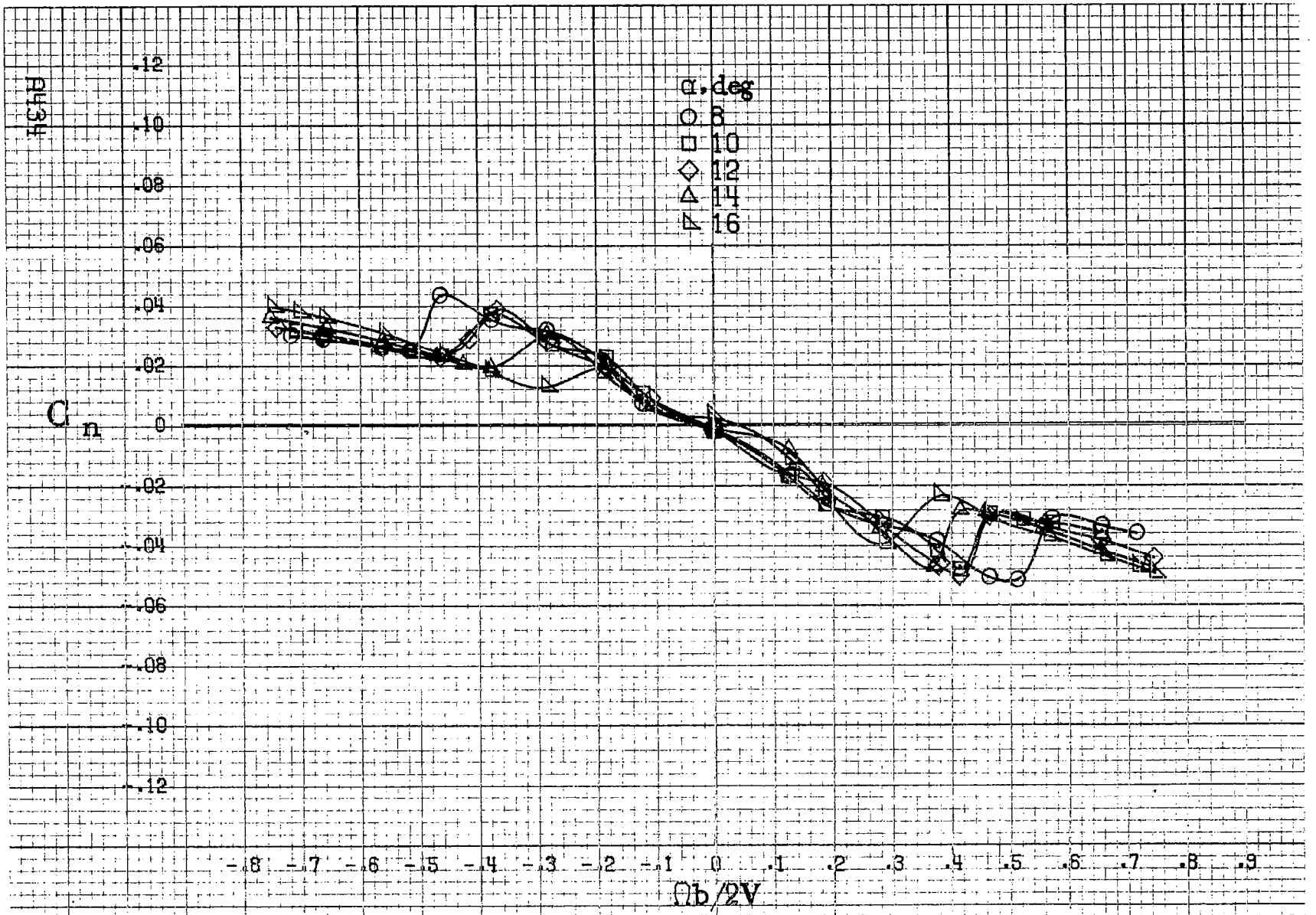

(a) α=8to16deg, SR=99cm(39in).

Figure A109. Effect of rotation rate and angle of attack on yawing-moment coefficient for configuration having outboard wing Kruger flap. $\delta_e = 0°$, $\delta_a = 0°$, $\delta_r = 0°$. $\beta = 0°$.

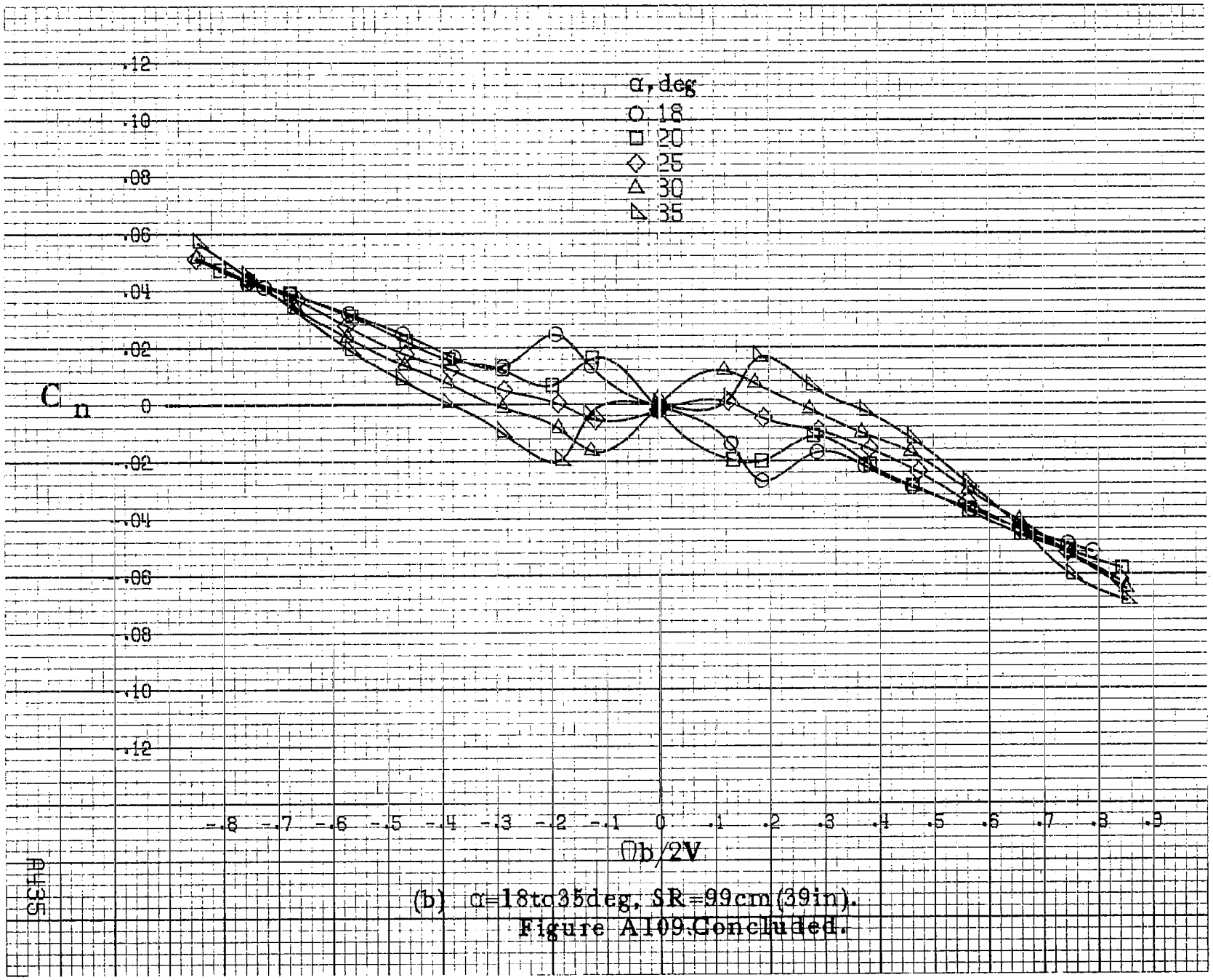

(b) α=18to35deg, SR=99cm(39in).

Figure A109.Concluded.

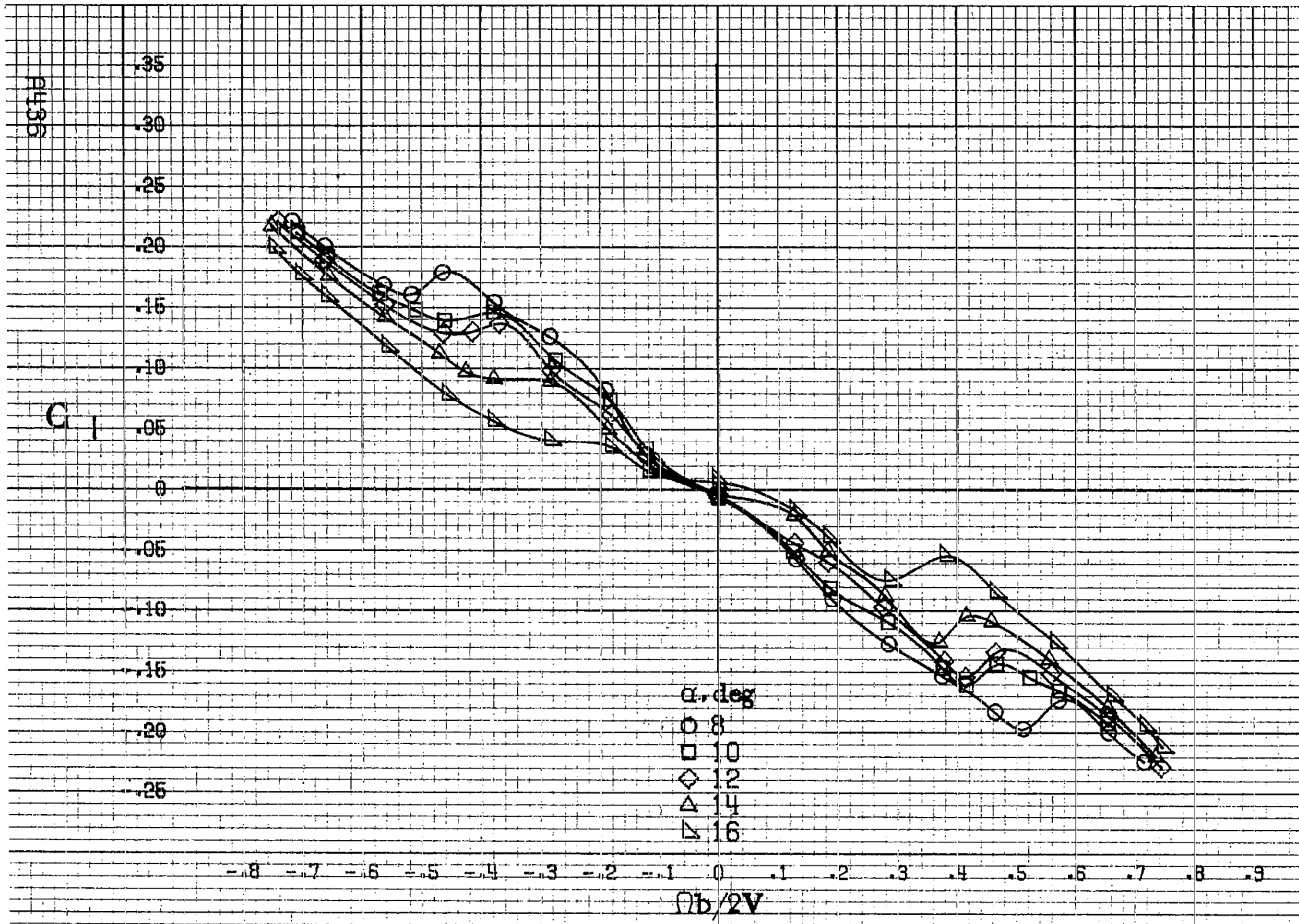

(a) α=8to16deg, SR=99cm(39in).

Figure A110.-Effect of rotation rate and angle of attack on rolling-moment coefficient for configuration having outboard wing Kruger flap. $\delta_e = 0°$, $\delta_a = 0°$, $\delta_r = 0°$, $\beta = 0°$.

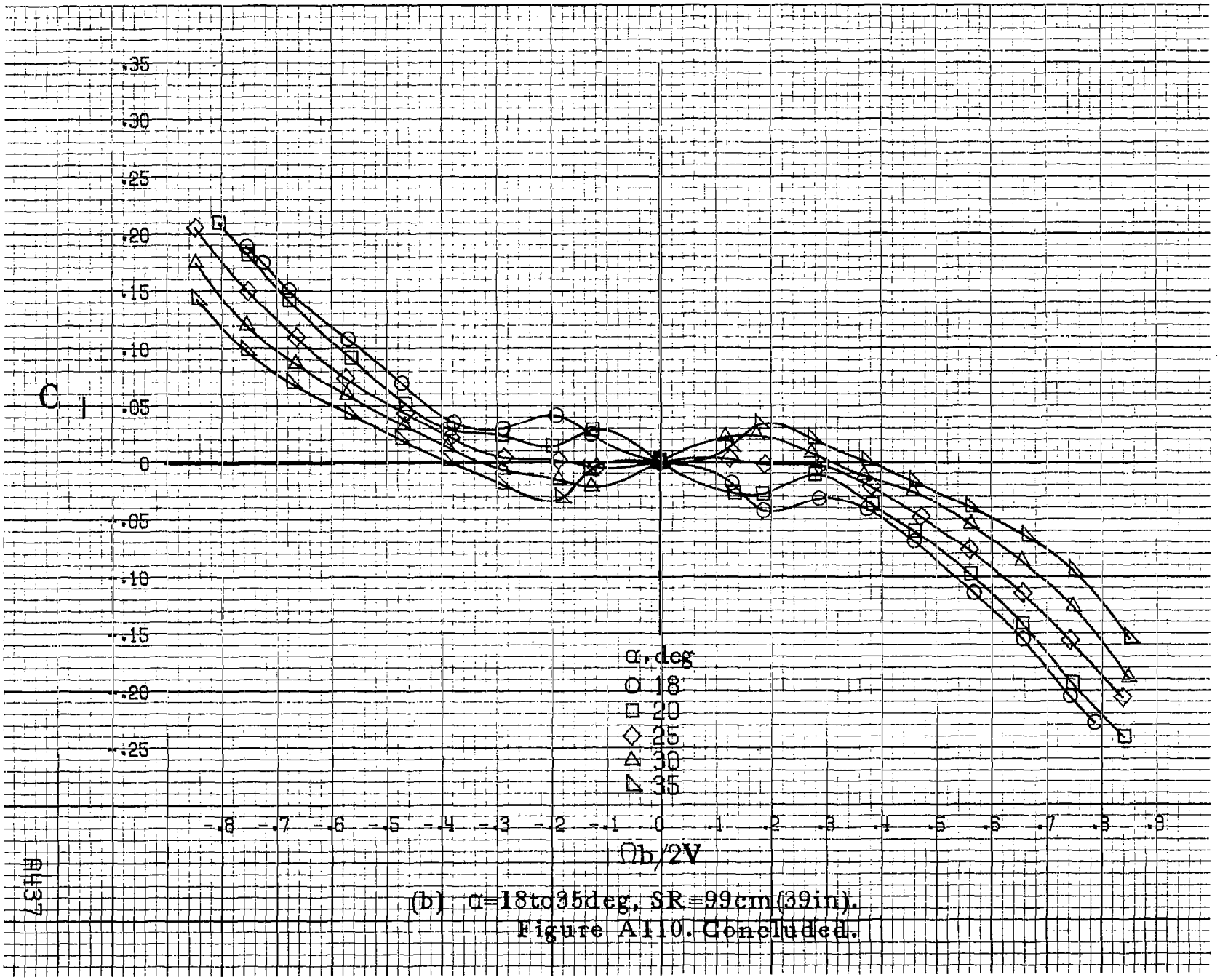

(b) α=18to35deg, SR=99cm(39in).

Figure A110. Concluded.

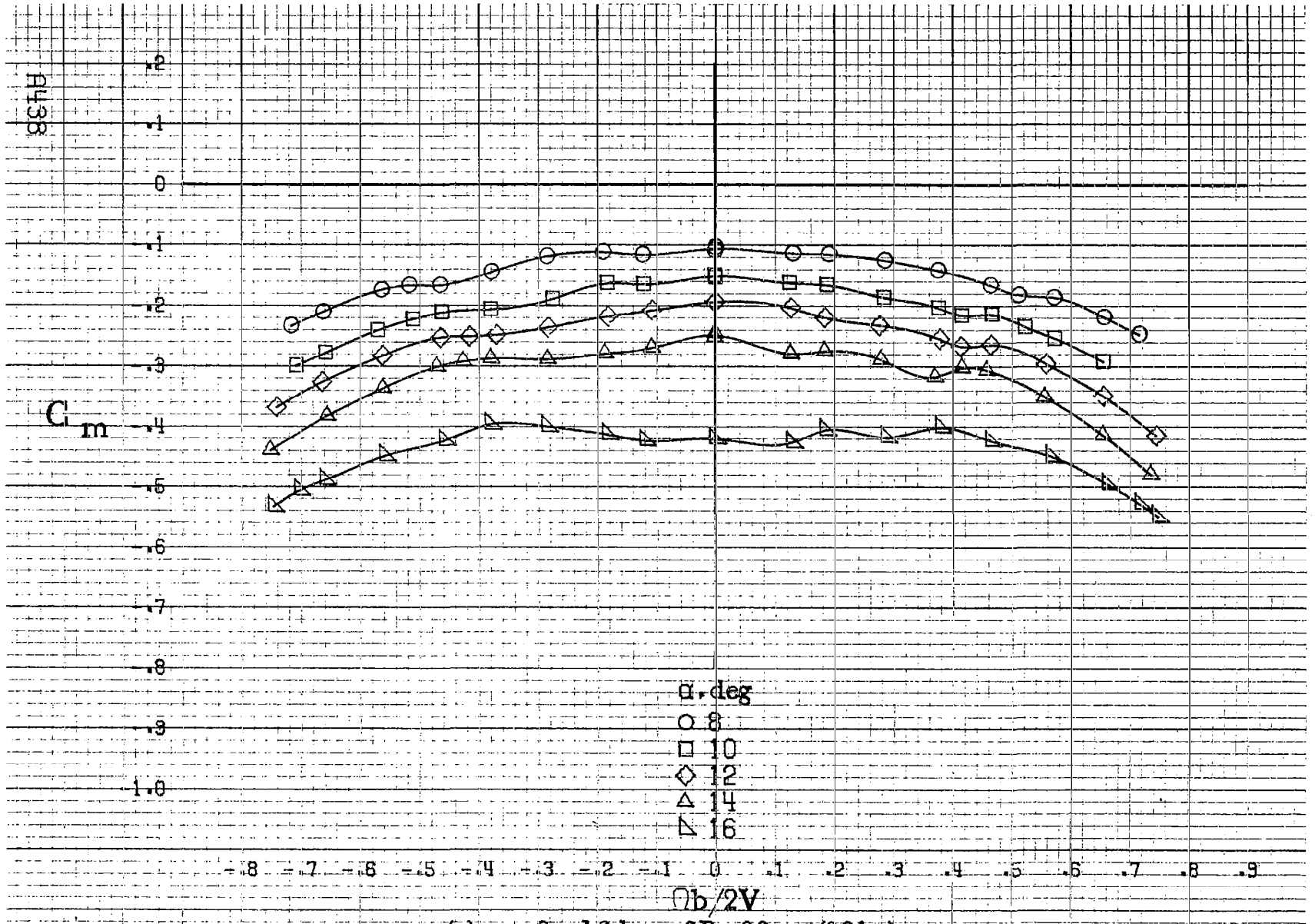

(a) α=8to16deg, SR=99cm(39in).

Figure A111.-Effect of rotation rate and angle of attack on pitching-moment coefficient for configuration having outboard wing Kruger flap. $\delta_e = 0°$, $\delta_a = 0°$, $\delta_r = 0°$, $\beta = 0°$.

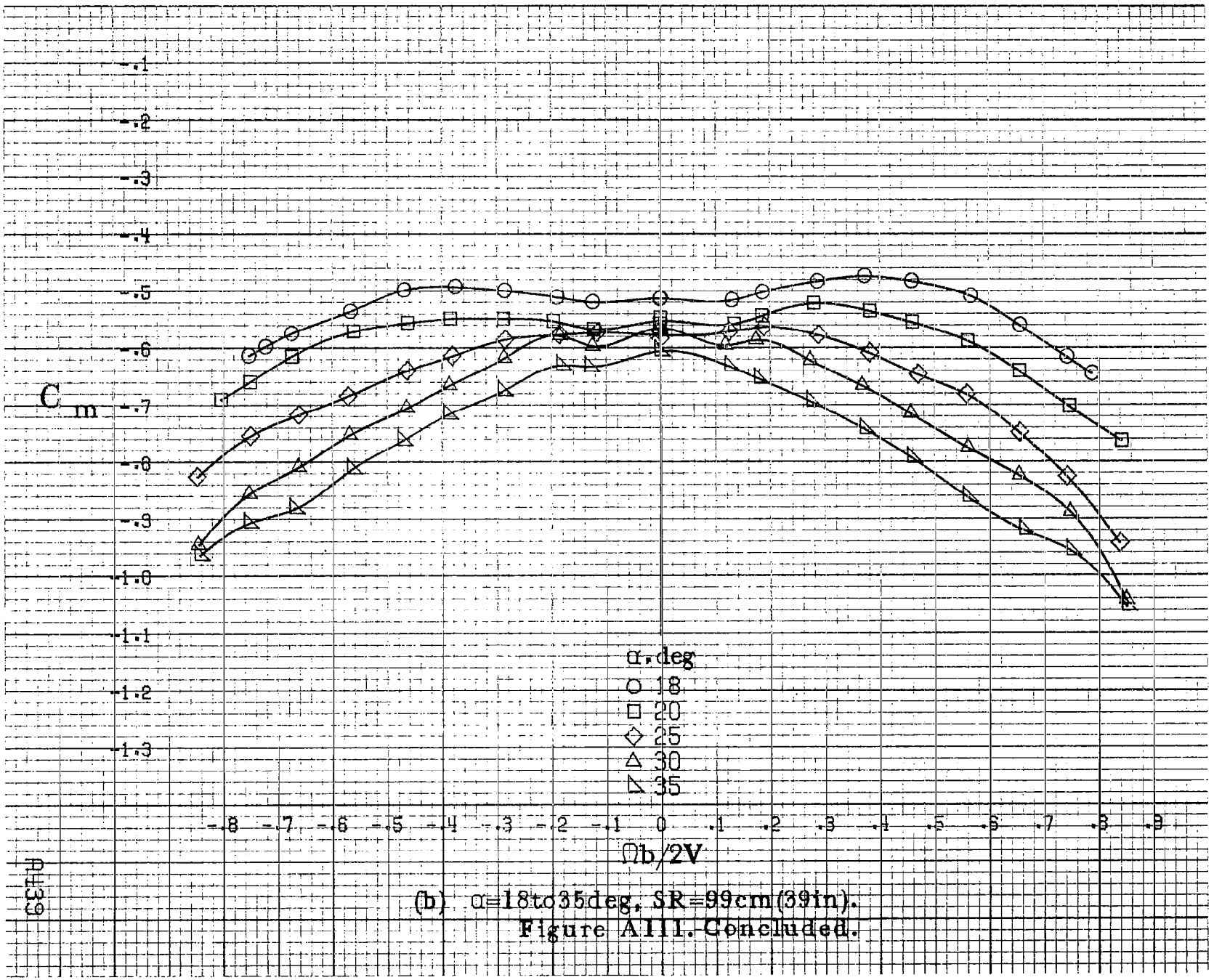

(b) α=18to35deg, SR=99cm(39in).

Figure A111. Concluded.

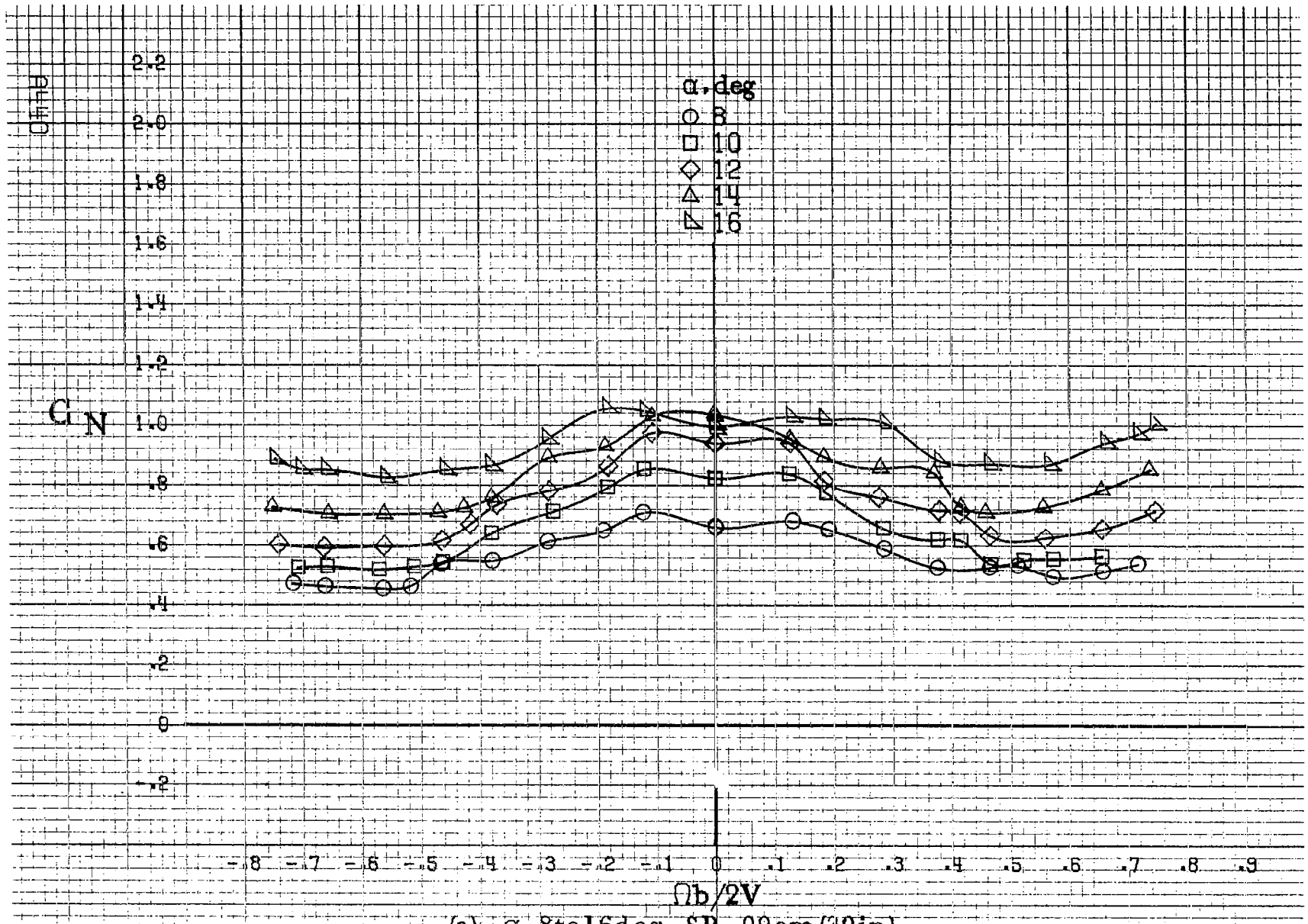

(a) α=8to16deg, SR=99cm(39in).

Figure A112.-Effect of rotation rate and angle of attack on normal-force coefficient for configuration having outboard wing Kruger flap. $\delta_e = 0°$, $\delta_a = 0°$, $\delta_r = 0°$, $\beta = 0°$.

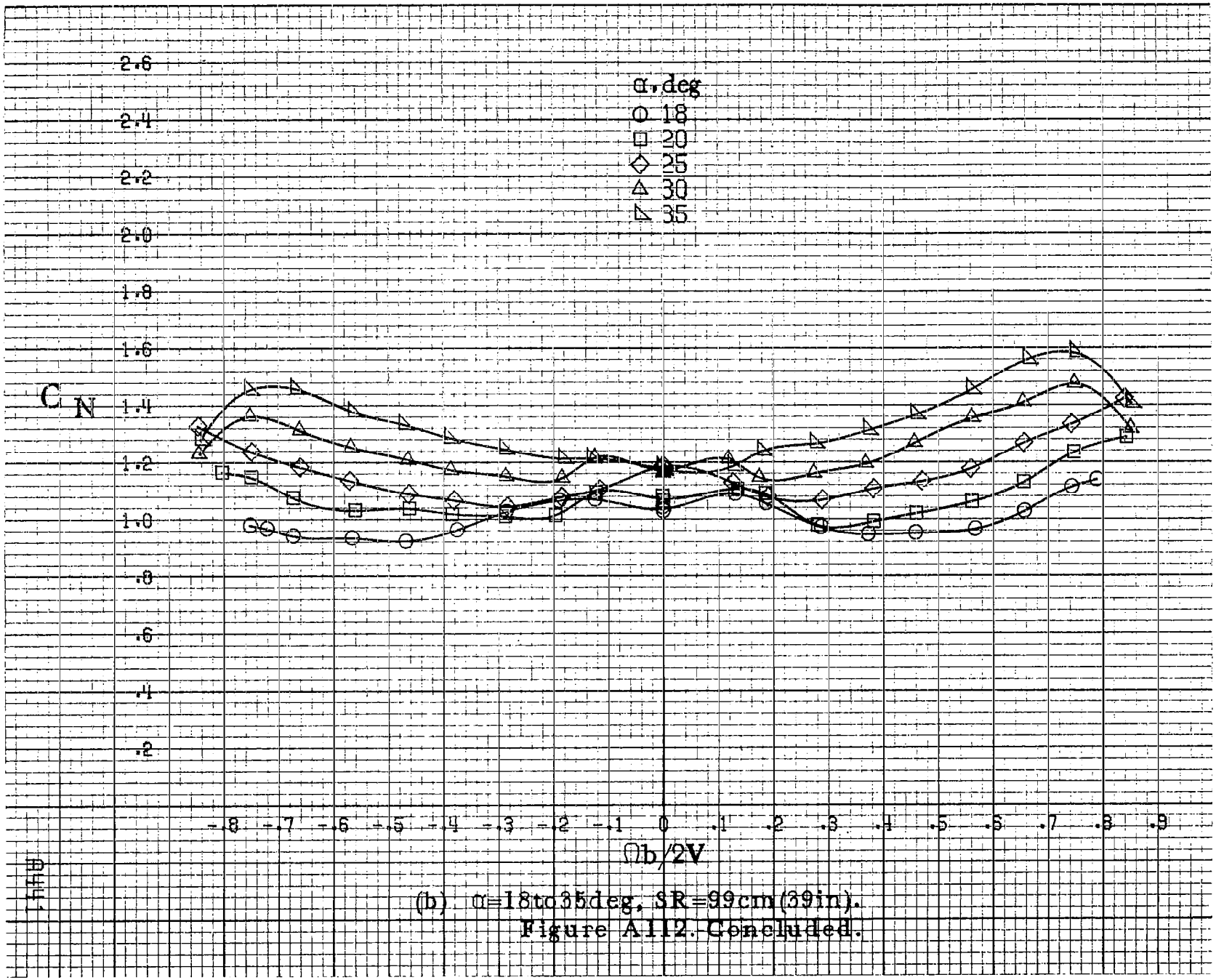

(b) α=18 to 35 deg, SR=99 cm (39 in).

Figure A112. Concluded.

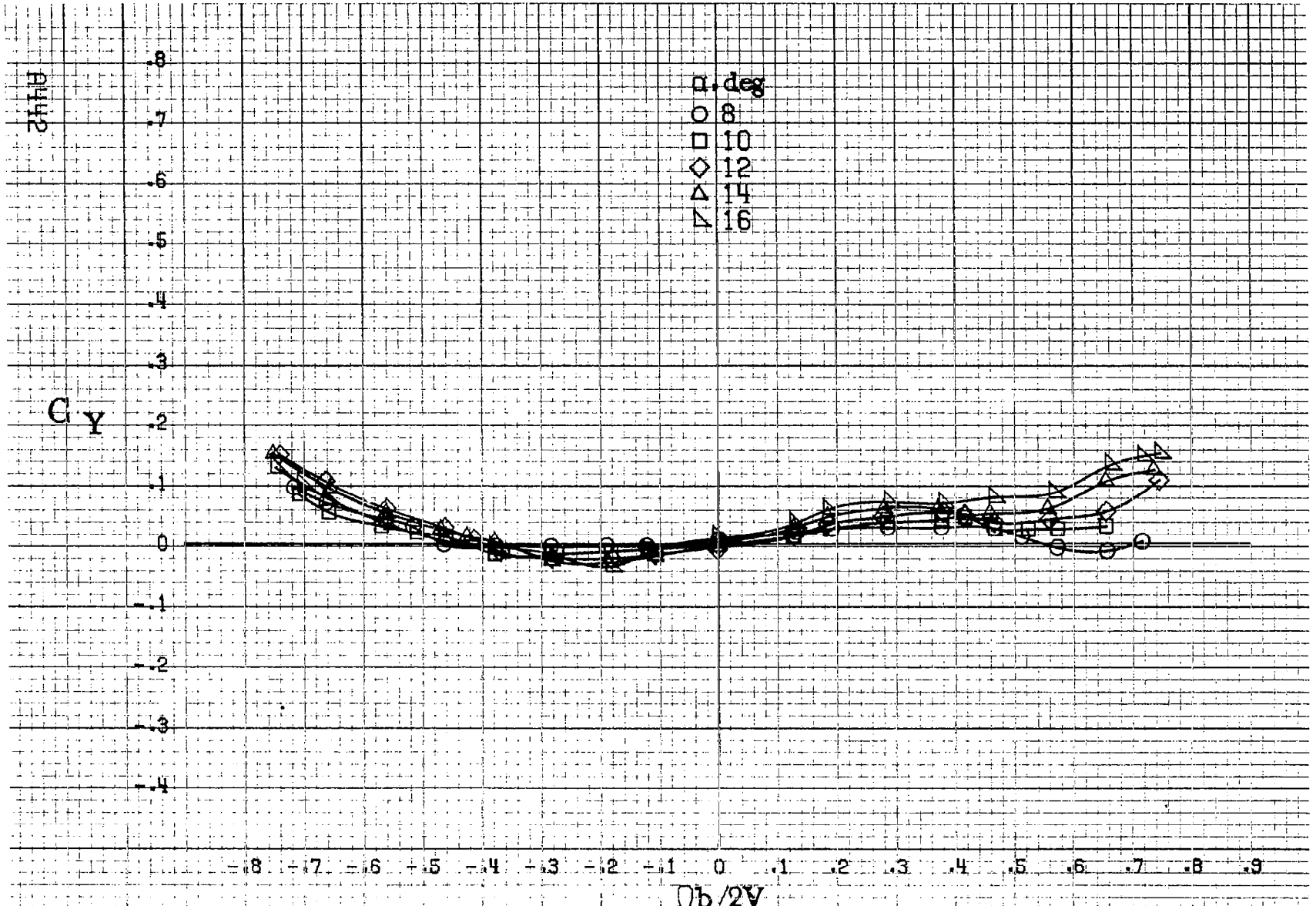

(a) α=8to16deg, SR=99cm(39in).

Figure A113.-Effect of rotation rate and angle of attack on side-force coefficient for configuration having outboard wing Kruger flap. $\delta_e = 0°$, $\delta_a = 0°$, $\delta_r = 0°$, $\beta = 0°$.

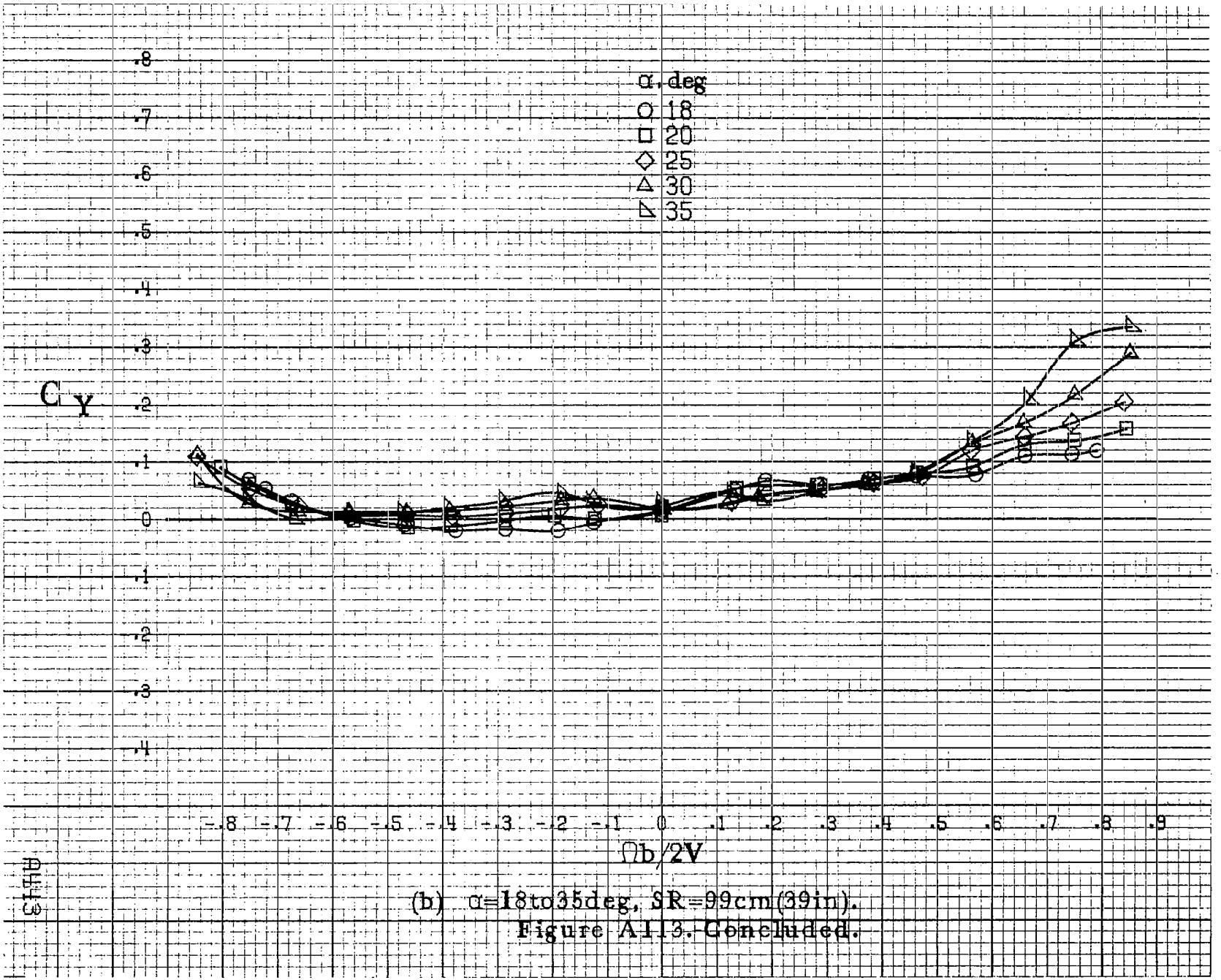

(b) α=18to35deg, SR=99cm(39in).

Figure A113.-Concluded.

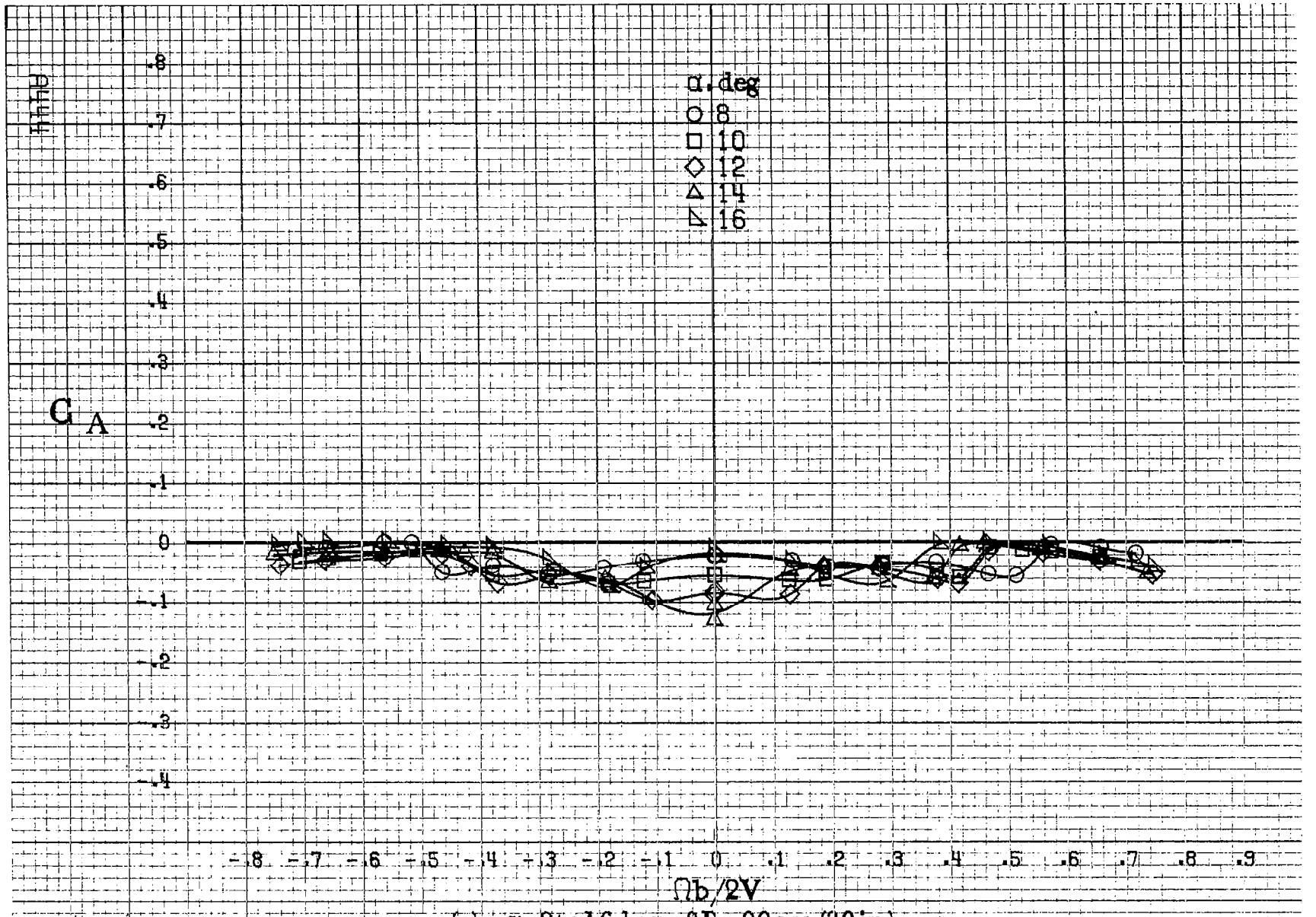

(a) α=8to16deg, $R=99cm(39in).

Figure A114.-Effect of rotation rate and angle of attack on axial-force coefficient for configuration having outboard wing Kruger flap. $\delta_e = 0°$, $\delta_a = 0°$, $\delta_r = 0°$, $\beta = 0°$.

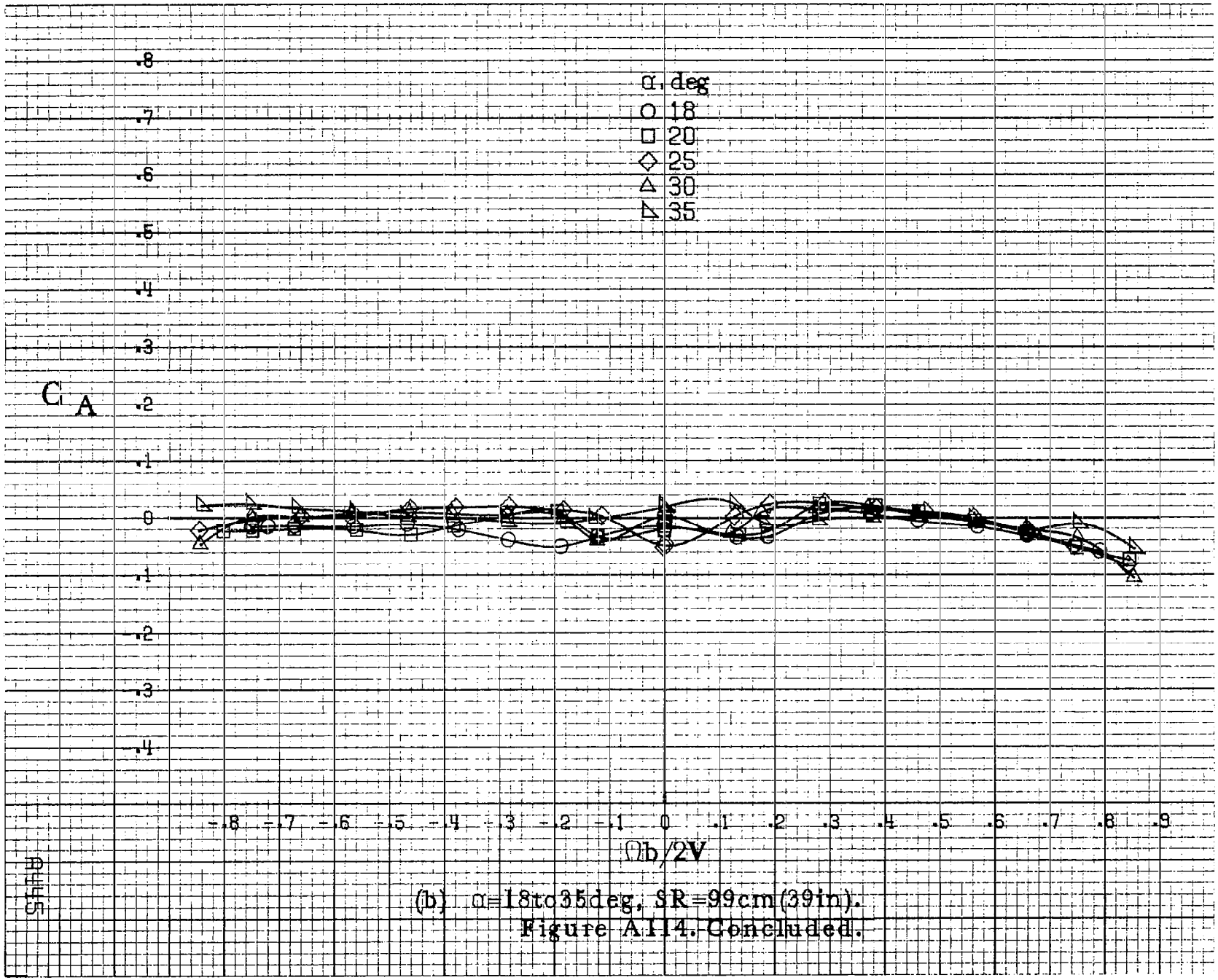

(b) α=18to35deg, SR=99cm(39in).

Figure A114.-Concluded.

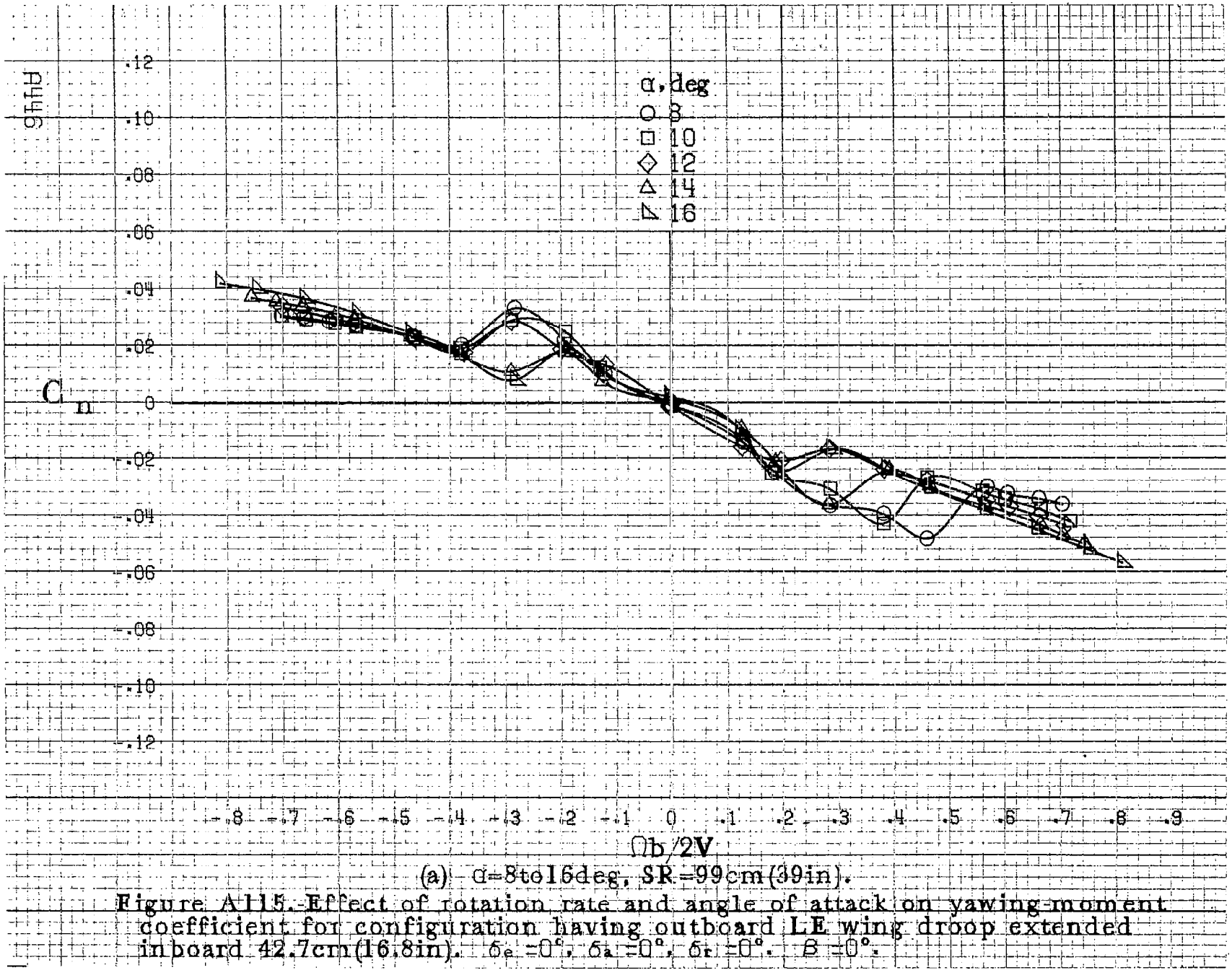

(a) α=8to16deg, SR=99cm(39in).

Figure A115.-Effect of rotation rate and angle of attack on yawing moment coefficient for configuration having outboard LE wing droop extended inboard 42.7cm(16.8in). $\delta_e = 0°$, $\delta_a = 0°$, $\delta_r = 0°$, $\beta = 0°$.

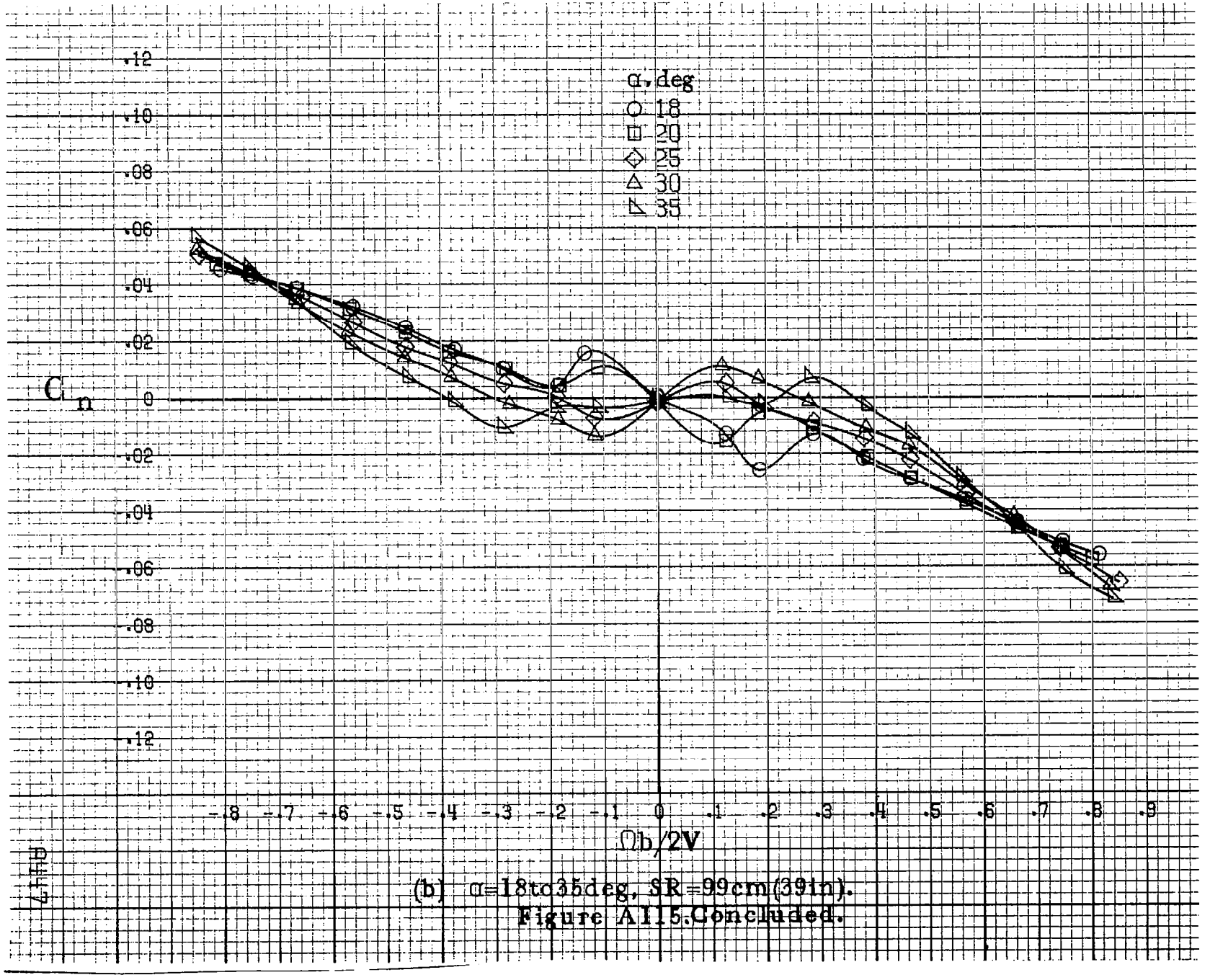

(b) α=18to35deg, SR=99cm(39in).

Figure A115.Concluded.

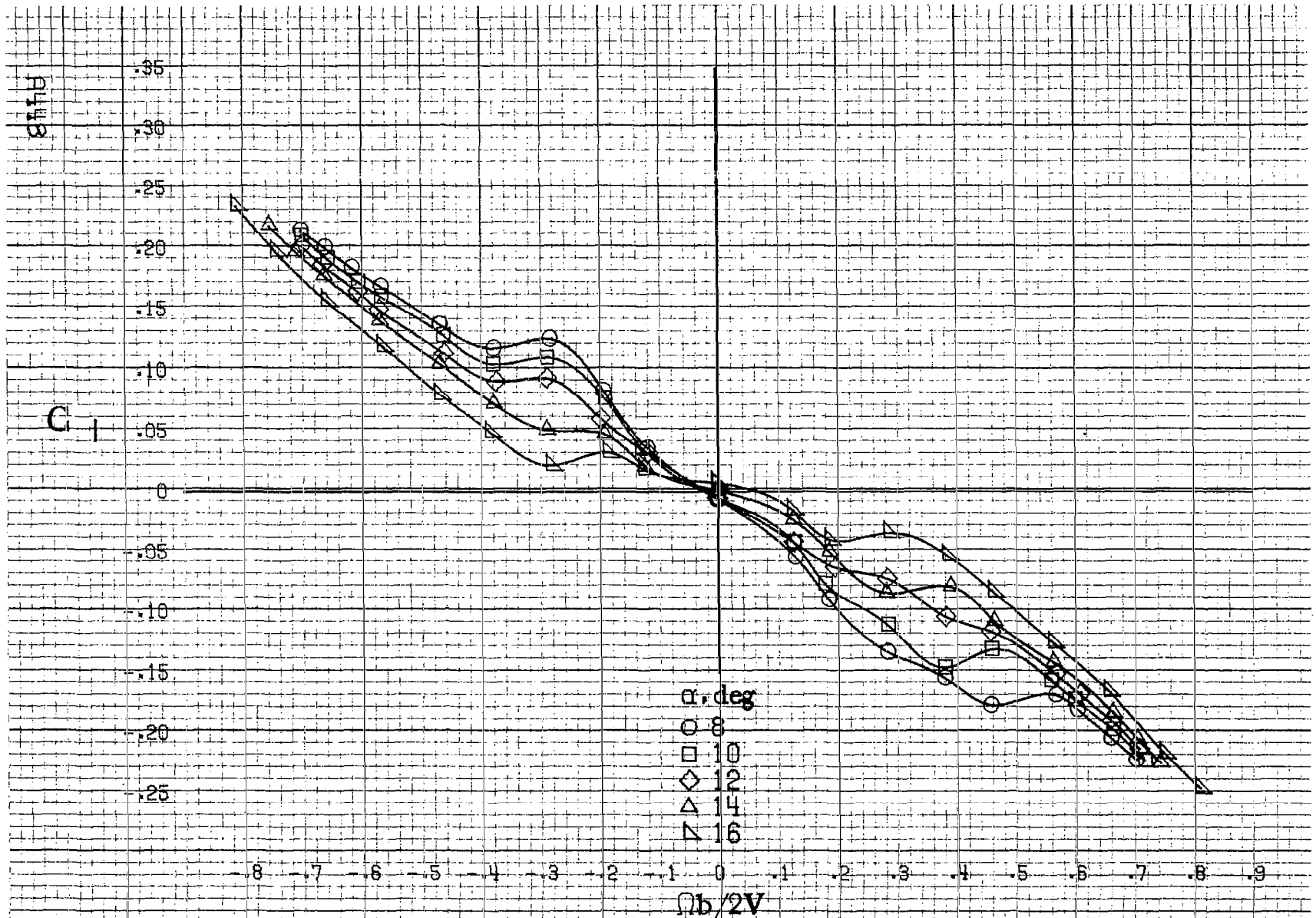

(a) α=8to16deg, SR=99cm(39in).

Figure A116.-Effect of rotation rate and angle of attack on rolling-moment coefficient for configuration having outboard LE wing droop extended inboard 42.7cm(16.8in). $\delta_e = 0^\circ$, $\delta_a = 0^\circ$, $\delta_r = 0^\circ$, $\beta = 0^\circ$.

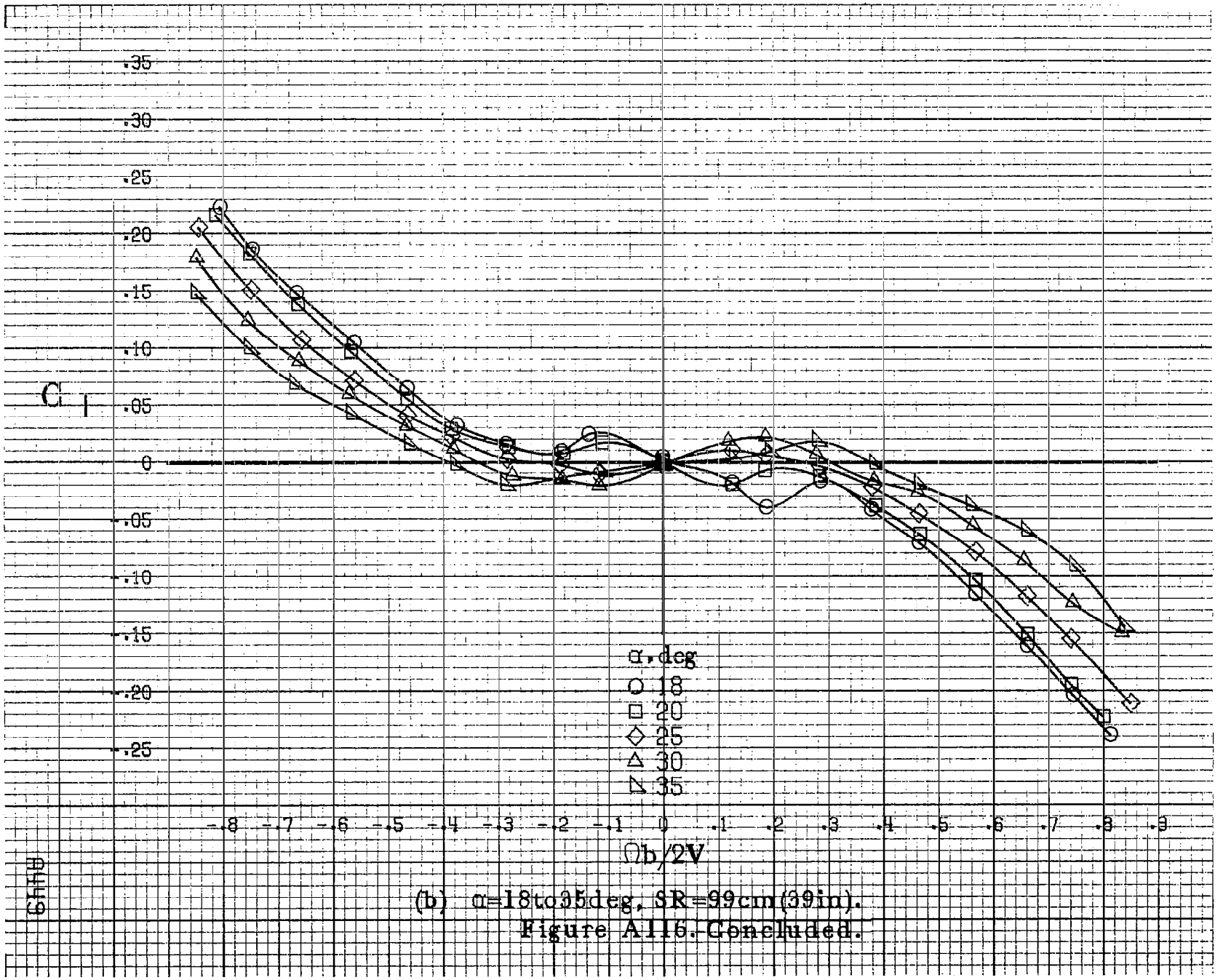

Figure A116.-Concluded.

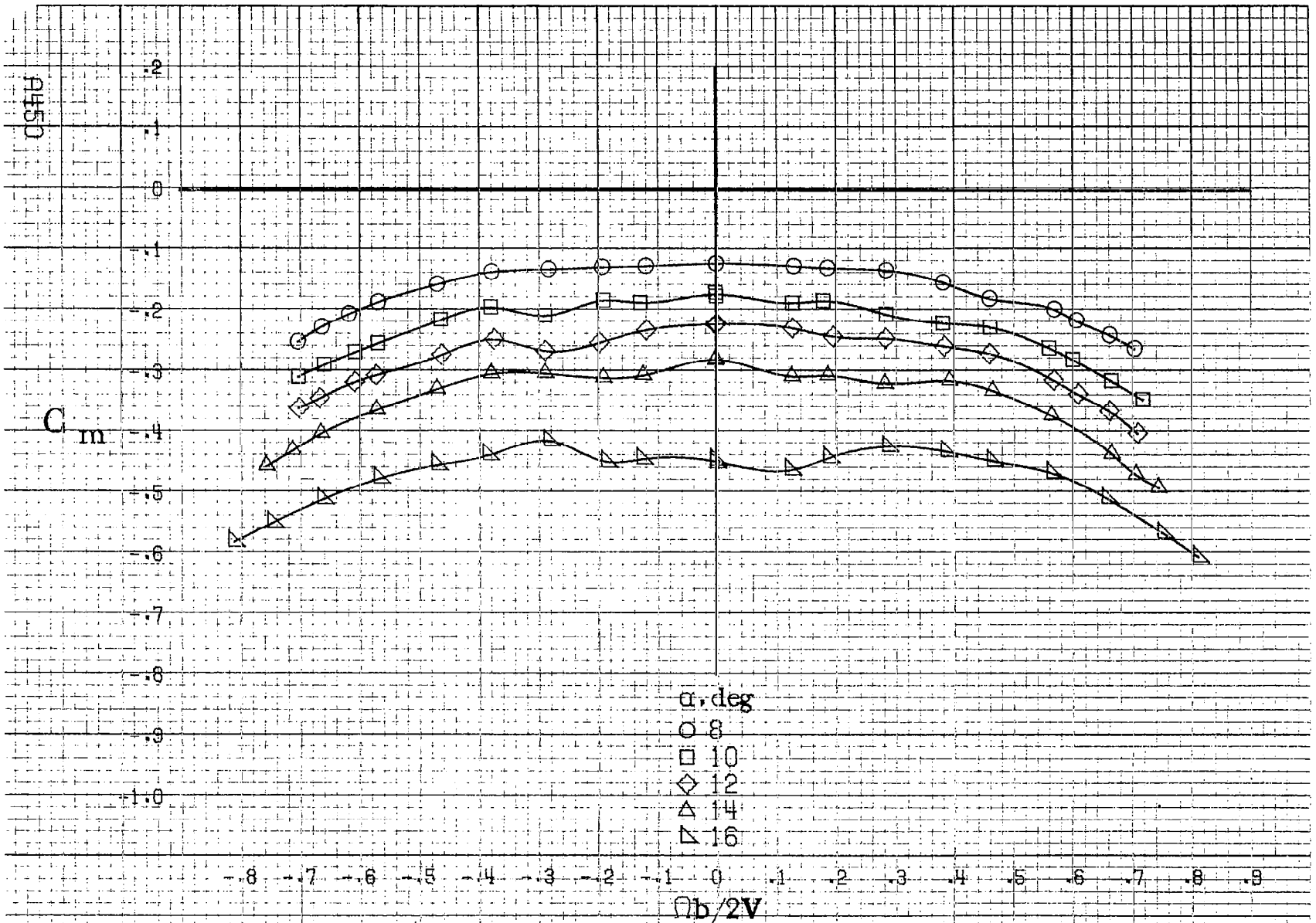

(a) α=8to15deg, SR=99cm(39in).

Figure A117.-Effect of rotation rate and angle of attack on pitching-moment coefficient for configuration having outboard LE wing droop extended inboard 42.7cm(16.8in). δ_e =0°, δ_a =0°, δ_r =0°, β =0°.

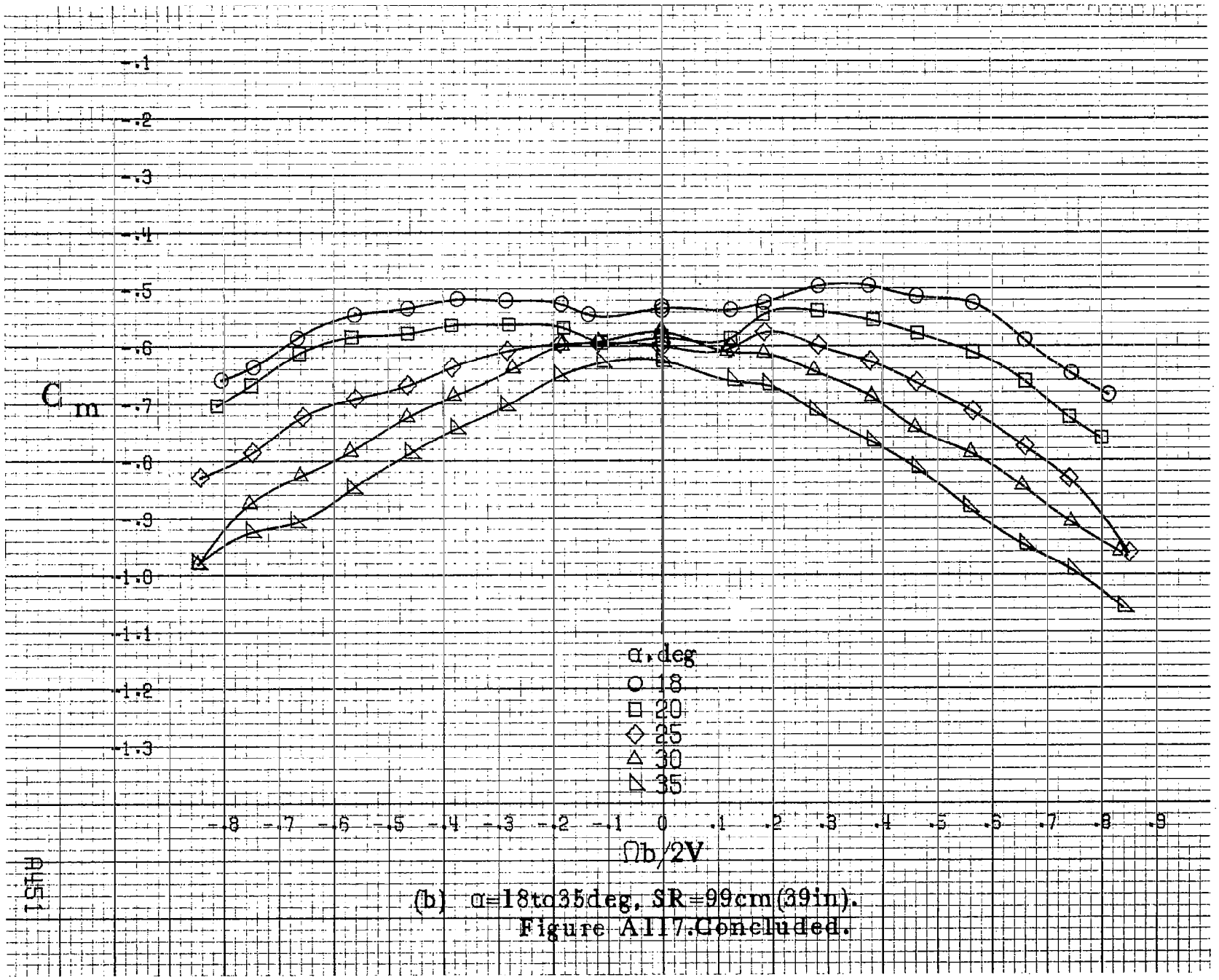

(b) α=18to35deg, SR=99cm(39in).

Figure A117.Concluded.

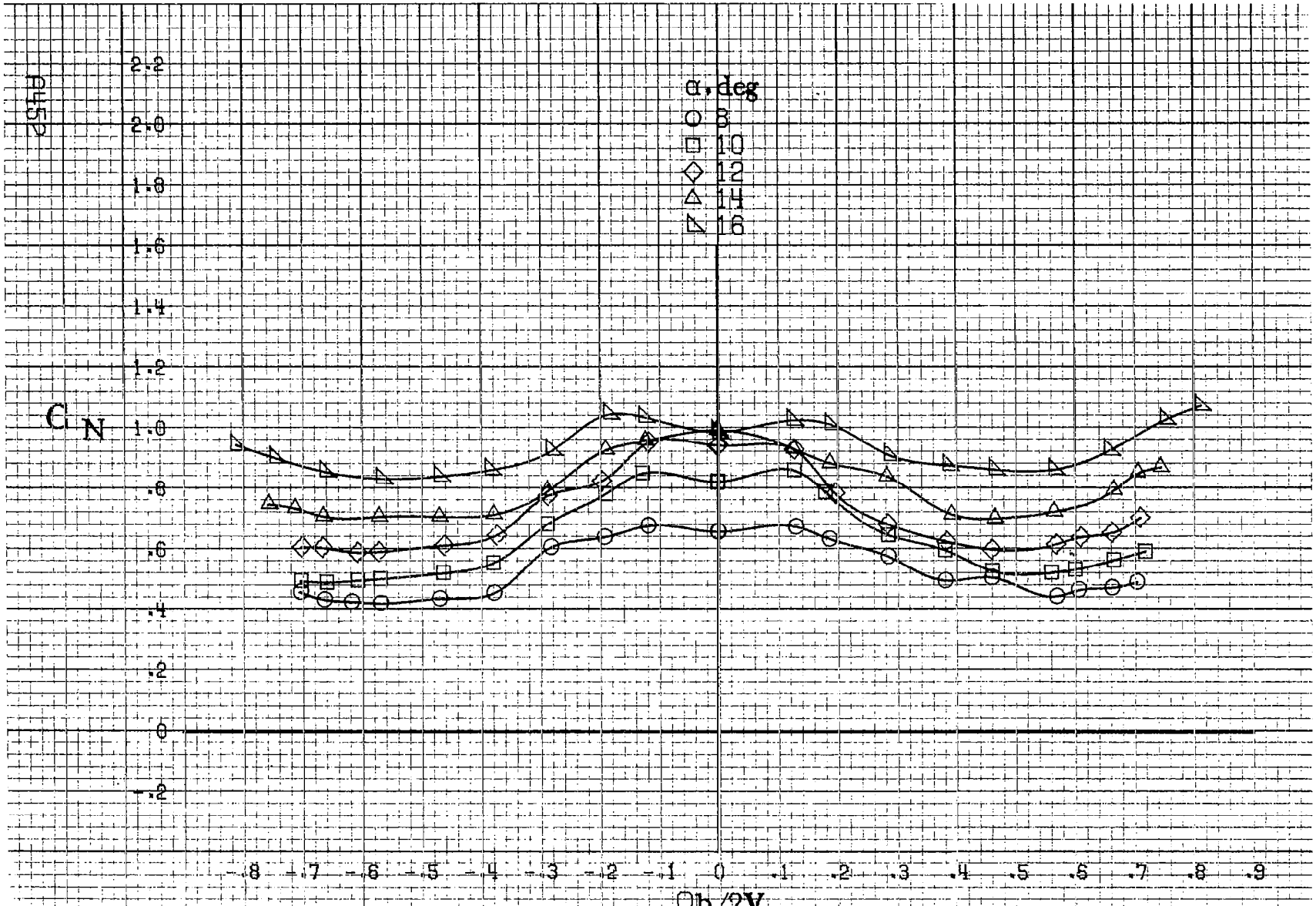

(a) α=8to16deg, SR=99cm(39in).

Figure A118.-Effect of rotation rate and angle of attack on normal-force coefficient for configuration having outboard LE wing droop extended inboard 42.7cm(16.8in). $\delta_e = 0°$, $\delta_a = 0°$, $\delta_r = 0°$, $\beta = 0°$.

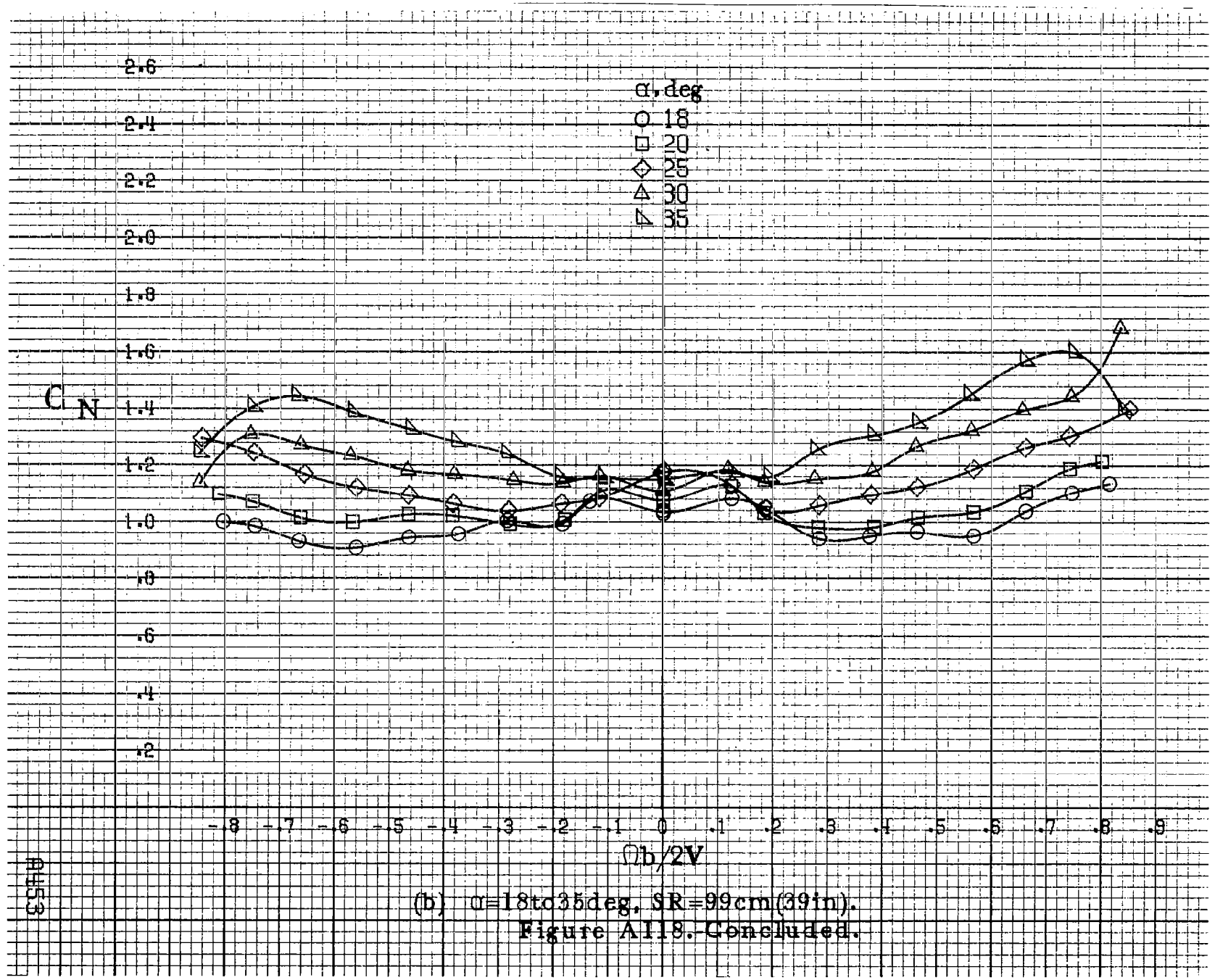

(b) α=18to35deg, SR=99cm(39in).

Figure A118.-Concluded.

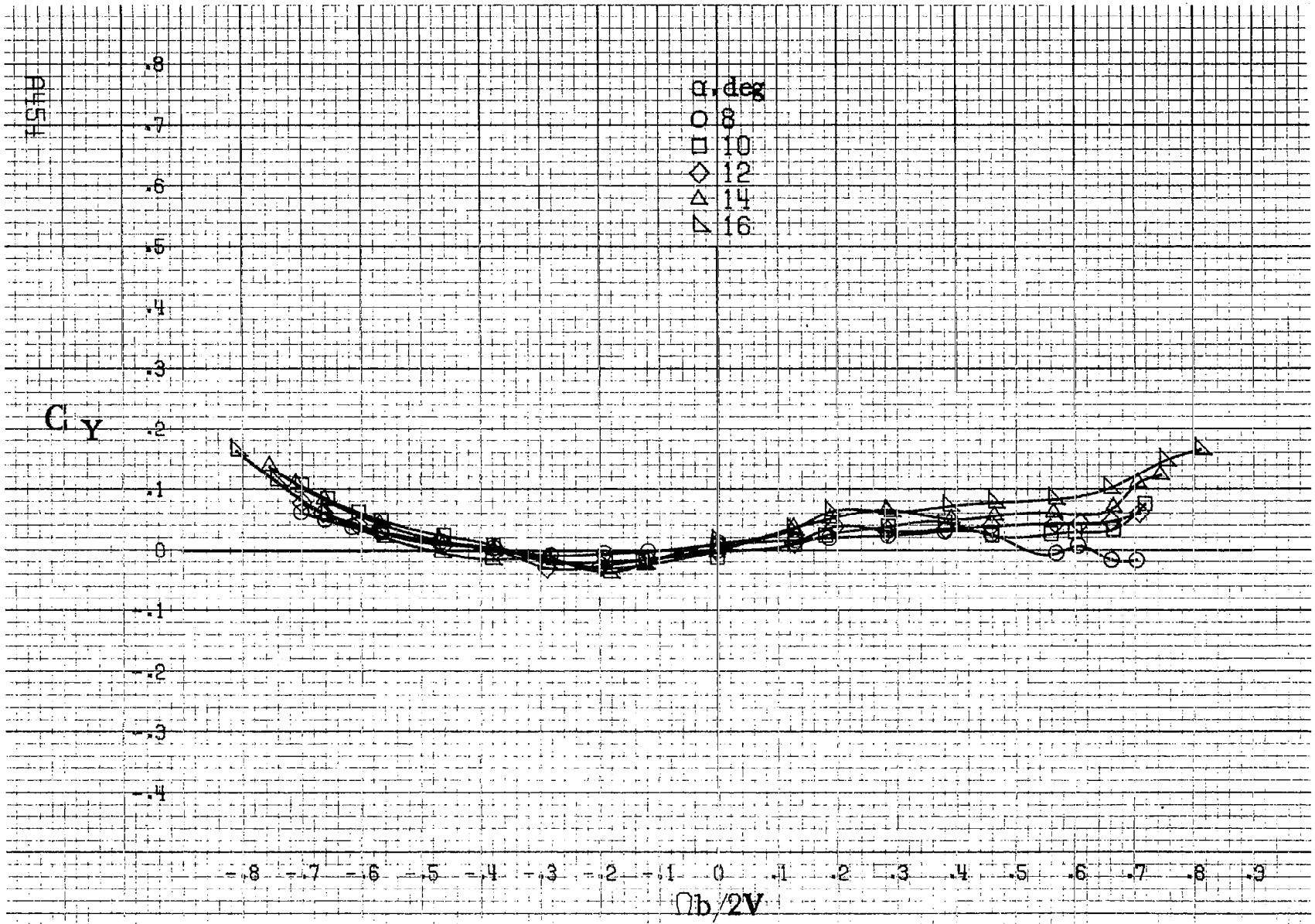

(a) α=8to16deg, SR=99cm(39in).

Figure A119.-Effect of rotation rate and angle of attack on side force coefficient for configuration having outboard LE wing droop extended inboard 42.7cm(16.8in). $\delta_e = 0°$, $\delta_a = 0°$, $\delta_r = 0°$. $\beta = 0°$.

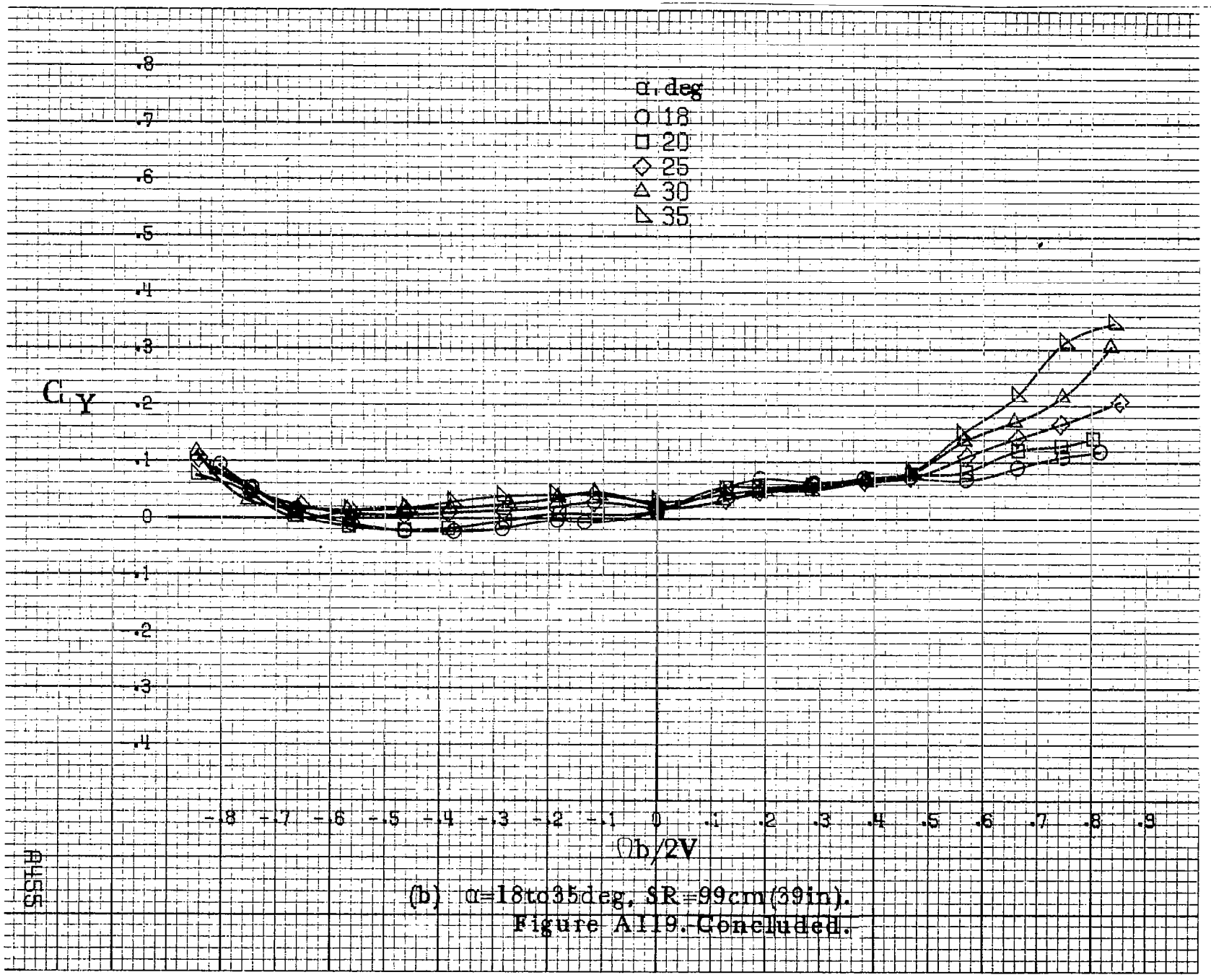

(b) α=18to35deg, SR=99cm(39in).

Figure A119.-Concluded.

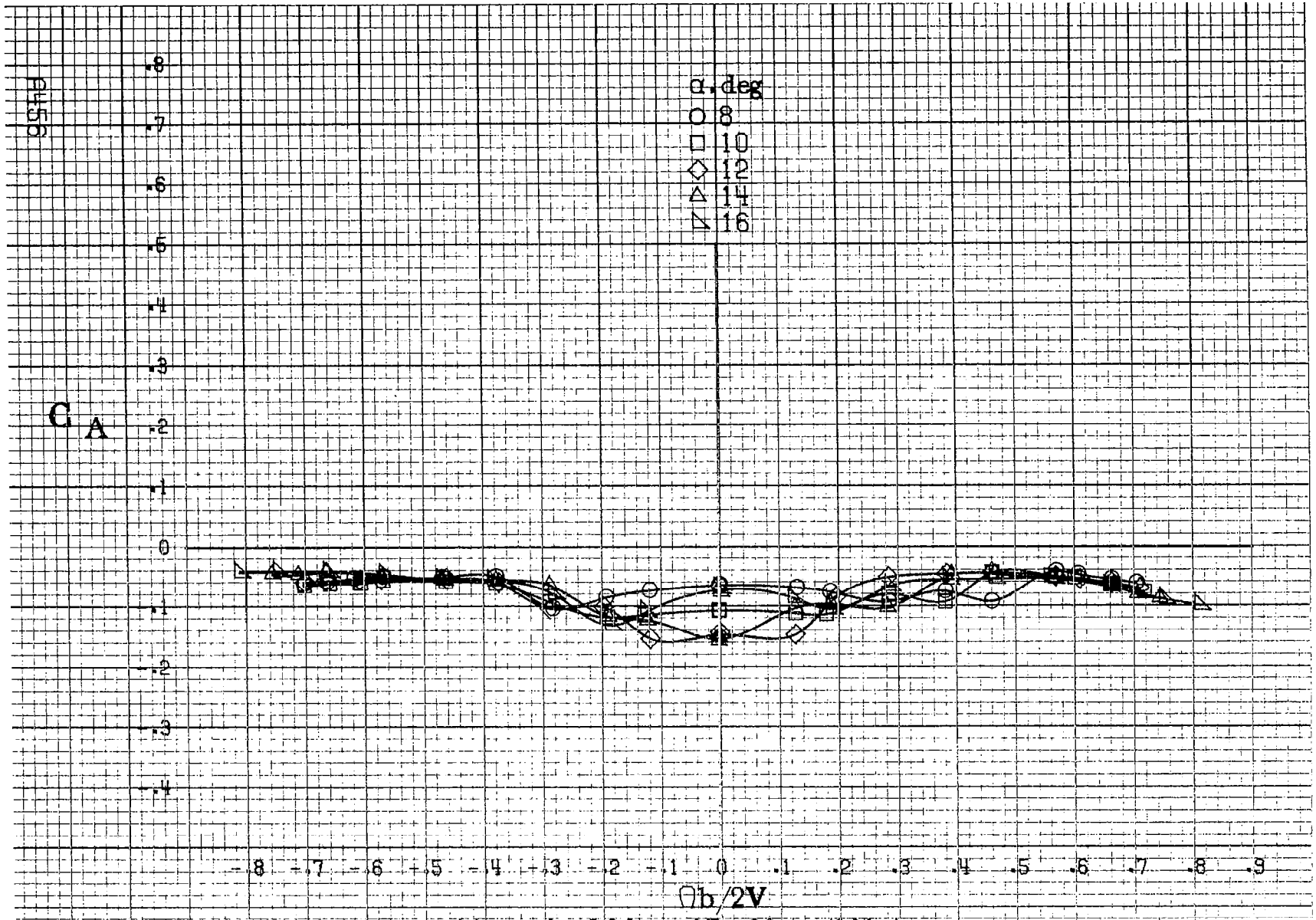

(a) α=8to16deg, SR=99cm(39in).

Figure A120.-Effect of rotation rate and angle of attack on axial-force coefficient for configuration having outboard LE wing droop extended inboard 42.7cm(16.8in). δ_e =0°, δ_a =0°, δ_r =0°, β =0°.

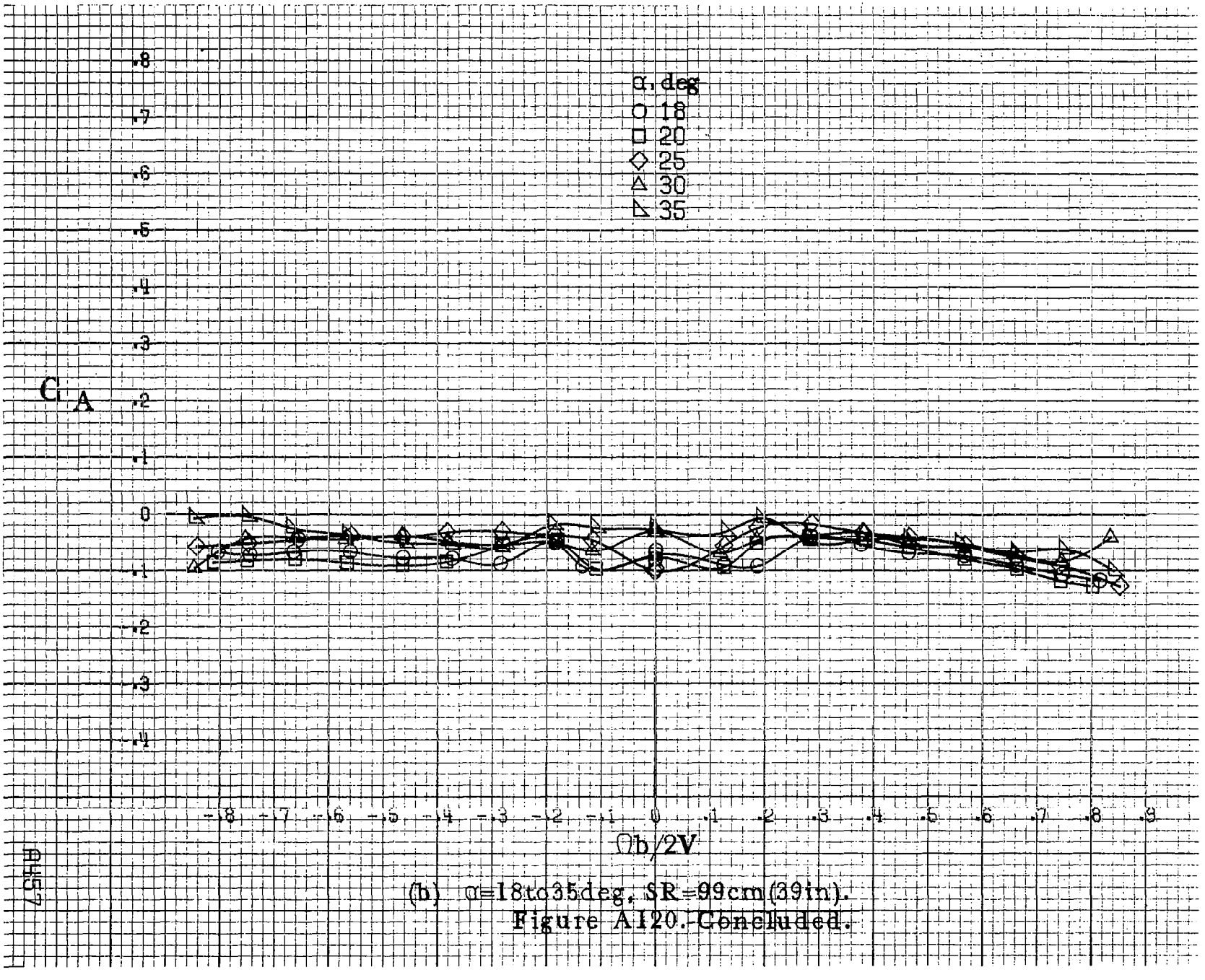

(b) α=18to35deg, SR=99cm(39in).

Figure A120.-Concluded.

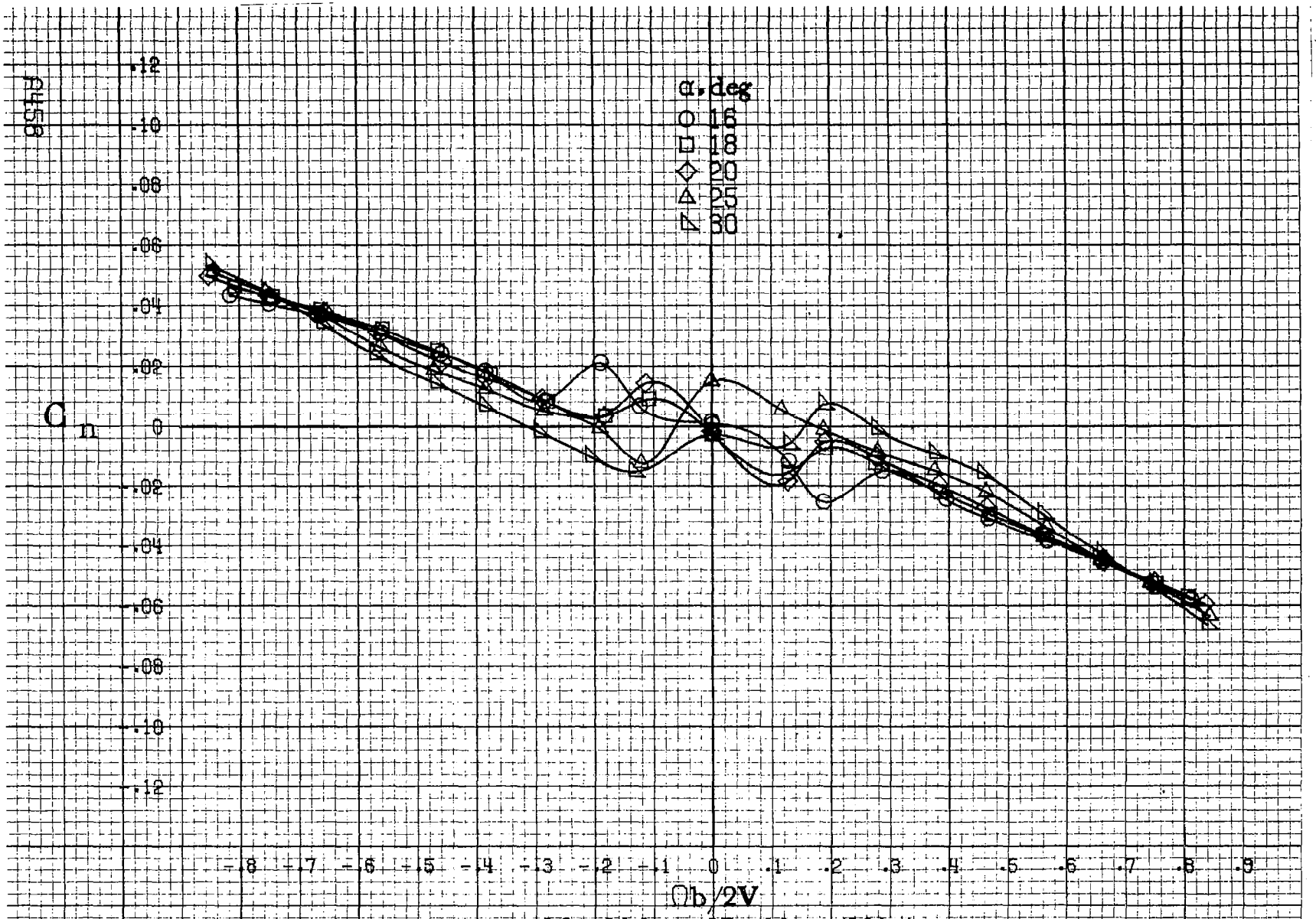

α=16to30deg, SR=99cm(39in).

Figure A121.-Effect of rotation rate and angle of attack on yawing-moment coefficient for configuration having outboard LE wing droop extended inboard 45.2cm(17.8in). δ_{a_1} =0°, δ_{a_2} =0°, δ_r =0°. β =0°.

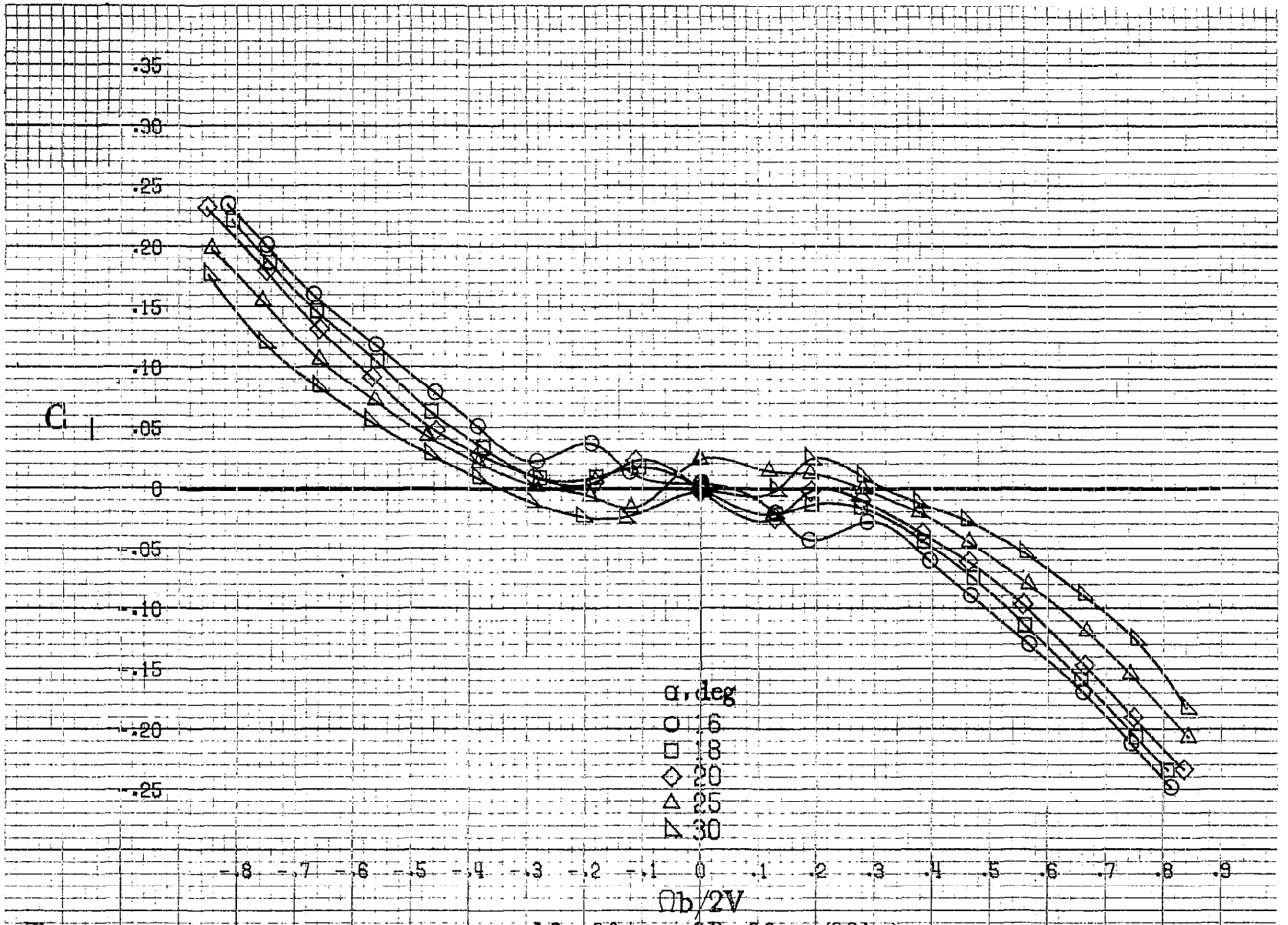

α=16to30deg, SR=99cm(39in).

Figure A122.-Effect of rotation rate and angle of attack on rolling-moment coefficient for configuration having outboard LE wing droop extended inboard 45.2cm(17.8in). δ_e =0°, δ_a =0°, δ_r =0°. β =0°.

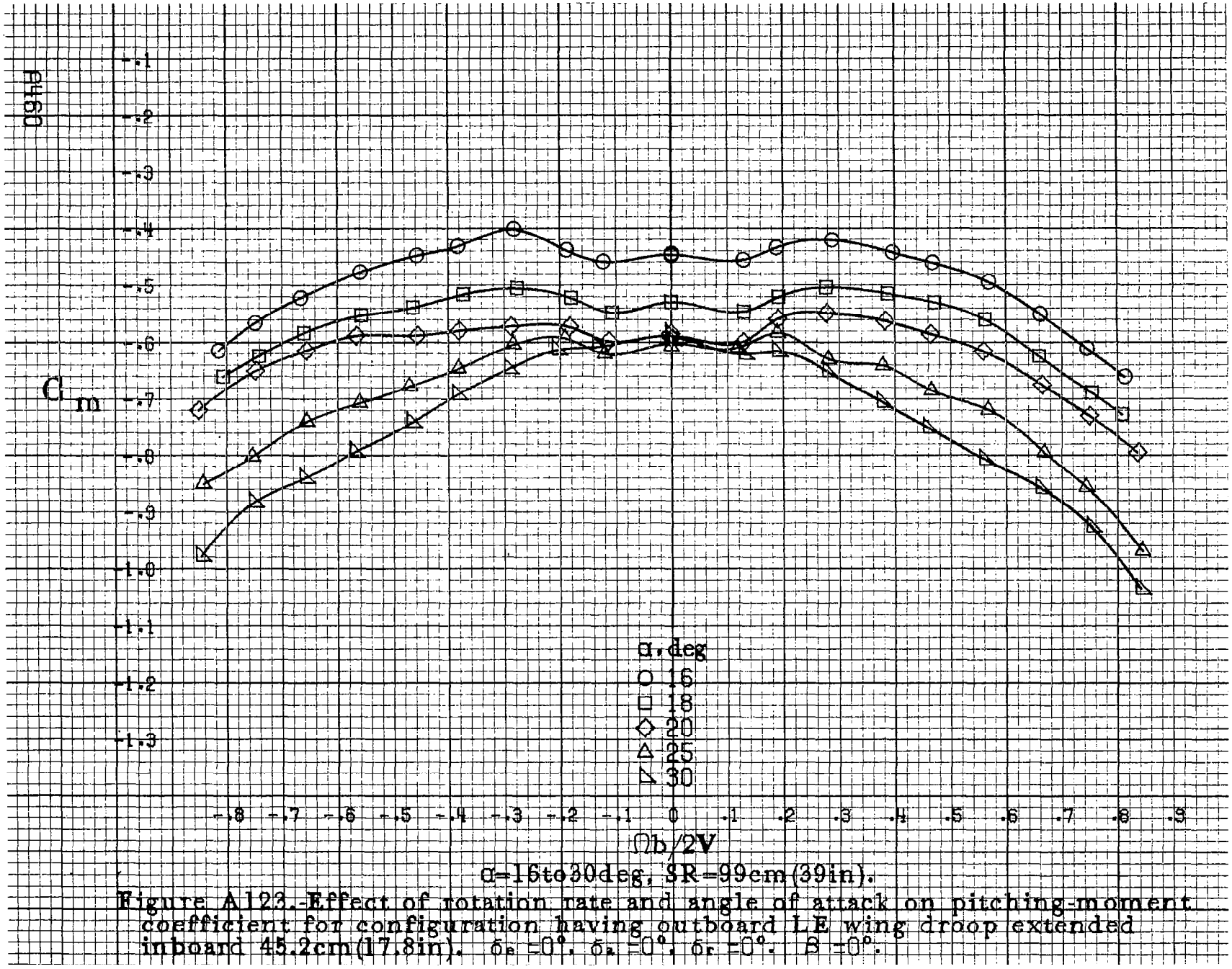

α=16to30deg, SR=99cm(39in).

Figure A123.-Effect of rotation rate and angle of attack on pitching-moment coefficient for configuration having outboard LE wing droop extended inboard 45.2cm(17.8in). δ_e =0°, δ_a =0°, δ_r =0°. β =0°.

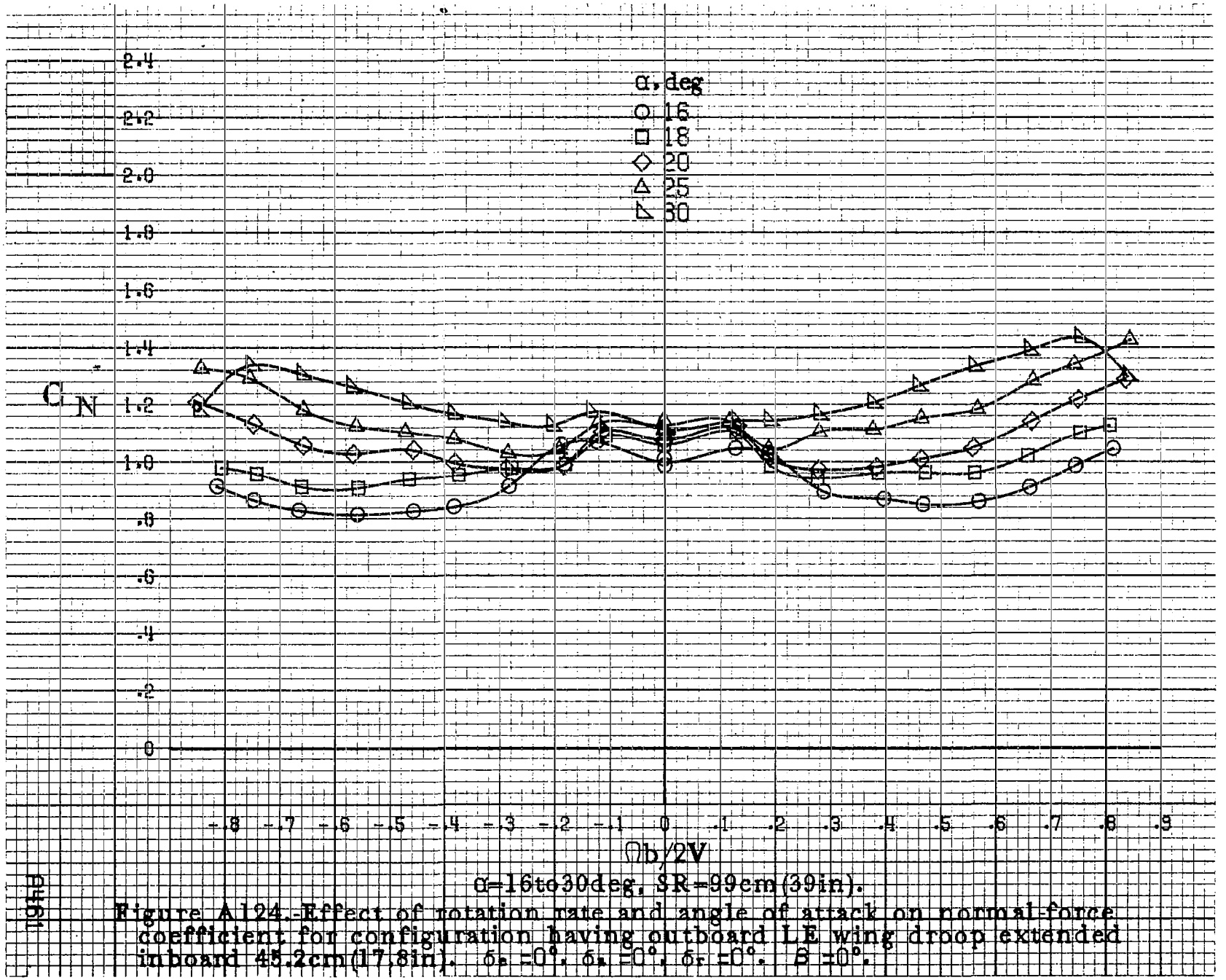

Figure A124.-Effect of rotation rate and angle of attack on normal-force coefficient for configuration having outboard LE wing droop extended inboard 45.2cm(17.8in). $\delta_a = 0°$, $\delta_s = 0°$, $\delta_r = 0°$. $\beta = 0°$.

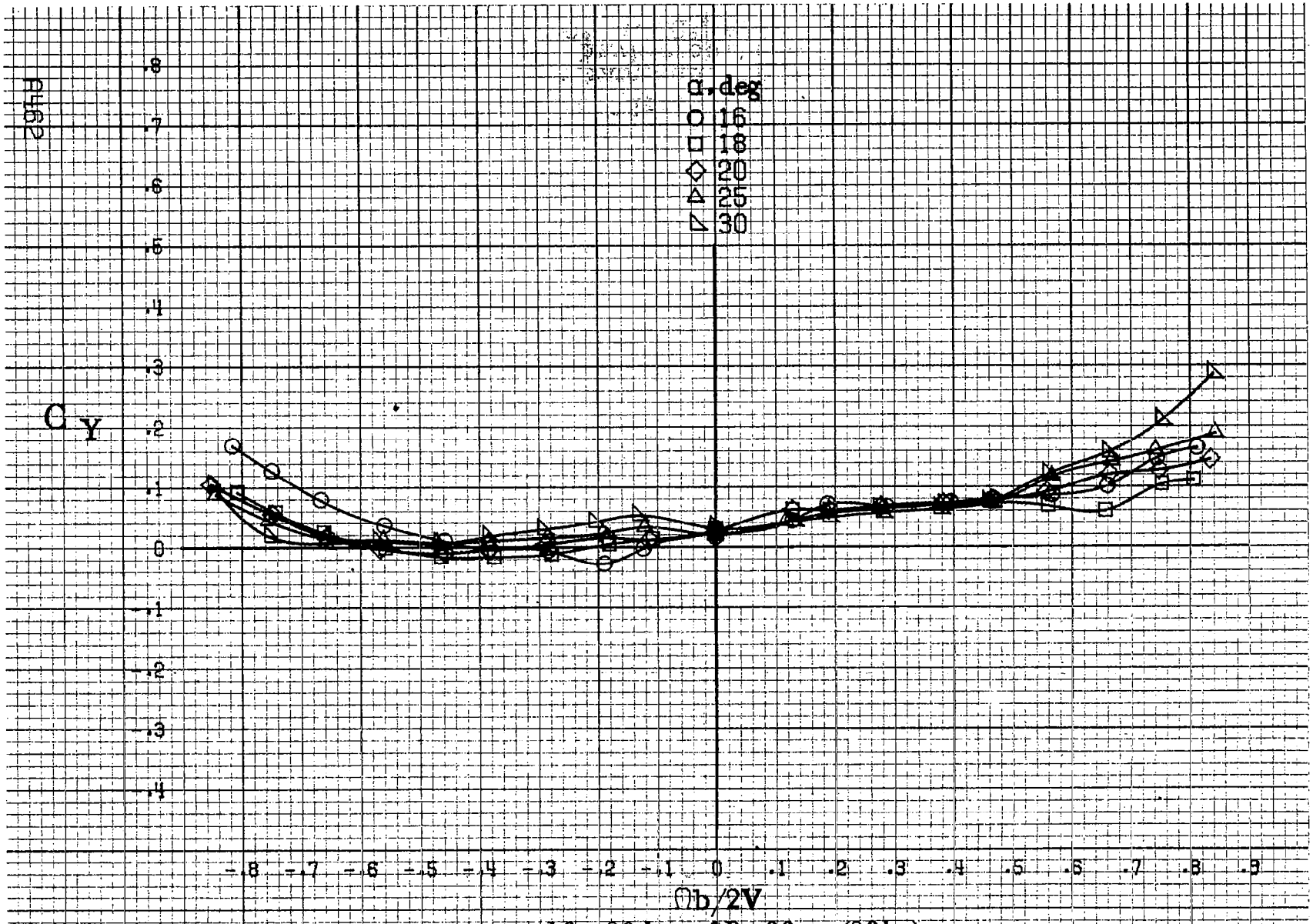

α=16to30deg, SR=99cm(39in).

Figure A125.-Effect of rotation rate and angle of attack on side-force coefficient for configuration having outboard LE wing droop extended inboard 45.2cm(17.8in). $\delta_a = 0°$, $\delta_s = 0°$, $\delta_r = 0°$. $\beta = 0°$.

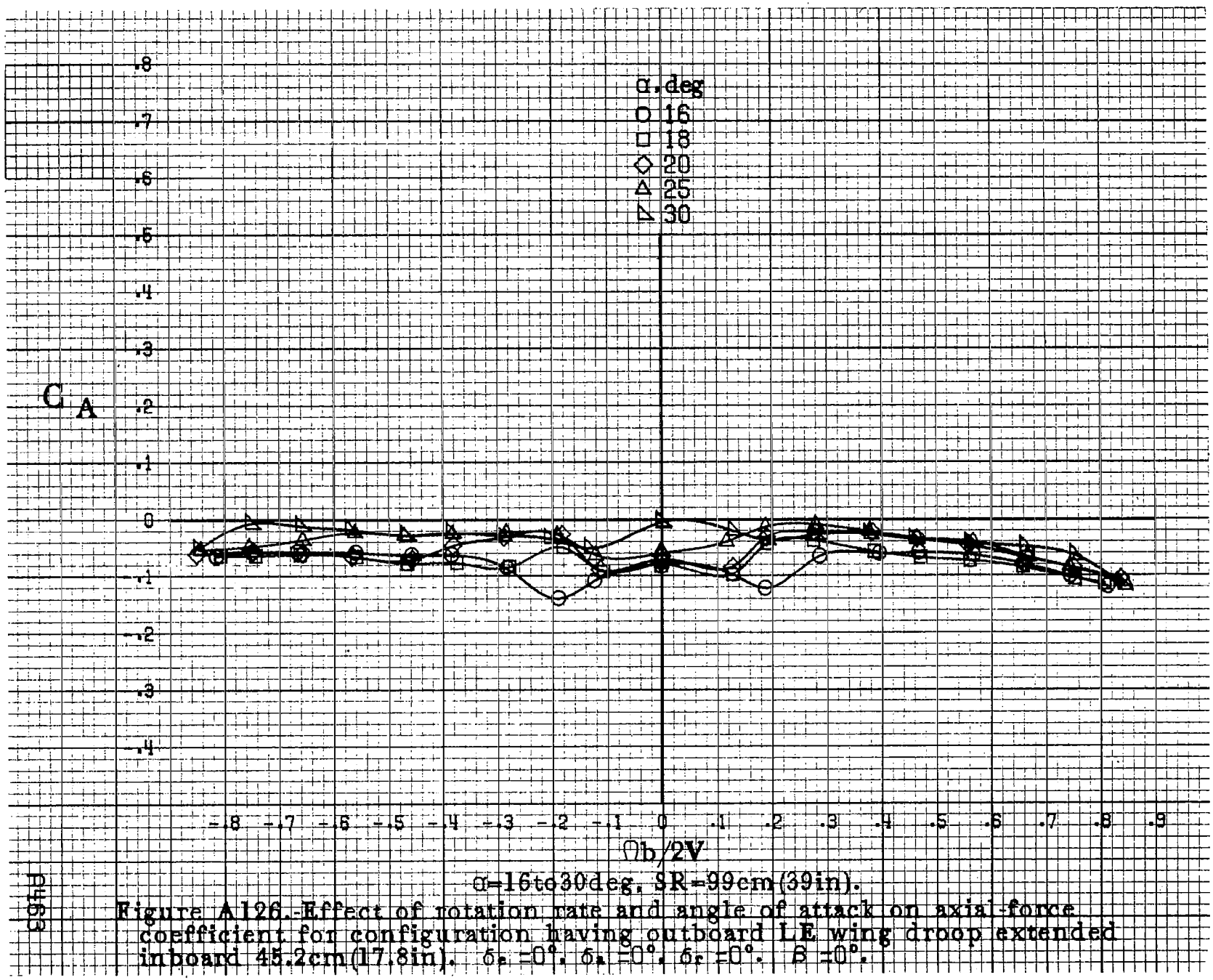

α=16to30deg, SR=99cm(39in).

Figure A126.-Effect of rotation rate and angle of attack on axial-force coefficient for configuration having outboard LE wing droop extended inboard 45.2cm(17.8in). δ_e =0°, δ_a =0°, δ_r =0°, β =0°.

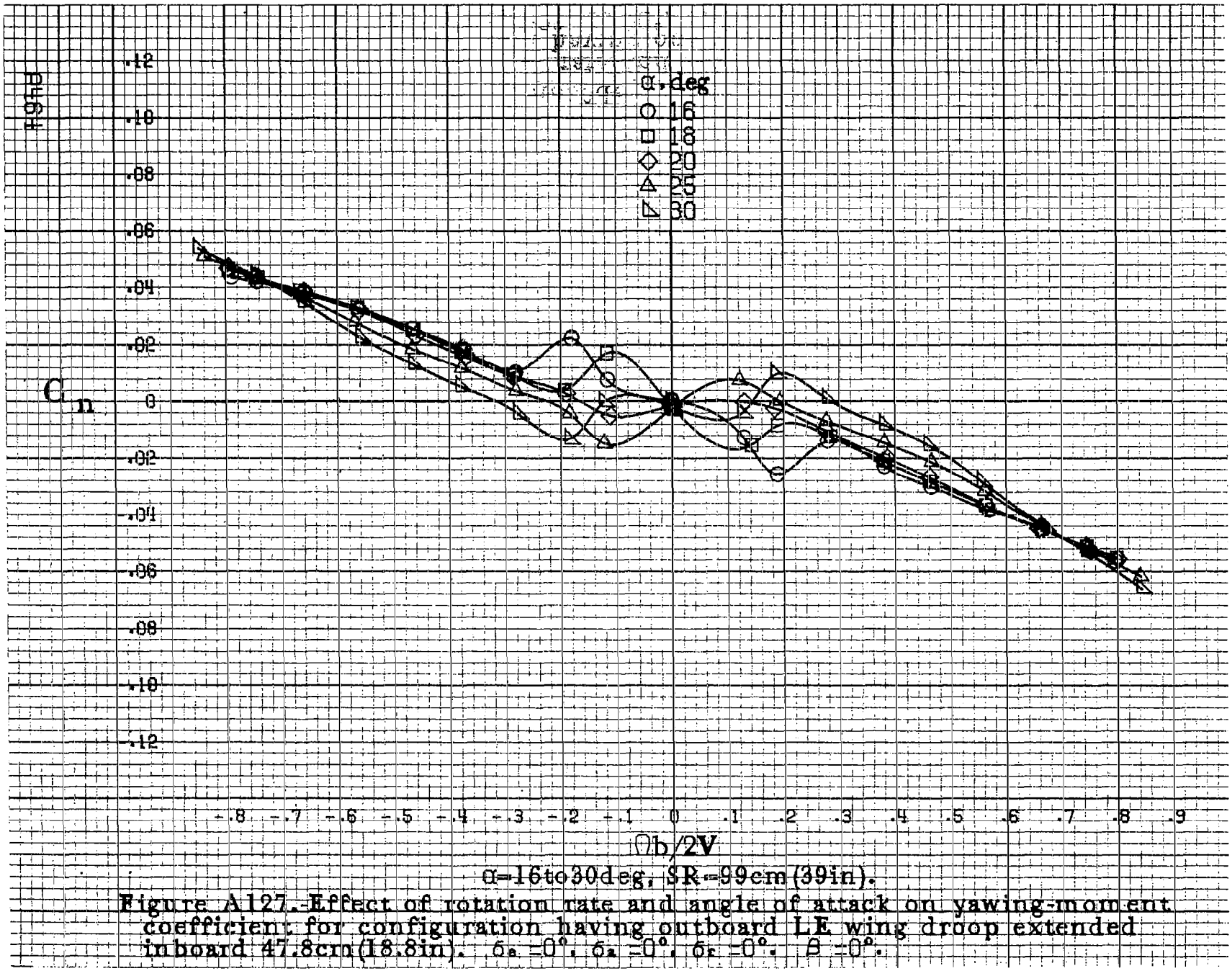

α=16to30deg, SR=99cm(39in).

Figure A127.-Effect of rotation rate and angle of attack on yawing-moment coefficient for configuration having outboard LE wing droop extended inboard 47.8cm(18.8in). δ_a =0°, δ_s =0°, δ_r =0°, β =0°.

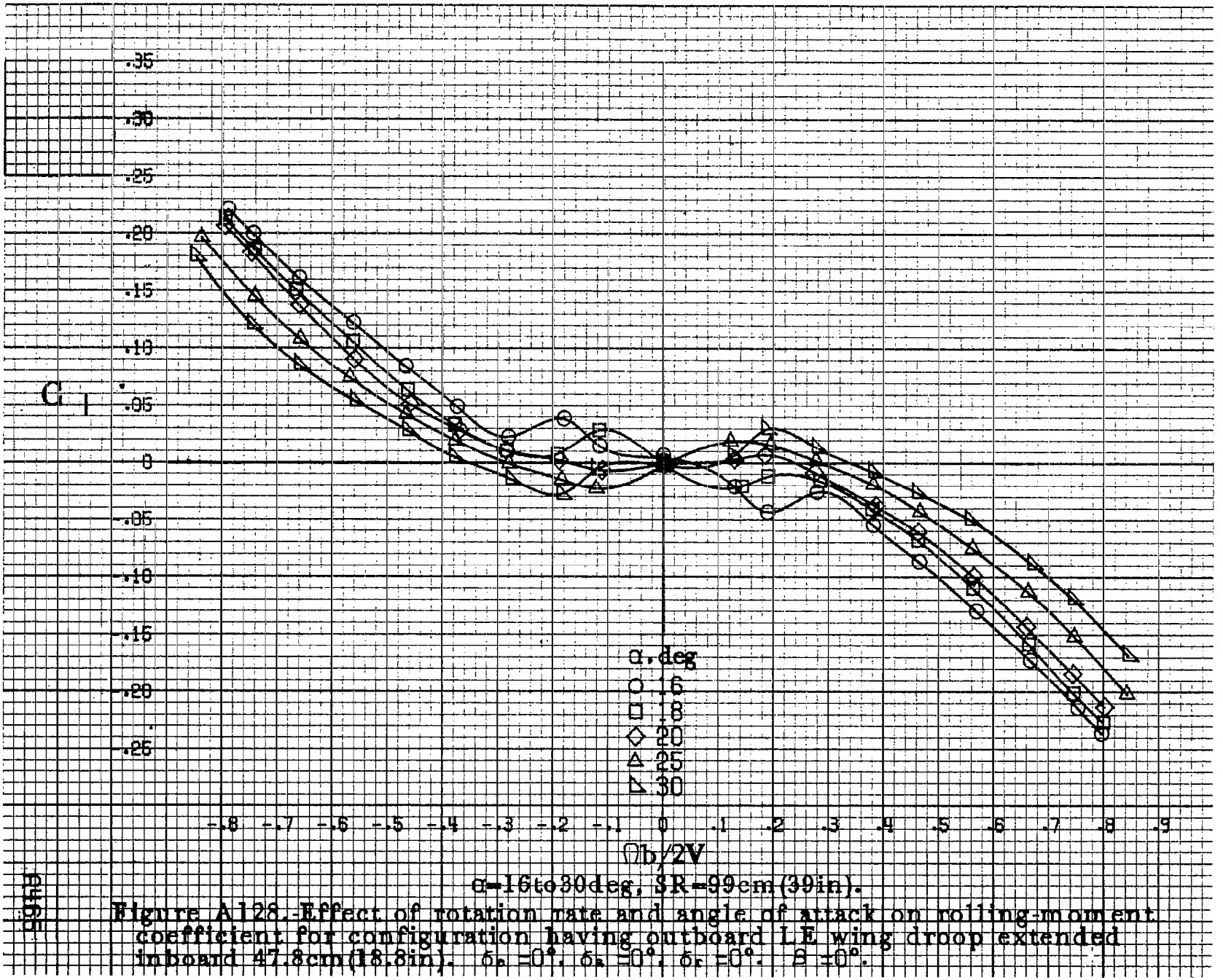

Figure A128.-Effect of rotation rate and angle of attack on rolling-moment coefficient for configuration having outboard LE wing droop extended inboard 47.8cm(18.8in). δ_a =0°, δ_s =0°, δ_r =0°. β =0°.

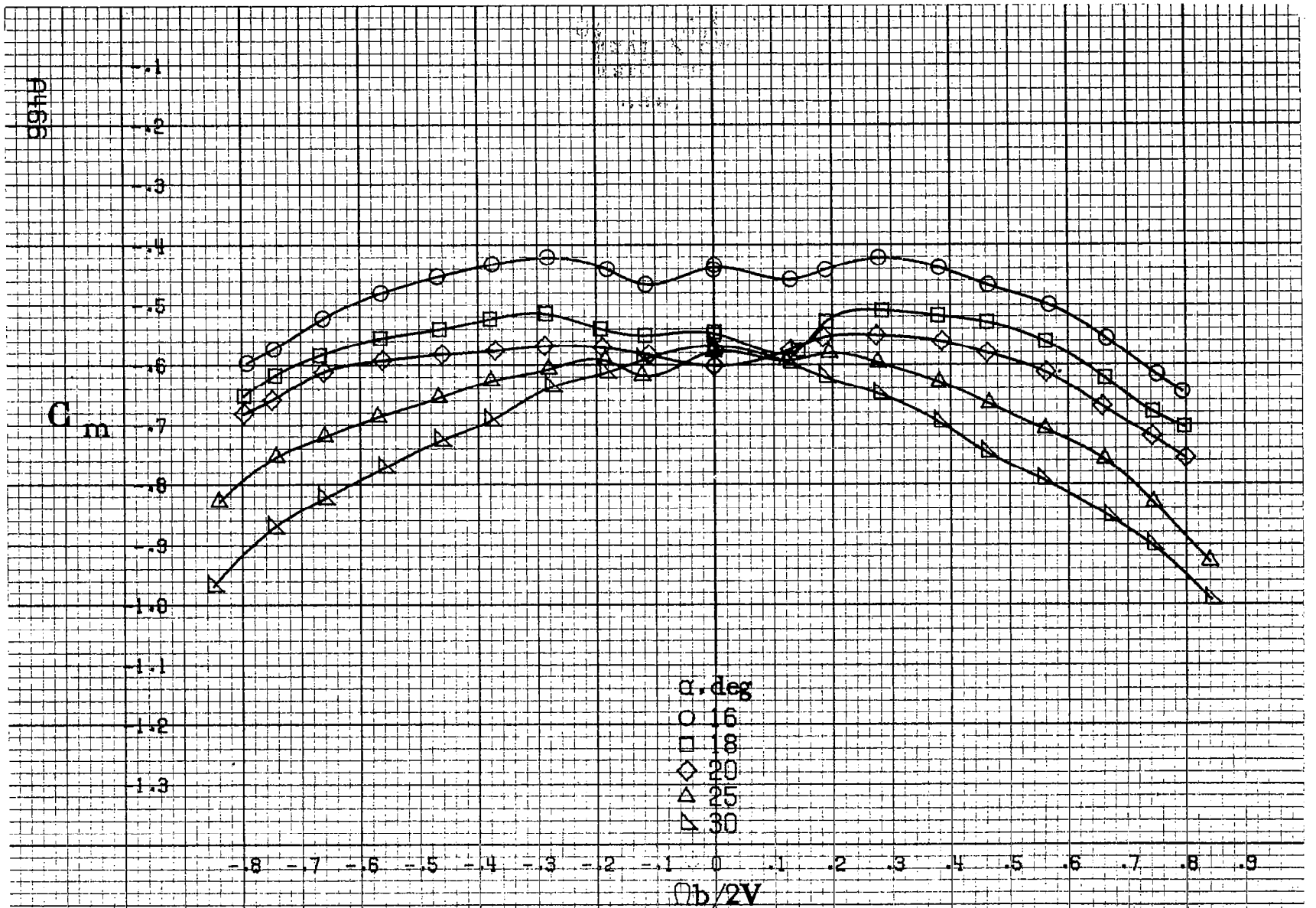

α=16to30deg, SR=99cm(39in).

Figure A129.-Effect of rotation rate and angle of attack on pitching-moment coefficient for configuration having outboard LE wing droop extended inboard 47.8cm(18.8in). $\delta_a = 0°$, $\delta_a = 0°$, $\delta_r = 0°$, $\beta = 0°$.

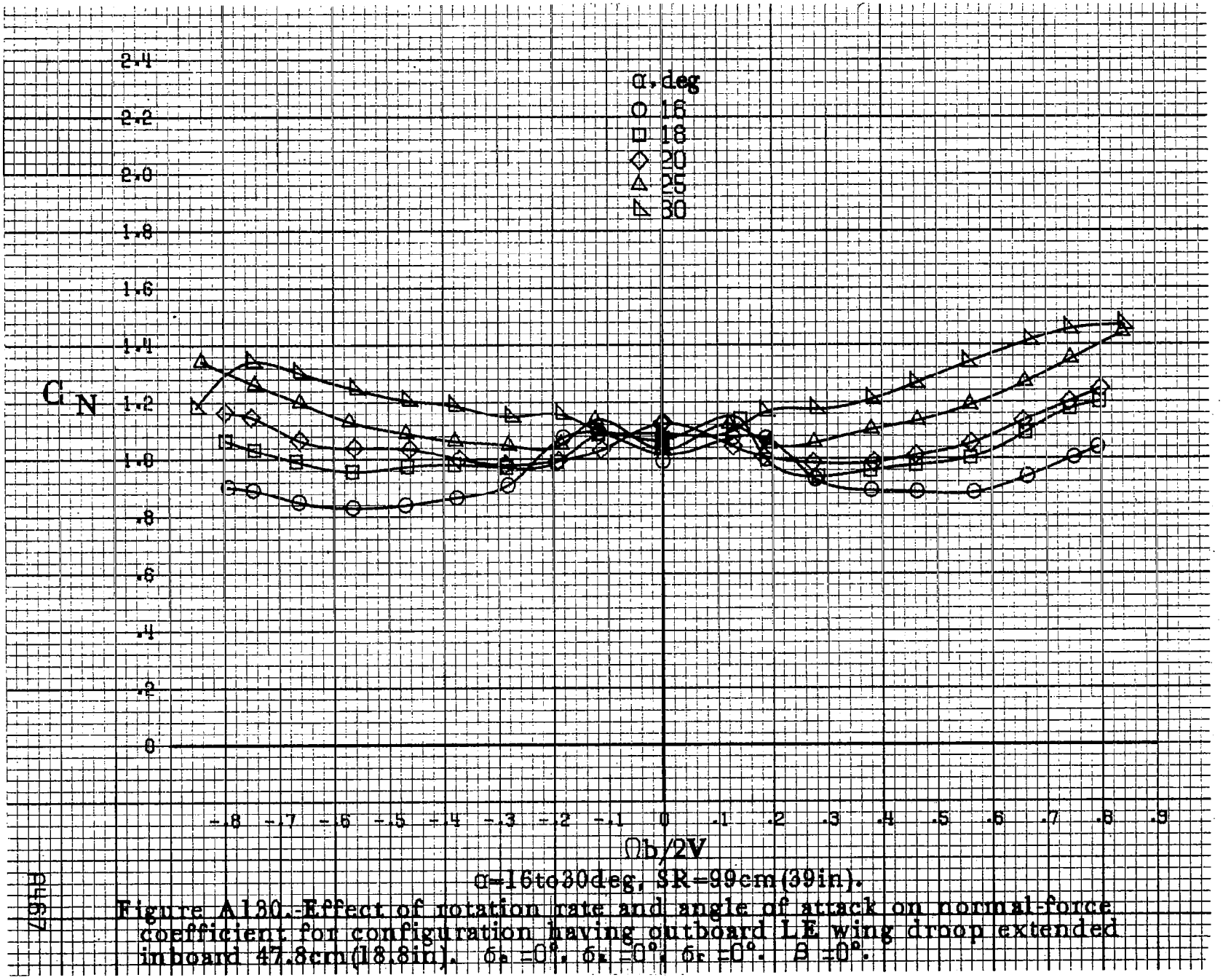

α=16to30deg, SR=99cm(39in).

Figure A130.-Effect of rotation rate and angle of attack on normal-force coefficient for configuration having outboard LE wing droop extended inboard 47.8cm(18.8in). $\delta_a = 0°$, $\delta_s = 0°$, $\delta_r = 0°$, $\beta = 0°$.

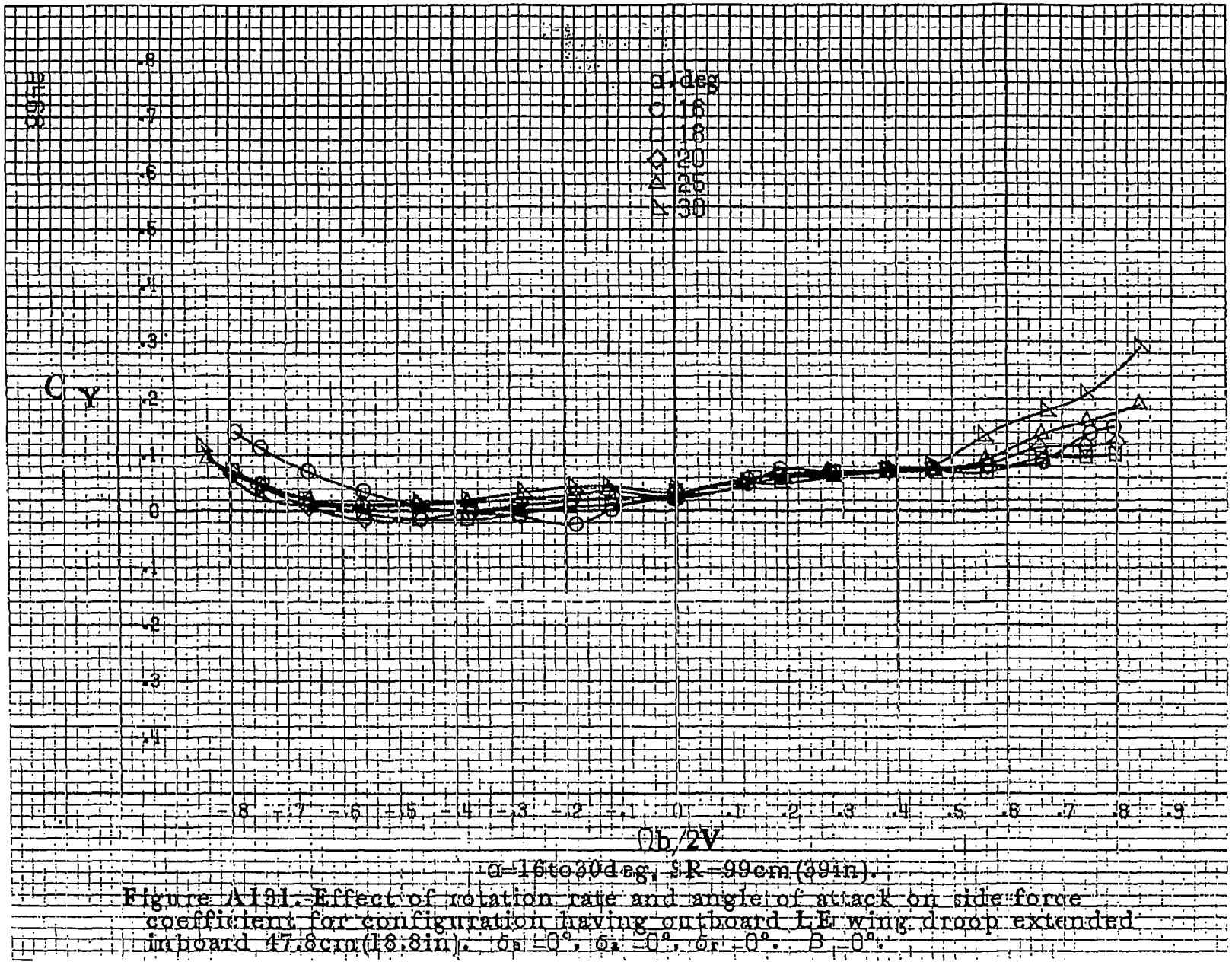

α=16to30deg, $\bar{c}$R=99cm(39in).

Figure A131.-Effect of rotation rate and angle of attack on side force coefficient for configuration having outboard LE wing droop extended inboard 47.8cm(18.8in). δ_a=0°, δ_s=0°, δ_r=0°, β=0°.

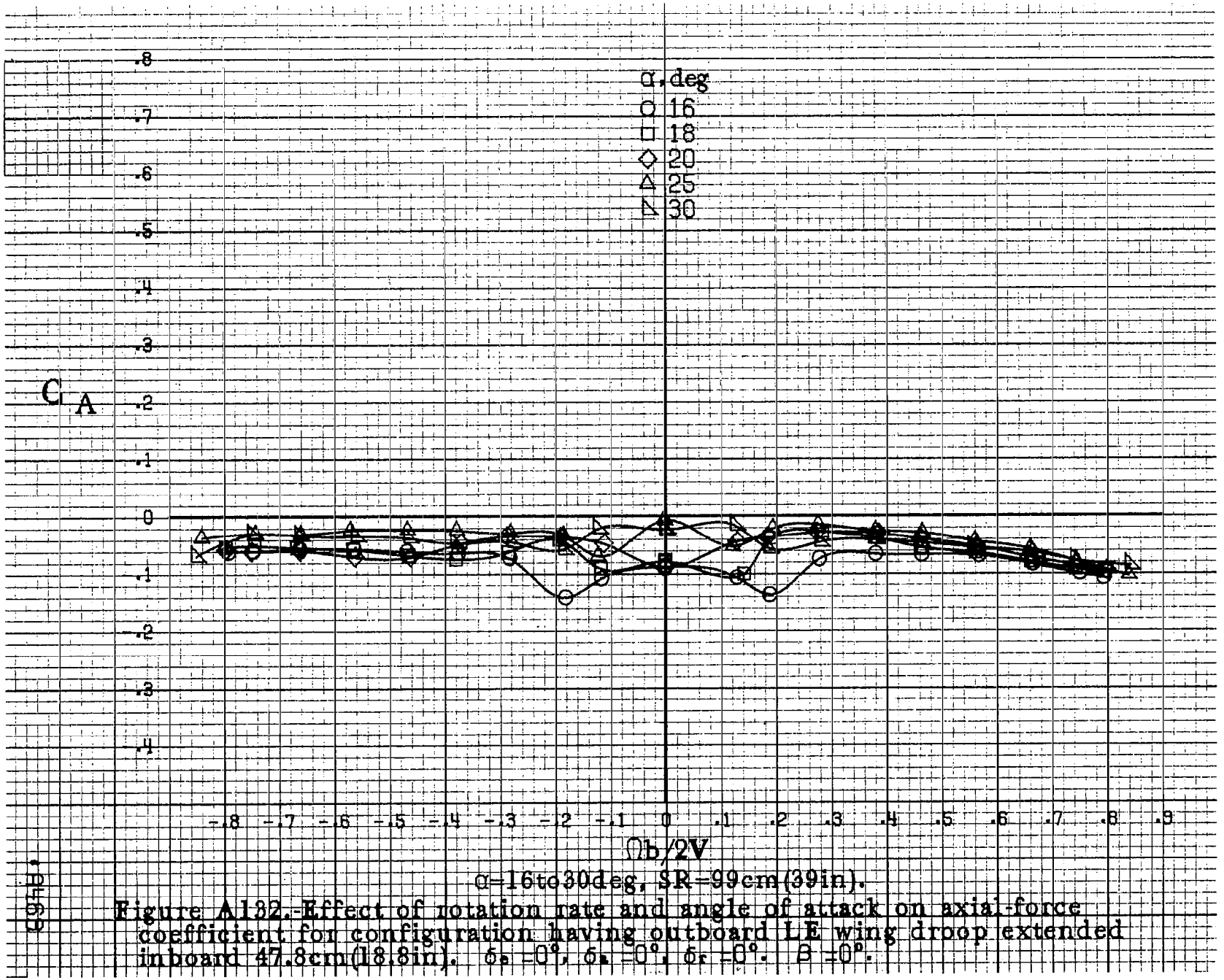

Figure A132.-Effect of rotation rate and angle of attack on axial-force coefficient for configuration having outboard LE wing droop extended inboard 47.8cm(18.8in). δ_a =0°, δ_s =0°, δ_r =0°. β =0°.

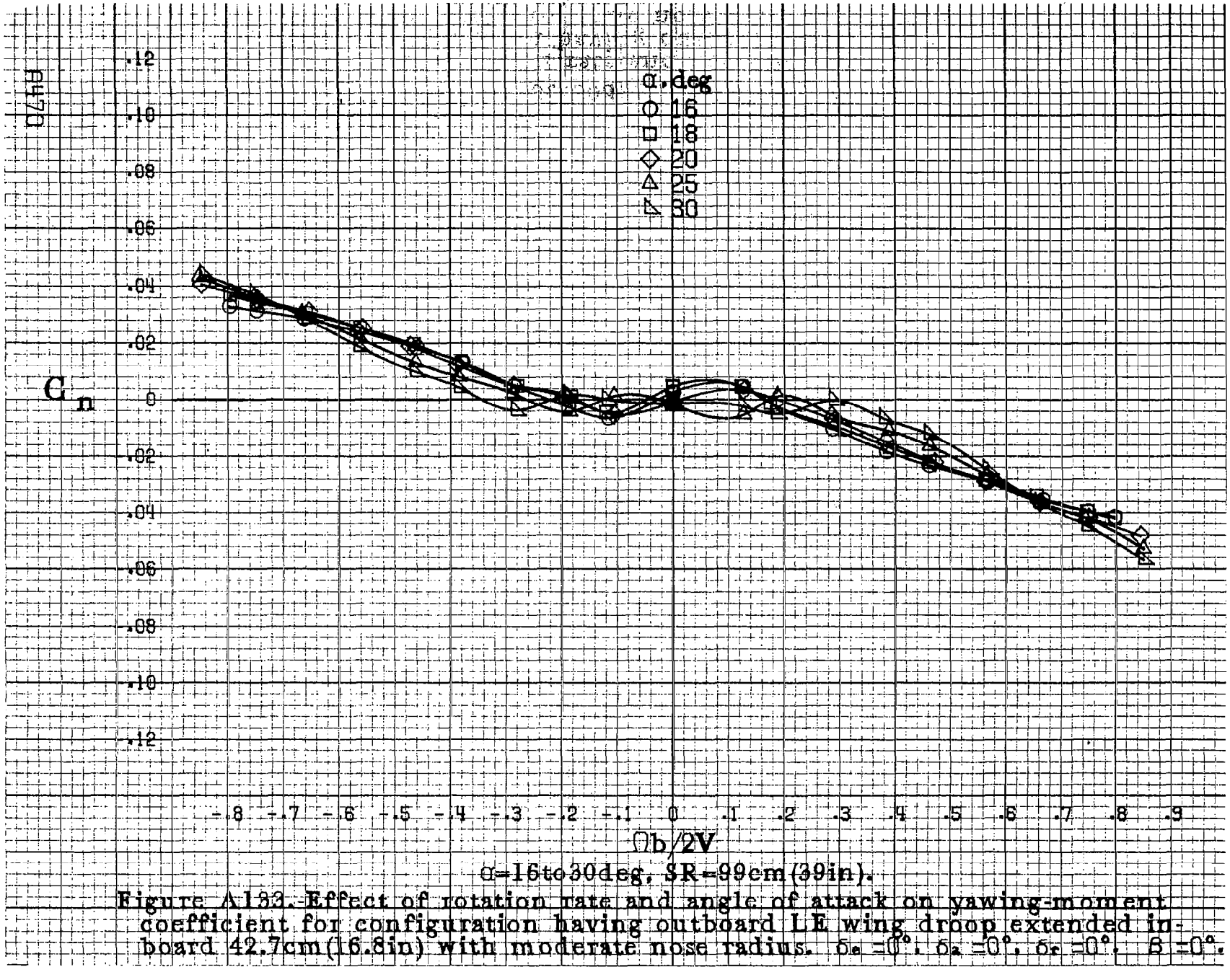

α=16to30deg, S_R=99cm(39in).

Figure A133. Effect of rotation rate and angle of attack on yawing-moment coefficient for configuration having outboard LE wing droop extended inboard 42.7cm(16.8in) with moderate nose radius. δ_e =0°, δ_a =0°, δ_r =0°, β =0°.

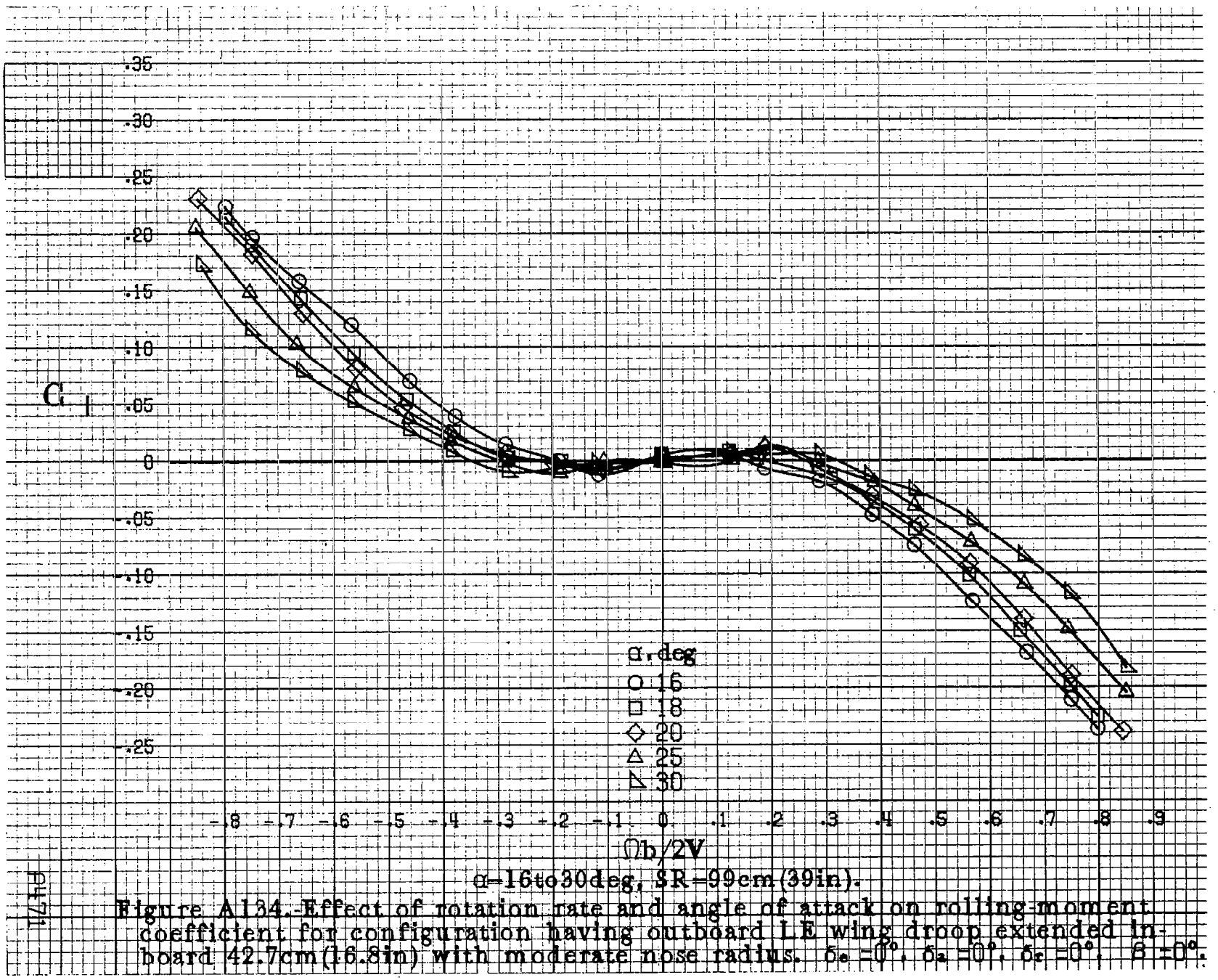

Figure A134.-Effect of rotation rate and angle of attack on rolling-moment coefficient for configuration having outboard LE wing droop extended inboard 42.7cm(16.8in) with moderate nose radius. $\delta_e = 0°$, $\delta_a = 0°$, $\delta_r = 0°$, $\beta = 0°$.

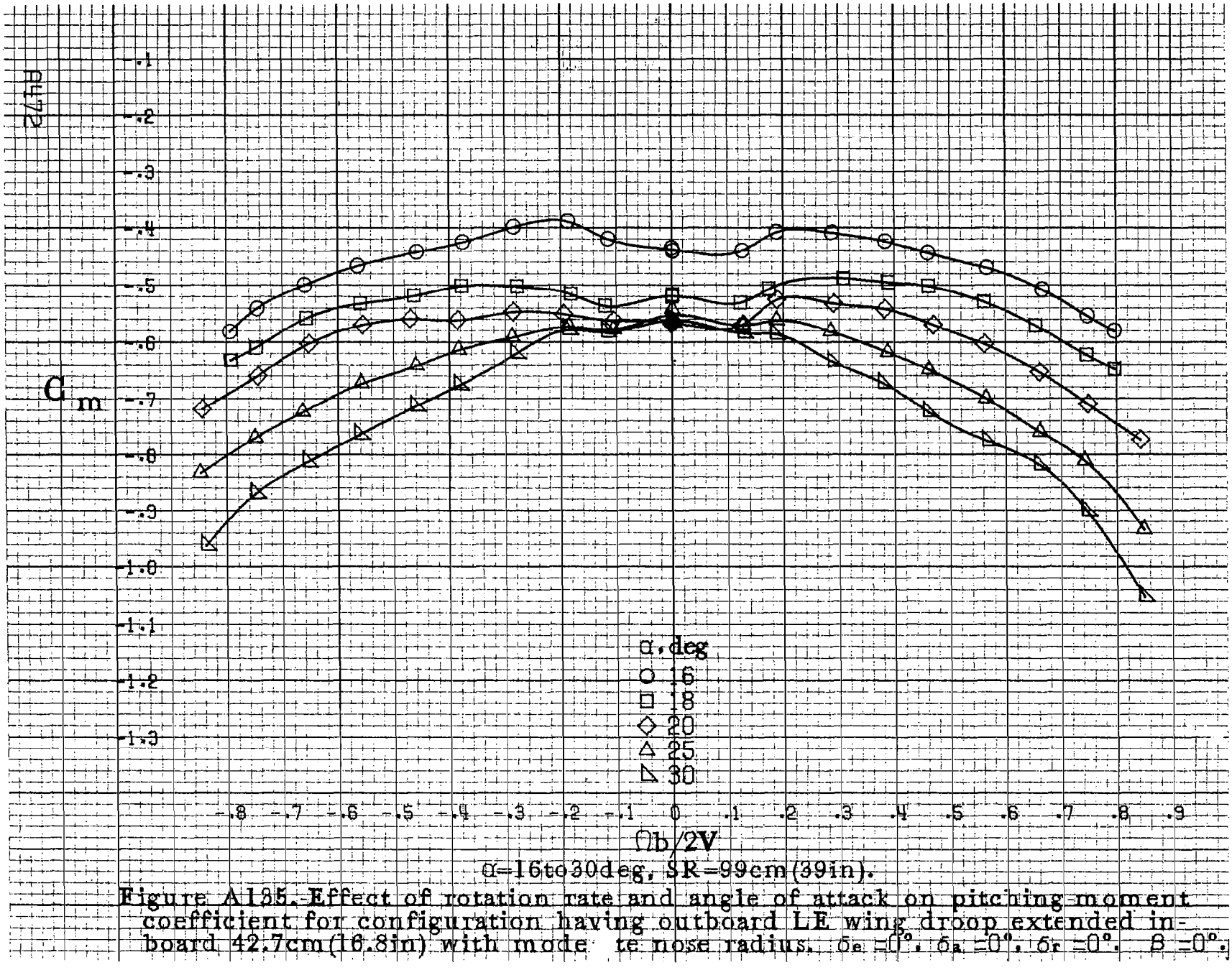

α=16to30deg, SR=99cm(39in).

Figure A125. Effect of rotation rate and angle of attack on pitching moment coefficient for configuration having outboard LE wing droop extended inboard 42.7cm(16.8in) with moderate nose radius. $\delta_e = 0°$, $\delta_a = 0°$, $\delta_r = 0°$, $\beta = 0°$.

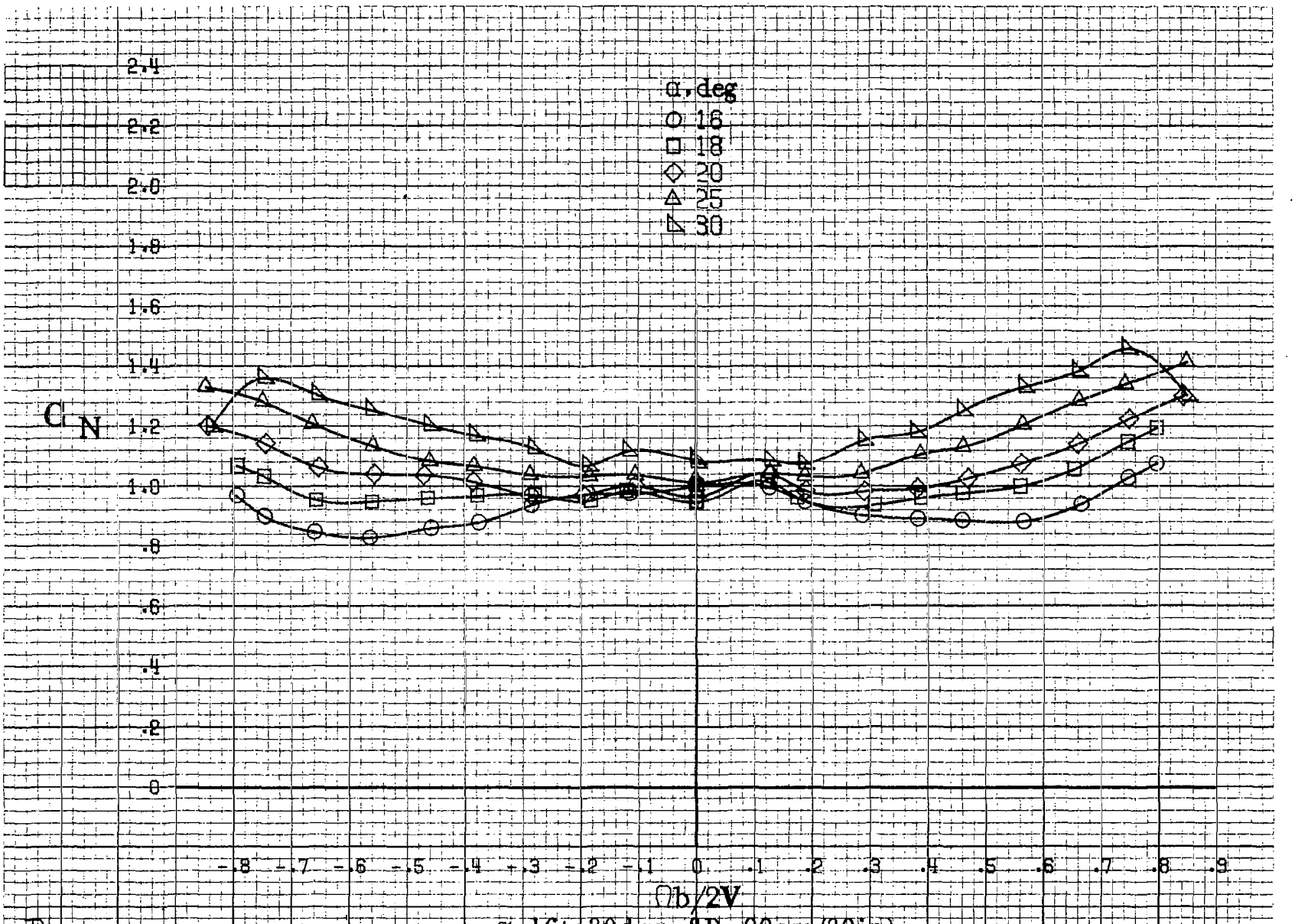

α=16to30deg, SR=99cm(39in).

Figure A136.-Effect of rotation rate and angle of attack on normal-force coefficient for configuration having outboard LE wing droop extended inboard 42.7cm(16.8in) with moderate nose radius. δ_a=0°, δ_s=0°, δ_r=0°, δ=0°.

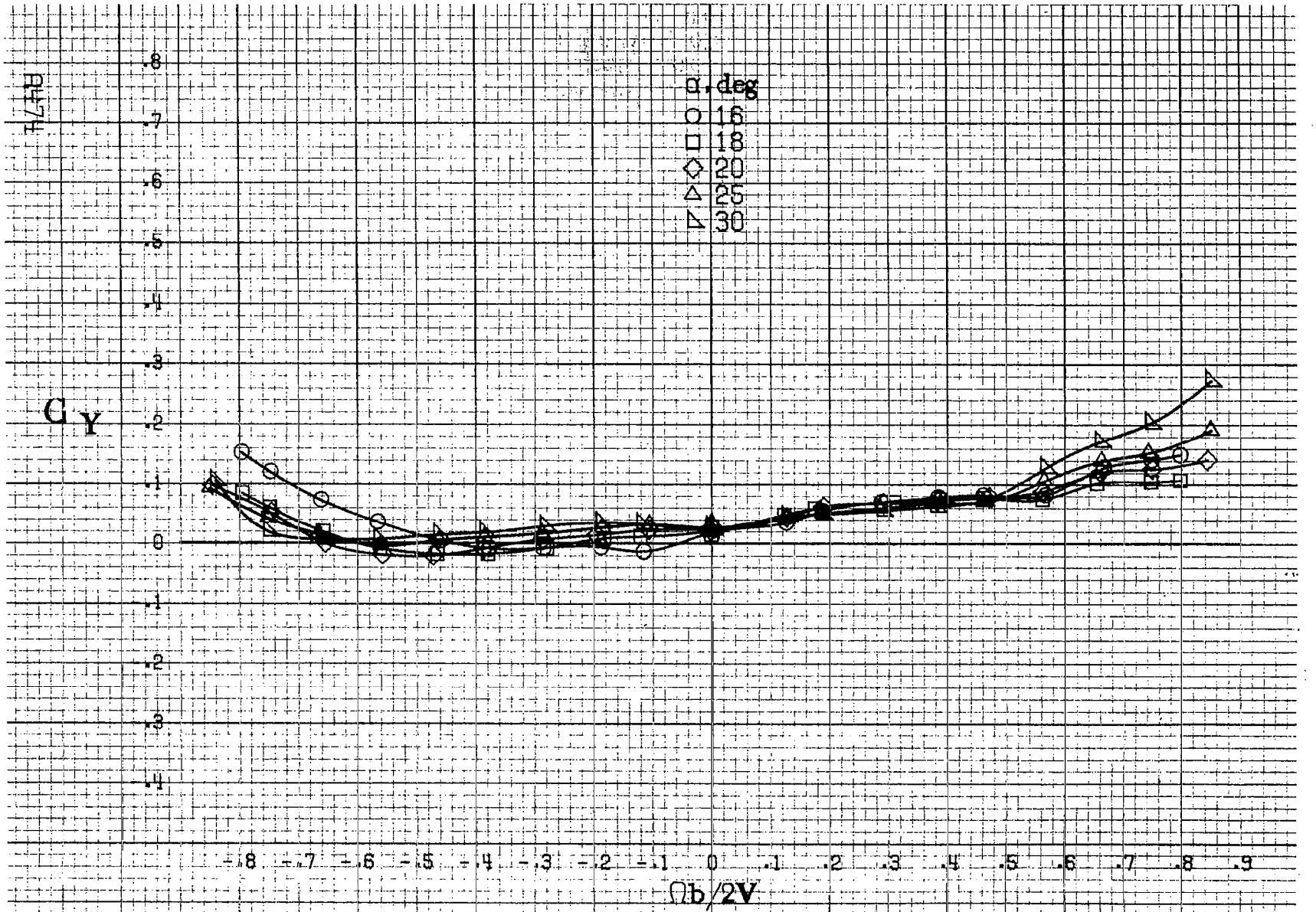

α=16to30deg, SR=99cm(39in).

Figure A137.-Effect of rotation rate and angle of attack on side-force coefficient for configuration having outboard LE wing droop extended inboard 42.7cm(16.8in) with moderate nose radius. $\delta_e = 0°$, $\delta_a = 0°$, $\delta_r = 0°$. $\beta = 0°$.

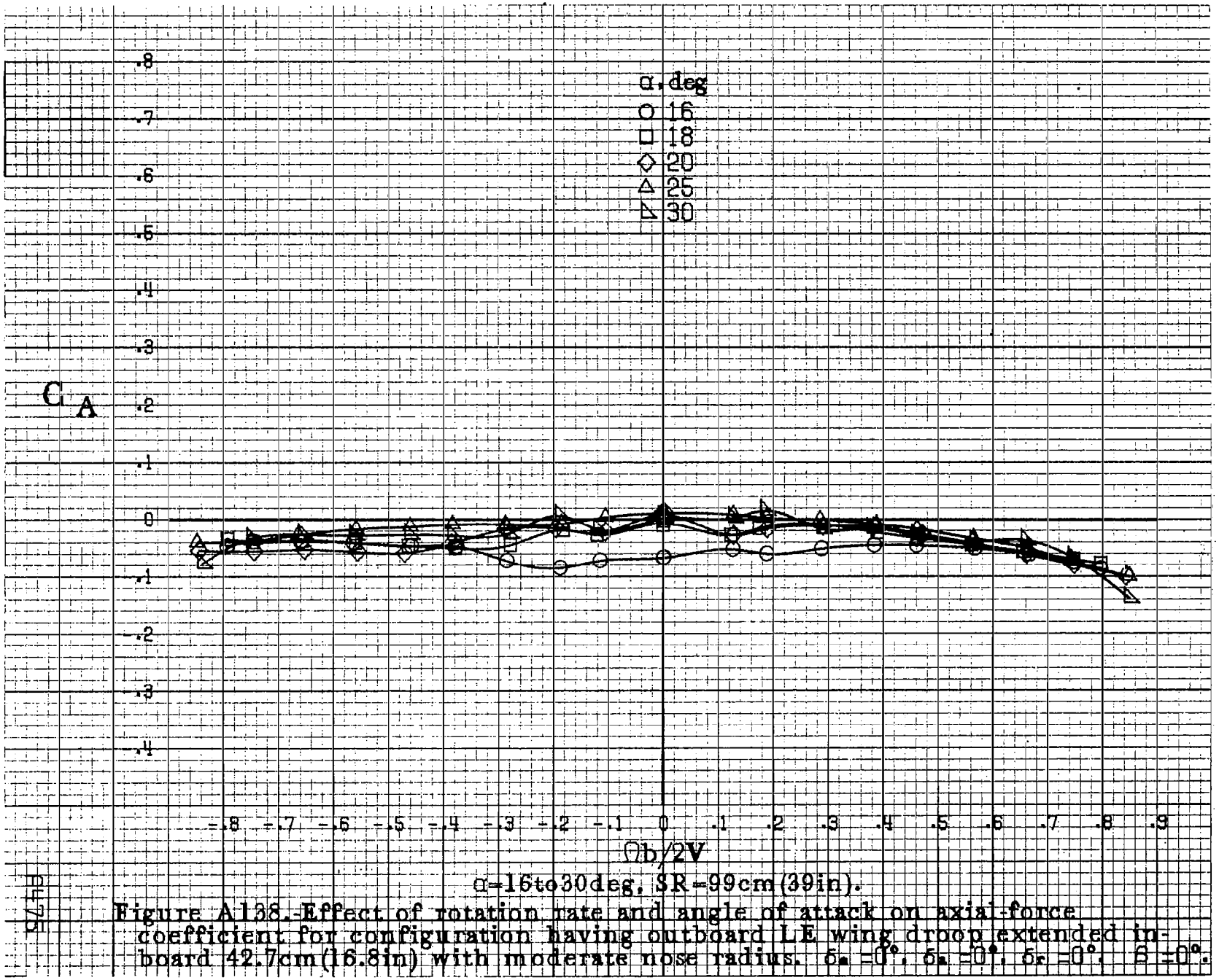

α=16to30deg, SR=99cm(39in).

Figure A138.-Effect of rotation rate and angle of attack on axial-force coefficient for configuration having outboard LE wing droop extended inboard 42.7cm(16.8in) with moderate nose radius. $\delta_e = 0°$, $\delta_a = 0°$, $\delta_r = 0°$, $\beta = 0°$.

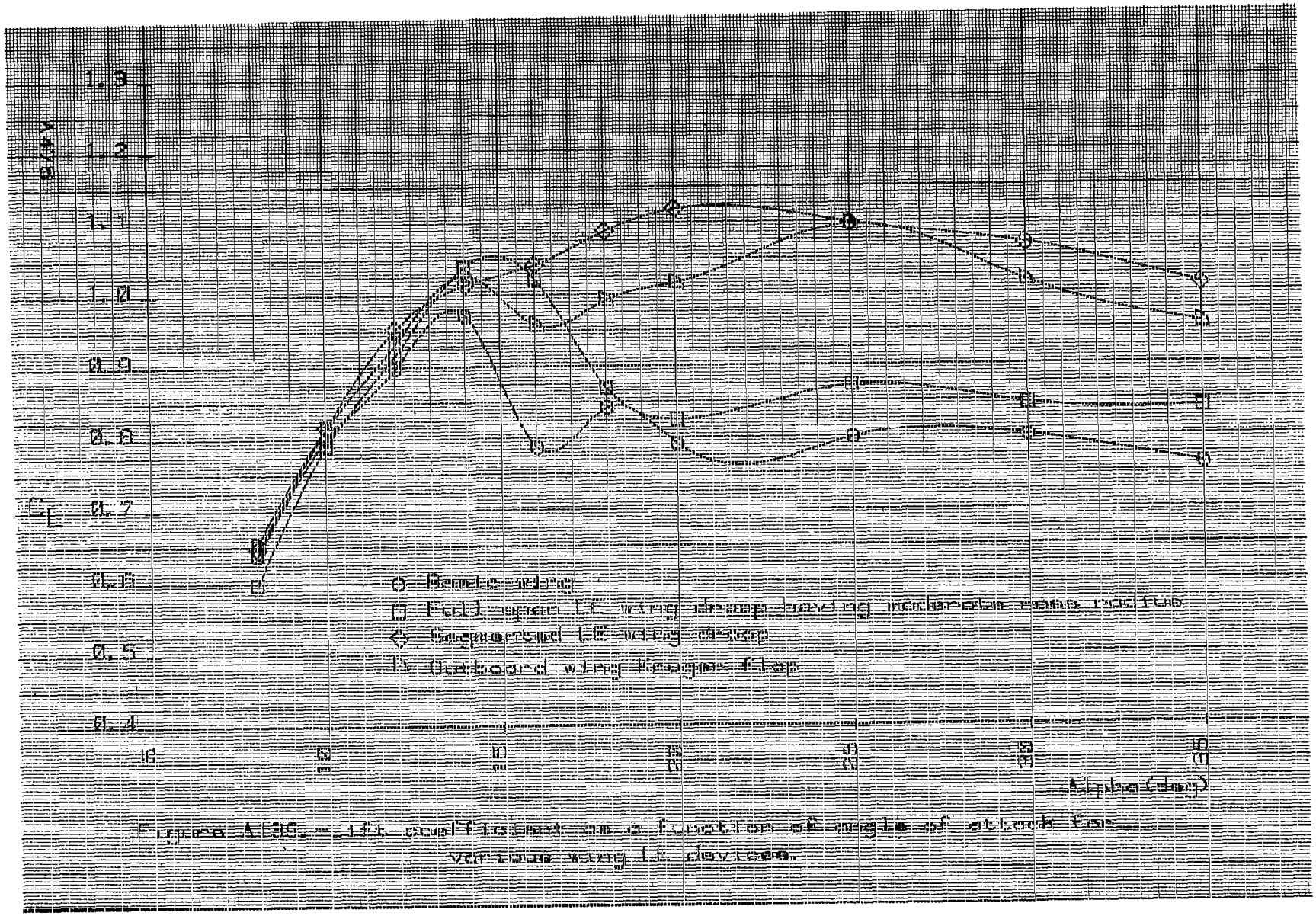

Figure A-30. Lift coefficient as a function of angle of attack for various wing LE devices.

Figure A148.- Lift coefficient as a function of angle of attack for various span LE outboard wing droops.

*U.S. GOVERNMENT PRINTING OFFICE: 1979 - 635-004/18

1. Report No.	2. Government Accession No.	3. Recipient's Catalog No.
NASA CR-3097		

4. Title and Subtitle	5. Report Date
Rotary Balance Data for a Typical Single-Engine General Aviation Design for an Angle-of-Attack Range of 8^{o} to 90^{o}. I - High-Wing Model B.	September 1979
	6. Performing Organization Code
7. Author(s) William Bihrle, Jr. Randy S. Hultberg	8. Performing Organization Report No.
	10. Work Unit No. 505-10-13-07
9. Performing Organization Name and Address Bihrle Applied Research, Inc. 400 Jericho Turnpike Jericho, New York 11753	11. Contract or Grant No. NAS1-14849
	13. Type of Report and Period Covered Contractor Report
12. Sponsoring Agency Name and Address National Aeronautics and Space Administration Washington, DC 20546	14. Sponsoring Agency Code

15. Supplementary Notes
Langley Technical Monitor: James S. Bowman, Jr.

Topical report

16. Abstract

Aerodynamic characteristics obtained in a rotational flow environment utilizing a rotary balance located in the Langley spin tunnel are presented in plotted form for a 1/6.5-scale, single-engine, high-wing, general aviation airplane model. The configurations tested included the basic airplane, various wing leading-edge devices, tail designs, and rudder control settings as well as airplane components. Date are presented without analysis for an angle-of attack range of 8^{o} to 90^{o} and clockwise and counter-clockwise rotations covering an $\frac{\Omega b}{2V}$ range from 0 to 0.85.

17. Key Words (Suggested by Author(s))	18. Distribution Statement
General Aviation Spinning Rotary Balance High angle-of-attack wind tunnel data	Unclassified - Unlimited Subject Category 02

19. Security Classif. (of this report)	20. Security Classif. (of this page)	21. No. of Pages	22. Price*
Unclassified	Unclassified	495	$15.00

*For sale by the National Technical Information Service, Springfield, Virginia 22161